CONF-9407103--

LA-UR- 95-1792

Title: AIP CONFERENCE PROCEEDINGS - INTERNATIONAL CONFERENCE ON ACCELERATOR-DRIVEN TRANSMUTATION TECHNOLOGIES AND APPLICATIONS, LAS VEGAS, NEVADA, JULY 25-29, 1994

Author(s): S. O. Schriber, E. Arthur, A. A. Rodriguez

Submitted to: Accelerator-Driven Transmutation Technologies & Applications,
Las Vegas, NV, July 25-29, 1994

Los Alamos
NATIONAL LABORATORY

Contents

An Overview of the
International Conference on Accelerator Driven Transmutation Technologies and Applications

MGM Grand Hotel
Las Vegas, Nevada,
July 25-29, 1994

This Conference was the first to bring together US and foreign researchers to define Accelerator Driven Transmutation Technology (ADTT) concepts in several important national and international application areas -- nuclear waste transmutation, minimizing of world plutonium inventories, and long-term energy production.

The Conference covered a number of diverse technological areas -- accelerators, target/blankets, separations, materials -- that make up ADTT systems. The meeting provided one of the first opportunities for specialists in these technologies to meet together and learn about system requirements, components, and interface issues. It was also an opportunity to formulate plans for future developments in ADTT.

The Conference also provided an occasion to describe the initiation of a Russian ADTT project which will be funded over the next two years by the International Science and Technology Center in Moscow. Approximately four-hundred Russian scientists will be working on concept definition and design, and beginning experiments.

During the Conference, over one hundred technical presentations were made describing ADTT system and technology concepts as well as the impact of ADTT on issues related to global plutonium management and the high-level nuclear waste problem areas. These included

- twenty-eight papers on accelerators,
- thirty-nine papers on target/blanket, and safety issues,
- twelve papers on materials properties and requirements,
- thirteen papers on technologies for materials separations,
- thirteen papers on planned or executed experiments as well as data needs, and
- fourteen papers on system performance and overviews of several international efforts.

The meeting also included

- a video address by Senator Pete Domenici (R-New Mexico) on the use of accelerator technology to address a number of significant problem areas and to meet important national requirements;

- a statement from the Governor of Nevada who expressed interest in the technology and related subjects because of their potential impact on high-level nuclear waste disposal;
- a panel discussion on the relationship of ADTT and repository approaches for high-level nuclear waste disposal;
- breakout groups in the several technical areas of the Conference -- accelerators, target/blankets, separations, materials, experiments -- that began to identify issues, development needs and next steps for demonstration and testing;
- a tour of the Yucca Mountain site which is being evaluated by the US Department of Energy as a potential disposal facility for high-level nuclear waste; and
a banquet speech by the new president of the American Nuclear Society,Alan Waltar, concerning the importance of nuclear power as a world-wide energy source, the excitement offered by accelerator-based technology concepts, and the need to intimately involve public participation as the technology is defined and developed.

Over two hundred participants attended the Conference. All major US Department of Energy laboratories (Los Alamos, Oak Ridge, Brookhaven, Argonne, Livermore, Sandia, Savannah River, Hanford) were represented along with a number of industrial companies (Northrop Grumman, General Atomics, Bechtel, Babcock and Wilcox, Litton, Rockwell International, Kaman Science). Significant foreign representation from Russian, Swedish, French, German, Italian, and Japanese efforts was also present.

We, the co-chairmen of the Conference, view the interactions as very successful and are grateful to all who helped organized it and participated in it. These Proceedings include a large fraction of the talks presented and represent an important resource for understanding the status and future directions of ADTT concepts and technology.

Based on the success of this Conference an International Planning and Program Group was organized to start preparations for a second such ADTT International Conference. Present plans are for Sweden to host the Conference in approximately two years (1996).

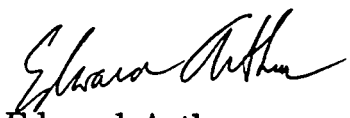

Edward Arthur
Conference Co-Organizer and
Technical Program Chairman
Los Alamos National Laboratory

Stan Schriber
Conference Co-Organizer
Los Alamos National Laboratory

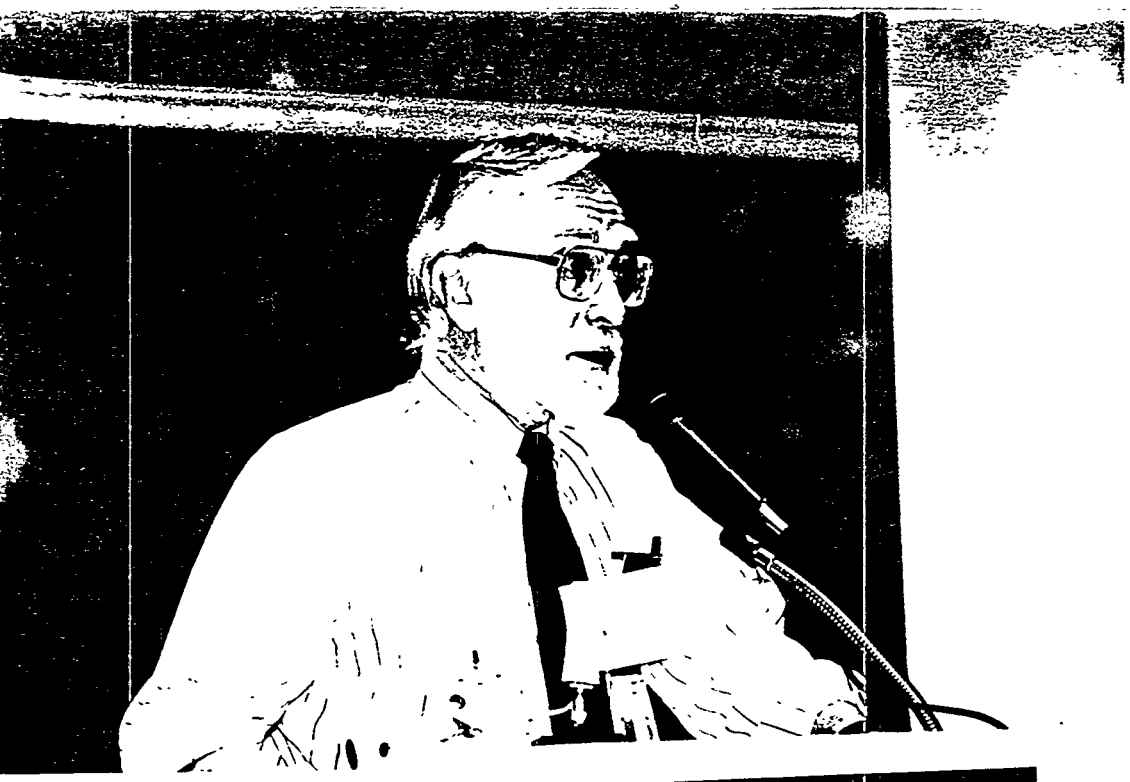

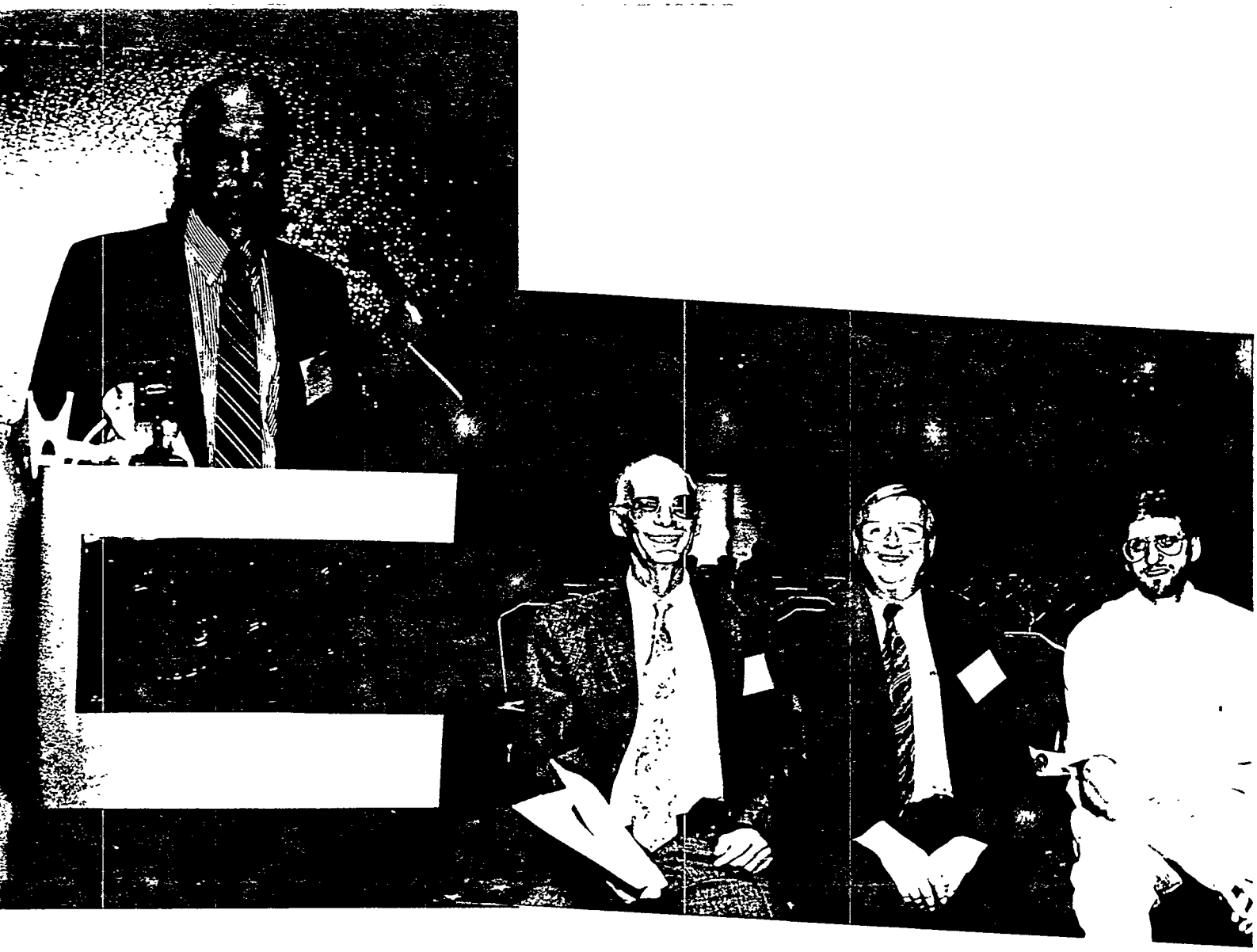

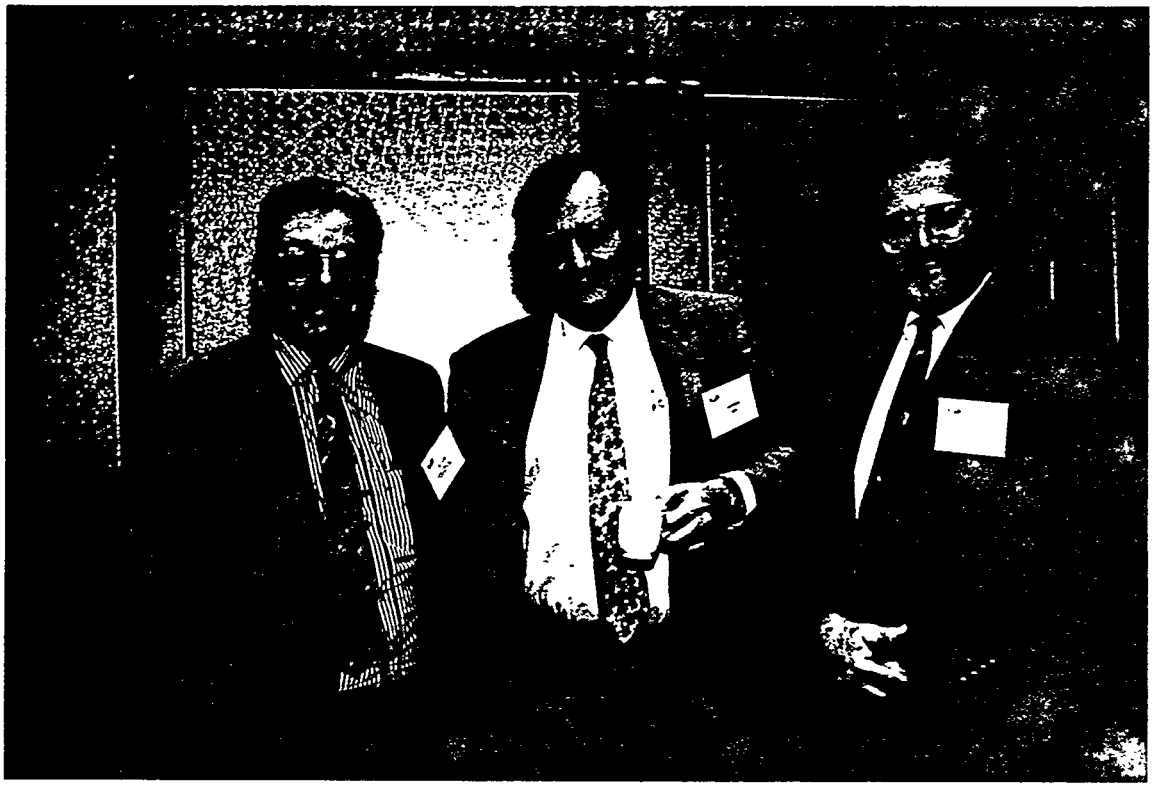

PARTICIPANTS

Abrahams, Kees—Netherlands Energy Research Foundation
Ackerman, John—Argonne National Lab.
Arthur, Edward—Los Alamos National Lab.
Bacha, Fabienne Wolff—
Barletta, Wm A—Lawrence Berkeley Lab.
Barnes, Peter D.—Los Alamos National Lab.
Baron, Seymour—Brookhaven National Lab.
Barthold, Wolfgang P.—Barthold and Assoc. Inc.
Batskikh, Guennadi I.—Moscow Radiotechnical Institute
Bauer, Guenther—Paul Scherrer Institute
Baxter, Alan M.—General Atomics
Beard, Carl—Los Alamos National Lab.
Bell, Charlie—Los Alamos National Lab.
Bell, Jimmy T.—Oak Ridge National Lab.
Bellan, Anthony P.—Texas A&M
Bergelson, Boris R.—ITEP
Bernstein Adam—Columbia
Berwald, David H.—Northrop Grumman
Bharadwaj, Vinod—FERMILAB
Bilpuch, Edward G.—Duke University
Bohn, Courtland—Argonne National Lab.
Bondarev, Boris—Moscow Radiotechnical Institute
Borden, Michael—Los Alamos National Lab.
Bowman, Charles D.—Los Alamos National Lab.
Browne, John—Los Alamos National Lab.
Brun, Torben—Los Alamos National Lab.
Buksa, John J.—Los Alamos National Lab.
Bullis, Robert—Northrop Grumman
Butler, Gilbert W.—Los Alamos National Lab.
Cammassa, Roberto A.—Los Alamos National Lab.
Cappiello, Michael W.—Los Alamos National Lab.
Carter, Thomas—Univ. of Wisconsin
Chan, Dominic—Los Alamos National Lab.
Cheng, Edward T.—TSI Research Inc.
Cho, Moo-Hyun—Pohang Accelerator Lab.
Cho, Yanglai—Argonne National Lab.
Chuvilo, Ivan V.—ITEP
Conde, Henri P.—Uppsala University
Cowell, Brian—Oakridge National Lab.
Croff, Allen G.—Oak Ridge National Laboratory
Cronhjort, Bjorn—Royal Institute of Technology
Cross, Eilene S.—EG&G
Cunliffe, John C.—Bechtel Corporation
D'Alessio, Gregory J.—Department of Energy
Daemen, Luke L.—Los Alamos National Lab.
Davidson, Wiley—Los Alamos National Lab.
DeMars, Richard V.—Babcock & Wilcox
Del, Cul G. D.—Oak Ridge National Lab.
Dewey, Harry—Los Alamos National Lab.
DiStefano, James R.—Oak Ridge National Lab.
Dietrich, Frank S.—Lawrence Livermore Nat'l Lab.
Dodson, Karen E.—Lawrence Livermore Nat'l Lab.

Doss, James D.—Los Alamos National Lab.
Eremeev, Petrovitch I.—Int'l Business Nucleonic LTD.
Erickson, John—Los Alamos National Lab.
Faltens, Andris—Lawrence Berkeley Lab.
Farish, Thomas J.—Los Alamos National Lab.
Faulkner, Roy—IPTM
Favale, Anthony—Northrop Grumman
Fomushkin, Eduard F.—Russia Federal Nuclear Center
Fontana, Mario H.—Oak Ridge National Lab.
Frehaut, Joel—Bruyeres-le-chatel
Furukawa, Kazuo—Tokai University
Gabriel, Tony A.—Oak Ridge National Lab.
Garner, Frank—Pacific Northwest Lab.
Gat, Uri—Oak Ridge National Lab.
Gay, Richard L.—Rockwell
Gillespie, George H.—G. H. Gillespie Assoc.
Gilpatrick, Doug—Los Alamos National Lab.
Goldman, Leonard M. L.—Goldman Consulting
Goodwin, David—Dept. of Energy /HENP
Grand, Pierre—Amparo Corporation
Grebyonkin, Konstantin—Russian Scientific Research Center
Grey-Morgan, Tim—Amersham International PLC
Gudowski, Waclaw—Royal Institute of Technology Institute
Guidee, Philippe J.—Thomson Tubes Electroniques
Guillebaud, Louis J.—Los Alamos National Lab.
Guzhovskii, Boris—Russian Federal Nuclear Center
Hardekopf, Robert A.—Los Alamos National Lab.
Heighway, Ed—Los Alamos National Lab.
Herrmannsfeldt, W.—Stanford University
Hill, Robert N.—Argonne National Lab.
Hoglund, Bruce N.—NWES Inc.
Ireland, John—Los Alamos National Lab.
Iyer, Natraj C.—Westinghouse Savanaah River Co.
Jameson, Robert A.—Los Alamos National Lab.
Janouch, Frantisek A.—Manne Siegbahn Institute of Physics
Jensen, Reed—Los Alamos National Lab.
Johnson, Gerald K.—Argonne National Lab.
Jongen, Yves—IBA
Kazaritsky, Vladimir D.—ITEP
Keenan, John—Northrop Grumman
Keiser, James R.—Oakridge National Lab.
Kim, Kyu C.—Los Alamos National Lab.
Klein, Horst—Inst. fur Angewandte Physik
Kloeg, Paul J.—KEMA
Kochurov, Boris P.—ITEP
Kolesov, Vladimir F.—Russian Federal Nuclear Center
Korovin, Yuri—INPE
Krakowski, Robert—Los Alamos National Lab.
Krasnykh, Anatoly K.—Inst. for Nuclear Research
Krawczyk, Frank L.—Los Alamos National Lab.
Kulikov, Evgeny V.—Ministry of Atomic Energy
Kupitz, Juergen—International Atomic Energy Agency
Laidler, James—Argonne National Lab.
Landeyro, Pedro A.—ENEA Italy

Landgren, Anders—
Lawrence, George—Los Alamos National Lab.
Laycock, Don—Litton Electron Devices
LeRay, Sylvie—Laboratoire National Saturne
Lee, Stacey K.—Los Alamos National Lab.
Leung, Ka-Ngo—Lawrence Berkeley Lab.
Li, Ning—Los Alamos National Lab.
Liljenzin, Jan-Olov—Chalmers Inst. of Technology
Lisowski, Paul W.—Los Alamos National Lab.
Lynch, Mike—Los Alamos National Lab.
Lynn, Larry L.—OSWR
Lypsch, Frank—ISR
MacCullum, Bill—Nordron International Inc.
Madic, Charles—Centr D'Etudes de Fontenay-Aux Roses
Maillard, Jacques—College de France
Martin, Ronald L.—ACCTEK Associates
McAdams, Roy—AEA Technology
McGowan, Thomas—
McMichael, Gerry E.—Argonne National Lab.
McNeese, James A.—Los Alamos National Lab.
Metzger, John D.—Northrop Grumman
Michaels, Gordon E.—Oak Ridge National Lab.
Michaudon, Andre—Los Alamos National Lab.
Mileikowsky, Curt—Scandatronix AB
Minguez, Emilio—Instituto de Fusion
Moeller, Erik J.—Royal Institute of Technology
Moore, Michael S.—Los Alamos National Lab.
Morgan, George L.—Los Alamos National Lab.
Myers, Timothy—Northrop Grumman
Nath, Subrata—Los Alamos National Lab.
Naumov, Valery S.—RIAR
Nelson, Ron—Los Alamos National Lab.
Newman, Eugene—Oak Ridge National Lab.
Novikov, Vladimir M.—Khurchatov Atomic Energy Inst.
Olson, Kenneth R.—Univ. of Wisconsin
Parish, Theodore A.—Texas A&M
Park, John—Los Alamos National Lab.
Perraudin, Claude—THOMSON - CSF
Piechowiak, Edward M.—Westinghouse
Pirozhenko, Vitaly M.—Moscow Radio Technical Inst.
Pitcher, Eric—Los Alamos National Lab.
Pleasant, Jack P.—Energy Frontiers Int'l
Popov, Yuri P.—Inst. for Nuclear Research
Potter, Christopher R.—Los Alamos National Lab.
Powell, James R.—Brookhaven National Lab.
Pynn, Roger—Los Alamos National Lab.
Rawlins, John—Westinghouse Hanford Company
Rawls, John M.—General Atomics
Reiser, Martin P.—University of Maryland
Rief, Herbert—CEC Joint Research Centre
Romero, Rick—Los Alamos National Lab.
Rose, Sewell C.—Los Alamos National Lab.
Rubbia, Carlos—CERN
Russell, Gary—Los Alamos National Lab.

Rusthoi, Daniel—Los Alamos National Lab.
Ryne, Robert D.—Los Alamos National Lab.
Sailor, Bill—Los Alamos National Lab.
Salvatores, Hassimo—CEA
Schneider, Dave—Los Alamos National Lab.
Schriber, Stan—Los Alamos National Lab.
Shafer, Robert E.—Los Alamos National Lab.
Sherman, Joe—Los Alamos National Lab.
Shubin, Yuri N.—Inst. of Physics & Power Eng.
Shvedov, Oleg V.—ITEP
Simonenko, Vadim A.—Institute of Technical Physics
Sisolak, James E.—Univ. of Wisconsin
Sommer, Walter—Los Alamos National Lab.
Stammbach, Thomas—PSI
Stansfield, Richard G.—AEA Technology
Stavissky, Yuri Y.—Academy of Sciences
Steinberg, Meyer—Brookhaven National Lab.
Steinhoff, R. Lewis—Department of Energy
Straalsund, Jerry—Pacific Northwest Lab.
Strottman, Dan—Los Alamos National Lab.
Stubbins, James F.—University of Illinois
Sullivan, Al—Los Alamos National Lab.
Symons, Robert S.—Litton Electron Devices
Takahashi, Hiroshi—Brookhaven National Lab.
Takizuka, Takakazu—Japan Atomic Energy Research Institute
Tallerico, Paul—Los Alamos National Lab.
Taussig, Robert T.—Bechtel Corporation
Thedeen, Torbjîrn—Center for Safety Research
Thorson, Ian M.—TRIUMF
Tinsley, James D.—EG&G/EM
Todd, Alan M.—Northrop Grumman
Todosow, Michael W.—Brookhaven National Lab.
Toevs, James W.—Los Alamos National Lab.
Toth, Mac—Oak Ridge National Lab.
Trujillo, David A.—Los Alamos National Lab.
Tubbs, Nigel A.—OECD
Van Tuyle, Gregory J.—Brookhaven National Lab.
VanDyck, Olin B.—Los Alamos National Lab.
Vassil'kov, Ratmir G.—Moscow Radiotechnical Institute
Venneri, Francesco—Los Alamos National Lab.
Victoria, Max—CRPP
Volk, Vladimir I.—Inst. Inorganic Materials Moscow
Wadlinger, Alan E.—Los Alamos National Lab.
Walter, Richard L.—Triangle Universities
Wangler, Thomas P.—Los Alamos National Lab.
Ward, Thomas E.—Brookhaven National Lab.
Wechsler, Monroe—North Carolina State University
Wender, Steve A.—Los Alamos National Lab.
Woods, Richard—Los Alamos National Lab.
Woosley, Michael—University of Virginia
Yefimov, Eugeni—IPPE
Young, Phillip G.—Los Alamos National Lab.
Ziomek, Christopher D.—Los Alamos National Lab.

A Long View of Global Plutonium Management

Richard L. Wagner, Jr.
2560 Huntington Avenue
Alexandria, VA 22303
Kaman Sciences Corporation

Abstract: Dealing with the large and growing world inventories of fissile materials from all sources is a major part of the long term challenge of limiting the danger from nuclear weapons. Providing clean, safe nuclear power may also be needed to prevent conditions from arising which could lead to large scale nuclear weapon (re)armament. ADTT technologies might reconcile the seeming dilemma of providing nuclear power while maintaining a very low world inventory of nuclear materials which can be used in weapons. This vision for ADTT should be tested in a variety of ways, including comparisons with competing approaches and with other objectives. Such testing is one part of constructing a path for a decades-long, worldwide implementation campaign for ADTT.

There has always been a close relationship between the civil and military dimensions of nuclear energy, principally, but not solely, because reactors make fissile material which can be used in nuclear weapons. That fact has constrained the growth of nuclear power. In recent decades. inhibiting potential proliferators from using reactors to produce fissile material for weapons has been a central objective in the non-proliferation regime. Strict separation of military and civil nuclear activities, wherever they occur, has been the main theme, and institutional approaches have been developed to promote it. With the major changes in the nuclear-weapon picture which are coming with the end of the Cold War, and with the increasingly urgent necessity for dealing in a more coherent way with civil fuel cycle issues, the question of the relationship between the military and the civil aspects of nuclear energy is likely to be reexamined. One of the major issues will be the very large and growing worldwide inventory of plutonium from all sources -- mainly power reactor operations and weapon dismantlement -- and in whatever form.

Mankind would be better off if nuclear weapons were physically impossible, but that is not the case. Even though the danger of nuclear war growing out of the confrontation involving the Soviet Union has disappeared, other nuclear weapon dangers remain or could arise. Over the long term, reducing or constraining the danger from nuclear weapons will remain as important as it was during the Cold War. There will always be at least a latent danger from nuclear weapons.

As reductions in existing nuclear weapon stockpiles continue, the danger from nuclear weapons will become more and more a latent one, and the roles of nuclear postures in security strategies will be increasingly related to dealing with this latency. At some point in nuclear reductions, a fuzzy threshold may be crossed where the latent danger would lie more in the potential for nations' reconstituting larger nuclear forces, than in the residual weapon inventories-in-being. In this regime, stability considerations of potential nuclear (re)armament will determine safety or danger.

Development of nuclear weapons by rogue nations like North Korea or Iraq is a serious problem. But a far more serious danger, over the long term, would be a world in which many

nations have (re)armed with large stockpiles of nuclear weapons. Paths to such a future are indistinct, but some time in the course of many decades -- a time frame invoked by the long shadows cast into the future by nuclear weapons -- the world could change in ways that could trigger such developments.

Of particular concern might be the period -- perhaps as short as a few years -- during which such widespread nuclear (re)armament might occur. If a nation could build substantial numbers of nuclear weapons more rapidly than an emerging adversary (or if a variety of such asymmetries were to exist among a number of potential adversaries) a dangerous situation could develop. Such N-sided asymmetries in weapon deployment rates, coupled with N-sided "first strike" instabilities among deploying forces, could trigger nuclear war and the use of large numbers of nuclear weapons. Global effects and/or fragilities in the infrastructure of modern civilization could threaten civilization worldwide or even the survival of mankind.

Such apocalyptic nightmares may seem overblown today, but during the Cold War, and especially its early phases, such things were understood to be at stake. We should never lose sight of such possibilities. Controlling the political and technical preconditions which would bear on major competitive, nuclear (re)armament involving many nations must be a major consideration in future control of the latent danger of nuclear weapons.

This view of the nature of the longer-term problems associated with nuclear weapons is different from the conventional "proliferation" concerns, which have mostly involved the "Nth country problem" -- i.e. the initial entry into the nuclear "club" of the next, and then the next, often relatively small nation. Of course, this sort of Nth country proliferation, if allowed to proceed to extremes, could evolve into, or trigger widespread nuclear (re)armament, but it is only one path to such a possibility.

We have always tried to reduce the danger from nuclear weapons. During the Cold War, deterrence was the principle mechanism, with arms control also playing an important and complementary role. Now we have an opportunity to construct, over some decades, a more multi-dimensional regime for dealing with the danger from nuclear weapons.

Controlling access to and production of, fissile material has always been a central feature of non-proliferation regimes, and the view that the fuel cycle for civil nuclear power holds the potential for the spread of nuclear weapons has, for decades, had an inhibiting effect on the development of nuclear power. As nuclear weapon inventories are reduced, the potential for the civil fuel cycle to exacerbate either Nth country nuclear proliferation or possible large scale nuclear (re)armament will undoubtedly come under increasing scrutiny, especially as the other technical and industrial limitations on nations' acquisition of nuclear weapon inventories are overtaken by the spread of technology and growth of industrial capacity.

Everything else needed to develop a significant nuclear weapon posture -- research, development, and production capabilities (with the exception of fissile material production) -- simply cannot be controlled and will be widespread and rapidly utilizable. For research and development capability, the horse is already out of the barn. The Manhattan Project, for example, developed

nuclear weapons in a few years from a scientific starting point less advanced than that available in hundreds of universities around the world today. And, except for production of the fissile material, there is nothing special about fabrication of nuclear weapon components. Industrial capacity needed to produce large numbers of nuclear weapons is a tiny fraction of the industrial capacity of many nations today. (During a few years in the mid 1950s, the U.S. built, from an industrial base smaller than that of at least a dozen nations today, capacity to produce several thousands of nuclear weapons per year.)

Thus, in the future we are addressing, dozens of nations, given the motivation and the fissile material, could be producing hundreds of nuclear weapons per year within two or three years from the decision to do so. Many nations could produce thousands per year. These weapons could be small enough to be delivered by many pre-existing conventional military aircraft or missiles, and they could have explosive yields larger than those of the nuclear weapons used in World War II. Many currently non-nuclear nations could design such weapons, with confidence adequate for the circumstances which might motivate such development, without nuclear tests. So the pressure will increasingly be on fuel cycle issues -- controlling availability of fissile materials and the technology to produce them.

About a thousand tons of plutonium exist on the planet today, with nuclear power plants making about fifty more tons each year. Over the next decade or so, the most attention is likely to be focussed on the weapons-grade material from dismantled weapons and on reprocessed (separated) plutonium from irradiated civil reactor fuels. Plutonium in unreprocessed irradiated fuel, which represents the bulk of the material existing today, is in a sense "protected" by being commingled with highly radioactive fission products in the irradiated fuel. But over the long term, the continued presence of large and growing quantities of this material, along with the inevitable development and spread of new technology which could be applied to faster, more efficient, and cheaper chemical (and isotopic) separation, will be, perhaps, the dominant issue. A world inventory of a few thousand tons of plutonium, when a percent or so of this can supply a large nuclear weapon inventory, is unlikely to be viewed as a satisfactory long-term state. Even with more extensive and stringent IAEA-like monitoring and controls, it is unlikely that diversion of, say, a few tenths of a percent of the world inventory could be prevented in the international circumstances which should be assumed. Long-term storage of either processed plutonium or unprocessed irradiated fuel is unlikely to suffice either; the pipeline to put the material in storable form is likely to contain large quantities, processing and storage facilities cannot be presumed to be secure over an indefinite period, and even deep geologic repositories could be mined.

The prudent plan, for the long term, is to (nuclearly) "burn" down this large and growing inventory and then maintain it at as low a level as possible. If low enough steady-state inventory levels can be achieved, international monitoring and control institutions more stringent than today's might suffice to significantly delay diversion or production of large quantities of fissile material for weapon use.

Reducing the nuclear weapon danger is only one of mankind's agendas. Raising standards of living worldwide and preserving and restoring the environment are others (and they are likely to be more focused on). Nuclear power is likely to play a continuing role, at some level. Reconciling

the seemingly contradictory objectives of continuing nuclear power and essentially eliminating fissile materials is where the long term promise of ADTT technologies lies, and it could play the pivotal role.

An extreme position, certain to be advanced by some, would be to phase out nuclear power altogether, over some decades. Even if this were adopted as a long term goal, it could not be implemented soon, because reactors would be an essential part, at least in the initial stages, of a strategy to burn down plutonium inventories. And of course it is far too soon to conclude that the world could do without nuclear energy, considering the tremendous complexity of the economic, environmental and climatological issues related to world energy futures. Furthermore, eliminating nuclear power would not completely eliminate the potential for nuclear (re)armament; fission (or fusion breeding) plants could be built, over a period of time, to make fissile material. The best solution, balancing all factors, may well be to burn down existing inventories and to maintain a low inventory, while generating needed power, by use of improved fission power technologies.

A vision for using ADTT to do this is shown in the Figure. After a development period, ADTT technologies are used to burn down, over a few decades, the thousands of tons of plutonium accumulated by that time in the worldwide inventories of plutonium from all sources (and to transmute fission products so that the residual "ash" is much more manageable). As this burn-down campaign is proceeding, other variants of ADTT technologies are replacing most or all fission reactors, so that after several decades world nuclear power generation is done with the lowest possible world inventory of fissile nuclei (and with the problem of nuclear waste also greatly reduced).

A VISION (AND A HYPOTHESIS TO TEST)

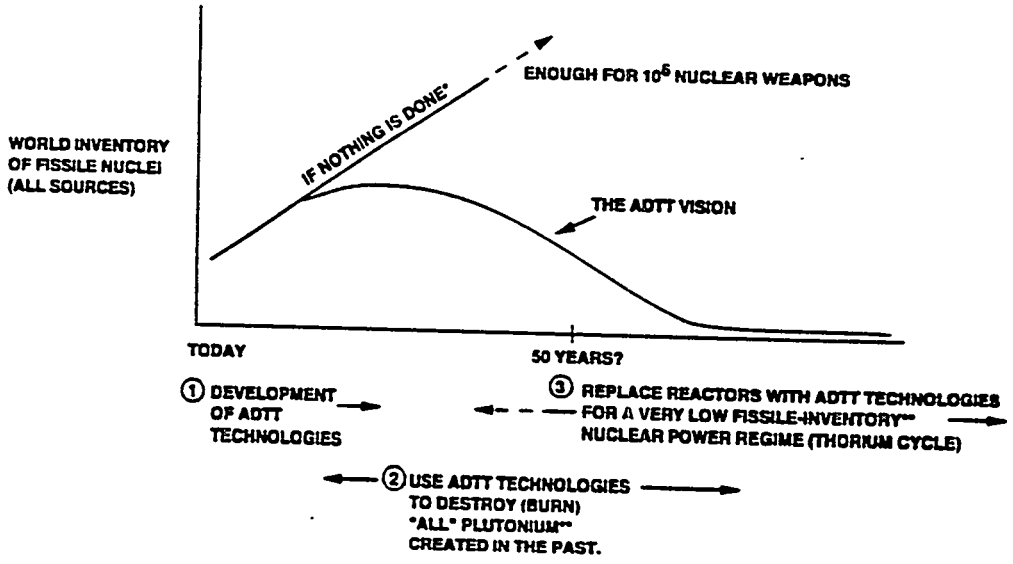

* e.g. CONSTANT FISSION POWER

**AND TRANSMUTE FISSION PRODUCTS, ETC.

Because the future is so uncertain in so many ways, this vision should also be thought of as a hypothesis to test. (Working toward a vision while also testing it, and adapting the vision as one learns from the testing, requires a special frame of mind. Many things we must do to shape our future in an increasingly complex and uncertain world are like this.)

Many things have to be considered in testing our vision, including:

- Competing approaches to achieving and maintaining low inventories of fissile nuclei

- The characteristics of various world situations in which various nuclear postures exist. (What makes up a "posture" are the nuclear technologies which are in use (such as ADTT), the world material inventories, and the institutional regimes related to them.)

- The development of the many other relevant technologies. One example is processing technologies. Another is military technologies; if (God forbid) other military technologies develop which could be as devastating as nuclear weapons and are easier, the nuclear weapon danger diminishes, and nuclear power postures could weigh weapon-constraining features less heavily.

- World nuclear weapon postures. The existence of some modest inventories of nuclear weapons (in stable force relationships) may stabilize against (re)armament asymmetries and uncertainties.

- Figures of merit for nuclear postures. If the objective is to inhibit nuclear (re)armament, all any posture can do is buy time. If nations feel driven to (re)arm with nuclear weapons, within a few years reactors or enrichment plants could be built to make fissile material. Thus, the value of a nuclear posture is determined (in part) by the accessibility of plutonium before these options could come into play. Any nuclear posture will have fissile isotopes in various stages of accessibility. One figure of merit (which would be scenario dependent) could be a time-weighted mass-accessibility function.

Let us amplify on a few of those things.

How far must world inventories of fissile material be reduced, and how stringently must the small, long-term inventories be controlled, in order to significantly mitigate the risk of widespread, rapid, and potentially unstable nuclear (re)armament? There are several relevant considerations, principally how many weapons, built over how long, make a difference. Consider first that the size of the residual inventories of nuclear weapons which would be retained by the current major nuclear weapon states would be an important factor. Weapon production less than these standing residual inventories would be less serious than rapid production of larger quantities. It seems likely on other grounds that these retained inventories will be at least several hundred weapons on the part of a number of nations. Second, we need not assume that international/institutional control regimes would break down completely and all at once. In many scenarios, perhaps only a fraction -- say ten or twenty percent -- of the global fissile material inventory might escape control over short enough

times to be of concern. Perfection is not attainable; but covering a significant part of "scenario-space" would be very worthwhile. Third, limits on nuclear testing could inhibit rapid development of weapon designs which make efficient use of small quantities of fissile material. Taking these and other factors together might mean that reducing the world plutonium inventory to levels achievable in an ADTT regime would buy as much time as can reasonably be hoped for.

Carefully designed international institutional arrangements for monitoring and controlling nuclear installations would be essential to complement a low-inventory technology regime. In fact, it is likely that neither part could be effective without the other. Arms control experience accumulated now over many years, in a wide variety of contexts (of which the IAEA regime is one), provides models for possible future institutions. A general feature of this experience has been to establish the correspondence between the accuracy, precision and certainty of the control desired and the institutional arrangements needed to provide for that control. If the consequences of even small non-compliance could be serious, arrangements must be based on detailed negotiations and rigorous monitoring (and in some cases, enforced inspection, as in Iraq). At the other end of the spectrum lie, for example, so-called confidence-building measures. The international arms control community now has useful experience across this entire spectrum, although the efficacy of some of the monitoring and control regimes constructed is still controversial, and the jury is still out on others.

In the long run, a low-inventory strategy for world fissile materials probably requires rather stringent institutional arrangements. But there is time to construct these arrangements, growing out of the IAEA regime augmented by other, near-term, less stringent methods involving government, industry, and the technical community. It is to be hoped that fissile-inventory control methods will be embedded in much broader and increasingly durable international non-proliferation and arms control regime.

Enriched uranium can be used to make nuclear weapons as well as plutonium, of course, though the quantities required are considerably larger. It is not clear that uranium-based nuclear power technology, with its attendant enrichment and fuel fabrication facilities, could meet the desired criteria for resistance to weapon applications. Use of ADTT technologies employing thorium for power generation, with inherently low inventories of fissile ^{233}U, might be the best alternative if the technologies prove feasible. Further, it might be possible to design a neutron spallation plant in such a way as to substantially increase the time needed for conversion to production of significant quantities of weapon material.

Technologies embodying low fissile material inventories do not completely guarantee against production of weapon material, of course. Any technology that uses neutrons to make power can be converted, over some time and with some degree of efficiency, to make fissile material for weapons, and neutron spallation plants would be no exception. Thus, even the most desirable technology will never be the entire solution. International control regimes, growing out of today's NPT/IAEA regime, but more stringent and/or with more dimensions, will be essential. But improving the proliferation-resistance of the technology being controlled by such a regime is certain to be beneficial in buying time, which is all any measure can do. A low-inventory approach to civil nuclear power, by the time such an approach becomes available, will be particularly suited to limit

the possibility of widespread production of substantial nuclear weapon stockpiles, which may have become the core problem in that time frame, in the risk/benefit calculus of nuclear weapons and nuclear energy.

While development of ADTT technologies is beginning, we need also to immerse ourselves in these considerations (and the many others I haven't mentioned or thought of), to understand better where we are trying to go and why, and how we might be deflected. This should be a planned, continuing activity, involving many points of view, and using a variety of tools (for example, "path gaming").

Realizing the vision for ADTT technologies will be an international enterprise because the objective is a global one, and it will be a campaign lasting several decades, spanning two or three professional careers. It is likely that during most of that time, the objective of limiting the danger from nuclear weapons will not be a top international priority, despite policy pronouncements. Thus, to the extent possible, its implementation should be accomplished by market forces, or at least be compatible with them. To the extent this is not possible, governments or international institutions will have to provide incentives, but these may be in tension with other national and international objectives. And the technical developments themselves will be full of twists and turns. In such a complex situation practically every decision will be contingent, its purpose being to set up conditions for a next decision, which will also be contingent, and so on.

Facing these complications, for ADTT development, it is essential to have close, effective, and sustained working relations among governments, laboratories (and the scientific community in general), and industry -- nationally and internationally. It is not too much to think of these relationships as institutions in their own right, and they should be carefully designed from the beginning.

Making this program work, in the face of the difficulties and uncertainties I have sketched out, is a daunting challenge, but containing the danger of nuclear weapons demands the best we have to give.

The concern this paper focusses on, while potentially the main concern related to nuclear weapons in mankind's future, is (we hope) a long way in the future. It may be like the concern for global environment changes in that regard. But like global change, it is not too soon to begin to build options, because it will take decades to reduce world inventories of fissile material to low levels and convert to (re)armament-resistant nuclear energy technologies.

Potential Benefits of Waste Transmutation to the U.S. High-Level Waste Repository

Gordon E. Michaels
Oak Ridge National Laboratory
P.O. Box 2009
Oak Ridge, Tennessee 37831

Abstract. This paper reexamines the potential benefits of waste transmutation to the proposed U.S. geologic repository at the Yucca Mountain site based on recent progress in the performance assessment for the Yucca Mountain base case of spent fuel emplacement. It is observed that actinides are assumed to have higher solubility than in previous studies and that Np and other actinides now dominate the projected aqueous releases from a Yucca Mountain repository. Actinides are also identified as the dominant source of decay heat in the repository, and the effect of decay heat in perturbing the hydrology, geochemistry, and thermal characteristics of Yucca Mountain are reviewed. It is concluded that the potential for thermally-driven, buoyant, gas-phase flow at Yucca Mountain introduces data and modeling requirements that will increase the costs of licensing the site and may cause the site to be unattractive for geologic disposal of wastes. A transmutation-enabled cold repository is proposed that might allow licensing of a repository to be based upon currently observable characteristics of the Yucca Mountain site.

INTRODUCTION

Accelerator-Driven Transmutation (ADT) concepts are being visualized as flexible neutron sources capable of "burning" or transmuting ^{99}Tc, ^{129}I, and actinide components of spent fuel and waste. While several nonrepository benefits are proposed for ADT system operation, the issue of whether transmutation will provide benefits to a geologic high-level waste repository has continued to be debated.

Several previous studies [1-4] have evaluated the effect of transmutation of actinides and fission products on the environmental and health risks of a high-level waste repository. In a particularly influential paper, Pigford [1] evaluated the effects of actinide burning technology and concluded that actinides were expected to be a relatively insignificant component of aqueous releases from a repository because of their very low solubility in water. Pigford pointed out that ^{99}Tc and ^{129}I were expected to dominate repository releases by groundwater and that little benefit could be realized by actinide transmutation.

Croff [5] and Cowell [6] have examined the impacts on repository areal capacity due to elimination of the long-term heat source presented by decay of the actinides, principally americium and plutonium. Croff's paper proposed a staggered emplacement pattern for high-level waste and concluded, based on fairly simple thermal calculations, that repository capacity could be increased due to actinide burning by a factor of four relative to spent fuel. Cowell performed more sophisticated thermal modeling and reported [6] that an increase in areal capacity by a factor of 2.6 could be realized by simple elimination of the long-term thermal power of the actinide waste inventory and reoptimization of the spacing between waste packages. In subsequent calculations [7], Cowell has assessed the staggered emplacement strategy proposed by Croff and calculated a potential increase in areal capacity by a factor of 4.9 due to actinide burning. The implications of these calculations are that the first U.S. repository site, for which

Basis and Objectives of the Los Alamos Accelerator-Driven Transmutation Technology Project

Charles D. Bowman
Los Alamos National Laboratory, MS H854
Los Alamos, NM 87544

Abstract. The Accelerator-Driven Transmutation Technology (ADTT) Project carries three approaches for dealing with waste from the defense and commercial nuclear energy enterprise. First, the problem of excess weapons plutonium in the U. S. and Russia originating both from stockpile reductions and from defense production site clean-up is one of significant current and long-term concern. The ADTT technology offers the possibility of almost complete destruction of this plutonium by fission. The technology might be particularly effective for destruction of the low quality plutonium from defense site clean-up since the system does not require the fabrication of the waste into fuel assemblies, does not require reprocessing and refabrication, and can tolerate a high level of impurities in the feed stream. Second, the ADTT system also can destroy the plutonium, other higher actinide, and long-lived fission product from commercial nuclear waste which now can only be dealt with by geologic storage. And finally, and probably most importantly the system can be used for the production of virtually unlimited electric power from thorium with concurrent destruction of its long-lived waste components so that geologic containment for them is not required. In addition plutonium is not a significant byproduct of the power generation so that non-proliferation concerns about nuclear power are almost completely eliminated. All of the ADTT systems operate with an accelerator supplementing the neutrons which in reactors are provided only by the fission process, and therefore the system can be designed to eliminate the possibility for a runaway chain reaction. The means for integration of the accelerator into nuclear power technology in order to make these benefits possible is described including estimates of accelerator operating parameters required for the three objectives.

INTRODUCTION

Concerns about waste from the defense and commercial nuclear sectors has grown to such an extent in recent years that it now dominates the nuclear enterprise. The emphasis in the nuclear technology field has moved from its earlier reactor-design focus into clean-up of defense production sites and a resolution of the commercial nuclear waste problem. The development of cleaner and safer systems for nuclear energy generation is almost at a standstill because of growing international concerns about the waste issues. The predominant approach to this problem for the past thirty years has been the geologic storage of waste whether it be from the defense or the commercial sector. Geologic storage offers the prospect of confining nuclear waste by the confinement features of a stable geologic structure rather than relying on long-term containment of the waste in man-made containers. In addition the waste is made much less accessible by its placement deep underground. Therefore many countries are providing significant funding for the development and siting of geologic waste storage facilities. While a number of sites might be under study in a given country, the intent is to provide a single site capable of confining the high level waste.

It has become increasingly difficult to convince a community to become host to a nation's single site for storage of waste which many consider to be the nation's most dangerous. The fact that the waste remains dangerous for many tens of thousands of years exacerbates these concerns. The concern that such repositories can become mines for plutonium has become of even greater concern as the U. S. has made it known that dangerous nuclear weapons can be made from commercial plutonium[1]. The natural

[17] U.S. Environmental Protection Agency, Title 40, Part 191, "Environmental Standards for the Management and Disposal of Spent Nuclear Fuel, High-Level and Transuranic Radioactive Wastes," FEDERAL REGISTER 50, 38066, September 19, 1985.

[18] Wilson, op. cit., p. 20-1.

[19] Wilson, op. cit., pp.14-62, Table 14-62.

transformation of commercial plutonium useful material for weapons into excellent weapons plutonium by radioactive decay[2] means that eventually many thousands of tons of weapons plutonium will be stored at many sites around the world. Some are becoming concerned about the possibility of natural or induced supercriticality of fissile material stored underground[3]. As a consequence of these and other concerns remaining to be resolved about geologic storage, no nation is expected to begin emplacement of high level waste in a geologic repository before the year 2010 and the ultimate viability of the geologic storage concept remains to be demonstrated.

The world therefore is in desperate need for an acceptably priced inexpensive and safe alternative to the geologic storage concept. In the U. S. commercial nuclear waste is accumulating at reactor sites and the defense site clean-up effort is struggling to understand what will happen to the plutonium and other high-level waste which will be gathered together after the clean-up has been completed. The Los Alamos National Laboratory along with a rapidly developing national and international community has therefore been studying Accelerator-Driven Transmutation Technology (ADTT) as a possible means of destruction of this nuclear waste and of generating nuclear power by systems which do not generate the most dangerous components of this waste and which concurrently destroy their own waste. If the full capability of the ADTT systems can be realized at acceptable cost, geologic storage of defense and commercial waste would not be required.

The main elements and function of an ADTT system are illustrated in Fig. 1 for a system which generates nuclear energy from thorium, avoids the production of plutonium and concurrently destroys its long-lived high-level fission product waste. This system is referred to as Accelerator-Driven Energy Production (ADEP). The system starts with benign ^{232}Th and converts it by neutron absorption into the excellent fissile fuel ^{233}U from which electric power is produced. The system consists of a reactor-like component referred to in the figure as the target-blanket which contains the fissile material and the waste to be destroyed. For a reactor each fission on average produces enough neutrons after losses to cause another fission so that the chain of fissions is continuous. For all ADTT systems, the losses are made somewhat larger by the expenditure of neutrons on waste destruction so that there are about 5-10 % fewer neutrons than necessary to maintain the chain. Therefore by itself the system is totally passive and inoperative. However, by making up for the 5-10 % loss of neutrons from an external neutron source, the system would function effectively even though the chain reaction would not be self-sustaining.

The essential conceptual difference between the ADTT system and a reactor is the presence of an accelerator to produce neutrons and the presence of a target inside of the reactor-like component to convert a beam of protons from the accelerator into neutrons. All electric-power-producing reactors presently operating have means for removing the heat from the system, converting it to steam, and driving generators for electric power production. These elements are also shown in Fig. 1 with most of the power being sent into the commercial grid except for 10-15 % being used to power the accelerator. Operation of the system stops when the accelerator stops because the system fission chain is not self-sustaining. For this reason the system can be made safe from a runaway chain reaction such as that which occurred at Chernobyl by entirely different means than that incorporated in other reactors, and many of the safety features required in accelerators such as control rods may be omitted.

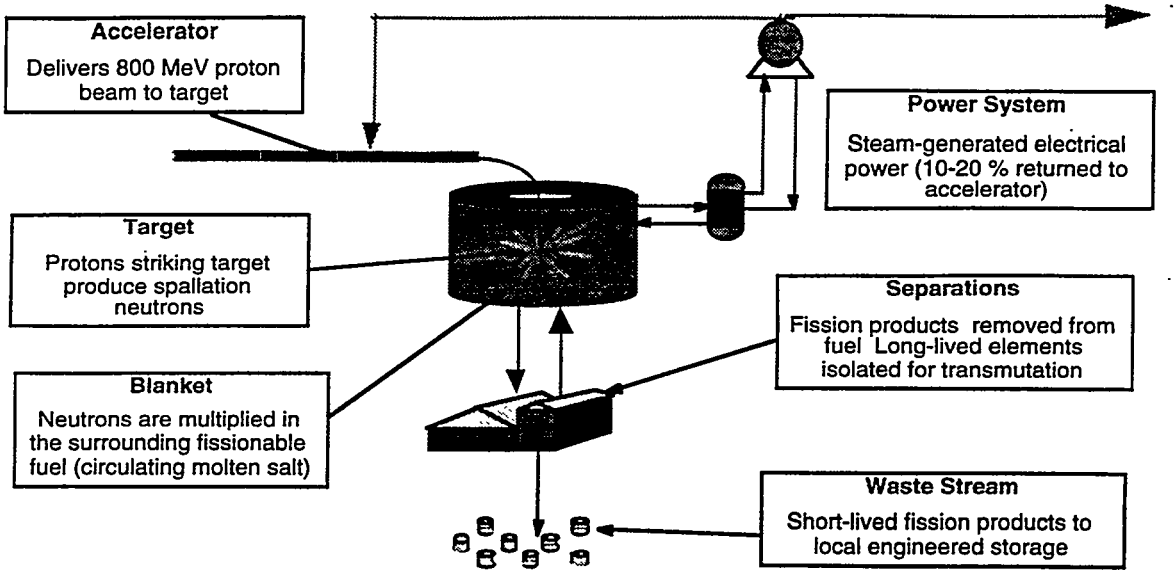

Fig. 1. ADTT System Components. An accelerator produces 800-MeV proton beam which is directed into a reactor-like assembly consisting of a lead target for the beam and a surrounding blanket containing fissile material. The beam strikes the liquid lead target and produces about 22 neutrons per proton. The neutrons are moderated in the surrounding blanket which consists mostly of graphite and molten salt which carries the fissile fuel as actinide fluoride. The system operates at $k_{eff} = 0.95$ so that the system multiplies the beam-produced neutrons by about a factor of 20. The blanket contains internal heat exchangers which transfer the heat from the working salt to a secondary external salt stream and then to a steam generator for electric power production. Most of the power is fed into the commercial grid but some of it is used to power the accelerator. The liquid fuel allows the system to be continuously refueled and allows the waste products from fission to be continuously removed.

To understand the value of the accelerator more clearly, consider a system containing ^{233}U fuel which undergoes fission with 92 % probability upon absorption of one thermal neutron and which releases 200 MeV per fission. Assume further that no neutrons are released in fission. The 100,000 MeV released by 500 such fission events would be converted with 42 % efficiency to 42,000 MeV of electric energy. The accelerator would convert this with 45 % efficiency to 18,900 MeV of proton beam power if all of the electric power were fed back to the accelerator. For a proton energy of 800 MeV, the accelerator would produce 18,900/800 = 23.6 protons. At the conversion rate of 25 neutrons per proton which probably can be achieved, a total of 23.6 X 25 = 590 neutrons per 500 fissions is possible. Upon absorption, 92 % of these neutrons would lead to fission of 543 nuclei of ^{233}U. Comparing this number with the original 500 fission events, we see that an accelerator-linked chain reaction is possible even if no neutrons were emitted from fission! Of course instead of no neutrons per fission 2.49 neutrons are produced per fission of a ^{233}U nucleus so that altogether one has 590 + 500 X 2.49 = 1835 neutrons per 500 fissions for an increase in the effective number of neutrons from fission from 2.49 to 3.67 if all of the electric power from the target blanket were fed back to the accelerator. This is an increase of more than one neutron per fission and is an enormous increase in the number

of neutrons per fission which are available to a nuclear system designer. The latter figure is far more neutrons than are required to maintain the fission process and to breed the ^{233}U from the thorium, so that only a small portion of the electric power must be consumed by the accelerator. The possibility to dial the neutron production requirement as desired and to operate effectively a system well away from criticality greatly broadens the parameter space available to the nuclear system designer

Owing largely to the enhanced safety of the system, one need no longer remain attached to solid fuel assemblies as in ordinary reactors. Liquid fuel becomes an option with all of the many advantages it provides. In Fig. 1 we show at bottom center a loop carrying the liquid fuel outside of the target-blanket in a continuous flow. An obvious advantage is that the fuel can be continuously added to the system to make up for that which is burned without shutting down for refueling as in the case of the reactor. Of course, the whole process and expense of solid fuel fabrication required for the reactor is avoided as well. But there is even greater benefit from the ability to remove the fission products from the liquid fuel on-line without stopping the system for removal of solid fuel assemblies. By means which will be described later, the liquid fuel can be continuously cleansed of the fission products which act as neutron poisons. Those long-lived fission products which would ordinarily require geologic storage can be returned to the system to be converted by neutron absorption to stable or short-lived fission product.

Since only fission product is removed from the system, there is no actinide waste except for a very small amount which slips through in the fission product separation process. Because the long-lived waste is destroyed, the only waste from the system is the short-lived and stable fission product. This waste is made up of a number of different species but none of the waste species have half-lives longer than 30 years. Containers can be made to confine this remnant waste until the radioactivity has decayed away by a factor of 1,000 or so. Geologic confinement of the waste is not required because, as is shown later, the remnant waste can be made to satisfy near surface disposal criteria of the NRC and the EPA. If the site of the ADEP system meets the criteria for near-surface disposal, the waste need not leave the site. Therefore only benign thorium need be brought to the site and no waste need be carried away.

More will be said later about the thorium-burning system, about weapons plutonium and commercial waste destruction, and the relationship between the latter two technologies.

TARGET-BLANKET DESCRIPTION

More detail on the target-blanket system is shown in Fig. 2. The system consists of a stainless steel tank which contains graphite blocks for neutron moderation and reflection and a molten salt carrier for the fertile and fissile fuel which will be described below. The graphite and molten salt are known to be compatible with one another from extensive experience at Oak Ridge National Laboratory with the Molten Salt Reactor Experiment (MSRE). The molten salt flows upward through holes in the graphite blocks across the top of the system to internal magnetic pumps and heat exchangers and back to the bottom of the system. The heat from fission is transferred in the heat exchangers to an external salt loop which carries the heat to steam generators for electric power production. The molten salt is a $LiF\text{-}BeF_2$ eutectic which melts at about 450 degrees centigrade and operates at between 650 and 720 degrees centigrade. Almost all elements react as fluorides and can be

dissolved in small but adequate amounts into the carrier salt for the transmutation and fission requirements. A cover gas of helium is circulated above the molten salt to collect and remove the noble gas and volatile fluoride fission products from the salt. The molten salt never leaves the tank, except for a small slip-stream for on-line refueling and waste removal, and therefore there is no possibility for spillage of the salt through pipe breaks.

Other liquids such as water could be chosen for the carrier. However the salt has the advantage of being an excellent solvent for almost any of the elements present in the system. It also has a low vapor pressure at high temperature which is a major safety advantage allowing operation without a pressure vessel which would be required for a higher vapor pressure medium such as water. The higher operating temperature allows a thermal-to-electric efficiency which might be as high as 44 %. Also the salt is non-reactive with air, nitrogen, or concrete, in contrast with for example, the liquid sodium coolant on which fast reactor technology is now based.

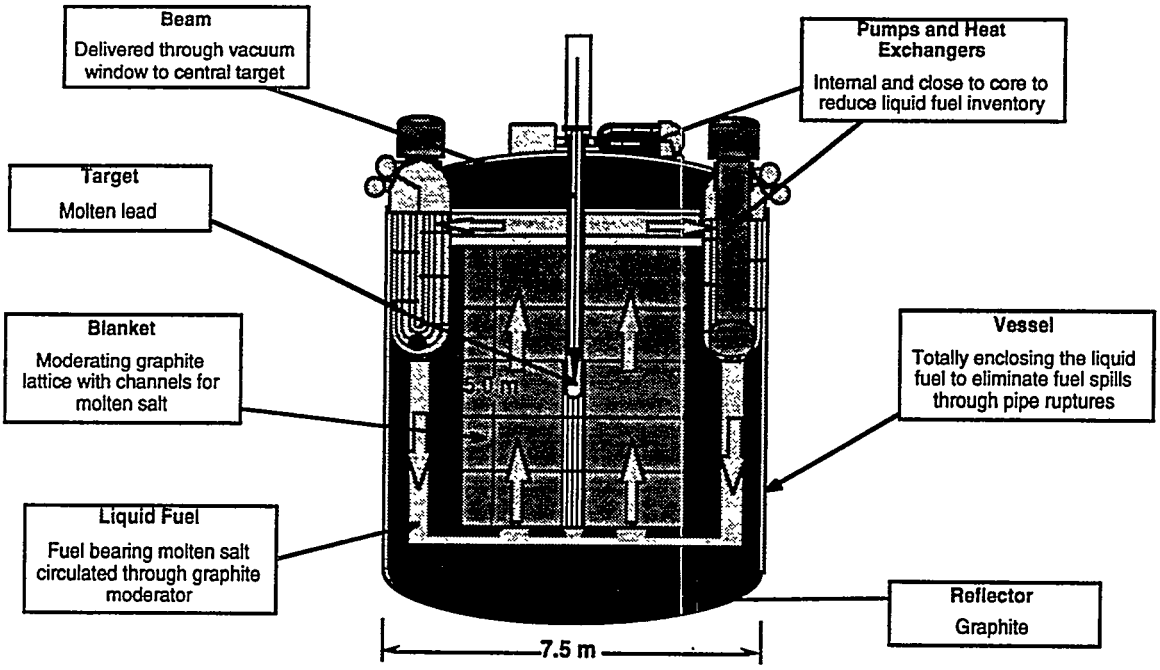

Fig. 2. Target blanket function. The proton beam enters through a window at the top of the system and strikes a liquid lead target at the center. The lead is circulated and cooled from above. Five layers of graphite blocks are shown which moderate the neutrons. The molten salt fuel flows upward through holes in the blocks and to the outside through pumps and heat exchangers and back to the bottom. Graphite on all sides serves as a neutron reflector. A cover-gas of helium collects the volatile species and carries them away for appropriate separations.

The neutrons are produced at the center in a liquid lead target. Protons enter from the top through a window and are stopped in the lead, with the lead pump and heat exchanger on top of the tank. The lead is confined by metal resistant to corrosion by the lead. Since the corrosion properties of the lead are different from those of the molten salt, the lead and salt are separated by an inner container compatible with the lead and an outer container

compatible with the salt. The metal for the salt containment probably will be Hastalloy-N developed for the MSRE and for the lead it probably will be Inconel.

The system operates at a k_{eff} of about 0.95 compared to $k_{eff} = 1$ for a reactor. The neutrons produced by the accelerator therefore are multiplied by a factor of about 20 for and therefore an ADEP system producing power from thorium with a fission power of 250 MWt for an electric power output of 100 MWe electric would require an accelerator capable of producing 6 ma at 800 MeV and consuming 11 MWe of electric power. The thermal-to-electric conversion efficiency for such a system would be 44 %. The bussbar-to-beam efficiency would be 45 %.

All systems which produce nuclear power from fission must protect against a potential loss of coolant accident (LOCA) which might occur when the primary coolant system fails and the fission product decay heat builds to dangerous levels. The nuclear reactors now operating have active redundant systems which come into action when the coolant system fails. Newer designs for reactors include passive means to deal with this situation. For example the power density and total power capacity of the reactor might be kept small enough so that the heat can be transferred to the outside of the reactor vessel and from there away from the system into the surroundings by convection or radiant heat loss. The power of such a passive system is usually limited by the rate of heat transfer to the vessel with the components at the center of the reactor being at highest risk.

The ADTT systems are also designed with passive capability for after-heat removal. They have the advantage over water-containing systems that the temperature can be allowed to rise much higher because the ADTT system contains mostly low vapor pressure high melting or vaporization temperature materials such as graphite and molten salt. Therefore much higher temperatures can be tolerated in the ADTT systems without risk of internal damage or dangerously high pressures. In addition to the use of liquid fuel, the incorporation of an internal inside-to-outside flow path and natural convection both contribute to enhanced heat transfer from the inside to the outer wall of the blanket. Threfore ADTT systems can be designed for substantially higher electric power capacity than conventional reactors while still maintaining the passive heat removal capability.

GEOLOGIC STORAGE AND THE ADTT SYSTEM

From the beginning of the development of the ADTT program, the discussion has continued as to whether the ADTT system requires a geologic storage facility as back-up for the untransmuted waste. The purpose of this section is to address the question of the requirement for geologic storage of remnant waste after destruction of the actinide and the long lived constituents of the fission products. It will be shown here that near-surface storage of this waste might be made consistent with existing NRC and EPA regulations with an addition to the regulations for storage of Cs, Sr, and Kr for about 200 years until they meet low-level radioactivity levels covered by existing regulations.

Review of Regulations

To begin the discussion, it is useful to review several aspects of near-surface waste storage. Waste destined for near-surface storage is divided into three classifications as class A, B, and C waste.

Class A waste is the most benign and it can be stored at the surface without stabilization. That is, no special precautions must be made to protect the system from natural dispersion mechanisms such as rainfall, wind, etc. There are of course some restrictions such as exclusion from flood plains and from unstable land. The site must be clearly marked, and monitored for 100 years but no fencing is required. After that time it is assumed that controls are no longer operative and that the site should not be dangerous to an inadvertent intruder. An inadvertent intruder is defined in NRC Regulation 10 CFR 61.2 as;

> "a person who might occupy the disposal site after closure and engage in normal activities such as agriculture, dwelling construction, or other pursuits in which the person might be unknowingly exposed to radiation from the waste."

Class B waste must be immobilized or contained by components in the waste site that maintain their "gross physical properties and identity" for 300 years. Surface storage is permitted and institutional control is required for 100 years. Productive use of the land during this 100-year period is possible so long as the "integrity and long-term performance of the site are not disturbed." Therefore the site perhaps might be used as a parking lot. Elsewhere in 10 CFR 61 the use of concrete in such systems is suggested and it is proposed later in this report to use that means for immobilization.

Class C is reserved for waste with even greater radioactivity concentrations. This waste also requires stabilized waste forms or waste containers. This waste must be stored at least five meters below the ground surface such that after 500 years the waste would not be a hazard to an inadvertent intruder or to the public health and safety.

There is no absolute limit on the amount of radioactivity which can be emplaced at one site, whether designated Class A, B, or C. The amount is only limited by the radiation released to the surroundings and risk to an inadvertent intruder. The radiation released from the site "must not result in an annual dose exceeding 25 millirems to the whole body, 75 millirems to the thyroid, and 25 millirems to any other organ of any member of the public." This release criterion for near surface disposal is the same as that for a single geologic storage system built to confine all of the radioactive waste of the nation. The siting criteria for surface storage of waste are specifically stated in 10 CFR 60 and are easily met so that such facilities can be sited almost anywhere except in flood plains, areas of unstable land, etc. Therefore there could be many such sites and almost certainly many more than one in every state. If there were 100 such sites in the U. S., the total radioactivity burden in a single site could be 1/100 of that at a national central repository. If in addition these sites were receiving the remnant waste from an ADTT system which reduces the long lived constituents by a factor of about 1000, the total long-lived radioactive waste burden would be smaller by a factor of 100,000 than that of a single geologic repository without transmutation. It therefore seems likely that the surface storage sites for remnant waste following transmutation could meet the whole body and specific organ dose limits for a much smaller radiation source term even though the confinement capability of the surface site would be less than that from a geologic site. This probably would have to be demonstrated on a site-by-site basis.

It might be argued that if the waste is distributed over 100 sites instead of a single geologic site, that more people would be endangered. The spirit of the release limit

however is that the dose received be too low to risk harm to the surrounding population. Therefore the same release limits apply to each of the many low-level waste sites as apply to a geologic storage site for the nation's entire commercial spent fuel. The number of people exposed is considered not to be a factor because no member of the public is to be subjected to a dangerous dose from any waste site...either high or low level.

The other type of restriction for the inadvertent intruder into the site relates to the concentration of the waste and to whether the waste stream from a transmutation system meets the concentration limits for class A, B, or C waste. Classes B and C waste require stabilization before emplacement. The method of stabilization chosen for this report is mixing with concrete, a material already mentioned in 10 CFR 60 as appropriate for use in surface storage systems. The stabilization before emplacement as required by the regulations will obviously result in the dilution of the waste. There are no statements in the regulations about the degree of the dilution allowable....only limits regarding radiation release to the surroundings and dose to the inadvertent intruder , which depend on dose concentration. Weakly contaminated dirt which is being cleaned up from some of the sites at Los Alamos and elsewhere can be disposed of in surface storage if the contaminated material meets the regulatory limits for radiation release or dose to an inadvertent intruder. For the remnant waste after transmutation from a 3000 MWt commercial reactor, we assume stabilization with 50 m^3 of concrete per year. Assuming the waste to be Class C, these blocks which might be 1m X 1m X 2 m = $2m^3$ would have to be stored under 5 meters of overburden according to 10 CFR 60. If stacked end-on, one year's remnant waste from a 3000 MWt system would occupy a surface area of 5m X 5m. The waste from 35 years of operation of the facility would therefore occupy approximately a 30 m by 30 m area. Since the land can be put to some beneficial use, this area would be much smaller than a 3000 MWt plant's parking lot and could be used as a small part of the plant's parking lot.

It would be correct to argue that stabilization amounts to dilution, but *stabilization is required* for class C storage and *dilution is not forbidden* by the regulations. In fact stabilization, which is required, demands some level of dilution by the stabilization medium. The operating criteria are (1) dose to an inadvertent intruder and (2) leakage of radiation from the site into the surrounding environment.

Disposition of Remnant Waste from ADTT Systems

For ADTT the issue then is what should happen to the remnant waste stream. This stream may be considered to have three components for the accelerator-driven transmutation of waste system (ATW). We assume here a system designed to deal with the actinide and fission product waste from a single 3000 MWt LWR thermal reactor destroying the waste at the rate that the waste is being produced in the reactor. The first components of the waste encountered in transmutation are the uranium, which is the primary constituent of the spent fuel, and the zirconium cladding. These components probably could be stored for reuse and are discussed later. The liquid fuel system allows the continuous feed of all of the waste left over after uranium and zirconium removal including both higher actinide and fission products. The ATW system destroys the higher actinide waste by fission generating an average fission power of about 750 MWt per 3000 MWt reactor. The liquid fuel system also allows the continuous removal of fission

products. The only actinides which escape are those which contaminate the fission product removal process. We assume that the atom fraction of actinides in the fission product removal stream can be held to 1 part per 10,000 and next compare the actinide loss rate with the Class C criteria for actinides.

This is illustrated in Table 1 where the first four columns show the isotopes, the annual production rates, the half-lives, and the decay rates. The fifth column shows the decay rate of the 1/10,000 of the actinide escaping from the transmuter through the separations process into the fission product stream. Stabilization of this annually escaping quantity of actinide waste with 50 m^3 of concrete as described above gives the decay rate per gram of column 6. This may be compared with the class C decay rate limits for these actinides given in 10 CFR 61 and shown in column 7. Except for the shorter half-life nuclides ^{238}Pu, ^{241}Am and ^{244}Cm, the concentrations are about a factor of 10 lower than the limits. For ^{238}Pu we use the limit given in 10 CFR 61.55 for the parent ^{242}Cm. For ^{241}Am we use the limit given for the parent ^{241}Pu. Applying the sum-of-fractions rule for combining the decay rates for several isotopes as given in paragraph (a)(7) of 10 CFR 61.55, the sum is still well below the decay rate limits. Therefore if the separations can be accomplished at the 1/10,000 level, the remnant could be disposed of as Class C waste.

A similar evaluation of fission products is summarized in Table 2 where those isotopes with half-lives 10 years or greater are listed along with their production rates, half-lives, and decay rates. The isotopes are divided into groups according to the treatment received and each group is discussed below.

Table 1. Actinide Amounts and Concentrations

Isotope	Annual Production (Atoms/Year)	Half life (Years)	Decay Rate (Curies)	Reduction by Separation[c] (Curies)	Concentration After Stabilization[d] (Nanocuries/ gram)	Class C Decay Rate Limit[a] (Nanocuries/ gram)
^{238}Pu	1.13×10^{25}	88	7.5×10^{4}	7.5	68	20,000[b]
^{239}Pu	41.6×10^{25}	24,100	1.0×10^{4}	1.0	9.1	100
^{240}Pu	19.2×10^{25}	6,560	1.7×10^{4}	1.7	15.	100
^{241}Pu	6.4×10^{25}	14.4	2.7×10^{6}	270.0	2454.5	3500
^{242}Pu	3.9×10^{25}	375,000	6.1×10^{1}	.006	0.05	100
^{237}Np	3.7×10^{25}	2,140,000	1.1×10^{1}	.001	0.009	100
^{241}Am	4.1×10^{25}	433	5.5×10^{4}	5.5	50.	3500[b]
^{243}Am	0.73×10^{25}	7,370	5.9×10^{2}	.059	0.54	100

[a] Used decay limits from 10 CFR 61.55

[b] Used decay limit for parent from 10 CFR 61.55

[c] For a separation factor of 10,000

[d] Stabilization with 50 m^3 of concrete

Table 2. Fission Product Amounts and Concentrations

Isotope	Annual Production (Atoms/Year) x10^{25}	Halflife (years)	Decay Rate	Separation factor and (Curies)	Decay rate (Curies)	Concentration After Stabilization[a] (Curies/m^3)	Class C Decay Rate Limit (Curies/m^3)
^{79}Se	0.13	65,000	11.9	10	1.2	0.024	0.2
^{90}Sr	9.0	29.1	1,860,000	10	190,000	3800	7000
^{93}Zr	15	1,500,000	60	1	60	1.2	2.0
^{99}Tc	15	213,000	426	100	4.26	0.85	3.0
^{107}Pd	4.1	6,500,000	3.8	1	3.8	0.076	2.0
^{126}Sn	0.46	100,000	27	10	2.7	0.054	0.2
^{129}I	2.7	15,700,000	1.0	10	0.1	0.002	0.08
^{135}Cs	4.2	2,300,000	8.4	100	0.084	0.0017	0.08
^{137}Cs	14	30.2	2,800,000	100	28,000	560	4600
^{151}Sm	0.16	90	11,000	300	37	0.74	2.0
^{85}Kr	1.0	10.7	560,000	1	560,000		

[a] Stabilized with 50 m^3 of concrete

1. ^{137}Cs, ^{135}Cs, and ^{90}Sr. These isotopes cannot be handled as near-surface low-level waste and they cannot be transmuted with significant beneficial effect using accelerators. Therefore they must be removed from the waste stream with a separation factor of 10-100. Column 6 shows the decay rate of the isotope left after the separation. Once isolated, the cesium and strontium must be stored until their radioactivity decays by about a factor of 100 or for about 200 years before they can also be disposed of as Class C waste. Containers can be built for containment for this storage period so that geologic storage is not necessary. The cans must be isolated from the public and protected so that they maintain their integrity. They must be stored with passive means for decay heat removal through this storage period. While geologic containment is not required for these relatively short-lived nuclides, they do not qualify for near-surface storage and new regulations must be developed for handling them on the transmutation site or at a central limited period storage site.

2. ^{107}Pd and ^{93}Zr. These nearly noble metals materials are almost benign with long half-lives and weak decay energies. No Class C limit is given explicitly for these in 10 CFR 61.54. However the limit for the semi-noble metal ^{94}Nb is given as 0.2 curies/m^3. It is more chemically active than either zirconium or palladium and its decay energy is more than a factor of ten higher than both. Therefore we assume that the Class C limit for ^{107}Pd and ^{93}Zr would be at least a factor of ten higher than for ^{94}Nb and use the ^{94}Nb limit increased by a factor of ten to 2 curies/m^3 to estimate the regulatory limit . With this limit no separation of these isotopes from the rest of the fission product waste would be required before storage as Class C waste and transmutation would not be necessary.

3. ^{79}Se and ^{126}Sn. No regulatory limit has been established for these nuclides. We assume their chemical reactivity is comparable to ^{94}Nb as are their decay energies. Therefore we use the Class C limit for ^{94}Nb of 0.2 Curies/m^3. A separation of a factor of ten must be achieved to reach the assumed Class C limit for each of these. These isotopes must be transmuted.

4. ^{99}Tc, and ^{129}I. These nuclides are perhaps the most chemically mobile of the long-lived fission products and regulatory Class C limits exist for them. To reach these limits, the ^{99}Tc must be separated by a factor of 100 and the ^{129}I by a factor of 10. These nuclides must be transmuted.

5. ^{151}Sm. This nuclide exhibits a very weak decay energy and we therefore assume the limit of 2.0 curies/m^3 derived from the established limit for ^{94}Nb. To reach this limit, the separation factor must be about 300. The separated material must then be transmuted.

6. ^{85}Kr. This noble gas is difficult to transmute because its cross section is small and gas-containing systems inside a nearly critical system must be avoided for criticality safety reasons. According to regulation, it must therefore be stored in 100 Curie or smaller amounts in separate containers with a volume of about 100 ml. These containers must then be immobilized in the Class C waste in accordance with 10 CFR 61.54. There are no regulatory limits to the number of containers, but 5600 would be required per year. It would therefore probably be preferable to collect the gas in yearly production volumes of about 10 m^3 and store it along with the cesium and strontium. After 200 years the container confining the remnant could be stored as Class C waste according to regulations.

Of the eleven long-lived fission products, two require no action. The other nine must be separated using eight chemical separations and five of these must be transmuted and stored as Class C waste with the other fission product. The remaining four (Kr, Sr and Cs) must be placed in engineered storage for about 200 years. After the 200-year period, the latter four can be stored permanently as Class C waste also. The five isotopes to be transmuted constitute about 6 % of the fission product and will require about 300 moles of neutrons per 3000 MWt-year of reactor operation. These neutrons may come either from an accelerator or from the excess neutrons produced by the fission of weapons plutonium or highly enriched uranium. Once the five long-lived fission products have been destroyed, the remnant fission product waste can be diluted and stored in concrete at the rate of 50 m^3 per year per 3000 MWt fission power. For the Los Alamos thorium burner, which transmutes its own fission product and produces 200 MWe (500 MWt) for 35 years, the subsurface storage area required for Class C waste immobilized in concrete if stored two meters thick would be about 12 m X 12 m.

The uranium and zirconium cladding are nearly benign materials and could be stored in containers at some central site for probable future use. There is no apparent reason now to place them in geologic storage where they would be almost inaccessible by definition.

In summary with transmutation and separations factors which need not exceed 10,000 and more nearly 1,000 for actinides and about 100 for fission product remnant waste would not require geologic storage. For the on-site transmutation of the waste from a

commercial nuclear power plant, the fission product immobilized in concrete could stay on the reactor site as Class C near-surface waste. The Cs, Sr, and Kr could stay or be moved in accordance with state and local government decisions. Without the need for a central geologic repository, the federal government need not become involved in the siting of waste storage facilities. Its role would be limited to providing the regulatory framework for near-surface storage.

WEAPONS PLUTONIUM DESTRUCTION (ABC SUBPROJECT OF ADTT)

This is the first of the three applications which were mentioned at the beginning of this paper and has been pursued under the acronym ABC for Accelerator-Based Conversion. Excess weapons plutonium (w-Pu) is being made available by major reductions in the U. S. and Russian stockpile of nuclear weapons and by the clean-up of U. S. and Russian w-Pu production sites. Altogether more than 100 tons of this material exists[1] with perhaps 20 % of it eventually being material reclaimed from the production sites. The ultimate disposition of w-Pu has been the subject of recent intensive study in the U. S. The options considered basically include three options; (1) burning of the plutonium to the point where it has roughly the same isotopic composition as commercial plutonium (c-Pu), referred to as the "spent fuel standard" followed by geologic storage, (2) geologic storage of the w-Pu without burning after vitrification with defense radioactive waste, or (3) complete burn-up of w-Pu.

Since there is about ten times as much c-Pu as w-Pu in the world today and the c-Pu is increasing rapidly, present U. S. policy appears to favor burning the w-Pu to the spent fuel standard. The advantages of this seem to be that the w-Pu then becomes a small increment on the already larger c-Pu inventory, the w-Pu is less effective as weapons material, the radioactivity of the burned w-Pu is a deterrent to the handling of this material in nuclear weapons fabrication, geologic storage of the burned plutonium makes it much less accessible than it now is, and the technology to burn the w-Pu to the spent fuel standard exists now even if it is replicated for the destruction process. The arguments against the spent fuel standard are that the resulting material is still quite effective for weapons construction, that it probably could be recovered from geologic storage without great difficulty, and that there is very little near-term political advantage because it will probably take 30-50 years to complete the conversion to the spent fuel standard and the placement of the material in geologic storage.

Perhaps most importantly, disposing of the material this way costs money or yields negative value from the w-Pu whereas there are clearly large positive-value uses for this material for start-up of the ADEP system and for ADTT commercial waste destruction. The destruction of commercial nuclear waste requires supplemental external neutrons all of which could be supplied by an accelerator. However the neutrons could also be supplied by fission of weapons material. The weapons materials are valuable for weapons precisely because they are an excellent source of neutrons. Each fission of ^{239}Pu produces 2.88 neutrons of which one per fission must be used to sustain the chain reaction. An additional 0.35 per fission are lost because not all neutron absorptions in ^{239}Pu lead to fission and a total of about 10 % of the neutrons per fission are loss to parasitic capture and leakage. After subtracting off these losses of neutrons, one is left with about 1.2 excess neutrons per fission available for other uses. The number of neutrons from HEU is

slightly smaller. In the burning of commercial waste using the ADTT technology, the accelerator supply of neutrons can be reduced by about a factor of two by the use of w-Pu or HEU. Since the accelerator source can be reduced significantly and we know roughly what the cost of the accelerator-produced neutrons is, the price which could be paid for w-Pu and HEU in this application can be estimated from the savings in cost of the accelerator, which are relatively well known. The value for w-Pu is found to be perhaps as high as $250,000 per kilogram[4]. This value is far more than the value of HEU blended down for commercial reactor fuel. An even higher price could be paid for w-Pu and HEU for the one initial load required for the ADEP system without bootstrapping from the commercial grid using the accelerator.

If one compares the present inventory in the U. S. and Russia of w-Pu and HEU to the amount required for destruction of the world's nuclear waste, there is a surprisingly good match, so that all of these materials could be used for commercial waste destruction. It can be argued that the price quoted above is artificially high because HEU can be separated from natural uranium at a much smaller price and that therefore a major need for either w-Pu or HEU would be satisfied by lower priced newly produced HEU. However continued production of HEU would not be consistent with international agreements to forego the enrichment of uranium to HEU when much smaller enrichments are quite sufficient for use as fuel in all of the world's commercial nuclear power plants. International political agreements therefore probably would make it difficult or impossible to produce HEU for commercial waste destruction. Nevertheless, a user of HEU or plutonium would argue effectively against paying the high accelerator-displacement value when it could be produced anew much more cheaply. A value higher by a factor of two than that for new HEU might be paid for existing HEU or w-Pu in which case the 100 tons of w-Pu might be valued at about $50 billion and the ten times larger amount of HEU at about $500 billion. Such high positive values for these weapons materials would be good news from the perspective of weapons material security since we willing guard our valuables and grudgingly pay to dispose of our waste. Fortunately Russia still considers its weapons material valuable and we can expect that it will be more carefully guarded if the U. S. policy is directed toward maintaining the high value perspective. Furthermore, since the value for the material is not received until the weapons material is sold for the desired purpose, one can expect the desire for converting the book value to real value to drive the sale of the material as soon as the waste destruction facilities are able to use it. The temptation to hold on to the material for weapons purposes is countered by the high value which could be obtained when it is sold.

Quite obviously these arguments for use of the weapons material for high value purposes are inconsistent with w-Pu destruction which is the purpose of the discussion in this section of the paper. None of the three options for near-term negative value w-Pu disposition identified by the National Academy Study[1] would be favored from the perspective of ADTT. This is especially true since the burning of w-Pu (or HEU) produces many more neutrons than are required to sustain a chain reaction so that the main purpose of the accelerator, which also is to produce surplus neutrons, is superfluous. The accelerator is however useful if high burn-up of the plutonium is required so that there is virtually no plutonium in the waste stream and the isotopic composition is incompatible with use of the remnant as weapons material.

Thus the Los Alamos National Laboratory has proposed an accelerator-driven subcritical system[5] in which fission product poisons are allowed to build up until not only sufficiently to consume the excess fission neutrons from w-Pu fission, but also the supplemental neutrons from the accelerator. The system achieves very high burn up without fuel reprocessing or fuel fabrication and refabrication. Also no chemistry for fission product removal is required. The General Atomic Corporation has proposed a program with a similar objective. Its helium-cooled graphite-moderated reactor with w-Pu fuel particles suspended in the graphite has been proposed as the first stage of w-Pu destruction. After the Pu has been burned sufficiently that it will not sustain criticality, the fuel is transferred to an accelerator-driven assembly which continues to destroy the plutonium using accelerator-generated neutrons until k_{eff} of the system has dropped to about 0.6. The burn-up of the Los Alamos and the General Atomic systems are similar and are the highest of any of the proposed w-Pu-burning systems; neither require fuel reprocessing or fuel refabrication. Present U. S. DOE policy towards w-Pu burning seems to be to burn the Pu only to the spent fuel standard. The Los Alamos ADTT Project Office position is that preferably the w-Pu either should be burned completely or reserved for enhancing commercial spent fuel waste transmutation as described above with the latter choice much preferred.

ACCELERATOR-DRIVEN ENERGY PRODUCTION (ADEP SUBPROJECT OF ADTT)

Perhaps the most important element of the ADTT project over the long term is Accelerator-Driven Energy Production (ADEP) which uses thorium as a nuclear fuel. The system is based on the Th-U cycle which in which ^{232}Th is converted by neutron capture to thermally fissile ^{233}U. This cycle has been studied extensively[6] for use in commercial nuclear reactor power generation. The primary objective of the molten salt reactor experiment was to show that an effective breeder reactor could be built on this cycle which produced more ^{233}U than it consumed. This reactor technology lost out to the fast breeder based on the U-Pu cycle because its breeding ratio was barely larger than unity even when fission products were promptly removed from the fuel. The U-Pu cycle showed much higher breeding ratios at a time when plutonium was in demand rather than in excess.

A major advantage in the present climate is that the Th-U cycle produces almost no plutonium. The Th-U cycle development program was also focused on a molten salt liquid fuel program with on-line removal of fission products, and the operation of a liquid fuel reactor was demonstrated with the several-year Molten Salt Reactor Experiment (MSRE) at the Oak Ridge National Laboratory. Not only could fission products be continuously removed from this system but the liquid fuel allowed the reactor to be continuously refueled. For this reason the MSRE still holds the world record for the longest continuous chain reaction. A great deal of successful research was done on the materials to contain the salt and all of the ADTT projects rely on the materials work done for the MSRE. While the MSRE had virtually no actinide waste stream, it had the usual fission product waste and its neutron economy did not allow it to breed as much ^{233}U as it burned and still have excess neutrons left for transmutation of its fission products.

By preserving many of the design features of the MSRE and introducing an accelerator into the system, one achieves the capability to produce as much ^{233}U as is burned so that

the nearly unlimited energy available in thorium can be accessed. In addition the extra accelerator-produced neutrons enable the long-lived fission products to be avoided so that there is no long-term high-level waste stream from this system. Because of the subcriticality of the system a runaway chain reaction can be made much smaller than any reactor and perhaps the probability for such an event can be reduced truly to zero. These three features of "unlimited" energy, criticality safety, and absence of high-level waste are the highly touted features of fusion systems which have been heavily studied for the many years. We believe that we can demonstrated these benefits to society during the coming decade by merging established reactor technology with the existing highly developed accelerator technology. The system produces almost no plutonium and it is has excellent non-proliferation features. This system has already been described in some detail at the beginning of this report so we will concentrate mostly here on the non-proliferation features which are of vital importance for any new nuclear power system

All existing commercial reactors for production of nuclear power produce plutonium as a by-product which is seen by many as an asset because of the additional power which can be derived from it. Others see it as a serious liability since it can be used for nuclear weapons and because of radiological concerns. The established means for separating the plutonium for reuse in reactors produces a stream of "naked" plutonium. This plutonium is pure and unmixed with other material which would inhibit its usefulness in nuclear weapons. This material might be diverted in the separation facility, in storage, in transport to fuel fabrication facilities, etc. There is the fear that in some countries it will simply be stockpiled for planned or possible future use in nuclear weapons. Therefore the U. S. has followed a policy of discouraging the reprocessing of commercial spent fuel and the use of plutonium for energy generation.

Instead the U. S. and Sweden follow a once through cycle where the spent fuel would go directly from reactor storage to geologic repository storage. Some are concerned about the consistency of U. S. policy if the once-through policy is proposed as the waste management solution which will promote the much greater use of nuclear power throughout the world. In that case there eventually would be many repositories spread all over the world which could be mined for plutonium. Furthermore the reactor-grade plutonium decays into weapons-grade plutonium. Therefore neither reprocessing, as it is presently performed, nor once through geologic storage are entirely satisfactory solutions. The ADEP program offers the opportunity to have the benefits of nuclear energy without the weapons potential from plutonium or other material which could be used for nuclear weapons.

The ADEP system is fed ^{232}Th and transforms it to ^{233}U which is then fissioned to obtain the nuclear electric power. After a stable equilibrium is reached, there will always be a fixed amount of ^{233}U in the system which might be accessed for nuclear weapons.
A number of non-proliferation features of the ADEP system will be described below which limit the amount of ^{233}U available to a much lower amount than ^{239}Pu in current LWRs, limits its accessibility, allows simple detection of any diversion attempt, and allows low impact actions to forcefully terminate diversion underway if necessary.

Limiting the Amount of Fissile Material Present

Fast reactor technology which is being pursued in many countries around the world carries a large inventory of plutonium. The fundamental reason for this is that the fission cross section for ^{239}Pu in the fast neutron spectrum is smaller by about a factor of 100 than that for thermal spectrum fission of ^{239}Pu. Therefore, other things being equal, the inventory for the thermal spectrum system is smaller by about a factor of 100 than for a fast spectrum system. The neutron flux for the thermal system is about a factor of ten smaller so that as a practical matter the thermal system requires about 10-30 times less material than a fast spectrum system. The same situation is true for ^{233}U when fast and thermal spectrum systems are compared. Generally speaking the ADEP system will carry about the same amount of ^{233}U as an LWR has of ^{235}U and ^{239}Pu together if the flux and power level are the same. The primary point here therefore is that the ADEP system carries a much smaller inventory of potential weapons material than the fast reactors under development in other countries.

Isotopic dilution of ^{233}U in ADEP

If the ^{233}U were diluted with ^{238}U to the 20 % level or lower, the ^{233}U would be classified as non-weapons material according to present regulations. A 500-MWt thermal ADEP system can be brought immediately into power production by a start-up inventory of 10,000 kg of Th and 700 kg of 20 % low enriched uranium (LEU) where the 20 % is ^{235}U. The original ^{235}U will be burned out over time and replaced with ^{233}U derived from the thorium. The distribution of isotopes reached after ten years of operation is given in Fig. 3 where the amount is given in grams. At ten years, which is essentially equilibrium, the uranium fissile material inventory will be 100 kg of ^{233}U along with 10 kg of ^{235}U for a total fissile content of 110 kg. The amount of ^{238}U present at this time is about 600 kg so that the required isotopic dilution of about 20 % is maintained. However the inclusion of ^{238}U in the systems will result in the production of a small amount of ^{239}Pu. The isotopic distribution of plutonium as 239, 240, 241, 241, and 242 is present in the amounts of 1.2, 1.2, 0.3, and 2.5 kilograms. The ratio of fissile to total plutonium is 0.29 so that the plutonium would be very poor quality weapons material and there would be only 5.2 kg of plutonium altogether to be accessed.

"Raiding" the Adep for ^{233}u Through ^{233}pa

The conversion of ^{232}Th to ^{233}U is a three-step process involving neutron capture by ^{232}Th to produce ^{233}Th which decays almost immediately to ^{233}Pa, which itself subsequently decays with a 26-day half-life to ^{233}U. Fig. 3 shows that the inventory of ^{233}Pa in the system is about 22 kilograms. If operation of the ADEP system were interrupted and the molten salt removed, it would be possible in principle to separate the ^{233}Pa before it decayed to ^{233}U from the 8000 kg of other actinide. If such a separation could be completed in about 26 days, about half of the ^{233}Pa could be recovered. When this half decayed to ^{233}U, the 11 kilograms of ^{233}U resulting would be useful weapons material. The separation in question would be a dangerous activity in view of the very high radioactivity of the salt so soon after shut-down. Ordinarily spent reactor fuel is allowed to

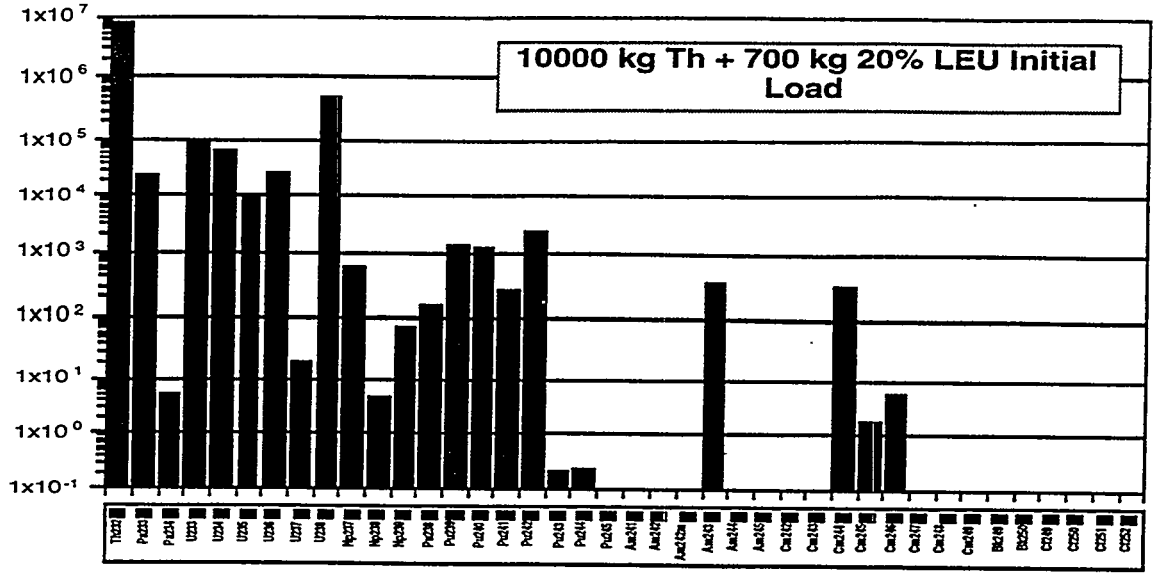

Fig. 3 Actinide isotopic distribution for the ADEP system. The distribution of actinide isotopes for the ADEP system is given ten years after start-up long after the system has reached equilibrium. The fission power level of the system is 500 MWt. The system was started with 10,000 kg of thorium and 700 kg of 20 % enriched uranium. The inventory is given on the ordinate in grams for isotopes from ^{232}Th to ^{246}Cm. The ^{233}U is diluted with ^{238}U such that the ^{233}U is never useful weapons material. The amount of plutonium in the system is very small and is of a very poor isotopic ratio. The ^{233}Pa decays in 26-days to ^{233}U. As described in the text it might be possible, using heroic measures, to extract a fraction of the 22 kg present. The loss of this material would have a significant effect on k_{eff} and probably could be readily detected remotely.,

decay 300 times longer (about 10 years) before separations begin. A further operational factor would be that the value for k_{eff} for the system would have dropped to about 0.85 from the normal value of about 0.95 by the removal of the 11 kg of ^{233}Pa. This may be compared with about 100 kg of plutonium which could be recovered from the interruption of operation of an LWR operating at the same thermal power level. A fast spectrum reactor of similar power would carry about 1000 kg of accessible plutonium.

With the removal of the 11 kg of ^{233}Pa, the thermal power level would have decreased by a factor of three and the net electric power into the commercial grid by a factor of about five while the accelerator power would have remained the same. The power level would recover over a period of several months, but the inconsistency between the accelerator power and the electric power output would be readily observed by infrared mapping from satellites or by other means.

Benefits from "Lock-Up" of ^{233}pa

There are two disadvantages if the ^{233}Pa is allowed to circulate freely in the salt. The first is that a "raid" on the ^{233}Pa might be started by draining the salt, although the follow on separations would be exceedingly sophisticated and dangerous. The second is that performance degradation through neutron capture on ^{233}Pa limits the flux to about

2×10^{14} n/cm^2-s. Five times higher flux at the same power level would mean only about 4.5 kg of ^{233}Pa inventory or of any of the other major constituents of the internal inventory. The gain from internal isolation of the ^{233}Pa during its decay period would offer many benefits in overall system performance.

Start-up without Fissile Material

There might be nations which could benefit greatly from nuclear power but which are considered to be substantial proliferation risks. In those cases providing non-radioactive LEU at 20% enrichment to start up the system might be considered a proliferation risk in that much of the enrichment towards highly enriched uranium has already been done. The start-up load might be diverted for enrichment for weapons use instead of being used for its intended purpose. The ADEP system can be brought into operation with no fissile material at all. For a system initially containing only ^{232}Th, the accelerator can be powered off the commercial grid and the neutrons produced used to produce ^{233}U. As the fission of the ^{233}U increases, the neutron flux also increases generating even more ^{233}U so that over a period of six to twelve months the system bootstraps itself to full power. No reactor existing or under development can operate with absolutely no fissile fuel load.

Remote Detection of Anomalous Operation and Possible Diversion

All conventional nuclear power systems deployed or under development use solid fuel which must be enriched, fabricated, brought to the site, burned, stored, eventually removed from the site, perhaps reprocessed, returned to the site, and finally placed into a repository. Each of these transfers might require a measurement to confirm the amount of fissile material present in the system. If each measurement could be done to 1 % accuracy and nine were required, the total uncertainty over the fuel cycle for nine independent measurements would be about $9^{1/2} \times 1\% = 3\%$. Since a 3000-megawatt reactor typically burns about 1200 kg of fuel per year, the real uncertainty in the fissile fuel in the system is about 36 kg. About half of this might be plutonium which could be diverted into nuclear weapons without being missed.

In contrast, no power is generated in ADEP without the operation of the accelerator and all of the fuel is generated internally. No actinide must be removed from the system in the course of normal operation of the system. The accelerator beam power, the fission power, the electric power generated, the electric power consumed by the accelerator and the plant, and the power fed into the external grid must all be internally consistent. If the accelerator power is increased, all of the other power levels must increase in a fixed relationship. If the plant is found to be operating out of balance, for example by power meters at the strategic points or by satellite infrared mapping, it is a signal that material diversion might be underway. A more detailed study of these anomalous conditions and their dependence on the rate of feed of thorium and the rate of removal of fission products might provide means to sense remotely when the source of the anomaly is nuclear material diversion.

Limited Consequences of Extreme Measures to Control Diversion

If an existing operating reactor is suspected or determined to be used for production of nuclear weapon material, the ultimate response by those alarmed could be the destruction of the nuclear reactor. There is a significant possibility that such action could lead to widespread death for the surrounding public and land contamination near the reactor. With such consequences the destruction of a reactor after it has begun operation is probably impractical. The accelerator component of the ADEP system is large and easily damaged into inoperation without significant possibility of damage to the target-blanket itself and the release of radiation. Diversion therefore can be terminated without exposing the surrounding population to significant danger.

COMMERCIAL WASTE TRANSMUTATION (ATW SUBPROJECT OF ADTT)

The objective of the Accelerator Transmutation of Waste (ATW) subproject of ADTT is to destroy the actinide and long-lived fission product waste from commercial nuclear reactor spent fuel. If the separations can be done sufficiently well, storage of the remnant waste could be in near-surface sites rather than in geologic storage facilities. The amounts of material requiring transmutation and the selectivity of chemistry separations has already been described in the section of this report entitled, "Geologic Storage and the ADTT System." Separation factors of about 1/100 are shown to be adequate to meet Class C storage criteria for fission product and about 1/10,000 for the plutonium and other minor actinides.

The ATW system also has means for continuous feed of waste from commercial light water reactors. To many this would appear to require the separation of plutonium and other components of the waste before feeding them into the system. This is referred to as reprocessing which was forbidden in the U. S. by President Carter by Executive Order. Even though this order expired when he left office, as a practical matter it has continued to govern U. S. internal policy on spent fuel and our foreign policy position has strongly attempted to discourage the reprocessing option for commercial spent fuel. The purpose is to reduce the opportunity for diversion of commercial plutonium to nuclear weapons purposes and to prevent the accumulation of large inventories of this material which is considered by many to be highly dangerous. Because of the excess neutrons provided by the accelerator, front end reprocessing is not required. The ATW system would require only the removal of the zirconium cladding and the uranium. All of the other actinide and all of the fission product can be fed into the blanket, because the capabilities for removal of the fission product already exist in the back-end separations system.

The front-end removal system has not been selected but there are at least two options under consideration. One would involve the crushing of the spent fuel assemblies which contain mostly UO_2 and the oxidation of this to U_3O_8. The volume expansion on the transformation to a higher oxide and the resulting conversion of the spent fuel to fine powder allows the spent fuel to be poured out of the spent fuel assemblies. Separation of the spent fuel from the cladding might approach 99 % for this process, but that might not be adequate and it might be difficult to clean the hulls further. Another means of removing the cladding might be to burn the spent fuel assemblies in a chlorine atmosphere over a

plasma torch converting the zirconium to volatile $ZrCl_4$. The oxide in the cladding however would fall as rubble into the bottom of the chlorination facility and be collected for subsequent fluorination. The bulk of the spent fuel is uranium and this would be removed as volatile UF_6. All of the other spent fuel material including the fission products, the plutonium and other higher actinides would be converted to fluorides and fed directly into the ATW system by dissolving them in the molten salt carrier.

In contrast to the aqueous reprocessing system developed long ago and now in common use, the processes described do not produce a pure stream of "naked" plutonium. The plutonium is never separated from the most highly radioactive components of the spent fuel, but only from the relatively benign zirconium and uranium. The front-end separation required for the ATW therefore produces a stream which is mostly highly radioactive fission product and separation of the plutonium from this fission product and from the other actinides would be required before it could be used in weapons. It is also important to mention that the front-end separations for the ATW system would be an integral part of the ATW system so that product stream from the Zr and U removal would be difficult to access.

Commercial nuclear power plants are typically sized at 3000 MW thermal and produce about 300 kg of plutonium and other higher actinide per year while fissioning 1200 kg of fissile material per year. Therefore an ATW system operating at the same fission power level of the LWRs could burn the waste from four LWRs if its operating life were the same as the LWRs. Destroying the LWR waste arising from the roughly 100 LWRs in the U. S. using ATW systems would require the deployment of about twenty five 3000-MWt ATW systems if the waste were to be destroyed in about 30 years. Unless the income from electric power sales were sufficient to offset the capital and operating costs of the ATW system, the cost of destroying the waste by this means could be prohibitive. The economic picture for the ATW system will be less favorable than for the ADEP system because the ADEP system need only destroy its own waste and only a modest accelerator is required for the modest neutron supplement. However the ATW system must destroy not only its own waste but also that from the four LWRs. Substantially more accelerator-produced neutrons are required therefore with greater capital cost for the larger accelerator and for the additional power which the accelerator consumes.

There is an attractive way around this. Presently the U. S. and Russia are reducing their weapons stockpiles and freeing up large amounts of highly enriched uranium and plutonium. Both are excellent sources of neutrons, which is part of the reason why they are ideal weapons materials. Over the long run it is probably unsafe to store these materials and so they will have to be destroyed almost certainly by fission. If some of these weapons materials are consumed in the ATW system, the excess neutrons can make up for some of the neutrons which otherwise would have to be supplied by the accelerator. Therefore by burning these weapons materials concurrently with the destruction of the commercial nuclear waste, the size of the accelerator probably can be reduced by at least a factor of two. With the resulting benefit to the economic picture for the ATW system, the destruction of the waste using the ATW system might be practical. A comparison between the amount of LWR waste and the amount of excess weapons material available shows that there is a satisfactory match.

There are other practical matters concerned with the practical deployment of the ATW systems. These systems will probably have to be located at government reservations and

operated in clusters both because of the sheer size and the use of the weapons material. If four ATWs were located on the same site, the electric power output into the local commercial grid would be about 3-4 gigawatts electric from each reservation and there would have to be about three sites if all of the waste was to be burned in 60 years. It is not easy to reliably estimate the U. S. power requirements over the next 30-50 years and how the power will be produced, but having access to a commercial market for the electric power from the ATW systems is an important consideration for this deployment option for the ATW system.

There is a second ATW deployment option for the destruction of the LWR waste which is a hybrid of the ATW and ADEP systems. This would involve the replacement of existing LWRs at the end of their life with an ATW system on the same site feeding the same amount of electric power into the grid. The ATW system would over its life destroy the waste from the LWR and also its own waste stream. About 25 % of its power would be derived from the actinide waste from the LWR and the rest from thorium. The accelerator requirement would be about the same as that for the other ATW deployment option, but no weapons material would be required. Of course it probably would not be desirable to have these weapons materials being delivered to the approximately 100 ATW systems operating in follow-on to the existing 100 LWRs. An advantage of this deployment scenario is that the waste need not leave the site, some level of radioactivity inventory already exists on the site, and there is probably a clear market for the ATW electric power and an existing distribution system. Under this scenario, the amount of nuclear power would continue to be at least as large as that produced today. The present system would have been replaced with systems which do not produce the waste stream of existing LWRs, which avoid the criticality and after heat safety concerns of existing reactors, and which nullify the requirement for a nuclear infrastructure of mining, enrichment, fuel fabrication, reactor, fuel storage, reprocessing plants, and fuel refabrication. The requirements for geologic storage of remnant waste would be greatly reduced or perhaps made entirely unnecessary depending on the technical and economic performance of the system.

In summary, the first ATW deployment option carries more of the features which might be associated with a nuclear close-out option. The second option could provide a bridge over the next 30-50 years from the present LWRs with their major infrastructure requirements to the ADEP systems which operate with little infrastructure support.

PRESENT STATUS AND SUMMARY

This paper describes a new accelerator-based nuclear technology which offers total destruction of the weapons plutonium inventory, a solution to the commercial nuclear waste problem which greatly reduces or perhaps eliminates the requirement for geologic waste storage, and a system which generates potentially "unlimited energy from thorium fuel while destroying its own waste and operating in a new regime of nuclear safety. The accelerator technology is already rather mature after 50 years of development and is being driven by other programs. Reactors are also well understood after 50 years of development of many different reactor types. The next essential step in the ADTT program is demonstration of the successful integration of reactor and accelerator technology in an experiment of significant size. Such an experiment has been proposed for the Los Alamos

Meson Physics Facility (LAMPF) at Los Alamos and for the Moscow Meson Factory at Troitsk, Russia. For a system operating at a $k_{eff} = 0.96$, LAMPF would drive the system at a power level of 40 MWt thermal. Of course lower powers are contemplated for the earlier stages of the experiment which might extend over about seven years including both construction and operation.

The experiment would be accompanied by research and demonstration, at about the same technical effort as the experiment, on the required separations in the molten salt context. Perhaps seven years hence, an integrated demonstration of the ADTT system could be in operation at the 200 MWt level, with the deployment of the ADTT system beginning in about fifteen years. This time scale is approximately the same as the earliest planned opening of a geologic repository in the U. S. or elsewhere.

REFERENCES

[1] Management and Disposition of Excess Weapons Pluronium, National Academy of Sciences, Committee on International Security and Arms Control, National Academy Press, Washington, DC 1994

[2] The isotope that makes the principle difference between commercial plutonium and weapons plutonium is ^{240}Pu which decays with a half life of 6,600 years. After about 13,000 years commercial plutonium containing about 24 % ^{240}Pu transforms to weapons plutonium containing about 6 % ^{240}Pu.

[3] R. W. Benjamin, Savannah River Laboratories, Private communication, 1994; P.J. Sentieri and K. B. Woods, Idaho National Engineering Laboratory, Private Communication, 1994

[4] C. D. Bowman, "High Value use of Weapons Plutonium by Burning in Molten Salt Accelerator-Driven Systems or Reactors," International Seminar on Nuclear War and Planetary Emergencies, 18th Session, pp. 400-411, E. Majorana Center for Scientific Culture, Erice, Italy, 1993

[5] "The Los Alamos Accelerator-Based Conversion Concept for Plutonium Dispositon," transparency set prepared for review by the JASON Group in January 1994, available from The ADTT Project Office, Los Alamos National Laboratory, Los Alamos, New Mexico; and C. D. Bowman, "Weapons and Commercial Plutonium Ultimate Disposition Choices...Destroy Completely or Store Forever," in Managing the Plutonium Surplus: Applications and Technical Options, pp 125-138, Kluwer Academic Publishers, Dordrecht, The Netherlands, 1994

[6] Alvin M. Weinberg, "Molten Salt Reactors," in Nuclear Applications and Technology 8, 102-219 (1970)

A High Gain Energy Amplifier Operated with Fast Neutrons

Carlo Rubbia
CERN, Geneva, Switzerland

Abstract. The basic concept and the main practical considerations of an Energy Amplifier (EA) have been exhaustively described in Ref. [1]. Here the concept of the EA is further explored and additional schemes are described which offer a higher gain, a larger maximum power density and an extended burn-up. All these benefits stem from the use of fast neutrons, instead of thermal or epithermal ones, which was the case in Ref. [1]. The higher gain is due both to a more efficient high energy target configuration and to a larger, practical value of the multiplication factor. The higher power density results from the higher permissible neutron flux, which in turn is related to the reduced rate of ^{233}Pa neutron captures (which, as is well known, suppress the formation of the fissile ^{233}U fuel) and the much smaller k variations after switch-off due to ^{233}Pa decays for a given burn-up rate. Finally a longer integrated burn-up is made possible by reduced capture rate by fission fragments of fast neutrons. In practice a 20 MW proton beam (20 mA @ 1 GeV) accelerated by a cyclotron will suffice to operate a compact EA at the level of $\approx$ 1 GW$_e$. The integrated fuel burn-up can be extended in excess of 100 GW d/ton, limited by the mechanical survival of the fuel elements. Radio-Toxicity accumulated at the end of the cycle is found to be largely inferior to the one of an ordinary Reactor for the same energy produced. Schemes are proposed which make a "melt-down" virtually impossible. The conversion ratio, namely the rate of production of ^{233}U relative to consumption is generally larger than unity, which permits production of fuel for other uses. Alternatively the neutron excess can be used to transform unwanted "ashes" into more acceptable elements.

1.— INTRODUCTION

The Energy Amplifier (EA) has been extensively discussed in Ref.[1]. The main feature of such a concept, when compared to the conceptual design of Bowman et al. [2], is that it operates in conditions which ensure no chemistry on line is required in order to extract quickly the ^{233}Pa which is the essential ingredient of the Thorium breeding into ^{233}U. At sufficiently low flux, a "decay dominated regime" sets in, in contrast with the "capture dominated regime" chosen for instance by Bowman et al. [2].

Both schemes, as well as most of the work on the subject [3] refer to the use of thermal neutrons, for which much is known from the experience of Nuclear Reactors. We shall denote such broad class of devices as Thermal Energy amplifiers, (T-EA). In Ref. [1] we had already proposed to use epi-thermal neutrons in order to extend the technology of Pressurised Water Reactors (PWR) to the EA (PW-EA). In this operating mode a significant part of the action is taken over by the resonance region.

The present note explores the possibility of building an EA which operates in analogy to a Fast Breeder Reactor in the region of fast neutrons, namely well above the resonance region, with an average neutron energy of the order of $10^5 \div 10^6$ eV. In contrast with the T-EA we denominate this novel device as a Fast Energy Amplifier (F-EA). The conceptual sketch of the three devices, namely T-EA, PW-EA and F-EA is shown in Fig. 1.

The extensive exploration of such a device performed in this paper shows that it has remarkable features and it overcomes several of the limitations of the T-EA. However, in contrast with the PW-EA, which relies largely on the well mastered technique of the PWR's, a non-moderating coolant must be chosen. In view of the considerable safety problems related to

liquid Sodium, chosen almost universally in the Fast Breeder Reactors, we have opted for definitess for liquid Lead, for which so far little experience exists, if not for some small reactor developed in the former Soviet Union and for the use in the USA of the rather similar metal, Bismuth as cooling agent [4]. Another overwhelming reason for choosing Lead (or Bismuth, or an eutectic mixture of the two) is the fact that these materials are high energy targets which offer an excellent neutron yield and therefore the coolant material can also be the first target for the high energy proton beam.

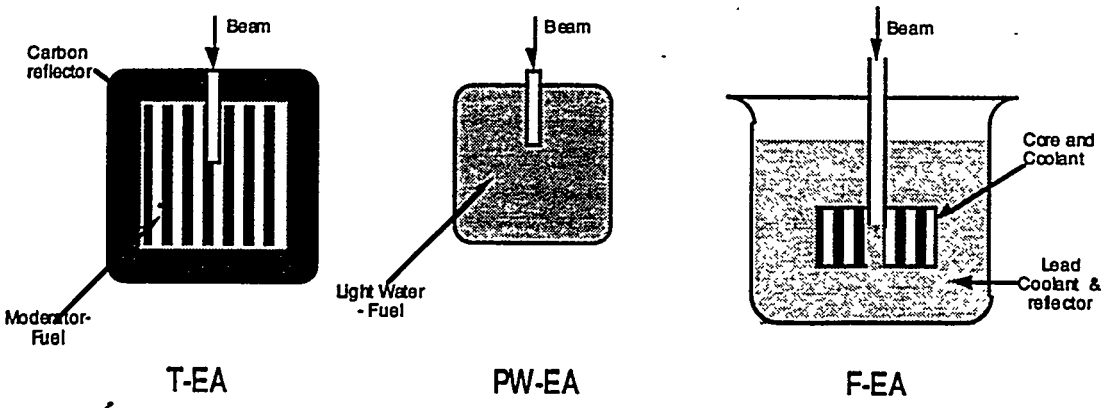

Fig. 1. Alternative Energy Amplifier schemes.

A second major difference of F-EA when compared to a T-EA is that the neutron flux and the related radiation damage are now some one hundred times larger. This is a well known problem of the Fast Breeder reactors and apparently has been solved [5] at least for burn-ups of the order of 100 GW(t) day/ton.

The motivations in accepting these additional changes is in our view overwhelming in view of the considerable improvement in performance when compared with a classic T-EA, namely (1) a higher gain ($G \approx 100 \div 150$) , (2) a larger maximum power density ($\approx$ 160 MW(t)/ton(Th)) and (3) an extended burn-up ($\geq$100GW(t) day/ton(Th)).

The higher gain is due both to a more efficient high energy target configuration and to a larger, practical value of the neutron multiplication factor k. The higher power density results from the higher permissible neutron flux, which in turn is related to the reduced rate of ^{233}Pa neutron captures (which, as well known, suppress the formation of the fissile ^{233}U fuel) and the much smaller k variations after switch-off due to ^{233}Pa decays for a given burn-up rate. Finally a longer integrated burn-up is made possible by reduced capture rate by fission fragments of fast neutrons and it is limited by the mechanical survival of the fuel elements.

In practice a 20 MW proton beam (20 mA @ 1 GeV) accelerated by a cyclotron will suffice to operate a compact EA at the level of $\approx$ 1 GW_e. The integrated fuel burn-up can be extended in excess of 100 GW d/ton, limited by the mechanical survival of the fuel elements.

The F-EA has a larger neutron yield than the T-EA and smaller losses associated to poisoning due to fission fragments and higher isotopes of Uranium. Therefore one can breed fissile ^{233}U in excess to what is normally regenerated by the main breeding process which is creating new ^{233}U exactly at the pace at which ^{233}U is burnt in the fuel. In this way one should be able to breed about 20% excess ^{233}U with respect to the one burnt in the central, high concentration, core. In practice this permits a doubling time of the available fuel every about 10 years, without relying on "start-up" procedures [1] based on enriched ^{235}U or surplus ^{239}Pu and ^{241}Pu from spent fuel or military applications. A doubling time of the installed power of F-EA of about ten years,

seems quite an adequate rate of growth, naturally after an initial number of installations have been started with different fuels.

Neutron capture cross sections for fast neutrons are much smaller both in the case of fission fragments and of newly produced Uranium, Protactinium and Neptunium isotopes. In the F-EA, most of these elements become useful fuels since they exhibit appreciable fission and (n,2n) cross sections. Concentrations of the Actinides are very different of the ones of a T-EA. While new elements become important because of the enhanced (n,2n) channels, like for instance ^{231}Pa and ^{232}U, the production of higher mass actinides is very strongly suppressed. Even the production of the lower Neptunium and Plutonium isotopes, like ^{237}Np and ^{238}Pu is now virtually suppressed (levels of less than 1 gr/ton after 100 GW(t) day/ton). A-fortiori this applies to higher Plutonium, Americium, Curium, Californium isotopes etc., which are the main source of long lived toxicity of ordinary Nuclear Reactors.

The F-EA constitutes also an important reduction in the toxicity of Actinides when compared to the already remarkable performance of the T-EA, provided two problems are mastered, namely the one associated to the presence of ^{232}U and the one of ^{231}Pa. The presence of a relatively large amount of ^{232}U, which is about 50 times more abundant than in a T-EA for comparable burn-up could indeed be considered as an advantage since it positively "denaturates" the Uranium extracted from the F-EA making it very hard, albeit impossible, for any military diversion of the material. As yet, the added toxicity due to the presence of ^{232}U is not so large to make the processing of the spent fuel impossibly expensive.

The ^{231}Pa represents a source of additional radio-toxicity which must be mastered. It is possible to separate chemically the ^{231}Pa from the spent fuel. Methods can be envisaged in order to neutralise it. One could introduce such an element inside an F-EA and transform it in ^{232}U by neutron capture and subsequent β-decay. The ^{231}Pa thermal neutron capture cross section is very large and dominated by a large resonance. An appropriate device based on thermal neutrons is therefore conceivable. Alternatively, if ^{231}Pa is simply re-injected with the next fuel load of the F-EA, its concentration will eventually saturate at a constant value after long burn-up, as a result of competing production and incineration.

We have already pointed out that the F-EA requires the use of coolants other than pressurised water. Although this last form of coolant is well known due to the waste experience of PWR's, its high pressure ($\geq$ 160 bars) in the T-EA is not without potential problems and for instance a massive loss of the coolant due to a leak could lead to melt-down problems. The presence of the window which must withstand such a large pressure and permit the injection of the high energy beam complicates the problem further. These problems can be strongly attenuated by reducing the temperature and hence the operating pressure of the water, but at the cost of a lower thermodynamical efficiency.

The F-EA operates instead with a liquid metal coolant which has a very low vapour pressure ($<<$ 1 mm Hg) in spite of the higher operating temperature. There is no way in which a major part of the coolant can be lost or spilled out, provided its tank is sufficiently strong and eventually double-walled. The radioactivity heating will in practice sufficiently maintain the Lead in the main tank in its liquid form. It suffices then to introduce a convective, passive and permanent heat dissipation from the tank to the outside of an amount larger than the radioactivity heating (a few percent of the full thermal power). This will suffice to dissipate safely away the residual power due to radioactive decays after shut-off and eliminate all risks associated to an uncontrolled temperature rise with the risk of melt-down accidents in an automatic and credible way. The cooling system should be entirely passive and involve convection cooling either with water or air or both.

The fact that the F-EA lends itself to an intrinsically safe protection against accidental melt-down is an important asset of this new kind of EA.

2.— PHYSICS CONSIDERATIONS AND PARAMETER DEFINITION.

The EA makes use of a fertile material, namely one or more of the isotopes ^{232}Th, ^{234}U, ^{238}U and ^{240}Pu. For many reasons illustrated for instance in Ref. [1], the by far preferred fertile material is ^{232}Th, but specific applications based on higher actinides could be of interest in burning Plutonium and similar surpluses. Neutron capture in these materials leads to production of fissile material, ^{233}U, ^{235}U, ^{239}Pu and ^{241}Pu respectively. The main breeding process for instance for ^{232}Th is then

$$^{232}\mathrm{Th}(n,\gamma)^{233}\mathrm{Th}\ \xrightarrow[22\ \mathrm{m}]{\beta^-}\ ^{233}\mathrm{Pa}\ \xrightarrow[27.4\ \mathrm{d}]{\beta^-}\ ^{233}\mathrm{U}$$

The dynamics of the breeding in an EA has been described in detail in Ref. [1] to which we refer for more details. In steady conditions, the EA will tend to the breeding equilibrium, namely in a situation in which each fissioned nucleus is replaced by a newly bred fuel nucleus. The equilibrium condition for the above reactions can be summarised by the equations:

$$N(^{232}Th)\sigma_\gamma(^{232}Th)\phi = N(^{233}Pa) / \tau(^{233}Pa \rightarrow ^{233}U) = N(^{233}U)\sigma_{fiss+\gamma}(^{233}U)\phi$$

where cross sections are averaged over the neutron spectrum of integrated flux ϕ. In brief, after a sufficiently large integrated neutron flux, the fuel/breeder concentration $\xi = N(^{233}U) / N(^{232}Th)$ will tend to the value for which the macroscopic (n,γ) breeding cross section becomes equal to the sum of the absorption macroscopic cross sections

$$\Sigma_\gamma(^{232}Th) = \sigma_\gamma(^{232}Th)N(^{232}Th) = \Sigma_a(^{233}Pa) + \Sigma_a(^{233}U) \cong \Sigma_a(^{233}U)$$

The last approximation is justified since the rate of captures in ^{233}Pa is proportional to the neutron flux and it can be made negligible by an appropriate choice of the burning rate [1]. Hence $\bar{\xi} \le \bar{\sigma}_\gamma(^{232}Th) / \bar{\sigma}_a(^{233}U)$. The quantities indicated are of course integrals over the spectral distribution of neutrons. As already pointed out in Ref.[1], the equilibrium concentration of fuel element with respect to the breeder element, while it is about $\xi = 1.35\ 10^{-2}$ for thermal energies, it grows to $\xi = 0.10$ for fast neutrons. An EA based on fast neutrons (F-EA) will then require a fuel concentration which is about seven times the one of a thermal device (T-EA). However as we shall see, the F-EA can operate with much higher burn-up rates and hence the total mass of fuel can be correspondingly reduced: for the same output power, the stockpile of ^{233}U is in general comparable for a F-EA and a T-EA.

The energetic gain G, namely the energy produced in the EA relative to the energy dissipated by the high energy proton beam is given by the expression [1]

$$G = \frac{G_o}{1-k} = \frac{2G_o}{2-\bar{\eta}(1-L)}$$

where G_o is the gain proportionality constant, typically 2.6 ÷ 3.0 for a well designed EA ; k is the fission-driven multiplication coefficient $k = \bar{\eta}(1-L)/2$; L is the sum of fractional losses of neutrons (absorbed in a variety of ways, like captures in structures and coolant, in fission-product poisons, diffused outside the EA and so on) ; $\bar{\eta}$ is the (spectrum averaged) number of fission neutrons produced by a neutron absorbed in the fissile isotope. As well known, in order to achieve criticality the denominator must become zero, namely $\bar{\eta} = 2/(1-L)$. More precisely, criticality is achieved when neutron losses are reduced to the value $L_{crit} = 1 - 2/\bar{\eta}$. Note that

since L > 0 in order to reach criticality $\overline{\eta} > 2$, one neutron being required to maintain the chain reaction and the second being absorbed by the fertile material.

The quantity $\overline{\eta}$ is an appropriate average over the neutron spectrum in the EA. Note that $\overline{\eta}$ is a function of the energy spectrum inside the EA, which in turn is a function of the moderator parameters and of the presence of other materials which may modify the neutron spectrum. In order to separate the cross section dependence from the details of the spectrum, we introduce an energy dependence in η. The parameter $\eta(E)$ has a rather complicated behaviour, with a somewhat lower value in some parts of the resonant region, before rising to large values for fast neutrons.

The F-EA has the advantage, when compared to an T-EA that it operates in a region where $\eta(E)$ is significantly larger. In addition because of the higher energies, additional neutrons are produced at each generation by different processes, like for instance fast fissions in the fertile material ^{232}Th and (n,2n) reactions in the fuel and the moderator. It should be noted that in the fast neutron regime most even-even nuclei like ^{232}U, ^{234}U, ^{236}U and so on exhibit a significant fission cross section. In order to take into account these contributions it is customary to replace the parameter $\overline{\eta}$ with $\overline{\eta}\varepsilon$ where ε is the ratio of all neutron produced to the ones from the main fissile material. For a F-EA we expect $\overline{\eta}\varepsilon \approx 2.4 \leftrightarrow 2.5$, conveniently and significantly larger than two and larger than $\overline{\eta}\varepsilon \approx 2.1 \leftrightarrow 2.2$ [6], appropriate for a T-EA. The consequent larger allowance for losses (f.i. $L_{crit} = 1 - 2/\overline{\eta}\varepsilon = 0.167 \leftrightarrow 0.200$ vs. $L_{crit} = 0.048 \leftrightarrow 0.091$) is an important asset of the F-EA. These extra neutrons do not have necessarily to represent losses; they may for instance be used to breed new fuel or to eliminate radio-toxic substances.

3.— FLUX DEPENDENT EFFECTS

It has been pointed out in Ref. [1]that there are sharp limitations to the neutron flux at which the T-EA can operate in acceptable conditions. The burn-up rate in turn is directly proportional to the neutron flux. We define with ρ such fuel specific power in units of thermal kWatt produced by one kg of fuel. The mass of the fuel is dominated and closely equal to the mass of the fertile ^{232}Th. At the breeding equilibrium the fluxes for thermal and fast neutrons respectively are

$$\phi_{thermal} = 1.80 \circ 10^{12} \times \left[\frac{\rho}{kW(t)/kg}\right] cm^{-2} s^{-1} \quad ; \quad \phi_{fastb} = 5.94 \circ 10^{13} \times \left[\frac{\rho}{kW(t)/kg}\right] cm^{-2} s^{-1}$$

For thermal neutrons, a power of ρ = 55.5 kW(t)/kg corresponds to a flux $\phi = 1.0 \times 10^{14}$ cm^{-2} s^{-1} , which is considered optimal for a T-EA [1]. Note that for the same power yield, the neutron flux in a F-EA is approximately 33 times larger. As is well known, it simply reflects the fact that cross sections are generally smaller at higher energies. As we shall see the practical burn-up of a F-EA is about ρ = 160.0 MW(t)/ton , i.e. the flux of fast neutrons will be about 100 times larger than the one optimal for a T-EA, $\phi = 1.0 \times 10^{16}$ cm^{-2} s^{-1} .

There are several flux dependent effects which have a direct influence on the value of the multiplication factor k, and hence on the gain:

1) Neutron capture by the intermediate elements of the breeding process and specifically by the ^{233}Pa which destroys a nascent ^{233}U atom at the price of an extra neutron. Such a loss involves a competition between neutron capture and radioactive decay, and it is proportional to the total flux ϕ through the parameter $\Delta\lambda_1 = \sigma_a(^{233}Pa) \times \tau(^{233}Pa \rightarrow ^{233}U) \times \phi << 1$ where the average of the absorption cross section is performed over the actual spectrum and τ represents the

mean life. The cross section $\overline{\sigma_a(^{233}Pa)}$ is about 43 b at thermal energies, a resonance integral of 850 b and 1.0 b for fast neutrons (E $\approx 10^5$ eV). The corresponding value for a T-EA is $\Delta\lambda_1 \approx 1.45\times10^{-16}\phi$, corresponding to a contribution to L of $\Delta L = (1-L)\overline{\eta\varepsilon}/2\Delta\lambda_1 \approx 1.4\times10^{-2}$ for the typical flux of 1.0×10^{14} cm^{-2} s^{-1}. For fast neutrons the cross section is much smaller but the flux is correspondingly larger: for a given burn-up rate ρ , $\Delta\lambda_1$ is 0.67 times of the value for thermal neutrons. Note however that the allowance for neutron losses is much greater for the F-EA and therefore larger burn-up rates are practical: for ρ = 160.0 MW(t)/ton , $\Delta\lambda_1 = 0.021$ which is quite acceptable.

2) A consequence of the relatively long mean life of ^{233}Pa(τ=39 d) is that a significant reactivity addition occurs during an extended EA shut-down. Conversely, any prolonged increase in burn-up rate produces a temporary reduction of reactivity until the ^{233}Pa inventory has not re-established, with the time constant of approach to saturation of 39 days. Such a reactivity change following a shut-down need not to be problem, but appropriate measures would be required to correct its effects. The density of ^{233}Pa is given by

$$N(^{233}Pa) = \tau(^{233}Pa\rightarrow^{233}U)\overline{\sigma_{\gamma+fiss}(^{233}U)}N(^{233}U)\phi =$$

$$= (1+\alpha)\tau(^{233}Pa\rightarrow^{233}U)\times\left[N(^{233}U)\overline{\sigma_{fiss}}(^{233}U)\phi\right]$$

where α is the fraction of the inelastic cross section involving non-fission (n,γ) reactions and the last term $N(^{233}U)\overline{\sigma_{fiss}}(^{233}U)\phi$ is directly proportional the ^{233}U burn-up rate, ρ. If the accelerator beam is shut down, following the characteristic decay lifetime $\tau(^{233}Pa\rightarrow^{233}U)$, the concentration of ^{233}U will increase by an amount asymptotically equal to $N(^{233}Pa)$, essentially independent of the mode of operation of the EA for a given equilibrium burn-up rate. However since in the case of the F-EA the equilibrium concentration ξ of ^{233}U is about seven times larger, its effect on reactivity $\max(\Delta k/k) = (\overline{\varepsilon\eta}/4)N(^{233}Pa)/N(^{233}U)$ will be only 1/7 of the one for a T-EA. For the chosen examples of burn-up rates ,$\max(\Delta k/k) \approx 0.072$ for the T-EA and only $\max(\Delta k/k) \approx 0.030$ for the F-EA, in spite of the factor three in ρ in favour of the present option.

3) Neutron losses to the high cross section fission product ^{135}Xe are well known [7]. The Xenon poison fraction is neutron flux dependent, since it relates, like in the case of ^{233}Pa to an equilibrium between captures and decays. For thermal neutrons and at the breeding equilibrium, the fraction of neutrons captured by ^{135}Xe is given by the expression $\Delta\lambda_3 \approx 0.9\times10^{-19}\phi/(2.1\times10^{-5}+3.5\times10^{-18}\phi)$ which tends to an asymptotic value $\Delta\lambda_3 \approx 0.028$ for fluxes $\phi \geq 1.0\times10^{14}$ cm^{-2} s^{-1} Following a reactor shutdown or reduction in power, the xenon poisoning temporarily increases even further [7] because decays producing Xe continue to occur, passing through a maximum 10 to 12 hours after the shutdown. The magnitude of this transient additional poisoning is also dependent on the neutron flux. Although the temporary loss is not significant, a reactivity reserve, if normally compensated by control rods, would represent a permanent loss of neutrons. The Xenon type poisoning effect is essentially absent in the case of F-EA, since there is no fission fragment nucleus which has the required features in the energy domain of importance.

4.— BURN-UP DEPENDENT EFFECTS

One of the most serious limitations in the T-EA is due to the losses of neutrons due to slowly saturating or non saturating fission products. In contrast to ^{135}Xe and ^{149}Sm, which have a very large neutron cross section and therefore reach saturation in a short time, the majority of the fission products have cross-sections which are comparable or smaller than the one of the fuel

itself. Hence the aggregate poisoning effect of such fission products is roughly proportional to the fractional burn-up of the fuel. The accumulated effect depends significantly on the past history of the fuel. Computer calculations have been used to analyse the poisoning as a function of the integrated burn-up for a variety of different conditions.

One important result is that losses due to fission fragment poisoning are much less important for a F-EA, when compared to a T-EA. (Fig. 2). Hence with a F-EA much longer burn-ups are possible without reprocessing of the fuel.

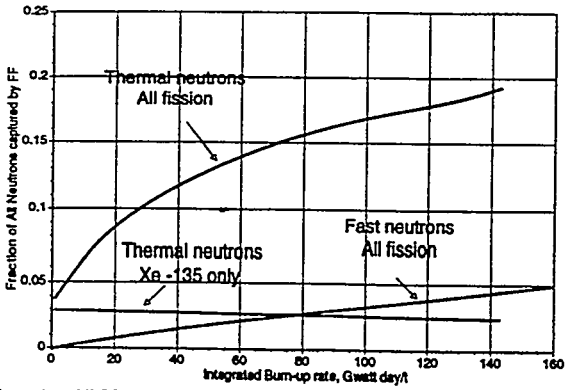

Fig. 2. Effect of Fission Fragment poisoning

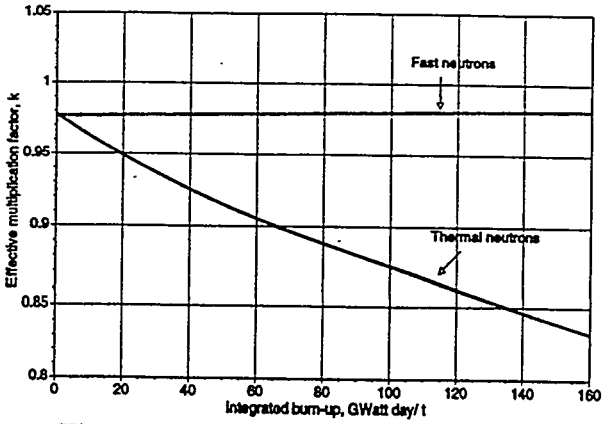

Fig. 3 . Burn-up dependence of factor k

Higher Uranium isotopes and eventually higher Actinides are produced by successive neutron captures. The time evolution of an initially "pure" ^{232}Th and ^{233}U fuel can be easily calculated and it was given in Ref. [1]. The build-up of the several isotopes (Figs. 4a-4c) introduces more captures and some fissions. Consequently we expect as a function of time a slight reduction of the parameter k. The value of k in steady conditions as a function of burn-up is given in Fig. 3.

The energetic gain of a T-EA, as discussed in Ref. [1] is of the order G= 30÷50. This appears well matched to the current produced by a 1 GeV cyclotron [8] and the relatively low optimal power due to the above indicated limitations in the permissible neutron flux. In practice this is realised operating the EA at an effective multiplication k in the range $0.92 < k < 0.95$. As we have already said, $k = \overline{\varepsilon\eta}(1-L)/2$. The parameter $\overline{\varepsilon\eta} \approx 2.2$ is relatively small for thermal and epi-thermal neutrons and one can expect in practice to achieve k_o=1.04 for a well designed EA, when only losses in the moderator and containment are included. The allowance for all other losses is then related to the actual k in the case of breeding equilibrium by the formula $\Delta L = 2(k_o - k)/\overline{\varepsilon\eta}$, which amounts to ΔL = 0.082 (0.109) for k = 0.95 (0.92). Hence the allowance for other sources is small and the details of the schemes in Ref. [1] were dominated by the neutron inventory. Fission poisoning limits the burn-up of the T-EA to some 30-50 GW day/t.

There are of course other reasons which suggest operation of the T-EA with relatively small values of k, namely its relatively large variations due to decay mechanisms after shut-down or power variations (^{232}Pa and ^{135}Xe) so as to leave enough margin from risk of criticality.

The same type of considerations would however suggest a much greater gain for a F-EA, for which an operating point in the vicinity of k = 0.980 is an optimal operating point, corresponding to an energetic gain in the interval G= 100÷150. A first reason for this choice stems from the much larger value of $\overline{\varepsilon\eta} \approx 2.5$, which implies $k_o \geq 1.20$ and ΔL = 0.136 for k = 0.980. On the other hand the fission poisoning is much smaller and linearly growing with the burn-up, amounting to about ΔL = 0.03 after 100 GW day/t. The flux dependent ^{135}Xe effect is absent and the time dependent k variation due to ^{233}Pa decays is seven times smaller for a given burn-up rate. All these considerations suggest that $k \approx 0.98$ as quite appropriate for a F-EA.

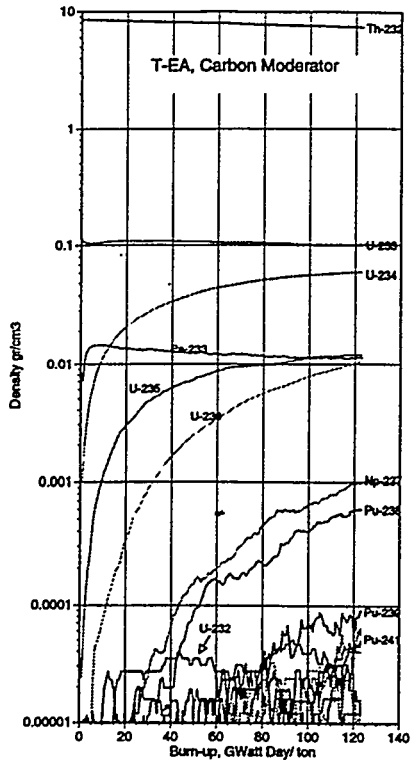

Fig. 4a Carbon Moderator (T-EA)

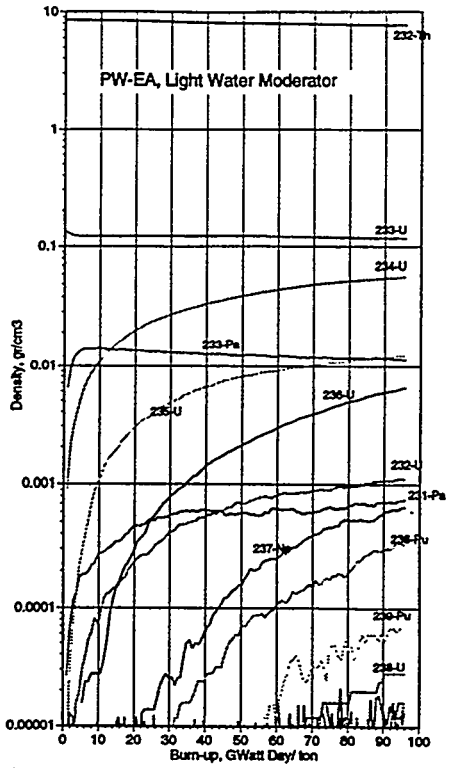

Fig. 4b. Pressurised Water (PW-EA)

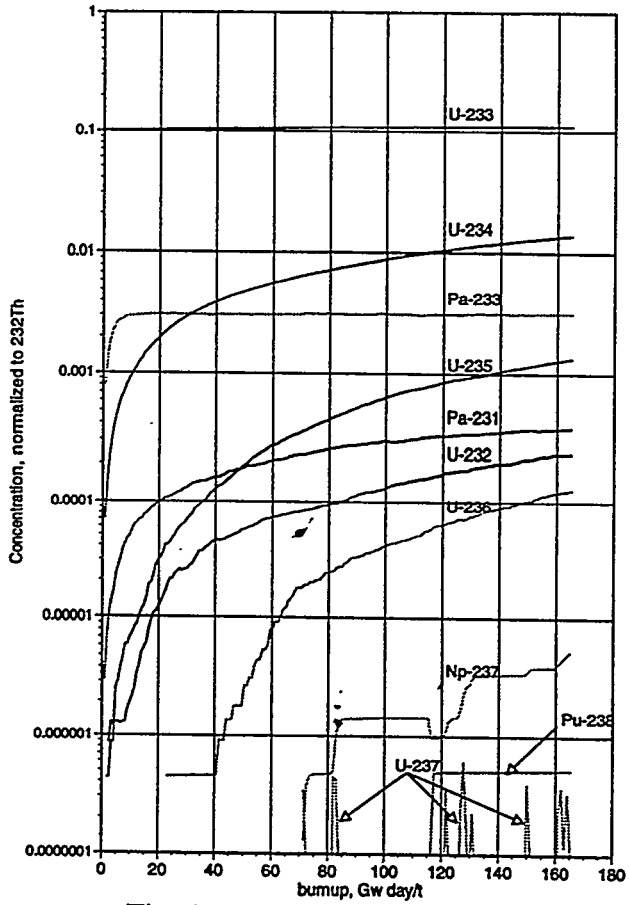

Fig. 4c. Fast Neutrons (F-EA)

5.— BREEDING OF ADDITIONAL FUEL

The EA is operating normally at the breeding equilibrium, namely it produces from initial Thorium exactly as much fuel as it burns. This permits to maintain an amount of "seeds" which, after fuel reprocessing, will be re-used indefinitely and repeatedly within the lifetime of the EA [1]. It might however be of interest to produce more fuel to be used as seeds for new installations or other similar applications.

In the simplest configuration the core is inserted in a large liquid Lead bath which has the function of reflector. Such a configuration will not make proper use of the excess of neutrons due to the high value of η. It is therefore necessary to determine which use one intends to make of them, like for instance (1) breeding new fuel (2) incineration of unwanted waste or eventually (3) absorbing them in "control rods". This choice would then define how the criticality parameter will be tuned to the wanted value, dissipating the excess criticality.

In the present note we shall make the assumption that the extra criticality of a F-EA is to be deployed essentially to breed additional fuel. The excess of neutrons is of the order of 10% of the total inventory, once the effects of higher actinides and the moderator captures have been taken into account. These neutrons can be conveniently captured in blanket of pure Thorium, in the form of ThO_2 oxide or metallic arranged at the periphery of the core. Contrary to the main core, in which ^{232}Th and ^{233}U have essentially equal macroscopic cross sections, all neutrons contribute here to the breeding of ^{232}Th. This will continue to be so, at least as long as the build-up of ^{233}U produces to a concentration which is much smaller than the equilibrium concentration $\xi = 0.10$. Therefore one expects to accumulate in the breeder about 20% of the 233U which is bred by the core. In practice this permits a doubling time of the available fuel every about 10 years, without relying on "start-up" procedures [1] based on enriched ^{235}U or surplus ^{239}Pu and ^{241}Pu from spent fuel or military applications. A doubling time of the installed power of F-EA of about ten years, seems quite an adequate rate of growth, naturally after an initial number of installations have been started with different fuels.

6.— A PRACTICAL LAYOUT.

On the basis of the previous considerations, a model example F-EA is now outlined with the objective of generating 1 GW(e). Because of the high(er) operating temperature ($\geq$ 600 °C) of the Lead coolant, one can safely assume a thermodynamical efficiency of the order of 42 % . Hence the thermal nominal power is 2.4 GW(t). At k = 0.98 the beam power is then 20 mA × 1 GeV. Following Table 1, the fuel mass is 2.4 GW/160 MW = 15 Tons of fuel material in the form of ThO_2–UO_2 mixture filling thin stainless steel pins. The ^{233}U "seeds" (at equilibrium concentration, ξ=0.1) have then a weight of 1.5 tons. Space must be allowed for the cooling liquid to circulate between pins. As an orientative figure we assume that the volume occupied by the cooling liquid is of order of 50% of the one occupied by the pins. Somewhat arbitrarily, we choose for the central core a cylindrical shape with the diameter of 1.75 m. A central hole of 20 cm diameter without pins but with Lead acts as the high energy target. Including the presence of a ThO_2 breeder, the k-dependence on burn-up is the one shown in Fig. 3. The heat produced by beta decay heating should be extracted from the core by natural convection. We have verified that (in the case of residual beta heating only) the flow of the coolant between the parallel pins can be made approximately laminar, because of the close spacing if the pins and the small convective driving force. The large molten Lead "swimming pool" has approximate diameter

and height equal to 6 m. A secondary Lead loop and a heat exchanger inside the pool are used to extract the heat. Electromagnetic pumping inside the pool with the help of a $\mathbf{E} \times \mathbf{B}$ field is being investigated. Amongst the many outstanding effects which must be examined we would like to mention (1) Corrosion due to molten Lead (2) Additional fragments are produced by the spallation processes due to the high energy beam (3) Radiotoxicity build-up in the Lead Coolant.

Table 1- Main parameters of a typical fast breeder fuel pin [5]

Material	UO_2,PuO_2, (ThO_2)	
Fuel pellet diameter	6.0	mm
Thickness of clad	0.35	mm
Type of clad	SS 16Cr13Ni	
Smear density	0.80 ÷ 0.85	
Linear rod power	450	W/cm
Fuel rating(ThO_2 + breeding), ρ	160	kW/kg
Gap between fuel pellet and clad	80.0	μm
Max. midway, hot spot clad temperature	700	°C
Burn-up	>100	GW day/t
Duration of an element @ 100 GW day/t	2 years	@ 85% util.

ACKNOWLEDGEMENTS.

The active participation to this work of S. Buono, F. Carminati, P. Cennini, J. Galvez, C. Gelès, I. Goulas, R. Klapisch, P. Mandrillon, J.P. Revol, C. Roche, J.A. Rubio and F. Saldana has been essential to this work.

REFERENCES.

[1] Carminati F. et al.. " An Energy Amplifier for cleaner and inexhaustible Nuclear Energy Production driven by a Particle Beam Accelerator", CERN/AT/93-47 (1993)

[2] Bowman C. et al. Nucl. Instrum. Methods, **A320** , 336 (1992)

[3] Furukawa K. et al. Journal of Nuclear Science and Technology, **27**,1157 (1990) and references therein

[4] Miles, F. T. et al. " Liquid metal Fuel Reactor with recycled Plutonium", Proc. Second UN Intern. Conf. on Peaceful Uses of Atomic Energy, Geneva, vol. 9 pt. 2 180, 1958
Heusener G.et al. "Seminar on the concept of the High Safety and Economy Lead Cooled Fast Reactor", Moscow, Oct.-24 1990, unpublished

[5] Häfele W. "Fast Breeder Reactors" Ann. Rev. Nucl. Sci., **20**, 393 (1970) and references therein

[6] Perry A.M. and Weinberg A. M. "Thermal Breeder Reactors", Ann. Rev. Nucl. Sci., **22** ,317 (1972)

[7] See for instance in Glasstone S., "Nuclear Reactor Engineering", D. Van Nostrand Company Inc. (1955)

[8] Rubbia C., Mandrillon P. and Fietier N. " A high intensity Accelerator for Driving the Energy Amplifier for Nuclear Energy Production", in Proceeding of EPAC94, London June 1994, to be published
Stainmbach Th. et al. "Potential of Cyclotron based Accelerators for Energy Production and Transmutation" , contribution to this Conference

Transmutation studies at CEA in frame of the SPIN program Objectives, results and future trends

M. Salvatores, C. Prunier, Y. Guérin, A. Zaetta
Direction des Réacteurs Nucléaires
Commissariat à l'Energie Atomique
CE Cadarache, FRANCE

1. INTRODUCTION

In order to respond to the public concern about wastes and in particular the long-lived high level ones, a French law issued on December 30, 1991 identified the major objectives of research for the next fifteen years, before a new debate and possibly a decision on final wastes disposal in Parliament. These objectives are :

1) improvement of the wastes conditioning ;
2) extraction and transmutation of the long-lived wastes in order to minimize their long term toxicity ;
3) research performed in underground laboratories in order to characterize the capacity of geological structures to confine radioactive wastes (two sites have to be selected for these underground laboratories, in concertation with the local population) ;
4) last, the study of conditioning and prolonged surface storage of wastes.

To comply with the requirements of the December 1991 law related to the management of long-lived high level wastes, the CEA has launched an important and long term R & D programme. A part of this programme called SPIN is devoted to separation and incineration of these wastes and it includes two sub-programmes :

- In short and mid term perspectives (1991-2000), PURETEX aiming primarily at reducing the volume of wastes from reprocessing from 1.5 m^3 to 0.5 m^3 per ton of reprocessed heavy metal. This value is to be compared with the 1.7 m^3 announced for direct disposal of irradiated fuel.
  This results will be obtained by modifying the PUREX process (decreasing or eliminating sodium salt, new management of liquid streams) in order to be able to eliminate bitumen and by improving the conditioning of solid wastes (hulls compaction or melting for example).
- In a long term perspective, ACTINEX devoted to the separation and transmutation of long-lived elements in view of reducing wastes toxicity.

Once separated, elements have to be mixed with fuel or manufactured into target elements for transmutation.

Transmutation studies of Minor Actinides (MA) and long-lived fission products (LLFP) are conducted on a wide range of options :

- fission reactors (fast reactors and thermal reactors),
- homogeneous or heterogeneous recycling of MA,
- LLFP transmutation in fission reactors,
- accelerator - based systems, mainly for LLFP transmutation.

The studies are performed in order to reduce the potential source of radiotoxicity in a deep geological repository and/or to reduce the residual radiotoxicity risk represented by mobile LLFPs.

These studies are conducted consistently with parallel studies devoted to Pu management, both in thermal reactors (MOX recycling in PWRs and its optimisation) and in Fast Reactors (the CAPRA project to burn Pu in a fast neutron core).

The transmutation programs cover the following areas :

1. *Basic data studies :*
   a) Sensitivity and uncertainty analysis.
   b) MA and LLFP Data evaluation and measurement (e.g. Tc-99 capture cross-section measurement and Np-237 (n,γ) cross-section measurement at the GELINA accelerator of IRMM-Geel).
   c) Intermediate energy data and codes for accelerator - based systems (e.g. : impact of uncertainties in neutron production double differential cross-sections).
   d) Integral experiments for MA and LLFP data validation (e.g. fuel pin irradiation experiments in power reactors).
2. *Fuel studies :*
   a) Fuel fabrication and irradiation for homogeneous recycling of Np and Am both in thermal and fast reactors.
   b) Inert matrix basic research, fabrication and irradiation for targets in the heterogeneous recycling mode, in particular for Am.
   c) Experiments for Tc-99 irradiation in power reactors.
3. *Reactor and fuel cycle studies :*
   a) Core characteristics when MA and/or LLFP added to the fuel / core constituents (e.g. : reactivity coefficients).
   b) Fuel cycle impact (Pu-238 content, decay heat, n sources, etc).
   c) Strategic studies for different scenarios (cost / benefit analysis).
   d) Hybrid systems physics and conceptual studies (as illustrated in a companion paper at this meeting).

Some results will be shown and future trends will be indicated in the following paragraphs.

2. BASIC DATA STUDIES

Most data and codes are presently available to perform a wide range of feasibility studies.

As an example, very tight (± 10 %), and probably not justified, target accuracies on relevant quantities such as the source of potential radiotoxicity and its evolution in time, give rise to data accuracies on minor actinides which are generally already met, see Table 1 and ref. 1.

Other requirements studies and data intercomparisons are performed in the frame of the Nuclear Energy Agency Working Party on Evaluation Cooperation.

As far as data validation for transmutation studies in fission reactors, irradiated fuel analysis plays an essential role. The excellent C/E comparison on the SUPERFACT experiment related to Np and Am has been reported [2].

In the field of accelerator - driven transmutation, intranuclear cascade (INC) codes and intermediate energy data, the CEA studies are mostly performed in the frame of the OECD Nuclear Energy Agency initiative.

First attempts have been devoted to define target accuracies and data requirements in this field.

First estimates indicate that a $\pm$ 10 ÷ 20 % target accuracy on a hybrid system energy balance, would require a corresponding $\pm$ 10 ÷ 20 % accuracy on the neutron yield, as calculated with an INC code. The radiotoxicity balance of the system can suggest a target accuracy of $\pm$ 100 % on the radiotoxicity source due to spallation products. This target accuracy can require new measurements with increased precision of the (A,Z) distribution of spallation products in different types of targets (Pb, W, U or Th, etc ...).

Table 1. Target accuracy on Radiotoxicity source term R and data uncertainty requirements

Basic data	Initial (a) uncertainties	Required uncertainties
σ_c Pu-240	25 %	16 %
σ_f Pu-241	20 %	14 %
σ_c Pu-242	50 %	12 %
σ_f Pu-242	50 %	30 %
σ_c Am-241	50 %	8 %
σ_f Am 241	50 %	14 %
σ_f Am-242M	50 %	21 %
σ_f Am-243	50 %	24 %
Radiotoxicity of a standard S/A of large fast reactor (EFR-type)	29 % (b)	8 % (c)
Radiotoxicity of S/A containing minor actinides for the same reactor	31 % (b)	10 % (c)

(a) Initial guess of uncertainties on σ
(b) Uncertainty on R due to initial guess of $\delta\sigma/\sigma$
(c) Target accuracy : $\pm$ 10 %

The neutron balance in the subcritical region of a hybrid system, is mostly responsible for the transmutation potential of the system [3]. This neutron balance is very little affected by specific features (e.g. energy / angle dependence) of the spectrum of the neutrons issued from spallation, since the properties of the multiplying region are dominating in the establishment of the average spectrum and, as a consequence, of the average cross-sections which enter in the neutron balance.

However, there is a need to know with sufficient precision the high energy (> 20 MeV) component of the neutron spectrum, to evaluate e.g. damage and activation in materials. As an example, the high energy component of an evaporation spectrum typical of a system like the PHOENIX system [4] produces a ~ 20 % contribution to the Fe DPA defined as :

$$DPA = \int_o^\infty \sigma_{dpa}^{Fe}(E)\,\phi_n(E)\,dE$$

3. FUEL STUDIES

Fuel studies have been reported previously (see for example refs 3 and 5).

Here we will recall that a significant irradiation program has been defined, both in fast reactors (PHENIX) and in thermal reactors (experimental reactor OSIRIS). The irradiation program is devoted to the validation both of the heterogeneous recycling mode and of the homogeneous recycling mode, and both for Am and Np.

Fig. 1, 2 and 3 show respectively :

a) the irradiation device for inert matrix tests (MATINA experiment in PHENIX to be launched in 1994) ;

b) the capsule for a new SUPERFACT-2 experiment in PHENIX, aiming to reach higher burn-ups ($\geq$ 10 % h.a.) than in the previous SUPERFACT-1 experiment [5] ;

c) the ACTINEAU experiment related to transmutation studies in PWRs (to be launched in 1995).

An experiment of Tc-99 irradiation will start in 1994 in a S/A of PHENIX (core periphery), using a moderator to increase the epithermal captures.

Demonstration experiments are foreseen in SUPER-PHENIX starting in 1995, which will involve 1 to 4 full subassemblies, with fuel pins containing ~ 2 % Np homogeneously mixed to the standard MOX fuel and few Am targets on inert matrix.

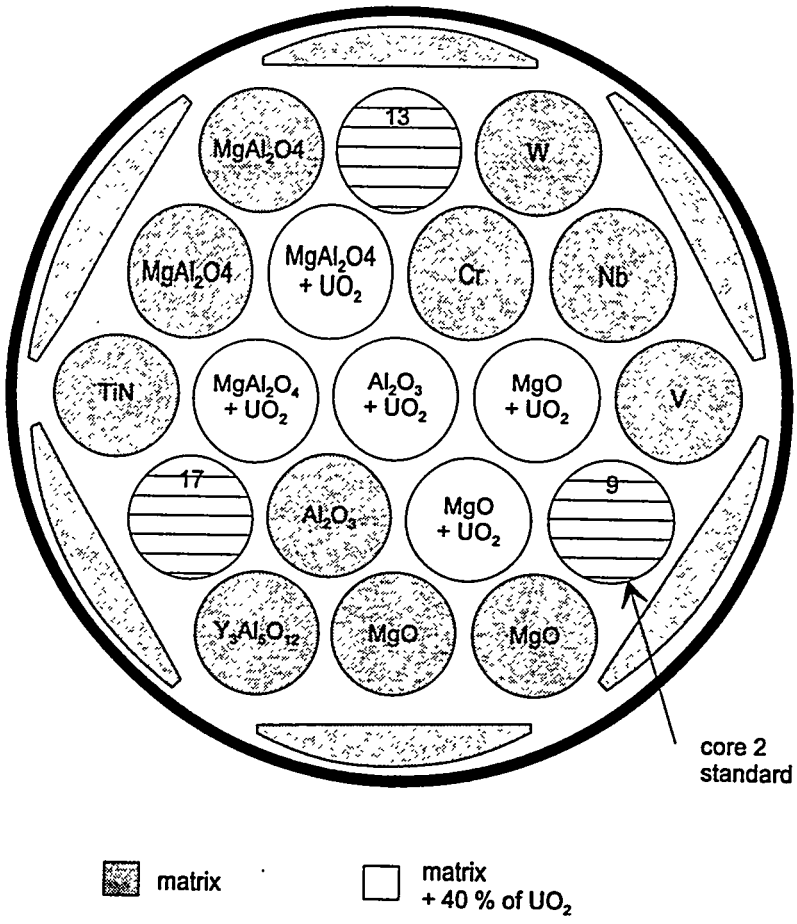

Fig. 1 Heterogeneous Concept. Behaviour of the inert matrix. Experiment MATINA in PHENIX

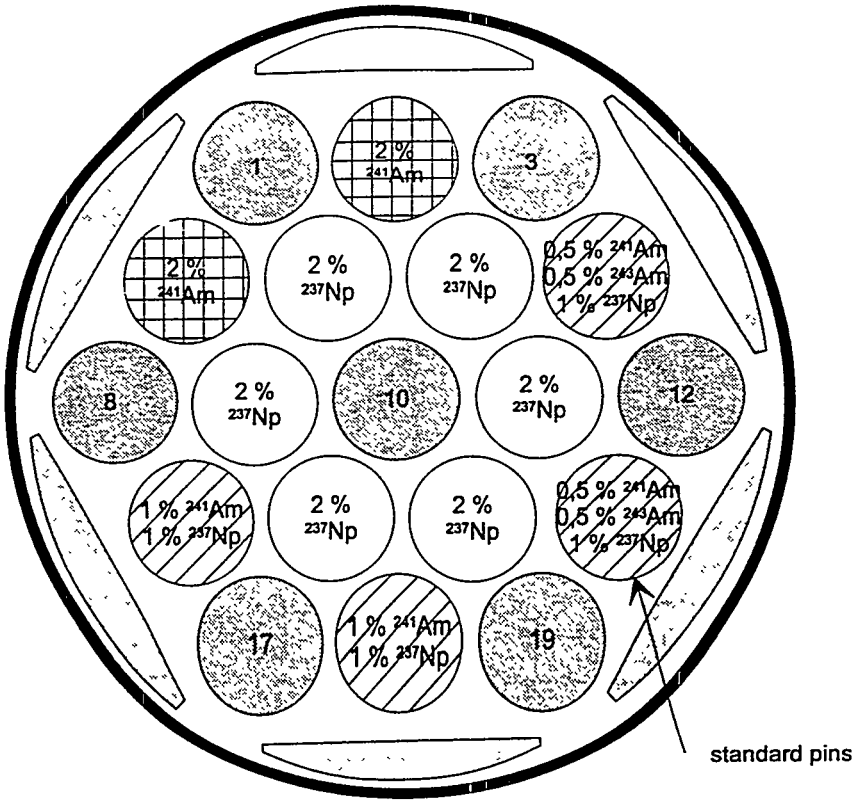

Fig. 2 SUPERFACT 2

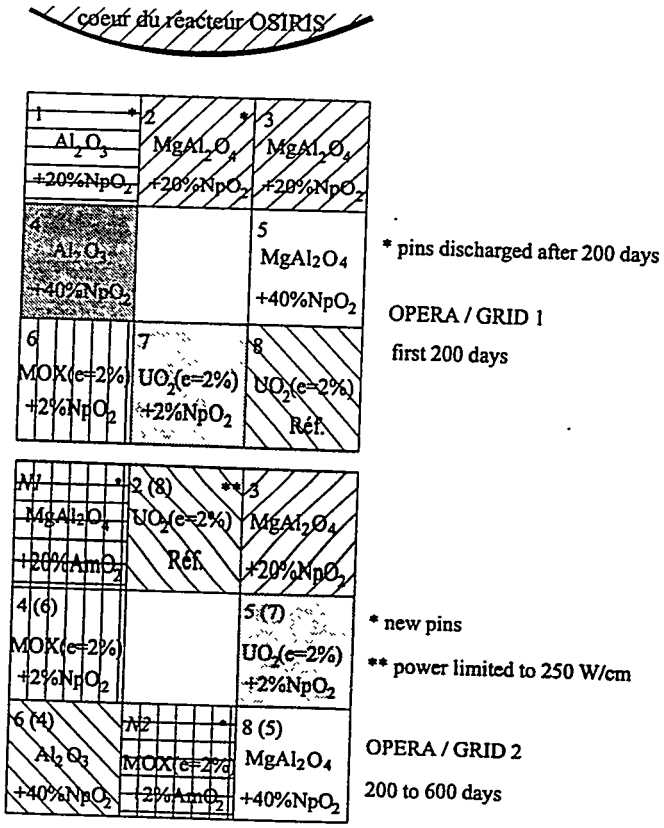

Fig. 3 ACTINEAU EXPERIMENT in the OPERA loop of OSIRS REACTOR
Pins positions in grid 1 (Np) and grid 2 (Am)

4. REACTOR AND FUEL STUDIES

4.1 Fission reactors

Results have been reported recently [3, 6, 7].

We will recall that if we consider the potential radiotoxicity source associated with an irradiated PWR fuel (33 GWd/t), the Pu component is dominating (Table 2). If one wants to quantify the theoretical effects of reprocessing and partitioning with respect to an open cycle, the curves of Fig. 4 are obtained.

Table 2. Components of the radiotoxicity source term Evolution with time (Sv/TWhe) (PWR fuel irradiated at 33 GWd/t)

	10^3 y	10^4 y	10^5 y
TOTAL	$3.1\ 10^8$	$7.7\ 10^7$	$4.2\ 10^6$
Components (%)			
Pu	90	97	88
Np	/	/	1.3
Am	9.2	2.5	2.7
Cm	0.3	0.4	/
P.F.	$6.0\ 10^{-4}$	$2.4\ 10^{-3}$	$3.2\ 10^{-2}$
URANIUM COMPONENTS			
Depleted U	$2.4\ 10^4$	$3.5\ 10^4$	$1.4\ 10^5$
U from reprocessing	$2.1\ 10^4$	$4.8\ 10^4$	$2.2\ 10^5$
Mill tailings	$7.2\ 10^5$	$6.6\ 10^5$	$2.6\ 10^5$

As far as Pu, an optimal strategy seems to be a limited number of its recycling in PWRs (possibly with 100 % MOX fuel and an appropriate moderator-to-fuel (M), ratio, see ref. 7), followed by recycling in a Fast Reactor (FR). For the medium term (2010 ÷ 2020), an appropriate strategy should be based on the development of Pu-burner FRs (e.g. of the CAPRA type, see ref. 8). A scheme of this strategy is given in Fig. 5.

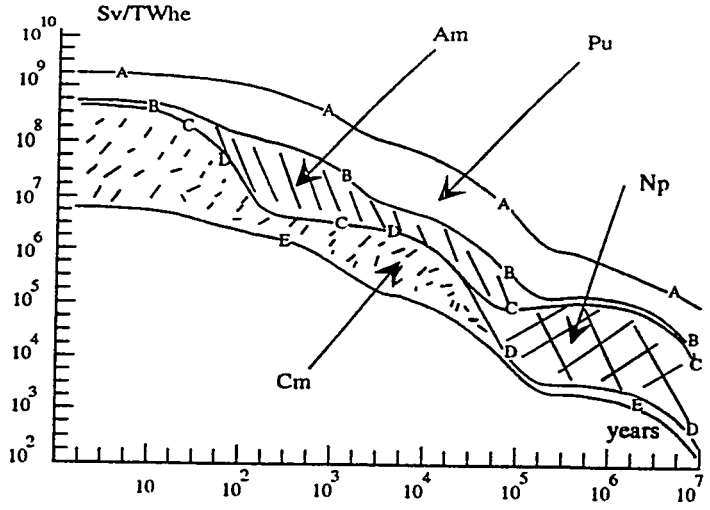

Fig. 4 Theoretical scenarios

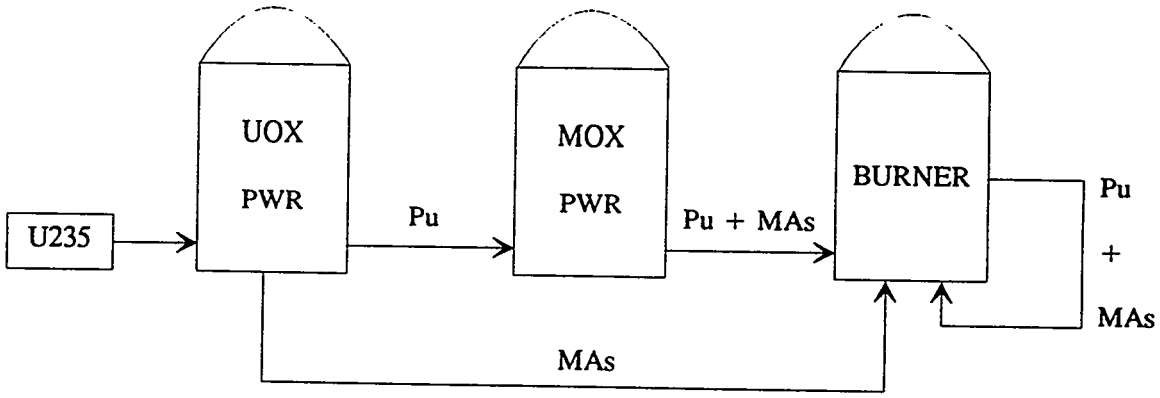

Fig. 5 Schematic flowpath for the Pu+MA burning strategy

The interest to go to Pu recycling in Fast Reactors can be easily seen in terms of radiotoxicity reduction. For example, in Fig. 6 we show the radiotoxicity balance in the case of an hypothetical shut-down of nuclear energy after :

1 recycling of MOX in a PWR (M = 2)	(curve 1)
1 recycling of MOX in a PWR (M = 3)	(curve 2)
2 recyclings of MOX in a PWR (M = 3)	(curve 3)
3 recyclings of MOX in a PWR (M = 3)	(curve 4)
2 recyclings of MOX in a PWR (M = 3) followed by a recycling in a burner FR	(curve 5)

The reference is the open cycle (R = 100).

To give an example of the potential of partitioning / transmutation scenarios, and on the basis of the indications of previous studies (e.g. see ref. 3), we can show the result [6] for an electronuclear power generating park which includes :

- 1450 GWe UOX PWRs (65 GWd/t burn-up),
- 1450 GWe MOX PWRs (65 GWd/t burn-up),
- (Pu + MA) burner FR (same power as above and 150 GWd/t burn-up).

The UOX PWRs plutonium output is directed to 100 % MOX PWRs for a single recycling, in order to reduce the Pu feed to the burner FRs.

MAs are recycled as follows : Np is recycled homogeneously in the core, Am heterogeneously in the radial blanket. Cm is left to decay into Pu isotopes and then it is recycled. The elementary losses at reprocessing are assumed to be 0.3 % for plutonium and 1 % for MAs. The evolutions for the burner FR are performed with an initial reactivity of 10000 pcm down to a final zero reactivity. The core residence time is 640 EFPD and the blanket irradiation time is 4 x 640 EFPD (compatible with damage doses target values).

According to this scheme, the reactor park power splits into 70 % of UOX PWRs, 9 % of MOX PWRs, and 21 % of FR burners.

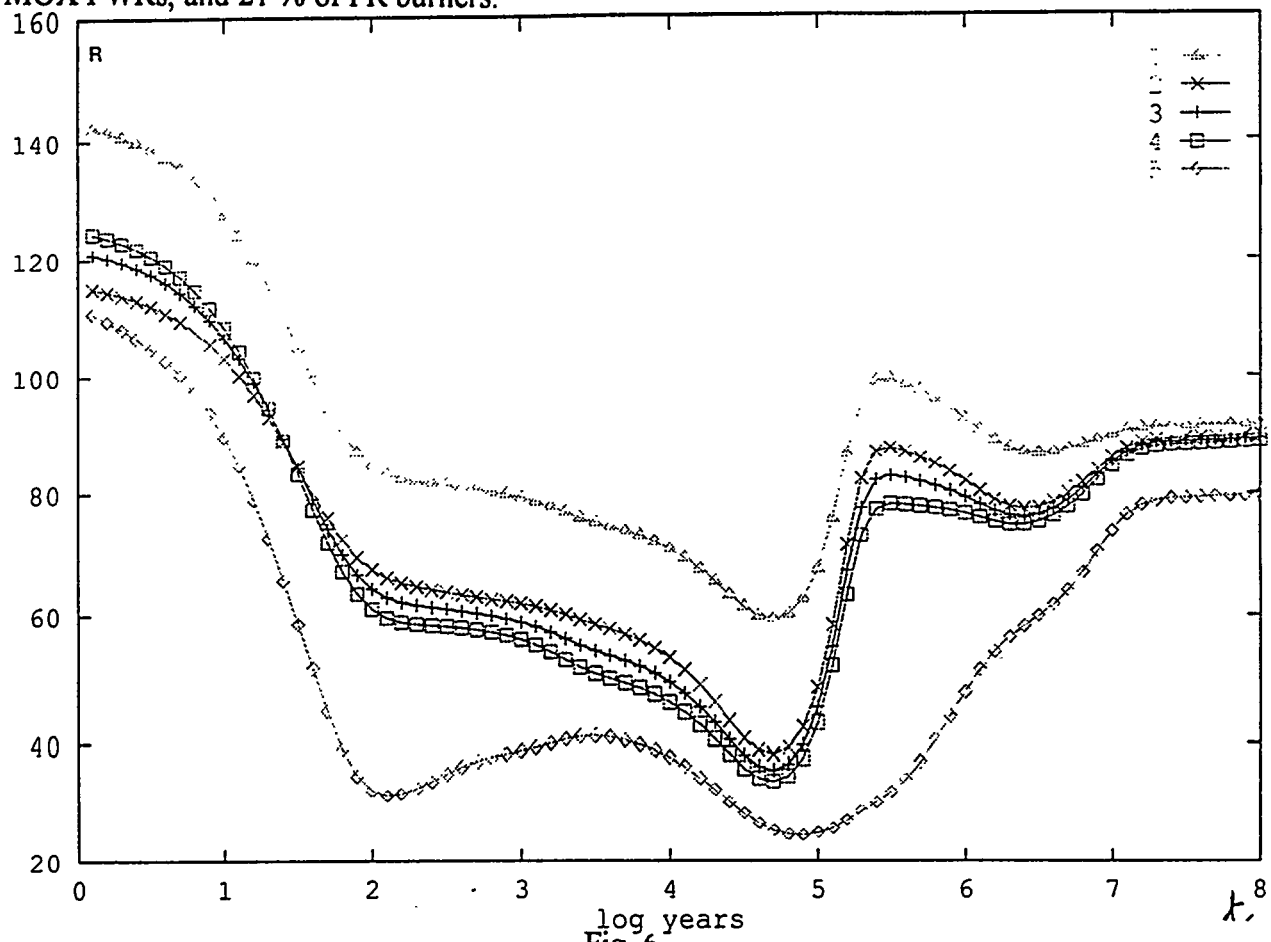

Fig. 6

Radiotoxicity R balance with respect to open cycle (R=100)

The radiotoxicity reduction factors (f_R) with respect to an open cycle, are as follows :

Storage time (years)	10^3	10^4	10^5	10^6	10^7
f_R	44	42	59	37	41

Associated fuel cycle studies are performed, in order to provide elements to very preliminary economical evaluations. One of such studies is performed at CEA under contract with the European Union [9].

4.2 Accelerator - based systems

Physics studies are performed at CEA on accelerator - based hybrid systems (see for example ref. 3). The potential role of these systems is investigated for long-lived fission product (LLFP) transmutation. The physics analysis of ref. 3 has shown that the potential interest of such system is to provide an "excess" of neutrons, available for transmutation. The accelerator provides in fact an external neutron source to a subcritical multiplying medium.

The maximum additional n source per fission (μ) that one can get, is dependent on the fraction f of the energy produced in the subcritical system that is used to produce the additional neutron source :

$$\mu = \frac{f}{K} \quad \text{where} \quad K = \frac{E_p}{E_{fiss} \cdot z \cdot \eta}$$

with : E_p proton energy ;
z number of neutrons per proton ;
η efficiency of the energy transformation into neutrons ;
f fraction of energy produced to be fed back to the accelerator.

For example, if $E_p \approx 1.5$ GeV, $z \approx 50$ and $\eta \approx 0.2$, we have $K \approx 0.75$. This means that if all the energy produced in the subcritical system is used to feed the accelerator to produce additional neutrons, in that case $\mu_{max} = 1.3$ n/fission.

The maximum additional neutron source per fission corresponds to a high subcriticality :

$$k_{eff} = \frac{\nu}{\nu + \mu}$$

As for proton current I, we can define /7/ a simple relationship between μ and I :

$$\mu \approx \frac{zI}{5} \frac{mA}{MWth} \approx 0.1\, I \frac{mA}{MWth} \qquad (\text{for } z \approx 50)$$

This relationship simply illustrates the need for an intense proton current if one wants to achieve a high value of μ (i.e. in a strongly subcritical system).

Finally, we get for an hybrid system a total neutron surplus G_H :

$$G_H = G_S + \mu$$

where G_S is the neutron surplus in the subcritical system, and which is maximum for a fast neutron spectrum, whatever the neutron flux level [3].

An example of a hybrid system, capable to burn Pu and Tc-99 is given in a companion paper at this conference [10]. In more general terms one can try to intercompare the different features of nuclear energy systems which can contribute to reduce all the long-term radiological risks. Subcriticality is one of these features. In table 3, we intercompare subcriticality together with other features in their effectiveness to reduce the integrated radiotoxicity associated to the full fuel cycle.

Table 3.

	S	L
• Closed cycle effect Vs open cycle	3.2	3.9
• Subcriticality (K = 1 → K = 0.8)	1.5 ÷ 2	1.5 ÷ 2
• Doubling of burn-up (from 4 % → 8 %)	2.5	2
• Fast neutron spectrum Vs thermal neutron spectrum	2.5	2.5
• Th cycle Vs U cycle (with fast neutron spectrum) (4 ÷ 8 % burn-up)	20	$\frac{1}{2}$ (a)

Reduction factors of the integral fuel cycle toxicity for the "short" time range (S : $t \leq 10^4$ y) and for the "Long" time range (L : $t \leq 10^6$ y) for different parameter variations in a power system.

(a) : Means : "increase of factor 2".

5. CONCLUSIONS

France choice to reprocess irradiated fuel can meet two major goals : possible re-use of the large amounts of residual fissile materials and optimisation of the waste management, according to their physical and chemical characteristics.

The transmutation program at CEA in the frame of the SPIN program and with the support of the industrial partners EdF and FRAMATOME provides the technical background to evaluate a wide range of options, from fission reactors (fast or thermal) to accelerator - based concepts.

6. REFERENCES

1. Palmiotti, G., Salvatores, M., Hill, R., *"Data Uncertainty Impact in Radiotoxicity Evaluation connected to EFR and IFR Systems"*, Nucl. Sci. Eng. to be published.
2. Salvatores, M., et al., *"The SPIN Program at CEA - Transmutation Aspects", Proc. Int. Conf. GLOBAL'93*, Seattle, 12-17 Sept. (1993), page 548.
3. Salvatores, M., Slessarev, I., Uematsu, M., Nucl. Sci. Eng., 116, 1 (1994).
4. Van Tuyle et al., *"The PHOENIX Concept"*, BNL-52279 (1991).
5. Prunier, C., et al., *"Some Specific Aspects of Homogeneous Am and Np Based Fuel Transmutation Through the Outcomes of the SUPERFACT Experiment in PHENIX", Proc. Int. Conf. GLOBAL'93*, Seattle, 12-17 September (1993), page 158.
6. Tommasi, J., et al., *"Long-lived waste Transmutation in reactors ", Ibidem*, page 1252.
7. Salvatores, M., et al., *"Nuclear Waste Transmutation : Physics Issues and Potential in Neutron Fields", Proc. Int. Reactor Physics Conference, Tel-Aviv*, 23-26 January (1994).
8. Rouault, J., et al., *"Physics of Pu burning in Fast Reactors : Impact on Burner core design", Proc. ANS Topical Mtg on Advances in Reactor Physics*, Knoxville, April 11-15 (1994).
9. Hugon, M., *"Potentialities of Partitioning and Transmutation for Nuclear Waste Management", Proc. RECOD'94*, London, 24-28 April (1994).
10. Slessarev, I., et al., *"Waste Transmutation with minimal fuel cycle long-term risk"*, This Conference.

JAERI R&D on Accelerator-Based Transmutation under OMEGA Program

T. Takizuka, T. Nishida, M. Mizumoto, and H. Yoshida
Japan Atomic Energy Research Institute
Tokai-mura, Naka-gun, Ibaraki-ken
319-11 Japan

Abstract. The overview of the Japanese long-term research and development program on nuclide partitioning and transmutation, called "OMEGA," is presented. Under this national program, major R&D activities are being carried out at JAERI, PNC, and CRIEPI. Accelerator-based transmutation study at JAERI is focused on a dedicated transmutor with a subcritical actinide-fueled subcritical core coupled with a spallation target driven by a high intensity proton accelerator. Two types of system concept, solid system and molten-salt system, are discussed. The solid system consists of sodium-cooled tungsten target and metallic actinide fuel. The molten-salt system is fueled with molten actinide chloride that acts also as a target material. The proposed plant transmutes about 250 kg of minor actinide per year, and generates enough electricity to power its own accelerator. JAERI is proposing the development of an intense proton linear accelerator ETA with 1.5 GeV-10 mA beam for engineering tests of accelerator-based transmutation. Recent achievements in the accelerator development are described.

INTRODUCTION

One of the most important problems with nuclear energy is the management of high-level radioactive waste (HLW) arising from the reprocessing of spent nuclear fuels. The hazard potential of transuranic actinides and fission products in the HLW is high due to their radioactivity. Of particular concern are the nuclides with very long half-life whose hazard remains high for millions of years.

The major candidate scheme for the long-term waste management in most nuclear countries is the permanent disposal of unpartitioned HLWs, or unreprocessed spent fuels, into a stable geological formation to isolate them from the human environment. However, considerable attention has been directed toward the partitioning and transmutation (P-T); separating long-lived nuclides from HLWs and converting them into shorter-lived or non-radioactive ones. Improvements of long-term safety assurance in the waste management and possible beneficial use of valuable resources in the wastes can be expected through establishing the P-T technologies.

In Japan, a national program called "OMEGA" has started from 1988 for research and development of new technologies on nuclear waste partitioning and transmutation. Under the OMEGA program, the Japan Atomic Energy Research Institute (JAERI) is carrying out R&Ds for advanced partitioning technology, transmutation with burner fast reactor, and proton accelerator-based transmutation. This paper describes the outline of the OMEGA program and JAERI's R&D activities with an emphasis on accelerator-based transmutation.

OMEGA PROGRAM

National policy for managing the HLW in Japan is based on disposal into a deep underground repository in a stable geological formation after solidification into a stable form and decay heat cooling for 30—50 years. Many R&D efforts have been devoted to establish technologies for its safety disposal and methodologies for its safety assessment.

In addition to this national project, Japan Atomic Energy Commission submitted in October 1988 a report entitled "Long-Term Program for Research and Development on Nuclide Partitioning and Transmutation Technology" to widen options of future waste management and to explore the possibility to utilize HLW as useful resources. The report plots a course for technological development up to the year 2000. This program is called "OMEGA," which is the

acronym derived from "Options Making Extra Gains from Actinides and fission products."

The program is led by the Science and Technology Agency (STA) under the collaboration of three major research organizations; JAERI, the Power Reactor and Nuclear Fuel Development Corporation (PNC) and the Central Research Institute of Electric Power Industry (CRIEPI). The program is to be proceeded in two steps: the phase-I and II. The phase-I covers a period up to about 1996, and the phase-II covers a period from about 1997 to about 2000. In general, the basic studies and testings are to be conducted in the phase-I to evaluate various concepts and to develop required technologies. In the phase-II, engineering tests of technologies or demonstration of concepts are planned. After 2000, pilot facilities will be constructed to demonstrate the P-T technology.

It is to be noted that the program is conceived as a research effort to pursue benefits for future generations through the long-term basic R&D, and is not to seek a short-term alternative for established or planned fuel cycle back-end policies. The program is also expected to serve to revitalize the nuclear option into the 21st century in a healthy state. In addition, advancement of technologies such as accelerator technology, as advocated in this program, will provide potential spin-offs for other fields of science and technology.

The OMEGA program consists of two major R&D areas; the group separation of elements from HLW based on their physical and chemical property and potential value of utilization, and the transmutation of minor actinides (MAs) and long-lived fission products (FPs) into short-lived or stable nuclides. The outline of the program is shown in Fig. 1.

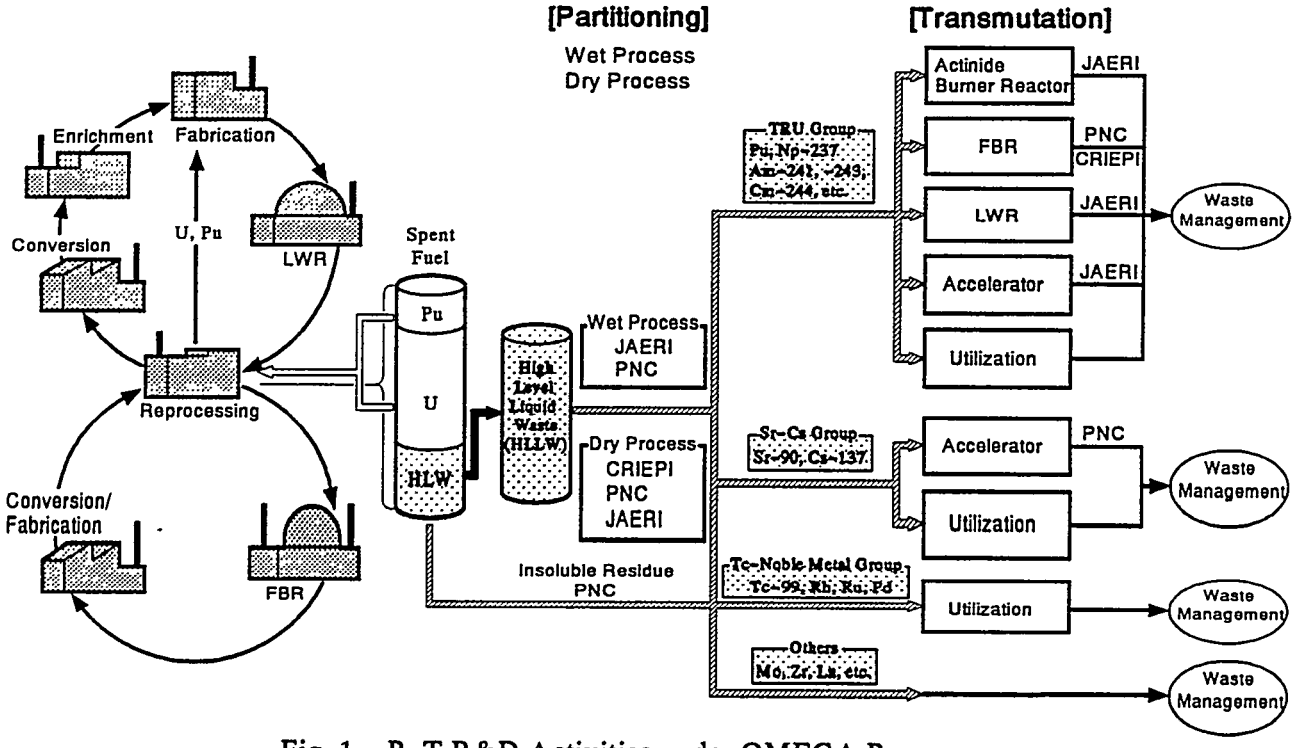

Fig. 1. P-T R&D Activities under OMEGA Program

Within the framework of the program, the following R&D activities are underway at JAERI, PNC, and CRIEPI.

JAERI : Four-group partitioning process
Actinide burner fast reactor
Proton accelerator-based transmutation

PNC : TRUEX-based partitioning process
Transmutation with oxide fuel fast breeder power reactor
Transmutation of fission products with electron accelerator
CRIEPI : Pyrometallurgical process
Transmutation with metallic fuel fast breeder power reactor

PARTITIONING AND TRANSMUTATION STUDIES AT JAERI

A partitioning process has been developed to separate elements in the HLW into four groups; transuranium elements (TRU), Sr-Cs, Tc-platinum group metals and the other elements [1]. A series of laboratory-scale tests with the actual or synthesized HLW indicated that the proposed partitioning process would be promising. The hot test of the entire process is to be conducted with the actual HLW at the Nuclear Fuel Cycle Safety Engineering Research Facility (NUCEF), Tokai. The chemical engineering test is also planed to start in 1996.

A special transmutor operated with very hard neutron energy spectrum and high neutron flux can be very efficient and effective for MA transmutation. In this context, JAERI has been pursuing the concepts of actinide burner reactor (ABR) and accelerator-driven system as dedicated transmutor, rather than the transmutation schemes using commercial power reactor.

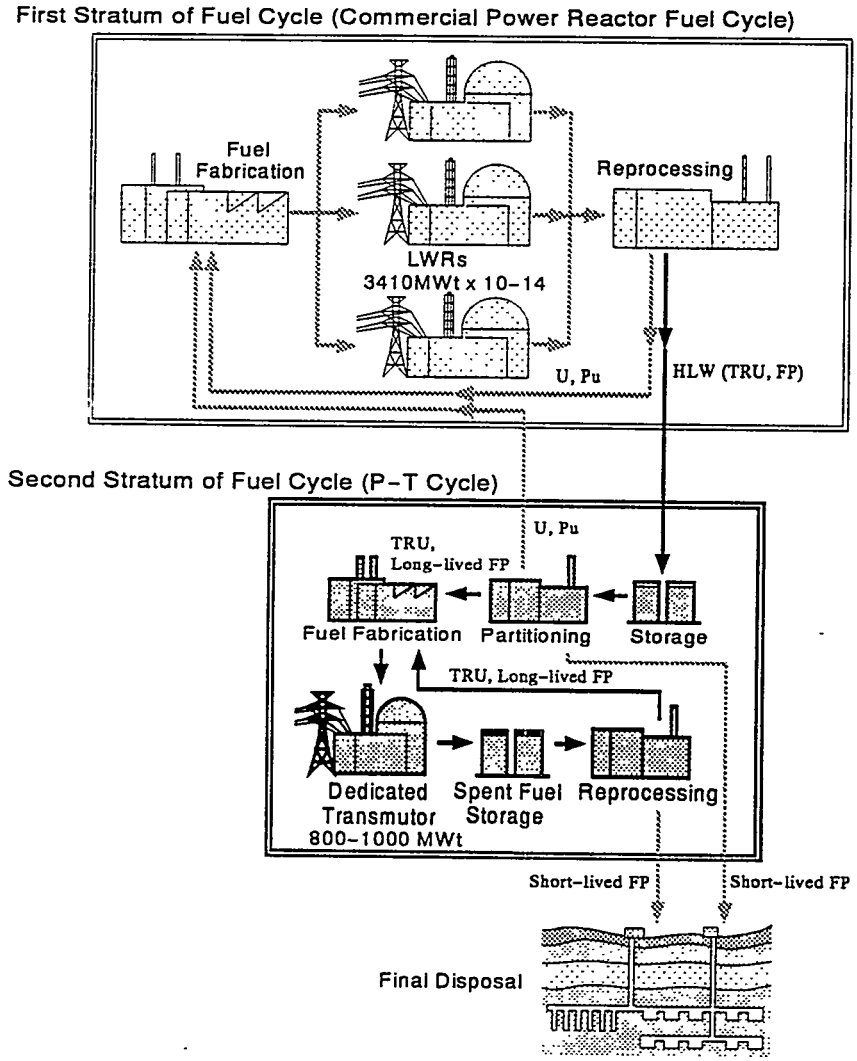

Fig. 2. Concept of Double Stratum Fuel Cycle

With the dedicated transmutor, the troublesome MA from the waste management view point could be confined in a P-T fuel cycle for transmutation, which is the second stratum separated from the first one of commercial fuel cycle for power generation. The concept of double-stratum fuel cycle is illustrated in Fig. 2. It will offer several advantages over the recycling of MA to the commercial power reactor. These are higher transmutation rate, effective confinement of MAs, and no impact on the power reactor operation. There will be no additional shielding and cooling requirements to the existing commercial fuel cycle.

Conceptual design studies have been carried out for ABRs and accelerator-driven transmutation systems. To support the design studies of these transmutors, several basic researches are in progress or planned. These include the nuclear data measurements of MAs and phase diagram, thermodynamic studies on MA compounds. The spallation integral experiments at the National Laboratory for High Energy Physics (KEK), Tsukuba are under way.

A high-intensity proton linear accelerator with 1.5 GeV-10 mA beam, named the Engineering Test Accelerator (ETA), has been proposed to conduct various engineering tests for the accelerator-driven transmutation system. In the course of the ETA development, R&D work for the Basic Technology Accelerator (BTA) with 10 MeV-10 mA beam is in progress.

ACTINIDE BURNER FAST REACTOR

Two types of reactor concept are proposed, one is the metallic fuel and sodium cooled type, called M-ABR, another is the nitride coated particle fuel and helium cooled type, named P-ABR [2]. Very hard neutron spectra, high neutron fluxes and high actinide burnups are obtained for these proposed actinide burner reactors.

M-ABR is a modular plant consisting of six 170-MWt reactors. The core is separated into two regions; an inner core composed of Np-Pu-Zr fuel and an outer core composed of (Am, Cm)-Pu-Y fuel. The mean neutron energy in the core is about 800 keV. One plant can transmute 300 kg/y of actinides.

P-ABR has fuel elements of particle bed formed in the annular space of concentric porous frits. Fuel particles are directly cooled with helium gas. Very high power density is obtained since a large heat transfer surface per volume is very effective for heat removal. A fuel particle consists of actinide nitride microsphere and thin TiN coating layers. P-ABR has a thermal power of 1200-MW and can transmute 360 kg of actinides annually.

R&D ACTIVITIES ON ACCELERATOR-BASED TRANSMUTATION

JAERI R&D includes the conceptual design study of accelerator-based transmutation plant, the development of spallation simulation code system, and the spallation integral experiments.

In the design study of transmutation plant, two types of system concepts are being investigated; solid system and molten-salt system. In either system, an MA-loaded subcritical core is driven by a high-intensity proton accelerator and uses fast neutrons to burn MAs efficiently. The design of the solid system is based on the status of sodium-cooled fast breeder reactor technology. Nuclear and thermal-hydraulic performance of the target/core was calculated and the engineering feasibility of the major components was assessed. The molten-salt system with chloride MA fuel is an another attractive option for accelerator-based transmutation. Its main advantage is the capability of continuous on-line chemical processing of MAs and reaction products.

A computer code system has been developed for the design of accelerator-based transmutation system [3]. The High Energy Nuclear Reactions and Nucleon-Meson Transport code NMTC/JAERI [4] simulates the proton-induced nuclear spallation, subsequent internuclear transport process for energies above 15 MeV. It also calculates high energy fission reaction as a competing process with evaporation. Neutronic calculation below 15 MeV is carried out using transport codes, TWOTRAN, MORSE, and MCNP. The time evolution process of transmutation products is calculated by SPCHAIN code and by ORIGEN-2 code for energies above and below

15 MeV, respectively. The code system has been upgraded and improved by incorporating current models and methods.

Spallation integral experiments [5] have been carried out to obtain data on the neutron and spallation product yields and to evaluate the validity of the simulation code system. The 500 MeV booster proton synchrotron facility at the National Laboratory for High Energy Physics (KEK) is used for the experiments. A lead/tungsten target was installed in the center of a lead assembly with a diameter of 600 mm and a length of 1000 mm. The activation samples of Al, Fe, Ni and Cu were inserted in the holes drilled through the assembly along the beam axis at various radial positions. The number of induced activities in the sample was obtained by measuring gamma rays with 100 cc Ge-detector. Experimental results agreed fairly well with prediction by NMTC/JAERI.

ACCELERATOR-BASED TRANSMUTATION SYSTEM CONCEPTS

Solid Target/Core System

A conceptual design study has been made on an accelerator-based MA transmutation plant with a sodium-cooled solid target/core [6]. Schematic diagram of the solid system is presented in Fig. 3. A 1.5 GeV proton beam is injected through beam window into the tungsten target located at the center of MA-loaded subcritical core. Spallation neutrons emitted from the target induce fission reactions in the MA fuel. Heat generated in the target/core is removed by primary sodium coolant, then transported through secondary loops to the power conversion system.

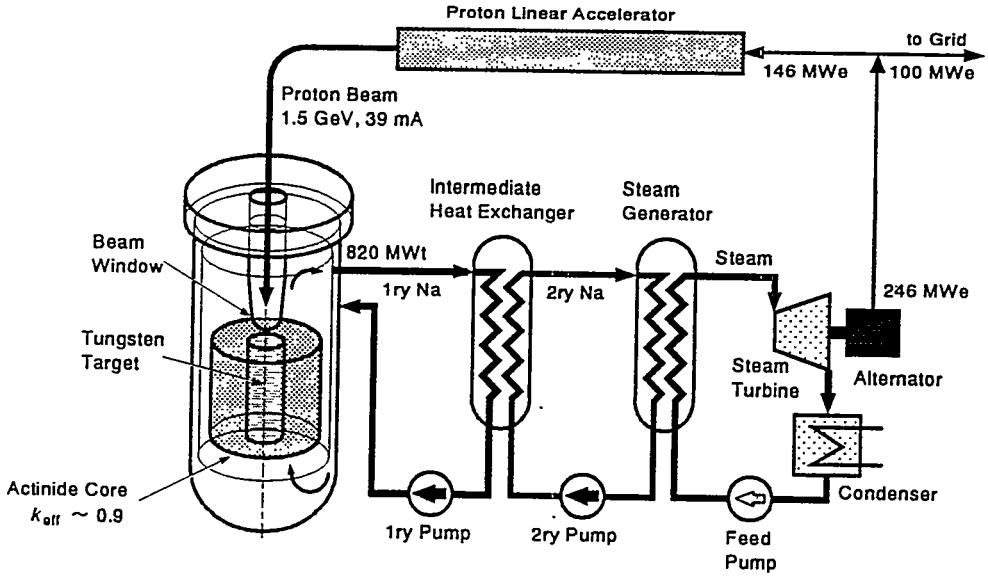

Fig. 3. Concept of Accelerator-driven Transmutation Plant

The fuel compositions are Np-15Pu-30Zr and AmCm-35Pu-10Y. These alloy systems are proposed for a sodium-cooled actinide burner reactor (M-ABR). Actinide fuel slug is clad in oxide dispersed strengthened (ODS) steel and sodium bonded. In the fuel subassembly design, measures are incorporated to ensure adequate fuel cooling during out-of-core handling operation.

The target subassembly is shown in Fig. 4. The target configuration consisting of layers of tungsten disk was chosen from the nuclear and thermal-hydraulic considerations. It is designed to maximize the number of emitted neutrons and to flatten the axial distribution of neutron flux. Coolant holes in the disk are arranged to stagger from layer to layer to avoid the direct penetration of high energy particles through the target.

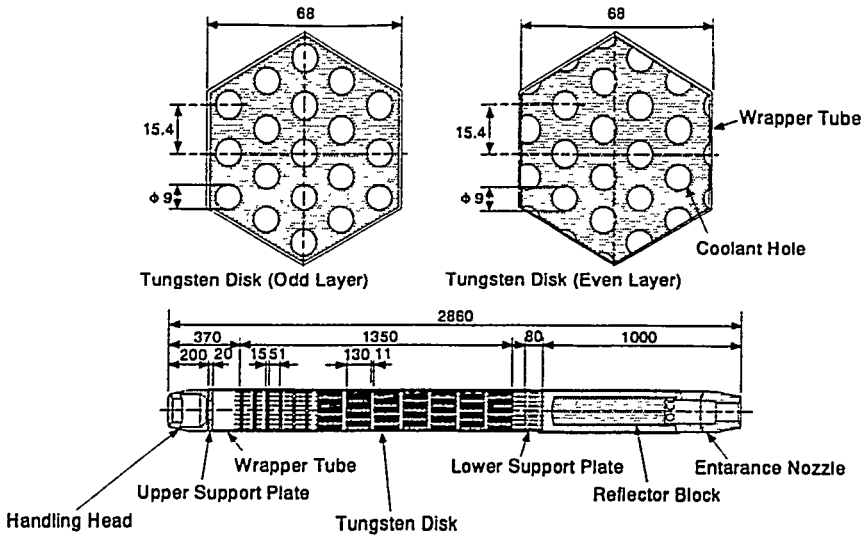

Fig. 4. Tungsten Target Subassembly

The fuel and target subassemblies are cooled by forced upward flow of sodium. The whole target/core including reflectors is contained within a steel reactor vessel as shown in Fig. 5. The vertical tube for beam path is vertically inserted into the reactor vessel down to just above the target. The bottom end of the tube forms the beam window. The beam window is cooled by a sodium flow from the target.

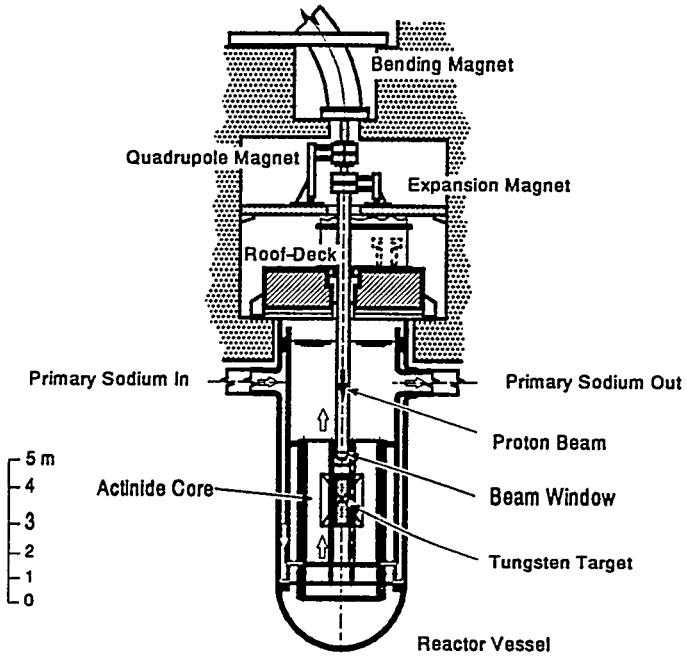

Fig. 5. Solid Target/Core System

Heat transport and power conversion systems are based on the current design practice for a sodium-cooled fast breeder reactor plant. A primary reactor auxiliary system with NaK loops is provided as an independent means of removing target/core decay heat.

With a 1.5 GeV-39 mA proton beam, the target/core having an effective neutron multiplication factor 0.89 produces 820-MW thermal power. Assuming a load factor of 80%, the

MA burnup (fission) is approximately 250 kg/y, or 8 %/y. The result shows that the system can support about 10 units of 1000-MWe light water reactor (LWR). An electric output of 246 MW is obtained at a plant thermal efficiency of 30%. The power required to operate the 1.5 GeV-39 mA accelerator is 146 MWe, assuming a 40% efficiency. This means that the system is more than self-sufficient in terms of its own energy balance.

Table 1 summarizes design parameters and operation condition of the solid system.

Table 1. Major Parameters of Solid Target/Core

Fuel	Metal Alloy Np-15Pu-30Zr AmCm-35Pu-10Y
Target	Solid Tungsten
Primary Coolant	Liquid Sodium
Actinide Inventory	3160 kg
Multiplication Factor	0.89
Spallation Neutrons	40 n/p
Proton Beam	1.5 GeV-39 mA
Thermal Power	820 MW
Burnup	250 kg/y (8.0 %/y)
Power Density, Max./Avg.	930/400 MW/m^3
Temperature, Core Inlet/Outlet	330/430 ℃
Coolant Maximum Velocity	8 m/s

Molten-Salt Target/Core System

A preliminary conceptual design study is being performed on an 800-MWt molten-salt core target/system as an advanced option for an accelerator-based nuclear waste transmutation system [7]. Chloride salt with a composition of 64NaCl-5PuCl$_3$-31MACl$_3$ is chosen for the molten-salt system based on the consideration mainly about actinide solubility. The molten-salt acts both as fuel and as target material, and at the same time it also serves as coolant in the molten-salt system. This significantly simplifies the core/target system configuration, as schematically shown in Fig. 6.

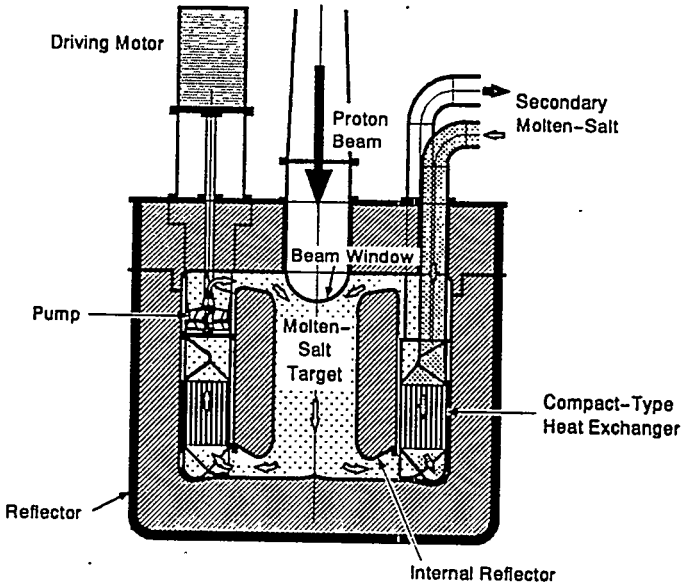

Fig. 6. Molten-salt Target/Core System

High energy proton beam at 1.5 GeV is injected into the central core/target region through the beam window. The core/target region is surrounded by an internal reflector. Intermediate heat exchangers and salt pumps are installed in the annular region around the internal reflector. This in-vessel heat exchanger design minimizes the total actinide inventory in the system.

The molten-salt target/core has an effective neutron multiplication factor of 0.92, and produces 800-MW thermal power with a 1.5 GeV-25 mA proton beam. In the molten-salt system, the maximum thermal power is limited not by the maximum fuel temperature or the maximum power density, but heat transfer rate through the heat exchangers. The maximum power density in the target/core region is about 1660 MW/m^3. Assuming a load factor of 80%, the actinide burnup is approximately 250 kg/y, or 4.6%/y. The system operates at molten-salt temperature in the range of 920—1020 K. With such a high operating temperature, a power conversion efficiency around 45% becomes feasible by using a supercritical steam cycle, which can improve the total energy balance of the system.

Table 2 summarizes design parameters and operating condition of the molten-salt system.

Table 2. Major Parameters of Molten-salt Target/Core

Fuel	Chloride Salt $64NaCl-5PuCl_3-31MACl_3$ (MA : Np, Am, Cm)
Target	Chloride Salt
Primary Coolant	Chloride Salt
Actinide Inventory	5430 kg
Multiplication Factor	0.92
Spallation Neutrons	38 n/p
Proton Beam	1.5 GeV-25 mA
Thermal Power	800 MW
Burnup	250 kg/y (4.6 %/y)
Power Density, Max./Avg.	1660/310 MW/m^3
Temperature, Core Inlet/Outlet	650/750 ℃
Coolant Maximum Velocity	3.6 m/s

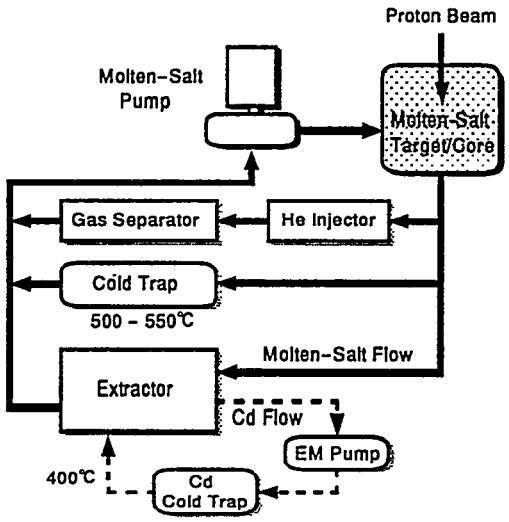

Fig. 7. Schematic Diagram of Continuous On-line Processing

The molten state of fuel salt offers several attractive features for the design of transmutation system. The main advantage over the solid system is the capability of the continuous on-line

processing. Schematic diagram of the continuous on-line processing in the molten-salt system is presented in Fig. 7. The fuel composition can be continuously controlled and fission and spallation products can be continuously removed from the fuel. Furthermore, rather laborious process of actinide fuel fabrication is not required for the molten-salt system. Core melt-down accidents can be impossible as the molten fuel is ready to be dumped from the core in case of emergency, which may add a high degree of safety.

PROTON ACCELERATOR DEVELOPMENT

The construction of a high-intensity proton linear accelerator called the Engineering Test Accelerator (ETA, 1.5 GeV-10 mA) has been proposed by JAERI for the purpose of performing various tests for accelerator-based transmutation and other possible nuclear engineering applications. The conceptual layout of the ETA is shown in Fig. 8.

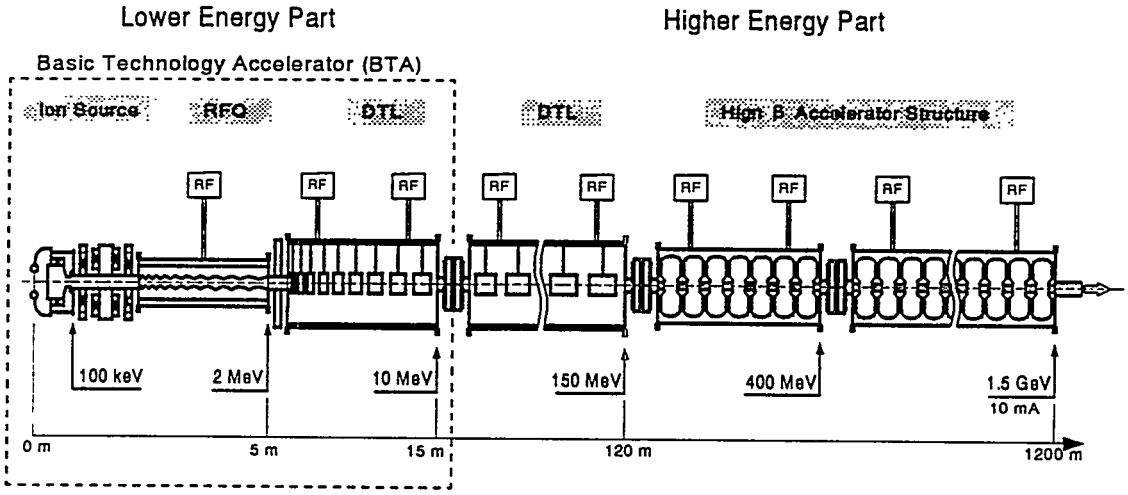

Fig. 8. Layout of Engineering Test Accelerator (ETA)

Table 3. BTA Basic Specification

Main Specification	
Accelerated Particle	Proton
Operation Mode	Pulse
Duty Factor	10 %
Output Energy	10 MeV
Average Beam Current	10 mA
Peak Beam Current	100 mA
Target Specification	
Normalized Tranverse Emittance	0.1 π cm•mrad (rms)
Energy Resolution	1 %

In the case of high-intensity accelerator, it is particularly important to minimize beam losses to avoid resultant damage and activation on the accelerator structures. The beam quality and maximum current are mainly determined in the low energy portion of the accelerator. As a first step toward the construction of the ETA, the Basic Technology Accelerator (BTA, 10 MeV-10 mA) is designed for the mockup test of the low energy potion [8]. The basic specifications of the BTA are shown in Table 3. Because of the high beam current and high duty factor (10%), heat removal from the accelerator structure is an important issue for the mechanical design. Temperature distribution, thermal stresses and displacements were carefully analyzed with the

3-dimensional modeling codes. The main accelerator components, such as ion source, radio-frequency quadrupole (RFQ), and radio-frequency (RF) sources, for the BTA have been developed and beam tests are successfully performed.

The conceptual studies for the ETA are underway in collaboration with the Los Alamos National Laboratory (LANL). These studies include design optimization for the operating frequency, the energy configuration, and the high ß structure based on beam dynamics and mechanical engineering considerations, aiming at ensuring low beam loss, hands-on maintenance capability and reduced construction cost.

SUMMARY

The background of the OMEGA program and its R&D areas were overviewed. The program pursues benefits for future generations through the long-term basic R&Ds.

The R&D activities at JAERI include the development of four-group partitioning process, the design study of MA burner fast reactor sand accelerator-based transmutation systems, the development of a high-intensity proton accelerator, and the related data measurement.

A conceptual design study of an accelerator-based transmutation plant with a sodium-cooled solid target/core has been carried out. The proposed plant transmutes about 250 kg of MA per year with a 1.5 GeV-39 mA proton beam and generates enough electricity to drive its own accelerator. The molten-salt system of chloride MA has been also examined as an another option with a capability of continuous on-line chemical processing. Simulation code development and spallation integral experiments have been made to improve the method and data for the design of accelerator-based transmutation systems.

The R&D work for prototype accelerator components (ion source, RFQ, DTL, and RF source) for high-power test is in progress. The detailed design of the BTA is followed in the next stage based on the results of the R&D work.

REFERENCES

[1] Kubota, M. et al.: "Development of Partitioning Process in JAERI," Proc. 2nd OECD/NEA Int. Information Exchange Meeting on Actinide and Fission Product Separation and Transmutation, ANL, 1992.

[2] Mukaiyama, T. et al.: "Higher Actinide Transmutation using Higher Actinide Burner Reactor," Proc. Int. Conf. Physics of Reactors, Marseille, 1990.

[3] Nishida, T. et al.: "Improvement of Spallation Reaction Simulation Codes NMTC/JAERI and NUCLEUS," 2nd Int. Symp. on Advanced Nuclear Energy Research , Mito, 1990.

[4] Y. Nakahara, Y. and Tsutsui, T.: "NMTC/JAERI — A Simulation Code System for High Energy Nuclear Reactions and Nucleon-Meson Transport Process," JAERI-M 82-198 (in Japanese) (1982)

[5] Takada, H. et al.: "Production of Radioactive Nuclides in a Lead Assembly with 500 MeV Protons," Proc. Specialists' Mtg. on Accelerator-Based Transmutation, PSI, 1992.

[6] Takizuka, T. et al.: "Conceptual Design Study of an Accelerator-based Actinide Transmutation Plant with Sodium-cooled Solid Target/Core," Proc. 2nd OECD/NEA Int. Information Exchange Meeting on Actinide and Fission Product Separation and Transmutation, ANL, 1992.

[7] Katsuta, H. et al.: "A Continuous Transmutation System for Long-lived Nuclides with Accelerator-driven Fluid Targets," ibid.

[8] Mizumoto, M. et al.: "High Intensity Proton Accelerator for Nuclear Waste Transmutation," 16th Int. Linear Accelerator Conf. LINAC-92, Ottawa, 1992.

Technologies Using Accelerator-Driven Targets Under Development at BNL*

Gregory J. Van Tuyle
Dept. of Advanced Technologies
Brookhaven National Laboratory, Upton, New York 11973

Abstract. Recent development work conducted at Brookhaven National Laboratory on technologies which use particle accelerator-driven targets is summarized. These efforts include development of the Spallation-Induced Lithium Conversion (SILC) Target for the Accelerator Production of Tritium (APT), the Accelerator-Driven Assembly for Plutonium Transformation (ADAPT) Target for the Accelerator-Based Conversion (ABC) of excess weapons plutonium, The PHOENIX Concept for the accelerator-driven transmutation of minor actinides and fission products from the waste stream of commercial nuclear power plants, and other potential applications.

INTRODUCTION

During its long history in designing, building, and operating particle accelerators and nuclear reactors, BNL has explored the application of hybrid technologies, with much of the early work being related to accelerator-driven breeder reactors [1]. More recently, advances in accelerator technologies, fueled largely by the Strategic Defense Initiative of the 1980s, have made viable much larger applications of hybrid technologies. In such applications, one uses the neutrons produced during spallation events, induced by driving charged particles into heavy targets, either to produce or destroy materials that would have previously been produced and/or destroyed in nuclear reactors. In some instances, these spallation neutrons are multiplied in a target containing actinides in some subcritical configuration.

Once one assumes the availability of large quantities of spallation neutrons, a wide array of potential applications becomes readily apparent, based in large part on missions previously undertaken using nuclear reactors. Given the recent difficulties in building nuclear reactors for any purpose, it is indeed tempting to take on any and all missions traditionally fulfilled by the reactors. However, it is essential for the proponent of accelerator-target applications to develop technically credible reasons for moving away from reactor solutions that could, in some cases, be simpler and cheaper. In the applications proposed by BNL, the justifications are generally based on significant environmental, safety, or/and economic or operational advantages.

Accelerator Production of Tritium (APT)

In the case of the Accelerator Production of Tritium (APT), for which BNL is developing the Spallation-Induced Lithium-Conversion (SILC) Target [2], the spallation target material is lead, and the surrounding blankets contain the lithium-6-bearing aluminum plates wherein the neutrons are captured to produce tritium (as is done at Savannah River). In this instance, there are no actinides involved, and the advantages include the avoidance of many reactor safety issues and the lack of high-level waste generation. The disadvantage with respect to reactors is the high electricity requirement, but that disadvantage diminishes with reduced tritium production requirements.

---

* This work was performed under the auspices of the U.S. Department of Energy.

The SILC Target is illustrated in Figures 1 (in exploded form) and 2 (as installed in the target cavity). The SILC Source region is the compact array (about two cubic meters) of aluminum pressure tubes, which each contain about five hundred 1-cm-diameter aluminum-clad lead pins, as well as the heavy-water coolant. Since none of these materials are significant neutron absorbers, most of the spallation neutrons escape the source and penetrate into the SILC Blanket. Once inside the blanket region, the neutrons are slowed by the light-water coolant, and then captured in the aluminum-clad plates of lithium (enriched to 50% Li-6) aluminum. As indicated in Figure 1, the Blanket is composed of three components, the U-blanket that fits below and beside the source region, the L-blanket the covers the top and back of the source region, and the beam-expander duct blanket, which captures most of the neutrons that come back off the front face of the source (towards the accelerator). (Note that a "dog-leg" in the beam transport line prevents these neutrons from ever reaching the accelerator.)

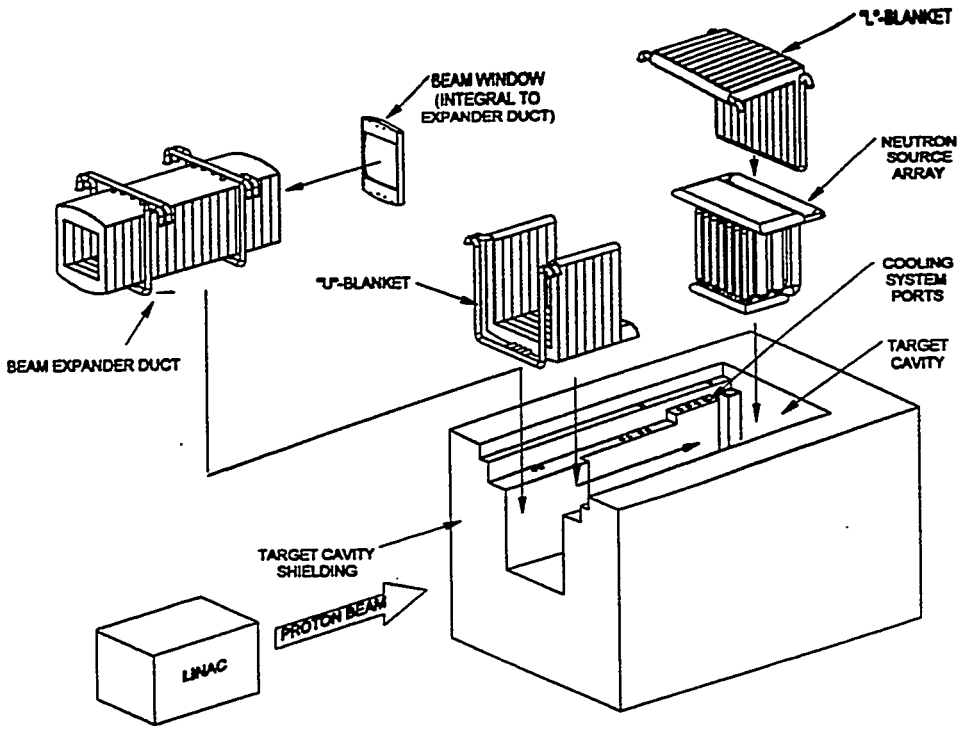

Fig. 1 SILC Target Exploded

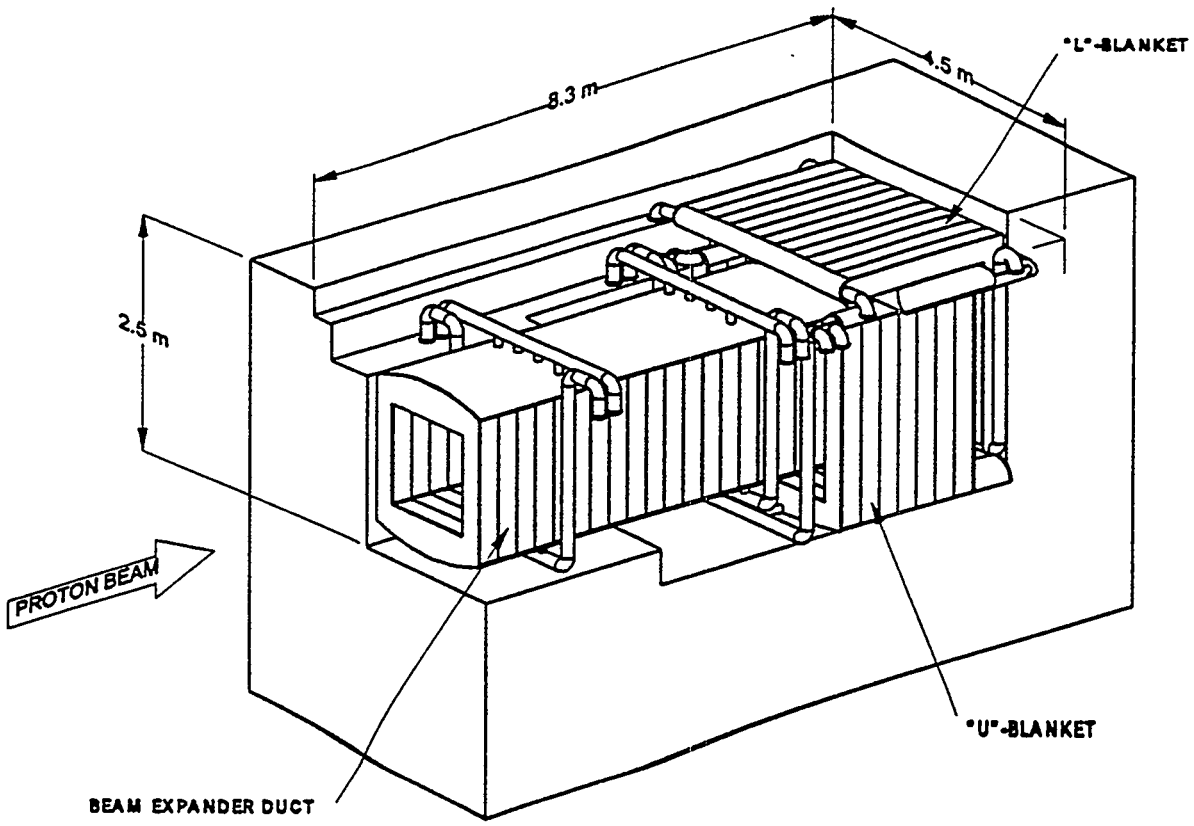

Fig. 2 SILC Target Installed

Extraction of the tritium from the lithium-aluminum plates is based on the Savannah River technology used in support of the production reactors for several years. Thus, in many respects, the SILC Target is an adaption of reactor technology, but with a different neutron source. However, in this case there are no actinides, which means no high-level radioactive wastes, no reactivity issues, very little after-heat, and a much-reduced "source term" (inventory of hazardous materials that might be released in worst-case accidents).

Accelerator-Based Conversion (ABC) of Weapons Plutonium Using ADAPT Target

Disposition of highly fissile plutonium from excess nuclear weapons is considered a national priority, and there is a healthy debate ongoing regarding the best candidate technologies for resolving this nontrivial mission. One of the difficulties has been to establish a common basis for comparison, especially regarding throughput and number of machines required. One can best compare options by postulating the complete fissioning of the roughly 50 metric tonnes of weapons plutonium being considered in the U.S (or possibly 100 tonnes). To do so, we postulate a reference *plant* as a 3240 MWt unit running on pure weapons Pu, and operating 75% of the time. Such a *plant* could fission 1 tonne per year, as shown in Figure 3. It is emphasized that this graph applies to both reactors and accelerator targets, as long as one is fissioning only the weapons plutonium and is not making additional plutonium in the process.

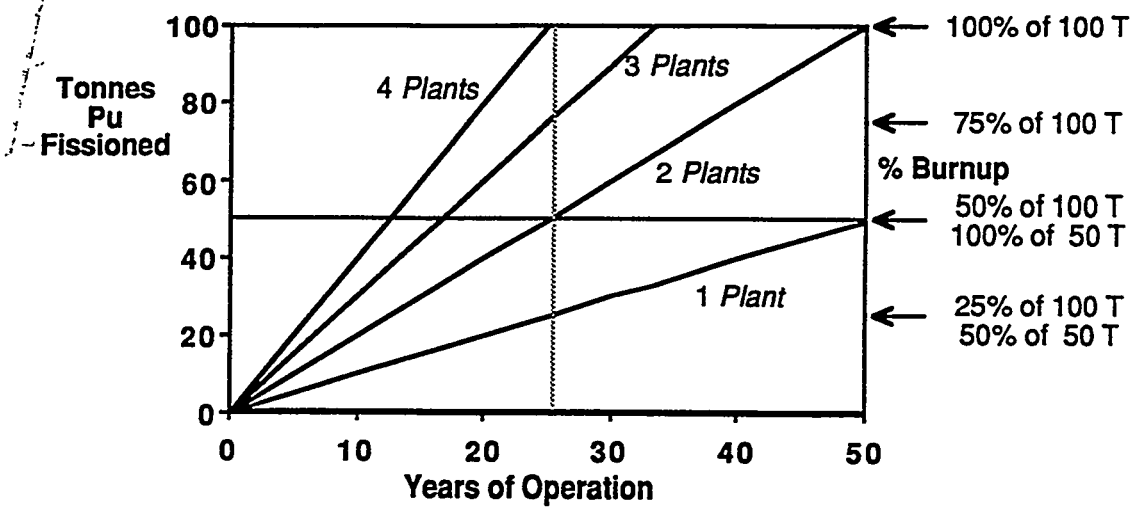

- Machine and System Capacity Dictated by Fission Energy, Plutonium Mass, and % Burnup
  - 190 MeV/Fission = 7.66 x 10^{10} MJ/Tonne of Pu (Fully Fission)
  - A 3240 MWt (1070MWe) *Plant*@ 75% Capacity Factor Fissions 1 Tonne/Yr
  - Assumes No New Plutonium Generated During Process

Fig. 3 Throughput of Plutonium for a 3240 MWt Plant

The Accelerator-Based Conversion (ABC) approach is categorized as an "ultimate disposition" candidate, and BNL is working on the Accelerator-Driven Assembly for Plutonium Transformation (ADAPT) target technology [3]. The spallation neutron source is similar to that used in the APT SILC Target, but the blanket is a subcritical reactor containing the 96% fissile plutonium contained in coated graphite beads (0.5 cm diameter). This fuel is based on a similar fuel developed for a Particle-Bed Reactor (PBR) that was to operate at much higher power densities and temperatures [4]. The degree of subcriticality is a key design issue, and will depend on the safety analysts assessment of the vulnerability to reactivity accidents. While much work must be done, some difficulties are expected due to a natural tendency for plutonium to give positive reactivity feedbacks, especially when overheated. Once the vulnerability has been assessed and the necessary safety margins have been quantified, one can set a suitable criticality limit, probably between 0.9 and 0.99. This would then determine the subcritical multiplication in the blanket, and the required accelerator current, as indicated in Figure 4.

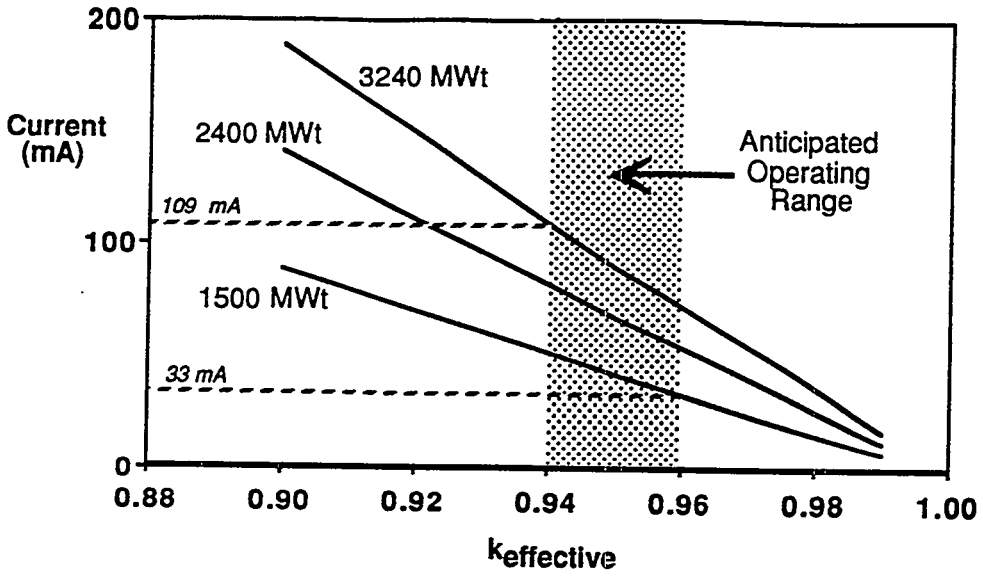

Fig. 4 Beam Current Required vs. K_{eff} for Candidate Power Levels

With a high power density and high throughput, this target is designed to convert the plutonium to fission products in a form ready for disposal, without producing new plutonium and with safe management of the difficult reactivity characteristics of plutonium. The formal design work (see Figure 5 and 6) is just beginning, with a reference or "Preconceptual" design expected by late 1995.

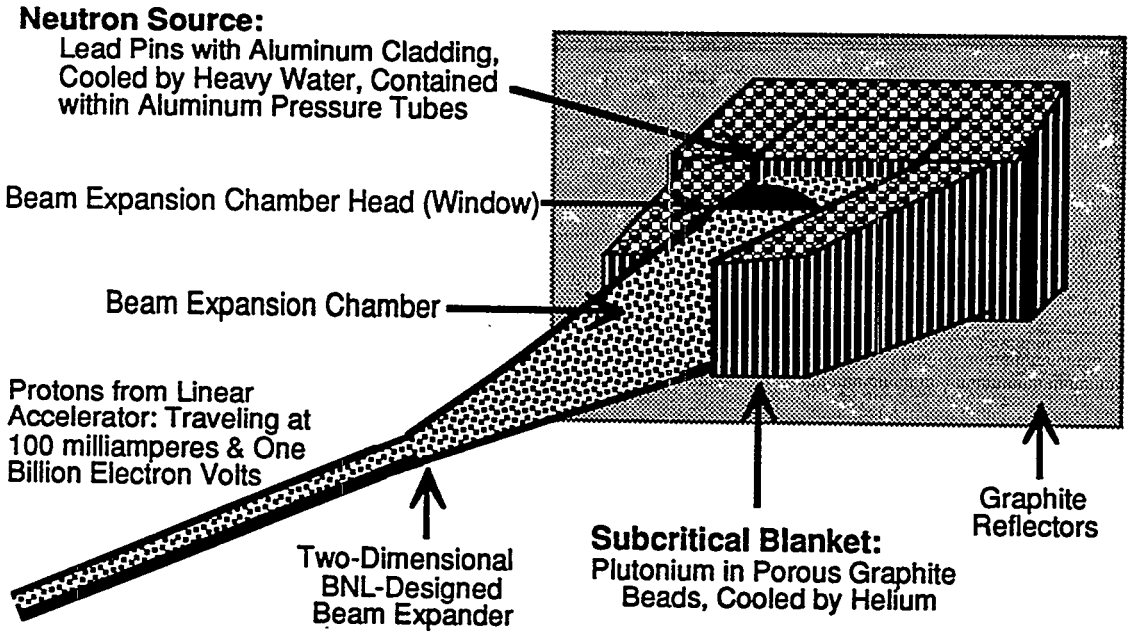

Fig. 5 ADAPT Target to Dispose of Excess Plutonium

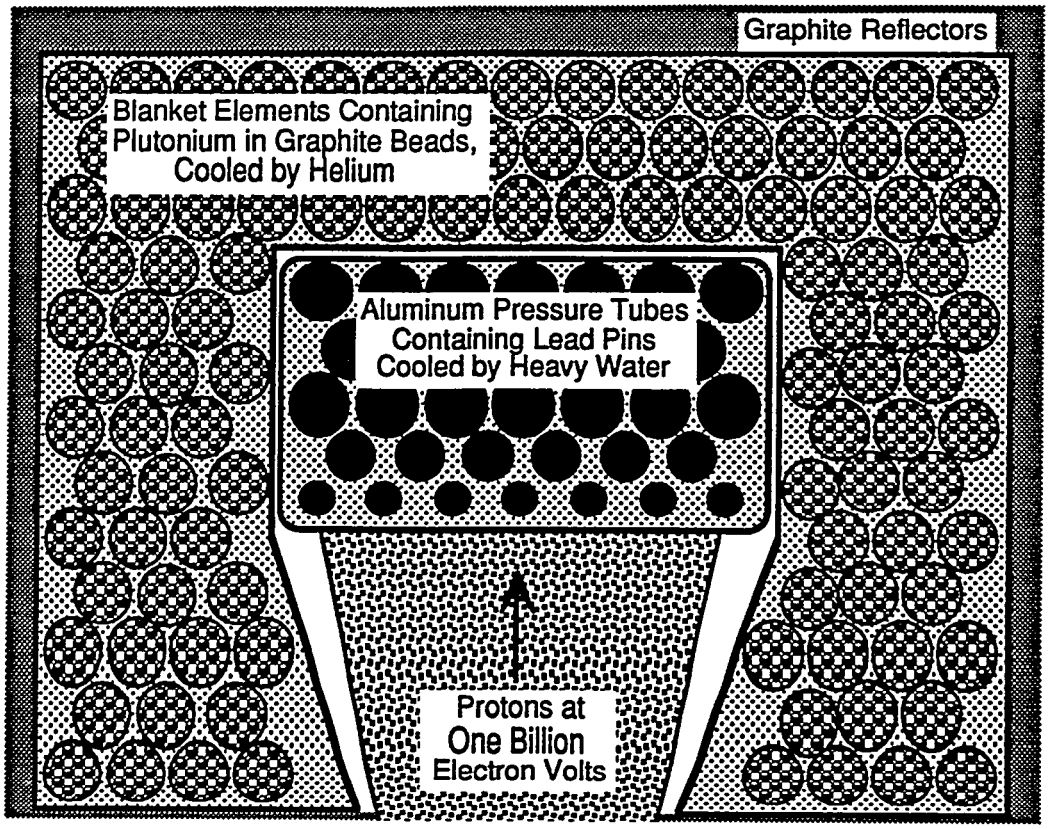

Fig. 6 ADAPT Target - Top View

The PHOENIX Concept

A few of the long-lived radioactive wastes in commercial spent fuel, including the plutonium, minor actinides, and a handful of fission products, cause most of the technical difficulties in assuring the adequacy of proposed waste repositories. The predicted mass flows from one hundred 1000 MWe nuclear power plants (slightly exceeds U.S. production levels) are shown in Figure 7 [5]. As shown, about 95.6% of the waste is 0.8% fissile uranium and 3% is either short-lived or stable fission products, with the remaining 1.4% containing long-lived actinides and fission products. While the LANL ATW Concept [6] attempts to transmute all of the components within the problematic 1.4%, BNL envisions the plutonium and technetium components being recycled back into power plants, due to the scope of this mission (the plutonium throughput could run at least seventeen 1000 MWe power plants). As a result, BNL has focused on the design of one or two machines to transmute the troublesome minor actinides and iodine, and assumes interim storage is the best option for the 30-year-half-life strontium-90 and cesium-137.

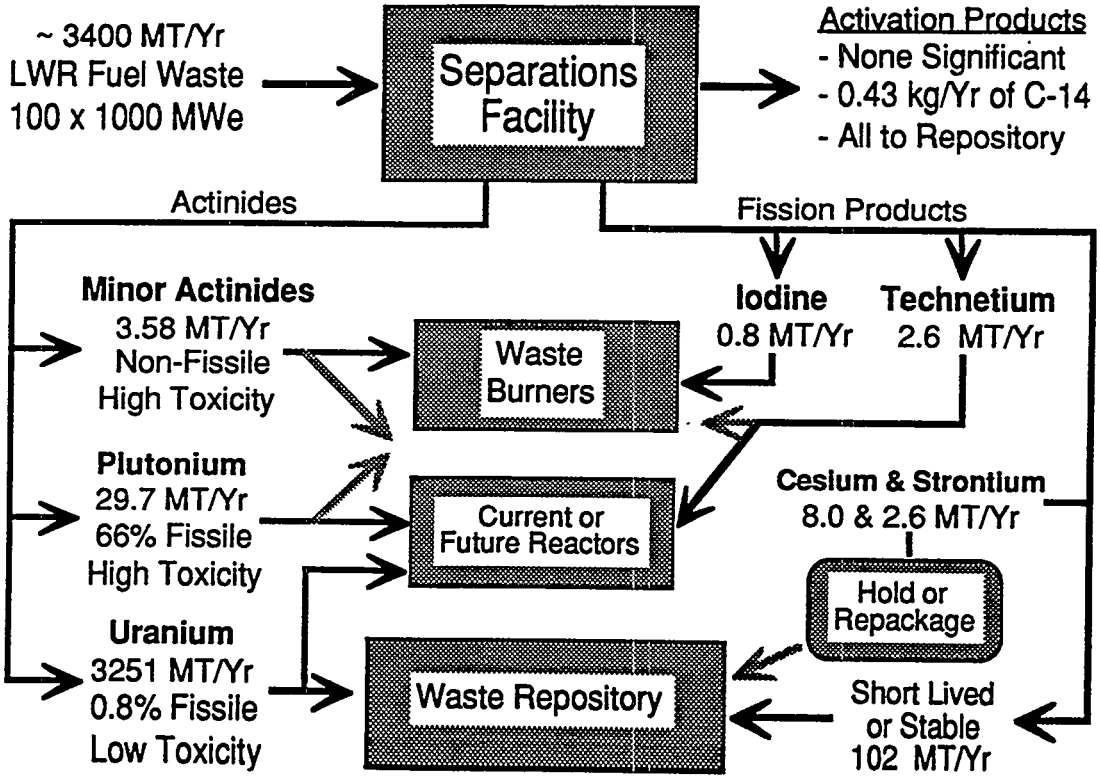

Fig. 7 Approximate Mass Flows From All U.S. LWRs in 1991
(Predicted, Not Measured)

The PHOENIX Concept [7] is illustrated in Figure 8. For this "waste" application, it is nearly impossible to make an assembly of minor actinides critical (initially the isotopes are all fertile, not fissile), even using a fast-spectrum, so the accelerator is essential to keep the target/blanket "source-critical". The eight modular targets closely resemble the Fast Flux Test Facility [8], except the fast reactor demonstration fuel is replaced by minor actinide oxide fuel, with the mix of neptunium, americium, and curium dictated by the composition from the LWR waste stream and the recycle flow from the PHOENIX fuel cycle. The machine would process 2.6 MT of Minor Actinides and about 300 kg of Iodine per year, producing 1.05 MT of fission products (mostly stable or short-lived, but with some recycling of iodine, etc.), 300 kg of stable xenon, and 1.55 MT of plutonium that is largely (about 85%) Pu-238. While NASA uses Pu-238 for deep-space missions, most of the Pu-238 produced by the waste burner would contain too much Pu-236 to be useful to NASA. However, the mix could be useful for blending with excess weapons plutonium, since it would make the mix hot (thermally) enough to make weapons design difficult [9].

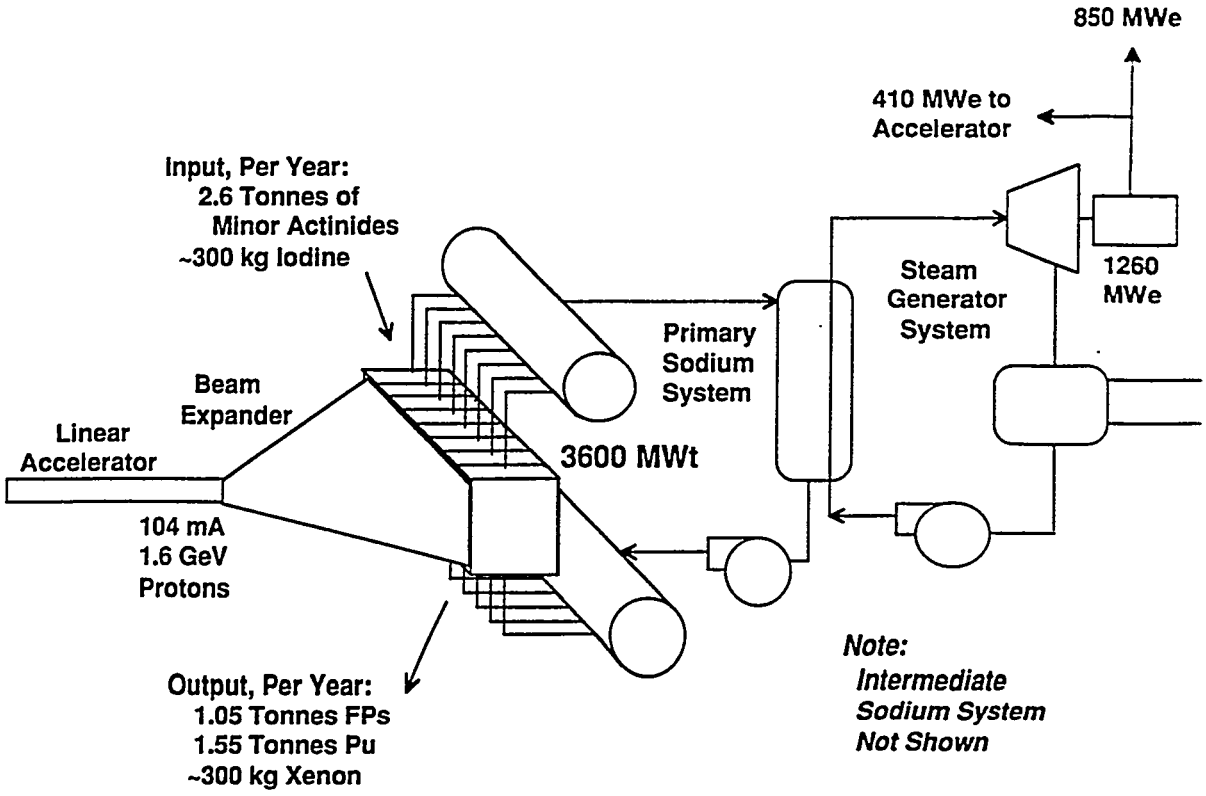

Fig. 8 The PHOENIX Concept

Other Accelerator Applications

Others accelerator-target applications envisioned and/or under development at BNL include spallation neutron sources [10] and isotope production facilities. In these instances, it is the difficulty and costs involved in building and operating reactors to perform these missions that drives the interest in looking at alternatives. Since some of these missions require modest beam power, it is possible to use smaller circular ("ring") accelerators, which would reduce the capital cost significantly. It is also possible to combine missions, and the addition of some isotope production to a tritium or weapons plutonium mission would not be technically difficult, although the programmatic aspects of such multiple missions could be challenging.

One intriguing mission would be the production of the Pu-238 needed by NASA, with the goal production being in the range of 15 kg/year. A major challenge would be the unavailability of americium 241 and the limited inventory of neptunium-237 in the U.S. (more of these materials would be available if the commercial wastes were to be reprocessed), especially when coupled with NASA's requirement for very low Pu-236 (about 2 ppm) content. (The decay chain of Pu-236 leads to Tl-208, which gives off a problematic 2.6 MeV gamma.) If Americium-241 were to be available, neutron capture and the subsequent alpha decay would yield highly pure Pu-238. However, Np-237 has a binding energy of 6.8 MeV, so neutrons or gammas above that energy are likely to produce Pu-236. So even though most Np-237 would capture lower energy neutrons and produce Pu-238, the Pu-236 must be carefully minimized. This would mean positioning the Np-237 out of the direct beam, and avoiding the use of structural materials that might introduce high-energy gamma decays in the proximity of the neptunium. At this time, BNL has not

performed detailed calculations for Pu-238 production, although some design features are readily apparent. Because neptunium and plutonium are relatively hazardous and toxic materials, the use of uranium in the spallation target / neutron source poses little additional safety burden, and provides neutron multiplication (subcritical) that could reduce the requirement for accelerator beam. However, as the target begins to function more and more like a reactor, the safety systems will evolve toward comparability, and the advantages associated with the accelerator driver would become significantly diminished.

SUMMARY

Several accelerator-driven target concepts are under evaluation at BNL, with the two largest efforts associated with tritium production (APT/SILC) and weapons-plutonium disposition (ABC/ADAPT). The availability of spallation neutrons opens up options to assume missions previously fulfilled using nuclear reactors, although the neutron economics are quite different. In general, the accelerator option is more economical when fewer neutrons are required, with reactors maintaining an advantage when many neutrons are necessary. Other potential advantages include better environmental, safety, and health characteristics (as for APT), potentially better safety and control characteristics (ABC), and additional operational options such as subcriticality (needed for transmuting minor actinides).

REFERENCES

[1] H. Kouts and M. Steinberg, Eds., Proceedings Information Meeting on Accelerator Breeding, Upton, NY, January 18-19, 1977, BNL-50838, Brookhaven National Laboratory, 1978.

[2] G.J. Van Tuyle, et al., "Topical Report on a Preconceptual Design for the Spallation-Induced Lithium Conversion (SILC) Target for the Accelerator Production of Tritium," Brookhaven National Laboratory Report, BNL-52401, September 30, 1993.

[3] G.J. van Tuyle, et al., "Brookhaven National Laboratory presentation to the DOE DP&NE", Washington D.C., Feb 17, 1994

[4] H. Ludewig, et al., "Design of Particle Bed Reactors for the Space Nuclear Thermal Propulsion Program," Brookhaven National Laboratory Report, BNL-60306, May 1994.

[5] S.E. Binney, et al., "CURE: Clean Use of Reactor Energy," WHC-EP-0268, Westinghouse Hanford Company, May 1990.

[6] C.D. Bowman, et al., "Nuclear Power Generation and Waste Transmutation Using an Accelerator-Driven Intense Thermal Neutron Source," Nuclear Instruments and Methods in Physics Research (Sec. A), Vol A320, Nos.1,2, August 15, 1992, pp 336-367.

[7] G.J. Van Tuyle, et al., "Accelerator-Driven Subcritical Target Concept for Transmutation of Nuclear Wastes," Nuclear Technology, Vol. 101, pp 1-17, Jan. 1993.

[8] "Final Safety Analysis Report for the Fast Flux Test Facility," HEDL-TI-75001, Westinghouse Hanford Company, Dec. 1975.

[9] R. G Cochran and N. Tsoulfanidis, The Nuclear Fuel Cycle: Analysis and Management, American Nuclear Society, La Grange Park, Illinois, 1990.

[10] A. van Steenbergen, et al., "Brookhaven National Laboratory 5 MW Pulsed Spallation Neutron Source - Preconceptual Design Study," Brookhaven National Laboratory Report in Preparation, 1994.

DEVELOPMENT OF ADVANCED TECHNOLOGICAL SYSTEMS FOR ACCELERATOR TRANSMUTATION

Guennadi I.Batskikh, Boris I.Bondarev, Alexsander P.Durkin, Arkady P.Fedotov, Boris P.Murin, Vitaly M.Pirozhenko, Oleg V.Plink, Boris S.Sychev, Ratmir G.Vassil'kov
Moscow Radiotechnical Institute (MRTI), Russian Academy of Sciences
Warshawskoe shosse 132, 113519 Moscow

Abstract. A development concept of the accelerator nuclear energy reactors is considered for energy generation and nuclear power plant waste conversion into short-lived nuclides along with the requirements imposed on the technological systems necessary for implementation of such projects. The state of art in the field is discussed.

INTRODUCTION

Development works on technological systems for accelerator transmutation started in MRTI at the end of 60-ies. The works were carried on in two aspects: development of high power accelerators and investigations on determination of nuclear constants which are necessary for feasibility studies and efficiency estimations for future accelerator transmutation facility.

The main field of MRTI activity is accelerators. However there exists in the institute a small group of researchers who started at the 60-ies the thorough experimental studies on the determination of neutron yields in targets irradiated by proton and light ion beams with the energy range of 0.1-10.0 GeV. Another research group is involved in the development of simulation methods for calculations of radiation processes associated with transport and absorption of high energy particles in materials.

Even in the 70-ies the solution of the accelerator transmutation problem (at the period it was associated with production of nuclear fuel Pu-239 and U-233) required creation of a huge accelerator with the energy of 1.0-1.5 GeV and mean current up to 300 mA. In the course of the design work on Moscow meson factory (MMF) [1] we were already considering the possibilities of creating an accelerator for transmutation in future. We were also examining carefully both the development and the operation of Los Alamos meson factory (LAMPF) [2]. Our longtime research works on the transmutation physics problems, consideration of Los Alamos National Laboratory (LANL) experience along with our own one on the development of MMF enable us to evaluate the problem and to formulate the tasks on creation of advanced technological systems for super high power accelerators.

DEVELOPMENT OF NUCLEAR DATA FOR ACCELERATOR TRANSMUTATION

Development and design works on accelerator transmutation facility require a detailed description of the variety of physical processes associated with transport and absorption of high energy particles in materials. These radiation problems can be subdivided into the following two groups: description of the target characteristics and the radiation safety for the accelerator facility.

Investigation of these problems related to the development of methods for radiation transport simulation have been carried out in MRTI for years. The systematization and evaluation of total [3,4] and differential [5-8] cross-sections for interactions of high energy hadrons with atomic nuclei were carried out. The nuclear data system is formalized in several options differing in details of energy spectra and angular distribution of secondary particles.

The developed nuclear data system was applied for solution of the transport equation system simulating hadron cascade in materials by successive collision method [9]. The ray method [10] based on effective technique for estimation of shielding configurations against hadron component of radiation at proton accelerators with energies from 20 MeV up to 1 TeV and more was created as well [11]. This method permits to determine the relations between the proton beam loss and the corresponding dose rates due to gamma radiation induced in linear proton accelerators [12]. The results are presented in graphic form [13] and are convenient for engineering evaluation and designing of high intensive accelerators.

The developed algorithms proved to be very powerful in solving some problems concerning a transmutation of nuclear fuel and wastes by intensive proton beams [14,15]. The most part of algorithms for simulation of radiation fields at accelerator facilities are realized in the form of computer programs and annotated [16,17].

Detailed experimental investigations of the bulky targets and blankets neutronics (metal U, Pb, Be, reactor graphite and their combinations) were performed in MRTI. Accelerated protons, deutrons, ions of He and C were used. Experiments with thin targets were also performed and used to evaluate the possible role of accelerators in nuclear power engineering as applied for industrial implementation of nuclear transmutation [18-19].

We were interested in obtaining the lacking experimental data on neutron yields and spectra, on fission reactions and neutron-gamma capture within and around the heavy-metal targets irradiated by various light ions accelerated up to the energies of 0.3-8 GeV per unit charge, as well as to apply the data for estimation of the basic parameters of future accelerator transmutation facility [20].

On big total absorption targets made of metal natural and depleted uranium (3.2-3.4t) irradiated by 300-600 MeV protons the data was obtained on yields of Pu and energy (Fig. 1) [26], which represents essentially the only experimental basis for estimation of the electronuclear breeding parameters (the Pu-239 generation rate, energy consumption at its production and accompanying release of energy) and for testing of computer programs describing the nuclear cascade in big masses of U.

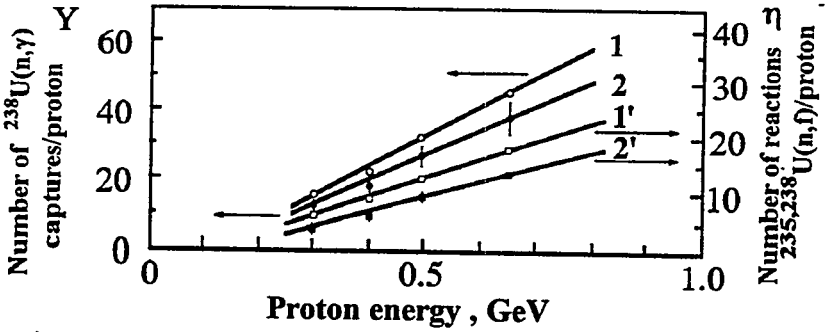

Fig. 1. Experimental data on ^{239}Pu yields: 1,2 - number of ^{238}U(n,γ) captures/proton; 1',2' - number of reactions ^{235,238}U(n,γ)/proton; 1,1' - naturalU; 2,2' - depleted U.

Two completely different experimental techniques were used within a wide range of kinetic energies of bombarding light relativistic ions (p,d,He-3,He-4,C-12) for studies of yields and spatial and energy distributions of neutrons emitted by a thick Pb target (cylinder of 10-26 cm in diameter and length of 4-76 cm) [22,23]. The data enabled us to determine the type of accelerated ion which provides for the maximum neutron yield per unit energy, to find the initial kinetic energy to which it is expedient to accelerate ions (minimization of the kinetic energy of primary ion spent for release of a neutron, Fig. 2).

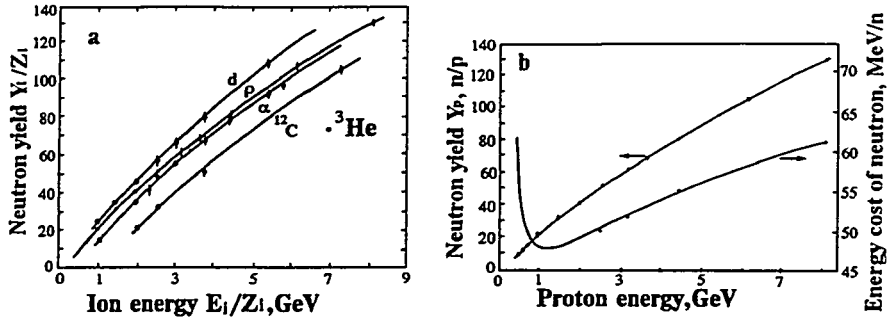

Fig. 2. Experimental data: a) Neutron yields for some bombarding particles; b) Neutron yield and energy cost of neutron for protons.

ACCELERATORS FOR TRANSMUTATION

Among the accelerator transmutation technologies there are the works on electronuclear breeding (production of U-233 and Pu-239), treatment of military plutonium, tritium production, neutralization of nuclear waste from nuclear power plant, electricity generation at nuclear power plant with reactors controlled by accelerated proton beams. These tasks require accelerated particle beams with parameters that are ranging within broad limits, the energy from 0.8 to 1.6 GeV and the current from 8 to 300 mA. Therefore every particular facility gives rise to specific requirements with regard to the beam of accelerated particles. Beam current value is defined by the required process rate. Accelerator energy decrease is accompanied by the accelerator cost fall but therewith it is necessary to remember that neutron yield reduces and transmutation process cost rises (Fig. 2). Therefore it is needed to find a cost optimum of transmutation facility as a whole.

Depending upon the required parameters, various transmutation processes differ with regard to their accelerator scheme and implementation technologies. With currents of up to ten mA and energy of up to 1.0 GeV, one can make use of the isochronous cyclotrons [24]. For higher currents and energies it makes sense to apply ion linear accelerators. If the beam current is up to 125 mA then the single channel scheme (Fig. 3) can be used with an RFQ accelerator as an initial part.

For the currents in excess of 125 mA, two versions of the scheme could be considered (Fig. 3): the two channel scheme with beam "funneling" [25] and with application of RFQ accelerators in the initial part, and the single channel scheme where a high current ion accelerator is used as an initial part, for instance HILBILAC (High Intensive Low Beta Ion Linear Accelerator) - linac with superconducting (SC) solenoid focusing [26].

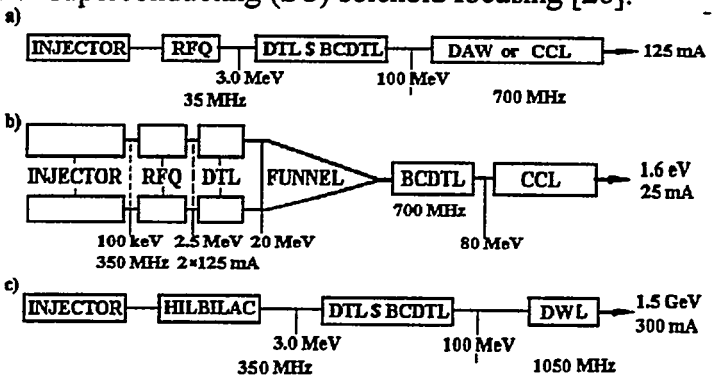

Fig. 3. The schems and main characteristics of linacs for transmutation.

TECHNOLOGICAL SYSTEMS OF LINEAR ACCELERATORS FOR TRANSMUTATION

Initial part of accelerator

Low injection energy and high value of the capture efficiency determine high effectiveness of RFQ accelerator. The H-cavities that are usually applied in the RFQ systems feature high shunt impedance combined with low coupling value (1%) thus imposing special requirements on the cavities manufacturing.

The modification of accelerating and focusing system of RFQ accelerator has been proposed in MRTI. The system features much higher coupling coefficient along with a sufficiently high level of the shunt impedance. Under these conditions one can obtain the accelerating field intensity increase along the accelerator thus providing for adiabatic beam bunching and particle capture with practically no loss. This structure represents a combination of a four-chamber H-cavity and a cavity with the opposite vibrators [27]*. The cavity design is presented in Fig. 4. There exist two types of plates: with quarter wavelength and with half wavelength cuts forming the resonant elements - vibrators. These cuts are also the coupling windows. Due to the size of the coupling windows and their location along the cavity, both the required coupling coefficient and the field distribution along the cavity are provided.

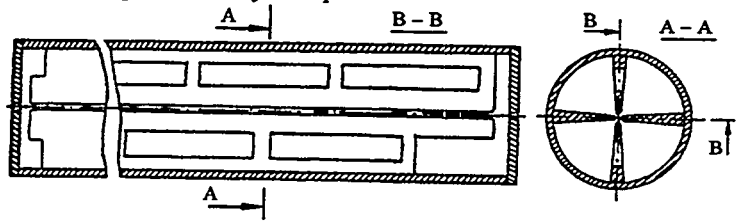

Fig. 4. The configuration of the RFQ with opposed vibrators.

H-cavity with four opposite vibrators at the end is capable of providing for the coupling coefficient of 10-15% combined with field increase along the cavity length by the factor of 2.5 - 4. Such structure is more effective as compared with the ordinary four-chamber H-cavity. It requires not so strict tolerances in the course of manufacturing, much simpler in tuning and more stable with respect to disturbances. Such accelerator could be used in a single channel accelerator facility with currents of up to 125 mA, and in the "funneling" scheme for higher currents.

In our opinion, funneling of beams results in the complications along with inevitable increase of the beam emittance and hence increased beam loss. One can use a single channel scheme for currents in excess of 125 mA, provided by the HILBILAC.*

HILBILAC advantages [28] are intensive beam with high operating frequency, high capture efficiency, small emittance growth and small longitudinal phase volume of the beam. The RF loss is basically in the elements that could be effectively water cooled and provide for the CW accelerator operation with the RF loss level of about 10 W / cm^2.

The design of 3 MeV HILBILAC is presented in Fig. 5. It consists of accelerating cavity, sectioned superconducting solenoid, helium envelope, thermal shields and vacuum envelope. RF power is injected into the cavity by a coaxial feeder through the end wall. H-wave is excited in the cavity. Basic 3 MeV HILBILAC parameters are presented in the Table 1.

---

* The work performed under the contract with Grumman Corporation

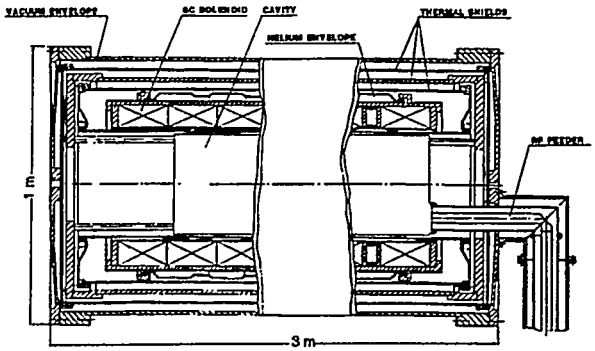

Fig. 5. 3 MeV HILBILAC design.

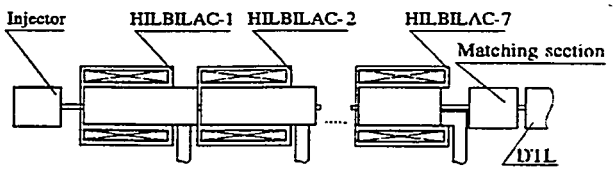

Fig. 6. Block-diagram of 20 MeV HILBILAC.

HILBILAC structure can be used to energy of 20 MeV with shunt impedance not less than 25 MΩ/m. The diagram of the 20 MeV HILBILAC is shown in Fig. 6. It consists of 7 accelerating sections similar to that for the energy of 3 MeV. The accelerating channel represents a continuous structure. Therefore there exists no need for longitudinal beam matching. The gaps between focusing coils are used for vacuum pumping and for RF power and cooling water supply. They are minimized to 150 mm. Compensation coils are used to compensate for field drops. The Fig. 7 demonstrates the magnetic field distribution and the beam envelope both with and without the magnetic field compensation. Basic parameters of the 2O MeV accelerator are presented in Table 1.

Table 1. 3 MeV and 20 MeV HILBILAC basic parameters

Parameter	3 MeV	20 MeV
Injection energy, MeV	0.15	0.15
Output energy of particles, MeV	3	20
Beam current, mA	250	250
Number of cavities	1	7
Operating frequency, MHz	352	352
Length of accelerator, m	3	14
Diameter of cryostates, m	1.0	1.0
Magnetic field induction, T	7	7
Maximum accelerating wave amplitude, MV/m	2.4	2.4
RF power injected into the cavity, kW	760	760-835

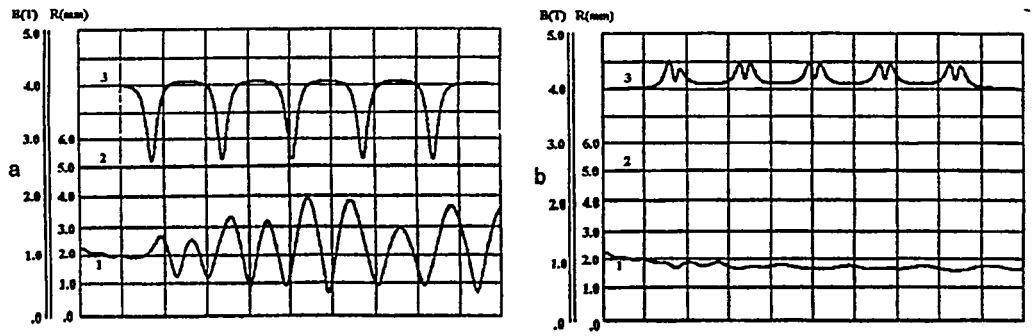

Fig. 7. Beam envelope along the 20 MeV HILBILAC:a - magnetic field without correction; b - magnetic field with correction (1 - Beam Envelope, 2 - Aperture, 3 - Magnetic Field).

Drift tube linac (DTL)

Various versions of DTL structure could be used within the energy range from 3 or 20 to 100 MeV. The structure has high shunt impedance within the energy range and used to be applied in many accelerator facilities. The versions differ with regard to the used magnetic systems. These are represented by either the quadrupole lenses (electromagnetic quadrupoles, or permanent magnet quadrupoles) placed inside of the drift tubes, or the quadrupole lenses between the cavities with bridge coupling (BCDTL) [25]. We considered the variant with superconducting solenoids focusing of beam (DTLSCF [29]).

The main part of accelerator

Two coupled cavity linac (CCL) structures are used with success for ions acceleration from 100 MeV to the higher energies: the structure with side coupled cavities (SCC) developed in LANL and the disc and washer (DAW) structure proposed in MRTI (Fig. 8). The former proved to be of use with good results at LAMPF. The latter was tested successfully at the MMF. The DAW structure features coupling coefficient between the cells that is almost by a factor of 10 larger than that of the SCC one. Therefore DAW structure provides for higher accelerating field stability with regard to the manufacturing errors, tuning defects and beam loading. Besides, it has the vacuum conductivity that is higher by a factor of magnitude.

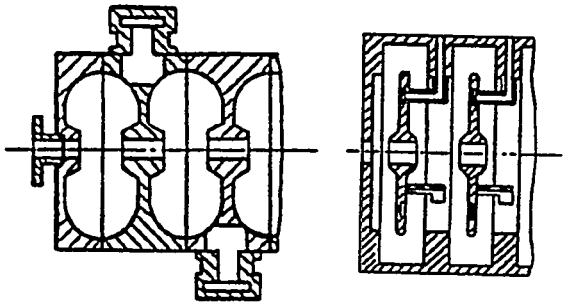

a) b)

Fig. 8. a) Side-coupled cavity structure; b) Disc and washer structure.

For years experts doubted the DAW structure potentials due to close location of non-operating and operating modes. Combined slots in disc (Fig. 9) are used to eliminate nonoperating oscillations. These slots are resonant elements which distort nonoperating oscillations and have practically no effect upon the operating one [30]. The operating and nonoperating modes with and without combined slots are shown in Fig. 10. The nonoperating modes are seen to be far beyond the operating band of the cavity and do not influence its performance.

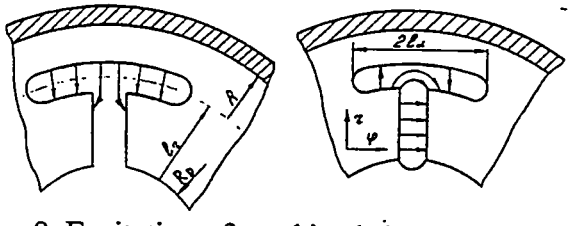

Fig. 9. Excitation of combined slot electromagnetic oscillations with the help of operating mode (left) and nonoperating mode.

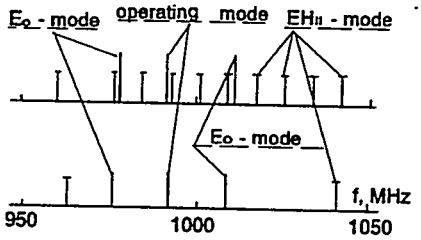

Fig. 10. The electromagnetic oscillation spectrum of DAW structure befor and after application combined slots into discs.

ACCELERATOR WITH SUPERCONDUCTING SOLENOID FOCUSING [29]*

General layout of the accelerator is presented in Fig. 11. The basic idea is to apply a one-type focusing (SC solenoids) all along the accelerator.

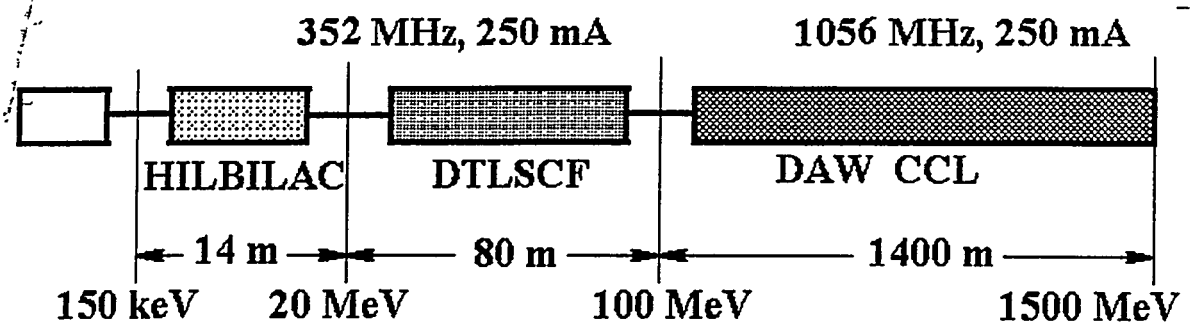

Fig. 11. 1.5 GeV, 250 mA CW proton linac with SC Solenoid focusing.

In the initial part the beam is accelerated up to 20 MeV by the above described 20 MeV HILBILAC.

From 20 to 100 MeV the beam acceleration is done by a DTLSCF. This accelerator is consisted of 24 cavities arranged in the form of four modules (Fig. 12). Basic parameters of accelerator are given in Table 2.

Table 2. DTLSCF and CCL parameters.

Parameter	DTLSCF	CCL
Injection energy , MeV	20	100
Output energy , MeV	100	1500
Operating frequency , MHz	352	1056
Accelerated current , mA	250	250
Number of cavities	24	120
Number of modules	4	-
Number of sections in a cavity	-	7
Diameter of cavities , mm	590-540	395-315
Length of cavities , m	2.4-2.15	12
Aperture radius , mm	10	10
Beam radius , mm	5	5
Drift tube diameter , mm	85	-
Magnetic field strength at the axis, T	5	5
Length of solenoids, m	1.1	0.5
Distance between solenoids , m	0.5	2.2
RF power injected into the cavity, MW	0.8	4.2

* The work performed under the contract with LANL

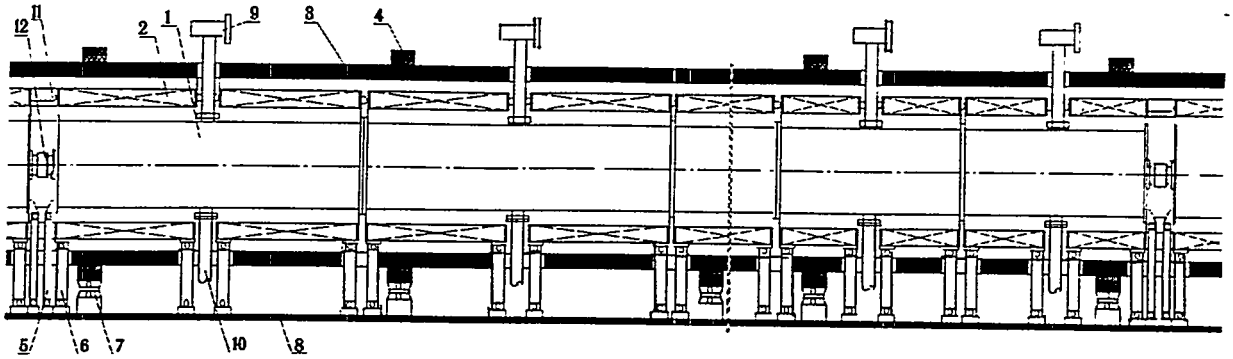

Fig. 12. DTL Module Design: 1 - accelerating cavity; 2 - superconducting solenoid; 3 - magnetic screen; 4 - assembly of transverse joint of magnetic screen; 5 - cavity adjustable support; 6 - solenoid adjustable support; 7 - adjustable support of magnetic screen section; 8 - solid support of accelerator; 9 - RF window; 10 - vacuum system branch pipe; 11 - screw-jack; 12 - bellows assembly.

In the main part of accelerator (CCL) the beam is accelerated from 100 to 1500 MeV by means of DAW structure with SC solenoid lenses. This part of accelerator is consisted of 120 similar cavities. Each of the cavities involves seven sections. The cavity is shown in Fig. 13. Basic parameters are given in Table 2.

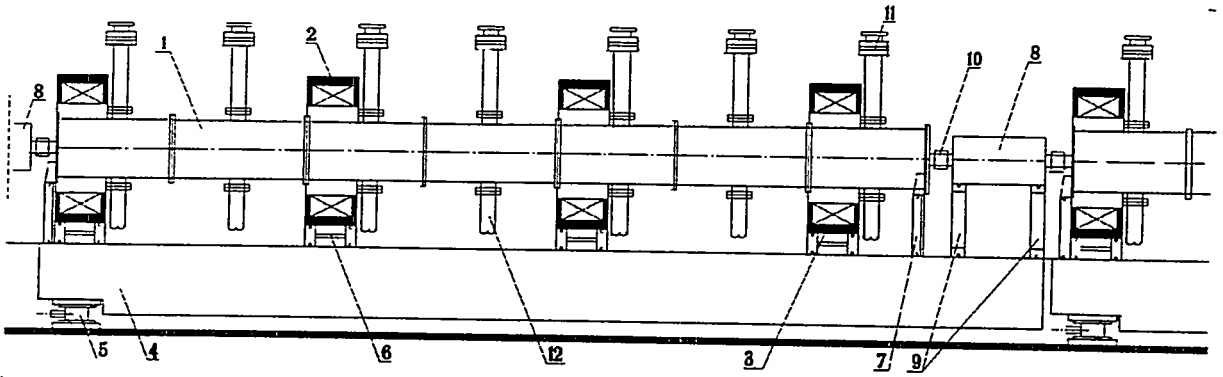

Fig. 13. Design of Main Accelerator Part Module: 1 - cavity; 2,3 - superconducting solenoid inside magnetic screen; 4 - girder; 5 - adjustable gider support; 6 - adjustable support of solenoid; 7 - adjustable support of cavity; 8 - measuring station of beam parameters; 9 - adjustable supports of measuring station; 10 - bellows assembly; 11 - RF window; 12 - vacuum system branch pipe.

RF power is injected into each section through discs as it was realized in Japan for the electron accelerator [31].

The one-type beam focusing by means of superconducting solenoids provides for the following advantages:

A. High current limit of the accelerating channel (700 mA in the present project).

B. Simplification of different accelerating structures (HILBILAC, DTLSCF, CCL) matching.

C. Replacement of quadrupole lenses by SC solenoids decreases by about a factor of magnitude the accelerating channel sensitivity with regard to disturbances.

However, transition to SC focusing along the whole accelerator gives rise to new engineering and technological problems that have to be solved.

RF system

RF power of about 750 to 840 kW has to be injected into the cavities of HILBILAC and DTLSCF. Taking into account the allowances for the control system, the 1.0 MW generators are required. In the capacity of the output stages of such generators, either CW flight klystrons YK 1350 (Philips) or TH-2089 (Tompson-CSF) can be used.

Two versions are possible for the CCL. Either application of 840 klystrons with power of 600 kW each, operating by 7 klystrons in parallel on each cavity, or use of 4.2 MW generators (Regotrons) [32] that is developed in MRTI. It will have 7 outputs each (one regotron will be capable of providing the RF power supply for one cavity).

PROBLEMS OF BEAM LOSS

Main sources of beam loss in the course of acceleration are associated with the beam halo and effective emittance increase due to Coulomb forces and to random disturbances of accelerating and focusing channel. Research work is carried out in MRTI on the halo elimination through application of filters along the length of accelerator [33,34].

If the SC solenoids are used, the high magnetic fields at the beginning of acceleration and with small beam radius will practically eliminate the influence of Coulomb forces.

As was already mentioned above, the SC solenoid focusing decreases by a factor of magnitude the effect of random disturbances on the beam as compared with quadrupole focusing. Therefore we believe that implementation of the present project will help to solve the problem of beam loss.

CONCLUSION

Presented material demonstrates the transmutation accelerator feasibility. One can consider various versions of technological systems that could be used in the course of designing such facility. The main problem to be solved is as follows: relation between reliability and cost.

The authors express their gratitude to our MRTI colleagues for their contribution into the present work, as well as to the specialists from Grumman Corporation and LANL for their valuable discussions.

REFERENCES

[1] Murin,B.P. et al., "High Current Ion Linear Accelerator for Medium Energy Physics (meson Factory)", *Proceedings of the 1972 Proton Linear Accelerator Conf.*, 1972, pp.387-395.

[2] Hagerman, D., *IEEE Trans., Nucl. Sci.*, NS-20, 3, 1974, pp.905-911.

[3] Sychev, B.S., et al., Cross Section of Hadron Inelastic Interactions with Nuclei. *MRTI Preprint* N34, 1983, Moscow.

[4] Sychev, B.S., et al., *Izv. AN BSSR*, Ser. of Physical & Energetic Sciences, 1987, 2, pp.13-18.

[5] Sychev, B.S., et al., Analytical Approximation of Differential Cross Sections of Secondary Particle Production in Nucleon-Nuclei Interactions in Energy Range above 20 MeV. *MRTI Preprint* N 799, 1979.

[6] Sychev, B.S., et al., *Izv. AN BSSR*, Ser. of Physical & Energetic Sciences, 1988, 4, pp.13-16.

[7] Sychev, B.S., et al., Analytical Approximation of Differential Cross Sections of Secondary Particle Production in High Energy Nucleon-Nuclei Interactions. *MRTI Preprint* N 8904, 1989.

[8] Sychev, B.S., and Kalmykov, A.R., Analytical Approximation of Differential Cross Sections of Nucleon Nuclei Elastic and Nucleon-Nuclei Quasi-Free Scattering. *MRTI Preprint* N 810, 1988.

[9] Gelfand, E.K., et al., "Sequence Collision Method for Accelerator Shielding Calculations", *MRTI Proceedings* n.20, 1974, pp.136-145.
[10] Sychev, B.S., "Method for Radiation Calculations around Accelerator Facilities and behind Their Shielding", *Proceedings of the Fifth All union Meeting on Particle Accelerators*, Moscow, 1977, pp.198-205.
[11] Gelfand, E.K. and Sychev, B.S., "Tables for Evaluation of Shielding against Secondary Hadrons Produced in Inelastic Interactions of Protons with Energies from 50 MeV to 1 TeV",*MRTI Proceedings* n.36, 1980, pp.98- 109.
[12] Gelfand, E.K., et al., "Irradiation of Proton Accelerator Elements under Linear Losses of Particles with Energies from 20 MeV to 1 TeV", *MRTI Proceedings* n.36, 1980, pp.78-84.
[13] Sychev, B.S., "Calculation of Activity Induced in Linear Proton Accelerators", MRTI Proceedings n.16, 1973, pp.287-294.
[14] Gelfand, E.K., et al., "Calculation of Neutron Yields in Bulk Uranium Target Irradiated by Protons with Energies from 0.1 to 10 GeV", *MRTI Proceedings* n.28, 1977, pp.187-195.
[15] Gelfand, E.K., et al., Integrated Nuclear Spallation Yields in Bulk Materials Irradiated by Accelerated Electrons and Protons, *MRTI Preprint* N211, 1992.
[16] Computer Codes in Accelerator Domain: Information Fund for Algorithms and Programs in Accelerator Domain, Moscow, 1992, pp.5-6, 9-10, 23-30, 43-48, 59-62, 73-74, 123-124, 129-130, 137-140.
[17] Computer Codes in Accelerator Domain: DESY M-92-07, 1992, pp.8, 13, 56.
[18] .Vassil'kov, R.G., et al., "The electronuclear Method of Neutron Generation and Production of Fissile Materials", *Atomnaja Energija*, 1970, vol.29, p.151.
[19] Vassil'kov, R.G., et al., "On the Electrical Breeding", *Uspekhi Physicheskikh Nauk*, 1983, vol.139, p.434.
[20] Vassil'kov, R.G., "Free Neutron Production with Hydrogen Ion Accelerators for Nuclear Fuel Cycle Needs", *Muon-Catalyzed Fusion*, 1992, 7, 245.
[21] Vassil'kov, R.G.,et al.,"Neutron Multiplication in Uranium Bombarded by Protons with Energies 300-660 MeV", *Atomnaja Energija*, 1978, vol.44, p.329.
[22] Vassil'kov, R.G., et al., "Neutron Emission from Extended Pb Targets under the Action of Light Ions in the GeV region", *Proceedings of the ICANS-11 Meeting*, 1990, Tsukuba, Japan, pp.340-353.
[23] Nikolayev, V.A., et al., "Neutron Production in Thick Lead Target by 1-3.7 GeV Protons and Deutrons", *Proceedings of ICANS-11 Meeting*, 1990, Tsukuba, Japan, pp.612-627.
[24] Carminati, F., et al., An Energy Amplifier for Cleaner and Inexhaustible Nuclear Energy Production Driven by a Particle Beam Accelerator, CERN/AT/93-47(ET), 1993.
[25] Lawrence, G., "Overview of Los Alamos High Power Accelerator Designs for ATW/ABC Applications", ATW/ABC Accelerator Workshop, Los Alamos, 1992.
[26] Murin, B.P., et al., "High Current Low Energy RF Ion Accelerator", *Proceedings of the 1990 Linear Accelerator Conference*, Albuquerque, 1990, pp.707-709.
[27] Bondarev, B.I., et al., "Development and Study of the Opposed Vibrator Resonator for RFQ Compact Ion Linac", *Proceedings of 3-rd EPAC*, 1992, pp.1337-1339.
[28] HILBILAC Basic Accelerator Concept Development, MRTI Report on the Grumman Corporation Contract, Moscow, 1993.
[29] Belugin, V.M., et al., "Design of High Current High Energy Linac with Focusing by Superconducting Solenoids (Conceptual Design)", MRTI Report on the LANL Contract, Moscow, 1994.
[30] Andreev, V.G., et al, "Parasitic Modes Removal Out of Operating Mode Neighborhood in DaW Accelerating Structures", *IEEE Trans. on Nuclear Science*, NS-30, 1983, 4, pp.3575-3578.
[31] Inagaki, S., "Disc-and-Washer Cavity for an Accelerators", *Nuclear Instruments and Methods in Physics Research*, A261, Amsterdam, 1986, pp.417-436.
[32] Batskikh, G.I., et al., "High-Power "Regotron"-Type Microwave Generator for Intensive Technological Accelerators", *Proceedings of the 11-th Meeting of International Collaboration on Advanced Neutron Sources*, Tsukuba, 1990, pp.218-223.
[33] Kabanov, V.S., et al., "Transverse Particle Motion Dependence upon Longitudinal Motion and beam Phase Volume Filtering in Proton Linear Accelerators", *Probory i Tekhnika Eksperimenta*, 1984, 4, pp.37-39.
[34] Bondarev,B.I., et al., "Design of High-Energy High-Current Linac with Focusing by Superconducting Solenoids", presented to this Conference.

Introduction to Spallation Physics and Spallation-Target Design

G. J. Russell, E. J. Pitcher, and L. L. Daemen
Manuel Lujan, Jr. Neutron Scattering Center
LANSCE, MS H805, P.O. Box 1663
Los Alamos National Laboratory
Los Alamos, NM 87545 U.S.A.

Abstract. When coupled with the *spallation* process in appropriate target materials, high-power accelerators can be used to produce large numbers of neutrons, thus providing an alternate method to the use of nuclear reactors for this purpose. Spallation offers exciting new possibilities for generating intense neutron fluxes for a variety of applications, including: (a) spallation-neutron sources for materials science research; (b) accelerator-based production of tritium; (c) accelerator-based transmutation of waste; (d) accelerator-based destruction of plutonium; and (e) radioisotope production for medical and energy applications. Target design plays a key role in these applications, with neutron production/leakage being strongly dependent on the incident particle type and energy, and target material and geometry.

INTRODUCTION

Nuclear transmutation was first demonstrated by Rutherford in 1919, who changed ^{14}N to ^{17}O using energetic alpha particles [1]. I. Curie and F. Joliot produced the first artificial radioactivity in 1933. They used alpha particles from naturally radioactive isotopes to transmute boron and aluminum (both light elements) into radioactive nitrogen and oxygen. It was not possible to extend this type of transmutation to heavy elements as long as the only available charged particles were the alpha particles from natural radioactivity, because the Coulomb barriers surrounding heavy nuclei are too great to permit the entry of such particles into atomic nuclei. The invention of the cyclotron by E. O. Lawrence [2], and the later construction and operation of high-power accelerators such as the Clinton P. Anderson Meson Physics Facility (LAMPF) [3] removed this barrier. (LAMPF, located at the Los Alamos National Laboratory [LANL], is the highest-power accelerator in the world, producing 1 mA of 800-MeV protons).

When coupled with the *spallation* process, high-power accelerators can be used to produce large numbers of neutrons, thus providing an alternate method to the use of nuclear reactors for this purpose. Spallation offers exciting new possibilities for generating intense neutron fluxes for a variety of applications. We will discuss basic spallation target physics, the calculational tools used at Los Alamos to simulate spallation, the fundamentals of spallation-target design, and the development of the split-composite target concept. Spallation is being considered for various applications including: (a) spallation-neutron sources for materials science research; (b) accelerator-based production of tritium; (c) accelerator-based transmutation of waste; (d) accelerator-based destruction of plutonium; and (e) radioisotope production for medical and energy applications.

WHAT IS SPALLATION, ANYWAY?

Spallation refers to nuclear reactions that occur when energetic particles (e.g., protons, deuterons, neutrons, pions, muons, etc.) interact with an atomic nucleus (the "target" nucleus). In this context, "energetic" means kinetic energies larger than about 100 MeV per nucleon. At these energies (where the deBroglie wavelength of the incident particle is short enough to allow the incident particle to interact with individual nucleons inside the nucleus), it is no longer correct to think of the nuclear reaction as proceeding through the formation of a compound nucleus. The initial collision between the incident projectile and the target nucleus leads to a series of direct reactions (intranuclear cascade) whereby individual nucleons or small groups of

nucleons are ejected from the nucleus. At energies above a few GeV per nucleon, fragmentation of the nucleus can also occur. After the intranuclear cascade phase of the reaction, the nucleus is left in an excited state. It subsequently relaxes to its ground state by "evaporating" nucleons, mostly neutrons.

The spallation process is depicted in Fig. 1, showing two stages of the process (intranuclear cascade and evaporation). For thick targets, high-energy ($\gtrsim$20 MeV) secondary particles (plus their progeny) can undergo further spallation reactions. For some target materials, low-energy ($\lesssim$ 20 MeV) spallation neutrons (i.e., the cascade-evaporation neutrons) can enhance neutron production through low-energy (n,xn) reactions. For heavier nuclei, high-energy fission can compete with evaporation in a highly-excited nucleus. High-energy fission competition with evaporation in a highly-excited nucleus is illustrated in Fig. 1. Tantalum, tungsten, and lead are examples of materials that can undergo spallation/high-energy fission.

Some spallation-target fissionable materials such as thorium and depleted uranium can (in addition to undergoing high-energy fission) be fissioned by low-energy (~1 MeV to ~20 MeV) neutrons. Spallation, high-energy fission, and low-energy neutron fission produce different nuclear debris (spallation and fission products) as discussed below.

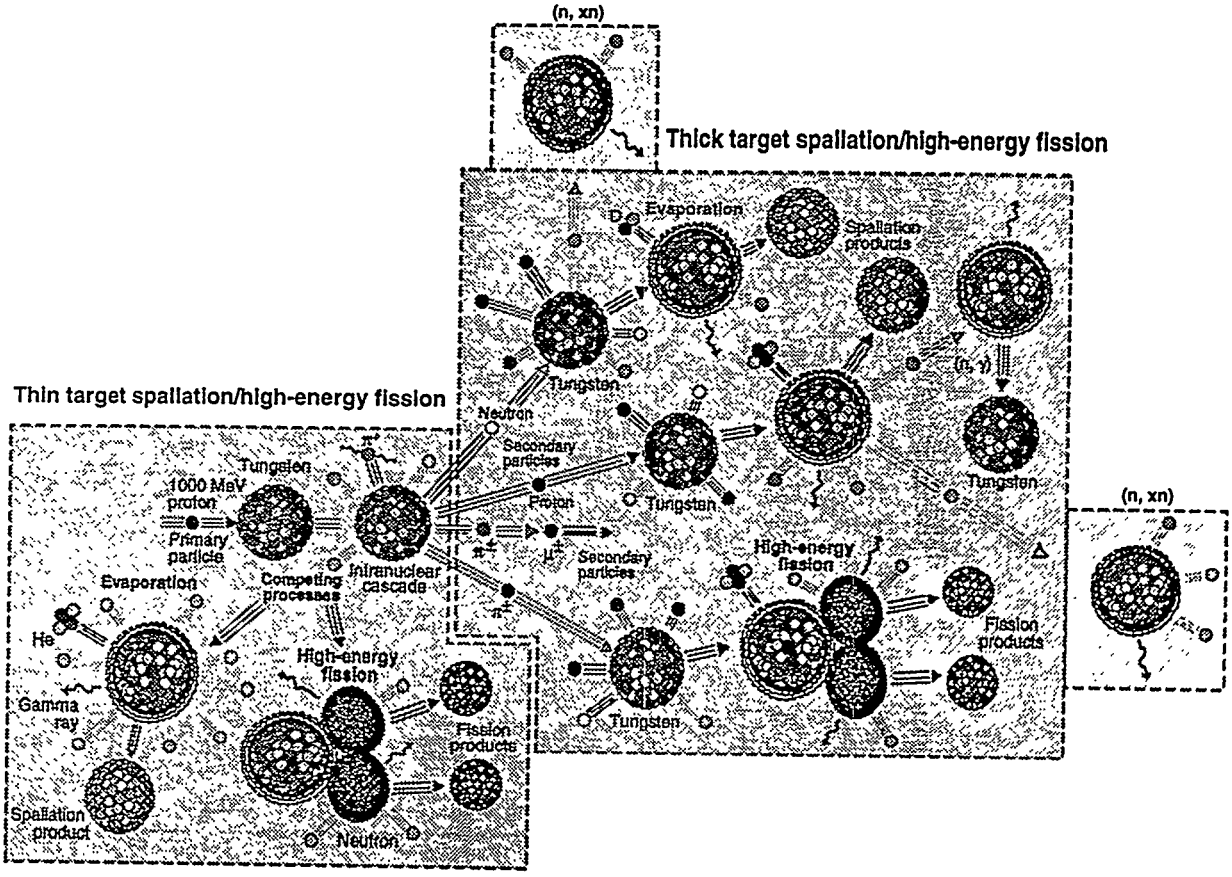

Fig. 1. Illustration of the spallation process in thick targets, with evaporation competing with high-energy fission in the de-excitation of highly-excited nuclei.

How Does Spallation Differ From Fission?

In The Number Of Low-Energy Neutrons Produced

Spallation and fission differ in several ways. One difference is in the number of (potentially) useful low-energy neutrons produced per spallation or fission event. The number of neutrons produced per fission event (about 2.5) is considerably less than that produced in spallation of heavy nuclei (typically in the tens of neutrons, depending on target material and size, and incident particle type and energy). Furthermore, one of the 2.5 neutrons produced by fission is needed to sustain the fission reaction; this neutron, therefore, is not available for other uses.

In The Amount Of Energy Deposited Per Neutron Produced

Spallation and fission also differ in the amount of energy deposited per (useful) neutron produced. For fission, about 180 MeV of energy is deposited in the reactor core per fission event, or about 120 MeV per useful neutron produced. For spallation (in an infinite tungsten target bombarded by 1000-MeV protons), the corresponding number is about 25 MeV. Power density in a reactor core limits the neutron flux that can be realized in a practical sense from fission reactors. The spallation process (by itself) is much more efficient than fission in this regard. Although there is less heat generated with spallation, the intensity of the incident particle beam (particles/cm^2) for a high-power spallation source can lead to cooling problems—equivalent to those of a high-power reactor source—in windows and targets, unless special care is taken.

In The Amount Of Gamma-Ray Energy Produced

For infinite tungsten and lead targets bombarded by 1000-MeV protons, ~3 MeV of gamma-ray energy is emitted for each neutron produced; about 12 MeV is released per fission event. Because spallation-neutron sources do not produce as much gamma-ray energy as equivalent reactor sources, gamma-ray heating problems in materials at a spallation source are less problematic than those at a reactor source. This difference can be important in practical applications—for example, when designing cold neutron sources for basic materials science research.

In The Energy Distribution Of The Neutrons Produced

On average, spallation neutrons have higher energies than fission neutrons. In a spallation source, high-energy secondary neutrons approach the energy of the incident particle. High-energy neutrons are extremely penetrating. Well-designed shielding is needed to prevent the escape of high-energy neutrons from the spallation-source environment. Also, the production of high-energy neutrons is angle-dependent, with higher-energy neutrons being generated in the forward direction. High-energy neutrons are useful for nuclear physics research, radiography, and in helping to understand radiation damage in a spallation environment. The low-energy neutrons are produced (more or less) isotropically.

In The Nuclear Debris Created

For low-energy neutron fission, the nucleus divides in two, typically producing a light fragment and a heavy fragment as fission products. For high-energy fission, the fission products

are more symmetric in their mass distribution than the asymmetric fission products caused by lower-energy particles. In spallation, the products created (nuclear debris) are distributed close to the original target material. The distribution of spallation products for tungsten and lead targets bombarded by 1000-MeV protons is illustrated in Fig. 2. Note that high-energy fission produces symmetric fission products peaking in the range around $Z = 40$.

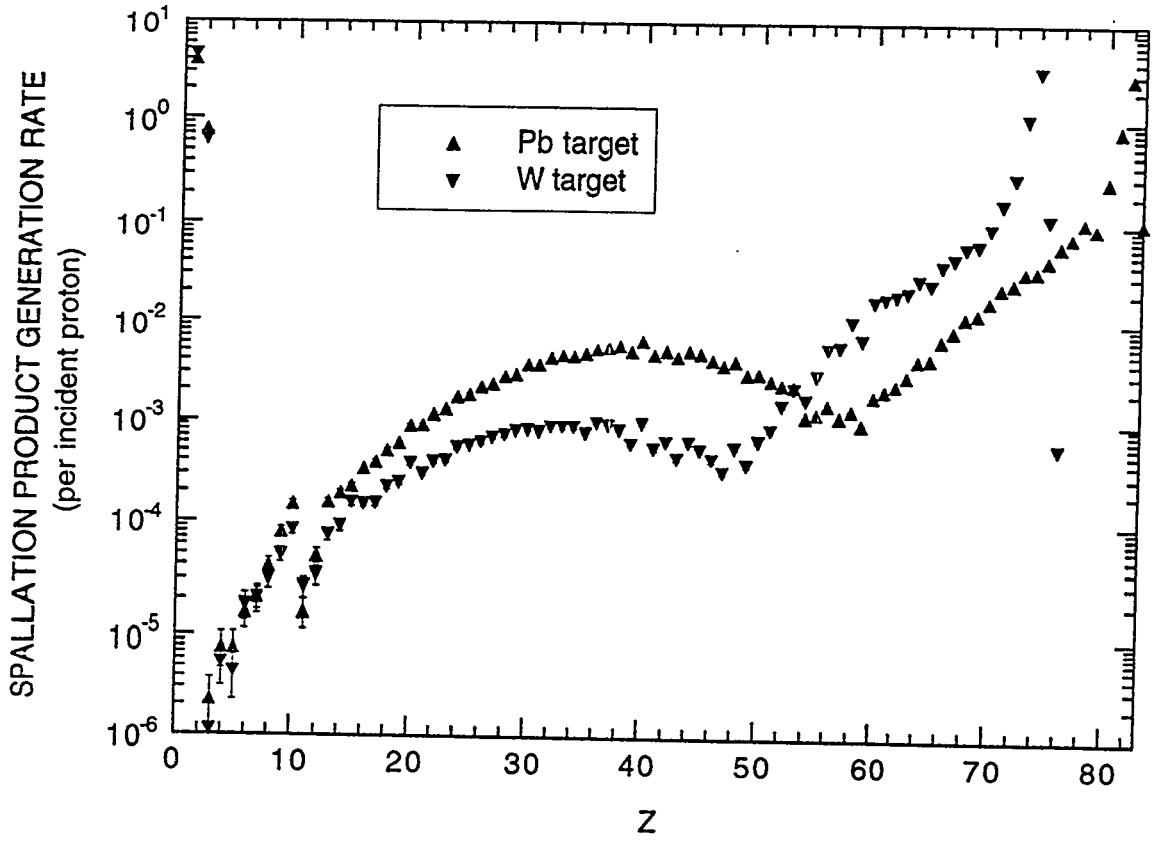

Fig. 2. Spallation product generation rate for 50-cm-diam 200-cm-long lead and tungsten targets bombarded on axis by 1000-MeV protons.

In The Radiation Damage To Materials

The type of radiation damage to materials at spallation neutron sources differs from that encountered at fission reactors in several respects. First, the evaporation phase of the spallation process produces enormous amounts of hydrogen and helium (one or two orders of magnitude more than at fusion reactors). Hydrogen can, for some materials such as zirconium, lead to the formation of metal hydrides; helium, at high operating temperatures, can form bubbles at grain boundaries and other defects which leads to material swelling and embrittlement. Second, the radiation field at a spallation source is much "harder" than the typical fission spectrum. Much remains to be learned about the effects of high-energy neutrons (and protons) on materials properties. Finally, the radiation field of a spallation source could have dramatic effects on the target coolant (e.g., light or heavy water) radiolysis that, in turn, could lead to radiation-enhanced corrosion problems.

COMPUTATIONAL TOOLS

LANL has world-class Monte-Carlo computational capability applicable to spallation-neutron source design; it also has the computer hardware and experienced people required to set up and run the codes and interpret the results. One part of the computational tool is based on the LANL version of the HETC Monte-Carlo code for the transport of nucleons, pions, and muons, which was originally developed at Oak Ridge National Laboratory (ORNL) [4]. Because of major modifications and additions made to the HETC code at LANL, this version of HETC has been renamed LAHET, and the system of codes based on LAHET is designated as the LAHET Code System (LCS) [5]. Below, we give a brief description of the breadth of capabilities that the LCS puts at the disposal of its users.

The LAHET Code System

The LCS (see Fig. 3) is a sophisticated code system based on several subcomponents, among which LAHET and MCNP are the major players. LAHET is a model-based Monte-Carlo code used for the transport and interaction of nucleons, pions, and muons at high energies (≤ 4 GeV). With the exception of measured nucleon-nucleon cross sections, LAHET uses nuclear models to describe particle interactions. LAHET uses the Bertini [6] or the ISABEL [7] model to describe the physics of the intranuclear cascade, and the Dresner evaporation model for the last phase of the nuclear interaction. The Fermi breakup model [8] replaces the Dresner model for describing the evaporation process for light nuclei. A pre-equilibrium model was recently added as an intermediate stage between the intranuclear phase and the evaporation phase. Two fission models (Rutherford-Appleton [9] and ORNL [10]) complement the set of physics models that LAHET uses.

The MCNP code [11] is a design-production code for low-energy neutron/photon/electron Monte-Carlo transport. The code is distributed and used internationally by nuclear system designers. The MCNP code is geared toward the transport of neutrons, photons, and electrons in matter. MCNP is a data-based code; it uses very detailed continuous-energy ENDF/B cross sections libraries for several hundred isotopes to describe the interaction of neutrons and photons with matter, down to sub-thermal energies. MCNP is a time-dependent Monte-Carlo transport code, capable of handling arbitrarily complex geometries.

Particle transport in both LAHET and MCNP is based on Monte-Carlo techniques. The philosophy used in the LAHET code is to treat all interactions by protons, pions, and muons within LAHET, but to treat neutron interactions only above a cutoff energy, typically 20 MeV. Any low-energy (< 20 MeV) neutron emerging from a reaction has its kinematic parameters recorded in a neutron file (NEUTP) for subsequent transport. For LAHET, a version of MCNP (called HMCNP) has been modified to accept the NEUTP file as an input source to complete the low-energy neutron transport. The low-energy transported neutrons can participate in nuclear reactions and produce additional neutrons and photons for transport within HMCNP.

Gamma-rays can also be transported by the LCS. During a LAHET calculation, a large quantity of information is recorded in a separate file, which another code (PHT—a photon source-generating code) can subsequently analyze to produce a gamma-ray source for HMCNP. The HMCNP phase of the calculation is then executed as a coupled neutron/photon transport problem. The photons produced in LAHET originate either from the decay of neutral pions produced in the intranuclear cascade phase or by the de-excitation of residual nuclei after the evaporation/high-energy fission phase. In a coupled neutron/photon problem, the neutron file NEUTP and the gamma-ray file GAMTP are merged (by the MRGNTP code in the LCS) to produce a combined neutron/photon file COMTP that describes the low-energy neutron source and high-energy-produced gamma-ray source for the entire system. HMCNP is then used to

transport these neutrons and photons plus gamma-rays produced from neutron-induced reactions below 20 MeV.

In addition, both LAHET and HMCNP can write history files (called HISTP and HISTX respectively), that contain a (nearly) complete description of events occurring during the computations. The code HTAPE (another code in the LCS suite of codes) is used to post-process the HISTP and HISTX files to extract a variety of information.

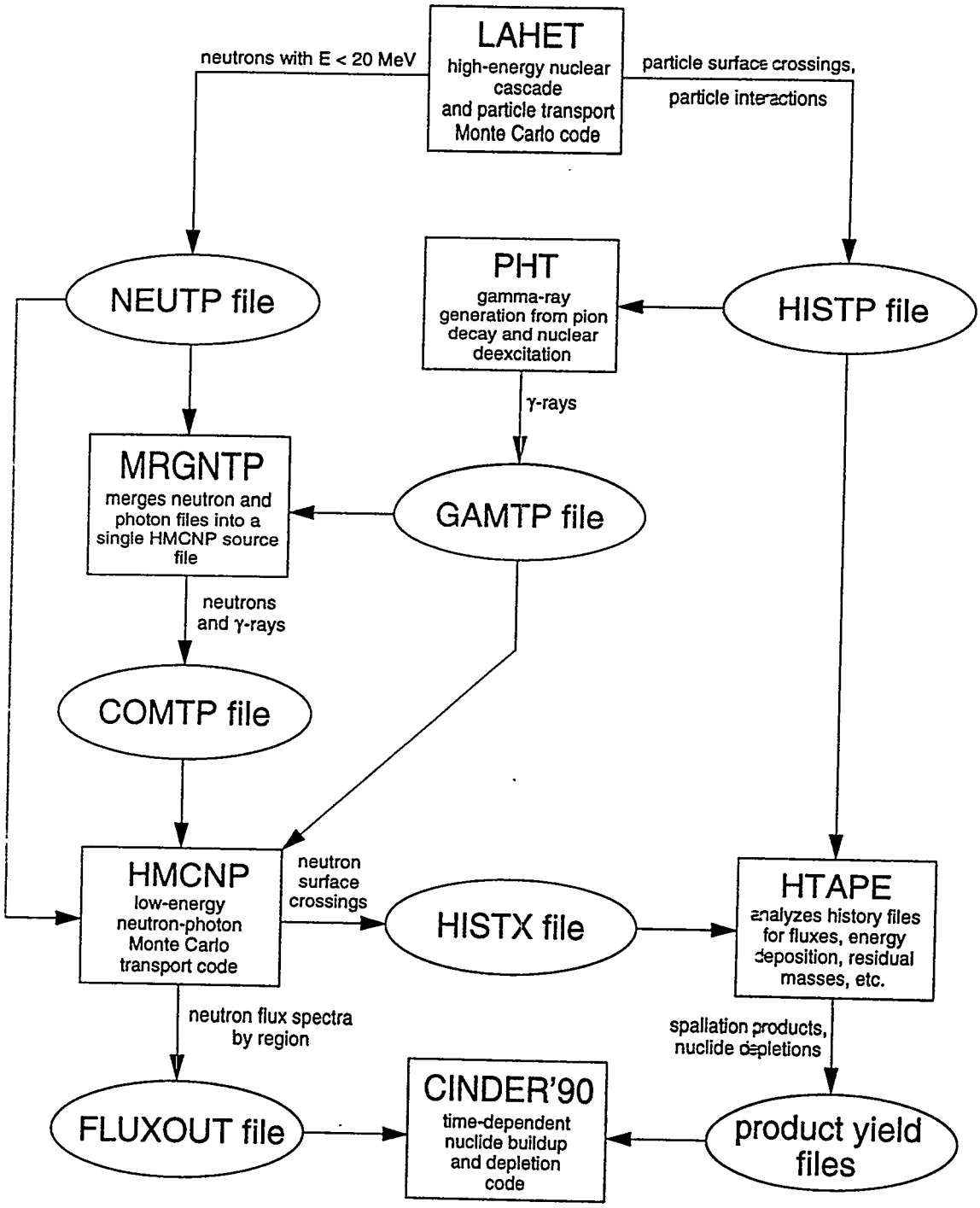

Fig. 3. LAHET Code System/CINDER'90 flow chart.

The CINDER'90 Code

CINDER'90 is a transmutation code used to follow the decay of nuclear species [12]. It uses nuclei production/destruction information from LAHET together with neutron fluxes from HMCNP to predict the time behavior of nuclear species through their production and subsequent decay. Each nuclide's concentration is determined by the history of gains from neutron-absorption reactions (spallation, fission, [n,γ], [n,2n], etc.) and radioactive decay of parent nuclides, as well as losses from its own decay and particle absorption. The total nuclide concentrations are obtained by summing partial concentrations. The CINDER'90 code uses a library of basic nuclear data to trace all possible transmutation paths, determining the partial concentration and associated activity of each nuclide as well as the integrated transmutation of each nuclide during a time increment. CINDER'90 accumulates nuclide concentrations and activities from nuclide properties as they are calculated. It then combines the post-processing data with decay and neutron-absorption data to obtain density (atoms/barn-cm and kg); activity (Ci/cm^3 and Ci); decay power (W/cm^3 and W); macroscopic neutron absorption (cm^{-1}); and decay spectra properties listed by nuclide, element Z, and mass A. The code also tabulates major contributors ($\geq$ 0.1%) to mass, activity, decay power, and macroscopic absorption. These results—activity inventory, decay power, macroscopic neutron absorption, etc.—have many practical applications. Some applications require the subsequent transport of the decay source in HMCNP to obtain a desired response, such as dose or dose-equivalent rates.

BARE-TARGET NEUTRONICS

Maximizing total low-energy neutron production, which depends on target material and geometry (as well as incident particle type and energy), is an important aspect of spallation-neutron-source target design—however, it is only part of the story. Once low-energy neutrons are produced inside the target, they must escape from the target before they can be moderated to energies that are *useful* in a variety of applications. Maximization of this leakage is another crucial aspect of target design. Target geometry and parasitic absorption in the target primarily control the leakage of low-energy neutrons. For example, for cylindrical targets, leakage from the front surface dominates total leakage at large target diameters (an undesirable effect). Parasitic neutron absorption in some spallation-target materials (such as tantalum and tungsten) is significant at large target diameters, whereas parasitic neutron absorption in lead is less important. Target neutronic performance is also a function of the energy and type of the incident particle, and of the target material and geometry.

Engineering realities (such as proton-beam windows, target canister material, target dilution by cooling material, and the profile and size of the incident particle beam) also affect the neutronic performance and design of a target; these practical matters must be explicitly dealt with in a realistic manner. The requirements of each particular application (*e.g.*, source brightness vs. total leakage) also affect target design. In addition, the neutronic coupling/decoupling of a target with its immediate environment plays an important role in the overall performance of a spallation-target system. This is particularly true when coupling a spallation target to a neutron-amplifying blanket (as in plutonium disposition).

Target Geometry

As mentioned above, leakage maximization is a crucial aspect of spallation-neutron-source target design. Geometry and parasitic absorption of the target control the leakage of low-energy neutrons for a given target material. Figure 4 illustrates these effects, comparing low-energy neutron production and leakage for two typical spallation-neutron-source target materials—lead

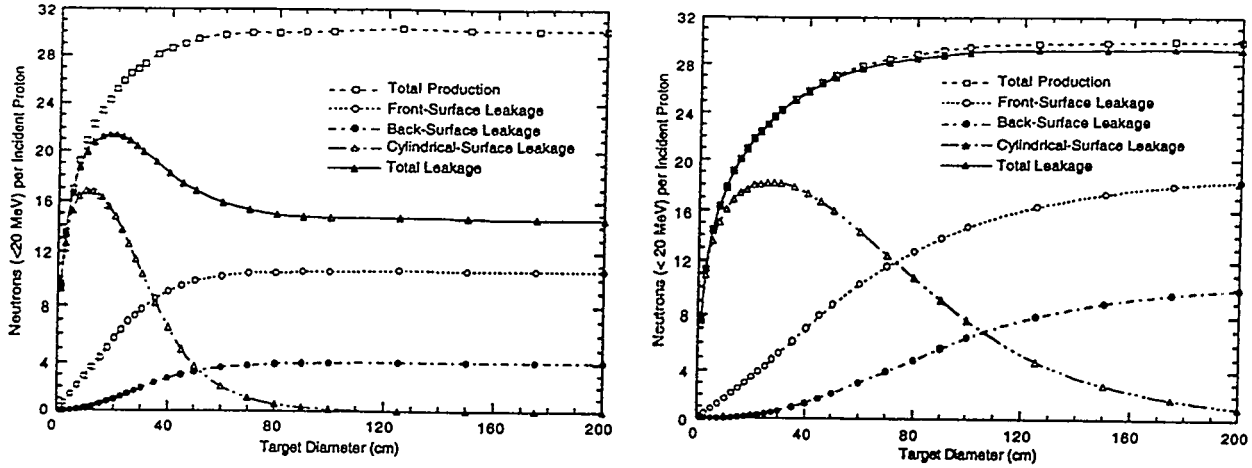

Fig. 4. Low-energy neutron production and leakage as a function of target diameter for solid right-circular cylindrical targets bombarded on axis by 1-GeV protons. (a) A 30-cm-long tungsten target; (b) a 55-cm-long lead target.

and tungsten. The increased parasitic absorption in tungsten is significant at large target diameters, yet tungsten produces more low-energy neutrons than lead, especially at small target diameters. At large target diameters (infinite targets) lead and tungsten produce roughly the same number of low-energy neutrons. As can be seen in Fig. 4, leakage from the front surface of the targets dominates the total leakage at large target diameters.

Figure 4 also illustrates both the flexibility and complexity of designing spallation targets. For example, if target compactness and neutron leakage from the cylindrical surface are important, then one would choose a tungsten target with a diameter of approximately 10 cm. Indeed, this is the case for the LANSCE pulsed spallation-neutron-source application for materials science research [13]. On the other hand, if total neutron leakage alone dominates the target design criteria, one would choose a solid lead target with a diameter of about 100 cm. However, engineering realities concerning target structural support and target cooling must be addressed; these criteria have a tremendous impact on spallation-target design.

Energy- and Material-Dependent Effects

In addition to geometry (size and shape), the neutron production and leakage from a spallation target depends on the target material and on the energy and type of the incident particle. Figure 5 shows the dependence of low-energy net neutron production—spallation plus (n,xn) and fission neutrons—on the energy of the incident proton and the target material. As can be seen in Fig. 5, fissionable targets produce more low-energy neutrons, but at a cost of more energy deposition in the target material. As mentioned before, neutron leakage (and not neutron production) is a better measure of target performance. Note (in Fig. 4) that neutron leakage from a solid lead target is much better than that from a solid tungsten target. Depending on the application, there are ways of mitigating this effect by employing the split-composite target idea [14].

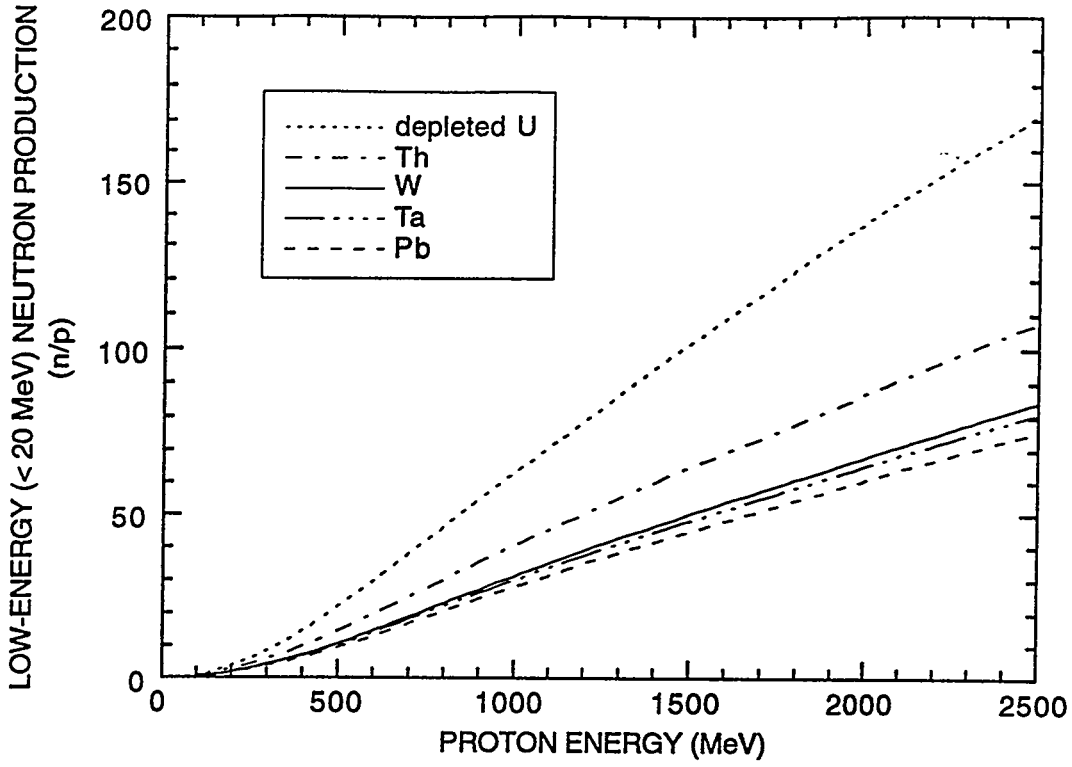

Fig. 5. Production of low-energy neutrons as a function of incident proton energy for various target materials. The targets are 50-cm-diam × 200-cm-long right-circular cylinders; the protons are incident on the cylindrical axis.

THE SPLIT-COMPOSITE TARGET CONCEPT

As discussed above, target geometry and parasitic absorption in the target primarily control leakage of low-energy neutrons from the target. The increased parasitic absorption in tungsten is significant at large target diameters. For tungsten (and any other neutron absorbing targets, such as tantalum), the detrimental parasitic absorption effect is decreased by splitting the target in the direction of the incident charged particle beam. This technique also helps mitigate excessive neutron leakage from the front surface of the target (by making the target neutronically reentrant). Splitting a target increases low-energy neutron leakage thereby reducing parasitic neutron absorption. However, low-energy neutron production is also degraded because secondary high-energy particles also escape from the central target zone. This loss in neutron production is diminished by employing a radially-composite target consisting of a central region and a radial zone. Depending on the application of the split-composite target concept, it may also be desirable to have a target both axially- and radially-composite as well as split. These target concepts are illustrated in Fig. 6.

The split-composite target concept has three unique features. *First* the split-composite target is neutronically reentrant: the central target zone is split axially (by flux traps) and the neutron production is spatially distributed deeper along the target axis. The term *flux trap* refers to the spaces between the target segments of a split target. Neutron leakage is reduced from the front target surface, allowing the use of large target diameters at reduced power densities without large front-surface leakage losses. *Second* splitting a target increases low-energy neutron leakage and reduces parasitic neutron absorption. The central target zone of a split-composite

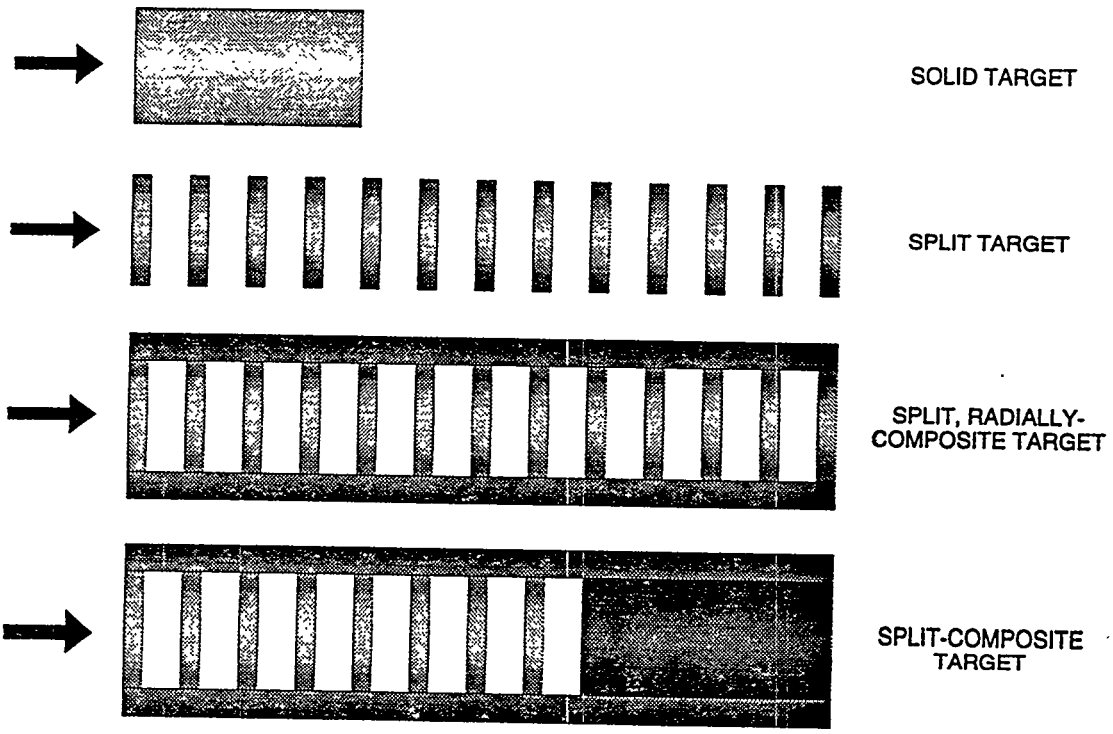

Fig. 6. Basic target concepts.

target provides *geometric decoupling* between the various regions in the central target; the axial splitting of the central target zone accomplishes this geometric effect. Geometric decoupling also enhances leakage of high-energy secondary particles into the radial/lateral target zone to cause spallation reactions. Production of low-energy spallation neutrons in the radial/lateral target zone increases their chance to escape (leak) from the split-composite target. *Third* a split-composite target allows for the possibility of using *neutronic decoupling*—employing neutron-absorbing material in and between target regions to reduce parasitic neutron absorption in the various target zones, and neutronically isolating target zones from each other and their surroundings. (The Los Alamos ^{3}He APT target system is an ideal application of the neutronic decoupling concept [14].)

The split-composite target concept also allows the use of high-temperature materials (such as tungsten) in the central target zone. Lead can be used in the radial or lateral target zone to enhance neutron production and utilization.

Figure 7 quantitatively shows the effects of splitting a target and making the target both split and radially composite. Note that splitting the target increases neutron leakage for flux-trap gaps that are ≥ 5 cm, decreases front-surface neutron leakage, but also decreases neutron production (as the flux-trap gaps increase). Making the target both split and radially composite enhances both the total low-energy neutron leakage and production. Split target and split-composite target concepts have been applied to projects as varied as pulsed spallation neutron source design [13]; Accelerator Production of Tritium (APT) [14], Accelerator Transmutation of Waste (ATW) [15], and are being studied for quasi-continuous and continuous spallation neutron source applications. Since splitting of the target distributes the neutron source over a larger volume, the split-composite target concept is more readily suited to applications where total neutron leakage, rather than peak flux, is the overriding design criterion.

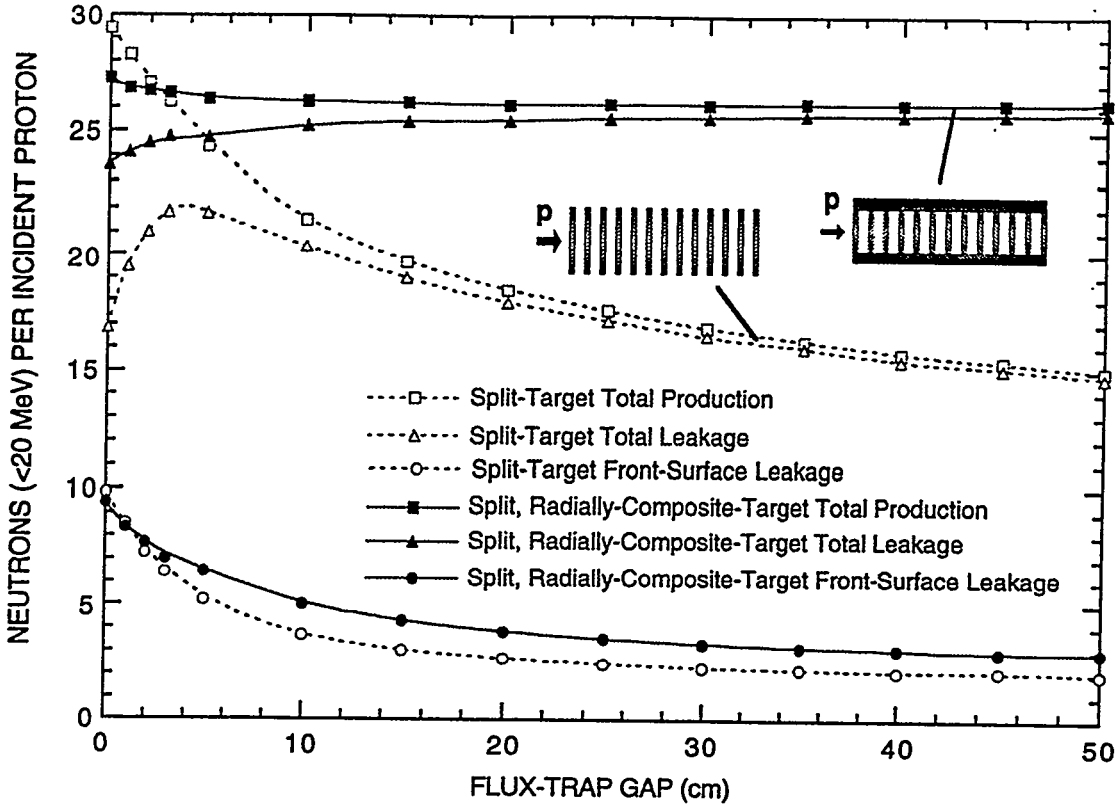

Fig. 7. Low-energy neutron production and leakage as a function of flux-trap gap for a split target and a split, radially-composite target. Both targets have twelve 2.5-cm-thick tungsten plates in the central target zone. For the zero-flux-trap-gap case, the targets are solid. The split target has 50-cm-diam plates, whereas the split, radially-composite target has 20-cm-diam plates surrounded by a 15-cm-thick lead annulus for a total diameter of 50 cm. The 1-GeV proton beam is incident on the target axes.

LIQUID TARGETS

For applications where high neutron flux is an important figure of merit, spallation targets must be compact and capable of handling high power densities. For such applications, liquid metal targets hold some promise. The main advantages of liquid targets are: a) high target mass density; b) high heat removal capability; c) reduced radiation damage; and d) no cooling water in the proton beam. The main disadvantage is how to contain the liquid target; however, this problem is under active study. The main liquid target materials under consideration are lead, lead-bismuth, and mercury. Polonium production from bismuth is a potential safety concern for a lead-bismuth target.

CONCLUSIONS

Because of recent advances in high-power accelerator technology, spallation is becoming an important alternative method to fission for producing high fluxes of neutrons for a variety of applications. Liquid targets will become important when high power density and heat removal dominate spallation target design. The low parasitic neutron absorption in liquid lead is an

important attribute for such applications as plutonium disposition and continuous (reactor-like) neutron sources. Mercury is being considered for pulsed neutron sources where parasitic neutron absorption is not such a critical factor [16]. As mentioned above, tantalum, tungsten, lead, and depleted uranium have found applications in the areas of pulsed and continuous spallation neutron sources, and tungsten and lead are being considered as target materials for accelerator-based production of tritium.

ACKNOWLEDGMENTS

We acknowledge useful discussions with Phillip Ferguson. This work is supported by the United States Department of Energy under contract W-7405-ENG-36 to the University of California.

REFERENCES

[1] Rutherford, E., "Collisions of α Particles with Light Atoms. IV. An Anomalous Effect in Nitrogen," *Phil. Mag.*, **37**, 581, January-June 1919.

[2] Lawrence, E. O. and Edlefsen, N. E., "On the Production of High Speed Protons," *Science*, **LXXII, NO. 1867**, 376, October 10, 1930.

[3] Livingston, M. S., LAMPF, a Nuclear Physics Research Facility, Los Alamos National Laboratory report, LA-6878-MS (1977).

[4] Radiation Shielding Information Center, "HETC Monte Carlo High-Energy Nucleon-Meson Transport Code," Oak Ridge National Laboratory report CCC-178 (August 1977).

[5] Prael, R. E. and Lichtenstein, H., "User Guide to LCS: The LAHET Code System," Los Alamos National Laboratory report LA-UR-89-3014 (September 1989).

[6] Bertini, H. W., *Phys. Rev.* **188**, 1711 (1969).

[7] Yariv, Y., and Fraenkel, Z., *Phys. Rev.* **166**, 2227 (1979).

[8] Brenner, D. J., Prael, R. E., Dicello, J. F., Zaider, M., "Improved Calculations of Energy Deposition from Fast Neutrons," in *Proceedings Fourth Symposium on Neutron Dosimetry*, EUR-7448, Munich-Nuremberg (1981).

[9] Atchison, F., "Spallation and Fission in Heavy Metal Nuclei under Medium Energy Proton Bombardment," in *Targets for Neutron Beam Spallation Sources*, Jül-Conf-34, Kernforschungsanlage Jülich GmbH (January 1980).

[10] Barish, J., et al., "HETFIS High-Energy Nucleon-Meson Transport Code with Fission," Oak Ridge National Laboratory report ORNL/TM-7882 (1981).

[11] Briesmeister, J., editor, "MCNP—A General Monte-Carlo N-Particle Transport Code—Version 4A," Los Alamos National Laboratory report LA-12625 (1993).

[12] Wilson, W. B., et al., " Accelerator Transmutation Studies at Los Alamos with LAHET, MCNP, and CINDER'90," in Proceedings of the Workshop on Simulating Accelerator Radiation Environments, Los Alamos National Laboratory report LA-12835-C (October 1994), pp. 115-133.

[13] Russell, G. J., Bowman, C. D., Whitaker, E. R., Robinson, H., and Meier, M. M., "LANSCE High-Power (200 uA) Target-Moderator-Reflector-Shield," in *ICANS-VIII: Proceedings of the Eighth Meeting of the International Collaboration on Advanced Neutron Sources*, Rutherford-Appleton Laboratory report RAL-85-110 (November 1985), pp. 272-293.

[14] Russell, G. J., Pitcher, E. J., and Daemen, L. L., "Split-Composite Spallation Neutron Source Targets and Accelerator Production of Tritium," Trans. Am. Nucl. Soc., **69**, ISSN: 0003-018X, 440-441 (1993).

[15] Daemen, L. L., Pitcher, E. J., and Russell, G. J., "Technetium-99 Burner for the Hanford Waste," Trans. Am. Nucl. Soc., **69**, ISSN: 0003-018X, 429-431 (1993).

[16] Bauer, G., private communication.

A Target Development Program for Beamhole Spallation Neutron Sources in the Megawatt Range

G.S. Bauer*, F. Atchison*, T.A. Broome[+], H.M. Conrad[$]

Paul Scherrer Institut, CH-5232 Villigen PSI
[+]*Rutherford Appleton Laboratory, Chilton, Didcot, Oxon OX11 0QX, UK*
[$]*Forschungszentrum Jülich, D-52425 Jülich*

Abstract: Spallation sources as an alternative to fission neutron sources have been operating successfully up to 160 kW of beam power. With the next generation of these facilities aiming at the medium power range between 0.5 and 5 MW, loads on the targets will be high enough to make present experience of little relevance. With the 0.6 MW continuous facility SINQ under construction, and a 5 MW pulsed facility (ESS) under study in Europe, a research and development program is about to be started which aimes at assessing the limits of stationary and moving solid targets and the feasibility and potential benefits of flowing liquid metal targets. Apart from theoretical work and examination of existing irradiated material, including used targets from ISIS, it is intended to take advantage of the SINQ solid rod target design to improve the relevant data base by building the target in such a way that individual rods can be equipped as irradiation capsules.

1. INTRODUCTION

Medium power spallation neutron sources, i.e. sources with a beam power between about 0.5 and 5 Megawatts have recently attracted considerable interest for various reasons:

- they offer an opportunity to devise high flux neutron sources for research applications without the difficulties of using fissionable materials or self-sustaining chain reactions
- they have the potential to operate with a time structure of the neutron flux which allows highly efficient exploitation of the neutrons produced and significantly expands their scientific use, as demonstrated by the existing low power facilities
- they are an important intermediate step on the way to potential high power commercial or industrial facilities, allowing one to gain relevant experience in accelerator as well as target technology.

So far, four pulsed spallation facilities used for neutron scattering are in operation, all of which use relatively low power beams (KENS, Japan, 3 kW, IPNS, USA, 7 kW, LANSCE, USA, 60 kW and ISIS, UK, 160 kW). A fifth active spallation target, at TRIUMF in Canada, mainly serves as a beam stop for the 50 kW continuous beam of the cyclotron and can be used as an irradiation facility. It is made up of a lead filled stainless steel container.

Although, taken together, these facilities represent many years of operational experience, the accumulated dose on any one of their targets only corresponds to about one to two weeks of beam time in a 5 MW facility.

2. DESIGN GOALS AND OPERATING CONDITIONS FOR MEDIUM POWER SPALLATION SOURCES

Proposals and design goals for new spallation sources range from little under a megawatt in beam power for the continuous source SINQ, under construction in Switzerland [4], to five megawatts for the ESS-project under study in the European Union, with the 1 megawatt level targeted also in various proposals by different US and Japanese laboratories.

proposal [7], and scoping studies are also carried out for ESS, it is generally felt that going to target rods to improve heat removal becomes necessary at or above this power level. For the 1 MW target of ESS, the reference target has hollow rods cooled at their inner and outer surfaces by separate cooling circuits. Its principal features are summarized in Table 2.

Table 2: *Summary of ESS-1MW rod target data*

Target rod outer diameter	9.5 mm
Target rod inner diameter	2 mm
Maximum temperature in rod	400°C
Maximum thermal stress in rod	15 MPa
Water fraction in target	20%
Water pressure	2 MPa

A similar concept, although with solid rods and a single cooling circuit is being built for the first SINQ target. Particular features of this target are the vertical beam injection from underneath and the large D_2O-tank that surrounds the target, because SINQ is a continuous neutron source designed for high time average neutron flux. This restricts considerably the freedom in the choice of materials, because absorption in the target and structural materials must be minimized. Table 3 gives an overview of the flux levels expected in the D_2O moderator for various target and container materials.

Table 3: *Calculated flux levels per mA of 570 MeV protons for different target concepts for SINQ*

Target System	Maximum thermal flux ($cm^{-2}s^{-1}$)	Useable flux at 25 cm ($cm^{-2}s^{-1}$)	Relative flux at 25 cm radius
Pb with weakly absorbing container	2×10^{14}	1.3×10^{14}	1
Pb-Bi with steel-container	0.9×10^{14}	0.85×10^{14}	0.65
W-plates in Al-container	0.8×10^{14}	0.6×10^{14}	0.46
Ta-plates in Al-container	0.55×10^{14}	0.45×10^{14}	0.35
Pb-rods in zircaloy tubes	1.5×10^{14}	1×10^{14}	0.70
Zircaloy rods	0.8×10^{14}	0.59×10^{14}	0.45

In order to have enough safety margin for reliable operation at all times, a staged concept of target development will be followed which starts with a less than optimum mark 1 target made up of zircaloy rods. The main goal of this target is to produce neutrons in the commissioning phase of the source and to prove the reliablility of a safety hull made up of two aluminium shells with water cooling between them (Fig. 1). This safety hull concept will be retained for all later target versions. As a second stage in the development program it is envisaged to replace the zircaloy rods by lead filled tubes to improve the neutron yield, but still run the target in a solid phase [8]. The question, whether zircaloy can be used as tube material still needs to be investigated. An overview of the operational parameters of the SINQ solid targets and the safety hull is given inTable 4.

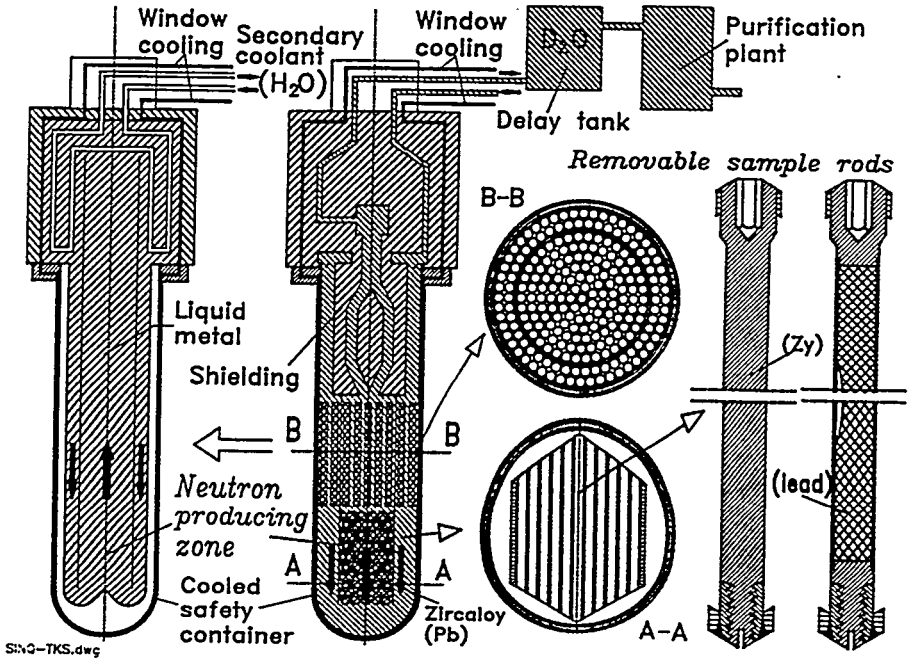

Figure 1: *Schematic representation of the SINQ-target design for beam injection from below. The mark 1 target will be a D_2O cooled solid rod target (right); the version shown at the left is the natural convection flow liquid metal target under study.*

Table 4: *Operating parameters of SINQ solid targets and safety hull*

Proton beam energy (MeV)	570	
Maximum beam current (mA)	1.5	
Design power in target (MW)	1	
Nominal beam current (mA)	1	
Nominal current density ($\mu A/cm^2$)	≤ 25	
Fault conditions current density ($\mu A/cm^2$)	≤ 350	
Power dissipation in beam window, Al, 2mm (kW)	5.5	
Max. hydrogen production in beam window* (appm/mA day)	14	
Max. helium production in beam window* (appm/mA day)	3.6	
Max. displacement damage in beam window* (dpa/mA day)	$1.1 \cdot 10^{-2}$	
Targets:	Zircaloy	Lead (in zircaloy)
Maximum power density (W/g mA)	39	35
Max. hydrogen production (appm/mA day)	32	35
Max. helium production (appm/mA day)	9	10
Decay power at beam turn off** (W/mA)	1100	921
Decay power after two weeks** (W/mA)	330	124
Total activity at beam turn off** (TBq)	5500	6700
Total activity after 1 year** (TBq)	145	925

* estimates for 800 MeV; effect of 600 MeV protons should be similar

** after 1 year of operation

As can be seen, the gas production rate is quite significant and, among others, its effect must be carefully assessed. Zirconium is known to have almost zero solubility for hydrogen at a few hundred °C but to form a hydride which deteriorates the material's mechanical properties significantly. Little or nothing is known on the effect of the helium produced, but in general, helium embrittlement is a severe problem in most metals. The cracking observed in the zircaloy cladding of the IPNS and ISIS uranium targets might indicate difficulties of that sort.

Another problem which may become increasingly severe as the beam power goes up is cooling water radiolysis and contamination. For SINQ, expected radioactivity data are given in Table 5.

Table 5: *Radioactivity data for SINQ cooling circuits at 1 mA*

Circuit	direct energy deposition (kW)	mass flow rate (kg/s)	pipe inner diam. (cm)	Dose rate at target exit per m of pipe mS/h from γ's	from n°	tritium production (10^{12} Bq) equil.	after 1 year	7-Be (10^{12}Bq) equil.	10-Be (10^{6}Bq per year)	14-C (10^{9}Bq per year)
Target	94	9	6.6	410	178	180	7.4	5.2	3	15
Safety hull	3.6	2.2	2.8	37	20	14	0.5	0.3	0.2	6

On top of the radioactivity either produced directly in the water or picked up by possible corrosion or erosion effects,- the latter being difficult to predict-, spallation products produced near the target surface can be expected to be ejected by recoil from a depth up to 50 μg/cm². For zircaloy this includes such problem nuclides as 90-Sr. Obviously, this becomes the more of a problem, the more the ratio of surface area to volume must be increased due to cooling requirements.

3.1.2 Water cooled moving solid targets

With little information available on the combined effects of the various operating conditions on the life expectancy and operational safety of the targets, the most obvious solution is dilution. This approach was chosen in the German SNQ-project in the eighties [9]: A 2.5 m diameter wheel built up of lead-filled aluminium tubes and cooled by water was to be rotated around its axis perpendicular to the proton beam. With the wheel circumference 200 times the beam diameter, the dilution effect in terms of average load, radiation effects and operating temperature was substantial. Of course, during one proton pulse the target remains essentailly stationary with the corersponding jump in temperature by some 42 K.

A similar approach is now being considered as reference concept for the 5 MW-ESS target [10]. Relative to the SNQ-concept it is different in two important ways: (a) it allows vertical beam injection and still covers all angles in the horizontal plane with beams from its various moderators and (b) it uses the split-target or flux trap concept first introduced in Los Alamos [11] and now considered as an option for virtually all new pulsed source projects. A schematic representation of this target is shown in Fig. 2. In order to minimize the mass of the moving part, only a total of 20 cm effective taget thickness is being rotated, separated into a lower section of 7 cm at the beam entrance and an upper section of 13 cm to produce about equal numbers of neutrons in both parts. About 85 % of the total power is deposited in this thickness for 1.33 GeV protons. The remainder can be handled in a stationary target, which is planned as a 20 cm diameter, 30 cm long cylinder above the target wheel. The outer diameter of the rotating part is about 1 m. With a revolution frequency of 1 Hz and an effective beam diameter of about 7 cm, consecutive pulses hit adjacent regions on the target. Thus,

while diluting the average load by a factor of 50, where it is high, this concept has the added advantage of allowing beams to be extracted across the target axis, which would not be possible in a stopping rotating target. The target material is arranged in water cooled rings of 12 cm lateral width and of varying thickness in order to keep the surface temperature on all rings approximately equal. Thus the cooling gaps between all rings can be the same, namely 0.18 cm. The cooling water, which is flowing outward resp. inward in half the number of gaps in each stack, enters the wheel through an annular space in the hub and leaves it again through the hub center. As in the SNQ-concept both, the wheel bearing and its drive are accomplished by hydraulic means.

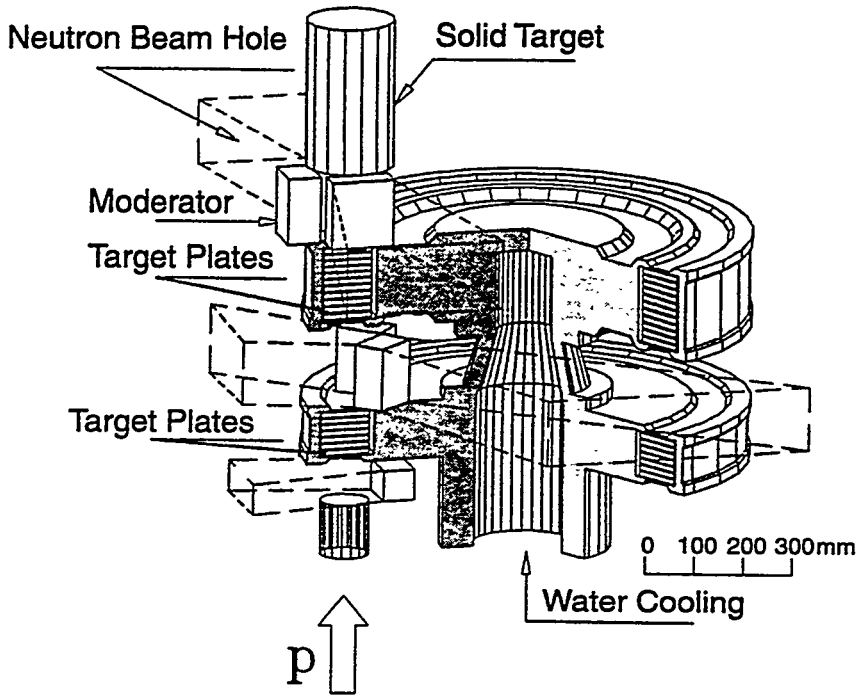

Figure 2: *Schematic representation of the rotating 5 MW-ESS split target.*

A fundamental issue with short pulses at these power levels (100 kJ/pulse) is the problem of shock waves. These occur, if the pressure rise caused by the power deposition cannot relax elastically via sound waves during the pulse. As mentioned before, the wheel is effectively at rest during the pulse. For tantalum the maximum power density at ESS reference parameters is obtained as 7 kW/cm^3 , corresponding to a temperature increase of 55 K or a pressure of 230 MPa. This is about 35% of the UTS of a Ta-10%W alloy (660 MPa), but it is known from the dynamical treatment of shock wave propagation that rarefaction stresses may exceed the static pressure value by as much as a factor 2 to 3, thus posing a real risk to the integrity of the target plates. Apart from the possibility to relax the situation by using a wider beam, mechanical subivision of the plates by very thin cuts in radial direction is being examined. Of course, changes of mechanical properties during target operation is yet another unknown.

3.2 Convectively cooled liquid metal targets

In view of the high damage levels expected for solid target materials and the difficulties of removing the heat without undue dilution of the heavy metal in the neutron producing zone, use of a flowing liquid heavy metal as spallation target was already considered in the Canadian ING-study in the sixties [12]. It was also studied as an option in the German SNQ-project [13]. Here, a concentric up and downward flow with a coalescence point in the downflowing material was evaluated with the

beam impinging on the coalescence point from above. In this way heated material would be removed quickly from the reaction zone and the need to have a stationary window in the beam to support the target could be eliminated.

Apart from requiring vertical injection from above, which is difficult to shield and to maintain, release of volatile spallation products into the vacuum space above the target was a problem that could not be fully assessed. In addition to the various hydrogen and helium isotopes mentioned earlier, this also includes heavier nuclei. Table 7 gives a summary of hazardous and potentially volatile species produced in a liquid lead-bismuth and lead target [14]. The production rates are for a target surrounded by a large D_2O-tank. This particularly affects the amount of 210-Po, an α-emitter which mainly results from thermal neutron capture in Bi. This contribution is therefore much lower in a lead target than in a lead-bismuth target. With a half life of 138 days, 210-Po is not a problem, as long as the target material can be kept in safe enclosure. If evaporation into a vacuum space or an atmosphere above the target must be considered, the operating temperature becomes very important. From experience with Pb-Bi- cooled nuclear reactors, a relation was derived [15], which gives the temperature dependence of Po-release from molten lead or lead-bismuth per unit molar concentration in the liquid.

Table 7: *The major contributors to radiotoxicity (in relative numbers) with the Pb target and the Pb-Bi target at SINQ after operation at 1 mA for 1 year*

Element	I	Sr	Ir	Hg	Y	Pb	Bi	Tl	Po*	Xe	Os	Pt	Cd	Yb	Ce	Others	Totals
Pb-Target	1.34	1.00	0.94	0.75	0.73	0.73	0.68	0.62	0.54	0.38	0.27	0.25	0.20	0.17	0.10	0.92	9.62
Pb-Bi Target	3.05	1.49	0.03	0.47	1.16	0.39	139	0.72	562	0.68	0.20	0.27	0.42	0.17	0.21	1.74	712

* The amount of Po given for Pb does not include the effect of possible small amounts of Bi contained in the lead.

This function is shown in Fig. 3. It can be seen to follow closely the temperature dependence of the vapour pressure of molten lead, which is included for reference. At the operating temperature of a molton lead target ($\approx$ 400°C), the evaporation rate is about 4 orders of magnitude higher than at 200° C, where a Pb-Bi-target can operate.This shows that, although down by three orders of magnitude in concentration in the liquid, more Po would evaporate from a molten lead target than from a Pb-Bi-target. This holds for a fully moderated source with a high thermal neutron flux at the target. For pulsed sources with small (and decoupled) moderators, the production rate of 210-Po from Bi is much lower, making the argument even stronger. This is very important, because the high operating temperature of a molten Pb-target also poses other problems related to the availability of suitable structural materials and to heat removal by a simple cooling system, in particular water. As for the mercury produced, all of it is expected to evaporate from the liquid, thus giving the main contribution to radiation burden in the space above the target.

A target which is fully contained under normal operating conditions and where the motion of the liquid is driven by natural convection (cf. Fig. 1) was originally studied for the SINQ-facility. Experiments showed that the natural convection flow can be started easily and is sufficiently stable [17]. However, such a concept still requires a large amount of detailed studies. Therefore it was postponed in favour of the rod target concept mentioned before.

For a medium-to-high power system, such as ESS, it is likely that a pumped circuit would be preferred for various reasons: target flow is independent of heat dissipation in the reaction zone, cooling of a beam window by the flowing target can be better controlled and there exists more freedom in the relative positions of the reaction zone, the heat sink and a potentially necessary target

material quality control circuit. Such a system could conceivably be used for a horizontal beam injection which, although presently not favoured for the 5 MW ESS-target for reasons of space around the target block, has not been completely dismissed so far.

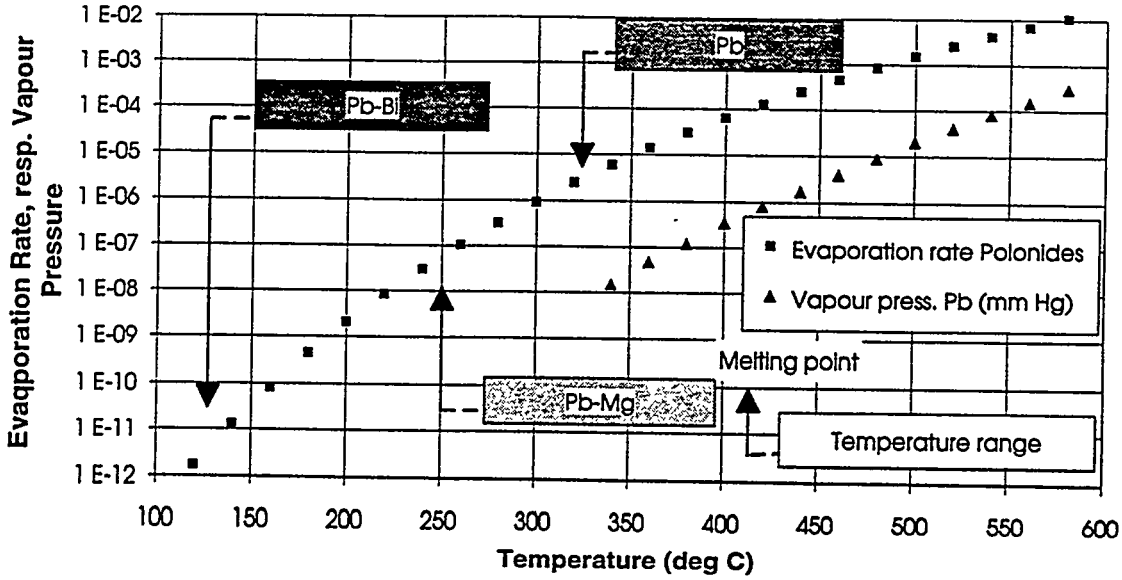

Figure 3: *Temperature dependence of the evaporation rate (kg/m²s per unit molar concentration) of polonides from liquid lead alloys and of the vapour pressure of molten lead. Melting points and operating ranges of potential target materials are indicated.*

Irrespective of whether the system is pumped or driven by natural convection, if it requires a beam window, this will always be the life-limiting component in a liquid metal target and will need to be assessed particularly carefully, because it has an obvious safety function.

A target configuration which is on the one hand largely compatible with the ESS-reference configuration (vertical beam injection from underneath, split rotating target) and on the other hand offers the advantages of a liquid metal target and a moving beam window is sketched very schematically in Fig. 4. The pumped liquid metal circuit is fully enclosed in a rotating container and the heat is transferred to a water reservoir by means of heat pipes in order to eliminate the risk of water ingress into the hot metal on the one hand and to have a relatively simple transition from the rotating to the stationary system on the other, at the same time relaxing the requirement on the coolant temperature and pressure.

Since the beam would pass through essentially flat windows in this case, problems might arise with the stress levels created during the pulses. These problems are much less serious in a curved window as the one shown in the left part of the drawing for the case of horizontal beam injection. Important advantages of such contained liquid metal targets are that most of the radioactivity is confined to the target volume itself, that only the structural materials are subject to radiation damage - where more freedom of choice exists than for the target itself - and that the cooling circuits are essentially "clean" and easier to maintain. They do, however, still require a large amount of study work.

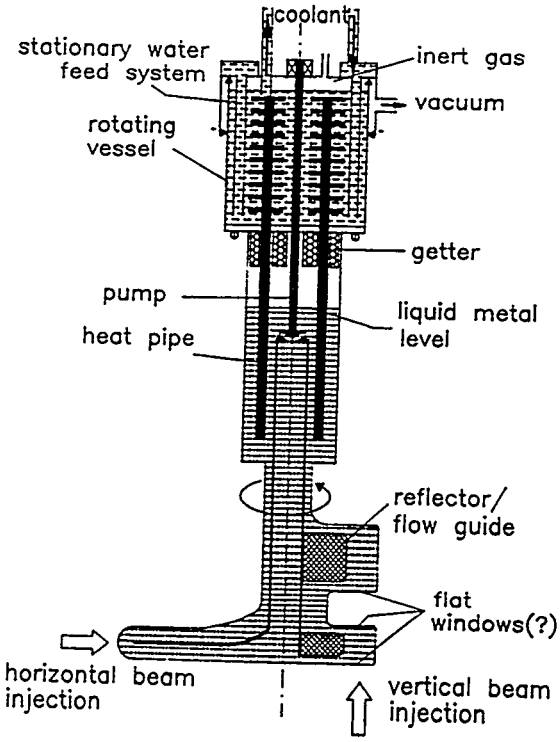

Figure 4: *Schematic of a rotating window liquid metal target concept.*

4. OPPORTUNITIES TO IMPROVE THE DATA BASE

The main problem one is faced with when trying to design a target for the load level as discussed is the lack of reliable data in particular about radiation damage, effects of thermal loads in conjuction with this damage and radiolysis in the coolant. Very few opportunities exist to carry out relevant research, in particular in a systematic way and under controlled conditions. Some sample irradiations were performed at the LASREF facility at Los Alamos, in general to a total dose of some 10^{20} protons/cm^2, in a few cases up to 10^{21}. At a current density of 200 μA/cm^2, this only corresponds to an irradiation time of one day or less. Obviously, target engineering will have to follow standard rules valid for non-irradiated materials to start with. This alone may mean that current densities must be limited to somewhere around 80 μA/cm^2. The effect of irradiation comes as an added difficulty. In this context it is important to analyse the available specimens, in order to have at least some "low dose" data. This is intended in the frame of the ESS-study work.

For the case of tantalum, stainless steel, and possibly tungsten, targets that have been in use over longer periods at ISIS (Ta, stainless steel) and LANSCE (W) might be a valuable source of information. The peak load on the ISIS target is about 1.75×10^{21} p/cm^2 (about 2 weeks of ESS-operation at 200 μA/cm^2 and for a stationary target).

An opportunity to do irradiations on a limited scale exists at the ISOLDE-facility at CERN: A 1 GeV-beam is delivered to the target in a 3 mm diameter spot and in pulses of about 3 μs length, containing 10^{12} protons per pulse. At present, the possibility is being studied, to place irradiation samples up to 10 mm thick in front of their target. However, due to their mode of operation, no more than a few times 10^{18} protons can be expected to be delivered to any particular specimen, leading, again, to a maximum load of less than 10^{20} p/cm^2. Nevertheless, it is planned to use this opportunity to study the effect of hydrogen and helium production in zircaloy for the mark 1 SINQ target. The specimens will be analyzed in the PSI-hot cells, where suitable equipment exists.

It should be noted that severe shock effects were observed in the hot ISOLDE-targets [18] sometimes leading to premature destruction in a matter of days, especially when molten metal (lead or lanthanum) was used. This effect is still a matter of investigation.

The most important source of information in the field of radiation effects on spallation targets to become available in the near future will, however, be SINQ itself. In order to take advantage of this opportunity, individual target rods shall be used as irradiation capsules. The methods for doing this must still be worked out in detail; one possible option is shown in Fig. 1: Selected rod positions are equipped with a threaded stub to which specially designed rods can be attatched. These might consist of an outer tube and some filling material to be investigated. For example, filling such tubes with lead or lead bismuth would allow investigation of the release of volatile products into a void space left inside the tube or to look at corrosion with potential container materials under the high radiation load. For this purpose the candidate container material should be placed in the hot centre of the Pb-Bi to make mass transport to cooler surfaces possible. Although safety issues will have to be assessed carefully in each particular case, the opportunities are manyfold. In this context it may be of interest to use different positions in the target, because, while the intensity and energy of the protons decrease as one goes deeper into the target, the fraction of the forward peaked high energy neutrons increases. Of course, due to the design characteristics of SINQ, one will always have a high flux of thermal neutrons.

In order to complement the data from microscopic and fracture analyses by information obtainable with neutrons, three of the neutron instruments at SINQ shall be equipped with the possibility to handle highly radioactive specimens: the radiography facility to determine the amount and distribution of hydrogen, the small angle facility to investigate large structural defects (precipitates, bubbles etc.) and a diffractometer to look for new phases, lattice strain, and texture. While the necessary shielding is relatively simple in the first two cases, which are essentially transmission measurements, construction of a time-of-flight Fourier diffractometer is contemplated to enable the full information to be obtained in a limited (backward) angular range.

5. STUDIES RELATING TO LIQUID METAL TARGETS

Although the rotating solid target as described in section 3.1.2 is the reference concept for the 5 MW ESS-target and will be studied in as much detail as possible, the parameter space to be explored is expanded in two ways: (a) the thermohydraulic and mechanical limits of a concept as followed for the 1 MW target are studied on a theoretical basis and options to realize a liquid metal target are investigated. As a starting point, 6 different configurations of a liquid metal target are considered:

- a coalescent configuration as in the SNQ-study
- an integrated target-reflector unit with vertical beam insertion tube [16]
- a stationary window target (SINQ-type) with beam insertion from underneath
- a rotating window concept as briefly outlined in section 3.2
- a target with horizontal beam injection through a stationary window
- an open surface flowing target with inclined beam injection

Theoretical studies relating to various feasibility problems will be used to eliminate those concepts, for which a solution cannot be found to any one of these questions.

These topics include:

- Volatile product control

- Thermal hydraulics and heat removal under variable load conditions
- Flow control and prevention of solidification
- Effect of short pulses on structural materials and flow stability
- Structural materials for the different load situations.

Problems of less fundamental nature such as general handling, neutronics, control of accident scenarios and implementation costs will be treated for those concepts surviving the first round to select a candidate concept for more detailed elaboration.

Much of the information obtained during this work will be of direct significance to the question, whether and how a liquid metal target can be implemented for SINQ and what the benefits of such a target over an optimzed solid target would be. It is also expected to provide guidance to the question, in what ways the research options provided by the SINQ rod target shall be exploited.

References

[1] J.M.Carpenter and A.G. Hins "Experience with IPNS Targets" Proceedings ICANS-XII, Abingdon 1993 Rutherford Appleton Report 94-025 (1994) p. T1-T11

[2] T.O. Brun private communication

[3] G.M. Allen, T.A. Broome, M.A. Clarke Gayther, and C.W. Planner "Measurement of Cooling Characteristics of the ISIS Tantalum Target" Proceedings ICANS-XII, Abingdon 1993 Rutherford Appleton Report 94-025 (1994) p. T12-T19

[4] G.S. Bauer, "SINQ- Status Report Oct. 1990" Proc. ICANS-XI, Tsukuba, 1990 KEK-report 90-25 (1991) p.41-60

[5] H. Lengeler, "Proposals for Spallation Sources in Europe"; paper presented at EPAC-94

[6] G.H. Rees, "Integrated Design Issues on High Output Current Proton Rings", paper presented at EPAC-'94

[7] J.M. Carpenter, R.K. Crawford, R. Kleb and A.E. Knox "Conceptual Design of the Target Stations of the IPNS Upgrade" Proceedings ICANS-XII, Abingdon 1993 Rutherford Appleton Report 94-025 (1994) p. T 95-T 104

[8] G. Heidenreich and G.S. Bauer, "The PSI-SINQ Target Development Programme"; in PSI-Proceedings 92-03 (1992) p. C1

[9] G.S. Bauer, "The general concept for a spallation neutron source in the Federal Republic of Germany"; Atomkernenergie-Kerntechnik 41 (1982) p.234-242

[10] H. Conrad, "Target-Moderator-Reflector Assembly for a High Power Pulsed Spallation Neutron Source"; Proceedings ICANS-XII, Abingdon 1993 Rutherford Appleton Report 94-025 p. T61-T70

[11] G.J. Russell, C.D. Bowman,E.R. Whitaker, H. Robinson, and M.M.Meier "LANSCE high power (200 μA) target-moderator-reflector-shield" Proceedings of the Eighth Meeting of the International Collaboration on Advanced Neutron Sources, report RAL-85-110 (1985) p.272

[12] J.S.Fraser and G.A.Bartholomew, "Spallation Neutron Sources"; in Neutron Sources for Basic Physics and Applications S. Cierjacks (ed) Pergamon Press, Oxford, New York (1983)

[13] G.S. Bauer, H. Sebening, J.-E. Vetter, and H. Willax (eds.) "Realisierungsstudie zur Spallations-Neutronenquelle" report Jül-Spez-113 and KfK 3175 Kernforschungsanlage Jülich und Kernforschungszentrum Karlsruhe (1981)

[14] F. Atchison and G. Heidenreich, "A Solid Target for SINQ based on a Pb-Shot Pebble-bed"; Proc. ICANS-XI, Tsukuba, 1990 KEK-report 90-25 (1991) p.551-568

[15] E.I. Yefimov and D.V. Pankratov "Contamination of Beam Transport System with Polonium in Accelerator-Based Plants with Liquid Metal Flow Target without Window" preprint, private communication

The Physics Design of Accelerator-Driven Transmutation Systems

Francesco Venneri
LER-ADTT, Los Alamos National Laboratory
Los Alamos, NM 87545 USA

Abstract. Nuclear systems under study in the Los Alamos Accelerator-Driven Transmutation Technology program (ADTT) will allow the destruction of nuclear spent fuel and weapons-return plutonium, as well as the production of nuclear energy from the thorium cycle, without a long-lived radioactive waste stream. The subcritical systems proposed represent a radical departure from traditional nuclear concepts (reactors), yet the actual implementation of ADTT systems is based on modest extrapolations of existing technology. These systems strive to keep the best that the nuclear technology has developed over the years, within a sensible conservative design envelope and eventually manage to offer a safer, less expensive and more environmentally sound approach to nuclear power.

SUMMARY

When a medium-energy intense particle beam interacts with a heavy metal target, neutrons are produced that are thermalized and multiplied in a surrounding moderating blanket containing fissile and fertile material. A neutron production of over 25 neutrons per incident particle per GeV is possible from such targets, with a multiplication of these neutrons by a factor of 10 to 20 in the subcritical blanket. Electricity is generated from the heat released by the fission processes, and a small part (between 10% and 15%) is used to drive the accelerator. A large excess of electric power is therefore available to the grid.

The basic elements, common to all the various ADTT systems, are a flowing lead spallation target driven by a GeV-class proton accelerator and a totally enclosed (pool-type) molten salt graphite moderated blanket.

The use of molten salt fuel allows the adoption of rather straightforward on-line fuel preparation (front-end) and cleanup (back-end) processes. Because no solid fuel extraction and refabrication is involved, these processes, under development at Los Alamos, do not introduce extraneous waste streams and have substantial proliferation and diversion barriers. Molten salt fuels also allow the attainment of substantially more powerful "passively safe" units, capable of unattended handling of loss of coolant transients, than possible with solid fuels, and owing to their high operating temperature and low pressure, they can achieve high thermal-to electrical efficiencies, well exceeding those of current light water reactor designs.

Thermal-subcritical, accelerator-driven systems can achieve safety from criticality accidents and have a neutron balance comparable to that of fast systems to enable them to perform the transmutation of the long-lived fission products. They also allow the complete burn of any nuclear fuel without reprocessing and, in the case of a thorium cycle, the full utilization of the fertile fuel without the use or production of enriched materials. Proliferation and diversion risks can be addressed effectively. End-of-Life inventories can be stored on-site as low level waste. As an example, the Accelerator Driven Energy Producer, based on the thorium cycle, is presented in some detail.

[16] G.S. Bauer, "Advanced Spallation Sources; Scientific Opportunities and Technical Feasibility" in "Advanced Neutron Sources 1988"; D.K. Hyer, ed. Proc ICANS-X, Los Alamos, 1988 Inst. Phys. Conf. Ser. 97 p.625-642 Bristol and New York (1989)

[17] Y. Takeda and W.E. Fischer "Thermofluid dynamics of liquid metal target of SINQ" Proc. ICANS-XI, Tsukuba, 1990 KEK-report 90-25 (1991) pp. 492-507

[18] J. Lettry, private communication

[19] W. Lohmann "Materialprobleme im Targetbereich" in "Realisierungsstudie zur Spallations-Neutronenquelle", Band II, p. A371 - A399, G.S. Bauer, H. Sebening, J.-E. Vetter and H. Willax (eds.) KFA Jülich and KfK Karlsruhe (1981)

THE IMPACT OF ADTT

Nuclear systems under study in the Los Alamos Accelerator-Driven Transmutation Technology program (ADTT) will allow the destruction of nuclear spent fuel and weapons-return plutonium, as well as the production of nuclear energy from the thorium cycle, without a long-lived radioactive waste stream. In the area of Global Plutonium Inventory, ADTT can phaseout production and eliminate world inventory of commercial plutonium from reactors in 30 years; excess weapons plutonium can be eliminated concurrently [1]. In the area of Nuclear Energy Production, ADTT can provide an alternative to conventional nuclear reactors and allow the complete utilization of fertile fuel (thorium) without excess breeding or the use of enriched material at any time in the cycle [2]. Finally in the area of Nuclear Waste Management, ADTT systems can drastically reduce the requirements for long-term storage of radioactive waste [3]. The same general ADTT nuclear design can be used in all three of these applications. ADEP (accelerator-Driven Energy producer) is a thorium based energy producer, ATW (Accelerator Transmutation of waste) is fueled by reactor spent fuel, ABC (Accelerator Based Plutonium Conversion) burns weapons-return plutonium. All these systems produce electricity and short-lived or stable fission product isotopes only (Fig.1).

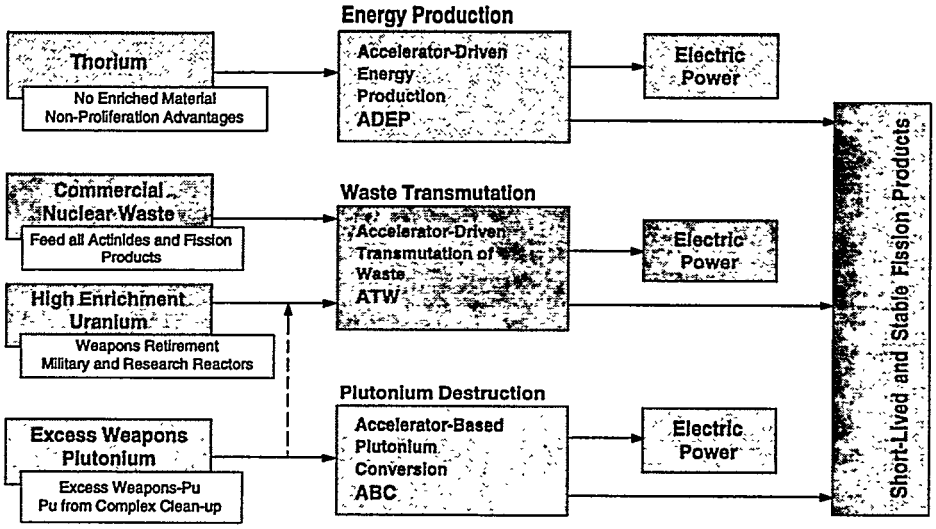

Figure 1. *ADTT systems based on the same technology can use thorium, commercial nuclear waste, highly enriched uranium and excess weapons plutonium to produce energy.*

The subcritical systems proposed by the ADTT program represent a radical departure from traditional nuclear concepts (reactors), yet they strive to keep the best that the technology developed over the years, within a sensible conservative design envelope.

OBJECTIVES OF ADTT

The Los Alamos ADTT concept is aimed at fulfilling the following 8 goals:

1) Can burn 100% of its fuel, any fuel, to produce energy
2) Does not require fuel enrichment, extraction or refabrication
3) Does not build up plutonium as it produces power
4) Can destroy its waste as well as previously generated waste
5) Offers substantial enhancements to safety
6) Is diversion and proliferation resistant
7) Does not cost more than alternative nuclear concepts
8) Does not require technological leaps of faith

Traditional nuclear reactor technology, based on critical, solid-fuel systems, has clearly never been able to meet all these objectives. However justified, the two assumptions of solid fuel and criticality have effectively negated the achievement of the 8 objectives. The adoption of the accelerator drive (subcritical systems) and of liquid fuel effectively widens the performance horizon of nuclear systems, to the point that all 8 objectives can be readily achieved.

The general features of the ADTT system proposed by the Los Alamos National Laboratory (LANL) group are shown in figure 2. The use of molten salt in the moderated blanket allows high thermal-to electrical efficiencies, exceeding those of current water-cooled reactors. A large excess of electric power is therefore available to the grid at rates that could be competitive with standard nuclear power costs.

In this system the molten salt fuel, a mixture of lithium, beryllium and actinides fluorides, flows through a matrix of moderating graphite. Power generation occurs within the molten salt in the moderated region. The fission products isolated for transmutation are placed in the higher flux regions near the center of the blanket, where they can absorb the extra neutrons necessary to convert them into stable species.

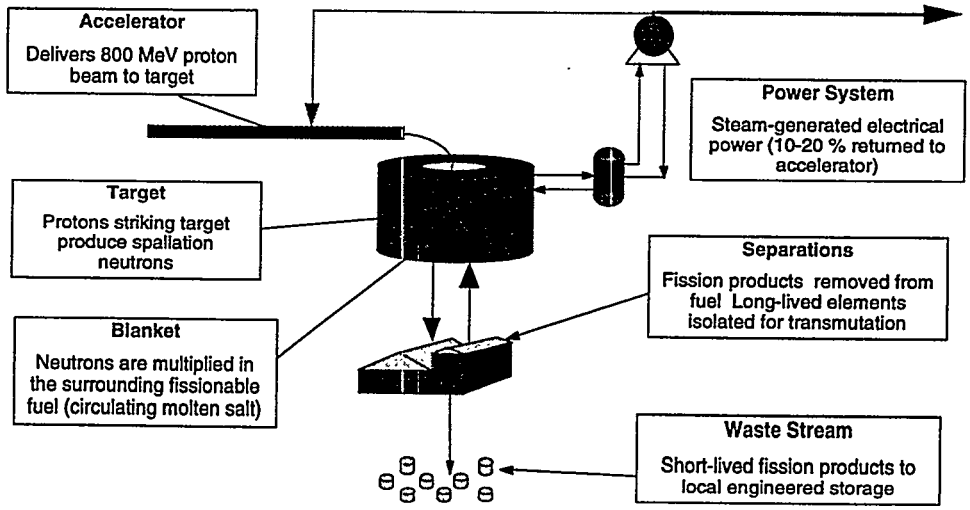

Figure 2. *Top-level illustration of the components of an ADTT system. ADTT is a closed nuclear system. A medium-energy intense particle beam (protons or deuterons, 10-20 mA at 500-1000 MeV) interacts with an appropriate target producing spallation neutrons that are thermalized and multiplied in a surrounding moderating blanket containing fertile and/or fissile material in liquid (molten salt) form. A neutron production from the target is 25 neutrons per incident particle per GeV, with further multiplication by a factor of 10 to 20 in the blanket. Power production is on the order of 25 MW (thermal) per MW of beam. Electricity is generated from the heat released by the fission processes, and a part (between 10% and 15%) is used to drive the accelerator. Physical type separation processes are used to keep the fuel clean of fission products. Since no isolation of actinides is required, nor fuel refabrication, the cleanup process is relatively simple and can be implemented in small size plants.*

The system described in this article (see fig. 3) is driven by a 15 mA beam of 800-MeV protons and operates at 500 MWt with a k_{eff} of 0.95. The subcritical margin is sufficient to insure subcriticality in all conceivable, off-normal conditions. The low power density of the system allows for a passively safe design, where the after-heat cooling can be handled by purely passive means in case of emergencies. By completely consuming the nuclear fuel and the most troublesome fission products, this system could obviate the need for transport and geological storage of the long lived actinide species and fission product waste.

The operation in a driven subcritical mode eliminates the possibility of a criticality accident and provides quick and absolute shutdown by simply turning off the accelerator. On a more

fundamental level the accelerator combines the traditional reactor control functions of control rods, burnable poison and chemical shim in one streamlined mechanism which is flux- and burnup-independent. Coupled with the features of a liquid fuel system with fuel cleanup, this allows the full utilization of the fuel without actinide extraction and excess breeding. The low-level and short-lived radioactive waste stream from power operation of these systems would be placed in near-surface managed storage at the power plant sites.

BASIC DESIGN CHOICES

Graphite moderated thermal neutron spectrum

Fast systems have potentially a better neutron economy than thermal systems, because of the better ratio of fission to capture cross-sections in actinides. However the extra (fast) neutrons are not very useful for fission product transmutations (because of the very low cross section) unless they are thermalized. We maintain that it may not be safe to have thermalized neutrons in fast systems. Therefore, while fast systems can burn all actinides, they cannot straightforwardly destroy fission products. The accelerator drive introduces the extra neutrons missing from thermal-spectrum systems, effectively improving the thermal system neutron utilization to the point where there is very little difference between fast reactors and thermal subcritical systems in terms of neutron economy; that is, they can use the same nuclear fuel.

Thermal systems however have much larger fission cross sections, and therefore can work

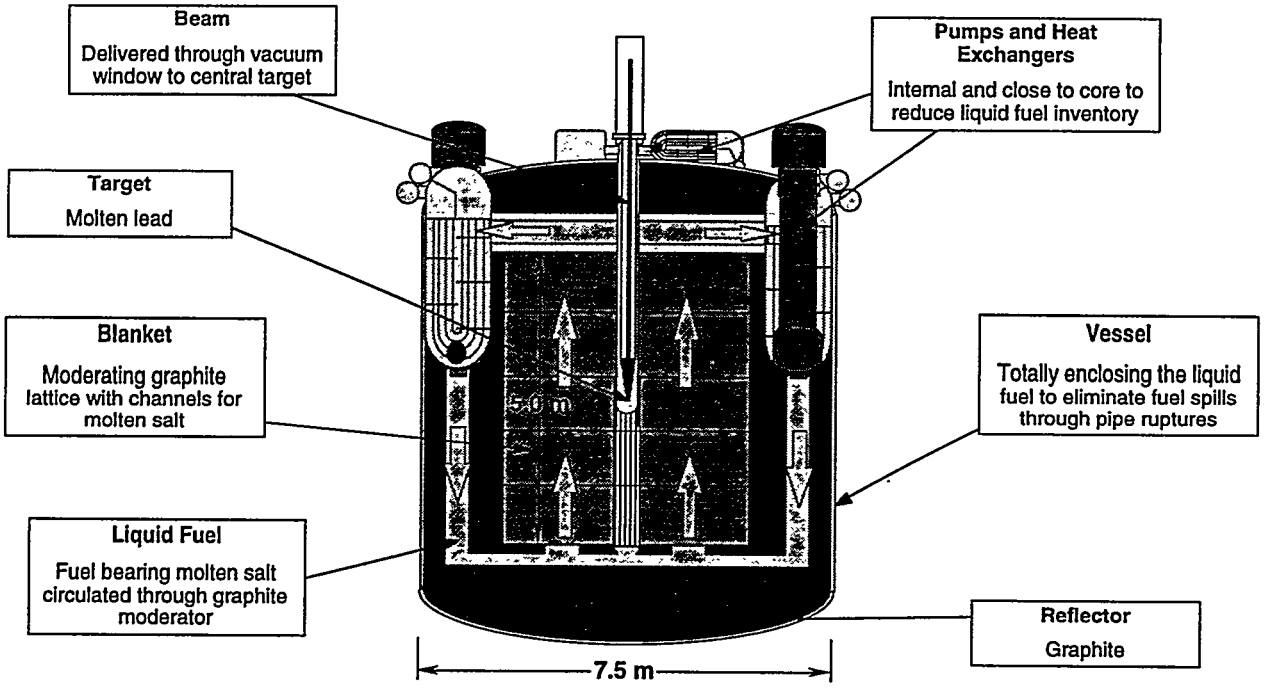

Figure 3. *The prototype 500 MWt ADTT molten salt blanket. This blanket can be used for all the ADTT applications (ADEP, ATW, ABC). Graphite-moderated and fueled by molten salt, the ADTT blanket improves on the 1960's Oak Ridge molten salt reactor concept, by incorporating the many design improvements introduced by the newer liquid-metal reactors "pool" designs.*

with much lower nuclear inventories and do not require enriched fuel to start. Looking at the thorium system, a thermal system might have an inventory of 100 kg of fissile uranium, whereas a fast system of the same size might require 10 tons of the same material. A thermal system driven by an accelerator can self-start in about 12 months, that is, drawing power from the grid a subcritical power system will produce enough uranium from thorium in one year to bring itself to full power, without having to use enriched start-up material. Based on its much larger equilibrium inventory, a fast system would require perhaps 100 years to do the same.

Fast systems operate in a region where absolute cross sections are very small. An accident that introduces a moderator into the fuel or fuel into a moderator will increase the reactivity. Water, for instance or even silicon dioxide (sand) will drastically increase the reactivity of fast systems fuels. The consequences of reactivity insertions in these systems can be quite severe.

Thermal systems on the other hand operate in an optimum combination of geometry and moderation so that cross sections are highest. An accidental departure from the operational configuration will likely lead to a less critical configuration.

While thermal systems can be conceived as inherently safer than fast systems, the compelling rationale to develop critical fast systems (fast reactors) has always been their superior neutron economy, which allows these systems to breed autonomally. Now, on the other hand. the accelerator drive can supply the extra neutrons needed to improve the neutron economy of thermal systems at a cost that is not too high, and therefore effectively provides ADTT systems the advantages of the fast spectrum while at the same time keeping the good safety and low inventory features of thermal systems.

Graphite is chosen as the moderator because of its high temperature compatibility with the liquid fuel choice, fluoride molten salt. In order for the graphite to last the entire life of the blanket, the power density is limited to 5-10 w/cc in the moderated region. Because the fuel is kept clean, even at such low power densities the neutron flux is anticipated to be in the range 10^{14} to 10^{15} n/cm^2s depending on whether a thorium bearing fuel is used or a pure actinide fuel.

Liquid fuel (Molten Salt)

The choice of liquid fuels (and molten salt in particular) for ADTT systems is based on the substantial advantages in the following 5 areas :

1)	Safety	Low-pressure operation
2)	Cleanup	On-line removal of fission products
3)	Complete Burn	No fuel fabrication and refabrication needed
4)	Efficiency	High temperature liquid
5)	Separations	Non-intrusive physical separations possible

Molten salts as reactor fuels and as coolants have been under study and development for over 40 years, and their chemical, physics, and irradiation properties are excellent. The Molten-Salt Reactor Experiment (MSRE) at ORNL, which was shut down in 1970 after about five years of very successful operation, contributed significantly to molten-salt reactor technology. The progress of the molten salt design study is covered in the entire February 1970 issue of Nuclear Applications and Technology, devoted to a review of molten salt reactor technology and to a description of a conceptual design for an molten salt breeder reactor [4]. The active work at Oak Ridge on the Molten Salt Breeder Reactor (MSBR) was phased out after the Liquid Metal Fast Breeder Reactor

(LMFBR) was selected as the choice breeder. The last published results on molten salt technology development at Oak Ridge date back to the late 70's. The successful operation of the Molten-Salt Reactor Experiment and the substantial amount of research and development accomplished on molten-salt reactor materials and processes at Oak Ridge indicate that with straightforward extensions in a few specific areas, a prototype Molten-Salt Accelerator-driven Transmutation Plant could be successfully constructed and operated.

The presence in the ADTT concept of the accelerator and separation subsystems, necessarily net drains on the energy balance, requires that the best possible efficiency be obtained in the power conversion process. Since the thermal to electrical efficiency is strictly related to the maximum temperature that is reached in the cycle, the liquid fuel should be able to operate at high temperatures without degradation of its physical and chemical properties. Safety concerns also require the use of liquid fuels that can reach high operating temperatures at low pressure. Molten fluoride salts can operate at temperatures well above 600 C at near-atmospheric pressure. This allows for the economical construction of rather large, low pressure vessels that can be all-enclosing, with integral pumps and heat exchangers, so that ducts and side-vessel penetrations can be eliminated, therefore reducing to extreme unlikelihood the event of a salt spill. In addition, since all the volatile fission products are continuously released and removed from the liquid fuel, and the others dissolved in the fuel itself are also removed, the source term important under severe accident conditions is substantially reduced vis-a-vis solid fuels.

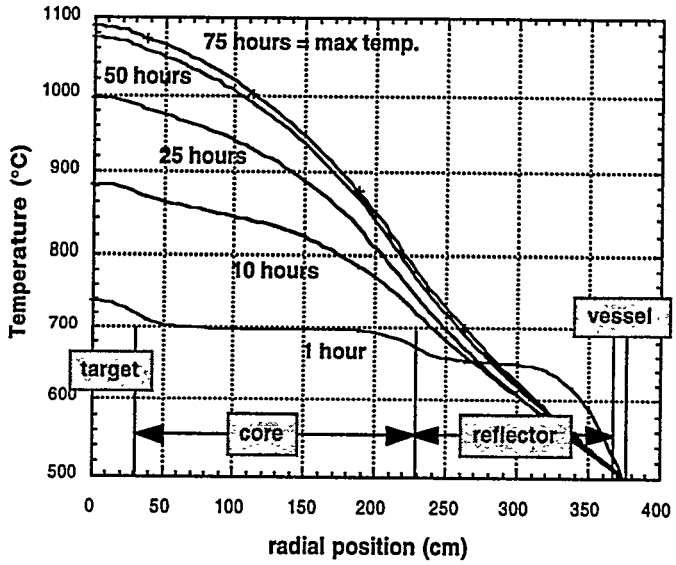

Figure 4. Temperature rise of a prototype 500 MWt ADTT blanket in a loss of coolant accident. Assuming only convective cooling and a passive heat removal mechanism, the maximum temperature is reached in 75 hours.

The substantially more centrally peaked flux of accelerator driven systems in comparison to reactors also favors the use liquid fuels, where the fuel is uniform and all potentially unstable build ups of poisons or excess fissile material in special locations are completely eliminated.

The use of molten salt fuel, as opposed to solid fuels or liquid slurries, allows the adoption of rather straightforward on-line fuel preparation (front-end) and cleanup (back-end) processes. Because no fuel partitioning and refabrication is involved with molten salt use, these processes, under development at Los Alamos, do not introduce extraneous waste streams and have substantial proliferation and diversion barriers.

Molten salt fuels also allow the attainment of substantially more powerful "passively safe" units than possible with solid fuels. The choice of power per unit is driven by the criterion that the unit should be passively safe in the event of a coolant failure, without need for salt drainage and removal. The 500 MW level per unit discussed later in the paper is a very conservative figure that might be the size of a first demonstration-type unit. Differing from solid fuel systems, molten salt systems in fact have a heat source that is distributed throughout the large blanket volume. There-

fore any residual decay heat can be removed more easily than for solid fuel systems, where the heat source is concentrated at the center of the core, where it is most difficult to remove when active cooling fails. The natural convection of the liquid fuel and the on-line removal of the fission products throughout operation also help considerably. A transient loss of coolant scenario is simulated in figure 4 for the 500 MW prototype module, which indicates a maximum temperature of 1100 °C reached 75 hours into the transient. We have performed calculations showing that the power per unit can be as high as 800 MWt and still satisfy the passive safety requirement that the salt not be drained in a loss of coolant accident. A much larger unit (3000 MWt) would require some means of draining the salt out of the blanket into a special passively cooled reservoir in the event of a coolant failure. Drainage in this case could still be obtained in a passive way through the use of melt plugs. Such a unit would have a power rating of 1200 MWe to the grid.

ADTT safety features

Because of their non-conventional design choices, ADTT systems have very important inherent safety features [5]. Design characteristics, such as deep subcriticality, low power density, low operating pressure, no enriched fuel feed, no vessel penetrations and a distributed heat source, translate into inherent safety features, such as: no possibility for overheating and core damage due to decay heat in emergency situations, no possibility for criticality due to feeding error, no possibility for salt leaks. Subcritical systems are obviously slower to respond to reactivity insertions than critical systems, to the point that it is conceivable to maintain positive temperature coefficients in subcritical systems. The negative power feedback into the accelerator from the electricity extracted from the blanket should also insure that in the event of loss of coolant the accelerator/target system will not continue to pump neutrons into the blanket.

High-current Accelerators

The high-power accelerator technology required for ADTT has been under continuous development for the past three decades at Los Alamos. Accelerators with up to five times more current than that required for the ADTT system described here have been proposed for the production of tritium for defense applications. These accelerators were reviewed by the Energy Research Advisory Board of the U.S. Department of Energy, subsequently by the JASONS, a scientific body which reviews proposed high technology programs of the U.S. Department of Defense, and were also evaluated by the General Accounting Office of the U.S. Congress. The result of these reviews was a general endorsement of the proposed accelerator technology with the provision that appropriate pilot and demonstration steps be made along the way towards the construction of a full scale facility [6].

The average power needed for the very largest of systems we propose (6 x 500 MWt), requires an accelerator average power of some tens of megawatts (100 mA beam). This can only be achieved with a linear accelerator. However, the highest power operational linear accelerator anywhere, (LAMPF), operates at around one megawatt (1 mA at 800 MeV). At first this seems like a very large extrapolation, but it is not nearly so bad as it appears. Firstly, in LAMPF, only every fourth bucket is filled with beam and so filling every bucket (if we use funneling) or every other bucket (if unfunneled) immediately gives a factor of four in average power respectively. Also LAMPF being a pulsed machine operating at 10% duty factor, going to 100% duty factor gives a factor of 10. The charge in each microbunch can be increased by about a factor of four and still stay

well within the stable space charge regime. Therefore an improvement by a factor of 160 (4x10x4) is possible by simple extension of proven technologies, so that up to 150 mA 1GeV LINACs can be built based on current technology [7]. Figure 5 shows a schematic view of a ADTT linac capable of driving 6 of the prototype 500 MW modules.

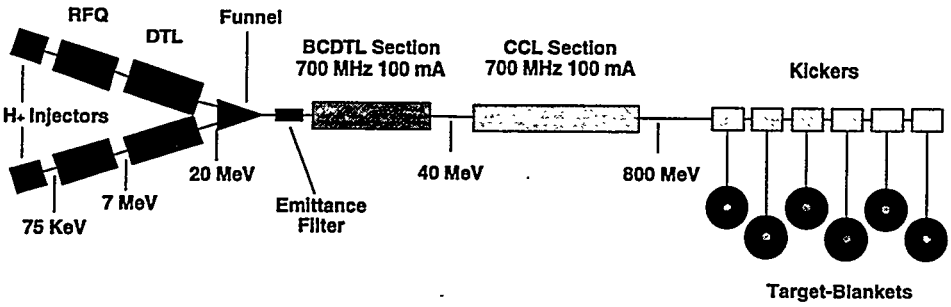

Figure 5. The ADTT linear accelerator design for multiple blankets. Single blankets of the size described in this paper (500MWt) would require smaller accelerators (15-20 mA, 800MeV) which could be compact cyclotrons.

For circular machines the situation is a little different. The highest average power machine at PSI operates CW at about. PSI (the Paul Scheerer Institute in Switzerland) believes that its machine can go to about 1 to 2 mA without major changes, but to go to 10 mA would require a new design, which could be the Intermediate Separated Sector Cyclotron, presently proposed and studied by Rubbia [8]. Rubbia's design of a very compact circular machine in particular promises to become an efficient and inexpensive driver for the individual subcritical systems later described in this paper.

Primary issues for the ADTT accelerator are the efficiency, reliability and maintainability appropriate to an industrial setting. Experience with the use of an accelerator in an ADTT application can be readily gained using the existing accelerator at Los Alamos National Laboratory (LAMPF). As is, LAMPF is capable of reliably providing up to 1 mA of 800-MeV proton beam to a scaled down target-blanket similar to the one described here. LAMPF could thus drive an experimental deeply subcritical facility with a multiplication of 5 to a fission power level of about 5 MWt, a sufficient level for a thorough testing of the ADTT concept [9]. With modest improvements, leading to an increase in reliable current to about 2 mA, LAMPF would be able to drive a full size prototype module (Keff=0.95, multiplication=20) to a fission power of 40 MW, sufficient for a full engineering testing of all the major components. With additional expenditures, small compared to the cost of a new accelerator, the LAMPF current could be increased to perhaps as much as 20 mA with a corresponding blanket power level easily exceeding 500 MWt, enough to power one of the prototype modules later described in the paper.

Liquid lead target technology

The function of a target in ADTT systems is the conversion of high energy (>500 MeV) protons to lower-energy (<20 MeV) neutrons and the delivery of these neutrons to the blanket in a useful manner. The conversion is achieved through the process of spallation, which is a simple way to describe the complex phenomena that take place when high energy protons hit a target. Through a series of internuclear cascades, neutrons and other charged particles are stripped off the target nuclei. Eventually neutrons will escape and propagate into the surrounding multiplying blanket. The ideal target should be simple in construction and operation, able to produce neutrons efficiently and to leak them to the surrounding blanket with minimal absorption losses.

At the high power densities generated by the beam currents proposed for ADTT systems,

liquid metal targets offer important advantages in practical implementations over solid targets. Besides the obvious ease of heat removal from liquid targets, there is no structural damage limit to the life of the target material, and the use of liquid targets would allow the primary target material to be reused beyond the structural life of the container material. This minimizes residual waste and maintenance time. High atomic weight, low melting point metals or alloys are needed. Among the low melting point heavy metals, lead and bismuth have very low neutron absorption cross-sections and therefore can be arranged in simple monolithic configurations. The lead-bismuth eutectic (LBE) has a lower melting point and operating temperature than either lead or bismuth and therefore should be favored in terms of structural consideration. The bismuth in the eutectic however creates greater materials compatibility problems with the structural container and produces radioactive polonium. Either lead or lead-bismuth eutectic would provide an adequate solution to the ADTT spallation target [10].

The liquid lead (or LBE) target used for the ADTT design is inserted vertically into the blanket from the top. The reasons for this choice are simple. A horizontal target would require very heavy shielding against forward directed high energy neutrons. It would also introduce the risk of a radioactive molten salt spill from a side penetration into the blanket. Vertical insertion of the target from the bottom would also introduce penetrations in the bottom part of the blanket or the presence of permanent metal structures in the center of the blanket where neutron damage is most severe. In the vertical insertion from the top, a window is placed upstream of the target along the beam path and it is of traditional design. Past the window, the proton beam enters a hydrostatic helium plenum which keeps the lead surface down in the bottom of the target. The helium region is 300 cm long and takes the beam with negligible loss into the central region of the subcritical blanket. There the beam hits the lead free surface and slows down in a 90 cm long liquid lead (or LBE) volume. The beam stops in this length, and also (n,xn) neutron multiplication reactions happen in this region. There would be no window between the beam and the lead. This configuration avoids the most serious cooling problems of a hot window at the center of the blanket. The liquid lead flows down on one side of the split pipe, across the target area receiving the beam directly on its free surface and then flows up on the other side (see Fig. 6).

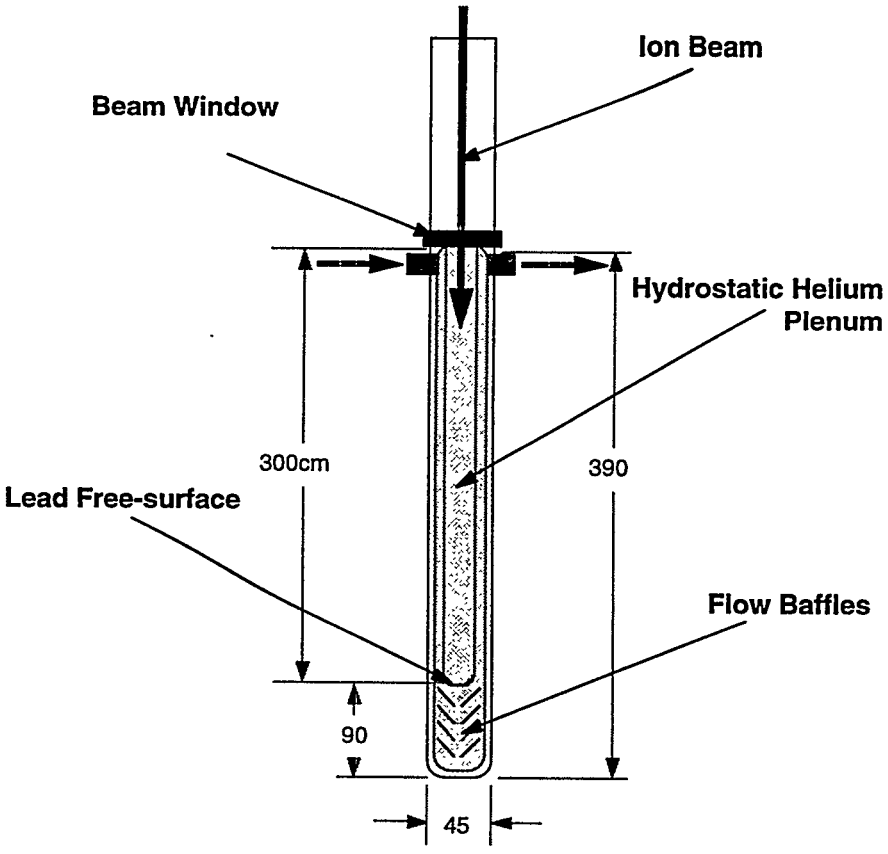

Figure 6. *A schematic view of the prototype ADTT lead target*

The target is a to-

tally enclosed structure, bolted on the lid of the blanket and capable of being rapidly inserted and extracted from the blanket. The container structure has a double wall: the inside is lead compatible HT-9 alloy, the outside is made of molten salt compatible Hastelloy-N. Due to radiation damage to the steel, it is anticipated that the structure of the target most exposed to the neutron flux will have to be replaced as often as every 1-2 years. The same lead is however recycled through the life of the plant and beyond to the next ADTT system.

FUEL PREPARATION AND CLEANUP

It has long been the policy in the US not to promote the reprocessing of spent fuel. If by fuel reprocessing we mean the extraction and refabrication of the actinides in spent fuel to extract new power and close the nuclear fuel cycle, then ADTT provides an answer to that seemingly impossible task: a closed nuclear cycle that does not require reprocessing. What ADTT requires are much simpler processes: Fuel Preparation at the front-end and On-line Cleanup at the back-end.

Front-end Processes (ATW)

Front-end processes in the Accelerator Transmutation of Waste (ADTT-ATW) concept are restricted to the removal of the undesireable uranium and zirconium, which are present in large amounts in the spent fuel feed to ATW systems. Uranium in particular needs to be separated from the rest of the feed, as the continued production of plutonium from neutron captures in uranium would be entirely undesirable in the course of the transmutation process.

The volatilization of fluorides is a well tested way to separate the uranium and the zirconium from the spent fuel. The proliferation risks of this approach however might not be acceptable, in that there are no strong barriers to the extraction of plutonium and other actinides from the fuel in this process. Very strong proliferation barriers are instead present in a second process, presently under investigation at Los Alamos: uranium electrowinning [11].

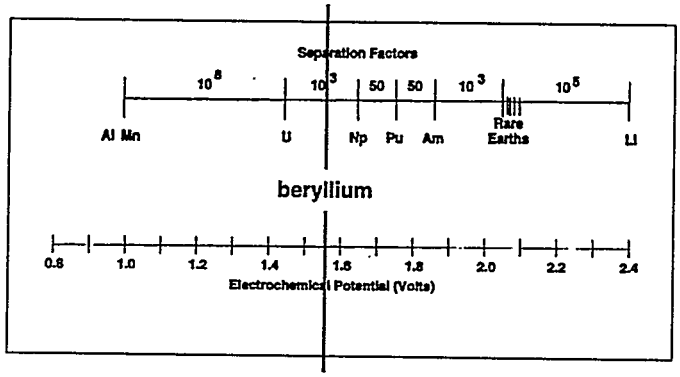

Figure 7. Electrochemical potential scale of the elements, showing the favorable position of beryllium, between uranium and the rest of the actinides. The presence of substantial amounts of beryllium in the salt prevents the isolation of plutonium or any of the higher actinides after uranium has been extracted.

The uranium electrowinning uses favorable differences in electrochemical potential to extract uranium and zirconium from spent fuel (see Fig. 7). If successfully implemented, it will allow the extraction of uranium from spent fuel without separation of plutonium and fission products, which is the goal of the fuel preparation processes for ADTT systems.

Briefly described, the process consists of three main steps:

First, the spent fuel rod is fluorinated in a stream of HF/H_2 so that fluorides are produced. Fluorination in HF/H2 prevents the formation of volatile hexafluorides.

Next, the fluorides are dissolved in molten Li_2BeF_4.

Finally, a beryllium anode is inserted in the molten salt and all the fluoride species less stable than BeF_2 will be reduced at the cathode.

Since beryllium is in between uranium and all the other actinides in the electrochemical potential scale, after the deposition of the uranium, all of the beryllium would have to come out of solution before any of the actinides including plutonium, or the rare earths could be isolated. Since the salt mixture after the uranium has been extracted is typically 74:24:2 of Lithium, beryllium and actinide (plus fission product) fluorides, the presence of beryllium is a strong barrier to the extraction of actinides or rare-earths fission products during the spent fuel preparation step. The species that remain in the molten salt will be Np, Pu, Am, Cm, and lanthanide fluorides which can be fed directly into the molten salt blanket. Fission products (rare earths) stay in solution with the actinides in the ATW feed (they are removed continuously at the back-end).

Back-end Processes (ATW, ABC, ADEP)

No actinide separation from the fuel is needed for ADTT operation and all actinide isotopes are fissioned and used for their energy content. The fission products, however, are continuously removed from the fuel. Short-life fission products can be left to decay naturally outside the blanket. Those with a longer half-life (>30 years) and which are of concern for long term storage, are transmuted into nonradioactive or short-lived nuclei through neutron capture.

The on-line cleanup processes envisioned for ADTT systems should not require introduction of external chemical agents.

Fission products in molten salt can be divided in three broadly different but roughly equivalent categories, and for each of these there is an appropriate physical means of cleanup. Volatile fission products and noble gases have low boiling points and tend to come out of the molten salt very easily. Removal of these volatile species and noble gases from the molten salt is obtained by helium flow or sparging. Because of the fast time scale of the sparging process, we call this "one-minute separation". Noble and semi-noble metals have low solubility in the salt and will plate out on internal surfaces. The process was observed at Oak Ridge in the molten salt experiment [4], and we plan to actively exploit it with the incorporation of passive extraction cells in the molten salt flow path. Again referring to the relevant time scale, these are the "one-hour separations". The remainder of the fission products, including the rare earths have good solubility in the salt and will tend to build up in concentration and stay in solution. Removal of lanthanides and other non volatile species will be done using liquid centrifugation and precipitation ("one-month separations"). Again the point should be emphasized that the ADTT back-end processing only requires fuel cleanup from fission products, not actinide isolation and extraction.

Helium Sparging of volatile fission products

Volatile fission products will be carried away by a flowing stream of helium at the top (free) surface of the molten salt. The efficiency of the removal might be improved by "sparging", that is by injecting helium bubbles in the molten salt stream [4]. These bubbles act as collectors of the gaseous fission products. Again the fission products are removed by the flowing helium stream at the top plenum. After extraction from the blanket the helium stream carrying the fission products undergoes fractional distillation processes to extract the different fission products at different temperatures according to their boiling point. Special care is dedicated to xenon and argon, which are collected on cold zeolites. If extraction from the blanket is effected promptly, there is the possibility of achieving separation of cesium isotopes from the fractional decay of xenon.

Electrolytic separation of noble and semi-noble metals

Electrochemical separation techniques are proposed for removing the "noble metals" fission products: Mo, Nb, Ru, Rh, Ag, Cd, etc. [12].

The electrochemical method has been used extensively to produce pure metals from oxide or halide feed materials that have been dissolved in a molten salt. In this application of the method, one is interested in purifying the molten salt and not in producing a pure metal. The electrochemical cell consists of a consumable anode, Zr or Be, which is placed in the molten salt and the "noble metals" are deposited on the cathode, a Ni rod. The fissile material, other actinides, and lanthanides remain in the molten salt. The reaction that describes the process is:

$$n\,Zr\,(s) + 4\,MFn\,(d) = n\,ZrF_4\,(d) + 4\,M\,(s)$$

where M is a "noble metal", n is the valence state of the "noble metal", and d refers to a fluoride species dissolved in molten Li_2BeF_4. The reaction is spontaneous because of the free energy difference between ZrF_4 and the "noble metal" fluorides. Therefore, in principle, the electrochemical cell can be operated in a passive fashion (i.e. no external source). Maintenance of this system involves the periodic replacement of the anode and cathode.

Molecular Centrifugation of soluble fission products

Molecular centrifugation uses the difference in molecular weight between carrier salt (light) fission product salt (medium) and actinide salt (heavy) to obtain effective separations of soluble fission products without recourse to chemical extractions [13]. The obvious consequence is the effective cleanup of lanthanides from fuel without acting on the chemically similar actinides.

Subjecting a liquid solution to large centrifugal fields will generate gradients of concentration increasing towards the outer edge of the spinning centrifuge rotor. These gradients and the speed at which they are attained are directly proportional to the square of the rotational velocity of the centrifuge and to the molecular weight of the solute. Other factors such as the solution viscosity and temperature also influence the process.

Centrifugal force can create solute concentration gradients in originally homogeneous solutions. The evolution of such processes is determined by the sedimentation coefficients and the mass diffusivities, which are predominantly dependent upon the molecular weights. A heavier solute will develop a steeper concentration gradient than a lighter solute. This leads to a relative enrichment of one solute in one section of the cen-

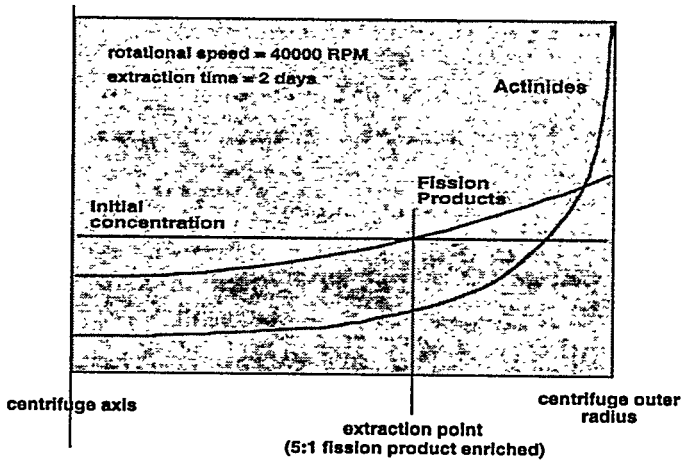

Figure 8. Working principle of cleanup centrifugation processes. Gradients of both light (fission products) and heavy (actinides) species are established. Note that at the extraction point the fission product-to-actinide ratio is higher than in the original feed, but the overall concentration of the salt has not changed.

trifuge with respect to the other. It is always possible to identify an extraction point in the radial concentration profile where there will be an enrichment in the concentration of the lighter solute with respect to the heavier solute or vice-versa (see Fig. 8).

The process can be used in liquid solutions of molten salt fuel to isolate and separate the fission products from the rest of the actinides. Since the process relies on physical properties and always operates in dilute solutions, it is capable of removing only the fission products from the fuel, regardless of their chemical affinity to the actinides and it will not give rise to extraneous waste streams. Very little of the actinides are ever disturbed and the process is benign from a proliferation and diversion point of view. Through a series of centrifugation stages, very high enrichments of light-to-heavy or heavy-to-light solute can be reached (>1000:1) without appreciably increasing the overall density of the solute in solution and therefore without concerns for precipitation or for non-ideal behavior of the solution constituents. The separated fission products can be concentrated in a final centrifugation stage to reduce the waste volume.

AN EXAMPLE: THE ACCELERATOR DRIVEN ENERGY PRODUCER (ADEP)

As an example of the ADTT concepts I will briefly describe the Accelerator-Driven Energy Producer concept. The design features discussed are very preliminary and by no means optimal .

The Accelerator-Driven Energy Production (ADEP) concept employs an accelerator to provide neutrons to a moderated multiplying blanket. This allows the breeding of fissile ^{233}U from thorium, the fission of the ^{233}U with consequent production of electric power, the concurrent transmutation of long-lived fission products wastes to stable or short-lived species and the burning of all actinide waste generated. Thorium is sufficiently abundant in the earth crust to allow electricity production for thousands of years at any foreseeable power production level.

Natural thorium is used as fuel and is completely utilized without excess breeding. All actinides generated during power production are fissioned and never removed from fuel. Unlike fast breeder reactor systems, new energy sites can be started without production and transportation of excess enriched nuclear fuel. Long-lived fission products are transmuted and the need for geological storage of waste drastically reduced. ADEP can fulfill all the promises of Controlled Nuclear Fusion using a reasonable extrapolation of current, proven technology.

When a thorium atom (^{232}Th) absorbs a neutron it is converted to an unstable thorium isotope (^{233}Th), which quickly decays into protactinium (^{233}Pa). In turn, the ^{233}Pa atom decays into ^{233}U with a half-life of 26 days. The nuclide ^{233}U has a large fission cross-section and a comparatively very small capture probability making it a very favorable fuel for nuclear energy production.

The thorium-uranium fuel cycle has two advantages over the traditional uranium plutonium cycle used in today's nuclear reactors:

1) The thorium-uranium cycle produces a very small amount of higher actinides (elements heavier than uranium), because of the small capture to fission ratio in ^{233}U and because of the presence of two other fissionable isotopes of uranium (^{235}U and ^{237}U) in the chain leading to plutonium and the other heavier actinides

2) The thorium-uranium cycle is regarded as safer than the uranium-plutonium cycle from a nuclear weapons proliferation standpoint, because of the presence of the hard-gamma emitter ^{232}U as a minor product of the cycle, and because of the possibility of straightforward isotopic dilution of ^{233}U with depleted or natural uranium in the feed or start-up fuel.

The thorium-uranium cycle has been extensively studied in the Oak Ridge Molten Salt Reactor Experiment (MSRE) and Breeder (MSBR) projects, and actually implemented in the origi-

nal High Temperature Gas Cooled Reactor proposed and built by General Atomic at Peach Bottom and Ft. Saint Vrain [14]. The conclusions of studies at Oak Ridge were that critical thermal breeders (reactor) could not breed fissile material in this cycle, unless the fuel could be kept painstakingly clean from fission product poisons and the protactinium precursor to ^{233}U could be promptly removed from the neutron flux and allowed to decay into ^{233}U. The use of the accelerator in ADEP largely eliminates these two problems and allows the thorium-uranium cycle to be exploited to its fullest in simple, practical systems.

The accelerator-driven spallation source supplements the number of available neutrons over that which can be achieved in a critical reactor by converting some of the electric power generated into neutrons. This increase in available neutrons allows ADEP designs to produce energy using only natural thorium as feed, without highly enriched fuels and without the chemical extraction of the protactinium precursor to ^{233}U, while at the same time transmuting the internally generated radioactive wastes. To do the equivalent functions, a critical reactor would require the use of enriched fuels, in excess of the breeding potential of the cycle.

What can ADEP systems transmute ?

ADEP systems can transmute all long-lived fission products ..... for a price. One concern with the geologic storage of radioactive waste is the possibility of migration out of the storage medium. In this regard, ^{99}Tc and ^{129}I are the most bothersome of the fission products. Fortunately, these isotopes have high thermal neutron capture cross-sections and are easily transmuted to stable ^{100}Ru and ^{130}Xe respectively. The next most important long-lived nuclide is ^{135}Cs; in this case, isotopic separation of the cesium nuclides is required before burning the ^{135}Cs, to make effective use of the neutrons in the transmuter. However, isotopic separation of ^{135}Cs and ^{137}Cs as well as ^{89}Sr and ^{90}Sr can be obtained naturally by radioactive decay in the ADEP system, exploiting the fast removal of their noble gas precursors from the liquid fuel. The small quantities of ^{126}Sn and ^{79}Se present among the fission products can also be readily transmuted. ^{90}Sr and ^{137}Cs are major components of the waste and are more difficult to transmute because of their very low thermal capture cross-sections.

The additional fraction of electricity needed to power the acceleration to accomplish the transmutation of key fission products is indicated in figure 9. In principle, the accelerator-driven neutron economy allows all of the long-lived fission products to be transmuted, but the value of performing the transmutation varies greatly among them and must be determined for each

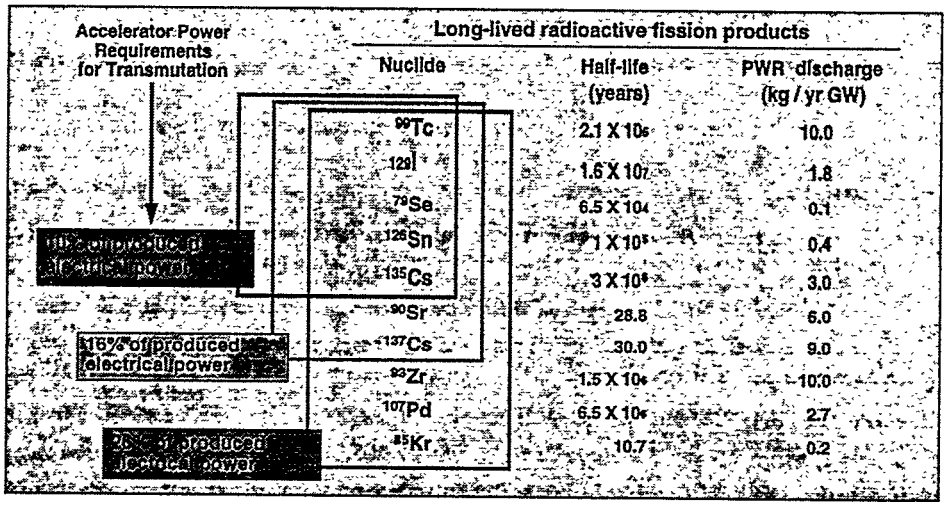

Figure 9. Fission product burning capabilities as a function of accelerator power . We think it is most appropriate to burn Technetium, Xenon,Selenium, Tin and ^{135}Cesium.

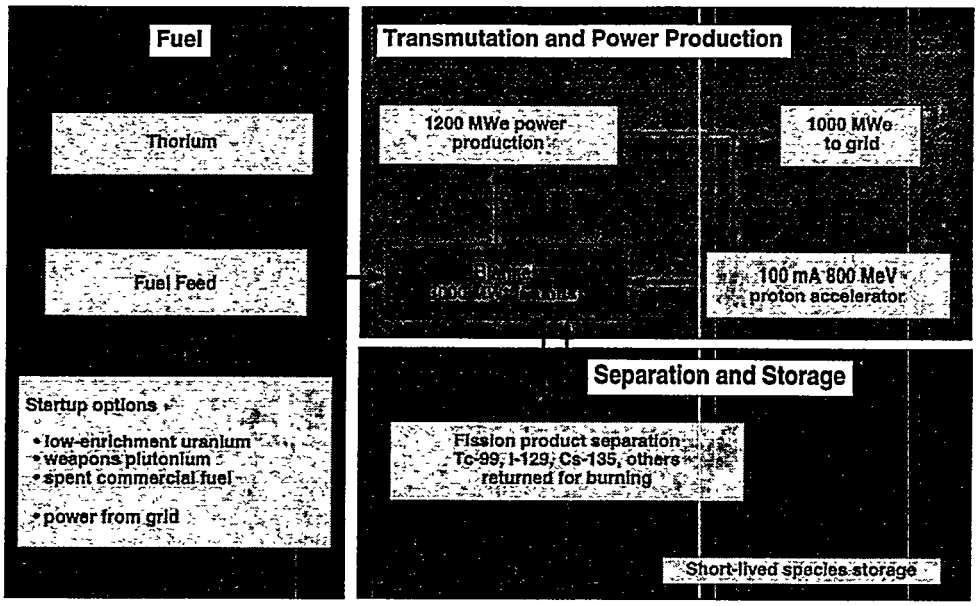

Figure 10. *General features of the ADEP system. Electricity is generated from the heat released by the fission process, and a part is fed back to drive the accelerator. While the system can be started with a variety of enriched materials, particularly interesting would be the option of starting the system purely from power from the grid. This would effectively enable ADEP to start and sustain a thorium breeding cycle without isolating enriched materials of any kind. Make-up thorium is continuously fed. back-end separations and transmutation of long lived fission products are performed concurrently. The back-end processing removes the fission products from the fuel and isolates the isotopes requiring transmutation (^{99}Tc, ^{129}I, ^{126}Sn, ^{79}Se, ^{135}Cs). The residual radioactive waste will be suitable for on-site burial.*

isotope through detailed cost, risk and benefit analyses.

Our fission product transmutation goal includes burning all of the ^{99}Tc, ^{129}I, ^{135}Cs, ^{126}Sn and ^{79}Se, which all together constitute 4.5% of the total fission products generated by the ADEP during power production. The remaining fission products are made up of stable nuclides, short-lived isotopes, and long-lived isotopes that do not present significant hazards. We believe, for instance, that it is unnecessary to transmute ^{93}Zr and ^{107}Pd because their radioactivity is very small, their decay modes have very low energies, and as noble metals they are not readily transported by natural means through the environment. ^{137}Cs and ^{90}Sr cannot be effectively transmuted inside the low-flux ADEP blanket because of their small cross-sections. A large fraction of these isotopes will however decay naturally due to their relatively short 30-year half-lives during the life of the ADEP power plant, and if a more complete transmutation of these fission products is desired, special high-flux, low-multiplication blankets should be used. The 300-year containment of these isotopes (10 half-lives) is however deemed feasible, and may be all that will be required to deal with them. (Figure 10 shows the functional block diagram of the ADEP system).

Start-up

While the ADEP could start-up by beaming ions into its target and breeding its ^{233}U from scratch, this process would require some time (typically 1 year) to build up the blanket to full power. A convenient start-up mechanism could be provided where appropriate by feeding an initial charge of high-enrichment uranium, weapons plutonium or spent reactor fuel at the beginning of life for the ADEP plant (about 100 kg per 500 MWt module). The use of this initial feed allows the quick jump-start of the thorium uranium breeding cycle, and time to full ^{233}U power under beam is estimated to be about 100 days in simple start-up scenarios.

THE DESIGN OF ADEP

The design of the ADEP plant consists of various systems, or facilities, categorized as:

1. The target-blanket system, in which source neutrons generated by the interaction of a ion beam with the molten salt target are thermalized and subcritically multiplied; the fission heat generated in the fuel salt in its passage through a graphite moderated region is removed in primary heat exchangers
2. A coolant-salt circulating system, steam generators, and a turbine-generator plant for converting the thermal energy into electric power
3. An off-gas system for purging the fuel salt of fission product gases and gas-borne particulates and an associated electrolytic system for plating out noble and semi-noble metals.
4. A separation processing facility for fuel salt cleanup and recycle; this facility would continuously process a slip stream of molten salt.
5. Auxiliary salt handling equipment
6. General facilities and equipment, including controls and instrumentation, maintenance tools, auxiliary power equipment, waste management, storage and disposal systems, condensing water systems, electrical switchyard, stacks, and conventional buildings and services.

It is not the purpose of this paper to describe in any detail the ADEP system. Therefore I will only cursorily describe subsystems 1 through 4 and then just those parts that are unique to the ADEP system.

Target-blanket primary system

In the reference concept the molten salt fuel (a mixture of lithium, beryllium, thorium and uranium fluorides) flows through a bed of graphite moderator elements, which form the multiplying part of the blanket where the heat is generated, and into heat exchangers.

The (750-cm diameter, 700-cm height) blanket vessel contains graphite for neutron moderation and reflection, with the power producing region 80 cubic meters in volume (500-cm height, 450-cm diameter). All pumps and primary heat exchangers are also contained in the vessel. Shutdown and power level of the subcritical assembly are controlled by the accelerator beam intensity. Fuel concentration can be changed during operation without affecting the control properties of the accelerator. The target/blanket assembly, fuel processing facilities and power generating equipment are all located underground.

The center of the blanket is occupied by the liquid lead target, a self-contained unit which is inserted and extracted from the top of the vessel. The primary salt is circulated through six loops feeding from and returning to a common central plenum. Each circuit contains a single-stage centrifugal pump and a heat exchanger, all placed within the first containment vessel. Construction is modular, so that any heat exchanger or pump can be independently removed for maintenance.

After-heat removal system

As a design feature, the hastelloy-N vessel is totally enclosed and without openings, except for the lid at the top, so that any spillage of the salt is extremely unlikely, as it would require a major break of the vessel. Extended removal of the after-heat in the event of loss of circulation in either the primary or the secondary salt systems is designed into the vessel and surrounding containment structure, and does not require the transfer of the salt to a separate storage tank.

Secondary-salt circulation and steam-power

Heat is transferred from the primary salt to a secondary fluid, sodium fluoroborate, having a composition of $NaBF_4$:NaF (92:8 mole %) and a liquidus temperature of 390°C. The secondary salt goes to the steam generators to obtain 550 °C-temperature steam. Turbines and power generating systems are entirely conventional.

Off-gas collection system

It is important to provide quick removal of the volatiles in order to improve the overall reactivity of the systems, limit reactivity excursions due to xenon decay, reduce the heat load of the molten salt in the event of loss of circulation or cooling power, and limit the radioactivity release in the event of direct fuel exposure to the environment. The molten salt fuel offers simple means for the separation of these volatile species. Almost all noble gas fission products and 30% of the noble metals are removed by flowing helium at the upper plenum surface within minutes from their formation, the rest of the noble metals plates out on special internal surfaces within a few hours.

Fuel-salt cleanup system

The cleaning cycle (Figure 11) must perform the following functions:

1. Remove all fission products from the molten salt.
2. Return all actinides to the blanket.
3. Isolate the long-lived fission products for return to the blanket for transmutation.

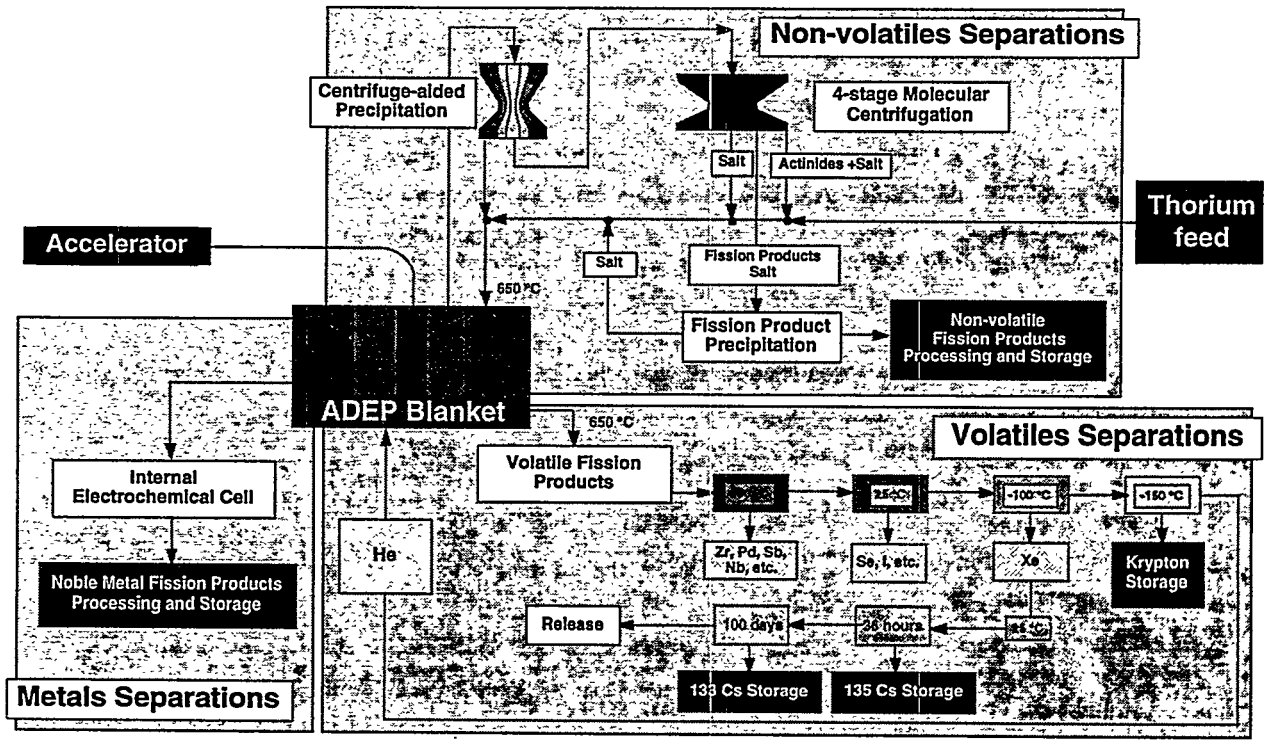

Figure 11. The molten salt ADEP flow-sheet for back-end cleanup processes. The three main groups of fission products receive different treatments.

The separation flowsheet proposed for ADEP is based on precipitation enhanced by centrifugation. It completely avoids the requirement for reagents, which might give rise to secondary waste streams. Starting with a nominal molten salt mixture of 12:1:69:18 ThF_4:UF_4:LiF:BeF_2 at an average temperature of 650 °C, the first process is a precipitation through cooled centrifugation. By the time the salt cools to about 400 °C, the salt composition will change to 2:54:44 of ThF_4:LiF:BeF_2. Nearly all of the ThF_4 precipitates, and the chemically similar UF_4 with it. These species can be returned to the transmuter blanket or be recycled through the centrifuge for further purification. The centrifugal fields required are modest and typical of those used in industrial centrifugation processes for removing precipitates from liquids.

Volatile fluoride fission products are removed throughout power production by the off-gas system. Low solubility fission product plate out in special places in the molten salt stream. Therefore only low volatility fission products and actinide fluorides are dissolved in the discharged salt. Because of their low concentration these fluoride salts will be carried with the LiF and the BeF_2 after the first precipitation.

A molecular centrifugation process follows this initial precipitation. During this centrifugation (4 parallel sets of 8 sequential stages) the residual fission products are extracted from the fuel. The end result is a stream of fission product bearing salt with less than 1 part per 1000 of actinides. This stream can be concentrated and fission products precipitated from it.

Waste Streams

Like the other accelerator-driven concepts originated at Los Alamos in the past few years, the ADEP concept is designed to limit its waste streams to a minimum. The ADEP transmutes the long-lived fission products generated during power production, and burns any higher actinide to a very low equilibrium level. It uses separation processes that do not involve external streams of reagents to be disposed and its high energy conversion efficiency limits the amount of waste heat released to the environment.

Four distinct radioactive waste streams have been identified from the ADEP operation at the end of its scheduled operational life: activated structural materials, short-lived solid fission products in fluoride form, noble metal fission products in metallic form, and noble gas fission products. The molten salt fuel is reusable in a new blanket and therefore is not considered a waste product.

All metallic components, including heat exchangers, vessel and all radioactively contaminated equipment will be cleaned using processes such as fluorine plasma etching that do not require the addition of solvents or reagents. The recovered actinides will be directly added to the molten salt fuel and burned in subsequent operations. The graphite moderator and reflector will be burned in a controlled environment, the residual fission products and actinides released by the burn will be scrubbed and recycled when appropriate in the blanket. Calcium carbonate or silicon carbide will be the final form of the decommissioned graphite. No carbon will be released. Thecalcium carbonate or silicon carbide will be mixed with the activated scrap metal and poured as low level radioactive concrete slabs for shallow burial on site.

All the troublesome fission products with long half-lives are transmuted to non radioactive materials in the ADEP blanket. Some shorter-lived isotopes, on the other hand, are too difficult to transmute, owing to their very small absorption cross section. No transmutation would probably be attempted on ^{90}Sr or ^{137}Cs. With a 30-year half-life, these isotopes will likely be lumped together with the other short lived and stable solid fission products, diluted with a salt of appropriate heat

capacity and then stored in supervised, engineered containers for up to 300 years before their radioactivity is down to safe levels. Alternatively, and at a high cost, both ^{90}Sr and ^{137}Cs, could be transmuted in special high-flux, low-multiplication blankets, where their effective half-life would decrease perhaps by a factor of 4. All noble metals recovered from the separation of fission products, including the weakly radioactive Zr and Pd, will be alloyed and stored in low level storage areas or recycled as seen appropriate. The noble gas Krypton, with a half-life of 10 years will have to be monitored for about 100 years in appropriate sealed containers.

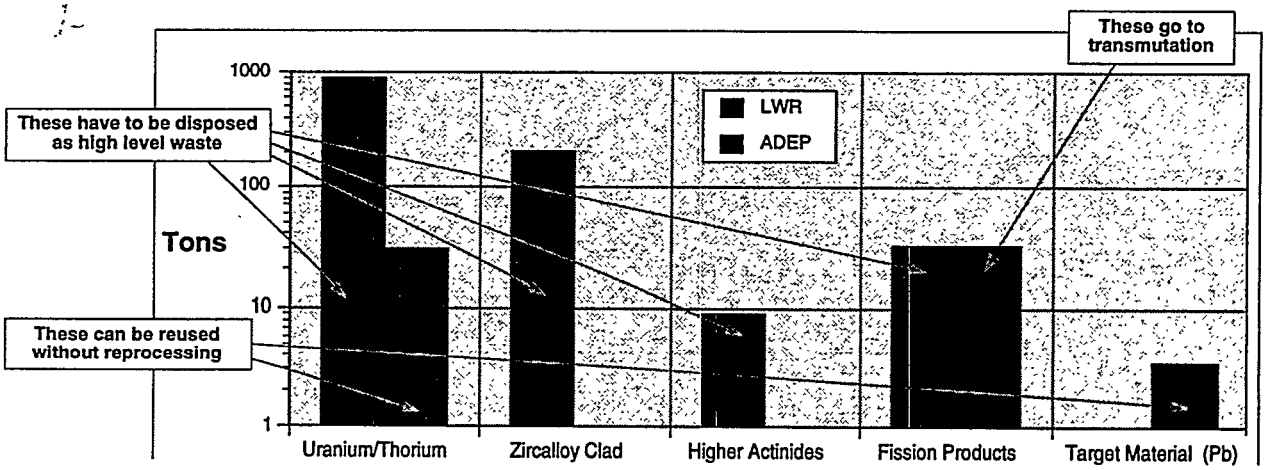

Figure 12. *The End of Life (EOL) Inventory (radioactive waste stream) of a typical Light Water Reactor (LWR, 30 years at 3000 MWt) compared with the inventory of an Accelerator Driven Energy Producer (ADEP, 6x500 MWt modules)*

Figure 12 compares the End of Life (EOL) radioactive waste stream of ADEP with that of a typical Light water reactor (LWR). LWR spent fuel must be reprocessed at plant EOL in order to be reused. The most optimistic estimates of fuel utilization for LWR systems range up to 40% following complex and repeated refabrication of fuel. On the other hand, ADEP fuel and target material are just as effective at End of Life as they were at the beginning of operations and ready to be placed in a new blanket without reprocessing. Full utilization of fuel and target material is readily achieved. Therefore the extent of the EOL radioactive inventory of ADEP and all other ADTT systems is driven by the cleanup efficiency, not inherently by the cycle.

A PROLIFERATION RESISTANT NUCLEAR SYSTEM

ADEP has very strong nonproliferation features:

- Complete fuel utilization without reprocessing
- No actinide waste stream
- ^{239}Pu production is very small and denatured with ^{238}Pu
- ^{233}U can be denatured with ^{238}U
- Power balance or thermal map can clearly identify diversion
- No fissile material is required for start-up or feed
- No fissile material needs to be extracted from the fuel
- On-line separations inhibit diversion
- System operation can be disrupted without radioactivity release

The ADEP concept could offer significant Safeguards and Non-Proliferation advantages over existing nuclear power production systems. The present system for nuclear power production involves different sites for fuel enrichment, fuel fabrication, commercial power production facilities, reprocessing plants and the disposal of high level wastes. The operations at each of these steps and the transfers between them offers opportunity for loss or diversion of nuclear material for clandestine purposes. The public is very concerned about the transport of spent fuel and high level waste in the back end of the fuel cycle and the safe storage of this high level waste for long periods. The ADEP system does away with the complex infrastructure of the current system and its transportation needs. Continued power generation at the site is possible through the use of the benign natural fuel thorium. Nuclear waste is destroyed at the same site without reprocessing, refabrication, or long-term actinide waste storage. Only one batch of thorium fuel need be delivered to the site every thirty years. With the full development of the concept, nothing need leave the site except electric power.

The primary measures for identification of attempts to divert nuclear material within the existing nuclear power infrastructure involve physical security and nuclear material accounting supervised by the International Atomic Energy Agency. This material balance accounting requires taking differences between large numbers, which places severe demands on measurement accuracy to detect diversion of small amounts of material. In the ADEP system, only thorium and (possibly) a small initial charge of fissile fuel are brought into the power production site. The thorium is fed into the system and no actinide is removed. The thorium and all other actinides are confined to the molten salt loops in the blanket. Therefore by monitoring the thorium input rate, by knowledge of the system efficiencies, and by measurement of the electric power output of the system, it should be possible to detect the production of any fissile uranium which was not used for electric power production, without nuclear material measurements at any point in the system.

No ^{233}U or ^{233}Pa is ever isolated either during the operation or during the fuel cleaning process, and because of the subcritical nature of the ADEP system, the inventory of fissile material can in principle be burned completely.

The addition of 7-10% ^{238}U in weight to the initial thorium load would ensure that the uranium present in an ADEP system at any time during its operating life will be unusable as weapons material without isotopic separation. Hardly any ^{239}Pu is produced (less than 3 kg is present in each 500 MWt modular blanket at any given time, dissolved in over 20 cubic meters of very hot salt and rendered unusable by the considerable fraction of the heat-laden ^{238}Pu isotope present). No buildup is possible because of the continuous cleaning of the fuel.

Even the surreptitious isolation of the protactinium inventory after a commandeered shutdown is not conducive to a high-risk proliferation scenario. Here again the dilution of the inventory (30 kg of ^{233}Pa at equilibrium 20 m^3 of salt) and the 27-day half-life of the protactinium would ensure that a significant isolation of the potential ^{233}U inventory will not be possible by terrorist groups. The uranium that would be produced in this scenario is also not as desirable as ^{239}Pu in the manufacturing of weapons. Whereas the nuclear properties of ^{233}U and ^{239}Pu are roughly equivalent, the hard gamma radiation associated with the ^{232}U isotope and its daughters, always present with the bred ^{233}U, would preclude hands-on work and allow easy detection of smuggled material and of secret warheads. Clearly there are easier ways to procure better weapons-grade material.

The ADEP technology offers new opportunities for improving protection against production and diversion of nuclear material. It is important to attempt to build in as many of these features into the design from the beginning, instead of attempting to retrofit them into otherwise unsatisfactory designs, as it has been the case with current nuclear power technology.

ADEP OPERATING PARAMETERS

fission power = 500 Mw power density = 6 w/cc
active core diameter = 450 cm
active core height = 500 cm
average core flux= 1.2 *10^{14} n/cm^2s average fuel flux= 5.0 *10^{13} n/cm^2s
molten salt composition = LiF-BeF2-Th(U)F4 69-18-13 mole % (nominal)
Fuel salt temperature in-out heat exchangers = 1000 - 850 °K
salt volume = 20 m3 (total)
graphite volume = 250 m3 (total) 80 m3 (core)
graphite mass = 180000 kg
salt volume in core = 8 m3
salt volume in heat exchangers and plenums = 12 m3
salt flow in heat exchangers = 0.63 m/s
salt flow in core = 1800 kg/s - 0.96 m/s
secondary salt temperatures = 770 °K (in) 840°K (out)
pump power = 0.14 Mw (total for 6 primary pumps)
target material = molten lead
target size = 40cm diameter x 90 cm length
target lifetime = 2 years (exposed structure) indefinite (lead)
target neutron production = 22 n/p at 800 MeV

REFERENCES

[1] Bowman,C.D., Venneri F., *"High Value use of Weapons Plutonium by Burning in Molten Salt Accelerator-Driven Systems or Reactors,"* International Seminar on Nuclear War and Planetary Emergencies, 18th Session, pp. 400-411, Erice, Italy, 1993

[2] Venneri, F., Bowman, C.D., Heighway, E.,*"Accelerators add a new option to our energy future"* Los Alamos Unclassified Report LA-UR 94-3905, submitted to Scientific American.

[3]. Venneri, F., Bowman, C.D., Jameson, R., *"Accelerators address nuclear waste problems"* Physics World 6,8 p.40 (Aug. 1993).

[4] The Molten Salt Reactor Experiment (MRSE) is described in a series of papers,Weinberg,A.M. editor, Nuclear Applications and Technology 8, pp 102-219, (1970).

[5] Bell, C., "Safety features of subcritical fluid fueled systems", included in these proceedings.

[6] *"Accelerator production of tritium"* Energy Research Advisory Board of the U.S. Department of Energy, Washington, DC (1990). and *"Accelerator production of tritium"* JASONS Report JSR-92-310, The Mitre Corporation, Mclean, VA (1992).

[7] Heighway, E.. private communication.

[8] Rubbia, C., et. al. *"Intermediate separated sector cyclotron"* (in preparation).

[9] Wender, S., Venneri, F. et. al. *" Accelerator driven transmutation experiments at the Los Alamos Meson Physics Facility"*, included in these proceedings.

[10] Beard,C.A., et al. *"Flowing lead spallation target design for use in an ADTT experimental facility located at LAMPF"*, included in these proceedings.

[11] Williamson,M.,Venneri, F., "Electrowinning of Uranium from Spent Fuel" (in preparation).

[12] Williamson,M., private communication.

[13] Li, N., Camassa, R., Ecke, R., Venneri, F., *"Centrifugal Separation for Miscible Solutions: Fundamentals and Applications to Separation of Molten Salt Nuclear Materials"* Los Alamos Unclassified Report LA-UR 94-3197.

[14] The thorium-cycle, gas-cooled reactors (HTGRs) are described in the Jan. 1974 issue of Nuclear Engineering and Design, pp.1-230.

The Results of the Investigations of Russian Research Center - "Kurchatov Institute" on Molten Salt Applications to Problems of Nuclear Energy Systems

Vladimir M. Novikov
Russian Research Center - "Kurchatov Institute", Moscow, 123182, Russia

Abstract. The results of investigations on molten salt (MS) applications to problems of nuclear energy systems that have been conducted in Russian Research "Kurchatov Institute" are presented and discussed. The spectrum of these investigations is rather broad and covers the following items: physical characteristics of molten salt nuclear energy systems (MSNES); nuclear and radiation safety of MSNES; construction materials compatible with MS of different compositions; technological aspects of MS loops; in-reactor loop testing.

It is shown that main findings of completed program support the conclusion that there are no physical nor technological obstacles on a way of MS application to different nuclear energy systems.

INTRODUCTION

Conceptual studies on molten salt technology application to problems of nuclear energy system are of the same age as nuclear power (NP) per se: the first experimental molten salt reactor (MSR) became critical in the USA at 1954 and the same year the first demonstration nuclear power plant (NPP) was commissioned in Russia. A half of century passed and a retrospective view fixes that times of extensive work on MSR followed by periods of stagnation or even cessation. It is interesting that periods of MS concepts revival correlates with occurrences of new problems or obstacles confronted traditional NES.

These correlations may be judged differently. Some could see it as an evidence of a persistence of MSR partisans. And it is partly true, as every idea has its followers. But more naturally to consider it as a proof of potential advantages of MS technology.

In favor of this statement speaks that for all cases such as fissile material breeding, effective use of natural resources, non-proliferation, inherent safety, etc MS technology demonstrated new qualities. Besides its flexibility manifests itself in the conceptual designs of molten salt NES based on fusion and accelerator technologies as well as in non-nuclear applications such as high temperature heat transport and heat accumulation.

In Russia the molten salt program started in the second half of 70th. Russian Research Center - "Kurchatov Institute" (that time Kurchatov Atomic Energy Institute) was a basic organization under which supervision a network of specialized institutions was formed and functioned.

A reduction of activity appeared after 1986 due to Chernobyl accident. Then at the end of 80th there was an increase of conceptual studies as a result of the interest to the inherent safe reactors of new generation. The political and economical changes in the former Soviet Union and its dissolution degraded the level of state support for scientific programs many of which stopped. MS program is among them. Now there are only a small level theoretical studies around this problem. All experimental works were stopped. Nevertheless the intellectual potential, technological experience and even some experimental installations do still exist and could be used if necessary.

The article aims at reviewing results of the works performed in Russia, mainly in RRC - "KI", relevant to the problems of MS technology application to NES.

MAIN ISSUES OF THE MS-PROGRAM

The concepts of MSNES based on a philosophy that presuppose the use of fuel in the form that permits continuous management of nuclear-physical, chemical and thermo-physical processes in fuel and regulation of its nuclides content. It means as if one includes an additional degree of freedom. This degree of freedom can be used for optimization of NES and gaining a maximal profits from physical potential of nuclear phenomenon.

This philosophy is an alternative to the traditional one, that presumes that fuel has to be used in a maximum condensed form (and volume) that excludes reprocessing and management while reactor operating. A consistent implementation of the traditional philosophy has an advantage of technological simplicity but it results in a loss of potential advantages of nuclear fission phenomenon and in deterioration of same nuclear plant indexes.

Sometimes the critics of MSR say, that the use of molten salt fuel means the loss of one safety barrier (solid fuel matrix) and thus diminishing the defence-in-depth principle. But it is a wrong way of understanding of defence-in-depth principle because:

- the use of molten fuel does not mean that fission products are more movable. Indeed, some fission nuclides are soluble and thus are kept in the melt. Others, that are volatile, could been removed from fuel during operation. Meanwhile they are being accumulated in solid fuel.
- the numbers of barriers is not a magic number. What is of real importance is a reliability of barriers. And if one wants to keep a number of barriers to be constant, why shouldn't we to put an additional guard vessel for MSR?

The question whether the philosophy of MSNES has ultimate advantages has to be solved in an open competition. This has predominated the objectives of the russian MS-

program. They were as follows:

- identify potential advantages and intrinsic pitfalls of MSNES,
- search for a way to maximize the use of advantages and minimize vulnerability,
- explore a feasibility of technical implementation of main MSNES design features.

The study was organized around the following issues:

- MSNES physics,
- exploration of possible use and niches for MSNES,
- safety aspects of MSR,
- construction materials,
- molten salt heat transfer,
- in-reactor loop experiments,
- radiation chemistry of MS.

The first three issues constituted theoretical studies, the rest - both theoretical and experimental studies. A comprehensive description of studies performed till 1990 were published in the book "Molten Salt Nuclears Energy Systems - Perspectives and Problems", Moscow, 1990 (in Russian).

The next sections composes materials based on this publication and those appeared afterwards. The restrictions on length allow to overview only a part of results. Physical characteristics, safety aspect and construction materials are of priority.

PHYSICAL CHARACTERISTICS OF MSR-DESIGNS

Molten Salt Breeder Reactor (MSR-B)

A well known ORNL design MSBR-1000 was optimized under supposition of linear growth of nuclear power (NP). It's breeding ratio is 1.06 and double time is 21 yr. Studies of potential breeding capacity of MSR showed that there were several reserves which might be used for increasing these characteristics, if necessary. They are: reduction of neutrons leakage, U-isotope corrections and increase of coolant heating in the core. Particularly, the construction materials study showed the possible upper level of molten salt temperature as of 800°C.

The use of these reserves can result in reduction of double time down to 7 years.

Molten Salt Convertor Reactors (MSR-C)

MSR-C were consider as a first stage of MSR-B, when MS reprocessing system did not work on full scale, and as MSR for technological applications, where breeding capacity associated with complex reprocessing system was not necessary. Nevertheless a part of fission products are expected to leave the molten salt fuel composition automatically due to low solubility. This improves neutron balance as compared with that of solid fuel thermal reactors. Efficiency of natural U and Th resources consumption was investigated for different MSR-C designs. The efficiency was defined as

$$\alpha = M\varphi T \times \left[\int_0^T g(t)dt\right]^{-1}$$

where M - power, φ - capacity factor, T - reactor life time, g(t) - rate of natural resources consumption.

The typical data are listed in Table 1. The comparison with data for modern VVER - (Russian PWR) reactor shows that from this point of view MSR-C are at least 5 times more effective than light water reactors.

Table 1. Efficiency of natural U and Th resources consumption by MSR-C and PWR (VVER-type)

Reactor	Fuel	Cycle	α,MW(el)·yr/t
VVER	UO_2	open, 3yr	3.5
		closed, 3yr	6.3
	Th-met.	open, 3yr	3
		closed, 3yr	12.6
MSR-C	UF_4	open, 30yr	17.2
		closed, 30yr	31.2

MSR with natural circulation

One of the serious problem of MSR technology is reliability of main circulation pumps. The use of natural circulation of molten fuel could be a good decision of this problem if it does not deteriorate the economic indexes very much.

Models of MS natural circulation were developed and verified in a series of experiments and applied for optimization of fuel circuit. Several designs were optimized:

- one is of MSBR-type, e.g. with graphite moderator in the core,
- the other is with homogeneous core and graphite reflector,
- next is High Temperature MSR (HTMSR) of integrated arrangement with graphite as construction material and radiant heat exchanger.

The efficiency of natural uranium resources consumption for these optimized designs was estimated as 20 MW (th)/t U^{nat} . This value should be compared with 10.5 MW (th)/t U^{nat} for PWR (open cycle) and 15.3 MW/t U^{nat} for HTGR (open cycle).

Another way to activate the fuel circulation is to use gaslift. The investigation of gaslift applied to HTMSR showed that modest value of gas volume fraction in lifting part of circuit (up to 0.15) resulted in two or three times increase of power level.

MSR and HTGR hybrid

The idea to combine a good compatibility of molten fluorides and graphite and developed technology of HTGR fuel balls leads to a conceptual design of VTRS (russian abbreviations) that is a kind of MSR and HTGR hybrid. Spherical fuel elements of HTGR form a core, as for coolant the compositions LiF - BeF2 or NaF - BeF2 are used. The former gives a better neutron balance while the letter excludes the problems due to T - generation.

The efficiency - α for this reactor is not so high as for MSR-C but still at the level of HTGR.

MS and MSR for industrial heat supply

Analysis of industrial heat demand shows that 80% of total refer to temperature interval up to 550°C. Further increase of 400°C results only in 3% of additional demand.

Only when temperature is substantially higher than 950°C the rest 17% of the total demand arises. It was proposed to use MSR-C as a heat source for industrial heat supply. Within this approach it is naturally to use molten salt as heat carrier in heat route connecting MSR-C and consumer. Several salt compositions, like LiCl-LiOH, NaF-$NaBF_4$, LiF-KF-NaF, $NaNO_2$-$NaNO_3$-KNO_3 were considered and corrosion of construction materials were investigated. The design has also received an economic examination that showed a specific cost of heat equal to that of AST - light water reactor for domestic heat supply.

Other applications

Among other applications the following were examined:

- use of MSR for alternating loads in electrical grids;
- MSR with gas-turbine cycles for electricity production;
- MS as coolant and working medium in blankets of thermonuclear reactor with magnetic confinement and with laser ignition;
- MS as coolant and working medium in targets of accelerator driven breeder or transmuter;
- MS in reactor loops for nuclear material breeding with manageable, isotopes content.

SAFETY ASPECTS

Safety problems of MSNES have been examined on several levels. The estimations on rather general, qualitative level showed that the majority of desired safety features of nuclear reactor for NPP are of MSR possession. It is illustrated at Table 2.

The on-line reprocessing of MS fuel permits to reduce residual heat release and residual radioactivity of the fuel. Calculations were made for two cases: reactor emergency shutdown with and without reprocessing system stop. For the former after 10hr the activity of fuel is about 10 times less as compared with no reprocessing MSR. The letter case gives additional 10 times reduction.

The quantitative evaluation of important parameters changes during transients were performed by use of codes developed for MSR accident analysis. The accidents of positive reactivity insertion (TOPWS), loss of forced coolant circulation (LOFWS), loss of heat sink (LOHSWS) as well as their combination were considered. The main result is that proper designing of MSR provides the core intact under practically all accidental conditions without using active safety system and personnel intervention.

Nevertheless a severe accident with the rupture of core vessel and fuel discharged on the reactor box bottom was also considered. The model describing main radionuclides distribution between the fuel salt, metallic surfaces of the primary circuit, graphite and the gas purging system was applied for calculation releases to the containment atmosphere.

The obtained results were compared to data on activity releases in solid-fuel reactor of the PWR-type for an accident with core melt and vessel rupture. It was shown that total release for MSR is significantly lower (by 1 - 2 orders of magnitude), though for several particular nuclides such I^{131} and I^{133} the differences are smaller.

Table 2. Comparison of qualitative safety features of different reactors.

Desired feature *	Reactor type			
	MSR	LWR	HTGR	LMFBR
low reactivity margin	+	-	-	-
low non-nuclear energy stored	+	-	+	-
low pressure in fuel	+	-	-	-
low pressure in primary circuit	+	-	-	+
low concentration of gaseous products in fuel	+	-	-	-
large temperature margins for phase transition in fuel and coolant	+	-	+	+
large heat capacity of fuel	+	-	+	-
cooling down whilst pumps failure	+	+	+	+
no local overheat on the primary circuit walls	-	+	+	+

* "+" for presence; "-" for absence.

MATERIALS FOR MSNES

The investigation of materials for MSNES was a major part of russian MS program. General requirements for materials were formulated as follows:

- they must be easily producible, i.e. easily subjected to treatment by pressure, cutting rolling, well weldable and in such a way to provide the possibility of fabricating complex elements of reactor constructions;
- pressure on walls in typical MS-circuit due to hydrostatic and hydrodynamic head of a circulating salt is less than 2 MPa. Thus, guiding by this limiting value and taking a ten-fold safety factor the candidate material must have the limiting value for lasting strength-bigger than 20 MPa (30 year of operation at temperature 700-800°C);
- metal construction in MSR are outside the peak neutron flux and neutron fluence is estimated as 10^{20} and $5 \cdot 10^{21}$ n/cm^2 for fast (> 0.5Mev) and thermal neutrons. It was demanded that limiting value for bending relative deformation after gaining a full neutron fluence would be not less than 4%. (The initial value of this parameter, for a non-irradiated Hastelloy-N amounts to 10% at 650°C);
- to keep the main sequences of corrosion on an acceptable level (heat exchanger wall thickness, molten salt content, mass transfer) it was demanded that the depth of corrosion should not exceed 10 μm/year and metal should not subject to a local corrosion (pitting or intergranular cracking).

The development of domestic structural material for MSR was essentially substantiated by available experience accumulated in ORNL MS-program). The alloy HN80MT was chosen as a base. Its composition is Ni(base), Cr(6.9), C(0.02), Ti(1.6), Mo(12.2), Nb(2.6).

Corrosion resistance of materials was studied by two methods. The first is the method of capsule static isothermal test of reference specimens in various molten-salt mixtures. The second is express-tests of materials in natural and forced convection loops with thermal gradient. Not only normal but also high oxidation conditions were preset in the loop. The last circumstance made it possible to estimate limiting corrosion characteristics of materials.

The information accumulated by ORNL on corrosion processes during thermal and forced convection loop tests allowed to compare them with data on our experiments carried out under similar conditions. Such a comparison enables in a number of cases to see new mechanisms of corrosion behaviors and predict an operability potential of presented materials. The development and optimization of HN80MT alloy was envisaged to be

performed in two directions:

- improvement of the alloy resistance to a selective chromium corrosion,
- increase of the alloy resistance to tellurium intergranular corrosion and cracking.

About 70 differently alloyed specimens of the HN80MT were tested. Among alloying elements there were W, Nb, Re, V, Al and Cu. The main finding is that alloying by aluminum at a decrease of titanium up to 0.5% revealed the significant improvement of both the corrosion and mechanical properties of the alloy. The chromium corrosion and intergranular corrosion have reached the minimum value at Al content in the alloy ~ 2.5%.

Irradiation effect on a corrosion activity of MS was also studies. It was shown that at least up to the power density 10 W/cm^3 in fuel composition Li-BeF_2-ThF_4-UF_4 there is no radiation induced corrosion.

Then the radiation study of 13 alloy modifications were carried out. Specimens were exposed to nitrogen atmosphere in the reactor neutron field to the fluence of $3 \cdot 10^{20}$ n/cm^2. Experimental results of alloy mechanical properties at temperatures of 20, 400 and 650°C for nonirradiated and irradiated specimens permits to rest only four modifications. These alloys modified by Ti, Al and V have shown the best postradiation properties.

At last corrosion under the stressed condition was studied. It is known that a material tensile strain promotes an opening of intergrain boundaries and thus boosts intergranular corrosion and create prerequisites for an intergranular cracking. The studies did not reveal any dependence of intergranular corrosion on the stress up to the value 240 Ma, that is 0.8 of a tensile yield of the material and 5 times higher than typical stresses in MSR designs.

The results of combined investigation of mechanical, corrosion and radiation properties various alloys of HN80MT permitted to suggest the Ti and Al - modified alloy as an optimum structural material for the MSR. This alloy named HN80MTY (or EK-50) has the following composition: Ni(base), Fe(1.5), Al(0.8-1.2), Ti(0.5-1), Mo(11-12), Cr(5-7), P(0.015), Mn(0.5), Si(<0.15), C(<0.04). The comparison with corrosion data obtained at ORNL for Hastelloy indicates that corrosion resistance of HN80MTY is higher and it's maximum working temperature could be up to 800°C. Still the weldability of the alloy deserves an improvement.

CONCLUSION

The MS-program performed in Russia, mainly in RRC-"KI", covered a wide range of theoretical and experimental studies. Calculations of physical and technical parameters of

MS NES showed the feasibility to get benefits practically in all spectrum of NES from nuclear fission reactors to thermonuclear reactors, accelerator breeders and transmutes. The main finding of experimental studies is that neither physical nor technical obstacles on a way to implement MS technology in NES were observed.

The stagnation of MS-program is partly caused by general stagnation of nuclear power. The other reason is deeper. The key feature of MS technology applications to NES is the use of fuel/fertile material flexibility for gaining additional profits as compared with solid materials. This approach presents important departures from traditional philosophy, applied in current nuclear power plants, and to some extent contradicts the straightforward interpretation of defence-in-depth principal.

As a matter of fact, any departure from current technology will be judged against "established rules" originated from "established" approaches, with question marks regarding all those "nasty non-compliances", even though one might agree that new approach is better from physical point of view.

It inevitably leads to some biases supported by traditional nuclear lobby, though the demand to consider core melt accident in solid fuel nuclear reactor makes the gap smaller.

Nevertheless it is naturally to expect that MS technology may meet an earlier application in new nuclear systems, e.g. nuclear waste transmuter or pulsed thermonuclear installation, that are likely not subjected to bias and where the use of MS flexibility may give a decisive profit.

An Active Target for the Accelerator-Based Transmutation System

K.F.Grebyonkin
Russian Federal Nuclear Center - Institute of Technical Physics.
P.O. Box 245, Chelyabinsk-70, 454070, Russia

Abstract. Consideration is given to the possibility of radical reduction in power requirements to the proton accelerator of the electronuclear reactor due to neutron multiplication both in the blanket and the target of an active material. The target is supposed to have the fast-neutron spectrum, and the blanket - the thermal one. The blanket and the target are separated by the thermal neutrons absorber, which is responsible for the neutron decoupling of the active target and blanket. Also made are preliminary estimations which illustrate that the realization of the idea under consideration can lead to significant reduction in power requirements to the proton beam and, hence considerably improve economic characteristics of the electronuclear reactor.

In recent time quite evident became the interest again to the idea of the electronuclear reactor (ENR), especially as applied to the problem of long-lived radioactive wastes transmutation. The basic ENR components are the high-current proton accelerator, the target made of material with high atomic number that is responsible for the protons-to-neutron transformation, and the subcritical blanket that multiplies neutrons leaving the target. The subcritival mode of the ENC operation gives grounds to hope that the elevated safety level can be achieved. But because of the accelerator high cost, the ENR-generated electric power cost, by some estimations [1], can appear to be considerably higher, if compared with traditional nuclear reactors. So, the search for methods of reducing power requirements to the ENR accelerator is of principal importance, and a progress in this direction could have changed present look at the perspectives of ENR practical usage.

Evidently, the power requirement to the ENR accelerator can be reduced by a trivial way, i.e. by increasing of the coefficient of neutron multiplication in the blanket. Then the major advantage of the electronuclear approach i.e. operation at a deep subcritical mode will be lost, and the ENR will have practically no differences from usual nuclear reactor in this respect.

The main purpose of this report is call to attention to the practical possibility of radical reduction in power requirement for the ENR proton accelerator due to neutron multiplication performed both in the blanket and in the target (active target). If the neutron flux from the blanket into the target is suppressed, these two subsystems will operate practically independently, and instead of the neutron multiplication in the blanket, which is $1/(1 - K_{eff})$, in the active target-blanket system it is possible to obtain the multiplication being equal to the product of neutron multiplications both for the blanket and for the active target. Of principal significance is the fact that in this case the target, the blanket and the system as whole will be deeply subcritical, and because of this the safety of the system with the active target will not practically degrade, i.e. the system transfer into the nearly-critical state is as just unlikely as in the ENR with the inert nonmultiplying target.

The idea of the sectioned blanket with one-way neutron coupling between its components is well-known [2,3] and has been investigated in detail as applied to

the pulsed aperiodic nuclear reactor [4]. Recently, some suggestions have been made regarding sectioned blanket usage to reduce the requirements to the accelerator for ENR [5,6].

Neutron one-way coupling of the active target and the blanket can be easily made, if the target has a fast-neutron spectra and the blanket has a thermal one, and the blanket and the active target are separated by the layer of a thermal neutron absorber. Hence, the target can be of an uranium oxide or MOX solid fuel rods and cooled by an liquid-metal coolant, e.g. the lead or lead-bithmuth one. Not only traditional absorbers, but materials undergoing transmutation with rather large thermal absorption cross-sections can be used as the thermal-neutron absorber. The problem of the absorber cooling can be solved by the forced circulation of the absorber solution through the core or by the coolant forced circulation through this zone. The active target reflector and the blanket shell of the hastelloy or other structural material could be used to create the one-way coupling, too.

Estimations show, that leaving the target fast neutrons absorption in the thermal neutrons absorber surounding the target will be not so large and these neutrons will efficiently cause fission in the blanket, where the neutron reverse flux from the blanket into the active target will be suppressed.

Let us estimate the proton beam current necessary to obtain 500 MWt of thermal power in the blanket proposed by LANL [7] with the active target. In order to obtain the given thermal power in the blanket, the neutron flux from the target should be

$$F_t = (1-K_b)\bullet(\nu - 1)\bullet P_b ,$$

where

F_t - neutron flux leaving the target,
K_b - multiplication coefficient of the blanket,
ν - mean number of the secondary neutrons per fission,
P_b - blanket power (fissions/sec).

For the obtaining the mentioned above blanket power at $K_b = 0.9$, the neutron yield from the target of about $4 \cdot 10^{18}$ neutrons/sec is required.

The target power P_t (fissions/sec) providing the specified value of the neutron flux going from it, is

$$P_t = F_t / \alpha ,$$

where α is the neutron yield from the target per one fission in it. For estimations we assume that $\alpha = 1$, then the target thermal power resulting from the neutron multiplication in it will be about 50 - 100 MWt and well over the the energy deposition from the proton beam.

Preliminary estimations have illustrated that the active target for the 500MWt blanket [7] can have the following parameters:

The target power	50 MW(th)
Volume of the target core	0.5 m^3
Fuel rodes	UO_2 or MOX
Fuel enrichement	up to 20 %
K_{eff} of the target/blanket system	up to 0.95
Accelerator power	
(800Mev protons)	
- with active target	3 - 5 ma
- without active target	15 ma.

The specific power in the active target will be near 100 MW/m^3 , that is no more than at existing fast reactors. So, the possibility to perform the active target cooling as well as to solve the problem of radiation stability of the materials is quite evident. Nuclear fuel burnup in the target will be close to this at the fast reactors, hence the active target fuel elements can be reloaded one or two times a year as for usual reactors. The active target is simply subcritical heavy-metal cooled reactor and it can be costructed at the present level of tecnologhy.

So, the estimations show the possibility of the essential reduction (some times) in the power and efficiency requirements to the accelerator for ENR due to usage of the active target essentialy multiplicating neutrons. The idea is worth to be developed in detail including neutron-physical and thermophysical simulations, experiments with coupled cores, thermophysical experiments, materials selection , safety analysis and preliminary designing. It is planed to perform this work in the nearest future.

REFERENCES

1.Rublev O.V.,Komin A.G. *Atomnaya Tehnika za rubezhom (in Rus.)*. **4**, 15-17 (1990).
2.Borst L.B. *Phys. Rev.* **107**, 905-906 (1957).
3.Dubovsky B.G. *Atomnaya Energya (in Rus.)*. **7**, 456 - 457 (1959).
4.Kolesov V.F., Malinkin A.A. *V A N T , Fiz. i Teh. Yad. Reakt (in Rus.)*. **4**, 10-23 (1991).
5.Kolesov V.F., Guzhovsky B.Ya. *Prepr. of Inst. of Exp. Phys.* N.27, Arzamas-16, 1993.
6.Grebyonkin K.F. *Prepr. of Inst. of Tech. Phys.* N. 41, Chelyabinsk-70, 1993.
7.Bowman C.D. "ABC Target/Blanket Physics and Engineering". *Presentation to the JASON Panel*, La Jolla, California, 18 Jan., 1994.

The ADAPT Concept - An Accelerator Driven System for the Rapid and Efficient Disposal of Plutonium*

James Powell, Michael Todosow, Gregory Van Tuyle,
Donald Schweitzer, and George Maise
Department of Advanced Technology
Brookhaven National Laboratory, Upton, New York 11973

Abstract. A new concept; termed ADAPT; for the rapid and virtually complete burning of plutonium is described. ADAPT employs a high current CW linear accelerator (linac) to generate neutrons in a lead/D_2O target. The neutrons are then absorbed in a surrounding subcritical ($K_{eff} \sim 0.95$) blanket assembly, that holds small ($\sim$ 0.5 cm diameter) graphite beads containing the plutonium to be burned. The graphite beads are coated and sealed to contain all fission products, including the noble gases. After destruction of virtually all ($\geq$ 90%) of the original plutonium loading, the fuel beads are discharged and sent to a geologic repository for ultimate disposal.

THE ADAPT CONCEPT

Fig. 1 shows the overall layout of ADAPT. The linear accelerator (linac) and target systems for ADAPT are similar in design and operating parameters to the systems developed for the APT concept [1] to produce tritium. The linac delivers a proton current on the order of 100 milliamps at 1 Gev ($=10^9$ev) onto the D_2O cooled lead target. The solid lead pins are contained in aluminum tubes, which are in turn assembled in a lattice inside aluminum pressure tubes, which also serve as the "window" that separates the high vacuum beam line from the pressurized heavy water coolant.

The ADAPT blanket consists of an outer assembly of zircalloy pressure tubes that contain annular beds of the plutonium containing graphite beads (Fig. 2). The fuel beads are held between two concentric porous cylindrical tubes (or "frits"). These frits allow the helium coolant to flow through the packed bead bed, directly cooling them, but hold the beads firmly in place during normal operation. Coolant flow through the packed bed is radially inwards, with the heated outlet gas exiting along the central channel inside the inner "hot" frit.

The directly cooled particle bed arrangement used in the ADAPT concept has been taken from the previous DOD SNTP development program on the Particle Bed Reactor (PBR) nuclear rocket [2]. This approach has a number of important advantages. First, the direct cooling of particles enables very high power densities - for example, the average bed power density in the PBR rocket was 40 Megawatts per Liter - with small ΔT's between the fuel particles and the coolant (typically on the order of 50 to 100K). This power density is much greater than the 0.5 to 1 Megawatts per Liter required for ADAPT, resulting in a very large thermal hydraulic margin. However, this large margin helps to ensure safe operation, and also allows the use of larger diameter particles, as described in the following section.

Second, the use of particulate fuel beads with high integrity coatings similar to those in HTGR fuel particles will enable virtually complete containment of all fission products, including noble gases, at all stages of the fuel cycle. Moreover, after discharge the ADAPT fuel beads will not require reprocessing and can be disposed of in a geologic repository without further

---

*This work was performed under the auspices of the U.S. Department of Energy.

ADAPT Target for Pu Disposition

ADAPT: Accelerator-Driven Assembly for Plutonium Transformation

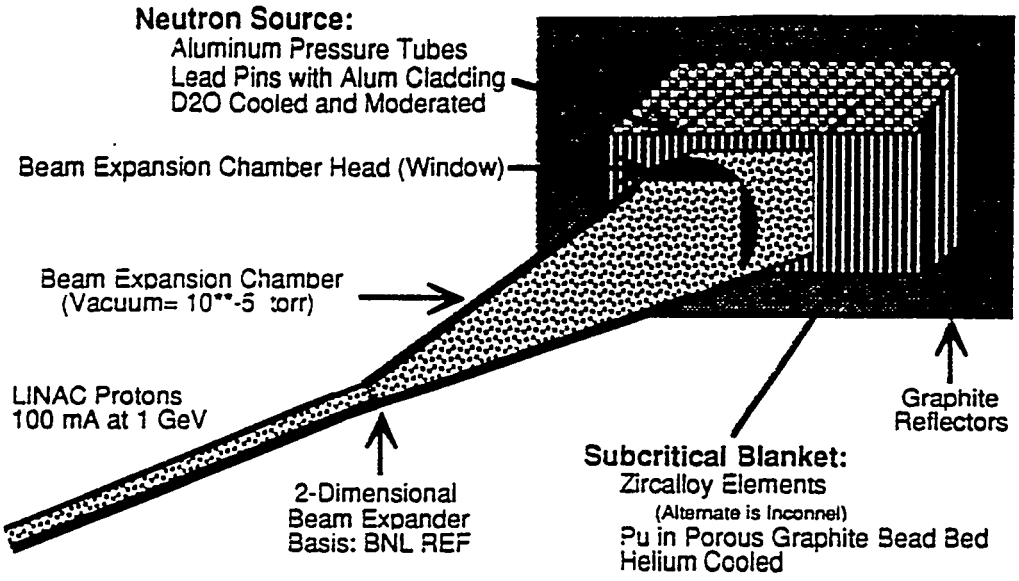

Fig. 1. Overall layout of ADAPT target for transformation of plutonium.

PLUTONIUM FUEL ELEMENT

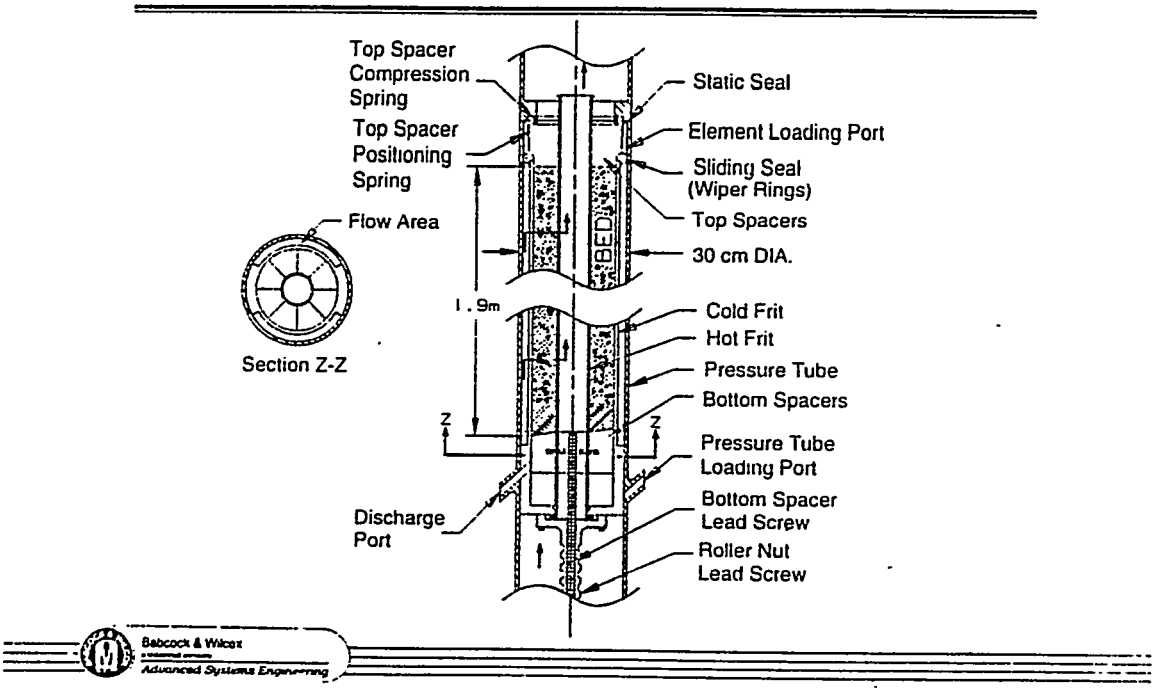

Fig. 2. Fuel element geometry for cooling ADAPT fuel beads.

treatment.

Third, the high power densities and fluxes enabled by direct cooling of fuel particles will permit in rapid burnup of the contained plutonium, with total residence times in the blanket on the order of 100 days.

Fourth, the fresh fuel beads can be loaded and spent fuel beads unloaded without inserting and removing fixed structures, using techniques similar to these for the pebble bed HTGR. This will allow fast throughput and minimum inventory of plutonium and fission products. The specific bead transfer arrangement depicted in Fig. 2 was devised by R. DeMars of B&W [3]. Alternate methods of bead transfer are also possible.

ADAPT FUEL DESIGN

Fig. 3 compares the ADAPT fuel bead design with second generation PBR fuel particles. Both use a porous graphite kernel that is loaded with the fissionable material (U-235 for PBR particles, Pu-239 for ADAPT beads) by the solvent impregnation process shown in Fig. 4. The impregnated plutonium nitrate salt is converted to a mixture of PuO_2/PC_2 by heat treatment at 1200K. Although plutonium impregnation using this process has not yet been demonstrated, it should behave much like the uranium and thorium impregnation processes which are very similar and well characterized. The beads would then be coated with pyrocarbon and/or silicon carbide using either a HTGR type CVD (chemical vapor deposition) process, or some alternate process, such as the molten silicon dip process.

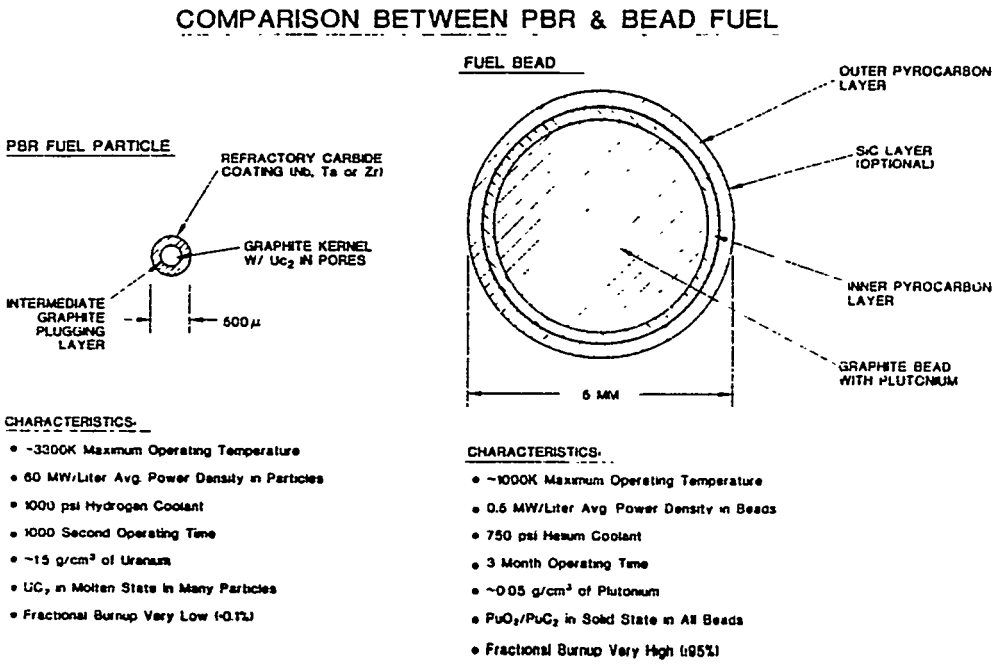

Fig. 3. Comparative characteristics of PBR fuel particles and ADAPT fuel beads.

The main differences between the two fuel forms, apart from the nature of the fissile material that is impregnated into the graphite matrix, are: 1) particle size, 2) fissile loading, and 3) coating composition. Tests of uranium impregnated graphite have found that maximum loading is uniform throughout the graphite matrix for samples to at least several centimeters in

thickness. Thus the impregnation behavior of the larger ADAPT fuel beads is expected to be the same as that of the smaller PBR fuel particles.

Second, the fissile loading for the ADAPT fuel particles will be in the range of 0.05 to 0.1 g/cm^3 of particle (depending on design), as compared to the much higher uranium loadings ($\sim$ 1.5 g/cm^3) required for PBR fuel particles. Depending on impregnation process parameters and graphite properties, on the order of 10 to 20 repeated impregnations are necessary to load the desired amount of uranium into PBR particles. For the lower fissile loadings in the ADAPT particles, 1 to 2 impregnations appear sufficient.

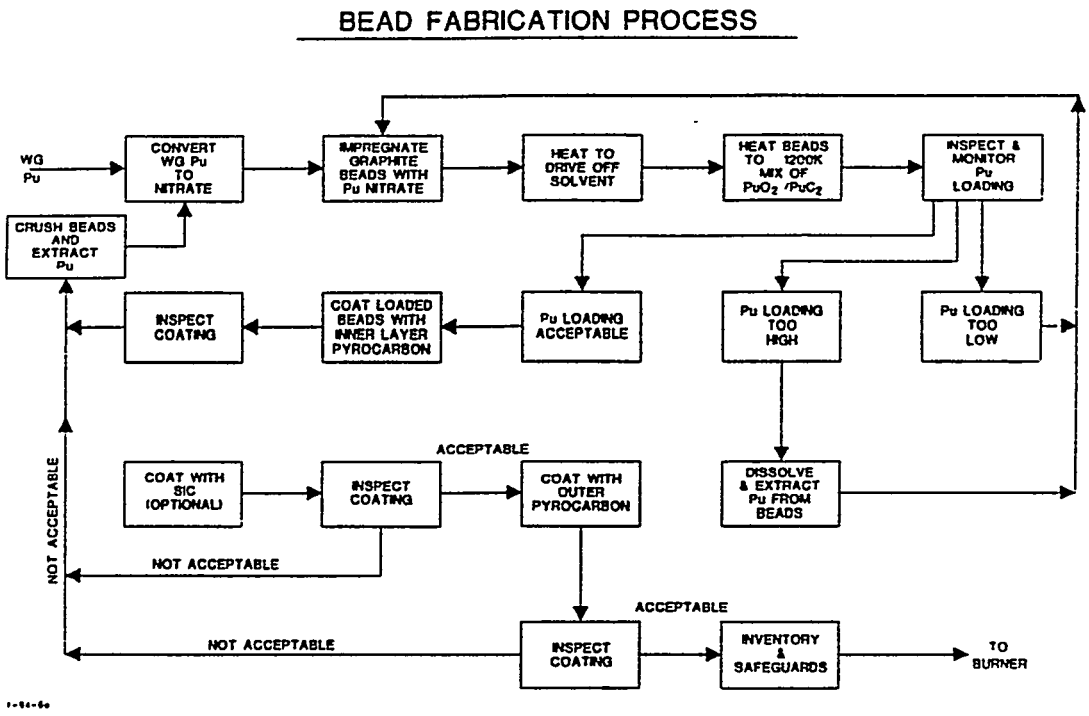

Fig. 4. Solvent impregnation and coating processes for the fabrication of ADAPT fuel beads.

The design value for plutonium loading will depend on the blanket parameters, as well as what fuel cycle is used. A once through cycle (OTTO) can be used, in which the inner and outer blanket regions utilize fuel beads with different fissile loadings, or a cycle (TITO) in which the fuel beads would be shuffled from the inner blanket to the outer after the appropriate burnup level is reached. Other fuel cycle options are possible, using a single fissile loading or several different loading levels in the beads.

Even with high fractional burnup of the fissile plutonium, internal gas pressures in the ADAPT beads will be low, as illustrated in Fig. 5. For a plutonium loading of 0.1 g/cm^3 and 95% burnup, the internal gas pressure will be 80 atmospheres for a 5 millimeter OD bead with a 0.75 millimeter coating thickness. The corresponding tensile stress in the coating will also be low, on the order or 1200 psi, which is much lower than the tensile stress in HTGR fuel particle coatings. Because the ADAPT fuel beads will be under considerably less stressing conditions than HTGR fuel particles, it is expected that they will exhibit even greater integrity than HTGR particles, where a failure rate of only 1 particle out of 10^5 has been achieved.

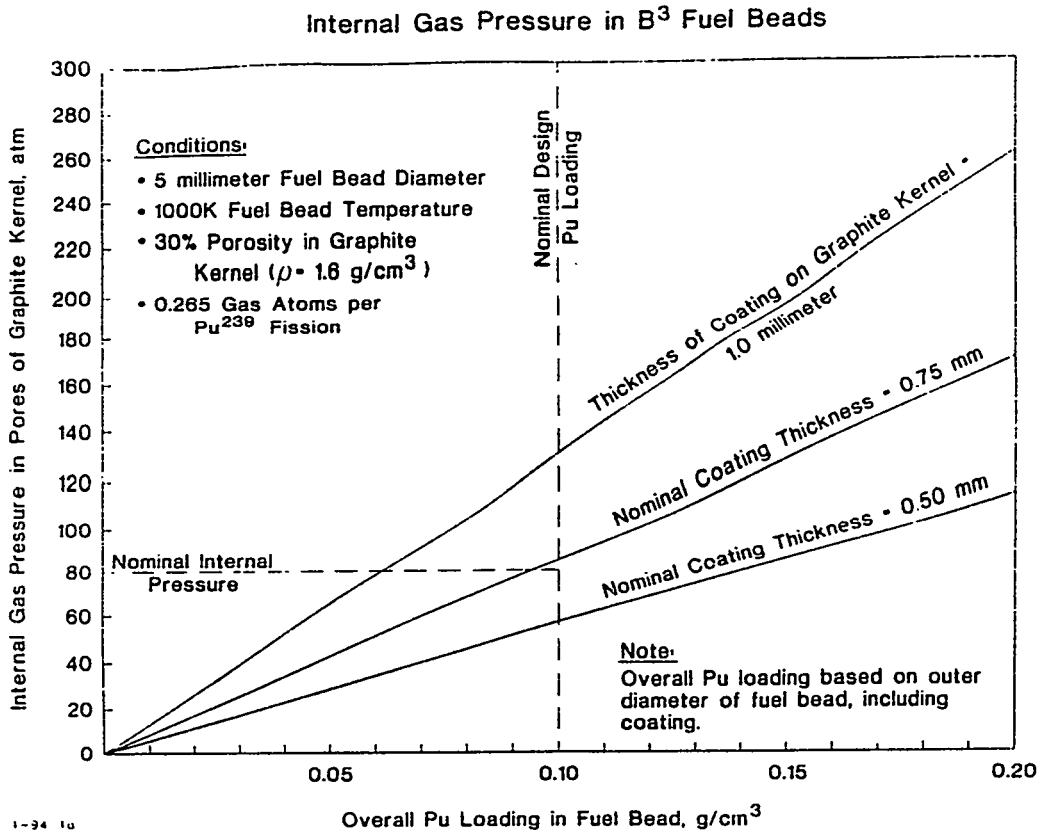

Fig. 5. Internal gas pressure in ADAPT fuel beads as a function of coating thickness and overall plutonium loading.

ADAPT NEUTRONICS AND BURNUP

Neutrons generated in the ADAPT lead D_2O target by spallation reactions from the 1 Gev proton beam enter the surrounding blanket assembly, inducing fission in the plutonium loaded fuel beads. The resultant K_{eff} of the blanket/target assembly depends on its geometry, the thickness of the blanket, plutonium loading in the fuel beads, and the nature of the neutron reflector surrounding the blanket assembly.

Fig. 6 shows a MCNP neutronics analysis of how K_{eff} varies with plutonium loading in the beads, for a typical ADAPT blanket assembly that is reflected by graphite. The height of the blanket assembly is 1.9 meters, and the radial thickness is 0.5 meters. For this particular lattice, a value of 0.95 is attained for K_{eff} at a plutonium loading of 0.08 g/cm^3. At a loading of 0.05 g/cm^3, which would correspond to the average loading in a shuffled lattice fed with fresh beads at a loading of 0.1 g/cm^3, the value of K_{eff} is 0.92.

With design optimization and improved neutron economy, it appears likely that a quasi steady state value of ~0.95 can be obtained for a shuffled lattice fed with beads that are initially loaded at 0.1 g/cm^3.

Fig. 7 shows the fractional burnup of the plutonium loadings as a function of time in the blanket, for initial loadings of 0.05, 0.10 and 0.20 g/cm^3, assuming an average bed power density of 1 Megawatt per Liter. For a 0.1 g/cm^3 loading, and a fractional burnup of 95% of the original Pu-239, the fuel beads would reside in the blanket for a total of 200 days.

K-EFF VS. PLUTONIUM LOADING FOR BNL ACCELERATOR-BURNER TARGET

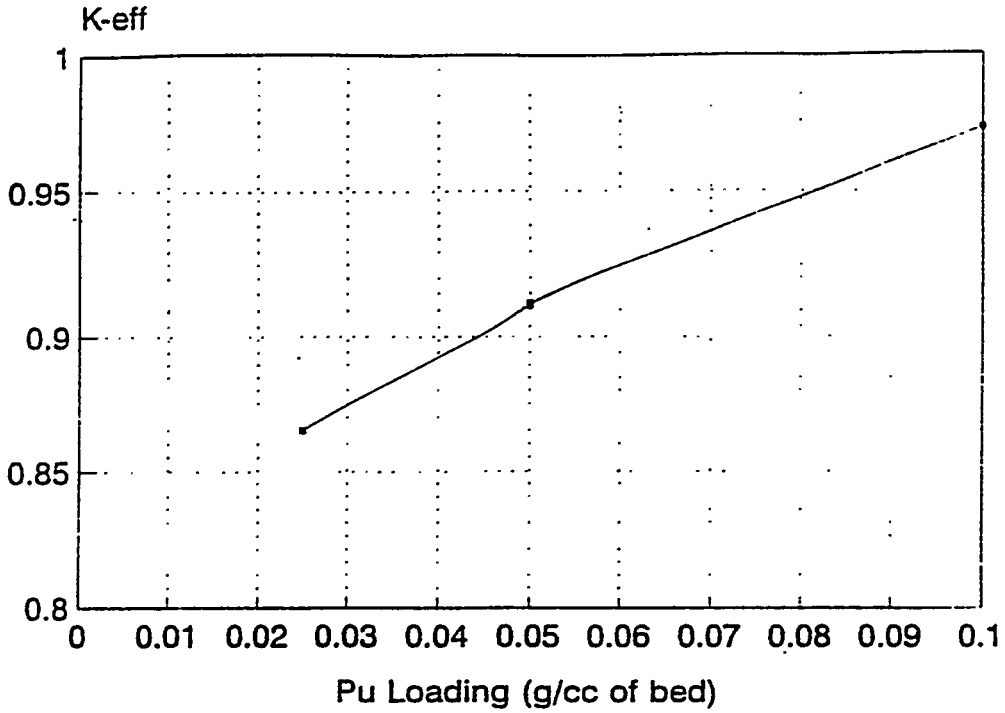

Fig. 6. K_{eff} of the ADAPT blanket/target assembly as a function of plutonium loading in the fuel beads.

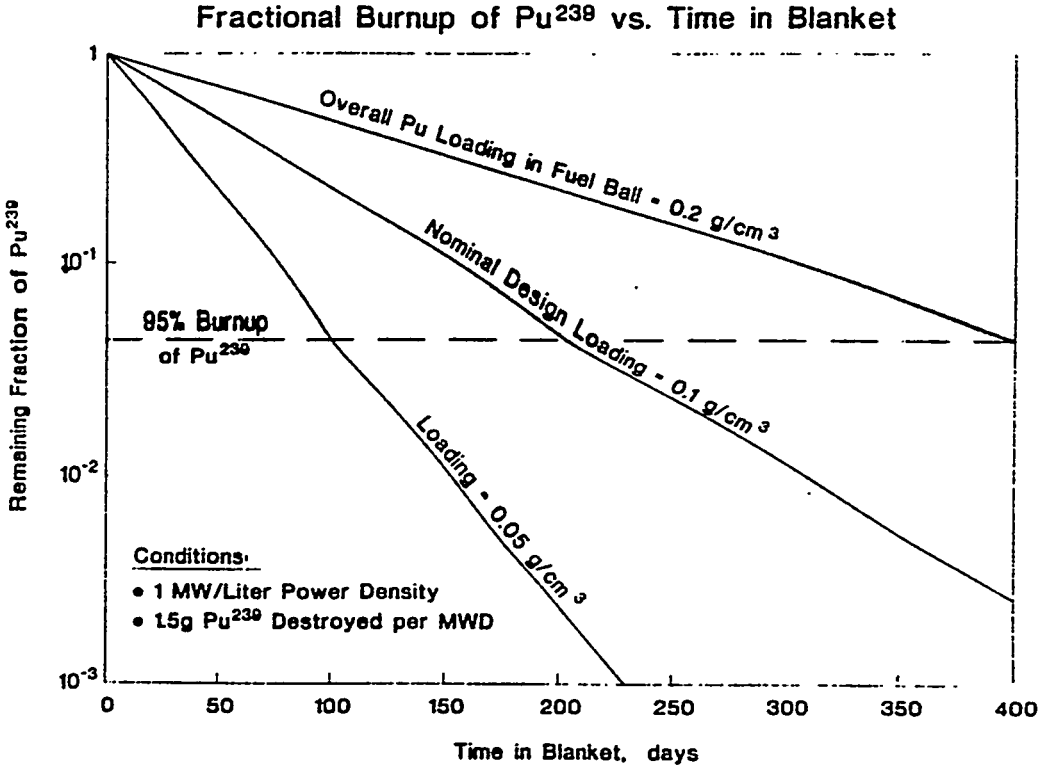

Fig. 7. Fractural burnup of plutonium fuel loading as a function of loading amount and residence time in the ADAPT blanket.

DISPOSAL OF ADAPT WASTES

At high fractional burnups, i.e., in excess of 90% of the original Pu-239, most of the plutonium remaining in the fuel beads would be present as Pu-240 and higher isotopes, rendering it unsuitable for use in nuclear weapons. Since the fuel beads then do not represent a proliferation hazard, are inert, and will have high integrity over geologic time intervals, they can be disposed of in a geologic repository without reprocessing.

Fig. 8 shows a possible approach for final disposal of the ADAPT fuel beads. The spent beads are imbedded in tar, and enclosed in a tar impregnated graphite container. This provides three lines of defense against leakage of long lived actinides and fission products. The first line of defense is the high integrity coatings on the fuel beads. The beads and coatings are chemically inert over geologic times in all types of environments. The failure rate for ADAPT beads is expected to be even lower than the very low failure rates measured for HTGR particles, i.e., less than 1 in 10^5.

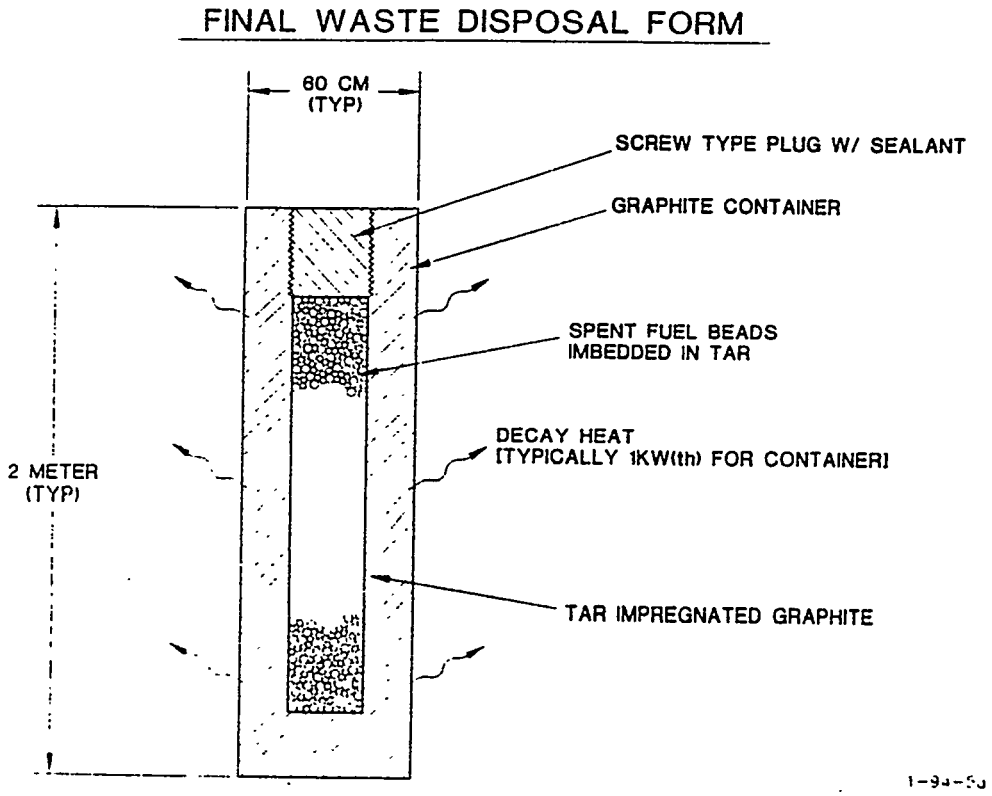

Fig. 8. Proposed containment approach for ADAPT fuel beads enabling burial in a geologic repository.

The second line of defense is provided by imbedding the beads in a tar matrix, and the third line by containing the tar matrix in a mechanically strong graphite container. As with the fuel beads, the tar matrix and the graphite container are chemically inert in a wide range of geologic environments over geologic time periods.

The proposed disposal method appears to offer an attractive combination of excellent containment capability, and minimum requirements for handling and reprocessing.

Safety and Control of Accelerator-Driven Subcritical Systems

H. Rief [1] and H. Takahashi [2]
[1] *Commission of the European Communities, Ispra Establishment, I-21020 Ispra, Italy*
[2] *Brookhaven National Laboratory, Upton, L.I. NY, USA 11973*

Abstract. To study control and safety of accelerator driven nuclear systems, a one point kinetic model was developed and programed. It deals with fast transients as a function of reactivity insertion, Doppler feedback, and the intensity of an external neutron source. The model allows for a simultaneous calculation of an equivalent critical reactor. It was validated by a comparison with a benchmark specified by the Nuclear Energy Agency Committee of Reactor Physics. Additional features are the possibility of inserting a linear or quadratic time dependent reactivity ramp which may account for gravity induced accidents like earthquakes, the possibility to shut down the external neutron source by an exponential decay law of the form $exp(-t/\tau)$, and a graphical display of the power and reactivity changes. The calculations revealed that such boosters behave quite benignly even if they are only slightly subcritical.

INTRODUCTION

In quite a number of studies presented in the recent past it has been shown that an integration of transmutation techniques could reduce substantially the long-term radiation hazard from radioactive waste. Transmutation could also contribute to a safe and even beneficial decommissioning of nuclear weapons. An additional benefit of this more economic use of fuel could be a reduction of radiation hazards from uranium mining.

In the search for transmutation concepts the first candidates were actinide fuelled (critical) reactors. But soon it turned out that they pose a particular problem of control. This is due to the fact that the fissile isotopes of Neptunium, Americium, and Curium have a considerably smaller fraction of delayed neutron emitters (as compared to the more common fuels U-235 and Pu-239) and a non-negative Doppler coefficient. As is well known, the fraction of delayed neutrons is essential for the control of a nuclear reactor in the critical state. To overcome these problems various concepts of accelerator driven subcritical systems aiming at the transmutation of actinides and long lived fission products have been proposed in the recent past.

The safety of multiplying systems depends to a large extend on fast transients caused by accidental reactivity insertions. To study the power changes in accelerator driven systems a kinetic model dealing with fast transients as a function of reactivity insertion, Doppler feedback and the intensity of an external neutron source, was developed and programed.

The model allows a comparison with an equivalent critical reactor. It was tested by a comparison with a NEACRP (Nuclear Energy Agency Committee of Reactor Physics) benchmark. As a general tendency it turned out that accelerator driven systems behave quite benignly even if they are only slightly subcritical

In the past, accelerator driven systems were proposed by several authors as an alternative to fast breeders [1,2,3,4,5] using the term "*electrical breeding*". However, cost estimates for such a hybrid system, consisting of a subcritical reactor and an accelerator coupled to it, led to unreasonably high figures. In the search for new transmutation concepts, accelerator driven systems are now considered competitors of critical reactors serving as actinide burners [6,7].

Especially in the US [8] and Japan [9,10] actinide transmuters of this kind have attracted a great deal of attention. The OECD Nuclear Energy Agency and the CEU have therefore been

SUMMARY AND CONCLUSIONS

The ADAPT concept for plutonium burning appears very promising. It provides high integrity containment for plutonium and fission products, utilizes HTGR technology, has high temperature capability, uses inert coolants and materials, does not require reprocessing of spent fuel, and enables a simple, effective waste disposal approach. More detailed study of the concept is recommended, with particular attention to neutronic burnup analyses and fuel shuffling strategies. Experiments on the fabrication of fuel beads and their capability for high burnup are also recommended.

REFERENCES

[1] Van Tuyle, G. J., et.at., "Preliminary Topical Report for Revision-1 of a Preconceptual Design for the Spallation-Induced Lithium Conversion (SILC) Target for the Accelerator Production of Tritium (APT)", BNL ATD/APT94-0008 (Rev. 0), June 24, 1994.

[2] Ludwig, H., et.al., "Summary of Particle Bed Reactor Designs for the Space Nuclear Thermal Propulsion Program", BNL52408 (1993).

[3] DeMars, R., B&W, *Personal Communication*, (1994).

carrying out studies of new transmutation strategies in an international co-operative effort.

Recent proposals [11,12] promote new accelerator driven fission systems based on the Thorium cycle which is almost free of actinides.

THE KINETIC MODEL

In the following considerations we use the conventional point kinetics equation to which the term $S(t)$ is added. It describes an external source which consists of the spallation neutrons generated by a proton accelerator.

$$\frac{dN}{dt} = \frac{\rho(t,N) - \beta}{\Lambda} N + \sum_{i=1}^{6} \lambda_i C_i + S(t) \qquad (1)$$

$$\frac{dC_i}{dt} = \frac{\beta_i}{\Lambda} - \lambda_i C_i; \quad i = 1, 2, \ldots, 6 \qquad (2)$$

where:

N = number of neutrons in the system (it is considered to be proportional to the power),

C_i = delayed precursor concentration of the *i-th* delayed neutron group,

λ_i = decay constant of the *i-th* delayed precursor group [sec^{-1}],

β_i = delayed neutron fraction of the *i-th* delayed precursor group,

β = total delayed neutron fraction ($=\beta_1+\beta_2+\ldots+\beta_6$),

$\rho(t,N) = \rho_R(t) + \rho_D(N)$ total reactivity variation caused by the time dependent ramp-rate $\rho_R(t)$ and the power (neutron population) dependent Doppler reactivity $\rho_D(N)$,

Λ = prompt neutron lifetime [s],

$S(t)$ = rate at which external neutrons are inserted. This is chosen so that a certain power level is maintained in the system.

The coupled equations (1) and (2) are solved by a numerical method employing a variable implicit technique [13]. The method yields an efficient and accurate solution. The general features of the program include time dependence of the total reactivity, prompt neutron generation time and time step size, and a maximum of six delayed neutron precursor groups. In addition, the total stored energy is also calculated by integrating the reactor power from $t = 0$ to the time of interest.

The solution of Equations (1) and (2) is based on the program described in [13] to which the following features were added:

- The possibility of inserting a linear or quadratic time dependent reactivity ramp. The quadratic time dependent reactivity ramp serves for the simulation of gravity induced accidents like earthquakes, etc.
- A negative reactivity feed-back mechanism to take the Doppler-effect into account.
- The possibility to shut down the external neutron source by an exponential, τ dependent, decay law of the form $exp(-t/\tau)$.
- A graphical display of the power and reactivity changes.

THE EXTERNAL SOURCE

The multiplication Factor of *fission neutrons* (per Spallation Neutron) for subsequent generations in a sub-critical assembly is

$$k_1 + k_1k_2 + k_1k_2k_3 + \ldots \approx k/(1-k) \text{ assuming that } k_1 \approx k_2 \approx k_3 \approx \ldots = k$$

Therefore the power production P_{fi} of a subcritical assembly fed by spallation neutrons can be quantified as:

$$P_{fi} = n_{sp} \frac{a \cdot k}{\nu(1-k)} \frac{I}{C} E_f \qquad (3)$$

where:

k = multiplication factor of the sub-critical system,

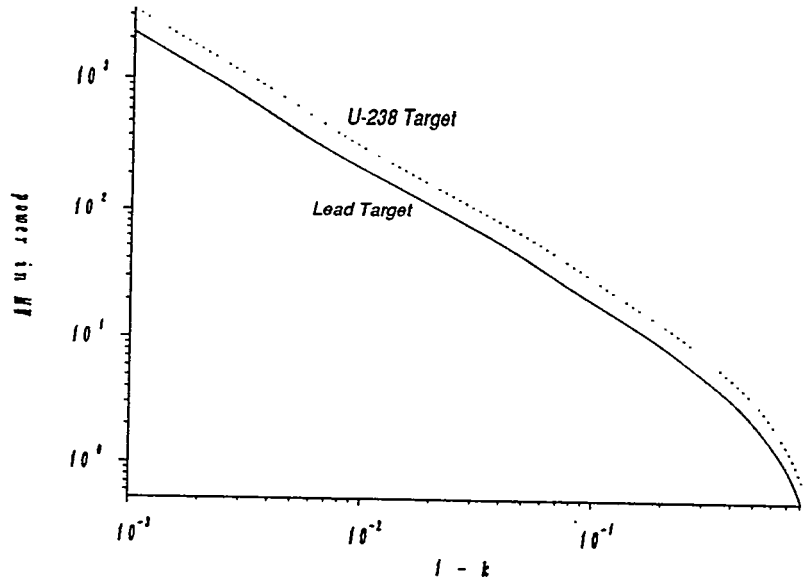

Fig. 1: Power production of an accelarator driven booster as a function of the sub-criticality ($1-k_{eff}$) assuming a proton beam of 1 mA at 1.5 GeV entering a lead or a U^{238} target.

a = importance of the target position and target neutron energy distribution (usually $a>1$ for a cen tral target position),

ν = mean number of neutrons in a fission process,

E_f = power release per fission (= $3.2 \cdot 10^{-11}$ Ws),

n_{sp} = neutron yield from one proton,

I = proton current,

C= proton charge (= $1.6 \cdot 10^{-19}$ A s).

It can be seen that near criticality, already a 1 mA current generates a relatively high fission power. For $k = 0.97$ more than 100 MW can be achieved.

One can assume that $S(t) \cong -\rho_0 n_{sp} / \Lambda$ is a good approximation since the spectrum of the spallation neutrons is quite similar to the fission spectrum, except for a tail of fast neutrons above 20 MeV. It follows therefore that

$$S(t) = P_{fi} \frac{\rho_0}{\Lambda} \frac{\nu(1-k)}{a \cdot k} \frac{C}{I E_f} \qquad (4)$$

THE EFFECT OF UNPROTECTED REACTIVITY ACCIDENTS

Usually three types of unprotected reactivity accidents are considered:
• Slow reactivity ramp insertion, • Fast reactivity ramp insertion, • LOF driven TOP (Fast reactivity ramp insertion due to sodium voiding caused by a loss of coolant accident.)

Slow reactivity ramp insertions without a scram are for example, the inadvertent withdrawal of a control rod(s) (*few cents/s* or *0.0001* k_{eff}/s). A typical fast reactivity ramp insertion occurred in the EBR-I accident which was caused by an inward bowing of the fuel pins. All later fast reactors were constructed with grids or helical wire spacers to prevent bowing. Other accidents of this category are earthquakes or diagrid failures without a scram (up to a *few \$ / s* or *0.01* k_{eff}/s).

Examples

The NEACRP Benchmark Problem. As a first example, the KfK benchmark problem defined as a rod ejection accident and proposed by the Nuclear Energy Agency Committee on Reactor Physics (NEACRP) is chosen. It consists of a fast reactor made up of a core with a bank of annular control rods, radial and axial blankets and sodium coolant. The essential features of the problem are: Axis-symmetry, two neutron groups and six delayed neutron precursor families and thermal feedback through Doppler effects in capture and fission cross sections.

The transient is obtained through steady control rod bank withdrawal. The reactivity insertion starts at *1 ms* and increases at a rate of *170 \$/s* for the duration of *16 ms*. (The speed of the control withdrawal is adjusted to produce a ramp of *0.548cm /ms*.) After this time the reactivity is kept constant.

The reactivity reduction by the Doppler coefficient was calculated from the sample data obtained from Beauwen (1992) as a heat generation coefficient of - *0.921 \$ / GJ*.

The analysis of this problem allows a comparison with transient calculations obtained by others to validate the code used in our analysis. It also gives a first indication of the mitigating effect of using a subcritical, accelerator driven system.

Figures 2a and 2b show the power and reactivity change in a critical reactor and in systems being sub-critical between *-1 \$* and *-3 \$* (dotted lines). These systems are driven by a spallation source dimensioned so that they generate in steady-state operation the same power as the critical reactor, which is assumed to be *1* GW_{therm}.

The power excursion curve which corresponds to a critical reactor oscillates and has two distinct peaks in a short time interval. Super-prompt criticality produces these peaks, as can be seen in Figure 2b. The power rises rapidly during the period of super-prompt criticality and reaches its peak value at the time when the Doppler effect reduces the reactivity to values below the super-prompt limit. (This characteristic is similar to a pulsed reactor).

In the case where the reactor is operated in a subcritical mode, the neutron source is determined so that the system generates *1 GW* thermal power and this source strength is maintained during the whole time the reactivity is increased. When the time reaches *17 ms*, or when the thermal power of the reactor reaches 50 times the initial power (50 GW), the neutron source is reduced by the shut-off function $exp(-t/\tau)$ ($\tau = 1$ *ms*).

For an initial sub-criticality of *-3* and *-2 \$* respectively, the power increases only to *2.2 GW* and *6 GW* respectively after *16 ms* and after *17 ms* the power decreases almost proportionally

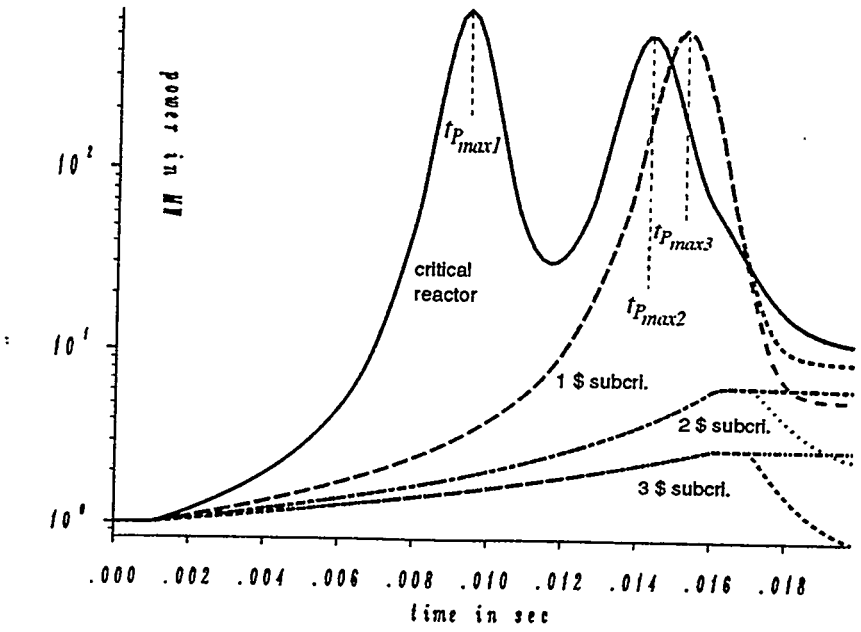

Fig. 2a: Fast reactor power excursion benchmark (as defined in a comparative NEACRP exercise) assuming a rod ejection accident. The reactivity insertion rate is 170 $/s during a period of 15 ms. The power release from a critical reactor is compared with 1$ to 3$ subcritical accelerator-driven systems of the same initial power.

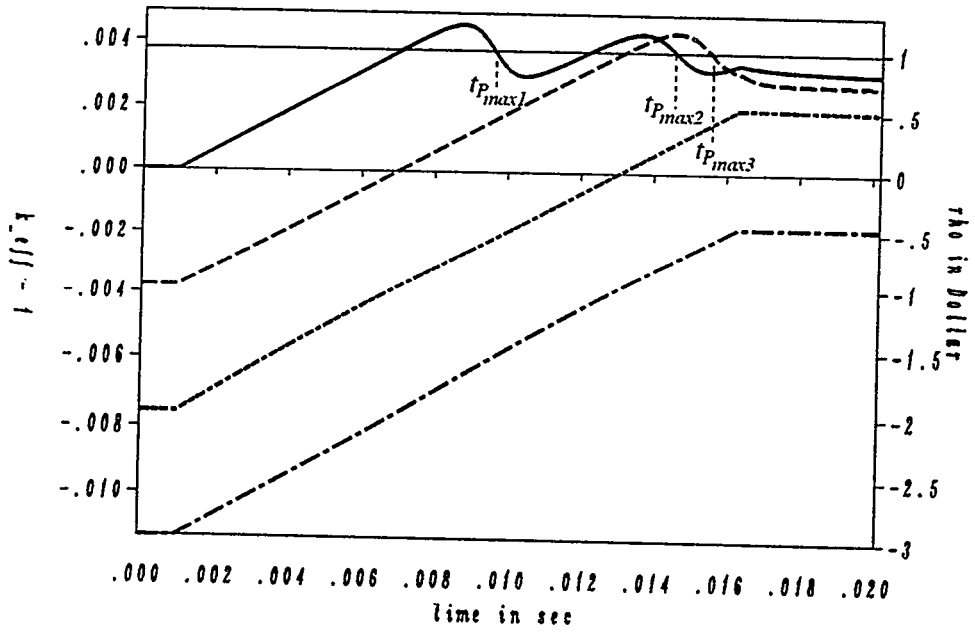

Fig. 2b. The Reactivity Behaviour During the Accident Scenario for the NEACRP Benchmark Exercise.

with the neutron source strength. If on the other hand the neutron source is maintained constant (the accelerator is not shut-off), also the power remains almost constant in this time range. For a subcriticality of only *-1 $*, a single peak-power of *530 GW* was calculated. Even though this value is similar to the peak value of the critical reactor, the integrated power, i.e. the total energy release during the excursion is much less than for a critical system.

An interesting result of this analysis is the fact that the power decreases even between the prompt and delayed critical state. This is due to the long time constant of the delayed neutrons. When the reactor is in an under prompt-critical condition, the neutron flux is controlled by

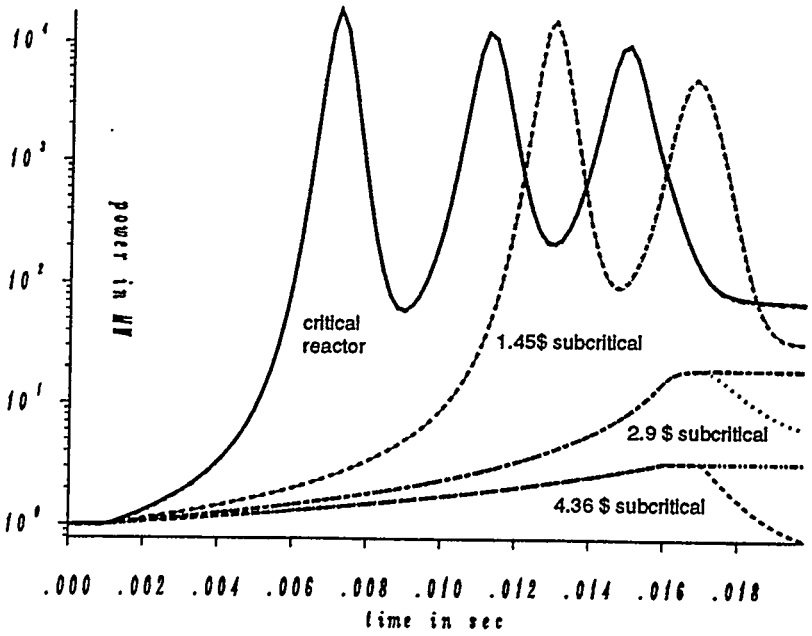

Fig. 3a: Comparison of power excursions in a critical actinide burner (as proposed by Mukaiyama, JAERI) with subcritical accelerator driven systems for an accidental reactivity insertion of 247 $/s of 15 ms duration.

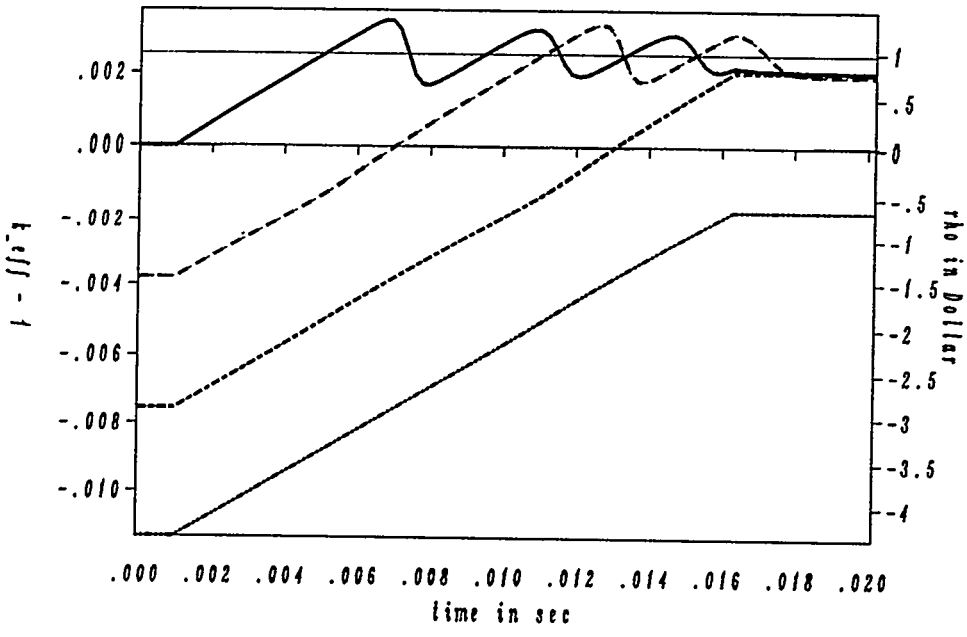

Fig. 3b: The reactivity behaviour during the accident scenario for a typical actinide burner.

prompt neutrons which decrease for a sub-supercritical condition. For the case of a critical reactor two power peaks of *700 GW* and *500 GW* resp. were calculated, which is in good agreement with the results obtained by participants of the NEACRP benchmark.

A Typical Fast Actinde Burner. The next example illustrated in Figures 3a and 3b deals with a typical actinide burner as for example proposed by [9]. Compared to the previous case this system has a shorter neutron generation time (*17 ns*), a smaller delayed neutron fraction (β= *.0026*) and a less effective Doppler coefficient (Δk_{eff} = *-0.0053 $/MJ*).

When the power change is slow, the reactor can be controlled by a mechanical movement of control rods or by a hydraulic dispersion of liquid neutron absorbers which are disolved by melting fuel elements like an electric fuse mechanism. In a subcritical reactor operated by spallation neutrons, the power change is much slower than in a critical reactor. This provides a great advantage from the point of view of reactor safety.

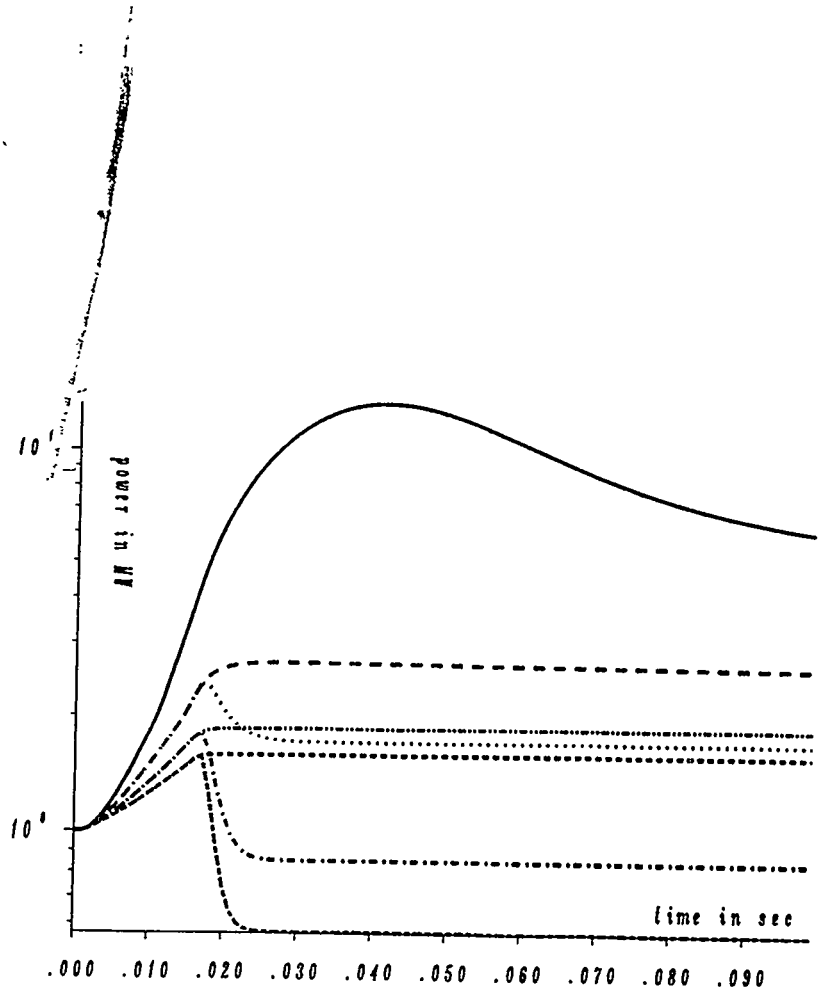

Fig. 3: Comparison of power excursions in a Light Water Reactor with subcritical accelerator driven systems for an accidental reactivity insertion of 66 $/s of 15 ms duration

Accelerator-Driven Thermal Systems. The last example deals with an accelerator-driven light water system. Again the same accident scenarios as in the previous examples are analyzed. The comparison with the critical reactor configuration shows first of all that for the same reactivity insertion as previously assumed, the power excursion is much smaller in the thermal system. Still it seems that the insertion of accelerator induced neutrons may be beneficial in avoiding power transients, but the gain in safety is less evident in this case since system-inherent mechanisms already mitigate such events. Almost all accident scenarios which cause reactivity changes in light water reactors make them less critical. In particular: depressurization, bubble formation, and loss-of-coolant. One of the few anticipated transients without scram is the ejection of control rods caused by a leak somewhere in the guide tubes and the "cold water" accident.

The main concern is the loss of coolant accident with subsequent fuel melt down and fission product release. This accident scenario typically occurs in the sub-critical state of the reactor.

CONCLUSIONS

A new one point kinetics program was developed. It allows the simultaneous calculation of a critical and sub-critical, externally driven system using the same input parameters. The code was validated by re-calculating a NEACRP specified benchmark dealing with the example of a rod ejection accident in a fast reactor.

The few examples treated show that even slightly subcritical systems which require only a low accelerator current, respond much more benignly to a sudden reactivity insertion than critical systems. In realistic accident scenarios with reactivity insertions of a few dollars, already a subcriticality of $\Delta k_{eff} \cong 1\%$ reduces the power transients by orders of magnitude if compared with those of a corresponding critical reactor. To most authors it appears that systems with a k_{eff} of around 0.9 ~ 0.95 (= -30 $ ~ -15 $ for a FR) would even look more attractive from the safety point of view. However, for a well designed multiplying system there are simply no credible accident scenarios which would require such an amount of subcriticality. On the other hand,

these systems would require an expensive high current accelerator. In addition they are characterized by an inhomogeneous power distribution with a sharp peak around the target area.

Accelerator-driven slightly subcritical systems show a relatively flat power distribution, and require a proton current of a few *mA* only. This can be achieved with today's technology, possibly even with Cyclotrons, presumably less expensive than LINACs. In addition, small proton currents facilitate considerably the target construction: less target cooling problems: less difficulties with the target window and less fission product poisoning in the target.

REFERENCES

[1] W. Lewis, Atomic Energy of Canada Ltd., Report AECL-969, (1953).

[2] W. Lewis, Atomic Energy of Canada Ltd., Report AECL-3190, (1968).

[3] M. Steinberg (ed.) Kouts H., in Proc. Inform. Meeting, Accelerator-Breeding, BNL, Report Conf. 770107, 1977.

[4] P. Grand, H. Kouts, J. Powell, M. Steinberg, H. Takahahshi: "Conceptual Design and Economical Analysis of Light Water Reactor Fuel Enrichment/Regenerator", BNL 50838, (UC-80, TID-4500), (1978).

[5] H. Takahashi, et al.: Atomkernenergie, Kerntechnik: 36, 195 (1980).

[6] P. Bonnaure, H. Rief, P. Mandrillon and H. Takahahshi, "Actinide Transmutation by Spallation in the Light of Recent Cyclotron Development", presented at the *4th International Conference on Emerging Nuclear Energy Systems*, Madrid, (1986) and NEACRP-A-910 (1987).

[7] H. Takahashi and H. Rief: "A Critical Review of Accelerator-based Transmutation Systems", invited paper in *Proceedings of the OECD-Nuclear Energy Specialists' Meeting on Accelerator-based Transmutation*, Würenlingen (CH), March 24-26, 1992.

[8] E.D. Bowman, E.D. Arthur et al., *Nuclear Energy generation and Waste Transmutation using an Accelerator-Driven Intense Thermal Neutron Source*, LA-UR-91-2601, 1991.

[9] T. Mukaiyama, H. Takano, T. Takizuka, T. Ogawa and M. Osakabe: "Conceptual Study of Actinide Burner Reactor": in *Proc. 1988 Int. Reactor Physics Conf.*, (Jackson Hole) 1988.

[10] Y. Kato et al., "Accelerator Molten Salt Target System for Transmutation of Long Lived Nuclides", in *Proceedings of the OECD-NEA Specialist's Meeting on Accelerator-Based Transmutation*, PSI Würenlingen/ Villigen, March 24-26, 1992.

[11] J. Toevs, et al., "Progress of ATW Project", in *Proceedings of 8èmes Journées SATURNE*, Saclay, May (1994).

[12] F. Carminati, R. Klapisch, J.P. Revol, Ch. Roche, J.A. Rubio and C. Rubbia, "An Energy Amplifier for Cleaner and Inexhaustible Nuclear Energy Production Driven by a Particle Beam Accelerator", CERN/AT/93-47 (ET), (1993).

[13] H.S.Cheng: "A Point Kinetics Program" BNL Memo, April 26.1976: Revised "Point Kinetic Solution by VIP", BNL Memorandum 8/31/90.

[14] R. Beauwens, N. Guessous, E. Mund and A.Van de Velde: "Intermediate Report on the development of HEXNODYN-2", Service de Metrologie Nucléaire, Unversite Libre de Bruxelles, 1050, February 21, (1992).

Safety Features of Subcritical Fluid Fueled Systems

Charles R. Bell
Technology and Safety Assessment Division
Los Alamos National Laboratory, Los Alamos, New Mexico 87545

Abstract. Accelerator-driven transmutation technology has been under study at Los Alamos for several years for application to nuclear waste treatment, tritium production, energy generation, and recently, to the disposition of excess weapons plutonium. Studies and evaluations performed to date at Los Alamos have led to a current focus on a fluid-fuel, fission system operating in a neutron source-supported subcritical mode, using molten salt reactor technology and accelerator-driven proton-neutron spallation. In this paper, the safety features and characteristics of such systems are explored from the perspective of the fundamental nuclear safety objectives that any reactor-type system should address. This exploration is qualitative in nature and uses current vintage solid-fueled reactors as a baseline for comparison. Based on the safety perspectives presented, such systems should be capable of meeting the fundamental nuclear safety objectives. In addition, they should be able to provide the safety robustness desired for advanced reactors. However, the manner in which safety objectives and robustness are achieved is very different from that associated with conventional reactors. Also, there are a number of safety design and operational challenges that will have to be addressed for the safety potential of such systems to be credible.

INTRODUCTION

Accelerator-driven transmutation technology (ADTT) has been under study [1] at Los Alamos for several years for application to nuclear waste treatment, tritium production, and energy generation. Recently, application of this technology to the disposition of excess weapons plutonium [2] has been considered. The goals for this application are to achieve efficient plutonium burning without involving fertile material, which would produce additional plutonium; to provide the potential for essentially complete destruction of unwanted plutonium; to minimize processing of fuel and wastes; to have inherent safety robustness; and to offset plutonium disposition costs through generation of electric power. Studies and evaluations performed to date at Los Alamos have led to the current focus on a fluid-fuel, fission system operating in a source-supported subcritical mode.

The molten salt technology [3] developed at the Oak Ridge National Laboratory is the basis for the fluid-fuel approach. The fission region is configured and a plutonium concentration is selected such that a desired level of subcriticality is achieved at the operating conditions. High energy protons from a nearby accelerator impinge on a neutron spallation target within the fission region (referred to as the blanket) to produce a continuous, intense neutron source to sustain the fission process at the power level desired. The LAMPF accelerator technology [4] at Los Alamos is the basis for the high current accelerator required. Spallation targets [5] that have been developed and used at Los Alamos and elsewhere for years form the technology base for the intense neutron source. The integration of these major elements into to a feasible system to achieve the desired goals is the thrust of ongoing activities at Los Alamos.

As part of the system conceptualization process, safety characteristics of such systems have been theorized and investigated. In this paper, key safety characteristics of molten salt, accelerator-driven systems are discussed and compared to the safety characteristics for conventional reactors from which the nuclear community, the scientific community, and the public have established their baseline safety perspectives. Through this comparison, a safety perspective for molten salt, accelerator-driven systems, which is radically different, is presented. This perspective also addresses the potential of this concept to conform to the safety expectations for advanced fission systems as delineated by the US Nuclear Regulatory Commission in its policy statement on the regulation of advanced nuclear power plants.

FUNDAMENTAL NUCLEAR SAFETY OBJECTIVES

Accelerator-driven subcritical systems involve sustained fission processes that produce power levels comparable to conventional power reactors. Thus, they can be expected to have large fission product inventories, which constitute hazards of a scale similar to those for conventional fission reactors. As such, a reactor-like nuclear safety approach should be employed. Fundamental nuclear safety objectives [6] universally applied to the design of fission reactors are 1) control of fission power, 2) adequate cooling, and 3) containment of radioactive materials. Because there are characteristics of fluid fueled systems that make them resemble nuclear processing systems, two additional safety objectives have been added. These additional objectives are 4) prevention of inadvertent criticality and 5) control of personnel exposure. All of these objectives should be emphasized during the design process. They also would be the focus of safety reviews and licensing processes.

Meeting these objectives is key to controlling the fundamental health and safety hazard associated with such systems, namely radiation exposure to operations personnel and the public. Control of power levels and provision of cooling, such that over heating does not occur at any location where power is generated, must be assured under all conditions (power operation, shutdown, cold or hot standby, various power levels, stages in systems life) and circumstances (component failures, system failures, accidents, etc.). Likewise, inadvertent criticality and large integrated radiation exposures to personnel must be prevented under all conditions and circumstances.

For such a system to be licensed in the United States, it also would need to have characteristics consistent with those delineated by the Nuclear Regulatory Commission (NRC) in its policy statement on regulation of advanced nuclear power plants [7]. This policy emphasizes the desirability of the following attributes:

- highly reliable and less complex shutdown and decay heat removal systems, using inherent or passive means;
- longer time constants and sufficient instrumentation to allow for more diagnosis and management prior to reaching safety system challenges and/or exposure of vital equipment to adverse conditions;
- simplified safety systems which, where possible, reduce required operator action, equipment subjected to severe environmental conditions, and components needed for maintaining safe shutdown conditions; such simplified systems should facilitate operator comprehension, reliable system function, and more straightforward engineering analysis;
- designs that minimize the potential for severe accidents and their consequences by providing sufficient inherent safety, reliability, redundancy, and independence in safety systems;
- designs that provide reliable equipment in the balance of plant (or safety system independence from balance of plant) to reduce the number of challenges to safety systems;
- designs that provide easily maintained equipment and components;
- designs that reduce potential radiation exposure to plant personnel;
- designs that incorporate defense-in-depth philosophy by maintaining multiple barriers against release of radioactive materials, and by reducing the potential for and consequences of severe accidents; and
- design features that can be proven by citation of existent technology or that can be satisfactorily established by commitment to a suitable technology development program.

These characteristics provide the safety robustness (simplicity, sluggish response, passive system reliability, reduced system interdependencies, reduced severe accident concerns, assured defense-

in-depth barriers, greater clarity in safety analyses and margins, etc.) that is desired for advanced systems, the initial versions of which will have little operational history.

SAFETY FEATURES AND PERSPECTIVES

In the this section, a qualitative perspective on the manner in which accelerator-driven subcritical systems and conventional reactors meet the five fundamental safety objectives is presented. The apparent safety robustness, or lack thereof, associated with accelerator-driven subcritical systems also is addressed.

Control of Fission Power

Control of the fission rate and therefore power generation has been recognized as an extremely important topic for fission reactors since the beginnings of reactor theory. The response of a neutronically critical system is highly nonlinear and rapid; the initial response being related to the prompt neutron generation time and the longer term response being related to the addition of delayed neutrons from particular decaying fission products. Indeed, it is these delayed neutrons that make practical reactor control feasible.

A key design objective has always been to ensure reactivity control (and therefore control of fission power) through an understanding the reactivity changes that can occur in a system and to provide an effective response to those changes using engineered control and safety systems and/or inherent reactivity feedbacks. Reactivity control systems must be capable of preventing power levels that exceed specific limits, which are set to ensure fuel stability (no significant melting, movement, or dimensional changes), cooling sufficiency, and first barrier (clad) integrity.

To obtain a general sense of the relative responses of critical and subcritical systems to postulated reactivity insertion events, simple point kinetics calculations were performed. The postulated reactivity insertion rate was 1 $/s, and its duration was assumed to be 0.5 s and 1 s. No reactivity feedbacks were assumed in either case to simplify the understanding of the results. The initial multiplication in the subcritical system was assumed to be 0.96, and the initial power for both systems was assumed to be 500 MW. The results are shown in Fig. 1. As expected for the critical system, the power rises rapidly and continues to rise after the reactivitiy insertion is terminated. Without negative reactivity insertions from inherent negative feedbacks and/or insertion of neutron absorbers, the transients are unterminated. The response of the subcritical system is markedly different in that the power changes very little. The power is proportional to the inverse of the degree of subcriticality of the system. The degree of subcriticality initially is 1-0.96 or 0.04. At the end of the 1 s reactivity insertion transient, one dollar (for the plutonium fueled molten salt system considered, some of the delayed neutron are released beyond the boundaries of the core, making a dollar of reactivity approximately equal to 0.002) of reactivity is inserted, making the final multiplication of the system equal to 0.962 and the degree of subcriticality equal to 0.038. The power change is approximately 5%, and a new steady state is established.

A subcritical system appears to be robust in accommodating postulated neutronic upset conditions because the system's response is predictable and relatively insensitive (small power changes for large reactivity changes) as long as the degree of subcriticality is substantial. If the system is assumed to be initially at a multiplication of 0.98 and the same reactivity insertion event is postulated (1 $/s for 1 s), the power would change by approximately 11%. If the system is assumed to be initially at a multiplication of 0.99 and the same reactivity insertion event is postulated, the power would change by approximately 25%. By selecting a substantial degree of subcritically for an operating point, the system would have large margins for reactivity changes without becoming critical and thereby transitioning to the nonlinear response regime or becoming prompt critical without hope of control.

Although these large margins and the decoupling of power changes from reactivity changes are attractive from the standpoint of the potential for power excursions, it is also true that desirable feedbacks such as those from system temperature changes only weakly affect the

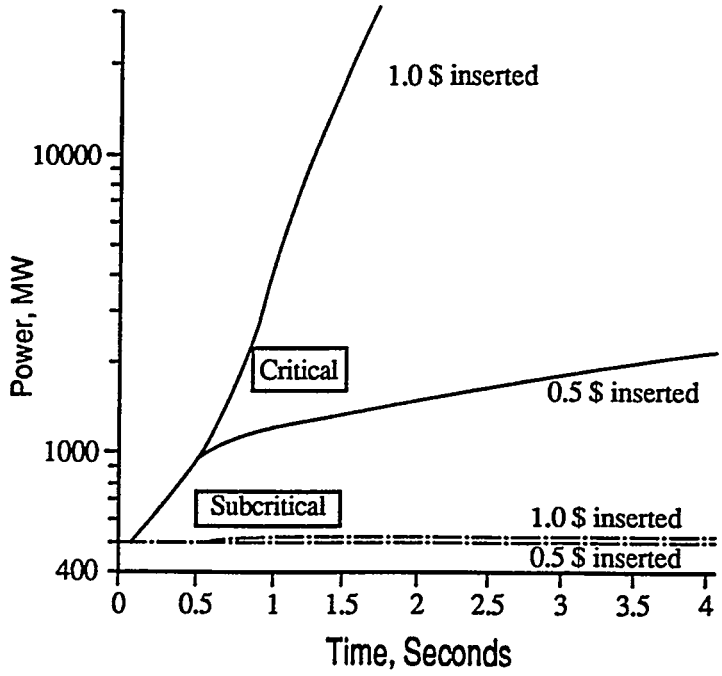

Fig. 1. Relative responses of critical and subcritical systems to reactivity insertions.

power. Thus, inherent power control is largely denied and must be replaced with active control. Active control with absorber rods also would not be particularly effective because of the power-reactivity decoupling. Thus, the active control would probably need to be done by varying the proton beam characteristics such that the neutron source intensity can be changed.

A second objective for reactor-type systems has always been to provide the capability for highly reliable and rapid termination of the fission process (scram) if the control system were to fail or unforeseen reactivity increases were to occur. Of particular importance is the prevention of the prompt-critical condition in which the power rises at such a high rate that the core and potentially other barriers against the release of radioactive materials could be compromised.

Normally reactors have mechanically inserted neutron absorber components (shutdown rods, safety rods, absorber balls, etc.) to provide the scram function. To achieve the desired high functional reliability of inserting these absorbers on demand, redundancy and diversity of components and systems are often employed. A high degree of assurance must be provided that core dimensional changes due to irradiation induced material swelling or thermal expansions do not prevent absorber insertion. Also a high degree of assurance must be provided that absorber insertion can be accomplished during seismic events. It is also important that the scram function be accomplished in the time interval required to intercept power excursions before safety limits are reached.

The situation is schematically portrayed in Fig. 2. For a typical reactor system, if the scram setting is reached, detectors sense the condition, the scram system sends signals to the actuation systems to insert the absorbers, the absorbers begin to move into the core as their inertia is overcome, negative reactivity is added to the core as the absorbers engage the core more and more, the power rise is arrested, and the system is shutdown after a short period of time. Because of the delays associated with absorber insertion, the power continued to rise above the scram point as shown. This power over-shoot for postulated transients must be predicted and included in the design of the shutdown system to ensure that safety limits are not exceeded. If a similar event were to occur in an accelerator-driven subcritical system, the delays would be limited to those associated with detection of the condition, scram system processing of the signals, and actuation of any number of beam interrupts. Once the proton beam is interrupted, the source neutron production stops nearly instantaneously and the power in the subcritical system drops promptly. Thus, the shutdown can be accomplished quickly,

predictably, and reliably following detection of the need for shutdown. The need for in-core neutron absorber insertion with the associated mechanical complexities is eliminated. The complexities associated with "managing" the power over-shoot also are eliminated.

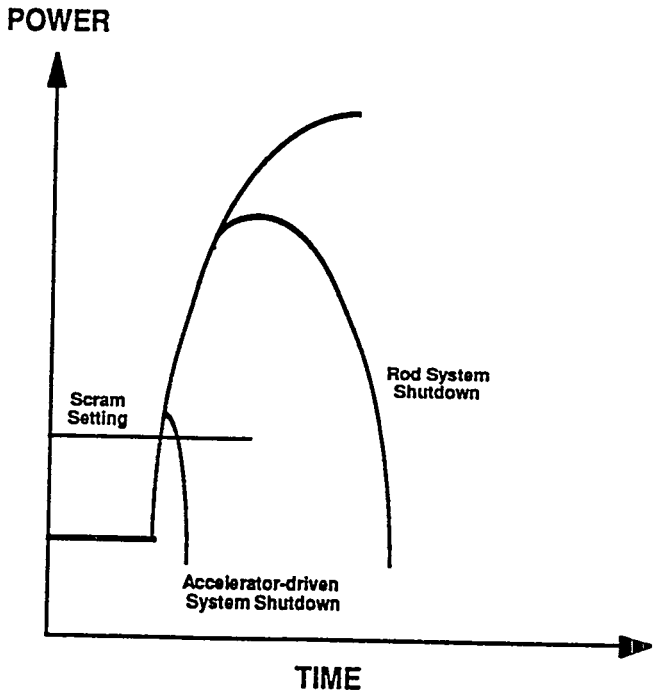

Fig. 2. Rapid shutdown potential for accelerator-driven fission systems.

Adequate Cooling

Assuring adequate cooling in all situations also has been recognized as an extremely important topic for fission reactors since the beginnings of reactor engineering. Because the integrity of the first barrier (for discussion purposes, the clad on fuel pins is considered the first barrier) is a key element in the defense-in-depth strategy for preventing the release of fission products and because this integrity is strongly linked to clad temperature, adequate cooling must be assured for normal power operations, for a variety of off-normal situations including accidents, and for shutdown with the associated decay heat from the fission products.

For conventional solid fueled reactors with high power densities and water coolants, the clad temperature can rise rapidly if cooling is interrupted locally. The rate of temperature rise is related primarily to the heat capacity of the core materials and the local power density. Because the clad temperature rise can be rapid, cooling interruptions due to degraded local heat transfer processes (such as departure from nucleate boiling) or insufficient coolant flow can not be tolerated. For the molten salt system, the first barrier is the primary system boundary (vessel, piping, heat exchanger tubes, etc.). The thermal response of this first barrier is linked to the heat capacity of the entire primary system, which is substantially larger than that of the core alone. As shown schematically in Fig. 3, the rate of temperature rise would be much lower if cooling is interrupted. This slow, system-wide response provides substantially increased opportunities to sense inadequate cooling conditions and to respond appropriately (such as scram, switching to emergency power, realigning valves, etc.). Thus, the molten salt system exhibits a thermal robustness that is attractive.

The molten salt system also exhibits robustness from the standpoint of heat transfer and heat transport in the core region. Again the point of reference is a solid fueled, rod-type core. The heat transfer situation is shown schematically in Fig. 4. The heat is generated in the solid fuel material and is transferred out of the fuel, across the fuel-clad gap, through the clad, and to

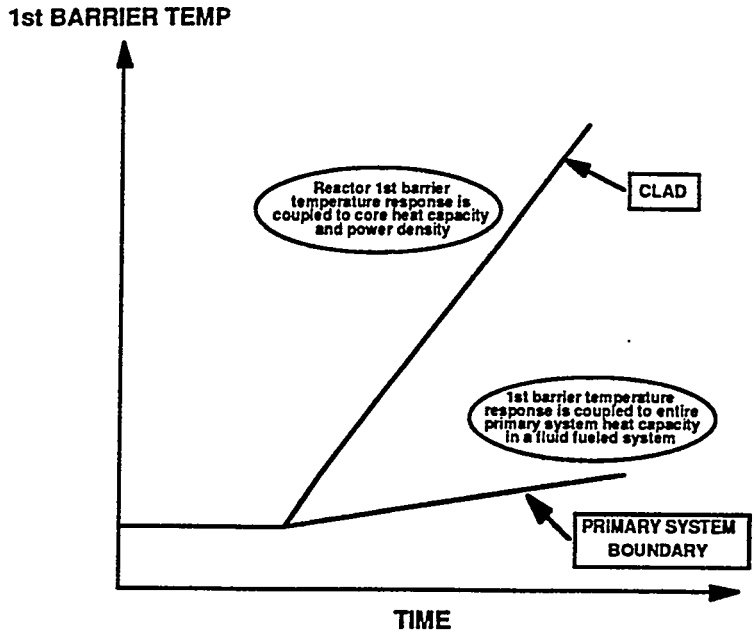

Fig. 3. Relative thermal response characteristics for solid and fluid fueled systems.

the surrounding coolant. The heat transfer processes include conduction, radiation, and convection. The overall heat transfer-heat transport process is sensitive to dimensional changes, fuel restructuring, fission gas content in the gap, coolant pressure, coolant subcooling, and coolant velocity. Many of these aspects can change substantially during core life, for different operating modes, and for off-normal and accident conditions. Thus, the overall heat transfer-heat transport process is complex yet must be known reasonably well to assure adequate cooling and protection of the first barrier under all circumstances. Also shown in Fig. 4 is a schematic of a typical molten salt core (in the accelerator-driven system it is referred to as the blanket) in which the salt flows through a graphite moderating structure. Because the fissioning materials are in the flowing molten salt, the heat is generated directly in the molten salt, which is also the heat transport medium. Thus, all coupled heat transfer-heat transport processes are eliminated in the core. This arrangement also appears to have a self limiting characteristic in that if cooling in the core (heat transport in this case) is inadequate, the coolant/fuel salt over heats, eventually boils, is ejected from the core, and effectively stops the fission process locally (fissioning materials removed).

The final aspect of assured cooling considered in this paper is that of decay heat removal, which also is extremely important for the protection of defense-in-depth barriers. A schematic comparison of the decay heat removal situation for the solid and fluid fueled systems is shown in Fig. 5. For both system, the challenge is to get the decay heat to an ultimate heat sink. The challenge of assuring an ultimate heat sink is the same for both systems. Again, however, there is the complexity in the solid fuel system of getting the heat from the compact core to the primary heat transport system. In the molten salt system, the decay heat is generated throughout the salt inventory in the primary system. Thus, this system has the possibility for predictable natural convection cooling to the primary system boundary and the possibility of radiant heat rejection from the primary system boundary to an external heat sink, if the individual systems are not too large. This could constitute a completely passive decay heat removal system.

Containment of Radioactive Materials

Because the accelerator-driven molten salt system operates at high power and involves a fission process, it has essentially all the hazards that are normally associated with conventional

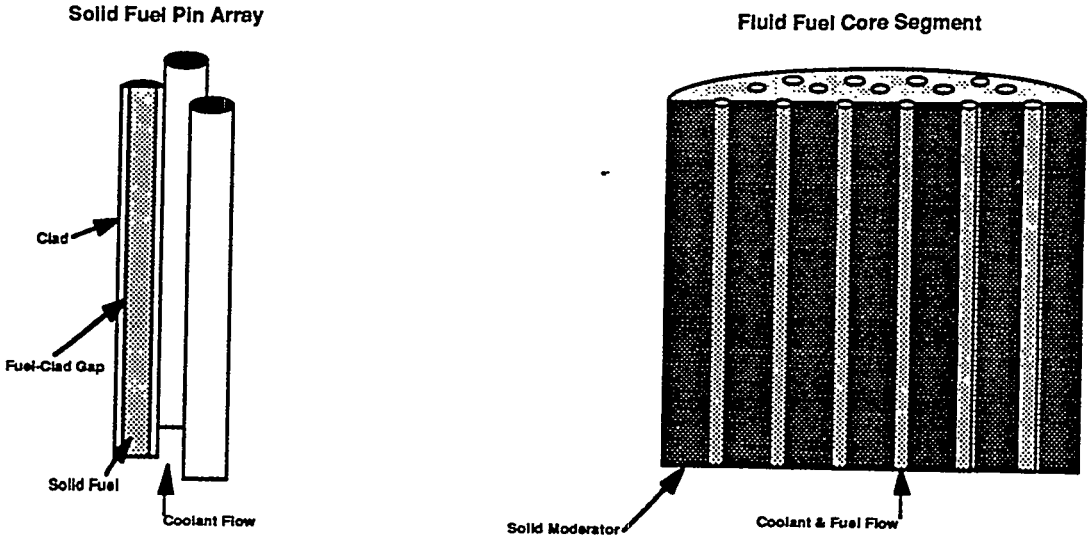

Fig. 4. Cooling arrangements for representative solid and fluid fueled systems.

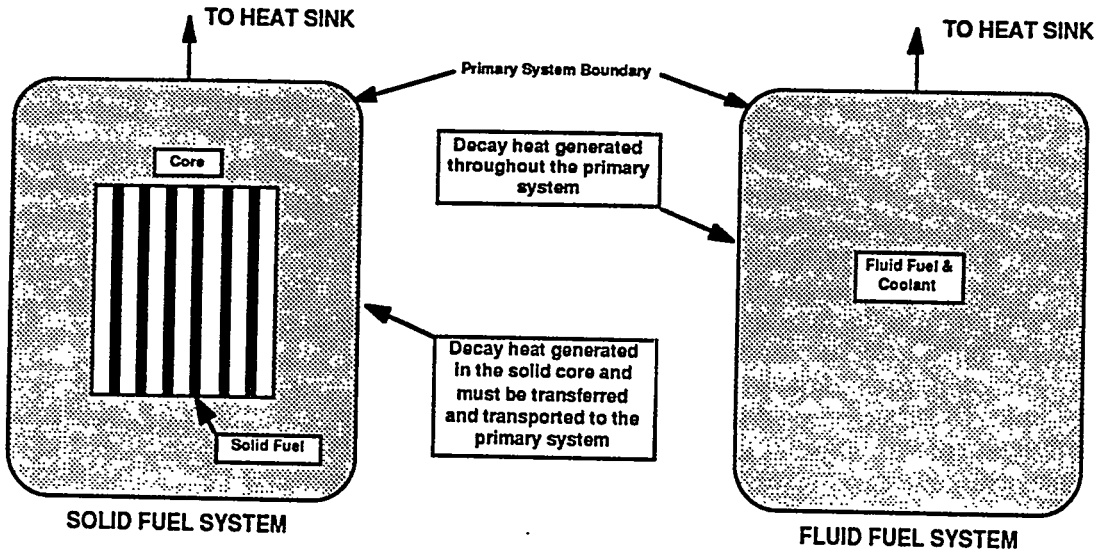

Fig. 5. Decay heat removal in solid and fluid fueled systems.

fission reactors, particularly with regard to fission products. The type and quantities of fission products are different for the molten salt system (gaseous fission products will not remain in the molten salt and will have to be collected and stored in special systems that are separate from the primary system), but will, never the less, constitute a formidable hazard. Thus, containment of the radioactive materials at all time and for all conditions must be accomplished for the molten salt system.

The challenge of providing appropriate defense-in-depth barriers will need to be met with a different approach for the molten salt system. In conventional reactors, the first barrier is a challenge to protect and to assure its function, but it has a limited life requirement (approximately 3 years and then it is replaced) and it is compartmentalized in the form of many individual sealed units (each fuel pin). Thus, if a few of the individual units of the first barrier fail for some reason, only a relatively small fraction of the fission product inventory is released to the next barrier. In contrast, if the first barrier (the primary system boundary) of the molten salt system fails for some reason, essentially all the fission product inventory in the salt will be released to the next barrier.

The options to deal with this challenge appear to be to assure high reliability in the performance of the primary system boundary, to provide a highly reliable and effective second barrier, or both. Because the first barrier is not in the core and therefore does not affect neutronic performance and is generally accessible, design flexibility should exist to make the primary system boundary highly robust and to provide inspectability by remote means. Although, engineering design layouts of various options for the second barrier have not been completed, the approach used for the Molten Salt Reactor Experiment [8] appears to have merit and to be feasible. Sealed vaults with appropriate heat removal systems, atmosphere control systems, spill recovery systems, etc. could be used. Finally, the defense-in-depth barrier strategy would be completed with a surrounding containment or confinement structure as appropriate. The barrier arrangements for a conventional reactor and for the molten salt system are shown schematically in Fig. 6.

Another special challenge for the accelerator-driven molten salt system is the integration of the beam transport equipment with the containment barriers. The proton beam can not pass directly through heavy-walled structures without substantial beam loss and the generation of significant heat and radiation. Some type of thin-window approach is necessary. To accommodate the conflicting requirements of barrier robustness and beam window thinness, it may be necessary to make the beam transport tube part of the barrier system. This would probably require the beam tube to be a reentrant thimble through the outer containment barrier, the vault barrier, and the primary system barrier. The target system and its associated thin window would be positioned entirely within this thimble.

Prevention of Inadvertent Criticality

Prevention of inadvertent criticality in conventional reactors is a relatively straightforward matter because it is a concern only for fuel handling, new fuel storage, and spent fuel storage. Because the fuel is in the solid state, is segregated into numerous individual assemblies, can be handled in a very controlled manner, can be monitored for structural deterioration, and can be stored in well characterized and robust structures (physical spacing and integrated neutron absorbers), it is extremely unlikely that an inadvertent criticality would occur.

In contrast, the molten salt system presents challenges in assuring that the location of all fissile material is known at all times. The potential for precipitation of fissile materials from the molten salt under various expected and postulated conditions must be considered. The

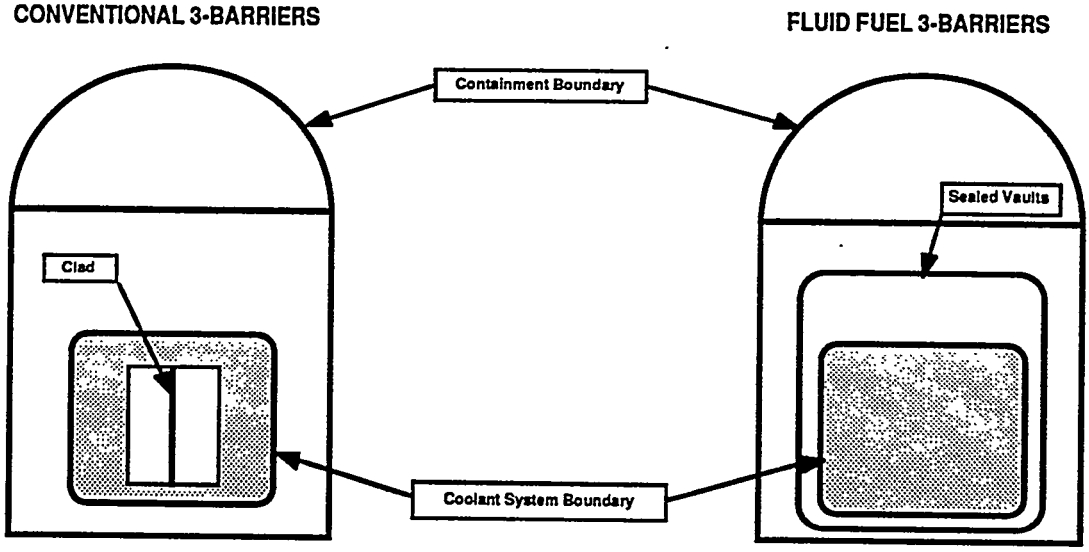

Fig. 6. Barrier arrangements for representative solid and fluid fueled systems.

potential for criticality in the fissile material feed system must be considered. The potential for criticality in the salt cleanup and processing system must be carefully considered. Salt storage

systems may need to be designed to accommodate some precipitation should the molten salt temperature drop to the freezing point. Care will also be required to assure that spills and leaks accumulate in subcritical configurations. The opportunities for inadvertent criticality are certainly greater in the fluid fueled molten salt system compared to conventional solid fueled systems. The criticality concerns should be mitigated somewhat by the subcritical character of the molten salt in an accelerator-driven system. However, the concerns will also be dependent on the degree of moderation provided in the core/blanket design and whether the opportunity exists to substantially increase neutronic multiplication in ex-core regions where substantial salt might accumulate. With the exception of the feed system, inadvertent criticality would occur only in unoccupied, robust, vault-type structures and therefore would not present a direct hazard to workers or the public.

Radiation Exposures to Personnel

Integrated exposure to the operating staff of a conventional reactor power station has become a figure-of-merit for the quality of the operation; reliability of equipment; and the provisions in the design for ease of maintenance, inspections, testing, and repairs. The accelerator-driven molten salt system has the potential to present a considerable challenge to designer and operators relative to this figure-of-merit. The challenge has its origin in four characteristics of the accelerator-driven molten salt system. First, the fissions products distributed throughout the primary system produce extremely high radiation fields in all areas adjacent to the primary system and potentially high exposures during incident recovery operations (spills) or eventual decontamination and decommissioning. Second, delayed neutron production throughout the primary system activates all primary system equipment resulting in radiation exposure potentials even after decontamination. Third, the target and thimble systems will have limited life and require frequent replacement, leading to exposure potentials. Fourth, the use of a lithium based salt will result in the generation of substantial tritium, which will diffuse through the metallic boundaries and produce exposure potentials. All of these exposure potentials will have to be recognized in the design process, including those associated with postulated off-normal events, and special provisions will have to be included to protect workers during inspections, testing, maintenance, and repairs. A high premium will need to be placed on highly reliable equipment.

SUMMARY

The accelerator-driven molten salt system has the potential to provide robust, predictable, straightforward, attractive safety characteristics in the areas of power excursion prevention, assured shutdown, assured cooling, and energetic severe accident prevention. Containment of radioactive materials through a defense-in-depth strategy is feasible for this system, but presents the challenge of integrating the proton beam tube with the desired robust barrier systems. Inadvertent criticality will require special attention in the design because of the decreased predictability of the location of all fissile materials in a fluid fueled system. Also special attention will be required in the design to manage the increased potentials for exposures to plant personnel arising from the distributed fission products in the primary system, extensive delayed neutron activation of equipment, target system replacement, and tritium control. It should be noted that the positive safety effects that result from subcritical operation can only be realized if the subcriticality status of the system is continuously known and within required limits. This is a challenge, but some plausible approaches have been defined.

The fundamental safety objectives for reactor-like systems can be accomplished in an accelerator-driven molten salt system, albeit by very different means. Many of the desirable characteristics of advanced reactor systems delineated by the USNRC can be provided by such a system. Others of these characteristics, such as providing easily maintained equipment and components and reducing the potential radiation exposure to plant personnel will be design challenges.

REFERENCES

[1] C. D. Bowman, "Overview of the Los Alamos Accelerator-Driven Transmutation Technology Program," presented at the International Conference on Accelerator-Driven Transmutation Technologies and Applications, Las Vegas, Nevada, July 25-29, 1994.

[2] R. J. Jensen et al, "Accelerator-Based Conversion (ABC) of Reactor and Weapons Plutonium," *Proceedings of the International Conference and Exposition on Future Nuclear Systems: Emerging Fuel Cycles and Waste Disposal Options Global 93*, 1993.

[3] R. O. Robertson, "Conceptual Design Studies of a Single-Fluid Molten-Salt Breeder Reactor," Oak Ridge National Laboratory report, ORNL-4541, 1971.

[4] G. Lawrence, "Los Alamos High-Power Proton Linac Design," presented at the International Conference on Accelerator-Driven Transmutation Technologies and Applications, Las Vegas, Nevada, July 25-29, 1994.

[5] G. Russell, et al., "Introduction to Spallation Target Requirements," presented at the International Conference on Accelerator-Driven Transmutation Technologies and Applications, Las Vegas, Nevada, July 25-29, 1994.

[6] International Nuclear Safety Advisory Group, "Basic Safety Principles for Nuclear Power Plants," International Atomic Energy Agency, Safety Series No. 75-INSAG-3, 1988.

[7] US Nuclear Regulatory Commission, "Regulation of Advanced Nuclear Power Plants; Statement of Policy," *Federal Register*, 51 FR 24643, July 1, 1986.

Los Alamos High-Power Proton Linac Designs

George P. Lawrence
Accelerator Operations and Technology Division,
Los Alamos National Laboratory, Los Alamos, New Mexico, 87545 USA

Abstract. Medium-energy high-power proton linear accelerators have been studied at Los Alamos as drivers for spallation neutron applications requiring large amounts of beam power. Reference designs for such accelerators are discussed, important design factors are reviewed, and issues and concerns specific to this unprecedented power regime are discussed.

INTRODUCTION

For the past few years Los Alamos has been studying designs of high-power medium-energy proton linear accelerators suitable for driving spallation-technology transmutation applications, including destruction of nuclear waste, plutonium disposition, production of nuclear materials (^{3}H and ^{238}Pu), and generation of fission power from the $^{232}Th/^{233}U$ cycle. Many of these applications are discussed in other papers in these proceedings and elsewhere.[1-5] Such accelerators span the energy range 600 MeV to 1600 MeV, and the (average) current range 10 mA to 300 mA. Los Alamos designs have focused on the higher power end of the range, a region where CW linacs offer a practical near term solution to the beam requirements.[6,7] Point designs based on conventional water-cooled copper accelerating structures have been evaluated at 1600 MeV/250 mA, at 1000 MeV/200 mA, and at 800 MeV/80 mA. These concepts have been examined by high-level review panels, including DOE's Energy Research Advisory Board, the JASONs, and the National Academy of Sciences, which have agreed in broad terms on the present practicality and feasibility of such accelerators, given the existing technology base.

FUNNELED REFERENCE DESIGN

A reference concept for a 200-mA CW 1000-MeV linac has been studied in some detail during the past two years. Several papers in these proceedings discuss considerations and designs for important components and subsystems.[8-11] The accelerator architecture, displayed in Fig. 1, consists of a front-end system in which two 100-mA beams from identical low-energy linacs are combined (funneled) at 20 MeV, followed by a high-energy linac that accelerates the 200-mA beam to 1000 MeV. In each of the two low-energy linacs, a microwave-driven ion source generates a 100%-duty proton beam that is injected at 75 keV through a solenoid-focused low-energy-beam-transport (LEBT) system into a 350-MHz radio-frequency quadrupole (RFQ), which bunches the beam and accelerates it to 7 MeV. The 100-mA bunched beams exiting the RFQs are further accelerated to 20 MeV in a 350-MHz Alvarez drift-tube linac (DTL). At this point, the two identical bunch trains are combined longitudinally in an RF funnel to produce a 700-MHz, 200-mA beam. This beam is accelerated to 100 MeV in a new hybrid structure called a bridge-coupled drift-tube linac (BCDTL), and then to 1000 MeV in a coupled-cavity linac (CCL) similar to the one driving the Los Alamos Neutron Science Center (LAMPF). The high-energy accelerating structures are powered by 1-MW CW RF amplifiers (klystrons), and constitute the bulk of the linac length.

Several key design parameters are displayed in Fig. 1. Additional parameters describing each of the accelerator sections are given in Table 1. The total RF power required to accelerate the 200-MW beam is 254 MW, which includes both the 700-MHz power systems

needed for the BCDTL and CCL, and the 350-MHz systems needed for the two front-end RFQs and DTLs. The power delivered at 700-MHz is 97% of the total. Because of the high .

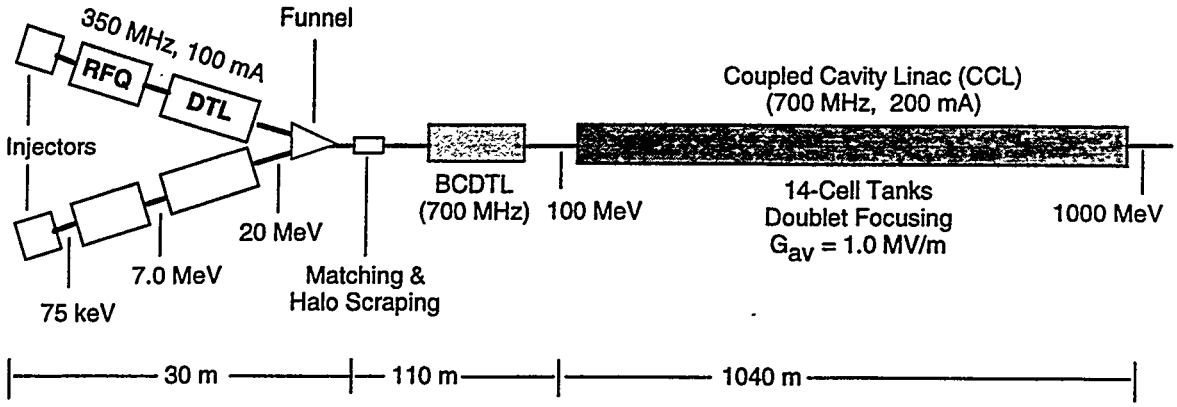

Fig. 1. Reference concept for funneled 1-GeV, 200-mA linac

beam current in the accelerator, and also the low average ("real estate") accelerating gradient of 1.0 MV/m, the RF efficiency of the CCL is very high (0.81). The efficiencies of the lower-β accelerating structures are smaller, but because of the dominance of the CCL in the power equation, the average for the entire linac is 0.79. Assuming an average efficiency of 0.58 for converting dc power to RF power in the klystrons, 0.01 losses in ac-to-dc power conversion, and 0.05 losses in RF transmission to the accelerating structures, the ac-to-beam efficiency is approximately 0.435, leading to a total ac power requirement for the accelerator of about 485 MW (including an allowance for focusing magnets, coolant pumps and other demands).

The overall linac design has been guided by a conservative philosophy, with key parameters justified by limited trade studies. The basic neutron production requirement determines the beam power. The balance between various cost factors determines a choice of energy and current that minimizes life-cycle costs while accounting for beam physics constraints. Other key parameters are selected to satisfy the criteria of low beam-loss, high electrical efficiency, and high availability and operability. An important design feature is the very large ratio of structure aperture to rms-beam-size (at the quadrupoles), which increases with particle energy from 4 at the DTL entrance to 26 at the CCL exit. The large aperture ratio is an essential criterion for assuring ultra-low beam loss, and is obtained through 1) using a large physical aperture (5.0 cm diameter in CCL), 2) maintaining a low transverse beam emittance, and 3) employing high transverse focusing strength per unit length.

Selection of the 350/700-MHz frequency combination is based on a number of factors, including the commercial availability of RF amplifiers and the need for DTL drift tubes large enough to house electromagnetic quadrupoles (EMQs). Permanent magnet quadrupoles (PMQs) are avoided in the DTL (and most other locations in the linac) because of their sensitivity to radiation damage, a significant concern because of the threat of high beam losses.

In the low-energy section of the linac (<20 MeV), the design emphasis is on providing a high-current low-emittance beam. This is addressed by 1) strong transverse focusing in the RFQs, 2) a high structure frequency and strong transverse focusing in the DTLs, 3) ramped accelerating fields (strong longitudinal focusing) in the DTLs, and 4) precise matching between adjacent accelerating structures. In the high-energy region of the accelerator (>20 MeV), a balance is struck between the need for very low fractional beamloss levels and the requirement of high RF-to-beam conversion efficiency. This leads to a design incorporating a large ratio of

accelerating-structure aperture to rms beamsize (10–26 in the CCL), short accelerating tanks for strong transverse focusing, smooth phase-space transitions between accelerating structures, and a relatively low accelerating gradient (1.00 MV/m averaged over accelerating structures and intertank regions). Because all the 700-MHz RF buckets are filled, and because the beam duty factor is 100%, the number of protons per bunch (1.78×10^9) is only 3.4 times greater than in LAMPF (0.52×10^9), even though the average current is 200 times higher. Thus the basic beam dynamics of the high-energy linac lie in a familiar (and benchmarked) physics regime.

Table 1. 1-GeV 200-mA Reference Accelerator Design Parameters

Parameter	RFQs (2)	DTLs (2)	BCDTL	CCL
Energy (MeV)	0.075–7.0	7–20	20–100	100–1000
Frequency (MHz)	350	350	700	700
Current (mA)	100	100	200	200
Structure Type	4-Vane	$1\,\beta\lambda$	$1\,\beta\lambda$	$\beta\lambda/2$
No. of Tanks or Segments	4 x 2	3 x 2	61	342
No. of RF Modules	2 x 2	3 x 2	24	342
No. of Assembly Units	—	3 x 2	24	302
No. of Cells per Tank	(433 total)	22 to 15	7	14
Length of Tanks or Segments (m)	2.03	2.44–2.50	0.615–1.281	1.29–2.62
Total Length (m)	8.10	7.98	93.66	1031.44
Radial Aperture (cm)	0.24	1.00	2.00–2.25	2.50
Aperture/Beamsize(rms) Ratio	–	4–5	8–13	13–26
Structure Gradient (MV/m)	0–1.75	1.04–2.80	1.70–1.50	1.50–1.36
Average Gradient (MV/m)	ramped	ramped	1.00	1.00
Synchronous Phase (deg)	-90 to -30	-35 to -25	-40 to -30	-30
Shunt Impedance (MΩ/m)	–	30.2–32.8	26.0–36.7	23.3–37.4
Structure Power (MW)	1.12 x 2	1.15 x 2	6.91	42.49
Beam Power (MW)	0.70 x 2	1.30 x 2	16.10	180.39
Total RF Power (MW)	1.82 x 2	2.45 x 2	23.01	223.18
Efficiency	0.385	0.530	0.711	0.806
Phase Advance/Period (deg)	30 (@ output)	80–70	80–70	70
Quadrupole Lattice	FD	FOFODODO	FDO	FDO
Quadrupole Length (cm)	–	5.7	8.2–9.5	11.0–18.0
Quadrupole Spacing (cm)	–	10.4–17.4	9.5	11.0–18.0
Quadrupole Gradient (T/m)	–	25.0–35.0	31.4–36.0	24.4–38.0
Emit_T, rms, norm (π·cm–mrad)	0.022	0.023	0.029	0.032
Emit_L, rms, norm (π·MeV–deg)	0.220*	0.216*	0.483**	0.608**

* 350-MHz RF cycle ** 700-MHz RF cycle

Most of the 200-mA 1-GeV linac is made up of well-established and well-tested accelerating structures. However, the baseline design incorporates two novel structures that are moderate extensions of the established technology base and offer significant performance advantages. These are 1) a high-energy (7-MeV) RFQ, and 2) a hybrid accelerating structure (BCDTL) which covers the 20-to-100-MeV energy regime. The BCDTL was evolved to provide a solution for accelerating beam in an energy region where traditional structures (DTL or CCL) would have been impractical or inefficient. The high-energy RFQ eliminates the mechanically-challenging first section of the 350-MHz DTL, and also provides a current-independent match to the DTL, greatly easing the accelerator turn-on process.

Beam funneling plays a key role in the 200-mA accelerator design,[10] reducing the injector and RFQ current requirements by a factor of two. Effectively it doubles the beam intensity delivered to the high-energy linac by the low-energy system without imposing an

emittance penalty. Funneling also fills all the RF cycles in the high-energy linac, minimizing the charge per bunch, beam emittance, and beam size. While no definitive demonstration of RF funneling has been completed, there is a high degree of confidence in the concept based on simulations and on tests carried out several years ago.[12] Beam measurements on a single-leg funnel prototype showed 100% transmission, no increase in transverse emittance, and only a small increase in longitudinal emittance. A remaining concern is the effect of transverse distortion of the longitudinal tails caused by sinusoidal deflection of the finite-length bunch in the RF deflector, which might cause beam halo enhancement and downstream losses. In the 200-mA linac design, the rms bunch width at the deflector is narrow (5°) so the divergence in the longitudinal tails should be minimal.

NON-FUNNELED REFERENCE DESIGN

For spallation applications requiring somewhat lower beam power (<100 MW), the funneling requirement can be eliminated. An example of such a system design is shown in Fig. 2, which represents an 800-MeV 80-mA CW linac specified for a plutonium burning (ABC) concept. The design frequencies and beam dynamics are similar to those for the 200-mA funneled system shown above. The major difference is that only every other RF bucket in the high-energy (700-MHz) linac contains a beam bunch. Because of the lower average current, the linac is less efficient in converting RF power to beam power; RF-to-beam efficiency is 0.60 instead of 0.79. Total RF power requirement to generate the 64 MW of beam power is 107 MW. Using the same klystron efficiency, ac-to-dc efficiency, and waveguide losses as in the funneled linac design, the ac-to-beam efficiency is 0.33 and the total ac power requirement is 214 MW. The beam serves four target/blanket assemblies simultaneously, so a beam distribution scheme (outlined below) is needed.

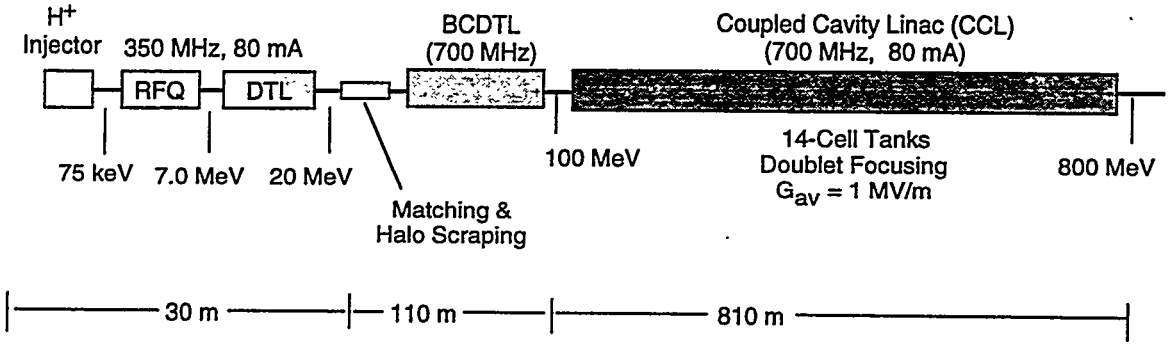

Fig. 2. Non-funneled 800-MeV, 80-mA CW linac scheme.

HIGH-ENERGY BEAM TRANSPORT SYSTEMS

A high-energy beam transport (HEBT) magnet system carries the beam from the end of the linac to one or more target-blanket assemblies or to a full-power beamstop at 0° for tuning the accelerator. A representative HEBT for directing beam alternately to two identical production targets is shown in Fig. 3. The system consists of 1) a periodic focusing lattice identical to that in the final portion of the linac, 2) a dc switching magnet, and 3) transport beamlines to the beamstop and production targets. Each target beamline begins with an achromatic bend (including the switching magnet), which is followed by a matching section and nonlinear beam expander. The expander is a system of quadrupole and multipole lenses (followed by a drift space) that converts the small-dimension Gaussian-like beam distribution leaving the linac into a large-area uniform-density rectangular distribution suitable for target

irradiation. The bends are designed to have a large momentum acceptance ($\delta p/p = \pm 0.02$) so that energy variations or errors in the beam from the linac have little effect on the beam positioning and intensity distribution at the targets. The 0° beamstop line is used primarily during linac turn-on and tuning operations. A small reverse bend (7.5°) at the end of each beamline enables shielding of the transport lines from target neutron backshine.

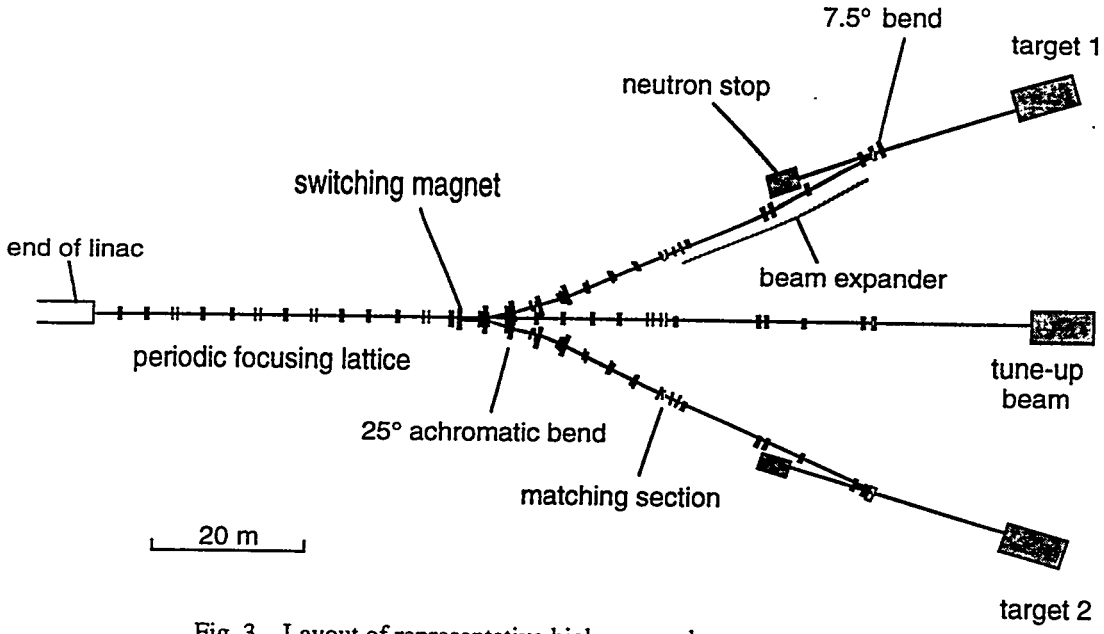

Fig. 3 Layout of representative high-energy-beam transport system.

An alternate beam distribution scheme is sketched in Fig. 4. In this arrangement, four production targets are served simultaneously, using a series of pulsed kicker magnets to direct 2.1-ms beam pulses sequentially into each transport line. A beam chopper in the linac LEBT opens synchronized time gaps in the output beam that allow for magnet rise times (typically 100 ms). In the scheme shown in the figure, each kicker operates at a pulse rate of 120/sec. Disadvantages of this pulse scheme are that significant extra performance demands are placed on the RF power control system in comparison with the requirements for a CW beam, and each production target has to be able to handle the pulsed deposition of beam energy at a 120-Hz rate. A beam distribution scheme based on RF separation of the beam micropulses has also been considered, but is not discussed here.

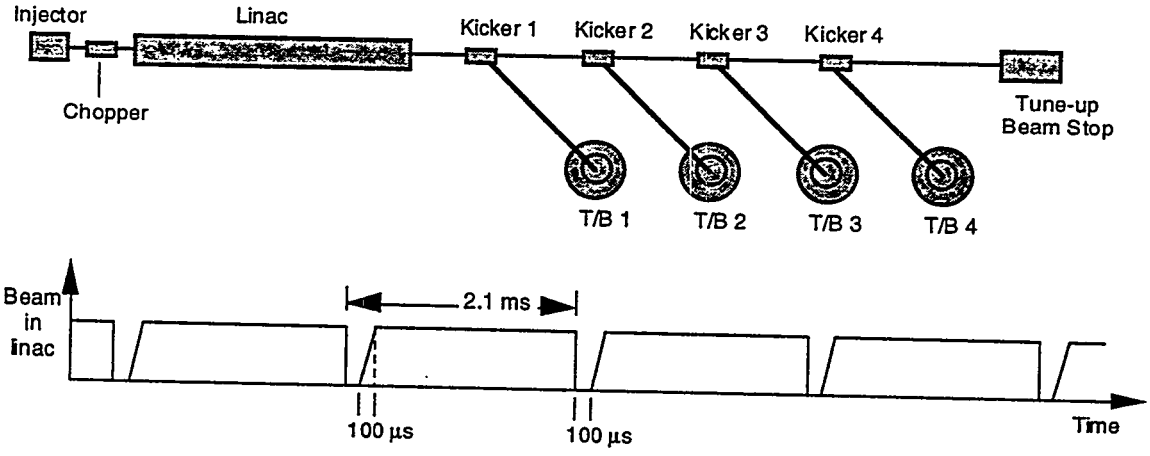

Fig. 4 Scheme for distributing beam to four target/blanket assemblies.

BEAM PHYSICS AND SIMULATIONS

In high intensity ADTT linacs, the main physics design goal is to accelerate the beam with extremely low loss and transport it to nearby targets. Control of the beam loss is the primary beam dynamics issue. Advances in theory and control of high-current beams achieved in the past decade (based on high frequencies, strong focusing, ramped gradients, equipartitioning, etc.) provide a rational starting framework for modern high-current accelerator design.[13] The results of applying this framework are seen in Fig. 5, which summarizes results from simulations of the 200-mA reference linac design. The figure displays the transverse and longitudinal rms emittances (as determined from simulation), with measured transverse emittance of the LAMPF 17-mA (peak) proton beam provided for comparison. The LAMPF linac was designed nearly 30 years ago, and there are significant transitions and mismatches in longitudinal and transverse space that account for the rapid emittance growth. The improvement resulting from modern design is readily apparent from the comparatively modest emittance growth in the 200-mA linac simulation.

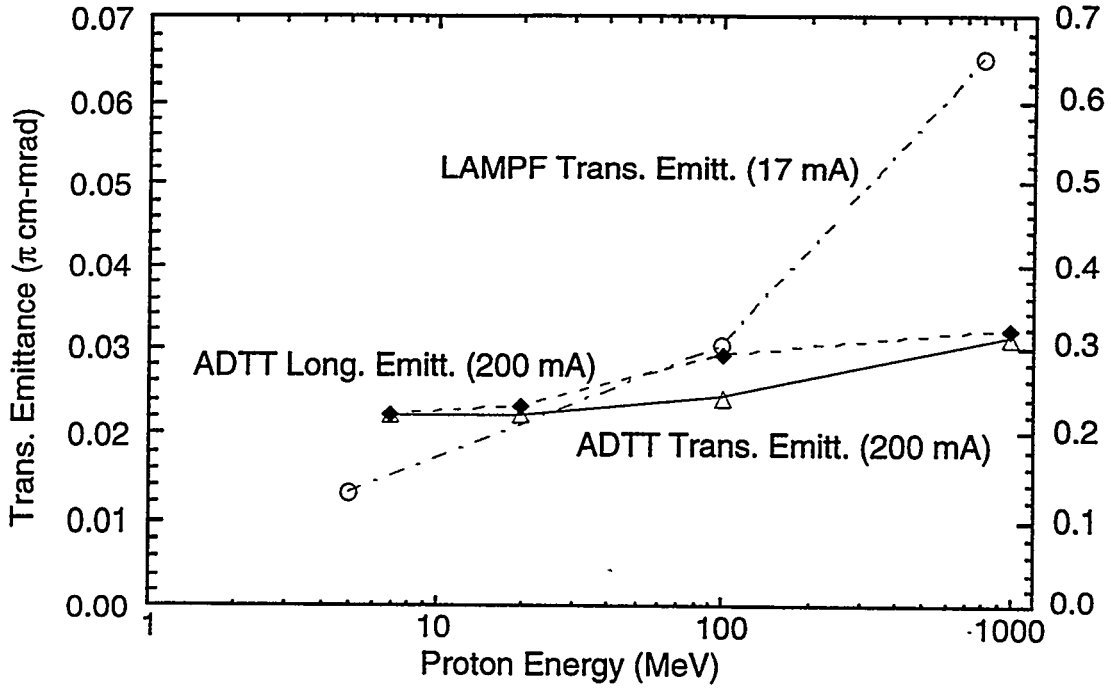

Fig. 5. Comparison of emittance growth for 200-mA high-intensity linac design and in LAMPF linac.

BEAM LOSS, HALO MODELS, AND DESIGN IMPACTS

ADTT linacs must achieve extremely low beam loss, in the range 0.1 nA/m to 1 nA/m (depending on proton energy) to assure maintainability without the use of remote handling. This translates to 10^{-8}/m to 10^{-9}/m fractional beam loss allowances. To reach such minuscule loss levels, the apertures in the accelerating structures and focusing elements must be large enough to contain not only the beam core but also the tails of the beam distribution (the halo) out to very low particle densities. A key measure of this containment is the aperture ratio mentioned earlier. In the LANL high-current linac designs this ratio is very large, increasing from 4-5 in the DTLs

to 13-26 in the CCL. In the LAMPF linac, for comparison, the ratio is 6.3 at the end of the CCL. Because of our present ignorance of the detailed intensity distribution in the halo, the design philosophy is to use the largest possible aperture factors consistent with maintaining reasonable efficiency in the accelerating structures and practical quadrupole pole-tip fields.

Operating experience at LAMPF provides the best hard information about the potential for achieving ultra-low losses in transmutation linacs. Figure 6 shows the estimated beam losses along the LAMPF CCL following an extended production run at 1-mA average current. The losses are inferred from an activation survey made soon after shut-down, using the approximate energy dependence of neutron production, and knowledge of the integrated beam loss between 100 MeV and 800 MeV. The figure shows two areas of high beam loss, located downstream from 100 MeV and from 200 MeV. A LAMPF simulation using as-built parameter values shows the same high loss regions, which are understood to be the result of mismatches and sudden transitions (reductions) in the longitudinal and transverse acceptances.[14] At higher energies in the SCL, beam losses are generally < 0.2 nA/m, which represents $< 2\times10^{-7}$/m fractional loss. The corresponding radiation levels 30 cm from the linac are a few mR/hr, a level that permits "unconstrained" hands-on maintenance. High-intensity linacs for transmutation applications need to achieve one to two orders of magnitude smaller fractional beam losses than LAMPF to permit this kind of maintenance. This is a challenging objective, but one that is reachable given the much larger aperture factors that can be provided in these machines, the greatly improved understanding of matching and emittance control now available, and the greater precision of beam diagnostics and control.

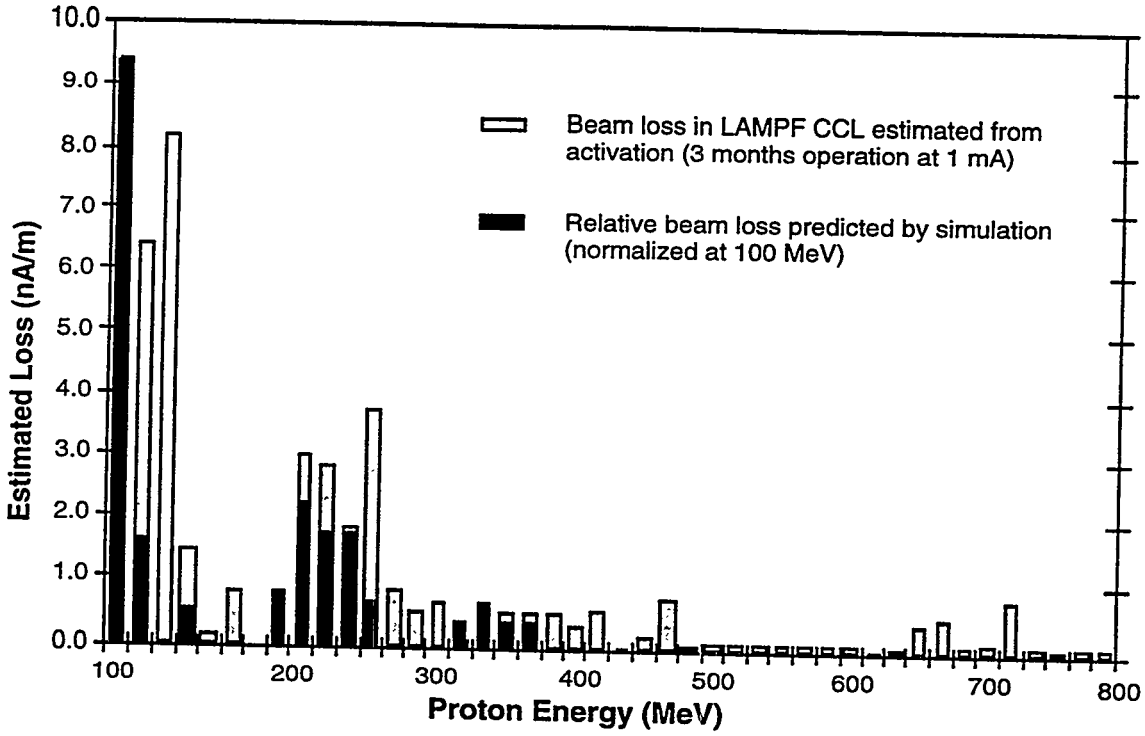

Fig. 6. LAMPF beam loss estimate and simulation.

Most of the beam loss in high-intensity linacs is due to the continuous interception of large-amplitude particles (the beam halo) by the accelerating structure apertures and beam pipes. Stimulated by the recognition that understanding (and control) of the beam halo could have major impacts on high-intensity linac design, theoretical investigations in this area are underway at several laboratories.[15-19] Recent Los Alamos results on beam halo production mechanics and

simulation studies are discussed in another paper at this conference. The most promising model representing halo production is one in which individual particles interact resonantly with a beam core whose envelope is oscillating due to a mismatch in a focusing channel. From the resonant interaction, particles initially near the core can receive significant transverse energy gain, and can move out into the halo. Two-dimensional uniform and alternating gradient focusing channels have been modeled, and simulations have been run using newly-available massively-parallel computers (such as the LANL CM-5). These simulations, which use 10^6 to 10^7 particles, are in general agreement with the main features of the core-halo model,[20] and provide a powerful new tool for performing numerical halo "experiments".

Preliminary results indicate that the main factor driving halo formation is the degree of mismatch between the beam and focusing channel, and to a lesser extent the space-charge density. The amplitudes of halo particles do not grow continuously, but appear to be bounded at a few times the beam core size. A major question for the design of high-intensity linacs is the effectiveness of halo-removal (scraping) systems. The simulations show that if the halo in a mismatched beam is removed, it repopulates in a relatively small number of plasma periods. However, if the beam distribution is allowed to equilibrate following a mismatch (so that the beam becomes matched to the channel), then scraping systems that remove the outer halo (beyond 5s) may be effective. Further work is needed to extend halo modeling and simulation to 3D geometry and more realistic situations before it will be possible to provide quantitative guidance in the design of high-intensity linacs.

The APT linac is designed to reduce halo production and to minimize interception of the halo by the accelerating structures.[21] There has been a strong emphasis on eliminating or minimizing transitions, especially at high energies. Above 20 MeV there are no significant acceptance transitions, and below this energy there has been careful attention to smooth matching between accelerating structures. Other key features incorporated into APT linac design to assure low beam loss include: (1) very large ratios of the accelerating structure apertures to the rms beam size, (2) large ratio of longitudinal acceptance to rms longitudinal emittance, (3) a high density of focusing elements, (4) tight RF amplitude and phase control, (5) precision transverse beam position alignment, (6) distribution of the beam among all available RF buckets in the high energy linac, and (7) the possible use of a halo scraping system following the last significant acceptance transition (the funnel).

ELECTRICAL EFFICIENCY

To minimize operating costs, the electrical efficiency of linacs for ADTT applications must be as high as possible. The wall-plug to beam efficiency can be written as:

$$\varepsilon_{tot} = \varepsilon_{ac/dc}\, \varepsilon_{tube}\, \varepsilon_{tr}\, \varepsilon_{rf/beam}$$

involving the efficiencies for ac-to-dc conversion, dc-to-rf in the RF generator, losses in RF transmission, and cavity RF efficiency (beam loading). Since cavity efficiency is simply

$$\varepsilon_{rf/beam} = I_{beam}/(I_{beam} + G/Z_{sh}\cos\phi),$$

the designer has three parameters available, the peak beam current, the cavity shunt impedance, and the structure accelerating gradient. The accelerating gradient also affects construction cost through the length factor. Simplified cost models based on estimates for power-related and length-related factors show that 1.3-1.5 MV/m structure gradient is optimum for CW operation in the 100-mA to 250-mA range. This is a result of the high cost of RF power systems relative to other components of the linac, as well as high electric power costs.

Shunt impedance in principle can be increased by using higher-frequency accelerating structures, since this quantity nominally scales with the square root of the frequency. However, this improvement is restricted by the need to maintain a large cavity aperture for low beam loss. For a fixed 5-cm aperture, the CCL shunt impedance vs. frequency has a dependence like that shown in Fig. 7, showing that the optimum operating frequency is between 600 MHz and 1000 MHz.

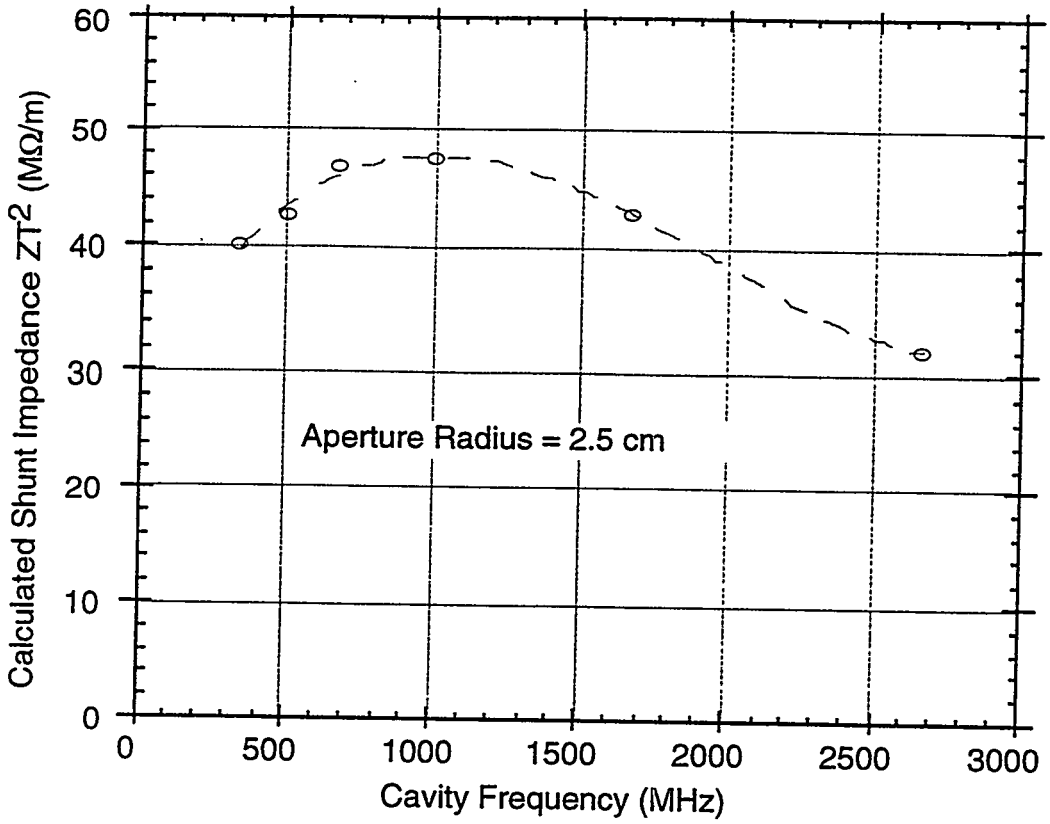

Fig. 7. Calculated SCL shunt impedance vs. frequency for fixed 5-cm aperture.

The beam current should be as high as possible, within the beam-physics constraints of the low-energy linac(s); values need to be well above 100 mA for highest efficiency.

Contemporary high-power klystrons have useful efficiencies around 0.55-0.60 when control margin is accounted for.[11] In future RF generator designs it is anticipated that this number could be raised as high as 0.75 (klystrode, magnicon, or advanced klystron). Thus, with all efficiencies optimized, the maximum ac-to-beam conversion efficiency that could be expected in future (conventional copper-technology) linacs might be as high as 0.55-0.60, an increase of 30 to 40% over present designs.

Superconducting RF accelerating structures based on niobium or niobium-coated cavities offer the potential for still higher linac efficiencies in the future,[22] but additional development work is needed to establish the basis for applying this technology to high-power proton accelerators. SCRF structures would essentially eliminate RF cavity wall losses in the linac, providing a 15-25% improvement in electrical efficiency, depending on the beam current. However, large low-temperature (4K) refrigeration systems are required to operate the superconducting structures, and the capital and electrical operating costs of these systems are significant. SCRF technology in principle also opens the way to higher gradient linacs, which

could reduce capital costs through reduced accelerator length. However, RF power coupling across the room-temperature/low-temperature interface is presently limited to < 150 kW per coupler. For high-current beams, this factor presently restricts the effective cavity gradients that can be employed to < 2 MV/m, which is not a large improvement over the gradients planned for conventional linacs.

REFERENCES

1. C.D. Bowman, et al., "Nuclear Energy Generation and Waste Transmutation Using an Accelerator-Driven Intense Thermal Neutron Source", NIM in Phys. Res., (Sec. A), Vol. A320, Nos. 1,2, August 15, 1992, pp. 336-367.
2. C.D. Bowman, "Overview of the Los Alamos Accelerator-Driven Transmutation Technology Program", Proc. of 1994 International Conf. on Accelerator-Driven Transmutation Technologies and Applications, Las Vegas, July 25-29, 1994.
3. C. Rubber, "The Energy Amplifier Concept: A Solid-Phase Accelerator -Driven Subcritical Th/233U Breeder for Nuclear Energy Production with Minimal Actinide Waste", ibid.
4. V.D. Kazaritzky, "Overview of Russian Experience and Capabilities for Development of ATW/ABC Systems", ibid.
5. D. Berwald, "Potential Role of ABC-Assisted Repositories in U.S. Plutonium and High-Level Waste Disposition", ibid.
6. G.P. Lawrence, et a.., "Accelerator Technology for Los Alamos Nuclear Waste Transmutation and Energy-Production Concepts", Proc. 6th International Conf. on Emerging Nuclear Energy Systems, Fusion Technology Vol. 20, No. 4, December 1991, pp. 652-656.
7. G.P. Lawrence, "High-Power Proton Linac for Transmuting the Long-Lived Fission Products in Nuclear Waste", Proc. 1991 Particle Accelerator Conference, San Francisco, May 1991, pp. 2598-2600.
8. K.C. Chan, "A Prototype Front-End Accelerator for Accelerator-Driven Transmutation Technologies", Proc. of 1994 International Conf. on Accelerator-Driven Transmutation Technologies and Applications, Las Vegas, July 25-29, 1994.
9. J.D. Schneider et al., "Design and Testing of a DC Ion Injector Suitable for Accelerator-Driven Transmutation", ibid.
10. S. Nath, "Funneling in LANL high intensity Linac Designs," ibid.
11. M. Lynch, et al., "Important Requirements for RF Generators for Accelerator-Driven Transmutation Technologies", ibid.
12. K.F. Johnson, et al., "The Single-Beam Funneling Demonstration: Experiment and Simulation", Proc. 1990 Linear Accelerator Conf., Albuquerque, NM, September, 1990, pp. 701-703.
13. T.P. Wangler, et al., "Linear Accelerator for Production of Tritium: Physics Design Challenges", ibid. pp. 548-552.
14. R.W. Garnett, et al., "Beam Dynamics Simulation of the LAMPF Linear Accelerator", ibid., pp. 347-350.
15. J.S. O'Connell, et al, "Beam Halo Formation from Space-Charge Dominated Beams in Uniform Focusing Channels", Proc. 1993 Particle Accelerator Conf., Washington, DC, May 1993, pp. 3657-3659.
16. B.I. Bondarev, "Emittance Growth and Halo Formation in Charge-Dominated Beams", ibid.
17. R.A. Jameson, "Beam Halo from Collective Core/Single-Particle Interactions", Los Alamos Report LA-UR-93-1209, March 1993.
18. J.M. Lagniel, "Chaotic Behaviour Induced by Space Charge", Proc. 1994 European Particle Accel. Conf., London, June 1994.
19. C.L. Bohn, "Mechanisms of Beam-Halo Formation in High-Intensity Linacs", Proc. of 1994 International Conf. on Accelerator-Driven Transmutation Technologies and Applications, Las Vegas, July 25-29, 1994.
20. R. Ryne, "Recent Results in Analysis and Simulation of Beam Halo", ibid.
21. R.A. Jameson, "Design for Low Beam Loss in Accelerators for Intense Neutron Source Applications", Proc. 1993 Particle Accelerator Conf., Washington, DC, May 1993, pp. 3926-3930.
22. J.R. Delayen et al. "Design Considerations for High-Current Superconducting Ion Linacs", ibid., pp. 1715-1717.

Linac Design for the European Spallation Source*

H. Klein
Institut für Angewandte Physik der Johann Wolfgang Goethe-Universität
Postfach 111 932, D-60054 Frankfurt am Main, Germany

Abstract. A study group has started to develop a conceptual design for a European Spallation Source (ESS). This pulsed 5 MW source presently consists of a 1.334 GeV linac and two compressor rings. In the following mainly the high intensity linac part will be discussed, which has some features of interest for accelerators for transmutation of radioactive waste too.

Introduction

At present two types of neutron sources are in use for neutron scattering resarch, the fission reactors and the accelerator based pulsed sources, where the neutrons are produced by spallation of a non fissile heavy metal target. Since the lifetime of the existing high flux reactors will end within the next two decades and the installation of new reactors is nearly impossible in many countries for political reasons, several studies on intense spallation sources are on the way. Another reason which speaks for the pulsed spallation source is the time structure of the beam allowing for time of flight experiments. In Europe - besides the SINQ and the Austron proposals - a site independent study project for a 5 MW European Spallation Source (ESS) has been launched, which shall produce neutron fluxes comparable with those of ILL's high flux reactor

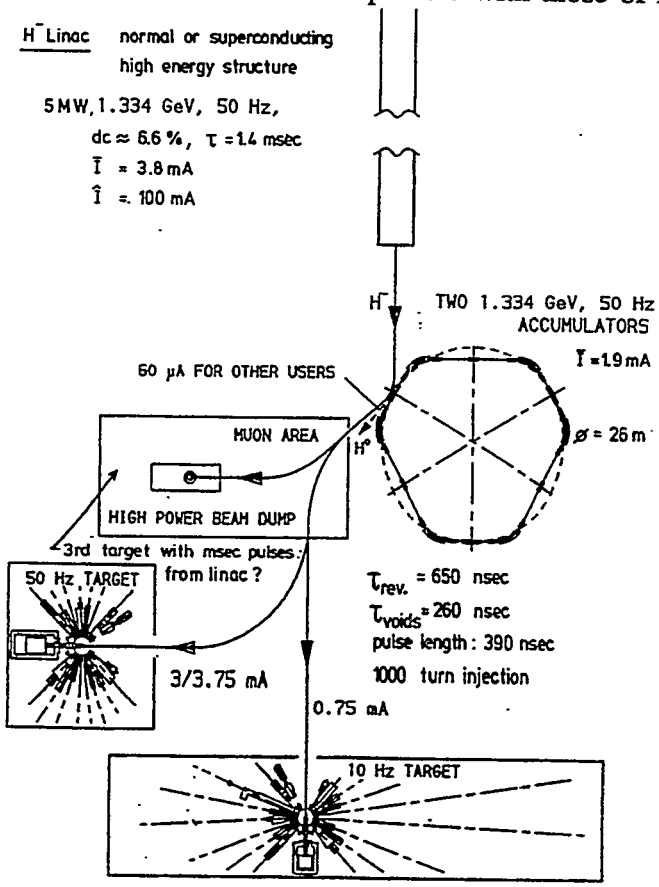

Fig. 1: Schematic layout of ESS.

*Work supported partly by BMFT and KFA Jülich

[1]. This two year study has been approved by the European Comunity and will start officially this year. It exists now an organization structure with a council representing 9 European countries, the EC and the two major labs involved (DRAL - G.B. and KFA Jülich), a scientific coordinator for the neutron physics issues (J. Finney), a project leader (H. Lengeler) and 3 group leaders (H. Klein, linac; I. Gardner, rings; H. Stechemesser, Target). The outcome of several workshops which have taken place already on ESS and its main parameters will be discussed concentrating on the linac part.

Parameters and basic layout of ESS

An average beam power of 5 MW (about 30 times more then ISIS) shall be achieved by accelerating an H^- beam (3.8 mA average, 100 mA peak) by a pulsed 1.334 GeV linac (τ = 1.4 ms, rep. rate 50 Hz). The beam is injected in two accumulator rings (1000 turn injection each), where it is compressed to 390 nsec. By successive ejection the required short pulse length of 1 µsec can be delivered to two targets (50 Hz, 10 Hz); an option for a 2 ms pulse direct from the linac is in discussion (see fig. 1). The main concerns for ESS are : Reliability, availability, hands on maintenance, low capital and operational costs. Particle losses have to be very small (~0.4 nA /m) along the linac and at injection and ejection. The emittance growth must be kept small; the formation of a halo has to be avoided - a major problem! Particle losses at the injection point due to exited H^0 states, which may decay shortly after the foil, can be minimized by the choosen energy, where the mainly exited states have a relative long live time [2]; for a clean extraction, the beam has to be chopped, providing 260 nsec long voids in the pulse.

The preliminary layout of the linac part is shown in Fig. 2. Two beam lines are funneled at 5 or 7 MeV, each consisting of an ion source, LEBT and 2 RFQs with a chopper in between. After the funneling section a drift tube linac (350 MHz) accelerates to 100-150 MeV, further acceleration will be done by a normal or superconducting coupled cavity linac. In the next chapters some of the different linac parts are discussed.

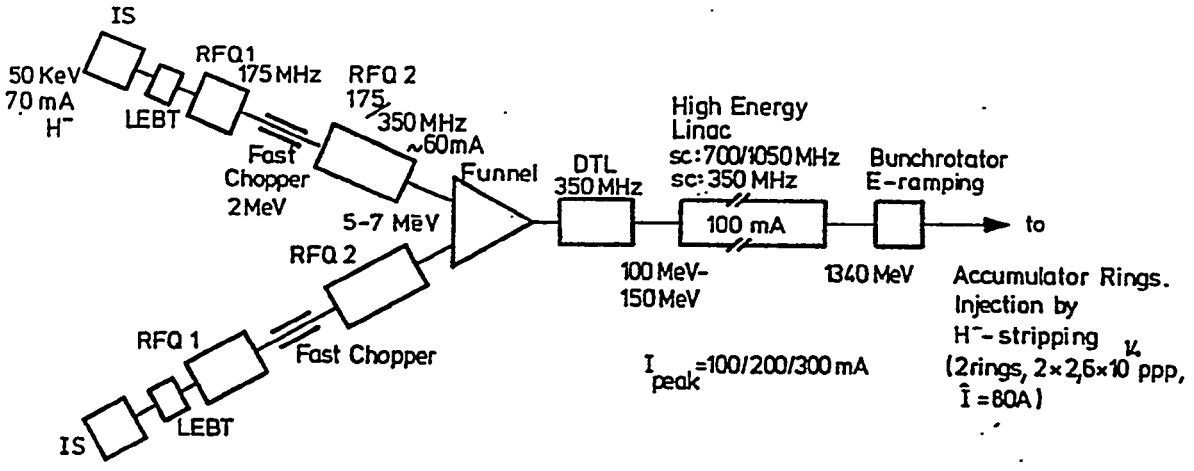

Fig. 2: Schematic layout of the linac part of ESS.

The H^- Source

The ESS facility requires a reliable 70 mA (dc=10 %) H^- source of excellent beam quality ($\varepsilon_{rms,norm} \leq 0.1$ πmmmrad) and long lifetime. Table 1 presents the performance of some existing H^- ion sources. At the moment, there is no source available which fulfils all the requirements for ESS at the same time; the Culham source is promising, but operates with cathodes.

Table 1. Performance of some H^- sources

	I [mA]	dc [%]
LBL	90	> 1
LANL	60	2
RAL	45	2.5
BNL	30	< 1
KEK	20	1
LAMPF	80	12
TRIUMF	9	100
Culham	86	100

Based on the high efficiency source (HIEFS) [3,4], developed in the Inst. für Angewandte Physik in Frankfurt an H^- source is under construction. A schematic drawing of the source is shown in Fig. 3. The plasma chamber is made of a water cooled cylindrical copper chamber (13 cm depth, 10 cm ∅). For high reliability the plasmaproduction is done by rf [5]. In order to increase the plasma density the plasma is confined by a solenoidal field [6]. The end of the chamber is enclosed by the plasma electrode, which is negatively biased with respect to the

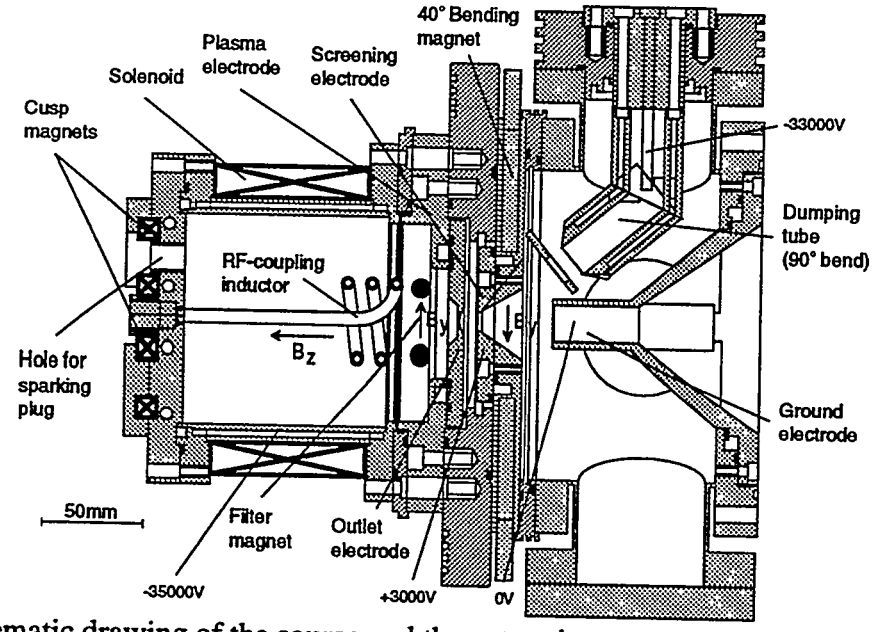

Fig. 3: Schematic drawing of the source and the extraction system.

anode. This arrangement serves to control the plasma potential near the plasma.electrode. A permanent magnet filter is installed near the plasma electrode, forming a transverse magnetic field with a magnitude of about 100 G at the axis. This way, the plasma is divided in an area of high electron energy round the antenna and an area of low electron energy near the plasma electrode. The rf-coupling inductor is positioned on the cylinder axis. To optimize its z-position the antenna is movable. For the experiments transmitters from 1.7 to 27 MHz with up to 100 kW are available. This allows us to investigate the source at different frequencies. At the beginning the source will be driven without cesium. Later on cesium will be injected to enhance the H^- yield, and a prechopping of the source will be tested. The work is been done in cooperation with LBL.

The experiments are divided in two steps. At first, the source will be equipped with an accel/decel system designed for 35 keV beam energy, a beam current of 35 mA and an aspect ratio of 0.36. For this arrangement a high current density, that means a high plasma density is required. In a second step the source will be driven with a 55 keV extraction system, leading to 70 mA H^- at lower current density. The most important parameters of the extraction system are presented in Table 2. A crucial point is the size of the extraction area. Both a low gas flow through the extraction channel and a low beam emittance require a small emitting area. However the larger the emitting area the larger the beam current. As a compromise we fixed the radius of the outlet electrode to 4 mm (2.5 mm), respectively the emitting size to 0.5 cm^2 (0.196 cm^2). As a result for a matched beam the extractable current density is 139 mA/cm^2. Fig. 4 shows the beam course in the extraction system for the given parameters, calculated with IGUN, Fig. 5 the facility which will dump the electron beam with 35 keV, 0.7 A after a 40^0 deflection outside the extractor.

Table 2 : Parameters of the extraction system for the different prototyps.

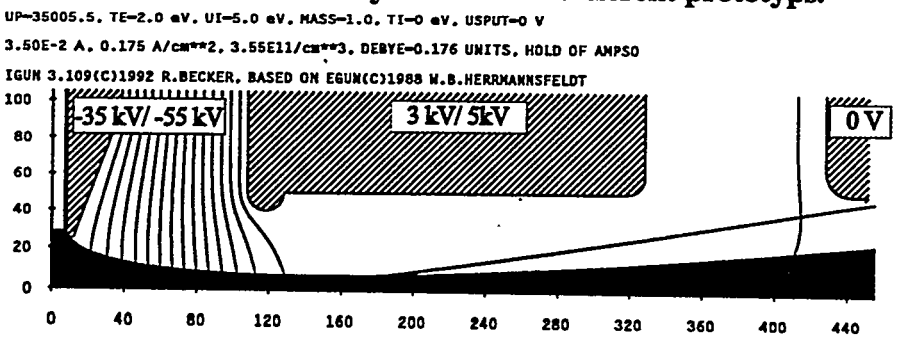

Fig. 4: Beam trajectories calculated with IGUN for a 3 5keV 3 5mA H^- resp. 55 kV 70 mA H^-.

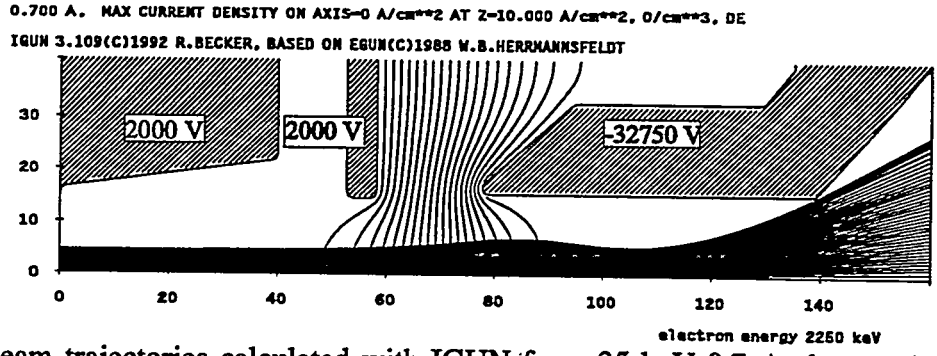

Fig. 5: Beam trajectories calculated with IGUN for a 35 keV 0.7 A electron beam in the dumping system.

		Prototype I	Prototype II
radius of the outlet aperture	[mm]	2.5	4
emitting area	[cm^2]	0.196	0.5
gap distance	[mm]	7	11
extraction voltage	[kV]	35	55
extraction current	[mA]	35	70
current density	[mA/cm^2]	179	139

Low energy beam transport

The LEBT system has to transport and match the beam from the ion source into the RFQ accelerator. For special applications beam chopping may be forseen at low energies. Depending on beam quality and intensity requirements, the main aspects for the design are minimization of emittance growth and/or particle losses. For the proposed ESS both aspects are very important.

The growth of the effective emittance of high perveance ion beams in a LEBT is not only caused by nonlinearities of the external focusing field but as well by nonlinear space charge forces. The first effect can be minimized optimizing the design with the help of simulation codes, for the second the space charge field has to be known which is only the case for decompensated ion beams and for known particle distribution. For these beams it has been shown that the electric self field energy U is minimum if the beam ion density distribution is homogeneous in real space (e.g. KV in phase space). Other density distributions have higher field energy. It is also well known that homogenization driven by space charge force is coupled with rms emittance growth which increases with increasing perveance and beam size [7,8,9] :

$$\frac{d}{dz}\varepsilon_{rms}^2 = -\frac{K}{2}\langle x^2\rangle \frac{d}{dz}\Delta U \qquad (1)$$

with $\varepsilon_{rms} = \sqrt{\langle x^2\rangle\langle x'^2\rangle - \langle xx'\rangle^2}$ and the generalized perveance $K = \frac{I e \zeta}{2\pi\varepsilon_o \beta^3 c^3 \gamma^3 m A}$

and the non linear field energy ΔU.

Space charge compensation

Space charge compensation can only occur in absence of external electric fields. Residual gas ions (positively charged) are produced by interaction between beam ions (BI) and residual gas atoms as well as electrons. For H^- beams the electrons are expelled from the electric self field of the beam and get lost at the beam line while the residual gas ions (RGI) stay in the beam potential and accumulate, reducing the space charge forces. Three different stages of compensation can be characterized (s. fig. 6).The gas focusing stage is similar (concerning the radial potential distribution as well as the net charge density distribution) to the case of a compensated positive ion beam (s. fig. 7). Therefore a lot of experimental experience [10] and computer codes are available [11].

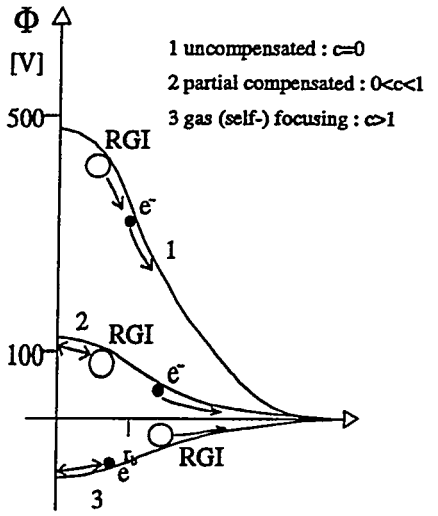

Fig. 6: Stages of compensation.
The compensation degree is defined by $c=1-\Phi_{comp.}/\Phi_{deco.}$. An H^- beam of 70 mA at 50 keV with an beam radius r_b of 10 mm was assumed.

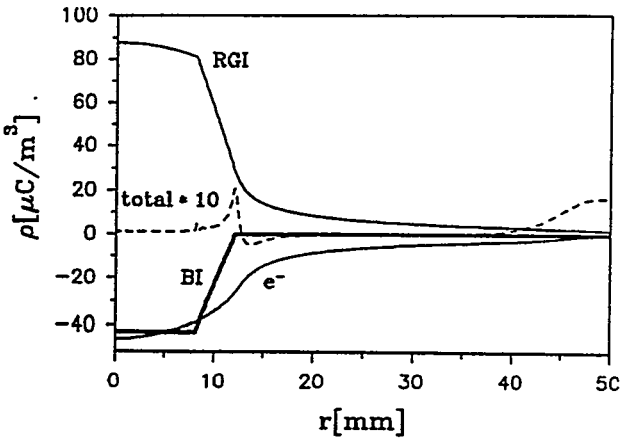

Fig. 7: Calculated self consistent radial density distribution for an 35 mA H^- beam of 35 keV and a beam radius of 12 mm. An Argon residual gas pressure of $2*10^{-5}$ hPa and a cross section for RGI production of $2*10^{-19}$ m^2 was assumed.

For DC-beams the lower pressure limit for self focusing can be calculated to be below $1*10^{-5}$ hPa which is not very critical for the subject of beam loss due to residual gas stripping (typ. 7 %/m, 50 keV H^- in Ar). Another reason for the use of self focusing transport is the occurence of longitudinal instabilities (caused by BI + RGI with a frequency in the low MHz range [12]) for conditions below the self focusing stage, destroying the transport of the beam at all.

For pulsed beam operation the rise time of space charge compensation is another issue of importance. For the process of space charge compensation by residual gas ionisation the rise time is mainly depending on the residual gas density and the cross section and can be estimated (neglecting RGI losses) to be in the range of 50-100 μs (for $1*10^{-5}$ hPa).

LEBT design

For the LEBT electrostatic as well as magnetic elements can be used, each having specific advantages and disadvantages.

In electrostatic systems space charge compensation can be avoided, so optimization of the LEBT can be performed with the help of simulation codes in a good quality. The main advantage of electrostatic systems is that short length designs with little particle loss are possible [13,14]. If the ion source delivers a nearly homogeneous beam, there will be only little emittance growth by space charge effects. On the other hand, there is usually no space for online beam diagnosis, steering elements or chopper devices. Fig. 8 shows for example an electrostatic injection system for H^+ with pentode extraction followed by an einzellens allowing independent variation of

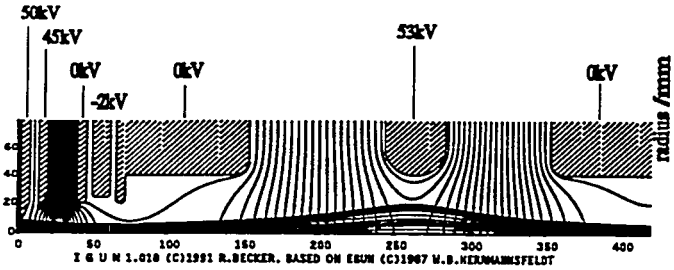

Fig. 8: Electrostatic LEBT line (1 unit = 0.5 mm).

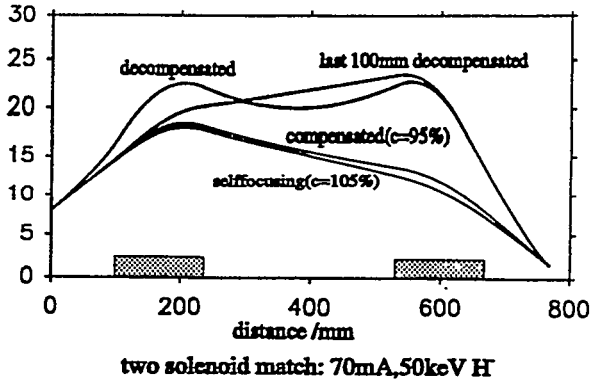

Fig. 9: Beam envelopes for variing degrees of compensation in a LEBT line with Solenoids (0.3-0.6 T).

envelope radius and angle for matching to the RFQ acceptance. But so far no successful experiment (under the aspects of emittance growth and transmisson) has been carried out with large beam current.

In contrary most operating accelerators are using magnetic systems allowing space charge compensation and therefore long distance beam transport with tolerable aperture filling and space for diagnosis and steering. Fig. 9 shows beam envelopes calculated for a two solenoid injection system. For this example the beam perveance has been variied for constant source emittance and RFQ acceptance. As expected the envelope of the compensated beam has a smaller radius compared to the decompensated case. Assuming 95 % compensation or self focusing (105 % compensation) does not change the situation drastically, but a decompensated drift of 10 cm in front of the RFQ strongly blows up the envelope and dominates the beam dynamics in the LEBT. Particle losses by interactions with the residual gas are higher compared to electrostatic systems and in the case of pulsed operation there is additional particle loss which is determined by the rise and decay time of compensation. From this aspect chopping in the LEBT has to be the subject of further investigations. Especially in the case of negative ions instabilities can occur for partly compensated beams which can be prevented by increasing the residual gas pressure and achieving self focusing.

One problem with space charge compensated transport is that the density profile of the compensated beam which is expected to be Gaussian like changes when the beam becomes decompensated in front of the RFQ. This change produces emittance growth wich cannot be predicted from our present knowledge of space charge compensated transport. Its magnitude can be estimated assuming a Gaussian shaped decompensated beam focused to the RFQ entrance. For 70 mA, 50 keV H^- with $\varepsilon_n = 0.1\pi$ the emittance grows by a factor of 2.8 at the last 10 cm (worst case scenario, in praxi the decompensation will take place in only 2-3 cm).

A LEBT line consisting of a HIEFS ion source, to soleniods (max 0.73 T, $\varnothing_i$ 100 mm) and multiple ring electrodes to influence the compensation has been set up in Frankfurt (see Fig. 10). For diagnostic Langmuir probes, RGI energy spectrometer, and emittance measurement device are available. First experiments with an high perveant ion beam (He^+, 10 keV,up to 5 mA) have been done with different emittance growth rates depending on the voltages on the ring electrodes (see fig. 11+12) [15].

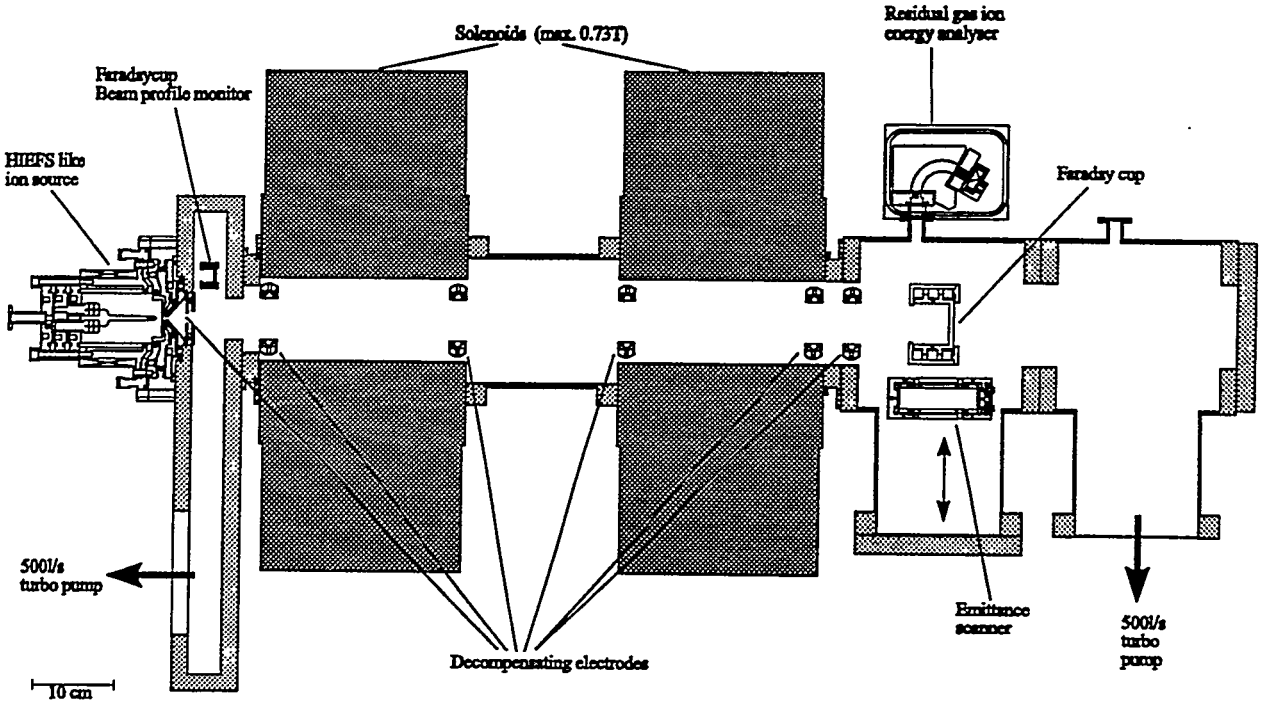

Fig. 10: Schematic drawing of the Frankfurt LEBT.

So emittance growth due to space charge effects is a very important problem of space charge compensated LEBT design for high perveance beams. Its solution requires more experimental and theoretical investigations in the next future.

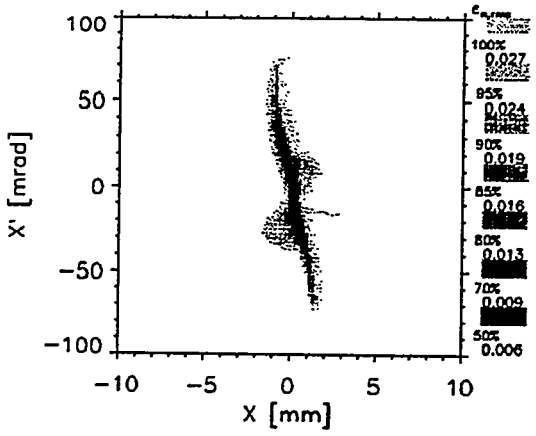

Fig. 11: Beam emittance after the second solenoid with space charge compensation (He^+, 10 keV, 2.5 mA). Source emittance: $\varepsilon_{n,rms,80\%} \approx 0.004\ \pi$mmmrad.

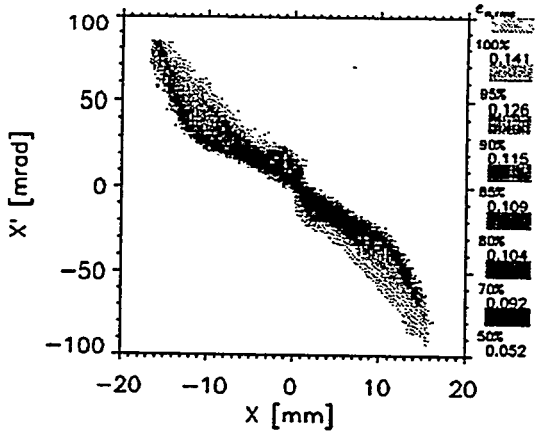

Fig. 12: Beam emittance after the first solenoid with all electrodes at positive potential (beam parameters see fig. 11).

RFQ part of the ESS - Injector

In nearly all operating as well as in planned new high current accelerator facilities formation and first acceleration of the beam coming from the ion source is done by the Radio Frequency Quadrupole (RFQ) structure [16,17]. This structure provides strong transverse rf focusing, a longitudinal field component is generated by a geometrical modulation to the quadrupole electrodes. Ion mass, beam current, beam quality, power losses and tolerances determine the choice of the rf structure and the main parameters frequency, current limit, electrode voltage and energy range, solutions for a wide range of parameters have been found already [survey in e.g. 18]. In the case of ESS an injector part is discussed (see fig. 2), which consists of two lines with ion source, LEBT, first RFQ, fast chopper and a second RFQ in each of them; both lines are then combined in a funneling section. The frequency of the normal conducting main linac was chosen to 700 MHz, for which proven rf accelerator structures and rf power supplies exist. The RFQ frequency could then be 175 MHz or 350 MHz resp., rf structures (four rod, four vane), transmitters and technical know how from operating RFQs are available for both. The proper choice has to be done from particel dynamics and technical requirements. In fig.13 current limits calculated from smooth approximation formulae [19] are plotted for the low energy first RFQ to allow a rough estimation of parameters. For the same input energy the current limit is lower for the higher frequency, which can be counteracted by a higher input energy (T_{in}=50 keV for 175 MHz and 100 keV for 350 MHz).

When assuming that the current limit should be about twice as high as the beam current only one injection line with I=100 mA is much more difficult to realize than the proposed two lines, but for both frequencies 50 mA can be handled with quite moderate parameters: electrode voltages of about 100 kV which is less then the rf sparking limit of 2 Kp (dashed line), mimimum aperture 4 mm, transverse phase advances of 30^0 or 20^0. In Fig. 14 results of PARMTEQ calculations for two preliminary design examples at 175 and 350 MHz resp. are plotted, where

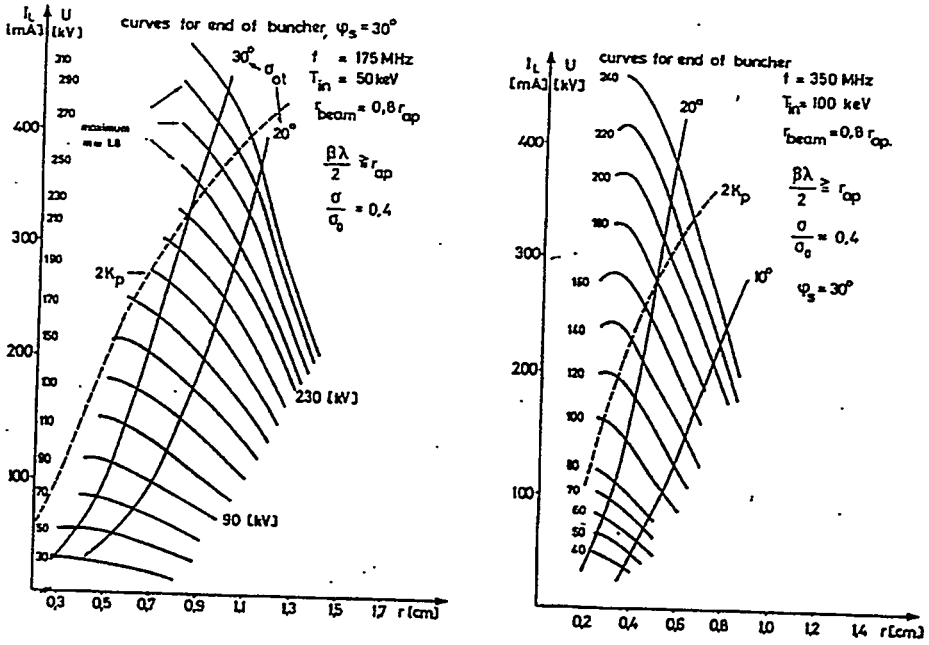

Fig. 13: Current limits calculated from smoth approximation for the first RFQ.

only small differences in beam size, emittance and transmission can be seen from the histograms of the beam behind the first RFQ [20]. The histograms are calculated from 100 % of the output beam and show a dense core with some particles around, for a reduction of this effect a more sophisticated design should be tried.

Between both RFQs a fast chopper will be installed to provide voids in the beam to give the necessary time for the extraction from the accumulator rings. The short rise time of the chopper, which still needs developement of suitable rf cavities, favours the lower frequency for the first RFQ; the achievable capability of the chopping line, which has to maintain the beam quality, especially the very small bunch width required for a frequency jump, will influence the final choice of frequency for the second RFQ.

First technical and beam dynamics layout of the RFQs have been done [21], some parameters are summarized in Table 3. Further investigations are necessary, both RFQs are not state of the art: they are long, will be operated at a duty cycle of up to 10 % with long pulses and have to perform an excellent beam quality at a rather high beam current.

Table 3 : Example of parameters of the ESS-injector-RFQs

		RFQ 1	RFQ 2	or RFQ 2
f	[MHz]	175	175	350
T_{in}	[MeV]	0.05	2.0	2.0
T_{out}	[MeV]	2.0	5.0 (7.0)	5.0 (7.0)
L	[m]	2.9	5.5	2.9
N_{rf}	[kW]	350	700	350
N_{beam}	[kW]	100	150	150
I_{lim}	[mA]	100	100	200

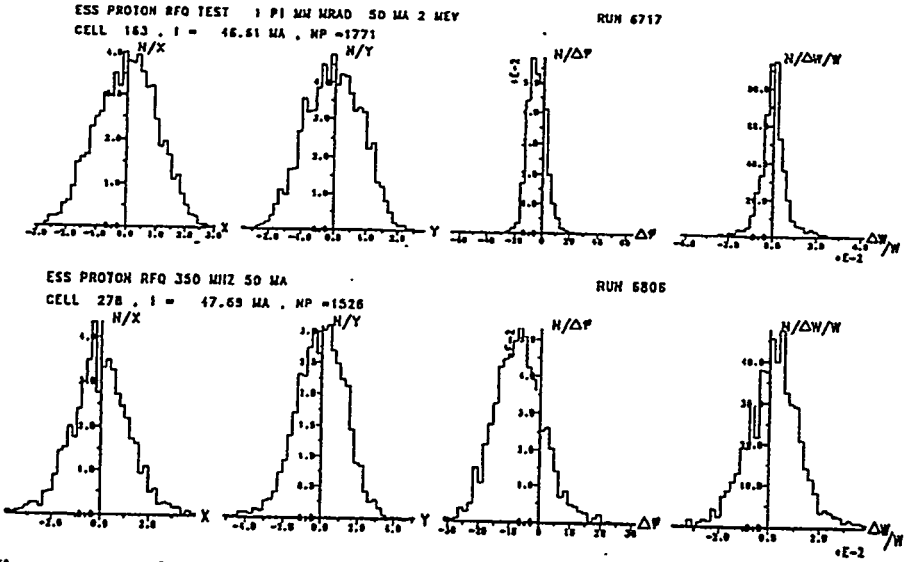

Fig. 14: Histograms of particle distribution for 100 % output beam, T=2 MeV, upper part f=175 MHz, lower part f=350 MHz.

Funneling

Without funneling the ion source has to deliver about 140 mA with the required good emittance, and the RFQs had to accelerate the full current. The preferred frequency would then be 350 MHz from the beginning to avoid a second frequency jump. This scenario is not impossible, but funneling relaxes the requirements for ion source and RFQ, promises a better beam quality and low emittance growth, allows the chopping at 175 MHz and improves the reliability. The investment costs for the front end is nearly doubled of course, but this is a small part of the overall cost anyway. For these reasons we propose to have a funnel section at about 7 MeV, where the two beams with a 175 MHz time structure are combined to a beam on one axis with a 350 MHz time structure and a doubled beam current without intrinsic emittance growth (Fig. 15).

Funneling [22] bas been successfully proven experimentally [23,24], but further work has to be done, especially for the deflecting and the rebuncher cavities, for which the IH-structure is advantagous [25]. Starting with a 350 MHz RFQ one could think of funneling also, if the high β linac is operated at 700 MHz; in this case the funneling could occur after 350 MHz DTL at a higher energy. In case of a superconducting high energy linac operated at 350 MHz, this option is not possible, of course.

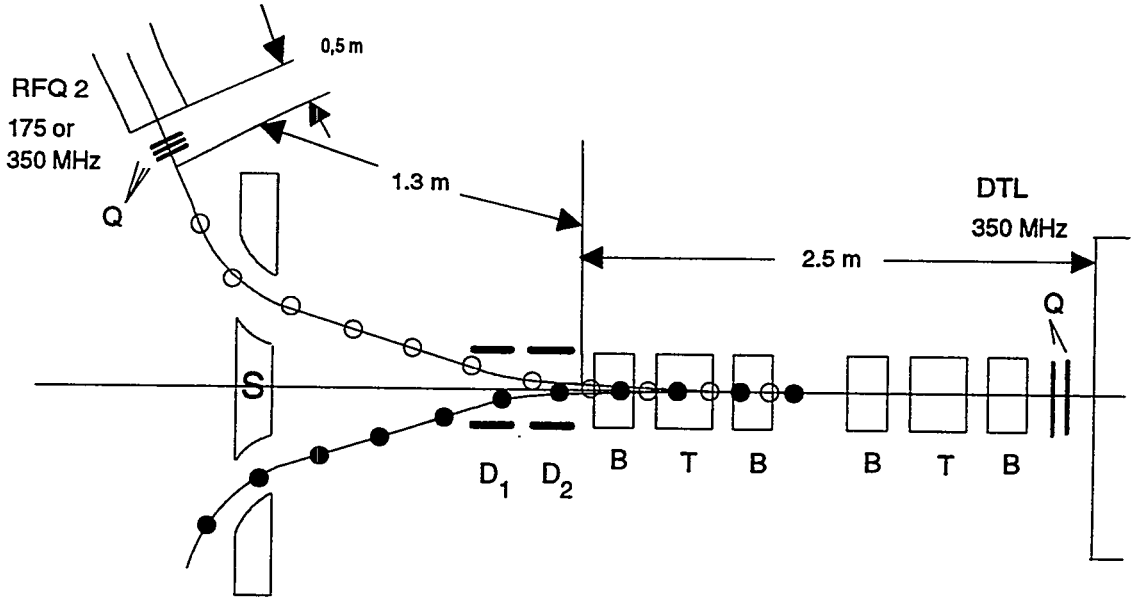

Fig. 15: ESS - Funneling line.
D_1, D_2 : rf-deflectors, 175 MHz,
S : septum magnet, Q: quadrupols
T: triplett, B : bunching cavity, 350 MHz.

DTL

The drift tube linac (350 MHz, l=75 m, cavity peak power=13 MW) has to accelerate from 5 (or better 7) MeV to 150 MeV. It is in principle state of the art, a post coupled Alvarez structure has been considered so far, but a bridge or cavity coupled DTL or an IH-structure are also possible structures.

High energy linac

The high energy linac will accelerate to the final energy of 1.334 GeV and may be normal or superconducting. For the n.c. linac a frequency of 700 MHz seems to be appropriate, leading to a peak current of 200 mA; but a frequency of 1050 MHz is not out of discussion. As a first option we consider side coupled cavities as used at LANL or Fermilab; the new SCC-linac at Fermilab serves as a good basis for the production techniques and cost estimations. An upgrade to the higher duty cycle of ≈ 7 % seems to be no severe problem. But other structures like the DAW are in consideration also. For a very good review of structures see [26,27,28]. An economic field gradient is about 2.8 MV/m, leading to Joule losses of about 100 MW peak in addition to the beam power of 70 MW peak. The linac length is about 570 m, the aperture radius 22 mm. For more details and beam dynamics see [29].

For a superconducting version a frequency of 350 MHz is preferred in the moment. The optimum acceleration field is about 10 MV/m ($Q_0 = 3*10^{-9}$, $Q_{load} = 3*10^5$), leading to a much shorter (≈ 320 m) and cheaper linac [30]. The large aperture of 10 cm reduces the non linear field components near the axis; this will reduce the emittance growth and the particle losses in the structure. Due to the pulsed operation (the pulse length is fixed by the 1000 injection turns allowed maximum) the s.c. linac looses a considerable part of its intrinsic efficiency by the long build up time in the order of 0.5-1 ms, which has to be taken into account. Fig. 16 shows an accelerator module. With one rf coupler only a two cell structure is fed, and even then the neccessary power per rf-window with 400 kW is much larger as the power that can be handled now a days (150-200 kW); therefore developments to improve the couplers are going on at several places. Of course one could reduce the accelerating field, but then the s.c. linac will loose some of its advantages. Other concerns connected with the low frequency and the high electric field are the detuning by the Lorentz force and the dark currents. In both cases a higher frequency (700 MHz) would help, but possibly cooling with superfluid Helium at about 2 K might be neccesary due to the increased rf losses. In any case, the use of superconducting cavities is very promising, but needs further investigations.

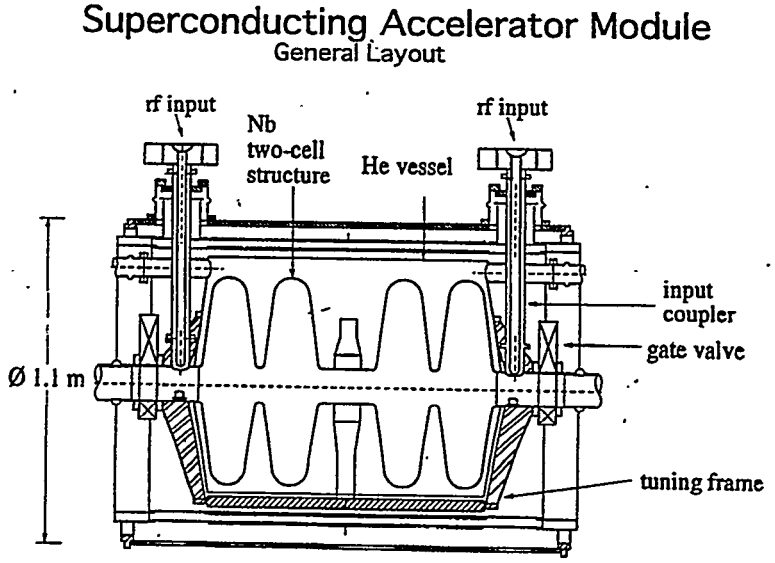

Fig. 16: Schematic drawing of a possible superconducting accelerator module.

Conclusions

Some design considerations and a preliminary layout of ESS have been discussed. We have concentrated on the combination of a linac with accumulator rings so far, but other possible solutions, as a combination of linac and rapid cycling synchrtrons or the use of induction modules, which are considered in other countries in detail, are not ruled out. Further work will hopefully lead us to a reasonable conceptional design in two years from now.

Acknowledgements

For information support and great help I express my warmest thanks to many colleagues, especally to H. Lengeler, K. Bongardt (KFA Jülich), H. Heinrichs, H. Piel (Univ. Wuppertal), I. Gardner, G. Rees (DRAL), H. Deitinghoff, P. Groß, A. Lakatos, J. Pozimski, M. Sarstedt, K. Volk (Univ. Frankfurt).

References

[1] Lengler, H., Proposals for spallation sources in Europe, EPAC94, London.

[1] Rees, G., Injection, Proc. of General Course of Cern Acc. School, Cern 94-01, 94, P. 737.

[3] Volk, K., Entwicklung einer effizienten Ionenquelle zur Produktion intensiver, hochbrillianter, atomarer, einfach geladener Ionenstrahlen, Dissertation 1993, Inst. Angewandte Physik, Frankfurt.

[4] Volk, K., Barth, W., Lakatos A., Ludwig, L., Maaser, a., Klein, H., A compact high brilliance ion source for RFQ injection, Proceedings of the EPAC 1994.

[5] Volk, K., Ludwig, T., Lakatos, A., Klein, H., Preliminary Studies of a rf-driven Bi^+ source, Annual Report 1993 on High Energy Density in Matter Produced by Heavy Ion Beams, GSI-94-10, June 1994, p. 34.

[6] Anderson, A., Chan, C.F., Leung, K.N., Soroka, L., Wells, R.P., Low-energy injector design for SSC, Rev. Sci. Instr. 63 (4), April 1992.

[7] Struckmeier, J., Klabunde, J., Reiser M., On the stability and emittance growth if different particle phase-space distributions in a long magnetic quadrupol channel. Particle Accelerators, 15:47-65, 1984.

[8] Wangler, T.P., Crandall, K.R., Mills R.S., Reiser, M., Relation between field energy and rms emittance in intense particle beams. IEEE Trans. Nucl. Sci., NS-32(5) 2196-2200, 1985.

[9] Anderson, O.A., Internal Dynamics and emittance growth in space-charge dominated beams. Particle Accelerators, 21:197-226, 1987.

[10] R. Dölling, Raumladungskompensation driftender intensiver Strahlen niederenergetischer Ionen und Techniken zu ihrer Vermessung, Dissertation in Vorbereitung, IAP Frankfurt.

[11] J. Pozimski, Groß, P., Dölling R., Klein H., Numerical calculation of charge density distribution in space charge compensated ion beams, GSI-Annual Report 1992 on High Energy Density in Matter, GSI-93-17, Mai 1993, p. 38.

[12] Gabovich, M.D., Dzhabbarov, D.Z., Naida, A.P., Effect of decompensation of a dense beam of negative ions. JETP Lett., 29(9):489-492, 1979.

[13] Anderson, O.A., L. Soroka, Kwan, J.W., Wells, R.P., Application of electrostatic LEBT to high energy accelerators, Proceedings of then EPAC 1990,pp. 1288-1290.

[14] Sarstedt, M., Untersuchungen zu Strahlformierung und Transport intensiver Ionenstrahlen und ihrer Injektion in einen RFQ-Beschleuniger , Dissertation 1994, Inst. Angewandte Physik, Frankfurt.

[15] Groß, P., et. al. , Experimental and theoretical investigations of emittance growth of space charge compensated beams in a magnetic transfer line, in prep. for LINAC 94.

[16] Kapchinsky, I.M., Teplyakov, M., Linear ion accelerator with spatially homogeneous strong focusing, Prib. Tekh. Eksp. Phys. 119,No. 2, 17-19 (1970).

[17] Crandall, K.R., Stokes, R.H., Wangler, T.P., RF quadrupole beam-dynamics design studies, Proc. 10 th LINAC Montauk, BNL - 51134, 205 ff. (1979).

[18] Schempp, A., RF Quadrupoles as accelerators, in: Advances of Accelerator Physics and Technology (ed. H. Schopper), World Scientific, Singapore (1993), 194 ff.
[19] Junior, P.H., Space-charge limits in heavy in RFQ linacs, Particle Accelerators, 13, 231 ff.(1983).
[20] Deitinghoff, D., First beam dynamics calculations for the ESS-RFQs, Int. Rep. 94-11, IAPFFM .
[21] Schempp, A., The low energy part of high intensity accelerators, Proc. EPAC94, ed. Frontiere, in print.
[22] Bongart, K., Funneling, ESS-Linac Meeting, Sept 93, Frankfurt.
[23] Johnson, K. F., et. al., The Single-Beam Funnel Demonstration : Experiment and Simulation, Linac92, AECL 10728 (1992) 64.
[24] Barth, W., A. Schempp, Funneling of Low Energy Ion Beams, Linac92, AECL 10728 (1992) 413.
[25] Krawczyk, F.L. et.al., Design of rf-cavities in the funnel of accelerators for transmutati0on technologies, this conference.
[26] Yamazaki, Y., Recent technological developments in accelerator structures, Linac 92, p 580.
[27] Schriber, S. , Survy of proposed High Intensity Accelerators, EPAC94, London.
[28] Lawrence, A.G., Critical Design Issues of High Intensity Hardron Linacs, EPAC 94, London.
[29] Pabst, M., Bongard, K., Design considerations of the ESS coupled cavity linac, in prep. for LINAC 94.
[30] Heinrichs, H., Piel, H., Univ. Wuppertal, ESS meeting Febr. 94 Jülich and private communication.

DESIGN OF HIGH-ENERGY HIGH-CURRENT LINAC WITH FOCUSING BY SUPERCONDUCTING SOLENOIDS

Guennady I.Batskikh, Vladimir M.Belugin, Boris I.Bondarev,
Arkady P.Fedotov, Alexander P.Durkin, Yury D.Ivanov,
Vladimir N.Mikhailov, Boris P.Murin, Kharis Kh.Mustafin,
Igor V. Shumakov, Nikolay I.Uksusov,
Moscow Radiotechnical Institute
Warshawskoe shosse, 132, 113519, Moscow, Russia

Abstract. The advancement of MRTI design for 1.5 GeV and 250 mA ion CW linac is presented in the report [1]. In new linac version all the way from input to output the ions are focused by magnetic fields of superconducting solenoids. The ion limit current is far beyond the needed value. The linac focusing channel offers major advantages over the more conventional ones. The acceptance is 1.7 times as large for such focusing channel as for quadrupole one. Concurrently, a random perturbation sensitivity for such channel is one order of magnitude smaller than in quadrupole channel. These focusing channel features allow to decrease beam matched radius and increase a linac radiation purity without aperture growth. "Regotron" is used as high power generator in linac main part. But D&W cavities need not be divided into sections connected by RF-bridges which denuded them of high coupling factor.

INTRODUCTION

A particles lossless transport through accelerating/focusing channel required a large margin of safety. The most critical areas are:

- initial space charge-dominated linac part (up to 3 MeV);
- interface between focusing channels with different types and structures;
- high-energy linac part with a great number of independent focusing elements and a high sensitivity to focusing field random perturbations.

It is evident that inadequate decision of above problems lead to beam quality degradation and to particle possible losses. Beam transport across matching sections is the most complex problem because we have no prior knowledge of beam mismatching.

The usual high-energy linac contains RFQ, DTL, BCDTL, CCL parts with quadrupole focusing. There are three matching sections: from RF quadrupole to magnetic quadrupole channel and between magnetic quadrupole channels with different period structures. The RFQ section does not give no possibilities for needed (250 mA) beam accelerating and gives necessarily the effective emittance growth due to beam parameter time dependent and beam funneling. HILBILAC was proposed in MRTI project of 1979 [2-4] as an initial part of a linac with higher ion current and higher channel acceptance.

In 1979 MRTI project HILBILAC - DTL interface problem was solved as usual matching of two time-independent periodical structures. But some distinguishing features remain unknown. Firstly, the quadrupole channel must be protected from magnetic field penetration by iron screen. Secondly, the matching must be made taking into account a rotation in (x,y)-plane with regard to quadrupole channel acceptance.

Because of this the idea of single-type focusing using come on the next design stage. The proposed superconducting solenoid focusing (SSF) has the following advantages:

a) high channel acceptance (from 1.5 to 2 times larger) and high limit current (700 mA) give promise that the beam with good transverse parameters can be formed after linac initial part passing in spite of the Coulomb effect action;

b) single-type focusing alleviates the good matching of different linac parts and an essential jump in periodicity takes place only during transition from DTL to HBL (High-Beta Linac);

c) replacing the quadrupole lenses by solenoids decreases the channel sensitivity to random perturbations by a factor of ten (numerical results will be presented in corresponding division).

Superconducting solenoids using makes linac practical design more complicated both in new systems emergence and in hard availability for some communications. Nevertheless, the proposed design has strong appeal and must be considered as having real possibility.

Let us consider the main special features of linac beginning part.

A CHOICE OF HILBILAC ACCELERATING CHANNEL PARAMETERS

Accelerating channel of linac beginning part must provide:

- full particle capture by virtue of adiabatically variation in RF amplitudes and phases along channel;
- smooth density variation during bunch generation (in the ideal case must has a nonincreasing density);
- reliable decisions for heat removal, cavity tuning and RF break-down problems in high magnetic fields.

The last requirement stands in need for drift tube length and number limits as well as RF amplitude limit in accelerating gaps. For example, in the first HILBILAC cavity in virtue of high frequency and low energy an accelerating period length equals $3\beta\lambda/2$ instead of $\beta\lambda/2$. The bunching part of linac contains so much accelerating periods that it must be divided into two cavities. The RF gap field intensity in high magnetic field must be no more then 5 MV/m.

The main task of conducted investigations was to show a potentialities of new approaches. The codes package **SSFL.Advisor** was generated. After drift tube and gap lengths calculation bunch density curve is indicated. It gives a possibility for designer to optimize linac version long before beam dynamics simulation.

The **SSFL.Advisor** was used for making investigations which lent support to the validity of the linac conception. At the same time some distinctive features had revealed. Firstly, the bunch optimal formation takes place at linac first two cavities with amplitude and phase concurrent variation, i.e. in these cavities the preset form for RF amplitude must be realized. Secondly, these two cavities must be sufficiently large in length in order to give full particle capture. For example, we can choose the first cavity (123 periods, 2.8 m) which accelerate protons from 0.15 MeV to 0.18 and the second cavity (107 periods, 5,6 m) for protons from 0.18 to 3 MeV. Thirdly, for operating frequency 350 MHz there are some difficulties with realization of beam bunch unincreasing density because of RF field radial nonuniformity.

In Table 1 are presented HILBILAC accelerating and focusing channels parameters obtained after preliminary optimization.

Table 1. HILBILAC Accelerating and Focusing Channels Parameters

	Tank 1	Tank 2
Input Energy, MeV	.150	.181
Output Energy, MeV	.181	3.01
Main Frequency, MHz	352.2	352.2
Ion Current, mA	250	250
Aperture Radius, mm	5	5
R_{beam}/Aperture	.75	.75
Drift Tube Length, mm	19	20-79
E_m-amplitude at Axis, MV/m	0.17-0.47	0.48-0.72
RF Gap Intensity, MV/m	0.9-2.6	2.6-3.9
Equilibrium Phase, deg	(-90)-(-81)	(-80)-(-31)
Tank Length, m	2.81	6.38
Tank Diameter,mm	200	200
Drift Tube Diameter,mm	20	20
Number of Periods	122	118
Cu Power, MW	.025	.05
Beam Power, MW	.01	.71
Total Power, MW	.035	.76
Magnetic Field Induction, T	6.5	6.5

FOCUSING CHANNEL PARAMETERS CHOICE AND BEAM MATCHING

Magnetic field permissible nonuniformity between adjacent solenoids and beam good matching are the main problems for beam focusing. The high-current matching beam transport in uniform longitudinal magnetic field is well-studied [5,6] and core + halo behavior is considered. The same results can be obtained for beam with smooth and slowly varying charge density. The required magnetic field induction equals 5-7 T for 250 mA proton beam with 4-5 mm radius and 0.2-0.3 π ¢m·mrad emittance. Beam dynamics investigations were carried out in order to verify that local magnetic field drop does not disturbed beam transverse motion when magnetic field average value does not changed because of additional coils using.

Two effects degraded the beam quality are the results of the phase motion influence on transverse one. The first is direct influence of accelerating field defocusing effects. It depends on RF-phase in a gap at the instant of the given particle pass it. This effect is more in evidence when bunch phase size is large (as in so called "adiabatic buncher" where phases may range up to 360 degrees). Because of moderate value of RF-amplitude in such buncher and because of defocusing effect decreasing with energy growth the considered factor rises beam effective radius no more than by 10%.

The bunch charge density variation during phase oscillations (both in its average value and also in its distribution) is the second factor. Generally, a particle moving along bunch may "sense" the essential transverse Coulomb force oscillations. With certain conditions the effect has some resonant features. As can be shown for considered linac version the first phase oscillation gives beam mismatching and effective emittance doubling.

Ion dynamics study verify that there are no intractable problems on the way of HILBILAC designing.

With respect to mechanical stability of SSF the most problem is axial ponderomotive forces on magnets (the force between small and long solenoid is about 10 tones).Even small relative displacement of solenoids with high current in

high magnetic field causes dangerous heat release. As this takes place, it is possible such negative effects as degradation and exercise of superconducting system.

Problem of mechanical stiffness of magnetic system is resolved by introduction of stiff elements between flanges of small and long solenoids, by using stiff telescopic supports and chain suspensions in cryostats.

Storage energy of magnetic field in HILBILAC SSF is as great as 20J. Safeguard problem of this system in passing from superconducting condition to normal one is most complicated problem.

During the transition of superconducting system to normal state it it necessary to use complex precautions for normal operation keeping such as:

- modules shunt;
- positioning of the modules in copper former aided uniform heating up of winding;
- compulsory "fire" of winding with the help of special heater placed inside superconducting modules; it is effected with change of state of normal zone origin detector.

HILBILAC LAYOUT

HILBILAC initial part (Fig.1) has relatively small length of about 10 m. It contains accelerating cavity 1, 2; superconducting solenoids 3, 5; magnetic screen 4; adjustable supports 7, 9, 11, 12 and so on. Cavities 1 and 2 are rigidly bound to unified construction and placed inside solenoid 3 with "warm" hole 400 m in diameter. Cavity 2 is joined with DTL cavity 13 with the help of bellows elements of its outward shell. DTL cavity is placed inside superconducting solenoid 14 with warm hole 800m in diameter. RF supply feeders, vacuum system brunch pipes, elements of cavity cooling system and cables of control-measuring system pass through gaps between solenoids 3, 5, 12 ends. To eliminate longitudinal displacement of solenoids under the action of mutual attraction of adjacent solenoid ends special screw-jacks 6 are designed.

HILBILAC accelerating/focusing channel is placed inside circular magnetic screen 4 about 1200m in diameter and about 150 m in thickness. The magnetic screen is lengthwise and transversely partitioned into sections. The construction of transverse joint assembly 8 is to provide a possibility of screen position adjustment (relative to solid support of accelerator) and to have small magnetic resistance of gap. RF windows 9 and vacuum system pumps are placed outside magnetic screen.

Cavities, solenoids and magnetic screen sections are placed on individual adjustable supports 11, 9, 12, 7 providing independent adjustment of its position relative to solid support of accelerator.

BEAM DYNAMICS PROBLEMS IN DTL

The beam acceleration from 3 to 100 MeV rises no additional problems if HILBILAC output beam can be taken as having high quality.

Focusing field is generated by sequence of closely-spaced identical superconducting solenoids slipped over tanks. There are two solenoids over one tank. Field distribution along the Z-axis smooth transit from continuous in HILBILAC to periodical in DTL. There are only two questions which must be answered:

a) how much can be magnetic field drop between adjacent solenoids?

b) what is the minimal beam energy starting from inter-tank practical intervals can be allowed?

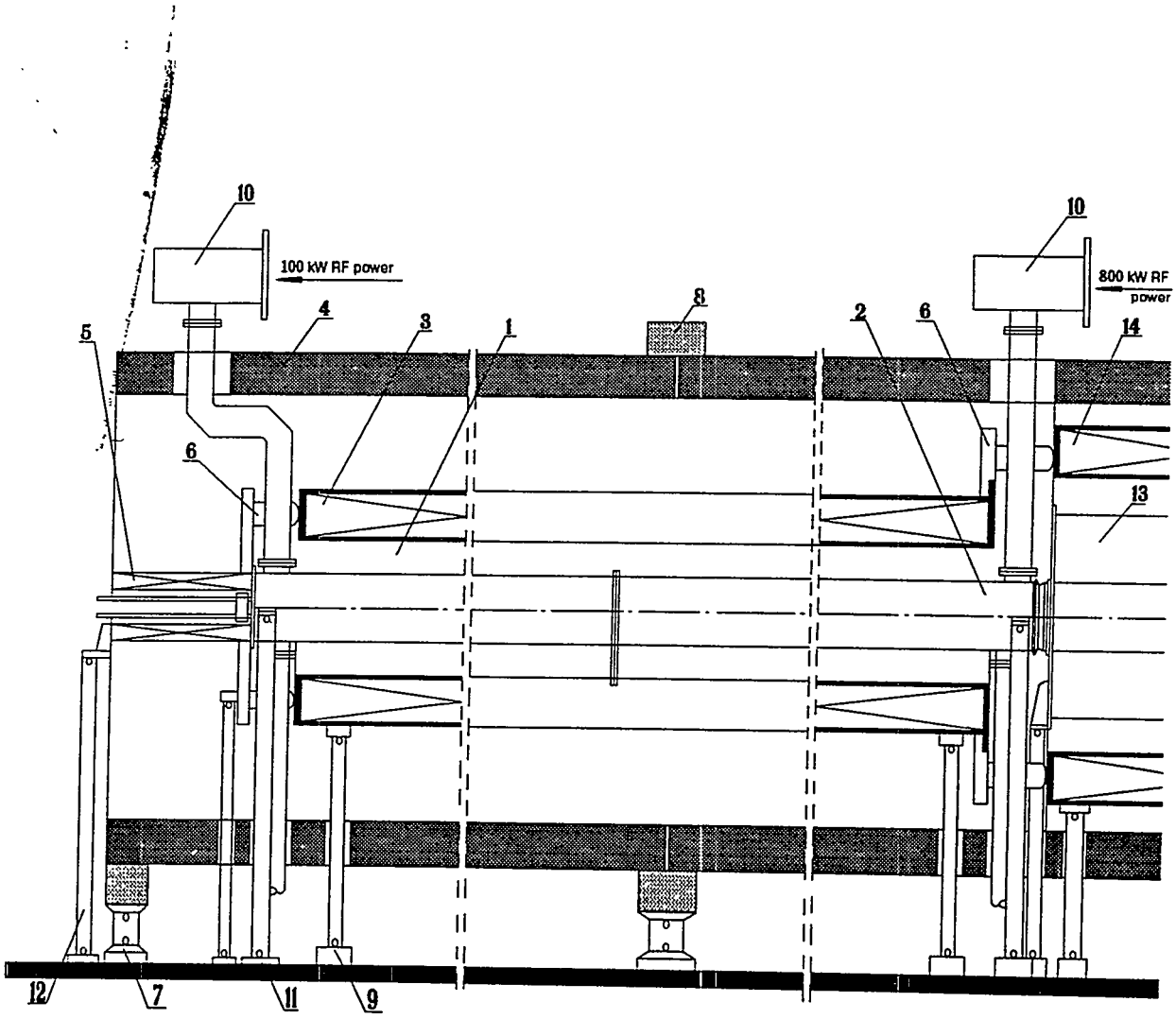

Fig. 1. HILBILAC (Initial Part)

1,2 - accelerating cavities; 3 - superconducting solenoid; 4 - magnetic screen; 5 - superconducting solenoid of transport channel; 6 - screw-jack; 7 - adjustable supports of magnetic screen; 8 - assembly of transverse joint of magnetic screen; 9,12 - adjustable supports of solenoid; 10 - RF window; 11 - adjustable supports of cavity; 13 - DTL cavity; 14 - DTL superconducting solenoid

It was shown by beam dynamics studies that 10-15% magnetic field drop (corresponding solenoid length 1.1 m and interval length from 0.25 m to 0.5 m) allows to transport beam along the channel length without its quality impairment.

The second problem study shows that intertank practical intervals with 200 mm and more lengths can be used for beam energy over 20 MeV.

One more SSF advantage must be noted. In usual quadrupole focusing channel a lens number exceeds 200. Each of lenses must be considered as a source of random errors connected with focusing channel manufacturing and tuning. It means that essential transverse motion perturbations and beam impairment can be expected at DTL output. A severe decrease in random perturbation influence take place if SSF channel is used. The SSF channel sensitivity is ten times smaller than FODO channel one and a solenoid number is no more then 70. That is why the SSF channel version is more reliable for required beam quality realization.

SOME PROBLEMS OF LINAC MAIN PART

It is customary to design the main (CCL) linac part as very long channel with 300 - 500 tanks and the twice number of quadrupole lenses. This numbers are bring forward in order to emphasized once more the random perturbation dangerous influence on beam quality. Very much sources of random errors can lead to beam transverse and phase sizes growths, particle losses and unfeasibility of linac operating.

The Regotron generator designed by MRTI with 5 MW unit power are used for increasing of linac operating reliability. In this case a tank number reduced in 5 times.

It is assumed that D&W accelerating structure will be used. It is customary to divide D&W tank into sections connected by RF bridges. Unfortunately, the bridge using reduce coupling factor and causes each section to become an independent source of random perturbations. If solenoid has a big diameter and is slipped over a tank the coupling factor remains big and the entire tank can be considered as one random source.

For the purpose of making comparison between solenoidal and quadrupole channels let us brief overview the results of beam radius growth under random perturbations [7,8]:

a) the most dangerous perturbations are magnetic field deviations, rotations of quadrupole lenses around longitudinal axes and lens/solenoid transverse displacements;

b) the channel sensitivity is determined by product $G \cdot R^2$, where G is refractive force gradient and R is an envelope maxi- mum over the period.

For quadrupole channel $G_q = eHLl/(mcp)$, for solenoidal one $G_s = (eB)Ll/(2mcp)$, where e and m are particle charge and mass, p is particle relative pulse, l is lens/solenoid length, L is focusing period length, H is transverse magnetic field gradient and B is longitudinal magnetic field induction.

Lens rotations around longitudinal axis as the most danger perturbation source is absent in solenoidal channel. This type of perturbations gives both radius and emittance growths. Comparing G_q and G_s we receive for G_q/G_s ratio that

$$G_q/G_s = (H/B)\cdot(4mcp/e)$$

For standard values $H = 15$ T/m, $B = 5$ T, $p = 0.9$, the ratio equals $G_q/G_s \doteq 6$. Taking into account that solenoidal channel acceptance is from 1.5 to 2 times larger than quadrupole one and acceptance is proportional to R^2 we obtain that a

solenoidal channel sensitivity is ten times smaller in comparison with quadrupole one.

In Table 2 the comparison between main tolerances for solenoidal and quadrupole channels of linac main part are presented. The following conditions are used for tolerances calculation: a probability of beam radius growth by factor 1.2 equals 0.9.

Table 2. The Comparison Between Main Tolerances for Solenoidal and Quadrupole Channels of Linac Main Part

Type of Tolerance	RMS-value of Tolerance in *Solenoidal Channel*	*Quadrupole Channel*
Magnetic Field Deviation	1%	0.1%
Lens Rotation	absent	0.15 deg

The rms-value of lens/solenoid displacement tolerance is 20 vicrons without system of beam transverse position correction and 120 microns with such system.

CONCLUSIONS

In proposed linac design the problem of lossless beam accelerating are solved with high reliability. An unique type of focusing channel with the greatest acceptance and the smallest sensitivity is used along the whole linac from its input to output. The beam matching between different linac parts is simplified.

Cost of the above-listed advantages is an increasing sophistication of focusing channel equipment. For example, the great number of superconducting solenoids with large diameter are used. For its safety operation reliable protection systems are needed.

The line of future trends in SSF linac advancing must be based on a trade-off of beam lossless transport efficiency against sophistication of focusing channel equipment. In future more closely must be investigate the following versions:

- 350 MHz H-resonators using up to 15-20 MeV,
- 700 MHz BCDTL using from 20 MeV to 100 MeV
- small aperture superconducting solenoids using between adjacent DTL tanks.

All above-listed versions have own advantages and disadvantages. For optimal version choosing both beam dynamics studies and technical researches must be made. The main question is trade-off of beam current transmission against sophistication of equipment.

Special investigations must be dedicated to linac reliability (including RF device redundancy) and to testing linac main part module.

ACKNOWLEDGMENTS

The authors would like to give special thanks to Dr. R.A.Jameson from LANL for constructive discussions, continuous encouragement and for work supporting.

REFERENCES

1. Batskikh, G.I., et al, "Development of Advanced Technological Systems for Accelerator Transmutation", *this Conference.*

2. Murin, B.P., Pirozhenko, V.M.,Plink, O.V.,"High-Current, Low-Energy RF Ion Accelerator" *Proceedings of the 1990 Linear Accelerator Conference.* Albuquerque, New Mexico, p.707-709.

3. Andreev, V.G. et al. "Basic Principles of Burner-Reactor Linac Design", *Specialist Meeting on Accelerator-Driven Transmutation Technology for Radwaste and other Applications,* 24-28 June, 1991, Stockholm, Sweden, LA-12205-C, SKN Report No 54.

4. Batskikh, G.I., et al. "High-Intensity Low-β Ion Linac (HILBILAC). *Report on ATW/ABC Accelerator Workshop*, 16-21 November, Los-Alamos, 1992.

5. Bondarev, B.I., Durkin, A.P., "Equilibrium States of Space Charge-Dominated Beam in a Longitudinal Magnetic Field, *Journal of Technical Physics*, v.56, N 11,1986.

6. Bondarev, B.I., Durkin, A.P., Murin, B.P., "Effective Emittance Growth, Contract 9-XG3-5167H-1 between LANL and MRTI, Phase 1, Moscow,1993.

7. Bondarev, B.I., et al., "Random Perturbation of the Transverse Motion of Protons in a Linear Accelerator and Their Correction, *Particle Accelerators*, v.6, N 1, pp. 27-40.

8. Murin, B.P., Bondarev, B.I., Durkin, A.P., "An Approach to Design of a Robust Focusing Channel", *Linac'92 Conf. Proc.*, AECL-10728, v.2, pp. 731-733.

Cost Optimisation Studies of High Power Accelerators

R. McAdams, M.P.S. Nightingale, D. Godden, A.J.T. Holmes and G. Proudfoot
AEA Technology, Culham, Abingdon,
Oxon, OX14 3DB, England

Abstract. Cost optimisation studies are carried out for an accelerator based neutron source consisting of a series of linear accelerators. The characteristics of the lowest cost design for a given beam current and energy machine such as power and length are found to depend on the lifetime envisaged for it. For a fixed neutron yield it is preferable to have a low current, high energy machine. The benefits of superconducting technology are also investigated. A Separated Orbit Cyclotron (SOC) has the potential to reduce capital and operating costs and initial estimates for the transverse and longitudinal current limits of such machines are made.

INTRODUCTION

The high power accelerators proposed for transmutation of material such as radioactive waste and plutonium are expensive both in terms of the capital and running costs. Acceptability of this accelerator technology rests not only on the benefits, the feasibility and the technical risks, but also on the delivery of the most cost effective solution. Thus it is important that the cost drivers are understood.

A required neutron yield can be met by an infinite number of combinations of beam current and energy as the yield is proportional to the product of beam current and the number of neutrons per incident proton which is a function of beam energy. This is illustrated in Figure 1 which shows curves of constant neutron yield, 5×10^{18}n/s in this case, for a proton accelerator with a lead target, a ^{238}U target, and an enriched uranium target where the neutron yield is assured to be ten times that of the ^{238}U yield. The curves are formed from neutron yield data obtained from the literature [1,2].

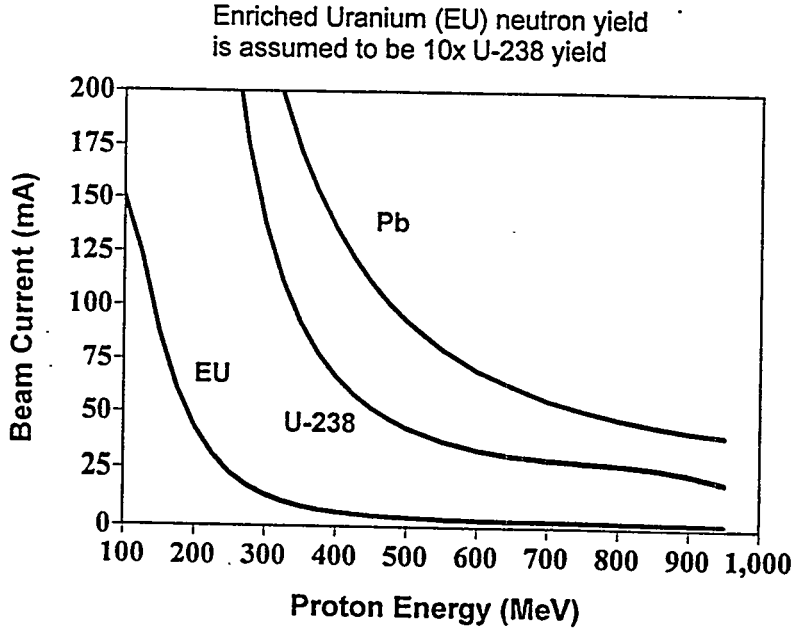

Fig. 1. Curves of constant neutron yield (5×10^{18} n/s)

The question then arises as to which combination of current and energy, whilst keeping the neutron yield constant, leads to the lowest cost accelerator. Furthermore each combination can be subject to a cost optimisation procedure in terms of overall power and length of the machine. This paper describes such cost optimisation studies for a linear accelerator with final energy greater than 100MeV. A simple cost model is used to calculate the capital and running costs of the accelerator. Following that the potential for cost reduction through the use of superconducting accelerators is illustrated.

The capital and running costs can be reduced through the use of a cyclotron. However the high currents need for transmutation applications have not been demonstrated in a cyclotron. The Separated Orbit Cyclotron (SOC) has the potential for high current beams and preliminary calculations are presented of the transverse current limit for such a machine.

BASELINE ACCELERATOR CHOICE

The cost optimisation studies were carried out for a baseline accelerator similar to that proposed by Los Alamos [3]. It is assumed to comprise of an injector up to 100keV, a Radio Frequency Quadruple (RFQ) up to 7MeV, a Drift Tube Linac (DTL) up to 20MeV, a Bridge Coupled Drift Tube Linac up to 100MeV and a Coupled Cavity Linac (CCL) up to the final energy. The ions species is protons, the accelerators are at room temperature and are driven by 350MHz klystrons to the end of the DTL after which 700MHz klystrons are then used for the BCDTL and the CCL. Figure 2 shows a schematic of the accelerator.

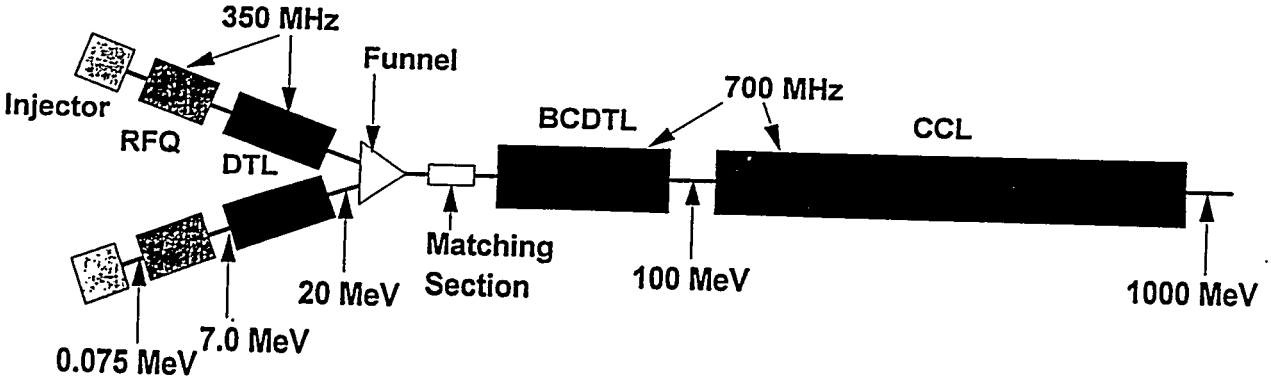

Fig. 2. Baseline accelerator choice

Bore Size Issues and Shunt Impedance Modelling

For such high power accelerators activation of the machine is a key issue and the bore size is usually many times the rms beam size. For the Los Alamos design this factor increases from 13 to 26 as the beam energy increases. From a model by Wangler [4] the beam size decreases with decreasing beam current. Thus we allow the bore to change with beam current whilst keeping a ratio between the bore to beam radius equal to that used by Los Alamos. Reducing the bore leads to increased power efficiency through an increase in the shunt impedance. Figure 3 shows the relationship between beam radius and beam current derived from

this model at 100MeV. This was assumed to be the case at all energies although at higher energies the beam size reduces giving further scope for shunt impedance improvement.

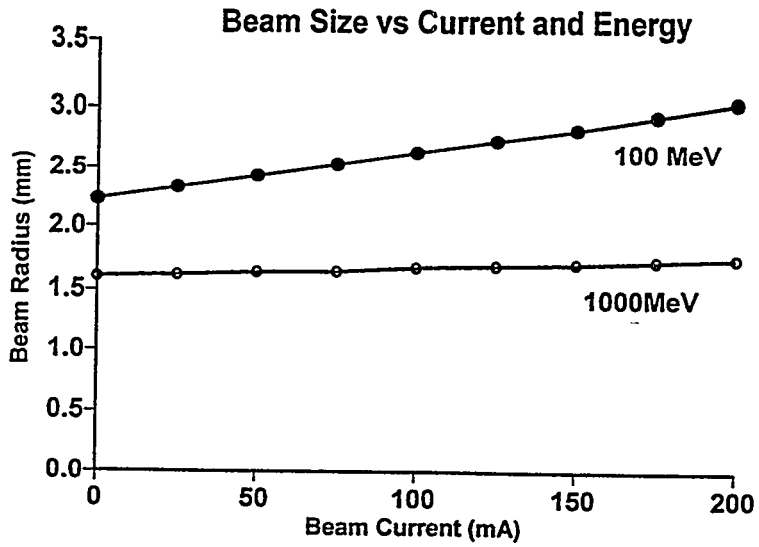

Fig. 3. Relationship between beam radius and beam current

In the modelling the design of the accelerator up to the 100MeV injection point of the CCL was assumed to be fixed. The generic Los Alamos CCL cavity design was optimised for highest power efficiency by varying the shape of the cavity to maximise the effective shunt impedance using the SUPERFISH code. This effective shunt impedance is defined as $0.85ZT^2$ where Z is the calculated shunt impedance, T is the transit time factor and the 0.85 factor allows for losses in coupling slits, coupling cavities and bridge cavities. In conjunction with the changing bore size at different currents, the shunt impedance for any current and energy can be obtained and this is shown in Figure 4. These shunt impedances can now be used in the cost modelling.

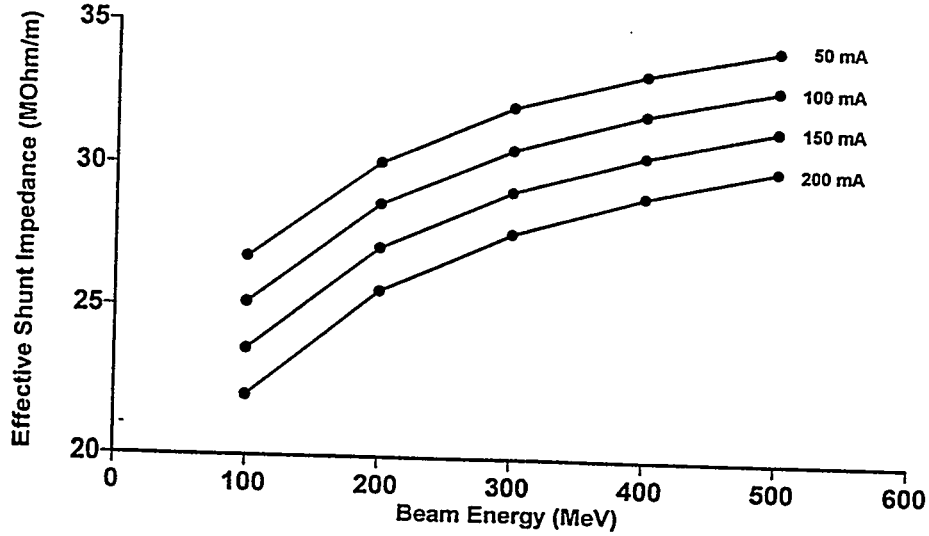

Fig. 4. Variation of CCL shunt impedance with beam energy and current.

COST MODEL

The aim of the cost modelling is to obtain the total costs (capital and running) of the accelerator for a matrix of currents and energies. Curves such as that shown in Figure 1 can be imposed on the matrix and the costs for a constant neutron yield obtained by interpolation.

The inputs to the cost model are given in Table 1 below.

Table 1. Inputs to the Cost Model

Parameter	Comment or Value
Shunt Impedance	Obtained from SUPERFISH
Cost of CCL Structure	£170k/meter
Capital Cost of RF System	£1/Watt for 1MW klystrons
Cost of Accelerator to CCL	Scaled from £50M for a 250mA machine
RF Tube Lifetime	50,000 hrs
RF Tube Replacement Cost	£350k
AC to RF Conversion Efficiency	58%
AC Power Costs	4.25p/kWhr for UK
Staff	100 at AEA rates
Availability	0.75
AC Requirement for Balance of Plant	25MW
Synchronous Phase	30°
Power Losses in RFQ, DTL, Funnel, BCDTL	11MW

A factor is added to the total capital cost for the cost of the linac tunnel and buildings.

The cost model is implemented in a spreadsheet. For a particular choice of beam current, beam energy and energy gradient in the CCL the total power requirements are calculated along with their cost over a chosen lifetime of the machine. Also calculated is the total capital cost of the machine. These are combined to give the total costs over the lifetime. The costs of the target systems, decommissioning and the cost of money are not included in the calculation at this stage of our studies.

This process is repeated for different accelerator energy gradients for each combination of current and energy to find the minimum cost for that combination. That such an optimum exists is demonstrated by writing the cost of a linear accelerator, C, as

$$C = C_F + C_L L + C_P P \qquad (1)$$

where C_F are fixed costs, C_L is cost of the structure per unit length, L is the length of the accelerator, C_P is the cost of power and P is the power required to operate the cavity. Since the power and length of the machines are related by

$$P = (E_o T)^2 \, L/ZT^2 \qquad (2)$$

where E_oT is the average electric field and also

$$\Delta W = E_oT\, L \cos\phi \qquad (3)$$

where ΔW is the energy gain over the length of the accelerator and ϕ is the synchronous phase. Hence we obtain

$$P = \frac{\Delta W^2}{(ZT^2)\, L \cos^2\phi} \qquad (4)$$

ie. the cavity power is inversely proportional to the length of the machine. Thus from equation (1) it can been seen that there is an optimum length and so an optimum energy gradient.

The cost model, using simple equations such as these above, is used to calculate the accelerator power, length, capital and operating costs for 50, 100, 150 and 200mA beams at energies of 100, 200, 300, 400 and 500MeV finding the optimum energy gradient for each combination.

COST OPTIMISATION FOR A ROOM TEMPERATURE MACHINE

An example of the cost optimisation for a 50mA, 400MeV accelerator is shown below in Table 2.

Table 2. Cost Optimisation of A 50mA, 400MeV Accelerator

	Energy Gradient (MV/m)	Total Linac Length (m)	Total AC Power (MW)	Linac Capital Cost (£M)	10-Year Cost (£M)	40-Year Cost (£M)
Capital Optimum	2.38	344	121	181	644	2034
10-Year Optimum	1.25	529	101	202	603	1807
40-Year Optimum	0.70	833	91	265	636	1749

The table shows three cases: firstly where the capital costs are optimised, secondly where the capital plus ten years running costs are optimised and thirdly where capital plus forty years costs are optimised. As the lifetime of the accelerator increases the energy gradient (E_oT) and the length increase whilst the power decreases. This is a direct consequence of the increasing dominance of the power costs for the accelerator over its lifetime. It is worth pointing out that the lowest cost machines also appear to be those of lowest technical risk ie. low Kilpatrick factor.

Turning now to the case of a constant neutron yield, Figure 5 shows the total ten and forty years costs as a function of beam current for two neutron yields (the second being three times the first). In this case the energy gradient is fixed at 1MeV/m. For both neutron yields there appears to be optimum beam current corresponding to minimum cost.

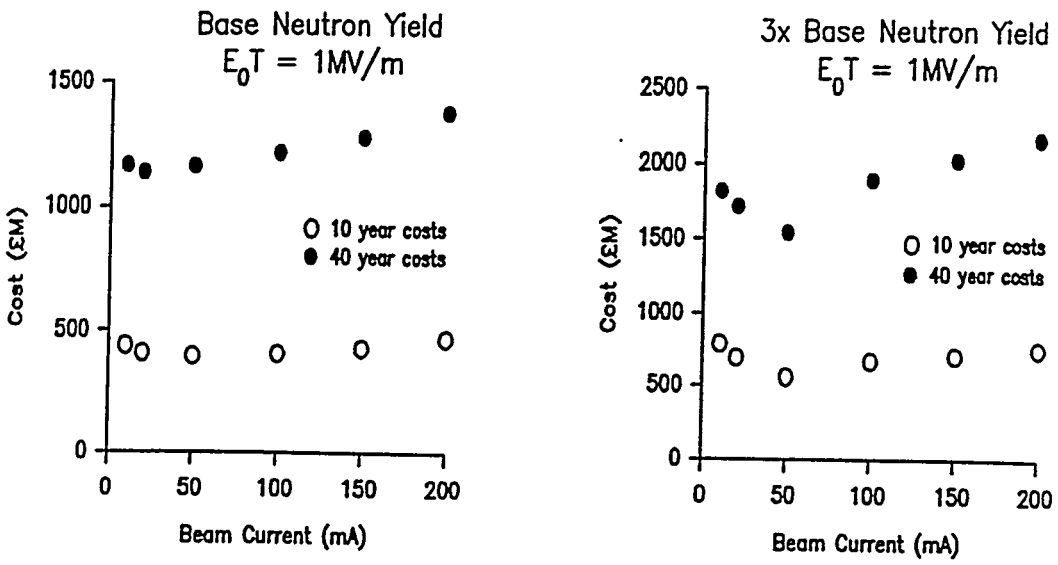

Fig. 5. Accelerator costs for a constant neutron yield and energy gradient

The results of optimisation including free choice of the energy gradient are shown in Figure 6. The beam energy, accelerator length, accelerator power and a relative unit cost over forty years, ie. £/neutron, are plotted against beam current. Here there is no minimum. The cost increases monotonically with the beam current. It is preferable to work at the lowest current and highest energy. This is due to the behaviour of the neutron yield with energy - the number of neutrons per sec per incident Watt of beam power is higher at higher energies than it is at lower energy.

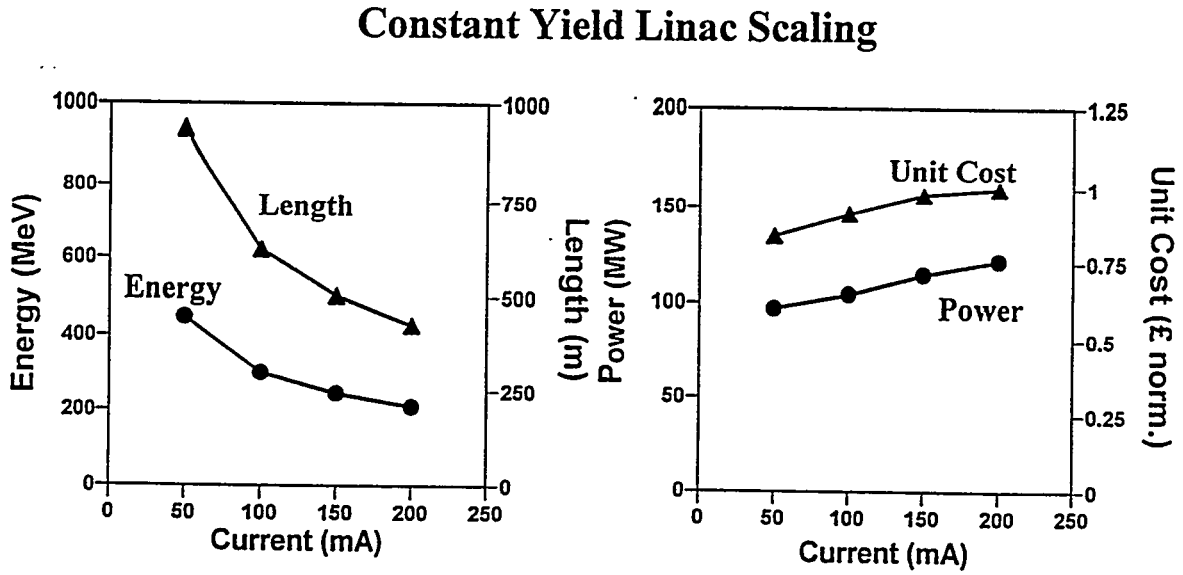

Fig. 6. Accelerator power, energy, length and relative unit cost (–£/neutron) for a constant neutron yield

Options for Cost Reduction

The costs over the lifetime are dominated by the annual power consumption and so means of reducing the electricity costs have been sought. Two methods have been identified.

The first option is to install a gas turbine generator on the site to provide the power required for its facility. The electricity costs over the lifetime are removed but this is balanced to some degree by the capital and running costs of the generator. Furthermore the generator can be available for up to 90% of the time whereas the accelerator may have an availability of 75%. The surplus electricity generated can be sold back to the utilities for additional income. For a 100MW power requirement this can lead to savings of ~ 45%. Furthermore, increasing the generation capacity beyond the power requirements can lead to increased income through electricity sales thus further reducing the costs.

A second option is to reduce the duty factor of the accelerator. Although the overall power requirements will increase for a fixed neutron yield the power consumed will reduce due to the decreased duty factor. This reduction in power must be compensated by an increase in accelerator energy and length. For the 100MW generator operating at 50% accelerator availability the forty year cost savings are ~ 55%.

Use of Superconducting Linear Accelerators

The power consumption in the accelerator which dominates the cost of the machine arises from the beam power and the power dissipated in the cavity walls. Although the beam power cannot be reduced the cavity power can be reduced to negligible levels through the use of superconducting accelerators.

The principle disadvantage of such accelerators is the present status of their development. A variety of superconducting linacs have accelerated electrons or heavy ions at low currents (less than a few mA) but their use at high currents such as that required for transmutation of material is untested. The work at Argonne National Laboratory [4] on a 355MHz cavity has concluded that gradients of ~7MeV/m are realisable at a power consumption of 20W with an extra 25% of length required for superconducting solenoids to focus the beam.

In superconducting accelerators loss of beam will not only lead to activation of the machine but may lead to quenching of the superconducting state. Furthermore availability may be affected due to the cool down/warm up times associated with maintenance and inspection of the accelerator.

In order to assess the implications for accelerator costs of superconductivity the following methodology is adopted

a) the superconducting accelerator begins after the RFQ
b) the accelerating gradient is 7MeV/m
c) cavity power loses are those as given by studies at ANL (~ 2.9W/MeV)
d) commercial helium liquefiers are used
e) cost of manufacturing the niobium coated copper linac structure is twice that of a room temperature structure.

The liquid helium plants for cooling the machine can be commercial units such as those used at the JET project at Culham. The specifications are given in Table 3 below.

Table 3. Helium Liquefier Specification

Cooling Capacity (W)	
Accelerator	270
Pipework	130
Total	400
Capital Cost (£M)	
Liquid He Plant	1.1
Liquid N_2 Plant	0.25
Electricity Usage	250kW
Maintenance Costs	£40k/yr

This data was used in the cost model for the case where there is a gas turbine generator with capacity in excess of that required by the facility. Table 4 shows the benefits to be gained in using superconducting technology for a 50mA, 320MeV accelerator.

Table 4. Parameter Ratios For Superconducting/Room Temperature Accelerator

Length	15%
AC Power	44%
Capital Costs	47%
Running Costs/Year	81%
40 Year Cost	59%

There are no proposals or designs for high current superconducting linear accelerators at present due to the lack of development of the technology. However, the potential benefits for future machines are clear subject to the solution of the problems associated with the use of superconducting technology in these high power accelerators.

THE SEPARATED ORBIT CYCLOTRON

So far it has been demonstrated that the costs of linear accelerators are high; the costs being driven by power usage over there lifetime such linacs are also large. A cyclotron is compact and makes efficient use of the cavities and so would seem to offer potential for overall cost reduction. The problem is that to date the comments available from cyclotrons have been limited at most to ~ 1-1.5mA [5]. However the Separated Orbit Cyclotron (SOC) appears capable of transporting much higher currents.

Figure 7 shows a schematic of an SOC. The machine consists of a number of sector magnets with rf cavities between them. There are radial gradients in the magnetic sectors (a FODO lattice is shown although it could be more complex) to provide strong focusing. It is this strong focusing that permits the transport of high current beams. Thus the SOC resembles a rolled up linac but since the same cavities are used many times as the beam follows its spiral path it is highly power efficient. The turn separation in an SOC can be made to be a constant, whereas in a conventional cyclotron the turn separation decreases with increasing radius. This feature not only aids injection and extraction, but allows a large bore size to beam size ratio to

be maintained thus reducing activation. In order to maintain a constant orbit separation, the energy gain per turn must increase with increasing energy and radius. The velocity of the particles increases to keep them in phase with the accelerating voltage.

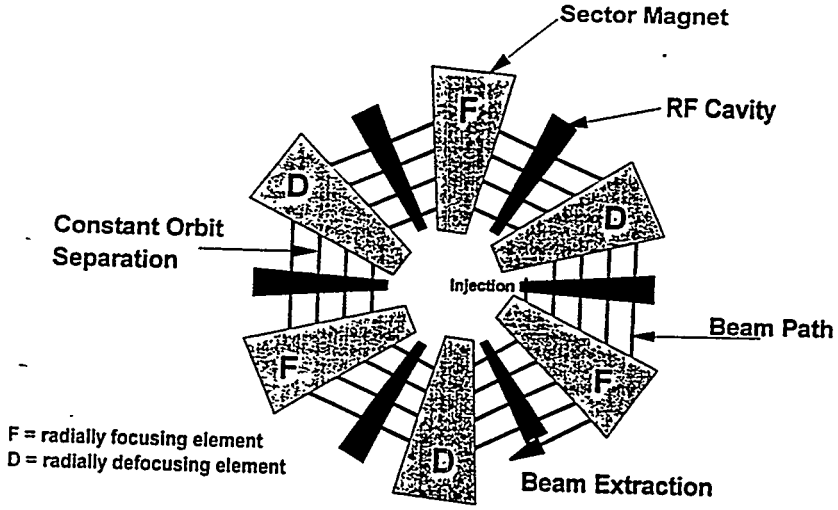

Fig. 7. The Separated Orbit Cyclotron

A 65mA, 1GeV three stage SOC was proposed in the mid-sixties at AECL in Canada [6] although no detailed evidence was presented to verify that the machine could transport such a current. A lower energy lower current (5μA, 43MeV) machine with superconducting magnets and cavities is being built in Munich [7]. Thus, as well as determining the potential cost reductions associated with an SOC, it is important to understand just what the current limits are for such a machine.

Due to the similarity between the SOC and the linac, the model by Wangler [4] for the current limits in a linac can be applied. This has been done for the case of the FODO lattice shown in Figure 7. The dependence of the transverse current limit, I_t , on the machine parameters is given by

$$I_t \propto \beta\, a^2\, B^2\, \Lambda^2\, H^2 \qquad (5)$$

where β is the relativistic factor, a is the beam radius, B is the magnetic field on the equilibrium orbit and Λ is the filling factor which is the fraction of the orbit occupied by the focusing elements and H is the number of focusing periods.

Usually in a linac the longitudinal current limit is far greater than the transverse limit but for the cyclotron consideration must be given to it. This is because the average accelerating field tends to be much greater in the linac. The longitudinal current, I_l , has the following dependence on the machine parameters

$$I_l \propto \beta\, \Delta r\, a\, B^2\, \Lambda^2\, H^2 \qquad (6)$$

where Δr is the orbit separation.

In Figure 8 the transverse current limit is plotted as a function of the number of focusing sectors for an injection energy of 20MeV, a B-field of 1.64T, a beam radius of 2.0mm, a filling factor of 0.55 and an orbit separation of 6cm.

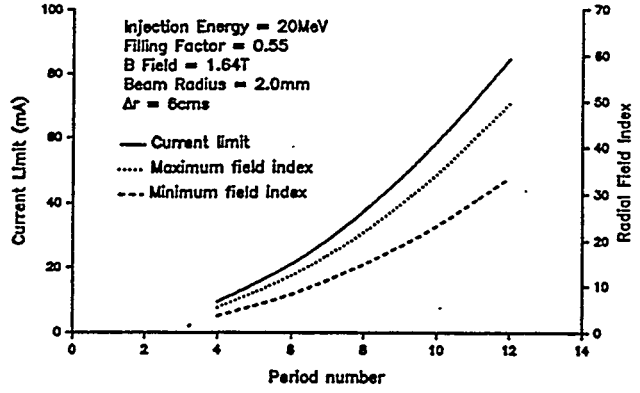

Fig. 8. The tranverse current limit in an SOC and the maximum and minimum radial field indices

From the diagram it can be seen that a current of ~ 80mA can be obtained. In practice the current used might be a fraction of that calculated in this way. Further optimisation of the parameters can lead to higher currents. Obviously, detailed beam dynamics calculations will be needed to verify the current limit. Also from Wangler's model the upper and lower limits to the radial field indices in the focusing channels can be calculated. This is based on the limits of the zero current phase advance, σ_o, where in order to limit emittance growth there is the requirement that $\sigma_o < \pi/2$ [4]. For the case above the longitudinal current limit is ~ 1A.

ACKNOWLEDGMENTS

The authors would like to thank Dr. George Lawrence and the Los Alamos team for some costing details and many helpful discussions.

REFERENCES

[1] Nakamura, T., et al, *Atomic Data and Nuclear Data Tables* 32, 471-501 (1985)

[2] Carpenter, J.M., *Nuc. Instr. Methods* 145, 91-114 (1977)

[3] Lawrence, G.A., *Nuc. Instr. Methods* B56/57, 1000-1004 (1991)

[4] Wangler, T.P., Space Charge Limits in Linear Accelerators, *Los Alamos Report* LA-8388 (1980)

[5] Schryber, U., Upgrading the PSI Accelerator Facility for High Intensity Operation, in *Proceedings of the Third European Particle Accelerator Conference*, 1992, pp. 173-177.

[6] Bartholomew, G.A., and Tunicliffe, P.R. The AECL Study for an Intense Neutron Generator, *AECL Report* 2600 (1966)

[7] Trinks, U., Assman, W., and Hinderer, G., *Nuc. Instr. Methods* A244, 273-282 (1986)

High Current Induction Linacs

William Barletta, Andris Faltens, Enrique Henestroza, and Edward Lee
Accelerator and Fusion Research and EngineeringDivisions
Lawrence Berkeley Laboratory
Berkeley, CA 94720

OVERVIEW

Induction linacs are among the most powerful accelerators in existence. They have accelerated electron bunches of several kiloamperes, and are being investigated as drivers for heavy ion driven inertial confinement fusion (HIF), which requires peak beam currents of kiloamperes and average beam powers of some tens of megawatts. The requirement for waste transmutation with an 800 MeV proton or deuteron beam with an average current of 50 mA and an average power of 40 MW lies midway between the electron machines and the heavy ion machines in overall difficulty. Much of the technology and understanding of beam physics carries over from the previous machines to the new requirements. The induction linac allows use of a very large beam aperture, which may turn out to be crucial to reducing beam loss and machine activation from the beam halo. The major issues addressed here are transport of high intensity beams, availability of sources, efficiency of acceleration, and the state of the needed technology for the waste treatment application.

Because of the transformer-like action of an induction core and the accompanying magnetizing current, induction linacs make the most economic sense and have the highest efficiencies with large beam currents. Based on present understanding of beam transport limits, induction core magnetizing current requirements, and pulse modulators, the efficiencies could be very high. The study of beam transport at high intensities has been the major activity of the HIF community. Beam transport and sources are limiting at low energies but are not significant constraints at the higher energies. As will be shown, the proton beams will be space-charge-dominated, for which the emittance has only a minor effect on the overall beam diameter but does determine the density falloff at the beam edge.

BEAM TRANSPORT

The equation of motion for the beam envelope in a focusing channel is

$$\frac{d^2a}{dz^2} = K(z)\,a + \frac{\varepsilon^2}{a^3} + \frac{Q}{a} \qquad (1)$$

where a is the beam radius, Ka is the focusing force as a function of the longitudinal coordinate, z, ε is the beam emittance, and Q is the perveance, a measure of space charge. By comparing the space charge term with the emittance term, we can solve for the radius at which the two types of forces would be equal. Based on beams for heating of magnetic

fusion energy plasmas, we assume a 100 ampere proton source of 25 cm radius with a temperature of 10 eV, for which, at 1 MeV,

$$a_e = \sqrt{\frac{\varepsilon^2}{Q}} \cong 4 \times 10^{-3}\,(m) \qquad (2)$$

Beams which are transported with radius small compared to a_e are emittance dominated, and beams which are large compared to a_e are space charge dominated. Beams considered here will be transported at large radius with modest fields, and thus are space charge dominated. There is little incentive to make the aperture smaller by using higher fields, and considerable difficulty in providing strong-enough fields which would make the beams emittance dominated. The solutions to the transport equation for our purposes are

$$I_s = 4 \times 10^5 \left(\frac{q}{A}\right) \beta\gamma (Ba)^2 \qquad (3)$$

$$I_q = 8 \times 10^5 (\beta\gamma)^2 (\eta Ba) \qquad (4)$$

The subscript s refers to solenoidal focusing, and the subscript q refers to quadrupole focusing with an effective field occupancy η. B is the magnetic field, and β, and γ are the relativistic factors. These results are shown graphically in Figure1.

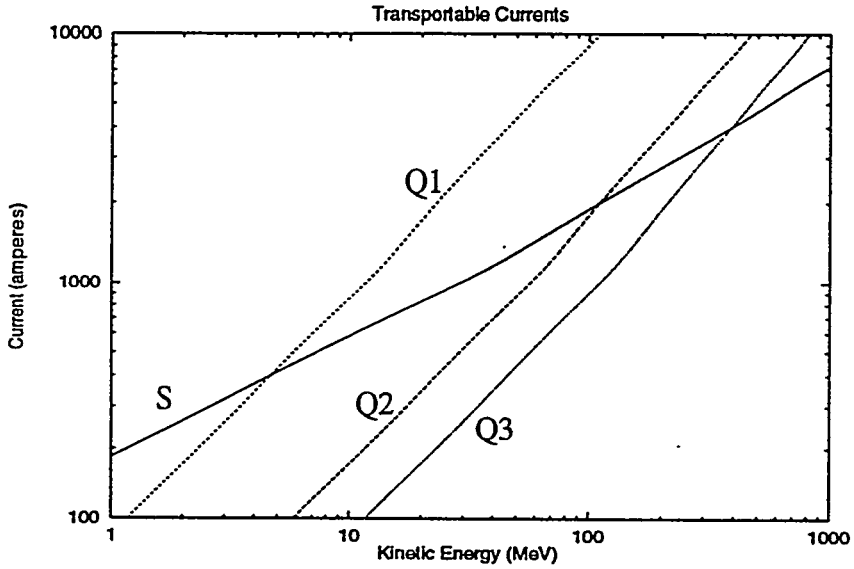

Fig. 1. Transportable proton currents for various solenoidal and quadrupole channels. For solenoids, B=1T, and for quadrupoles the field at the edge of the beam is 1T. 'S' denotes a solenoid channel with a=10cm; 'Q1' a quadrupole channel with a=10cm, η=0.5; Q2 a quadrupole channel with a=10cm and η=0.1; and Q3 a quadrupole channel with a=5cm and η=0.1.

Transverse focusing gives an upper bound to the beam current. There is a technological limit on attainable magnetic fields of about 10 Tesla and on practical occupancy of about 60% in a FODO lattice. The cost optimum lattices are sparse, with an occupancy close to 10% and fields close to 1Tesla. Beyond an energy of 100 MeV, focusing ceases to be a major constraint. Longitudinal focusing is mainly a balancing of the bunch field against some externally applied field ramps. It is uneconomical to devote most of the "effort" to just keeping the bunch together, so we choose a bunch shape which requires the focusing field to be small compared to the acceleration field. Longitudinally, the bunch can be thought of as undergoing an oscillation at the reduced plasma frequency where the focusing fields reverse the motion incurred by the beam space charge. Using the well-known approximation that a parabolic bunch maintains its parabolic shape from 1-D space charge expansion and that the fields are linear with z, the longitudinally defocusing space charge fields would be counteracted with occasional ramped focusing fields placed along the accelerator. For a long bunch with rounded ends, a pair of "ears" at the bunch ends, one positive and one negative, is sufficient.

For a space charge dominated beam, transported in a solenoid or quadrupole focused channel, the beam density is nearly uniform within the interior. The density at the edge decays abruptly as $\exp(-d/\lambda_D)$ with the characteristic decay distance,

$$\lambda_D = \frac{v_{th}}{\omega_p}. \qquad (5)$$

The beam size is 2.6 cm in radius with a decay distance, λ_D, of 2.6 mm for a 1 kA deuteron beam focused with 1T fields at an energy of 400 MeV, which is a midway point in the energy of the accelerator. To this we add an amount corresponding to the beam misalignment oscillation resulting from 500 quadrupoles each with an rms error of 0.1 mm in either plane, $\Delta x=\Delta y= 9$ mm. Another small contribution to the required aperture is the initial mismatch of the beam. As for the other errors originating at low energy, its effect decreases with distance along the machine. There is a small amount of scattering from the background gas which we neglect here. Taking all of these effects together, we expect a beam halo of about one cm. The standard prescription used for HIF for intense beams is that the clearance should be 1.25a +1 cm, which corresponds to a clearance of about 2 cm here, which is just adequate. There is an image effect which leads to emittance growth of the beam for closer approaches.

Beam Instabilities

The possibility of transverse and longitudinal instabilities must be considered for the transport and acceleration of any intense beam. Both the transverse and longitudinal instabilities are stabilized by a momentum spread in the beam and driven by resistance in the beam coupling impedances. On both accounts, the waste treatment accelerator is in a favorable situation. Because there is no stringent focusing requirement at the end of the accelerator, there is no significant constraint on the allowable momentum spread. Similarly, there is no need to bend the beams within the accelerator or afterwards. Starting with a monoenergetic beam, which is unstable, it is probably acceptable to let any instability grow and create its own stabilizing momentum

spread. The worst case scenario is stabilized with less than 10% momentum spread, which is transportable by the focusing channel.

The growth rates depend on the beam space charge intensity and the resistive part of the pulser or generator impedance. For the standard PFN and closing switch only type of pulser, the generator impedance is just the characteristic impedance of the PFN, which is roughly the voltage gain per meter divided by the beam current for a matched system. For the capacitor plus controllable switch circuit, the coupling impedance is very low. A pulser with a truly regulated output voltage, of course, would have no resistive impedance.

MACHINE DESIGN

The induction linac accelerates a single bunch of ions, whether deuterons or protons, which contains a fixed total amount of charge. The free variable is the repetition rate. To attain the desired average current of 50 mA, the rep rate could be 50 pps with a bunch charge of 1 mC, or 500 pps with 100 μC. Given the total charge within the bunch, we may also choose how it is to be accelerated, that is, at some point along the accelerator, we may choose the pulse duration, acceleration rate, and beam radius. Starting with a 100 A proton source, and using simple acceleration scenarios, the 50 pps machine would be 1664 m long and use a maximum induction core buildup of 40 cm, the 500 pps machine would be half as long and require a maximum core buildup of 13 cm, thus there is a major incentive to use the highest rep rate technologically possible. The minimum core inner radius would be about 12 cm at the low energy end, decreasing to about 7 cm at the high energy end. The maximum diameter of these machines would be 1m and 0.5 m respectively. The number of variables is large enough that for the HIF accelerators this selection process has been computerized in the two design programs LIACEP and HILDA. For each set of design choices, these programs calculate the incremental cost of acceleration, and choose the lowest cost design. The entire machine is the sum of these local design optima. In practice, we expect a slow and smooth variation in the character of the machine along its length. The principal beam dynamics activity is to ensure that the bunch is kept together with longitudinally focusing "ears" which overcome the repulsive effects of the space charge, and that a small amount of tilt is provided on the accelerating waveforms if it is desired to lengthen or shorten the bunch length downstream. The major increase in bunch current arises from the increase in velocity, so the bunch length control is a minor adjustment, provided that the bunch is short compared to the machine length.

The results of such a computerized design are shown in Figures 3-7, which display some of the trends along the accelerator. As it is presently set up, this program considers only high field superconducting magnets, which are the correct choice for heavy ions for energy production, and pulsed quadrupoles for machines designed for essentially single pulse operation. As seen in Fig.1, for the much lighter protons conventional magnets operating at the 1 T level are adequate, and lead to a smaller overall package, but we do not yet have an algorithm for such magnets in the code. Nevertheless, we show the general trends of decreasing bore size and increasing half-periods which result in reduced cost for the available magnet types in the programs. Because of the premium attached to reducing beam loss, the beam aperture was increased to 20 cm for these

cases, that is a clearance of about 10 cm instead of the minimum 2cm, which shows the realizability of the large clearance options.

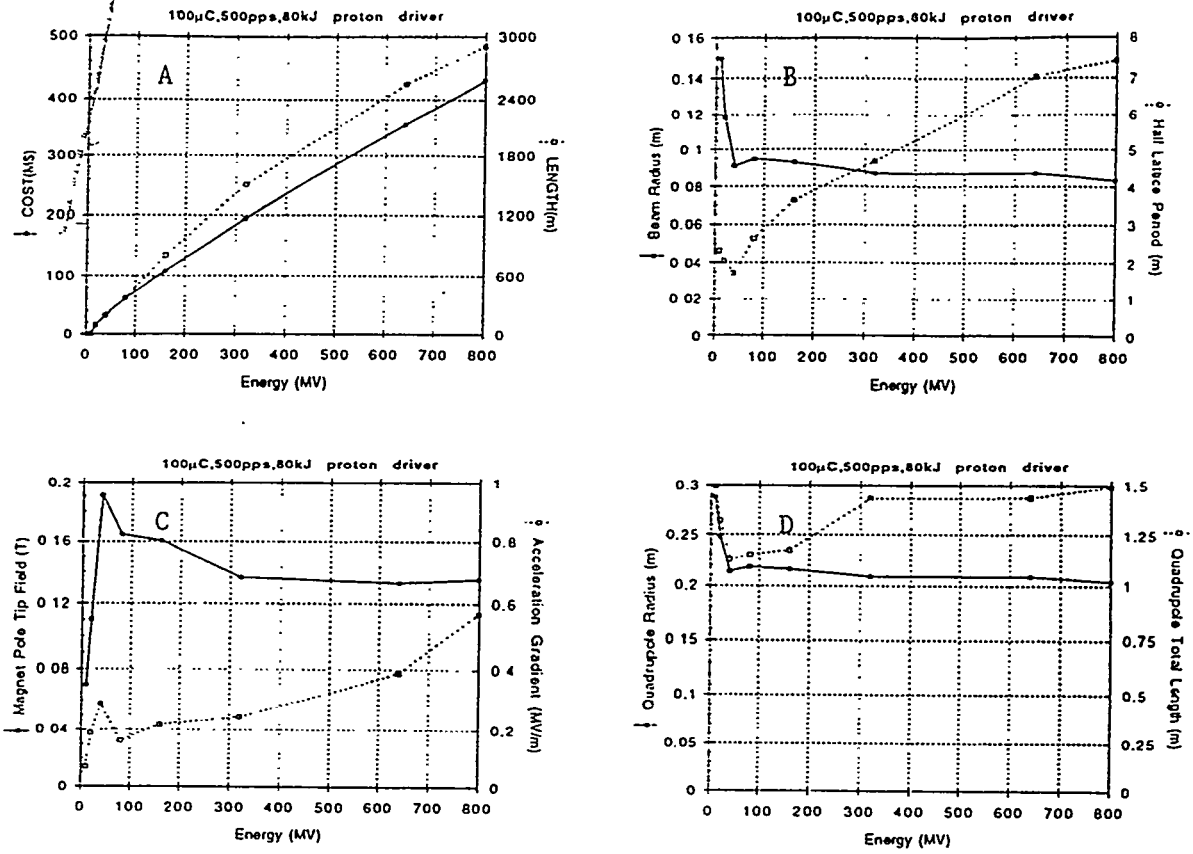

Fig. 2. Example of minimum cost machine designed with an imposed 10 cm clearance between the beam and the vacuum chamber. Panel A shows the cost and length as almost linear functions of energy; panel B shows the decrease of beam radius and increase of half-period with energy; panel C shows the quadrupole field and acceleration rates; and panel D shows the quadrupole radius and length.

The use of magnetic quadrupoles at low energies is inconvenient because of the required short half-periods. A continuous solenoid (or a solenoid with short breaks in it which are required for the acceleration gaps) at low energies can transport a current which is higher than can be transported in a similar strength quadrupole, therefore the first 10 MeV of the machine uses solenoidal transport of a beam of 10cm radius. After that, the beam radius can be gradually decreased. Figure 1 shows the beam transport limits for protons as a function of the particle energy for the continuous solenoid and the alternating gradient quadrupole systems. The corresponding currents for deuteron acceleration are roughly 0.35 times as great in the solenoidal section and 0.5 times as great in the quadrupole transport section. From these curves, it is evident that beam transport ceases to be a major concern past the 100 MeV point. The low-energy limit is not a major hindrance because it is desirable to maintain a low acceleration rate at the beginning of the machine. With a low acceleration rate, relatively less space is required for the acceleration gaps, and more can be devoted to the focusing elements. The low initial acceleration rate is desired for beam transport reasons. It is possible to accelerate at such a high rate that the energy

of the particles passing one location varies by a factor of several, that is, from the front of the bunch to the rear, with the result that a system matched for one energy and current is not well suited for the other. To keep the bunch within reasonable transport limits, we use the criterion that at any one location the energy at the rear of the bunch should be no higher than twice the energy which the front of the bunch had when it passed that location. This corresponds to a doubling of the energy in a distance equal to the bunch length, up to the point where high field or economics limits make this prescription undesirable. Past this point, the acceleration proceeds at a constant rate of 1 MeV/m, which is believed to be the technological limit.

Besides the usual beam transport considerations given above, there are at least two additional ones: whether the energy in the beam pulse may be so high that the machine is damaged by the beam in case of a fault; and whether the beam loss along the machine is sufficiently serious to lead to activation of the accelerator and a subsequent imposed lowering of the operating current. Our work on the HIF beams has shown that an intense beam must be kept within approximately 80% of the aperture, otherwise the nonlinearities associated with the beam image fields lead to emittance growth and beam loss. In addition, we have found that an off center beam is much more susceptible to emittance growth than a centered beam. For these reasons, for the waste disposal application, we have examined cases where the clearance is greatly increased. The induction linac differs from the rf linacs in that there is no significant penalty in the beam dynamics if the bore diameter is made very large. The induction linac could be thought of as a very-low-frequency rf system which is very tightly coupled to the cavity. The electric field distribution across the accelerating gap during the flat portion of the pulse is exactly the same as for a dc gap, and the energy gained by a particle crossing it is just the applied voltage, independent of the transverse dimension of the beam pipe. There actually is a vestige of a low frequency resonance in the induction modules, at a frequency around 1 MHz, but this is greatly swamped by the drive pulse circuitry. That is, the impedance of the induction module is much higher than the impedance of the generator or pulser that is connected across the module, so that the beam interacts with the pulser impedance, and we can neglect the resonant contribution.

Pulsers

The pulser is perhaps the most important component of an induction linac; besides its interaction with the beam it also largely determines the overall machine design.There are two major types of pulse generators in use: the line-type and the controllable switch type. In the line-type modulator a lumped or distributed element pulse forming line is discharged into the load, with the discharge initiated by a closing switch. The usual switch is a thyratron gas tube. The thyratron utilizes a low pressure plasma discharge and remains conducting until the plasma has recombined, which may require some tens of microseconds. The controllable switch type of pulser has the additional capability to be turned off, and in some cases to also regulate the output voltage. The usual controllable switches are hard tubes or transistor arrays. Because of the unfavorable economics or the technical limitations of some of these primary switches, it is also possible to use a magnetic pulse compression line (the Melville line) to increase the output power considerably above that available from the primary switch. Even in the magnetic compression line a single stage is usually limited in its performance by available magnetic materials and insulation, and it has been found preferable to use several stages, each of which handles the entire pulse energy in turn. This adds to the overall cost of the modulator and reduces its effi-

ciency. The ideal switch that can simultaneously handle the pulse energy, regulate the output voltage, present a low generator output impedance, and have a low cost does not exist now. A device which approximates some of these desirable characteristics and which has been declining in cost is the field effect transistor (FET) array. Because of the eventual promise of FETs, we have been making measurements on an FET-driven induction core. Similar and related work is ongoing at LLNL and at FM Technologies.

For the LBL HIF application, the most probable first use of FETs will be in providing small corrections, of the order of 1%, to the main acceleration voltages. The combination of a very high power but economical pulser with a controllable trimmer results in an overall package which has the best features of each constituent. Related developments at LLNL and FM Technologies center on pulsers that are capable at pulsing at several hundred kHz for use in induction accelerator recirculators. The FET pulser at LBL was designed and constructed by American Controls Engineering in San Diego, Ca. The pulser's nominal specifications are an operating voltage of 12 kV and a peak current of 1.5kA. The measured 10-90% risetime and falltime are 150ns and 100ns respectively. The pulser was initially intended to demonstrate burst mode operation at the 100 kHz rate with 1 μs pulses. It is also well suited to demonstrate the possible performance of induction linacs for other applications, such as the present one. In some respects, the output pulse is similar to that which can be obtained from a thyratron pulser, but using different means.

The circuit used to obtain the pulses shown in Fig.3 is very simple: a large capacitor and the FET array. The capacitor is large enough so that its voltage appears almost constant during the pulse; actually, there is a 1% droop during the pulse due to the charge removed from it. The charge to the capacitor is restored during the interval between pulses, at high efficiency, from a dc power supply which is isolated from the capacitor with a small resistor. The induction cores used in these tests were of several types, principally 50%Ni-50%Fe of 25 μm thickness and Metglas type 2506 SC of 30 μm thickness. These cores behave similarly and have essentially square loop character at low frequencies, which allows them to retain a remanent magnetization close to the saturation magnetization value. A dc bias current of 30 amperes was used to reset the cores to the negative remanent value. At constant current near the minimum required to saturate the outermost laminations of the core, the reset would occur in about 50 μs after the pulse, and of course faster with a higher current. A large choke of 2.5 mHy inductance was used in series with the dc current supply to isolate it from the high voltage pulses applied to the core

During the pulse, the dc level in the choke current changes abruptly by a few amperes. In addition, there is excitation of higher order mode oscillations in the choke. These processes contribute a very small amount to the losses of the system and to the top of the voltage waveform. The spurious oscillations die out in tens of μs, well before the next pulse. A resistive load was placed across the core to simulate a beam load. The load current could be increased above that shown with a small decrease in the pulse flatness. As shown, the "beam" current corresponds to roughly the middle of a long pulse /low rep rate machine. The nominal efficiency for this point is 50%, with points upstream being slightly lower in efficiency and points downstream being higher in efficiently. Efficiency is the power going into the "beam" divided by the dc power supply input; during the pulse the "beam"current is about twice the core current. The core magnetizing current shown during the pulse is not the minimum possible. Core excitation current can be related to various processes involving domain nucleation and domain wall movements. The

macroscopic result of these is that the drive current can be decreased by using a larger core and reducing the flux swing within it. The drive current is also decreased by avoiding hard saturation in either direction. As shown, about half of the possible flux swing is being utilized. In the design of an induction linac for efficiency instead of for lowest capital cost, it is also advantageous to obtain the required core cross sectional area by using as much axial distance and as little radial distance as possible, to arrive at a smaller core volume. Two good approximations are that the core losses are proportional to the core volume, and that the average drive current is proportional to the average core radius, for a fixed voltage and pulse duration. Improved efficiency comes at the increased cost of the beam transport for the longer accelerator, and the increased cost of the core material for the underutilized flux swing.

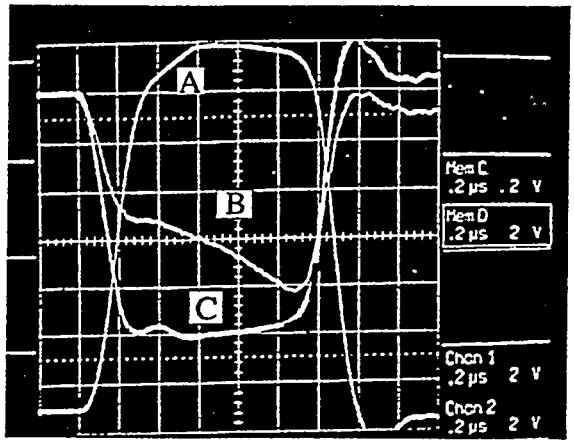

Fig. 3. Waveforms of the FET pulser driving an induction core at 72 pulses per second. A is the load (simulated beam) current (100A/division), B is the core current (80A/division), and C is the output voltage (2kV/division). Horizontal sweep is 200ns/division.

This pulser was operated at 72 pps intermittently for 25 million pulses during exploratory testing and at 100 pps around the clock for a total of 200 million pulses for a life and reliability test of the pulser and core assembly. It was also operated at 200 pps for brief periods. The core was convection cooled with ambient air in these tests. Higher repetition rates require the core package to be re-engineered for better cooling, and such an effort is presently underway.

Sources

High current long pulse sources have already been developed for heating of magnetic fusion energy plasmas. The available species include protons, deuterons, and H^-. The particular sources which are well matched to the front end of an induction linac produced 100 amps of protons at 120 kV and an equivalent deuteron current of 70 amps. The sources were developed in the 1970's and were used reliably for several years in TFTR and Doublet IIID. These sources used a large plasma chamber and an extraction surface made of sturdy, water cooled grid bars with typical dimension of 0.5 cm diameter with a separation of about 1 cm. The output beams went through an accel-decel region composed of similar grids. The grids were aligned to decrease beam loss. A typical source had dimensions of 12 cmx48 cm. For the induction linac using such a gridded source the geometry would need to be reconfigured toward a more circular

shape, and the emerging ribbon beams would be allowed to merge into one big beam of circular cross section, and accelerated to higher voltages. The emittance increase due to this process is reasonably well understood, and continues to be addressed by the HIF program. The major developmental task for the future is to work on a system which would produce faster risetimes on the injector pulse, either by longitudinal switching of the beam or by transverse deflections.

A considerable amount of hardware remains from the Magnetic Fusion neutral beam program from the previous two decades which could be modified for short pulse operation. It would be relatively inexpensive to look at the high current-short pulse operation while the knowledgable personnel and hardware are still available.

Needed Developments

In addition to the source development described above, work is needed on low cost induction cores and better switches. The metallic glass induction core material cost has declined dramatically in the past decade, to about $3/kg. The cost of annealing and insulating the material has not decreased as much, and some development is needed to arrive at a satisfactory solution. In the much more mature silicon steel and nickel iron induction core manufacturing processes the insulation is adequate and takes up negligible space. These are baked-on inorganic coatings which survive the annealing temperatures. For the newer metallic glass induction cores, several types of insulation have been tried, some of which survive the annealing temperatures but have relatively low voltage holding, and others which have very high voltage holding but do not tolerate the annealing temperature. The metallic glasses themselves can not tolerate the temperatures used on the previous silicon steel insulation processes. Several techniques have been suggested but there has not been sufficient investment in the field to follow through.

SUMMARY

The induction linac is used in a few applications which require very high peak currents, such as flash X-ray radiography and heavy-ion fusion. It has been considered for food irradiation, collective acceleration, free-electron laser drivers, and similar applications. The peak currents which have been accelerated have been in the vicinity of 10 kA. The particle used in these applications usually has been the electron. As far as the acceleration process is concerned, it doesn't matter what the particle is. The beam simply is a current source to the acceleration modules. The energy gained by the beam is the result of the drive voltage applied to the module minus the beam generated voltage. Electrically, the induction accelerator functions as a transformer which applies power to a particle beam without the intervening step of going through a radio frequency system. The induction module can be thought of as the equivalent of an rf cavity, but one which is so heavily coupled to the drive circuitry that the cavity is non-resonant. The drive circuitry is some kind of modulator, such as a pulse-forming line or a controllable switch with a capacitor bank. The difference between the two types of accelerators is partly in the power conversion train: the induction linac does not require the step between a modulator and the acceleration cavity, that is, the rf generation; on the other hand, the drive power required by the induction module to establish the acceleration fields is considerable, so the efficiency is high only for high beam currents. While clearly suited for the high peak power applications for which induction

linacs were originally built, they may also be well suited for some high average power applications. This is the subject of this present paper. The high average power is basically a quest for higher average current, since generally the output particle kinetic energy is specified. In some applications it is the upper energy which is limited, and even in these cases it may be desirable to use the highest energies because it is usually easier to increase energy by further acceleration rather than by increased current.The two main ways by which the average current may be increased are by increasing the pulse duration and by increasing the repetition rate. There is a maximum pulse duration which is related to subsequent downstream bunch dynamics, and a maximum rep rate which is related to present day technology. Another, less frequently used technique for increasing the average current is the use of multiple beams: this technique works best where the costs of the induction core and pulsers are dominant and the required core is very large. In this case, the central bore may be enlarged to carry several parallel beams with only a relatively small fractional increase in the core outer diameter and the attendant costs. In some instances, as the core inner diameter is increased to accommodate the multiple beams, the core outer diameter shrinks, because the increased current carrying capacity of the parallel transport channels allows the use of a much shorter pulse duration, which in turn requires the smaller core cross-sectional area. This last option has not been examined for the present application.

The development of a high current proton or deuteron induction linac, after the initial parameter selection for the overall configuration, becomes the development of a few representative modules for several locations along the machine. This is essentially a low cost process which answers most of the technical questions.

ACKNOWLEDGEMENTS

The authors are indebted for the indispensable help provided by Peter Seidl in the preparation of this manuscript and for valuable discussions.

Potential of Cyclotron based Accelerators for Energy Production and Transmutation

Th. Stammbach, S. Adam, H.R. Fitze, W. Joho and U. Schryber
Accelerator Division, Paul Scherrer Institute
CH-5234 Villigen-PSI, Switzerland

Abstract. PSI operates a 590 MeV-cyclotron facility for high intensity proton beams for the production of intense beams of pions and muons. The facility, commissioned in 1974, has been partially upgraded and is now operated routinely at a beam current of 1 mA, which corresponds to a beam power of 0.6 MW. At this current, the beam losses in the cyclotron are about 0.02%. By the end of 1995 we expect to have 1.5 mA of protons. Extensive theoretical investigations on beam current limitations in isochronous cyclotrons were undertaken. They show that the longitudinal space charge effects dominate.
Based on our experience we present a preliminary design of a cyclotron scheme that could produce a 10 MW beam as a driver for an "energy amplifier" as proposed by C. Rubbia and his collaborators. The expected efficiency for the conversion of AC into beam power would be about 50% (for the RF-systems only). The beam losses in the cyclotron are expected to be a few μA, leading to a tolerable activation level.

Introduction

PSI operates a 590 MeV-cyclotron facility for high intensity proton beams for the production of intense beams of pions and muons. This ring cyclotron, commissioned in 1974, was originally designed for a current of 0.1 mA. Since then the cyclotron was subject to several upgrades and the facility is now successfully operated at routine currents near 1 mA with beam losses in the order of 0.02% . A spallation neutron source is presently under construction, requiring a beam current of 1.5 mA, corresponding to a beam power of 0.9 MW. We hope to achieve this goal in 1995. This current level will be close to the theoretical limit of the cyclotron, given by the effects of longitudinal space charge forces.

Based on our experience with the 1 mA beam we propose a cyclotron scheme for the acceleration of a 10 MW beam, worthwhile to be investigated in more details. Such a facility could be an economic solution to the "energy amplifier" as proposed by C. Rubbia and his collaborators [1], for future spallation neutron sources and eventually for transmutation. The specifications for such an accelerator facility would have to fulfil the following requirements:

- A high beam power of about 10 MW.
- efficient conversion of electric input power to beam power, to ensure an acceptable efficiency of the "energy amplifier".
- An accelerator scheme that allows continuous operation with lowest possible beam loss to avoid prohibitive activation of the accelerator.

Over the past 20 years extensive efforts were made toward a better understanding of the effects that limit the beam current in isochronous cyclotrons. These effects will be discussed in the following chapter with special emphasis on the PSI ring cyclotron.

The PSI-Cyclotrons

The PSI - accelerator complex is shown in fig. 1. The protons are accelerated in two isochronous cyclotrons to the fixed energy of 590 MeV with an intermediate stage at 72 MeV. Both cyclotrons are of the "ring"-design with separated magnets, leaving room in between for powerful RF-cavities. A third cyclotron, built by Philips (NL) for variable energy operation with a large variety of ions is mainly used for low energy experiments and applications and, during several weeks per year, for the injection of polarized protons (up to 12 μA) into the 590 MeV ring.

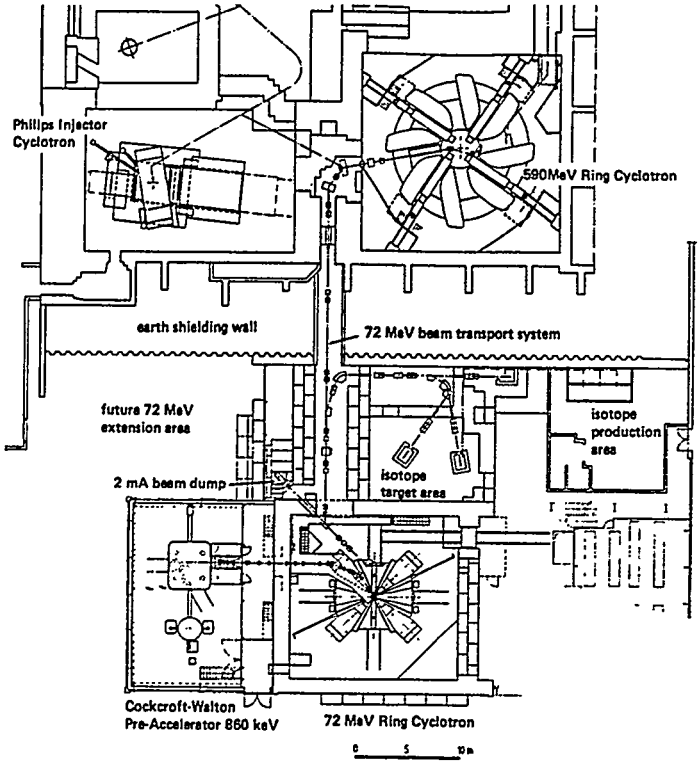

Fig. 1. Layout of the PSI cyclotron facility. The 590 MeV ring will deliver 1.5 mA of protons after completion of the upgrading program. The 72 MeV injector cyclotron (below) has produced 1.6 mA. The Philips cyclotron is occasionally used for the acceleration of polarized protons in the main ring.

The 590 MeV ring consists of 8 sector magnets, four large accelerating cavities for 50 MHz and one so called flattop-cavity for 150 MHz. It is specially designed for high beam currents. Main features are a good turn separation, so that the beam can be extracted with minimum beam losses. Two properties are important in this respect: The "flat-topping" and the high accelerating voltage. The flattop-principle means the flattening of the accelerating voltage by the superposition of a higher harmonic voltage to the fundamental accelerating voltage. This produces an almost constant acceleration voltage over a large phase range and provides a necessary condition for a constant turn number and a small energy spread. This method was for the first time demonstrated in a cyclotron at PSI in 1980 [2]. The second factor, the high accelerating voltage, reduces the turn number in the cyclotron which helps in two ways: It increases the turn separation which facilitates the extraction and it reduces the path length of the protons in the cyclotrons, an important factor to minimize the space charge effects. The RF-cavities provide a radially sinusoidal voltage distribution, with peak voltages of 730 kV in the 50 MHz-cavities and 420 kV in the flattop cavity. In 1995, after the completion of the upgrade of all four cavities [3] [4], this will result in an average energy gain

per turn of 2.4 MeV per revolution, corresponding to a total of 214 revolutions in the main ring. The extraction from the cyclotron is achieved by an electrostatic septum (thickness 50 μm) followed by a magnetic channel and a septum magnet. Around the first two elements radiation shields, made from concrete and marble, are installed. Fig. 2 shows the extraction losses in the ring versus beam current during 1994. The loss measurements were taken with ionization chambers located at strategic positions around the ring. It should be noted that the absolute calibration is difficult, with an uncertainty of about 30%.

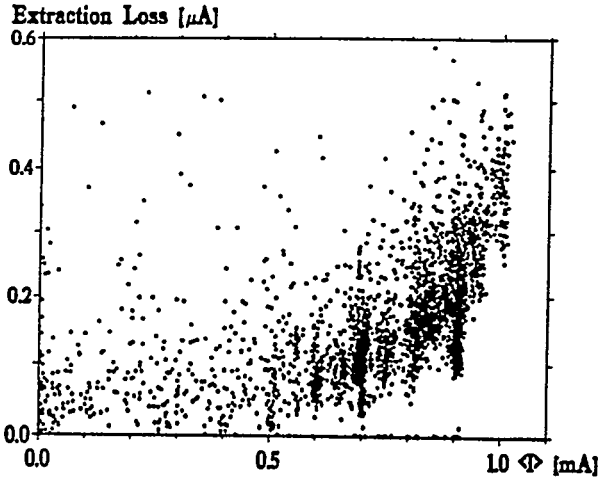

Fig. 2. Scatterplot of extraction losses vs. extracted beam intensity taken from the operation of the PSI 590 MeV ring during May and June 1994

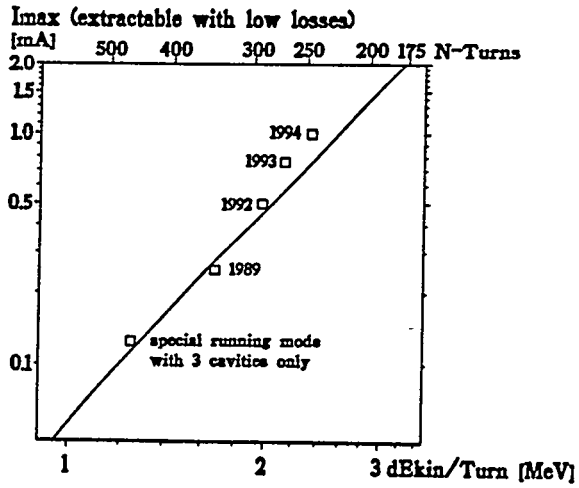

Fig. 3. The maximum intensity that can be extracted with low losses is proportional to $1/N^3$, N being the number of revolutions in the cyclotron. The datapoints are from the PSI 590 MeV ring, the line represents Joho's formula.

The injector 2 cyclotron has four sector magnets, two 50 MHz-resonators and two flattop cavities at 150 MHz. After about 100 revolutions a final energy of 72MeV is reached. The turn separations at injection and extraction are 80mm and 18mm respectively. The beam is extracted with an electrostatic septum followed by a septum magnet. Protons are injected at an energy of 870 keV from a Cockcroft-Walton type preaccelerator. A buncher is installed in the 870 keV beam line. The injector 2 has reached 1.6 mA in 1991 with typical extraction losses of 1μA. In order to keep the losses in the injector 2 and in the main ring minimal, a careful beam collimation in the center of the injector and after extraction is essential.

Beam Current Limits due to Space Charge Effects

Space charge effects become important when the charge density inside a beam bunch is so high that the repelling forces of the particles against each other are comparable to the external electromagnetic forces that guide and focus the beam [5]. In almost all accelerators the transversal (radial and vertical) space charge effects produce a widening of the radial and vertical beam width and in parallel a lowering of the focussing frequencies for the incoherent

betatron oscillations. The intensity limit imposed by transversal space charge effects has been estimated [6] for the injector 2 and PSI ring cyclotron to be at about 5 mA and 20 mA respectively. For the high power 1GeV cyclotron, to be discussed in the next chapter, the transversal space charge limit is estimated to be at 50mA. For the corresponding 120 MeV injector this limit is about 20mA.

In an isochronous cyclotron there is no focusing in the longitudinal direction (i.e. a cyclotron is always on transition). Leading particles e.g. stay ahead throughout acceleration and acquire thus an additional energy gain from the longitudinal space charge forces within the bunch. Without special measures this can result in an unacceptable energy spread [6].

The effect of the longitudinal space charge forces can be seen as a vortex motion of the particles in the longitudinal phase space of energy and phase [7] ... [14]. We can distinguish three stages:

1. Particles gaining or loosing energy drift adiabatically to the corresponding equilibrium orbit with larger or smaller radius respectively, thus producing a tilted bunch. This effect can be compensated by operating the flattop system in a "tilt top" mode[6].

2. The Coulomb forces that generate the tilt, however, are not linear and produce a distorted bunch. This effect, which dominates at higher beam energies, tends to smear out the turn structure at extraction. In [6] an approximation formula shows that the resulting intensity limit due to those longitudinal space charge forces is proportional to $1/N^3$, N being the number of turns in the cyclotron. This scaling law is quite well verified in the PSI ring cyclotron (see fig. 3) and it was taken as a basis to propose the high power 1GeV cyclotron to be designed with an extremely high energy gain per turn, resulting in only 140 revolutions of the beam.

3. The betatron oscillations, finally, introduce a coupling of radial and longitudinal motion and the vortex motion of the beam bunch leads towards the formation of a galaxy shaped charge distribution [15]. This effect dominates at the low energy end of the injector cyclotron.

It is obvious that such a distorted beam has to be collimated before acceleration. Experience from high beam intensity experiments at injector 2 has shown that this is indeed possible without major problems. The beam from the Cockcroft Walton preaccelerator is collimated to about 70 - 80% of the initial beam intensity in the first and fourth turn, which results in a clean and compact bunch at the extraction from this cyclotron [16] [17]

A Cyclotron for 10 MW Beam power

The layout of the cyclotron shown in figure 4 is based on the design criteria, techniques and components which proved to be successful in the high intensity operation of the PSI-ring cyclotron. The field of the sector magnets fulfils the condition of isochronism and has acceptable focusing properties. The exact value of the injection energy is still open and should be optimized together with the injector cyclotron and preinjector.

To build cavities for a peak voltage of 1 MV, with wall losses of < 500 kW and with a very high operational reliability, will be a very difficult task. In addition, such a cavity will have to handle about 1.2 MW of beam power, meaning that approximately 1.7 MW of

RF-power have to be coupled into the cavity. Most probably this problem can only be solved applying the multiple window technique. The PSI-experience is limited so far to couple 500 kW through one RF-window into a cavity at 50 MHz.

PSI plans to build new cavities with a peak voltage of 1 MV for the 590 MeV ring, an important step to clarify most of the questions mentioned above. The new generation of cavities will be equipped with an inner Cu-surface (instead of Al); this will improve the break down-behavior of the cavity (reliability!) and also increase the shunt impedance from todays 850 kOhm to >1000 kOhm. Fig. 5 gives a view of and a cross section through the new cavity. A 1:3 model of the new cavity is near completion.

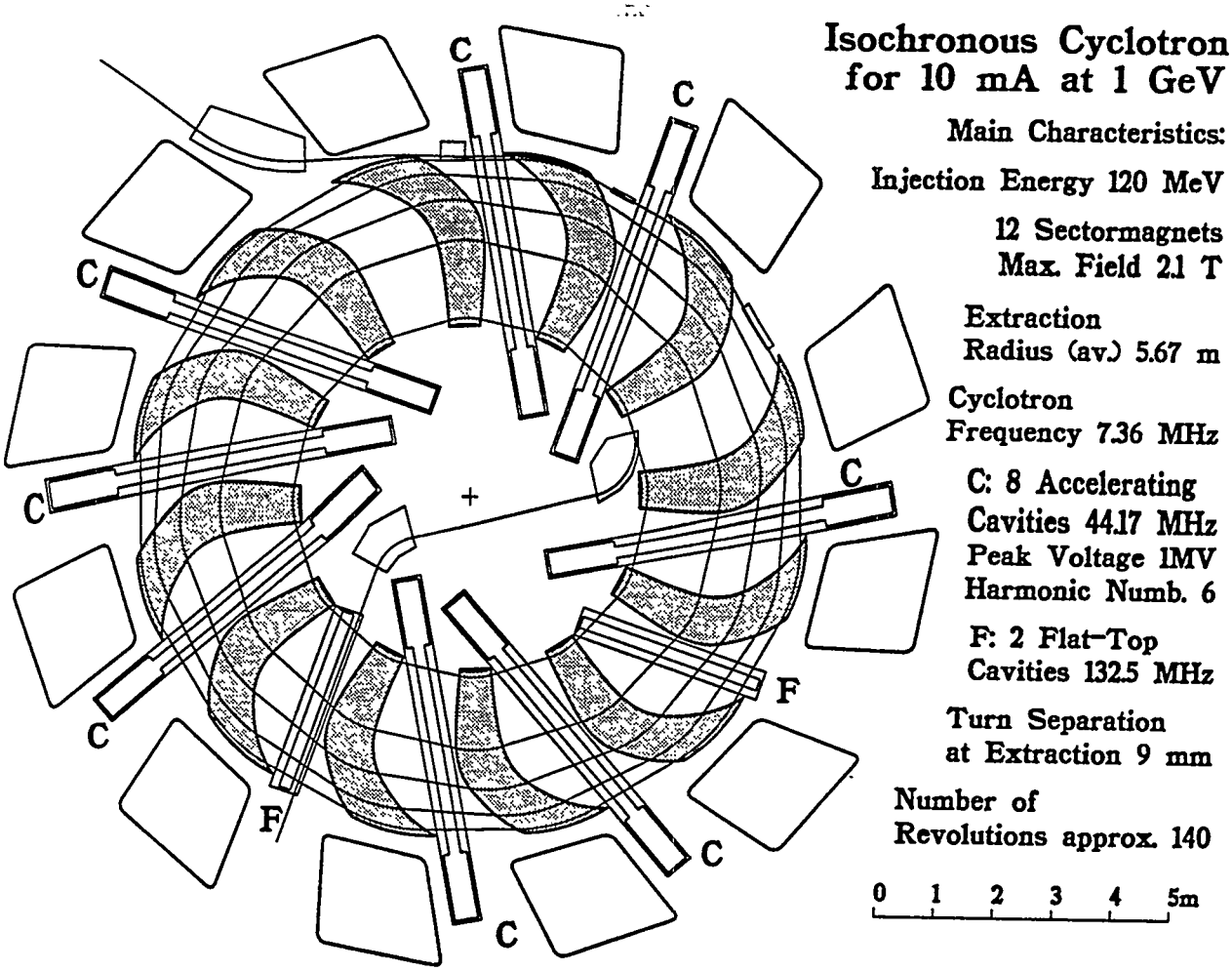

Fig. 4. Layout of the proposed high power cyclotron.

In an operating mode with a 3rd harmonic "flat-topping", these cavities absorb approximately 11% of the beam power, which will amount to more than 1MW and will exceed by far the wall losses of the flattop cavity at the operating voltage. (This extra power has to be delivered by the main cavities). This beam loading will lead to a collapse of the voltage and phase control systems unless effective measures are taken. At PSI this problem was solved by adding an external electrical damping to the flattop cavity.

The conversion efficiency of the RF-systems will be about 50%. This value is based on the following assumptions:

- The shunt impedance of the main cavities is 1000 kOhm. This is a realistic value for an optimized geometry at 44 MHz.
- The efficiency of the RF-systems is 75%.
- The power transferred from the main cavities to the flattop cavities by the beam is 10% of the beam power. The transferred power is assumed to be lost, although one could imagine that it could partly be recuperated.

The power consumption of the magnets could be kept below 1 MW when properly designed.

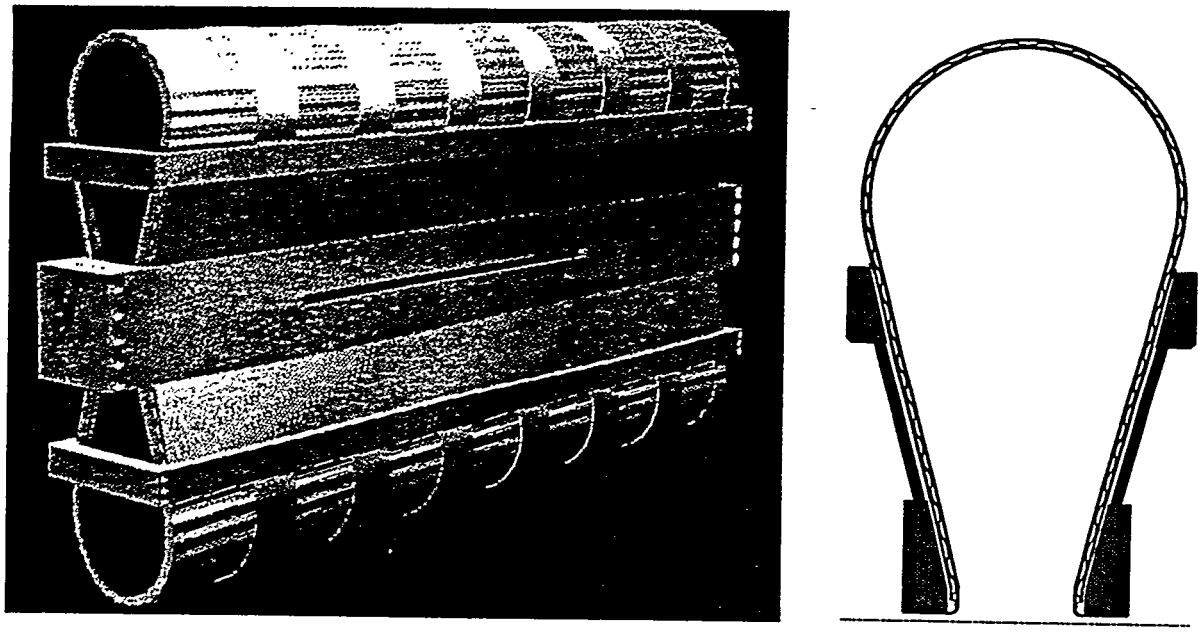

Fig. 5. The new 50 MHz cavities for the PSI ring cyclotron, presently under construction. The goal is to achieve 1 MV peak voltage with wall losses < 500 kW. The sketch on the right side shows the cross section of the upper half of the cavity. The corrugated design provides the cooling ducts for the inner copper mantle.

For the 10 MW cyclotron we forsee a similar extraction scheme as for the PSI-ring. The turn separation at extraction will be about 9 mm, which compares favourably with the 5.5 mm in the PSI-ring. It should be mentioned, however, that the turn separation can be increased by a limited amount by the superposition of a precessional motion to the accelerated orbits. The effective thickness of the electrostatic septum and the beam halos between neighboring turns at extraction are the factors which determine the beam losses. When the beam is carefully collimated at lower energies, we would expect the extraction losses to be in the order of a few μA. In the PSI-experience this is a tolerable value for a save operation and maintenance of the cyclotron, provided the extraction components are adequately shielded and adequate handling equipment is available.

The injector for the 1GeV ring would probably be a cyclotron as well, similar to the PSI Injector 2 described above, again with a not yet defined preaccelerator as a first stage.

While in the last accelerator stage, at the high energy end, longitudinal space charge forces are not expected to hinder the extraction of beams with currents up to several mA by simply reducing the turn number, the situation is different at low energies. The effect of space charge is inversely proportional to the momentum [6] and hence is much stronger in the preinjector and the injector cyclotron. Further detailed investigations are necessary to find the optimal solution to build an injector for a 10mA facility.

Conclusions

At present we do not see any fundamental reasons, neither from theoretical nor technical aspects, that would hinder the construction of a cyclotron for 10 MW protons with tolerable beam losses. A long list of open questions, however, would need to be clarified before such an accelerator could be declared to be feasible. On the top of the priority list we would like to set the following points:

1. A concept for an injector cyclotron and preinjector should be worked out.
2. Demonstrate a reliably operating cavity with a peak voltage of > 1 MV.
3. A deeper understanding of space charge effects in cyclotrons.
4. More detailed investigations which would help to predict the extraction losses.

References

[1] Carminati, F. et al., "An Energy Amplifier for Cleaner and Inexhaustible Nuclear Energy Driven by a Particle Accelerator", CERN Report, 1993, CERN/AT/93-47.

[2] Adam, S. et al., "First Operation of a Flattop Accelerating System in an Isochronous Cyclotron", Part. Accel. Conf. 1981, Washington DC, IEEE NS-28, #3 (1981) pp.2721-2723.

[3] Schryber, U. et al., "Upgrading the PSI Accelerator Facility for High Intensity Operation", 3rd Europ. Part. Acc. Conf., Berlin, 1992, pp.173-175.

[4] Sigg, P. et al., "Experience with the PSI Cyclotron RF-System under Heavy Beam Loading", 13th Int. Cycl. Conf., Vancouver 1992, pp.534-537.

[5] Reiser, M., "Space Charge and Current Limitations", IEEE Trans. NS-13 (1966) pp.171-178.

[6] Joho, W., "High Intensity Problems in Cyclotrons", 9th Int. Cycl. Conf., Caen, France, 1981, pp.337-347.

[7] Welton, T.A., "Factors Affecting Beam Quality", Proc.Informal Conf., Sea Island, Georgia, USA, Publ. NAS-NRC #656 (1959) pp.192-197.

[8] Gordon, M.M., "The Longitudinal Space Charge Effect and Energy Resolution", 5th Int.Cycl.Conf., Oxford, UK, 1969, pp.305-317.

[9] Adam, S., diss. ETH Zürich Nr.7694 (1985) and IEEE Trans. NS-32 (1985) pp.2507-2509.

[10] Chabert, A. et al., 7th Int.Cycl.Conf., Zurich, 1975, pp.245-248, and IEEE Trans. NS 22/3 (1975) pp.1930-1933.

[11] Baron, E. et al., 11th Int.Cycl.Conf., Tokyo, 1986, pp.234-237.

[12] Chasman, C. et al., NI&M - Phys.Res. 219 (1984) pp.279-283.

[13] Cazoll, V., thèse Univ. de Paris-Sud No 732 (1988), GANIL Report T 89.01.

[14] Kleeven, W.J.G.M., Thesis Techn. Univ. Eindhoven (1988).

[15] Koscielniak, S.R. and Adam, S., Part.Accel.Conf. PAC 1993, Washington DC, pp.3639-3641.

[16] Stetson, J. et al., 13th Int. Cycl. Conf., Vancouver 1992, pp.36-39.

[17] Stammbach, Th., 13th Int. Cycl. Conf., Vancouver 1992, pp.28-35.

Potential Role Of ABC-Assisted Repositories In U.S. Plutonium And High-Level Waste Disposition

David Berwald, Anthony Favale and Timothy Myers
Grumman Aerospace Corporation, Bethpage NY 11714

Jerry McDaniel
Bechtel Corporation, 50 Beal St., San Francisco, CA 94105

Abstract. This paper characterizes the issues involving deep geologic disposal of LWR spent fuel rods, then presents results of an investigation to quantify the potential role of Accelerator-Based Conversion (ABC) in an integrated national nuclear materials and high level waste disposition strategy. The investigation used the deep geological repository envisioned for Yucca Mt., Nevada as a baseline and considered complementary roles for integrated ABC transmutation systems. The results indicate that although a U.S. geologic waste repository will continue to be required, waste partitioning and accelerator transmutation of plutonium, the minor actinides, and selected long-lived fission products can result in the following substantial benefits: plutonium burndown to near zero levels, a dramatic reduction of the long term hazard associated with geologic repositories, an ability to place several-fold more high level nuclear waste in a single repository, electricity sales to compensate for capital and operating costs.

INTRODUCTION AND BACKGROUND

The ultimate disposition of spent reactor fuel and processed high level waste (HLW) has been a subject of much concern and little progress since the dawn of the nuclear era. In the U.S. today, the spent fuel from over 110 commercial Light Water Reactors (LWRs) continues to be stored on-site while highly toxic liquid HLW continues to be stored in tanks at DOE reservations in Hanford, Savannah River, Idaho Falls and West Valley.

The current U.S. HLW management policy is defined by the Nuclear Waste Policy Act (NWPA) of 1982 and its subsequent amendment of 1987. The NWPA requires the permanent disposal of spent fuel assemblies in geologic waste repositories, the first of which will presumably be located at Yucca Mountain, Nevada. The pace of process for implementing Yucca, discussed in a recent General Accounting Office (GAO) assessment, *Nuclear Waste: Yucca Mountain Project Behind Schedule and Facing Major Scientific Uncertainties* [1], remains frustratingly slow. By GAO estimation, an operational waste repository at Yucca Mountain could be delayed beyond the 2020 time frame.

The approach to formulating an acceptable HLW disposal strategy has always involved serious consideration of nonproliferation issues. Most recently, the nuclear weapon build-down following the cold war has stimulated a need for the U.S. and Russia to dispose of surplus plutonium. Consideration of this has motivated: (1) a recognition that all plutonium is a proliferation hazard [2] and (2) a renewed debate on the best approach to dispose of plutonium in general [3, 4].

From an international perspective, there is little agreement on the best strategy for ultimate disposition of HLW and plutonium. Plutonium recycle remains the policy of most of the nuclear powers including France, Britain, Japan and Russia [3]. They argue that the best way to limit the possibility of proliferation is to limit the total amount of plutonium by continuously recycling it in fission power reactors, consistent with the provisions of the Nonproliferation Treaty.

In this paper we consider a system for the back end of the nuclear fuel cycle that could provide an internationally attractive approach to solving the coupled HLW and nuclear material proliferation issues. The principal components of this system, based upon design studies recently performed by the U.S. National Laboratories [5,6], are a large chemical processing facility, several

Accelerator Based Conversion Systems (ABC), and a geologic repository. Together, these can perform the following functions, shown in Figure 1:

- Acceptance of weapon plutonium and spent commercial reactor fuel from commercial power plants,
- Extraction of plutonium, minor actinides and certain long-lived fission products,
- Elimination of the plutonium and minor actinides by fission,
- Generation of large quantities of electricity,
- Transmutation of the long-lived fission products to more benign species,
- Disposal of resulting shorter-lived HLW in a geologic repository.

Such a system could fundamentally improve the attractiveness and acceptability of permanent geologic disposal of HLW, stabilize and burn-down growing worldwide plutonium inventories, and do so in a safe and environmentally attractive manner that does not lead to or encourage the development of a plutonium economy.

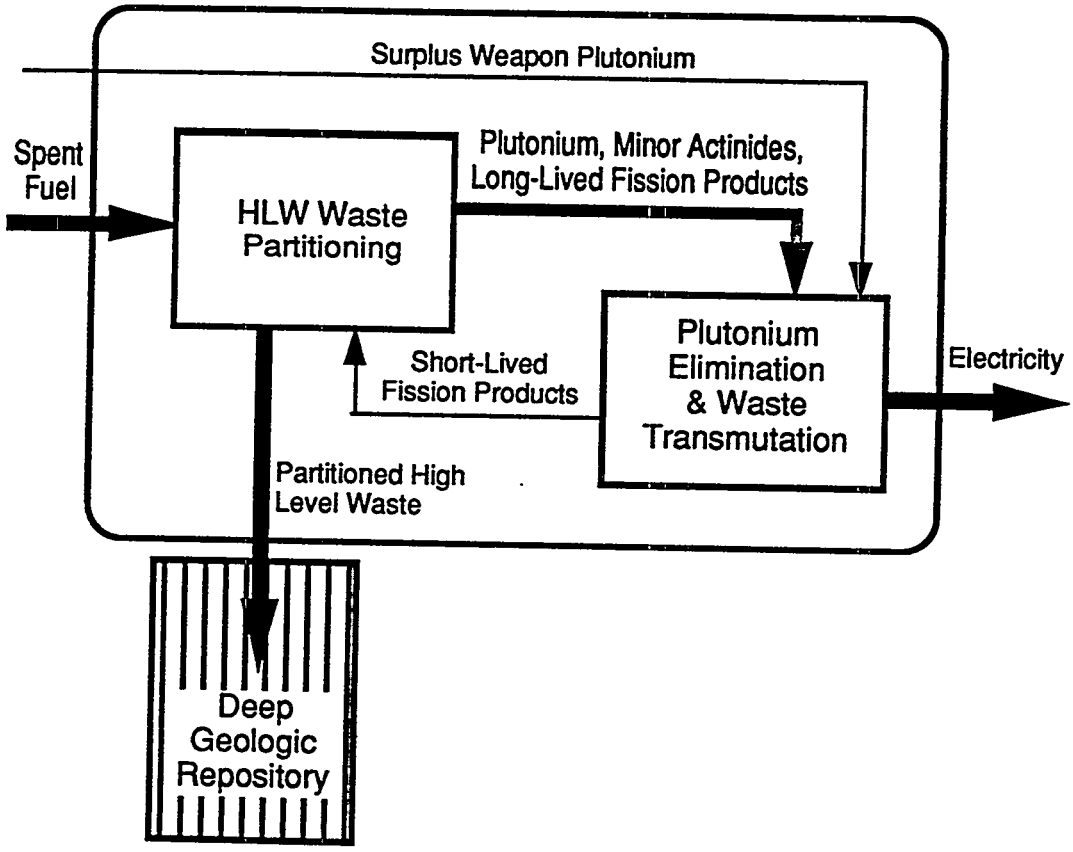

Fig. 1. Functional Requirements For Accelerator Based Conversion System

CRITICAL REVIEW OF CURRENT U.S. HLW MANAGEMENT POLICY

Before promoting the benefits of improved approaches to HLW and nuclear material management, it appears prudent to provide a critical review of the current HLW management policy, which reveals several areas for concern. These areas are highlighted below:

- Geologic disposal would appear to be a passive, therefore low cost, waste remediation technology. But it is, in fact, personnel intensive and very expensive. For example, the present value of the cost of the Yucca repository is likely to exceed $30 billion [7, 8].

- Geologic repositories will be limited in both area and volume. For example, the Nuclear Waste Policy Act limits the capacity of the Yucca site to 70,000 MT of spent fuel; the 30 year production of about 90, 1 GWe LWRs. DOE estimates that, by 2010 there will already be 61,000 MT of LWR-generated spent fuel [8]. Not including defense wastes, the capacity of the first repository is likely to be exhausted well before it begins operation.

- The statutory period of time for which EPA requires that the integrity must be guaranteed, 10,000 years, is somewhat arbitrary. The radiological hazard potential due to HLW waste constituents and their long-lived daughters does not substantially diminish between 1000 and 10,000 years [9]. Indeed, as shown in Table 1, nearly all of the long-lived waste initially charged to the repository remains well beyond 10,000 years. Given past experience and our current tools for projecting into the future, many experts argue that it will not be possible to guarantee the long term integrity for even 10,000 years [10].

Table 1. Long-Lived Isotopes From Spent LWR Fuel, Charged To A Repository

Long-Lived Waste Constituent	Fraction Remaining (%)					
	Initial Charge	$5 \cdot 10^2$ yr	10^3 yr.	10^4 yr.	10^5 yr.	10^6 yr.
Technetium - 99	100	100	100	97	72	4
Iodine - 129	100	100	100	100	100	96
Plutonium (All)	100	88	85	58	8	1
Neptunium-237	100	100	100	100	97	71

- As the radioactivity dies down, the repository becomes a "plutonium mine". For example, the 70,000 MT of spent fuel to be charged to the Yucca repository will contain about 600,000 kg of plutonium, or approximately 150,000 critical masses [2, 11]. Because the isotopes that cause difficulties in weapon design have shorter half-lives than ^{239}Pu, the plutonium quality for weapon use improves as the radioactivity diminishes. By encouraging other nuclear countries to emulate our HLW management approach within their own borders, the current U.S. policy runs the future risk of increasing the possibility that national or subnational groups will find a ready supply of plutonium should the current trend toward nuclear weapons build down and non-proliferation be reversed.

- In a more general context, the U.S. approach fails to engage other countries (where 70% of the plutonium and nuclear waste are being generated [12]) in the development of mutually acceptable alternatives that improve the proliferation resistance, safety and environmental impact of nuclear power.

PARTITIONING AND TRANSMUTATION: QUALITATIVE ADVANTAGES

HLW partitioning refers to the process whereby HLW may be chemically separated to extract plutonium, the minor actinides and certain long-lived fission products. Subsequent to this process, the balance of the HLW, highly depleted in long-lived sources of radiotoxicity, is disposed in a geologic repository. Transmutation refers to the process whereby the long-lived waste constituents extracted from the spent fuel are converted into more benign short-lived constituents by fission and transmutation. The advantages of HLW partitioning and transmutation are several:

- By removing the small number of radioactive isotopes that dominate the risk of radiotoxic release for long confinement times in the geologic repository, and by transmuting them into stable or short-lived isotopes using dedicated facilities, the radiotoxic hazard associated with these remaining waste constituents is dramatically reduced for time periods in excess of a few hundred years. Therefore, the acceptability of the geologic repository may be fundamentally improved, the reliance on long-term engineered barriers may be reduced and compliance with existing regulations may be facilitated [9].

- Recent results [13] indicate that by (1) removing the long-lived actinides from the high level waste charged to a deep geologic repository and by (2) keeping the repository waste storage drifts accessible during the entire filling to enable the emplacement of the remaining shorter-lived waste in a staggered manner, the amount of waste that can be contained in the Yucca repository might be increased by 4-5 fold. This compares with a smaller (perhaps 2-fold) increase in the amount of waste that can be loaded if the plutonium and actinides are not removed, but staggered waste emplacement is employed. With HLW partitioning, the U.S. could continue to rely upon a viable nuclear-electric generation capability while requiring only one repository for the foreseeable future.

- By destroying plutonium by fission, the growing plutonium inventory in spent reactor fuel can be capped and needed electricity can be produced. The most efficient transmutation alternatives, such as ABC systems, utilize high burnup fuels to avoid recycle and minimize the accessibility of separated material [5,6]. These alternatives avoid the risk of a "plutonium economy" while drawing down the plutonium inventory to near-zero levels, thus eliminating the long term legacy of the plutonium mine.

- Advanced technologies that use plutonium to generate power are more acceptable to the other nuclear powers. U.S. involvement in the development of waste partitioning and transmutation technologies can provide a basis for cooperation in the development of nuclear alternatives that promise improved proliferation resistance, safety and environmental impact.

The chemical process requirements for waste partitioning are, in general more challenging than for commercial fuel reprocessing (99% extraction of plutonium from spent fuel is typical). However, depending upon the waste disposal objective, the required separation requirements, the process complexity, and the level of technological difficulty can evolve in time. For example, as shown in Table 2, a range of requirements may be envisioned.

To demonstrate achievement of the required separation requirements, and to evaluate the possibilities for efficient waste transmutation, the French have launched a new R&D program, SPIN, which includes the following elements [14]:

- In the intermediate term (next 20 years), they will evolve PUREX to their ACTINEX process, which will reduce the long term toxicity of the partitioned waste by a factor of 100, with an ultimate reduction goal of 1000.

- Transmutation alternatives such as fast reactors (EFR-type) and subcritical accelerator-driven systems will be investigated. An experimental program, Superfact, involving high burnup irradiation of actinide-loaded fuel elements in the PHENIX fast reactor is underway.

Table 2. HLW Partitioning Separation Requirements

Goal	Approximate Separation Requirement
• Remove long term decay heat to expand repository	90%
• Eliminate plutonium mine	99%
• Reduce long-term repository risk (nominal goal)	99.9%
• Reduce repository lifetime to 1000 yrs.	99.997%
• Reduce repository lifetime to 300 yrs.	99.999%

COMPARATIVE COST SCENARIOS: QUANTITATIVE ADVANTAGES

To provide a realistic perspective, two nuclear power growth scenarios and three approaches to managing the HLW were investigated. The two growth scenarios were:

Scenario 1: Fission power in the U.S. terminated when current plants reach design lifetimes,

Scenario 2: The U.S. maintains an installed nuclear capacity of 80-100 GWe replacing nuclear plants as they retire.

The three HLW management approaches were:

Approach A: Baseline approach reflecting the current U.S. HLW management policy, deep geologic storage of spent fuel in Yucca-class repositories. For this approach, neither partitioning and transmutation or staggered HLW emplacement in the repository are considered.

Approach B: ABC assisted geologic storage repository. For this approach, an ABC HLW partitioning and transmutation system, providing the advantages described above, will be deployed. As indicated in Figure 2, this approach will require ten ABC facilities, one large aqueous fuel processing plant (Aqueous FPP) and one HLW repository.

Each ABC facility, required to operate for 40 years, will consist of:

- One high energy proton accelerator (100 mA, 1.2 GeV),
- Six target blanket assemblies (1000 MWth each) and the required power conversion and balance of plant equipment,
- One central pyrochemical fuel processing plant (Pyro FPP).

Operating with a 75% plant capacity factor, each ABC system will produce 2400 MWe of total power and 2000 MWe of net power. Thus, 20 GWe of new electric generation capacity would be available.

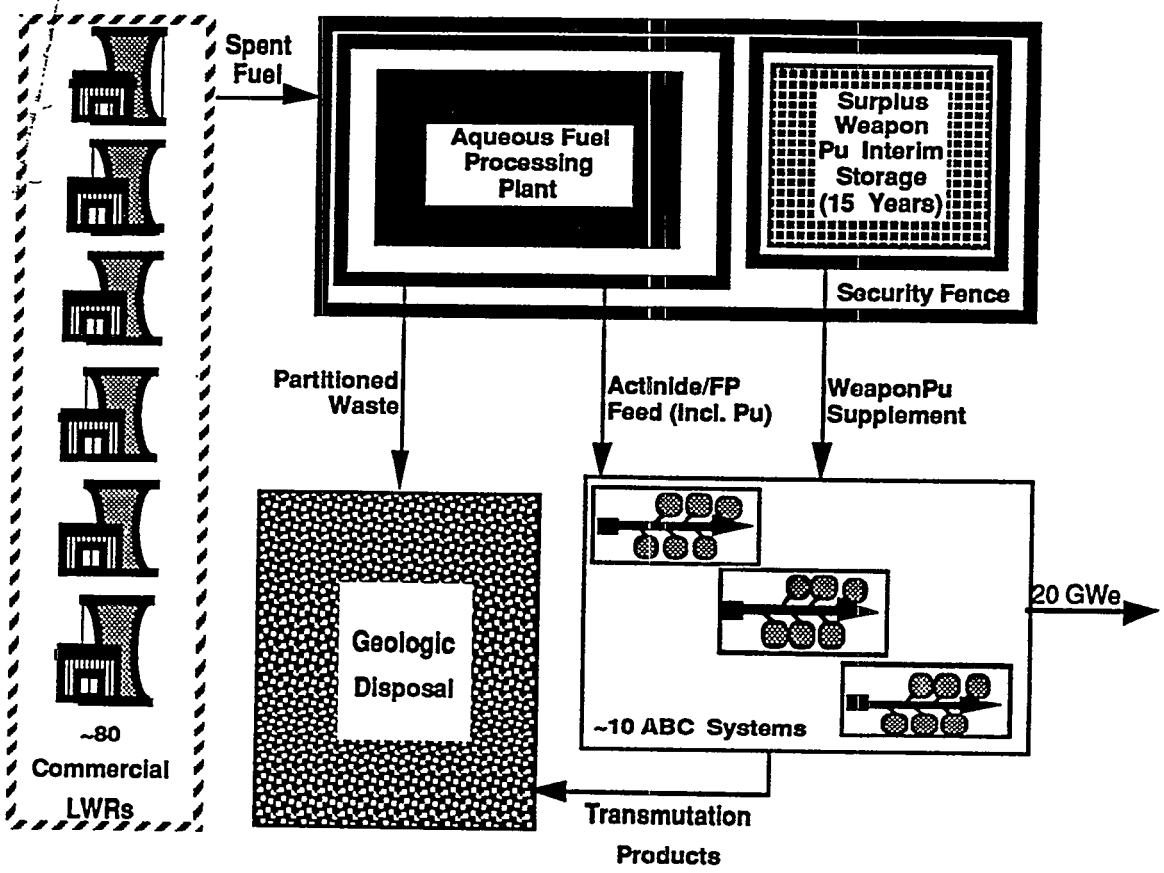

Figure 2. Accelerator-Based Conversion System Segments

The large aqueous fuel processing plant, similar in capacity to Cogema's La Hague fuel reprocessing facility (1750 MTHM/yr versus 1600 at La Hague) [15], will be required to

- Accept weapon plutonium and spent commercial reactor fuel,
- Extract of plutonium, minor actinides and certain long-lived fission products,
- Prepare the fuel feed streams for the ten ABC transmutation systems,
- Prepare all of the remaining waste streams for disposal.

This approach takes into account the repository volume gain enabled by partitioning and transmutation.

Approach C: Modified repository utilizing a 2-fold storage improvement enabled by Staggered Waste Emplacement (SWE). By including this approach, which does not involve waste partitioning or transmutation, we are able to separate the benefits of partitioning and transmutation from those that could result from a HLW management strategy that employs only SWE.

Financial Assumptions

The same financial assumptions were used to develop a levelized financial analysis that considers all of the above approaches: The assumptions included a real inflation rate of 4%, a discount rate (cost of money) of 8%, a cost recovery period of 40 years and a bus bar price of electricity to be sold by the ABC system of 50 mils/KWe-Hr. Learning curve effects, applied to all capital costs (including the geologic repository and the chemical processing plants), were used to account for transition from first-of-a-kind facilities to nth-of-a-kind production facilities [16]. All results are referenced to 1994 dollars.

Capital Costs

Capital cost estimates for the various major components of an ABC-assisted repository system are provided in Table 3. In reviewing these estimates, the reader should note that they

Table 3. ABC-Assisted Repository - System Capital Cost

	Value		Basis
Accelerators:			
• Number of ABC Accelerators	10		1.2 GeV, 100 mA
• First Unit Cost	1.0	$B	Largest cost: 185 MW RF @ 2 $/W
• Capital Cost of ABC Accelerators	8.6	$B	Learning curve applied to units 2-10
ABC Targets/Blankets:			
• Number of ABC Targets/Blankets	60		Includes balance-of-plant
• First Unit Cost	1020	$/kWth	1.25 cost of LWR @816 $/kWth
• Capital Cost of ABC Targets/ Blankets	51.2	$B	Learning curve applied to units 2-60
On-Site ABC Fuel Processing:			
• Number of ABC Pyro FPPs	10		
• Unit Cost of ABC Pyro FPP	0.26	$B	~1/10 throughput of aqueous plant
• Capital Cost of ABC Pyro FPPs	2.6	$B	
ABC Capital Cost	62.4	$B	
LWR Fuel Processing:			
• Number of Aqueous FPPs	1		1750 MTHM/yr, scaled from La Hague experience
• Capital Cost of Aqueous FPPs	12.2	$B	
Repository:			
• Number of Repositories	1		70,000 MTHM (partitioned waste)
• Capital Cost of Repository	14.6	$B	Reduced volume/toxicity/size
ABC-Related Research & Development Cost	3.2	$B	
Total Capital Cost	92.4	$B	

result from reasonable assumptions, but do not reflect the results of a thorough cost estimating activity, which must be supported by detailed design information. Therefore the estimates provided below should be viewed as budgetary estimates suitable for parametric evaluation in support of planning activities.

The accelerator capital cost is scaled from the projected cost of RF power, which is expected to be the dominant cost element. The capital cost of the ABC target/blanket (including balance of plant) is scaled from LWR construction experience [16]. The capital cost of the large LWR fuel processing plant was scaled from reported cost data for La Hague [15]. The total net present cost of the Yucca Mountain geologic waste repository (including all of its above ground support operations and facilities) was taken to be $30 billion [7,8]. The capital cost fraction of this total was developed by the authors based upon review of References 7 and 17. The remaining fraction was allocated to the annual operating cost of the repository. The ABC-assisted repository costs, shown in Tables 3 and 4, reflect a 20% savings that attempts to capture the savings due to reduced engineering requirements for a repository that contains waste forms with greatly diminished long term risks.

Table 4. Results Of Financial Analysis

	Scenario 1		Scenario 2		
	A	B	A	B	C
Includes Accelerator-Based Conversion ?	No	Yes	No	Yes	No
Includes Staggered Waste Emplacement ?	N/A	N/A	No	Yes	Yes
Capital Costs ($B):					
Cost of Repository	18.3	14.6	17.2	a	a
Cost of ABC System		64.6		61.24	
Cost of LWR Fuel Processing		13.2		11.45	
Total ($B)	18.3	92.4	17.2	72.69	
O&M Costs ($B/yr):					
Repository[b]	0.60	0.48	0.56	0.45	0.45
ABC System[c]		1.29		1.22	
LWR Fuel Processing[d]		0.66		0.57	
Elec. Sales Credit		-6.57		-6.57	
Total ($B/yr)	0.6	-4.14	0.56	-4.33	0.45
Annual Levelized Costs ($B/yr):					
Capital[e]	1.53	7.76	1.44	6.1	d
Operating[f]	1.02	-7.03	0.96	-7.35	0.77
Total ($B/yr)	2.55	0.72	2.40	-1.25	0.77

[a] Additional partitioned waste for Scenarios 2B and 2C charged to first repository. No additional capital cost, but repository O&M costs continue as required for additional emplacements

[b] O&M for repository includes construction activities associated with continuing waste emplacement. Estimated from analysis of Ref. 17, 18 projections.

[c] O&M for ABC plants taken to be 2%/yr.

[d] O&M for LWR fuel processing plant taken to be 5 %/yr

[e] Capital recovery factor = 8.4%/yr

[f] Levelized cost factor = 1.70

The cost estimate for ABC-related research and development (including the non-recurring costs associated with the first demonstration unit) are ROM (rough order of magnitude). They recognize that the development of ABC technologies can benefit from the substantial prior investment that the U.S. Government has already made in nuclear technology and experimental particle accelerator facilities such as the Los Alamos Meson Physics Facility (LAMPF).

Results For Scenario 1: Termination Of Fission Power In The U.S.

The results for the two nuclear growth scenarios examined are summarized in Table 4. As shown, the results for Scenario 1 indicate that, although the cost of both approaches is significant, the net annual levelized cost of the ABC assisted repository (1B) is expected to more than 3-fold lower than the cost of the current approach (1A). Although the capital and operating costs of the ABC system are much greater, the revenues from electricity sales cause the net cost of the ABC system to be significantly lower than for a stand-alone HLW repository. The ABC-assisted repository also eliminates the HLW and plutonium legacies, while adding 20 GWe to the grid.

Given the preliminary nature of the cost estimates, the sensitivity of these results to cost uncertainty is of interest. The results summarized in Figure 3 indicate the levelized cash flow for the ABC-assisted repository as a function of the price of salable electricity and the cost of the ABC target/blanket (a dominant system cost). For example, for a baseline ABC target/blanket cost of

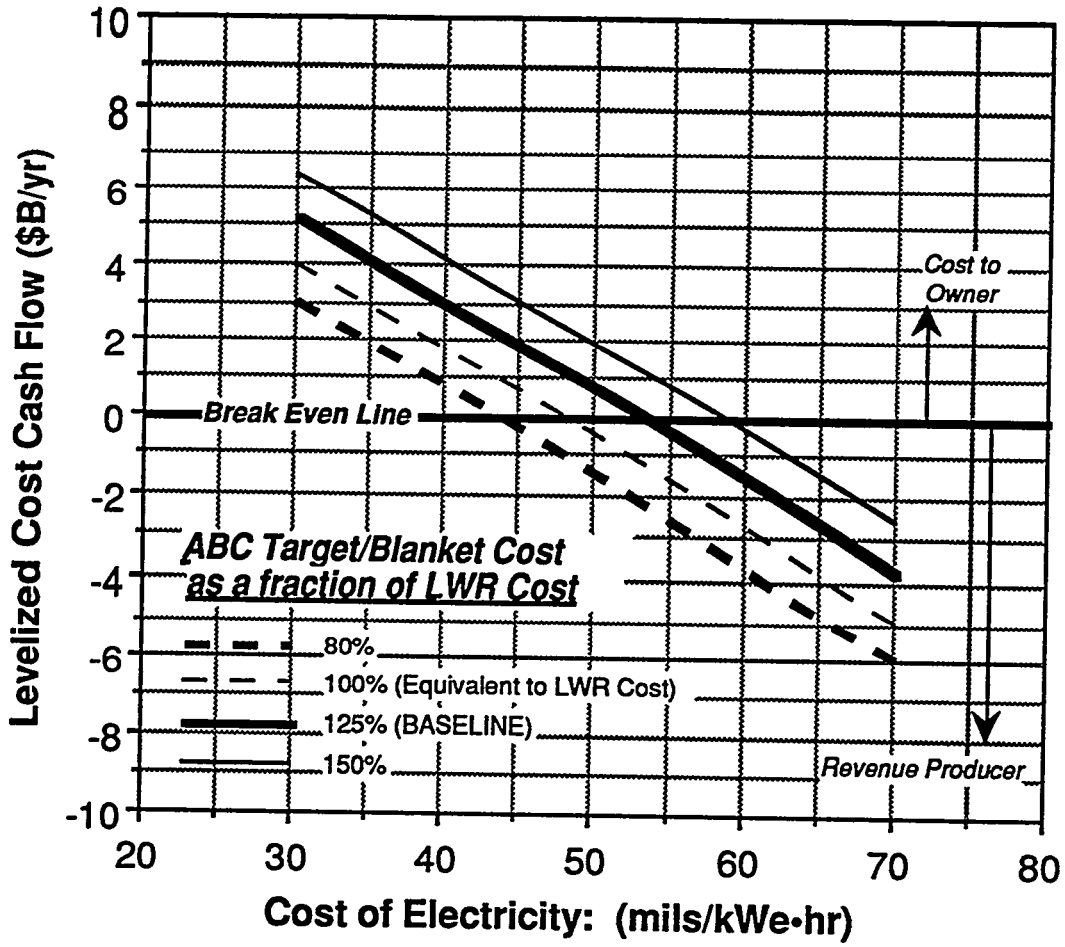

Figure 3. Cost Sensitivity Analysis

125% of the assumed cost of a LWR and a baseline electricity price of 50 mil/kWe-hr, the expected cash flow (indicated in Table 4) results in a net cost of $0.7 B/yr. If the electricity price increases

to 60 mil/kWe-hr, the cash flow improves to a net revenue of about $1.6 B/yr. However, if the electricity price decreases to 40 mil/kWe-hr, then the cash flow worsens to a net cost of about $2.9 B/yr (similar to the stand-alone repository). Similarly, if the achievable first unit cost of the ABC target/blanket is reduced to 100 % of the assumed cost of a LWR, then the ABC-assisted repository generates a net revenue stream of about $0.5 B/yr. However, if the cost increases to 150% of the assumed cost of a LWR, then the cash flow worsens to a net cost of about $2.0 B/yr.

Results For Scenario 2: Continued Operation Past Original 70,000 MT

Utilizing Approach A, a new repository (most likely located in the eastern half of the U.S.) would be required. This is reflected by the charges in the first column of Table 4, under Scenario 2. Including learning curve effects for the second repository (all other assumptions are the same) the result is an annual levelized cost of $2.4 B/yr.

In Approach B we assume that an additional fuel processing plant and an additional 10 ABC plants will be required. However, assuming that this approach is anticipated beforehand, the partitioned waste, which has a lower decay heat generation rate, can be charged to the original repository. All other assumptions are the same. The result, an annual levelized revenue of 1.25 $B/yr, is significantly better than for the approaches without partitioning and transmutation. As shown in Figure 4, the results indicate that, in comparison with geologic disposal, ABC-assisted repositories have potential to generate future revenue, and even a net revenue. [The reader should note that the cumulative cost shown in Figure 4 is less than the product of the annual levelized cost and the number of years because the costs incurred in a given year are adjusted [reduced] to reflect the 1994 equivalency.]

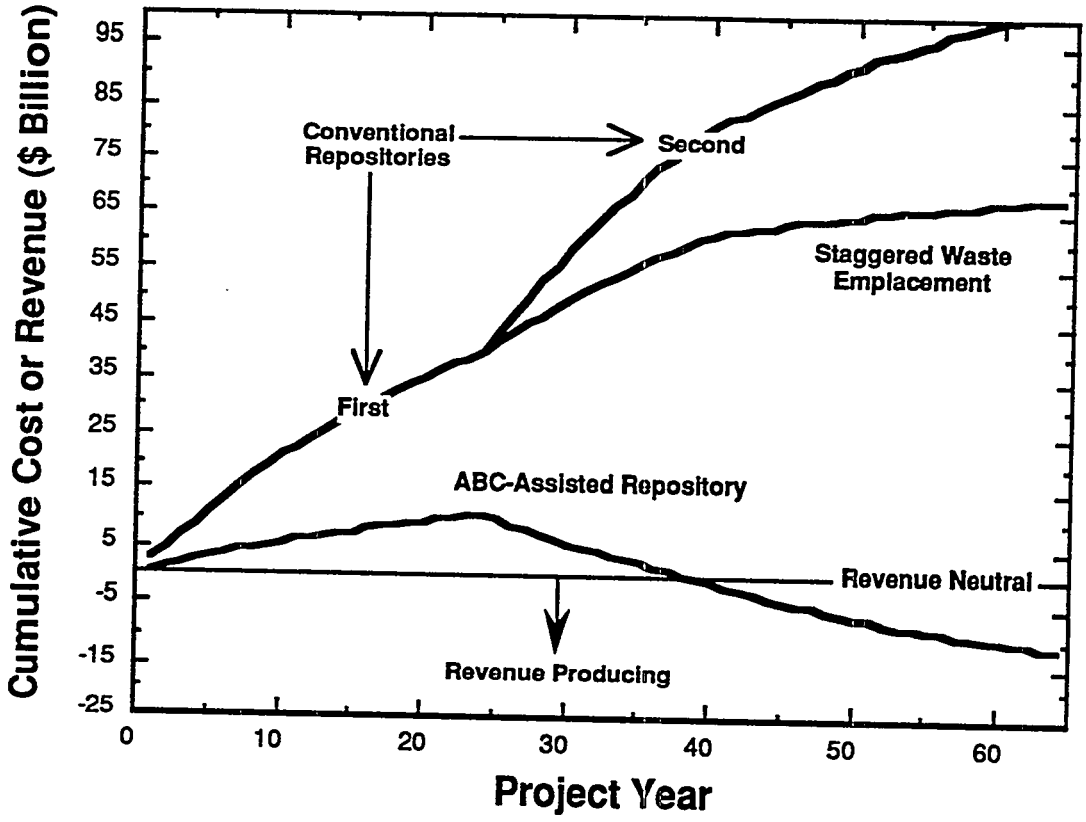

Figure 4. Comparison of Cumulative Cost For Alternative Waste Handling Approaches

In Approach C, we assume that a new repository is not required (again assuming that this approach is anticipated beforehand), but that the operating cost for the repository will continue. The results, indicated in Table 4 and Figure 4, indicate that the revenue requirement would continue, albeit at a rate of growth that would be much reduced in comparison with the initial loading (Approach 1A).

However, for the third 70,000 MT of spent fuel Approaches A and C would require new repositories. In contrast, the ABC-assisted repository, which has an overall capacity which is 4-5 fold larger than currently planned for Yucca Mountain, can continue for two additional cycles before a new repository is required. Under the assumptions of Scenario 2, a second ABC-assisted repository would not be required until the beginning of the 22nd century.

CONCLUSIONS

Emerging nuclear waste partitioning and transmutation technologies (e.g., Accelerator-Based Conversion) offer the potential to fundamentally mitigate the most controversial issues for geologic disposal, making it a more acceptable option for both technical experts and the lay public. The advantages are as follows:

- *Reduction in Long Term Hazard of Repository* - By removing the small number of radioactive isotopes that dominate the risk of radiotoxic release for long confinement times in the geologic repository, and by transmuting them into stable or short-lived isotopes using dedicated facilities, the radiotoxic hazard associated with these remaining waste constituents is dramatically reduced for time periods in excess of a few hundred years. Therefore, the acceptability of the geologic repository may be fundamentally improved, the reliance on long-term engineered barriers may be reduced and compliance with existing regulations may be facilitated.

- *Increased Repository Capacity* - By removing the heat generation associated with the long-lived species, it will be possible to increase the quantity of waste charged to the Yucca repository by 4-5 fold. Therefore, the U.S. will need only one repository for the foreseeable future.

- *Plutonium Destruction* - By destroying plutonium by fission, the growing plutonium inventory created by spent reactor fuel can be capped. The most efficient transmutation alternatives eliminate plutonium using high burnup fuels to avoid recycle and to minimize the accessibility of separated plutonium. These alternatives could avoid the risk of a "plutonium economy" while drawing down the plutonium inventory to near-zero levels, thus eliminating the long term legacy of the plutonium mine.

- *Electricity Generation* - ABC systems can create considerable quantities of electricity from fissioning of the waste plutonium and higher actinides. The sale of this electricity appears sufficient to finance the ABC-assisted waste repository system, including research and development and all other charges. If nuclear power is to be maintained at the current or expanded levels, then the financial benefit of waste partitioning and transmutation technologies, which would expand the capacity of a single repository, could be sufficient to transform the overall waste management system from a large consumer of funding resources into a net producer of revenue.

- *Proliferation Resistant Advanced Nuclear Systems* - By developing an advanced technology that consumes plutonium to generate power we can provide a basis for U.S. leadership and cooperation in the development of nuclear alternatives that promise improved proliferation resistance, safety and environmental impact.

REFERENCES

[1] *Nuclear Waste: Yucca Mountain Project Behind Schedule and Facing Major Scientific Uncertainties*, GAO, Report GAO/RCED-93-124, May 1993

[2] C. Mark, *Explosive Properties of Reactor Grade Plutonium*, Science & Global Security, Vol. 3, p. 111, Gordon and Breach Science Publishers, 1993

[3] Proceedings, *International Policy Forum: Management & Disposition of Nuclear Weapons Materials, Another Side of the Peace Dividend . . . Dealing with a Worldwide Excess of Plutonium and HEU*, Leesburg, VA, March 8-11, 1994

[4] *Management and Disposition of Excess Weapons Plutonium*, Committee On International Security and Arms Control, National Academy of Sciences, National Academy Press, Washington D.C., 1994

[5] C. Bowman, *Overview of the Los Alamos ADTT Project*, 1994 International Conference on Accelerator-Driven Transmutation Technologies and Applications, Las Vegas, Nevada, 25-28 July, 1994 (see also other Los Alamos papers from same conference)

[6] G. J. Van Tuyle, *Accelerator-Driven target Technologies Under Development at BNL*, 1994 International Conference on Accelerator-Driven Transmutation Technologies and Applications, Las Vegas, Nevada, 25-28 July, 1994 (see also other Brookhaven papers from same conference)

[7] *Cost Estimate of the Yucca Mountain Repository Based on the Site Characterization Plan Conceptual Design*, E. R. Gruer et. al., Sandia Report SAND85-1964, June 1987

[8] *Developing Technology to Reduce Radioactive Waste May Take Decades and Be Costly*, GAO, Report GAO/RECD-94-16, December 1993

[9] *Out of Sight, Out of Our Minds - Nuclear waste Buried Now In Haste Will Still Be Deadly In 12001 - What's The Rush?*, Prof. Kai Erickson, N.Y. Times Magazine, 6 March 1994

[10] M.J. Bell, *Heavy Element Composition of Spent Power Reactor Fuels*, ORNL-TM-2897, Oak Ridge National Laboratory, 1970

[11] *World List of Nuclear Power Plants*, Nuclear News, March 1994

[12] Forsberg, *Health and Environmental Risk-Related Impacts of Actinide Burning on High-Level Waste Disposal*, ORNL/M-1822, Oak Ridge National Laboratory, 1992

[13] B.S. Cowell, M. H. Fontana and G. E. Michaels, *Incentives and Techniques for Increasing the Capacity of the Geologic Repository*, Spectrum '94 Topical Meeting on Nuclear and Hazardous Waste Management, Atlanta, GA, 14-16 August 1994. Supplemented by preliminary results presented in informal discussions held at Oak Ridge National Laboratory, 8 June 1994

[14] J-Y Barre and J. Bouchard, *French R&D Strategy For The Back End Of The Fuel Cycle*, Global '93, Future Nuclear Systems: Emerging Fuel Cycles and Waste Disposal Options, Vol. 1, p 27, Seattle, WA, 12-17 September 1993

[15] S. Rippon, *First Phase of New Reprocessing Plant Opened at La Hague*, Nuclear News, June 1992

[16] J. G. Delene and C. R. Hudson II, *Cost Estimating Guidelines for Advanced Nuclear Power Technologies*, ORNL/TM-1007I/R3, Oak Ridge National Laboratory, 1993

[17] *Cost Analysis of Spent Nuclear Fuel Management*, 1993 American Power Conference Proceedings, p 1043-1049, 1993

STATUS OF ELECTRO-NUCLEAR FACILITIES DEVELOPMENT IN ITEP

I. V. Chuvilo
ITEP, Moscow, Russia

The concept of plutonium management, both weapon-grade and power, should be developed taking into account the history of previous stages of the nuclear industry and ideas which guided the process of their implementation.

Theoretical studies of several versions of a neutron multiplying subcritical system based on thermal and epithermal neutrons are conducted in ITEP. Systems with several neutron multiplying subcritical sections are considered connected by neutron flux propagating from a previous section to subsequent one.

This could be implemented by the use of neutron valves separating these sections that permits to decrease the requirements imposed upon proton beam power significantly. Heterogeneous and homogeneous approaches to implementation of such systems are studied.

There are many problems associated with nuclear constants and their classification. Measurements are performed of thermal effects in various materials under proton beam irradiation. Problems associated with materials are in the process of investigation too. Joint programs and division of labour should be organized.

Waste Transmutation with minimal Fuel Cycle Long-Term Risk

I. Slessarev, M. Salvatores, M. Uematsu
Commissariat à l'Energie Atomique
Direction des Réacteurs Nucléaires
CE Cadarache, FRANCE

1 - INTRODUCTION

Hybrid systems (source-driven subcritical reactors), are investigated at CEA, mainly from a conceptual point of view, in order to assess their potential to transmute radioactive wastes (mainly long-lived fission products, LLFP) and their potential to insure a minimal long-term radiological risk related both to the fuel inventory inside the system and to the full fuel cycle (mass flows, reprocessing, transport, waste disposal).

The physics of these systems has been explored [1, 2] and work is in progress both in the field of basic data and INC code validation [3], in the frame of international collaborations (see e.g. Ref. 4), and in the field of conceptual design studies [5]. The most interesting feature of subcritical source-driven system is related to the possibility to obtain an "excess" of neutrons per fission [1, 2], which can be used to reduce the long-term radiological risk. A specific example will be discussed here.

2 - BREEDER-BURNER SOURCE-DRIVEN SUBCRITICAL SYSTEM

In the present paper, a breeder-burner subcritical system concept will be discussed, which has the following objectives :

- To provide a significant reduction both of :
  - fuel waste toxicity in a closed fuel cycle (to reduce the "Fuel Cycle Long Term Radiological Risk"),
  - toxicity of a total fuel inventory (to reduce the "Fuel Inventory Long Term Radiological Risk").
- To transmute transuranium elements (TRU) or Pu, in order to reduce the initial long term fuel toxicity of a standard reactor discharge.
- To transmute LLFP, in order to reduce "Fission Product Long Term Toxicity".

The system under study should use [5] :

- the Th cycle,
- high fuel burn-up (~ 45 % of heavy atoms),
- fast neutron spectrum and a flux level ~ 2×10^{15} n/s.cm^2,
- subcriticality in the range of $K_{eff} \approx 0.85$,
- neutron balance improvements (e.g. leakage decrease),
- fuel breeding (to compensate for reactivity swing).

The system has an external neutron source via proton beam (E_p =1.5 GeV), and the fuel of the subcritical reactor acts as target and is made of molten salts $ThCl_3$ (60 mol %) + $PbCl_3$ (40 mol %). The choice of a molten salt fuel is not essential, but is taken as example of a high burn-up configuration.

3 - SYSTEM CHARACTERISTICS

To improve the potential of the Th-cycle breeding characteristics and its evolution in time (e.g. to transmute LLFP), some Pu fuel (or any other TRU fuel) is added at the start-up of the system.

The addition of Pu (or TRU) can be kept low enough : a 3 % ^{239}Pu (or 5 % TRU) addition to the Th fuel salt (i.e. (^{232}Th + ^{239}Pu (3 %)) Cl_3) keeps the level of K_∞ (and K_{eff}) inside the system high enough during an extended irradiation time (e.g. well beyond 10 years) such that a further addition of Tc-99 (~ 5 x 10^{20} atoms/cc) allows to obtain a K_{eff} value of the order of 0.8. The K_∞ of such system and its evolution with time is given in Fig. 1.

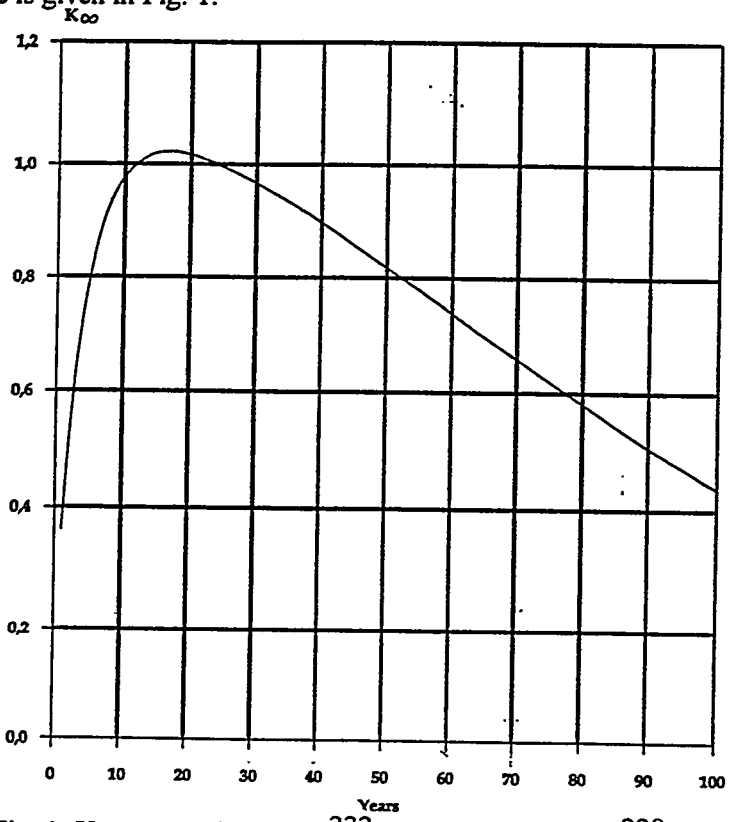

Fig. 1 K_∞ versus time for a $^{232}ThCl_3$ (57 mol %) + $^{239}PuCl_3$ (3 %) + ^{99}Tc composition (see text)

It is to be noted that the Pu (or TRU) concentration can be varied according to the target K_{eff} value, or according to the required LLFP transmutation potential. However, Pu (or TRU) concentration increase will increase the fuel inventory long term radiological risk : if we want to keep this risk low one has to limit the Pu (TRU) inventory.

In order to model a system with a rather constant K_{eff} in the range around 0.85, one can imagine a core geometry subdivided in five regions of equal volume (see Fig. 2). At equilibrium the loading will be as follows :

region 1 : fresh fuel
region 2 : fuel irradiated 10 years
region 3 : fuel irradiated 20 years
region 4 : fuel irradiated 30 years
region 5 : fuel irradiated 40 years

The fuel irradiated 40 years corresponds to a $K_\infty = 0.9$ (see Fig. 1). The evolutions with time of K_{eff} and of the fraction f of energy used to feed the accelerator, are given in Fig. 3 and 4. A 10 year fuel cycle is adopted, as illustrated in Fig. 5.

As far as the external source neutron distribution, two cases have been investigated and are shown in Fig. 3 :

a. homogeneous distribution over the whole core,
b. neutron source only in the centre of the core (region 1).

Height	:	600 cm	
Core 1	:	Radius	$R_1 = 111$ cm
Core 2	:	Radius	$R_2 = 157$ cm
Core 3	:	Radius	$R_3 = 192$ cm
Core 4	:	Radius	$R_4 = 221$ cm
Core 5	:	Radius	$R_5 = 248$ cm
Blanket	:	Radius	$R_B = 324$ cm
Reflector thickness			$H = 30$ cm

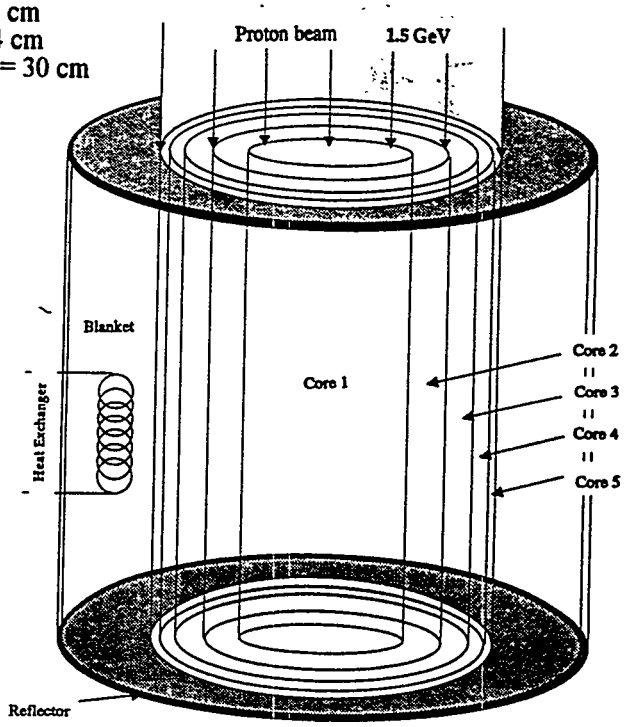

Fig. 2 Core geometry

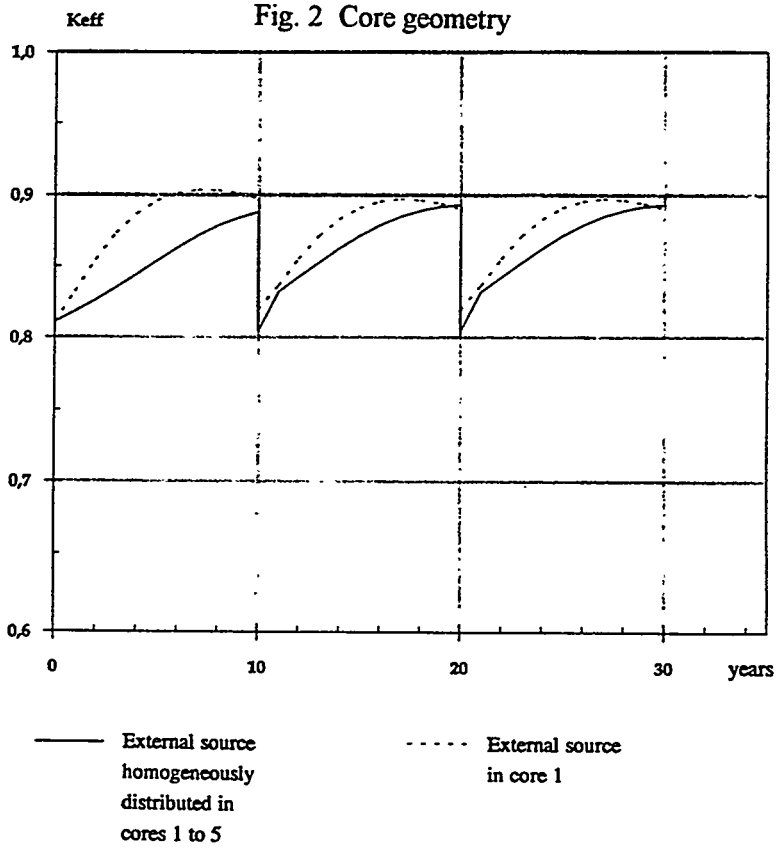

Fig. 3 K_{eff} variation with time

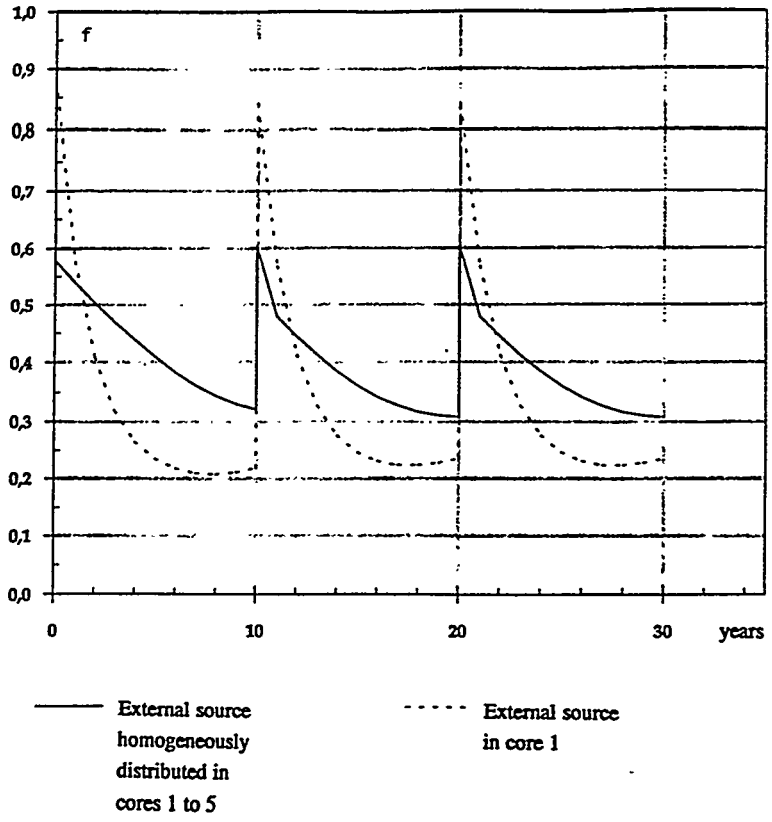

Fig. 4 Energy fraction f used to feed the accelerator

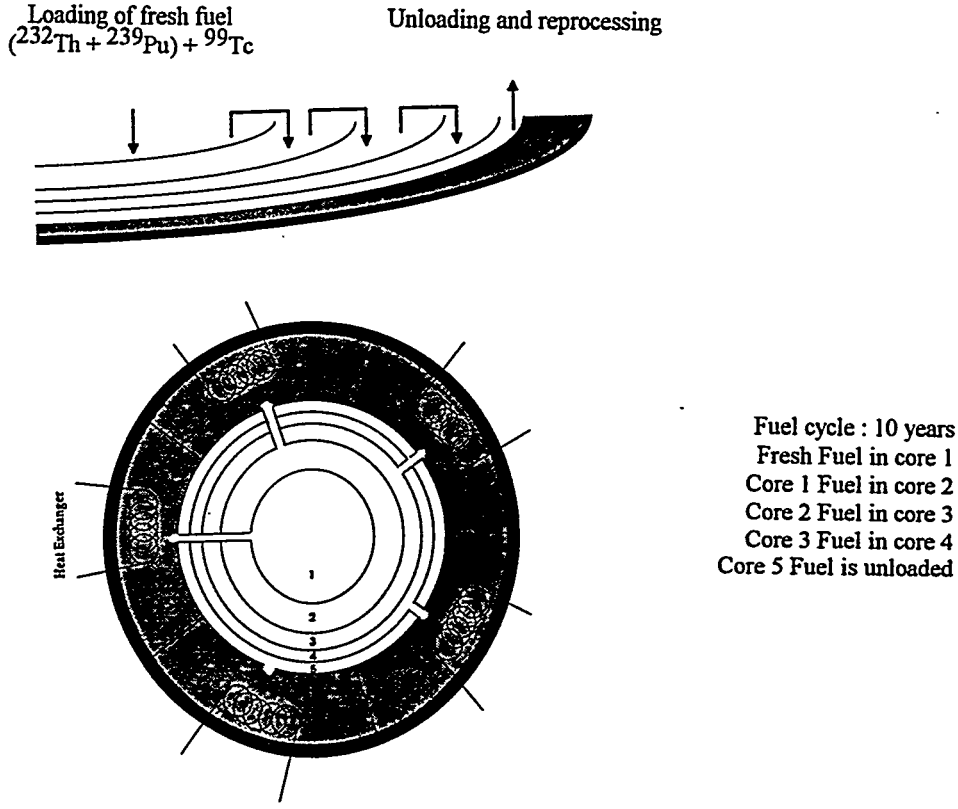

Fig. 5 Loading / Unloading Scheme

In the first case, the proton beam is spread and the whole core is a spallation target. In the second case, only the central part of the core acts as spallation target. As it can be seen in Fig. 3, the K_{eff} evolution is similar in the two cases, but the evolution of f is very sharp (see Fig. 4) and unfavourable in the case of a source concentration in the central region.

However, even in the most favourable case (i.e. a neutron source homogeneously distributed), the average f factor is relatively high (~ 0.4).

A calculation with the HERMES INC code system [6] gives a neutron yield for a beam of 1.5 GeV protons on the homogeneous salt fuel target ($^{232}Th + ^{239}Pu)Cl_3 + ^{99}Tc$ of approximately 40 neutrons per proton.

The neutron source below 20 MeV has been propagated by a transport S_N 2D dimensional code system (ERANOS) using multigroup neutron interaction cross-sections derived from the European data base JEF-2.

The main resulting system characteristics are given in table 1.

Table 1. System parameters of a Fast Molten Salt Hybrid

		BBR
Accelerator :		
• Type		Proton LINAC
• Particle		Proton
• Energy	(MeV)	1500
• Current	(mA)	270
Target :		
• Diameter	(cm)	495 (all core)
• Height	(cm)	600
• Material		Molten salt fuel
• Cooling material		None
Subcritical core :		
• Diameter	(cm)	495
• Height	(cm)	600
• Material composition of core		100 % of molten salt
• Chemical form of fuel		(Th, 3% $^{239}Pu)Cl_3$ - 60% mol + $PbCl_3$
• Average fresh fuel composition Th:Pu:^{99}Tc weights ratios		35:1.1:1.85
• Isotopic composition of Pu		100 % Pu^{239}, no TRU
• Isotopic composition of LLFP		100 % Tc^{99}
System Characteristics :		
• k_{eff}		0.85
• Thermal power in core		5000 MWt(t)
• Power density : average max	W/cm^3	40 / 70
• Neutron flux average in core	n/cm^3	2×10^{15}
• Residence fuel (target) time (full power years)		50
• Burnup reactivity swing	(% δk/k/365 EFPD)	0.003
• Burnup	% h.a.	45
• Reloading interval	(full power years)	10

The high accelerator current is closely related to the relatively high subcriticality.

As far as the molten salt core, the height z = 600 cm was chosen both to account for the penetration of the proton beam and to allow the molten salt natural convection. In that case one can envisage the keep the pressure at the atmospheric level (which is favourable for the beam / target interface technology). However, more technological studies will obviously be needed.

4 - SYSTEM PERFORMANCES

The fuel inventory and transmutation, together with a full mass balance over a 10 year irradiation cycle, is given in table 2.

Table 2. Fuel and transmutation material inventory and mass balance

Nuclides	Mass balance in EOC (after each 10 years) L-loading	U-unloading	Transmutation capability U-L kg/MWt(t)y
FUEL			
Thorium-232	35500	16700	- 0.38
Uranium			
U-233	-	1970	+ 0.039
U-234	-	570	+ 0.011
U-235	-	110	+ 0.0022
Plutonium			
Pu-238	-	5.7	+ 0.00011
Pu-239	1100	7.4	- 0.022
Pu-240	-	40	+ 0.0008
Pu-241	-	4.5	+ 0.00009
Pu-242	-	2.5	+ 0.00005
Americium			
Am-241	-	4.1	+ 0.00008
Am-242m	-	0.27	+ 0.000005
Am-243	-	0.75	+ 0.00001
Curium			
Cm-242	-	0.1	+ 0.000002
Cm-243	-	0.01	+ 0.0000002
Cm-244	-	0.36	+ 0.000007
Cm-245	-	0.05	+ 0.000001
LLFP (Tc-99)	1850	680	- 0.023

The installation is able to transmute (during 50 years) 5.5 t of ^{239}Pu and 6.0 t of ^{99}Tc, with extremely low fuel toxicity and fuel inventory toxicity.

In fact the integrated toxicity of the fuel waste (R) for the time interval ΔT_S between $t = 10^2$ y and $t = 10^4$ y and for the time interval ΔT_L between $t = 10^2$ y and $t = 10^6$ y after unloading is :

$$R = 10^{4.2} \text{ Sv/GWt (e) . year (for } \Delta T_L)$$

$$R = 10^{5.0} \text{ Sv/GWt (e) . year (for } \Delta T_S)$$

with the following hypothesis on fuel losses during processing : 0.3 % for U, 0.5 % for Pu, 5 % for Np and TRPu).

The decrease factors d of the waste toxicity as compared to the feed fuel are :

$$d = 40 \text{ (for } \Delta T_L)$$

$$d = 1500 \text{ (for } \Delta T_S)$$

The fuel waste toxicity is decreased as compared to the LWR open cycle by factors d' :

$$d' = 800 \text{ (for } \Delta T_L)$$

$$d' = 10^4 \text{ (for } \Delta T_S)$$

5 - CONCLUSIONS

Source-driven subcritical hybrid systems can have a potential to transmute radioactive wastes when a large "excess" of neutrons is needed, as it is the case for the long-lived fission products.

However, one has to look in a more general way to the potential of these systems to reduce the long-term fuel cycle radiological risk.

Advanced technologies (long fuel burn-up, possibly molten salt fuel, sophisticated proton beam / target interfaces, etc) seem to be necessary, together with the use of new fuel cycles (like Th fuel cycle), to obtain significant improvements.

Moreover, the energy balance of these systems can impose rather severe economic constraints to their deployment.

6 - REFERENCES

1. Salvatores, M., Slessarev, I., Uematsu, M., Nucl. Sci. Eng., 116, 1 (1994).
2. Slessarev, I., Salvatores, M., Uematsu, M., *"Transmutation Potential of Current and Innovative Power Systems", Proc. of GLOBAL'93 Int. Conf.*, Seattle, 12-17 Sept. (1993).
3. Salvatores, M., *"A first approach to Data Needs and Target Accuracies for Hybrid Systems"*, Proc. Spec. Meeting on.
4. Kadi, Y., Wydler, P., *"Neutronic Analyses of Hybrid Systems with TRU Targets"*, Ibiden.
5. Salvatores, M., Slessarev, I., Uematsu, M., to be published.
6. Filges, D., et al., *"The HERMES code system"*.

An Overview of Russian Experience and Capabilities for Development of ATW/ABC Systems

Vladimir D. Kazaritsky
Institute for Theoretical and Experimental Physics, Moscow, Russia 117259

Abstract. Several Russian institutes are expected to undertake a feasibility study of nuclear power systems based on proton accelerators. The examined systems are intended for conversion of surplus Pu and transmutation of long-lived radioactive waste. This research motivated by the demilitarisation agreements and criticism of traditional nuclear power is focused on environmental protection.

INTRODUCTION

In the former Soviet Union the intensity and the scientific level of the research in the field of applying accelerator to nuclear power have been inadequately reflected in the limited publications on "accelerator breeding". But for a few short contributions to international conferences it was only in 1970 that the first public discussion of the concept of using a powerful accelerator in nuclear power took place [1,2]. Shortly afterwards all the work was suspended to be resumed only at the beginning of the 80s. At the end of the 80s this trend in research was given a new impetus due to the idea that an accelerator can be used in systems for transmutation of long-lived radioactive materials (mainly nuclear power waste) into short-lived and stable materials (ATW) and later due to a proposal on accelerator based conversion of surplus Pu (ABC) [3-4].

At present time Russian research laboratories have a considerable technical experience necessary for developing and demonstrating ATW/ABC technologies. The approaches to the problem, which are currently being developed at the Institute for Theoretical and Experimental Physics, are based on the latest achievements in designing high current linear accelerators. Since the achieved results have become widely known, in particular due to the proposal on RFQ [5,6], which influenced most design of modern accelerators, they will not be discussed here.

This paper is a brief summary of some Russian-developed technologies concerning the reactor part of hybrid assemblies of ATW/ABC type and handling of nuclear materials, fractionating and partitioning of radioactive waste included. Some perspectives of joint Russian institutes research are also dealt with.

REACTOR TECHNOLOGIES OF TARGET-BLANKET

Seeing that in future nuclear power small losses in the full cycle will have to be guaranteed it is vital to examine the alternatives, characterised by minimal radio-toxicity of the fuel cycle. The drastic means of eliminating the most radiotoxic waste of nuclear power (Pu and other transuraniums) would be their non-production in the fuel cycle. That would be possible in case of change to a thorium-uranium cycle. The possibility of converting thorium to good nuclear fuel - uranium 233 - with the help

of beams of accelerated particles creates a basically new situation for thermal neutron reactors on thorium-uranium cycle for it becomes possible to give up altogether the critical breeder reactors and use only reactors-converters with high fuel recovery (CR of about 0.8-0.9 would be enough for the purpose).

In the process of transition to the thorium-uranium cycle it will be necessary to burn down the accumulated plutonium and minor actinides Np, Am, Cm. There have already appeared designs of proton accelerator-driven facilities for burning down both military and power Pu [7-9]. The burning down of the transuraniums being the immediate task for the proposed accelerator-driven systems, it will be necessary for them to operate in future in a fuel cycle with a less environmental burden while ensuring :

1) burning down of Pu, minor actinides and most hazardous fission products,
2) fuel production for thermal reactors - uranium-233,
3) electricity production by means of burning uranium-233 with a high rate of fuel conversion from thorium.

The technological experience in developing thermal neutron reactors, accumulated in Russian laboratories, can lie at the basis of designing accelerator driven facilities with fluid (circulating) fuel, which can perform the above-mentioned functions. The reason for such a choice is primarily connected with the peculiarities of the process of burning down military and power plutonium, minor actinides and the most hazardous fission products.

Heavy-water systems

Touching upon the Russian experience it is necessary to mention that the prototype of a heavy water power reactor of a channel type with the power of the 450 MWt and 150 MWe was made by ITEP's design and operated successfully for nearly 5 years [10]. The problems of using heavy water as a moderator have been completely solved. However, fuel on heavy-water carrier needs further consideration in spite of a great research and pilot data that have already been accumulated.

ITEP has proposed a design of a heavy water blanket with circulating fuel [11,12]. A lattice of power channels is placed inside a cold heavy water tank under normal pressure. The channels made of proven Zr-Nb alloy isolate the fluid fuel from the moderator and keep it constantly exposed to irradiation. Inside each channel there are two loops : a fuel loop (solution or slurry in heavy water) and a loop of pressurised heavy water coolant. The latter cools the fuel circulating in the channel while the fuel is continuously fed and removed in small portions for chemical reprocessing. After reprocessing the actinides come back to the fuel loop, while the remainder is fractionated and further sent for transmutation or storage and burial.

The heavy water fuel carrier in the channel is both heat depositing and cooling. Thus the changes in the temperature under power fluctuations are not too abrupt due to big heat capacity. An optimisation of the composition, structure, sizes and other parameters of the channel can make it possible to achieve negative coolant-void and temperature coefficients of reactivity.

A blanket with fluid fuel has an essential advantage of being loaded with fuel at a minimal level that can provide an excess reactivity only for compensating negative temperature and power reactivity changes as well as equilibrium poisoning by fission products, the latter depending on power density and the rate of fuel regeneration in the blanket. Small loading may considerably reduce the possibility of forming secondary critical masses under accidents while it may exclude introduction big positive reactivity.

Radiation safety for reactors with fluid fuel is provided by the same means as in the traditional nuclear power, namely by security in depth and control. The radiation situation in the suggested system can be improved, since on the one hand activity of the fission products is lessened through the continuous removal of the irradiated fuel for reprocessing, and on the other hand there is no need to open the reactor for reloading, as the fluid fuel channels will be produced in the form of separate modules. In order to replace the channels-modules the reactor should be stopped and the fuel removed. Lack of the swelling of the fuel makes it possible to provide better operation conditions. A better quality control can be achieved in fabricating fuel channels. All this must exclude fission products and fuel getting into the coolant.

It is assumed [11,12] that the concept of a fluid fuel channel with in-core circulation is universal enough to be used for the solution of all the three above-mentioned problems: burn-down of Pu, production of new fuel and burning of this fuel to generate electricity. The difficulties that may arise in realising the heavy water systems are primarily connected with radiolytic gas releases. The fission energy in heavy-water fuel mediums is released in the water in the form of kinetic energy of fission products, resulting in the high yield of molecular products of radiolisis with the negligible role of recombination of deuterium and oxygen.

There is some evidence, however, that in homogeneous fuel it may be possible to suppress radiolytic gas production completely with the help of some soluted substances, in particular, salt of bivalent copper which acts as a homogeneous catalyst for recombination of deuterium and oxygen in water solutions of fissionable nuclides. The rates of radiolytic gas recombination were determined for oxide suspensions [12,13]. By the estimates, made in ITEP, in the density of bivalent copper not exceeding 0.1 mole/l the macroscopic cross section of neutron capture is 2.2×10^{-4} cm^{-1}. Technologically acceptable concentration of soluted deuterium is equal to its partial pressure 1,0 MPa. If heavy water solutions are used the permissible power density is 20 kW/l at temperature 250 C and 130 kW/l at 300 C. If heavy water slurries are used the values would be 100 kW/l and 260 kW/l accordingly, which would allow for radiolytic gas production to be entirely suppressed.

Liquid Metal Cooling

In Russia considerable experience has been accumulated in constructing reactors with liquid metal cooling. The specific power in the target of an accelerator driven facility can be no less than the specific power of reactors with liquid metal cooling provided high level neutron fluxes are designed to be achieved (of about

$10^{15} - 10^{16}\, n / cm^2\, sec$). The use of liquid Pb or its alloys makes it possible to simultaneously generate neutrons and cool the target. It also offers the advantage of inserting a proton beam into the facility without a special diaphragm, separating the liquid metal from the beam transport channel of the accelerator. The Institute of Physics and Power Engineering (IPPE, Obninsk) has an experience in commercial scale reactors cooled with Pb-Bi (the reactor operation time - 100 reactor-years). On the developed research base integral experiments on the thermohydraulics of Pb-Bi loops have been carried out. Computer codes of hydrodynamic flow and heat exchange have been developed and tested for predicting velocity temperature fields in loops of real geometry.

Construction materials and technologies of ensuring the quality of the coolant have been developed. The corrosion resistance of the materials is ensured by protective oxide layers (films), formed and sustained on the surfaces exposed to the alloy. The developed technologies prevent both the dissociation of the films and their gaining excessive thickness. A continuous decontamination of the coolant from impurities is ensured. The problems of the mass transfer of the impurities, corrosion products and their compounds in the coolant have been investigated. Data have been obtained on corrosion-erosion resistance, physico-mechanical, thermal and radiation stability of different steels in the coolant depending on the operation conditions (temperature, flow rate, temperature drop, concentration and composition of the impurities in the loop).

The results of this work made it possible to choose construction materials for long-term operation of the loops at temperatures up to 600 C. Structural and phase changes as well as mechanical stress arising from freezing the coolant in the loop have also been studied. There is also a technology of melting and refrigerating the coolant in the loop, which prevents damage to the loop that may be caused by its periodical "freezing" and "defreezing".

A contribution to the radiation safety has been made by research of physico-chemical mechanisms of the formation of gas-aerosol activity over the free surface of the coolant. Using the experimental data Po expansion into vacuum and gas filled rooms over the liquid metal has been simulated. There have been developed ways and means of ensuring radiation safety of repairs, connected with the opening of the loop, decontamination of the equipment and the building after the repairs or emergency leakage of the coolant.

The Technology of Molten Salt

Though the fixed fuel reactors continue to be viewed in Russia as a basis for nuclear power in the immediate future, the possibilities of liquid fuel reactors have been closely examined. The main problem of liquid fuel is connected with the circulation of a big volume of radioactive fuel-coolant in the reactor loop. An attempt to solve this problem for the heavy-water carrier with the help of a in-core heat exchanger was described above. In the proposed fluid fuel channels the fuel circulates inside the irradiation core and does not enter the external heat exchanger for cooling,

while the fuel heat is removed with the help of pressurised coolant. Such a way among other advantages provides reduction of fuel leakage risk.

Besides fuel leakage accidents accompanied by loss of circulation in the first loop may present a serious danger. However, this danger can be diminished for accelerator driven systems, since their blanket is subcritical and, besides, the beam can be quickly shut down. There still remains the problem of reactor after-heat, which may be solved by a regime of the free circulation of the fuel. It is this trend of research that is being developed in Russia at the Kurchatov Institute of Atomic Energy (IAE, Moscow) [14]. Since 1976 an all-round study has been performed to substantiate the expediency and efficiency of using molten-salt reactors (MSR) in breeder and converter regimes in the nuclear power of the country. The potentialities of constructing MSR with the help of the technologies that had been developed in the country were demonstrated in research reactor and laboratory experiments which included :

- developing and testing construction materials of the first and intermediate loops;
- testing a technology of high temperature fluoride coolant;
- investigating radiation resistance of fluoride fuel compounds;
- investigating the chemical processes of removing U and Pa from the fuel compounds.

An analysis of safety problems shows that in MSR it may be possible to achieve ultimate safety. Study of the efficiency of free circulation of the molten salt fuel-coolant $(LiF - BeF_2 - ThF_4 - UF_4)$, as compared to Na, Pb and water, reveals great potentialities of the molten salt for the free circulation regime of operation. That is connected both with the thermal characteristics of the salt (density, heat capacity, heat expansion coefficient) and the greater admissible temperature drop of the liquid between the heating and cooling zones in normal and emergency conditions.

A potential use of the molten salt technology for the target-blanket of an accelerator-driven facility was studied in Japan [15]. It was suggested that the identical salt compound be used both for the target and blanket and that all solid materials, mainly graphite, be removed from the radiation zone. Upon this concept calculations were made in ITEP for U-233 yield and Pu transmutation rate for several salt compounds [16]. Among the advantages of such a homogeneous molten salt target-blanket there are a relatively small quantity of the stored non-nuclear energy, the minimal quantity of construction materials in the radiation zone, and finally the minimal hydraulic resistance, which is beneficial for the free circulation regime and eventually increases the safety and reliability of the facility.

FUEL REPROCESSING

Accelerator-driven facilities with fluid circulating fuel make it possible to create the most room-saving technology of handling the irradiated fuel, which is vital for effective transmutation. The system's characteristics allow to remove from the fuel just the poisoning fission products. The result is the smallest possible volume of the waste as compared to all the other existing systems for fuel processing.

At present time in Russia there exist commercial scale recycling of fissile materials (uranium, plutonium), extraction and isolation of neptunium (for production of Pu-238). The first plant for processing the fuel of VVER-440 was built in Chelyabinsk [17], another one is under construction in Krasnoyarsk for the fuel of VVER-1000. By 2000 the plant will be able to process 650 tons of spent fuel a year [18]. The processing of the fuel is based on the aqueous-extraction technology, with tributyl phosphate in some organic solvent used as the extractant. The resulting flow of the so-called high-level waste (HLW) contains transplutonium elements and fission products. The fractionating of HLW, i.e. the extraction of the elements with different nuclear and radioecological characteristics (decay type, life time, capacity for leaching and migration in the environment, toxicity), has been developed as a necessary stage of radioactive waste treatment. Fractionating is regarded as a stage prior, to incorporation of the waste in clays, glasses, or synthetic minerals it to be stored or buried, for different components of HLW have life times ranging from dozens to hundreds of thousands years and are selective as regards immobilising materials and storage conditions.

At present time there exists a process of fractionating transplutonium and rare-earth elements with further partitioning of the two as well as a process of isolation of the relatively short-lived strontium and cesium. Developed fractionating is vital for transmutation which requires partitioning of the discharged products into those, going back for transmutation, and the stable and short-lived transmutation products, removed from the cycle.

Though the traditional approach, which rests on fixed fuel elements, assemblies and targets, can be realised on the basis of the existing in Russia experience in producing nuclear fuel and its reprocessing, it may face considerable difficulties on all stages. The presence of transmuted elements will increase radiation and heat production, will aggravate the problem of nuclear safety.

Nowadays the evident way to minimise the secondary waste from a fuel cycle of transmutation and fractionating is to use the aqueous technology of fluid fuel with a nitrate solution loop, whose blanket may be designed as described in the section about the heavy water technology. Contrary to the fixed fuel technology there is only one problem left, that of transfer of actinide nitrates from the flow, formed after the fractionating of HLW of the PUREX process, into the heavy water loop of the blanket and back for regeneration [19]. The Institute of Non-Organic Materials (VNIINM, Moscow) suggests transfer technologies providing minimal mutual penetration of the light and heavy water flows [20]. The simple procedure of evaporating the blanket solution till dry residue, returning the condensate to the fluid fuel channel and solving the residue in light water is considered impractical since the residue produces power and contains concentrated fissile materials.

Slurries (stabilised oxide suspension), considered on a par with the nitrate solutions for introducing transmuted components in the fuel, must lead to the formation of salt wastes from conversion of chemical forms. However, in this case transfer of the transmuted components from the light water medium to the heavy water loop of the blanket will surely be simplified. Treating the molten salt blankets as an alternative to the heavy water blankets, it is necessary to realise that on a

commercial scale there exists only the fractionating technology based on aqueous extraction methods (mainly, on processing the nitrate solution of the PUREX process). In order to prevent formation of secondary waste in the form of salts, contaminated by radionuclides, the classical PUREX methods will have to be rejected and methods of pyrochemistry will have to be applied [21].

In 1968-72 at the Institute of Atomic Reactors (NIIAR, Dimitrovgrad) volatilisation of UF_6 and PuF_6 was investigated at the FREGAT assembly. An experimental load of 15 kgs of the spent UO_2- fuel of the experimental reactor was processed. In 1973 four kgs of the same fuel were processed in the medium of molten chlorides with the help of a pyrochemical method. In 1986-1989 the pilot plant with the designed capacity of 1 ton of the MOX fuel a year was reconstructed [22]. The data on the problem at issue, that have so far been accumulated, refer mainly to the use of fluorides in molten salt reactors on $LiF - BeF_2$ base with Th-U fuel. The missing data on solubility of fluorides of Np, Pu, Am, and Cm with their thermal dynamics characteristics can be partially compensated by calculations.

In NIIAR several schematic diagrams of the external fuel cycle of an accelerator driven facility fuelled with molten salt were worked out : a plant with a full fuel processing of the fuel flow, a plant with a partial fuel processing and a plant, removing only gases and volatile fission products from the fuel. The suggested diagrams take account of the realisable technological approaches to removing gas and volatile products from the fuel, which were developed in the 60-70s at the Oak-Ridge laboratory (USA). Some other of the included technologies must be proved experimentally. NIIAR offers to demonstrate the fuel cycle of ATW/ABC type assembly on molten $LiF - BeF_2$ fuel.

NUCLEAR AND OTHER DATA

For the purposes of the described project the Institute of Experimental Physics (VNIIEF, Arzamas-16) and the Institute of Technical Physics (VNIITF, Chelyabinsk-70) intend to work out system requirements and constraints, including a classification of the materials to be used and the products of their treatment with respect to their potential danger for non- proliferation of nuclear weapons and for developing facilities with a heavy environmental burden. An analysis will be performed of the potentialities of the facilities for recycling the materials into weapons programs even in the owner countries. VNIIEF,VNIITF, ITEP, FEI and Radium Institute (RI, St. Petersburg) are planning a joint program for augmenting the nuclear data : measurement of neutron and proton cross sections for transmutation, measurement of nuclide yields from particle radiation, measurement of the damages of materials, development and extension of related libraries and catalogues. Several suggestions on the target-blanket design, including the concept of the multisectional structure of the blanket, based on the idea of coupled reactors, will be tested in integral experiments [23].

The proposed studies are focused on the role and behaviour of Pu in an accelerator driven power system. The project concerns proton beams of 40 to 400 MW power. The current and energy parameters range from 50 to 200 mA (cw) at 800

to 1600 MeV. Such high power of the beam can only be provided by a linear accelerator, many times more powerful than the existing installations. The accelerator performance, target-blanket physics, chemical processing requirements and overall systems engineering must fit well in determining the economic incentives for ABC and ATW. Preliminary estimates of and insight into the economics of Pu conversion, transmutation of nuclear waste and a net-power-producing ATW will be provided by the Institute of Research and Design of Energo-Engineering (VNIIPIET, St. Petersburg). Comparison with the routine reactor systems will be performed with due regard for the cost of ensuring guaranties of environmental safety and the cost of non-proliferation and terrorism prevention.

CONCLUSION

The presented achievements are a technological background for a feasibility study of technologies for accelerator-based conversion of Pu and long-lived radioactive waste. Studies will include accelerator developments, a detailed protonics and neutronics analysis of target-blanket, the system's thermal hydraulics, its mechanical and structural analysis etc. The project will cover extensive calculations on the options, determination of an optimal system for safe incineration of power and weapon-grade Pu and efficient conversion of the heat to electricity. The quality of the chemical processes is deemed to be decisive for the success of the entire project. The on-line removal of fission products and continuous fuel regeneration are to be examined. The non-proliferation measures will be studied for the whole of the transmutation cycle. Recommendations will be given for a disposal of the low-level activity waste.

ACKNOWLEDGMENT

The author would like to thank his colleagues from LANL (USA) who initiated the project and also his colleagues from the Russian institutes for helpful discussions.

REFERENCES

[1] Vasilkov R.G.,Goldanskii V.I.,Dgelepov V.M.,Dmitrievskii V.M., Atomnaya Energiya **29**, N3, 151-158 (1970).
[2] Davidenko V.A., Atomnaya Energiya **29**, N3, 158-162 (1970).
[3] Blagovolin P.P., Dubinskii V.D., Kazaritsky V.D. et al, Atomnaya Energiya **65**, N5, 326-329 (1988).
[4] Blagovolin P.P., Kazaritsky V.D., Kiselev G.V. et al, Atomnaya Energiya, **70**, N6, 380-386 (1991).
[5] Kapchinskii I.M.,Teplijakov V.A., Pribory i Tekhnika Esperimenta, N2, 19-22 (1977)
[6] Kapchinskii I.M., Pribory i Tekhnika Esperimenta, N4, 23-25, (1977)
[7] Cappiello M., Ireland J., Sapir J., Krohn B. "Los Alamos Aqueous Target/Blanket System Design for the Accelerator Transmutation of Waste Concept", In Proceedings of International Conference and Technology Exhibition on Future Nuclear Systems : Emerging Fuel Cycles and Waste Disposal Options, September 12-17,1993, Seattle,Washington,V.1, 397-401.

[8] Jensen R.J., Trapp T.J., Arthur E.D., Davidson J.W., Linford R.K., ibid.,V.2, 833-841.
[9] Venneri F., Bowman C., Jameson R., "Accelerator Driven Transmutation of Waste (ATW) : A New Method for Reducing the Long-Term Radioactivity of Commercial Nuclear Waste", Preprint LANL, LA-UR-93-752, Los Alamos, 1993.
[10] Abramov V.M. et al, Keger J. et al,1974 Atomnaya Energiya, **36**, N2, 113-125 (1974).
[11] Kazaritsky V.D, Blagovolin P.P., Zolotarjeva E.A., Mladov V.R., Nicolaevsky E.S., Okhlopkov M.L., "Plutonium-Doped Incineration of Minor Actinides in Fluid Fuel Elements of Accelerator Driven Heavy Water Blanket", Moscow, Preprint ITEP, 1993, N72.
[12] V.D.Kazaritsky, P.P.Blagovolin, V.R.Mladov, M.L.Okhlopkov, E.B.Strakhov, "Problem of Fluid Agent for Blankets with Fuel Circulation", Moscow, Preprint ITEP, 1994, N20.
[13] Byakov I.M., Nichiporov F.G., Radiolis vody v yadernykh reaktorakx, Moscow, Energoatomisdat,1990, ch 3, pp 129-138.
[14] Novikov V.M. et al, Zhidkosolevye YEU : pespektivy i problemy, Moscow, Energoatomisdat, 1990, ch 5-8.
[15] Furukawa K., Tsukada K., Nakahara Y., Journal of Nuclear Science and Technology, **18**, №1, 79-87, (1981).
[16] Kazaritsky V.D., Furukawa K., Kiselev G.V., Hirakawa N., "Practical Treatment of Minor Actinides by Single-Fluid Molten Salt Reactor Concepts", in Proceedings of International Conference on Design and Safety of Advanced Nuclear Power Plants, October 25-29, 1992, Tokyo,V.1, pp.P3.8-(1-5).
[17] Nikipelov B.V., Kudryavtsev E.G., Egorov N.N. et al, "On the Management of Radioactive Wastes in the Community of Independent States; Problems of Long-Lived Nuclides and Partitioning", in Proceedings of the Symposium on Waste Management, Tucson, Arisona, March 1-5, 1992,V.1,p.19-22.
[18] Romanovskii V.N., Galkin B.Ya., Lazarev L.N. et al, "New Appoaches to Reprocessing in Russia", in Proceedings of International Conference and Technology Exhibition on Future Nuclear Systems : Emerging Fuel Cycles and Waste Disposal Options, September 12-17, 1993, Seattle,Washington,V.1,pp. 71-77
[19] Kazaritsky V.D., Blagovolin P.P., Volk V.I., Vakhrushin A.Yu., "Nuclear Power Systems Based on Accelerator and Fluid Fuel Technologies" ibid, V.1, pp.229-231.
[20] Volk V.I., Zakharkin B.S., Vakhrushin A.Yu. et al, "Optimization of PUREX-Process Aimed at Volume Reduction of Aqueos Waste from NPP Spent Fuel Reprocessing", in Proceedings of International Conference on Nuclear Waste Management and Environmental Remediation, Prague,1993, V.1, pp.673-679.
[21] Skiba O.V., Savochkin Yu.P., Bychkov A.V. et al, "Technology of Pyroelectrochemical Reprocessing and Production of Nuclear Fuel", in [30], V.2, pp. 1344-1350.
[22] Skiba O.V., Mayorshin A.A., Porodnov P.T., Bychkov A.V., "Nuclear Fuel Cycle Based on "Dry" Methods for Fuel Reprocessing and Fuel Elements Manufacture Automated Processes" in [30], V.2, pp. 934-942.
[23] Kolesov V.F., Guzhovski B.Ya., "On Possible Improvement of Efficiency of Electronuclear Transmutating Device on the Base of Going over to the Multisection Structure of the Blanket", Arzamas-16, Preprint VNIIEF, 1993,N 27.

On the ATW- concepts: ITP Approach and Opportunities

V.A. Simonenko, K.F. Grebyonkin
Theoretical Division, Institute of Technical Physics
P.O. Box 245, Chelyabinsk-70, 454070, Russia
Phone: (351-72)-32930 *E-mail: sva@ch70.chel.su*

Abstract. It is discussed the interest of Russian Federal Nuclear Center - Institute of Technical Physics at Chelyabinsk-70 in the research of Accelerator Driven Technologies applications for radioactive waste transmutation, cumulated actinides burning, energy production. The ITP background and opportunities for this research are presented. It is shown the ITP possibilities for testing and experimental development of Accelerator Driven Technologies.

THE ITP INTERESTS

One of the most important directions for diversification of scientific and engineering activity of the Russian Federal Nuclear Center - All-Russian Scientific Research Institute of Technical Physics (ITP) at Chelyabinsk-70 is research of perspective technologies of nuclear energy production for civilian needs, and exploration and development of technologies for treatment of civilian and military nuclear waste and accumulated actinides. The specialists fulfill conceptual comparative studies of perspective alternative nuclear directions for energy production such as

- use of explosion energy, yielded by special nuclear devices in large strengthening underground chambers equipped by technical facilities for energy transfer and radioactive waste treatment (e.g., [1]),
- thermonuclear energy production by magnetic confinement systems like ITER or similar (e.g., [2]),
- inertial confinement fusion systems under impact of powerful lasers or charged particles beams (e.g., [3, 4]) etc.

Our specialists involved in various problems of nuclear waste treatment. Their activity embrace development of traditional technologies, estimation of long-term scenarios of behavior for burial radioactive materials in temporal storage and stationary repositories located in various climatic conditions and different geological formations [5,6].

In this respect, the Accelerator Driven Technologies (ADT) proposed and developing by specialists of Los Alamos National Laboratory (e.g., [7,8]) have a great interest for the ITP in spite of limited experimental opportunities of the Institute.

The problems of Accelerator-Waste-Transmutation (ATW) technology is attractive for the ITP in two aspects. The ITP has long-termed general interest in research of wide-scope problems on various directions of nuclear energy production including non-traditional and acute aspects of energy production technologies such as waste treatment, thermal consumption, material properties etc.

We are interested in estimation of different conceptual aspects and approaches of ATW technology and its adjacent perspective applications such as high intensive neutron sources [9] for material study or special blanket system for tritium production [10], in search of optimal solutions for the technology components. In particular, we are developing an original proposal for target-blanket system with active core [11].

EXPERIENCE AND OPPORTUNITIES

On the specific aspect for ATW concept the ITP has an experience and opportunity to facilitate the solution of several key problems. These opportunities include conceptual evaluation and choice of separate subsystems of the ATW technology, theoretical design of some subsystems, development of physical models and mathematical codes for target physics, thermophysics etc., material properties research, neutron processes experimental verification for fast neutron moderation, neutron data corrections for separate materials and required energy range, data-bank creation for material properties, neutron data and kinetic characteristics of the processes, data-base for bench-mark experiments, technical design works for several subsystems, experimental verification for several technological processes, experimental modeling and testing facilities for separate subsystems of ATW technology.

More efficient fast reached results can be obtained in the following areas.

1. Physical models, numerical methods, mathematical codes and numerical simulation for

- neutron and other particles transport (Monte-Carlo and finite-difference methods),
- hydrodynamics coupled with neutron transport,
- nuclear burning simulation coupled with neutron transport.

To provide complete simulation of target-blanket systems we ought to develop our codes to add the proton-nuclei interaction, to broaden energy range for neutron cross-sections, to verify and improve neutron cross-sections for some actinides and fission fragments.

2. The use of experimental facilities of the Institute, specifically

- pulsed nuclear reactors with metal and solution cores,
- different critical assemblies,
- tritium handling subsystems,
- material testing facilities, in particular for tritium saturated systems.

All these facilities can be fitted directly to the ADT separate problems solution.

3. Technical design and experimental mock-up of target-blanket composition and its separate subsystems using the experience of our personal in design of facilities and devices with radioactive material, in distance electronic control systems, diagnostic systems etc.

4. Technological testing and development of separate processes on active blanket core, energy outflow, material separation and processing.

THE ITP PROSPECTS

The program for ATW activity can be essential part of works on diversification of our Federal Nuclear Center. It corresponds the experience and opportunities of our scientists, engineers, and separate facilities in many aspects. There is no direct financial support of the program by Russian Government however and it hardly be expected in essential degree during nearest future. On this reason the work can progress mainly under condition of stationary funding by foreign sources. It can be conducted by means separate contracts on specific directions of the ATW as mentioned before. We have two contracts now with the LANL and Grumman. We are in the initial stage of works on joint contract for the International Science and Technology Center in Moscow together with the Institute of Theoretical and Experimental Physics (Moscow), RFNC - Institute of

Experimental Physics (Arzamas-16) and other institutions. However all these contracts are small and can not embrace all the directions of possible effective activity on the ATW in the ITP which was mentioned before.

Besides the use of existing facilities there are opportunities for more wide experimental research on the base of the ITP and other institutions in cooperation with the ITP. There is under construction in the ITP of Multi-channel Pulsed Graphite Reactor - MPGR (MIGR in Russian abbreviation) [12]. Its core of 370 cm high will have main channel of ~60 cm in diameter. Maximum neutron fluence will be of $3 \cdot 10^{17} n/cm^2$. Beside the set of reactor safety experiments the reactor can be used for testing of separate loops of the ATW target-blanket, material properties research etc.

Another opportunity will be given by our close collaboration with Productive Combine "Mayak" (Chelyabinsk-65) on the base of heavy-water reactors.

For the success of the ATW works in the ITP it is highly important to have a program of long-term activity for our specialists on the project. On this reason, besides the separate small-scale contracts, we need to have the long-tern end-goal aimed plan on ATW technology.

ACKNOWLEDGMENT

We are thankful to our colleagues from LANL Drs. E.D. Arthur, E. Highway for attraction of our attention to the ADT perspective and fruitful discussions on separates aspects the concepts, technologies, and their applications. Different problems of ADT were widely discussed with specialists from experimental and design divisions of the ITP. All the works are supported by the ITP Scientific Director Academician E.N. Avrorin and Minister of MAE RF Professor V.N. Mikhailov. We highly grateful to all our colleagues.

REFERENCES

[1] Ivanov, G.A., Shibarshov L.I., "Ecologically Safe Deuterium Power-Plant", Preprint ITP #25, 1992.

[2] Karlykhanov, N.G., Litvinenko, I.A., Matveenko, Yu.I., Martynov, Yu.V., Moscovkin, P.G., Politov, V.Yu., and Simonenko, V.A., "Interaction of ITER Plasma Flow with Solid Targets", Preprint ITP #68, 1994.

[3] Avrorin, E.N., Feoktistov, L.P., Bunatyan A.A., and Lykov, V.A., "On Hybrid Reactor for Laser ICF", *Quantum Electronics* 5, #2, 349-358 (1978).

[4] Avrorin, E.N., Bunatyan, A.A., Lykov, V.A., and Strotseva, L.S., "Targets and Parameters Laser Installations Burn-up and Hybrid Reactor", *Pis'ma v ZhETF* 32, #7, 457-460, 1980.

[5] Simonenko, V.A., Chernukhin, Yu.I., Shybarshov, L.I., "Concepts on Containment and Terminal Liquidation of Radioactive Waste and Special Equipment", ITP Report, Chelyabinsk-70, 1991.

[6] Simonenko, V.A., Vasil'ev, A.P., and Shubin, O.N., "Burial of Toxic Chemical Waste or Their Controlled Destruction with the Help of Underground Nuclear Explosions", ITP Report, Chelyabinsk-70, 1991.

[7] "A Loss Alamos Concept for Accelerator Transmutation of Waste and Energy Production", Los Alamos Report LA-UR-90-4432, December 1990.

[8] Lawrence, G.P., Jameson, R.A., and Schriber, S.O., "Accelerator Technology for Los Alamos Nuclear-Waste-Transmutation and Energy production Concepts", Los Alamos Report LA-UR-91-2797.

[9] Arthur, E.D., "Comparison of Accelerator-Driven Intense Neutron Sources and Reactors for Various Applications, Los Alamos Report LA-UR-92-2453.

[10] Wangler, T.P., Lawrence, G.P., Bhatia, T.S., Billen, J.H., Chan, K.S.D., Garnett, R.W., Guy, F.W., Liska, D.J., Nath, S., Neuschaefer, G.H., and Shubaly, M., "Accelerator Production of Tritium: Physics Design Challenges", in *Proceedings 1990Linear Accelerator Conference*, Los Alamos Report LA-12004-c,553 (March1991).
[11] Grebyonkin, K.F., An Active Target for the Accelerator-Based Transmutation System, in *Proceedings of International Conference on Accelerator-Driven Transmutation Technologies and Application,* 1994.
[12] Avrorin, E.N., and Vasil'ev, A.P., Pavshuk, V.A., Kiryushkin A.I., and Sikharev Yu.P., Main Research Goals for Multi-channel Pulsed Grapgite Reaktor MIGR", Paper for Meeting of American Nuclear Society, December 1994 (to be publishrd).

Accelerator-Driven Nuclear Synergetic Systems - An Overview of the Research Activities in Sweden

H. Condé*, A. Bäcklin**, S. Carius**, E. Traneus**,
W. Gudowski†, E. Möller†, T. Thedéen††,
J-O Liljenzin†††, M. Skålberg††† and M. af Ugglas††††
C. Mileikowsky¤, E. Tenerz¤, K. Hannerz¤, C. Sundqvist¤ and Ch. Pind¤

** Department of Neutron Research and **Department of Radiation Science*
Uppsala University, Box 535, S-751 21 Uppsala, Sweden
† Department of Neutron and Reactor Physics and ††Centre for Safety Reseach
Royal Institute of Technology, S-100 44 Stockholm, Sweden
†††Department of Nuclear Chemistry,
Chalmers University of Technology, S-412 96 Göteborg, Sweden
††††Manne Siegbahn Laboratory, S-106 91 Stockholm, Sweden
¤Drottninggatan 101, S-113 60 Stockholm, Sweden

Abstract. The rapid development of the accelerator technology which enables the construction of reliable and very intense neutron sources has initiated a growing interest for acceleratordriven transmutation systems in Sweden. After the Specialist Meeting on Accelerator-Driven Transmutation Technology for Radwaste and other Applications on 24-28 June 1991 at Saltsjöbaden, Sweden the research activities oriented towards accelerator-driven systems have been started at several research centres in Sweden. Also the governmental agencies responsible for the spent fuel policy showed a positive attitude to these activities through a limited financial support, particularly for studies of the safety aspects of these systems. Also the nuclear power industry and utilities show a positive interest in the research on these concepts.

The present paper presents an overview of the Swedish research activities on accelerator-driven systems and the proposed future coordination, organizations and prospects for this research in the context of the national nuclear energy and spent fuel policy. The Swedish perspective for international cooperation is also described.

BACKGROUND

At present, about 50 percent of Swedens electrical power or about 70 TWh is generated yearly by 12 nuclear power reactors. The reactors are located at 4 different sites along the coast of Sweden, two at the North Sea and two at the Baltic Sea. All of the reactors are light water moderated of which 9 are of the boiling water type (BWR) built by the ABB-ATOM company and 3 of the pressurized water type (PWR) built by Westinghouse. The oldest reactor (Oskarshamn #1) went commercial in 1972 and the newest one (Forsmark #3) in 1985.

The Government, which came into power after the election in 1976, asked the utilities to present a safe method to handle the nuclear waste before any licenses could be given to start up the remaining reactors being in a construction phase at that time. The utilities established the Swedish Nuclear Fuel and Waste Management Company (SKB) which, since then, runs the R&D program for waste managements. In the middle of the 70-ties, a safe method involving reprocessing followed by a geological deposition was investigated. Later, the SKB presented a method with a direct deposition of the high level radioactive waste deep in solid rocks which was generally accepted by the Government. The method is called KBS-3, named after the investigation made by the utilities.

A referendum about the use of nuclear power in Sweden was held in 1980 triggered by the Three Mile Island accident. The outcome of the referendum was a "no" to further building of nuclear power reactors. Subsequently, the Parliament decided that no more nuclear power reactors were to be built after the 12 reactors, of which 7 of them were in operation and the rest (5) were in

a more or less final construction phase at that time. Furthermore, it was decided that the reactors should be phased out at the latest in year 2010.

The R&D of SKB is paid from a special fund which is set up by the Government for the dismantling of the nuclear power reactors including the treatment of the high level nuclear waste. The fund is at present about 13 billion SKR (about 1.7 billion US $) and will amount to about 50 billion SKR at year 2010 (about 6.5 billion US $) and is created by charging the consumers of electrical power about 0.02 SKR/kWh. The research plans of SKB are updated each third year. The plans are screened by the the Swedish Nuclear Power Inspectorate (SKI) and are approved by the Government. The Government has also set up a consultative committee the "Swedish Consultative Committee for Nuclear Waste Management (KASAM)" which consists of members from the National Institute of Radiation Protection (SSI), the Nuclear Power Inspectorate (SKI) and leading Swedish scientists.

The Government pointed out in the comments to the last 3 years R&D plan of SKB in 1992 that the deposition of the waste should be arranged in such a way that the material can be taken in return. Furthermore, it was stated that SKB should keep track of alternative methods of handling the nuclear waste.

A big effort was needed by Swedish standards to implement the nuclear power and nuclear waste programs. As a result, a fair number of experts entered the field of nuclear engineering during a few decades of research and construction. At present, the expertise is not renewed in a speed to compensate for retirements, partly because of the impact of the nuclear power moratorium on the efforts to recruit students. This fact has been observed to be a threat against the present nuclear power program in Sweden and the universities have been asked to counteract this development.

With the twofold aim to find better methods for treating the high level nuclear waste which could be more easily accepted by the public than the geological deposition, and at the same time recruit students to the nuclear energy field, a national collaboration has been initiated on the research of accelerator based nuclear waste transmutation systems (ATW). The ambition to start research in this field was positively influenced by the Specialists' Meeting on "Accelerator-Driven Transmutation Technology for Radwaste and other Applications" which was held at Saltsjöbaden, Sweden on 24-28 June 1991.

RESEARCH COLLABORATION ON ATW

The research groups participating in the collaboration are from the Department of Neutron Research and the Department of Radiation Science, Uppsala University, the Department of Neutron and Reactor Physics and the Centre for Safety Research, Royal Institute of Technology (KTH), the Department of Nuclear Chemistry, Chalmers University of Technology (CTH) and the Manne Siegbahn Laboratory (MSL). Besides, a more industrial oriented group of reactor physicists, formerly at ABB Atom, and neutron physicists from Uppsala University and KTH have investigated the technical and economical possibilities to implement a nuclear reactor construction based on the concept which recently has been presented by C Rubbia et al. The combined research program of these different groups will cover most problem areas within the proposed systems for nuclear transmutation. Thus, it will also give a broad base for an educational program related to the nuclear energy field.

The main technical constituents of an accelerator based transmuter of nuclear waste are a high power accelerator, a target system to convert the charged particle beam from the accelerator to an intense neutron source and a blanket/core system that creates a neutron field which incinerates the waste in the core by neutron interactions. Furthermore, a chemical separation of the waste would be necessary, on-line or not, to efficiently burn the waste. A repository for the remaining short lived products from the transmutation process is also a part of the ATW concept technologies. The more general issues are safety and enviromental aspects and public acceptance.

There is competence in most of these research areas within the collaboration. Several of the research projects already in progress will be reported in separate contributions to this conference why only the main research field and a few examples of on-going research projects for each group is presented in the present report.

Department of Neutron Research and Department of Radiation Science
Uppsala University

Basic and applied experimental neutron and nuclear research at the Uppsala University is centred around two laboratories administrated by the University, namely the The Svedberg Laboratory (TSL), Uppsala and the Neutron Research Laboratory (NFL), Studsvik.

The main facilities of TSL is a cyclotron, a storage ring (CELSIUS) on-line the cyclotron and a tandem van de Graff-acclerator.The cyclotron can operate in an isochronous mode allowing acceleration of protons up to 100 MeV and heavy ions to $196Q^2/A$ MeV and in a synchrocyclotron mode which allows acceleration of protons to 180 MeV. Light ions are produced with an internal PIG ion source while heavy ions and polarized protons and deutrons are produced by an external ECR ion source and a Balzers/Pfeiffer polarized source, respectively. The storage ring CELSIUS is equipped with acceleration and electron cooling capabilities. It takes both light and heavy ion beams. The maximum proton energy is 1.36 GeV. The tandem is a High Voltage 6 MV EN-tandem mostly used for applied research as ^{14}C-dating, PIXE, ion-surface studies etc.

The NFL is located at the research reactors R2 and R2-0 at Studsvik. The main facility aside of the neutron diffractometers at the R2 reactor is an isotope separator on-line the R2-0 reactor (OSIRIS) for studies of nuclear structure and decay data for fission products and fission yields.

Measurements in progress or planned by different Uppsala groups of relevance for the research on the ATW concept at the TSL and NFL facilities are.

1. Fission yields of ^{233}U thermal fission and ^{232}Th fast fission at the OSIRIS facility at the R2-0 reactor, Studsvik.

2. Cross sections for residual nuclide production by proton- and neutron induced reactions in the energy interval from 70 to 180 MeV. Participation in collaboration with Universities in Hannover, Cologne, Kossuth Debrecen and Bordeaux-Gradignan, KFA Jülich and ETH Hönggerberg.

3. Cross section measurements of proton and neutron induced fissons of ^{208}Pb, ^{209}Bi and ^{238}U in the energy region 50 -180 MeV. Collaboration with the Khlopin Radium Institute, S:t Petersburg.

4. Cross sections of (n,p)-reactions and the n-p scattering in the energy region 100-160 MeV. Model calculation of intermediate energy reaction cross sections.

5. Research and development of measuring procedures and instrumentations for isotopic analysis of burned nuclear fuels.

The Uppsala group is also participating in an experiment at SATURNE, Saclay, France to study the neutron production in thin targets of several elements (Pb, Bi, W, Fe etc) between 0.6 and 2 GeV. The study is a collaboration between Centre d'Etudes de Bruyères-le-Châtel, Laboratoire National SATURNE, I.P.N. Orsay, Centre d'Etudes de Saclay, Collège de France Paris and Uppsala University.

A report about the LANL ATW and AXE concepts have been prepared on the request of the Studsvik ECO & SAFETY Co [1].

Department of Neutron and Reactor Physics and Centre for Safety Research Royal Institute of Technology (KTH)

Alternative nuclear fuel handling has been discussed within a working-group at KTH through a number of years. The group consists of about 25 experts of different disciplines as reactor physics, nuclear chemistry, physics, material sciences, hydrology, geology and risk analysis. The group has worked actively to broaden the interest for transmutation after the Conference in Saltsjöbaden in 1991. The Conference also initiated a study at KTH resulting in a report on "Acclerator Transmutation of Wastes. Safety and Prospects" which was published by the Swedish Nuclear Fuel and Waste Management Company (SKB) [2].

The prestudy resulted in a research project with the title "Safety analysis and neutronics safety problems in connection with accelerator-driven transmutation of nuclear waste with energy production", which is sponsered by SKB. The research program has at present the following components:

1. Safety analysis of transmutation systems

   a) Criticality
   b) Minimizing the amount of actinides in the system
   c) Neutronics for the ATW/AXE systems
   d) Calculation of fuel cycle and activation

2. Studies of waste streams and the change of those streams during irradiation

3. Analysis of a synergetic system containing transmutation and geological deposition

A large potential exist at KTH to enter other research areas as nuclear chemistry, material research, reactor technology, accelerator technology etc.

Research collaborations about transmutation concepts are at present established with the LANL Accelerator Operations & Technology Division, JAERI, Nuclera Fuel Development Corporation, University of Tokyo and CERN.

Department of Nuclear Chemistry
Chalmers University of Technology (CTH)

A research project was initiated at the Department of Nuclear Chemistry at CTH in 1976 to develop a process for separation of actinides from high level radioactive waste from the PUREX process. The project run for about 10 years time and resulted in the so called "CTH-process".

When the US and Japan separation and transmutation programs were presented around 1990 a new interest come into the field. This resulted in the creation of a new separation and transmutation project at the Department of Nuclear Chemistry at CTH which started in 1991. Initially, a comprehensive survey was made of national and international activities in the field [3]. Since 1993, the Department has started an own research project linked to the activities in other countries within the same research area.

The aim of the project is to study separation processes in cooperation with research groups in US, Japan and EU proposed for use in connection with nuclear transmutation. The project contains both experimental investigations as well as modelling of different separation systems. The project is mostly directed towards fundamental research and aim to help judging the realism of different proposed separation and transmutation processes.In particular, the proposed separation systems by LANL and within the OMEGA project in Japan will be screened.

A very important issue to get a reasonable reduction of radionuclides through transmutation is a high separation efficiency. In turn, this means that one has to have a good control over what happens in the separation process. The separation process has to be optimized which requires separation data for a number of different elements and a sensitive analysing technique. The most important elements are the actinides, which are long-lived and highly radiotoxics. The development of analysis techniques for the actinides is, for that reason, an important research area.

Collaboration has been established with LANL, JAERI and the Technische Universität Dresden.

Manne Siegbahn Laboratory (MSL)

The Manne Siegbahn Laboratory has a long tradition in accelerator design and operation. The present main accelerator facility at MSL is a 52-m circumference synchrotron storage ring called CRYRING [4]. It includes both an injection line for light ions, the MINIS separator, and a line for highly-charged heavy-ions, the INIS-CRYSIS electron-beam ion-source system. Intermediate acceleration is provided by a radiofrequency quadrupole structure, RFQ, and the quality of stored ions in the ring is improved by an electron cooler.

Within the collaboration the group at MSL has proposed studies of critical issues connected to the construction of high current accelerators. The issues involve studies of space-charge current-limitation in the low energy part of the accelerator and a minimization of the particle losses due to rest gas collisions in the vacuum system. Furthermore, the injection lines feeding CRYRING allow and can hence be used to investigate how to merge two beams into the RFQ as has been proposed for the high current ATW-facility at Los Alamos. Another research area of concern for the construction of a high power accelerator is ultra high vaccum technology. Experienced scientists in this area are available at both MSL and TSL.

MSL has the competence and experimental resources to measure nuclear reaction data of importance for the spallation concepts. A small van de Graff accelerator (2 MeV) is available near the CRYRING facility for this purpose.

The Industrial Group

As a first goal, this group of reactor and neutron physicists will investigate the technical and economical possibilities to realize a nuclear energy production facility based on the concept that recently was presented by C Rubbia et al. The strategy choosen by the group is to start with a LWR-construction and to just marginally modify the construction, with state-of-the-art technology, and if necessary supplement it with an autogenous rescue cooling system of the PIUS-type or similar. After this study is carried out the group will look into other concepts.

SUMMARY

The competence distribution of the proposed collaboration between the three universities and two national laboratories in Sweden on accelerator transmutation studies is schematically shown in table 1. The funding for the present activities are coming separately to the research groups from different governmental agencies and private industry. The intention for the future is to find a joined funding, at least, for the international collaborations and the PhD students linked to the program.

Tabell 1. Distribution of competence

University	Accelerator	Spallator		Separation	Safety
		N-source	Transm.		
CTH				X	
KTH		X	X		X
U.U.		X	X		
Nat. lab.					
TSL	X				
MSL	X				

REFERENCES

[1] A Bäcklin, S Carius and H Condé, "The LANL accelerator based nuclear waste transmutation (ATW) and energy generation (AXE) concepts", Studsvik ECO & SAFETY Report (to be published)

[2] W Gudowski, K Petterson and T Thedéen, "Accelerator Transmutation of Wastes (ATW)- Prospects and Safety", SKB Report 93-23 (1993)

[3] M. Skålberg and J-O Liljenzin, "Partitioning and Transmutation. A Review of the Current State of the Art", SKB Technical Report 92-19, October 1992 (A summary of the SKB report is published in Nuclear Engineering International, Febr 1993, p 30)

[4] K. Abrahamsson et al, "CRYRING - a Synchrotron, Cooler and Storage Ring,Proc.Conference on the Application of Accelerators in Research and Industry, Denton USA 1992, NIM vol B79 (1993) 269

SPECIFIC CONTRIBUTIONS of THE DUTCH PROGRAMME "RAS" TOWARDS ACCELERATOR-BASED TRANSMUTATION

K. Abrahams, W.M.P. Franken, J.H. Bultman, J.A. Heil, and A.J. Koning
Netherlands Energy Research Foundation (ECN), Petten, The Netherlands

Abstract. Accelerator-based transmutation is being studied by ECN within its general nuclear waste transmutation programme RAS. In this paper the following contributions are presented:
1) Evaluation of cross sections at intermediate energies, within an international frame given by NEA,
2) Cell calculations on the equilibration of transuranium actinides in thermal molten-salt transmuters,
3) Irradiation facilities at the European research reactor HFR in Petten, which have been constructed with the purpose to demonstrate and investigate the transmutation of waste in a high neutron flux,
4) Studies of accelerator-based neutron generating systems to transmute neptunium and technetium,
5) Comparison of several systems on the basis of criteria for successful nuclear waste-management.

THE DUTCH PROGRAMME RAS

In contrast to an OECD average of 25 %, The Netherlands produces only 5% of its required electricity by means of nuclear power. Exploitation of the apparent growth potential would require a broad acceptance of an appropriate waste management strategy. Deep geological disposal of the high level waste is considered, but due to the long half-life of some of the radionuclides, integrity of the isolation-barriers would have to be guaranteed for a period of at least 100.000 years. In order to study complementary options a research programme (RAS) on the recycling actinides and on the transmutation of long-lived fission products has been defined by ECN. One of the aims of this programme is the compilation and evaluation of various schemes proposed for reducing environmental risks. Within this RAS programme there is a small but significant study on the subject of accelerator-based transmutation and on its competing demands of safety, economy, and aspects of proliferation. Ref. [1] considers evolutionary scenarios on low-waste producing systems, the thorium/uranium cycle, and end-scenarios in which very large amounts of actinide waste are offered. The present paper treats more specific contributions:

Cross Sections at Intermediate Energies

On behalf of the design of systems for accelerator-based transmutation, contributions are given in the form of evaluations of cross sections at intermediate energies. Lead-208 is taken as a target material for a "sample evaluation" (ref. [2] and table 1), which fits as a benchmark of evaluation methods in an international frame given by NEA (Working Party on Evaluation Coordination of the Nuclear Science Committee). In earlier work [3] the most urgent data needs have been prioritized and translated in terms of intermediate energy data libraries. This work is a contribution to the subgroup on Intermediate Energy Nuclear Data Evaluation of the above mentioned Working Party. In Fig. 1 the complicated set of relevant reactions are indicated. Some studies on nuclear data needs for ATW [4, 5, 6] have revealed that single- and double-differential neutron and proton cross sections of proton- and neutron- induced reactions up to 1500 MeV have a very high priority. Also important are total, elastic, gamma production, fission and activation/transmutation cross sections. Most relevant nuclides are actinides, target materials (Ta, W, Pb and Bi), and materials in structures, shielding, and coolants (H, C, N, O, Na, Mg, Al, Ar, K, Ca, Cr, Mn, Fe, Co, Ni, Zn, Zr). Extensions of the numerical data base EXFOR with high-priority intermediate-energy data are made and evaluation programmes on intermediate-energy

nuclear data are being defined in the framework of the above mentioned NEA activity. In addition ECN evaluates the European Activation file (EAF), which consists of a huge set of activation and transmutation cross sections, so far up to 20 MeV [7].

MF	MT	Description
1	451	General information
3	2	Elastic cross section
3	5	(p,anything) cross section
6	2	Elastic angular distribution
6	5	(p,anything) yields and energy-angle distributions

Table 1: Directory of proton data up to 100 MeV for Pb-208 (ENDF-6 Format).

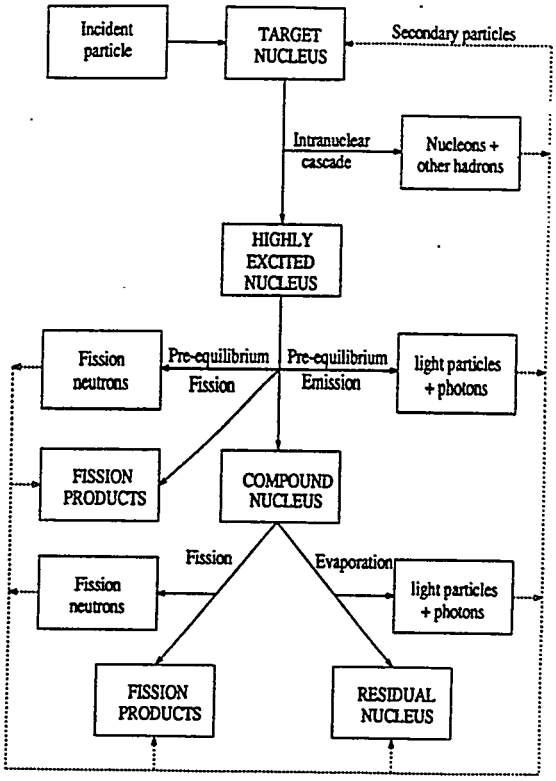

Fig.1: Intermediate-energy nuclear reactions. Solid arrows refer to an intranuclear cascade process (thin target and single proton nucleus reaction), whereas dotted arrows represent an internuclear cascade process (thick target and multiple transport processes).

Equilibration of actinides in a molten salt reactor

There are many advantages of actinide transmutation in a thermal reactor with molten salt as fuel: it allows for on-line reprocessing of the molten salt, continuous and easy refuelling, and for small neutron loss in fission products. Calculations show [7] that due to reactivity feedback, the operation of critical molten salt transmuters fuelled with transuranic LWR mix, is possible in only a very limited range of its design parameters. This could make it necessary to operate the system sub-critically like an ATW. For the various levels of the neutron flux in such a molten-salt reactor, fig. 2 presents equilibrium masses of the actinides. Heavier actinides, being products of shorter-lived trans-uranium isotopes, will increase with the flux-level, whereas the plutonium isotopes decrease. As is discussed later, this causes a lack of delayed neutrons in the system.

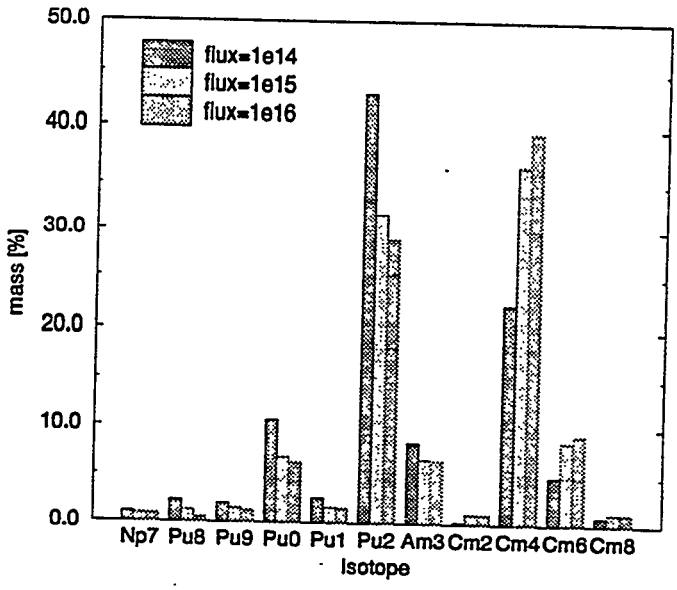

Fig. 2: Actinide masses in a molten salt transmuter.

Demonstrations and Experimental Work

For experimental and technological research on transmutation a European network EFTTRA (Experimental Feasibility of Targets for TRAnsmutation) has been founded. In this network ECN participates together with the French organisations CEA and EdF, the German KfK and the EC-establishment TUI. Targets are prepared in the laboratories of TUI, CEA and ECN, irradiations are being performed in the Petten HFR by ECN (see fig. 3 and ref. [8] for a description of the setup), and will later also be performed in the French Phénix reactor. After finishing the irradiations, targets will be examined to study transmutation efficiency and material aspects. The EFTTRA programme is focused on irradiation of the actinides (especially the americium isotopes), but also the fission products iodine and technetium are being studied. Chemical and material properties of candidate target materials will be studied before and after irradiation of about one year.

From the shielded one-group cross section of the fission products I-129 and Tc-99 (about 12 and 7 b, respectively), one might conclude that in a high flux research reactor such as the Petten HFR, about 50% transmutation is feasible within about three years [9]. This 45 MW(th) reactor is excellent for R&D on high-flux (10^{14}-10^{15}) systems, but it is not designed to cope with the huge amount of fission product waste from power reactors. Drastic changes in reactor parameters would be needed for transmutation of such amounts.

Fig. 3a: The facility (shown on the right) consists of a thimble, which forms an irradiation chamber for specific instrument-insets. Primary reactor-cooling water is being used for cooling.

Fig. 3b: A sample holder (shown below) consists of ring-shaped aluminium blocks with peripheral holes for positioning test capsules. Stainless steel 100 mm long capsules are used, and targets are 50 mm long and have a diameter of 5 mm. The instrumentation consists of thermocouples and of neutron fluency detectors. The sample holders are surrounded by three stainless steel containments. Containments have gaps for inert gas (He or Ne) used for temperature control near about 450 °C.

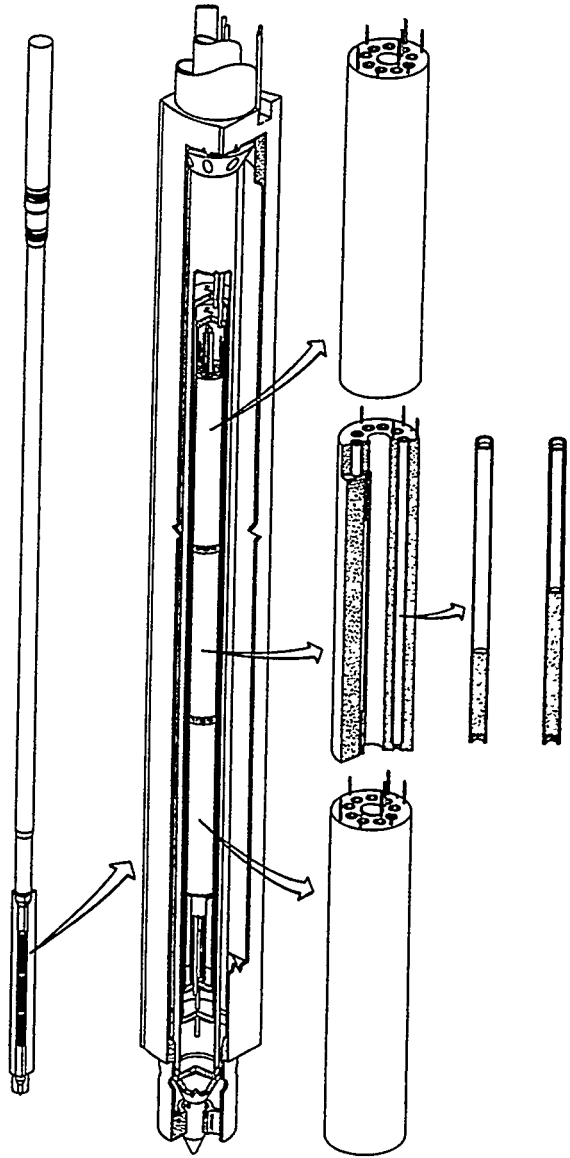

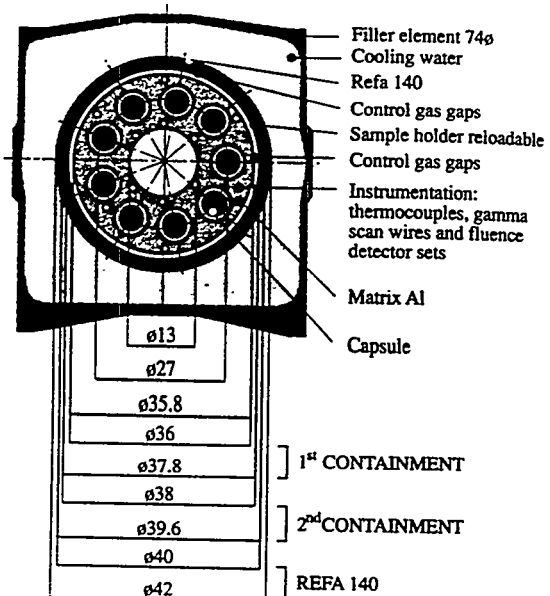

A Study of the Stability of an ATW System

A study has been made [13] of the high-flux ATW system of ref. [12], which transmutes Np-237 and Tc-99. Although the Los Alamos group has recently proposed another ATW system [10], the first system had quite some interesting aspects due to the fact that it is non-linear. A surprising nature of some solutions of differential equations for flux ϕ, concentrations N, and rates of transmutation R, originates from the likelihood that in a very high flux Np-238 will fission before it decays with a half-life of about two days. This fission process will convert neptunium at high flux [14] from an absorber into a fuel. Because of the retarded build up and the small decay constant λ_8 of Np-238, instabilities will not have a run-away behaviour, but will rather be of a controllable and creeping kind (time constants are of the order of days). A feature related to this fuel/ absorber conversion is the occurrence of several branches in the flux-concentration diagram for the steady state (see fig. 4). If the fractional load N_7 of Np is far below a critical value of about $2 * 10^{-4}$, only the fixed amount N_{Tc} of technetium acts as an absorber of neutrons [12], and the neutron loss n is equal to the transmutation rate R_{Tc} of technetium, and the source strength is given by: $n = \phi * N_{Tc} * \sigma_{Tc}$. In approaching the above-mentioned critical value of the fractional neptunium load N_7, the neptunium starts to act as a fuel and the flux ϕ will slowly rise until the value of N_7 has decreased again. In an intermediary region (up to a second critical value of the fractional load of about $1.5 * 10^{-3}$) a "chaotic" behaviour of the system is found, where the flux will change unpredictably but slowly to either lower or higher values. For selected values of N_{Tc} a third region starts above a second critical point with a solution at high flux, for which the Np acts mostly as a fuel, and a solution at low flux, for which the Np acts more as an absorber. This "post-critical" region will be stable in its "absorber" branch into which the "fuel" branch will decay.

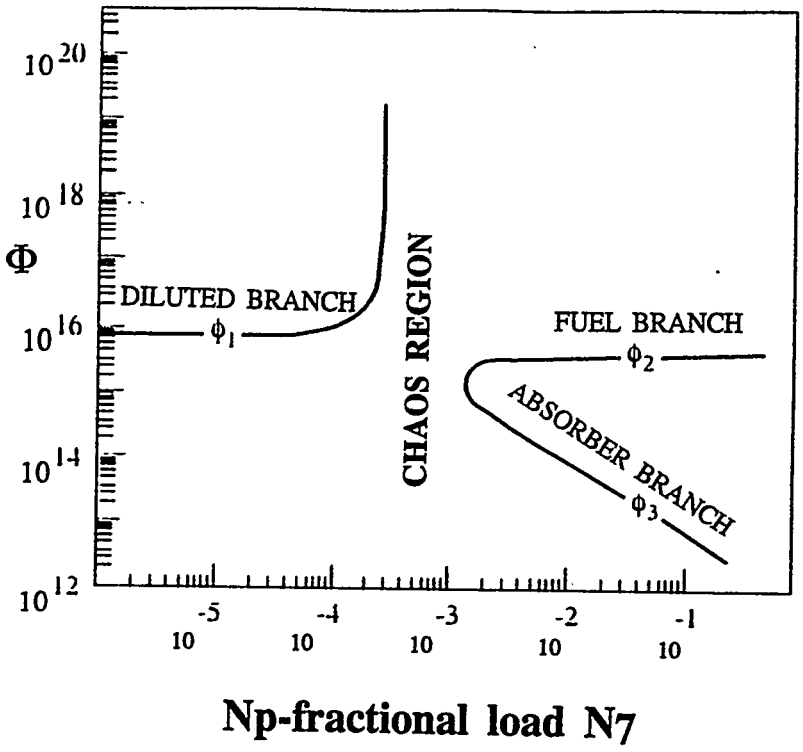

Fig. 4: Steady flux states in a Np-Tc transmuter [13]

Addendum to fig.4: Values for the parameters N_{Tc} and for n are from [12]. If the flux ϕ and fractional load N_7 of neptunium are constant, the rates of change R_7, R_8 of Np-237 and Np-238 will be connected by:

$R_7 = \lambda_8 * N_8 + R_8$,

$n = R_7 + R_8 * \{H\} + R_{Tc}$,

with $\{H\} = (1+\alpha-\nu)/(1+\alpha)$.

If N_7 approaches zero, then $R_8=0$, $n=R_{Tc}$ and:

$\phi_1 = n/(N_{Tc} * \sigma_{Tc})$.

If $N_7 >> (n, R_{Tc})$,
the asymptotic solutions are:

$\phi_2 = (\lambda_8/\sigma_8) * [-1/(1+\{H\})]$,

and $\phi_3 = n / (N_7 * \sigma_7)$.

COMPARISON OF ACCELERATOR-BASED SYSTEMS

Large energy flows should be dealt with, during any effective incineration of fissile material. For accelerator-based hybrids [10-12], the accelerator power P_A can be expressed as a function of the hybrid power P_H according to: $P_A = C * P_H * (1 - k_{eff}) / k_{eff}$. Here the hybrid power P_H depends on the accelerator power P_A, the reactor variable k_{eff} and on a conversion factor C; it can be deduced that this design parameter C lies between one and two for competing proposals. Economy of incineration might require an approach to k_{eff}=1 to allow for a reduction of the electric power P_A in the accelerator beam [17]. Approach towards a critical system will lead to a more homogeneous neutron flux and less flux-peaking in the window of the GeV proton beam. This window should be cooled by non-pressurized liquids like sodium or molten salt, as it is the weakest spot of the system.

Accelerator Transmutation of Waste (ATW) systems, in which a very high powered (100 MWe) high-energy proton beam plays a key role, were proposed by Los Alamos as special hybrid accelerator-reactor systems [10,12] that operate at $k_{eff} < 0.95$. If a very high flux and diluted fission material inventories are used, the transmutation rate will be very high. This actinide-transmuter can be equipped with a molten salt reactor [12], in which thorium fuel can be used as well. Because liquid reactor fuel (D_2O moderated slurries or molten salts) could lead to safety problems, an ATW system with solid fuel was proposed. In this proposal [10] the solid fuel is cooled with low cross-section liquid metals like Li-7. Further studies are needed to see how efficient this system can transmute fission products.

A fast reactor setup as a sub-critical booster has been proposed in Ispra, Brookhaven and JAERI. Relative to ATWs, these systems require only a small accelerator [15]. In fact these slightly sub-critical fast reactors are partly regulated with an accelerator beam, which also acts as an "electronic safety rod". Such fast reactor-boosters have very attractive features to fission minor-actinides and even-isotopes of plutonium. Because these systems have only a small surplus of thermal neutrons, transmutation of long-lived fission products would require application of moderated sub-assemblies. However combined transmutation of fission products and actinides simultaneously has not yet been foreseen for these systems.

A thermal Th/U breeder, with external neutrons has been proposed by CERN [11]; it will have intrinsic safety parameters, and some degree of protection against diversion of weapons-grade material. The fissile U-233 will always be diluted isotopically with less fissile U-234 (table 2 shows the fuel composition as derived from [11]). However there are two drawbacks, both of which are related to a non-compliance with the need to reduce future dose-risks: first of all the simultaneous transmutation of the long-lived fission products and actinides is not foreseen, and secondly the amount of U-234 in the waste might be rather high, which could lead to long-term risks due to radon-emanation [1].

Table 2 presents data relevant to safety and efficiency, and also compares the mass balance for some accelerator-based hybrids with an LWR (once-through). The delayed neutron fraction ν_d is an important safety parameter in reactor kinetics. For even-odd fissile nuclides it is fitted empirically by: $\nu_d = \exp\{16.46 - 0.5\ (3Z - A)\}$. For actinides with an even number of neutrons this value of ν_d should be divided by: $\{\ 6.4 - (3Z - A)/8\ \}$. Too small values of ν_d are found for thermal transmuters of transuranic waste, especially for high-flux thermal molten-salt systems (see earlier discussions on molten salt systems). Low values of ν_d could be compensated for by a reduction in k_{eff}, and by a corresponding increase in P_A; this however would not be economical nor be gentle towards the window.

Table 2: Actinide mass Balance EOC and delayed neutron fractions (both in percents)

	Type of transmuting system:	Energy producing systems		Waste burners	
		LWR (U/Pu) once through typical case	(Th/U) Energy-Amplifier	LWR waste molten-salt system	Metal fuelled system
	Delayed neutron fraction (ν_d in %)	k_{eff} =1	k_{eff} =0.92	k_{eff} =0.92	k_{eff} =0.89
		Efficiencies ε *) of the four transmutation-systems are:			
		ε = 1	ε = 0.86	ε = 0.86	ε = 0.81
Nuclide:	Exp. [16] /Systematics	Mass balance EOC of the four transmuting systems			
Th-232	5.27(40) / 4.78	-	97.3	-	-
U-232	0.44(3) / 0.44	pm	pm	pm	pm
U-233	0.74(4) / 0.65	-	1.1	-	-
U-234	- / 0.93	2*10-2	0.8	2*10-2	< 10-2
U-235	1.67(7) / 1.76	0.9	0.1	5*10-2	-
U-236	- / 2.07	2*10-2	0.6	-	< 10-2
U-238	4.60(25) / 4.78	98.1	< 0.1	-	-
Np-237	1.07(10) / 0.93	3*10-2	< 0.01	1	50
Pu-238	0.46(7) / 0.44	2*10-2	< 0.01	2	10
Pu-239	0.65(5) / 0.65	0.5	< 0.01	2	11
Pu-240	0.90(9) / 0.93	0.2	< 0.01	8	10
Pu-241	1.57(15) / 1.76	0.1	< 0.01	3	2
Pu-242	1.86(9) / 2.07	3*10-2	< 0.01	34	2
Am-241	0.44(5) / 0.44	2*10-2	-	-	8
Am-242m	0.69(5) / 0.65	-	-	-	0.2
Am-243	- / 0.93	1*10-2	-	7	4
Cm-242	- / 0.22	-	-	0.2	-
Cm-243	- / 0.24	-	-	< 10-2	-
Cm-244	- / 0.44	3*10-3	-	32	2
Cm-245	0.59(4) / 0.65	-	-	0.7	0.3
Cm-246	- / 0.93	-	-	8	-
Cm-248	- / 2.07	-	-	2	-
Cf-249	0.27(2) / 0.24	-	-	-	-

*) System-efficiency is defined by: $\varepsilon = P_H / (P_H + P_A) = k_{eff} / \{ k_{eff} + C (1 - k_{eff}) \}$, For a critical reactor ε is obviously equal to 1; for proposed energy producing systems the design parameter C turns out to be about 1.9 and ε should be rather close to one.

Systems which have been treated in this chapter were compared by means of earlier defined criteria [1]. From point of view of delayed neutrons LWRs and Energy-Amplifiers are stable and safe energy-producing systems, the latter being more secure with respect to safe-guarding than high-flux Th/U systems. The temperature- and voiding- behaviour should be evaluated for all systems. Metal fuel systems are most efficient in end-scenarios [18].

REFERENCES

1. K. Abrahams, "Benefits and Risks of P & T of Nuclear Waste", to be published.

2. A.J. Koning, "Present status of intermediate energy data evaluation for accelerator-based transmutation of radioactive waste, Contribution to the International Conference on Nuclear Data for Science and Technology, Gatlinburg, Tennessee USA, May 1994, and in:

   M. Blann et al, "International Code Intercomparison for Intermediate Energy Nuclear Data", NEA Data Bank report, 1994.

3. A.J. Koning, "Review of High Energy Data and Model Codes for Accelerator-Based Transmutation", NEA Data Bank Report, NEA/NSC/DOC (92) 12, (1992).

4. Y. Nakahara in Nuclear Data for Science and Technology, Jülich, May 1991, 23.

5. S. Cierjacks, in OECD/NEA Specialist's Meeting on Accelerator-based Transmutation, Würenlingen, 24-26 March 1992, 23.

6. A.J. Koning, "Requirements for an Evaluated Nuclear Data File for Accelerator-Based Transmutation", NEA Data Bank Report NEA/NSC/DOC (93) 6, (1993).

7. J. Kopecky, H.A.J. van der Kamp, H. Gruppelaar, D. Nierop, "The European Activation File EAF-3 with Neutron Activation and Transmutation Cross-Sections", ECN-C--92-058 (1992).

8. R.J.M. Konings et al, "Technological Aspects of Transmutation of Technetium and Iodine". Proc. of the GLOBAL '93 conference, September 1993, Seattle page 1260.

9. J.H. Bultman, "Calculation of the Transmutation Rates of Tc-99, I-129 and Cs-135 in the High Flux Reactor, in the PHENIX reactor and in a Light Water Reactor", Netherlands Energy Research Foundation. ECN--I-92-013, April 1992.

10. F. Venneri, C. Bowman and R. Jameson, Accelerator-driven Transmutation of Waste, LA-UR-93-752, Physics World 1993.

11. F. Carmati, R. Klapisch, J.P. Revol, Ch. Roche, J.A. Rubio, and C. Rubia, "An Energy Amplifier for Cleaner and Inexhaustible Nuclear Energy Production by a Particle Beam Accelerator", CERN/AT/93-47.

12. C.D. Bowman et al, "Nuclear Energy Generation and Waste Transmutation using an Accelerator-driven Intense Thermal Neutron Source", Nuclear Instruments and Methods in Physics Research A 320, 336-367 (1992).

13. J.A. Heil, ECN report to be published.

14. C.D. Bowman et al, "Specialist Meeting on Accelerator Driven Transmutation Technology for Radwaste and other Applications", 24-28 June 1991, Stockholm.

15. Hiroshi Takahashi and Herbert Rief, Concepts of Accelerator Based Transmutation Systems, presented at NEA meetings (Wuerenlingen/Villigen 26 March 1992, and later).

16. R.W. Waldo, R.A. Karam, and R.A. Meyer, "Delayed neutrons yield: Time dependent measurements and a predictive model", Phys. Rev. C 23, 1113, (1981).

17. A. J. Janssen, Transmutation of fission products in reactors and accelerator-driven systems: some critical remarks, ECN-R--94-01 (1994).

18. J.H. Bultman, Reduction of nuclear waste by introducing Advanced Liquid Metal Reactors, GLOBAL'93 Conference, Seattle, September 1993.

Site Layout and Balance of Plant Design for an Accelerator-Driven Materials Processing Complex

John Cunliffe*, Robert Taussig*, Sunil Ghose*, and Louis Guillebaud†
** Research and Development, Bechtel Corporation, 50 Beale Street, San Francisco California 94105, and*
† The Los Alamos National Laboratory, Los Alamos, New Mexico 87545

Abstract. High energy proton beam accelerators are under consideration for use in radioisotope production, surplus weapons material destruction, radioactive waste transmutation, and thorium-based energy conversion cycles. While there are unique aspects to each of these applications that must be accommodated in the design of the associated facility, all share a set of fundamental characteristics that in large measure dictate the site layout features and many balance-of-plant (BOP) design requirements found to be common to all. This paper defines these key design determinants and goes on to discuss the manner in which they have been accommodated in the pre-conceptual design for a particular materials production application. An estimate of the costs associated with this BOP design is also presented with the aim of guiding future evaluations where the basic plant designs are similar to that of this specific case.

INTRODUCTION

As with any engineered commodity, the determinants of the BOP design for an accelerator-based facility are multi-dimensional in nature: In addition to the physical characteristics of the facility's equipment and site and the interface requirements imposed by its fundamental processes, there are also institutional, financial and societal constraints that must be considered. While many of these may introduce an element of tension by tending to drive the design in different directions, all must be accommodated in an adequate and appropriately balanced fashion in order for the facility to be deployed and operated in a successful and cost effective manner. The challenge for the integrator/designer is to determine what constitutes an "adequate and appropriately balanced" accommodation. However, before these determinants and constraints can be considered, they must first be clearly defined and, if possible, quantified.

KEY DESIGN DETERMINANTS

Physical Constraints

The most distinctive feature of any linear accelerator-based facility — a generally long and relatively narrow site plan (see Figure 1) — is a direct reflection of the physical characteristics of its fundamental constituent, the accelerator itself. The length of the linear accelerator (linac) and, thus, of the overall facility for a given application is mainly a function of the beam particle energy which must be delivered to the target to produce the desired output. The other significant linac-imposed impact on the site layout is the substantial space required for the equipment which converts AC electrical power to the high voltage DC (HVDC) needed to energize the klystrons which, in turn, provide the radio frequency (RF) power used to drive the accelerating process. For low power applications, the linac may still require the same length as a high power application, but the space for AC/DC and DC/RF conversion may be much reduced.

The layout impact of the target- and associated process-related systems is very much application-specific. The principal structure at the target end is the Target Building (TB) itself. In all cases, it can be expected to house a full power beam stop for accelerator tuning and one or more

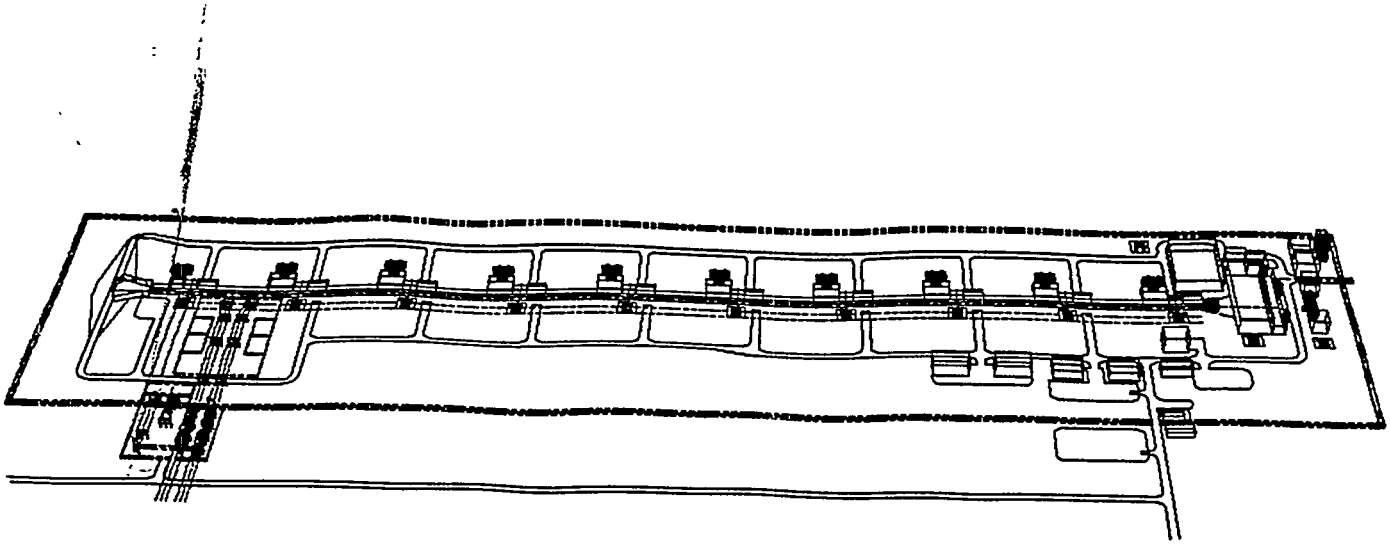

Fig. 1. Site layout of an accelerator-driven material processing facility

target assemblies. Beyond this, the process-related interface requirements setting the size, configuration, and other significant characteristics of the TB will vary significantly from application to application. This also holds true for facilities housing the associated process equipment, radioactive waste handling and storage facilities, and target heat removal equipment.

The elongated layout characteristic of a linac-based facility imposes significant constraints on accelerator support services such as ventilation, cooling water and electrical power. Further complexity exists for those systems cooling the accelerating structures themselves as the cooling water temperature is used to control their resonant frequency and, thus, maintain the beam in tune.

Process Interfaces

Key interfaces between the material processing equipment and the BOP include the connections between the target and pre- and post-process units for continuous flow feedstocks; remote handling equipment, overhead cranes and manipulator tools for removing and replacing target elements for batch processing; target and shield coolant systems; and safety monitoring and control within the larger space of the TB. Material process throughput will govern the size of the BOP components; the levels of activation will determine the amounts of shielding required around the processed materials as they are being transferred from one unit to the next. After the materials have been exposed for the appropriate length of time to the neutron flux, they generally will require remote handling for removal from the target region and will need to be transferred to a building for storage, controls (e.g., assaying, weighing, etc.) and post-processing (e.g., isotopic and chemical purification). The post-process building should be physically connected to the TB to guarantee safe transport of the irradiated materials. The connection may be via a water-filled passageway to further reduce the external radiation dose rate from the activated materials.

ES&H Considerations

Regulatory Criteria/Mandated Requirements

Accelerator-driven materials processing facilities built for DOE fall under the aegis of DOE's radiological safety assurance orders. The DOE radiological safety requirements distinguish between reactor and non-reactor nuclear facilities depending on whether or not fertile and fissile materials are present. DOE Order 5480.30 prescribes that large Category A facilities (e.g., nuclear reactors having

a steady-state power level of greater than 200 MWt) be equipped with a containment system. Equivalently, if the equilibrium radionuclide inventory in the target region is comparable to such a reactor, the same rationale applies. If the inventory is less than that amount, the facility may be treated as a non-reactor nuclear facility subject to substantially less demanding prescriptions, as DOE Order 6430.1A stipulates that confinement systems are sufficient for non-reactor facilities. The accelerator and its supporting systems can be treated generally as a non-nuclear facility under DOE Order 5480.25 [Safety of Accelerator Facilities], though draft 9 of DOE-STD-1027-92 does provide guidance to determine if any portion should be treated as a nuclear facility. Accelerator-based systems without fertile/fissile target materials especially gain in safety requirement simplicity as the requisite neutron flux is supplied by an accelerator-driven source rather than by a self-sustaining reaction, in contrast to nuclear reactor facilities.

Limiting Routine Radionuclide Releases/Exposures

Safety requirements covering routine releases or exposures are phrased in terms of the maximum allowable dose rates that may be incurred at the site boundary and within the facility where radiation workers might be exposed on a routine basis. Under normal operating procedures, compliance with these limits is achieved by providing adequate shielding of portions of the accelerator, the high energy beam lines, the beam stops, the target regions, and other systems or areas containing radioactive materials. In addition, waste water and exhaust air which may become activated will be monitored with the aim of accumulating them before they are released to the environment. In some cases, filtration is necessary to clean up these effluents so that they can be safely released; in other cases, a few hours or days of hold-up is sufficient for the activated material to decay to levels that meet the allowable release limits.

Accident Preclusion

Implementation of the "defense-in-depth" concept in general indicates that the design should provide several layers of accident preclusion or termination mechanisms as well as redundancy in cooling systems that prevent a failure in one portion of the system from propagating to other components and which might thereby result in a breach in the confinement/containment or other portion of the radionuclide retention system. The BOP design will also need to include methods to remove decay heat from the target region during shutdown, off-normal or otherwise, to limit the release of spallation- or activation-generated radionuclides normally held fast in the target structures and solid target materials as well as to preclude failure of radionuclide-retaining target assembly fluid boundaries. Finally, in those applications where radioactive isotopes are being produced deliberately, they must be carefully contained in the target component itself so that individual targets can be removed without dispersing their contents accidently.

Accident Mitigation

Accident mitigation and accident preclusion are complements rather than substitutes in assuring adequate protection of public health and safety; achieving such assurance both effectively and efficiently requires an appropriate balance of the two. Contemporary analytical techniques (e.g., safety risk assessment) and the on-going evolution toward a performance-based safety review regime increasingly make it possible to reap the potential benefits of pursuing safety assurance strategies emphasizing severe accident preclusion by obviating the need to unnecessarily

include prescribed design features intended to mitigate such events. Nonetheless, while it may be possible to sufficiently reduce the expected occurrence of large consequence events that they are insignificant contributors to the safety risk posed by an accelerator-driven facility, it may be more cost-effective to implement a balanced approach which includes aspects of mitigation as well as preclusion in meeting performance- and/or risk-based criteria. Further, the principle of "defense-in-depth" would also indicate that any design should include aspects of both. Finally, the design will also require a capability to adequately mitigate more likely but lower consequence events. It should be left to the designer, however, to select, on a disciplined and analytical basis, the most appropriate combination of mitigation and prevention features as well as their required performance capabilities, given the characteristics of the specific application and the other constraints and requirements which must also be satisfied.

Shielding

Particle beam energies and target materials determine the shielding requirements to a large extent. With energies of several hundred MeV or more associated with this class of accelerator applications, the spallation neutron spectra created by the protons is hard enough to initiate a variety of nuclear transitions not seen with the neutron spectra of ordinary reactors. The spallation neutrons are created principally in the direction of the beam, with a smaller percentage of lower energy neutrons produced isotropically. Shielding must accommodate neutron energies up to the maximum energy of the incident proton beam.

Concrete is probably the cheapest form of shielding. Only when spatial constraints dominate is it useful to consider using steel and/or heavier forms of concrete to reduce the depth of shielding required. Initial target shielding calculations indicated that 6 to 8 meters of concrete may be required in the forward beam direction for incident proton energies on the order of 1 GeV. Smaller amounts of shielding are needed around the accelerator tunnel, especially at the higher energy end where occasional beam scrape-off may activate local components and spray neutrons into adjacent portions of the facility. The design of shielding needs to be considered carefully to include provisions for efficient removal incident to target repair or replacement. Ultimately, the permissible dose rate to facility workers, impact of remnant neutron flux on groundwater, and surface dose rates (i.e., at grade) will be specified by the permitting and safety requirements for the facility and will determine the amount of shielding required in each particular application.

Availability/Reliability/Investment Risk Factors

Models using well-established reliability/availability/maintainability (RAM) methods are used to predict the expected performance of these accelerator-driven concepts. Where possible, these models are based upon reliability data obtained at accelerator facilities world-wide or in other comparable applications. However, when, as in the case of high energy, high current proton accelerators, some of the key components are still under development, considerable uncertainty exists in the estimates of their performance. It then becomes necessary to compensate for this uncertainty in the reliability of one portion by increasing the expected reliability elsewhere in the design. These compensatory measures may increase the costs of initial accelerator-driven systems until sufficient performance data is obtained to jusitify simplification of follow-on facilities. For this reason, it is very worthwhile to invest in pilot demonstrations of performance to justify a more economical design for a full-scale system from the outset. Present value calculations serve as

standard methods for determining the level of development and final engineering design that should be carried out to reduce the final capital and O&M costs to "profitable" levels, whether for the Government or for a private owner.

Schedule and/or Construction-Related Constraints

The primary schedule constraints encompass such critical activities as achieving performance milestones in key technologies; site, safety and environmental permitting; acquisition of long-lead time equipment; and, installation/startup of the accelerator and target subsystems. The project has some control over their duration, though several tend to be rather immutable. Additionally, for government funded installations, initiation of Title I and Title II engineering, construction, and start-up of the facility all require that an explicit decision to proceed be made. Delays may occur if the prerequisites for such decisions are not all met in time for the acquisition authority to review and approve the results as scheduled.

Construction constraints are a principal determinant of the achievable deployment schedule (e.g., the physical nature of the accelerator tunnel allows only a limited number of personnel to be engaged in accelerator installation at a time). However, the tension induced by countervailing construction and schedule constraints is not unidirectional, tending only to increase the schedule duration. Instead, the client's required deployment date may dictate that more costly design features or construction techniques be employed than if the schedule were less constrained. As an example, site conditions might favor cut-and-cover embeddment or even at-grade berming of the accelerator tunnel. However, the required deployment schedule may dictate that klystron gallery and tunnel construction proceed in parallel, requiring in turn an embedded accelerator installed in a bored tunnel. Conversely, there may be cases where construction or fabrication techniques, e.g., modularization or pre-fabrication, can be applied which serve to reduce both cost and schedule. To reiterate, it falls to the designer/integrator to develop the most efficient approach to deploying a particular application within the specified requirements and constraints.

Potential Site-Specific Considerations

Principal site-specific features that may affect both site selection and facility design are:

- Geology and seismology
- Labor rates
- Capacity and costs of local utilities (electricity & water)
- Pre-existing environmental conditions
- Infrastructure (shops, storage, shipping/receiving, rail/road transportation, ...)

As shown in Table 1, data drawn from a preliminary site study for a radioisotope production application illustrate the differences in these factors which can exist from site to site. Other less objective, but no less important, site selection criteria include the need to sustain employment at such sites, the existing experience mix of that labor force, and the ways in which such a facility might provide diversity to the missions of a given site.

In those instances where, for a selected site, local labor rates are high, consideration should be given to off-site pre-assembly as a way to minimize on-site labor content. If electric power must be purchased, gas turbine combined cycle power units placed on-site may be more cost-effective than use of higher-priced (and/or under-capacity) public utility power. If the application produces excess electric power, it may be important to site the plant where the current price of power is higher in order to realize a greater financial gain from the sale of the excess electricity.

Table 1. Site-Specific Factors

Factors	Site 1	Site 2	Site 3	Site 4	Site 5
Avg.Labor Rates ($/hr) (Davis-Bacon Rates)	8.85	14.90	25.24	10.29	29.87
Electric Power Costs (mills/kW-hr)	31.8	66.5	31.0	53.4	42.5
Water Table Depth (m)	-76 to -91	-2	-30	-2	-200
Seismic Factors					
General Facilities	0.08g	0.08g	0.12g	0.15g	0.21g
Moderate Hazard	0.10g	0.11g	0.14g	0.19g	0.27g
High Hazard	0.17g	0.19g	0.21g	0.32g	0.46g

IMPLEMENTATION/ACCOMMODATION ON A SPECIFIC MATERIALS PRODUCTION CONCEPT

Constraints on Integrated and Structured Design Development

For the specific materials production concept serving as the basis for this paper, the design constraints included a specified annual production goal, facility siting at one of the five sites listed in Table 1, and the need to accommodate either of two possible target/production technologies. The exigencies of producing a pre-conceptual design to support the client's schedule for selecting between alternative technologies to fulfill this particular materials production mission did not allow for the prior formulation of a systems engineering program supporting an integrated and structured development process. Rather, a point design for the facility was developed, driven in large measure by an accelerator designed to be capable of achieving the specified goal quantity with either target technology under the assumption that the overall availability factor would be 75 percent. It is intended that further development will be conducted under a formal, structured systems engineering process, which will serve to ensure that the resultant design satisfies all requirements and constraints in an adequate and appropriately balanced fashion.

Key Features of Current BOP Design

The site layout for this particular application would be similar to that of Fig. 1. The plant is approximately 1 km long, with the accelerator tunnel roughly 15 m below grade as measured to the roof of the tunnel. The targets, beam injectors, beam stop and high energy beam transport tubes are all on the same horizontal plane to simplify turning magnet design and beam alignment. Electric power requirements are on the order of 500 MW(e), with the greatest proportion of power being used to drive the accelerator. Cooling water, HVAC, and station electrical systems serving the accelerator, accelerator tunnel and klystron gallery are distributed in 10 stations located along the accelerator's length. Additional stations serve the TB and associated systems. While the design incorporates passive means for post-accident target residual heat removal, an active system and rotating emergency power source are also provided for investment protection purposes.

Preliminary assessments indicate that, based on the relevant safety requirements as well as the concept's accident response characteristics, the TB need only serve as a confinement and not as a low-leakage containment. While the degree of post-event radionuclide retention which the confinement must provide remains to be fully determined, the pre-conceptual point design leverages off of precedent with commercial boiling water reactors by providing both a primary and a secondary confinement. The primary confinement, which will have some pressure retention capability, will contain the targets and their primary cooling loops. Target replacement, which is analogous to reactor refueling, will occur within the secondary confinement envelope, which will also contain the targets' secondary cooling loops, coolant purification system, and other target-related ancillary equipment. To limit routine radionuclide releases to as low as reasonably achievable, the accelerator tunnel will be isolated during operation, with cooling provided by recirculating the tunnel air through distributed unit coolers. Following shutdown under normal conditions, short-lived air activation products will be allowed to decay before once-through ventilation of the tunnel commences.

Use of Alternative Design Selection Trade-Offs and Concept Optimization

Even if systems engineering has not been applied from the outset of concept development, an existing point design may be optimized by constraining the overall system against one set of requirements and varying it against another. As an example, the design may be held constant to a gross production level providing the specified net production at a pre-set availability factor and the other aspects of the design varied to develop a least-cost solution using the present value of life-cycle costs as the basis for comparison. Alternatively, the gross production level and availability factor may both be allowed to vary in arriving at a least-cost solution which still achieves the prescribed net production. The greater the number of characteristics which are allowed to vary, the closer the design can be taken to the optimum solution. Potential alternatives in this optimization process include increased target density to enhance the rate of reaction for a given number of incident protons and increased accelerator efficiency to reduce electric power consumption (reductions of 20 to 40% may be possible).

Estimated BOP-Related Costs

Table 2 summarizes the best-estimate BOP-related life-cycle costs for this specific application in comparison with those for the entire facility. In addition to the costs shown here, a contingency of $906M intended to take the estimate to a 75% confidence level has been established on the basis

of the overall facility's preoperational and capital costs; this contingency cannot be directly prorated to the corresponding BOP cost figures.

Table 2. BOP-Related Costs Compared to Total Facility Costs

	BOP	Total Facility
Pre-Operational Costs	**$ 88M**	**$ 414M**
Capital Costs		
Engineering & Design	$ 130	$ 346
Construction (Site & Bldgs)	319	1469
Proj. Mgt. & Admin.	84	94
Subtotal	**$533M**	**$1909M**
Annual O&M Costs (M$/yr)	**$ 40M**	**$ 346M**
D & D Costs	**$160M**	**$ 160M**

CONCLUSIONS

Accelerator-driven materials processing facilities all share a set of fundamental characteristics that in large measure dictate the site layout features and many BOP design requirements. Thus, while there are requirements and constraints unique to each application, considerable synergy between applications does exist. Further, careful consideration of all of these design determinants in an integrated and structured engineering process will serve to ensure that all are satisfied in an adequate and appropriately balanced fashion. The result will be an accelerator-based facility that can be a strong contender — technically, environmentally, and economically — amongst the competing options for a particular application or mission.

SIMULATION OF RADIOACTIVE WASTE TRANSMUTATION ON THE T.NODE PARALLEL COMPUTER [1]

F.Bacha, J.Maillard, J.Silva
LPC Collège de France.IN2P3
11, Place Marcelin Berthelot
F-75231 Paris Cedex 05, France

Abstract. Before any experiment on reactor driven by an accelerator, computer simulation supplies tools for optimization. Some of the key parameters are neutron production on a heavy target and neutronic distribution flux in the core. During two code benchmarks organized by the NEA-OECD, simulations of energetic incident proton collisions on a thin lead target for the first one, on a thick lead target for the second one, are described. One validation of our numeric codes is based on these results. A preliminary design of a burning waste system using benchmark result analysis and fission focused simulations is proposed.

INTRODUCTION

To study the indirect transmutation, the neutron production by a heavy target has been simulated during an intercomparison of codes (benchmark 1 and 2) with a specified target geometry.

The design of a hybrid system is approached with a succession of intermediate studies, for instance on the interface between reactor and accelerator, on the criticity of a simulated pressurized water reactor (PWR) core filled with natural uranium and bombarded with energetic protons according to the direct transmutation.

Energy production from nuclear waste is not provided in this scheme - even if our system would be quite reliable for later simulations putting other actinides in place of uranium - but the aim is only to destroy them in the more efficient, secure, safe way without energy profitability for the accelerator feeding.

I BENCHMARKING SIMULATIONS

1.1 Simulation codes

Within the framework of the code intercomparison, the simulation code which has been used is GEANT 3.15 [1], a current code for high energy physics experiments. Two code interfaces, GHEISHA [2] and FLUKA [3] belonging to the main code GEANT, intervene when hadronic interaction, especially particle-nucleus collisions, happens. They represent the base code in the thin and thick target simulation exercises.

GEANT, a Monte-Carlo calculation based code, allows the simulation of varied processes such as bremsstrahlung, δ-ray production, Compton scattering, photo electric effect,

[1]This work was supported by the Direction des Etudes et Recherches, Electricité de France, Clamart

Rayleigh scattering, photon induced fission in heavy materials, gaussian multiple scattering, ionisation processes, e^+e^- production, muons-nucleus interactions.

The simulated events are generated from a standard MC generator. GEANT capacities are the description of the experimental set-up, the particle tracking through various regions of a medium -taking into account geometrical volume boundaries and all physical effects concerning the produced particles- , the graphical representation of particle trajectories - and its records- and the prevision of the detector response. Calculations of physical values like trajectories, energy deposition, decay length, multiplicities can be obtained during the simulations.

The GHEISHA code acts under 50 MeV energy of neutrons and simulates hadronic shower development. It is based on the intra-nuclear cascade, evaporation model and thermal fission. Cross section calculations, final multiplicity and kinematics, neutron nuclear capture, nuclear fission, elastic and inelastic scattering are described in this interface. The cross sections on nucleus are known only for pions and protons. For 2 GeV -and above- protons, the general law is:

$$\sigma(A) = 1.25\sigma_{tot}(protons)A^{1/3} \quad (1)$$

The FLUKA [4] code comprises three energetic domains. Above 50 MeV, calculations and generation of secondary particles from inelastic and elastic cross sections can be obtained; between 50 MeV and 5 GeV, experimental or interpolated cross sections and a resonance production model are used; between 5 GeV and 10 TeV, a multistring fragmentation is the main model.

1.2 The T.Node

The parallel computer is adapted to these considerable time consuming calculations. The T.Node calculation power is equivalent to 4 IBM 30.90 calculation power.

Without any major change in GEANT structure, the GEANT parallelization has been possible because the physical problem, proton collisions on nuclei, constitutes similar events which can be distributed between the 64 "slave" transputers with an appreciable executing time reduction (cf.fig.1).

The master sends the initialisation to the slaves; after the slaves' running, they send back their results to the master. Only the master can access the files.

1.3 Benchmark 1 and 2

1.3.1 Description

In the benchmark 1 framework, a thin (^{208}Pb and ^{90}Zr) target [6] is bombarded with 25, 45, 80, 160, 256, 800 and 1800 MeV protons. The result comparison turned to the (p,xn) and (p,xp) double differential cross sections. Nuclide distribution is asked for ^{208}Pb and ^{186}W at 800 MeV.

In the benchmark 2 framework, the specified thick target [7] [8] (^{208}Pb and ^{186}W) is a cylinder (cf. the figure of this target divided in meshes) bombarded with 800 MeV protons

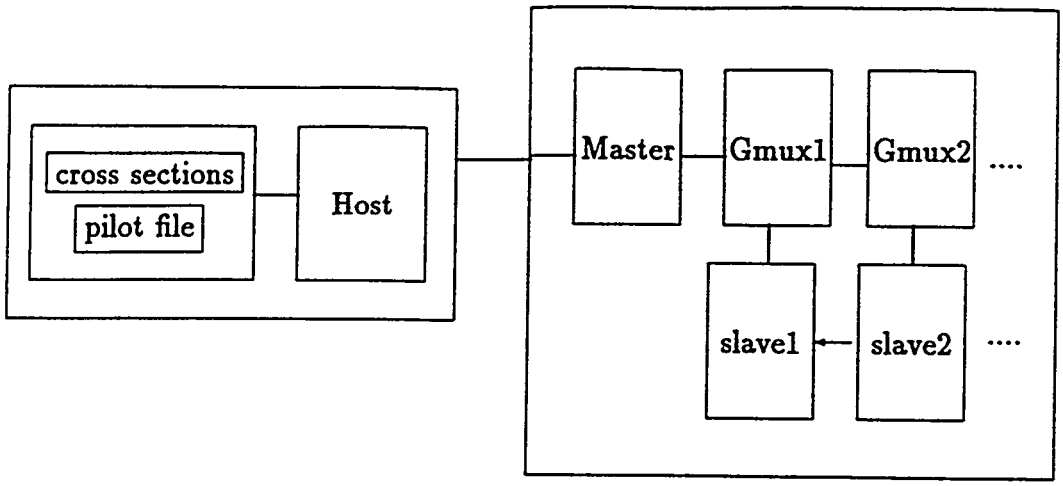

Figure 1: The T.NODE structure.

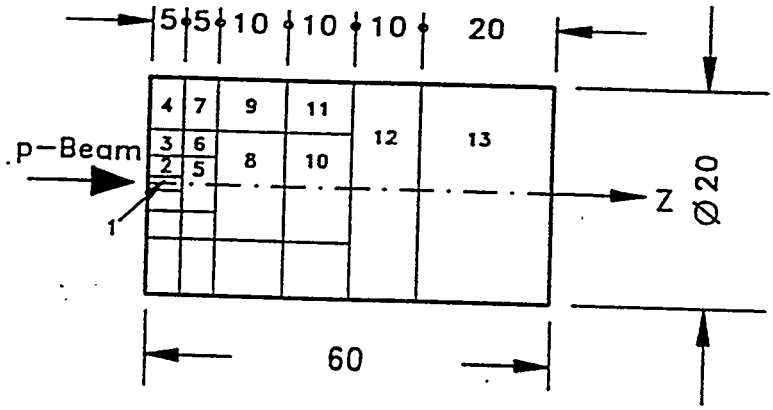

Figure 2: The target mesh grid for benchmark 2.

(pencil beam on the axis); the neutron production per proton, the neutron yield spectra, are required over the whole target. For the surfaces of different meshes, total neutron flux leakage distributions, above and below 20 MeV, have been simulated at 300°K. The spallation distribution product has been asked for after the beam shutoff, after one year cooling and after 100 years.

1.3.2 Summary of some results

The comparison between the results for the double differential cross sections on ^{208}Pb (p,xn) shows that:

- all codes have no results for 25 MeV protons at the angle 0° and 80 MeV protons at 25°.
- the whole energetic range has been approximately simulated by GEANT from 80 MeV to 800 MeV.
- lacks in GEANT are perceptible for the 25, 45 MeV for all angles of the double differential cross sections.

- benchmark 1 has demonstrated some discrepancies between the varied code results and the view of some large uncertainties on the experimental values. But even a high particle code such as the one used, was able to participate in the validation test.

Benchmark 2 results permit these remarks:

- under 20 MeV, the total neutron yield spectra from heavy target is not satisfying; over 20 MeV, its values rejoin the other codes results.
- the values of the neutron production on the whole target are also underestimated at low energy;
- the inhomogenous neutron production from the target indicates that the heavy target, even if it makes it possible to multiply neutrons, raises problems because the criticity would be easier under control with neutrons well distributed in the space.
- the back-scattering neutron phenomenon was highlighted by our simulations. These neutrons can damage the window and also the accelerator.

1.3.3 Code improvements

Problems distinguished by the benchmarks results are a consequence of GEANT limits. Microscopic calculations have to be improved by a modification in the physical model of the nucleus. The treatment of the intranuclear cascade and the evaporation code has to incorporate the precompound model (multistep equilibrium, exciton model) in the GEANT code [9][10].

Our code was improved by the addition of a tracking neutron code between a few meV and 10 MeV because of its deficiency at low energy. But the spallation and fission products distribution after the reactions have not yet been described.

II FEASIBILITY OF A HYBRID SYSTEM

2.1 Description of the core geometry

This study uses GEANT 3.15 with the addition of Lefièvre's code [11], which tracks low energy neutrons down to their thermalization, using the Drozdov model.

One of our concerns will be to reproduce quantitative results as near as possible to a classical PWR filled with natural uranium fuel. Its set-up is composed of a large vessel (diameter: 2 meters, height: 4 meters); the features of the core geometry, the rod size, the space between them, the coolant and moderator -light water- are similar to those of a PWR. We use for simplicity steel clads which capture more neutrons than zircalloy one.

Using this subcritical reactor, we begin to work without a whole description of cross-sections. In fact, above 10 eV, it is very complicated to introduce them accurately because of the multitude of resonances. One of the main input data is the fuel enrichment (0.7% in natural uranium). To watch over the criticity, we generate neutrons in the center of the reactor and we measure the fission number. This give the 1/1-k factor (k: effective factor of neutron multiplication in the target for the fission reaction). For the further simulations, a proton beam (200 particles) is sent through the vessel side.

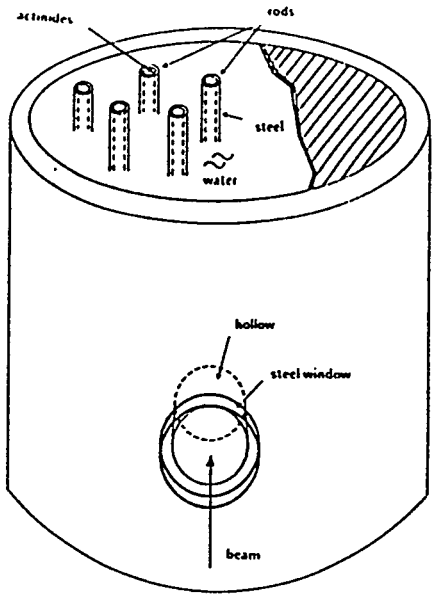

Figure 3: Geometry of the PWR simulated core.

2.2 Interface proposal

2.2.1 Preliminary

In every hybrid system, whatever direction the beam takes among the possibilities, it is not secure and safe to suppress any interface between the accelerator and the reactor. In case of an accident, the reactor would work without a radioprotection barrier, the accelerator would be polluted and the risks of radioactive coolant dissemination or even nuclear waste dissemination in the environment are not negligible.

2.2.2 Proposal of the window design

Many constraints act on the interface between the reactor and the accelerator. The pressure on the accelerator side is very low (vacuum level) whereas on the reactor side, it can overtake 155 bars typically because of the water cooling system. The heat transfer problem and the mecanical damage by the intense incident proton flux and the back-scattering neutrons from the core have to be considered. The window compound activation -but the vessel activation particularly- induces a radioactive pollution of the water and the core.

Compatible with all of these constraints, the metallic alloy of such a window could be an austenitic stainless steel (AISI 316 L)[12] which composition corresponds to:
molybdenum 2-2.5 %, chromium 16-18 %, nickel 10 %, carbon 0.060 %.

If the window diameter is proposed as 200 mm, hence its thickness must be at least 20 mm for the range of temperatures (from 600 to 873°K).

Above 873°K, the thickness has to be greater. These data represent only an order of magnitude. It is not sure, for instance, that the window thickness has to be exactly the same everywhere.

A meshing of this area has been carried out with the Accord-Coquepoutre code; the boundary conditions, critical constraints, forces on the meshing nodes, the displacement of the nodes has been calculated. Table 1 shows the slightness of node displacement.

Table 1. Simulation of maximal displacement and constraint for an austenitic stainless window (diameter: 200 mm) at the temperature 873°K.

thickness (mm)	*displacement max (mm)*	*constraint N/m²*
20	0.23	$0.229\ 10^9$
25	0.118	$0.147\ 10^9$
30	0.068	$0.102\ 10^9$

The critical austenitic steel resistance to the constraints is approximately $0.62\ 10^9$ N/m² at 873°K. The maximal constraint on the nodes is $0.229\ 10^9$ N/m² which square with 37% of the limit value.

2.2.3 Beam energy choice with an arbitrary window thickness

The beam efficiency is studied in relation with the incident particle energy (1, 20, 40 GeV). The number of fissions per proton in the core, for a window of 50 mm and without a window (cf. table 2.) characterizes indirectly the energy lost by the beam in the window.

Table 2. Number of fissions per incident proton in the core.

energy (GeV)	*with window of 50 mm*	*without a window*
1	40	72
20	1 499	1 760
40	2 769	3 060

The greater the incident energy, the less fission is lost in the core. With a window, 41% of number of fissions to the number of fissions without a window are lost at 1 GeV whereas less than 10% are at 40 GeV. The number of fissions in the core per incoming GeV increases with the energy until a maximum (around 30 GeV) depending on window thickness.

2.2.4 Connection between the fission production in the core and window thickness

Simulations with a protonic beam (200 protons) on a PWR reactor were made with and without a window:

Table 3. Number of fissions for 1 GeV protons.

thickness (mm)	*number of fissions*
0	13 963
20	11 307
50	8 803

As it is expected, the number of produced fissions in the core decreases exponentially with the increase of the window thickness because of the incident particle and energy loss in the window.

2.3.4 Heat deposition and the number of reactions in all parts of the reactor.

For 200 protons of 1 GeV and 20 GeV energy respectively and a window whose diameter is 200 mm and thickness 50 mm, the heat transfer to the window relatively to the beam energy and also the different nuclear mechanisms in the different parts of the system (cf. table 4 and 5) are considered.

Table 4. Parameters evaluation for 1 GeV protons.

	window	*vessel*	*clads*	*rods*
energy loss all part. (MeV)	153	121	87	459
number of elas.react.(low en. neut)	237	7 334	40 722	96 211
number of inelas.react.(low en.)	3	277	3 132	3 223
number of fissions	0	0	0	7 957

Table 5. Parameters evaluation for 20 GeV protons.

	window	*vessel*	*clads*	*rods*
energy loss all part. (MeV)	708	1 386	2 630	14 600
number of elas.react.(low en. neut)	950	126 607	1 524 000	3 600 000
number of inelas.react.(low en.)	19	4 535	113 900	594 800
number of fissions	0	0	0	298 000

Two contributions to radiation damage exist: the first resulting from the incoming proton, the second resulting from secondary particles coming essentially from the reactor.

Some experiments at Framatome have proved that the power limit for a water cooled window (thickness: 25 mm) on its back side was 0.4 MW/m^2. In our case it corresponds to 12.6 kW on a window of 200 mm diameter.

This seems rather incompatible with the beam intensity needed for the nuclear waste transmutation. Our simulations show an energy loss of about 75 MeV for a 1 GeV proton and of 350 MeV for a 20 GeV proton i.e. for a 1 mA beam intensity, 75 kW at 1 GeV and 350 kW for 20 GeV.

Nevertheless, for the same amount of fissions in the core and the same amount of beam energy, the 20 GeV case is more easy to get (17:5 kW against 75 kW) with a factor of about 5. But, only beams of the order of a few mA can be accepted.

An energy rise allows us to increase the window thickness without a large relative energy loss; in this case, the heat evacuation must be specially evaluated. If the halo problem is attenuated, the window size can be reduced. For an efficient transmutation system, we have to gain several orders of magnitude.

A minimal surface of window and a minimal beam width are required. Knowing the nuclear interaction length in iron -16.6 cm- and given a thickness of 1 mm, we can estimate the contribution of proton as 0.1/16.6 per mm of steel depth, for each incoming proton i.e. 0.006 interaction. The number of deleted atoms of the bombarded window per year corresponds to 0.14 g of steel for a beam of 1 mA and for a depth of 1 mm. The critical hole damage in the volumic fraction of the window [12] is evaluated at 1%. This requires at least a beam spread of 20 cm^2, given a beam radius of about 3 cm. To avoid a halo problem, a radius of 10 cm is taken for the window, corresponding to a factor 10^{-4} of halo for a gaussian beam. The above number must be considered as optimistic, since we secondaries are not taken account. As we saw in benchmark 2 at least, one energetic neutron per incident proton can hit the window.

2.3 Fission expansion in the core

Important problems of the reactor are the inhomogeneity of the power distribution and the isotopic modification which may induce local overcriticity and risks for the system. For accelerator based concepts, this is significant because a hadronic shower is a totally inhomogeneous phenomenon.

2.3.1 Beam on the lateral side

The size of a hadronic shower increases logarithmically (cf. fig. 4) both laterally and longitudinally with the energy. For 1 GeV and 20 GeV, the penetration depth of the shower increases by about 18 cm. Above 10-20 cm distance, the number of fissions in the core decreases rather linearly with the distance from the maximum. This fact can be a start to realize systems where the source term is homogenous at least on one plane.

2.3.2 Comparison of fission production in the core

We have looked at the possibility of injecting neutrons from the top. It does not seem to change drastically the number of fissions. The fission production for the two positions of the beam are almost equal (cf.table 6). We are also investigating the shape of the beam.

Table 6. Fission production in the core for a proton beam ($E_{prot.}$ = 1 GeV) sent along the core axis, above the reactor and for the same beam sent laterally.

beam along axis	*beam laterally*
20 249	19 781

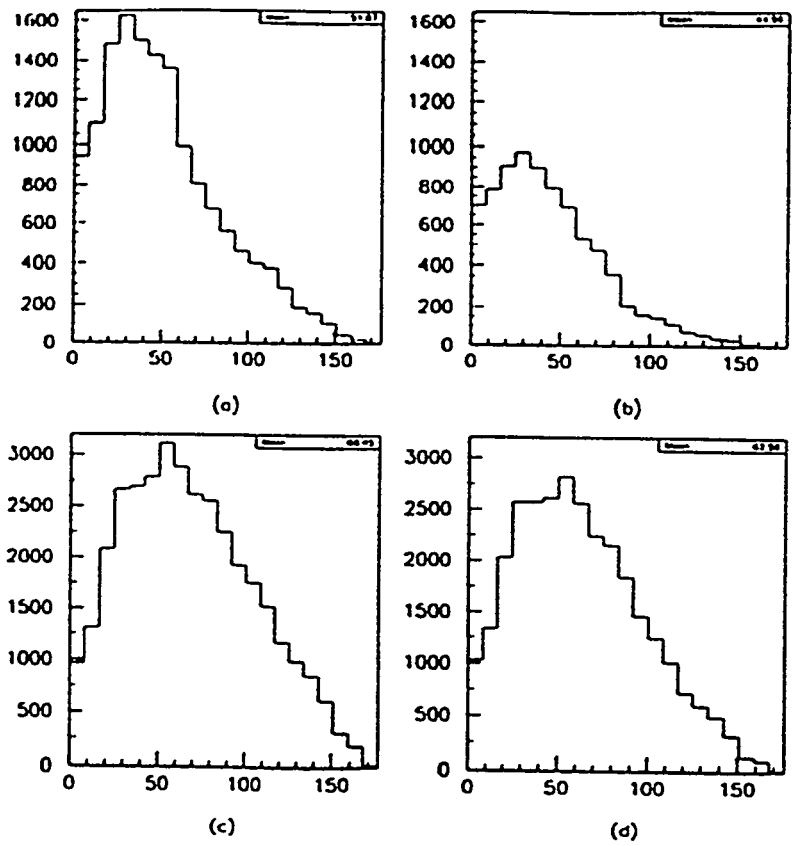

Figure 4: Penetration of the hadronic shower; (a) 1 GeV without a window; (b) 1 GeV with a window; (c) 20 GeV without a window; (d) 20 GeV with a window.

2.3.3 Comments on the homogeneity conditions for a subcritical core

To realize a homogenous subcritical core, our proposals are to increase incident energy and to multiply beams. Higher energy allows the expansion of the shower in the core space. The multiplication of beams avoids window problems and homogenizes the neutron source. More difficult to optimize is the isotopic distribution of neutrons and the power distribution.

2.3.4 Improvement needed

Full description of fission, with time delayed neutrons and gamma emission, fission product distribution and a complete set of cross-sections, has to be included in the code.

The heat transfer in the window and the local criticity in the core are still unsolved questions. More generally, main difficulties are: how to decrease the inhomogeneity of the system, how to evaluate the power distribution in this particular geometry and to obtain the neutron balance, how to take into account the modification with the time of the material compound (nuclear waste, target) and avoid the nuclear risks because of its radiotoxicity.

CONCLUSION

The problem of safety lies essentially in the problems related to the backward neutron flux, window resistance and the reactor homogeneity in fission products and power. This

appears to be crucial questions for an accelerator-based burning concept. High energy beams and volume repartition of the incident particles seem to be a way of tacke with them.

In these conditions, an interface with its mechanical features seems to be foreseen. Distribution of neutrons in the core for various beam conditions seems particularly important to study, because such parameters as a change of target composition can affect the dynamical properties of the reactor, the power distribution, the local criticity and even cause bursts.

Programs to simulate more accurately these concepts needs to be improved: time dependence of neutron production, variation of the materials with the irradiation dose, precision in physical events and cross sections are needed.

ACKNOWLEDGMENTS

We are deeply indebted to Professor M.Froissart for his interest and support. We thank Y.Meyzaud (Framatome) for his careful advice on the interface materials, F.Vinchon (LPC) for the simulations with the Accord Coquepoutre code. Special thanks go to Professor H.Takahashi (BNL) for his technical suggestions. We wish to thank J.Vergnes (EDF DER) for his technical support.

REFERENCES

[1] Brun R., Bruyant F., Maire M., McPherson A. et al., *User's Guide GEANT 3.15*, CERN 1992.

[2] Fesefeldt H., *GHEISHA, The Simulation of Hadronic Showers - Physics and Applications* - , Aachen, Report PITHA 85/02, CERN.

[3] Aarnio P.A., Lindgren J., Ranft J. et al., *FLUKA User's guide*, CERN TIS-RP, 1990., CERN TIS RP-190, 1987.

[4] Fassò A., Ferrari A., Ranft J. et al., FLUKA 92, presented on worshop on *Simulating Accelerator Radiation Environment*, Santa Fè, January 11-15, 1993.

[5] Bacha F., De Moura C., Duflot C., Jejcic A., Maillard J., Maurel G., Silva J., Tembely F., *Mise en oeuvre de grands programmes de simulation sur ordinateurs parallèles: l'exemple du T.Node*, LPC 93 07, 1993.

[6] Blann J.M., Gruppelaar H., Nagel P., Rodens J., *International code comparison for intermediate energy nuclear data*, NEA OECD report, 1994.

[7] Bacha F., Lefièvre B., Maillard J., Silva J., Analysis of benchmark results presented at the *Specialists Meeting on Intermediate Energy Nuclear Data*, Issy-les-Moulineaux, France, on May 30. - June 1. 1994.

[8] Filges D., Neef R.D., OECD Thick Target Benchmark (Preprint), *Specialists Meeting on Intermediate Energy Nuclear Data*, Issy-les-Moulineaux, France, on May 30. - June 1. 1994.

[9] Shubin Yu.N., Lunev V.P., Konobeyev A.Yu., Korovin Yu.A., Comparison Between Preequilibrium and Intranuclear Cascade Models at intermediate Energies presented at the *Specialists Meeting on Intermediate Energy Nuclear Data*, Issy-les-Moulineaux, France, on May 30. - June 1. 1994.

[10] Prael R., A Review of Physics Models in the LAHET Code, LA-UR-94-1817, presented at *Specialists Meeting on Intermediate Energy Nuclear Data*, Issy-les-Moulineaux, France, on May 30. - June 1. 1994.

[11] De Kerret H., Lefièvre B., Simulation de neutron de basse énergie par Monte-Carlo, *rapport interne*, LPC 8801, 1988.

[12] Private discussion (Framatome).

ACCELERATOR DRIVEN REACTORS AND NUCLEAR WASTE MANAGEMENT PROJECTS IN THE CZECH REPUBLIC

František Janouch
The Royal Institute of Technology,
Stockholm, Sweden

and

Rostislav Mach,
Institute of Nuclear Physics,
Řež near Prague, Czech Republic

ABSTRACT

The Czech Republic is almost the only country in the central Europe which continues with the construction of nuclear power reactors. Its small territory and dense population causes public worries concerning the disposal of the spent nuclear fuel. The Czech nuclear scientists and the power companies and the nuclear industries are therefore looking for alternative solutions. The Los Alamos ATW project had received a positive response in the Czech mass-media and even in the industrial and governmental quarters.

The recent scientific symposium "Accelerator driven reactors and nuclear waste management" convened at the Liblice castle near Prague, 27 - 29. 6. 1994 and sponsored by the Czech Energy Company ČEZ, reviewed the competencies and experimental basis in the Czech republic and made the first attempt to formulate the national approach and to establish international collaboration in this area.

INTRODUCTION

NUCLEAR ENERGY

The former Czechoslovakia - and presently both the Czech and the Slovak republics are very poor in conventional energy resources: the hydroenergy - fully exploited -provides less then 3% of the total electricity production, fossils reserves (concentrated predominantly in the Czech part) are reduced to coal only, most of it being low quality and sulphur rich brown coal and lignites. Its use for electricity production caused and still causes heavy environmental damages especially in the north part of the Czech republic which is in fact declared to be a catastrophe region. The atmospheric pollution is causing grave concerns even in the neighboring countries. At the end of eighties, Czechoslovakia, having a population of about 0.3% of the total world population, was burning apr. 10% of the total world production of lignites.

The energy situation is even worse in the Slovak republic, where even the coal reserves are absent.

At the beginning of nineties up to 90% of Czechoslovakia's consumed oil and natural gas were imported from the former USSR i.e. from abroad, making the country economics very vulnerable and dependable.

At the same time the Czech republic had considerable reserves of uranium ores. Although a large part of it was depleted between 1945 and seventies by the Soviet union and taken without any control out from the country, not a negligible amount of uranium ores is still available.

These are in short the reasons why Czechoslovakia accepted in 1956 the Soviet offer to start both an intensive and extensive nuclear power program and to build basic nuclear research facilities.

Taking into consideration the fact that Czechoslovakia was the most industrially developed country of the former Soviet bloc, it was decided, most probably in Moscow, that the country will develop, jointly with the Soviet specialists, its own reactor type: a graphite moderated gas-cooled (CO_2) reactor using natural uranium. It was called A1 and the designed net electrical output was of 150 MW(e).

The construction of the first Czechoslovak NPS near the Slovak city of Jaslovské Bohunice A1 started in 1958. Its completion was very much delayed -- the A1 NPS went into operation only in December 1972. The A1 should be in fact taken placed in the Guiness book of records: Its construction lasted 172 months and it was in operation for only about 55 months. From February 1977 the A1 NPS was practically out of operation due to severe technological problems and two larger accidents (1976 and 1977). The A1 NPS was officially shut down in May 1979. The A1 nuclear power station was not yet disposed - everything was left there as it was for over 15 years and this is causing environmental concern not only in the Slovak republic but also in neighboring Austria and elsewhere.

Due to the design problems and construction delays of A1, in the relatively free period of the spring of Prague in 1968 it was seriously considered a possibility to change the country's nuclear power program to the CANDU type of reactors. The Soviet led occupation of the country in 1968 put end to these discussions and plans. Instead, in 1970 a decision was taken to orient Czechoslovakia's nuclear power program to the Soviet designed and produced VVER reactors.

The first two VVER 440 (type V-230) reactors were constructed in Jaslovské Bohunice in Slovakia at the end of seventieth and connected to the grid in 1979 and 1980. The safety level of these reactors is causing some legitimate concern both inside and outside the country. The second pair of reactors was constructed at the same location but was of newer and more modern series VVER 440-213 and was connected to the grid between 1984-85.

In the Czech part of Czechoslovakia four reactors of newer VVER-440 type (V-213) were constructed in Dukovany near Brno and put into operation between 1985 and 1987. In the middle of eighties a construction of eight new reactors was started: Four VVER-440 (type V-213) reactors near the Slovak town of Mochovce, another four VVER-1000 (type V-320) in the Czech republic near Temelín.

The collapse of the communist regime in 1989 met both of these power plants uncompleted. After thorough discussions and analysis it was decided in 1990 to complete the Mochovce power plant with Siemens responsible for its modernization, mainly for the control and steering systems and also for overall improvement of safety systems. In 1993-94 it was also decided to complete the two already constructed Temelín reactors with Westinghouse being responsible for both control-steering system and for the fuel.

The decision to complete two of the originally planed reactors at Temelín was heavily opposed and protested not only by different green groups both in the Czech republic and Austria but also by the Austrian government and not only in different bilateral negotiations but even during the hearing in the US congress considering the Washington EXIM bank loan to complete the Temelín nuclear power plant.

SPENT FUEL MANAGEMENT

Together with the decision to continue and further develop nuclear energetics it was necessary to find a domestic and economically reasonable solution for spent fuel disposal.

Until 1986 the spent fuel did not represent any problem since the manufacturing country - i.e. USSR - made obligation at signing the contract to take care about it: the spent fuel was deposited at Jaslovské Bohunice and then transported back to the country where it was produced at practically no costs charged to Czechoslovakia. One can only speculate about the reason of such a generous arrangement. Most probably it was a way of keeping control over the plutonium.

During the period of perestrojka and the introduction of elements of market economy in the Soviet Union, the situation changed dramatically. Since 1986 the Soviet union, and later Russia, were ready to fulfil the initial deal only at additional costs which were gradually climbing sky high. Since 19.12.1991 when a law of Russian Federation was passed by the parliament, prohibiting to accept the spent fuel from abroad, the Soviet/Russian variant of handling the spent fuel became completely out of question.

This is the reason why Czechoslovakia started already in 1987 to build an interim storage capacity for spent fuel at Jaslovské Bohunice designed originally for all the Czechoslovak nuclear power stations from where the spent fuel should had been eventually further transported to the Soviet union.

Already before the split of Czechoslovakia the Slovak authorities opposed using this interim storage for the spent fuel from the nuclear power station at the territory of the Czech republic.

This is why the Czech republic had since 1992 to reconsider the whole problem of the

spent waste. The Czech energy board tried unsuccessfully to negotiate the storage of spent fuel abroad in Germany, Italy, Finland, Belgium and Sweden - i.e. in countries disposing with a free storage capacity. After rejecting the reprocessing variant it was decided to build both an interim and a final depository at the territory of the Czech republic.

The whole project is presently under the responsibility of the Czech energy board, the owner of all Czech nuclear power plants, and is financed by it. The spent fuel management program consist of several steps:

1. Increasing the capacity of the cooling basins at the nuclear power stations.
2. The construction of an interim storage capacity at the territory of the nuclear power station at Dukovany with a capacity of 600 t which will be used up to 2005.
3. Construction of a second interim storage capacity which will be used during cca 50 years. The interim storage capacity will be of surface type with containers produced by Škoda and will be in operation from approximately 2005.
4. Preparation and construction of a final depository which will be opened cca 2050-2070.

Under the assumption that no new nuclear power stations will be built and that the Dukovany NPP will be operated until 2018 and the Temelín NPP until 2028 - i.e. for thirty years only - the Czech republic will have to take care about 2872 t of uranium or of heavy metals. (See table I).

FINANCING

It is estimated that the handling and disposal of spent fuel and of final disposal of all the six reactor blocks operating today at the territory of the Czech republic will cost around 120 billions Kč (cca 4 billions of US $).

The whole project will be financed by the Czech energy board which is putting about 0.10 Kč from every produced Kwh to a special fund. (The production costs of nuclear electricity are presently about 0.45 Kč - i.e. one is keeping about 20% for the end part of the fuel cycle.)

PUBLIC OPINION

Due to the circumstances I referred to earlier (devastation of whole regions by coal power stations, heavy impact on health) the public opinion in the Czech republic is essentially pro-nuclear. Most of the antinuclear activities are imported from abroad: Austrian antinuclear activities, Green peace etc.

The public opinion pool performed in April 1993 shows that over 61 % of the population is either definitely pro-nuclear or probably pro-nuclear, with only 7% definitely anti-nuclear and 19% with no opinion. (See table II).

LEGISLATION

A weak point in the Czech republic is presently its nuclear legislation or better to say - the absence of it. The Czechoslovak Atomic Energy Commission (which existed since late fiftieth) ceased to exist when Czechoslovakia was divided in 1993. A corresponding Czech

atomic Energy commission was never constituted.

Even a more serious problem is that both the conception of nuclear energetics and the nuclear safety is handled at the department level of the Ministry of Industry and Commerce - certainly not a level possessing sufficiently high authority to decide, to promote and to regulate.

The Czechoslovak atomic legislation is in preparation - the nuclear law should be discussed in the parliament by the end of this year or latest in the spring of 1995 prior commissioning the first Temelín block. Unfortunately it is barely reflecting the existing situation and it is questionable whether it could bring any considerable improvement.

THE LIBLICE SYMPOSIUM

These are in short the reasons why the new ideas presented in the Los Alamos ATW project an later on the Rubbia energy amplifier met a positive response not only in the political quarters but also in the nuclear industry and in the management of the power plants. Even the mass-media were mainly positive and published several reports about the Los Alamos project already several months before Rubbia's press conference.

The initiative group for the accelerator driven transmutation of wastes and reactors was created in September 1973. Its activities are financially supported by the Czech Energy Company (ČEZ) and this allowed to convene on June 27-29, 1994 a small symposium at the Liblice castle near Prague on ACCELERATOR DRIVEN REACTORS AND NUCLEAR WASTE MANAGEMENT PROJECTS IN THE CZECH REPUBLIC.

The symposium met with a considerable interest of Czech scientists and nuclear engineers. Over 40 person, including several scientists from Sweden, Slovakia and Russia, took part in its work and around 20 papers, covering different aspects of this problem and reporting related activities in the Czech republic were presented. Encouraging was participation of a group of engineers from ŠKODA Nuclear Machinery Co who presented several papers showing that these new ideas are seriously discussed and studied in the industry.

The Liblice symposium allowed to review the competencies of Czech scientists and engineers in the field of accelerator driven reactor and transmuters. Many interesting proposals, topics were presented at the symposium.

COMPETENCE

The main centers in the Czech republic which possess know-how and a competence for the future accelerator driven transmutation studies.

Institute of Nuclear Physics, Czech Academy of Sciences, Řež
Institute of Nuclear Research, Řež
Institute of Special Anorganic Chemistry, Řež
Institute of Physics, Czech Academy of Sciences, Prague
Faculty of Mathematics and Physics, Charles University, Prague
Faculty of Nuclear Physics and Engineering, Czech Technical University, Prague

Institute of Nuclear Fuel, Zbraslav near Prague
Škoda, Nuclear Machinery Co, Plzeň

Institute of Thermomechanics, Prague
Institute of Electrotechnics, Prague

Let us shortly characterize these centra:

Nuclear Research institute, Řež near Prague:

Two experimental reactors (LVR-15 and LR-0 developed for testing fuel for the VVER reactors)
Reactor department.
Division of theoretical reactor physics.
Division of radiation chemistry (hot cells).,
Division of fuel cycle.
Division of metallurgy of uranium and of reactor materials, .

Institute of Nuclear Physics, Řež near Prague:

Cyclotron (U120M, energy for protons 36 MeV, alpha-particles 40 MeV)
Van de Graaf (protons 2-5 MeV).
Accelerator department.
Department of Nuclear reactions.
Department of Nuclear spectroscopy.
Collaboration with the Joint Institute for Nuclear studies in Dubna, Russia and access to its facilities.

Institute of Special Anorganic Chemistry, Řež

Considerable experiences with partition, extraction, solidification etc.

Institute of Physics, Czech Academy of Sciences, Prague

High Energy physics, detectors.
Collaboration with CERN.

Faculty of Mathematics and Physics and Faculty of Nuclear Physics and Engineering, Prague

Experimental reactor VR-1
Nuclear Physics
High energy physics
Dosimetry
Nuclear Chemistry
Neutron Physics,

Reactor Engineering.
Reactor safety.

Škoda Nuclear Machinery Co, Plzeň.

Considerable experiences and know-how in reactor construction. This company built at least 14 reactors (12 VVER 440, 2 VVER 1000), testing loops, production of transport and storage casks for spent fuel, reactor safety studies.

CONCLUSIONS

The 1994 Liblice meeting concluded that the Czech republic has not a negligible theoretical, experimental and engineering potential and know-how in several fields important for the rapid development of ATW and Accelerator driven reactor.

Reflecting the strong interest of Czech scientists and engineers and a favorable attitude of Czech industry and of Czech political quarters it was decided to establish an information and coordination center, based at the Institute of Nuclear Physics in Prague. Presently the main task of this Center will be the formulation and coordination of the national policy in this field. The center will also collect information about the development of transmutation technologies and assist in establishing contacts and collaboration with similar centra abroad.

The interest and financial support for this center both from the Czech Energy Board and Škoda company and the interest shown to these programs by the Ministry of Industry and Commerce is noted as positive and promising.

At the same time the Czech scientists and engineers are fully aware of the fact that the accelerator driven transmutation and reactors are too big projects to be handled individually by small European nations. Scientists and engineers from the Czech republic consider therefore a large scale international collaboration as an essential condition for further progress in this important and perspective project and would welcome a creation of an international coordination body as the first step. In a more - but not too - distant perspective also creation of an international institute, laboratory or center specialized on accelerator driven transmutation and energy production is desirable and will be supported by Czech specialists.

Table I

TIME-TABLE FOR THE FINAL DEPOSITORY IN THE CZECH REPUBLIC

1993-1994	approval of the conception, creating the basis of the spent fuel management system (legislation, fund, agency)
1995-2000	general geological survey, selection of the appropriate regions, comparison
2000-2010	detailed conception of the depository, underground laboratory, tests
2010-2015	decision about the location
2015-2022	detailed evaluation, discussion and approval of the selected location
2022-2030	final project and the construction of the depository
2030-2070	use of the depository and its sealing

BENEFITS and RISKS of P & T of NUCLEAR WASTE

K. Abrahams
Netherlands Energy Research Foundation (ECN), Petten, The Netherlands

Abstract. Efforts on waste transmutation are coordinated in a research programme called RAS. One of the aims of this RAS program is to inform the public and advise the authorities on methods for transmutation/ conditioning of nuclear waste, and on techniques which are being developed. Such new procedures for the treatment of waste should of course not lead to significant risks for the present population. Small risks might be accepted, but these should sufficiently be compensated for by favours to future generations.

CRITERIA TO JUDGE TRANSMUTATION SCENARIOS

Spent fuel from light water reactors contains about 100 kg of long-lived fission products, 300 kg of toxic actinides and 900 kg of short-lived fission products for each GWe year generated. For the actinides the mass balance depends strongly on the fuel cycle history, for the fission products this is less so. The long-lived fraction of fission products consists for about one third of the geochemically mobile fission products Tc-99 and I-129. Partitioning and transmutation (P & T) might have the following benefits and risks:

1) *Exploitation of the full energy content of the actinides will reduce fuel costs and waste streams from mining as well as from spent fuel.* A higher long-term toxicity in the fuel and a change in reactor parameters (delayed neutrons, temperature- and void-dependent efects) could be the price one has to pay for this benefit. If the corresponding risks would be low enough, one could reach acceptable waste-storage strategies, in which the life-time of long-lived radioactive components is shortened and actinides would be harmles in any waste-disposal scenario even if it is falsified by human intrusion.

2) Untreated waste transforms itself into a manageable form of partly fissile matter by decay of short-lived products, and disposal sites might become attractive actinide mines. *Future proliferation risks could be eliminated by transmutation.* The price for this benefit would be that one could risk an actual proliferation during the P & T process itself. If the risks and costs are controlled the P & T process could generate broad public acceptance.

3) *Dose-risks by leakage of mobile elements like Rn-222 and the metalloid fission products technetium and iodine could be reduced.* The price which should be paid relates to the avoidance of ecological risks of the partitioning process itself [1], as one should not spread radiotoxicity by procedures as machining or spilling of solvents.

Above mentioned points should be judged in a cost-risk analysis. For oil and coal the loss of human lives to the present generation for a constant production of one GW(e) lies between 1 and 10 per year. Casualties are lower for nuclear energy [2], and also the long term risks ought to be lower than long-term risks from the use of fossil fuel. As each scenario will have a price, it could be an approach to see this price expressed in an amount of dollars needed to save a life. On behalf of protecting contemporary individual radiological workers from harmful overdoses, one might offer a price of for example about 100 000 US $ for each man Sv avoided [3]. If however risks for any individual are low enough, collective risks will only be handled according to a strategy called ALARA (As Low As Reasonably Achievable), after all it is considered to be "more important to avoid one man to be hit by a bag of barley than to avoid every one to be hit by some grains".

TRANSMUTATION IN SUB-CRITICAL SYSTEMS AND IN REACTORS

Each proton of high energy (GeV or more) will liberate dozens of spallation neutrons from a heavy-metal target [4]. Either directly or after moderation these neutrons can be used to transmute actinides or fission products. In a slightly subcritical booster setup the number of neutrons might be multiplied with a factor $k_{eff}/(1-k_{eff})$. Cost and safety aspects of neutron generation and the amount of excess neutrons both depend on the value of k_{eff}. For small values the safety of the system might be best; on the other hand costs for electricity and capital investment in the accelerator would be less if k_{eff} would be close to one. In comparing the different proposed systems, the safety-cost balance should include special arguments for fission products as these are no potential source of neutrons in a reactor like actinides [5]. Although fast neutrons will have some advantages for actinide-transmutation, it is easy to show that fission-product transmutation rather takes place by capture of thermal neutrons [6].

In thermal incinerators some actinides could be used as fuel. Commercial thermal reactors are however energy and plutonium producing entities, which are not dedicated to waste transmutation. These LWRs may of course transmute Pu-239, and application of plutonium in MOX fuel for electricity generating LWRs will clearly diminish its growth. However the amount of transuranium elements will increase anyway due to the continuous capture of neutrons in U-238. It is difficult leave out the U-238 because this capture process is essential to economy and safety of LWRs: it increases the reactivity swing of the fuel by breeding fissile plutonium, and Doppler broadening of capture resonances will keep temperature coefficients negative even for large systems. As long as U-238 is the main component in the fuel, the accumulated plutonium mass will increase in any recycling scenario (fig. 1). Due to the build-up of even plutonium isotopes the multi-recycled fuel will become much less fissile in thermal spectra, whereas it remains fissile in fast spectra. If no external neutron source would be applied, an LWR would require an increasingly higher fissile enrichment, and this would create a less economical situation. High concentrations of even-N transuranium isotopes in LWR fuel would also give safety problems due to the fact that the number of formed fission neutrons in such multi-recycled fuel increases with a hardening of the neutron spectrum (see table 1). This problem should be solved, either by integrating the fuel with the moderator or by applying an external neutron source to a sub-critical system, otherwise the reactor could become a prompt critical fast reactor after an accidental loss of its moderator! Thermal systems will have as a further disadvantage that the toxicity in the U/Pu cycle will rise due to heavier actinides, as the amount of even plutonium isotopes and trans-plutonium elements will continuously grow by neutron capture. Calculational exercises on a liquid-salt reactor with graphite moderator show that continuous feeding of LWR waste would lead to unpractical equilibria up to 40 % curium in the fuel [7]. For any reshuffling scheme in any thermal system which tries to eat its own waste, similar toxic mixtures will be produced in the fuel.

Fast incinerators have therefore been proposed for transmutation of actinides. Possibly the breeding mantles of fast incinerators could be replaced by moderated sub-assemblies, which could then also be used for the transmutation of fission products. From several studies it has been concluded that critical fast reactors could only have a minor-actinide fraction in the fuel up to 5%. If the transuranium concentrations in the fuel would be higher, the number of delayed neutrons per fission could become too small, especially for the lighter isotopes [7]. Reactivity problems could either be enhanced by positive voiding-feedback or by insufficient Doppler-damping of temperature excursions. If critical reactors

are not considered safe enough one could consider systems with $k_{eff} < 0.95$. External neutrons could then be supplied by another reactor (possibly a fusion reactor), or by a spallation source with a GeV proton beam. Such external sources could even provide enough excess neutrons for transmutation and generation of energy at the same time. Advanced reactor systems could be developed to reduce not only the amount of plutonium, but also to reduce the very long-term toxicity due to americium and neptunium.

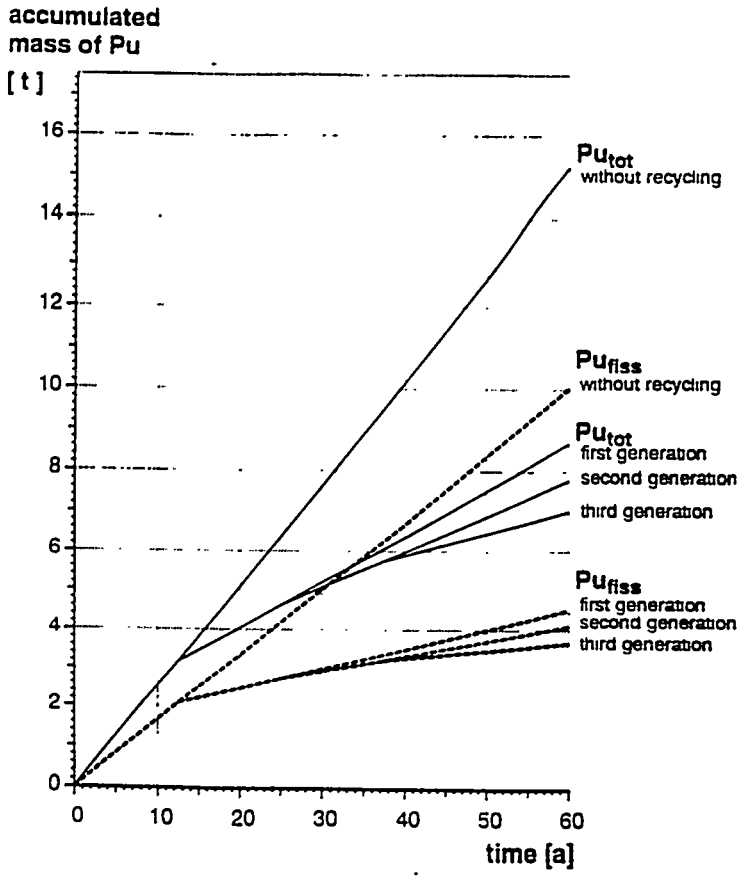

Fig.1: Evolution of the total mass Pu_{tot} and of the total fissile mass of plutonium Pu_{fiss} in a multi-recycling scenario for a PWR, 1300 MWe, 45 MWd/kg, and recycling time 12.5 years [8].

Table 1: Average amount of fission neutrons for a single neutron, which has been absorbed in a fuel pin of a Light Water Reactor or of a Liquid Metal Burner Reactor. This amount is given for several actinides.

Nuclide	LWR	LMFBR
U -235	1.98	1.92
U -236	0.11	0.43
U -238	0.29	0.39
Np-237	0.05	0.49
Pu-238	0.25	2.02
Pu-239	1.84	2.29
Pu-240	0.02	1.24
Pu-241	2.20	2.45
Pu-242	0.05	1.10
Am-241	0.04	0.46
Cm-242	0.64	1.33
Cm-243	2.94	2.99
Cm-244	0.20	1.58

Special arguments in case of transmutation of fission products

In contrast to the situation described for the actinides any thermal reactor could be used to diminish the toxicity of fission products, and in principle even commercial LWRs could be used to get rid of Tc and perhaps also of I. Costs might however be prohibitive as an efficient transmutation at low flux would require huge loadings of waste, additional fuel enrichment and recanning and reprocessing efforts. Reactors with a somewhat higher flux (HWRs like CANDU) and with possibilities for refuelling on-line, are therefore being studied. High-flux thermal reactors could be entirely dedicated to transmutation, and moderated sub-assemblies of high flux fast reactors might also have potentials. For large scale transmutation of long-lived fission products a feasible and economic technology is however not yet available due to several limitations related to safety and cost aspects.

Fission products with low cross sections would require a rather high thermal flux, and one might consider application of neutron boosters just as for actinides. In fact a sub-critical system will be more economical than any accelerator-based system without a booster. The argument is as follows: One 1.5 GeV neutron produces 30 neutrons in a tungsten target without a booster. Suppose the accelerator efficiency is about 50% (a very optimistic statement). In this case the price of one thermal neutron in terms of electrical energy is 1500/(30*0.5) = 100 MeV. As this electrical energy had to made from thermal energy one would have required about three times more energy. It is unrealistic to assume that each neutron will transmute a nucleus, but even then one would need more than 300 MeV thermal energy to transmute one nucleus. If this 300 MeV would have been generated by means of a nuclear reactor, this would mean that more than one fission in the reactor is needed to transmute one nucleus at the accelerator. Direct transmutation in a reactor seems more economic because also one free neutron might become available for each fission in the reactor itself. Reactor-based transmutation of a technetium nucleus is clearly more direct because the 200 MeV, which is generated by fission, will still be useful to generate electricity, which is no longer needed for the accelerator. In sub-critical systems with fissionable material each neutron from the accelerator-target system might produce again up to ten new fission neutrons, and transmutation costs of such systems will be in between that of pure accelerators and that of critical reactors [9]. Other costs might however be lower for hybrid systems, as a good neutron economy [5] allows for a better loading.

REDUCTION OF DOSE-RISKS FROM LEAKAGE

As long as the integrity of a disposal site is guaranteed, *long-lived fission products will determine the leakage-risks*, which are defined by the triple product of toxicity, leakage probability and geochemical mobility. For an unperturbed granite repository [10] table 1 shows the risk due to spent LWR fuel in a once through scenario [6]. It is seen that the unspent uranium would give the main residual actinide contribution, and that Tc and I dominate dose-risks. Diffusion of anions of iodine and per-technate in ground water is more rapid than flow of the ground water itself. This fact is now again being realized.

TABLE 2: TIME-INTEGRATED LEAKAGE-DOSE DUE TO SPENT LWR FUEL
(direct storage of spent fuel, due to nuclear generation of one GW(e) year)

Period : Nuclides :	One million years	Hundred million years
Tc-99	98 %	46 %
I -129	2 %	1 %
Cs-135		24 %
U -235		6 %
U -238		14 %
Np-237		5 %
Pu-239		4 %
man Sv	9000 *)	20 000 *)

*) Collective dose for the global population. The average yearly individual dose may be obtained by dividing by the affected number of people and the indicated period.

Any collective dose rate could be compared with the natural rate from radon, and even for the most relevant long-lived fission product Tc-99 the collective dose-risk is only marginal, if it can be assumed that in due time the Tc will distribute itself evenly in time and space over the world. A value of 10^{-12} Sv/year would then be the order of magnitude for the personal average dose-rate due to electro-nuclear production of one GW(e) year, which is about one part per billion in terms of the natural radon dose-rate.

Arguments on the collective leakage-dose should be treated with some caution. First of all it is questionable whether the risk should be ranked as in table 2 (a collective integrated dose from leakage out of a repository). If one would for example rank according to the highest possible individual dose, the I-129 risk could dominate for repositories of clay [11] or rock salt [6]. Local dose-risks are almost entirely due to uptake of iodine in the thyroid. This gland contains about 10 mg of iodine, and risks could be made marginal by diluting the I-129 isotopically with natural iodine. In some scenarios the collective leakage dose might even increase due to transmutation: Due to the fact that U-234 will in the long run lead to mobile Rn-222 one could for example double the local dose due to emanations for a few hundred thousand years by spilling only a few hundred milligrams of U-234 or one of its precursors into the soil. This isotope of uranium, which also occurs naturally (with an isotopic abundance of 0.0055 %) is responsible for most of the present radiation dose to mankind. Its most dangerous daughter Ra-226 has a half life of 1600 year, and about 60 t of radium in the soil emanates almost 6 litre of radon each day, which builds up an equilibrium value of about 20 litre of radon in the total biosphere of our planet. This tiny amount nevertheless gives about 60 % of the total radiation dose, which averages to about 10^{-3} Sv per person yearly and this leads to an estimate of the collective dose of the order of $5 * 10^6$ man Sv/year. It would therefore be environmentally very unwanted if the present amount of U-234 would increase, and it might very well be that build-up of U-234 in the soil gives a higher dose than a corresponding build-up of the heavier actinides.

Dose risks for the Th/U Cycle

Competing demands of safety, economy and non-proliferation have been defined and rated for the thorium cycle, in which capture breeds Pa-233, which decays into the fissile U-233. The U-233 will be isotopically diluted with U-234, which is formed by parasitic capture, and as a consequence the risk for proliferation would be reduced as long as the decaying Pa-233 would remain in the fuel. In this case however the breeding cycle suffers from neutron shortage due to absorbtion in Pa-233. High-flux systems to transmute non-fissile waste, would not only need extra fissile additives or a powerful accelerator as a neutron source [13], but also frequent refuelling and partitioning of the Pa-233 would be needed to reduce parasitic absorbtion. Such a cycle needs a regular clean-up by removal of intermediary daughter nuclei because otherwise high radiation levels at reprocessing facilities could result from the build-up of U-232 and its daughter Th-228, that would soon lead to the hard gamma-emitter Tl-208. In a low-flux system only a small external neutron source [12] or the addition of little extra plutonium to the fuel could compensate for capture losses in Pa-233, and on-line reprocessing would no longer be required. This is important, because as was discussed above, any spilling of U-234 should be avoided. Nevertheless isotopic contents in the fuel of the Th/U cycle could range from 30-50 % for U-233,234 and because in the long term the dose-risks due to Rn-222 might dominate over dose-risks from any actinide, *the Th/U cycle gives a high long-time dose-risk due to radon emanation, in any scenario in which the waste would come to the surface either by intrusion or by accident.*

STUDY OF END SCENARIOS

Some study ought to be focused on accelerator-based waste management for the case that production of nuclear energy would be ended and large quantities of fissile waste are to be disposed of at once. Similar situations would occur if large quantities of weapon plutonium would have to be transmuted. Procedures would depend on the criteria to be adopted. In case of ultimate safeguarding requirements one could pollute the Pu-239 with less fissile material by irradiating it with thermal neutrons. This renders the plutonium less useful as a weapons material, and makes it hard to divert. Either LWRs, HWRs, or ATW systems could be used to denature plutonium isotopically by its even isotopes. This procedure would however increase the toxicity considerably, and one would need to store the irradiated plutonium for a long time, and possibly in an irreversible and geologically secured way. As this storage procedure would hardly comply with present public demands for waste disposal, any acceptable end-scenario should be followed by fission of actinide waste. This could be achieved by means of an extended use of fast reactors, and possibilities to generate a fast spectrum in a safe way, and to develop a hybrid with a proper neutron economy should therefore be investigated [14].

CONCLUDING REMARKS and RECOMMENDATIONS

Transmutation of the existing plutonium is priority number one. After all proliferation risks are most clear for plutonium, and possibilities for future mining for this element should be eliminated to prevent very long lasting proliferation risks. No exclusive LWR-scenario has yet been found, which entirely solves the plutonium problem by transmutation.

Reduction of minor-actinides in fast reactors might profit from a special control of the reactivity in accelerator-based options [14]. Accelerator-based systems, have safety aspects in common with purely reactor-based waste transmuters. As an energy of 200 MeV will be liberated per fission, energy densities and meltdown risks due to Loss of Cooling (LOC) scenarios will be similar for any efficient burner. In order to avoid window problems low currents should be applied and windows ought to be cooled by non-pressurized liquids.

Criteria on the reduction of dose risks disfavour transmutation scenarios in which the waste will be contaminated with U-234 or with one of its precursors, unless a disposal method is applied that prevents radon emanation from the waste to reach the atmosphere.

Reductions of collective dose-risks, which are far below the natural dose-risks seem at first sight to be of less relevance. In proper disposal scenarios the world- and time-integrated collective dose is almost 10 000 man Sv for each GWe year, and thereby less than a fraction 10^{-9} of the natural dose risk. Resistance against the dumping of low-level nuclear waste into the ocean has shown that there are incentives to reduce the dose even below marginally small values. These incentives seem hardly motivated by the wish to reduce dose risks to human beings, and in this respect it is illuminating to recall the argument on the dose risk from the fission product I-129, for which other people argue that "isotopic dilution with natural iodine should reduce the highest individual doses". As long as no agreement exists on the existence of safe thresholds for dose-risks, priorities are a matter of taste, and are therefore subject to changes.

"What is reasonable?" is the main question relevant to reduction of collective dose-risks, as the ALARA principle extends apparently to the price of electricity as well as to risks.

REFERENCES

1. T.H. Pigford, Trans. of the ANS 62 (1990) 97, and 63 (1991) 80.

2. A.F. Fritzsche, "The Health Risk of Energy Production", Risk Anal. 9 565-577, 1992.

3. E. Schmidt, E. Zamorani, W. Hage, and S. Guardini, "Assessment Studies on Nuclear Transmutation of by-product Actinides". Commission of the European Communities, Joint Centre ISPRA Establishment, S.A./1.05.03.83.13.

4. L.H. Baetsle, "Role and Influence of Partitioning and Transmutation on the Management of Nuclear Waste Streams" NEA/P&T REPORT No 3 1992".

5. M. Salvatores, I. Slessarev, and M. Uematsu, "A Global Physics Approach to Transmutation of Radioactive Nuclei", Nuclear Science an Engineering, 116 (1994), 1.

6. K. Abrahams, "Transmutation of Long-Lived Fission Products", ECN-RX-94-003, IAEA Technical Committee Meeting on: Safety and environmental aspects of partitioning and transmutation of actinides and fission products, Vienna, 29-11-93.

7. K. Abrahams, Specific contributions of the Dutch programme RAS towards accelerator-based transmutation

8. G.J. Schlosser, S. Winnik, IEAE-SM-294/33 (1987), and draft status report from H. Küsters and G. Schlosser to the NSC on Pu utilization.

9. A.J. Janssen, Transmutation of Fission Products in Reactors and Accelerator-driven Systems: Some Critical Remarks, Report to the CEC, and ECN--I-94-001 (1994).

10. S.F. Mobbs et al, "Comparison of Waste Management Aspects of Spent Fuel Disposal and Reprocessing: Post-Disposal Radiological Impact", EUR 13561 EN (1991).

11. L.H. Baetsle, Proc. of the Information Exchange Meeting on Act. and Fiss. Product Separation and Transmutation, Mito city, Japan, 7-11-90, OECD 37290 (1991) 299.

12. F. Carmati, R. Klapisch, J.P. Revol, Ch. Roche, J.A. Rubio, and C. Rubia, "An Energy Amplifier for Cleaner and Inexhaustible Nuclear Energy Production by a Particle Beam Accelerator", CERN/AT/93-47.

13. C.D. Bowman et al, "Nuclear Energy Generation and Waste Transmutation using an Accelerator-driven Intense Thermal Neutron Source", Nuclear Instruments and Methods in Physics Research A 320 (1992) 336-367

14. Hiroshi Takahashi and Herbert Rief, Concepts of Accelerator Based Transmutation Systems, OECD Specialists' Meeting on Accelerator Based Transmutation (Wuerenlingen/Villigen 26-3-'92).

    H. Takada et al, Proc. Int. Conf. Emerg. Nucl. Energy systems (1991).

Flowing Lead Spallation Target Design for Use in an ADTT Experimental Facility Located at LAMPF

C. A. Beard, R. R. Bracht, J. J. Buksa, W. Chaves, B. G. DeVolder, H. O'Brien, J. J. Park, R. B. Parker, C. Pillai, R. C. Potter, R. S. Reid, D. A. Trujillo, O. A. Vela, F. Venneri, D. J. Weinacht, S. A. Wender, W. B. Wilson, K. A. Woloshun
Los Alamos National Laboratory
Los Alamos, NM 87545

Abstract. A conceptual design has been initiated for a flowing lead spallation target for use in an ADTT experimental facility located at LAMPF. The lead is contained using Nb-1Zr as the structural material. This material was selected based on its favorable material properties as well as its compatibility with the flowing lead. Heat deposited in the lead and the Nb-1Zr container by the 800-MeV, 1-mA beam is removed by the flowing lead and transferred to helium via a conventional heat exchanger.

The neutronic, thermal hydraulic, and stress characteristics of the system have been determined. In addition, a module to control the thaw and freeze of the lead has been developed and incorporated into the target system design. The entire primary target system (spallation target, thaw/freeze system, and intermediate heat exchanger) has been designed to be built as a contained module to allow easy insertion into an experimental ADTT blanket assembly and to provide multiple levels of containment for the lead.

For the 800-MeV LAMPF beam, the target delivers a source of approximately 18 neutrons/proton. A total of 540 kW are deposited in the target. The lead temperature ranges from 400 to 500 C. The peak structural heating occurs at the beam interface, and the target is designed to maximize cooling at this point. An innovative thin-window structure has been incorporated that allows direct, convective cooling of the window by the inlet flowing lead. Safe and reliable operation of the target has been maximized through simple, robust engineering.

INTRODUCTION

The design of a high-power spallation target is essential for almost all Accelerator-Driven Transmutation Technologies (ADTT). Although the optimal target material and target design is strongly dependent on the system in which it is to be used (and its associated goals), many ADTT applications (Accelerator Transmutation of Waste (ATW), Accelerator-Based Conversion of plutonium (ABC), Accelerator-Driven Energy Production (ADEP)) would benefit from using a simple monolithic target design. To avoid large parasitic neutron losses in such a design, the use of a low-neutron-absorbing material (such as lead, bismuth, or a lead-bismuth eutectic) is required. Additionally, the low melting points of these materials and the high target power densities needed for the ADTT applications require that the target material be used in liquid form.

The design and operation of a flowing-liquid-metal spallation target presents many technical challenges with regard to material compatibilities, heat transport from the target material as well as its structural container, handling of the liquid metal, as well as obtaining the required target lifetime for use in an ADTT system. All of these issues must be dealt with while still delivering the required neutron source to the transmutation system. In order to resolve these issues, an effort has been initiated to design and operate an experimental flowing lead spallation target at the Los Alamos Meson Physics Facility (LAMPF). This effort includes the design of the primary target and required subsystems (pump, heat exchanger, secondary heat transport system, lead freeze/thaw control, lead injection/removal system, and associated instrumentation), as well as a series of developmental experiments (material irradiation, flow modeling, lead handling, etc.) ultimately leading to the operation of the flowing lead spallation target in the LAMPF proton beam.

PRIMARY TARGET DESIGN

A diagram of the primary target is shown in Fig. 1. The lead is contained using Nb-1Zr as the structural material. This material was selected based on its favorable material properties as well as its compatibility with the flowing lead[1]. The 800-MeV, 1-mA LAMPF proton beam impinges upon the target with a beam distribution assumed to be a Gaussian with a 1.25-cm standard deviation which is similar to the beam distribution incident on the Los Alamos Neutron Scattering Center (LANSCE) spallation target. The actual beam distribution will ultimately depend on the physical location of the target along the beam line, but in no case will be smaller than stated above. The LAHET Code System (LCS)[2] was used to characterize the neutron source. This configuration produces a total neutron source (leakage) of 18.13 neutrons/proton. The leakage distribution is given in Table 1.

Table 1. Calculated Distribution of Leakage Neutrons from Spallation Target

Target Face	Leakage (neutrons/proton)
Front	6.58
Rear	2.23
Radial	9.32
Total	18.13

Flow-characterization within the target has been performed. The flow enters vertically from the top into an inlet plenum located in the outer radial region at the rear of the target. The flow is injected into the center core of the target where it is forced through the hole in the second window and upon the center of the first window, where it is then redirected outward between the two windows into the outlet plenum and upward out of the primary target region. It should be noted that although both the primary structural interface between the target and beam, as well as the flow guide behind it are referred to as "windows", the actual window confining the vacuum along the beam line will be the typical water-cooled inconel-718 window currently used at LAMPF. For a target employed in an ADTT system, it is envisioned that the first window will be the actual vacuum interface for the beam line, but this will not be the case for the experimental assembly. The flow distribution between the two windows is shown in Fig. 2. Two recirculation zones exists: one between the two windows, and a second in the outlet plenum. Neither of these is expected to present a problem; however, efforts are underway to reduce or eliminate this behavior.

Stress analysis on the target has centered on the mechanical response of the target to internal pressure loading. Three-dimensional, one-quarter symmetry, static ABAQUS analyses have been used to determine stress levels within the walls of the target assembly. Typically, the models are composed of beam entrance windows that intersect the outer wall of the pressure vessel. The outer window was modeled with a varying thickness throughout its diameter because of the volumetric heating of the window material by the proton beam. The window initially has a constant thickness of 3/16 inch from the center of the window to a radius of 2 inches. From the 2 inch radius to the outer edge of the windows the thickness linearly varies from 3/16 inch to 3/8 inch with radius. The outer cylinder and double radius end cap are all 3/8 inch thick. All other walls and cylinders are 1/16 inch thick. The entire structure was modeled with Nb-1Zr. The outer surfaces were subjected to an internal 45 psi pressure to simulate the load created by the internal liquefied lead.

Areas with von Mises stress levels approaching a stress level greater than a percentage of yield (typically 30 to 50%) indicated areas of the model that were weak and needed modification. If areas of high stress were found, the model was changed to reduce the stress. This process continued until the peak stresses in the tank were less than 1/3 the yield value of 11,000 psi at

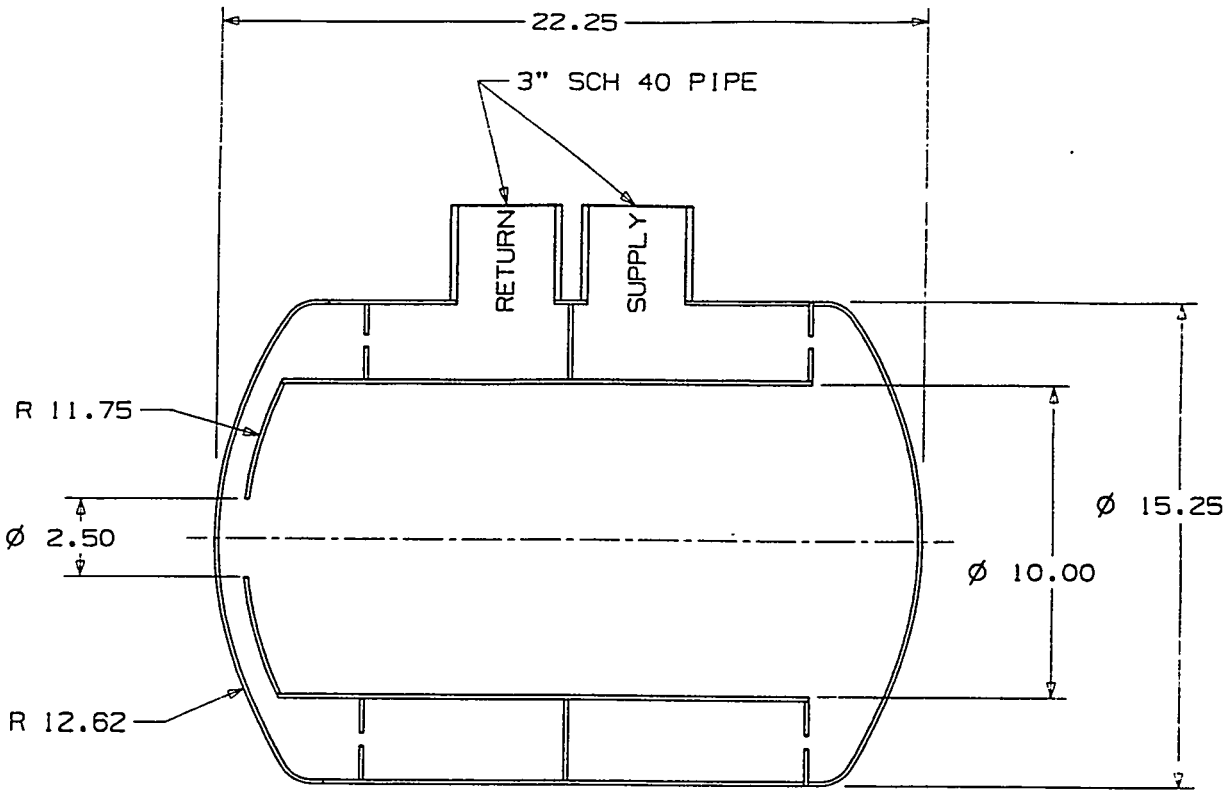

Fig. 1. Diagram of the primary spallation target. All units are in inches.

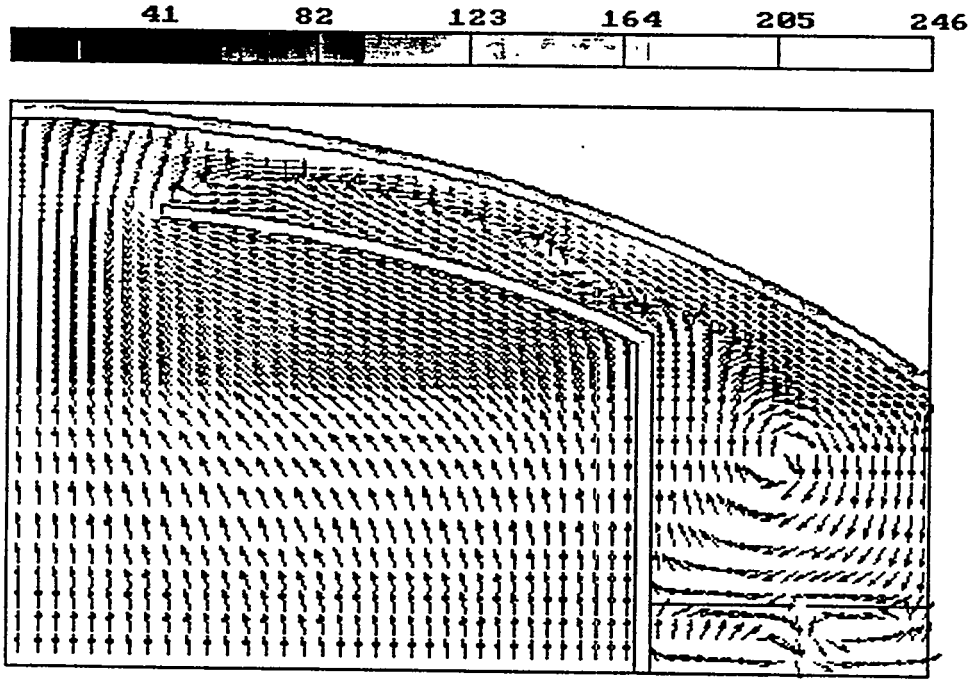

Fig. 2. Flow characterization of the lead flow between the two windows with velocity vectors (cm/sec) included.

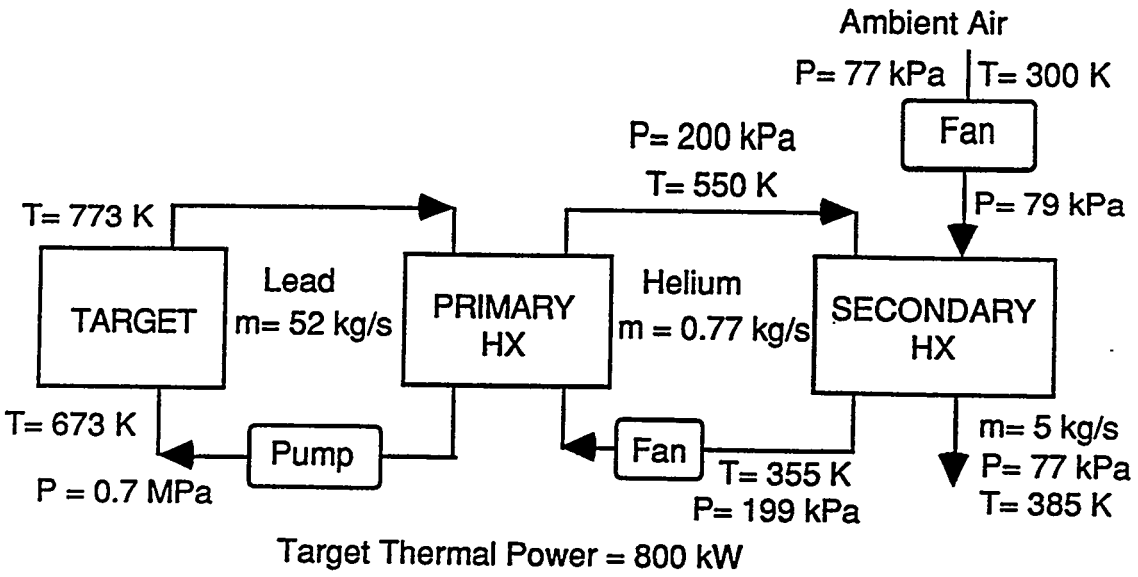

Fig. 3. Operating conditions for lead target system.

900 °C for Nb-1Zr. Although this temperature is the temperature reported for the center portion of the window, the actual temperature at the edge of the tank may be much less than the 900 °C maximum. Since the areas of highest stress levels were typically encountered at the intersection of the beam entrance window and the outer tank wall, the use of the maximum stress at the higher temperature provides for a conservative approach to the design of the target.

HEAT REMOVAL SYSTEM

Heat removal is accomplished by circulating the lead *via* an electromagnetic (EM) pump through an intermediate heat exchanger which uses helium as the secondary working fluid. The total power deposition was computed using the LCS and was found to be 540 kW. However, for conservatism, the primary and secondary heat transport systems were designed to remove 800 kW. This translates into a required mass flow rate of 52 kg/s. A systems diagram which shows the temperatures and pressures throughout both the primary and secondary loops is shown in Fig. 3.

Heat removal from the structural container is accomplished through convective cooling using the flowing lead. This places the most stressing heat removal requirements on the first window which is directly exposed to the beam. Using the LCS, a spatially dependent power distribution in the first window was calculated by dividing this structure into a series of concentric annuli. The peak power density occurs in the center of the beam and is equal to approximately 2000 W/cc. A best estimate of heat transfer coefficient for direct impingement cooling on the target window with flow through a 6.35-cm diameter hole is 17400 W/m^2-K. This is based on flow impinging on a large diameter sphere, whereas the actual flow condition looks more like a submerged jet impingement. Therefore, there is a large uncertainty in this prediction, and there is no correlation in the literature for a liquid metal from a better geometry match. With this coefficient, and at 450 W/cm^2 surface heat flux (resulting from 2000 W/cc in a 0.24 cm thick window), the inside window temperature will be 775°C at a Pb temperature of 500°C. The temperature gradient through the window is 100°C, resulting in a peak window temperature of 875°C. Issues such as wetting and effects of gases or other impurities are recognized as serious issues in maintaining the required heat removal from the structure. These

issues can not be resolved satisfactorily through analytical techniques, however, and (as will be described later) are included in the developmental experiments which precede the final spallation target operation.

The intermediate heat exchanger has the lead contained within the shell and the secondary fluid (helium) flowing within the tubes. The lead is contained within the shell so as to provide easier draining and eliminate the chance of plugging the tubes' interior bore. The tubes are formed in a U-tube shape to aid in absorbing thermal expansion. The heat exchanger is designed to transfer 800 kW of heat with an additional over-capacity factor of 35%. Calculations include an allowance for compressive heating of the helium by the blower. Helium enters through a duct in the side of the assembly at 102 °C and flows at an average velocity of 134 m/s downward on one side of the U-tubes, and then flows upward on the other side and exits at a temperature of 277 °C back out the side horizontally. The liquid lead enters at a temperature of 500 °C through distribution pipes at the rear of the tube bundle and flows forward in crossflow across the tubes, making a single pass, and then exiting at a temperature of 400 °C at the front through another set of distribution pipes. Because the heat conduction of the lead to the tubes is much better than the heat conduction of the helium to the tubes, the lead flows at a relatively low average velocity of 0.07 m/s.

A compact plate-fin cross-flow heat exchanger transfers heat from the secondary cooling loop to the ambient environment. The secondary cooling loop pressure and temperature at the compact heat exchanger inlet are 200 kPa and 277°C temperature. Several heat exchanger candidate designs have been examined to maximize heat exchanger effectiveness with minimum pressure drop and heat exchanger size. A typical heat exchanger configuration has an exit temperature of 75°C with a 840 Pa pressure drop. The power requirement for the secondary loop heat exchangers is about 50 kW for a blower with a 50 percent adiabatic efficiency. The heat exchanger is cooled with ambient air supplied by a blower. After passing through the heat exchanger the heated air is exhausted to the atmosphere. The required power for the air blower with 50 percent adiabatic efficiency assuming a 77 kPa inlet pressure, a 1770 Pa static pressure rise, and a 5 kg/s mass flow rate is about 20 kW.

Lead circulation in the ADTT experimental target will be produced using an A. C. electromagnetic (EM) conduction pump. EM pumps offer the advantage of being nonintrusive to the piping; no seals or mechanical coupling to the lead are necessary. The selected pump will circulate the lead at the required 52 kg/s with a 20 psi pressure boost at an efficiency of 11%. Physically, the pump is approximately cubical, 22 inches on a side, and weighs 360 lb.

LEAD HANDLING SYSTEM

To facilitate safe and efficient handling of the lead, only liquid lead will be used in the primary target system. Thaw, freeze and lead storage will be performed below (allowing gravity drainage) the primary target system in a "reservoir" specifically designed for this purpose. Outside the primary target system the lead is handled in a "foundry" of similar design (but twice the volume) to the "reservoir". A diagram of the foundry is shown in Fig. 4 and the features of the reservoir can be seen in Fig. 5. In each, heaters are located around the sides and bottom of the lead in clusters or zones to allow for spatially dependent heating of the lead. A free surface of lead at the top accommodates the increase in volume (3%) and any lead oxide that might form. The heaters in the foundry produce 20 kW allowing for a 4 hour melt. In the reservoir they produce 10 kW which translates into a 6.6-hour period to melt the volume of lead to an operational temperature (450°C) prior to injection, including estimates for heat losses to the vessel and surrounding environment. In both systems lead is maintained in an argon atmosphere to minimize the formation of lead oxide which can prohibit flow. Initially, the lead is 0.9999 pure; this purity is commercially available[3]. Also, lead injected into the primary target system

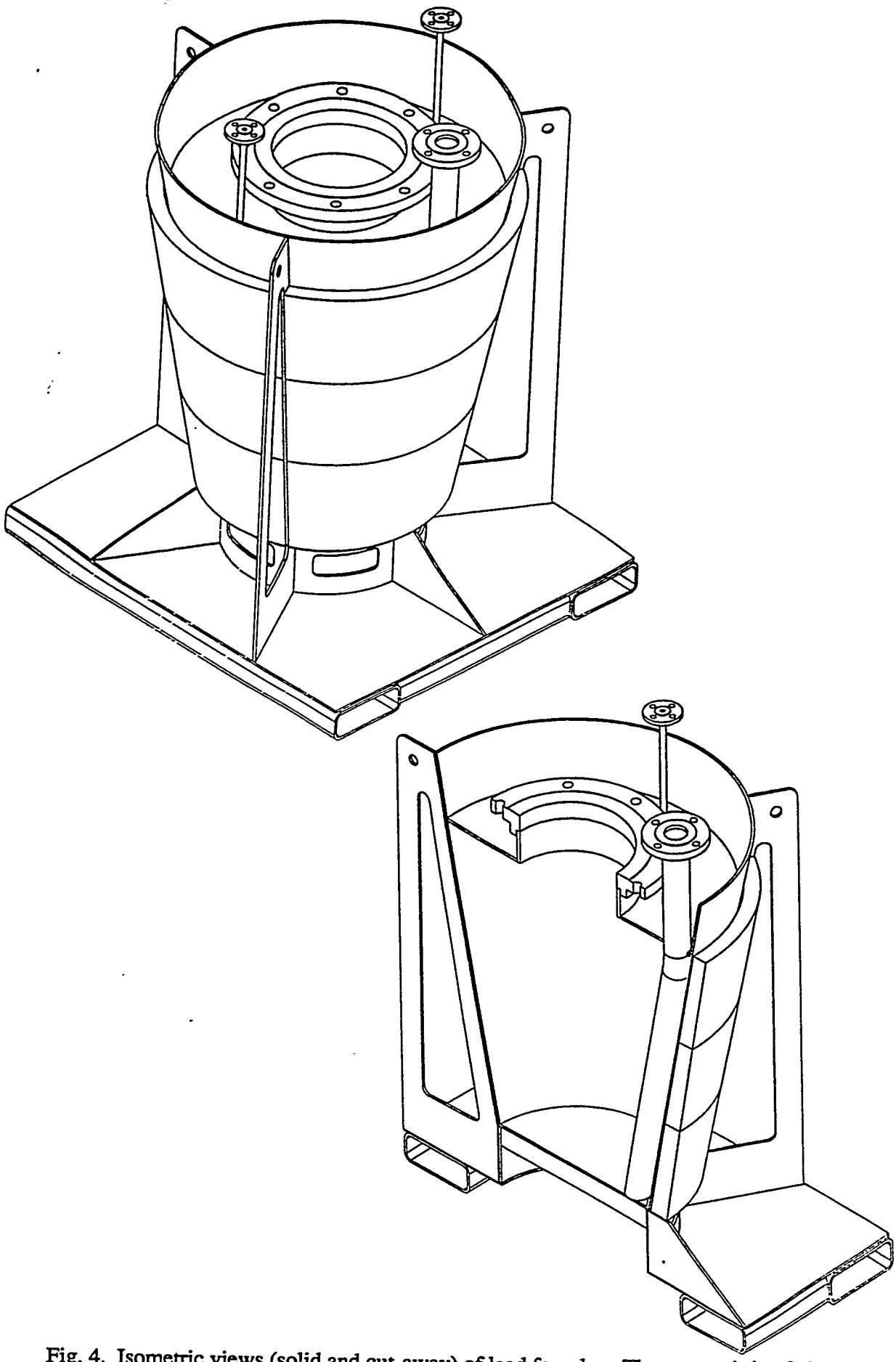

Fig. 4. Isometric views (solid and cut-away) of lead foundry. The reservoir is of similar design, but smaller.

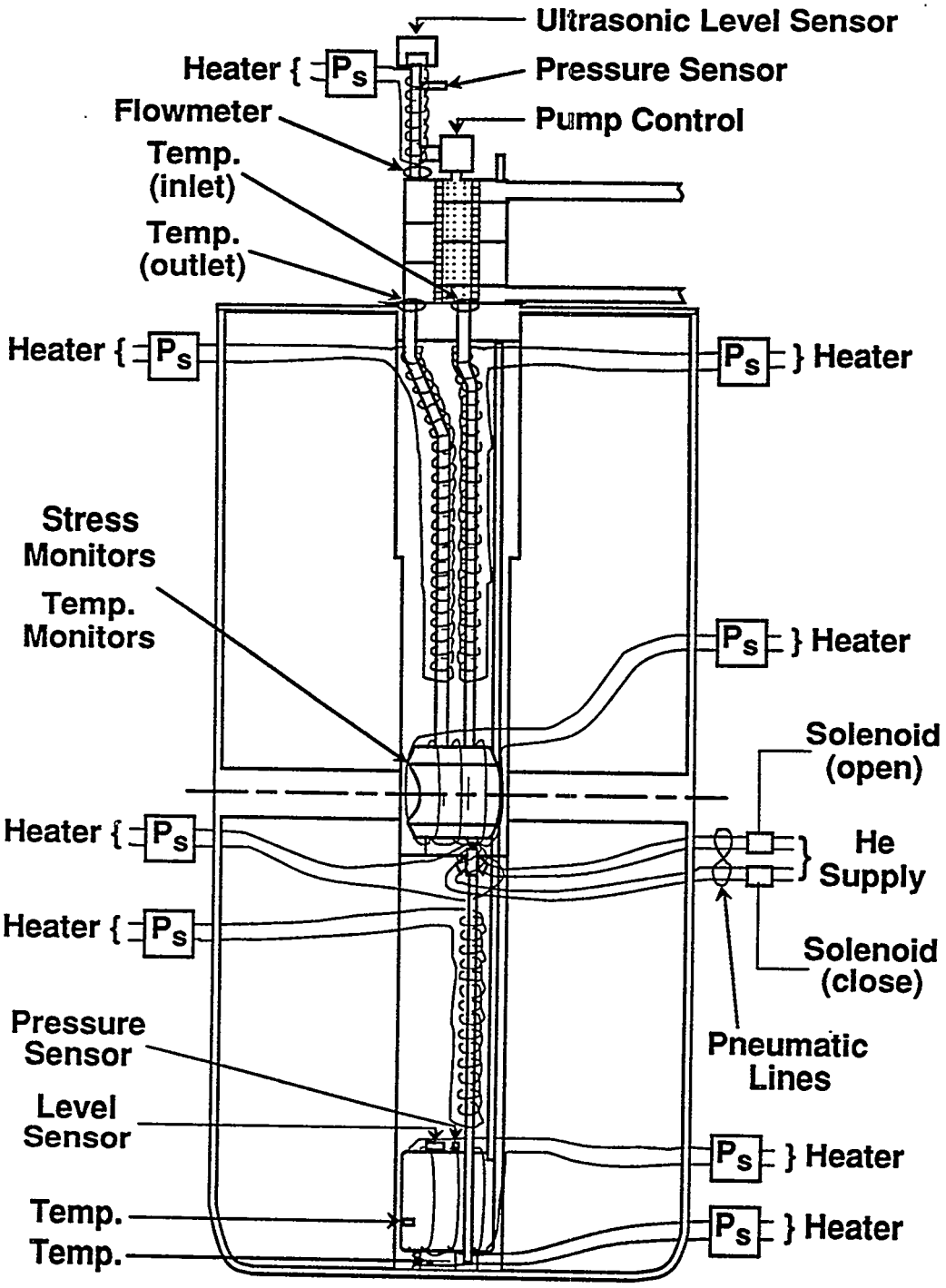

Fig. 5. Diagram of experimental target system showing primary target loop, lead reservoir, and planned instrumentation

is taken from the bottom of the foundry or reservoir to help reduce injection of any oxide into the system because the less-dense oxide will float on the top of the free-surface in both the foundry and the reservoir. The lead is injected using argon pressure into the target system initially from the foundry and subsequently from the reservoir. A level sensor located at the top of the primary loop detects when the system is full, closing a pneumatic valve and separating the primary loop from the reservoir. These features can be seen in Fig. 5. The valve can be remotely operated to drain the lead into the reservoir for storage and freezing. The valve will automatically open during off-normal conditions to drain the lead from the system. Lead can be pumped outside the target chamber, from the reservoir to the foundry, using argon pressurization.

INSTRUMENTATION

The planned instrumentation is also shown in Fig. 5. The ADTT instrumentation will be centered around dual personal computers (PCs) with one PC running in hot standby mode. A heartbeat between the two PCs will provide automatic switchover in case the active computer should fail. All interfaces to temperature sensors, level detectors, etc. will be handled through standard process control boards plugged into the PC. The hardware will use off-the-shelf products wherever possible. All process control and user interface will be handled in LabView. LabView is a process control/programming environment that allows maximum flexibility in modifying the process when needed. At the same time, a process flow chart can be easily implemented that maintains safety of operation by not allowing process actions that could produce unintended results. As an added safety measure, both audible and visual alarms will be controlled from within LabView.

DEVELOPMENTAL EXPERIMENTS

Prior to the final operation of the experimental target, a number of developmental experiments are planned. The purpose of these experiments is to eliminate as many uncertainties as possible prior to the final target operation that can not be eliminated through analysis, as well as benchmark the analytical techniques used in the target design.

Irradiation Experiments

Although the high temperature strength of Nb-1Zr is well characterized, both unirradiated and thermal-reactor irradiated, its long term behavior in a mixed proton and high energy neutron environment is unknown. The effect of irradiation on surface topology will also impact Pb wetting and heat transfer. Consequently, several material irradiation experiments are planned which address the irradiated strength of Nb-1Zr:

Neutron Irradiation of TEM Samples

TEM samples in a sample holder will be irradiated at LAMPF in neutron-irradiation ports. The irradiated TEM samples will be used for subsequent micro-hardness testing, surface examination, and Transmission Electron Microscopy (TEM). Material damage induced by the entire spallation neutron flux spectrum can be estimated from the results of this experiment. The calculated spallation neutron flux from the LAMPF A-6 target station differs from the fission flux in two ways: there is a high energy tail above 5 MeV and there is an increased flux component below approximately 0.1 MeV; both of these are not present in a fission flux.

Proton Irradiation

In order to expose material samples directly to a high-energy (700-800 MeV) proton flux, thin sheet samples will be inserted into a standard isotope production stringer. The irradiated samples will be used for subsequent micro hardness test, tensile test, and TEM microscopy to

identify the material damage induced by protons. Depending on sample location within a stringer and the stringer's relative position to other stringers, nearly prototypic proton and neutron conditions can be achieved.

Thermal-Hydraulic Experiments

Key to the performance and lifetime of the active target region is the ability of the flowing lead to cool the window and other important locations within the active target region. Locating stagnation points and predicting flow patterns within the complex geometry of the target is very important and analytical predictions for the lead system must be validated experimentally. Another uncertainty stems from the inability of lead to readily wet surfaces. Heat transfer coefficient correlations are sometimes 50% lower for lead than predicted for lighter liquid metals. This fact, coupled with the target's complex flow geometry, results in a large uncertainty in the ability of the lead to remove energy generated within the containment structure walls. Cleaning procedures and design features, such as surface polishing, may be used to enhance wetting and reduce surface resistivity. The following experiments are planned to quantify performance and eliminate these uncertainties.

Scaled Plexiglas Model with Simulant Fluid (Dye Visualization)

This experiment consists of a scaled model of the active target region constructed of Plexiglas. Room temperature water, or another applicable simulant fluid, will be circulated through the model and dye injection used to examine the flow topology throughout the target. Various dye injection locations will be used to validate predictions to the extent that water has similar hydraulic characteristics as molten lead.

Convective Heat Transfer Test with Flowing Pb

This experiment will consist of a forced convection molten lead loop centered around a test fixture. The fixture will be heated and relevant heat transfer coefficient measurements will be made. In addition, the effects of wetting and gas build-up will be characterized.

Full-Scale, Fully Instrumented Flowing Pb Loop (w/o Nb-1Zr)

This purpose of this test is to qualify the target by repeated operation of a liquid-lead loop through all anticipated normal events (such as drain, rethaw, refill, and drain) and anticipated off-normal events (such as drain valve failure or loss of cooling). The system will be fully instrumented with pressure transducers, thermocouples, strain gauges, and flow meters and can be constructed of non-prototypic material such as ferritic steel. Included in this test will be a pre-test of the experimental target with RF and I^2R heating used to simulate actual heating conditions.

CONCLUSIONS

Preliminary analyses with regard to an experimental flowing-lead spallation target to be located at LAMPF have been performed. While many technical issues remain to be resolved either through further calculations or experimentally, no serious deficiencies have been identified. Safe and reliable operation of the target has been maximized through simple, robust engineering, and a developmental experimental program has been identified to resolve the majority of design uncertainties before final operation of the target in the proton beam. The successful completion of this experimental program will be a key component in proving the practical feasibility of ADTT systems.

REFERENCES

[1] Park, J. J., et al., "Selection of Structural Materials for Flowing Liquid Lead Target for the Accelerator Based Conversion of Plutonium/Accelerator Transmutation of Waste," this conference, 1994.

[2] Prael, R. E., and Lichtenstein, H., "User Guide to LCS: The LAHET Code System," Los Alamos National Laboratory document LA-UR-89-3014 (September 1989).

[3] DOE RUN Inc., personal communication (1994).

EURAC: A Liquid Target Neutron Spallation Source Using Cyclotron Technology

J.M. Perlado, E. Mínguez, J. Sanz, M. Piera
Instituto de Fusión Nuclear (DENIM)
Universidad Politécnica de Madrid
E.T.S.I. Industriales de Madrid
José Gutiérrez Abascal 2, 28006 Madrid

Abstract. Euratom/JRC Ispra led some years ago the design of an accelerator based neutron spallation source EURAC, with special emphasis as a fusion material testing device. DENIM was involved in the development of the last version of this source.

EURAC proposes to use a beam of 600 MeV or 1.5 GeV protons, produced by an effective and low cost **ring cyclotron** with a current of 6 mA impinging in a **liquid lead, or lead-bismuth, target.** It will use an advanced cyclotron technology which can be implemented in the next future, in the line of the actual technology of the upgraded SIN-type cyclotron.

The adjacent rows to the target correspond to the lead, or $Li_{17}Pb_{83}$, cooled channels where the samples will be located. The available volumes there were shown enough for material testing purposes. Here, proposal of using those experimental areas to introduce small masses of radioactive wastes for testing of transmutation in spallation source is made. In addition, extrapolation of present conceptual design to make available larger volumes under flexible conditions seems to be possible.

Neutrons leaking from the test zone drive a subcritical booster (< 10 MW) which could provide a thermal neutron flux trap with a liquid hidrogen moderator in the center.

INTRODUCTION

It is presently a general understanding of the fusion materials research community that the **end-of life** of the first wall or blanket materials will be determined by competing complex phenomena. Effects of neutron radiation damage in fusion can be performed to some extent with charged-particle interaction, D-T sources or high flux fission reactors. However, none of these possibilities have been found to be good for technological and engineering materials data base.

Accumulated damage in structural materials of first walls of magnetic fusion reactors, after 30 years irradiation, is so large as 400-1000 dpa [1,2], being the fluences of 10^{22}-10^{23} n.cm^{-2} with fluxes of 10^{14} n.cm^{-2}s^{-1}. To obtain those fluences in short irradiation times (e.g. ≤1 year), neutron fluxes of 10^{15} cm^{-2} s^{-1} are needed, with appropriate spectra. This problem was the starting motivation of EURAC.

A decade ago, spallation neutron sources were first considered [3,4] for solving the previously enunciated problem, but considering simultaneous uses of the facility, such as transmutation of radioactive wastes, isotope production, cold neutron source. Additional contributions from different authors (compiled in [5]) produce a final picture of this proposal.

The encouraging relevance of the concept of Partitioning and Transmutation (P&T) of high-level radioactive wastes (HLW) incorporates EURAC in the mainstream of potential accelerator-based facilities.

Here, we present EURAC without modifications of the last presented version [5,6], but introducing two considerations as linkage with the transmutation problem:

- its former presentation as multipurpose facility, with small volumes of irradiation where simple canisters of radioactive wastes could be introduced for transmutation.
- available upgrading for higher masses of wastes in efficient large scale operations; we considerer the possibility to include the booster area here presented (for multiplication and thermalization of neutrons) in the single use facility.

A critical point to justify this facility is the choice of the accelerator and its low range parameters, a beam of 600 MeV protons, produced by a **ring cyclotron**, with a current of 6 mA impinging in a liquid lead target. It has been shown [7], that almost with the actual technology of the SIN-type cyclotron and its upgraded current is realistic to attain good conditions for our purpose. Of course, this solution will reduce some of our performances, but remains as an efficient approach to low cost (to be considered as a simple experimental facility in its low-grade version).

CONCEPTUAL LAYOUT OF EURAC

In Fig. 1, the general layout of the facility is given, showing arrangement and dimensions of the full facility.

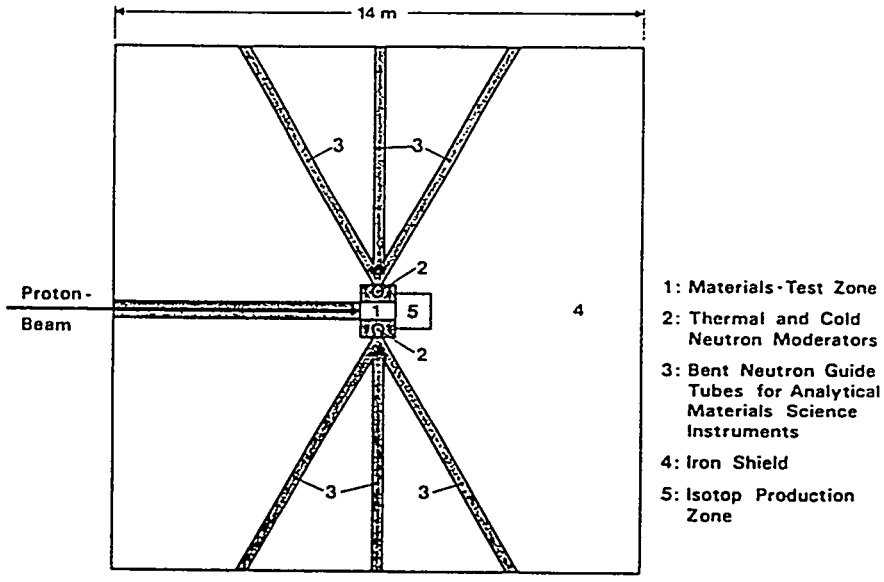

Fig. 1. Lay-out of the neutron target station.

In Fig. 2 a three-dimensional view of the full installation is given including target, material test zones and booster area for cold neutron uses.

The proposed target, which is represented in a longitudinal view along the beam axis in Fig. 3, consists in a 1 cm wide liquid lead target which can tolerate beam power densities higher that 15 MW/cm^2. The liquid lead, which could also be lead-bismuth, is flowing downward at a speed of 10 m/s, and the fins are guiding the liquid in such a way that along the beam axis the centrifugal forces are generating an increasing pressure in the liquid lead suppressing any violent boiling of the lead. Explosive boiling is not dangerous since the target can be made long enough and, consequently, the proton beam does not hit in a solid wall. The liquid passing through the 6 mA, 5 mm wide proton beam changes its temperature by 550°C. It is clear that when using liquid metal at high temperatures, effects like corrosion need to be more carefully analyzed. A vetical section, Fig. 4, is also given showing alternative solution of neutron reflector/multiplier.

In the actual design concept, the first three rows adjacent to the target correspond to the lead or $Li_{17}Pb_{83}$-cooled channels where the material samples could be located for performing the irradiation. That supposes to have a lead reflected non-leakage lead target instead of the original approach or iron reflected high leakage lead target Kley [6, 7]. This material test zone has a total radial wideness of ~4 cm, with a length of 50 cm and height of 30 cm. The available volumes have been discussed elsewhere [5,6].

The neutrons leaking from the test zone drive a subcritical booster (< 10 MW) which provides a thermal neutron flux trap with a liquid hydrogen moderator in the center. The neutron multiplication is obtained by using the fission reactions produced in a small mass of enriched uranium surrounded by natural or enrichment tails of uranium. This arrangement is proposed to be reflected by lead or beryllium. The ZrH_2-thermal neutron moderator will be gas cooled in

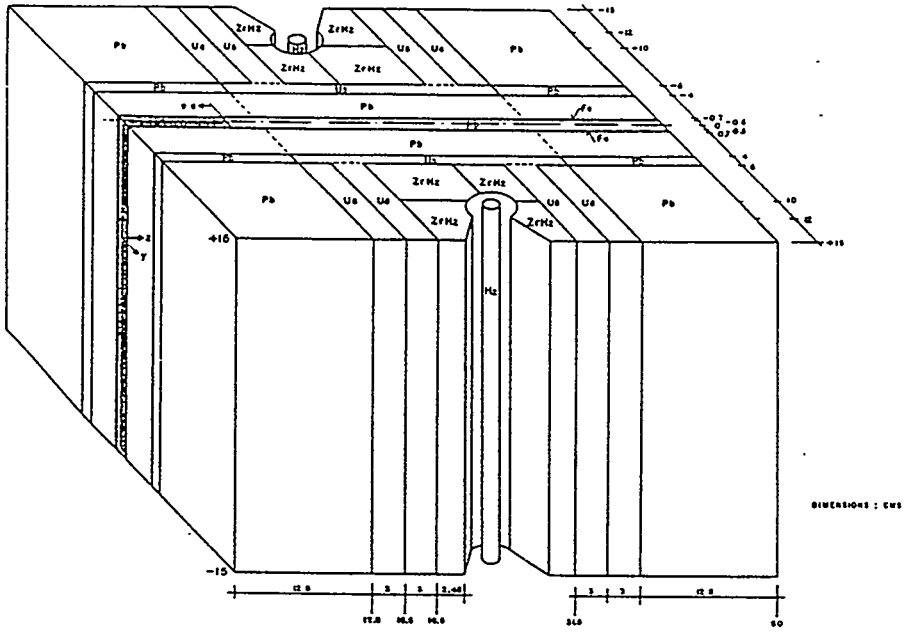

Fig. 2. Three dimensional view of EURAC target station. Material test zone and booster area.

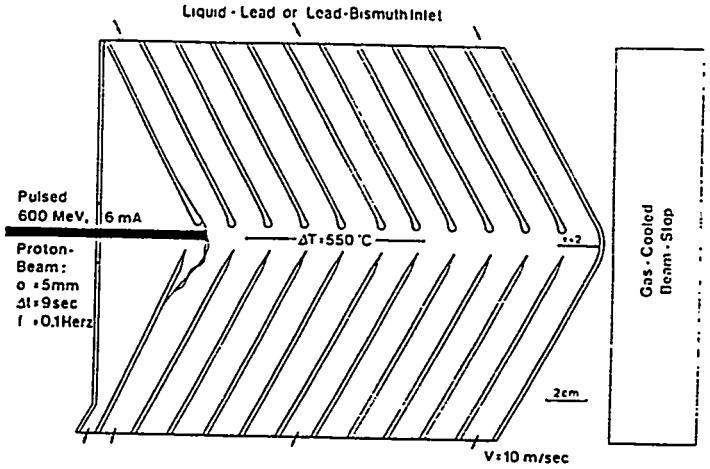

Fig. 3. Conceptional design of the liquid lead target. Vertical cross section.

order to avoid any light or heavy water in the liquid metal-cooled target station by safety consideration. All this ensemble can be viewed as a bos of (50x30 cm) horizontal dimensions and ~30 cm height.

The appropriate shielding will be provided inserting this chamber together with those for other purposes (incineration, isotope production, μ production) and the neutron guide tubes in an iron chamber of 12 to 14 m side.

NEUTRON FLUXES

Neutron transport calculations have been performed in two different areas: those concerning to material test zones and those related to the final design of the booster part.

The HETC [8] code for direct reactions and scattering at high energy, and the MCNP[9] code for the low energy range have been used. A consistent treatment of the geometry considered by

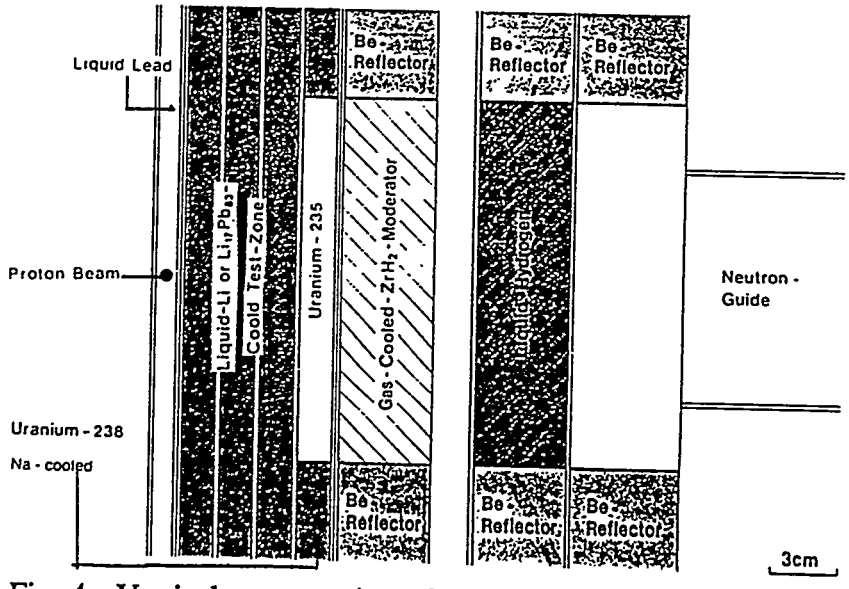

Fig. 4. Vertical cross section of conceptional SNS target station.

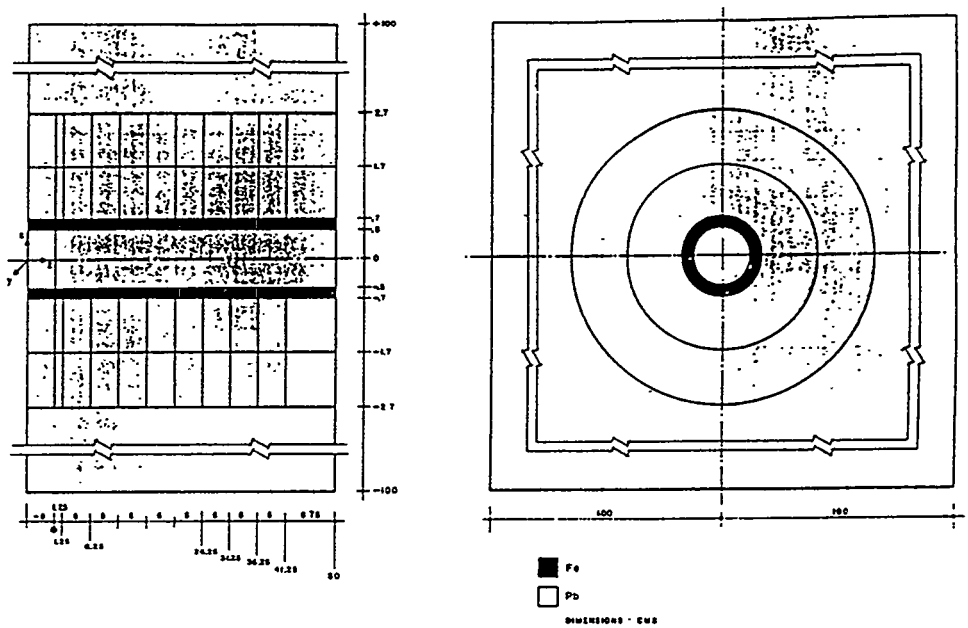

Fig. 5. Geometrical arrangement of target and material test zones used in MCNP calculations.

HETC and that of MCNP has been used, through the checking routines in MCNP, correlating each source neutron coordinates with the corresponding new sections to be used in MCNP. The procedure has been shown to work properly and introduces minor corrections in the programming flow of the code.

Adjacent areas to the target

The description of the geometry of the test material zones used in the calculations is given in Fig. 5, concerning a lead target station reflected by lead.

The results in the canister areas are represented in Fig. 6 and 7 corresponding to the central transversal point of the first and second rows and along the beam axis.Three main energy groups are given corresponding to 0<E< 0.1 MeV, 0.1<E<1 MeV, and 1<E<15 MeV.

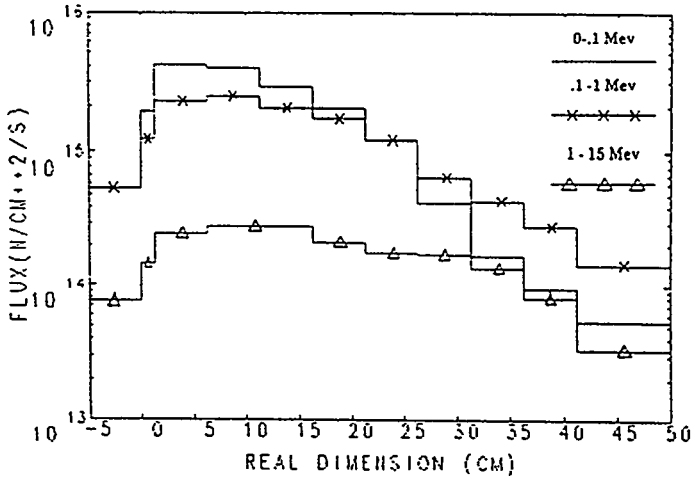

Fig. 6. Axial (Z) neutron flux distributions in three energy groups in the first radial test zone (r = 1.3 cm).

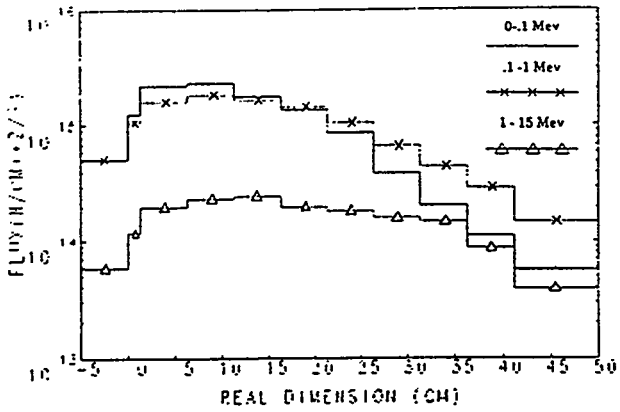

Fig. 7. Axial (Z) neutron flux distributions in three energy groups in the second radial test zone (r = 2.0 cm).

It is important to note the significance of the neutrons with E<1 MeV in the points of maximum flux. This effect could be important in concerning the solid transmutants production, and a more careful analysis of this aspect need to be provided. It is clear that the slowing down effect is reduced along the axis leading to a much less contribution to the total flux. Those numbers are given for a proton current of 6 mA.

The Fig. 8 gives the neutron spectra in two radial points (1.3 cm/2.0 cm) at a longitudinal distance of 3.75 cm. At the closest point, neutrons E>40 MeV are in a fraction of 3.3%, and those with E>15 MeV in 5.75%.

Booster area

The goal of the booster part of EURAC facility is to multiply and moderate the neutron flux escaping from the test area, in order to obtain a high enough cold neutron flux which could be useful for implementing neutron scattering techniques as diagnosis in many areas of physics like

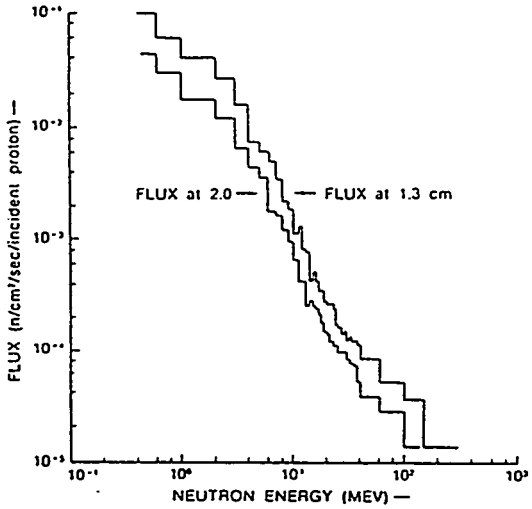

Fig. 8. Neutron spectra at Z = 3.75 cm for lead-shielded neutron source and 600-MeV protons for two radial positions (1.3, 2.0 cm) corresponding to center points of the adjacent rows to the beam.

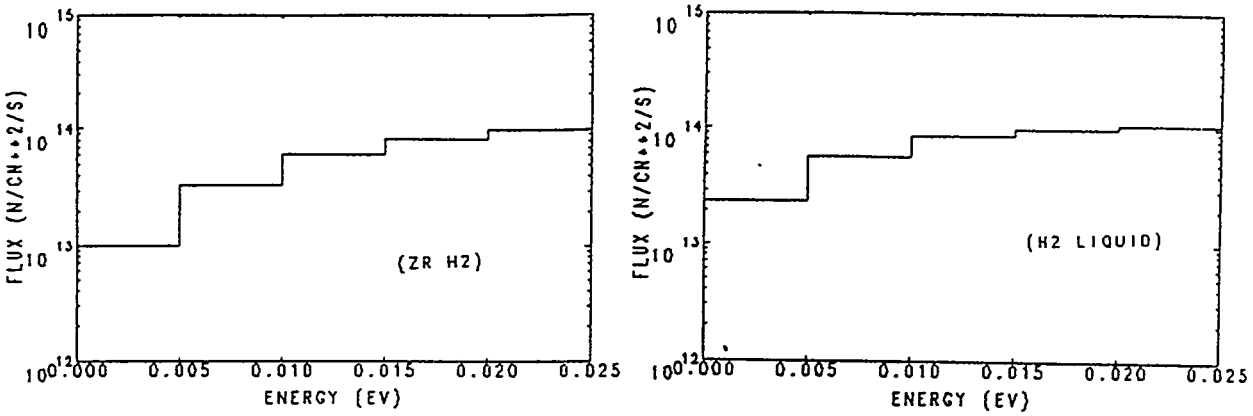

Fig. 9. Neutron flux for a proton current of 6 mA in the parts of the booster corresponding to the H_2 and Zr H_2.

solid state, biology and microscopic analysis of material samples.

To attain our purposes we make use of fission reactions in U^{235}, or highly enriched uranium, and fast fission in U^{238}. The ensemble is reflected by lead in a first approach, but this element could be changed by beryllium. In our calculations here performed we use lead as reflector. The selected moderator has been ZrH_2, and finally the beam tube of liquid H_2.

The neutron fluxes, in the case of a proton current of 6mA, for the useful part of the booster are given in Fig. 9 corresponding to the H_2 and ZrH_2 sections. It can be observed that cold fluxes (E<25 meV) in the range or 10^{14} n/cm^2. are reported.

REFERENCES

[1] Mattas, R.F., et al., *Nuclear Technology/Fusion* **1**, 169 (1981)

[2] Sanz, J., de la Fuente, R., Perlado, J.M., Impact of the neutron flux on transmutation products at fusion reactor first-walls, *J. Nucl. Mat.* **155-157**, 592-596 (1988).

[3] Kley, W., Bishop, G.R., The JRC Ispra Fusion Reactor Materials Test and Development Facility, EUR 9753 EN (1984)

[4] Kley, W., Bishop, G.R., EURAC, the JRC proposal for a european fusion reactor materials test and development facility, EUR 10337 EN(1985).

[5] Perlado,J.M., Piera, M., Sanz, J., Option for spallation neutron sources, *Journal of Fusion Energy* **8**, 3/4, 181-192 (1989)

[6] Kley, W., Bishop, G.R., Sinha, A., Perlado, J.M. EURAC: A concept for a European Accelerator Neutron Source, Proceedings of the 14th ASTM International Symposium on Effects of Radiation on Materials, 1988 pp. 607-622

[7] Mandrillon, P., Ostojic, R., Susini, A., A proposal for 600 MeV-6 mA Ring Cyclotron Accelerator Complex, Final Report on Work carried out for Contract No. 3061-86-11 ED ISP-F (1988)

[8] Chandler, K.C., Amstrong, T.W., HETC Montecarlo High Energy Nuclear Meson Transport Code System, RSIC CCC-161 (1970)

[9] Los Alamos Radiation Transport Group (x-6), MCNP. A general Montecarlo code for Neutron and Photon Transport, LA-7396-M (1981)

Conceptual Design Of A Thorium Target For Molten Salt Transmutation Systems

John J. Buksa, Carl A. Beard, Francesco Venneri, Jay S. Elson,
John J. Park, Richard E. Prael, Laurie S. Waters, J. Wiley Davidson
Los Alamos National Laboratory
Los Alamos, NM 87545

Abstract. A spallation target constructed of thorium metal has been designed for applications using molten-salt as the target coolant. The design consists of an array of wire-wrapped, hastelloy-clad, thorium rods in which a parabolic void region is introduced in the upper regions. Each target rod is approximately 1 m in length, 3.1 cm in diameter, and has a clad thickness of 0.05 cm; 140 rods are arranged in a triangular lattice with a pitch of 3.2 cm, which results in a cylindrical target configuration with a radius of 20 cm and an estimated yield of 17 neutrons/proton for 800 MeV protons.

INTRODUCTION

Spallation target-driven, subcritical, molten-salt blanket systems are being pursued at Los Alamos National Laboratory for plutonium disposition, nuclear waste transmutation, and power production applications [1]. In the process of investigating various concepts for realizing these goals, a spallation target has been designed that uses the blanket fluid-fuel as the target coolant. This fluid-fuel is a molten-salt based on fluorinated lithium, beryllium, and zirconium, and has been studied in depth during the molten salt reactor program at Oak Ridge National Laboratory in the 1960s and early 70s [2]. For the target/blanket concept being pursued here, the circulating molten-salt fuel is directed by orificing from a lower plenum to both the active blanket region and the target. In this configuration, sufficient salt is forced up through the target and then recombined in the upper plenum with salt that has passed through the blanket. Another paper at this conference presents an overview of this target/blanket concept [3].

For the purposes of this design effort, a number of design goals and constraints were specified early on. A safe and reliable target subsystem was the highest goal, which translated into a target that is safe during normal and off-normal operation and that has a maximum lifetime. The target must also have a reasonable neutron yield with a minimum axial peak to average neutron yield distribution. Any design that meets these goals was also constrained by an inlet salt temperature of 850 K, and a bulk exit salt temperature of 1000 K. Although thorium metal melts at 2000 K, the maximum thorium temperature was limited to 1500 K everywhere. The target design was also required to interface with both the accelerator beam transport tube (in vacuum) and blanket subsystems.

After investigating a number of solid-target ideas, a Hastelloy clad thorium target was selected for further design and analysis. Similar to that of a light water reactor fuel rod bundle, the target consists of a bundle of wire-wrapped pins in a triangular pitch that is cooled by molten-salt. Each pin is 1-m long and is made of a thin-walled Hastelloy tube containing a stack of thorium metal pellets. Each pellet has a fabricated central void region that varies in diameter according to the axial location of the pellet. This axially varying central void is tailored to yield a parabolic profile, which is necessary to limit the peak temperature of the thorium during operation. This peak temperature occurs at the inner pellet radius and is a function of the power density and coolant heat transfer characteristics at that axial location. A number of thermal, hydraulic, and physics models were constructed and used to arrive at a consistent baseline design. This baseline target consists of about 140, 3.1-cm OD pins with a 0.5-mm thick clad. Based on inlet and outlet coolant temperatures of 850 K and 1000 K, respectively, an axial and radial central void distribution was determined by iterative analysis. For a 20-mA beam of 800 MeV protons, this target design produced 17 leakage neutrons per incident proton.

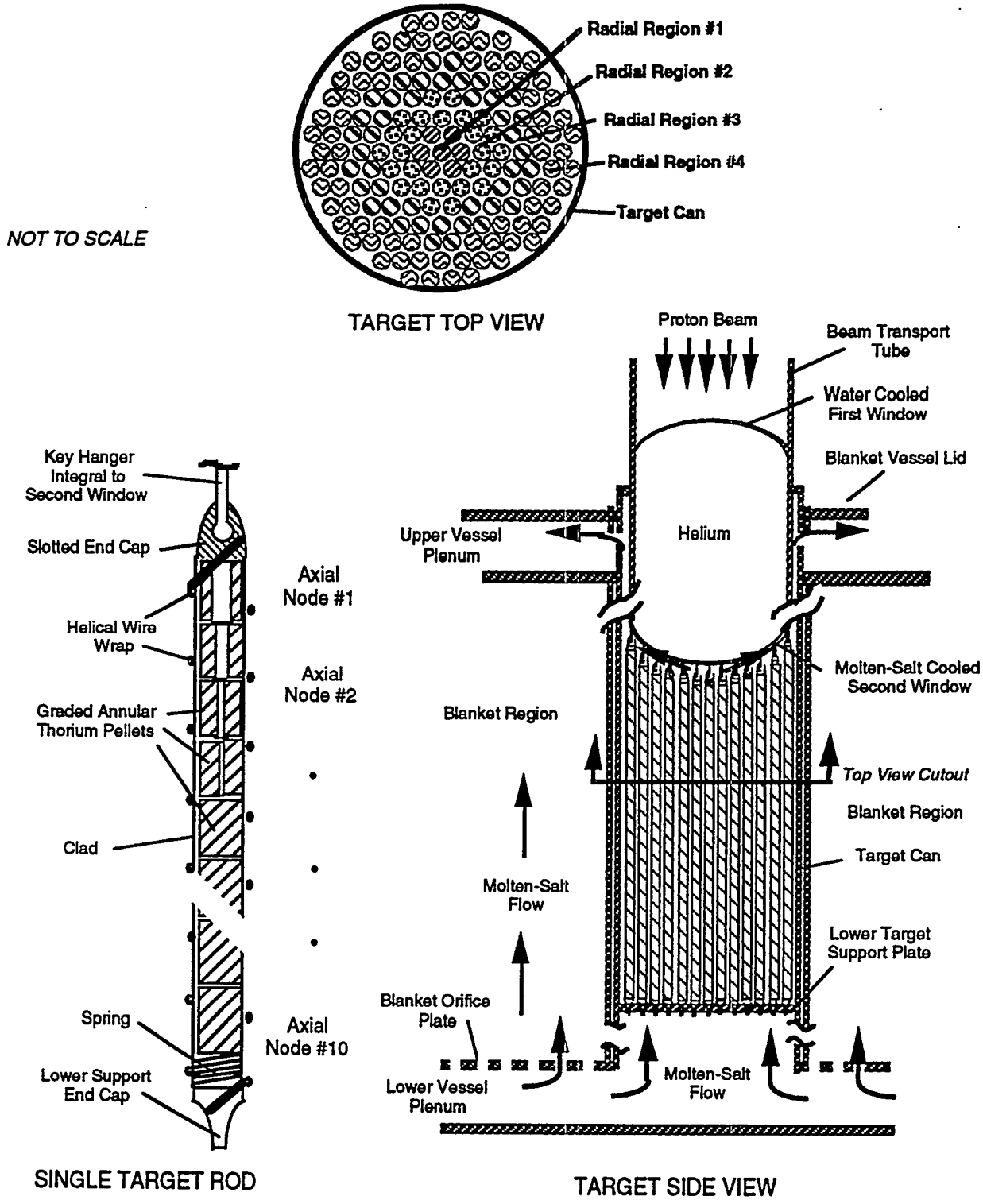

Fig. 1. Sketch of ABC/ATW molten-salt cooled thorium target.

MECHANICAL DESIGN

The mechanical structure required to integrate the target bundle into the blanket and beam transport tube is similar to that of advanced liquid metal reactors and the LANL APT tungsten target [4]. Figure 1 presents a sketch of the target and indicates several important design features and accelerator/blanket interfaces. Each pin is both hung from a customized slotted-key hanger that is an integral part of the secondary window and constrained by a rod support lattice that is located in the lower target plenum. Each pin has a hastelloy wire wrap that acts to mechanically integrate the target and enhance heat transfer from the pins. This design assures that the bundle will not vibrate during operation, and that the window is cooled by the up-flowing molten-salt coolant. The entire target assembly is contained within a thin hastelloy outer can that mechanically seals with the primary window assembly. The primary window consists of a water-cooled double wall structure that separates the hard vacuum of the beam transport tube from the target assembly. Pressurized helium resides in the volume between the water-cooled primary window and the molten-salt cooled secondary window. The design of the target and window assemblies are such that replacement of each is easily accomplished. Table 1 presents a summary of several key design parameters.

Table 1. Key Target Design Parameters

Parameter	Value
Target Fuel Material	Thorium Metal
Target Clad Material	Hastelloy N
Target Coolant Composition	LiF-BeF_2-ZrF_4-UF_4 (65-29-5-1 mole %)
Nominal Pin Length	1.0 m
Nominal Fuel Outer Diameter	0.03 m
Clad Thickness	0.0005 m
Bundle Pitch/Diameter Ratio	1.0329
Approximate Number of Pins in Target	140
Target Fuel Fraction	65.6 %
Target Clad Fraction	5.4 %
Target Coolant Fraction	15 %
Target Void Fraction	14 %

PHYSICS DESIGN

The use of a solid target material in a monolithic form (i.e. an array of rods) typically produces a highly localized neutron source with an intense heat generation rate at this location. This can cause problems in cooling the target, as well in producing power peaking in the blanket. To limit the maximum thorium metal temperature, voids were introduced into the rods. Parametric analyses were performed to determine the optimal method for distributing the neutron source and power distribution, including investigating homogeneously grading the fuel density, or the introduction of discrete void regions with conical, elliptical, or parabolic shapes. It was determined that a discrete, pellet-by-pellet tailored parabolic void produced the most uniform distribution among the investigated options, and was used to define the reference performance for the thorium target. Figure 2 shows the fuel inner radius as a function of axial and radial location required for the conditions of maximum neutron yield and thorium temperature. Note that the lower 10 cm of rods in the inner radial regions (1,2 and 3) contain solid thorium and that the outer radial region (4) contains all annular pellets (the proton beam does not directly impact this outer region).

The LAHET Code System [5] was used to predict the neutron production and energy deposition in the target due to spallation, as well as the resulting spatial and energy dependent neutron flux in

the target, including the contribution from a surrounding 500 MW_t subcritical multiplying blanket. An assumed proton energy of 800 MeV, uniformly distributed over a 15-cm radius circle (radial regions 1, 2 and 3), was used in the calculations. Because thorium is a fertile material, and produces the fissile isotope ^{233}U when exposed to a neutron flux, the power deposition due to subsequent ^{233}U fission must be accounted for in the target design. To accomplish this, the isotopic depletion code ORIGEN2 was coupled with MCNP to produce a spatial and time dependent ^{233}U fission power density in the target. Figure 3 shows the time dependent ^{233}U fission power as a function of operating time for the four radial zones depicted in the top view of Figure 1. This value was then added to the energy deposition contributions from the proton, neutron, and gamma interactions to produce the required heat removal rates. Figure 4 shows the combined spallation and fission power density in the target after two years of operation when the fission power in region four (the region closest to the blanket region) peaks.

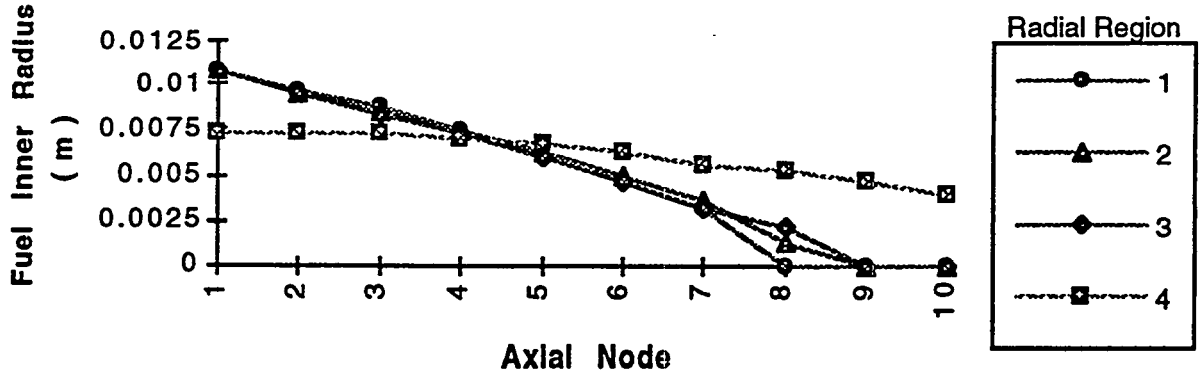

Fig. 2. Target thorium annular pellet inner radius.

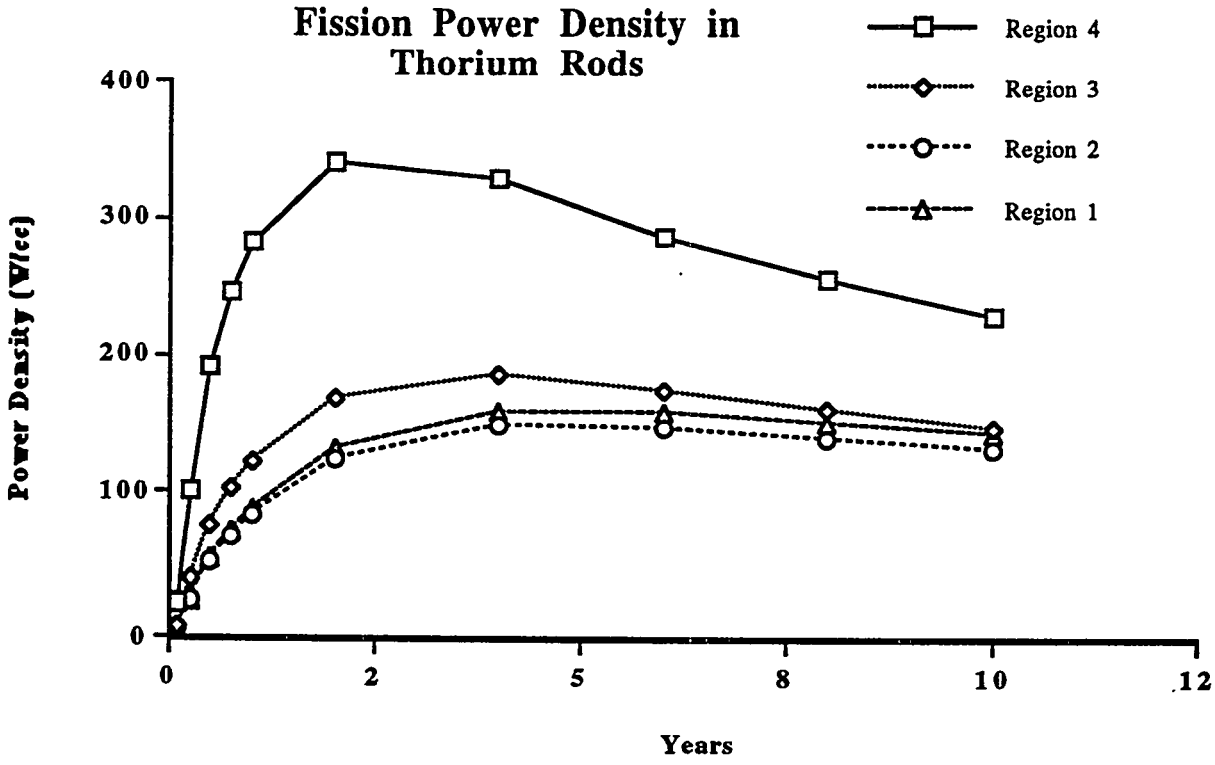

Fig. 3. Fission power density in the target as a function of operating time and radial location.

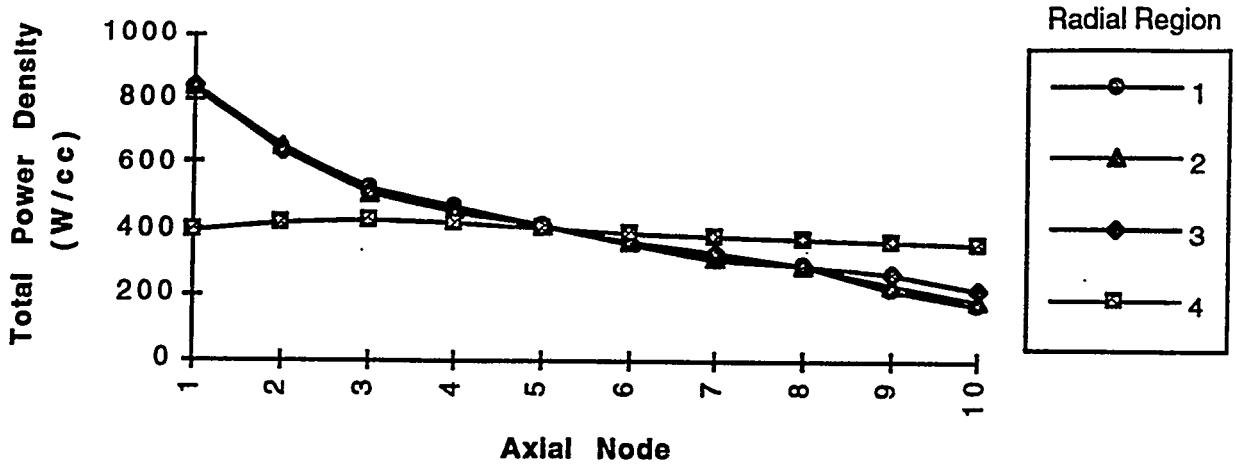

Fig. 4. Axial and radial total (spallation and 2-year fission) power density.

THERMAL-HYDRAULIC DESIGN

The key to maximizing the neutron yield of the thorium target is the maximum temperature in each pin when the ^{233}U fission power peaks after two years of operation. In order to couple the physics and thermal-hydraulic performance of the target, an axially discretized, one-dimensional (radial) thermal-hydraulic model of a pin was constructed and used to model the thermal and hydraulic performance of an individual pin. At the four radial target locations shown in Figure 1, the power densities shown in Figure 4 were used to design an optimum target that is coolable under nominal conditions. An iterative procedure using both the physics and the thermal-hydraulic models was used to arrive at a consistent design. Two key assumptions are that the molten-salt coolant produces no thermal power and that the thorium metal swells into good mechanical contact with the clad after two years of operation (i.e. there is no fuel/clad gap). Several key operating parameters for this design are shown in Table 2. Figures 5 and 6 indicate the peak thorium and bulk coolant temperature distributions under these conditions. Note that the thorium pellet inner radii were adjusted to yield a nearly flat axial and radial peak fuel temperature.

Table 2. Key Target Operating Parameters

Parameter	Value
Coolant Inlet Temperature	850 K
Total Coolant Mass Flow Rate	112 kg/s
Total Thermal Power	32 MW
Average Coolant Exit Temperature	995 K
Average Target Fuel Power Density	388 MW/m^3
Maximum Target Fuel Power Density	833 MW/m^3
Peak Fuel Surface Heat Flux	3 MW/m^2
Coolant Velocity	2.77 m/s
Total Pressure Drop	45 kPa

SUMMARY

For single fluid applications, where the target is cooled by molten-salt, the thorium target presented here is worthy of further development. Although the stage of the design presented here is preliminary, the potential for using thorium as a target material is evident. Several analyses must, however, be completed before the thorium target is deemed successful. Firstly, the ability to keep the secondary window sufficiently cool by the (relatively) hot molten-salt coolant must be shown. Secondly, the penalty on neutron yield due to the secondary window mechanical structure and molten-salt boundary layer, and the target canister needs to be addressed. Current analysis did not consider these features in calculating a 17 n/p yield; this value will be reduced accordingly. And thirdly, the lifetime of the Hastelloy clad under the thermal, neutron, high-energy proton, and corrosive environments of the target region needs to be addressed.

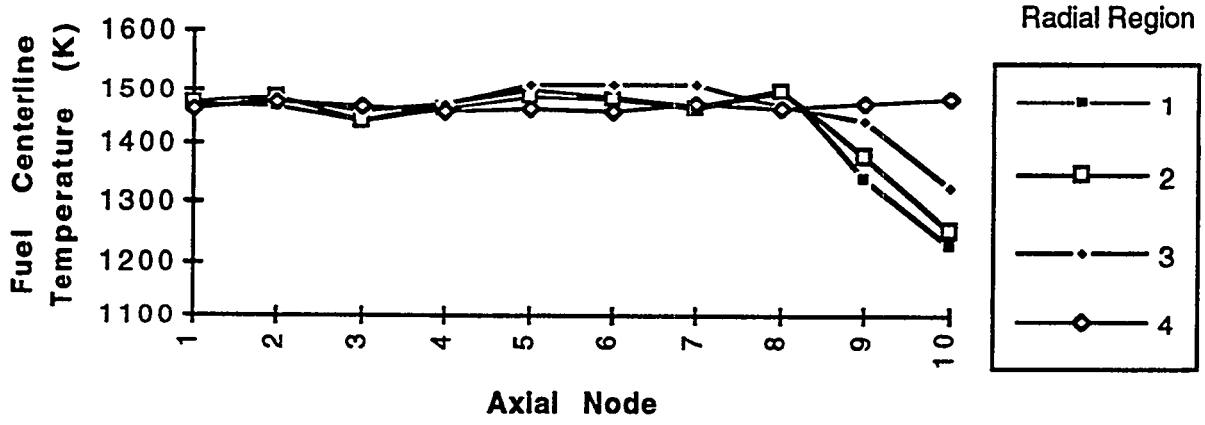

Fig. 5. Axial and radial peak thorium centerline temperature.

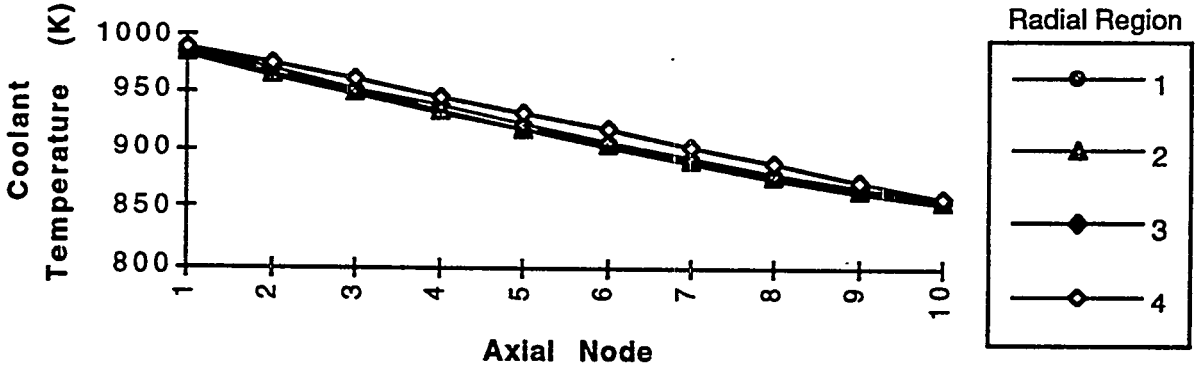

Fig. 6. Axial and radial bulk molten-salt coolant temperature.

REFERENCES

[1] Bowman, C., "Overview of the Los Alamos ADTT Project," presented at the 1994 International Conference on Accelerator-Driven Transmutation Technologies and Applications, Las Vegas, NV, July 25–29, 1994.

[2] Robertson, R. C., "Conceptual Design Study of a Single-Fluid Molten-Salt Breeder Reactor," Oak Ridge National Laboratory report ORNL-4541, June 1971.

[3] Venneri, F., "Overview of ADTT Target/Blanket Configurations," presented at the 1994 International Conference on Accelerator-Driven Transmutation Technologies and Applications, Las Vegas, NV, July 25–29, 1994.

[4] "APT ^{3}He Target/Blanket Topical Report," LA-CP-94-27, Vol. 1, Rev. 1, Los Alamos National Laboratory, March, 1994.

[5] Prael, R.E. and H. Lichtenstein, "User Guide to LCS: The LAHET Code System," LA-UR-89-3014, Los Alamos National Laboratory, September, 1989.

Proton-beam Window Design for a Transmutation Facility Operating with a Liquid Lead Target

Christoph Jansen, Frank Lypsch, Pablo Lizana, Peter W. Phlippen
Institute for Safety Research and Reactor Technology, Research Centre Jülich, 52425 Jülich, Germany

Abstract. The proton beam target of an accelerator-driven transmutation facility can be designed as a vertical liquid lead column. To prevent lead vapor from entering the accelerator vacuum, a proton-beam window has to separate the area above the lead surface from the accelerator tube. Two radiation-cooled design alternatives have been investigated which should withstand a proton beam of 1.6 GeV and 25 mA. Temperature calculations based on energy deposition calculations with the Monte Carlo code HETC, stability analysis and spallation-induced damage calculations have been performed showing the applicability of both designs.

INTRODUCTION

A vertical liquid lead target has been discussed for operation in an accelerator-driven transmutation facility. Spallation induced nuclear reactions in the target will produce a high neutron flux which will be used to transmute the radioactive waste in the surrounding blanket. Besides several advantages concerning neutron physics and heat removal from the target, it can be applied with a pressureless upper end. Thus there is no need for a barrier between the target and accelerator tube in order to maintain the vaccum of the accelerator.

The proton beam (1.6 GeV, 25 mA as calculated in our group to be suitable for transmutation) which impinges onto the target will deposit approximately 15 MW thermal power in the liquid lead mainly caused by the slowing down of the spallation products. The question to be answered is whether there is any need to separate the accelerator tube from the target section by a proton beam window or not. In fact, lead has a vapor pressure of only $1.33*10^{-8}$bar at 758 K, which is the expected temperature at the surface of the target. Using an industrial processing engineering formula [1]

$$E = 0.583\, p \sqrt{\frac{M}{T}} \qquad (1)$$

with knowledge of the temperature T (K), the vapor pressure p (torr) and the molecular weight M (kg kmol^{-1}) the evaporation rate E (kg m^{-2}s^{-1}) can be estimated to be just 11 g/(m^2 h) of lead at T = 758 K. Because of the radioactive spallation products in the target material, the contaminated lead vapor should not only be inhibited from entering the beam tube by cold traps but also by a mechanical barrier, called a proton beam window. Apart from the low vapor pressure, the window does not have to withstand any pressure difference between the target and accelerator. With the support of cold traps surrounding the window, it will not have to be absolutely gas-tight.

As shown in **fig. 1**, the window is to be installed in the horizontal part of the accelerator tube just in front of a 90°-return of the beam into the vertical axis. The main reason for the decision not to place the window close to the target is to protect it from heat radiation from the hot target. Another advantage is that the secondary particles produced in the lead by interactions with the protons will not cause additional radiation damage of the window material.

The window will only be cooled by thermal radiation. As it does not have to withstand a high pressure difference it can be very thin. Therefore the temperature gradients inside the window can be reduced to a rate such that the window will not be destroyed by

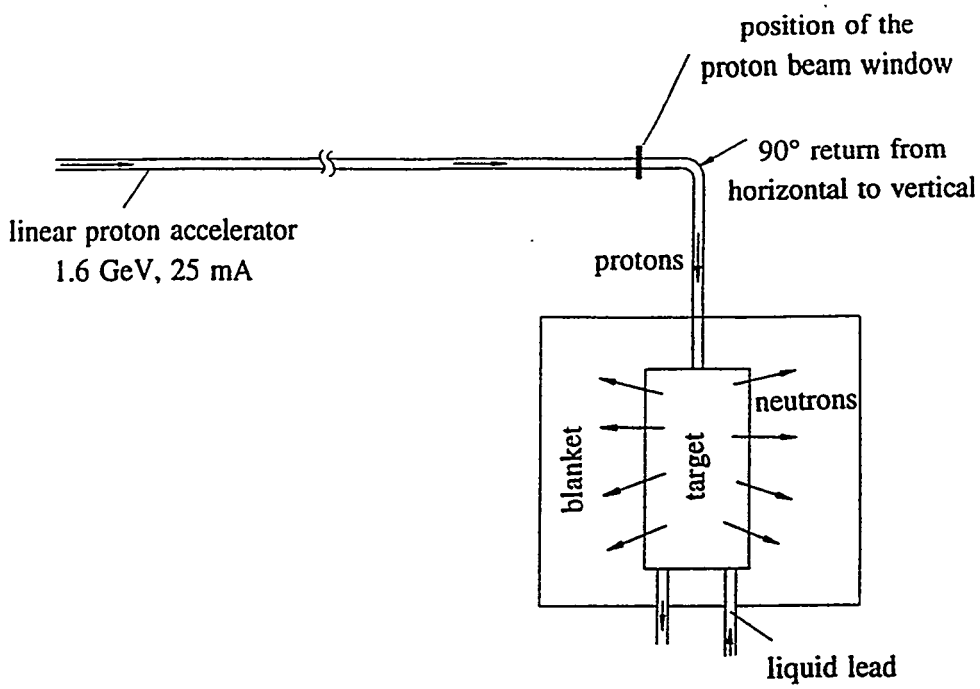

Fig. 1. Transmutation facility: possible arrangement of the window in a transmutation facility

thermomechanical stresses. In contrast, a window cooled by a liquid has to be designed to withstand a pressure of some bars to overcome the pressure losses of the cooling loop. Consequently more energy will be deposited which has to be removed from the window. Some calculations on such a system have been performed for a window made of steel (AISI 304) with sodium cooling. Temperatures and stresses are high to withstand these loads. Thus we decided to solve this problem with a radiation-cooled window.

Some major requirements for a proton beam window are listed below:

- low energy absorption,
- little influence on the proton beam,
- low damage and He production,
- high thermal stability,
- good thermal conductivity (to avoid large temperature gradients) and
- long service life.

Two alternative designs will be presented: a rotating window made of silicon carbide (SiC) and a gas-tight one made of chemical vapor deposition (CVD) diamond.

ROTATING PROTON BEAM WINDOW (SiC)

SiC has been investigated as a candidate first wall material for fusion. Its main advantages are the high thermal stability (up to 2000°C in inert atmosphere), the good thermal conductivity (up to 200 W/(m K)) and its rather good fracture toughness.

The window itself will be designed like a rotor with slightly convex SiC-plates as rotor blades, see **fig. 2.** The beam axis is perpendicular to the plates which will pass through the proton beam because of the rotation of the window.

The construction is not gas-tight, but the ingressing lead vapor will be recoiled by the slight ventilation effect of the rotating window and afterwards it will be caught by cold trapping. The energy deposited was calculated by the Monte Carlo code HETC [3] while the temperature field was predicted by a finite difference model. Because of the rotation (ν = 0.5 to 1 Hz) the

material will be only heated locally and in a short time interval with a thermal power of 36.7 kW (material thickness 2 mm, Gaussian standard deviation of the beam σ = 3 cm). Afterwards it will be cooled down by thermal radiation before entering the proton beam again. (The ambient temperature is set arbitrarily to T_U = 80°C). Therefore the maximum temperatures will only rise to 630°C, see **fig. 3.** The temperature difference in the hottest part of the window between entering and leaving the beam is 18 K, which is more than 10 times less than the thermal stress parameter R_1 of SiC [2].

Table 1. Material characteristics of HIPSiC [2]

Density	Flexural strength[a] 4-pt. bending	Fracture toughness	Max. operating temperature	Thermal conductivity
3.21 g/cm^3	610 N/mm^2	4.0 MPa m$^{1/2}$	2000°C[b]	180 W/(m K)

[a] result obtained from a series of standard test pieces, [b] in inert atmosphere
Note: All data (apart from maximum operating temperature) are valid for T = 20°C.

The stresses which will result from the temperature gradients inside the window were calculated with finite elements. The maximum stress was determined as approx. 100 N/mm^2 with respect to the maximum principal stress criterion. The average ultimate tensile strength of ceramics are determined from a series of standard test pieces. The maximum UTS can be plotted over the failure probability (Weibull plot). It has to be recalculated to obtain the value for a certain failure probability. Another transformation has to be performed due to the geometrical dimensions of the structural member and that part of it which is stressed in comparison to the volume of the test pieces. Calculations on the SiC-plates indicate that the UTS will

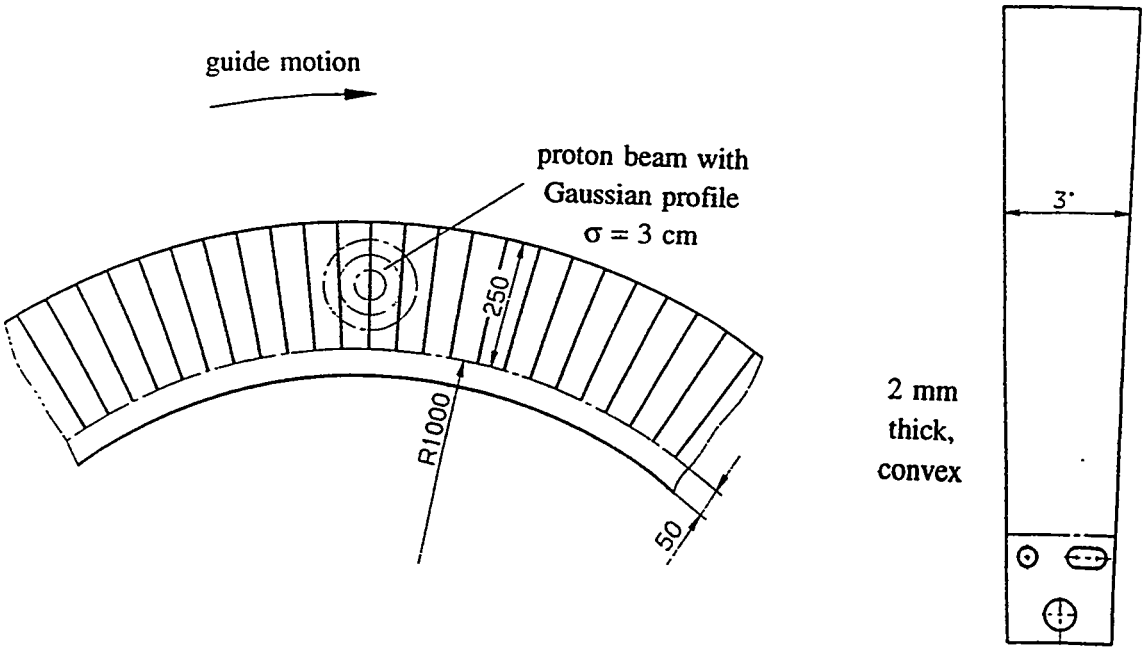

Fig. 2. Window design: schematic drawing of the rotating SiC-proton beam window; on the left side: part of the rotating window, on the right side: one single SiC-rotor blade; 2 mm thick, convex shape; dimensions in mm

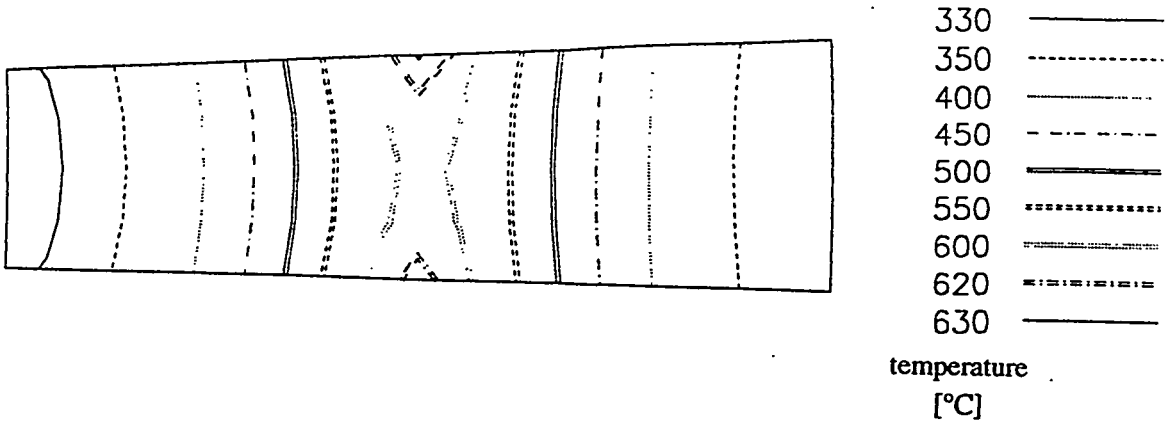

Fig. 3. Temperature field: maximum temperatures in an unirradiated SiC window plate through the proton beam (**Note:** The temperature peaks on the left and the right side of the plate are caused by the overlap of the adjacent SiC-plates.)

be reduced from 610 N/mm^2 to 271 N/mm^2 with a failure probability of 10^{-3}. Therefore it is probably possible to operate this window.

Irradiation experiments have shown that mainly the thermal conductivity of SiC is influenced. It will be reduced by neutron irradiation to approx. 15 W/(m K) [4]. Thus thermal gradients and mechanical stresses will increase during operation in the transmutation facility. Calculations on the worst case, i.e. if thermal conductivity is be diminished in the whole SiC-plate, show that the maximum temperature does not exceed 760°C and the mechanical stresses are less than 215 N/mm^2, calculated again with the maximum principal stress criterion.

Damage and gas production by spallation were calculated using the damage code (SID) [5] which is implemented in the HETC-code. With its help damage- and helium-production cross sections have been generated. The peak proton dose Φ_P in a time interval Δt can be estimated with respect to the rotation of the window and the two-dimensional Gaussian distribution of the proton beam as

$$\Phi_P = \frac{\dot{n}_p \, \Delta t}{(2\pi)^{2/3} r \, \sigma} \qquad (2)$$

where $\dot{n}_p$ is the number of protons transported in the beam per time interval, r the distance from the rotation axis of the window to the midpoint of the Gaussian distribution of the proton beam and σ the standard deviation of the Gaussian distribution - The damage in the window is expected to be very low, s. **table 2.**

Table 2. Material damage to SiC caused by proton irradiation

threshold energy[a]	average p^+ dose	peak p^+ dose	peak damage rate[b]	peak H prod. rate[b]	peak He prod. rate[b]
[eV]	[p/(m^{2}a)]	[p/(m^{2}a)]	[dpa/a]	[appm/a]	[appm/a]
27	3.9*10^{24}	9.3*10^{24}	0.314	355	90

[a] $E_{D,C}$ = 31 eV, $E_{D,Si}$ = 25 eV [6]
[b] calculated for monoenergetic protons (1.6 GeV)

The service life of the window is limited due to its material damage and He-production caused by the interaction of the proton beam with the SiC. Hydrogen production is considered

to be less important because the smaller atomic radius facilitates the diffusion of hydrogen in SiC. Several investigations have been carried out concerning irradiation damage with fast neutrons. The ultimate tensile strength and the Weibull modulus will be severely reduced at neutron fluences $\geq 1x10^{26}$ n/m^2 (E > 0.1 MeV, temperatures 500 ° up to 1150°C) [4]. A neutron fluence of $1.2x10^{26}$ n/m^2 (E > 1 MeV at a temperature of approx. 420 K) with the neutron spectra of the High Flux Beam Reactor (HFBR) at Brookhaven National Laboratory corresponds to approximately 2.6 dpa [7]. Data on He-effects in SiC are scarce. In [8], a critical concentration of a few 1000 ppm is mentioned as producing a significant loss of mechanical strength. Moreover, it is mentioned that He-bubble formations only occur at temperatures higher than 1200°C due to a higher mobility of the He-atoms. In comparison to the corresponding data calculated for the proton beam window it can be estimated that the latter will withstand irradiation damages for at least one year.

CVD-DIAMOND PROTON BEAM WINDOW

Chemical vapor deposited (CVD) diamond has been produced in self-supporting layers of some nm up to 1 mm and 9 cm in diameter. It will be possible to generate CVD-diamonds 40 cm in diameter in the near future. The price of 500 µm thick layers with 3 cm in diameter and a good thermal conductivity is US$ 3000.

CVD-diamond has an excellent thermal conductivity of more than 2000 W/(m K) which is dependent on the purity of the synthetic material (compare: copper 400 W/(m K)) [9]. Another advantage of this material is its high ultimate tensile strength (UTS, between 800 and 5000 N/mm^2, depending on size and manufacturing process [10]). Finally the low Z-number of 6 guarantees for little energy absorption in the diamond. Some typical material characteristics are given in **table 3.**

Table 3. Material characteristics of CVD-diamond

Density [11]	UTS [10]	Thermal exp. coefficient[a] [11]	Max. operating temperature [12][b]	Thermal conductivity[c] [11]
3.52 g/cm^3	0.8-5 kN/mm^2	$0.8*10^{-6}$ K^{-1}	1700°C	≃ 20 W/(cm K)

[a] at T = 20°C, [b] in vacuum, [c] at T = 25°C

The proton beam window made of CVD-diamond is stationary. It is only a simple self-supporting layer (50 µm thickness) which is fixed so that thermal expansion will not cause extra stresses. The temperatures and thermal stresses arising in the window are calculated for the same beam parameters as mentioned above. Energy deposition in the window was calculated again with HETC. Temperatures have been estimated by striking a balance between the heat flows, and mechanical stresses are computed by a FE-program. Radiation-induced damage is calculated with SID. The results are listed in **table 4.**

The CVD-diamond is obviously able to withstand the thermal and mechanical stresses. Besides this it will be a problem to predict how the thermophysical and mechanical properties of the diamond will change after irradiation as few data can be found in the literature. Temperatures and mechanical stresses have also been calculated for a loss of thermal conductivity as λ = 200 W/(m K) and even 20 W/(m K). The resulting temperature profiles are plotted in **fig. 4.** The highest stress is expected to be σ = 720 N/mm^2 for the lowest thermal conductivity. There will probably be a loss of ultimate strength too. Diamond has only a metastable atomic state. It can be supposed that there will be some graphitization of the diamond, resulting in a dramatic loss of strength. The service life of the window made of CVD-diamond will probably

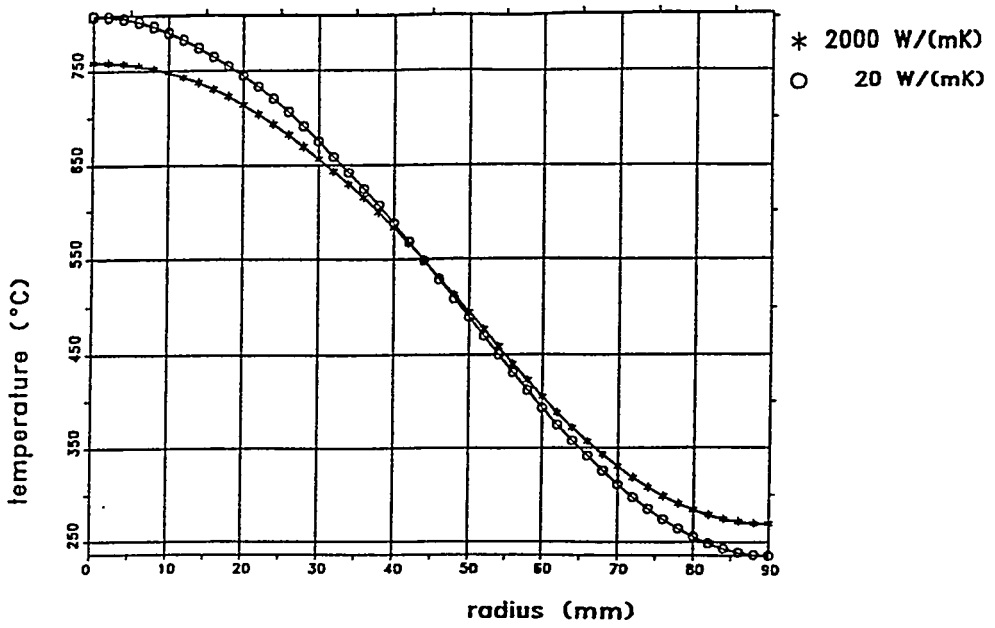

Fig. 4. Temperature profiles in the CVD-diamond: different thermal conductivities

be limited by this effect. In future, investigations concerning this phenomenon have to be undertaken.

Table 4. Calculated results of a proton beam window made of CVD-diamond

material thickness:	50 μm
thermal power deposited by the proton beam:	890 W
peak thermal power density:	3150 MW/m^3
max. temperature, λ=2000 W/(mK):	760°C
max. stress, λ=2000 W/(mK):	510 N/mm^2
max. temperature, λ=20 W/(mK):	810°C
max. stress, λ=20 W/(mK):	720 N/mm^2
threshold energy: [13]	55 eV
average annual proton dose:	$1.9*10^{26}$ $p^+/(m^2a)$
peak annual proton dose:	$8.7*10^{26}$ $p^+/(m^2a)$
peak annual material damage:	2.9 dpa/ a
peak annual H-production:	480 appm/ a
peak annual He-production:	145 appm/ a

Conclusions

Two different design alternatives for a proton beam window have been investigated for operation in an accelerator-driven transmutation facility. It has the function of inhibiting radioactively contaminated lead vapor from the target from entering the accelerator tube.

There is no need to withstand a pressure difference between the accelerator tube and the proposed liquid metal target. Furthermore both windows will be radiation cooled so a very thin construction is possible.

Due to their good thermal conductivity, high ultimate strength and low ordinal number, both SiC (silicon carbide) and CVD-diamond (CVD: chemical vapor deposition) are suitable candidate window materials.

Thermal and mechanical analysis have been made based on energy deposition calculations performed with the Monte Carlo code HETC. Due to the respective thickness of the windows (SiC type: 2 mm, CVD-diamond: 50 μm), temperatures do not exceed the maximum allowed in inert atmosphere. The mechanical stresses are also calculated to be tolerable for both materials. The radiation damage in the rotating SiC window has been found to be very low. A comparison with data from the literature enables to predict that the service life of this construction will be longer than one year of full operation. - In contrast, only few data can be found concerning the change of physical properties of CVD-diamond due to radiation damage. Therefore it is not possible to estimate the service life of a window made of diamond.

Both alternatives are the basis for further investigations. Mainly material questions have to be considered. Experimental analysis of the proton damage and the resulting change of physical and mechanical properties of SiC and CVD-diamond has yet to be carried out.

ACKNOWLEDGMENT

One of the authors (P.L.) would like to thank the Konrad Adenauer Foundation for supporting his scientific work at the Research Centre Jülich.

REFERENCES

[1] Grassmann, P., Physikalische Grundlagen der Chemie-Ingenieur-Technik, Aarau, Frankfurt am Main: Verlag H.R. Sauerländer & Co., 1961, ch. 3, pp. 217-220.

[2] N.N., Elektroschmelzwerk Kempten GmbH, Munich, Germany.

[3] Cloth, P., Filges, D. et al., HERMES - A Monte Carlo Program System for Beam-materials Interaction Studies, KFA-report Jül-2203, 1988.

[4] Dienst, W., Fusion Eng. Des. **16**, 311-316 (1983).

[5] Armstrong, T.W., Colborn, B.L., Software Development for Predicting Materials Damage from High-Energy Spallation Radiation, Armstrong & Associates, La Jolla, California, USA, Report No. AA-844910, Dec. 1984.

[6] Greenwood, L.R., Neutron source characterization and radiation damage calculations for material studies, J. Nucl. Mat. **108 & 109**, 21-27 (1982).

[7] Harrison, S.D., Corelli, J.C., Microstructure of neutron irradiation-induced defects in sintered and siliconized SiC, J. Nucl. Mat. **122 & 123**, 833-839 (1984).

[8] Bolt, H., Nonmetallic materials for plasma facing and structural applications in fusion reactors, Fusion Eng. Des. **22**, 85-98 (1993).

[9] Ositinskaya, T.D., Podoba, A.P., Shmegera, S.V., Influence of point defects on the thermal conductivity of diamond single crystals: state of the art, Diamond Relat. Mat. **2**, 1500-1504 (1993).

[10] Windischmann, H., Epps, G.F., Ceasar, G.P., Tensile strength and biaxial Young's modulus of diamond films, in: Messier, R., Glass, J.T., Butler, J.E., Roy, R., New Diamond Science and Technology, Proc. Conf. Washington 1990, pp. 767 f.

[11] Angus, J.C., Diamond and diamond-like films, Thin Solid Films **216**, 126-133 (1992).

[12] Wilks, J., Wilks, E., Properties and Applications of Diamond, Oxford: Butterworth-Heinemann, 1991, p. 342.

[13] Prins, J.E., Derry, T.E., Sellschop, J.P.F., Volume expansion of diamond during ion implantation, in: Phys. Rev. B, **34**, 8870-8874 (1986).

EVALUATIONS FOR THE CHOICE OF THE BEST TARGET MATERIAL IN A ACCELERATOR-DRIVEN REACTOR

Piero Neuhold
Ansaldo

From the point of view of the overall credibility of the machine the choice of the best target material plays a fundamental role. That has to fulfill at least three requirements: (1) the maximum number of neutrons produced per incident proton; (2) the maximum melting point; (3) the minimum activation under neutron irradiation.

A number of different candidates can be investigated, keeping in mind that the first requirement is roughly fulfilled by high atomic number elements: the most popular among them appear to be W, Pb and Np.

While the characteristics for the second point are well known (3410 C, 327 C and 640 C), as well as many evaluations are done about the first point, even if showing numbers ranging roughly a factor of 2 between the lowest and the highest ones, poor attention instead has been given to the third one.

As far as the operation/maintenance of the machine is concerned, is important to know the dose rate of the target due to its neutron activation. According to my calculations, for example after one year of 800 MeV/62.5 mA proton irradiation of W, we can have, after one day of decay, dose rates as high as 2*10**6 Sv/hr, cumulative of the effects due to the direct proton beam and to the arising neutron flux.

I made use of the codes MSMPN (1), ANITA (2) for the neutron activation analysis and of NMTC (3), ORIGEN (4) for the proton interaction analysis. In particular it's worth noting how dramatic differences can arise from different isotopic composition, that is for example between natural W or only W-186, due to the very different behavior of the daughter elements as decay time and gamma-energy. For example the dose rate due to the neutron activation alone, after one month of decay, for natural W is a factor of 500 greater than for W-186.

It can be concluded that, at least taking into account the above mentioned requirements, the best material could be W, but enriched in its isotope 186 which is about the 30% of natural composition.

References

(1) Moving Source Model Proton Neutron, An Ansaldo/University of Moscow computer code for proton spallation calculations.
(2) ANITA: Analysis of Neutron Induced Transmutation and Activation. EUR 12622 EN — EURATOM.
(3) NMTC: A Simulation Code System for High Energy Nuclear Reactions and Nucleon-Meson Transport Processes. JAERI-M-82-198.
(4) ORIGEN: The ORNL Isotope Generation and Depletion Code.

345

Combining a Gas Turbine Modular Helium Reactor and an Accelerator and for Near Total Destruction of Weapons Grade Plutonium

A.M. Baxter, R.K. Lane, and R. Sherman
General Atomics
P.O. Box 85608
San Diego, California 92186-9784
USA

Abstract. Fissioning surplus weapons-grade plutonium (WG-Pu) in a reactor is an effective means of rendering this stockpile non-weapons useable. In addition the enormous energy content of the plutonium is released by the fission process and can be captured to produce valuable electric power. While no fission option has been identified that can accomplish the destruction of more than about 70% of the WG-Pu without repeated reprocessing and recycling, which presents additional opportunities for diversion, the gas turbine modular helium-cooled reactor (GT-MHR), using an annular graphite core and graphite inner and outer reflectors combines the maximum plutonium destruction and highest electrical production efficiency and economics in an inherently safe system.

Accelerator driven sub-critical assemblies have also been proposed for WG-Pu destruction. These systems offer almost complete WG-Pu destruction, but achieve this goal by using circulating aqueous or molten salt solutions of the fuel, with potential safety implications.

By combining the GT-MHR with an accelerator-driven sub-critical MHR assembly, the best features of both systems can be merged to achieve the near total destruction of WG-Pu in an inherently safe, diversion-proof system in which the discharged fuel elements are suitable for long term high level waste storage without the need for further processing. More than 90% total plutonium destruction, and more than 99.9% Pu-239 destruction, could be achieved. The modular concept minimizes the size of each unit so that both the GT-MHR and the accelerator would be straightforward extensions of current technology.

THE WEAPONS PLUTONIUM DESTRUCTION PROBLEM

Plutonium can be used as a basic material in a fission weapon or as a trigger for a fusion (thermonuclear) weapon. The threat posed by the diversion of plutonium for such purposes has received increased attention as a result of the strategic arms reduction treaty (START) agreements which will make surplus, in both the United States (U.S.) and the Newly Independent States (NIS) of the former Soviet Union, tens of metric tons of weapons-grade plutonium. The safe, permanent disposition of this material presents a difficult challenge.

Unlike uranium, there is no plutonium feedstock that can be blended with weapons plutonium to produce a "non-weapons usable" (i.e., denatured) plutonium. The use of physical security and institutional barriers to provide secure storage of the weapons-grade plutonium in its present form, or in a slightly altered form, for centuries is questionable when considering governmental instability and the possibility of national recidivism in Russia or elsewhere. Blending the plutonium with high-level waste and disposing of it in glassified waste form in geological repositories provides a higher level of diversion resistance. However, it does not effectively preclude subsequent "mining" and recovery of weapons-grade plutonium.

Fissioning the weapons plutonium in a reactor appears to be the most effective means to render the stockpile non-weapons useable. Material can be consumed and the isotopic composition of the remaining material degraded to make it a less attractive weapons material, also the fissioning leads to dilution of the material with highly radioactive fission products. Further, the enormous energy content within the plutonium is released by the fission process can be captured and converted to produce valuable electric power. However, the degree of degradation induced during irradiation is an important consideration.

No fission option has been identified that can accomplish the destruction of more than 70% of all of the plutonium without the repeated reprocessing and recycle of the irradiated fuel from the reactor, a politically sensitive action that may present additional opportunities for diversion. Further, the time required to accomplish total destruction levels (>95%) is extended, for some scenarios exceeding 100 years.

Of all the fission options, the Gas-Turbine Modular Helium Reactor (GT-MHR) can provide the maximum plutonium destruction without reprocessing, and generate electricity at the highest efficiency (Ref 1).

By using an accelerator and target to provide a neutron source in a subcritical modular helium reactor (AD-MHR) the remaining plutonium discharged from the GT-MHR core can be further irradiated to almost complete destruction in the same inherently safe, diversion proof manner.

THE GT-MHR AND ACCELERATOR COMBINATION FOR WEAPONS PLUTONIUM DESTRUCTION

The destruction of weapons plutonium using a GT-MHR and accelerator would be accomplished in the following manner:

- First the weapons plutonium would be Irradiated to high burnup in a GT-MHR. 90% of the original Pu-239 and 65% of the total plutonium would be destroyed in this "deep burn" step.

- Then the discharged fuel elements would be placed in a GT-MHR core which is driven by an accelerator through a target located in the central annulus (AD-MHR). The fuel elements would be used "as is", and no reprocessing of the fuel would be required before irradiation in the AD-MHR. These discharged fuel elements would then be irradiated to obtain the desired plutonium destruction using the accelerator/target as a neutron source. Over 99% Pu-239 and 83% total plutonium destruction can be achieved in less than one year; and over 99.99% Pu-239 and 90% total plutonium destruction possible. during a three year burnup.

- The fuel elements finally discharged from the AD-MHR core could be disposed of directly in a geologic repository as high level waste without further reprocessing.

This system achieves near total destruction of weapons plutonium in a single pass, with minimum potential for diversion of the material, and no reprocessing of the plutonium required.

The current GT-MHR design for "deep burn" of plutonium utilizes a three year fuel cycle in which one-third of the core is discharged each year. Since the AD-MHR is batch loaded, combining the annual discharge from three GT-MHR modules into a single AD-MHR core permits the destruction over 99% of the Pu-239 in 4 years. This combination is shown schematically in Fig 1, and the basic parameters of the system are given in Table 1. Note that, with the very high efficiency of the Gas Turbine, the AD-MHR averages 195 MW(e) annually. Additionally, since the accelerator requires only 72 MW(e), the combined system of 3 GT-MHRs and 1 AD-MHR has a net electrical output of almost 1000 MW(e).

Table 1. Basic Parameters of the GT-MHR Accelerator Combination

Basic Unit	3 GT-MHRs + 1 AD-MHR
GT-MHR Power Level	600 MW(t)
GT-MHR Fuel Cycle	1/3 core per GT-MHR/year
AD-MHR Power Level	600 MW(t) to 207 MW(t) at constant beam power
AD-MHR Fuel Cycle	Full core per AD-MHR year
tonnes of WG-Pu destroyed per year	0.8
Net Electrical Power	975 MW(e) per year per MT

The GT-MHR uses plutonium-oxide coated particles which has been successfully tested to 750,000 MWD/MT, and up to 1400°C, in irradiations carried out in the Peach Bottom reactor in the United States,and in the DRAGON and Studsvik reactors in Europe (Ref 2,3).

Er-167 in the form of coated particles of natural erbium oxide is used as a burnable poison to control excess reactivity and ensure a negative core temperature coefficient under all conditions. Since no fertile material required, no additional plutonium is created in the irradiation process, thus the system maximizes plutonium destruction, and does not support a plutonium recycle economy.

Studies have shown (Ref 4) that the discharged fuel elements are suitable for direct disposal in standard multipurpose canisters as high level waste in a geologic repository.

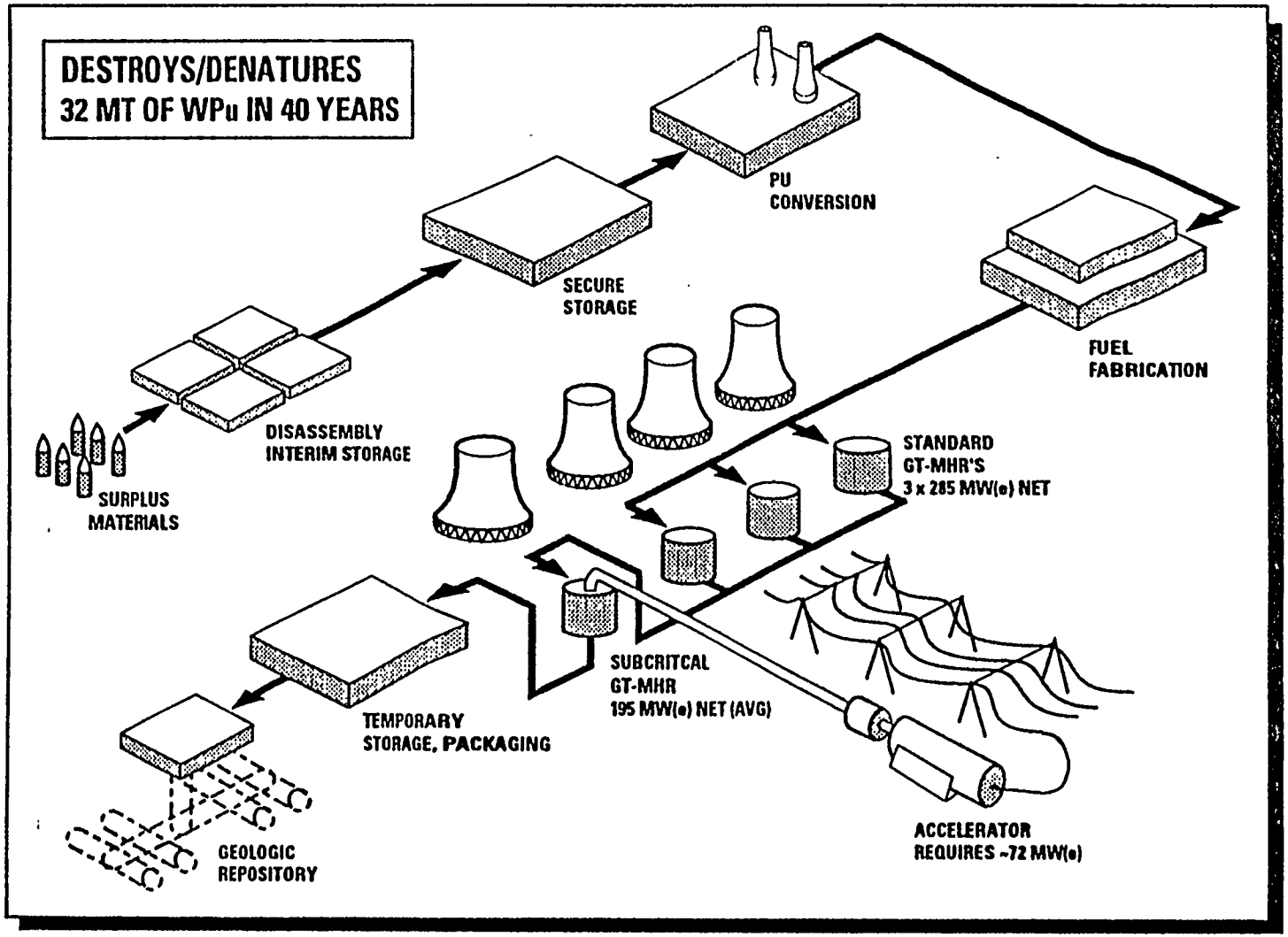

Fig.1 AD-MHR Plutonium Disposition System Layout

The MHR, being graphite moderated and helium cooled, is capable of operating at sufficiently high temperatures that it can be used in a Brayton cycle to drive a Gas Turbine which converts thermal energy to electricity at the highest possible efficiency, almost 50%. This produces excellent economics for the system when the electricity produced from the plutonium fission is sold to the grid; and minimum thermal discharge to environment. The GT-MHR also provides inherently safe operation because of the high temperature capability of the all-graphite construction of the core, and the annular design of the core which limits fuel temperatures below damage values during a loss of coolant or coolant pressure accident. The core is also designed to have a negative temperature coefficient of reactivity under all conditions. The temperature coefficient is the only significant contributor to the overall power coefficient.

The smaller modular design of the overall system means that the beam power requirements for the accelerator are relatively small so that it represents a straightforward extension of current technology.

THE GT-MHR

The GT-MHR module arrangement is shown in Fig 2; and a detailed description of the GT-MHR is given in Ref 5. The reference GT-MHR plant consists of four such modules. The components for each module are contained within a steel vessel system which includes a reactor vessel, and a power conversion vessel in a side-by-side configuration connected by a cross vessel as shown in the figure. The vessel system is sited underground in a concrete silo which serves as an independent pressure containment structure. The reactor vessel is made of high strength modified 9Cr-1Mo-V alloy steel, and is approximately 8.5 m (28 ft.) in diameter and 23.8 m (78 ft.) high.

The basic parameters of the GT-MHR core are summarized in Table 2, and a simplified flow diagram is shown in Fig 3. The reactor core is an annular assembly of hexagonal graphite fuel elements, shown in cross section in Fig 4. The annular shape helps to keep peak fuel temperatures during loss of coolant flow or pressure accidents below the damage limit of the fuel particles so that no fission product release will occur.

The GT-MHR plutonium destruction fuel cycle in a once-through three-year cycle with one-third of the core refueled approximately every 12 months at a power level of 600 MWt.

Core reactivity is controlled by control rods in the core and reflectors. A completely independent and redundant reserve shutdown system provides a diverse reactivity control capability using boronated graphite pellets stored in hoppers above special channels in the core. The inherent features that control reactivity, and thus heat generation, include a strong negative temperature coefficient of reactivity, and a single phase (no void coefficient), and neutronically inert coolant. These characteristics cause the reactor to shut down without operator or safety system action if core temperatures increase above normal fuel temperatures.

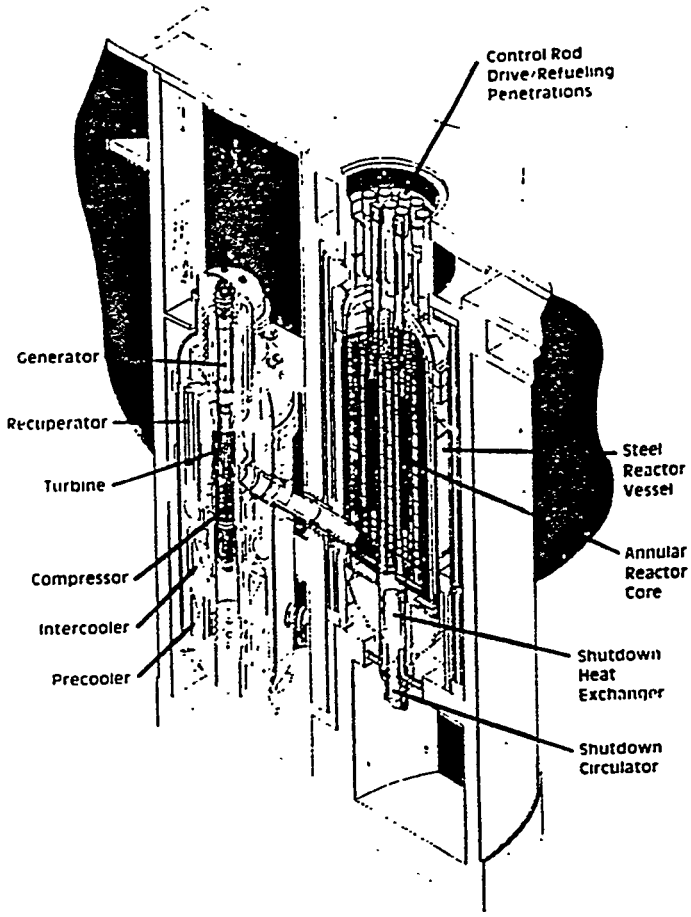

Fig 2. GT-MHR Module Arrangement

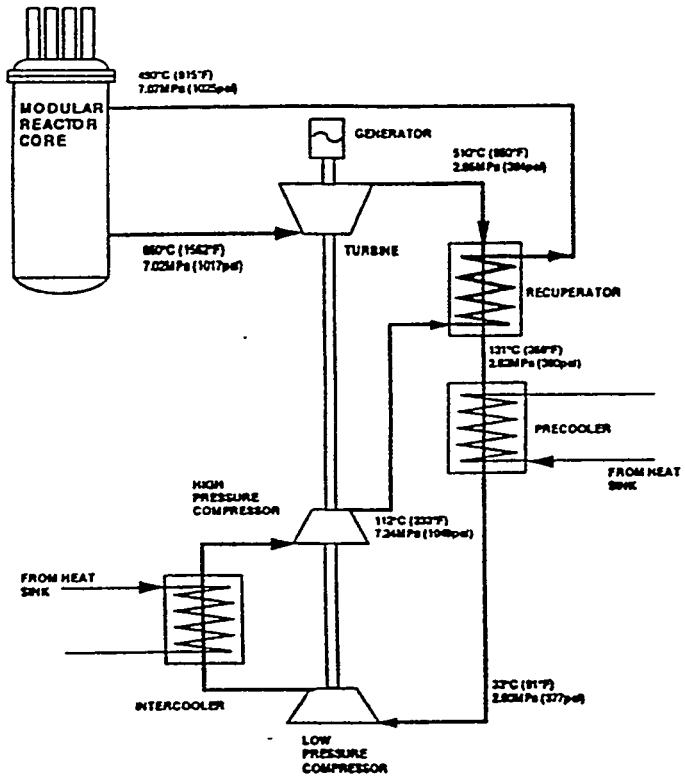

Fig. 3. GT-MHR Flow Schematic

Table 2. Basic Parameters of the GT-MHR

Core Power Level	600 MW(t)
Core Power Density	6.58 w/cc
Core Coolant & Pressure	Helium @ 7.07 MPa
Core Inlet Temperature	490°C
Core Outlet Temperature	850°C
Core Shape	Cylindrical Annulus
Core Size:	
Height	7.93 m (10 blocks)
O.D.	4.86 m
I.D.	3.0 m
Number of Fuel Elements in Core	1020
Fuel Cycle Length	3 years

The design of the fuel for the PC-MHR is based on fuel designs for high-burnup plutonium and uranium developed and tested for use in a number of HTGRs in the U.S., Europe, and Japan

The basic unit of the PC-MHR fuel is the coated particle. The coated particle consists of a tiny, 195 μm diameter, sphere of plutonium oxide (referred to as a "kernel") coated with multiple layers of refractory material, called a TRISO coating. The kernel is surrounded by a low density buffer coating, which is in turn enclosed in a silicon carbide (SiC) coating contained between an inner and outer pyrolytic carbon (IPyC and OPyC) coating. The TRISO coating forms a strong pressure vessel for containing both gaseous and metallic fission products and is the primary barrier to the release of radionuclides.

The composition selected for the kernel is a hypostoichiometric form of plutonium oxide with O/Pu ≈ 1.61. The specification for the kernel for the particle is the same as the kernel successfully tested in the Peach Bottom reactor at peak temperatures up to 1440°C, peak burnup of 737,000 MWd/MT, and peak fast neutron fluence of 2.2×10^{25} n/m^2.

The TRISO coating design is based on past successful uranium and plutonium irradiation experience with coating designs tested in similar service conditions (Ref. 6). Figure 5 illustrates the TRISO fuel particle coating concept.

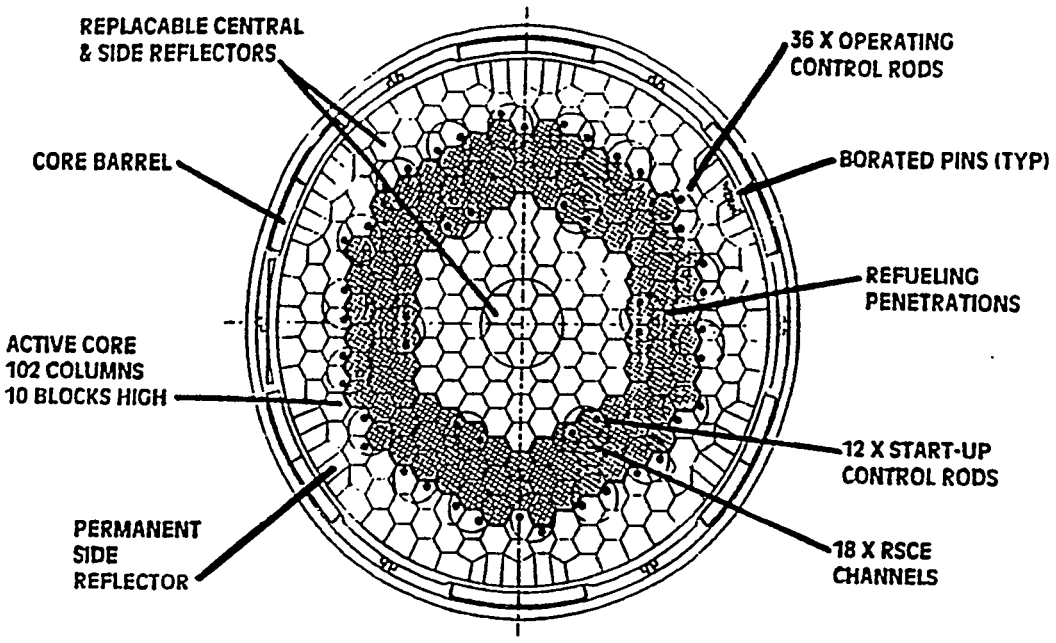

Fig 4. GT-MHR Annular Core Layout

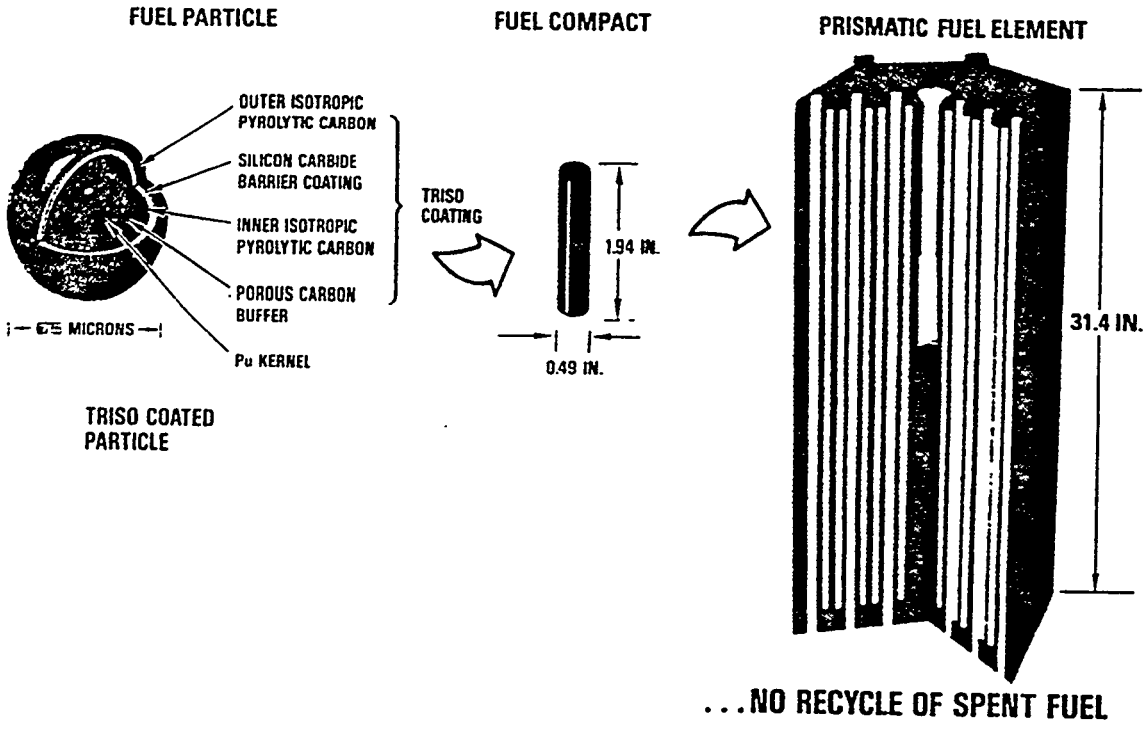

Fig. 5. Fuel Element Components

THE AD-MHR AND TARGET

As shown in Fig 6, the AD-MHR core is very similar to the GT-MHR core, the primary difference being the provision for an accelerator target for neutron production by spallation, and a surrounding pressure vessel, both located in the central graphite reflector as shown in the figure. This graphite reflector serves to moderate the spallation neutrons and produce a thermal flux spectrum in the fuel annulus. A vertical cross-section of the AD-MHR core showing the centrally located target tube is given in Fig 7, and a summary of the basic core parameters is given in Table 3 The reactor core components and fuel plus all the power conversion system components are identical to those in the GT-MHR and are described in the previous section.

Table 3. Basic Parameters of the AD-MHR and Accelerator

Core Power Level:	
Maximum	600 MW(t)
Average	410 MW(t)
Minimum	210 MW(t)
Fuel Cycle Length	300 days
Accelerator:	
Proton Beam	800 Mev, 33 mA (avg)
Beam Power	28 MW
Power Requirements	72 MW(e)
Neutron Source Strength	~ 6 x 10^{18} n/s

Several options are available for the accelerator target in the AD-MHR. However, based on studies by Los Alamos, the best design appears to be one using molten lead flowing through the target, cooled by helium. A sketch of the target is shown in Fig 8. The lead has a very low parasitic absorption cross section for neutrons, can handle the energy deposition from the accelerator without damage, and does not have stress or other problems from the spallation process (Ref 7). The heat deposited in the target by the proton beam would be removed by the flowing lead and transferred to the helium coolant via a conventional heat exchanger. Calculations indicate a production rate of about 23 neutrons per incident proton; and the graphite reflector elements surrounding the target ensure an excellent thermalized neutron spectrum in the core assembly. As shown in Fig 7, the target would be contained in the subcritical assembly within its own pressure vessel. Additional helium cooling around this inner pressure vessel can be provided as required, by diverting flow from the core regions.

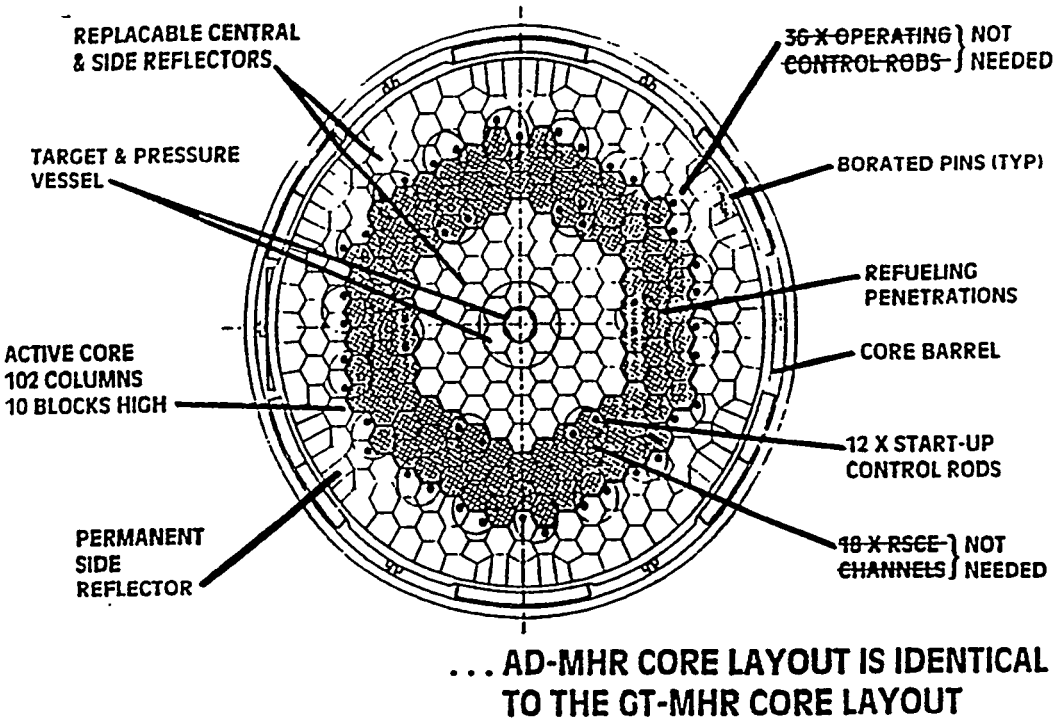

Fig 6. AD-MHR Annular Core Layout

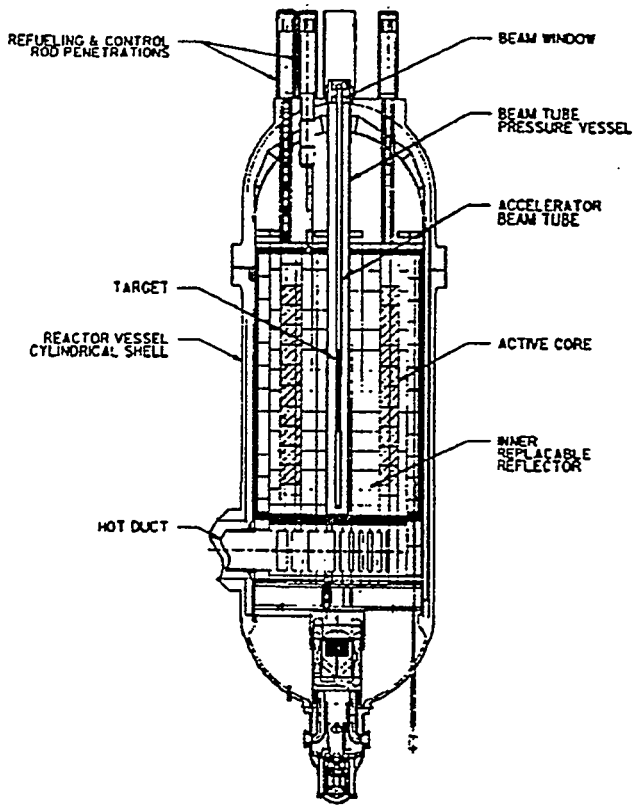

Fig. 7. AD-MHR Elevation View

The accelerator represents a fairly straightforward extension of current technology, since the power level requirements are not excessive. A pulsed accelerator configuration appears the most promising, and a sketch of a possible configuration is shown in Fig 9. This system would produce a 800 MeV beam at 32 mA average current. Total AC power requirements are 72 MW. As indicated in Table 4, the components for this accelerator design are based on demonstrated technologies.

Table 4. The Accelerator is Based on Demonstrated Technologies

COMPONENT	STATUS	REQUIREMENT
Injector	> 100 mA demonstrated	≤125 mA
RFQ	70 mA, 0.6 MeV demonstrated	≤125 mA
Drift Tube Linac	100 mA pulsed configuration operated at LANL. 250 mA at CERN	250 mA peak, pulsed operation
Coupled Cavity Linac	17 mA in operation at LAMPF	30 to 250 mA
RF Generators	1 MW klystrons available from industry	1 MW Tubes

PERFORMANCE EVALUATION

The plutonium destruction capability of the GT-MHR has been evaluated previously (Ref 8), and the results are presented in table 5. The performance of the sub-critical, AD-MHR was studied using a detailed, two-dimensional diffusion theory model. The subcritical assembly was assumed to be batch loaded with plutonium fuel discharged after a single pass through the GT-MHR. A total neutron source of $6x10^{18}$ neutrons/sec was assumed to be provided in the center of the reactor from the accelerator target.

The discharged fuel from the GT-MHR is still quite reactive when loaded into the AD-MHR since most of the erbium poison has been burned away. Therefore, erbium loaded poison rods were placed in the inner reflector adjacent to the core to bring the beginning-of-cycle reactivity (K-eff) to ~0.96. This poison distribution has the additional advantage of reducing the power peaking in the inner ring of core fuel elements at the start of the irradiation cycle because they are closest to the target neutron source.

- **Flowing heavy metal**
  - Lead
- **Efficient**
  - High neutron production
  - Low neutron loss
- **Flexible**
  - Can handle wide beam power range
  - Compact
- **Significant experience base**
  - Russian expertise in Pb-cooled nuclear systems
  - Canadian ING program
  - Swiss neutron source program

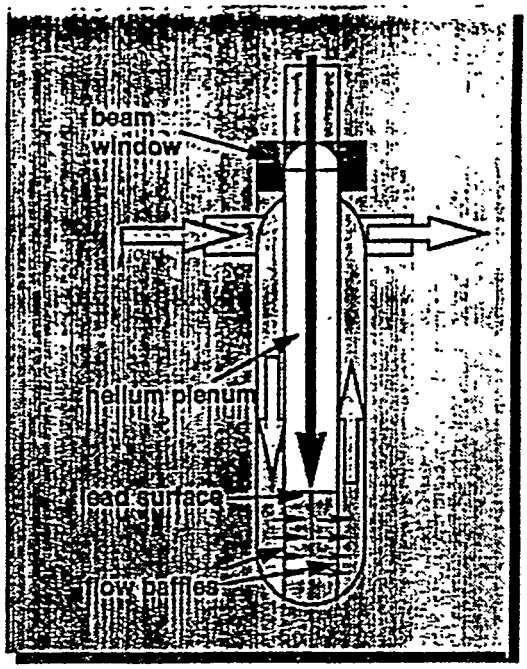

Fig 8. Schematic of AD-MHR Neutron Production Target

- Accelerator beam power requirements significantly less than APT (26 MW vs 200 MW)
- Significant technology base exists
- Maximum electrical utilization efficiency desirable for AD-MHR
- Pulsed accelerator configuration promising option
- Beginning design and optimization effort needed

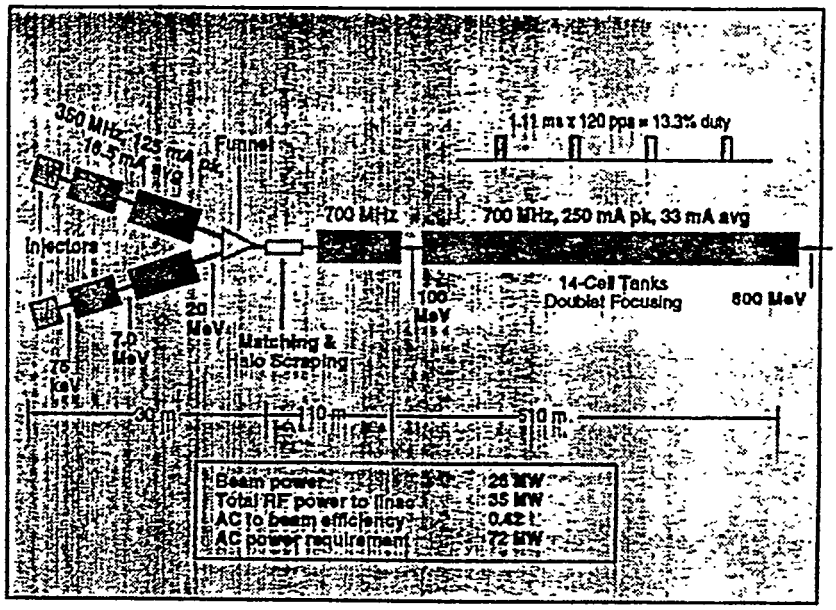

Fig. 9. Accelerator Concept for the AD-MHR

The resulting burnup of Pu-239 and total plutonium is shown in Fig 10, and the core reactivity behavior and power production as a function of burnup are shown in Fig 11. As Fig. 10 shows even a one year (300 day) exposure in the AD-MHR results in 99% Pu-239 destruction and 83% total plutonium destruction. A three year (900 day) exposure yields 99.9% Pu-239 and 90% total plutonium destruction.

The detailed burnup analysis shows that the power peaking in the core remains within acceptable limits throughout the cycle. The power peaks shift from the inner to the outer core ring as burnup proceeds. The maximum fast neutron fluence ranges from 0.93×10^{25} n/m^2 after 300 days to 1.2×10^{25} n/m^2 after 900 days. These values are within acceptable limits for the graphite and fuel particles.

MEASURES OF PROLIFERATION RESISTANCE

Table 5 summarizes the diversion resistance of the spent plutonium fuel from both the GT-MHR and AD-MHR, including the isotopic composition of the fuel relative to the original WG-Pu. As can be seen from the table, the AD-MHR fuel cycle offers an extremely high level of resistance to diversion and proliferation. The plutonium content of each spent fuel element is very low (about one-tenth a kilogram), and the plutonium is much more difficult to recover from spent MHR fuel than from spent MOX fuel. Since over 150 AD-MHR fuel elements are required for a critical mass, it would be very difficult to divert a sufficient quantify of this fuel to obtain a weapons-useful quantity of plutonium; the technology for separating plutonium from MHR spent fuel has not been developed; and the isotopic mixture of the spent fuel makes it unattractive for weapons applications.

The radiation level in the AD-MHR discharged plutonium is extremely high, even after it has been separated from the fission products. The internal heat generation rate in the plutonium, and the spontaneous neutron emission rate are both large enough to preclude the use of this material as a weapon even by a country with sophisticated weapons technology. Fig 12 graphically shows the WG-Pu destruction achieved in the GT-MHR and AD-MHR as compared to other options being considered for dealing with this material.

CONCLUSIONS

The gas-turbine modular helium reactor can provide a very high level of weapons-grade plutonium destruction, without the need for recycle, in an inherently safe system which provides maximum efficiency for electrical energy production, and minimum environmental impact. This system is also very cost effective because of its high thermal efficiency.

By combining the GT-MHR with an accelerator driven subcritical assembly, this high efficiency, minimum environmental impact, and inherent safety can be retained while providing near total destruction level of weapons plutonium without recycle.

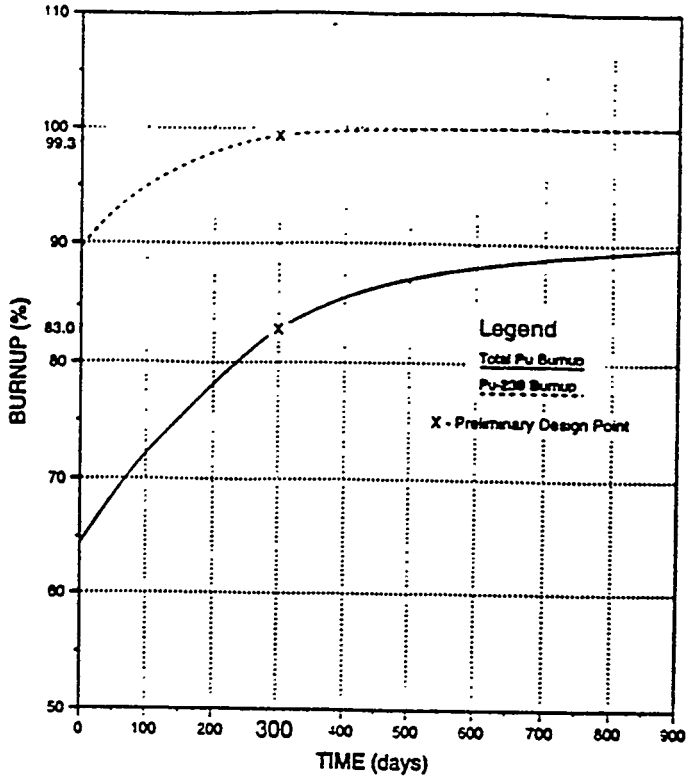

Fig 10. AD-MHR Plutonium Burnup vs. Time

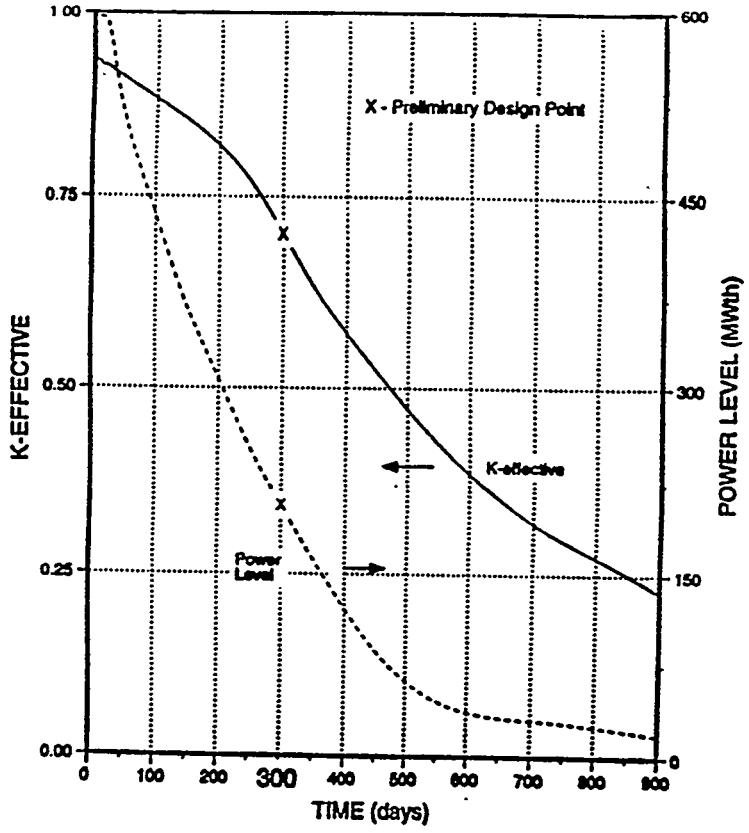

Fig. 11. AD-MHR Reactivity and Power Level vs. Time

Table 5. Diversion Resistance of AD-MHR Discharged Plutonium

	WG-Pu	LWR Discharge	PC-MHR Discharge	AD-MHR Discharge
Composition, % of WG-Pu				
Pu-238	0%	0.1%	0.1%	0.3%
Pu-239	94%	47.9%	9.8%	0.7%
Pu-240	6%	18.7%	10.7%	5.0%
Pu-241	0%	10.6%	11.6%	4.3%
Pu-242	0%	4.0%	3.3%	6.8%
Reflected Sphere:				
Critical Mass, Kgs	8.0	9.6	15.2	20
Elements req'd	N/A	1	55	150
Volume, litre	N/A	170	4,977	13,575
Weapons usefulness	extreme	useful	very low	not useful

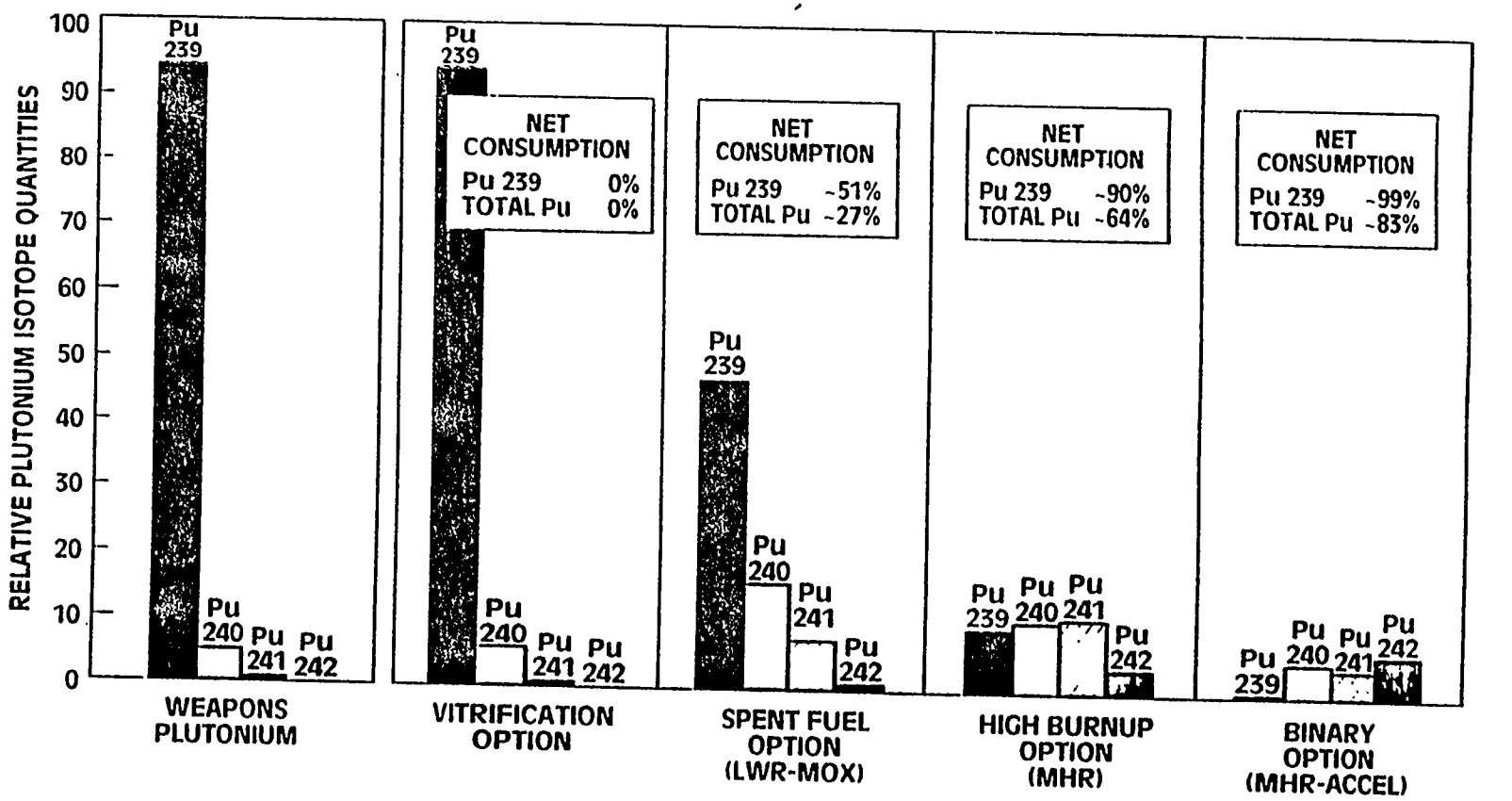

. . . THE MHR OPTIONS ARE MOST EFFECTIVE AT DESTROYING AND DEGRADING

Fig.12 Effectiveness of Disposition Options to Consume and Degrade Plutonium

ACKNOWLEDGEMENTS

The authors wish to express their appreciation to E. Arthur, F. Venneri, and the other members of the Accelerator-Driven Transmutation Technology (ADTT) group at Los Alamos National Laboratories for their valuable technical review and comments regarding the AD-MHR concept. The ADTT group also supplied the Target and Accelerator sketches shown in figures 8 and 9 of this paper.

REFERENCES

[1] *Removing the Threat of Weapons Plutonium*, General Atomics report, Pu-005, September 24, 1993.

[2] Barr, P., Pollitt, N., and Redding, G.B., *High-Temperature Irradiation Experiments on Plutonium-Bearing Coating Particle Fuel*, in Plutonium as a Reactor Fuel, IAEA, 1967, SM-88/38, pp. 391-417.

[3] Formann, E., et al., *The Irradiation Behavior of Plutonium Coated Particle Fuel in the Dragon Reactor Experiment*, Dragon Project Report 526, 1967.

[4] Lotts, A.L., et al., *Options for Treating High Temperature Gas-Cooled Reactor Fuel for Repository Disposal*, ORNL/TM-12627, Oak Ridge National Laboratory, February 1992.

[5] *Gas Turbine-Modular Helium Reactor (GT-MHR): A Multipurpose Passively Safe Next Generation Reactor*, General Atomic Report, GA-A21920, November 1994.

[6] Scheffel, W.J., *Design and Operational Evaluation for the Plutonium Test Element (FTE-13)*, Gulf-GA-B12271, Gulf General Atomic, August 1972

[7] Beard, C.A., et al, *Flowing Lead Spallation Target Design for Use in an ADTT Experimental Facility Located as LAMPF*, Los Alamos report LAUR-94-2495

[8] Alberstein, D., A.M. Baxter, and W.A. Simon, *The Plutonium Consumption Modular Helium Reactor (PC-MHR)*, IAEA Technical Committee Meeting on Unconventional Options for Plutonium Disposition, 7-11 November, 1994, Obninsk, Kaluga Region, Russia.

Beam Physics Design Strategy for a High-Current RF Linac

Martin Reiser
Institute for Plasma Research
University of Maryland, College Park, MD 20742-3511

Abstract

The high average beam power of an rf linac system for transmutation of nuclear waste puts very stringent requirements on beam quality and beam control. Fractional beam losses along the accelerator must be kept at extremely low levels to assure "hands-on" maintenance. Hence, halo formation and large-amplitude tails in the particle distribution due to beam mismatch and equipartitioning effects must be avoided. This implies that the beam should ideally be in near-perfect thermal equilibrium from injection to full energy – in contrast to existing rf linacs in which the transverse temperature, $T_\perp$, is higher than the longitudinal temperature, $T_\parallel$. The physics and parameter scaling for such a system will be reviewed using the results of recent work on high-intensity bunched beams. A design strategy for a high-current rf linac with equilibrated beam will be proposed.

1. INTRODUCTION

Accelerator driven transmutation of nuclear waste (ATW) offers an attractive solution to one of the most difficult environmental problems of our time – disposal of the large inventories of past and future long-lived radioactive waste from nuclear power plants [1, 2]. The rf ion linac is a natural candidate for the accelerator in view of its demonstrated capability of handling high beam currents and average power. It is also being considered for other advanced high-current applications such as neutron spallation sources, heavy-ion inertial fusion, and materials testing facilities. The extensive experience with the high-current, low-duty factor linacs at LAMPF, at the various high-energy accelerator laboratories in the world, and at other places provide a valuable technological base for the design of the CW-type machines required for ATW systems and other applications. The three most important problems – extending the duty factor to CW operation, increasing the average power to the 100 MW level, and the concomitant stringent beam control – must be solved in future R&D work.

The high average beam power of an ATW system puts extremely tight constraints on the beam quality. To insure "hands-on" maintenance, without remote manipulators, over the lifetime of an accelerator, fractional beam losses along the linac system must be kept below 10^{-5} to 10^{-8} per meter and even lower at high energy [1, 2]. Thus all the effects resulting in emittance growth, formation of halos and Gaussian tails in the particle distribution, as observed in existing linac operation and in computer simulation work must be minimized or, if possible, avoided altogether. It will be argued in the next section that the prevailing design philosophy for rf linacs is incompatible with these requirements on beam quality.

The proposed alternative strategy, a linac design in which the beam is in or near three-dimensional thermal equilibrium throughout the entire system from the RFQ injector to full energy will be presented in Section 3. The advantages and special design requirements of such an equilibrated rf linac will be summarized in Section 4.

2. EQUIPARTITIONING AND EMITTANCE GROWTH IN THE CONVENTIONAL LINAC DESIGN

The applied transverse and longitudinal focusing forces keeping the bunches confined during the acceleration process in an rf linac can be represented by the wave numbers $k_{x0} = 2\pi/\lambda_{x0}$ and $k_{z0} = 2\pi/\lambda_{z0}$, respectively. They define the wavelengths λ_{x0} and λ_{z0} of the transverse and longitudinal particle oscillations in the absence of space charge. The transverse focusing wave number, k_{x0} is determined by the phase advance σ_{x0}, of the transverse ("betatron") oscillations without space charge in one period of length $S = n\beta\lambda$ by

$$k_{x0} = \frac{\sigma_{x0}}{n\beta_0\lambda}. \tag{1}$$

Here, $\beta_0 = v_0/c$ is the ratio of the beam centroid velocity v_0 to the speed of light c, $\lambda = c/f$ is the wavelength, and f the frequency of the accelerating rf field while n is an integer (usually $n \geq 2$) that depends on the machine design. The longitudinal focusing wave number is given by

$$k_{z0} = \left(-\frac{2\pi q E_m \sin\phi_0}{\lambda m c^2 \beta_0^3 \gamma_0^3}\right)^{1/2}. \tag{2}$$

With the applied accelerating rf electric field defined by $E_{az} = E_m \cos\phi$, E_m is the peak field (including a transit-time factor in the accelerating gap); ϕ_0 is the phase angle of the beam-centroid ("synchronous") particle ($\phi_0 < 0$ for longitudinal focusing), $\gamma_0 = (1-\beta_0^2)^{1/2}$ is the relativistic energy factor, q the charge, and m the mass of the particle.

For a given average current, emittance, and rf wavelength, λ, the two wave numbers determine the size of the bunch and the beam physics. Specifically, as we will see in the next section, if $\tilde{x}$ and $\tilde{z}$ denote the transverse and longitudinal rms widths of the bunch, $a = \sqrt{5}\tilde{x}$ and $z_m = \sqrt{5}\tilde{z}$ the semi-axes of the equivalent uniform-density ellipsoidal bunch, the aspect ratio $z_m/a = \tilde{z}/\tilde{x}$ is directly related to the ratio k_{x0}/k_{z0}.

The traditional rf linac design is based on a constant phase advance σ_{x0} and a constant product of field gradient E_m and $|\sin\phi_0|$, that is

$$\sigma_{x0} = \text{const}, \tag{3}$$

$$E_m|\sin\phi_0| = \text{const}. \tag{4}$$

Hence, we get the scaling

$$k_{x0} \propto \frac{1}{\beta_0}, \tag{5}$$

$$k_{z0} \propto \frac{1}{(\beta_0\gamma_0)^{3/2}}, \tag{6}$$

and

$$\frac{k_{x0}}{k_{z0}} \propto \beta_0^{1/2}\gamma_0^{3/2}. \tag{7}$$

Thus, the ratio of transverse-to-longitudinal focusing strength increases with energy and, as a result, the aspect ratio z_m/a also increases: the radius a usually becomes smaller while the bunch length $2z_m$ becomes larger as the beam is accelerated. Thermodynamically, such a beam is not equilibrated; it becomes cooler longitudinally, and the difference between transverse and longitudinal temperature increases during the acceleration process as will be shown in the next section. The strong space-charge forces in a high-current linac beam couple the longitudinal and transverse particle motion and drive the beam in the direction of an equipartitioned equilibrium state. Due to the nonlinear, stochastic, and hence non-Liouvillean, nature of the forces involved, the equipartitioning process leads to significant emittance growth, especially in the longitudinal direction, and to a lesser extent also in the transverse direction where it produces halos and particle losses to the drift tube walls. This effect was first recognized and studied systematically in computer simulation work by R. Jameson [3] who tried to correlate his findings with the instability modes due to coupling forces in an anisotropic K-V beam investigated theoretically by I. Hoffmann [4] at about the same time. Further work following these early papers, such as the computer simulations by Wangler et al [5] and the very detailed studies by Jameson [6], have added a wealth of information on the equipartitioning effect. But so far in the framework of the traditional linac design ($\sigma_{x0} = \text{const}$, $E_m|\sin\phi_0| = \text{const}$), no satisfactory solution with tolerable minimal emittance growth has been found.

3. SCALING LAWS AND DESIGN RELATIONS FOR AN EQUIPARTITIONED RF LINAC

Since early spring of 1993 we have conducted at the University of Maryland an extensive investigation of the Boltzmann distribution (as the "natural" stationary state of a charged particle beam), the effects of image forces on bunched beams, and the coupled envelope equations in bunched beams. Some aspects of this work have been published [7, 8] or have been submitted for publication [9, 10], and some work is still in progress. A detailed and comprehensive theoretical description that includes a considerable amount of unpublished material can be found in the author's book [11]. The present paper is based on this material, in particular the section on equipartitioning in rf linacs in Appendix 4. While referring to the book for details and derivations, I will present here only a brief summary of the main features of the theory, the scaling laws and design relations for an equipartitioned linac.

Theoretically, for a matched beam in a smooth-focusing system, the transverse and longitudinal temperatures, $T_\perp$, $T_\parallel$, can be related to the rms beam widths, $\tilde{x}$, $\tilde{z}$ and rms normalized emittances $\tilde{\epsilon}_{nx}$, $\tilde{\epsilon}_{nz}$, by [11]

$$\frac{T_\perp}{T_\parallel} = \frac{\tilde{\epsilon}_{nx}^2}{\gamma_0\tilde{x}^2}\,\frac{\gamma_0^3\tilde{z}^2}{\tilde{\epsilon}_{nz}^2}. \tag{8a}$$

In terms of the effective normalized emittances $\epsilon_{nx} = 5\tilde{\epsilon}_{nx}$, $\epsilon_{nz} = 5\tilde{\epsilon}_{nz}$ and effective widths $a = \sqrt{5}\tilde{x}$, $z_m = \sqrt{5}\tilde{z}$ of the equivalent uniform-density ellipsoid, this relation may be written in the alternative form

$$\frac{T_\perp}{T_\parallel} = \frac{\epsilon_{nx}^2}{\epsilon_{nz}^2} \frac{\gamma_0^2 z_m^2}{a^2}. \tag{8b}$$

We see that for constant emittances, the temperature anisotropy increases when the ratio $\gamma_0 z_m/a$ increases, as mentioned above.

A two-temperature Boltzmann distribution with strong space-charge forces is not a stationary solution of the Vlasov equation [11] which explains why the beam is driven towards thermal equilibrium. The beam is equipartitioned ($T_\perp = T_\parallel$) when

$$\frac{\epsilon_{nx}}{\epsilon_{nz}} \frac{\gamma_0 z_m}{a} = 1. \tag{9}$$

For a space-charge dominated beam with small aspect ratio, say $0.8 \leq \gamma_0 z_m/a \leq 4$, image effects can be neglected, and one can find analytic relations for a and z_m which yield for the ratio z_m/a the relation [11]

$$\frac{z_m}{a} = \frac{2}{3\gamma_0}\left(\frac{k_{x0}^2}{k_{z0}^2} + \frac{1}{2}\right) \tag{10}$$

which is independent of the average beam current $\overline{I}$.

By using the equipartitioning condition (9) we can eliminate z_m/a and find the result

$$\frac{k_{x0}}{k_{z0}} = \left(\frac{3}{2}\frac{\epsilon_{nz}}{\epsilon_{nx}} - \frac{1}{2}\right)^{1/2}, \tag{11}$$

which relates the wave numbers to the emittances for an equilibrated beam. If the beam is in thermal equilibrium, the normalized emittances do not change during the acceleration process. If the beam is to remain in thermal equilibrium, the ratio of the focusing wave numbers must remain constant and obey the relation (11) along the entire linac. Thus, in contrast to the scaling (5) to (7) for the conventional design, we must vary the transverse focusing like the longitudinal focusing, as

$$k_{x0} \propto \frac{1}{(\beta_0\gamma_0)^{3/2}} \tag{12}$$

so that k_{x0}/k_{z0} remains constant while the energy changes, in accordance with Eq. (11).

As an example, consider a high-current rf linac accelerating protons from a nonrelativistic energy of 2 MeV ($\gamma_0 \approx 1$, $\beta_0 \approx 0.065$) to a relativistic final energy of 938 MeV ($\gamma_0 \approx 2$, $\beta_0 \approx 0.866$). Assume that the normalized longitudinal emittance is twice as large as the normalized transverse emittance so that $\epsilon_{nz}/\epsilon_{nx} = 2$. To satisfy the equipartitioning condition (11), the transverse and longitudinal focusing strength must be designed so that $k_{x0}/k_{z0} = \sqrt{2.5} \approx 1.58$ remains constant while at the same time both k_{x0} and k_{z0} decrease along the linac as $(\beta_0\gamma_0)^{-3/2}$. From (9) the bunch width ratio for this design is $z_m/a = 2$

at injection and decreases to $z_m/a = 1$ (spherical shape) at full energy. The analysis shows that the beam radius scales as [11]

$$a \propto \frac{N^{1/3}}{k_{z0}^{2/3}} \frac{1}{\beta_0^{2/3}\gamma_0^{2/3}} \propto N^{1/3}\beta_0^{1/3}\gamma_0^{1/3} \tag{13}$$

and the longitudinal semi-axis as

$$z_m \propto \frac{N^{1/3}}{k_{z0}^{2/3}} \frac{1}{\beta_0^{2/3}\gamma_0^{5/3}} \propto \frac{N^{1/3}\beta_0^{1/3}}{\gamma_0^{2/3}}, \tag{14}$$

where N is the number of particles in the beam. Thus, for a given particle number N or average current $\overline{I} = qNc/\lambda$, one finds that the bunch radius a increases from 2 MeV to 938 MeV by a factor of about 3 while z_m increases by about 1.5. This increase can be reduced by making a transition at an appropriate energy to a linac that operates at a higher frequency (shorter wavelength). For a fixed total power loss in the walls of the rf system one can increase the accelerating field with frequency as $f^{3/4}$. Using the more conservative scaling $E_m \propto (1/\lambda)^{1/2}$ and combining with the factor λ in the denominator of Eq. (2), one finds that k_{z0} scales with the rf wavelength as

$$k_{z0} \propto \frac{1}{\lambda^{3/4}} \tag{15}$$

so that the radius varies as

$$a \propto \lambda^{1/2}. \tag{16}$$

Thus by doubling the frequency in the high-energy linac stage one can reduce the radius increase to $3/\sqrt{2} = 2.1$. If one steps up the frequency by a factor of 4, as in LAMPF (200 MHz to 800 MHz), the semi-axes of the bunch will increase by only 50%. For example, using numbers similar to the study by Wangler et al [5], i.e. a 200 MHz drift tube linac with average current of $\overline{I}$=100 mA, emittances $\epsilon_{nx} = 6.85 \times 10^{-7}$ m-rad, $\epsilon_{nz} = 1.37 \times 10^{-6}$ m-rad, field gradient E_m=1.6 MV/m, and phase $\phi_0 = -40°$, one finds that the bunch radius and half-length at 2 MeV are $a \approx 2.5$ mm and $z_m \approx 5.0$ mm. For our equipartitioned linac design with a frequency change to 800 MHz one would then have $a = z_m \approx 3.8$ mm at 938 MeV. These numbers fit very well with typical drift-tube bore radii of 2 to 4 cm and they indicate that an equilibrated linac is a realistic and very attractive alternative to the conventional design.

4. SUMMARY AND CONCLUSIONS

Our results and the conclusions can be summarized as follows:

1. The prevailing rf ion linac design (with $\sigma_{x0} = \text{const}$, $E_m|\sin\phi_0| = \text{const}$) is intrinsically anisotropic in temperature and unstable for high-current operation even when the beam is carefully matched transversely and longitudinally at injection. Theoretically, such

a two-temperature beam does not satisfy the stationary Vlasov equation. Due to the equipartitioning effect, which is a manifestation of the instability, there is unavoidable emittance growth and halo formation, and the theoretical studies done so far [3-6] have not produced a satisfactory solution.

2. As a logical alternative, a design strategy is proposed in which the beam is in, or near, three-dimensional equilibrium from injection to full energy. By definition such a beam is in a state of minimum total energy and stable against perturbations that would cause undesirable emittance growth and halo formation.

3. The parameters for the equilibrated beam look very attractive from a scientific, technical, and practical point of view. Moreover, since the beam is space-charge dominated and z_m/a is close to unity, simple analytical formulas can be derived to calculate the bunch radius a and semi-length z_m as a function of average current, focusing wave numbers, and kinetic energy. This is of great value for establishing scaling relations and developing the design for a high-current linac.

4. A space-charge dominated (cold) equilibrated beam has a relatively uniform (flat-top) density profile with well-defined boundaries, unlike the Gaussian tail of an emittance-dominated beam. It should therefore be much easier to satisfy the stringent beam loss requirements. A clear advantage of the equipartitioned beam is that the phase width $\Delta\phi = 2\pi z_m/\beta_0\lambda$ of the bunch is shorter than in the conventional design and hence the linearity of the accelerating force along the bunch is better.

5. Careful transverse and longitudinal matching of rms width, divergence, and beam profile from the ion source through the low-energy beam transport, the RFQ, and the linac system will be necessary to keep the beam in thermal equilibrium and avoid creation of free energy that could cause emittance growth and halo formation [12]. Particularly important are the transitions between accelerator sections. The figures and tables in References [7] to [11] regarding the Boltzmann profiles and the effects of image forces should be of great value to the designers of such rf linacs. The RFQ design must be re-examined and modified, if necessary, to assure that it produces an equipartitioned beam.

6. The proposed design strategy for an equilibrated beam is relevant not only to ATW rf linacs but also to other high-current linac applications such as spallation neutron sources, high-energy colliders, heavy-ion fusion drivers, and materials testing facilities.

ACKNOWLEDGEMENTS

Research supported by the U.S. Department of Energy.

REFERENCES

[1] Jameson, R.A., Lawrence, G.P., and Bowman, C.D., *Nucl. Inst. and Meth. in Phys. Res. B* **68**, 474-480 (1992).

[2] Venneri, F., Bowman, C., and Jameson, R., *Physics World* **6**, 40-44 (1993).

[3] Jameson, R.A., *IEEE Trans. Nucl. Sci.* **28**, 2408-2412 (1981).

[4] Hofmann, I., *IEEE Trans. Nucl. Sci.* **28**, 2399-2401 (1981).

[5] Wangler, T.P., Bhatia, T.S., Neuschaefer, G.H., and Pabst, M., *Conference Record of the 1989 IEEE Particle Accelerator Conference*, 89CH2669-0, (1989), pp. 1748-1751.

[6] Jameson, R.A., *AIP Conference Proceedings* **279**, 969-998 (1993).

[7] Reiser, M. and Brown, N., *Phys. Rev. Lett.* **71**, 2911-2914 (1993).

[8] Allen, C.K., Brown, N., and Reiser, M., *Part. Accel.* **45**, 149-166 (1994).

[9] Allen, C.K. and Reiser, M., "Zero-temperature equilibrium for bunched beams in axisymmetric systems," CPB Technical Report #94-005, March 25, 1994, Institute for Plasma Research, University of Maryland, College Park, MD 20742; to be published.

[10] Brown, N., "Three-dimensional thermal distribution for bunched beams," presented at BEAMS Conference, San Diego, CA, June 20-24, 1994; to be published in Conference Proceedings.

[11] Reiser, M., *Theory and Design of Charged Particle Beams*, New York: John Wiley & Sons, Inc., 1994.

[12] Reiser, M., *J. Appl. Phys.* **70**, 1919-1923 (1991).

Mechanisms of Beam-Halo Formation in High-Intensity Linacs

C. L. Bohn and J. R. Delayen

Technology Development Division, Argonne National Laboratory, Argonne, Illinois 60439

An rms-mismatched beam with space-charge forces can evolve rapidly, and during the course of evolution its emittance grows and a diffuse halo forms. The halo is of particular concern for long-term operation of linacs such as those envisioned for accelerator transmutation of waste (ATW) because too much particle impingement on the accelerating structures would cause enough radioactivation to prohibit routine hands-on maintenance. Thus, halo suppression is a design consideration for these linacs. In this paper, we summarize both the physical processes associated with the rapid evolution of the rms-mismatched beam and a semianalytic formalism which was recently developed to account for them. We also provide representative results derived from the formalism.

INTRODUCTION

Space-charge forces in high-intensity linacs are known to complicate the beam dynamics significantly. If at injection the beam is mismatched, charge redistribution takes place. This injects free energy associated with the mismatch in rms beam size into a spectrum of collective modes. As individual particles interact with the time-dependent global field and with clumps of particles within it, their orbits can be chaotic. The ensemble of particle orbits rapidly tends to cover the accessible phase space in a coarse-grained manner, and its range of energies widens. In this sense, the collective interactions cause violent relaxation toward a stationary state which leads to quasi-thermalization of the free energy and of the beam. This scenario, which has been seen in both laboratory and numerical experiments, results in particles being ejected into high-amplitude orbits, causing the emittance to grow and a halo to form.

Much of the recent work on this problem concerns the interaction of single particles with an oscillating uniform-density core [1, 2]. In this simplified model, single particles with the requisite initial conditions are rapidly ejected from the core through parametric resonance [3], and so halo formation is not a surprising phenomenon. However, a proper treatment must include the evolving mode spectrum to self-consistently account for the rapid changes in the electrostatic self-field of the beam. We recently developed a self-consistent, semianalytic formalism which uses the Fokker-Planck and Poisson equations to govern the rapid evolution of the coarse-grained distribution function in the single-particle phase space [4, 5]. In what follows, we shall briefly summarize the physics of the problem and present representative results for ATW-class linacs calculated with the semianalytic formalism.

EVOLUTIONARY PHASES

A beam which is matched at injection is stationary because it is in equilibrium and

characterized by the Maxwell-Boltzmann distribution function. If the beam is mismatched, it will evolve through a complicated evolutionary sequence toward Maxwell-Boltzmann. Ref. [5] includes a detailed account of this sequence, and here we list highlights extracted from the reference.

A mismatched beam will first undergo charge redistribution, a phase lasting about one quarter of the beam's plasma period t_p. If the beam is rms-matched, it then becomes quasi-stationary, and most of the free energy associated with mismatch of the shape of the density profile appears as emittance growth. The relaxation time for further evolution, t_r, which is the time needed for a typical particle to lose memory of its initial orbit, is of the order of the very long time scale t_b associated with binary Coulomb interactions, *i.e.*, collisions in the absence of strong multiparticle correlations. On the other hand, if the beam is rms-mismatched, it continues to oscillate. If the Debye length λ_D is much larger than the beam size a, then space charge is unimportant, the beam oscillates in response to the external focusing force, and the free energy associated with mismatch thermalizes on the time scale t_b so that $t_r \sim t_b$. If λ_D is comparable to or smaller than a, then collective space-charge forces enter. Free energy associated with rms mismatch then distributes itself in a spectrum of collective modes, and these modes are subject to Landau damping. Modes with wavenumber $k \gtrsim \lambda_D^{-1}$ damp on a time scale $\sim t_p$, and modes for which $k \ll \lambda_D^{-1}$ are long-lived. Thus, if $\lambda_D \gtrsim a$ (a warm beam), we can expect the modes to damp within a few core oscillations, but if $\lambda_D \ll a$ (a cool, space-charge-dominated beam), the large-scale global modes will persist.

There are many degrees of freedom available by which a space-charge-dominated beam may release the free energy of rms mismatch. It will pass through a state of strong turbulence triggered by wave breaking associated with charge redistribution if $\Delta E_m/E_t \gg \Delta k^2 \lambda_D^2$, where ΔE_m is the free energy per particle due to rms mismatch, E_t is the thermal energy per particle, and Δk is the effective half-width of the mode spectrum. As a rule of thumb, this inequality will generally be satisfied for cold space-charge-dominated beams.

Localized collective modes in a strongly turbulent beam release their free energy very quickly (on a heating time scale $t_h \sim t_p$) via Landau damping. The short-wavelength modes dissipate, and single particles efficiently gain energy by resonant interactions with the dissipating modes. The particles continue to interact with the residual weak turbulence, and the beam relaxes on a short time scale compared to t_b. For example, in three-dimensional beams which are strongly turbulent, the average "collision frequency" is $\sim g^{-1}$ times larger than in a quiescent beam, where $g \equiv 1/n\lambda_D^3$ is the plasma parameter. In space-charge-dominated beams g^{-1} is large and interactions between particles and localized fluctuations are important. In weak turbulence the average collision frequency is $\sim g^{1/2}$ times smaller than in strong turbulence.

An increase in energy spread, or "heating", reveals itself in the relative growth of the rms beam size $\tilde{x}$ and rms emittance $\tilde{\epsilon}$. For example, suppose the injected beam is in thermodynamic equilibrium at temperature T_0 and the ejected beam is in thermodynamic equilibrium at temperature T_∞. Then the ratio of emittance to beam size is proportional to the rms velocity $\tilde{v} \propto \sqrt{T}$ at both $t = 0$ and $t \to \infty$, so $\tilde{\epsilon}_0/\tilde{x}_0 \propto \sqrt{T_0}$ and $\tilde{\epsilon}_\infty/\tilde{x}_\infty \propto \sqrt{T_\infty}$. If heating were absent, $\tilde{\epsilon}$ and $\tilde{x}$ would evolve together in lock-step, but when heating occurs, $\tilde{\epsilon}$ grows to a relatively larger amplitude than $\tilde{x}$, *i.e.*, by the factor $(T_\infty/T_0)^{1/2}$. This circumstance typifies what is observed in laboratory and numerical experiments, and heating ($T_\infty > T_0$) is prevalent. Using the principle of conservation of energy, Reiser developed a recipe for

estimating the final rms size $\tilde{x}_\infty$ and rms emittance $\tilde{\epsilon}_\infty$ from the free energy of mismatch [6], and this theory provides the basis for calculating T_∞/T_0 from the accelerator parameters and the degree of mismatch.

It is clear from these considerations that both systematic global oscillation of the potential and transient, local stochastic fluctuations can influence the violent relaxation of a beam. These processes increase the energy spread of the particles, and they inject some particles into large-amplitude orbits, yet the ways they influence the particle distribution are qualitatively different.

Calculations of the orbits of test particles in the electric potential of a globally oscillating core show that some particles gain energy, but the process is self-limiting [1–3]. This is easily explained as a resonance phenomenon. A particle will gain energy if it enters the core when the core is large and leaves the core when the core is small. The space-charge force of the core then imparts a net boost to the particle, and the process repeats itself as long as the particle orbits in phase with the core oscillations. This oscillating-core/single-particle interaction ejects resonant particles to large amplitudes in a short time, *i.e.*, within a few core oscillations [5]. However, as the particle increases its energy, its orbital period changes, the orbit eventually falls out of phase with the core oscillation, and the energy gain is accordingly self-limiting. There is consequently a maximum amplitude which a particle can attain from this systematic process.

By contrast, interactions with a broad spectrum of modes are not self-limiting. A statistically small sample of particles may be expected to interact in phase with many localized fluctuations over several orbital periods, and the orbits of these particles would thereby achieve very large amplitudes. Moreover, these interactions will divert some particles from orbits which are nonresonant with respect to the core oscillation to resonant orbits, and these particles will then experience the self-limiting energy gain. Inasmuch as these mode-particle interactions are stochastic, the attendant dynamics is very difficult to analyze, but it is clear that particles can quickly lose memory of their initial conditions. There is both experimental and numerical evidence for ongoing population of the halo by particles having small initial energy [1, 7].

FOKKER-PLANCK-POISSON FORMALISM

The Fokker-Planck-Poisson formalism is based on a two-component model of the distribution function of particles in the phase-space of a single particle. The Fokker-Planck equation governs the evolution of the coarse-grained component of the distribution function and drives it toward Maxwell-Boltzmann equilibrium. Although there is no guarantee that violent relaxation takes the beam all the way to thermodynamic equilibrium, we nevertheless assume it does as a working hypothesis. The coefficients of dynamical friction and diffusion in velocity space result from fluctuations about the coarse-grained distribution function. Turbulence excited as a consequence of charge redistribution enhances these coefficients and converts free energy due to mismatch into thermal energy. Dynamical friction and diffusion generate emittance growth and halo by injecting particles into higher-amplitude orbits. They also dissipate any fine structure present in the beam at injection. Poisson's equation provides the coarse-grained space-charge force.

The spectrum of electric-field fluctuations determines the friction and diffusion coef-

ficients. In general, the diffusion coefficient and relaxation rate may be expected to be functions of position, velocity, and time. For simplicity, and since we do not know these functions *a priori*, we ignore the position and velocity dependencies and model the beam as a fluctuating fluid in which particles execute Brownian motion. The diffusion coefficient is expressed as $D = \beta T/m$, in which β is the relaxation rate, m is the single-particle mass, and T is the "diffusive temperature" in energy units. We adopt a physically plausible phenomenological model of the diffusion coefficient by letting $T = T_\infty + (T_0 - T_\infty)\exp(-\beta_s t)$. Starting from temperature T_0, the beam strives to reach a Maxwell-Boltzmann distribution with temperature T_∞, and the heating occurs at the rate $\beta_s \geq \beta$ associated with "strong" turbulence.

To solve the coupled Fokker-Planck and Poisson equations self-consistently, we decompose the coarse-grained distribution function into complete sets of orthogonal polynomials [5]. The decomposition results in an infinite set of first-order, nonlinear differential equations for the time-dependent expansion coefficients which is fully equivalent to the Fokker-Planck-Poisson equations. Upon solving this set of equations, we have a self-consistent expression for the distribution function from which we may calculate any desired moment as a function of time, including the particle-density profile, the rms beam size, and the rms emittance.

We have written a FORTRAN code to solve for the time-dependent expansion coefficients associated with a cylindrically symmetric beam. The code has been benchmarked against a closed-form, analytic solution of the Fokker-Planck equation in which the orbits are all modeled as harmonic oscillators. It has also been verified to provide the correct final distribution function corresponding to thermodynamic equilibrium and for which the density profile can be calculated numerically directly from Poisson's equation. The solution process involves truncating the series of equations, solving the truncated series, then increasing the number of equations and solving the bigger series. If the solutions substantially agree, then one knows that a sufficient number of terms has been retained in the truncation.

We provide here an example which is representative of ATW-class linacs. We consider a linear focusing channel into which a beam with a Gaussian particle-density profile and Maxwellian velocity distribution is injected. The rms radius of the Gaussian beam is 1.2, where the unit of length is $(2T_0/m\omega^2)^{1/2}$, and ω is the angular betatron frequency without space charge. The rms radius of the equilibrium (matched) beam is 1.458. This example therefore resembles a transition to weaker focusing. The input beam is therefore modestly (20%) rms-mismatched, and it is believed that existing techniques for accelerator design would keep mismatches at transitions to about this level [8]. The ratio of the average Debye length [9] of the matched beam to its rms radius is 0.471, which indicates explicitly that space-charge forces are important to the beam dynamics, and therefore the beam is also mismatched in shape. The ratio of final-to-initial temperature is calculated from Reiser's theory to be $T_\infty/T_0 = 1.211$. Because the mismatch is modest, we assume the turbulence is always weak and take $\beta_s = \beta$. Furthermore, we let $\beta = 0.05\omega$, a relaxation rate compatible with results of numerical simulations.

Evolution of the rms radius and rms emittance normalized to their initial values is shown in Figure 1. For comparison, curves calculated analytically by modeling all the orbits as harmonic oscillators are also shown. Space charge clearly has a significant quantitative effect on the evolution. It tends in this example to push particles out, increasing the size of the core both in configuration space and in phase space.

Evolution of the "halo" is illustrated in Figure 2. This figure shows the number of particles lying outside fixed radii equal to 1, 1.5, and 2. Curves calculated analytically with model harmonic-oscillator orbits are also shown, and once again it is seen that the nonlinear space-charge forces tend to push particles farther away from the beam axis, as is consistent with Figure 1. It is also seen that, in this example, the process is somewhat more prominent in the earlier stages of evolution than in the later stages.

In summary, we have developed a semianalytic formalism for calculating emittance growth and halo formation in high-current beams for which space charge is important. Unlike oscillating-core/single-particle models, this formalism strives for self-consistency. It also leads to relatively fast computation of the transient dynamics compared to N-body simulations. However, it incorporates an oversimplified model of the very complicated microscopic dynamics which involves at least one free parameter representing the relaxation rate. Thus, while the formalism accounts for all halo-formation mechanisms, its predictive accuracy is limited, particularly with regard to the detailed halo structure. Accordingly, future work should focus on improvements with the ultimate goal of including a self-consistent calculation of the Fokker-Planck coefficients.

ACKNOWLEDGEMENTS

This work was supported by the U. S. Department of Energy under contract W-31-109-ENG-38 and by the Accelerator Operations & Technology Division, Los Alamos National Laboratory, under contract 9142K0014-2R.

REFERENCES

[1] J. S. O'Connell, T. P. Wangler, R. S. Mills, and K. R. Crandall, "Beam halo formation from space-charge dominated beams in uniform focusing channels", in *Proceedings of the 1993 Particle Accelerator Conference, Chicago, IL*, edited by S. T. Corneliussen (IEEE, Piscataway, NJ, 1993), p. 3657.

[2] J.-M. Lagniel, Nucl. Instr. and Meth. in Phys. Res. A, **345**, 46 (1994).

[3] R. L. Gluckstern, "Analytic model for halo formation in high current ion linacs", Phys. Rev. Lett. (submitted).

[4] C. L. Bohn, Phys. Rev. Lett., **70**, 932 (1993).

[5] C. L. Bohn and J. R. Delayen, "Fokker-Planck approach to the dynamics of mismatched charged-particle beams", Phys. Rev. E, **50**, August 1994 (in press).

[6] M. Reiser, J. Appl. Phys., **70**, 1919 (1991).

[7] D. Kehne, M. Reiser, and H. Rudd, in *Proceedings of the 1993 Particle Accelerator Conference, Chicago, IL*, (Ref. [1]), p. 65.

[8] R. A. Jameson, private communication (1993).

[9] M. Reiser and N. Brown, Phys. Rev. Lett., **71**, 2911 (1993).

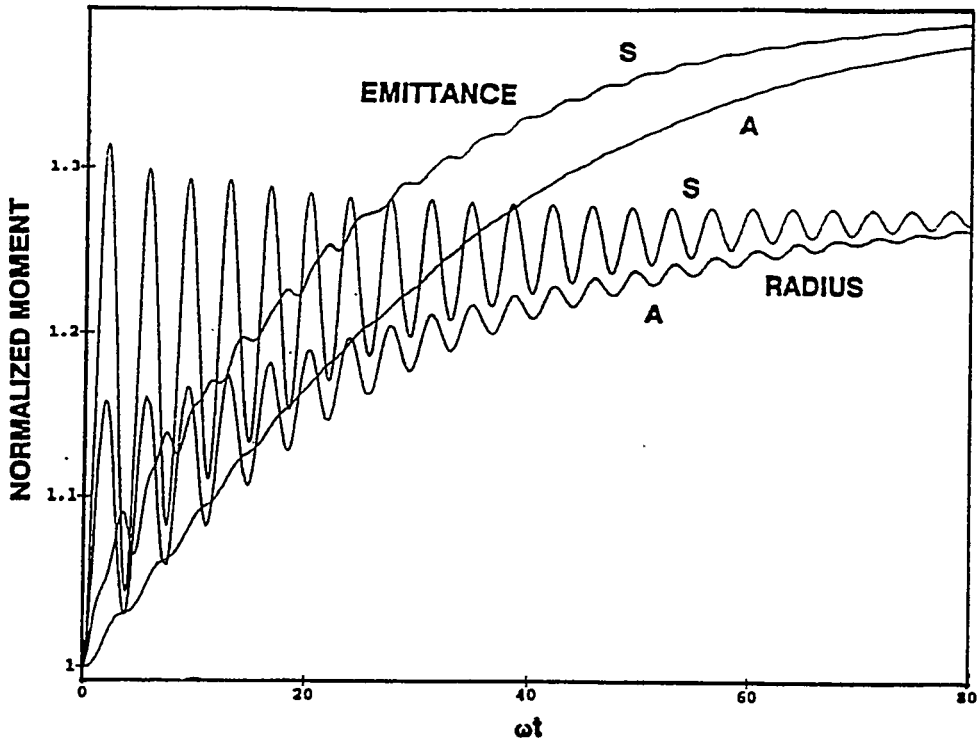

Fig. 1. Rms radius, emittance normalized to $t = 0$. Self-consistent solutions are denoted "S". Analytic solutions with harmonic-oscillator orbits are denoted "A".

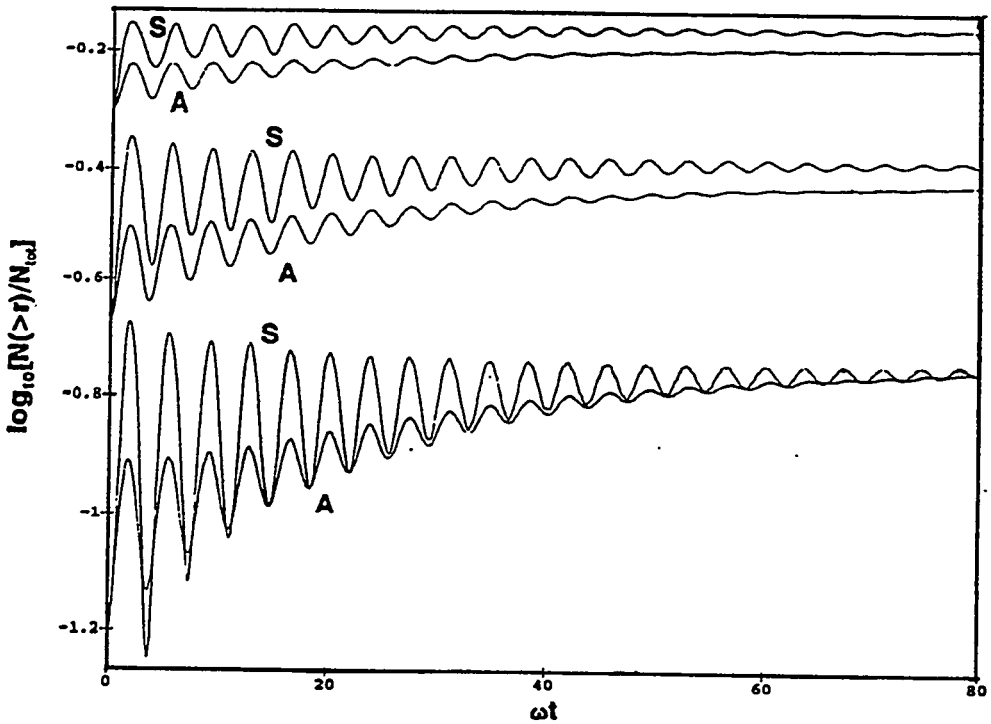

Fig. 2. Fractional number of particles outside r=1 (top), r=1.5 (center), and r=2 (bottom). "S": self-consistent solutions; "A": analytic solutions.

EMITTANCE GROWTH AND HALO FORMATION IN CHARGE-DOMINATED BEAMS

Boris I. Bondarev, Alexander P. Durkin and Boris P. Murin
Moscow Radiotechnical Institute
Warshawskoe shosse, 132, 113519, Moscow, Russia

R.A.Jameson
Los Alamos National Laboratory
P.O.Box 1663, MS H811, Los Alamos, NM 87545

Abstract. The optimization of high-current high-energy linacs against the low beam loss requirement is not straightforward or well- codified. Outlying particle losses at the 10^{-5} up to 10^{-8} level might have only a small effect on the rms properties of the beam, and thus the total beam size must be constantly kept under observation. RMS-physics has gained wide-spread acceptance as a necessary design tool, but its sufficiency is an issue for ATW/ABC accelerators.

INTRODUCTION

Rms-parameters knowledge is deficient for designing of linacs with low beam loss requirement. Both the high-density core and low-density long-extended halo must be described with the same accuracy. The halo particles have only a small effect on the rms properties of the beam and are the main reason why the rms-physics gives not the full information about beam size. For example, the matching section may be the position where wide fluctuation of beam halo size takes place without beam rms-size changing. It is why the "effective emittance" has been proposed as main parameter for describing the beam quality at any linac position. The "effective emittance" is the area of minimum phase ellipse with all beam points during RF time period inside it.

Another key parameter is total transverse beam size, because particle loss to the bore is the primary concern.

A simple model must be chosen for better understanding of process of halo formation.

It can be a continuous cylindrical beam transported in longitudinal magnetic field. In this case the model dimension is equal two and a Coulomb force calculation is very much simplified. Within the framework of this model there are only a few characteristics for understanding the cause and effect of halo formation. For halo study a model of a single-particle interaction with uniform charged cylindrical kern can be used.

THE MATHEMATICAL MODELS

The mathematical model describes the motion of continuous cylindrical beam in uniform longitudinal magnetic field. The magnetic field is a piecewice periodical function of longitudinal coordinate z. The constant field is a special case. It is assumed that input beam was born outside of magnetic field. The Coulomb fields have been calculated as the beam with cylindrical form and a formed transverse charge distribution.

The equations of motion inside magnetic lens has a unitless form

$$\begin{cases} \tilde{x}'' + 2\Lambda\tilde{y}' - \alpha\cdot\dfrac{Q(\tilde{r})}{\tilde{r}^2}\tilde{x} = 0 \\ \\ \tilde{y}'' + 2\Lambda\tilde{x}' - \alpha\cdot\dfrac{\tilde{Q}(\tilde{r})}{\tilde{r}^2}\tilde{y} = 0 \end{cases} \qquad (1)$$

$$\Lambda = \frac{eB_z L}{2m_o c\beta\gamma}, \qquad \alpha = \frac{2IL}{I_o E\cdot(\beta\gamma)^2}$$

where e, m_o are particle charge and rest mass, β - the ratio of particle longitudinal velocity to light velocity c, $\gamma = (1 - \beta^2)^{-1/2}$, B_z is magnetic field value, I is beam current, $I_o = 3.13\cdot10^{-7}$ A is Alfven current for protons, $Q(r)$ is proportion of particles charge inside the circle with radius r ($Q(\infty) = 1$), $r^2 = x^2 + y^2$. The difficulties connected with singularity of radial equation near the origin can be circumvent by using the Cartesian coordinates.

In the framework of chosen variables the product of phase ellipse semiaxes is equal 1. The parameter A can be considered as R_m/ρ_{max}, where ρ_{max} is maximum value (for the length of period) of matching beam unitless envelope, R_m - matching beam radius. In the case when $\Lambda^2 = \alpha$ and matching beam emittance equals zero it is believed that $A = R_m$.

This is evident from general form of equations (1) that beam characteristics during its transporting are determined by input particle distributions in the space of transverse coordinates and velocities and also by two parameters Λ^2 and α.

The combinations of uniform and Gauss distributions are used as input particle distributions in the space of transverse coordinates and velocities.

THE INVESTIGATION RESULTS

Some deductions about mismatching beam transporting in a longitudinal magnetic field can be made.

1) There are kern oscillation damping and halo oscillation growth.

2) All parameters of oscillations are limited.

3) The uniform kern distribution has established in spite of diffuse boundary for the most part.

4) As would be expected the relative emittance growth is larger with a larger mismatch factor.

5) The relative rms-emittance growth practically is the same for particle distributions considered here.

6) A beam with relatively great mismatching factor $f = R/R_o$ generates rms-emittance growth and this growth is greater and faster when $f > 1$ as compared with $f < 1$ in spite of f and $1/f$ are the same.

7) For beam with the same input mismatching factor rms-emittance growth is greater in periodical channel as compared with continuous channel.

8) A rms-emittance growth practically takes place at the points where kern

radius increased.

A MECHANISM FOR EMITTANCE GROWTH AND HALO FORMATION IN A HIGH CURRENT BEAM

The phase volume projections on (R,W_k)- and (R,R')-planes contain a part of particle with low density and high kinetic energies moved on phase plane outward from main beam part. It mean that there are particles which gain energy. In order to explain this effect let us consider a single particle motion in external magnetic field and in space charge field of uniform charged kern mismatched with focusing channel.

The equations of particle motion inside and outside of a kern are not the same. We have outside of a kern

$$r'' + \Lambda^2 r - \frac{\alpha}{r} = 0$$

The motion equations inside of a kern have a form

$$r'' + \left(\Lambda^2 - \frac{\alpha}{r_k^2} \right) \cdot r = 0$$

The Coulomb force in the equation outside of a kern not depends from τ and motion integral (energy conservation law) has a form

$$\frac{(r')^2}{2} + \frac{\Lambda^2 r^2}{2} - \alpha \cdot ln(r) = W_k + W_p = W_t$$

A change of W_t after kern passing gives rise to halo particle oscillations or, on the contrary, decreases this oscillation amplitudes.

Let us consider a particle motion inside the kern. Multiplying both parts of equation by r' and integrating them over τ we find

$$\Delta W_k = \int_{\tau_{in}}^{\tau_{out}} \frac{\alpha}{r_k^2} r\, r'\, d\tau$$

Transforming the integral in the right part we take the relations

$$W_{out} - W_{in} = - \int_{\rho_{in}}^{\rho_{out}} r^2\, d\rho$$

where $\rho = \alpha/r_k^2$ (if during a particle motion inside kern its oscillation pass through its maximum or minimum and r dependence from ρ is ambiguous then the above integral can be divided into some parts with a single-valued function $r(\rho)$.

Comparing a particle energies at kern entrance and exit we find its difference

$$\Delta W_t = - \int_{\rho_{in}}^{\rho_{out}} r^2 \, d\rho - \alpha \cdot ln(\rho_{out}/\rho_{in})$$

In the right part of above equation the first term defines a kinetic energy change, the second term - a potential energy change. A particle that passes through the beam kern can either gain energy or loose energy depending on time of the particle transit through the kern and depending on kern density change during the time interval from particle entrance into kern and its exit. The equations for kinetic and potential energies show that if during the transit of the particle through the kern the envelope of the kern has a monotonically change (monotone increasing or monotone decreasing) the changes in kinetic and potential energies have the opposite sighs.

In order to compare the changes in kinetic or potential energies let us consider the case of a monotonically change in kern size. The changes in kern radius and in particle radius can be taken as being approximately linear during the transit of the particle through the kern. Then the particle radius dependence on the kern radius at the same time describes by a equation

$$r(r_k) = r_{in} + \frac{r_{in} + r_{out}}{r_{in} - r_{out}} \cdot (r_k - r_{in})$$

where r_{in} and r_{out} are the kern radius values at the moments of particle entrance into the kern and its exit correspondingly. Substituting this equation into a equation for kinetic energy and integrating it we obtain

$$\Delta W_k/\alpha = - 4 \frac{\kappa + 1}{\kappa - 1} + 2 \left(\frac{\kappa + 1}{\kappa - 1} \right)^2 ln(\kappa)$$

where $\kappa = r_{out}/r_{in}$.

The general change in energy in this case is defined by equation

$$\Delta W_t/\alpha = - 4 \frac{\kappa + 1}{\kappa - 1} + 2 \left(\frac{\kappa + 1}{\kappa - 1} \right)^2 ln(\kappa) - 2ln(\kappa)$$

It is easy to check that replacing κ by reciprocal $1/\kappa$ we change the sign of above relation. It means that in the case of monotonically change in the kern radius there is antisymmetry for energy gain.

At Fig.1 are indicated changes in kinetic, potential and total energy versus the ratio κ ($\Delta W_k/\alpha$, $\Delta W_p/\alpha$, $\Delta W_t/\alpha$). It can be seen that in considered case the change in potential energy is some times greater in magnitude then

the change in kinetic energy.

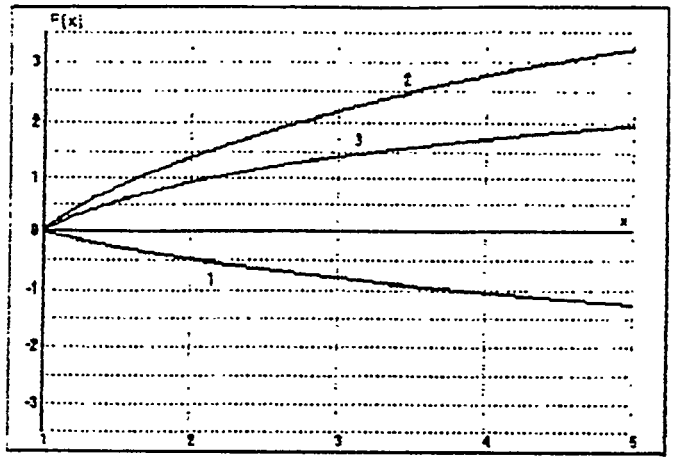

Fig.1 **x = Rinp/Rout** **F(x) = -F(1/x)**
Energies: 1 - Kinetic, 2 - Potential, 3 - Total

The above qualitative analysis gives an opportunity to understanding a mechanism for halo production and emittance growth. The codes for analytical estimates supporting codes have been generated. This codes allows to visualize phase-space dynamics for uniform-density kern model. The codes are based on concurrent solutions of kern envelope equation and equations of particle motion in the superposition of external magnetic field and kern space-charge field.

The simulation shows that the resulting separation of particles depends on the moment of kern entrance (phase of kern oscillation). If the particle enters and exits when kern density is increasing it gains the energy and in phase plane we see their "repulsion" from kern phase-plane projection. If the particle enters and exits when kern density is decreasing, it loses energy and in phase plane we see their "attraction" to kern phase-plane projection.

There is a mechanism which desynchronized the oscillations of kern and halo particles. The particle gaining the energy increases its duration of stay outside the kern. Its next kern traversal take place in another phase of kern oscillation and it can loose the energy. That is why the maximum size of kern is dictated by different particles. The right upper window shows spiral-wise phase trajectories which twists or untwists depending on the sign of energy gain after kern transit. In this window can be seen also the space clear from halo particles. This space is the intersection of kern phase volume projections at different points of kern oscillation period.

CONCLUSION

The some conclusions about the halo formation and effective emittance growth can be made:

1) The change in kern density while a halo particle passes through the kern leads to the change of the full energy of this particle. The kern density change can be caused by beam particle redistribution in transition regime as well as kern radius oscillations.

2) The change of particle energy after kern passage is added from kinetic and potential energy changes. With the availability of all factors changed the kern density the main is a potential energy change caused by change of transverse kern size. It explains the large emittance growth of mismatched beam and this growth increasing when mismatching factor is increased. With the same mismatching factor the amplitude of kern oscillations is grater in a periodical channel rather then

in continuous channel. That is why the emittance growth are greater in a periodical channel.

3) If the particle enters into the kern when kern density is smaller with regarding the kern density at the moment when the particle exits the kern then the kinetic energy of particle will be decreased and the potential energy will be increased. The particle total energy and the amplitude of its oscillations are increased. If the ratio of kern densities at the entrance and the exit will be changed by reciprocal value the energy gain changes its sign.

4) The duration of particle being outside the kern is increased with increasing of the particle total energy. That is the phase of a kern envelope oscillation will be changed in the next kern traversal. It means there is a mechanism which desynchronized the oscillations of kern envelope and halo particles which limits the halo transverse size.

The above results can be considered as a development of works [1-6].

REFERENCES

1. J.O'Connell "Stationary Phase Space Density Distribution for High Current Beams with Linear Focusing" Linear Accelerator Conference Proceeding, 1992, Ottawa, pp.522-524

2. J.O'Connell, S.Butler, Ju.O'Connell "Evolution of Simple Phase Space Distributions Using the Vlasov Equation" Computational Accelerator Physics Conference, Pleasanton,CA,1993, pp.560-567.

3. Th.P.Wangler "Beam Halo in High-Intensity Beams" Computational Accelerator Physics Conference 1993, pp.9-18.

4. R.A.Jameson "On Scaling & Optimization of High-Intensity, Low-Beam-Loss RF Linacs for Neutron Source Drivers" LA- UR-92 2474

5. R.A.Jameson "Beam Halo from Collective Core/Single Particle Interactions". LA-UR-93-1209, LANL 1993

6. J.S.O'Connell, T.P.Wangler, R.S.Mills and K.R.Crandall "Beam Halo Formation from Space-Charge Dominated Beams in Uniform Focusing Channels". Report on PAC'93

Recent Results in Analysis and Simulation of Beam Halo

Robert D. Ryne and Thomas P. Wangler
AOT-1, MS H817
Los Alamos National Laboratory, Los Alamos, NM 87544, USA

Abstract. Understanding and predicting beam halo is a major issue for accelerator driven transmutation technologies. If strict beam loss requirements are not met, the resulting radioactivation can reduce the availability of the accelerator facility and may lead to the necessity for time-consuming remote maintenance. Recently there has been much activity related to the core-halo model of halo evolution [1-5]. In this paper we will discuss the core-halo model in the context of constant focusing channels and periodic focusing channels. We will present numerical results based on this model and we will show comparisons with results from large scale particle simulations run on a massively parallel computer. We will also present results from direct Vlasov simulations.

INTRODUCTION

Several countries are now involved in efforts aimed at utilizing accelerator-driven technologies to solve problems of national and international importance. These technologies have both economic and environmental implications. The technologies include waste transmutation, plutonium conversion, neutron production for materials science and biological science research, neutron production for fusion materials testing, fission energy production systems, and tritium production. All of these projects require a high-intensity accelerator that operates with extremely low beam loss (approximately one part in 10^8 per meter). It is now known that a major source of beam loss is the formation of a very low density beam halo at a displacement exceeding several *rms* beam radii. Understanding the nature of this halo and finding ways to minimize it is crucial to the future of the above mentioned technologies. We are using both analytical and numerical tools to study beam halo.

CORE-HALO MODEL: CONSTANT FOCUSING CHANNEL

In the core-halo model of beam halo evolution [1-5], halo particles interact with a beam core of an assumed density profile, whose *rms* radius is governed by envelope equations. We begin by considering a uniform linear focusing channel with no acceleration; the channel and the beam are assumed to have axial symmetry. We will assume that the beam core has a uniform density, though the main features of the core-halo model have been observed to be insensitive to the choice of the core density profile. Figures 1 and 2 show stroboscopic plots of 32 test particles in the core-halo model; points are plotted in (x, p_x)-space each time the core radius reaches a minimum. The main features of the plots are: (1) a central region that has an extent of slightly more than the core radius; (2) a large amplitude region where particles exhibit betatron motion perturbed by the core space charge; (3) a period-2 resonant structure (associated with the fixed points to the left and right of the central region); and (4) a separatrix with an inner branch that encloses the central region and outer branches that separate the period-2 resonance from the betatron-like trajectories. The period-2 resonance is a parametric resonance corresponding to the fact that resonant particles have an oscillation frequency which is one half the envelope frequency [5]. In these figures the separatrix is actually a narrow chaotic band, and the outer edge of the chaotic band

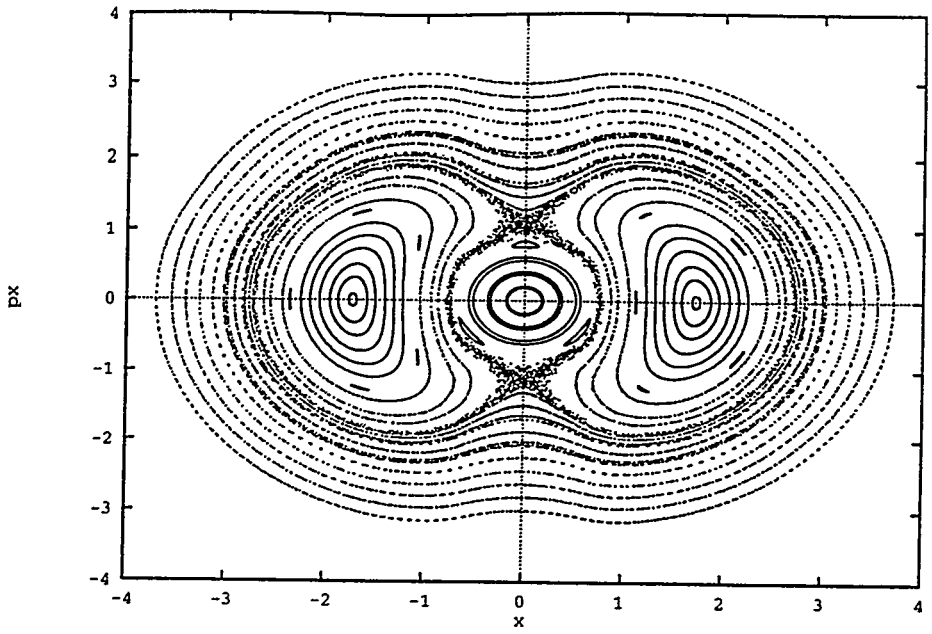

Figure 1: Stroboscopic phase space plot based on the core-halo model (uniform density core, tune depression=0.4). The initial core mismatch is 1.5 (*i.e.* the beam oscillates with a maximum amplitude 1.5 times the matched value). The location of 32 test particles is plotted every time the beam envelope reaches a minimum, for a total of 1000 oscillations.

has the approximate shape of a peanut. This "peanut diagram" provides a useful picture for describing halo formation: if particles in an initially well-defined uniform core reach the separatrix (by transport mechanisms not included in this model [1]), then they will be carried to large amplitudes along the outer branch of the separatrix. Also, deviations from an exact uniform core, in which a low-density tail extends into the resonance region, will produce the same result. Figure 1 (with the obvious chaotic region) corresponds to a system with a core mismatch of 1.5 and a space-charge tune depression of 0.4; Figure 2 corresponds to a slightly less intense beam with a tune depression of 0.5 and the same mismatch as in Figure 1. Features of the core-halo model agree well with detailed particle simulations run on the massively parallel CM-5 at the Advanced Computing Laboratory. Figure 3 shows simulation results of an initial Kapchinskij-Vladimirskij (KV) distribution with a mismatch of 1.5 and a tune depression of 0.5. For these parameters the system is unstable, and Figure 3 shows the distribution after the instability has set in. The simulation was run with 2 million particles. The first curve bounding the chaotic band in Figure 2 is also shown in Figure 3 for comparison. For this configuration (an axially symmetric beam in a solenoid channel), the CM-5 results show that the maximum particle amplitudes will be approximately confined within the outer separatrix of the core-halo model.

[1]Two examples of processes beyond the scope of the core-halo model which could lead to transport from the core toward the inner branch of the separatrix are (1) nonlinear instabilities of the core and (2) particle collisions inside the core. The presence of observable chaos, and its effect on the rate of diffusion toward the inner branch of the separatrix, is a topic that is presently being studied.

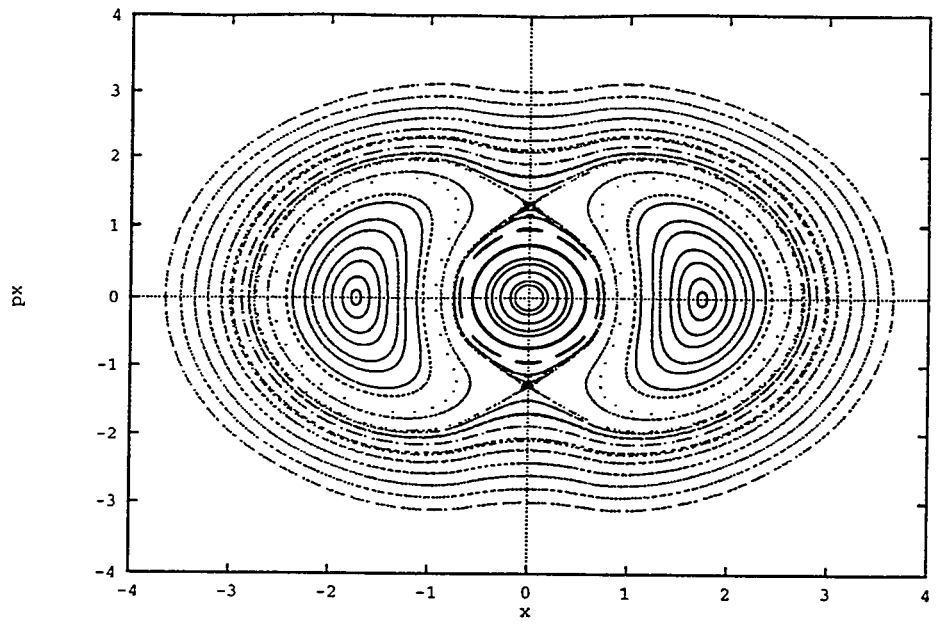

Figure 2: Stroboscopic phase space plot based on the core-halo model (uniform density core, tune depression=0.5, mismatch=1.5).

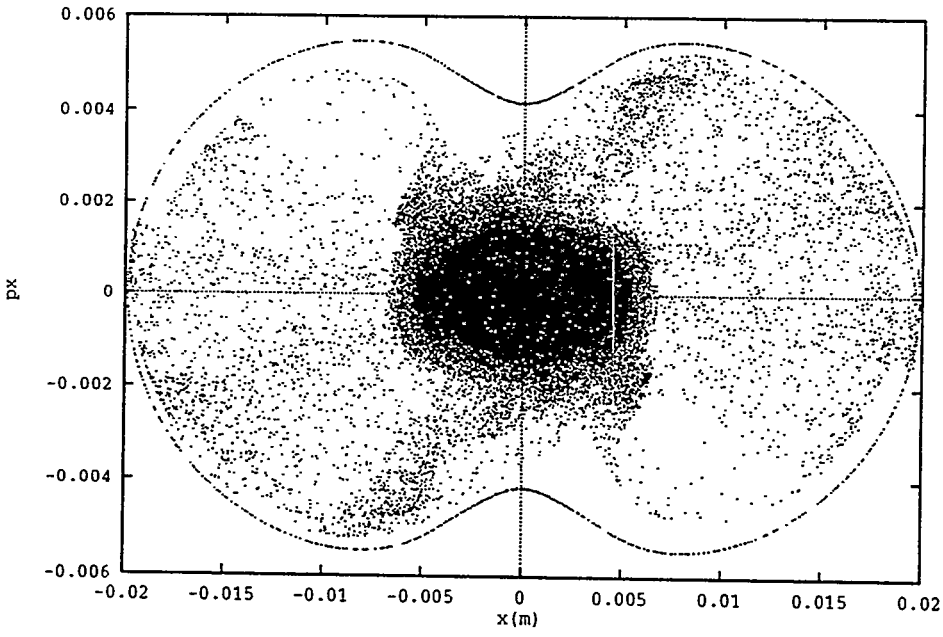

Figure 3: Beam phase space from a 2 million particle simulation on the CM-5 (65536 points are plotted). The outer peanut-shaped set of points were obtained from the core-halo model shown in Figure 2.

CORE-HALO MODEL: ALTERNATING GRADIENT CHANNEL

As shown above, the mismatch of intense beams in constant focusing channels can result in large amplitude growth for the particles. This leads naturally to the following question: Can the envelope oscillation of a matched beam in an alternating gradient channel have similar deleterious effects? The study of the core-halo model for beams in periodic focusing systems was first performed by Lagniel [3]. Consider, for example, a matched uniform beam in a FODO channel with a zero-current phase advance per focusing period of 70 degrees/cell which is depressed by space charge to 35 degrees/cell. A stroboscopic plot for an array of particles in such a system is shown in Figure 4; the data points are recorded at the center of a horizontally focusing quadrupole, where the matched horizontal beam size is $x_{edge} = 4.6$mm (*i.e.*, $x_{rms} = 2.3$mm). It is clear that the period-2 resonance that was such an important feature for a mismatched beam in a constant focusing channel is not present here. This is to be expected, since a halo particle in this example oscillates with a period roughly one tenth the quadrupole period (*i.e.*, the period of the drive in the single particle equation of motion). Though resonant structure and weak chaos are present, this does not appear to be a major source of halo formation, since the resonance structure does not provide a path by which particles can be transported to large amplitudes. Figure 5 shows simulation results for an initially *rms* matched Gaussian beam in this channel after 22 periods. A large amplitude halo is *not* present. A low amplitude halo is present due to charge redistribution (since the initial Gaussian beam was not an equilibrium distribution in this channel), accompanied by a small emittance growth of approximately 7 percent. In contrast, Figure 6 shows the same system as Figure 5, but the beam is *rms* mismatched by a factor of 1.5. Now a significant halo is present; the emittance growth in this case is approximately a factor of two.

DIRECT VLASOV/POISSON SIMULATIONS

Particle simulations provide a means of modeling the Vlasov equation by following the trajectories of a large number of interacting particles. (Since the Vlasov equation does not include the effects of two-particle collisions, the above statement assumes that collisions between particles in the simulation have a negligible effect). With the advent of large-memory computers, another approach is now possible: the direct numerical solution of the Vlasov/Poisson equations. In this approach, the distribution function is specified on a grid in phase space, and the values of the function on the grid are stepped forward in time. At present we have developed a 2-dimensional (x, p_x, y, p_y) code that runs on the CM-5 [6]. An example output is shown in Figure 7, which corresponds to an initially mismatched 4-dimensional Gaussian beam in a quadrupole channel. The figure, which shows the beam density, was obtained by integrating the 4-dimensional distribution over the variables p_x and p_y. This simulation utilized a 128^4 grid, for a total of 268 million grid points. At present, we see no clear advantage to using direct Vlasov simulations: though the resulting data are smoother than that obtained from particle simulations (because binning the output of a particle simulation generally results in noise from poor statistics), a high resolution Vlasov code requires a very large amount of memory. We will continue to develop both particle simulations and Vlasov/Poisson simulations so that we can make further comparisons of these two approaches.

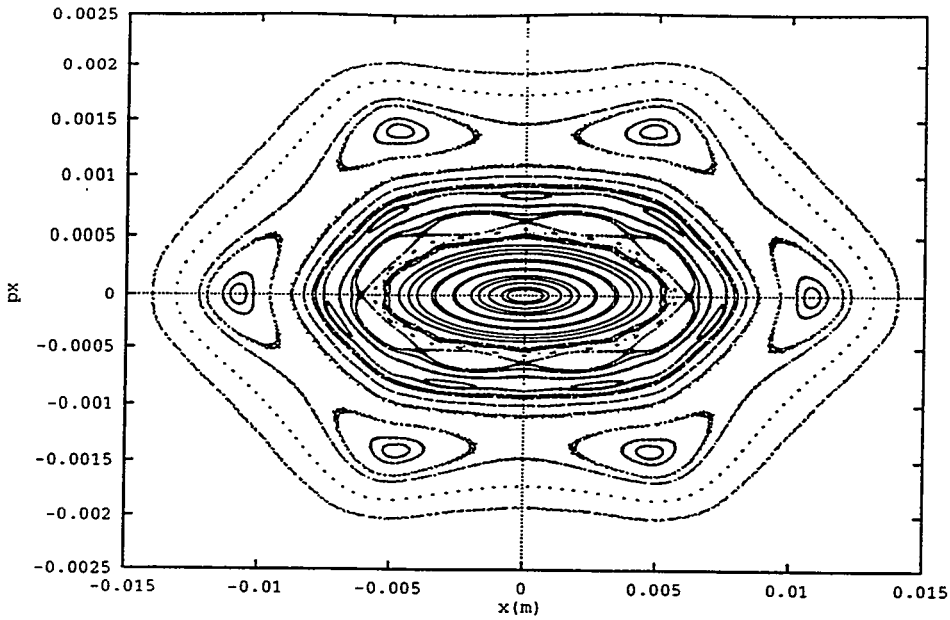

Figure 4: Stroboscopic phase space plot based on the core-halo model for a matched uniform beam in a quadrupole channel. Zero-current phase shift/cell and depressed phase shift/cell are $\sigma_0 = 70\,\text{deg}$, $\sigma = 35\,\text{deg}$, respectively.

CONCLUSIONS AND FUTURE WORK

There is strong evidence that core breathing oscillations due to transverse mismatch of intense charged particle beams can lead to significant halo formation. This is evident in the core-halo model, and it is supported by large scale particle simulations. In contrast, it appears that the flutter associated with matched beams in quadrupole channel does not lead to serious halo formation. Based on our experience with the CM-5, we believe that particle simulations with 10 million particles are easily achievable, and simulations with 100 million particles are possible but with some difficulty. Though such simulations will provide high precision beam loss estimates of linac designs, it is worth stressing that understanding the physics of halo formation and propagation through analytical models is essential for the systematic design and optimization of linacs for accelerator driven technologies.

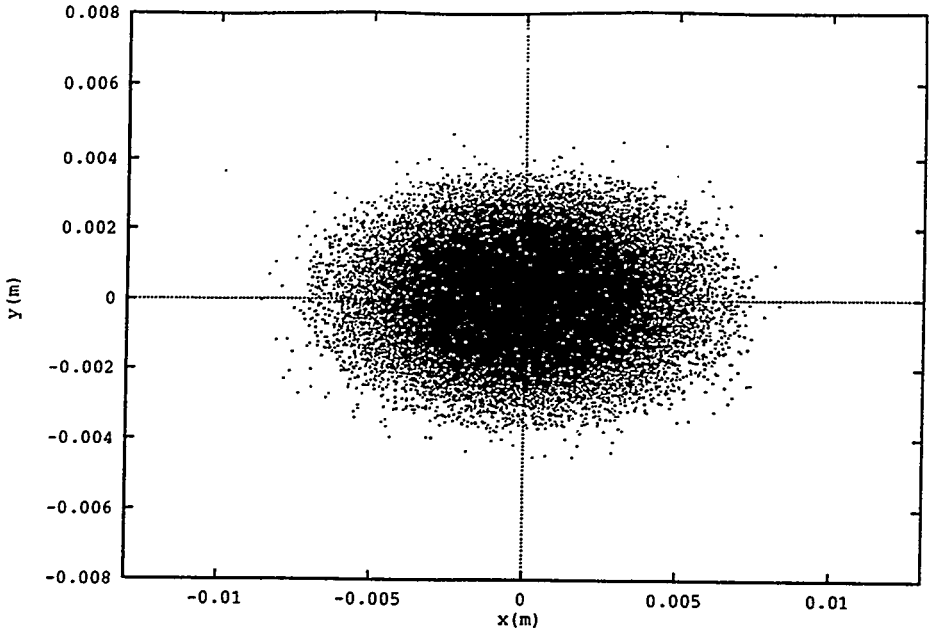

Figure 5: Simulation results showing the beam phase space after 22 focusing periods in a FODO channel. The initial distribution is an *rms* matched Gaussian beam. ($\sigma_0 = 70\,\text{deg}$, $\sigma = 35\,\text{deg}$)

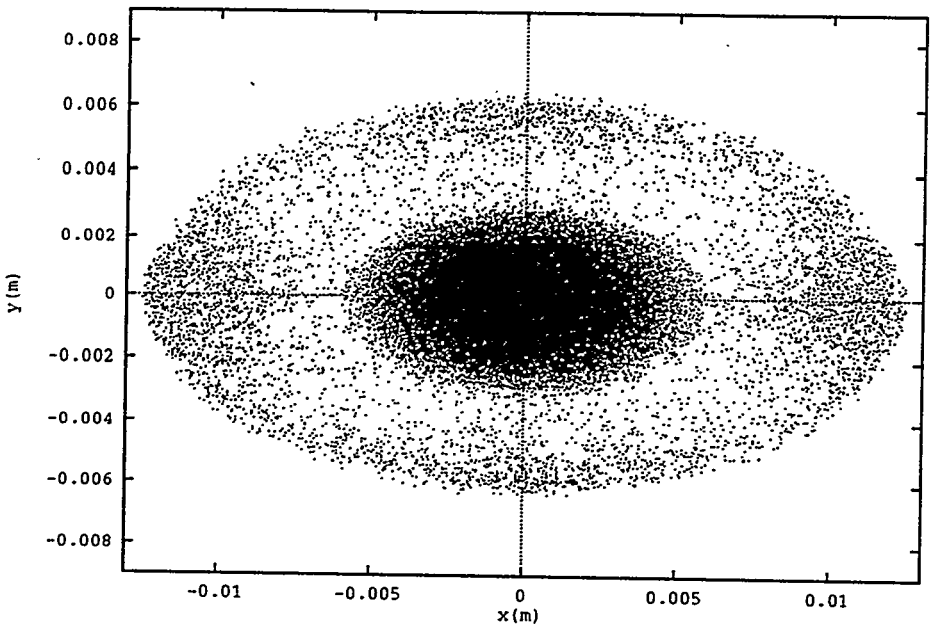

Figure 6: Simulation results showing the beam phase space after 22 focusing periods in a FODO channel. The initial distribution is an *rms* mismatched Gaussian beam. ($\sigma_0 = 70\,\text{deg}$, $\sigma = 35\,\text{deg}$)

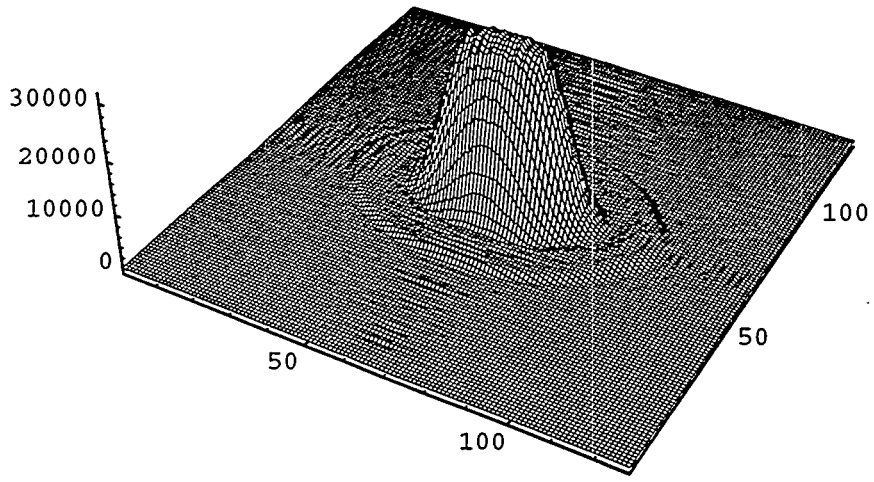

Figure 7: Output from a direct Vlasov/Poisson simulation. The 4-dimensional distribution function was integrated over p_x and p_y to obtain the beam density on a 128x128 grid.

ACKNOWLEDGEMENT

This research was performed in part using the resources located at the Advanced Computing Laboratory of Los Alamos National Laboratory, Los Alamos, NM 87545

REFERENCES

[1] J.S. O'Connell, T.P. Wangler, R.S. Mills and K.R.. Crandall, "Beam Halo Formation from Space-Charge Dominated Beams in Uniform Focusing Channels," Proceedings of the Particle Accelerator Conference, Washington, DC, p. 3657 (1993).
[2] J.M. Lagniel, "On Halo Formation in Space-Charge Dominated Beams," Nucl. Inst. Meth A345, No. 1, p. 46 (1994).
[3] J.M. Lagniel, "Chaotic Behaviour and Halo Formation from 2D Space-Charge Dominated Beams," Nucl. Inst. Meth A345, No. 3, p. 405 (1994).
[4] T.P. Wangler, "Dynamics of Beam Halo in Mismatched High Current Charged Particle Beams," Los Alamos preprint, LA-UR-94-1135 (1994).
[5] R.L. Gluckstern, "Analytic Model for Halo Formation in High Current Ion Linacs," to appear in Phys. Rev. Lett. (1994).
[6] S. Habib and R. Ryne, in preparation.

Funneling in LANL High Intensity Linac Designs*

Subrata Nath
AOT-1, MS H817
Los Alamos National Laboratory, Los Alamos, NM 87544, USA

Abstract: The Los Alamos design approach to Accelerator driven transmutation applications is based on high power proton linacs. Most of the accelerators that have been studied have one important element in common. That component is a funnel, where beams from two separate but identical front end linac systems are merged to form a collinear beam of twice the initial beam intensity. The nominal linac design for Accelerator Transmutation of Waste (ATW) consists of an ion source-injector / Radio Frequency Quadrupole (RFQ) / Drift Tube Linac (DTL) combination operating at 350 MHz. The output beam at 20 MeV from each of the DTLs is then funneled to a single high energy linac operating at 700 MHz which accelerates the beam to 800 MeV. In this paper, we present the rationale behind the choice of funneling to achieve higher beam intensity, a beam dynamics design, and simulation results through the funnel section, together with the present experimental status of funneling.

INTRODUCTION

In a funnel section, two beams from two separate low energy legs, each consisting of one ion source, LEBT, RFQ, and DTL, are combined to form a single collinear beam. The two legs carry bunched beams that are phased 180^0 apart and of frequency f_0 which are then merged forming a single beam of frequency $2f_0$. The beams are interlaced as shown in Fig. 1. The interlacing is done in a deflector cavity by alternating rf transverse deflecting fields operating at frequency f_0. It is to be noted that the funneling doubles the effective current of the output beam but does not increase the charge per bunch.

Funneling becomes a necessary feature of a linac design as soon as very high power is required of the machine as is the case for some transmutation of waste applications. All ion sources and low energy sections of the linac, i.e., RFQs and DTLs, have beam current limits. We avoid these limits by reducing our injector and RFQ current requirements in half

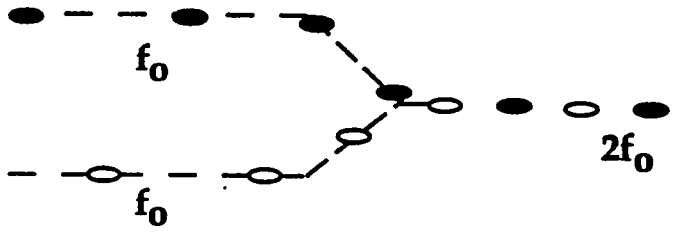

Fig. 1. Interlacing of the bunches in a funnel section

* Work supported by the US Department of Energy

and funneling at an appropriate stage. It allows us to fill all the rf cycles with beam in the high energy portion of the linac and thereby increase the efficiency of the machine. Assuming that emittance growth effects can be controlled, the beam size, and the charge per bunch are also smaller compared to an unfunneled beam of the same effective current. This provides an effective design strategy to achieve lower beam loss at the high energy end of the linac, a foremost concern and a must for hands on maintenance of such a high power, high energy machine.

In the proposed LANL design [1], the energy of funneling was chosen to be 20 MeV. The choice of energy was a compromise between several conflicting requirements. This energy was chosen to keep space charge forces relatively small and to have high enough velocity so that the 700-MHz linac following the funnel would accept the funneled beam. Also, a relatively high energy was needed to provide interquad distances that were large enough to meet engineering and diagnostic requirements. The 20-MeV beam-energy is still low enough to result in a beam that is not too rigid for deflection in the rf deflector.

DESIGN ISSUES

In designing a complete configuration for the funnel, i.e., the layout of the components, choosing the quadrupole focusing lattice, and the component strengths etc., one has to strike a compromise between a number of physics as well as engineering issues. These have been discussed at some length elsewhere [2].

The final kick at the rf deflector is time dependent which translates into transverse beam spreading [3]. For a short bunch, the difference in deflection between the synchronous particle and a particle of phase σ with respect to the synchronous particle is approximately proportional to σ^2. Thus, the head and tail of the bunch will be deflected less compared to the center of the bunch even if the deflector is optimized for maximum deflection. To minimize this "head-tail" effect, longitudinal beam width of the beam should be made as small as possible. The shorter the bunch, the less transverse emittance growth. Reduction of the longitudinal beam size is also required for accommodating the beam inside the bucket as it enters the accelerating structure operating at twice the frequency that follows the funnel section. A real deflector structure will also have non-uniformities in the deflecting electric field at the edges and ends. The fringe field-effect would contribute to undesired emittance growth unless beam size is small enough to traverse the central section of the deflecting field. The maximum gap between the deflector plates in the bending plane is constrained by sustainable electric field across the gap and thermal management considerations. In the orthogonal plane, however, the plate dimensions could be larger consistent with the cavity dimension. This puts constraint on the transverse size of the beam i.e., the transverse size in the bend-plane should be made as small as possible.

From beam dynamics point of view, the funnel lattice should follow the same pattern as the previous accelerating structure. In the present LANL design, the DTL structure which precedes the funnel, has a FOFODODO lattice with a $4\beta\lambda$ focusing period. The transverse phase advance per focusing period should be kept less than 90^0 to avoid the so called

envelope instability. This puts a constraint on the inter-element spacing at the merging end of the layout. The beam as it travels through bunchers and bending magnets, suffers momentum dispersion. Minimizing this effect requires that the total bending and bunching be done in small steps, distributing them as evenly along the length of the funnel as possible.

The physics considerations outlined above, are often in conflict with the engineering requirements. The layout must provide adequate spacing for placement of quadrupoles, bending magnets, and bunchers with minimum deviation from a truly periodic lattice. The space constraint is particularly severe in and around the merging section. The physical size of the deflector is dictated by the rf structure and cooling considerations. This also imposes a constraint on the space to be provided for the deflector cavity. Room needed for placement of appropriate diagnostic elements along the length of the funnel also places additional demand on the available space.

LAYOUT

The arrangement of the components in the 20-MeV funnel is shown in Fig. 2. Each leg of the transport region consists of eight electromagnetic quadrupoles (EMQ) and two conventional two gap 700-MHz bunchers (R3 and R2). These elements transport the beam with about the same transverse and longitudinal focusing strengths as in the exit of the DTL.

The funnel legs are designed with 700 MHz bunchers operating at the second harmonic of the beam, resulting in smaller cavities and a savings of power and space in a fairly tight configuration. All the buncher cavities used are two-gap drift-tube linacs. Three distinct types of buncher cavity designs are used. The second of the two buncher cavities (R2) in the two legs has a special tapered geometry to enable the bunchers in the two adjacent legs fit together. SUPERFISH [2] was used for both the types i.e., R3 and R2 calculations because of their cylindrical symmetry. The final buncher (R1) is located where the two legs of the funnel are very close together. In this case, a common cavity is used as the bunching cavity for the beams. This buncher cavity has two beamlines through it. It may be best described as a drift tube linac with two beamlines. Since this cavity is not cylindrically symmetric, MAFIA [4], a 3-D code, was used for this structure. A detailed discussion on this cavity is presented in an accompanying paper [5].

The deflector is the key component in the funnel. A detailed discussion on the rf properties, thermal analysis and rf tuning of this structure is also contained in Ref. 5. After the initial configuration was established with CHARGE2D code [3], MAFIA was used for this axi-asymmetric structure. The beams enter the cavity at an angle to the symmetry axis. The electric field of the cavity's fundamental mode with a dominant amplitude between the two electrodes, normal to the symmetry axis, deflects the beam on the axis. The rectangular shape of the electrodes and the gap between the plates are chosen to provide a fairly homogeneous field. It is practically constant ($\Delta E_z < 0.5$ %) in a transverse range of $\pm$ 10 mm about the central axis. The tuning of the cavity could be achieved by either

adjustment of the cavity radius or the radius of the base of the circular cones holding the electrodes or a combination of the both consistent with lowest heatload to the structure. The peak gap-field used for the structure is 24 MV/m, which is less than 1.5 E_k.

The last two quadrupoles in each leg are made of permanent magnet materials (PMQ) for compactness, while the final defocusing quadrupole in the "merge" section in front of the deflector cavity is a large bore EMQ with both beams entering off-axis. The dipoles in each leg of the funnel bend the beam by 9.77^0. The common large bore EMQ (where the beams enter off-axis) deflects each beam by another $\sim 1^0$. The remaining $\sim 2^0$ of bend, to merge the beams on symmetry axis, is done in the rf deflector cavity. The parameters of the current 20-MeV funnel design are contained in Table 1.

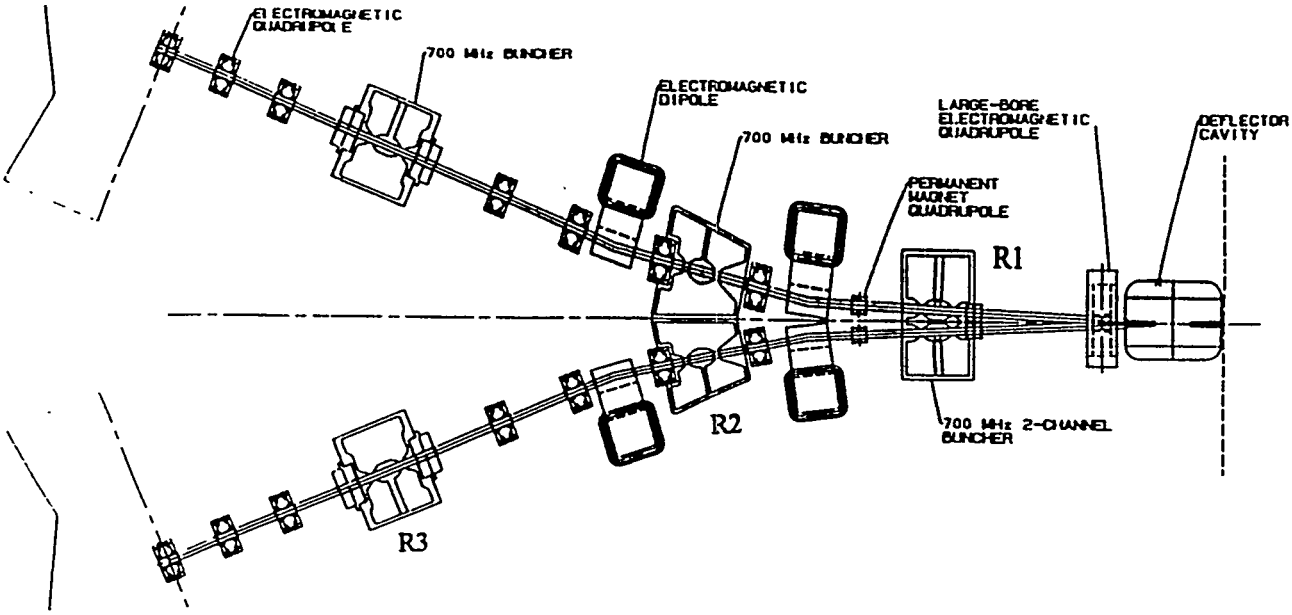

Fig. 2. Layout of the 20-MeV Funnel

Table 1. General Parameters of the 20-MeV Funnel

Energy	20.0 MeV
Length	295.0 cm
No. of Quadrupoles	2 X 10 + 1 = 21
No. of Dipoles	4
No. of Bunchers	2 X 2 + 1 = 5
No. of Deflectors	1
Initial Beam Approach Angle	22.4 degree
Initial Separation of Beams	137.8 cm
Quadrupole Lattice	FOFODODO
Effective Quadrupole Lengths	5.7 cm

SIMULATION RESULTS

For funnel simulation studies, a modified version of PARMILA is used. It has a deflector subroutine that transports particles stepwise through a time dependent electric field map between the deflecting plates. Calculations were done with a simulated distribution of ten thousand macro-particles (10,000) at the input. The phase space distributions at the output of the funnel are shown in Fig. 3. Results of end-to-end simulation (particle distribution at

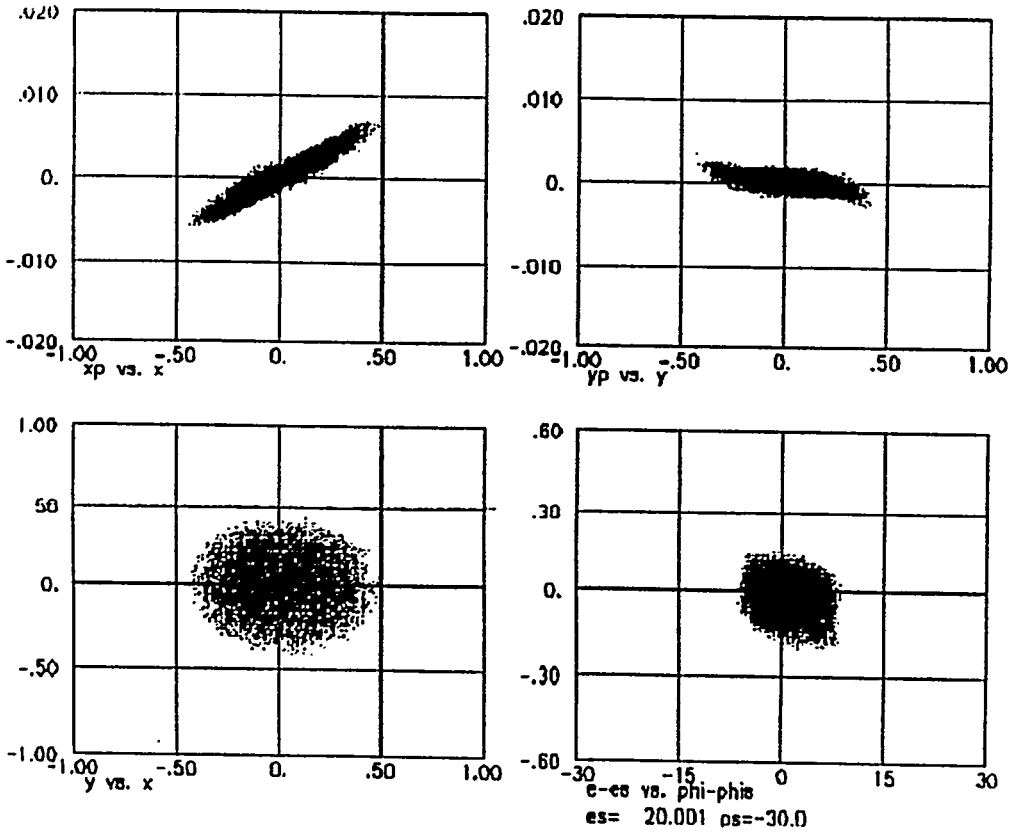

Fig. 3. Phase Space Plots at the Output to the Funnel

Table 2. Beam Parameters for the 20-MeV Funnel

Beam Current	Input Output	100 mA in each leg 200 mA
Radial Aperture		1.00 cm (0.6 cm between deflector plates in the bend plane)
Aperture /Beam Size (rms)		4.3 @ Deflector 5.5 @ PMQs
Longitudinal Beam Size (rms)	Input Output	~ ± 5.5 degree ~ ± 3.3 degree
Transverse Emittance (rms, norm.)	Input Output	0.023 π cm-mrad 0.026 π cm-mrad
Longitudinal Emittance (norm)	Input Output	0.0216 π deg-MeV @ 350 MHz 0.0219 π deg-MeV @ 350 MHz

the input to the RFQ transported all the way through the funnel to the end of the CCL) are contained in an earlier publication [2]. A 3-D space charge algorithm (a point-to-point treatment) were used . A summary of the beam characteristics are included in Table 2.

An error study of the funnel section was also carried out. Four types of error conditions were examined : 1) input beam errors, 2) quadrupole errors, 3) buncher errors, and 4) deflector errors. In addition, a longitudinal acceptance study was also done. All the error studies were done with a simulated distribution of ten thousand macro-particles at the input. Simulation results using 2D or 3D space charge subroutines did not show any significant differences. Since the computation time for 3-D space charge calculations vary approximately as N^2 (N is the number of particles), and it required 10,000 particles to perform statistically meaningful simulations, the 2-D space charge subroutine was used in the error studies.

EXPERIMENTAL STATUS

An experimental demonstration confirming the beam dynamics of funneling was completed on the Accelerator Test Stand (ATS) at Los Alamos National Laboratory [6]. The experiment used a single leg layout. The funnel input beam was from the ATS H⁻, 425 MHz, 5 MeV DTL. The details of the experiment can be found in Ref. 6. A schematic of the experiment is shown in Fig. 4.

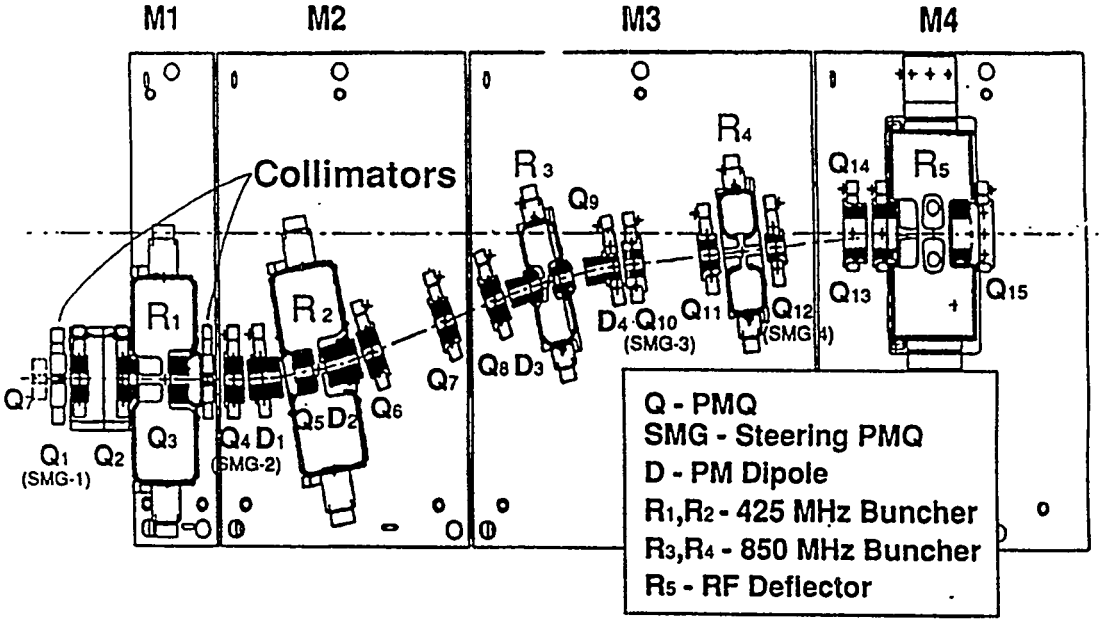

Fig. 4. Schematic of the Los Alamos Single Beam Funnel Experiment

The experimental results showed ~ 100 % beam transmission through this single leg funnel, with good steering control. Transverse and longitudinal emittance growth were demonstrably controlled. Transverse emittance growth agreed with computer simulations to within experimental errors. Non-optimum operation of the rf bunchers also failed to

produce any measurable transverse emittance growth. The observed longitudinal emittance growth was ~ 15 % with an uncertainty of 5 %. This observed level of longitudinal emittance growth had no effect on the funnel's performance. The results with non-optimum buncher operations were basically the same.

A two-beam funnel experiment was also attempted at the McDonnell Douglas site [7] in 1991. The purpose of this two beam experiment was to resolve funnel issues not addressed in the earlier ATS experiment at Los Alamos. The experiment used two beams from two separate linacs, each providing a 2 MeV, H^+ beam with a nominal current of 25 mA at 425 MHz. The beamline was optically similar to the ATS beamline, except that the input beams entered the funnel at 20^0 from the output axis, as is the case in our current funnel design. This also used a two hole bunching structure. Unfortunately, the experiment was cut short prematurely before a complete beam characterization was performed. However, it demonstrated operational feasibility of a two hole-buncher and resolved some of the engineering concerns on the placement of components in the adjacent legs.

SUMMARY AND CONCLUSIONS

An example design of a funnel for high intensity proton linac is presented. Thorough optimization of the individual components and layout should precede actual fabrication. Particular attention needs be paid to the deflector cavity and the two hole buncher designs. The ATS single-beam funnel experiment showed that, with present methods and techniques, one can design a funnel and its key component, i.e., the deflector, with very low emittance growth. Very good agreement between calculations and the ATS experimental results showed that rf and beam-dynamics design procedures are essentially correct and no important physics issues were omitted in the codes.

REFERENCES

[1] K. C. D. Chan, "A Prototype Front-End Accelerator for Accelerator-Driven Transmutation Technologies", contribution to this conference.
[2] APT Accelerator Topical Report, Los Alamos National Laboratory Report LA-CP-94-48, vol. 1, March 1994.
[3] F. W. Guy, et al., "Beam-Dynamics Design and Performance of the RF Deflector in the Los Alamos Single-Beam Funnel Experiment", Proceedings of the IEEE Particle Accelerator Conference, vol. 1, p 578, 1991.
[4] M. Bartsch, et al., "Solution of Maxwell Equations", Computer Physics Communications, vol. 72, p 22, 1992.
[5] F. L. Krawczyk, et al., contribution to this conference.
[6] K. F. Johnson, et al., "A Beam Funneling Demonstration:Experiment and Simulation", Particle Accelerators, vol. 37-38, p 261, 1992.
[7] McDonnell Douglas Report, MCD91E0028, August 1991.

Design of RF-Cavities in the Funnel of Accelerators for Transmutation Technologies[1]

Frank L. Krawczyk*, Nathan K. Bultman**, K.C. Dominic Chan***, Rick L. Martineau**, Subrata Nath*, Lloyd M. Young*
**AOT-1, MS H817, **ESA-7, MS H821, ***AOT-17, MS H851*
Los Alamos National Laboratory, Los Alamos, NM 87544, USA

Abstract. Funnels are a key component of accelerator structures proposed for transmutation technologies. In addition to conventional accelerator elements, specialized rf-cavities are needed for these structures. Simulations were done to obtain their electromagnetic field distribution and to minimize the rf-induced heat loads. Using these results a structural and thermal analysis of these cavities was performed to insure their reliability at high average power and to determine their cooling requirements. For one cavity the thermal expansion data in return was used to estimate the thermal detuning.

INTRODUCTION

High intensity CW proton accelerators are proposed candidates as drivers for waste transformation systems and spallation neutron sources. An essential component of such a structure is a funnel. In a funnel two beams are merged into a single beam. This is accomplished by using an arrangement of lenses and special rf-cavities [1]. An example is the recent design of the Accelerator Performance Demonstration Facility in Los Alamos[2] (APDF). The design of the APDF funnel's special deflector and buncher cavities will be discussed here.

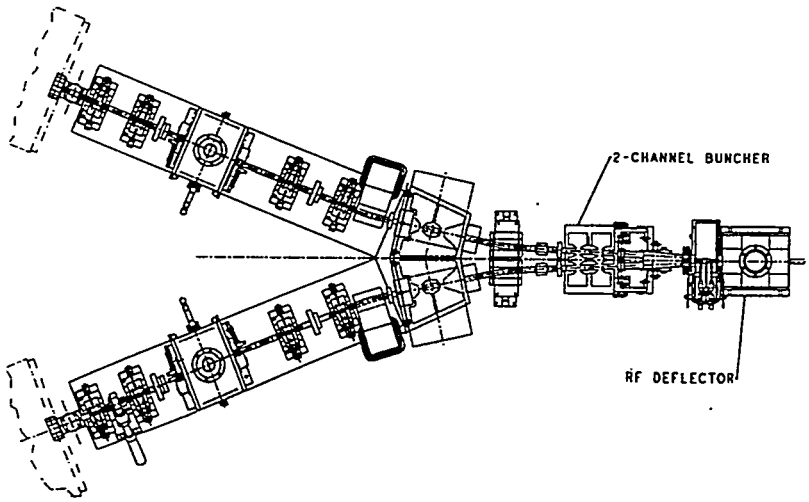

Fig. 1. This plot shows the front-end part of the APDF. The beams from the two ion-sources are deflected into a common channel. The deflector and two-beam buncher cavity for the final step of the deflection will be discussed here.

For the electromagnetic analysis preliminary calculations have been done with the 2D code SUPERFISH [3]. As these cavities are not axis-symmetric, their final modeling requires a 3D-analysis. The estimated parameters from the 2D-calculations were the starting point for

[1]Work supported by Defense Nuclear Agency

this analysis to determine their final shapes and measurements that should yield structures with reasonable wall losses and the desired operational frequencies. These simulations have been done using the finite difference electromagnetic program package MAFIA (Rel 3.2 [4]). Besides the 3D capabilities MAFIA has a flexible input language allowing a variable description of grid and structures. This significantly simplifies the parameter studies to tune and optimize these structures. Also the extended post-processing helped to easily evaluate secondary quantities like wall losses, Q and shuntimpedance for the appropriately normalized field solutions. For the transfer of loss data to the structural analysis code command macros and an interface have been programmed [5] within the MAFIA code.

The structural analysis has been done with ABAQUS (V5.3), a finite element code. The heat flux data provided by the MAFIA code was used as a boundary heat source condition on the finite element model. This data was imposed on the finite element mesh by using the closest element surface to a MAFIA output point. This produced a very good mapping between the the two differently discretized models.

Despite the necessity to do a final 3D-modeling it is remarkable that already the 2D-calculations gave good approximations of the final structures. For example, the estimated deflector gap voltage (24MV/m) derived from these calculations agreed within $< 1\%$ with the one derived from the 3D-model. The modeling process for this parameter study has been significantly accelerated by the preliminary 2D-calculations.

THE DEFLECTOR CAVITY

In the funnel the beams from the two ion-sources are combined into a single beam by deflection. To conserve the beam quality this deflection has to be done in several steps. The

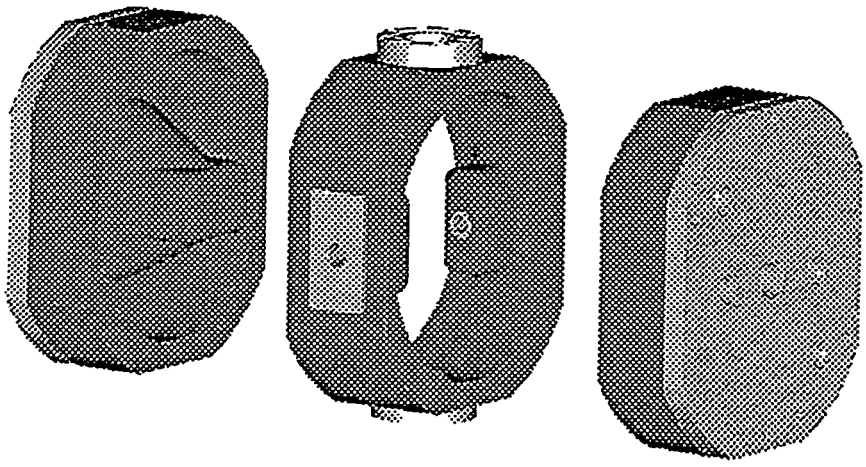

Fig. 2. This is the structural model of a deflector cavity. The end caps hold the electrodes fixed to circular cones. The central ring holds the noses housing the common beam pipe.

final deflection has to be done by the same optical element for both channels, since they already are very close to each other. Static electric or magnetic fields cannot be switched

or reversed fast enough to provide both beams with the needed change in momentum. The fastest method is a rf-field, whose frequency is an odd multiple of half the bunch repetition rate. The deflector geometry has to be chosen to have a harmonic electric field orthogonal to the beam direction providing the opposite deflections for each of the two beams. Figure 2 shows the model of such a deflector cavity.

The beams cross the cylindrical cavity radially, not on the cylinder axis. They are guided close to the electrodes by a beam pipe sitting inside a rectangular metal nose. The electrodes sit on top of cylindrical cones aligned with the cavity's cylinder axis. The electric field of the cavity's fundamental mode with a dominant amplitude between the two electrodes, normal to the beam directions, deflects the beams when they pass the gap between the electrodes.

The rectangular shape of the electrodes as well as the electrode distance have been chosen to provide a fairly homogeneous field where the beam passes them. It is practically constant ($\Delta E_z < 0.5\%$) in a transverse range ± 10 mm around the central axis.

Calculations show that a gap longer than $\beta\lambda/2$, despite a partial compensation of the achieved deflection, allows a lower overall field level in the cavity than a shorter gap. Any arrangement with a shorter electrode results in a less effective deflection that requires an even higher field amplitude. For a final deflection of 1.9 degree the APDF deflector cavity needs a deflection of 2.02 degree associated with the passage between the two electrodes.

The tuning of the cavity can be done by changing the cavity radius or the radius of the base of the circular cones holding the electrodes. A combination of these two parameters has to be found that yields the desired frequency and the lowest possible heat loads. Our final model is not necessarily the optimal one. We just searched for a parameter set that reduced the losses to a tolerable level and fits the tight longitudinal space requirements at the deflector position of the accelerator. The APDF deflector cavity has a radius of 121 mm. The cone base radius is 73.5 mm. Table 1 shows some of its calculated properties for a peak gap-field of 24 MV/m.

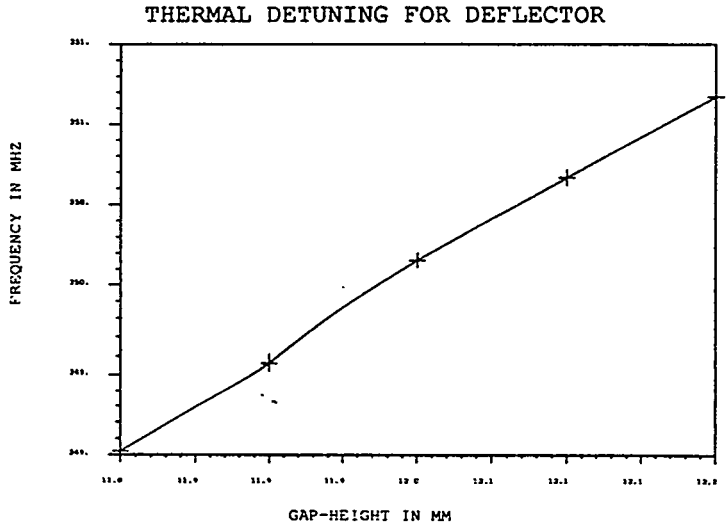

Fig. 3. Here the frequency variation for an assumed gap height variation due to thermal expansion is displayed. The change seems to be linear. For a gap variation of ± 0.2 mm the frequency changes by only $\pm 0.3\%$.

Table 1. Important Parameters of the Deflector Cavity

Frequency	Integrated Loss	Peak Loss Density	Deflection Angle
350 MHz	48 kW	68 W/cm^2	1.9 deg

The loss data from the numerical field calculation have been transferred to ABAQUS for the stress and thermal analysis. This analysis will be described in the next section. From the stress analysis the change of gap-height has been determined as the dominant deformation of the structure. With the electromagnetic field calculation program the resulting detuning that can be expected for this cavity has been estimated (see figure 3).

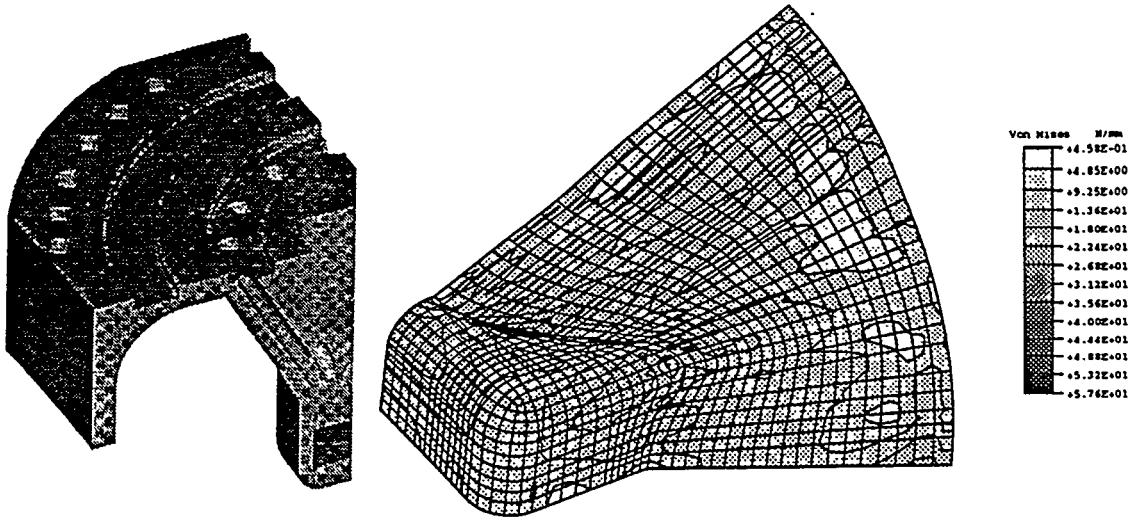

Fig. 4. Left the cooling passages in the deflector electrode are shown. They provide an adequate cooling for the heat loads predicted by the MAFIA field calculations. The right part shows the Von Mises stresses taking into account the heat loads and the cooling provided.

THE THERMAL ANALYSIS OF THE DEFLECTOR CAVITY

The thermal analysis for the deflector to date has been limited to the nose region of the electrode. The heating varies considerably around the circumference of the electrode. The left part of figure 4 shows a cut-away of the cone region and the location of the cooling passages drilled into the wall of the cone. Cooling water flows into the end cap of the cavity and through the the drilled passages in the cone wall. It then flows across the surface and end of the deflector electrode and returns through the center of the cone. The analysis predicts a peak temperature of 63 C, this is a rise above inlet water temperature of 43 C. Peak stresses (right part of figure 4) are predicted to be 58 MPa, or about 85% of the yield stress. This is adequate for this stage of the design effort; probably additional cooling will be required and will be added during the overall detailed design phase.

THE TWO BEAM BUNCHER

There is one disadvantage of the rf-deflection scheme. Bunches not short enough will experience different deflections at head, center and tail due to the harmonic change in the electric field amplitude. To minimize this effect bunches have to be longitudinally compressed shortly before entering the deflector. As the two beams are already very close at this point they need a common buncher cavity. Also for very short bunches a single buncher would need an unreasonably high field level. To reduce the needed amplitude two buncher cavities can be used. Since these in cw-operation still dissipate a huge amount of power, a combined two beam and double gap buncher (figure 5) has been proposed. As this double gap structure has two endwalls less than two single buncher cavities, this arrangement has significantly reduced wall losses.

The two beams enter the circular cavity tank under angles of approximately ±2 degree symmetric to the cylindrical axis. The gaps for each beam are defined by two half drift tubes attached to the end walls and a central drift tube held by a circular stem. The cavity is

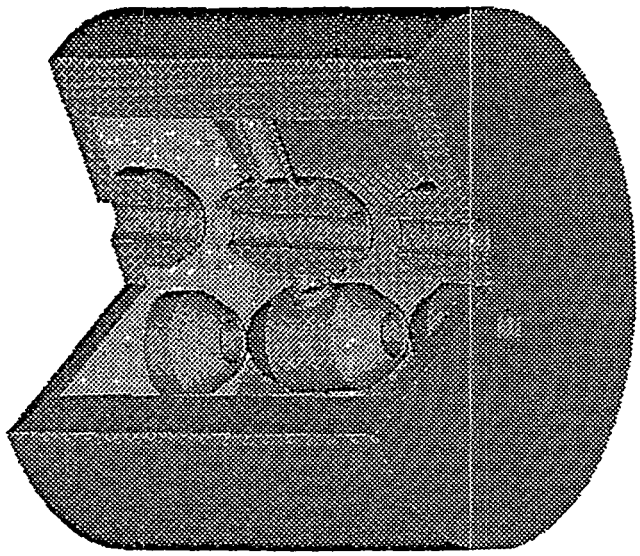

Fig. 5. This is a structural model of the two beam buncher cavity. The strong bunching required for the deflector is achieved by using two gaps within this cavity. This reduces wall losses significantly compared to a single gap or two single gap cavities.

operated in the mode shown in figure 6 at twice the frequency of the deflector. The distance between the two gaps is $\beta\lambda$, thus the particles see the same bunching in both gaps.

The electromagnetic field calculations were used to tune the cavity to the desired frequency and to find the induced wall losses for the mode of interest. The tuning parameters were the radius of the cavity tank and the length of free space between the drift tubes. The length of free space was chosen long enough to minimize the electric peak fields necessary to achieve the desired E_0T. The cavity radius should be as big as possible to reduce the wall losses. Here again not the optimal cavity was designed. Losses were only reduced to a tolerable level. The following table includes some of the calculated cavity properties for a field achieving an E_0TL of 0.472 MV.

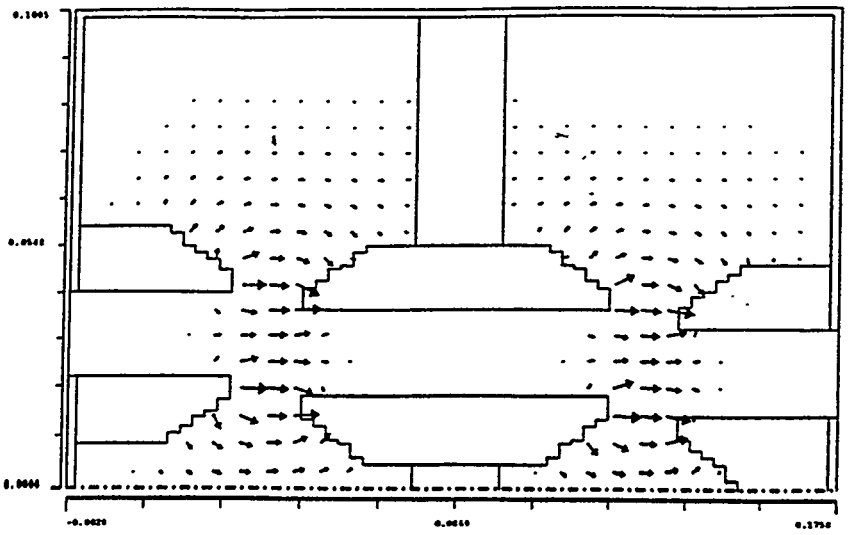

Fig. 6. This mode is used for bunching. The plot shows the electric field in one of the symmetry planes. The frequency of this mode is twice the frequency of the deflector following this cavity.

Table 2. Important Parameters of the Two Beam Buncher

Frequency	Integrated Loss	Peak Loss Density	Average Loss on Tubes
700 MHz	45 kW	220 W/cm^2	100 W/cm^2

THE THERMAL ANALYSIS OF THE TWO BEAM BUNCHER

In the two beam buncher model the surface heating is highest near the drift tube stem and body junction on the surface of the drift tube, here the heat flux is about 220 W/cm^2. The heating drops to near zero on the tube body at a location 180 degree from the stem joint, at the point closest to the drift tube of the neighboring channel. Cooling water flows in through the stem on one side of the buncher cavity. From there around the circumference of each drift tube in sequence and out through the stem on the opposite side. This scheme puts cooling water in close contact with the highly heated regions and provides good thermal control. In addition there is substantial circumferential heat flow in the wall of the drift tube due to the high thermal conductivity of the copper. These two factors combine to smooth the thermal peak near the stem joints and significantly redistribute the energy flow in the tube body away from a purely one-dimensional situation. In the body of the cavity simple axially drilled passages provide the cooling channels for a good and simple heat removal design. Figure 7 shows the calculated temperature contours on the drift tube body considering the heat loads and the proposed cooling. The temperature rise above the coolant inlet temperature is about 30 C; this coupled with the internal pressure stress of the water gives a peak stress in the drift tube surface of about 33 MPa, or about half the yield strength of annealed copper. This is adequate for the service anticipated.

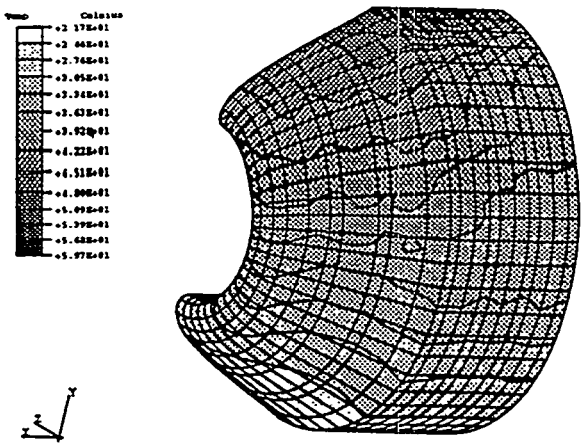

Fig. 7. Taking into account the heat loads from the magnetic field and the proposed cooling scheme described in the text the above final temperature distribution results.

OUTLOOK

These simulations indicate that the special cavities required in the funnel-section of an accelerator-driven transmutation technology can be reasonably controlled.

The internal field distribution in both cavities is very asymmetric to the beam channel axes and thus produces a strongly position dependant surface heating. The ABAQUS evaluation to date has been done only for the most critical parts of the structures. A structural evaluation for the full structure will follow.

For the detailed design phase of the APDF minor adjustments could be done to further improve the thermal behavior of the cavities. This should especially reduce the stresses expected in the electrode of the deflector from the present design.

An interfacing between electromagnetic and structural codes has proven important for a successful overall design of high power rf-structures.

REFERENCES

[1] Nath S. "Funneling in LANL High Intensity LINAC Designs", presented at this conference

[2] Chan K.C.D. "A Prototype Front-End Accelerator for Accelerator-Driven Transmutation Technologies", presented at this conference

[3] *APT Accelerator Topical Report, LA-CP-94-98* , Vol 1, Rev 1, Chap. 5, (March 94)

[4] Bartsch M. et al. "Solution of Maxwell's Equations", *Computer Physics Communications* **72** 22-39(1992)

[5] Krawczyk F.L. "Data-Transfer from MAFIA Rel3.x to other Applications as an Example for Writing Complex Applications with the MAFIA Codes", Los Alamos National Laboratory, AOT-1:94-115, (1994)

HILBILAC Development for Accelerator-Driven Transmutation*

Vitaly Pirozhenko, Oleg Plink and HILBILAC Study Team,
Moscow Radiotechnical Institute, Russian Academy of Sciences
Warshawskoe shosse 132, 113519, Moscow

Abstract. High-Intensity Low-Beta Ion Linac (HILBILAC) is intended for acceleration of ion beams with current of about 1 A and higher. The CW HILBILAC with beam current of 250 mA is under development at MRTI. Concept of parameters choice is presented along with results of beam dynamics and resonator parameters calculations. A pulse prototype HILBILAC-TEST will have to be constructed and tested for the CW accelerator development, its scheme and parameters are presented.

INTRODUCTION

The accelerator under development is designed for application in an initial part of the CW proton accelerator for transmutation [1]. Basic requirements for the initial part are the following: beam current is 250 mA, transverse rms emittance is 1.2 mm·mrad, operating frequency is about 350 MHz. Output energy of the initial part is 20 MeV, it may be obtained by a few accelerating sections. The main problems are concentrated on the first 3-MeV section, another sections are similar to it [2].

A high current accelerator scheme based on HILBILAC (High Intensity Low Beta Ion Linac) had been earlier proposed [3]. The acceleration method has been tested on SIU-1 pulsed proton accelerator where the record value of beam current (400 mA) for RF ion accelerator was achieved [4].

GENERAL DESIGN CONSIDERATION

The rough drawing of HILBILAC is shown in Fig. 1 along with HILBILAC-DTL matching device. The HILBILAC section includes a resonator located inside a bore of superconducting focusing solenoid which is placed in a cryostate. The solenoid is cooled down to liquid helium temperature. The resonator may be cooled down to liquid nitrogen or to room temperature.

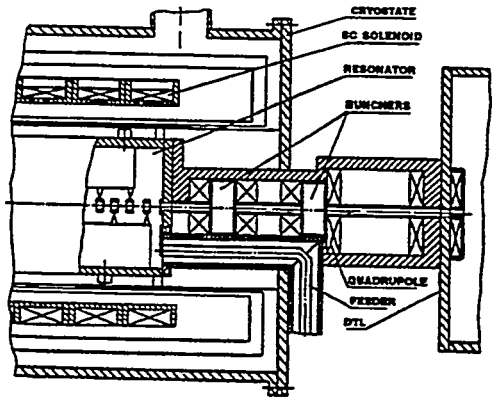

Fig.1. HILBILAC and matching device

* Work supported by Grumman Aerospace Corporation under Contract No 53-40876.

Experience in HILBILAC designing is based on the mathematic simulation and the experimental results. Now we use 3D BEAMPATH and 2D LIDOS beam dynamics codes, 2D GNOM, 2D REAL and 3D ISFEL electrodynamics codes [2]. The physical modelling with electron beam has demonstrated the beam current of 5.2 A (scaling on proton beam) [5]. SIU-1 experimental results and another investigations [6] have indicated the parameters we now use in projects including available accelerating and focusing fields. The accelerating resonator parameters are defined by means of cold modelling.

The HILBILAC basic features are the following. As calculations show the beam current limit may be up to 15 A [7]. Therefore HILBILAC is capable of acceleration a 250 mA proton beam with a large margin at a frequency about 350 MHz. HILBILAC allows to use the injection energy of 75 - 150 keV for acceleration of such beam. Separation of focusing and acceleration in HILBILAC allows to optimize beam dynamics for providing a high capture efficiency. High values of accelerating and focusing fields enable the beam with diameter of 3 - 5 mm to be accelerated thus providing the low value of beam emittance. Use of adiabatic bunching in HILBILAC allows to form the bunch with a small longitudinal phase volume. And finally, accelerating structures with high effective shunt impedance may be used in HILBILAC.

The basic parameters of 3-MeV HILBILAC section are given in Table 1 and Fig.2.

Table 1. Parameters of accelerating sections

Accelerator	CW HILBILAC	HILBILAC-TEST
Beam current, mA	250	250
Injection energy, MeV	0.15	0.1
Output energy, MeV	3	1.5
Operating frequency, MHz	352	352
Accelerating resonator length, m	3	1.2
Accelerating wave amplitude, MV/m	0.4 - 2.4	0.5 - 3
Magnetic field, T	7	7
Transverse rms emittance, mm·mrad	1.2	1.2
Capture efficiency	> 90 %	> 85 %
RF power supply, kW	760	370
Accelerating resonator efficiency	93 %	94 %
Resonator temperature, K	300	77
Solenoid temperature, K	4.2	4.2

Choice of accelerating wave amplitude is realized with due allowance for SIU-1 experimental results and for special investigations of electrical strength of RF gaps in the strong magnetic field [6]. The maximum value of accelerating wave amplitude is taken to be 1.5 times less then the one achieved in the SIU-1 accelerator. Such an approach will provide for a reliable continuous mode operation of the accelerator. The above value of magnetic field is easily obtained by modern SC solenoid technology.

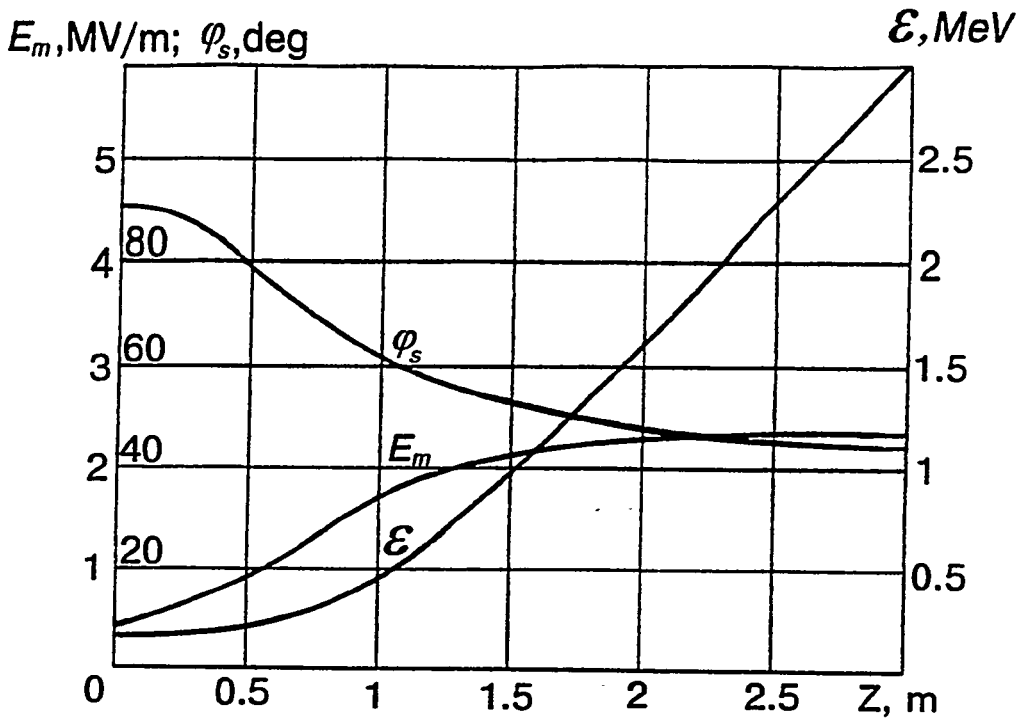

Fig. 2. Distributions of accelerating wave amplitude E_m, synchronous phase φ_s and particle energy $\mathcal{E}$ along the HILBILAC low energy section

Initial part of the section (about 1 m long) represents an adiabatic beam buncher. Within its length, the synchronous phase decreases gradually starting from 90 deg, while accelerating wave amplitude increases. Main acceleration of the particles is realized within the subsequent part of section. The posibility of obtaihing of such field distribution is tried out by resonator modelling.

BEAM DYNAMICS COMPUTATION

Earlier studied HILBILAC accelerators were mainly oriented to achieve high beam current values. The problem of obtaining low emittance beam in HILBILAC was not investigated. A new problem is also combining HILBILAC sections with each other or with other accelerator types.

The series of beam dynamics simulations have been performed with 3D BEAMPATH code [8]. Various variants of both beam model and HILBILAC parameters have been studied. The number of "big particles" was varied from 1000 to 8000 in the computations. The initial beam phase distributions were KV and Gaussians ones. Dipole component of accelerating field have been taken into account.

The study shows that to achieve beam matching and high capture efficiency it is expedient to use adiabatic beam bunching in rising accelerating field. A small value of transverse Coulomb parameter of the beam is desirable in order to have a small emittance growth. The beam envelope and rms emittance variations along the section are given in Fig. 3 for magnetic field of 4 T.

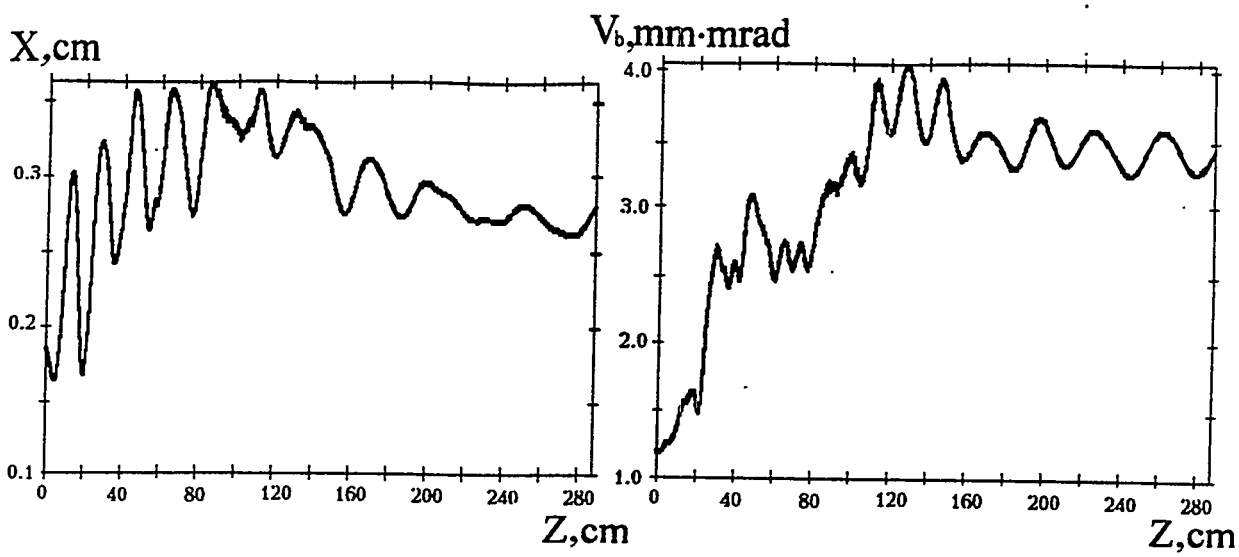

Fig. 3. Beam envelope and rms emittance for magnetic field of 4 T.

The magnetic field of 4 T is determined by analitical calculations. As one can see the beam radius growth is about two and the emittance growth is about four. The beam envelope and emittance values for magnetic field of 7 T are given in Fig.4. The growth of both beam radius and emittance is small.

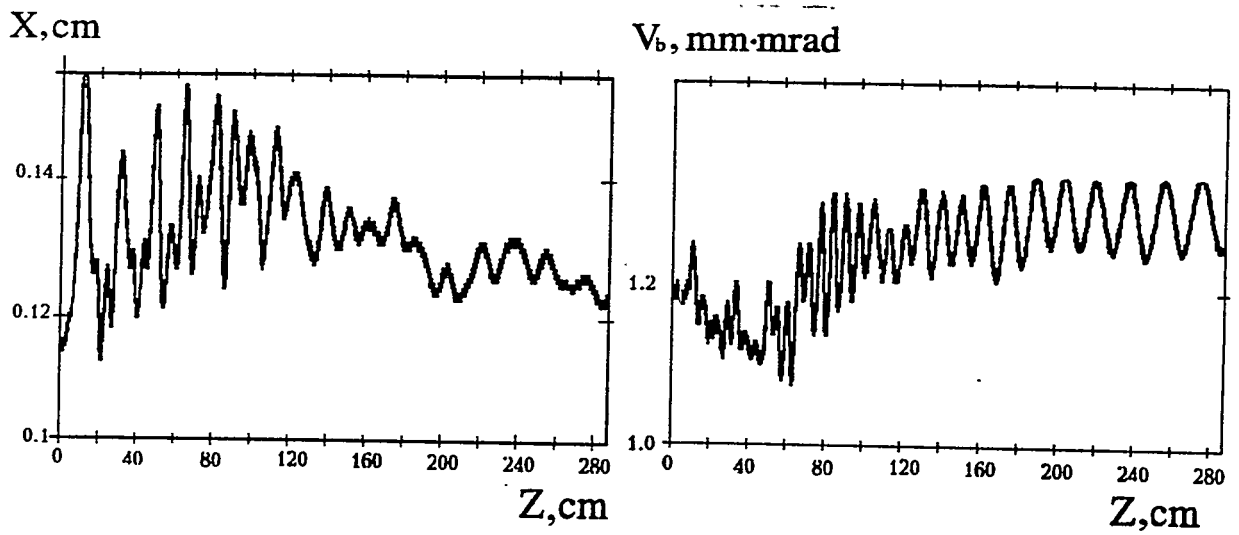

Fig. 4. Beam envelope and rms emittance for magnetic field of 7 T.

The high value magnetic field allows also to reduce influence of phase oscillation frequencies dispersion along the beam bunch on transverse beam matching. Main beam losses are distributed along the buncher beginning where the beam energy is 150 keV. The beam with minimal halo is formed at the section for 7 T magnetic field (Fig. 5).

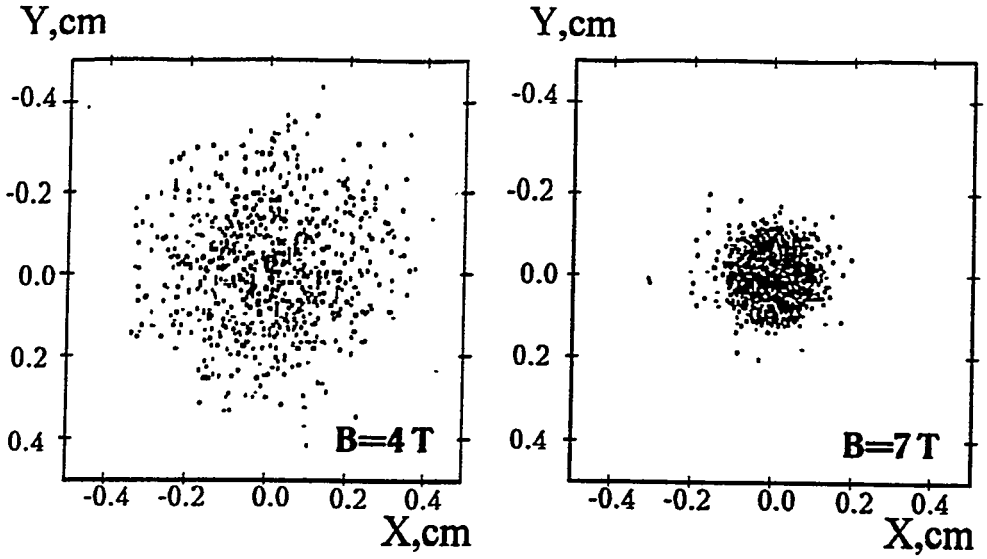

Fig. 5. Cross sections of the beam at CW HILBILAC section output.

ACCELERATING RESONATOR

The resonator with longitudinal RF magnetic field (H-resonator) has the highest efficiency in the low beta range [9].

The resonator (see Fig.1) consists of cylindric cavity with channels for cooling liquid in walls; two rows of vanes with cooling liquid channels inside; drift tubes attached in turn to the vanes and forming the accelerating gaps; coaxial feeder with a coupling loop at its end.

Electrodynamic parameters of the resonator had been calculated with the help of the GNOM and REAL codes based on the mesh method. The GNOM code is used for a computation of the field in transverse cross-section of H-resonator, the REAL code - for the field in accelerating gaps near the axis. The calculation techniques have been checked experimentally through measurements on RF models.

The shunt impedance of the H-resonator versus the relative particle velocity is given in Fig.6 for the frequency of 352 MHz. The values of the shunt-impedance are very high, it is roughly inverse to particle velocity.

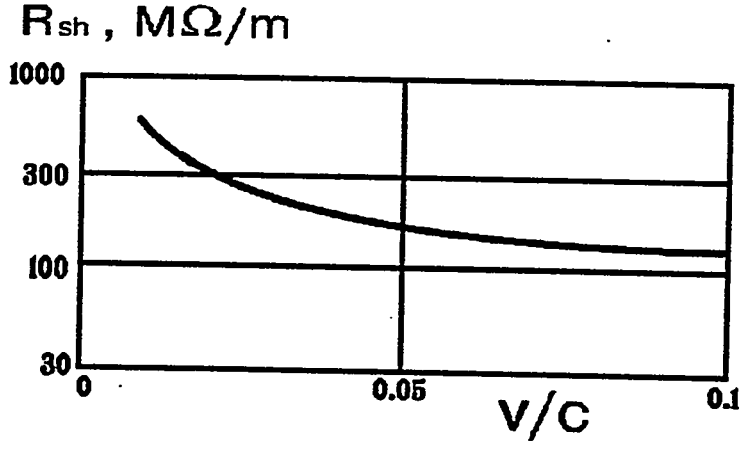

Fig. 6. Shunt impedance of the H-resonator vs relative particle velosity

The important issue is thermal mode of resonator operation. The resonator is cooled by the water. As a basic criterion for CW accelerator, local power dissipation in resonator elements should not exceed 10 W/cm^2. The main electrodynamic and thermal parameters of the resonator are presented in Table 2.

Table 2. Parameters of the CW HILBILAC accelerating resonator

Resonator length, m	3
Internal diameter of resonator, m	0.13 - 0.23
Aperture diameter, mm	10
Maximum surface electric field, MV/m	9
RF power losses, kW	50
Average local power dissipation, W/cm^2	1.5
Maximum local power dissipation, W/cm^2	10
Maximum overheating of elements, deg	10

RF supply of the resonator may be provided by a powerfull klystron amplifier. YK-1350 CW klystron of Philips is suitable for the RF power system. Operation of an accelerator with a high resonator efficiency results in some difficulties. Heavy beam loading may produce the disturbance of the complex amplitude of electric field, it may be decreased and redistributed along the resonator. Therefore the resonator with strong coupling between cells will have to be used for due field stabilisation. The method of field stabilisation was tried out in course of SIU-1 experiments, the resonator efficiency being of 75 %.

HILBILAC-TEST ACCELERATOR

Because of both the unique nature and high cost of the CW accelerator development, it is expendient to test and work out basic scientific and engineering approaches by means of a pulsed accelerator HILBILAC-TEST. The pulse duration will have to be long enough in order to try out and test all effects including possible beam charge compensation at the accelerator input and output.

The equipment earlier developed and manufactured in MRTI for the SIU-2 accelerator [10], can be used for the HILBILAC-TEST constructing. Power supply can provide the beam pulse duration of 100 - 300 microseconds and beam pulse repetition rate of 1 pulse per second.

Main parameters of the accelerator are presented in Table 1. They are selected to be as close as possible to the parameters of CW HILBILAC. Beam current, operating frequency, magneting field and accelerating resonator efficiency are the same. Accelerating wave amplitude is higher and injection energy is lower because of limitation on the resonator length. This enables not only the bunching but the beam acceleration to be obtained as well. During of our experiments with SIU-1 accelerator, the accelerating wave amplitude of 4 MV/m had been achieved. So there exists a fairly good evidence that HILBILAC-TEST accelerator will be reliable in operation.

CONCLUSION

Above listed parameters of CW HILBILAC accelerator are preliminary. Careful study and optimization of beam injection, H-resonator electrodynamics, profiles of RF losses and temperatures are needed to accomplish the project along with HILBILAC-TEST experiments.

REFERENCES

[1] Favale,A.J., et al., "Accelerator Based Conversion (ABC) for Utilization of Surplus Plutonium", *White Paper*, July 20, 1992.

[2] Pirozhenko,V.M., Plink,O.V., and Myers,T.J., "Scheme and Parameters of a 250 mA, 20 MeV CW Proton Accelerator", presented to European Particle Accelerator Conference EPAC-94, London, June 27 - July 1, 1994.

[3] Bondarev,B.I., et al., "Application of the Superconducting Focusing Solenoid to the Problem of Increasing the Limiting Current in a Linear Ion Accelerator", in *Proceedings of the 6-th All Union Conference on Charged Particle Accelerators*, vol.1, pp. 260-263, 1978 (in Russian).

[4] Pirozhenko,V.M., and Plink,O.V., "Linear Proton Accelerator with Superconducting Focusing Solenoid and Opposed-Vibrator Accelerating Resonator", in *Problems of Nuclear science and Technology*, no 6, pp. 30-33, 1989 (in Russian).

[5] Zharkov,Ju.D., et al., "Optimization and Investigation of Characteristics of Physical Model of the 4.7 MeV Proton Linac", ibid, pp. 67-70.

[6] Pirozhenko,V.M., Porunov,V.A., and Ruzin,V.V., "Influence of Strong Magnetic Field on Electric Strength of Accelerating Resonator", ibid, pp. 104-107.

[7] Bondarev,B.I., et al., "High-Current RF Ion Accelerators with Longitudinal Magnetic Field Focusing", in *Proceedings of the BEAMS-90*, pp. 860-865, 1990.

[8] Batygin,Yu.K., "BEAMPATH: A Program Library for Beam Dynamics Simulations in Linear Accelerator", in *Proceedings of 3 rd European Particle Accelerator Conference EPAC-92*, pp. 822-824, 1992.

[9] Likharev,A.N., Pirozhenko,V.M., and Seleznyov,I.B., "Calculations of H-Resonators for Ion Linear Accelerators", in *Theory and Engineering of Accelerators*, MRTI, Moscow, pp. 32-45, 1978.

[10] Murin,B.P., Pirozhenko,V.M., and Plink,O.V., "High-Current, Low-Energy RF Ion Accelerator", in *Proceedings of the 1990 Linac Conference*, pp. 774-776, 1990.

Argonne CW Linac (ACWL) -- Legacy from SDI and Opportunities for the Future*

G.E. McMichael and T.J. Yule
Argonne National Laboratory, Argonne, IL 60439

Abstract. The former Strategic Defense Initiative Organization (SDIO) invested significant resources over a 6-year period to develop and build an accelerator to demonstrate the launching of a cw beam with characteristics suitable for a space-based Neutral Particle Beam (NPB) system. This accelerator, the CWDD (Continuous Wave Deuterium Demonstrator) accelerator, was designed to accelerate 80 mA cw of D^- to 7.5 MeV. A considerable amount of hardware was constructed and installed in the Argonne-based facility, and major performance milestones were achieved before program funding from the Department of Defense ended in October 1993. Existing assets have been turned over to Argonne. Assets include a fully functional 200 kV cw D^- injector, a cw RFQ that has been tuned, leak checked and aligned, beam lines and a high-power beam stop, all installed in a shielded vault with appropriate safety and interlock systems. In addition, there are two high power (1 MW) cw rf amplifiers and all the ancillary power, cooling and control systems required for a high-power accelerator system. The SDI mission required that the CWDD accelerator structures operate at cryogenic temperatures (26K), a requirement that placed severe limitations on operating period (CWDD would have provided 20 seconds of cw beam every 90 minutes). However, the accelerator structures were designed for full-power rf operation with water cooling and ACWL (Argonne Continuous Wave Linac), the new name for CWDD in its water-cooled, positive-ion configuration, will be able to operate continuously. Project status and achievements will be reviewed. Preliminary design of a proton conversion for the RFQ, and other proposals for turning ACWL into a testbed for cw-linac engineering, will be discussed.

INTRODUCTION

The Continuous Wave Deuterium Demonstrator (CWDD), a cryogenically-cooled ground-based accelerator facility, was being built to test components and concepts for a space-based Neutral Particle Beam (NPB) system. The CWDD research and development program was set up to pursue four main objectives: cw operation, deuterium (D^-) beams, operation at cryogenic temperatures, and high beam brightness. The CWDD accelerator included a D^- ion source, cw RFQ and a cw ramped-gradient drift-tube linear accelerator (RGDTL). Grumman Aerospace Corporation, the prime contractor, had overall system responsibility. Culham Laboratories UK was a major subcontractor for the injector, beam lines, diagnostics and controls and Los Alamos National Laboratory assisted with design, prototyping and cold-model testing. Site, services, and cryogenics were being provided by Argonne National Laboratory, and CWDD was to be turned over to Argonne for ongoing programs upon demonstration of compliance with contract specifications. CWDD was being installed and commissioned at Argonne when the NPB program was cancelled in October 1993, and subsequently was turned over to Argonne "as is".

Presently, the facility is being maintained in its nearly-completed state while we consider modifications to the accelerator and beam stop to prepare it for new missions and sponsors. All plans for cryogenic operation have been dropped; we will instead change to water cooling and will operate the structures at room temperature. This change removes both the expense of a

*This work was performed under the auspices of the U.S. Department of Energy and funded by the U.S. Army Space and Strategic Defense Command.

cryosystem and its operating-time limitation (as designed, CWDD would have required over one hour to lower the refrigerant temperature from 30K to 26K after 40 seconds of full-power cw operation). The name "CWDD" is strongly associated with both the previous mission and operational parameters; these are now changing and to mark these changes, a new name, the Argonne Continuous Wave Linac (ACWL) has been adopted for the facility. Thus, we will use "CWDD" when referring to the original design goals and what was accomplished prior to the NPB program termination, and "ACWL" when discussing future plans and proposals.

We are proposing to use ACWL to generate engineering and operational data relevant to the high-current cw accelerators being proposed for spallation neutron sources (the Los Alamos' proposals that have made "Axy" a generic term for intense cw proton linacs[1], the Japanese OMEGA program[2] etc.) and the fusion community's International Fusion Materials Irradiation Facility (IFMIF)[3]. We also propose to use the ACWL beam with a low-Z target and moderator/collimator to generate neutron beams for neutron radiography (NR) or boron neutron capture therapy (BNCT), believing that such a dual use of the facility reaps maximum benefit from the assets and shares operating costs between two or more sponsors.

THE CWDD PROGRAM - DESIGN AND ACCOMPLISHMENTS

General

A schematic layout of the CWDD facility is shown in Figure 1. With the exception of the RGDTL, all items and subsystems shown have been installed and most have been commissioned or are awaiting final hookup to cooling or power. Funding constraints postponed acquisition of the 150,000 standard cubic feet of neon (required to commission the cryo refrigerator) in FY93, which as a consequence prevented high-power operation of the RFQ. Low-power operation could have started late in FY93, but to do so would have interrupted the schedule for high-power operation. By the time such a schedule change could have been considered (when it was apparent that the CWDD program would not be funded for completion) the opportunity had passed.

200 keV D^- Injector

The CWDD injector, designed and built at Culham Laboratory, comprises a volume ion source, triode accelerator, high-power electron traps and low-energy beam transport (LEBT) with a single focusing solenoid.[4] The injector control systems were designed to produce beam pulses variable from a few microseconds to 20 seconds (consistent with the beam requirements of the accelerator as a whole). However, the source is capable of continuous (dc) operation and was operated briefly in dc mode to deliver more than 20 mA of D^- to a beam stop in the LEBT line. It is expected that the D^- current could be doubled by adding cesium to the source.[5] However, with no further requirement to demonstrate neutral-beam capability, operation can be simplified and current capability significantly increased by changing the source to deliver D^+.

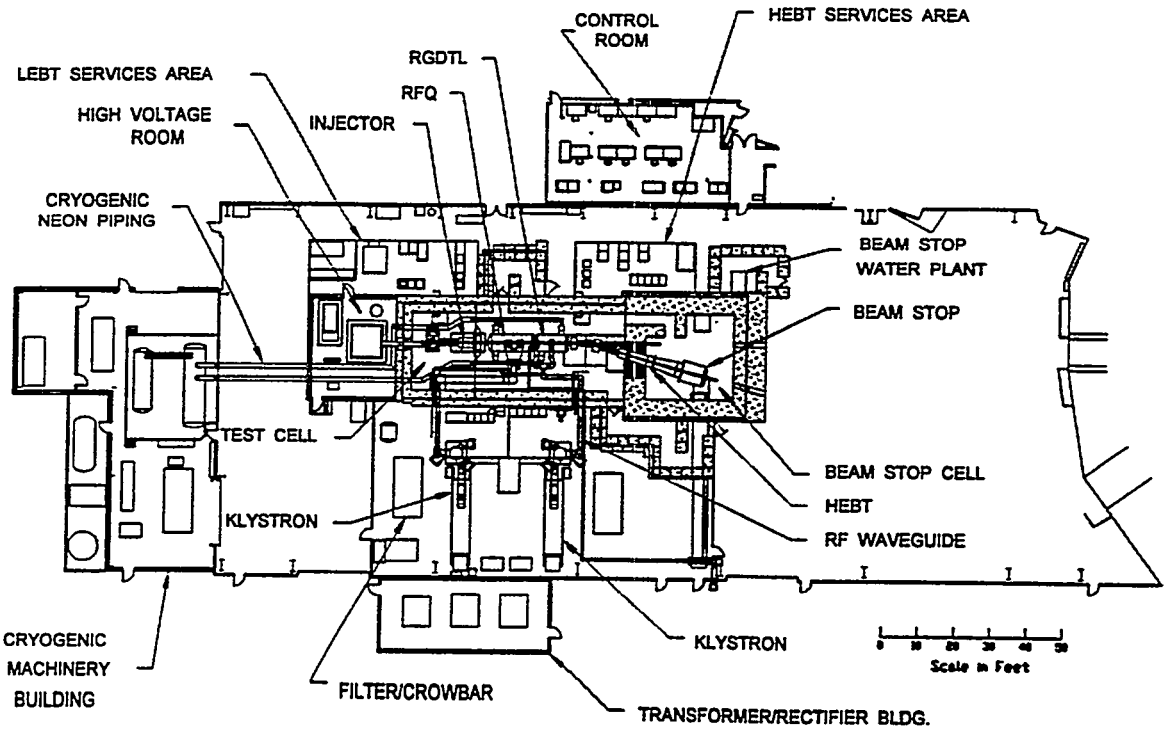

Fig. 1. CWDD Facility layout showing key accelerator components, shielded vault and ancillaries.

2 MeV CW Radiofrequency Quadrupole Accelerator (RFQ)

The RFQ is a four-meter long rf cavity, made by assembling four one-meter long segments. The segments are made from solid tellurium copper, machined and then electroformed into a four-vane configuration. The RFQ has extensive internal cooling channels and all ancillary components (tuners, rf power couplers, end walls) are actively cooled. RF power dissipation at design fields at room temperature is 600 kW. The RFQ has been installed in its cryostat (which also serves as the vacuum chamber), and has been aligned with the injector and exit beamline, and connected to the rf drive lines. It is presently connected to the cryo refrigerator, but those lines will soon be removed to prepare for water cooling.

7.5 MeV CW Ramped-Gradient Drift Tube Linac (RGDTL)

Deuterons were to be accelerated from 2 MeV to 7.54 MeV in a 47 cell RGDTL in which the fields were ramped from 2.0 to 4.0 MV/m over its 2.6 meter length.[6] The 46 drift tubes have been assembled and leak checked, and the tank has been machined, but no work has started on the vacuum chamber (cryostat) or end flanges.

RF Power Systems

The 352.2 MHz rf power systems were designed and manufactured by GE Marconi Communications Systems Ltd and comprise two 1 MW cw klystron amplifiers (to power the RFQ and RGDTL respectively) and a 25 kW tetrode amplifier (for the matching section cavity between the RFQ and RGDTL). All three amplifiers are complete and installed, and two (the tetrode amplifier and the triode amplifier for the RFQ) have been commissioned into resistive loads. The tetrode has operated to full power; but problems with the 1 MW load for the klystron amplifier limited cw operation to 550 kW.

Controls, Diagnostics, Ancillary Subsystems

Most of the control and diagnostics systems are completed and major parts, such as the injector/LEBT controls and diagnostics, the PASS (personal access safety system), fire and radiation protection systems etc., have been in service now for over two years. The water cooling systems are completed and in service, except for connections between the pump station and the RFQ.

ACWL - PLANS AND PROPOSALS

Completion Choices

Commissioning plans for the RFQ were well advanced when the NPB Program was cancelled, but only parts of the RGDTL had been fabricated. We have consequently deferred planning for the RGDTL, and have been concentrating on completing the RFQ as a water-cooled cw structure and on adding a neutron-producing target and moderator to produce neutron beams suitable for neutron radiography (NR) and/or boron neutron capture therapy (BNCT). Making dual or multi-use of the facility (operating the accelerator to extract cw engineering, reliability and control data while also using the beam for target studies, radiography or therapy) would split operating costs between sponsors, providing maximum return at minimum cost.

The proposed change to water cooling is greatly facilitated by the fact that the original plans for CWDD called for both water and cryo cooling; water cooling for initial full-power cw rf conditioning of the structures and then cryo cooling to 26K for accelerated-beam operation. Later in the program, tests at Grumman[7] established that cw structures could be successfully conditioned at cryo temperatures. However, by then most of the major components had been designed or were being built and were not changed to take advantage of the lower power dissipation and improved thermal conductivity that comes from cooling the structures to 26K. The exception for the RFQ was with the rf drive-line windows, which are Rexolite© disks and were only tested to 70 kW. These will almost certainly not be suitable for the 200 kW required for room temperature operation. That a solution is possible is shown by the successful operation of a cylindrical alumina window[8] at >225 kW on the Chalk River cw RFQ[9]. A similar design could be adopted for ACWL if the simple replacement of the Rexolite disks by low-loss alumina disks proves insufficient.

The CWDD RFQ will accelerate a deuteron beam (either D^- or D^+) to 2 MeV. The present D^- source limits the available current to about 20 mA. However, this source could be converted for D^+ operation[10] to provide the design 90 mA input current for the RFQ that will

give 80 mA of 2 MeV deuterons. Such a beam, impinging on a thick beryllium target, should give about 6×10^{13} n/s, the same production rate as obtained with the same current of 3.5 MeV protons on a beryllium target or 2.5 MeV protons on a lithium target.[11] Beam power (and hence target cooling problems) varies with energy, and since the melting point for beryllium is 1280°C, while that of lithium is only 186°C, target engineering would appear to favor Be(d,n). However, the maximum neutron energy is less with protons (1.6 MeV for Be(p,n) and 0.8 MeV for Li(p,n) for the proton energies above), and are therefore more efficiently moderated to obtain the thermal neutrons wanted for NR or the epithermals wanted for BNCT. Thus the choice of proper beam and target is not just a question of yield, but also depends on neutron energy and the thermo-mechanical properties of the target. Unfortunately, there is a distinct paucity of data in all these areas for 2-5 MeV deuterons or protons on low-Z targets. The MCNP transport code is being used to estimate the yield of thermal and epithermal neutrons for different moderator materials and the beam/target combinations discussed above. We do not expect definitive answers because of uncertainties (factors of 2 to 4 in some instances) in yield, energy and angular distribution for these beam-target combinations,[12] but hope for some indication of the trade-offs between higher neutron yield (deuteron beams) and lower neutron energy (proton beams).

We are also looking at the possibility of modifying the CWDD RFQ to produce a 2.5 or 3.5 MeV proton beam should this be necessary. Calculations[13] with the RFQUIK and PARMTEQ codes show that by merely changing the vane profile (and without exceeding the 1.8 Kilpatrick design field of CWDD), the RFQ could be modified to accelerate over 75 mA of protons from 75 keV to at least 3 MeV. Such a change would expand the range of data that ACWL could provide for programs like Axy. An RFQ can in general be used to accelerate particles of a smaller mass-to-charge ratio, but the output velocity of a fixed-frequency RFQ is constant, so without modification, a 2 MeV deuteron RFQ will only accelerate protons to 1 MeV. To get higher-energy protons, the tip geometry would have to be changed. Such a modification (building up the tip by electroforming and machining a new profile) was performed on one section during the original manufacturing process[14], however based on original manufacturing times, the electroforming for reassembly after machining would keep the RFQ out-of-service for at least one year. There is a lot of engineering data, relative to either a proton or deuteron linac, that can be obtained from CWDD in its original configuration. Therefore, even if an eventual change to protons becomes necessary, we envisage starting operation with deuterons and doing a shutdown to modify for protons after obtaining this data.

Staged Program

CWDD was being built to a very ambitious schedule to generate engineering data (demonstrate cw-cryo operation and a D^- beam that would be suitable for an NPB system) for a soon-to-follow space experiment. The cancellation of the NPB program does not remove the requirement for the type of data CWDD (now ACWL) can generate. In fact, such data is even more critical for "Axy" or IFMIF accelerators because the economics and practicality of such systems are tightly tied to the lifetime and dependability of the basic accelerator components. To be viable, an IFMIF or Axy must provide very high availability (90% or greater) over many years. Thus the requirement for such data is still there, but the time frame is not as tight as neither appear likely to receive major funding for several years. Consequently we are proposing a more extended program for ACWL than had been followed for CWDD, one that is more affordable, that can

generate the longer-term data relevant to Axy, and that can evolve as such data is accumulated. Although deuterons are of primary interest for IFMIF, it is likely that for Axy and for either NR or BNCT neutron source development, that ultimately a change from deuterons to protons will be warranted. First however, benefit should be taken of the potentialities of the nearly completed deuteron linac, so an ACWL program will probably extend over four or more years. For an assumed dual mission of engineering development for Axy and development of a high-resolution neutron radiography facility, the program highlights and types of information that could be obtained for the Axy mission could be as follows (with major NR mission milestones in italics to show how the two missions are harmonized):

Year One

- commission water cooling for RFQ and condition RFQ to design cw power
- obtain information on stability of a 4 meter long cw RFQ, information on multiple rf drive loops (4) and on sparking rates and spark damage in a long RFQ (stored energy a factor of 4 greater than Chalk River RFQ1[15])
- *{design NR beryllium target and neutron moderator/collimator}*

Year Two

- commission RFQ accelerator and get operating experience with 20 mA D^- beam
- continue accumulating operating data with 1 MW cw rf amplifier
- complete design modifications to the injector to permit change from D^- to D^+
- *{fabricate and install NR target and obtain first beam-on-target results}*

Year Three

- complete design of modifications to RFQ for change from deuterons to protons
- gain RFQ operational experience with >50 mA deuteron beam
- commission proton injector and begin injector long-term-reliability tests
- *{commission NR moderator/collimator and demonstrate production runs with industrial products}*

Year Four

- modify RFQ for protons, install and commission
- continue proton injector long-term-reliability testing
- accelerate >75 mA cw proton beam in RFQ
- *{complete design and confirm performance predictions for accelerator-based NR facility}*

CONCLUSIONS

SDIO, through the U.S. Army Space and Strategic Defense Command (SSDC), invested significant resources in the CWDD facility prior to cancellation of the NPB program. This nearly-operational facility is now available for other missions, and offers a very cost-effective means of obtaining critical cw linac engineering and operational data.

ACKNOWLEDGMENTS

The "CWDD Technical Team" included physicists, engineers and technicians from Grumman Aerospace Corporation (now Northrup-Grumman), Culham Laboratory, Los Alamos National Laboratory and Argonne. Their efforts are gratefully acknowledged, and it is hoped that those efforts will be rewarded through the completion of the facility and the verification that it "meets specifications". However, it also takes another group to accomplish a program like CWDD, and the authors would like to acknowledge the efforts of Dr. M. Lavan and his group at the Army SSDC in Huntsville. They conceived the program, kept it on track through several turbulent years, fought hard for its completion and continue to lend their support to our efforts to redirect it.

REFERENCES

[1] C.D. Browman, E.D. Arthur, et al., "Nuclear Energy Generation and Waste Transmutation Using an Accelerator-Driven Intense Thermal Neutron Source", NIM in Phys. Res., A320, Nos.1,2, 1992, pp. 336-367.

[2] M.Mizumoto, K.Hasegawa, H.Yokobori, M. Mino, H.Murata, K.Sakogawa, H. Oguri, Y. Okumura, H. Takada, T. Nishida and T. Takizuka, "High Intensity Proton Accelerator for Nuclear Waste Transmutation", Proc. 1992 Lin. Accel. Conf., AECL Rep. #10728, 1992, pp. 749-751.

[3] T. Kondo, D. Doran, K.Ehrlich and F. Wiffen, "The Status and Prospects of High-Energy Neutron Test Facilities for Fusion Materials Development", J. Nucl. Mater. 191-194, 1992, pp. 100-107.

[4] J. Carwardine, G. Pile and T. Zinneman, "Management of High Current Transients in the CWDD Injector 200 kV Power System", Proc. 1993 Part. Accel. Conf., IEEE 93CH3279-7, 1993, pp. 3210-3212.

[5] K. Leung, "State of H^- Source Development", Proc. 1991 PAC Conf, IEEE 91CH3038-7, 1991, pp. 2076-2079.

[6] A. Todd, M. Nightingale and T. Yule, "The Continuous Wave Deuterium Demonstrator (CWDD) Design and Status", Proc. 1993 Part. Accel. Conf., IEEE 93CH3279-7, 1993, pp. 1777-1779.

[7] P. Den Hartog, J. Dooling, M. Lorello, J. Rathke, J. Carwardine, D. Godden, G. Pile, T. Yule and T. Zinneman, "Commissioning Status of the Continuous Wave Deuterium Demonstrator", Proc. 1993 Part. Accel. Conf., IEEE 93CH3279-7, 1993, pp. 1709-1711.

[8] T. Tran-Ngoc, G. McMichael, G. Arbique and F. Adams, "Components for CW RFQ's", Proc. 1990 Lin. Accel. Conf., LANL Report #LA-12004-C, 1991, pp. 48-50.

[9] G. Arbique, B. Chidley, G. McMichael and J. Sheikh, "Beam Parameter Measurements on the CW RFQ1-1250 Accelerator", Proc. 1992 Lin. Accel. Conf., AECL Rep. #10728, 1992, pp. 55-57.

[10] M. Mead, AEA Technology, Culham Laboratory, private communication, 1994.

[11] M. Hawkesworth, "Neutron Radiography: Equipment and Methods", Atomic Energy Review 15, 1977 pp. 169-220.

[12] C.Fink, D. Smith and J. Meadows, "Use of a High-Current Accelerator (CWDD) for Neutron Radiography", Proc. 1991 PAC Conf, IEEE 91CH3038-7, 1991, pp. 547-549.

[13] L. Sagalovsky, Argonne National Laboratory, private communication, 1993.

[14] J. Rathke, Northrup-Grumman, private communication, 1993.

[15] J.Sheikh, A. Davidson, G. McMichael, L. Shankland and B. Smith, "Operation of a High-Power CW Klystrode with the RFQ1 Facility", Proc. 1993 Part. Accel. Conf., IEEE 93CH3279-7, 1993, pp. 1175-1177.

A PROTOTYPE FRONT-END ACCELERATOR FOR ACCELERATOR-DRIVEN TRANSMUTATION TECHNOLOGIES*

K. C. Dominic Chan
Los Alamos National Laboratory

Abstract. The Accelerator Performance Demonstration Facility is the front-end prototype of a CW accelerator useful for accelerator-driven technologies. Its purpose to evaluate the reliability, availability, and maintainability of a high-current and high-power machine. This paper describes the design and technology development of the facility.

INTRODUCTION

During recent years high-power proton accelerators have been proposed as the spallation neutron sources for various applications. These applications include the transmutation of waste, production of tritium, and the disposition of weapon plutonium, collectively referred to as the Accelerator-Driven Transmutation Technologies (ADTT) [1]. ADTT require a CW proton accelerator, nominally at 1 GeV with a current up to 200 mA, with high reliability and availability.

An accelerator useful for ADTT applications has been proposed for the Accelerator Production of Tritium (APT) Project. The APT-accelerator design [2], although well received in various design reviews, is technically challenging and is a large extrapolation from any existing proton accelerator. To date, the highest average-power proton accelerator is the Los Alamos Meson Physics Facility (LAMPF) at 1 MW. There are no operation data on machines at a power level of hundreds of megawatts like the APT accelerator. The accelerator's reliability and availability need to be demonstrated.

Los Alamos National Laboratory has proposed to build the Accelerator Performance Demonstration Facility (APDF), which is the front-end prototype of the first 40-MeV of the APT accelerator. The goal is to gain experience operating a high-current CW accelerator. The facility will evaluate the engineering and operational aspects of the design as well as the reliability, availability, and maintainability of the components and system. APDF will also develop funnel technology and will establish beam performance and benchmark simulations.

In the summer of 1993, the Defense Nuclear Agency funded the conceptual design of APDF. The work was completed and reviewed in February 1994 [3] and is described in this paper.

DESCRIPTION

Figure 1 shows a schematic of the APDF accelerator. It consists of two identical 20-MeV, 350-MHz linacs, each generating a CW proton beam of 100 mA. Each of these 20-MeV linac system has a microwave protonsource, a low-energy beam transport (LEBT), a radio-frequency quadrupole (RFQ) accelerator, a drift-tube linac (DTL), and a matching section between the RFQ and the DTL. The two beams are combined (funneled) together at 20 MeV and further accelerated to 40 MeV in a 700-MHz bridge-coupled drift-tube linac (BCDTL).

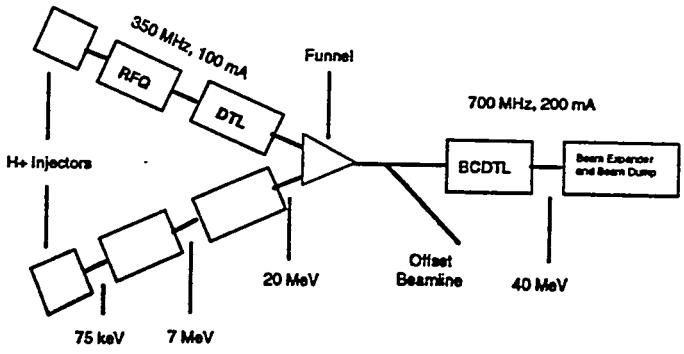

Figure 1: A schematic of the APDF

* Work supported by the Defense Nuclear Agency, US Department of Defense.

The beam dynamics has been designed so that similar transverse and longitudinal focusing strengths are maintained along the accelerator. By doing this, matched beams with currents between zero and full current can be transport through the accelerator with no loss without any retuning. This current-independence property allows easier beam startup and higher tolerance of beam fluctuation. The accelerator is equipped with diagnostics such that good matches of beam parameters can be maintained throughout the accelerator.

APDF INJECTOR

The APDF Injector (Fig. 2) consists of a microwave proton source and a low-energy beam transport (LEBT). The source is designed to operate at 75 keV and is required to provide more than 110 mA of proton current at the RFQ input. The normalized rms emittance is required to be less than 0.02 π cm mr with a beam fluctuation of better than 1% at 1-MHz bandwidth. For beam commissioning and reliable beam turnon, the dc proton source will have pulsing capability. The LEBT is equipped with non-interceptive beam diagnostics. The two solenoids can be used to provide the proper match needed for the RFQ. The system has been designed with automatic-fault recovery, variable-current operation, and beam-interrupt systems.

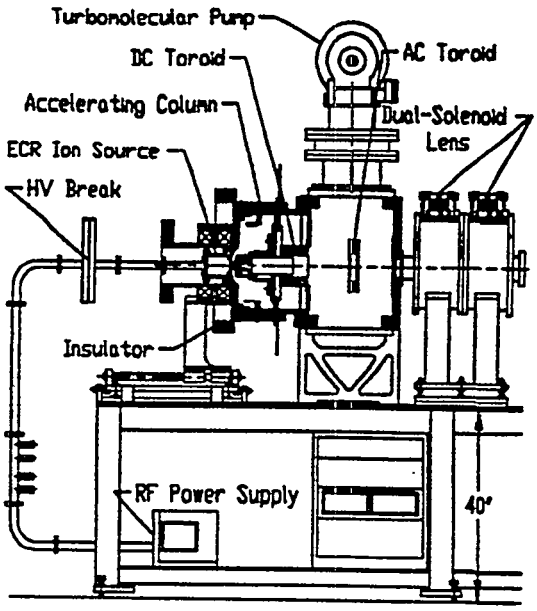

Figure 2: A schematic of the APDF Injector

The design of the APDF Injector is completed and a prototype has been built. An experimental program to study the reliability and stability of this injector is now in progress. This program will be described in detail by Schneider in this Conference [4].

Radio-Frequency Quadrupole Linac

The APDF RFQ is an 8-meter-long RFQ accelerating the beam to 7 MeV and is the longest RFQ ever proposed [5]. Table 1 shows the RFQ parameters. A schematic of the APDF RFQ is shown in Figure 3. The high energy of the RFQ is chosen for two reasons. First, the transverse focusing strength of the RFQ is better matched to the DTL allowing for a current-independent accelerator design. Second, the longitudinal-length scale is higher at higher energy, allowing more space at the RFQ-DTL matching section for diagnostics and the use of electromagnetic quadrupoles that are more radiation resistant.

A long RFQ, because of the high multiplicity of modes and their spacing, will be difficult to tune and difficult to obtain the required field uniformity. This issue is being addressed by coupling four 2-m long RFQs to form the required 8-m-long RFQ. This concept of a resonantly-coupled RFQ has been recently verified with a full-scale cold model. A field flatness better than 2% with a dipole component less than 2% has been obtained. The mode spectra for the quadrupole and dipole modes show mode separation of better than 2 MHz around the operating mode. The cold model is currently used to investigate the possibility of waveguide coupling to the RFQ. If successful, the complication in using multiple coupling loops can be eliminated.

Table 1: RFQ Parameters

Energy (MeV)	0.075–7.000
Frequency (MHz)	350
Input Beam Current (mA)	105
Transmission	95.2%
Structure Type	4-vane
No. of Segments	4
No. of RF Modules	2
No. of Cells	433
Total Length (m)	8.10 (9.45 λ)
Radial Aperture (cm)	0.235
Peak Surface Field (Kilpatrick)	≤1.8
Synchronous Phase (deg)	-90 to -30
Average Power Density (W/cm^2)	≤12
Structure Gradient (MV/m)	0–1.75
Structure Power (MW)	1.12
Beam Power (MW)	0.70
Total RF Power (MW)	1.82
Efficiency	0.385

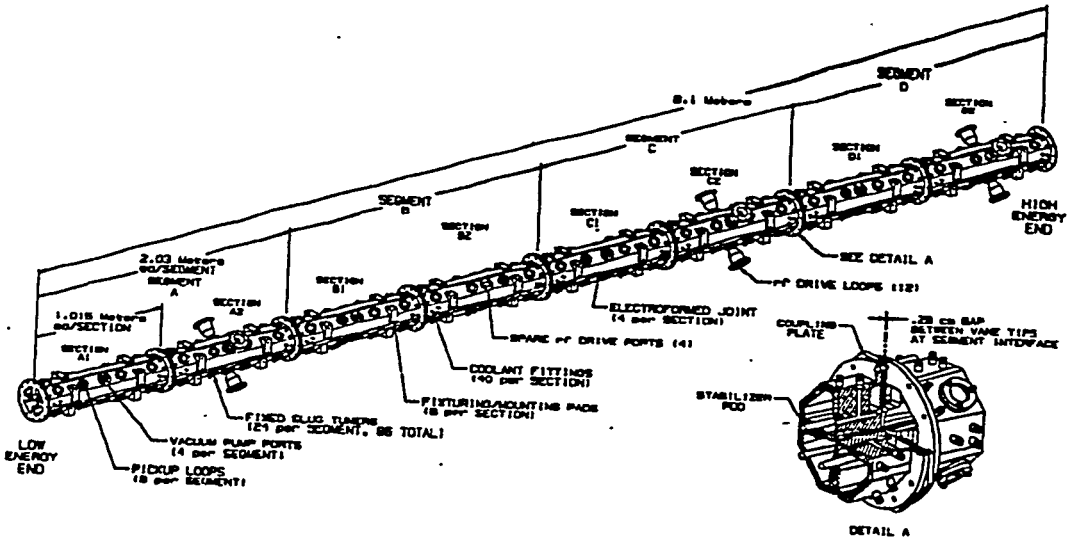

Figure 3 A schematic of the APDF RFQ

Building a long RFQ can be expensive and time consuming using the conventional method of electroforming. A Fabrication Development Program [6] to investigate fabrication of RFQs using hydrogen-furnace brazing as a joining technique has recently been successfully completed. Under this program, it was demonstrated that the required alignment tolerances, vacuum integrity, and structural properties could be achieved and the performance, cost, and schedule can be reliably predicted.

RFQ-DTL MATCHING SECTION

The RFQ-DTL matching section matches the beam between the RFQ and DTL. The DTL quadrupole gradients and accelerating gradients are chosen to match the RFQ output focusing strength. The matching section is designed to have a focusing lattice that is an extension of both the DTL and RFQ focusing lattice to achieve a current-independent design [7]. Figure 4 is a schematic of the matching section. The matching section has been equipped with diagnostics to monitor the current, centroid position, and profile of the beam to insure that the optimum beam characteristics exist at the RFQ output.

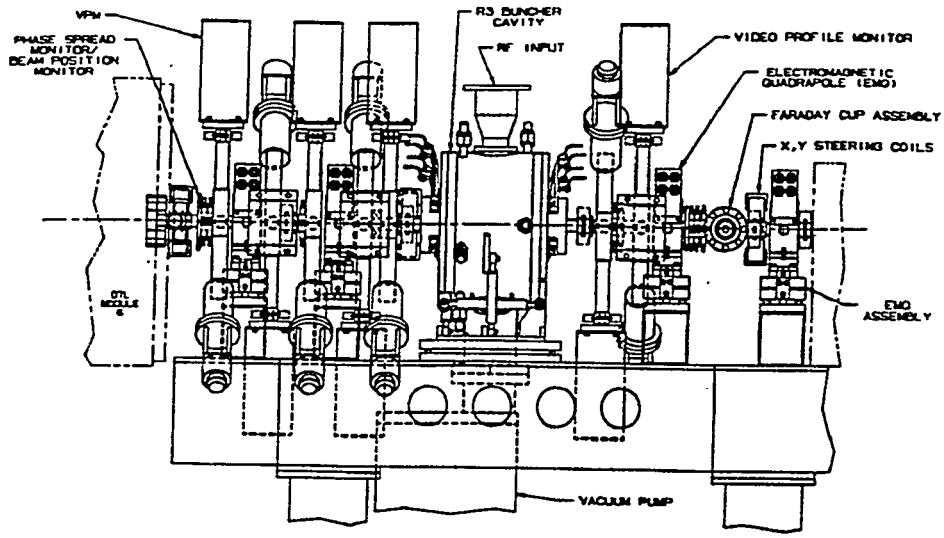

Figure 4 A schematic of the RFQ-DTL Matching Section

DRIFT-TUBE LINAC (DTL)

The DTL design is in an advanced design stage [2]. There are three DTL modules on each leg of the funnel (Fig. 5). Table 2 lists the parameters for the DTL modules. Each tank is designed to be driven by an 1-MW klystron station. The drift tubes are mounted on for ease of alignment and repair. They have knife-edged RF seals and flex-membranes with the tank wall for CW operation. The drift tubes contain radiation-hardened EMQ's for reliability and adjustability.

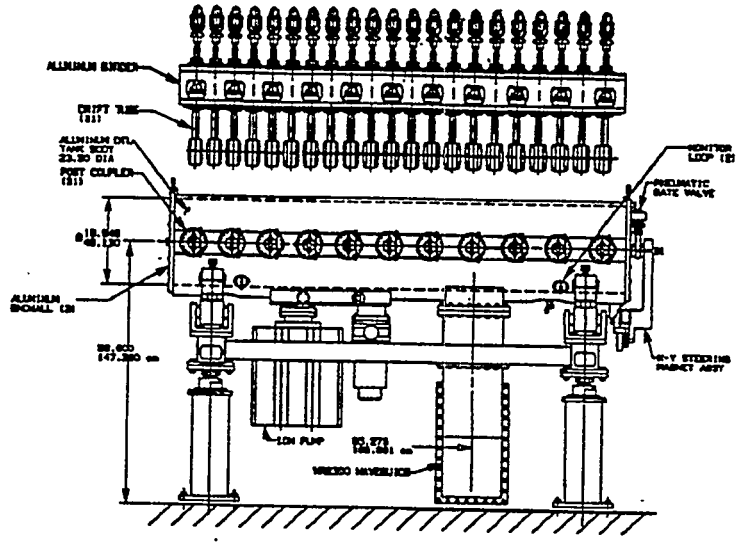

Figure 5: A schematic of DTL Module

As with all CW room-temperature accelerator systems, temperature control and thus, resonant-frequency control of the module is critical and difficult. A constant-flow system is used with the DTLs with the maximum temperature differential kept to less than 10°C. Thermal stress analysis has been completed and shows no serious problems.

Table 2: Parameters of DTL Modules

Energy (MeV)	7.0–20.0
Frequency (MHz)	350
Beam Current (mA)	100
No. of RF Modules	3
No. of Tanks	3
No. of Cells per Tank	Tank 1 (22), 2 (18), 3 (15)
Length of Cells	$1\beta\lambda$
Length of Tanks (m)	2.44–2.50
Total Length (m)	7.98
Intertank Spacing	$2\beta\lambda$
Radial Aperture (cm)	1.00
Aperture/Beamsize(rms) Ratio	4–5
Peak Surface Field (Kilpatrick)	<1.0
Synchronous Phase (deg)	-35 to -25
Average Power Density (W/cm^2)	~22
Structure Gradient (MW)	1.04–2.80
Shunt Impedance (MΩ/m)	30.2–32.8
Structure Power (MW)	1.153
Beam Power (MW)	1.300
Total RF Power (MW)	2.453
Efficiency	0.530
Quadrupole Lattice	FOFODODO
Quadrupole Effective Length (cm)	5.7
Quadrupole Gradients (T/m)	25.0–35.0
Quadrupole Spacing (cm)	10.4–17.4 ($1\beta\lambda$)
Quadrupole Phase Advance/Period (deg)	80–70

FUNNEL

A funnel is employed so that when the current is at low energy, it is halved to minimize the space-charge effect [8]. It is also the matching section between the DTLs and the BCDTL. Significant effort was put into packaging the required bunchers, transverse focusing elements, and diagnostics in the specified limited space where the two low-energy beams merge. Figure 6 shows the present design. Because of the importance in maintaining the emittance while it is in the funnel, sufficient diagnostic sensors have been provided to fully characterize the beam before and after funneling.

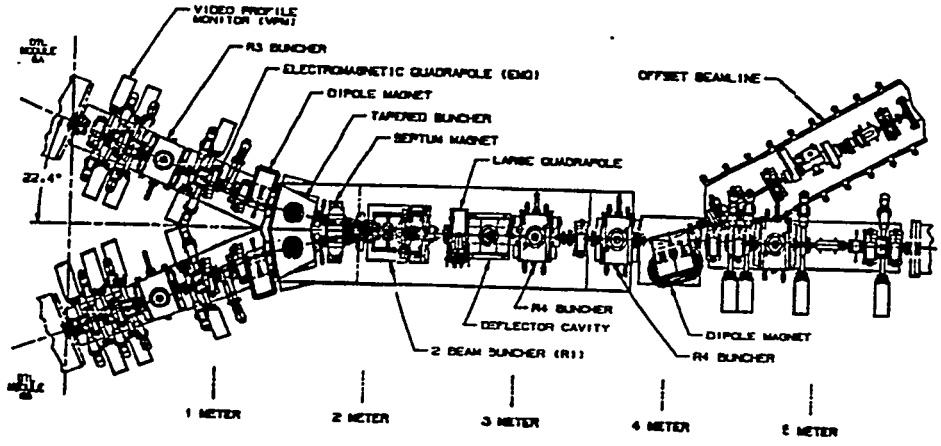

Figure 6: A schematic of the funnel

There are two special rf cavities in the funnel. These are the two-beam buncher and the deflector cavity. With two beams going through these cavities, their electromagnetic field distributions do not have axial symmetry. Both cavities have high thermal losses and significant cooling is required to keep them in tune. Detailed thermal calculation was performed with 3-D codes because of the lack of axial symmetry. MAFIA codes have been used to calculate the electromagnetic fields and the thermal loads. These load data are then transferred to an engineering code, ABAQUS, to calculate the thermal distribution and stresses. Results show that the cooling designs in these cavities are adequate [9].

BRIDGE COUPLED DRIFT-TUBE LINAC (BCDTL)

The BCDTL [2] is the type of accelerating structure chosen to accelerate the beam from 20 to 40 MeV. Seven-$\beta\lambda$ long drift-tube tanks are bridge-coupled together over intervening 5-$\beta\lambda$ gaps that carry the quad doublets (Fig. 7). Since no quadrupoles are carried in the drift tube, the bores of the drift tubes can be increased to 4-cm diameter. The alignment of the drift tubes is no longer particularly critical. The drift-tube can be hard-socketed to the tank wall to provide a good rf seal. Table 3 shows the parameters of BCDTL modules.

Table 3: BCDTL Parameters

Energy (MeV)	20–40
Frequency (MHz)	700
Beam Current (mA)	200
No. of RF Modules	6
No. of Tanks	19
No. of Cells per Tank	7
Length of Cells	$1\,\beta\lambda$
Length of Tanks (m)	0.615–0.843 ($7\,\beta\lambda$)
Intertank Spacing	$5\,\beta\lambda$
Total Length (m)	23.8
Aperture/Beamsize (rms) Ratio	8
Structure Gradient (MV/m)	1.70
Average Gradient (MV/m)	1.00
Shunt Impedance (MΩ/m)	26.0
Average Power Density (W/cm^2)	≤25
Peak Surface Field (Kilpatrick)	≤1.0
Structure Power (MW)	1.74
Beam Power (MW)	4.0
Total RF Power (MW)	5.74
Efficiency	0.7
Length of Focusing Period	$12\,\beta\lambda$
Synchronous Phase (deg)	-40 to -30 (20-37.6 MeV) -30 (37.6-100 MeV)
Quadrupole Lattice	FDO
Quadrupole Length (cm)	8.2–9.5
Quadrupole Doublet Spacing (cm)	9.5
Quadrupole Gradients (T/m)	31.4–36.0
Quadrupole Pole-tip, Maximum (T)	0.810
Quadrupole Phase Advance/Period (deg)	80–70 (20-37.6 MeV) 70 (37.6-100 MeV)

Recently, a new structure called the Coupled-Cavity Drift-Tube Linac (CCDTL) has been proposed. This type of structure is expected to be much less sensitive to tuning errors than BCDTL. The BCDTL is presently under study and cold-model test is planned [10].

RF SYSTEM

There will be four types of basic rf-power modules. First, each RFQ will be powered by a module that has two 350-MHz 1.1-MW klystrons. Second, each DTL tank will be powered by a module that has one 350-MHz 1.1-MW klystron. Third, BCDTL tank will be powered by modules that have one 700-MHz 1.1 MW klystron. These

modules, because of restrictions on available electricity, will be pulsed at 6% duty factor. Fourth, the buncher cavities will be powered by modules that have 700-MHz, 50-kW klystrodes.

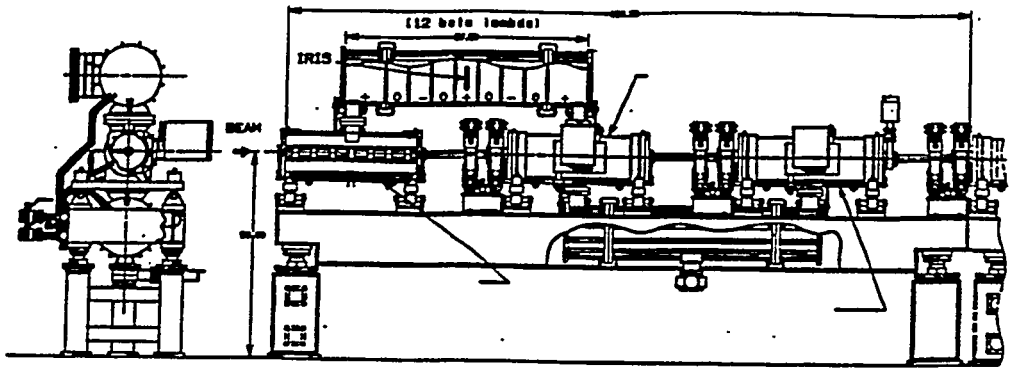

Figure 7: Schematic of a BCDTL Module

The rf-field stability will be maintained with feedback and feedforward control. With the accelerator heavily beam loaded, beam current fluctuation is a major disturbance to the rf fields. In the APDF rf control system, the beam current fluctuation will be detected early upstream and fed to the rf generator downstream to anticipate the current induced rf fields. This "feedforward' control is possible because the beam bunches are nonrelativistic. In addition, the feedforward control will have automatic gain control such that operator intervention will be minimized [11].

To maintain a regular periodicity of the focusing lattice for current independence, the rf power needed from accelerator module varies. Subsequently, the klystron efficiency is reduced because it is not operated in maximum design power. Simulation and experiments [12] have been carried out to understand klystron efficiency at reduced power under various operation conditions. Results show that lowering output power by decreasing both the beam voltage and beam current while maintaining a constant beam impedance has the least impact to efficiency. The next desirable way is to reduce the output power by only reducing the beam current and maintain the same voltage. This way has the advantage of having one operating voltage for all klystrons. Both of the above methods compare favorably to decreasing output power by lowering drive power.

SUMMARY

The conceptual design of the Accelerator Performance Demonstration Facility is now complete. Documentation of the work is being prepared [3].

REFERENCES

1. Bowman, C., "Overview of the Los Alamos ADTT Project," Presented in this Conference.
2. "APT Accelerator Topical Report," Los Alamos National Laboratory Report LA-CP-94-48, March 1994, Vol. 1, Rev. 1.
3. Chan, K. C. D., "Final Report of theAPDF Integrated Design," edited by K. C. D. Chan, in preparation.
4. Schneider, J. D., "Design and Testing of a DC Ion Injector Suitable for Accelerator Driven Transmutation," presented in this Conference.
5. Schrage, D. L. , et al, "Conceptual Design of a 7 MeV RFQ Linac for the Accelerator Production of Tritium," Los Alamos National Laboratory Report LA-UR-93-1790.
6. Schrage, D.L., et al, "A New RFQ Linac Fabrication Technique," to be presented in the 17-th International Linac Conference, August 21-26, 1994, Tsukuba, Ibaraki, Japan.
7. Garnett, R., and Smith, P., "Design of a Current Independent Matching Section for APDF," ibid.
8. Nath, S., "Funneling in LANL High-Intensity LINAC Designs," presented in this Conference.
9. Bultman, N. K., etal, Designs of RF Cavities for CW Operation, to be presented in the 17-th International Linac Conference, August 21-26, 1994, Tsukuba, Ibaraki, Japan.
10. Billen, J., "A New RF Structure with Intermediate-Energy Particles," ibid.
11. Ziomek, C. D. "Low-Level RF Control System Issues for An ADTT Accelerator," presented in this Conference.
12. Rees, D. E., etal, Techniques for Maintaining Design Efficiency when Operating Klystron Amplifiers at Levels Below the Maximum Output Power, Los Alamos National Laboratory Report LA-UR-94580.

ITEP Subcritical Neutron Generator Driven by Charged Particle Accelerator

Oleg V. Shvedov, Ivan V. Chuvilo, Evgeny V. Kulikov*, Valery V. Vasiliev, Mikhail M. Igumnov, Alexander M. Kozodaev, Evgeny B. Volkov, Alexander V. Lopatkin**
Institute of Theoretical and Experimental Physics, 117259 Moscow, Russia
** Ministry of the Atomic Power, 101000 Moscow, Russia*
*** Research and Design Institute for Power Technology, Moscow, Russia*

Abstract. A research facility prototype including a combination of a linear accelerator, a neutron generating target, a subcritical multiplying system is discussed. Principles of the nuclear safety ensuring and means of its attainment for Subcritical Neutron Generator are considered. The scheme of the multiplying is shown. The assembly will be mounted in the body of the partly dismantled ITEP HWR. Reqirements for subcritical assembly are worked out and their feasibility within the framework of the heavy-water blanket is shown. The facility's application as a full-scale model of more powerful installations of this kind and for fundamental experimental research has been investigated (see Fig. 1).

INTRODUCTION

ELECTRO-NUCLEAR NEUTRON GENERATOR of low power is planned to be constructed in ITEP that uses the decomissioned HWR for placement of a subcritical blanket with fast and thermal neutron multiplication zones, heavy-water and graphite reflectors, and experimental devices. Berillium target irradiated by protons from ISTRA linear accelerator is the source of fast neutrons.

Table 1. GENERATOR main parameters

Accelerator proton energy, E_p	36 MeV
Proton pulse time, T_p	150 μs
Proton pulse current, I_p	1 mA
Mean proton current, I_p	0.5 μA
Proton pulse frequency, F_p	25 Hz
Proton pulse power, W_p	5.4 MW
Target fast neutrons intensity	$1.5 \cdot 10^{14}$ n/s
K_{eff} start-up blanket	0.95
Start-up blanket power	25 kW
Thermal neutron flux in reflector	$1.5 \cdot 10^{12}$ n/cm$^2 \cdot$s
Start-up blanket load ^{235}U (90%)	2 kg

The purpose of the facility is:

- to be applied as a full-scale physical model of the power transmutation facility blanket;
- to check and improve the control and protection system for electro-nuclear complex;
- to conduct fundamental research (actinide constants in the range of fast neutrons, parameters of proton interaction with blanket and accelerator materials, ultra cold neutrons production and their use, etc.);
- to conduct radiation research on fast neutrons;
- to solve applied problems: production of radiation sources for positron tomography, development of medical neutron beams, large diameter (up to 200 mm) silicon doping;
- to serve as a possible version of decomissioned reactors destiny.

PECULIARITY OF BLANKET FOR NEUTRON GENERATOR

The choice of physical, neutron and structural parameters of the blanket is determined by the following considerations (see Fig. 2):

- the berillium target is surrounded by a "fast" multiplication zone which effectively utilizes fast neutrons emitted by the target. The gain is provided by fission of "fast" zone material nuclei and (n, xn) - reactions. ^{237}Np and ^{9}Be are the most suitable (productive) materials for the "fast" multiplication zone;
- the berillium target should have the shape and size providing fast neutron yield sufficiently uniform across the target's volume, power generation, and temperature. The implementation of heat removal guaranties the absence of the coolant boiling on the target's surface;
- the whole space outside fast neutron multiplication zone could be used for placement of the multiplying lattices of the transmutation facility blankets or thorium lattices with possibility of rapid change in radial and axial composition of lattices being investigated;
- a compact thermal neutron multiplication zone with highly enriched uranium (used in GENERATOR comissioning, in studies of the CPS peculiarities, in solving applied problems), makes it possible to place large irradiated volumes and experimental devices in the reflector. High neutron flux of the optimum spectrum will be achieved due to heavy water application as moderator, coolant, and reflector in the thermal neutron multiplication zone in those cases because of the absence of neutron absorption in it and its diffusion features;
- the dismantling and replacement of the ITEP HWR graphite reflector with heavy water was recognized as inadvisable first of all because of high capital spending and radiation safety considerations;
- the blanket design should provide the possibility to change its composition with the aim of change in reactivity, optimization of neutron fluxes and neutron spectra, provision of the neutron fluxes uniformity in experimental devices, irradiated volumes and channels.

PECULIARITIES OF THE GENERATOR CONTROL AND PROTECTION SYSTEM

The principal salient feature of the GENERATOR control and protection system compared to the critical system is the need in permanent measuring and controlling blanket power and reactivity. The GENERATOR control and protection system, its logic, the quantity and quality of components should provide its function while operating:

- in a subcritical state (K_{eff} = 0.95 - 0.98) when accelerator operates in pulse mode (pulse duration is 150 μs at repetition frequency of 10 - 25 Hz). The control over blanket power and protection against excess in a specified power level is performed using pulse and current channels. Continuous control of the subcriticality by analysis of decay constant of instantenous neutrons (characteristic times are 10 - 100 s) after neutron pulse completion. Because of considerable theoretical difficulties in correlation with the decay constant and subcriticality level (caused by multiplicity of blanket zones) it is necessary to have independent precision method to control subcriticality. To implement it a reactimeter developed in ITEP could be used based on analysis of neutron density behaviour after introduction of positive or negative reactivity. The method requires periodical achiving of critical and slightly overcritical (to provide accelerating period value of 30 -60 s) or slightly subcritical (0.5%) condition;
- with a constant neutron ^{252}Cf source from the moment of the first fuel channel placement in the core up to achiving a critical state in facility's comissioning and performing of the experimental program aimed at relaible estimation of its neutron, physical and performance parameters. While operating with a constant neutron source the power control and protection against excess in power level is performed by two pulse and nine current channels. The control and protection against rise in power is performed using two pulse and three current channels.

The GENERATOR CPS automatically provides:

- the regulation of neutron power while working with a constant external neutron source;
- the emergency protection action when the necessary blanket subcriticality level is not provided while operating in pulse mode;
- the emergency protection action when the power level exceeds the specified power level (while operating in pulse mode or with a constant neutron source), or with the failure of technical system components affecting the GENERATOR operation safety;
- the accelerator stop according to the emergency protection signal with simultaneous introduction in blanket a constant neutron source to perform a reliable control over the blanket state;
- the rise in subcriticality level while performing procedures associated with change in blanket composition, introduction of compensating rods, etc.;
- the necessary authorization and blocking of the GENERATOR operation when CPS or systems affecting the safety are not ready to work.

The CPS rods are located in the heavy-water reflector; by doing so the minimum disturbance in neutron field is provided in experimental channels.

PROVISION OF THE GENERATOR SAFETY

The following principles and considerations are placed into the basis of the GENERATOR nuclear and radiation safety provision:

- a specified level of the blanket subcriticality should not decrease neither due to the change in blanket neutron and physical properties nor because of the external effect even in the case of overlapping in effects of several accidents. In this case it is necessary to exclude or limit unauthorized rise of the protection operating controls, mechanical effects and blanket "disintegration", unauthorized change in blanket configuration including fuel replenishment, collapse of experimental channels or their rupture with filling water;
- a small fuel burnup (1%) in the long run (3 - 4 years) leads to the relatively low build-up of fission fragments;
- the GENERATOR CPS ensures reliable operation and speed of response both in critical and subcritical state providing safe control over power level and reactivity, necessary blanket lock in accident situations or under diversion from normal operating mode;
- the possibility to achieve and fix critical states increases reliability in evaluation of the lattice subcriticality level to a great extent;
- the absence of the excess reactivity in blanket;
- the possibility of the blanket coolant loss is excluded that permits to accumulate the residual power generation of the fuel;
- the GENERATOR service will be performed by a staff of HWR and MAKET reactors having unique, long-term experience in operating heavy-water critical and subcritical lattices.

CHARGED PARTICLES ACCELERATOR AND NEUTRON PRODUCING TARGET

Although it is known that irradiation of light targets (lithium, berillium) with deuterons appears to be slightly more effective in providing maximum neutron yield in 15 - 30 MeV region the 36 MeV ISTRA proton accelerator that is considerably (70-80%) completed has been chosen as the GENERATOR component.

The proton beam of 36 MeV energy and 0.5 mA average current will be supplied from ISTRA-36 linac which consists of RFQ, DTL-1, and DTL-2 resonators and is placed in two levels near the reactor vessel.

The linac characteristic features are the following:

- the application of RFQ-section at its input;
- the application of the wavelength (λ = 1 m) in DTL-resonators which is twice lower compared to RFQ;
- development and application of hard magnetic quadrupoles in drift tubes opened into vacuum in DTL-resonators. This provides the lowering of injection energy, increasing of particles

capture into acceleration, decreasing of the diameter in DTL-resonators and RF-power as well as heat generation in them, simplification of heat removal, increasing of relability. This allows to anticpate the rise in the average beam current value up to 2-4 mA in the future.

The choice of berillium as the target material is explained first of all by its rather high neutron yield, good mechanical and thermal physics properties (T_{melt} = 1283°C, sufficient strength, high thermal conductivity). Due to the choice of target shape in the form of empty cone it is possible to reduce the surface thermal power generation in target and provide the target wall temperature in the most stressed place approximately equal to 100°C. The berillium target has an aluminium shell. The power generation uniformity across the target surface with the use of proton transportation channel from accelerator to target (in this case it is necessary to provide beam spot diameter equal to 80 mm, beam uniformity across the spot diameter equal to +/- 10%).

EXPERIMENTAL AND ANALYTICAL SUBSTANTIATION OF THE GENERATOR

Results obtained during implementation of the HWR-M high flux heavy-water reactor in ITEP have been used in the choice of the blanket start-up version. The full scale physical model of this reactor's core has been thoroughly studied on ITEP MAKET zero power reactor (see Fig. 3) that makes it possible to use unique precision experimental data obtained for testing TREC, TREC-S, DISHER small group three-dimensional heterogeneous analytical programs. The same programs and their versions are used for calculation of neutron and physical parameters of the GENERATOR blanket including lattices with experimental devices and channels that ensures reliability and representativeness of calculations. Experiments with blanket full scale model will be conducted on MAKET reactor in the period of the GENERATOR development. The pulse D-T generator will be used in studying subcritical lattices as neutron external surces that permits receiving of indformation on neutron and physical as well as dynamical parameters of blanket lattices and investigation of the possibility to control reactivity by neutron pulse analysis.

CONCLUSION

Electro-nuclear generator of neutrons is being constructed using building and structures of the ITEP HWR decomissioned reactor and ISTRA-36 proton accelerator. The GENERATOR integrates reactor and accelerator lines of research traditionally developed in ITEP. The facility permits to solve a set of problems associated with development of power electro-nuclear facilities by conducting fundamental research in the field of neutron physics as well as applied ones. The facility's level of completion is 70 - 80%. The proposed term for facility's commissioning is 1997.
The work is supported by Ministry of Atomic Power of the Russian Federation, Russian Fund for Fundamental Investigations, Grumman Aerospace Corp. (USA).

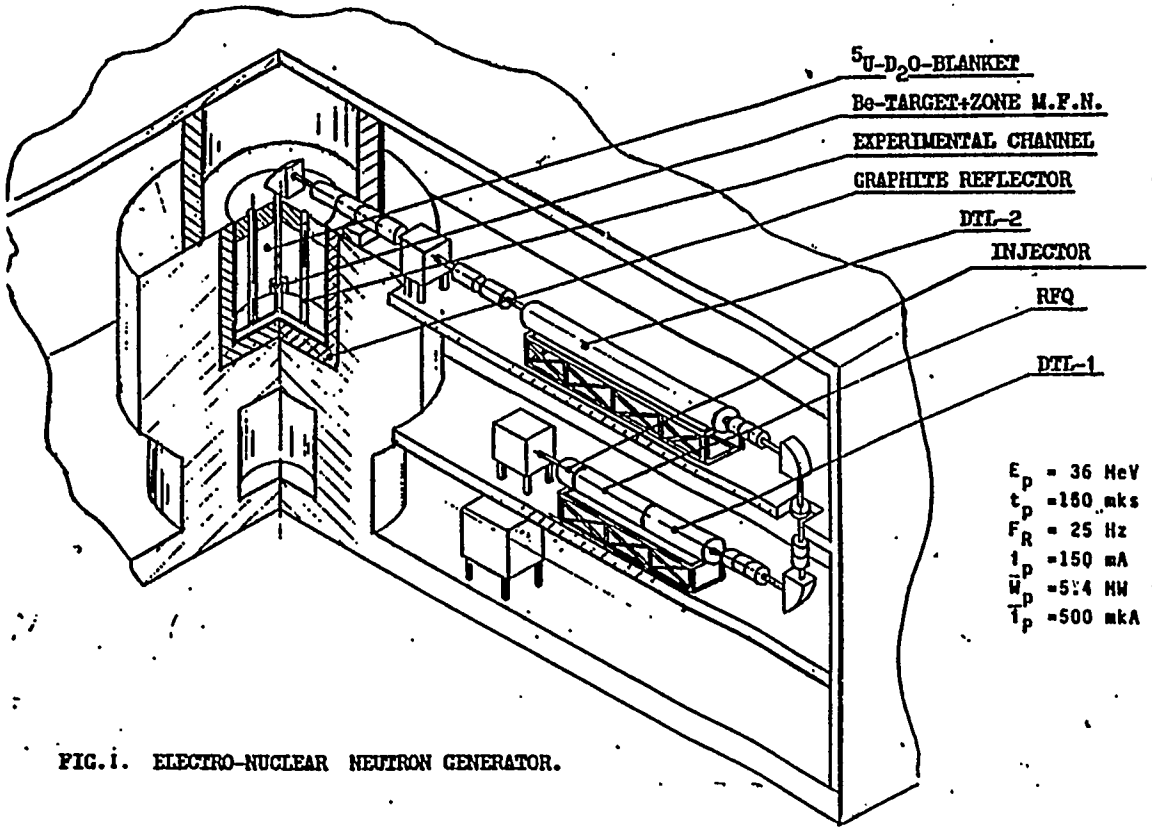

FIG. 1. ELECTRO-NUCLEAR NEUTRON GENERATOR.

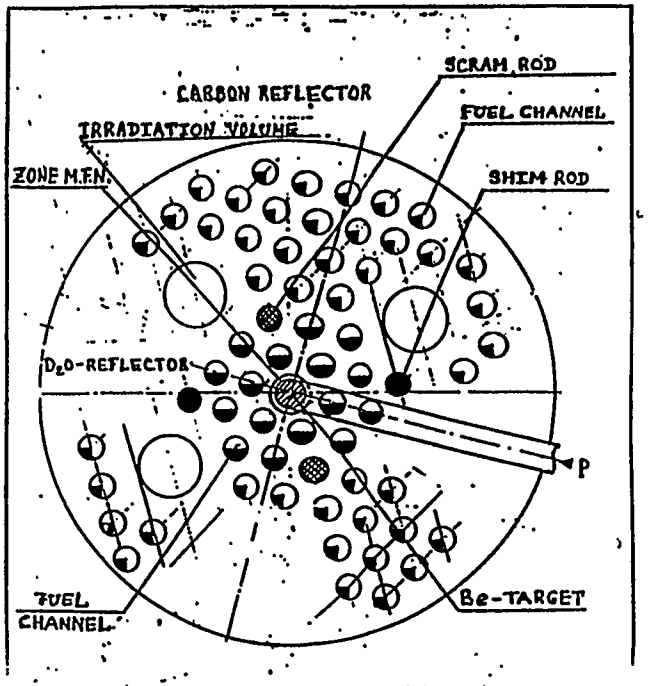

FIG.2. NEUTRON GENERATOR BLANKET.

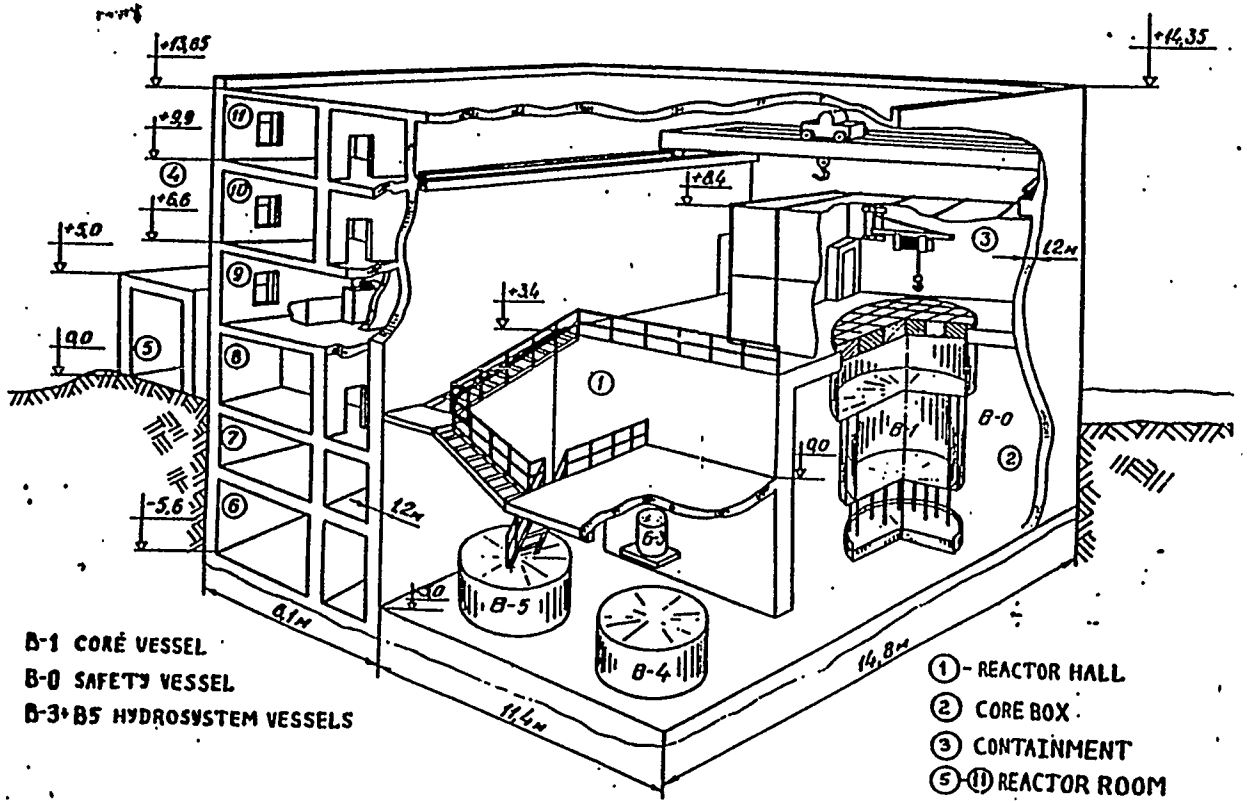

FIG.3. ZERO POWER REACTOR MAKET.

BASIC PARAMETERS OF THE ZERO POWER REACTOR MAKET

1. Core vessel B-1	diameter	2.6 m
	height	3.6 m
	volume	19 m^3
2. Safety vessel B-0	diameter	3.4 m
	height	3.7 m
	volume	33 m^3
3. Automatic control rod compensation and safety rods		1 2
4. Automatic heavy water level meters in vessel B-1		2
measurement accurency of absolute level		1.5 mm
of relative level		0.5 mm
5. Limitater of heavy water level in vessel B-1		1
measurement accurancy of absolute level		1.5 mm
6. Signaller of heavy water level in vessel B-1		1
measurement accurancy of absolute level		1.5 mm
7. Maximum rate of heavy water pumping into vessel B-1		0.7 l/s
8. Channals of control and safety system		11
9. Channels of radiation control system		
neutrons		6
γ-radiations		30
10. Maximal power of the reactor		1 kW

Direct-Current Proton-Beam Measurements at Los Alamos*

Joseph Sherman, Ralph R. Stevens, J. David Schneider, and Thomas Zaugg
AOT-10, Los Alamos National Laboratory, Los Alamos, NM 87545 USA

Abstract. Recently, a CW proton accelerator complex was moved from Chalk River Laboratories (CRL) to Los Alamos National Laboratory. This includes a 50-keV dc proton injector with a single-solenoid low-energy beam transport system (LEBT) and a CW 1.25-MeV, 267-MHz radiofrequency quadrupole (RFQ). The move was completed after CRL had achieved 55-mA CW operation at 1.25 MeV using 250-kW klystrode tubes to power the RFQ. These accelerator components are prototypes for the front end of a CW linac required for an accelerator-driven transmutation linac, and they provide early confirmation of some CW accelerator components. The injector (ion source and LEBT) and emittance measuring unit are installed and operational at Los Alamos. The dc microwave ion source has been operated routinely at 50-keV, 75-mA hydrogen-ion current. This ion source has demonstrated very good discharge and H_2 gas efficiencies, and sufficient reliability to complete CW RFQ measurements at CRL. Proton fraction of 75% has been measured with 550-W discharge power. This high proton fraction removes the need for an analyzing magnet. Proton LEBT emittance measurements completed at Los Alamos suggest that improved transmission through the RFQ may be achieved by increasing the solenoid focusing current. Status of the final CW RFQ operation at CRL and the installation of the RFQ at Los Alamos will be given.

INTRODUCTION

Accelerator-Driven Transmutation Technologies (ADTT) address many current societal concerns - energy production, disposition of nuclear wastes, reduction of fissionable material inventories, and safe production of critical nuclear materials. Part of the ADTT requires the development of very powerful and reliable proton beams. In 1986 a program using CW RFQ technology was undertaken at CRL in collaboration with Los Alamos [1], and continued through April 1993, when CRL terminated this development program. While at CRL the RFQ produced 600-keV, 75-mA and 1250-keV, 55-mA CW proton beams. Subsequently the equipment has been moved to Los Alamos.

One of the present program goals is to establish the experimental 1250-keV RFQ current limit which will depend on the LEBT performance [2]. Beam measurements on the 50-keV single-solenoid [3] LEBT system completed at Los Alamos are discussed here. The LEBT function is to preserve beam quality and match the low-energy beam into the RFQ.

50 keV INJECTOR DESCRIPTION

The major injector components are a proton microwave ion source [4], a single-lens LEBT system with online diagnostics, and a dc emittance measuring unit (EMU) [5]. The EMU is inserted in the normal RFQ position (offline mode) to characterize the injected proton beam.

The microwave ion source has several desirable features. It has already demonstrated good reliability [6], and sufficiently low emittance to meet ADTT linac requirements [4]. Proton discharge efficiencies (390 mA/cm^2kW) and gas efficiencies (0.31) measured at Los Alamos are quite attractive compared to other candidate ion sources [7]. Higher ion source efficiencies have been measured at CRL [4]. Improved efficiencies result in minimum injector vacuum pumping and cooling requirements, leading to higher reliability and ion source longevity. Typically, 75-mA dc hydrogen ion beams are generated with 600 - 700 W of 2.45-GHz discharge power P_d. Less than 100-W isolation power (power at the 50-kV high voltage deck) is required to run the gas flow

* Work supported by the Defense Nuclear Agency under the auspices of the U.S. Department of Energy.

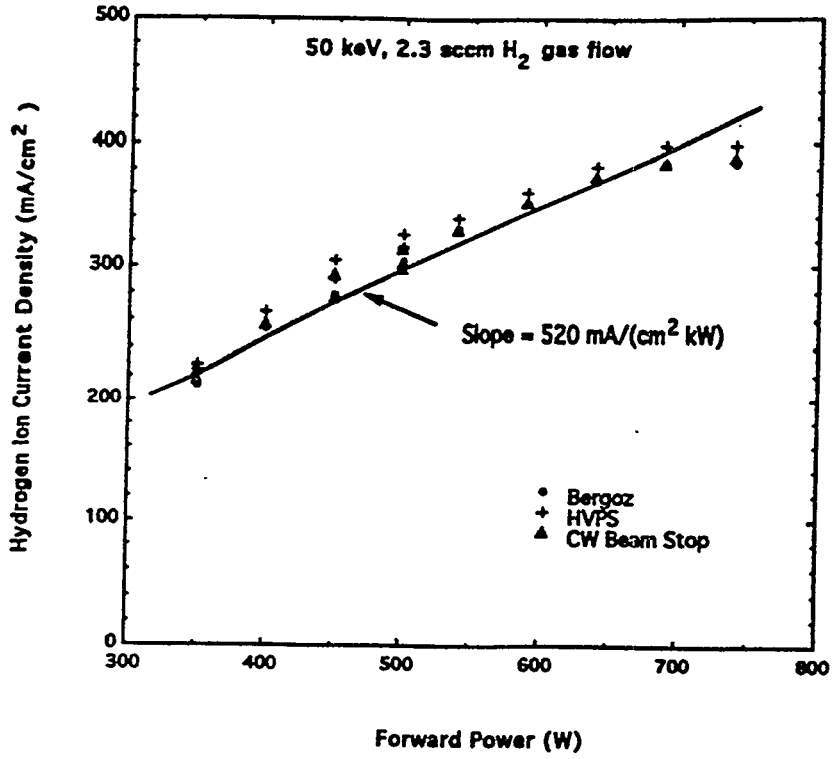

Fig. 1. Forward power vs. the hydrogen ion current density. A hydrogen ion beam production efficiency of 520 mA/(cm^{2}kW) is derived from this plot which corresponds to 390 mA/(cm^{2}kW) proton efficiency.

system. All other power supplies are located at ground voltage, eliminating the need for high power isolation transformers.

The dependence of the extracted current density, j, on P_d is shown in Fig. 1 for 50-kV extraction potential. The beam current is $I_b = j(\pi R_e^2)$ where R_e = 2.5 mm = emission aperture radius. At f = 2.45 GHz the solenoidal field required to establish an electron cyclotron resonance condition is B_s = 875 G. Optimal operation for this microwave ion source is at 5 - 10% greater magnetic field. The scaling of this source to an ADTT linac (140-mA hydrogen ion current at 75-keV beam energy) is discussed in an accompanying paper [8].

Beam current monitoring is accomplished with three diagnostics: the high voltage power supply (HVPS) drain current, a Bergoz dc current monitor [9], and a CW beam stop capable of handling the full beam power. Secondary electron emission is suppressed at the beam stop by the application of a 160-G transverse magnetic field. Error among these diagnostics is ≤ 5% (cf. Fig. 1).

A 50-mm aperture dipole magnet has been installed after the EMU main slit to measure proton fraction. Typical data are shown in Fig. 2 where the beam currents at the Faraday cup are plotted as a function of the magnetic field ramp time. The species ratio H^+:H_2^+:H_3^+ equals 75:17:8% with P_d = 550 W and gas flow Q = 2 sccm. The LEBT solenoid was turned off during these measurements to ensure a homogeneous hydrogen ion beam at the EMU. The ion source current and beam fraction measurements are comparable with those reported by CRL [4,10].

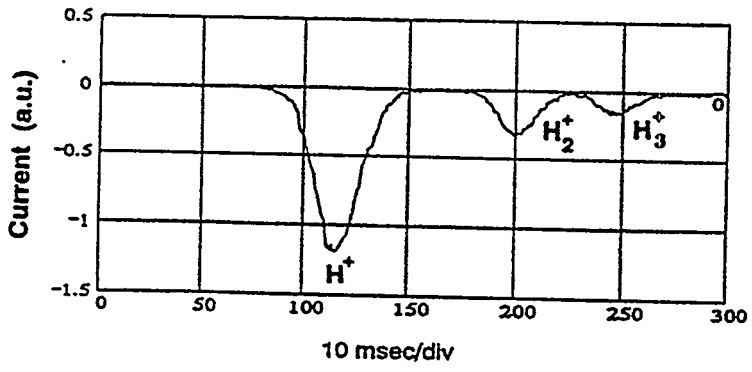

Fig. 2. Measurement of the hydrogen ion species at the LEBT exit.

Beam extraction is accomplished with a triode accelerator system, composed of a 5-mm diam emitter, a 4.5-mm diam extractor/ suppressor electrode, and a 5-mm

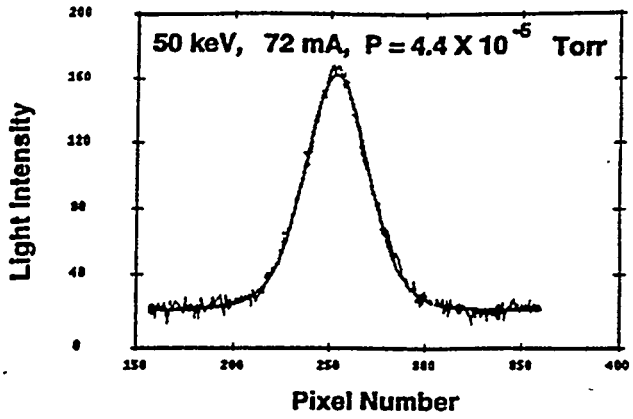

Fig. 3. Beam profile extracted from the Cohu data.

diam ground electrode. The extractor electrode is over-biased by 2 kV to suppress electrons backstreaming from the LEBT. The gap between the emission and extraction electrodes is g_1 = 6.9 mm, and the gap between the extraction and ground electrodes is g_2 = 2.9 mm.

Beam profile monitoring located in the beam diagnostics station is accomplished with a two dimensional Cohu imaging system [11]. It is located 35 cm from the ion source. Fig. 3 shows the profile of a 50-keV, 72-mA hydrogen ion beam in H_2 gas at $P = 4.4 \times 10^{-5}$ Torr. The FWHM of this distribution is 1.10 cm.

A 50-keV emittance measurement sample is shown in Fig. 4(A). The LEBT solenoid is excited to 102 A. The intense central part of the phase space contains the proton component (≥10% threshold contour) while the unfocused components at 1% contour are primarily the H_2^+ and H_3^+ species. A plot of total emittance at beam fraction F vs. F (in the form $\ln(1-F)^{-1}$) is shown in Fig.

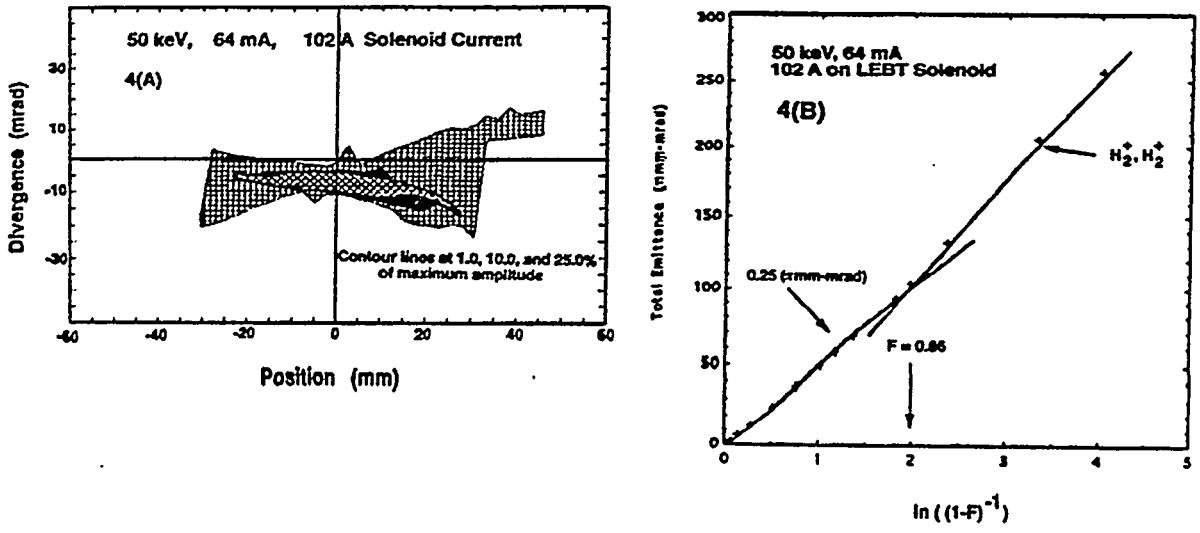

Fig. 4. (A) A sample emittance measurement. (B) Total emittance at beam fraction F vs. $\ln(1-F)^{-1}$ for the emittance measurement in (A).

4(B). For a Gaussian beam distribution [12] a linear plot would indicate a beam distribution characterized by an ion temperature kT. The data contain two separate linear relations with a break at F ≈ 0.86. The curve for F < 0.86 is characteristic of the proton distribution while the distribution for F > 0.86 includes the H_2^+ and H_3^+ species. The lower curve yields the Gaussian-extrapolated rms normalized emittance= $\varepsilon_{rms,n}$ = 0.25 (πmm-mrad) for the proton beam. All proton beam emittance data presented here have been analyzed by using the Gaussian extrapolation procedure on 10% and 25% threshold emittance data. The phase-space distributions expected for the $H_2^+$and H_3^+ components were calculated from the TRACE code and agree with the observed

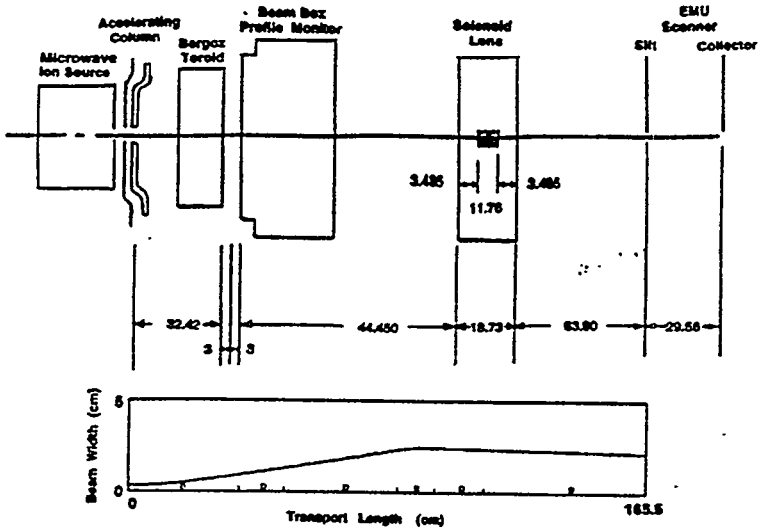

Fig. 5. Schematic layout of the single-solenoid LEBT system for beam transport to the EMU. The TRACE 50 keV beam envelope calculation for 102 A solenoid excitation with I_{eff} = 1 mA is shown below.

data for the 1% threshold contour. The break in the emittance vs. ln(1-F)$^{-1}$ plot is very similar to a single-species beam with aberrations [13].

The LEBT solenoid field has been mapped at Los Alamos to 260-A excitation current. Measured multipole fields have revealed a 170 G-cm dipole component which significantly steers a 50-keV proton beam.

MEASUREMENT RESULTS

Figure 5 shows a schematic layout of the single solenoid LEBT system with TRACE calculations [14] superimposed below. The distance along the beam is in the z direction, and the distances transverse to z are the x and y directions. This figure shows the relative locations of the microwave ion source, Bergoz current monitor, diagnostics box, focusing solenoid, and the EMU. In principle, the Courant-Snyder beam parameters at the ion source can be determined by transporting the emittance measurement results backward through the LEBT using the TRACE code. The only unknown in this procedure is the effective current, I_{eff}. I_{eff} in the TRACE code was varied to give the best fit to the known ion source emission aperture size. The best fit obtained over a series of solenoid settings gave a 3-mm beam envelope size at I_{eff} = 1 mA, yielding the Courant-Snyder parameters $\alpha = 0.513$ and $\beta = 0.16$ (mm/mrad) for $\varepsilon_{rms,n} = 0.20$ (πmm-mrad). These projected calculations were made as a function of the LEBT solenoid current using the 10% threshold emittance results. Below 70-A LEBT solenoid current not all of the proton current is scanned by the EMU, and for this reason these data are not included in the TRACE projections for determining I_{eff}. Ion source beam size predictions for I_{eff} = 2 mA varied from 3.5 to 7.5 mm depending on the solenoid current, and are clearly inferior to the I_{eff} = 1 mA results.

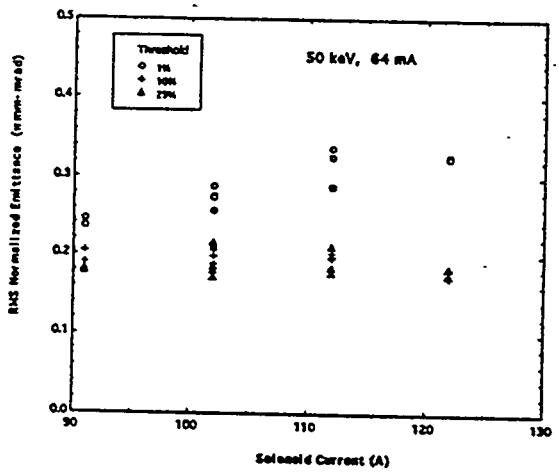

Fig. 6. Measured LEBT emittances as a function of solenoid coil current. The measured emittances at 10 and 25% beam thresholds have been used in a Gaussian beam model to derive the proton beam rms normalized emittances.

Calculations [15] for the voltage drop within a 50-keV, 90-mA proton beam show that for our beam radius (1.0 cm) and gas density (6.6 X 10^{11} (cm)$^{-3}$) we should have a residual beam space potential = $\Delta\phi_n$ =5 V. For a totally unneutralized beam, $\Delta\phi = I_b R/\beta = 218$ V where $R = 30\ \Omega$ and β is the relativistic velocity factor. Most of the positive-ion-beam space charge is neutralized by the accumulation of electrons generated by ionization of the background gas by the hydrogen ion beam. Taking I_{eff} =

$I_b(\Delta\phi_n/\Delta\phi) = 1.4$ mA, which is in good agreement with I_{eff} derived from the TRACE calculations.

Extracted $\varepsilon_{rms,n}$ for $P_d = 600$ W are plotted vs. the LEBT solenoid current in Fig. 6. The Gaussian projections at 10 and 25% beam thresholds are clustered at ≈ 0.20 (πmm-mrad) while projections using the 1% threshold emittances are 50% greater. This is expected because the 1% threshold data includes H_2^+ and H_3^+ contributions to the phase-space area. Ion-source-only emittance measurements (no LEBT transport) from CRL give ≈ 0.12 (πmm-mrad) [ref. 4,10], thus indicating a 70% emittance increase observed at Los Alamos is brought about by beam transport through the LEBT.

Average beam position at the EMU location was measured for five EMU data sets on different days with different LEBT solenoid excitations. Translation of these EMU measurements to the RFQ location shows that 0.5 - 3.2 mm steering may be expected at the RFQ matchpoint. The steering effect is quite reproducible, and is consistent with the observed solenoid dipole field.

DISCUSSION

Predictions have been made with the TRACE code for RFQ matching by using the derived Courant-Snyder parameters. Figure 7 shows the (α,β) tuning plot [2] for the single-solenoid LEBT; as solenoid current is increased from 205 A to 230 A the α–β tune moves from right to left down the solid curve. The design matched beam [16] parameters for RFQ input beam currents of 80 and 70 mA with the rms normalized input emittances varying from 0.1 to 0.4 (πmm-mrad) are shown as crosses and open circles in this figure. The best match would occur at ≈ 213 A LEBT solenoid current, 13 A higher than CRL was able to obtain in their last RFQ measurements because of power supply limitations.

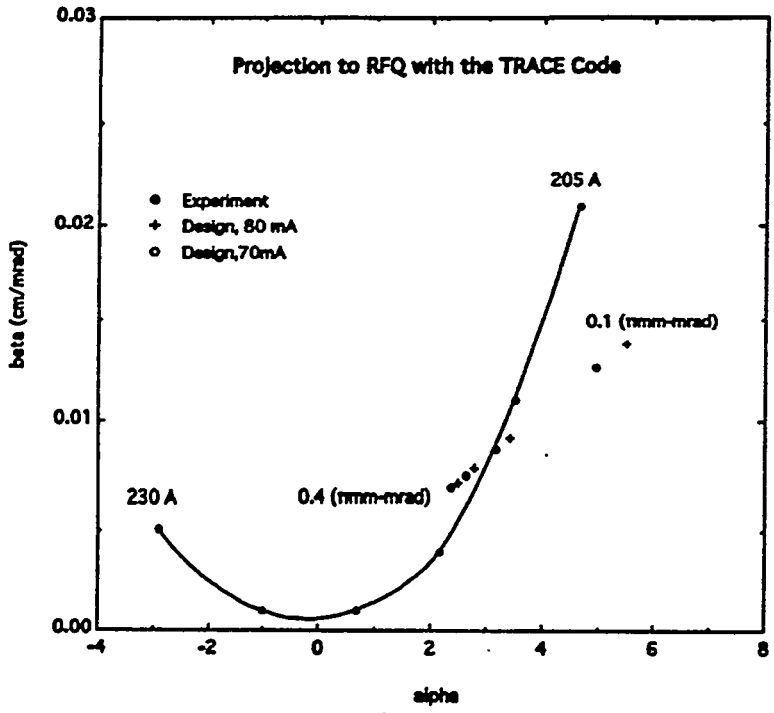

Fig. 7. Single-solenoid LEBT (α,β) tuning plot derived from EMU beam measurements.

A higher-order beam transport LEBT model using the SCHAR code [17] predicts an emittance growth of 40% using the projected Courant-Snyder parameters and taking the $\varepsilon_{rms,n}$ = 0.12 (πmm-mrad) for the initial emittance. Figure 8(A) shows the SCHAR beam phase space (transverse velocity = v_x vs. x position) representation at the ion source. Figure 8(B) shows the phase space at the solenoid entrance where the beam has expanded to 36 mm diameter. Figure 8(C) shows the beam phase space focused to approximately 1mm at the RFQ matchpoint. Figure 8(C) also shows (1) the effect of the solenoid dipole field as the beam is displaced to x ≈ -1mm and (2), the onset of focusing and space-charge aberrations. These calculations were performed with I_{eff} = 1 mA and initial ion source beam radius equal to 2.5 mm. Taking an initial beam radius equal to 1.3 mm, a LEBT emittance growth of 3.5X has been

calculated. A smaller beam at the ion source with constant emittance results in a larger beam at the solenoid position because of increased ion source divergence. Emittance preservation in this LEBT is thus crucially dependent on the ion source operation.

The SCHAR calculation takes into account the solenoid dipole field, and an approximate 1 mm displacement is noted at the RFQ matchpoint. RFQ simulations [16] predict that a 1 mm displacement will reduce the beam transmission through the RFQ from 89 to 80%. Beam steering of this magnitude has now been both observed and calculated, and control of the beam centroid parameters going into the RFQ will be an important parameter in determining its transmission.

A primary goal of this work is to study possible LEBT problems in achieving the RFQ design current. Three potential problems with the direct injection scheme have become apparent: mismatch of the 50 keV beam into the RFQ, solenoid steering problems, and emittance growth in the LEBT. In future RFQ studies, influence of these effects will need to be considered.

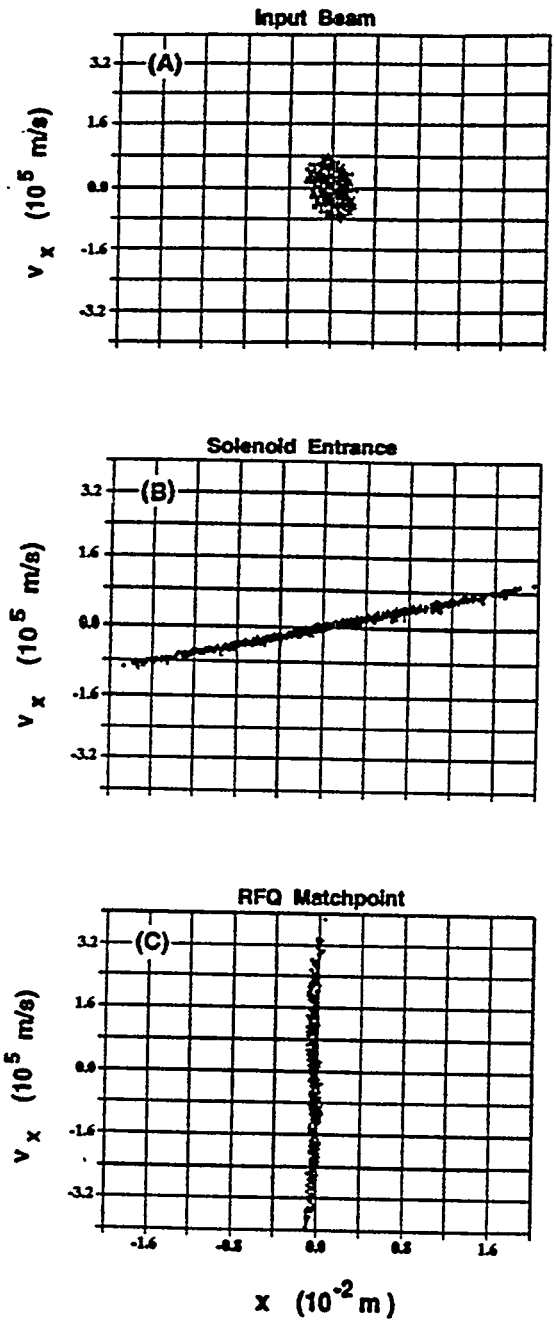

Fig. 8. SCHAR predictions for the beam phase space at (A) the ion source, (B) entrance to the solenoid focusing magnet, and (C) the RFQ matchpoint. All three plots have the same scale on both coordinate axes.

ACKNOWLEDGMENTS

Cooperation of the CRL staff in helping Los Alamos operate the 50-keV injector is deeply appreciated. Special thanks to Gerry McMichael (CRL) and Robert Hardekopf (LANL) for making the move possible, and to Terence Taylor and Walt Michel for many helpful discussions on the microwave ion source and computer control system. Los Alamos technical staff led by Patrick Schafstall were instrumental in getting the 50 keV beam operational.

REFERENCES

[1] McMichael, G. E., Arbique, G. M., Birney, L. F., Brown, J. C., Chidley, B. G., Davidson, A. D., M. S. de Jong, Hutcheon, R. M., Michel, W. L., Sheikh, J. Y., Taylor, T., Tran Ngoc, T., Walton, A. A., and Wills, J. S. C., "The RFQ1 Project at CRNL - A Status Report", CRNL-4126, February, 1987.

[2] Sander, O. R., Atkins, W. H., Bolme, G. O., Bowling, S., Brown, S., Cole, R., Connolly, R., Gilpatrick, J. D., Garnett, R., Guy, F. W., Ingalls, W. B., Johnson, K. F., Kerstiens, D., Little, C., Lohsen, R. A., Lloyd, S., Lysenko, W. P., Mottershead, C. T., Neuschaefer, G., Power, J., Rusthoi, D. P., Saadatmand, K., Sandoval, D. P., Stevens, Jr., R. R., Vaughn, G., Wadlinger, E. A.,

Weiss, R., and Yuan, V., "Commissioning the GTA Accelerator", in *Proceedings of the 1992 Linear Accelerator Conference*, AECL-10728, August, 1992, pp. 535-539.

[3] Arbique, G. M., Taylor, T., Davidson, A. D., and Wills, J. S. C., "High Current Direct Injection to a CW RFQ Using an ECR Proton Source", in *Proceedings of the 1992 Linear Accelerator Conference*, AECL-10728, August 1992, pp. 52-54.

[4] Taylor, Terence and Mouris, Jozef F., "An Advanced High-Current Low-Emittance DC Microwave Proton Source", *Nucl. Instrum. and Methods in Physics Research* A336, 1993, 1-5.

[5] Taylor, T., M. S. de Jong, and Michel, W. L., "An Emittance Measuring System for High-Current High Brightness Multi-Beamlet Multi-Species Heavy Ion Beams", in *Proceedings of the 1988 Linear Accelerator Conference*, CEBAF-Report-89-001, June, 1989, 100-102.

[6] Arbique, G. M., Chidley, B. G., McMichael, G. E., and Sheikh, J. Y., "Beam Parameter Measurements on the CW RFQ1-1250 Accelerator", in *Proceedings of the 1992 Linear Accelerator Conference*, AECL-10728, August, 1992, 55-57.

[7] Stevens, Jr., Ralph R. , Sherman, Joseph D., and Schneider, J. David, "Injector Design for High-Current CW Proton Linacs", in *Proceedings of the 1993 Particle Accelerator Conference*, IEEE Catalog No. 93CH3279-7, May, 1993, 3166-3168.

[8] Schneider, J. David, Meyer, Earl, Stevens, Jr., Ralph R., Hansborough, Lash, and Sherman, Joseph "Design and Testing of a DC Ion Injector Suitable for Accelerator-Driven Transmutation", these Conference Proceedings.

[9] Unser, K. B., "Design and Preliminary Tests of a Beam Intensity Monitor for LEP", in *Proceedings of the 1989 Particle Accelerator Conference*, IEEE Catalog No. 89CH2669-0, March 1989, 71-73.

[10] Taylor, Terence and Wills, John S. C., "A High-Current Low-Emittance DC ECR Proton Source", *Nucl. Instrum. and Methods in Physics Research* A309, 1991, 37-42.

[11] Sandoval, D. P., Garcia, R. C., Gilpatrick, Doug, Johnson, K. F., Shinas, M. A., Wright, R., Yuan, V., and Zander, M. E., "Video Profile Monitor Diagnostic System for GTA", in *Proceedings of the 1992 Linear Accelerator Conference*, AECL-10728, August 1992, 247-249.

[12] Allison, Paul, "Some Comments on Emittance of H^- Ion Beams", in *Proceedings of the 1986 Production and Neutralization of Negative Ions and Beams Symposium*, AIP Conference Proceedings No. 158, Brookhaven, NY 1986, 465-481.

[13] Stevens,Jr., Ralph R., York, R. L.,Leung, K. N., and Ehlers, K. W., "Operation of a Magnetically Filtered Multicusp Volume Source", in *Proceedings of the 1986 Production and Neutralization of Negative Ions and Beams Symposium*, AIP Conference Proceedings No. 158, Brookhaven, NY 1986, 271-281.

[14] Crandall, K. R., and Rusthoi, D. P., "Documentation for TRACE: An Interactive Beam-Transport Code", Los Alamos Report LA-10235-MS, January, 1985.

[15] Soloshenko, I. A., "Space-Charge Compensation of 50 and 75 keV Proton Beams", Institute of Physics Ukrainian Academy of Sciences, (Kiev, Ukraine), Contract No. 9424L0014-9G, May, 1994.

[16] Neuschaefer, George, Internal Los Alamos Report, AT-1:93-164, July, 1993.

[17] Jakobson, Mark J. and Hayden, Richard J., "Dependence of Emittance Degradation on Beam Angular Momentum for Charge Exchange in Solenoids", *Nucl. Instrum. and Methods in Physics Res.* A258, 1987, 536-541.

Design and Testing of a DC Ion Injector Suitable for Accelerator-Driven Transmutation

J. David Schneider, Earl Meyer, Ralph R. Stevens, Jr., Lash Hansborough, and Joseph Sherman
Accelerator Operations and Technology Division, Los Alamos National Laboratory, Los Alamos, New Mexico 87545 USA

Abstract. For a number of years, Los Alamos personnel have collaborated with a team of experimentalists at Chalk River Labs (CRL) near Deep River, Ontario, Canada who were pursuing the development of the front end of a high power cw proton accelerator. At the termination of this program last year, Los Alamos acquired this equipment. With the help of internal Laboratory funding and modest defense conversion funds, we have set up and operated the accelerator at Los Alamos. Operational equipment includes a slightly modified Chalk River Injector Test Stand (CRITS) including a 50 keV proton injector and a 1.25 MeV radio-frequency quadrupole (RFQ) with a klystrode rf power system. Substantial upgrading and modification of the ac power system was necessary to provide the required ac voltage (2400 vac) and power (2 MVA) needed for the operation of this equipment. A companion paper describes in detail the first ion source and beam-transport measurements at Los Alamos.

Many of the challenges involved in operating an rf linear accelerator to provide neutrons for an accelerator-driven reactor are encountered at the front (low energy) end of this system. The formation of the ion beam, the control of the beam parameters, and the focusing and matching of a highly space-charge-dominated beam are major problems. To address the operating problems in this critical front end, the Accelerator Operations and Technology Division at the Los Alamos National Laboratory has designed the APDF (Accelerator Prototype Demonstration Facility). The front end of this facility is a 75 keV, high-current, ion injector which has been assembled and is now being tested.

This paper discusses the design modifications required in going from the 50 keV CRITS injector to the higher current, 75 keV injector. Major innovative changes were made in the design of this injector. This design eliminates all the control electronics and most of the ion source equipment at high potential. Also, a new, high-quality, ion-extractor system has been built. A dual-solenoid lens will be used in the low energy beam transport (LEBT) line to provide the capability of matching the extracted beam to a high-current ADTT linac. This new injector is the first piece of hardware in the APDF program and will be used to develop the long-term, reliable cw beam operation required for ADTT applications.

INTRODUCTION

High power cw proton injectors have been built in the past two decades at several national laboratories both for neutral beam experiments and for neutron production applications. One of the first such injectors was the 600 kV, 100 mA proton injector built by Morgan et al at the Oak Ridge National Laboratory using a duoplasmatron ion source in the DCX-2 injector [1]. At Sandia Laboratory, a 200 kV, 150 mA injector was built by Brainard using a single ring, cusp ion source for tests of a medical neutron source [2]. At the Lawrence Livermore Laboratory, the rotating target neutron source (RTNS-II) employing a 300 kV, 200 mA duopigatron ion source was built to provide neutrons in a production facility for material testing [3]. At the Los Alamos National Laboratory, a 75 keV injector was built and tested for the Fusion Materials Irradiation Test (FMIT) facility with a cusp-field bucket ion source [4]. This injector produced 240 mA of total hydrogen ion current; the associated RFQ accelerator accelerated 60 mA of H_2^+ ions to 2 MeV. More recently, the accelerator group at Chalk River Labs built a proton test stand with a microwave proton source [5]. This 50 keV injector and RFQ demonstrated beams of greater than 100 mA from the injector and over 55 mA accelerated by the RFQ to 1.25 MeV. Thus, there have been several successful demonstrations of the feasibility of high-current, dc injectors. However, implementing reliable, long-term operation in a production mode remains to be demonstrated.

ADTT DESIGN REQUIREMENTS

Injector requirements for ADTT applications entail producing sufficient total beam current from the ion source (140 mA) to give a 100 mA proton beam at the RFQ match point from an injector

which is capable of long-term, stable operation in a production environment [6]. The transverse beam emittance requirement at the RFQ input is 0.20 πmm-mrad rms normalized, and the longitudinal emittance must have energy error less than ± 1kV. Matching to the RFQ requires precise control of the Twiss and centroid parameters. An injector employing a dual solenoid lens system with beam steering coils can effect this matching.

In addition to matching the transverse and longitudinal phase space to the RFQ, the injector must also provide a means of turning on the ion beam in a controlled manner. This will probably require ramping the beam current to the accelerator with a ~100 μs ramp time thus permitting the rf control loops to remain locked. Injected beam current modulation with a small (few percent) amplitude modulation may be needed to permit an on-line measurement of the K_{eff} of the accelerator-driven assembly.

Long-term reliability is the key issue in the design of this injector. The concept of simplicity, ease of access, and modularity in system design are used throughout. The ion source was chosen on the basis of low power, stability, efficiency, simplicity, and proven performance. Ion source component lifetimes must be increased and means must be provided to implement automated fault recovery after high voltage trips. Routine maintenance will be necessary to carry out replacement of critical components prior to on-line failure. A computer control system will set and monitor injector parameters and has the potential for automatic sequencing procedures and turn-on algorithms. This control system can keep critical parameters within specified limits and can provide closed-loop feedback. Development of these control functions will be done after the injector hardware is commissioned.

DESIGN FEATURES OF THE 75 keV APDF INJECTOR

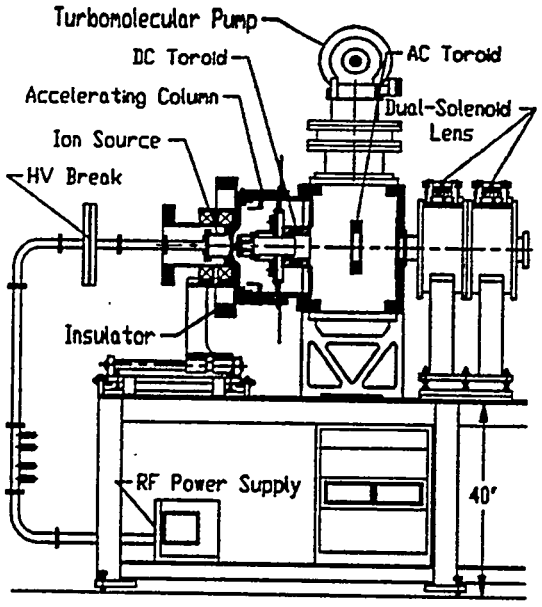

Fig. 1. Schematic diagram of the APDF Injector.

Key features are the simple ion source structure, the proven single-gap 75 kV extractor, and a simple, compact beam transport system with non-interceptive diagnostics. The ion source is at high potential (75 kV) and a solid, integral, insulator unit allows all of the ancillary ion source components and electronics to remain at ground potential. A schematic diagram of this injector is shown in Fig. 1 and a photograph of the assembled system is shown in Fig. 2.

This injector uses the same microwave proton source that was developed for CRITS [7]. This source has high gas and discharge-power efficiencies and provides a 75% proton fraction in the extracted beam. Operational details are discussed in a companion paper [8]. A mechanical hydrogen gas flow system is used. An insulated ion source coil design is employed so that the coils are operated at ground potential. Thus, no gas controller or power supplies are required at high potential.

Vacuum pumping is provided by a 2500 l/s turbomolecular pump that is capable of uninterrupted operation with only minor periodic maintenance. This pump is mounted on top of the beam diagnostic box located just after the extractor in the LEBT line. All these design features have been chosen to ensure long-term reliability and stability of operation.

All beam line components are water cooled and collimators are placed both at the exit of the accelerating column and the beam diagnostic box to intercept beam halo. Non-interceptive beam

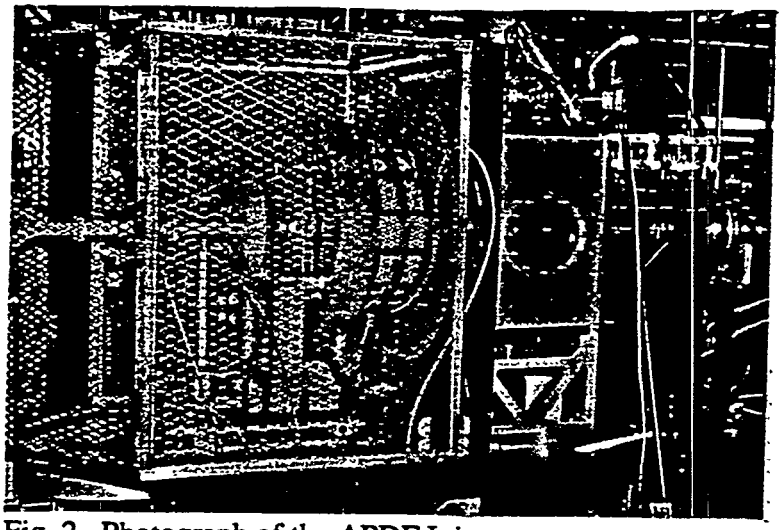

Fig. 2. Photograph of the APDF Injector.

diagnostic systems permit on-line monitoring of beam parameters. A current transductor measures the low-frequency components of the beam current while a conventional ac toroid monitors frequencies up to 4 MHz. CCD cameras measure horizontal and vertical beam profiles at both the exit of the accelerating column and at the RFQ entrance. These profile monitors permit continuous on-line beam measurements and provide input to the closed-loop feedback systems.

Beam simulations similar to those done for the CRITS injector were carried out using both the beam envelope code TRACE [9] and the macroparticle code SCHAR [10]. The expected beam envelopes for the design beam are shown in Fig. 3. The input beam was determined by scaling the observed beams from the CRITS injector with the same extracted current density (250 mA/cm^2). We are therefore assuming that the input beam parameters are determined only by the beam perveance. Simulations were also done with SCHAR assuming a 4-D waterbag phase space distribution. These simulations predict that the emittance growth in the LEBT due to solenoid aberrations is only 1.0%. Experiments on the CRITS injector show that the beam is 99% space-charge neutralized. Assuming the same neutralization for the APDF injector, SCHAR predicts there is an additional emittance growth of 2.2% due to the relaxation of the input phase space distribution as the beam is transported from the source to the RFQ. Thus, we expect an overall emittance growth in the LEBT of 3.2%. The calculated phase space distribution at the RFQ match point as predicted by SCHAR is shown in Fig. 4.

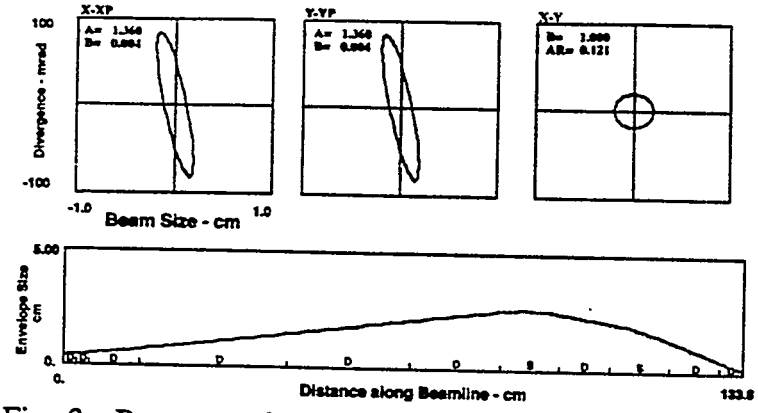

Fig. 3. Beam envelopes for the design beam of the APDF Injector.

APDF INJECTOR SYSTEMS

The engineering of the APDF injector is patterned after the successful designs of previous cw injectors, but includes enhancements to obtain better long-term reliability. The microwave ion source is identical to that used on CRITS except that the plasma electrode was modified to have an 8.4 mm-dia. emission aperture, thus giving a more conservative 250 mA/cm^2 extracted current density at the design current (140 mA) [8]. Electrode shapes for the extraction system were confirmed by SNOW simulations after optimizing the design with an extensive parameter search. The accelerating column design is based on the FMIT column and employs a single accelerating gap and subdivides the voltage with an intermediate electrode so that each of the two insulator rings in the column runs at half the total voltage. This intermediate ring is held at proper potential by a

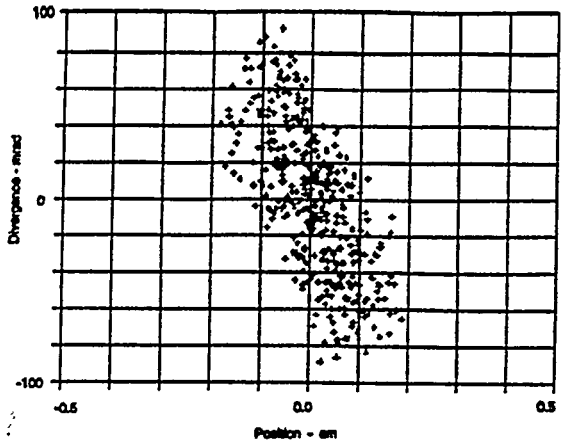

Fig. 4. Expected APDF phase space distribution at the RFQ match point.

water resistor that also provides cooling to the ion source baseplate. High voltage shields are incorporated in the column to shield the insulators and an electron trap is placed at the interface of the accelerating column and the beam transport line. Extractor shield tubes prevent the insulators from seeing the beam or the beam-induced plasma. Pressed alumina insulator rings are assembled into a column by G-10 insulating rods and sealed with O-rings. All beam tubes and other surfaces that can be exposed to beam impingement or radiation are water cooled.

The beam diagnostics are located in the beam diagnostic box just after the extractor. A Bergoz dc current transformer measures the beam current and CCD cameras (COHU Model 4810) are used to measure the beam profiles. A Balzers 2500 l/s turbomolecular pump backed by a Leybold-Hereaus DK-60 provides the vacuum pumping. This pumping system produces an ultimate vacuum in the low 10^{-7} torr region and can maintain a beam line vacuum in the low 10^{-5} torr range for a hydrogen flow of 4 to 5 sccm.

The ground level rack for this injector has been configured with the water manifolds on one side and with the ac power distribution on the other side of the rack. Thus, all utilities needed for the injector are located in a single area and brought in from this rack on a common duct. This arrangement provides a compact package, permitting easy installation of the injector onto any accelerator.

The LEBT focusing system employs a dual-solenoid lens located just after the beam diagnostic box. A dual-solenoid lens was chosen instead of the conventional separated, two-solenoid lens system [11] for simplicity and compactness. This choice should permit easier alignment and can be operated as a non-rotational lens by operating with the solenoid fields opposing. This mode of operation limits steering effects in the solenoids if there are centroid errors in the input beam. Each solenoid lens is constructed with simple, rugged, bifilar pancake coils that are enclosed in an assembly with steel yoke and pole pieces for a design field of 0.4 Tesla. A photograph of this lens system is shown in Fig. 5. The dual-solenoid provides the required two-knob tuning capability needed for an optimal RFQ match. Magnetic field measurements confirmed the Flux-2D design calculation and showed that there are no saturation effects in the magnet steel for fields well above the design field. Both the calculated and the measured axial magnetic field strengths at the expected operating field are shown in Fig. 6 for one of the lenses in the dual-solenoid system; the other lens is identical. There are sufficient ampere turns to operate the lenses with the fields opposing, which may be useful if the input beam errors are significant. The dipole and higher multipole field components were also measured and are well

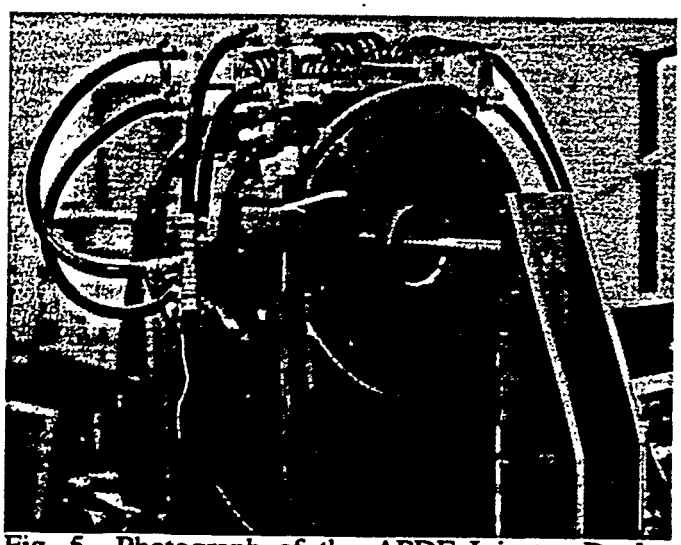

Fig. 5. Photograph of the APDF Injector Dual-Solenoid Lens.

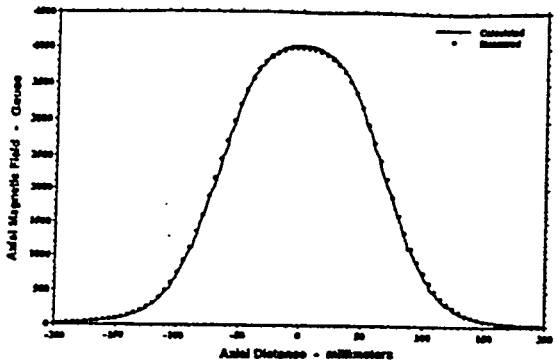

Fig. 6. Axial magnetic field measurement for one of the solenoids in the APDF LEBT.

below the 0.1% level and thus are not important. No steering was incorporated into the original design of this injector, but provision has been made to place Lambertson coils in the solenoid lenses when the injector is mounted onto the RFQ.

The injector employs a computer control system to monitor and control the setpoints of the various injector subsystems. This control system uses a Motorola 68040 microprocessor in the input-output controller and runs with EPICS™ software. A software-based run permit system is employed for proper turnon and hardware protection. A hard-wired safety interlock system is used for personnel protection.

INITIAL OPERATING EXPERIENCE

The injector has been assembled and initial beam tests carried out. Low current (7mA) beams were extracted at 30 kV. Although the accelerating column alone (no ion source) had been operated at 100 kV without corona, high voltage problems were encountered at 50 kV with the ion source support structures. A number of modifications were subsequently made both to the ion source coil support stands and to the electrostatic guard rings to limit corona and prevent sparking. The injector was then conditioned to 75 kV without beam. Beam currents up to 60 mA were then obtained for a short time at 50 kV. Based on the operating experience on CRITS, we anticipate that the design current of 140 mA will be achieved at 75 kV after the ion source operation is optimized.

DISCUSSION

The initial beam tests at 50 kV demonstrated that this injector was operating close to the current levels expected from the previous work on CRITS where 75 mA beams had been observed at this voltage. Based on the experimental results obtained on CRITS and on the SNOW simulations of the extractor system, we can predict the beam parameters that should be produced with the APDF extraction system. We anticipate running the ion source with a 8.4 mm-dia. emission aperture and with an extracted current density of 250 mA/cm^2. Data taken on the microwave ion source [7] has shown that as the emission aperture diameter is increased from 5.0 to 7.0 mm, there is only a 20% increase in the beam emittance; thus the ion source emittance for the APDF injector is predicted to be 0.13 πmm-mrad, rms normalized. Simulations with SNOW for an ion source with an 8.4 mm-dia. emission aperture operated with 250 mA/cm^2 extracted current density at 75 kV extraction voltage, show that the maximum divergence angle of the extracted beam at perveance match remains at the same 26 mrad as predicted for the 50 kV case with a 5.0 mm-dia. emission aperture. Assuming that the beam envelope size at the exit of the extractor is equal to the emission aperture radius of 4.2 mm, the phase space parameters of the extracted beam are determined and we can model the beam transport line in this injector. The results of the TRACE

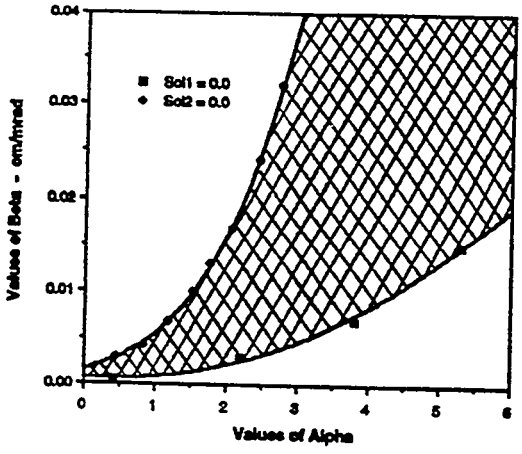

Fig. 7. Alpha-beta tuning diagram for the APDF Injector.

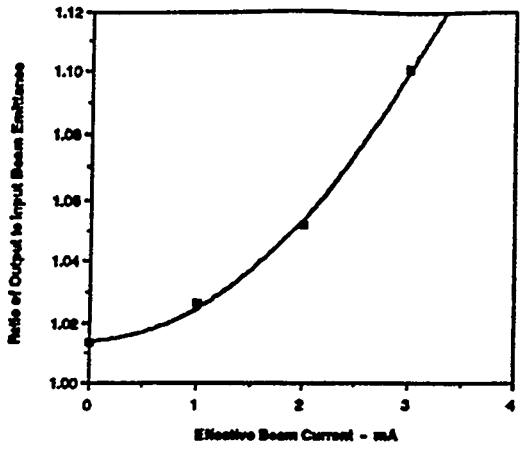

Fig. 8. Calculated emittance growth in the APDF LEBT.

calculation are shown in Fig. 3 where the above input beam is transported through the dual-solenoid lens to the RFQ match point. The solenoid lens strengths are adjusted to give a matched beam with α = 1.36 and β=0.004 cm/mrad, which are typical RFQ match parameters. The alpha-beta tuning diagram for this lens system is then calculated for the two extreme zero excitation cases and is shown in Fig. 7. The cross-hatched area shows the region in alpha-beta space that can be reached for this dual lens system. This region is more than adequate to match the expected input beams to an RFQ accelerator for the ranges of beam currents and emittances expected in these applications. The beam transport line was then simulated with the SCHAR code to determine the expected emittance growth due to solenoid aberration and to non-linear space-charge effects. The overall emittance growth predicted in these simulations as a function of effective beam current is presented in Fig. 8.

CONCLUSIONS

We anticipate carrying out an experimental program of beam measurements similar to those done on CRITS in order to characterize the beams produced by this injector. The results that we have obtained together with the simulations of the expected performance of this injector indicate that we should be able to meet all the requirements needed for ADTT applications.

ACKNOWLEDGMENTS

The authors wish to acknowledge the work of Thomas Zaugg, Patrick Schafstall and David Hodgkins in building and testing this injector and of Richard Martinez for engineering design. This work was supported by the Defense Nuclear Agency under the auspices of the U. S. Department of Energy.

REFERENCES

[1] Morgan, O. B., Kelley, G. G., and Davis, R. C., "Technology of Intense dc Ion Beams", Rev. Sci. Instrum. 38, 467, (1967).

[2] Brainard, J. P. and O'Hagen, J. B. "Single-Ring Magnetic Cusp Ion Source", Rev. Sci. Instrum. 54 (11), 1497-1505, 1983.

[3] Davis, J. C., Heikkinen, D. W., Held, J. L., Logan, C. M., and Osher, J. E., "RTNS-II Neutron Sources: Status Report", IEEE Trans. on Nucl. Sci., NS-26, No.3, 3058-3060, June, 1979.

[4] Cornelius, W. D., "CW Operation of the FMIT RFQ Accelerator", IEEE Trans. on Nuclear Science, NS-32, No. 5, October, 1985

[5] Taylor, Terence and Wills, John S., "A High Current Low-Emittance DC ECR Proton Source", Nucl. Instrum. and Methods in Physics Research A309, 1991 37-42.

[6] Stevens, Ralph R., Jr., Sherman, J. D., and Schneider, J. D., "Injector Design for High-Current CW Proton Linacs", Particle Accelerator Conference, Washington DC, 3166-3168 May 1993.

[7] Taylor, Terence and Mouris, Jozef F., "An Advanced High-Current Low-Emittance DC Microwave Proton Source", Nucl. Instrum. and Methods in Physics Research A336, 1993, 1-5.

[8] Sherman, Joseph, Stevens, Ralph R., Jr., Schneider, J. David, and Zaugg, Thomas, "Direct-Current Proton-Beam Measurements at Los Alamos", these conference proceedings.

[9] Crandall, K. R., and Rusthoi, D. P., "Documentation for TRACE: An Interactive Beam-Transport Code", Los Alamos Report LA-10235, January, 1985.

[10] Jakobson, Mark J. and Hayden, Richard J., "Dependence of Emittance Degradation on Beam Angular Momentum for Charge Exchange in Solenoid", Nucl. Instrum and Methods in Physics Research; A258, 536-541, 1987.

[11] Stevens, Ralph R., Jr., "High Current Negative-Ion Beam Transport", Sixth Int. Sym. on the Production and Neutralization of Negative Ion Beams, Brookhaven National Laboratory, 646-657, November 1992.

Important Requirements for RF Generators for Accelerator-Driven Transmutation Technologies (ADTT)

Michael T. Lynch, Paul J. Tallerico, and George Lawrence
AOT Division
Los Alamos National Laboratory
Los Alamos, NM 87545

Abstract. All Accelerator-Driven Transmutation applications require very large amounts of RF Power. For example, one version of a Plutonium burning system requires an 800-MeV, 80-mA, proton accelerator running at 100% duty factor. This accelerator requires approximately 110-MW of continuous RF power if one assumes only 10% reserve power for control of the accelerator fields. In fact, to minimize beam spill, the RF controls may need as much as 15 to 20% of reserve power. In addition, unlike an electron accelerator in which the beam is relativistic, a failed RF station can disturb the synchronism of the beam, possibly shutting down the entire accelerator. These issues and more lead to a set of requirements for the RF generators which are stringent, and in some cases, conflicting. In this paper, we will describe the issues and requirements, and outline a plan for RF generator development to meet the needs of the Accelerator-Driven Transmutation Technologies. The key issues which will be discussed include: operating efficiency, operating linearity, effect on the input power grid, bandwidth, gain, reliability, operating voltage, and operating current.

ACCELERATORS NEEDED FOR VARIOUS ADTT OPTIONS

There are many versions of ADTT which require varying amounts of beam current, beam power, and beam energy. The consistent feature in each version is a need for large amounts of continuous (CW) RF power. A selection of some of the options is shown in Table 1.

Table 1. Current, Energy, and RF power for various ADTT options.

Type of Machine	Current (mA)	Energy (MeV)	RF Power (MW-CW)
Commercial Waste Transmuter	250	1600	500
Accelerator Production of Tritium	200	1000	255
Accelerator Based Conversion (ABC) of Pu	80	800	110

It should be noted that the RF power in Table 1 is the amount of power needed for the accelerator, beam acceleration, transport losses, and control. In actuality, because each acclerator module requires a different amount of RF power, the RF generators will in general be capable of providing more power than what is needed in each module. As a result, the purchased RF generation capability will be approximately 40% above the numbers in Table 1. Therefore the range of purchased RF generation capability for the three options listed in Table 1 goes from 155 MW to 360 MW. As a point of reference the largest CW accelerators in the world are CERN in Europe (with 16 MW of CW RF) KEK in Japan (with 38 MW of CW RF). CERN is in the process of upgrading, but even after the upgrade will have 31 MW of installed CW RF power. See Table 2.

In any of the ADTT options, high beam loading is important in order to maximize the operating efficiency. In addition, to achieve the best efficiency, the match of the accelerator to the RF source is very important. A proper match is obtained with two parameters, the coupling of the drive line to the accelerator and the resonant frequency of the accelerator. In essence the coupling loop or iris acts as an impedance transformer to match the impedance of the accelerator (with beam) to the drive line impedance. In addition because the beam is not synchronized with the peak of

Table 2. A Comparison of one ADTT Accelerator with Current Accelerators

Machine	Location	Frequency (MHz)	# of Stations	Peak MW	Duty Factor	First Beam
LAMPF	LANL	805	44	55	12%	1972
LEP	CERN	352	28*	32	cw	1989
TRISTAN	KEK	508	34	38	cw	1986
SLAC	SLAC	2856	247	16000	0.03%	1966
INR-MMFL	Moscow	991	28	130	1%	1990
ABC		**350/700**	**156**	**156**	**cw**	

*by end of 1994

the RF waveform (it is typically 30° before the RF peak), it looks like a reactance to the drive system. The reactance can be eliminated by detuning the cavity (setting the resonant frequency at a frequency different from the drive frequency) so that the cavity presents a compensating reactance to the drive line. The sum of the two reactances then adds to zero. Table 3 shows the result of operation with a properly detuned and matched cavity as well as two other situations which show the effect of incorrect operation. The third column indicates that the tube must be robust. If normal operation is occurring and the beam suddenly stops because of a failure of the injector, the RF generator could see a sudden 3:1 mismatch and a reflected power level of almost 25%. If the tube cannot tolerate this type of condition, costly protection devices such as circulators must be used.

Table 3. Results of Variation of Detuning and Coupling for ABC 800-MeV CCL Cavity*

Parameter	Coupling and Detuning for Full Current	Coupling for Full Current, No Detuning	Coupling and Detuning for Full Current, I=0
Current (A)	0.08	0.08	0
Cavity Power (kW)	299	299	299
Beam Power (kW)	464	464	0
Generator Power (kW)	764	787	393
Reflected Power (kW)	0	23.5	94.1
VSWR	1.0	1.4	2.9
% Power Reflected	0	3	24

*(F=700 MHz, Synchronous Phase =-30°, Beam Loading= 60%

OVERVIEW OF RF GENERATOR PARAMETERS AND IMPACT ON THE ADTT APPLICATIONS

High voltage, operating efficiency (not saturated efficiency), gain, linearity, reliability, lifetime, cooling, ancillary power, robustness, reaction to input power grid, cost, and size are all issues for these applications. Each of the parameters can generally be traded off against one or more other parameters. For instance, the high voltage for a klystron can be reduced by operating the tube at a higher perveance (more current). However, best efficiency is obtained with a low perveance tube. In another example, each klystron can be optimized for output efficiency by varying both the current in the tube and the high voltage so as to run all tubes at constant perveance. That complicates the high voltage system in a very large way. Each klystron would

require its own high voltage system. To reduce cost and improve the reliability, we are considering the use of very large AC-DC converters and a high voltage bus for the entire set of RF generators. This allows us to borrow from the electric power industry and use AC-DC converters designed for DC power transmission systems. While this means all RF generators run at the same high voltage, there are important advantages in the lack of system complexity and in the reduced system cost. The primary disadvantage is the need for a HVDC isolation switch.

The Operating Efficiency is a key Issue

The operation of linear beam tubes (e.g. klystron, magnicon, regotron, MBK) must be near saturation in order to minimize the power lost to the collector and to maximize the efficiency. On the other hand the usual rule-of thumb is that at least 20% excess drive capability is neaded for adequate control response. These two conditions lead to conflicting requirements. The first leads to a decision that all generators will be operated with 10% or less overdrive, and the second that all generators have 20% or more. The ADTT accelerator designs make it very difficult to operate with a very small overdrive capability, simply because the power needed in each station varies throughout the accelerator. Every RF station has a different power level to achieve a specific overdrive percentage. Figure 1 shows the power needed for each module for one ADTT option. The IOT shows promise for excellent operating efficiency in the ADTT applications. Typical efficiencies for the IOT are over 70%, and the degradation in efficiency is only a few percentage points in dropping the output power to 50% of the maximum for the tube.

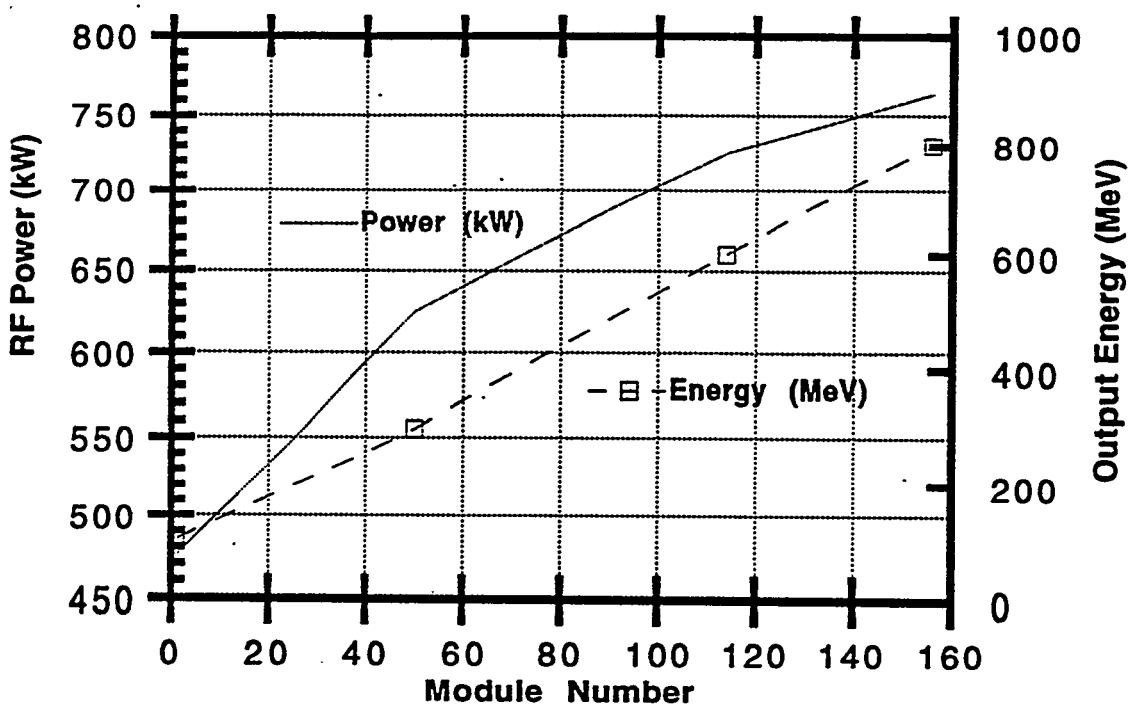

Fig. 1. RF Power and Output Energy versus Module Number for one version of an ABC

Types of RF Generators

There are several types of RF generators in addition to the klystron which can be considered for the ADTT applications. Each of the generators has features which make it attractive

for these applications and features which make it unattractive. A short list of some of the leading candidates and a brief comparison is given in Table 4. The klystron is the baseline choice for current ADTT accelerator designs, primarily because of its technological maturity. Almost all RF driven accelerators in use today use klystrons. Other devices look interesting however. One issue which must be considered with any tube choice is the impact on the power grid. If the RF is reduced because of sudden failure of the injector, the power grid could see a large transient- particularly in the high efficiency options such as the IOT or the Depressed Collector Klystron.

Table 4. A Selection of RF Generators appropriate for ADTT Applications

Type	Frequency (MHz)	CW Power (MW)	Efficiency (%)	Maturity
Klystron	352	1.3	67	Very High
IOT	267	0.25	75	Medium
Klystron-(Depressed Collector)	476	1.2	70	Medium
MBK	425	0.1	60	Low
Magnicon	700	>2.0	80	Very Low
Regotron	991	5.0	70	Very Low

Baseline RF Source: The Klystron

The klystron has been the generator of choice for RF accelerators for decades now. It is a very mature device, with long lifetimes (>30,000 hours) and robust operation (especially with the use of a circulator on the output). However, there are negative attributes of the klystron which lead one to at least consider other options. Figure 2 shows a graph of conversion efficiency of a typical klystron versus percent of maximum output power.

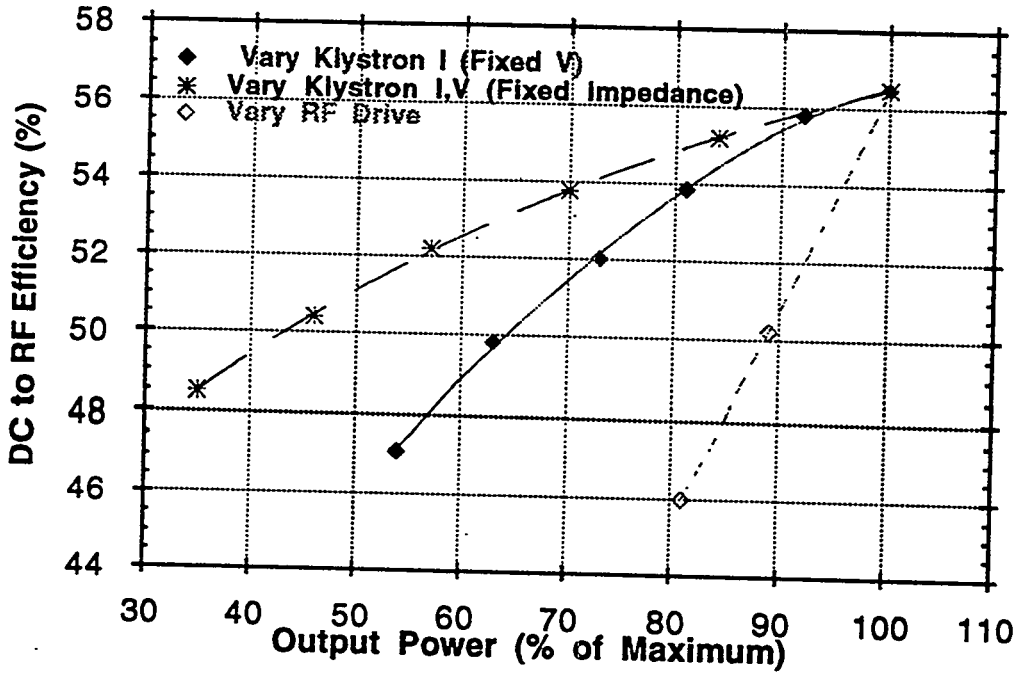

Fig. 2. Measured Output Efficiency of a klystron when output is varied by 3 different methods.

The good efficiency of the klystron (approaching 70% in the best exemples) is achieved only at saturation. The overdrive capability required for the feedback control system reduces the operating efficiency to levels much below the saturated efficiency. If the saturated power level of the klystron is not adjusted somehow and there is no input RF signal or if the input RF signal is small, then most or all of the energy in the klystron electron beam is lost as heat. If the output is varied by changing the RF drive only, the efficiency falls off linearly with output power. Dramatic improvements in the klystron operating efficiency can be made by changing the saturation condition. In one case, by changing the modulating anode voltage, the current in the kystron can be changed. This varies the outut power capability while maintaining the efficiency. This method is used on many accelerators (CERN and LAMPF are two examples). The efficiency can be maintained even higher by varying both the current and the operating voltage in the klystron to maintain constant impedance of the klystron beam.[1] This is much more complicated than just varying the klystron current, and it requires that each klystron have its own high voltage power supply..

Another property of the klystron is that it does exhibit classical saturation. The output power grows more slowly with input power as the level grows until the output achieves a maximum. In addition, while the tube is going into and past saturation, the RF phase is exhibiting large changes. These changes put very large stresses on the feedback control system. [1] Figure 3 shows the amplitude and phase variation of one type of klystron as the tube is driven into and past saturation. At levels well below saturation the gain of the klystron is constant and the loop parameters do not change. Operation near saturation (which is needed to maximize the operating efficiency) makes the setup parameters of the feedback loops very sensitive.

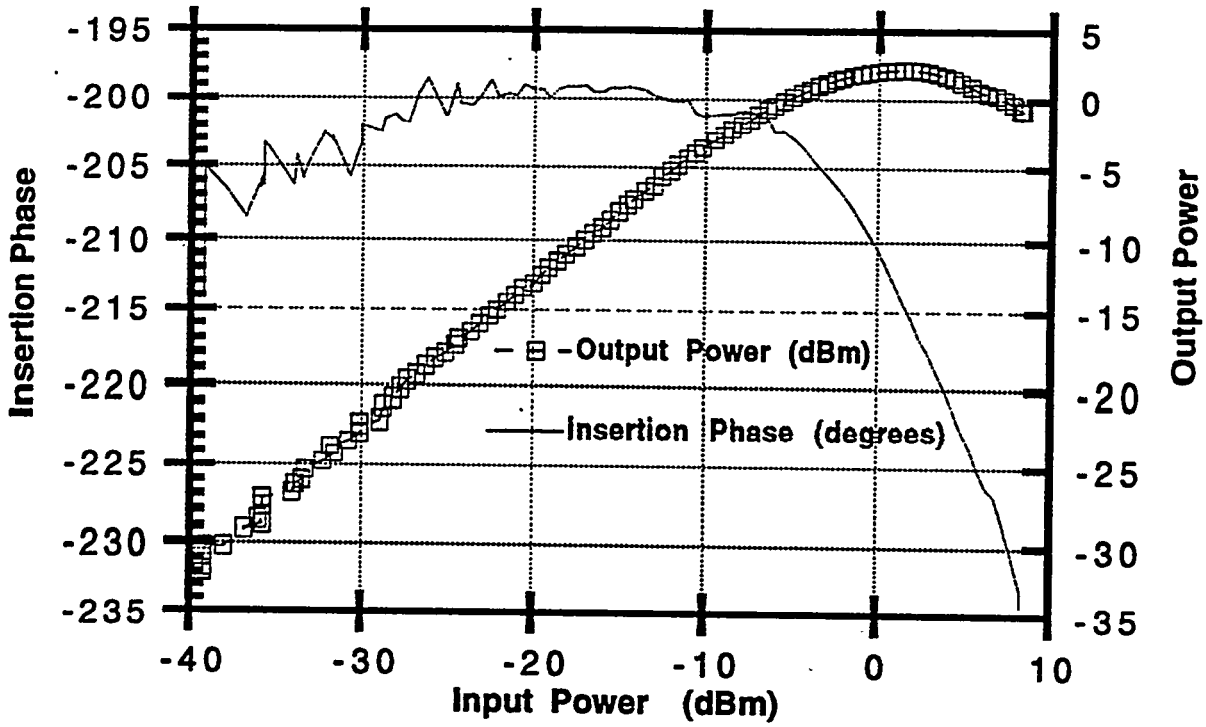

Fig. 3 Output Power and Insertion Phase versus Input Power of a Klystron

1) Method first suggested by Robert Symons and Don Laycock of Litton Electron Devices

Near saturation, the loop can be optimized and very little degradation in performance is seen-unless the output power requirements change (even by a small amount). If more power is needed, the loop gain parameters are set too low for optimal performance and the response is sluggish (at best). If less power is needed, the loop gain parameters are set too high and damped oscillations occur. The insertion phase creates corresponding difficulties for the feedback loops because the klystron exhibits large changes near saturation.

AVAILABILITY

Availability is a very important issue for any ADTT application. In all of the applications, the production plant must operate for approximately 75% of a year. This generally means that the accelerator availability must be ≥ 85%. In the energy producing versions of the ADTT, the high availability is coupled with a requirement for minimal shutdowns which might impact the production of power. The availability issues are addressed in other papers at this conference [2,3]. A key point for consideration in availability analysis is the need for all RF systems to be operating in order to have beam. This is unlike high power CW electron linear accelerators. CERN and KEK are both electron machines in which the beam is relativistic. Synchronism with the beam is not lost if one station is not operational. In a proton machine at the 1-GeV energy level, the beam is never completely relativistic. This means that the beam's velocity varies with every new acceleration. In order to maintain synchronism, the beam must see acceleration at every station. However, we have done a beam dynamics analysis that says the accelerating process continues if the RF station failure is above some energy level (> 350 MeV in this particular simulation).

An issue for the availability analysis is the commissioning process. There is often a difficult startup process in which many more tubes fail than when steady state operation is reached. The KEK Tristan project is a good example of this. A plot of the number of failed tubes versus the number of filament operating hours is shown in Figure 4. [4]

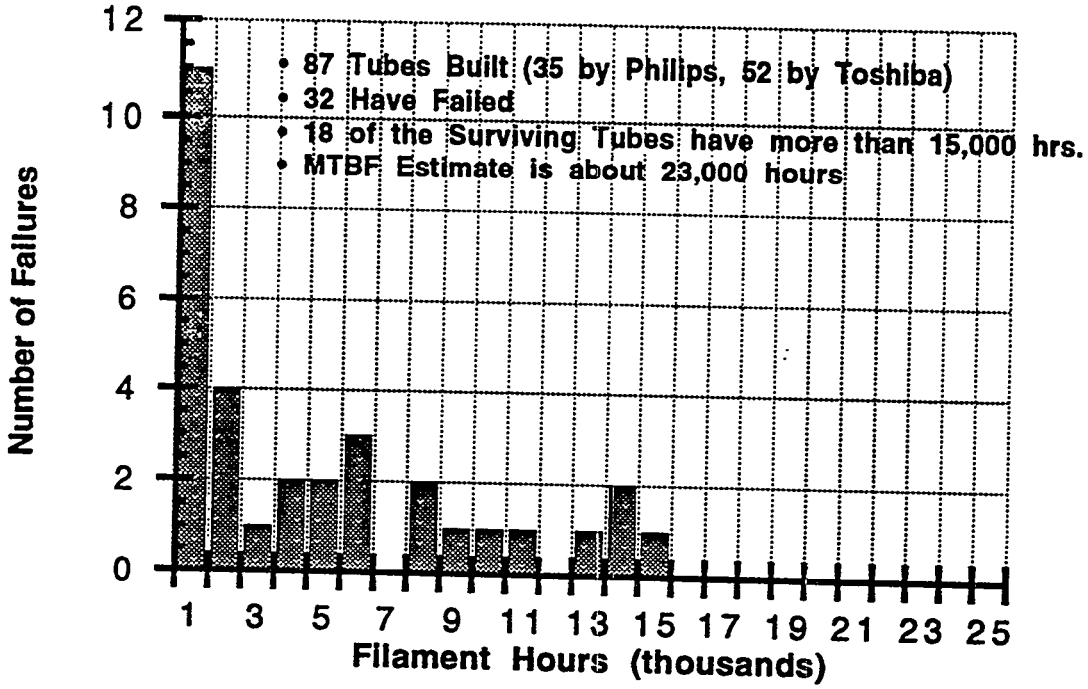

Fig.4. The number of failed klystrons vs. the filament operating hours at the KEK Tristan project

There is a very clear pattern of several early failures with a slowly decreasing failure rate. This is due to manufacuring process development, changes in the machine parameters, infant failures, etc. In order to meet the stringent availability requirements of the ADTT applications, some level of redundancy is probably needed. The important tradeoff that accompanies redundancy is increased cost and (perhaps) complexity.

TUBE DEVELOPMENT PLAN

It should be kept in mind that devlopment of a new high power RF generator can take two or more years, and an additional few years of initial operations are needed to completely solve all initial problems. A few examples will help to illustrate this point.

CERN began its operation with 16 1-MW CW klystrons in 1989. In 1990, 4 of the 16 tubes had to be replaced, and in 1991 another tube had to be replaced. The following year, no tubes were replaced. In those years they had achieved 14,000 hours of operation on the original 11 which had continued to operate successfully.

KEK has had a somewhat similar experience on the Tristan project. This project uses three different CW klystrons at 508.58 MHz. They have Philips klystrons with either 0.8 MW or 1.0 MW output power capability, and they have a Toshiba klystron with 1.2 MW output capability. There are a total of 34 klystrons installed. Figure 4 shows the number of failed tubes versus the filament operating hours.

The final choice for the RF Generator for ADTT applications needs a comprehensive study and design effort. Included in this effort must be: 1) a complete analysis of the tradeoffs, 2) prototyping of several tube options to ensure complete understanding of the tube parameters, and 3) consideration of the feedback control issues. The strict reliability requirements, the large number of generators, and the potential payback in efficiency dictate the need for this design effort.

REFERENCES

[1] Ziomek, C.D., Regan, A.H., Lynch, M.T., and Bowling, P.S., "Low-Level RF Control System Issues for and ADTT Accelerator", these proceedings (WE1-07).

[2] van Dyck, O., "LAMPF Reliability History and Program:, these proceedings (TH1-01).

[3] Tallerico, P.J., Lynch, M.T., and Lawrence, G., "Reliability and Availability Considerations in the RF and Power Systems of ATW-Class Accelerators", these proceedings (TH1-03).

[4] Isagawa, S., et al, "Operational Experience and Recent Upgrading of TRISTAN High Power CW Klystrons", Third European Particle Accelerator Conference, Berlin, Germany, March 24-28, 1992.

Low-Level RF Control System Issues for an ADTT Accelerator

C. D. Ziomek, A. H. Regan, M. T. Lynch, P. S. Bowling
Los Alamos National Laboratory, Los Alamos, New Mexico 87545

Abstract. The RF control system for a charged-particle accelerator must maintain the correct amplitude and phase of the RF field inside the accelerator cavity in the presence of perturbations, noises, and time varying system components. For an accelerator with heavy beam-loading, fluctuations in the beam current cause large perturbations to the RF field amplitude and phase that must be corrected by the RF control system. The ADTT applications require a high-current, heavily beam-loaded, continuous-wave (CW) accelerator. Additional concerns created by the CW operation include system start-up, beam interruption, and fault recovery. Also, the RF control system for an ADTT facility must include sophisticated automation to reduce the operator interaction and support. This paper describes an RF control system design that addresses these various issues by evaluation a combination of feedback and feedforward control techniques. Experience from the high-current Ground Test Accelerator (GTA) is drawn upon for this RF control system design. Comprehensive computer modeling with the Matrix$_X$ software has been used to predict the performance of this RF control system.

INTRODUCTION

The proposed design for the accelerator-driven transmutation technologies (ADTT) requires a high current, heavily beam-loaded, continuous-wave (CW) accelerator. The heavy beam-loading and the CW operation necessitate advanced low-level RF control techniques. With a 200 mA beam, the ADTT accelerator will have greater than 70% beam loading. The RF field control accuracy for an accelerator with heavy beam loading is very sensitive to fluctuations in the beam current. To enable particle acceleration, the RF field control system must be able to maintain the correct RF field amplitude and phase in the presence of strong perturbations caused by beam current fluctuations. Similar problems were addressed by the low-level RF control system for the high-current GTA accelerator [1,2]. Many of the same feedback and feedforward techniques used on GTA apply to the ADTT low-level RF control system. CW operation results in high average RF power levels that cause thermal effects within the RF system. These thermal effects cause large shifts in the resonance characteristics of the coupled-cavity LINAC (CCL) accelerating structures. Consequently, the low-level RF control system must allow efficient, reliable operation in the presence of these resonance shifts. Also, CW operation creates additional concerns regarding accelerator start-up, beam interruption, and fault recovery. It must be possible to turn on and tune up the accelerator from a variety of initial conditions, including first-time commissioning, cold starts after maintenance shutdowns, short interruptions caused by RF station faults, and extremely brief beam absences due to chopping or fast protection aborts. From the perspective of the RF system, there are only two levels of start-up modes: 1) when the beam and/or RF abort momentarily but can return to operation before the temperature changes in the CCL cavity, or 2) when the RF has been off for more than a few seconds and the CCL cavity resonance has shifted. In the first case, the low-level RF system must maintain the correct RF field level while experiencing the transient disturbances of the beam and RF switching on and off. The second case is further complicated by the resonant frequency shift and requires a method to retune the cavity to accept RF power at the design frequency. Automation is a fundamental component to the low-level RF system. Embedded computer programs perform many of the tracking and regulation functions, reducing the need for manual intervention. From the perspective of the low-level RF system, these various concerns reduce down to two basic issues: field control and resonance tracking. Figure 1 shows a simplified block diagram of a low-level RF system. This diagram depicts the fundamental components of the low-level RF system needed to perform the two basic functions. The field control electronics use a sample of the field in the RF cavity along with a beam feedforward signal to maintain the proper amplitude and phase in the RF cavity. The resonance detection electronics use the reflectometer signals to

calculate the resonance condition of the RF cavity. This calculated resonance condition is used for both frequency tracking and cavity tuning.

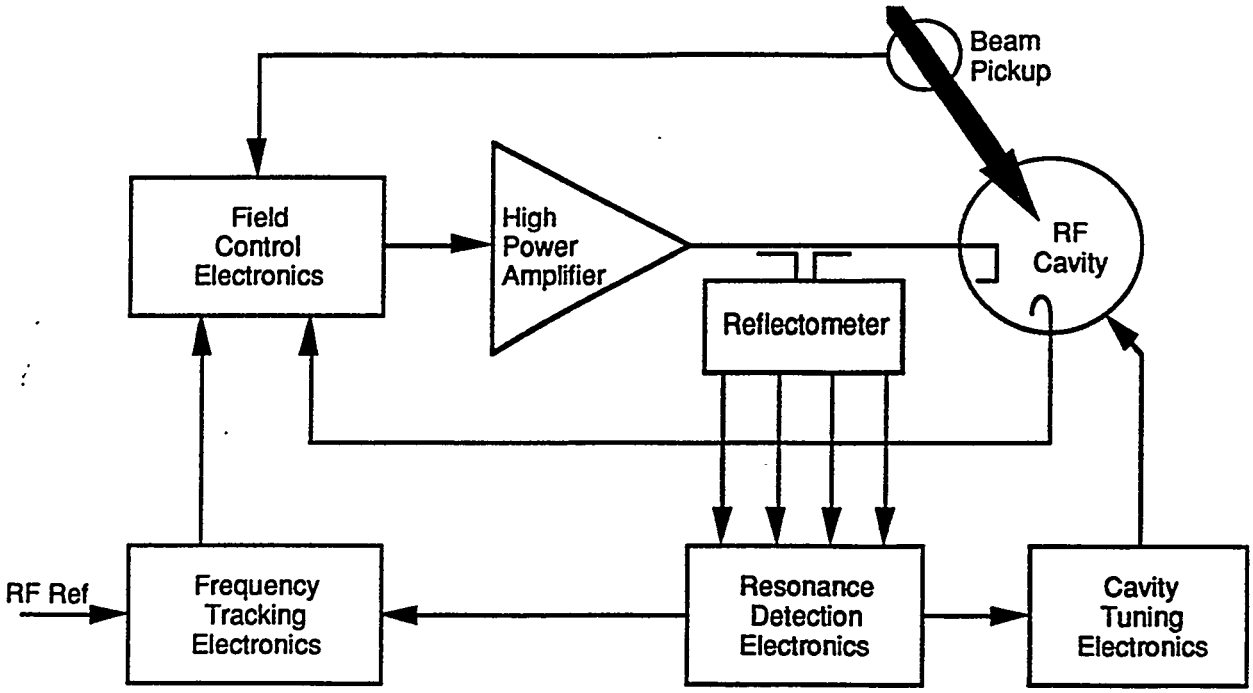

Fig. 1. Simplified block diagram of low-level RF control system for ADTT accelerator

FIELD CONTROL

The field control requirements for the ADTT accelerator address many of the preceding issues. As a fundamental objective, the low-level RF control system must regulate the RF field of each accelerator cavity at a predetermined amplitude level and phase angle. Fluctuations in beam current in the heavily beam-loaded ADTT accelerator adversely affect the cavity RF field. Beam noise and beam chopping are two phenomena that cause these fluctuations in beam current. In addition, fault conditions where the beam and/or RF abort momentarily affect the RF field control system design. The RF field control system must compensate for the transient effects of the beam and/or RF switching on and off. Faults should be resolved quickly enough to prevent the RF accelerator structure from drifting off resonance due to the loss of RF power. This allows the RF to be returned on without having to address the more complicated issue of tracking resonant frequency changes. Frequently, RF field regulation is accomplished with a feedback control system. A feedback system uses the measured RF field parameters to adjust the drive signal and maintain the correct amplitude and phase. Because an error must occur in the field output before a correction can be made, a feedback system always has an inherent bandwidth limitation and corrects low-frequency disturbances only. The modeling results indicate that a typical feedback control system operating on the ADTT accelerator can reject beam-noise disturbances in the RF field for frequencies below 10 kHz. Beam-noise frequencies between 10 kHz and 1 MHz are not completely rejected by the feedback system. The worst-case errors occur between 100 kHz and 200 kHz. Also, during CW operation, any brief beam interruptions cause transient errors in the RF field parameters that require some time for the feedback loop to respond. These transient errors also occur during beam turn-on, beam chopping, and beam-fault recovery.

Feedforward control is an enhancement to feedback RF field regulation. For a pulsed accelerator, many of the disturbances to the RF field repeat with each pulse of the accelerator. This allows adaptive feedforward techniques to be used where the past error information is used to predict the current feedforward correction function [3,4]. For a CW accelerator, disturbances

do not repeat in any definable pattern. A more direct feedforward approach must be used where a measured system input is used to predict errors in the output. For the ADTT accelerator, beam-current fluctuation is the dominant disturbance to the RF field. Consequently, the amplitude and phase of the beam current are measured and used to derive feedforward correction functions that negate any errors in the RF field parameters before they occur. The system topology for such a beam feedforward implementation requires that a single beam diagnostic sensor just after the beam source be used to derive the feedforward signals for all of the RF cavities in the system. This feedforward concept relies upon the fact that the charged-particle beam is non-relativistic at the beginning of the accelerator. Because the beam travels at less than the speed of light and the measurement signals are transmitted near the speed of light with air-core cables, the measured beam feedforward signals arrive before the beam does. This allows a correction function to be applied at the RF generator such that the beam fluctuations and a corrected RF field occur concurrently. Because the beam causes both amplitude and phase disturbances, the feedforward correction signal must include both amplitude and phase information. This requires that the amplitude and relative phase information be available from beam diagnostic sensors with bandwidths of at least 10 kHz to 1 MHz. Also, the absolute phase at each insertion point must be determined to compensate for the propagation phases within the system.

Feedforward systems tend to require frequent manual adjustments due to drifts in the gain parameters that are determined in an empirical manner. The feedforward signal levels must be consistent with the effects of the beam on the RF field parameters. If a device in the system changes (like the gain of the RF amplifier or the sensitivity of the beam diagnostics), there is no mechanism to automatically correct the feedforward signal level. As a result, feedforward systems typically require frequent manual gain adjustments. As an alternative to manual adjustments, a cross-correlation algorithm can be used to automatically adjust the feedforward signal levels. The cross-correlation algorithm uses a time-averaged product of the RF field error and beam signals. The goal is that an RF field error resulting from a beam fluctuation causes an adjustment of the feedforward signal level. Figure 2 shows a simplified block diagram of the implementation of the automatic gain adjustment. The first delay aligns the measured beam and the measured RF field error corresponding to that beam. The two aligned signals are multiplied together and the product integrated. The integrator output provides the feedforward gain function that varies over time. This gain is multiplied by the original beam signal to give a feedforward signal with the correct signal level. The feedforward signal is delayed to compensate for any excess advance resulting from the different propagation speeds between the beam and the feedforward signal and, thus, aligns the feedforward signal with the corresponding beam.

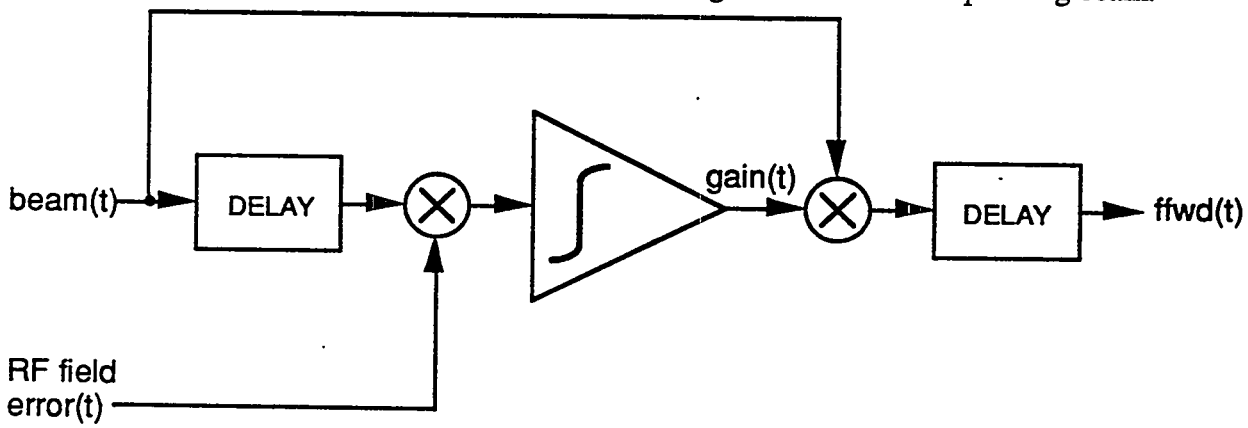

Fig. 2. Simplified block diagram of automatic beam feedforward correlation algorithm

The results of RF system simulations demonstrate that beam feedforward does enhance RF field regulation and that automatic gain adjustments are possible. Figure 3 shows the effects of beam current fluctuations of 20% on the RF field of a typical ADTT accelerator cavity. Three

control system configurations are shown: open-loop operation without a control system, regulation with a feedback control system, and combining both feedback and feedforward control systems. Notice that for beam-noise frequencies below 10 kHz, the RF field parameters are well regulated by the feedback control system. For beam-noise frequencies above 1 MHz, the damping of the narrow-band accelerator cavity negates any effects of the beam on the RF field. Beam-noise frequencies between 10 kHz and 1 MHz are not completely rejected by the feedback system, with the worst-case errors occurring between 100 kHz and 200 kHz. A beam feedforward system does reduce the RF field errors caused by beam fluctuations for the frequency range over which feedback does not function adequately (10 kHz to 1 MHz). **With both feedback and feedforward, the RF field amplitude and phase errors could be maintained at less than 0.5%/0.5° in the presence of beam current fluctuations of 20% at any frequency.** In the presence of a pulsed beam (simulating beam turn-on and interruption), the RF field fluctuations were maintained at less than 0.5%/0.5°. This indicates that the beam feedforward concept could be used to significantly improve the performance of the RF field control system.

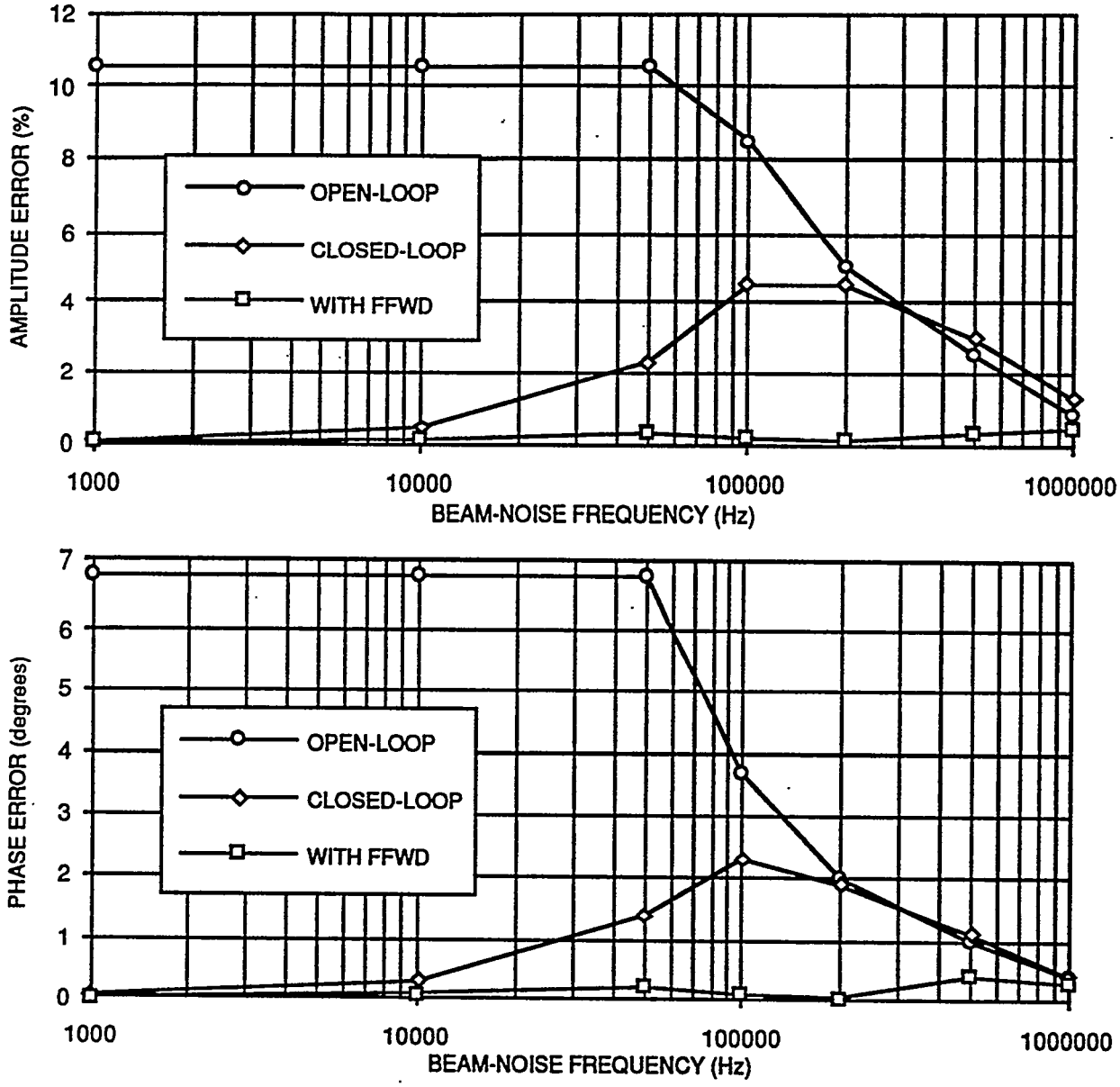

Fig. 3. RF field errors cause by 20% beam fluctuations at various frequencies.

RESONANCE TRACKING

The CW nature of the ADTT accelerator results in high average RF power levels dissipated in the accelerator structures during operation. The high-average power levels cause significant thermal changes to the RF cavities, which affect their mechanical dimensions, which in turn affect their resonant characteristics. Because an accelerator cavity has a high quality factor (Q), it accepts RF power over a narrow frequency range only. A thermal change may cause a resonant frequency shift that prohibits the cavity from accepting RF power at the fundamental machine RF frequency. The low-level RF control system must provide a resonance tracking mechanism that retunes the cavity to accept RF power at the machine frequency.

The proposed ADTT accelerator consists mainly of coupled-cavity LINAC (CCL) accelerating structures. A CCL cavity cannot be easily tuned by disrupting the fields with an external tuning mechanism like a paddle or slug. Consequently, resonance is typically maintained by regulating the temperature of the cavity, and thereby its physical dimensions and resonant frequency. The temperature is typically regulated by applying cooling water to the structure to offset the heating effects of the RF field inside the cavity. Maintaining the proper temperature in the presence of the large thermal transients at turn-on and fault shut-down has not been demonstrated to be feasible. The mixing chambers, flow valves, and other mechanical devices associated with a water cooling system respond very slowly. When the RF drive is shut down for more than a few seconds, a high Q cavity drifts off resonance due to its immediate cooling. This prevents the cavity from accepting RF power at the fundamental machine RF frequency and makes it difficult to heat the cavity back to its nominal temperature. Without an alternative heating mechanism, the system will experience long delays in achieving the proper operating temperature and frequency. Using water heating is inadequate for the same reasons that cooling water is inadequate: the response time is too slow. Also, the mechanical devices associated with water systems tend to require on-going maintenance. Consequently, another means to quickly heat a CCL cavity must be used to resolve the problems with turn-on and fault-recovery. One option is to drive the RF cavity with an alternative frequency source so that it will accept power when its resonance condition has drifted from the machine frequency. This resonance tracking system requires a swept frequency source that can search out and track the resonant frequency of the CCL cavity as its temperature changes. Once the cavity is heated to its nominal operating conditions in temperature and frequency, it can be driven at the machine frequency with the normal RF reference source. The swept frequency source is only used for structure heating and a fixed low-noise frequency source is required for accelerator operation. Figure 4 depicts the resonance tracking system.

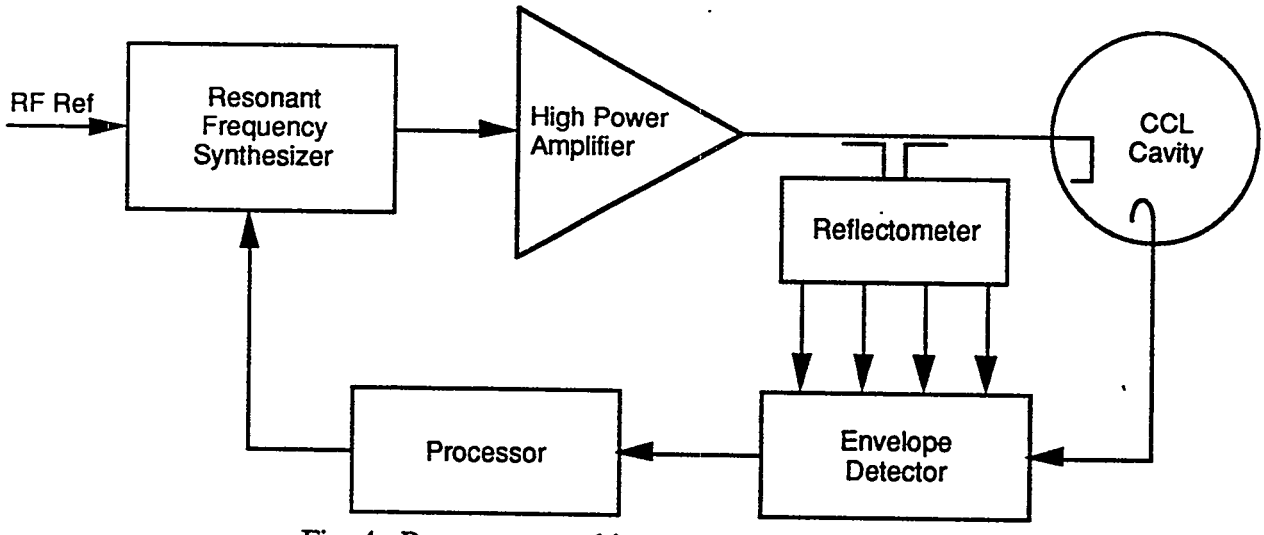

Fig. 4. Resonance tracking system block diagram.

The resonance tracking system uses a reflection analyzer to monitor the match condition between the high-power RF amplifier and the CCL cavity by measuring the incident and reflected waves in the transmission line connecting the two. The reflection analyzer is based upon an RF device called a reflectometer that enables precision transmission line measurements. The magnitudes of the reflectometer output signals are detected and converted to digital values by the envelope detector electronics. These digital values are used by the processor in an error-correction algorithm to compute the resonance condition of the CCL cavity. The resonant frequency synthesizer uses the calculated resonance condition to adjust the frequency of its output to track the resonant frequency of the CCL cavity when its temperature varies during start-up and fault-recovery situations. During normal accelerator operation, the cooling water system maintains the CCL at its nominal temperature and frequency, and the frequency-tracking functionality is disengaged.

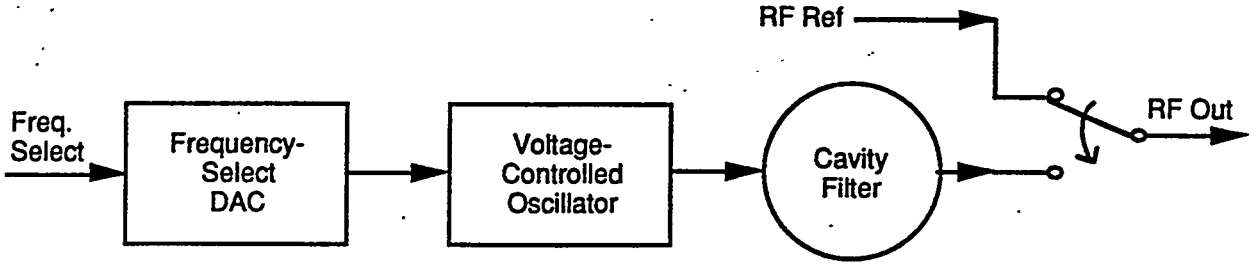

Fig. 5. Detail of VCO-based resonant frequency synthesizer.

Figure 5 shows the details of a possible Resonant Frequency Synthesizer based upon a voltage-controlled oscillator (VCO). The VCO provides a second RF source that can be switched in to replace the machine RF reference. This approach has been demonstrated on the accelerators for the Beam-Experiments-Aboard-a-Rocket and the National Institute of Standards and Technology Racetrack Microtron. The VCO would be operated in a frequency-locked loop configuration with filtering for stability and noise reduction. This configuration requires a conversion step to convert the digital processor output to the analog input needed by the VCO. Due to the noisy nature of the VCO, a stored-energy device like a resonant cavity can be used to filter out the phase noise of the VCO output. This adds size and physical complexity to the design. Also, switching between the VCO and the machine RF reference would cause a transient disturbance due to the phase discontinuity.

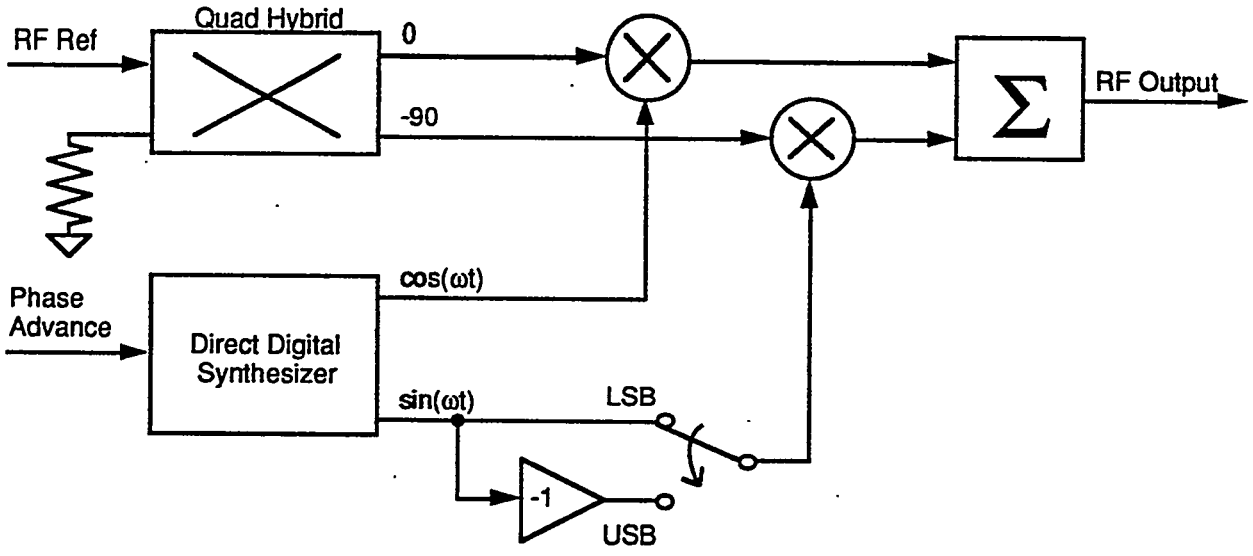

Fig. 6. Detail of DDS-based resonant frequency synthesizer.

Figure 6 shows the preferred design for the Resonant Frequency Synthesizer which is based upon a direct digital synthesizer (DDS). The DDS uses a digital phase advance value from the processor to create two sinusoidal analog IF outputs that are in phase quadrature. These IF signals are used in a single-side band heterodyne modulator to adjust the frequency of the RF output. Notice that the RF output is derived directly from the machine RF reference source. The switch allows the modulator to perform both upper and lower side-band modulation. If the phase advance is set to zero, the RF reference input passes through the Synthesizer without being affected. The DDS configuration is preferred for its simplicity and because it provides phase-continuous switching.

The entire resonance tracking system consists of electronic devices. This provides many inherent advantages including reliability, automation, and flexibility. The mathematics for the resonance tracking are accomplished using a digital processor, allowing flexibility in the resonance tracking algorithm. The algorithms could be modified for transmission measurements instead of reflection measurements. Empirical data could be added to the control algorithms. Undesired operating conditions (frequencies that excite other cavity resonance modes) could be strictly avoided. As a result, this frequency tracking system enables an ADTT accelerator to be turned on and tuned up as quickly and automatically as possible.

CONCLUSION

The low-level RF system implementation for a ADTT accelerator is feasible with little technical risk. The concepts and designs that were developed for the GTA accelerator could be modified slightly for application to an ADTT accelerator. The RF field control can be accomplished with a combination of feedback and beam feedforward. The frequency tracking can be accomplished with a reflection analyzer and an off-line RF source heating the RF cavity during turn-on and fault recovery. The implementation for this equipment should be accomplished entirely with electronic circuitry to provide the most reliable system possible. Automation should be designed into the system to take advantage of modern digital processing capabilities that will eliminate the costly hands-on operator intervention. It is not surprising that the Los Alamos Meson Physics Facility (LAMPF) is experiencing similar issues with high beam currents and quick fault recovery. The next step in this development would be to build a proof-of-principle prototype of the low-level RF equipment. This prototype should be used within experiments at LAMPF to verify and refine its functionality.

REFERENCES

[1] Jachim, S.P., et. al., "The Los Alamos VXI-Based Modular RF Control System," *Proc. IEEE Particle Accelerator Conference*, 1993.

[2] Denney, P. and Jachim, S.P., "Measured Performance of the GTA RF Systems," *Proc. IEEE Particle Accelerator Conference*, 1993.

[3] Ziomek, C.D., "Adaptive Feedforward in the LANL RF Control System," *Proc. LINAC Conference*, 1992.

[4] Ziomek, C.D., et. al. "Results of Adaptive Feedforward on GTA," *Proc. IEEE Particle Accelerator Conference*, 1993.

Overview of Superconducting RF Technology and its Application to High-Current Linacs

J. R. Delayen, C.L. Bohn
Argonne National Laboratory, Engineering Physics Division
9700 South Cass Avenue, Argonne, Illinois 60439

Abstract. Superconducting linacs may be a viable option for high-current applications such as copious neutron production like that needed for transmutation of radioactive waste. These linacs must run reliably for many years and allow easy routine maintenance. Superconducting cavities operate efficiently with high cw gradients, properties which help to reduce operating and capital costs. However, cost effectiveness is not the sole consideration in these applications. For example, beam impingement must be essentially eliminated to prevent unsafe radioactivation of the accelerating structures, and thus large apertures are needed through which to pass the beam. Because of their high efficiency, superconducting cavities can be designed with very large bore apertures, thereby reducing the effect of beam impingement.

I. INTRODUCTION

Questions regarding the design of linear accelerators with high duty factor for the long-term production of high-current ion beams center as much on beam physics as on hardware. The pervasive concern is whether dynamical phenomena which generate a diffuse halo of beam particles can be sufficiently controlled to limit radioactivation induced by beam impingement to safe levels. For example, as indicated in Section III below, the maximum tolerable amount of beam impingement is of the order of 0.03 nA/m for 1 GeV protons. The heat load associated with this level of impingement is 30 mW/m. The rf losses on a superconducting cavity will be ~20-40 W/m, and therefore radioactivation is by far the dominant concern related to beam impingement on superconducting structures. This concern is equally important for copper accelerators. Because shunt impedance is of less concern in superconducting cavities, they can be designed to operate at low frequency and with large bore-hole apertures to mitigate impingement. These constitute additional degrees of freedom which are available in the design of high-current linacs. In Section IV below, we provide four generic superconducting cavity geometries designed specifically for use in these high-current linacs.

II. SUPERCONDUCTING ACCELERATORS

Superconducting accelerators now have a long history which spans almost 20 years [1-8]. Both low-velocity ion (and proton) accelerators and high-energy electron accelerators have been developed and are operating. With the exception of a few high-energy electron accelerators, all of them have been low current machines where the power delivered to the beam was much smaller than the rf power which would have been required had the accelerator been normal-conducting. The main driver in the development of superconducting accelerators has been the substantial reduction of electrical power required to achieve the beam energy. As the beam current is increased the rf power delivered to the beam also increases and, if the current is sufficiently high, even a normal-conducting accelerator becomes beam loaded. Thus, for very

high-current beams, the relative reduction in power provided by superconductivity is not large, while the absolute reduction remains approximately the same.

Another important characteristic of superconducting cavities and accelerators is that they can sustain high cw gradients. This usually translates into accelerators which are substantially shorter than their normal-conducting counterparts and a corresponding reduction in construction and capital costs. As the beam current is increased, however, the maximum operating gradient will not be set by the maximum value that can be sustained by the cavities but by the maximum amount of rf power that can be transmitted by each coupler from room temperature to cryogenic temperature. For accelerators of the ATW class it is expected that, indeed, the couplers would limit the achievable gradient otherwise attainable but that it still would be higher than that of a normal-conducting accelerator.

Superconducting accelerators (especially at low velocity) have traditionally been built from a large number of small, independent accelerating cavities. The main reason is that those accelerators had to be able to accelerate particles with widely different charge-to-mass ratio and thus had to be able to tailor their velocity profile to the particle to be accelerated. This feature had the added advantage that each cavity could be operated at its optimum field value instead of at a predetermined design value. Additionally, these accelerators displayed very good reliability and availability since they could operate in the presence of a number of local point failures-- all that was needed was to readjust the phase and amplitude of the cavities past the failure point. This enhanced reliability could be of major importance in accelerators of the ATW class which must provide high availability. The amount and location of point failures that can be tolerated would, however, be dependent on the beam current and would be determined by detailed beam dynamics studies. Preliminary studies on a deuteron accelerator for IFMIF indicate that loss of a cavity or focusing element could be tolerated while maintaining a reasonable bunch size and beam emittance.

While all the previous considerations have been crucial for low-current superconducting accelerators and may still be important for high-current accelerators, the main advantage that the superconducting technology may have for the latter is in offering a way to reduce beam loss and activation of the accelerator, thus possibly allowing hands-on maintenance instead of the required remote maintenance when beam loss exceed a certain value. Because the surface resistance of superconductors is a quadratic function of frequency, it is usually more efficient to design superconducting accelerators for lower frequencies than one would for normal-conducting ones. Thus a large bore size is often a natural feature of superconducting structures. Additionally, since optimizing the shunt impedance of a superconducting structure is not an overarching consideration as it is in the case of normal-conducting structures, at a given frequency, the former can be designed with much larger apertures than optimal, further reducing the amount of beam impingement.

III. LIMITS ON PERMISSIBLE RADIOACTIVATION

Studies of the amount of beam impingement that can be tolerated while still allowing hands-on maintenance have been done in the case of 35 MeV deuteron accelerators. Typically,

dose rates of the order of 2 mrem/h, 30 cm from the accelerators and 24h after shutdown are obtained for beam losses of the order of 1 nA/m for either copper or niobium [9].

For high-energy proton accelerators, detailed calculations are much more difficult to perform. Neutron yields increase with higher Z for proton bombardment; the range of 1 GeV protons in both niobium and copper is of order 40 cm,[2] and, because the wall thickness of the cavities is much less than the range, radioactivation of niobium should be slightly more, but comparable to, that of copper. Thus, for a proton beam, the current loss in both niobium and copper needs to be less than 0.2 nA/m at 200 MeV, and less than 0.03 nA/m at 1 GeV, to be under 2.5 mrem/hr at a distance of 1 m from the linac one hour after shutdown [10].

IV. SUPERCONDUCTING STRUCTURES

1. General considerations

Geometries of low-velocity superconducting resonators generally incorporate an inner conductor which provides a TEM-like accelerating mode [11]. The center-gap to center-gap distance in these structures is of order $\beta\lambda/2$, where $\beta=v/c$ is the beam velocity, and λ is the rf wavelength. For velocities less than $\sim 0.1c$ and frequencies of several hundred MHz, this distance becomes too small for practical resonators, and this consideration is a principal motivator for superconducting RFQs which provide proton energies to ~ 8 MeV [12]. For proton energies ranging from 8 MeV to 2 GeV, the corresponding velocity range is $\beta=0.1$-0.9. Superconducting resonators have recently been developed for frequencies in the range 350-850 MHz and optimized for velocities up to $\beta=0.3$. Off-line experiments with these structures have yielded high accelerating gradients [13,14]. Of these structures, the easiest to fabricate is the spoke resonator shown in Fig. 1. This geometry is also modular, for several units can be stacked together to make a multigap cavity. For these reasons, we use the spoke as the baseline geometry for superconducting cavities to be used in high-current linacs.

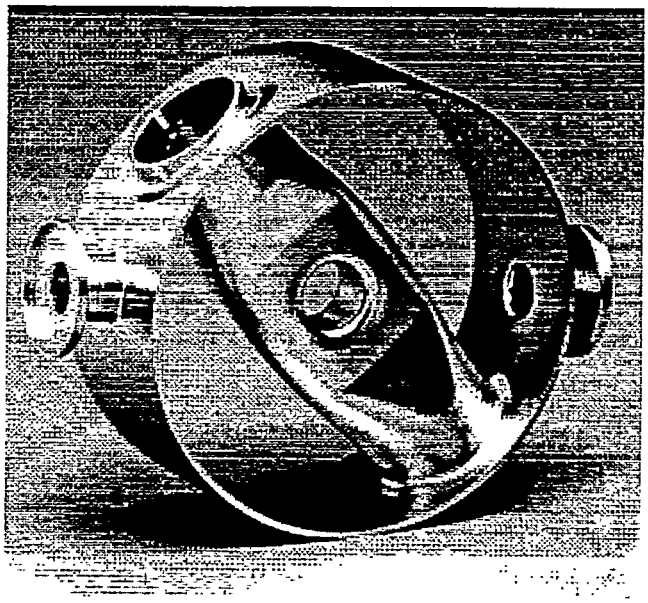

Figure 1. 850 MHz, $\beta=0.28$, 2-gap spoke resonator prior to the welding of the end plates.

The choice of frequency hinges on a number of considerations. One of them is the ability to provide large-bore apertures for the beam, and this favors lower frequencies and larger cavities. Large bores also provide lower transverse shunt impedances which reduce cumulative beam breakup. The availability of rf power is a second concern.

On the other hand, it has been inferred from numerical simulations that high frequencies mitigate emittance growth by lowering the charge per bunch [15]. This is a major consideration when emittance preservation is crucial. For most of the high-current applications, however, emittance growth is a concern only in connection with halo formation and beam transport. A detailed understanding of the effects of bunching on high-current beams is a fundamental building block for the design of these linacs, and this will be the topic of future investigations.

One possible strategy for achieving high currents is to combine two beams by funneling them together at a relatively low energy, a process which doubles the rf frequency. To achieve large bores and use a common frequency for rf power amplifiers, we shall assume the linac operates at 350 MHz, and that prior to funneling, the frequency is 175 MHz.

2. Large-bore superconducting cavity geometries

As shown in the examples of Figs. 2 and 3, the spoke geometry can be adapted to span a wide velocity range. For high velocities it becomes more practical to introduce single-cell structures like that shown in Fig. 4, or multicell structures like that shown in Fig. 5. The properties of these large-bore geometries, which were calculated with MAFIA in the case of the spoke resonators and SUPERFISH in the case of the "elliptical" cavities, are given in Table 2 below. In the Table, resonators #1-#4 refer to the 175 MHz, ß=0.125 spoke, the 350 MHz, ß=0.45 spoke, the 350 MHz, ß=0.45 single-cell, and the 350 MHz, ß=0.8 two-cell, respectively.

Compared to two-gap spoke resonators, two-cell "elliptical" cavities generally have higher shunt impedances and lower rf surface fields. They are also comparatively simple and easy to fabricate. However, for a given frequency, these structures are also much larger than the spoke, and are likely to be less mechanically rigid.

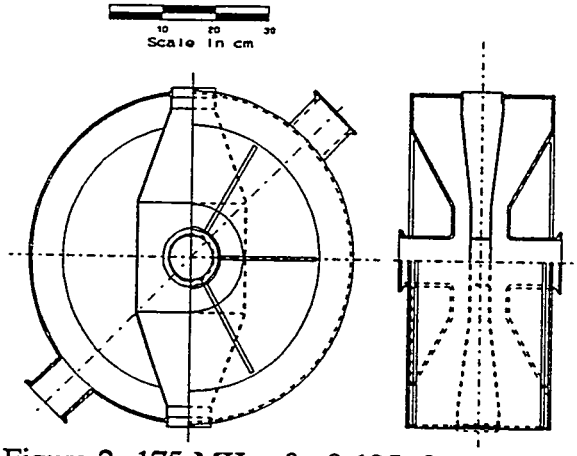

Figure 2. 175 MHz, β=0.125, 2-gap spoke resonator.

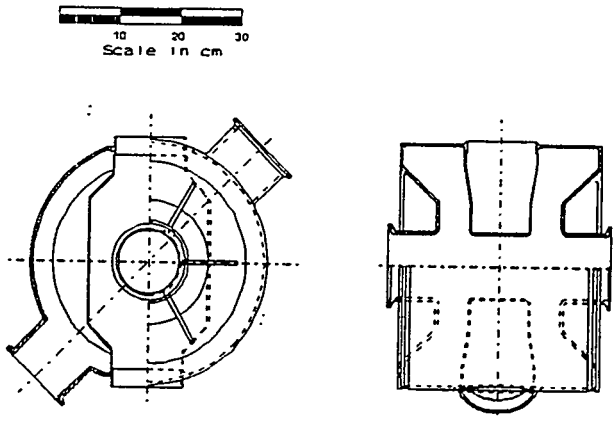

Figure 3. 350 MHz, β=0.45, 2-gap spoke resonator.

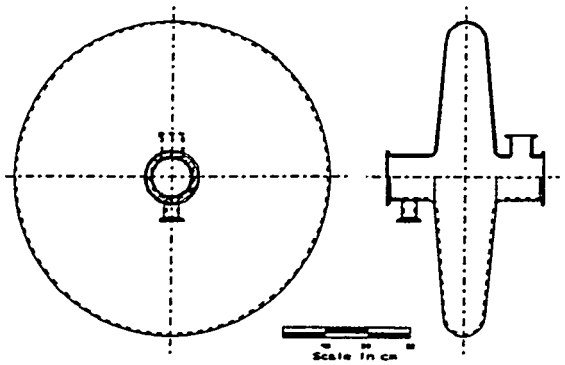

Figure 4. 350 MHz, β=0.45, single-cell TM_{010} resonator.

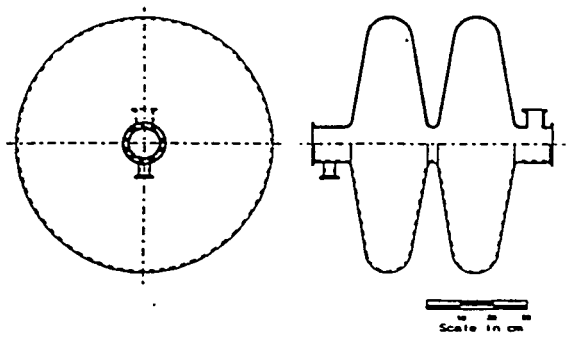

Figure 5. 350 MHz, β= 0.8, 2-cell TM_{010} resonator.

Table 1. Comparison of resonator properties.

	#1	#2	#3	#4
B_p/E_{acc}[G/(MV/m)]	122	125	41.6	35.9
R_{sh}* (10^5 MΩ)	1.3	1.5	1.2	6.7
R_{sh}/Q (Ω)	47.1	121	51.3	205
P (W)*†	2.73	9.65	9.0	14.5
ΔV (MV)†	0.6	1.2	1.0	3.1
Diameter (cm)	60	38	74	76

*Assumes BCS R_s at T = 4.2 K, †At E_{acc} = 6 MV/m.

It remains to be determined where to transition from the spoke geometry to multicell structures in a full linac design. It is also of interest to determine the optimum number of gaps or cells for each structure. Beam dynamics and the availability of rf power influence this question. The required lattice period of focusing elements will be shorter at lower velocities. A requirement that the linac be operable when one or more structures have failed will place an additional constraint on structure length. The amount of rf power which may be input to the cavity will be limited by the capability of the coupler, and this places the most stringent restriction on structure length in high-current linacs.

V. CONCLUSIONS

Radiofrequency superconductivity offers a number of advantages for high-current, high-duty-factor linacs, among these is the ability to open up the cavity apertures to mitigate beam impingement and its associated radioactivation. The cavities also may be expected to operate at a higher real-estate gradient than their normal-conducting counterparts. There are no known show-stoppers for rf superconductivity in these applications; the associated beam physics is beginning to be understood [16-18], and appropriate accelerating structures have been designed.

An important uncertainty in the design of these linacs is the projected capability of rf power couplers. Coupler development and continued beam-physics research are key components of the development path. A more important and fundamental component, however, is a high-current ion-beam test of superconducting structures [13].

ACKNOWLEDGEMENTS

This work was supported by the U.S. Department of Energy under contract W-31-109-ENG-38 and by the Accelerator Operation & Technology Division, Los Alamos National Laboratory, under contract 9142K0014-2R.

REFERENCES

[1] Proceedings of the Workshop on Rf Superconductivity, Karlsruhe, Germany, 2-4 July 1980. M. Kuntze Ed., KfK Report 3019.

[2] Proceedings of the Second Workshop on RF Superconductivity, CERN, Switzerland, 23-27 July 1984, H. Lengeler Ed.

[3] Proceedings of the Third Workshop on RF Superconductivity, Argonne National Laboratory, 14-18 September 1987, K.W. Shepard Ed., ANL report ANL-PHY-88-1.

[4] Proceedings of the Fourth Workshop on RF superconductivity, KEK, Japan, 14-18 August 1989, Y. Kojima Ed., KEK Report 89-21.

[5] Proceedings of the Fifth Workshop on RF superconductivity, DESY, Germany, 19-23 August 1991, D. Proch Ed., DESY Report M-92-01.

[6] Proceedings of the Sixth Workshop on RF Superconductivity, CEBAF, 4-9 October 1993.

[7] Bollinger L., "Superconducting Linear Accelerators for Heavy Ions", *Ann. Rev. Nucl. Part. Sci.*, **36**, 475-503 (1986).

[8] Proch D., "SRF Cavities for Future Applications", in *Proc. of the 1993 Particle Accelerator Conference*, p. 758.

[9] Delayen J.R., C.L. Bohn, B.J. Michlich, C.T. Roche, L. Sagalovsky, in *Proc. of the 1993 Particle Accelerator Conference*, p. 1715.

[10] N.I. Golubeva, A.S. Pashnekov, Yu.V. Senichev, and E.N. Shaposhnikova, "Problems of Beam Loss in Intense Ion Linear Accelerators", *Proceedings of the 1988 Linear Accelerator Conference*, 669 (1988).

[11] J.R. Delayen, C.L. Bohn, and C.T. Roche, "Niobium Resonator Development for High-Brightness Ion Beam Acceleration", *IEEE Trans. Magnetics*, **MAG-27**, 1924 (1991).

[12] J.R. Delayen, C.L. Bohn, W.L. Kennedy, L.Sagalovsky, "Design Considerations for High-Current - Superconducting RFQ", *Proc. 1993 Particle Accelerator Conference*, p. 838

[13] J.R. Delayen, C.L. Bohn, W.L. Kennedy, G.L. Nicholls, C.T. Roche, and L. Sagalovsky, "Recent Developments in the Application of RF Superconductivity to High-Brightness and High-Gradient Ion Beam Accelerators", *Proceedings of the 5th Workshop on RF Superconductivity*, **DESY Report No. M-92-01**, 376 (1992).

[14] J.R. Delayen, W.L. Kennedy, and C.T. Roche, "Design and Test of a Superconducting Structure for High-Velocity Ions", *Proceedings of the 1992 Linear Accelerator Conference*, **AECL Report No. 10728**, pp. 695-697 (1992).

[15] T.P. Wangler, "High-Brightness Injectors for Hadron Colliders", in Frontiers of Particle Beams: Intensity Limitations, (Springer-Verlag, Berlin, 1992), pp. 542-561.

[16] C.L. Bohn, "Transverse Phase-Space Dynamics of Mismatched Charged-Particle Beams", *Phys. Rev. Lett.*, **70**, 932 (1993).

[17] C.L. Bohn, J.R. Delayen, "Fokker Planck Approach to the Dynamics of Mismatched Charged-Particle Beams", *Phys. Rev. E*, **50**, August 1994 (in press).

[18] C.L. Bohn, J.R. Delayen, "Mechanisms of Beam-Halo Formation in High-Intensity Linacs", these proceedings.

Basic Aspects of Spallation Radiation Damage to Materials

Monroe S. Wechsler*, Chubin Lin* and Walter F. Sommer+
*Department of Nuclear Engineering, North Carolina State University, Raleigh, North Carolina 27695
+Los Alamos National Laboratory, Los Alamos, New Mexico 87545

Abstract. The nature of radiation effects, as learned from investigations using reactor neutron irradiations, is reviewed, and its relevance to spallation radiation damage to materials in accelerator-driven neutron sources is discussed. Property changes upon irradiation are due to (1) displaced atoms, producing vacancy and interstitial defect clusters, which cause radiation hardening and embrittlement; (2) helium production, the helium then forming bubbles, which engenders high-temperature grain-boundary fracture; and (3) transmutations, which means that impurity concentrations are introduced. Methods for analyzing displacement production are related, and recent calculations of displacement cross sections using SPECTER and LAHET are described, with special reference to tungsten, a major candidate for a target material in accelerator-driven neutron systems.

INTRODUCTION

Accelerator-driven transmutation technologies (ADTT) rely on the production of spallation neutrons that occurs when high-energy protons are incident upon target materials lying in their path. To increase the number of spallation neutrons produced, a heavy target material is strongly preferred. As is pointed out in a recent report on the selection and qualification of materials for the accelerator transmutation of waste project [1], the target of choice may be tungsten or a tungsten alloy. In illustrating basic aspects of spallation radiation damage, we shall attempt to concentrate on radiation effects on tungsten.

By far, the preponderance of information concerning radiation effects on materials stems from studies of the effects of fission neutrons in nuclear reactors. The reactor neutrons in the fission spectrum have a most probable energy of about 0.6 MeV and an average energy of about 1.9 MeV. By contrast, the neutrons in ADTT spallation facilities have energies that extend up to the incident proton energy. For spallation to take place, the protons incident on materials must have a DeBroglie wavelength, λ, (given by $\lambda = h/p$, where h is Planck's constant and p is the proton momentum) that is short compared to the size of the target nucleus. As a result, the protons that produce spallation neutrons will have energies above several hundred MeV and typically near or above 1000 MeV, and the resulting spallation neutrons will extend up to these energies as well. A question of major importance is the extent to which radiation effects due to reactor neutrons can be safely applied to spallation systems where the neutron energies extend up to energies that are so much higher than those in a nuclear reactor.

RADIATION EFFECTS ON MATERIALS

True solids are, of course, characterized by a crystal structure, i.e., by the arrangement of atoms in a regular periodic array of lattice atoms. The major type of radiation damage to materials stems from the *displacement* of lattice atoms resulting from the collision of the projectile particle upon the target atom or from the recoil energy that the atom receives upon emission of a nuclear particle, for example the atom recoil upon absorption of a neutron and emission of a

capture gamma ray. The critical transferred energy to allow the struck or recoiling atom to be displaced is known as the threshold displacement energy, T_d . Typical values are 25 eV for Al, 30 eV for Ti and Cu, 40 eV for Cr, Fe, Co, and Ni, 60 eV for Nb and Mo, and 90 eV for W [2,3]. When an atom is displaced from its lattice site and comes to rest in between lattice atoms, a vacancy and an interstitial have been created. The vacancies may aggregate together and similarly for the interstitials, forming vacancy-type and interstitial-type *defect clusters.* These defect clusters may be observed in the electron microscope, and they are primary agents for causing radiation hardening and embrittlement.

While neutron irradiations have been the principal tool for studying radiation effects on materials, electron irradiations have been useful in the determination of T_d. Electrons, typically from a Van de Graaff accelerator, bombard a wire or foil of the target material, and the electrical resistivity increase per unit electron fluence is measured as a function of electron energy. The T_d is then determined by the value needed to get best agreement to the shape of the curve as calculated theoretically using analyses similar to the ones presented by Oen [4]. The reason for using electrons instead of neutrons in determining T_d lies in the fact that electron beams can be employed at energy levels (below about 5 MeV) such that only a few displacements are created even in a head-on collision. By contrast, a single neutron-atom collision can result in many displacements. Consider a reactor neutron of energy E = 1 MeV making a head-on collision with a tungsten atom at rest. The energy transferred to the tungsten atom in such an elastic collision is given by

$$T = T_{\max} = \frac{4mM}{(m+M)^2} E = \frac{4A}{(1+A)} E \tag{1}$$

where m and M are the masses of the neutron and tungsten atom, respectively, and A is the atomic weight of tungsten. Since for tungsten $A \cong 184$, we see that $T_{max} \cong 0.022$ MeV. Thus, since T_d is only 90 eV, there is enough transferred energy not only to displace the primary struck atom, but also to produce many secondary displacements as the primary struck atom strikes other atoms and they in turn strike still other atoms, resulting in a displacement cascade. In order for the electron to produce a displacement in a head-on collision with a tungsten atom, the electron must have an energy greater than its rest energy of 0.511 MeV. Therefore, the relativistic form of (1) must be used, viz.,

$$T_{\max} = \frac{2ME(E+2m_e c^2)}{(m_e+M)^2 c^2 + 2ME} \tag{2}$$

where m_e and E are the mass and energy of the electron, M is the mass of the target atom, and c is the speed of light. For electrons of energies below 5 or 10 MeV, (2) may be approximated by

$$T_{\max} = \frac{2E(E+2m_e c^2)}{Mc^2} \tag{3}$$

and for 5 MeV electrons on tungsten we find that T_{max} is only about 350 eV. As a result, electron radiation damage is largely a reflection of isolated single displacements, with less complication due to the aggregation of vacancies and interstitials into defect clusters than is the case for neutron radiation damage. One measure of this may be found in the report by Oen [4] where calculated cross sections are given for a primary collision between an electron and a lattice atom, σ_P, and for producing a displacement, σ_d. For 5 MeV electrons on tungsten with $T_d = 90$ eV, we find by interpolating data in [4] that $\sigma_P = 53.6$ b and $\sigma_d = 57.3$ b. The fact that σ_d is only slightly

higher than σ_P indicates that most of the electron-atom collisions do not produce more than one displacement.

An issue of some importance for radiation effects due to neutrons is how the moving struck atom partitions its energy between nuclei and electrons as it moves through the material. At lower energies the moving atom delivers energy mostly to nuclei producing secondary displacements, and at higher energies to electrons producing ionization and electronic excitation, but causing no lasting effect in metals. At one time, displacement cross sections were calculated using the concept of an ionization cutoff energy, T_I, given as a rule of thumb by the atomic mass number in keV. Thus, a moving tungsten atom would give its energy to the electron system until its energy fell below ~184 keV, at which point it delivered energy only to nuclei and produced displacements. However, Lindhard and co-workers [5] developed a more sophisticated approach in which there is a gradual transition from electronic energy loss to nuclear energy loss as the moving atom is slowed down. This has given rise to the concept of *damage energy*, T_{dam}, the portion of the energy of the moving atom that is transferred to nuclei. T_{dam} is given by

$$T_{dam} = \xi(T)\, T \tag{4}$$

where T is the recoil energy transferred to the primary knocked-on atom (PKA), e.g., the energy transferred to a tungsten atom by an incident neutron. Figure 1 shows the representation by

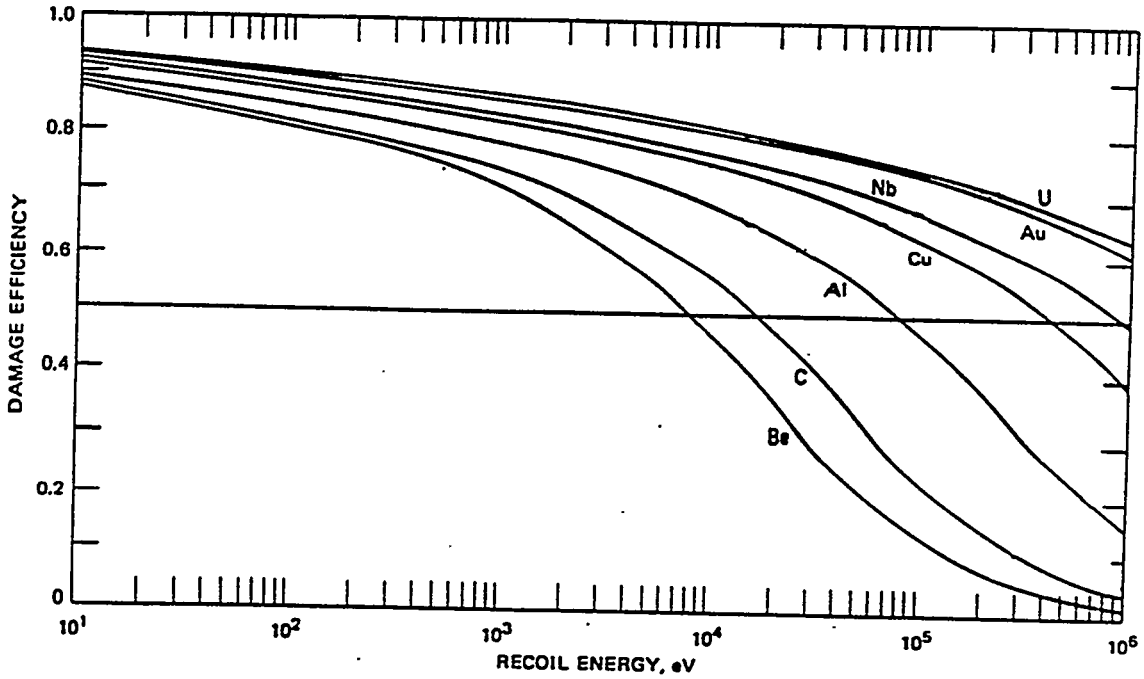

Fig. 1. Damage efficiency $\xi(T)$ versus transferred recoil energy, T. After [5,6],

Robinson [6] based on the Lindhard model for the damage efficiency $\xi(T)$ for various irradiated materials. In recent years, the convention has developed to express the number of displacements resulting from a PKA of damage energy T_{dam} as

$$n_d = \beta T_{dam}/2T_d \tag{5}$$

where $\beta = 0.8$ is intended to compensate for forward scattering in the displacement cascade and the factor 2 in the denominator is to allow for energy loss in subthreshold interactions. In connection with Eq. (1), above, we noted that a 1 MeV neutron transfers about 22,000 eV to a

tungsten atom in a head-on collision. Fig. 1 indicates that the corresponding damage efficiency for tungsten is about 0.8, so that Eq. (4) gives T_{dam} = 17,000 eV, and Eq. (5) suggests that the resultant number of displacements is about 77. Furthermore, one defines a damage energy cross section σ_E with typical units b keV, where σ_E is the rate of damage energy transferred per lattice atom per unit flux. For elastic collisions, the damage energy cross section is given by

$$\sigma_E = \int \sigma_T'(E,T) T_{dam} dT \tag{6}$$

where σ_T'(E, T) is the differential scattering cross section for transferring energy within unit energy range at T by a neutron of energy E and the integral is taken normally from T_d to T_{max}. The rate of energy transfer to the lattice atoms is given by

$$K_E = \int_0^\infty \sigma_E \phi_E' dE \tag{7}$$

where ϕ_E' is the differential flux. By (5), the displacement cross section is related to the damage energy cross section by

$$\sigma_d = (\beta / 2T_d)\sigma_E \tag{8}$$

and the spectrum-average displacement cross section is

$$<\sigma_d> = \frac{\int \sigma_d \phi_E' dE}{\int \phi_E' dE} \tag{9}$$

The above discussion of energy transfer to lattice atoms is framed largely in terms of elastic collision interactions. Substantial energy can be imparted to atoms, however, due to recoil from inelastic interactions. Reference [7] shows for 1 MeV neutrons on tungsten that 36.7% of the reactions are inelastic; at 14 MeV the fraction is 8.9%. Also, recoil from (n,γ) reactions may be important for ADTT systems since they employ highly thermalized neutrons for which the (n,γ) cross section is high. For thermal neutrons on tungsten, [7] indicates that (n,γ) reactions comprise 78.4% of the total and elastic reactions 21.6%. When a capture gamma ray of energy E_γ is emitted, its momentum is $p_\gamma = E_\gamma/c$, and to conserve momentum the atom acquires this momentum also. If the atom mass is M after absorbing the neutron, its recoil energy is

$$T_R = \frac{p_\gamma^2}{2M} = \frac{E_\gamma^2}{2Mc^2} \tag{10}$$

If we consider a typical tungsten atom to have mass number 185 after absorbing a neutron, then we calculate that the gamma ray energy to produce a recoil energy of $T_R = T_d$ = 90 eV is about 5.6 MeV. Since many capture gamma rays may have energies greater than this, we may expect displacement production in tungsten due to (n,γ) capture events. The energy balance or Q-value for the capture (n,γ) reaction in tungsten is listed in [7] as 7.4 MeV. Radiation damage in metals due to thermal neutron capture (n,γ) events was studied by Coltman et al. [8].

Radiation damage calculations using the SPECTER code [9] are presented below. SPECTER contains displacement and damage energy cross section libraries for 38 elements, including separate outputs for the tungsten isotopes of mass numbers 182, 183, 184, and 186. The displacement calculations are based on the DISCS program [10], they embrace elastic and inelastic scattering including thermal neutron capture (n,γ) events, and they assume the Lindhard model to partition the available recoil energy into nuclear and electronic components. In addition, cross sections are given for gas production, and PKA energy distributions are also available. The underlying cross sections stem from the ENDF libraries [11], and they extend up to neutron energies of 20 MeV.

It should be realized that the calculations of displacement production do not take into account the annealing of radiation-produced defects that will occur during irradiation at ambient temperatures or upon warming up following low temperature irradiation. Annealing stages tend to be keyed to the absolute melting temperature, and since tungsten melts at such a high temperature (3410 C), annealing stages are expected to be quite elevated in temperature for tungsten. Coltman et al. [12] have neutron-irradiated tungsten at 4.2 K and observed the annealing out of the radiation-induced increase in electrical resistivity as a function of isochronal annealing temperature. As shown in Fig. 10 of [13], about 75% of the resistivity increment remains upon annealing up to 140 K. In addition, Keys et al. [14] studied the high-temperature annealing of tungsten after neutron irradiation at ~70 C. Three resistivity annealing stages were observed: at 100-450 C, 450-650 C, and 650-1000 C. There was also some residual radiation-induced resistivity remaining after annealing up to 1900 C, which is believed to be due to the formation of rhenium.

SPALLATION RADIATION DAMAGE

As mentioned above, spallation occurs when the energy of a proton incident on matter is so high and its deBroglie wavelength so short that the proton is able to interact with individual nucleons in the nucleus. As envisaged by Serber [15], spallation reactions take place in two stages: an intranuclear cascade and evaporation or, alternatively, fission. The probability that fission will occur in the second stage is proportional to Z^2/A, where Z and A are the atomic and mass numbers of the target nucleus, respectively. The Serber two-stage model was adapted by Bertini [16] in the High Energy Transport Code (HETC) to describe the nuclear products resulting from the inelastic proton-nucleus interaction. For each such interaction, HETC calculates the energy and direction of emitted cascade and evaporated particles and the mass and recoil energy of the residual target nucleus. After creation of cascade and evaporation particles, HETC transports them through the geometry until they degrade down to their cutoff energies, which are 20, 1, 0.149, and 0.113 MeV for neutrons, protons, pions, and muons, respectively. Any neutrons emitted from a reaction with energy below 20 Mev has its kinematic parameters recorded in a file (NEUTP) for subsequent transport by a Monte Carlo code using ENDF/B-based neutron cross section libraries. The Monte Carlo code for this purpose is usually the Monte Carlo Code for the Transport of Neutrons and Photons (MCNP) [17].

The current LANL version of HETC is LAHET [18], which contains a number of new features. The user has the option of employing either the Bertini-Serber intranuclear cascade model or the ISABEL intranuclear cascade model, which is an extension by Yariv and Fraenkel [19,20] of the VEGAS code [21]. As indicated by LAHET benchmark calculations of neutron yields from stopping-length targets from 113 MeV and 256 MeV protons, there does not seem to be a clear advantage of one intranuclear cascade model over any other [22]. Other new features in LAHET are the Fermi breakup model for excited light nuclei (instead of the evaporation model), and a multistage preequilibrium exciton model functioning between the intranuclear cascade model and the evaporation (or Fermi breakup) model.

Since [18] was published, a PKA option (option 16) was added to LAHET. Based on a user-designated recoil energy group structure, option 16 gives the energy distribution of PKA's in terms of the following kinds of energy: (1) the raw recoil energies imparted to target atoms, (2) the portion of (1) for elastic interactions only, (3) the damage energies corresponding to (1), using

the Lindhard model as described above, and (4) the portion of (3) for elastic interactions only. In addition, option 16 gives, in particular, the average damage energy per incident particle, $<T_{dam}>/n'$, where the averaging is done over the n′ histories being run. The thin-target damage energy cross section is then given by

$$\sigma_E = \frac{<T_{dam}>/n'}{N_V x} \tag{11}$$

where N_V is the atom density and x is the target thickness. The displacement cross section is then given by Eq. (8).

For tungsten as the target material, Fig. 2 shows the results of our LAHET calculations for neutron energies from 20 to 1600 MeV and SPECTER calculations from 1 to 20 MeV. The results are based on 150,000 histories, an atom density of 6.3011 x 10^{22} atoms per cm^3, and target thickness and radius of 1 and 50 cm, respectively. We note in Fig. 2 that in the region of 20 MeV the SPECTER cross sections lie above the LAHET ones. This was observed also to be the case,

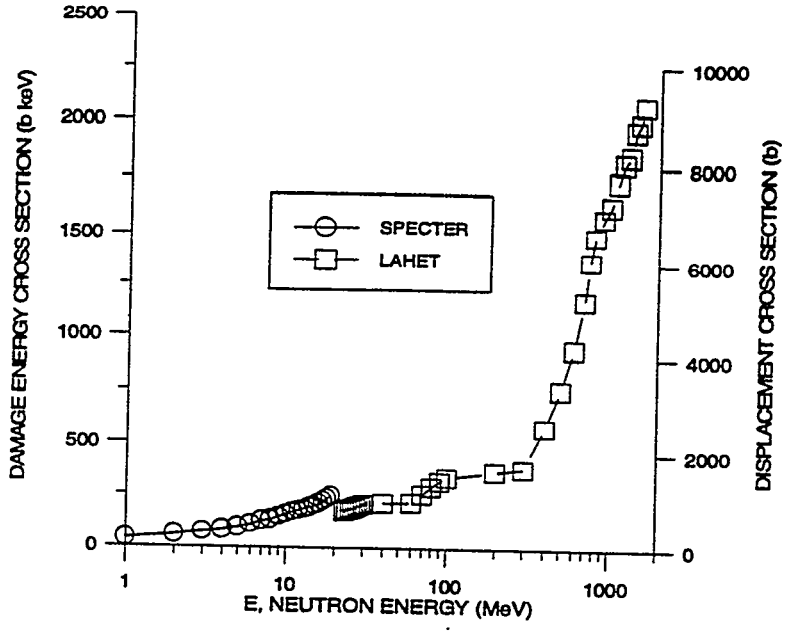

Fig. 2. Damage energy and displacement cross sections for tungsten as calculated by SPECTER and LAHET. Threshold displacement energy, 90 eV.

for similar calculations for neutrons on copper [23], although the discrepancy is larger for copper. It may be that conditions for spallation are no longer met at energies near 20 MeV, but the reason for the discrepancy has not been definitely established.

Eq. (11) gives the damage energy cross section assuming that the target is thin, so that the projectile neutrons can be considered to have the same energy throughout the target volume. To test the validity of this assumption we varied the target thickness from 0.01 to 10 cm for the LAHET calculations for 800 MeV neutrons on tungsten. Fig. 3 shows that the damage energy

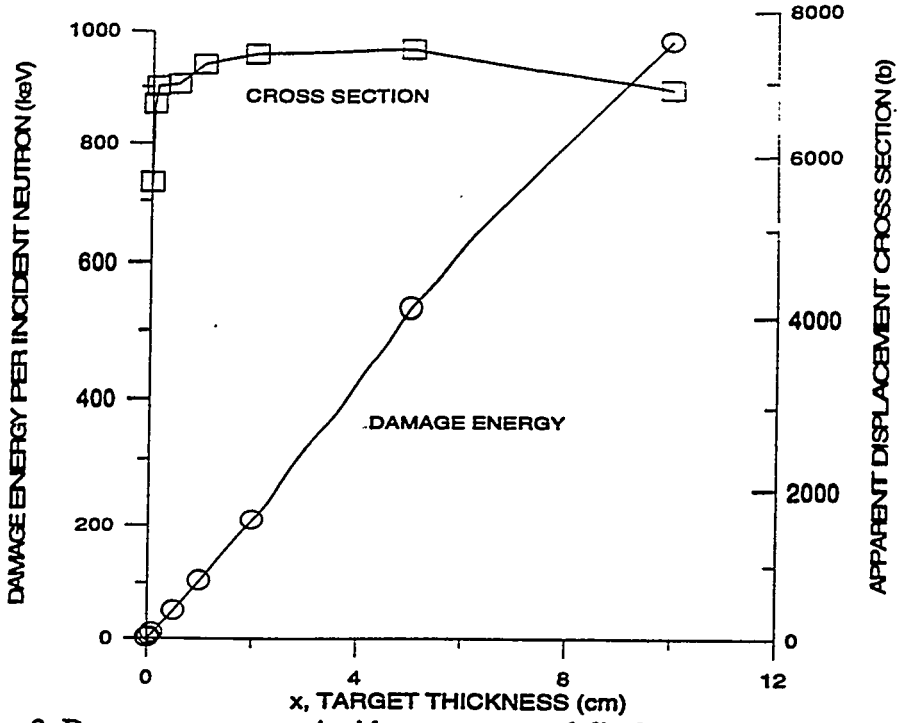

Fig. 3. Damage energy per incident neutron and displacement cross section versus target thickness for 800 MeV neutrons on tungsten.

per incident neutron increases linearly for thicknesses up to 5 cm and almost linearly up to 10 cm. By contrast, the apparent displacement cross section, calculated by Eq. (11), is rougly constant over most of the range of target thickness, although it is low for x = 0.01 cm (possibly due to poor statistics for such a thin sample) and again slightly low for x = 10 cm. We conclude that the thin-target approximation and Eq. (11) are valid over most of the range tested.

Radiation effects due to incident protons on tungsten have also been investigated using LAHET. The damage energy and displacement cross sections are about the same as shown in Fig. 2 for neutrons for 200 MeV and higher. For lower energies, the cross sections for protons lie below those for neutrons.

Calculations have also been made for helium production, for transmutation yield, and for PKA spectra, but space does not permit further discussion of these here.

CONSEQUENCES OF RADIATION EFFECTS

The primary effects of concern with regard to the use of materials in radiation environment are changes in mechanical properties and dimensional stability. The major mechanical property changes are hardening and embrittlement, and the embrittlement manifests itself in several ways. One type of embrittlement is illustrated in Fig. 4, which shows stress-strain curves for Ta, a body-centered cubic (BCC) refractory metal like tungsten. The irradiated samples were proton irradiated with 800 MeV protons at LAMPF [24]. They were maintained in contact with liquid Pb-Bi eutectic liquid, and they received fluences of 0.48 and 5.4 x 10^{20} protons/cm^2 at a temperature of about 673 K. Fig. 4 shows that the yield stress is increased upon irradiation, i.e., the tantalum is hardened. But, immediately upon yielding the metal undergoes plastic instability with a decrease in its load-carrying capacity until it fractures prematurely at a strain below 5%.

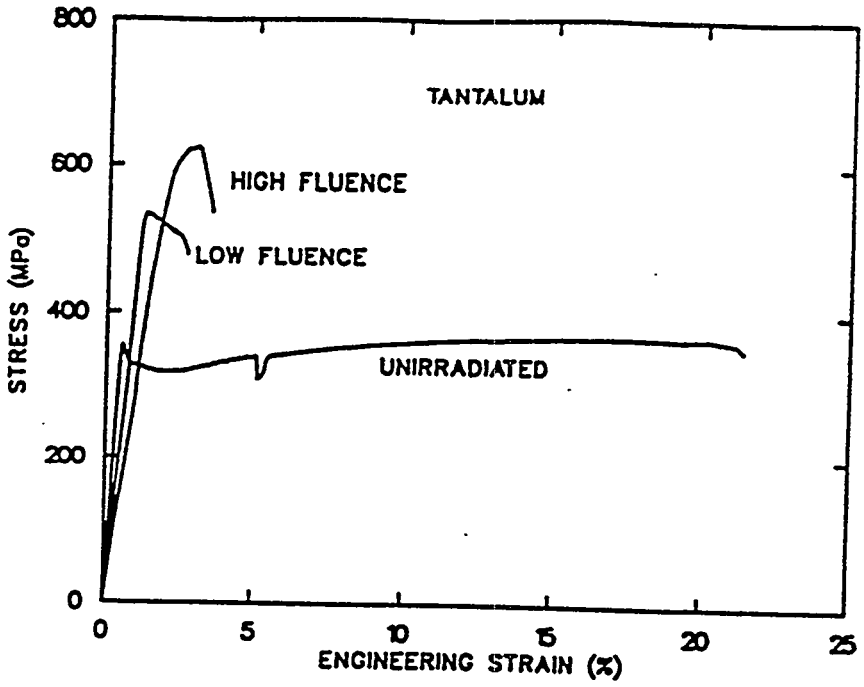

Fig. 4. Stress-strain curves for unirradiated and 800 MeV proton irradiated Ta. After [24].

We have mentioned that radiation-produced defect clusters (aggregates of vacancies and interstitials) are observable in the electron microscope. Experiments have been conducted on BCC refractory metals like V, Nb, and Mo, as well as on metals of other crystal structures, that illustrate the phenomenon of *dislocation channeling* [25]. When irradiated metals are examined by transmission electron microscopy, the defect clusters appear as black spots. But, if the irradiated metal is plastically deformed before insertion in the electron microscope, channels cleared of the black spots are observed along the slip planes where the deformation occurs. As a result, the deformation becomes concentrated in the softer defect-cluster-free channels, separated by undeformed regions. This inhomogeneity of plastic deformation can result in the premature plastic instability and embrittlement indicated by the curves in Fig. 4 for the irradiated tantalum.

A second type of radiation embrittlement is associated with the production of helium and its aggregation into bubbles concentrated at grain boundaries. The bubbles decrease cohesion between the grains and promote high-temperature grain-boundary fracture.

The third type of radiation embrittlement is particularly prevalent in body-centered cubic metals. These metals exhibit a ductile-brittle transition temperature (DBTT), such that the material is ductile at higher temperatures and brittle at lower ones. With this property is associated a well-known syndrome of failures in large steel structures [26]. In connection with the development of target materials for the German spallation neutron source SNQ project, tungsten samples were irradiated in a fission reactor to a fluence of about 10^{21} neutrons per cm^2 (E>0.1 MeV). The DBTT was observed to increase from 75 C to 240 C as a result of the irradiation ([1], page 74).

A large body of information has been accumulated in the course of development of cladding alloys for liquid-metal breeder reactors, that documents the role of radiation-produced voids in the swelling of irradiated metals (see, for example, [27,28]). The voids form upon irradiation from about 0.3 to 0.55 of the absolute melting temperature (from 832 to 1753 C for tungsten). In stainless steel, the swelling is predicted to amount to about 20% for neutron fluences of the order of 2.5×10^{23} neutrons per cm^2 [29]. Voids have been observed in irradiated tungsten; for fluences of about 1.5×10^{20} neutrons per cm^2 at 1000-1300 C, the swelling amounted to about 0.05% [30].

A further type of radiation damage consists of the impurities introduced by virtue of the formation of transmutation products. Our LAHET calculations for tungsten indicate that the major impurities are those with atomic numbers immediately below tungsten (Z = 74). For example, in tungsten irradiated with 1600 MeV neutrons or protons, tantalum (Z = 73) and hafnium (Z = 72) are produced with cross sections of about 0.5 and 0.2 barns, respectively.

CLOSURE

The limited experimental observations of spallation radiation effects on materials are recounted in [1]. The radiation-induced degradation in properties appears to be similar in kind to those observed upon reactor neutron irradiation. The exposures anticipated for materials in ADTT systems, however, are of a severity in terms of neutron and proton fluxes and energies that has no parallel in previous experience. The major concerns are associated with displacement, helium, and transmutation production. The nature and consequences of displacements, in particular, are described above with special reference to tungsten, a major candidate as a target material.

ACKNOWLEDGMENTS

We are indebted to L. R. Greenwood for providing a recent version of the SPECTER Code and to R. E. Prael, G. J. Russell, and J. R. Seal for assistance in running LAHET. We also appreciate helpful comments by L. L. Daemen.

REFERENCES

[1] Wechsler, M. S., Stubbins, J. F., Sommer, W. F. Ferguson, P. D. and Farnum, E. H., Selection and Qualification of Materials for the Accelerator Transmutation of Waste Project, Report LA-UR-92-1211, Los Alamos National Laboratory, Los Alamos, NM, 1992.

[2] "Standard Practice for Neutron Radiation Damage Simulation by Charged-Particle Irradiation," ASTM E 521-83, 1986 Annual Book of ASTM Standards, Section 12, Volume 12.02, American Society for Testing and Materials, Philadelphia, 1986.

[3] Thompson, M. W., *Defects and Radiation Damage in Metals*, London, Cambridge University Press, 1969, page 38.

[4] Oen, O. S., Cross Sections for Atomic Displacements in Solids by Fast Electrons, Report ORNL-4897, Oak Ridge National Laboratory, Oak Ridge, Tennessee, 1973.

[5] Lindhard, J., Nielsen, V. Scharff, M. and Thomsen, P. V., Integral Equations Governing Radiation Effects, Notes on Atomic Collisions, III. Kongelige Danske Videnskabernes Selskab, Matematisk-Fysiske Meddelelser, Vol. 33, No. 10, Copenhagen, 1963.

[6] Robinson, M. W., "The Dependence of Radiation Effects on the Primary Recoil Energy," in *Radiation-Induced Voids in Metals*, 1972, pp. 397-429.

[7] Fisher, H. M., A Nuclear Cross Section Data Handbook, Report LA-11711-M Manual, Los Alamos National Laboratory, Los Alamos, NM 87545, 1989.
[8] Coltman, R. R., Klabunde, C. E., and Redman, J. K., *Phys. Rev.* **156**, 715 (1967).
[9] Greenwood, L. R., and Smither, R. K., SPECTER: Neutron Damage Calculations for Materials Irradiations, Report ANL/FPP/TM-197, Argonne National Laboratory, Argonne, Illinois, 1985.
[10] Odette, G. R., and Doiron, D. R., *Nuclear Technology* **29**, 346-368 (1976).
[11] Ozer, O. and Garber, D., ENDF/B Summary Documentation, Report BNL-17541, National Cross Section Center, Brookhaven National Laboratory, Upton, NY, 1973.
[12] Coltman, R. R., Blewitt, T. H., Klabunde, C. E., Redman, J. K., and McDonald, D. L., Annealing Studies of Various Neutron-Irradiated Metals, Report ORNL-3213, Oak Ridge National Laboratory, Oak Ridge, Tennessee, 1961, page 15.
[13] Wechsler, M. S., "Radiation, Diffusion, and Body-Centered Cubic Metals," in *Diffusion in Body- Centered Cubic Metals*, American Society for Metals, Metals Park, Ohio, 1965, pp. 291-315.
[14] Keys, L. K., Smith, J. P. and Moteff, J. M., *Phys. Rev.* **176**, 851-856 (1968).
[15] Serber, R., *Phys. Rev.* **72**, 1114-1115 (1947).
[16] Bertini, H. W., *Phys. Rev.* **18**, 1711-1730 (1969).
[17] Briesmeister, J. F., Editor, MCNP--A General Monte Carlo Code for Neutron and Photon Transport, Version 3A, LA-7396-M, Rev. 2, Manual, Los Alamos Monte Carlo Group, Los Alamos National Laboratory, September 1986. See also, J. F. Briesmeister, MCNP3B Newsletter, Los Alamos National Laboratory memorandum X-6:JFB-88-292, July 18, 1988.
[18] Prael, R. E. and Lichtenstein, H., User Guide to LCS: The LAHET Code System, Report LA-UR 89-3014, Radiation Transport Group, Los Alamos National Laboratory, Los Alamos, NM, September 1989.
[19] Yariv, Y., and Fraenkel, Z., *Phys. Rev. C*, **20**, 2227-2243 (1979).
[20] Yariv, Y., and Fraenkel, Z., *Phys. Rev. C*, **24**, 488-494 (1981).
[21] Chen, K. et al., *Phys. Rev.*, **168**, 949- (1968).
[22] Prael, R. E., "LAHET Benchmark Calculations of Differential Neutron Production Cross Sections for 113 MeV and 256 MeV Protons," LA-UR-89-3347, Los Alamos National Laboratory, Los Alamos, NM 87545, September 1989.
[23] Wechsler, M. S., D. R. Davidson, D. R., Greenwood, L. R. and Sommer, W. F., "Calculation of displacement and helium production at the LAMPF irradiation facility," in *Effects of Radiation on Materials: Twelfth International Symposium*, STP 870, edited by F. A. Garner and J. S. Perrin, American Society for Testing and Materials, Philadelphia, 1985, pp. 1189-1198.
[24] Brown, R. D., Wechsler, M. S., and Tschalär, C., "Tensile properties of several 800 MeV irradiated BCC metals and alloys," in *Influence of Radiation on Material Properties*, STP 956, edited by F. A. Garner, C. H. Henager, and N. Igata, American Society for Testing and Materials, Philadelphia, 1987, pp. 131-140.
[25] Wechsler, M. S., "Dislocation Channeling in Irradiated and Quenched Metals," in *The Inhomogeneity of Plastic Deformation*, American Society for Metals, Metals Park, Ohio, 1973, Chapter 2.
[26] Tipper, C. F., *The Brittle Fracture Story*, Cambridge University Press, Cambridge, England, 1962.
[27] Corbett, J. W. and Ianniello, L. C., Editors, *Radiation-Induced Voids in Metals*, U. S. Atomic Energy Commission, April 1972.
[28] Bleiberg, M. L. and Bennett, J. W., Editors, *Radiation Effects in Breeder Reactor Structural Materials*, American Institute of Mining, Metallurgical and Petroleum Engineers, New York, 1977.
[29] Bennett, J. W. and Horton, K. E., *Met. Trans.* **9A**, 143-149 (1978).
[30] Rau, R. C., Ladd, R. L., and Moteff, J., *J. Nucl. Mater.* **33**, 324-327 (1969).

Materials Considerations for Molten Salt Accelerator-based Plutonium Conversion Systems

J. H. DeVan, J. R. DiStefano, W. P. Eatherly, J. R. Keiser, and R. L. Klueh
Oak Ridge National Laboratory
P. O. Box 2008
Oak Ridge, Tennessee 37831

Abstract. A Molten-Salt Reactor Program for civilian power applications was initiated at the Oak Ridge National Laboratory in 1956. In 1965 the Molten Salt Reactor Experiment (MSRE) went critical and was successfully operated for several years. Operation of the MSRE revealed two deficiencies in the Hastelloy N alloy that had been developed specifically for molten-salt systems. The alloy embrittled at elevated temperatures as a result of exposure to thermal neutrons (radiation damage) and grain boundary embrittlement occurred in materials exposed to fuel salt. Intergranular cracking was found to be associated with fission products, viz. tellurium. An improved Hastelloy N composition was subsequently developed that had better resistance to both of these problems. However, the discovery that fission product cracking could be significantly decreased by making the salt sufficiently reducing offers the prospect of improved compatibility with molten salts containing fission products and resistance to radiation damage in ABC applications. Recommendations are made regarding the types of corrosion tests and mechanistic studies needed to qualify materials for operation with PuF_3-containing molten salts.

INTRODUCTION

Fused fluoride mixtures containing PuF_3 are being considered as the blanket material for accelerator-based systems proposed for plutonium disposition. Because of their high boiling points, these mixtures can be contained at low pressures even at relatively high operating temperatures. Their chemical and physical properties impart additional advantages such as stability under irradiation and chemical compatibility with a variety of containment and neutron moderator materials. The reference salt mixtures under consideration for accelerator-based plutonium conversion systems (ABCs) are modelled after mixtures that were developed for the Molten Salt Reactor (MSR) program, conducted at Oak Ridge National Laboratory during the 1950's to early 1970's. These mixtures were based on the eutectic LiF-BeF_2 system containing small percentages of UF_4 and, for some concepts, larger percentages of ThF_4. The present paper reviews the materials developments underlying the MSR program and relates them to the materials requirements for the ABC PuF_3-containing blanket. The selection of structural and moderator materials is discussed in terms of their chemical compatibility with the fluoride fuel mixtures and their neutron radiation damage characteristics. The paper then addresses the ABC materials issues and needs in the implementation of a molten fluoride blanket.

SELECTION OF CONSTRUCTION MATERIAL

The development of reactors that incorporate a circulating molten fluoride fuel is predicated on the availability of a construction material that will contain the salt over long time periods and also afford useful mechanical properties. The container material must also be resistant to air oxidation, be easily formed and welded into relatively complicated shapes, and be metallurgically stable over a wide temperature range. For initial MSR studies, several commercially available high temperature alloy systems were evaluated with respect to the aforementioned requirements [1,2]. As a result of these initial studies, Inconel 600, a nickel based alloy containing 15% Cr and 7% Fe, was found to afford the best combination of desired properties and was utilized as a container for the construction of the

Aircraft Reactor Experiment [3]. Corrosion rates encountered with this alloy at 700°C and above, however, were excessive for long-term use with most fluoride fuel systems. Utilizing experience gained in corrosion testing of commercial alloys, an alloy development program was conducted to provide an advanced container material for MSR systems. The reference alloy system was composed of nickel with a primary strengthening addition of 15-20% Mo. This composition afforded exceptional resistance to salt attack but lacked sufficient mechanical strength and oxidation resistance at the desired service temperature. To augment these latter properties, additions of various solid-solution alloying agents were evaluated, among them Cr, Al, Ti, Nb, Fe, V, and W. An optimum alloy composition was selected on the basis of parallel investigations of the mechanical and corrosion properties which were imparted by each of these additions. The composition best suited to reactor use was determined to be within the range 15-17% Mo, 6-8% Cr, 4-6% Fe, 0.04-0.08 C, balance Ni. This alloy was commercialized under the trade name Hastelloy N.

A 7.4 MW test reactor, the Molten Salt Reactor Experiment (MSRE), was constructed of Hastelloy N and became critical in 1965. The reactor operated successfully for four years and verified the excellent corrosion resistance of the alloy to the UF_4-containing LiF-BeF_2 salt mixture. However, operation of the MSRE revealed two potential problem areas that were of concern in the utilization of the Hastelloy N alloy for more advanced Molten Salt Breeder Reactors (MSBRs), where greater concentrations of fission products and greater neutron fluences would be encountered. Radiation damage, in the form of helium embrittlement from n,α reactions, was found to have reduced the creep ductility of the Hastelloy N in post-operation examinations. Also grain boundaries of the Hastelloy N directly exposed to the fuel salt were shown in post-operation tensile tests to have been embrittled to depths of 0.15-0.25 mm. Subsequent studies showed the embrittlement to be associated with the presence of fission product tellurium on grain boundaries that intersected with the salt-exposed surfaces. Accordingly, the earlier alloy Hastelloy N development program was extended to improve the alloy's radiation damage characteristics and resistance to penetration by sulfur-like fission products, such as tellurium. (These alloy modifications are discussed in later sections of this report.) In addition, compatibility tests were conducted to re-examine the possibility of using iron-based alloys as containment materials for the MSBR. These alloys are more resistant to tellurium penetration and also generate less helium from n,α reactions than nickel-based alloys. However, their use would severely limit the oxidation potential of the salt (in effect, the fluoride ion activity), whereas the Hastelloy N composition could resist attack by the reference MSBR salt components under virtually all sustainable reactor operating conditions. As will be discussed, these same materials concerns are key issues in selecting the ABC salt blanket structural material, but with the condition that PuF_3 has replaced UF_4 in the salt mixture.

Corrosion by Fluoride Mixtures

The selection of a structural material for containment of molten fluoride salts begins with a consideration of the reduction-oxidation (redox) potentials of the component elements of the material with respect to components of the salt. Table 1 lists the standard free energies of formation, per gram atom of fluorine, of fluoride compounds at 527 and 727°C associated with salt constituents and metals commonly used in high temperature alloys. It is evident that the major salt components, LiF and BeF_2, are considerably more stable than any fluorides of the structural metals listed, so they are unreactive with the structural metals. The corrosion of a variety of structural alloys by reference MSR salt mixtures has been found [4] to result from a combination of reactions involving impurities in the salt, $2HF + M = MF_2 + H_2$ (M = Ni, Cr, Fe) and $XF_2 + Cr = CrF_2 + X$ (X = Ni, Fe); and reactions involving fuel components, e.g., $2Cr + 2UF_4 = CrF_2 + 2UF_3$.

Table 1. Standard Free Energies of Formation of Fluorides in a Molten Salt System

Fluoride	$-\Delta G_f$ (800 K) (kcal/gram-atom of F)	$-\Delta G_f$ (1000 K) (kcal/gram-atom of F)
LiF	128.9	124.3
ThF_4	111.4	107.9
PuF_3	108.2	104.5
BeF_2	107.8	104.4
UF_3	104.3	100.9
UF_4	99.3	95.9
TiF_2	84.2	80.7
CrF_2	79.8	76.6
NbF_5	73.7	71.0
FeF_2	71.0	67.9
MoF_3	67.3	64.2
NiF_2	63.7	60.1

In all cases, the corrosion product fluorides are readily dissolved by the molten salt mixture. The impurity reactions can be minimized by maintaining low impurity concentrations in the salt and on the alloy surfaces. However, the reaction with UF_4 is intrinsic and depends on the redox potential of the salt, which is reflected in the activity of quadrivalent uranium ions in the salt compared to trivalent uranium ions. Although this redox potential can be adjusted to make the salt less oxidizing (for example, by exposing the salt to beryllium or chromium metal), the UF_3 must be restricted to a sufficiently low activity in the salt to avoid its disproportionation and the alloying of uranium with the containment alloy. The relationship between the U^{+4} and U^{+3} ratios and the effective fluoride ion oxidation potential is given in Fig. 1. The cross-hatched area in the figure indicates the ratios that were generally studied in corrosion tests and that were maintained in the MSRE. Relative to the reactions listed above, assuming equilibrium is attained, those structural metals with the lower free energy fluorides, such as nickel and molybdenum, are less susceptible to oxidation, while those with the higher free energies, such as chromium, are more prone to oxidation. The chemistry of Hastelloy N was tailored to achieve compatibility with UF_4-containing salt mixtures by simply allowing the salt to "equilibrate" with the alloy. In any heat transfer

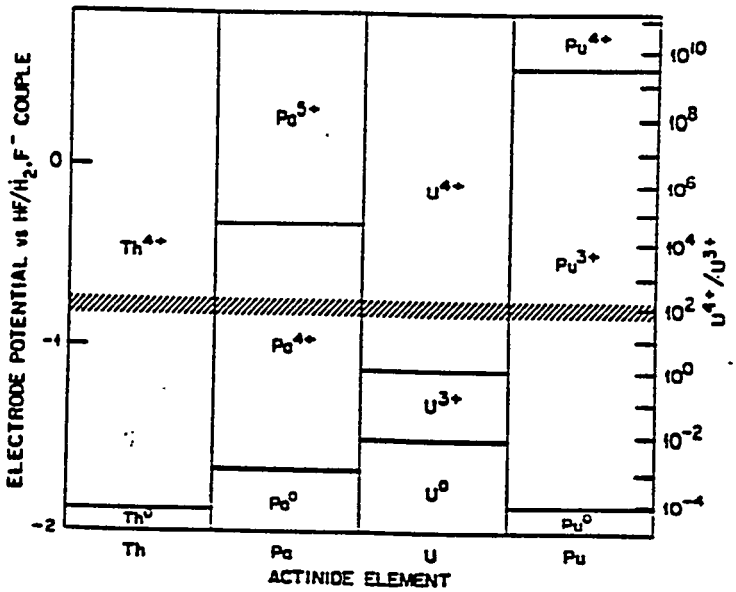

● BAR INDICATES MSR OPERATING RANGE (CONSTRAINED BY LIMITED SOLUBILITY OF U^{+3} IN SALT)

Fig. 1. Oxidation states of actinides in LiF-BeF_2-ThF_4-UF_4.

system, true equilibrium between the salt and the alloy is precluded by temperature differences in the system. Nevertheless, in a Hastelloy N closed loop system operating at 600-700°C, a steady-state U^{+4}/U^{+3} ratio is reached within a few hundred hours [5] and has been shown experimentally to be in the range 100 to 350. Corrosion proceeds by the selective oxidation of chromium at the hotter loop surfaces and the reduction and deposition of chromium at the cooler loop surfaces. In the case of the MSR fuel salts, the resultant maximum corrosion rate of Hastelloy N measured in extensive loop testing was below 4 μm/y, and a similar rate was measured on surveillance specimens in the MSRE [6].

If a 300-series stainless steel (18%Cr-10%Ni-balance iron) is exposed to UF_4-containing salts under the same closed system conditions as described above, corrosion again is manifested by the selective removal of chromium from hotter loop surfaces with concomitant chromium deposition at cooler surfaces. However, because of the much higher chromium activity in the stainless compared to Hastelloy N, the extent of chromium mass transport is considerably greater than for Hastelloy N. Table 2 lists the operating conditions and corrosion rates of two stainless steel thermal convection loops that circulated LiF-BeF_2 salts containing 1 mole % and 0.3 mole % UF_4, respectively [7]. The 304L loop operated successfully for nine years at a maximum temperature of 688°C and exhibited an average corrosion rate equivalent to 21.8 μm/y, based on uniform wall reduction. However, corrosion was actually manifested by subsurface void formation to depths ≥1.5 mm below the exposed surface. A second loop was constructed of type 316 stainless steel and operated for 4490 h. The corrosion rate of this loop at 650°C was slightly less than the 304L loop, but corrosion again was manifested by subsurface voids, in this case to a depth of 76 μm. A second 316 stainless steel loop, whose conditions are also shown in Table 2, was operated with a LiF-BeF_2 salt that contained no uranium, so that the oxidation potential of the salt could be lowered by buffering with metallic beryllium without concern for the disproportionation of UF_3. Before adding beryllium, the corrosion rate of the loop averaged 8 μm/y over 25,000 h at 650°C. After contacting the salt with a small beryllium rod, the corrosion rate was lowered to 2 μm/y over a 2000-h period [8].

Table 2. Operating Conditions of Stainless Steel Thermal Convection Loops Involving LiF-BeF_2 Based Molten Salts

Loop material	Salt composition (mole %)	Maximum temperature (°C)	Δ T (°C)	Time (h)
304L SS	LiF-BeF_2-ZrF_4-ThF_4-UF_4 (70-23-5-1-1)	688	100	83,520
316 SS	LiF-BeF_2-ThF_4-UF_4 (68-20-11.7-0.3)	650	110	4,490
316 SS	LiF-BeF_2 (66-34)	650	125	25,100

Based on the above observations, the corrosion characteristics of a LiF-BeF_2 salt containing PuF_3 in place of UF_4, i.e., the reference ABC blanket salt, would depend on the redox potential set for the salt system. If the potential is maintained in the same range as for the MSR program, the corrosion rate of the containment material, in terms of chromium and iron oxidation, should be unaffected by the replacement. However, as shown in Fig. 1, the oxidation potential at which the plutonium activity associated with PuF_3 becomes unity is lower than the potential at which the activity of uranium associated with UF_3 becomes unity. Accordingly, it may be possible to maintain a lower oxidation potential in the PuF_3-containing salt than in the case of the uranium-containing salt without encountering alloying

with the containment. If this can be demonstrated, then the corrosion rate of an austenitic stainless steel may be in an acceptable range to be used as the structural material for the ABC blanket.

Transmutation Effects

Depending on the neutron energies and fluxes in the ABC blanket, transmutation reactions may affect the salt chemistry and, accordingly, the redox potential of the salt [9]. The overall reactions can be represented as

$$^{6}LiF + n \rightarrow {}^{4}He + TF$$
$$^{7}LiF + n \rightarrow {}^{4}He + TF + n'$$

$$^{10}BeF_2 + n \rightarrow 2\,n' + 2\,{}^{4}He + 2\,F$$
$$^{10}BeF_2 + n \rightarrow {}^{6}He + {}^{4}He + 2\,F \text{ followed by}$$
$$^{6}He \rightarrow {}^{6}Li, \text{ and } {}^{6}Li + F \rightarrow {}^{6}LiF$$

$$^{19}F^{-} + n \rightarrow {}^{16}N^{-} \rightarrow {}^{4}He \text{ followed by}$$
$$^{16}N^{-} \rightarrow {}^{16}O^{-} + \beta^{-}$$

The TF and F produced by the transmutation of lithium and beryllium, respectively, will act to increase the oxidation potential of the salt. The effect is similar to that encountered in the fission of UF_4 in the MSR salt, where effectively one fluorine atom per fission is free to oxidize or corrode the container (i.e., is not tied up with fission products). In the MSRE the small concentration of UF_3 in the fuel provided a reductant to buffer any oxidants resulting from transmutation, and a redox couple similar to UF_4/UF_3 could be added to the ABC blanket to control the transmutation effect. The selection and use of redox additions is discussed in a companion paper [10]. The transmutation of fluoride ions ultimately results in the formation of O^{2-} ions in the salt; however, whatever reductant is used to reduce fluorine to fluoride should also reduce the oxygen [9].

Fission Product Effects

As previously described, the corrosion rate of Hastelloy N measured during operation of the MSRE was relatively low and of the same order as that for forced convection loops operating under similar temperatures. However, Hastelloy N tensile specimens which had been exposed to the MSRE fuel salt showed shallow surface cracks along the gage length at grain boundaries that connected to the salt exposed surfaces (Fig. 2). These cracks generally extended to depths of about 0.13 mm, but were as deep as 0.33 mm in parts removed from the salt plenum region of the pump bowl. Because this grain boundary embrittlement was found in the heat exchanger tubes where the neutron flux was insignificant as well as in samples exposed in the reactor core, it was concluded this cracking was not due to radiation effects. Controlled dissolution of samples detected a number of fission products within the material; tellurium was the fission product found at the highest concentration. Subsequent tests showed that grain boundary embrittlement could be caused in Hastelloy N samples when tellurium was applied to the sample surface. Since the depth of cracking observed in the MSRE would not have been acceptable when extrapolated to the 30-year design life of a Molten-Salt Breeder Reactor, a program was undertaken to identify ways to prevent tellurium embrittlement of Hastelloy N.

Investigation of the problem was approached in several ways. In-reactor experiments were used to evaluate the embrittlement resistance of various alloys. In another study, over sixty alloys were electroplated with tellurium and annealed for extended times before being tensile tested. No cracks formed on a number of alloys including stainless steels and nickel-base alloys containing more than 15% chromium. Most heats of Hastelloy N

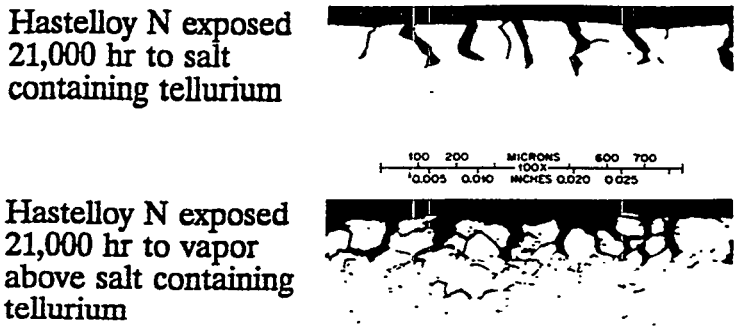

Fig. 2. Hastelloy N used in experimental molten salt reactor showed intergranular cracks when strained.

developed cracks, but modifications that contained 2% niobium showed better crack resistance than standard Hastelloy N [6]. Other tests were developed that involved exposure of alloy samples to molten fluoride salts containing telluride compounds. Telluride compounds used included Li_2Te, $LiTe_3$, Cr_2Te_3, Cr_3Te_4, Cr_5Te_6, and Ni_3Te_2, and cracking resulted in Hastelloy N samples exposed to salt solutions of all but the first of these compounds. Modifications of Hastelloy N were independently being developed to address the problem of radiation embrittlement, so samples of alloys modified with different combinations of titanium, niobium, and chromium were also exposed in the salt solutions containing the tellurides. Results indicated that niobium as an alloying agent reduced embrittlement of Hastelloy N, but neither chromium nor niobium exhibited as strong an effect when titanium was included. The extent of the effect of niobium on reducing grain boundary embrittlement is shown in Fig. 3 [ref. 11].

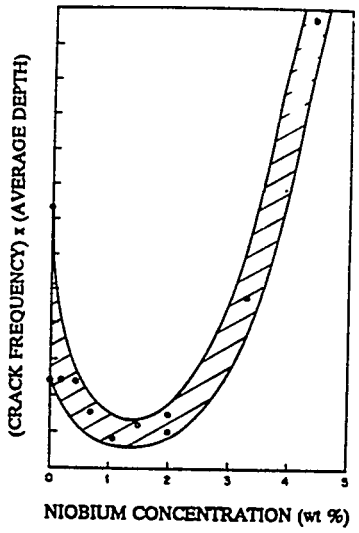

Fig. 3. Effect of niobium in modified Hastelloy N on grain boundary cracking when exposed in salt-Cr_3Te_4 + Cr_5Te_6 for 250 hr at 700°C.

Although the effort to prevent tellurium embrittlement of grain boundaries was primarily directed at alloying modifications of Hastelloy N, some work was done to determine if chemical changes in the salt could also alter tellurium behavior. On the basis of electrochemical studies conducted at ORNL, which indicated tellurium could exist as a telluride rather than as elemental tellurium in a relatively reducing melt, standard

Hastelloy N samples were exposed to molten salt solutions containing Cr_3Te_4 with variable oxidation potentials. The oxidation potential of the salt solution was described in terms of the U^{+4}/U^{+3} ratio (Fig. 1), and this ratio was varied between 10 and 300. Results of these studies are shown in Fig. 4 where it is apparent that below an oxidation potential of approximately 70, tellurium embrittlement of grain boundaries is greatly reduced [12]. This finding may be particularly significant for the PuF_3-containing ABC blanket salt, which, as discussed above, appears more amenable to operation at lower redox potentials than the UF_4-containing MSR fuel salts.

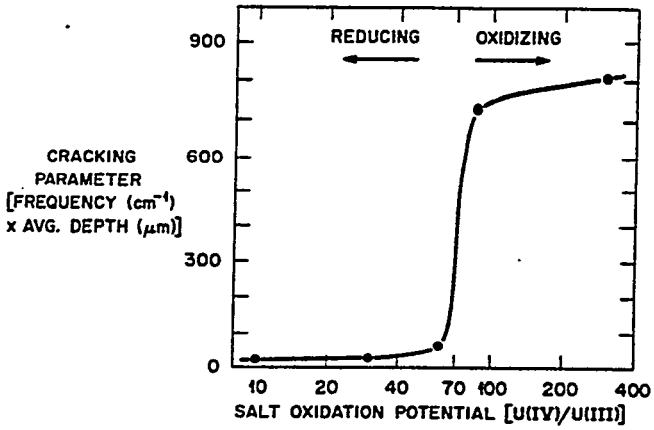

Fig. 4. Extent of tellurium embrittlement of Hastelloy N is strongly affected by oxidation potential of salt.

Irradiation Damage of Structural Alloys

Nickel-Based Alloys

Nickel-based alloys of the type proposed for an ABC with a molten salt blanket are relatively resistant to void swelling [13-15]. However, a high cross section for (n,α) reactions exists between thermal neutrons and ^{58}Ni (68% of natural nickel is ^{58}Ni). At elevated temperatures, helium can diffuse to grain boundaries and embrittle the alloy. Helium can also cause swelling by bubble formation at elevated temperatures. Finally, in certain nickel alloys, irradiation enhances precipitate formation, which can degrade mechanical properties.

The irradiation damage properties of several high-nickel superalloys were studied in the liquid metal reactor (LMR) program [13,14]. When irradiated in the Experimental Breeder Reactor (EBR-II) at 465 to 575•C and tensile tested at 234 to 785•C, ductility decreased to zero at test temperatures of 600 to 800•C [14]. The temperature of zero ductility decreased with increasing neutron fluence. This ductility loss was attributed to an irradiation-enhanced formation of a grain-boundary precipitate. However, the alloys were dropped from the LMR program before the mechanism was completely understood. Embrittlement was not due to elevated-temperature helium embrittlement, because little helium is produced by irradiation in EBR-II.

In view of the potential application of Hastelloy N in the ABC concept, it is of interest to examine the radiation-damage experience for this alloy in the MSRE [6]. The major differences between the MSRE and the ABC involve the neutron fluxes (and fluences). The high-energy (>0.8 MeV) neutron flux in MSRE was only 1.2×10^{11} n/cm^2-s, and the thermal neutron flux was limited to 6.5×10^{12} n/cm^2-s [15]. Much larger fluxes are expected in the ABC.

During irradiation at 650•C in the MSRE, no swelling or hardening was observed in Hastelloy N. However, helium formed by (n,α) reactions of thermal neutrons with nickel and residual boron caused elevated-temperature helium embrittlement of the Hastelloy N,

as exhibited by a loss of ductility measured in tensile and creep tests at 650°C. Fracture strains depended on strain rate and thermal fluence (Fig. 5). Creep-rupture strains of less than 0.1% were observed for the highest fluence, compared to strains that exceeded 16% at all strain rates for specimens aged in fluoride salt for 15,189 h at 650°C. Embrittlement was attributed to helium gas bubbles that were observed on grain boundaries.

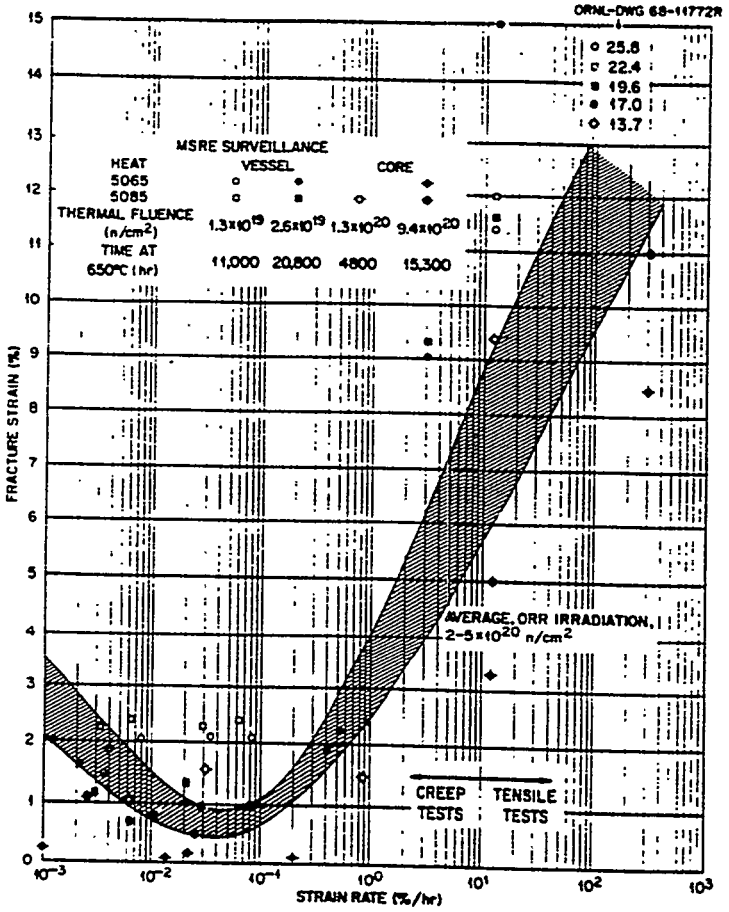

Fig. 5. Variation of fracture strain with strain rate for Hastelloy N specimens irradiated in the MSRE and tested at 650°C.

An alloy-development program demonstrated that the radiation resistance of the Hastelloy N could be improved by alloying. A niobium addition increased creep strength and fracture strain (Fig. 6). Titanium also proved beneficial. This work resulted in the modified Hastelloy N composition in Table 3, where it is compared to the standard Hastelloy N.

Alternative Materials

As an alternative to high-nickel alloys, austenitic stainless steels may offer enhanced radiation resistance for the ABC. Because these alloys contain less nickel, less helium will be generated in an austenitic stainless steel than in a nickel-based alloy. Although conventional austenitic stainless steels (e.g., type 316) tend to be embrittled by even relatively small amounts of helium, their resistance to embrittlement has been enhanced through alloying development studies under the U.S. fusion reactor program [16]. Helium embrittlement can be minimized by the precipitation of a fine dispersion of carbide particles in the matrix and grain boundaries. Fine helium bubbles form on the particles and, because

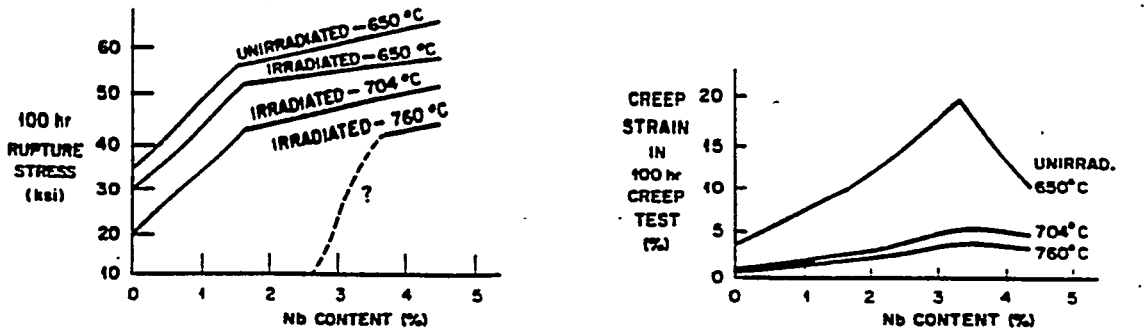

Fig. 6. The effect of niobium additions on the creep-rupture behavior of irradiated Hastelloy N.

Table 3. Nominal Composition of Standard and Modified Hastelloy N

Norminal Composition of Hastelloy N (%)		
	Standard	Modified
Ni	bal	bal
Mo	16	12
Cr	7	7
Fe	4	0.5
Mn	0.5	0.2
Si	0.5	0.1
C	0.05	0.05
Ti+Nb	—	2
Re	—	0.01

of their large number and small size, do not grow to critical size for embrittlement. After irradiation at 600°C in the mixed-spectrum High Flux Isotope Reactor (HFIR) to 17 dpa and 1750 appm He, the tensile ductility of the most promising of these improved alloys was essentially unchanged. However, irradiation behavior at temperatures greater than 600°C has not been determined. More advanced alloys have also been developed, but their irradiation properties remain to be determined.

GRAPHITE

Graphite in a molten-salt reactor serves no structural purpose other than to define the flow patterns for the salt and, of course, to support its own weight. The requirements on the graphite derive almost entirely from nuclear considerations-namely, stability of the material against radiation-induced distortion, resistance to penetration by the fuel-bearing salt, and non-trapping of Xe within the free-volume of the graphite pores [6].

Radiation Damage

Neutron bombardment produces atomic displacements which result in vacancy-interstitial pairs. Vacancies migrate to dislocations and collapse, interstitials combine into ordered interlaminar planes which assume a graphite structure with stacking faults. The result is that individual crystallites contract in the a-axis direction and expand in the c-axis direction. This is reflected in an initial macroscopic bulk contraction of the polycrystalline graphite, followed by bulk expansion as damage proceeds. Eventually the expansion induces macroscopic cracking of the graphite until mechanical disintegration occurs. During this progression, all of the thermo-mechanical properties are affected, and radiation-activated creep occurs, resembling in some detail its high-temperature thermal analogue.

During reactor operation, internal stresses develop within the graphite due to temperature and flux gradients. These internal stresses are relaxed due to the radiation creep. At shutdown, the thermal gradients disappear and a reversed stress field immediately appears in the graphite. The most detailed creep data exist on the US and German Graphites for the high temperature gas-cooled reactor. But these graphites, because of their coarse granularity and large pore size, are unsatisfactory for molten salt applications. Conversely, the IG-100 graphite grade produced in Japan for their gas-cooled reactor program is generically much closer to the MSR requirements [17]. However, the dominant term in the constitutive equations describing mechanical properties in the presence of neutron and thermal gradients is the creep term [18], and the creep behavior of the fine-grained, low porosity graphites needs further evaluation.

The operating temperature of the ABC blanket, which is on the order of 600° to 700°C, will be advantageous in terms of the graphite lifetime. It is precisely this temperature range over which graphite is the most long-lived, i.e., the point in fluence at which graphite has expanded back to its original unirradiated volume. For graphites of the type needed in for ABC service, this fluence will be of the order of 25-30 x 10^{22} nvt (E > 50 kev) [19].

Salt and Gas Entrapment

The unique character of the graphite required for a molten salt reactor relates to the necessity to prevent the molten salt from "soaking" into the graphite. Artificial graphites are generally fabricated from petroleum cokes and pitches or polymers which, on heat treatment to high temperatures (≥ 2500°C), leave a relic carbon structure capable of crystallization. By necessity the evolving gases, predominantly hydrogen, must escape the structure, and this produces a pore texture within the graphite. Completely sealing these pores is impractical—the material will simply "blow-up" due to internal gas pressure developed during heat treatment. However, since the molten salts are non-wetting to graphite and possess a high surface tension, it is only necessary to reduce the entrance pore diameter to ≤ 1 μm to prevent salt intrusion. Fortunately, the industry is quite capable of producing materials with the very small pores required. Also, in the last decade, isostatic molding has become a standard forming technique. As a result quality has been significantly improved and cost has decreased for materials of the type used in the MSRE some twenty years ago.

Gas entrapment in the graphite, specifically Xe^{135} and Xe^{137}, was an additional problem in the MSBR because of its effect on breeding uranium from thorium and the resultant fuel doubling time. Fortunately, this problem should be of lesser significance in a Pu-burner reactor.

SUMMARY AND RECOMMENDATIONS

Corrosion studies and reactor operation have shown that Hastelloy N (both standard and modified) has excellent resistance to molten fluoride salts. As a result of studies conducted for the MSR program from 1956 through 1976, an extensive corrosion data base exists on both nickel- and iron-base alloys for UF_4-containing salts. This data base provides a roadmap for establishing the corrosion properties for PuF_3-containing salts, but additional corrosion testing under ABC conditions will be required to quantify corrosion rates of candidate structural alloys.

Use of Hastelloy N as a containment material allows a wide latitude in possible system operating parameters such as the temperature and salt redox potential. However, operating experience in the MSRE did show that Hastelloy N was embrittled at elevated temperatures due to radiation-induced internal helium generation, and shallow intergranular cracking was associated with interactions with fission products (tellurium). Alloy development studies showed that Hastelloy N modified with 1-2% niobium had better resistance to irradiation embrittlement and to intergranular cracking by tellurium. It was also found that the severity

of cracking by tellurium could be diminished by lowering the redox potential of the salt. However, since the spectrum of products from transmutation of plutonium or actinide wastes would be different from that investigated in the MSR program, corrosion reactions specific to the ABC salt chemistries must be evaluated. Included in this evaluation should be an assessment of lower salt redox potentials from the standpoint of allowing the use of austenitic stainless steels as structural materials and establishing the potentials that must be maintained to avoid uranium alloying with the containment.

The radiation fluence and energy spectrum poses a serious challenge for any structural alloy in an ABC system. A combination of high energy and thermal neutrons introduces different conditions from previous applications. Calculations of neutron energy spectra and fluxes are required so damage parameters can be determined and a better assessment of candidate alloys can be made. Stability of potential structural alloys under high-energy neutron irradiation should be determined (i.e., whether irradiation-enhanced precipitation in combination with helium generation causes embrittlement of nickel-base alloys). Techniques developed under the fusion reactor program to improve the resistance of austenitic stainless steels to helium embrittlement should be extended to include nickel-base alloys, particularly Hastelloy N.

Graphite has long been successfully employed in nuclear reactor applications, and commercial graphites are available with adequate physical, corrosion, and structural properties for ABC service. Based on available data, it should be possible to estimate the lifetimes of these graphites at ABC neutron fluences once the ABC design parameters have been finalized.

In summary, the selection of materials for ABC systems will require trade-offs between the system operating parameters and material properties in order to achieve adequate resistance to salt corrosion, fission product cracking, and radiation resistance.

REFERENCES

[1] Adamson, G. M., Crouse, R. S., and Manly, W. D., *Interim Report on Corrosion by Alkali-Metal Fluorides*, ORNL-2337, Oak Ridge National Laboratory (1953).

[2] Adamson, G. M., Crouse, R. S., and Manly, W. D., *Interim Report on Corrosion by Zirconium-Base Fluorides*, ORNL-2338, Oak Ridge National Laboratory (1961).

[3] Manly, W. D., et al., Aircraft Reactor Experiment-Metallurgical Aspects, ORNL-2349, Oak Ridge National Laboratory (1957).

[4] Manly, W. D., et al., *Progr. Nucl. Energy, Ser. IV* 2, 164 (1960).

[5] DeVan J. H., and Evans, R. B., Corrosion Behavior of Reactor Materials in Fluoride Salt Mixtures, ORNL/TM-328, Oak Ridge National Laboratory (1962).

[6] Rosenthal, M. W., Haubenreich, P. N., and Briggs, R. B., The Development of Molten Salt Breeder Reactors, Vol. II, Oak Ridge National Laboratory (1972).

[7] Koger, J. W., Alloy Compatibility with LiF-BeF_2 Containing ThF_4 and UF_4, ORNL/TM-4286, (1972).

[8] Keiser, J. R., DeVan, J. H., and Manning, D. L., The Corrosion Resistance of Type 316 Stainless Steel to Li_2BeF_4, ORNL/TM-5782, Oak Ridge National Laboratory (1977).

[9] Cantor S., and Grimes, W. R., *Nucl. Technol.* 22, 120 (1974).

[10] Toth, L. M., "*Molten Fluoride Fuel Salt Chemistry*," Invited Paper-Session XII, 1994 International Conference on Accelerator-Driven Transmutation Technologies and Applications, Las Vegas, Nevada, July 1994.

[11] McCoy, Jr., H. E., Status of Materials Development for Molten Salt Reactors, ORNL/TM-5920, Oak Ridge National Laboratory (1978).

[12] Keiser, J. R., Status of Tellurium-Hastelloy N Studies in Molten Fluoride Salts, ORNL/TM-6002, Oak Ridge National Laboratory (1977).

[13] Sklad, P. S., Clausing, R. E., and Bloom, E. E., "*Effects of Neutron Irradiation on Microstructure and Mechanical Properties of Nimonic PE-16*," Irradiation Effects on the Microstructure and Properties of Metals, ASTM STP 611, 1976, pp. 139–155.

[14] Vaidyanathan, S., Lauritzen, T., and Bell, W. L., "Irradiation Embrittlement in some Austenitic Superalloys," Effects of Radiation on Materials: Eleventh Conference, ASTM STP 782, 1982, pp. 619–635.
[15] McCoy, Jr., H. E., An Evaluation of the Molten-Salt Reactor Experiment Hastelloy N Surveillance Specimens - Third Group, ORNL/TM-2647, Oak Ridge National Laboratory (1970).
[16] Maziasz, P. J., and Braski, D. N., *J. Nucl. Mat.* **141–143**, 973 (1986).
[17] Oku, T., Eto, M., and Ishiyama, S., *J. Nucl. Mat.* **172**(1), 77 (1990).
[18] Kelly, B. T., *Physics of Graphite*, 114, Applied Science Publishers, London (1981).
[19] Burchell, T. D., and Eatherly, W. P., *J. Nucl. Mat.* **179–181**, 205 (1991).

Radiation Damage Effects at Spallation Neutron Sources

L.L. Daemen[1], P.D. Ferguson[1], W.F. Sommer[1], M.S. Wechsler[2]
[1] *Los Alamos National Laboratory, Los Alamos, New Mexico 87545 and*
[2] *North Carolina State University, Raleigh, North Carolina 27695*

Radiation damage effects at accelerator-based spallation neutron sources correspond to a new regime, distinct from that encountered at fission reactors. We characterize the radiation environment of a spallation neutron source in some detail, and review the major issues associated with radiation damage at these sources. As a first step toward better understanding of radiation damage effects at such sources, we are trying to link together radiation transport codes with a variety of other codes such as CINDER'90 for activation calculations and the Jülich code SID for the calculation of basic radiation damage parameters. Several examples of the application of these codes to the determination of radiation effects at spallation sources are presented.

INTRODUCTION

Accelerator-driven spallation neutron sources (SNS) are becoming popular for a variety of applications ranging from cancer therapy and the production of medical radio-isotopes to accelerator production of tritium (APT), from accelerator transmutation of nuclear waste (ATW) and accelerator transmutation of plutonium (ABC) to accelerator-based neutron sources for neutron scattering studies of materials. Such projects are currently under study in the US, Europe, Japan, and the former Soviet Union. There are several spallation sources in operation at Los Alamos National Laboratory at the Los Alamos Neutron Scattering Center (LANSCE), the Los Alamos Meson Physics Facility (LAMPF), and the Weapons Neutron Research group (WNR). All these neutron sources have in common certain elements, such as an accelerator, a neutron production target, and a blanket system surrounding the target. The nature of the blanket is specific to the application considered, but it generally includes a reflector and/or moderator.

In view of the extreme conditions under which many materials used at SNS operate, it is hardly necessary to emphasize the importance of understanding and controling the change in physical properties these materials undergo in the spallation radiation environment. These effects have usually a dramatic impact on material properties, and ultimately determine important characteristics of the SNS such as failure modes or component lifetime, among others. While these effects have received considerable attention for fission reactors, there is a lack of theoretical and experimental studies devoted to radiation damage in the radiation environment of an accelerator-driven spallation neutron source, particularly for high-power applications.

The complexity of the radiation environment at a SNS, coupled to the desire to do most of the design calculations within a coherent framework lead us to try to couple well-known radiation transport codes such as LAHET and MCNP to other codes more directly relevant to radiation effect calculations such as CINDER'90 for activation calculations and SID for gas production and microstructural damage parameters.

COMPUTER CODES

For the benefit of the reader unacquainted with LCS and SID, this section contains a very brief description of both code systems.

The LAHET Code System (LCS) is, broadly speaking, a set of analog Monte-Carlo radiation transport codes. It has two main components: LAHET and MCNP. LAHET is based on the Bertini

intranuclear cascade/evaporation model and deals with the spallation physics and the transport of most of the particles born in spallation reactions. Photons and low energy (< 20 MeV) neutrons, however, are passed to MCNP for transport. MCNP uses ENDF/B-VI continuous cross sections, and a large number of complex laws to transport photons and neutrons. Both codes have a sophisticated geometry interface that allows the modelling of arbitrarily complex geometries. The interested reader will find more details in Refs.[1,2].

The Spallation-Induced Damage code was developed in Jülich, and implements the ideas of Lindhard et al.[3] to calculate a few basic radiation damage parameters. It makes use of a history tape dumped by LCS and containing detailed transport histories to calculate quantities such as damage energy cross sections, atom displacement cross sections, recoil spectra, spallation products, gas production, etc. SID is also capable of providing the contribution of various particle types and interaction mechanism (elastic scattering, non-elastic interactions, and fission events) to the various damage parameters calculated. We refer the interested reader to the complete manual [4] for more information.

Many essential features in these codes have been extensively benchmarked by comparison with other codes or with experimental results, see Refs.[4,5].

RADIATION ENVIRONMENT OF A SNS

Several important features distinguish the radiation environment of a spallation neutron source from that of a reactor, namely:

- The presence of high-energy (hundreds of MeV) charged particles from the accelerator (typically protons);
- The neutron spectrum resulting from spallation reactions is harder than a typical fission reactor spectrum;
- The spallation reactions induced by high-energy particles produce a large number of impurities in the form of spallation, fission, and transmutation products that alter the physical and chemical properties of the materials.

These considerations underscore the importance of assessing radiation damage to the various components of high-power accelerator facilities for accelerator-driven transmutation technologies. Although many components of a SNS are subjected to radiation in various degrees, the target and its associated components (containment vessel, window, etc) are more likely to be affected by the conditions outlined above than other components. This is especially true in view of the fact that in many SNS applications, the neutrons are often moderated after leaving that target, thereby softening the energy spectrum to a more familiar regime similar to that encountered at fission reactors. Thus we will focus essentially on the neutron production target in what follows.

In order to illustrate these points, we calculated (with LCS) the neutron energy spectrum for a 1 GeV proton beam on a stopping-length solid tungsten target, and compared it to a typical fission reactor spectrum. Fig.1 clearly show that the spallation neutrons produced when an 800 MeV proton beam hits a tungsten target have, on average, a larger kinetic energy than fission neutrons.

There are several broad classes of radiation damage parameters of interest to metallurgists and material scientists: (a) The production of hydrogen and helium isotopes via (n,α) reactions.

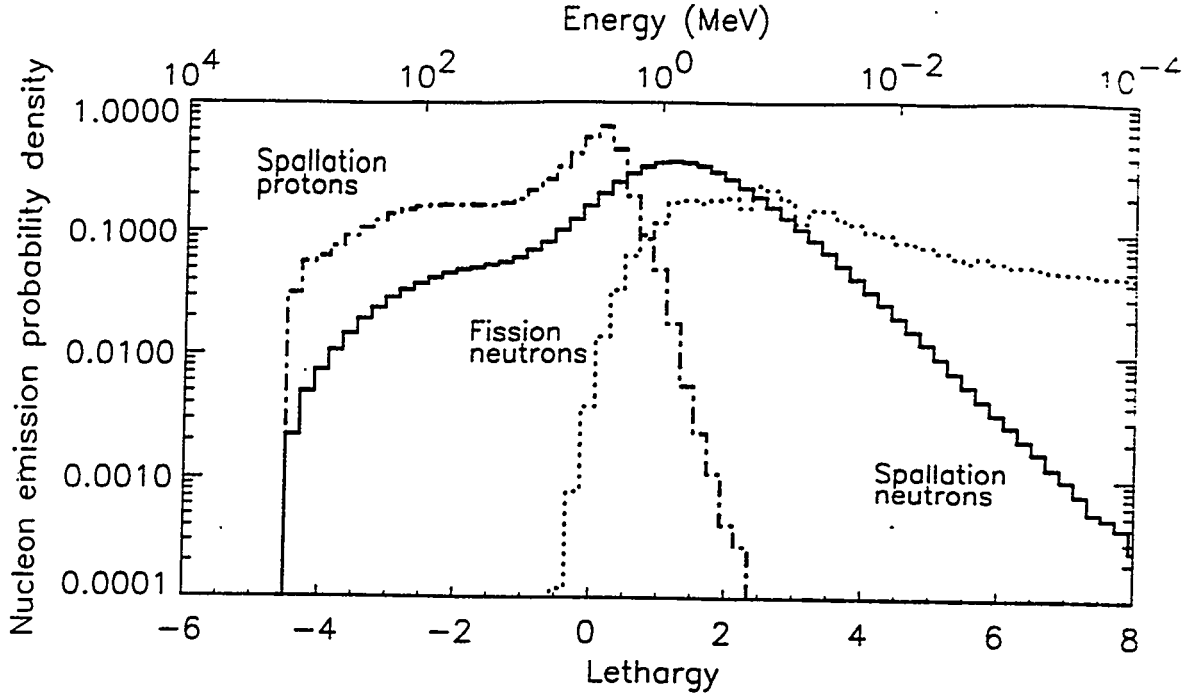

Figure 1: Probability density of observing a nucleon with energy E in a W target bombarded by 800 MeV protons. The corresponding quantity for a typical LWR is shown for comparison. The curves are normalized to unity.

However, notice the possibility of (p,α) or (d,α) reactions at SNS. (b) Atomic displacements leading to the formation of microstructural defects, and corresponding changes in the mechanical properties of the metal or alloy. (c) The formation of chemical impurities (spallation, fission, and transmutation products).

The next two sections are devoted to various aspects of these problems in relation to the SNS radiation environment. It should be emphasized that, although essential, these parameters are not enough to determine radiation *effects*. Indeed, the kinetics of the defects formed during irradiation must be taken into account to calculate the effect of irradiation on the physical properties of metals. There are also other basic radiation damage mechanisms and effects worth mentioning. For instance, many components have to be actively cooled during operation. The coolant of choice -light or heavy water- undergoes decomposition in the radiation field with the formation of highly reactive atomic or molecular species that contribute to accelerated metal corrosion. Another example is the effect of irradiation on the kinetics of various transport processes (e.g., displacement mixing in alloys, segregation, enhanced-diffusivity, etc). These effects are out of the scope of the present work.

GAS PRODUCTION

Hydrogen and its isotopes are soluble, to various degrees, in many metals. Occasionally, hydrogen can form stoechiometric compounds with metal leading to drastic chemical and physical changes. Zircaloy is an example of a material that is important for nuclear technology where hydrogen effects must be controlled. The effects of hydrogen in metals have been documented extensively in the nuclear technology literature and will not be considered here.

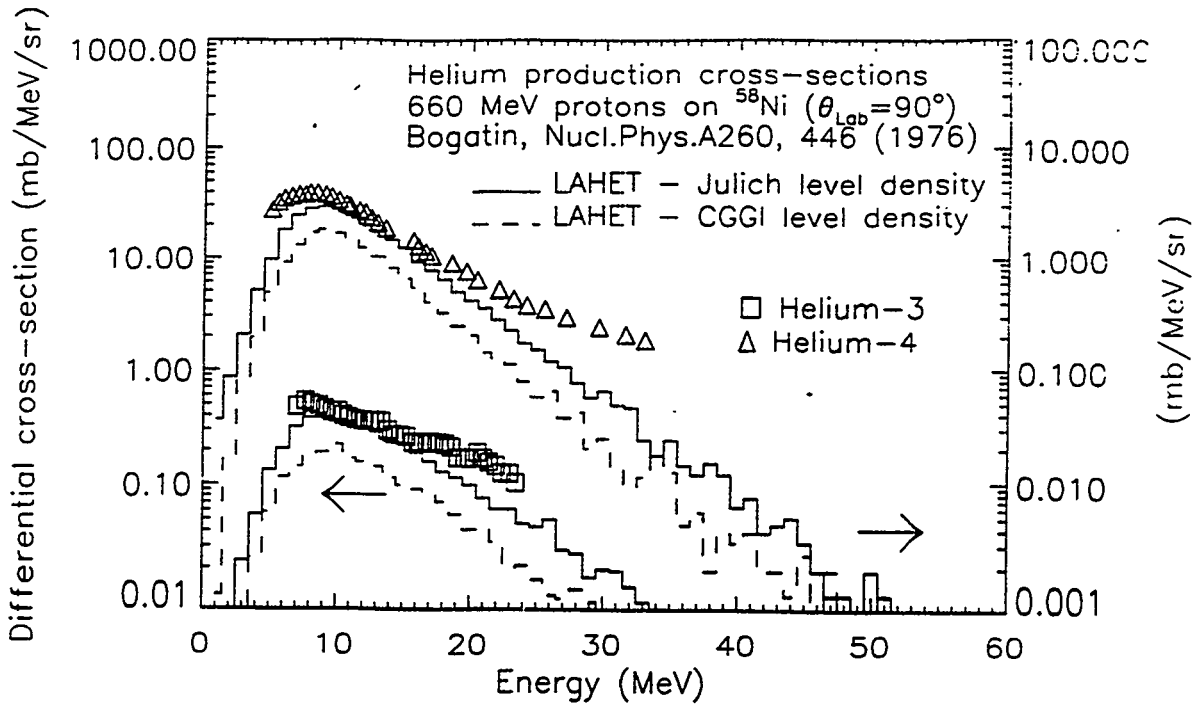

Figure 2: ^{3}He and ^{4}He production cross sections for 660 MeV protons on a thin ^{58}Ni target.

Perhaps more important than hydrogen formation is helium production. Because of their large enthalpy of solution, helium atoms are largely insoluble in most, if not all, metals. They tend to migrate, congregate at defects, and form large bubbles that ultimately embrittle the irradiated metal, particularly at high temperature. Helium embrittlement of metals has been extensively studied. A review can be found in Ref.[6].

We will focus on the calculation of hydrogen and helium production rates, particularly at SNS, rather than the consequences of hydrogen and helium formation in irradiated metals. In principle, codes such as LCS are capable of calculating gas production rates *ab initio*. In order to evaluate the accuracy and reliability of the gas production rates calculated by LCS, we compared the results of detailed calculations with a variety of nuclear models to experimental results. Fig.2 is a representative example of our calculations. Generally speaking, nucleon production can be predicted rather accurately [5] (and is not very sensitive to the physics model used). The prediction of production rates for light composite particles, however, is much more sensitive to the particular nucleus model used. Furthermore, although the order of magnitude of the production cross section is, most of the time, within a factor of a few of the measured cross section, certain qualitative features are not reproduced by the calculation. Fig.2 is an example where reasonably good agreement was obtained between the experimental results and the LAHET calculation. Other isotopes did not fare nearly as well. In calculating the results shown in Fig.1, we used all the default physics parameters in LAHET, but varied systematically the nuclear energy level density parametrization. We also calculated gas production cross sections for other isotopes and elements (^{120}Sn, ^{209}Bi, U, ^{27}Al, ^{54}Fe, ^{58}Ni, ^{12}C, ^{197}Au). There appears to be no single combination of model options in LAHET that leads systematically to better agreement with experimental measurements. Worse yet, for a given

isotope, different sets of options lead to better agreement depending on the gas being produced. These results will be described in detail elsewhere.

System (target)	Proton beam	Power density MW/l	^{1}H appm/d (at/p)	^{2}H appm/d (at/p)	^{3}H appm/d (at/p)	^{3}He appm/d (at/p)	^{4}He appm/d (at/p)
ATW-aq. (W)	E_p=1 GeV I_p=0.2 A W=200 MW	~2	60 (2.7)	9 (0.4)	4 (0.2)	0.6 (0.03)	12 (0.5)
APT (W)	E_p=1 GeV I_p=0.2 A W=200 MW	~2	58 (2.7)	9 (0.4)	4 (0.2)	0.6 (0.03)	12 (0.5)
LANSCE-II (W)	E_p=800 MeV I_p=1.25 mA W=1 MW	~0.6	14 (3.0)	1 (0.3)	0.6 (0.1)	0.06 (0.01)	1.6 (0.3)
ISIS (Ta)	E_p=800 MeV I_p=0.2 mA W=0.16 MW	~0.07	2 (2.7)	0.2 (0.3)	0.1 (0.1)	0.006 (0.007)	0.3 (0.3)
LANSCE (W)	E_p=800 MeV I_p=0.08 mA W=64 kW	~0.04	1 (2.7)	0.1 (0.2)	0.04 (0.1)	0.003 (0.007)	0.1 (0.3)
FBR core	W=2500 MW_t					0.03	
Fusion reactor (first wall)	1 MW/m^2		1.5		0.3		
HFIR	W=100 MW		1.2		0.07		

Table 1: Gas production rates at various SNS. The numbers between parentheses are gas production per incident proton. For comparison, we give helium production rates at a typical fast breeder reactor and in the first wall of a typical fusion reactor. The power density is an average for the neutron production target.

In all fairness, we ought to emphasize that the experimental cross sections are measured at a fixed angle in the laboratory frame of reference, and thus part of the discrepancy observed may be due to the inability to calculate accurately the angular dependence of the cross section. Indeed, comparison with angle-integrated cross sections reveals, generally, better agreement [7].

We used LCS to study gas production in the neutron production target of a variety of SNS (listed in Table 1). SID was used to extract gas production rates and cross sections. The SNS listed in

Table 1 operate at a variety of power levels, but they all have in common a water-cooled tungsten (or tantalum in the case of ISIS) target. For comparison, we include in Table 1 typical numbers (when applicable) for other nuclear systems. It can be seen immediately that gas production at SNS is significantly higher than that at other nuclear facilities, especially at higher accelerator power. Thus swelling and embrittlement problems can be expected to be much more severe at SNS.

RADIATION-INDUCED DEFECTS

SID uses the well-known Lindhard formalism [3,8] to calculate a number of useful radiation parameters such as damage energy and damage energy cross sections, dpa's and dpa cross sections, recoil spectra, etc. It has important limitations that are not easily overcome. Going beyond these limitations requires a drastically different approach such as that adopted by MARLOWE or molecular dynamics codes. Nonetheless, SID can provide useful insight into the severity of the radiation damage problem under consideration.

System	dpa/yr
APT	24
ATW-aqueous	65
LANSCE-II	16
LANSCE	1
HFIR (SS-316)	41
Fusion reactor (first wall)	13

Table 2: Displacements per atom (dpa) in the W target of the SNS listed in Table 1. Typical dpa for other nuclear system have benn included for comparison (see Ref.[10]).

Basic radiation damage parameters for medium- to high-energy proton irradiation of thin W targets have been studied extensively [9]. Coupling SID to LCS enables us to use the actual geometry of the system under study to calculate the radiation environment which is responsible for damage production. Table 2 shows the results of LCS/SID calculations for the W target of most of the SNS listed in Table 1. Typical numbers for other facilities have been included for comparison. The numbers quoted in Table 2 for SNS correspond to damage produced by the high-energy part of the radiation field, i.e., it includes everything except the effect of low-energy (< 20 MeV) neutrons.

CONCLUSION

The use of SID in conjunction with LAHET produces useful information for scoping, radiation damage calculations. Ultimately, more refined calculations (and experimental checks) are needed if one is to assess carefully the impact of radiation damage on component lifetime and failure modes. LCS and SID are useful to direct one's attention to potential problems for further study.

As illustrated by the gas production benchmark calculations more benchmarking and code validation is necessary to assess the reliability of primary yields of light composite particles. Clearly, improvements are needed. This implies an extensive reworking of the physics models

used. In all fairness, it should be mentioned that, to this day, the calculation of light composite particle yields remains a challenge to theoretical nuclear physicists.

We have shown that gas production rates are much higher at SNS than at fission reactors, and thus that the familiar embrittlement and swelling problems are likely to be felt more accutely at SNS, especially at higher power levels.

Similarly, dpa's are high at SNS, and it is likely that materials considerations will be an essential part of SNS design, particularly at higher accelerator power. Finally, it is worth emphasizing the importance of calculating damage parameters in the actual radiation environment of a SNS, with the appropriate geometry. It is thus highly desirable that LCS or similar codes be coupled directly to radiation effects computer codes.

ACKNOWLEDGEMENTS

This work was supported by the US Department of Energy. We thank R.E. Prael, L.S. Waters, and R. Kidmann for useful discussions.

REFERENCES

[1] R.E. Prael and H. Lichtenstein, "User guide to LCS: The LAHET Code System", Los Alamos National Laboratory report LA-UR-89-3014 (September 1989); R.E. Prael, "A review of physics models in the LAHET code", submitted for Specialists' Meeting on Intermediate Energy Nuclear Data, Nuclear Energy Agengy, OECD, Paris, May 30 - June 1, 1994, LA-UR-94-1796, Los Alamos National Laboratory (May 1994)

[2] "MCNP - A general Monte-Carlo code N-particle transport code - Version 4A", Judith F. Briesmeister, editor, Los Alamos National Laboratory report LA-12625, (1993).

[3] M.T. Robinson and I.M. Torrens, Phys.Rev.**B9**, 5008, (1974) and references therein.

[4] T.W. Armstrong, P. Cloth, D. Filges, "SID - User's manual", Jülich internal report.

[5] T.O. Brun, L.L. Daemen, E.J. Pitcher, G.J. Russell, C.A. Beard, and W.B. Wilson, "LAHET Code System/ Cinder'90 validation calculations and comparison with experimental data", Proceedings of the Twelfth Meeting of the International Collaboration on Advanced Neutron Sources, Rutherford-Appleton Laboratory (May 1993) RAL-94-025, p.T-26.

[6] H. Ullmaier, in "Atomic defects in metals", Landolt-Börnstein (Springer-Verlag, Berlin, 1991), Chapter 3. See also, H. Ullmaier and H. Trinkaus, "Helium in metals: Effect on mechanical properties", in Materials Science Forum, Vol.97-99, G.Szenes Ed., (Trans Tech Publications, Zürich, Switzerland), pp.451-472.

[7] S.L. Green et al., "Production of helium by medium energy protons.", J.Nucl.Mater., **155-157**, 1350 (1988).

[8] M.T. Robinson, "The theory of radiation-induced defect production", in 'Radiation Damage in Metals', Papers presented at a seminar of the American Society of Metals, Nov. 9 and 10, 1975, N.L. Peterson, Ed., (American Society for Metals, Metal Park, 1975), p.1.

[9] M.S. Wechsler, private communication.

[10] T.A. Gabriel, J.D. Amburgey, N.M. Greene, "Radiation damage calculations: primary recoil spectra, displacement rates, and gas production rates", ORNL/TM-5160 (1976).

Materials Considerations in Accelerator Targets

H. B. Peacock, Jr., N. C. Iyer and M. R. Louthan, Jr.

Materials Technology Section, Savannah River Technology Center,
Westinghouse Savannah River Company, Aiken, SC 29808

Abstract Future nuclear materials production and/or the burn-up of long lived radioisotopes may be accomplished through the capture of spallation produced neutrons in accelerators. Aluminum clad-lead and/or lead alloys has been proposed as a spallation target. Aluminum was the cladding choice because of the low neutron absorption cross section, fast radioactivity decay, high thermal conductivity, and excellent fabricability. Metallic lead and lead oxide powders were considered for the target core with the fabrication options being casting or powder metallurgy (PM). Scoping tests to evaluate gravity casting, squeeze casting, and casting and swaging processes showed that, based on fabricability and heat transfer considerations, squeeze casting was the preferred option for manufacture of targets with initial core cladding contact.

Thousands of aluminum clad aluminum-lithium alloy core targets and control rods for tritium production have been fabricated by coextrusion processes and successfully irradiated in the SRS reactors. Tritium retention in, and release from, the coextruded product was modeled from experimental and operational data. The model assumed that tritium atoms, formed by the 6Li(n,a)3He reaction, were produced in solid solution in the Al-Li alloy. Because of the low solubility of hydrogen isotopes in aluminum alloys, the irradiated Al-Li rapidly became supersaturated in tritium. Newly produced tritium atoms were trapped by lithium atoms to form a lithium tritide. The effective tritium pressure required for trap or tritide stability was the equilibrium decomposition pressure of tritium over a lithium tritide-aluminum mixture. The temperature dependence of tritium release was determined by the permeability of the cladding to tritium and the local equilibrium at the trap sites. The model can be used to calculate tritium release from aluminum clad, aluminum-lithium alloy targets during postulated accelerator operational and accident conditions. This paper describes the manufacturing technologies evaluated and presents the model for tritium retention in aluminum clad, aluminum-lithium alloy tritium production targets.

INTRODUCTION

Conventional production of nuclear materials for atomic weapons has relied on neutron capture in specially designed targets exposed to a neutron flux in a nuclear reactor. Future nuclear materials production and/or the burn-up of long lived radioisotopes generated during previous production campaigns may be accomplished through the capture of spallation produced neutron in accelerators. High energy protons from an accelerator bombard lead targets and cause spallation reactions that generate neutrons. The free neutrons strike aluminum-lithium targets located in blanket positions around the spallation targets. Both the lead and the aluminum-lithium target cores are clad and placed inside pressure tubes. The cladding material will be selected through evaluation of its nuclear, thermal and metallurgical properties and the cost and ease of fabrication.

Fabrication technologies for the spallation source target are not as well established as the aluminum clad aluminum-lithium core target technology. Coextrusion of a metallurgically bonded cladding over the very soft, low melting temperature lead will be

extremely difficult. Without coextrusion or some other elevated temperature metal working process to break the protective oxide film on the clad material, a metallurgical bond between the clad and core is unlikely. The low melting temperature of lead precludes most of the elevated temperature working processes; thus, fabrication technologies which do not produce a clad-core bond may be required for the spallation target. Scoping experiments to establish the potential for direct casting and cold swaging of the spallation target were therefore conducted (1).

Fabrication of aluminum clad aluminum-lithium alloy targets from tritium is a proven technology which has been used at the Savannah River Site (SRS) for over thirty years. The primary target fabrication technology at SRS has been billet casting and coextrusion although direct casting, powder metallurgy and swaging technologies have also been applied. These technologies should be easily modified and transferred to a commercial fabricator for the production of accelerator targets. Billet casting and coextrusion will require only minor modifications before that technology is directly applicable to the fabrication of tritium producing, aluminum-lithium targets. Additionally, the SRS operating experience may be coupled with an understanding of tritium behavior in the target to provide the model necessary to predict tritium retention under postulated operating and accident conditions. This paper summarizes the results of the scoping experiments on fabrication of the spallation targets and presents a model for tritium retention in the aluminum clad aluminum-lithium alloy tritium production target.

FABRICATION OF SPALLATION TARGET

Cladding Materials

Cladding for the lead spallation target must have a low thermal neutron absorption cross section, an established data base for neutron damage, good weldability and workability, reasonable thermal conductivity, experienced significant use in accelerators and resist degradation in the accelerator environment. Potential cladding materials include aluminum and its alloys, Inconel and Type 304L stainless steel. Aluminum is the primary candidate because of the excellent experience base and its low neutron absorption cross section, fast radioactivity decay, high thermal conductivity, and excellent fabricability. However, aluminum alloys are very susceptible to mercury induced degradation processes such as liquid metal embrittlement and amalgamation.

Mercury is produced during the spallation of lead. The Spallation Induced Lithium Conversion (SILC) accelerator concept, for example, may produce about eight kilograms of mercury during six months of operation (2). The mercury content in the 24,000 kgs of lead used in the SILC concept is only about 0.03 wt. %; thus, most if not all the mercury should be soluble in the lead (3) and only the mercury vapor should be available for the degradation processes. The vapor pressure of mercury at 250°C, a potential operating temperature for the spallation targets in the SILC concept, is about 9.9 kPa. This pressure may be adequate to cause degradation of an aluminum cladding, if the protective oxide film were compromised. If mercury induced degradation of aluminum alloys is determined to be a significant problem, Inconel, or even Type 304 stainless steel, could become a compromise cladding candidate. However, mercury induced degradation and compromise of the aluminum cladding is currently considered to be unlikely and aluminum alloys remain the preferred cladding alloy and the only cladding material studied in these scoping experiments.

FABRICATION PROCESSES

Gravity Casting

An aluminum clad-lead core target was fabricated by direct casting lead into a preheated Type 1100 aluminum alloy tube. The 41 cm long aluminum tube had a 2.4 cm outside diameter and a 0.35 cm wall. Molten lead, at approximately 400°C, was bottom poured from a graphite crucible into the aluminum tube which had also been preheated to 400°C. The pseudo target was air cooled (the lead solidified in approximately three minutes), then sectioned for evaluation. A small pipe formed at the top of the casting and, because of differences in thermal contraction during cooling, a gap developed between the lead core and the aluminum cladding.

The gap was measured by preparing vacuum/epoxy impregnated metallographic sections. The gap width in these right circular cylindrical sections was measured at an arbitrary position and at every 45° from that position. The average gap width varied from 0.008 mm near the top of the target to 0.057 mm near the bottom. There were wide variations around the average and in isolated locations the lead wetted the aluminum forming a metallurgical bond, Figure 1. Typical gaps between the lead and aluminum are illustrated in Figure 2.

The maximum lead, or target centerline, temperature at any given set of accelerator operating parameters is a sensitive function of the gap width. Heat transfer across a gap decreases as the gap width increases and is improved if the gap contains helium rather than air or a vacuum. Parametric studies of the target centerline temperature as a function of gap width demonstrate that the calculated target centerline temperature in an Inconel 601 clad-lead core target increases from 220°C to 265°C as the gap size increases from 0.025 mm to 0.076 mm (Figure 3). This centerline temperature calculation was based on the assumption that heat is uniformly generated, 100 W/cm^3, within a one centimeter diameter lead target clad with 0.08 cm of Inconel 601 and exposed to cooling water at 90°C. The calculated centerline temperatures for an aluminum clad target are anticipated to be lower because the 100°C thermal conductivity of aluminum (235W/m°C) is significantly higher than that for Inconel 601 (13W/m°C). In addition to affecting the margin against melting, the gap size may also affect the susceptibility to cladding degradation because the mobility of spallation products, including mercury, will decrease significantly as the temperature decreases. Therefore, fabrication techniques that minimize gap width may be desirable. Squeeze casting of pseudo target was therefore attempted.

Squeeze Casting

Squeeze casting is the process of solidifying metal under pressure. The high pressure promotes melt feed from hot spots to incipient shrinkage pores, keeps trapped gases in solution and promotes intimate contact between the casting (lead) and the tooling (the cladding).

A pseudo lead-aluminum target was squeeze cast by bottom pouring lead at 400°C into a system (an aluminum tube and associated tooling) that was preheated to 200°C. A 8.6 MPa pressure was applied to the lead during solidification. The system preheat temperature was selected to assure that the 8.6 MPa pressure did not deform the aluminum cladding. This casting process reduced the average gap but has little apparent affect on the tendency for the lead to wet the aluminum cladding. The average gap width varied from 0.004 mm near the bottom of the target to 0.016 mm near the target top.

These gaps are partially due to thermal gradients that develop during solidification and to the differences in thermal expansion among lead and aluminum alloys. Similar thermal effects will develop in an operating target. Thus even if a zero gap target were fabricated, accelerator operation would produce a core-clad gap during cyclic operation without a metallurgical bond.

Finite Element Analysis

Finite element analysis was done to determine the clad-core response of a spallation target operating under hypothetical conditions. The analysis was for a target that had no gap between the Type 1100 aluminum cladding and pure lead core. This postulated zero gap, zero residual stress target was heated to steady state operation conditions where the centerline temperature was 250°C and the aluminum cladding was at 90°C at the coolant-clad interface. A linear radial gradient was imposed on the 150 cm long target and no axial or angular variations in temperature were assumed. Temperature dependent values for thermal expansion coefficients and yield strength were used in the calculation. Elastic-perfectly plastic material behavior was also assumed. The coefficient of friction at the clad-core interface was based on engineering judgment and was chosen to be 0.6 with a stiffness in stick of 1MPa.

The finite element analysis showed that, at the operating conditions, the lead core expanded against the aluminum cladding with sufficient force to cause the lead to yield axially (Figure 3). This axial expansion is approximately 0.6% and creates a need for expansion chambers at the target ends. On cooling to room temperature, the lead is permanately deformed and has an axial plastic strain of 0.3%, thus leaving a gap of approximately 0.0075 mm between the cladding and the core (Figure 4). Therefore, the minimum average gap sizes observed in both the gravity cast and the squeezed cast pseudo targets are similar to the gap that would developed during service, even if a zero gap target were fabricated. However, clad-core wetting could provide a metallurgical interface which may inhibit gap development during service.

Cast and Swaged

The strength of the lead-aluminum metallurgical interface was apparent is a gravity cast pseudo target which was cold swagged in an attempt to reduce the as fabricated gap size. The pseudo target was cast to duplicate the gravity cast target, than cold swagged in an attempt to reduce the as-fabricated gap size. The room temperature swaging process reduced the rod diameter by 9.6%. Metallurgical evaluation of the swaged target showed that the gap width varied from 0.005 mm to 0.038 mm. The swaging process caused fracture of the lead core underlying the wetted or metallurgically bonded regions (Figure 5).

A metallurgically bonded interface will improve heat transfer between the target core and cladding and therefore lower the centerline temperature of an operating spallation target. However, the metallurgical bond may also facilitate the core to clad migration of spallation products. Mercury, which is generated in the lead, could accumulate at the lead-aluminum interface. In contrast to the normal oxide film which prevents metallurgical contact between mercury and aluminum, this interface is not protective. Additionally, the aluminum will be in tension because of the thermal expansion gradients and the differences in thermal expansion. The combination of metallurgical contact with mercury and an operating tensile stress could cause liquid metal embrittlement and splitting of the aluminum cladding. This liquid metal embrittlement scenario has received only minimal attention. Until this potential

degradation process is more fully understood, the satisfactory performance of a metallurgically bonded lead core-aluminum clad spallation target is questionable.

The tendency for metallurgical bonding at the clad core interface of a direct cast target can be minimized, if not eliminated through the use of aluminum tubing with anodized coatings on the interior surfaces. Nunerous commercial anodization processes are available. These processes can produce uniform, relatively defect free coatings similar to the 6000 angstrom thick coating shown in Figure 6. The actual thickness of coating required would be a compromise among the desire for a thin coating for heat transfer purposes and a thick coating to protect against metallurgical bonding. Other barrier layers, such as a nickel plate on the interior surface of the aluminum, may be effective in preventing degradation by the spallation products while permitting metallurgical bonding and thereby improving the heat transfer characteristics. However, the desirability of a metallurgical bond in the spallation target has not been established. This contrasts the aluminum clad-aluminum lithium tritium production target which can be coextruded to assure a metallurgical bond at the clad-core interface.

MODELING THE TRITIUM PRODUCTION TARGET

The ability to accurately model tritium retention in, and release from, aluminum clad-aluminum lithium alloys is vital to the safe and efficient production of tritium in an accelerator. The Savannah River Site's operational experience has demonstrated that essentially all the tritium produced during irradiation is retained in the target until extraction processes are initiated. The model developed in the following paragraphs provides the technical basis to calculate tritium release as a function of the target temperature. Heat production in the tritium target is minimal, thus the target temperature may be considered to equal the temperature of the accelerator coolant.

Model Development and Assumptions

The flux of hydrogen through a metallic wall is dependent on the permeability (f) of the wall material, the area and thickness of the wall, and the driving force (G), which is related to the difference in hydrogen activity on the entrance and exit surfaces. Permeability is simply the product of the diffusivity (D) and solubility (S). Hydrogen solubility can be related to either a real or an effective hydrogen pressure (p) on the wall. Permeability, diffusivity and solubility can be expressed as: $f = SD$, where

$$D = D_o \exp(-Q_d/RT) \text{ and} \qquad [1]$$

$$S = S_o (p)^{1/2} \exp(-Q_s/RT) \qquad [2]$$

The hydrogen pressure is generally assumed to be one in the expression for permeability.

Experiments to determine the permeability of metals and alloys to hydrogen isotopes generally involve the exposure of one side of a relatively thin, foil-like sample to gaseous hydrogen and the measurement of the hydrogen flux through the foil. Under these conditions, molecular hydrogen dissociates on the entrance surface, dissolves and diffuses as an atom or screened proton, reaches the exit surface and combines with another hydrogen atom to form a molecule. The driving force for such permeation is a function of the hydrogen pressure on the two sides of the foil,

$$G = \sqrt{P_1} - \sqrt{P_2} \qquad [3]$$

If the hydrogen concentration on the exit side of the foil is zero, the driving force for permeation is $\sqrt{p}$, where p is the hydrogen pressure, either real of effective, on the entrance side of the foil. The $\sqrt{p}$ relationship results because hydrogen is a diatomic gas molecules which dissolves as an atom.

The tritium (^3H) which is created in an Al-Li alloy through the $^6Li(n,a)^3$ the reaction is not in equilibrium with a real hydrogen pressure. However, if hydrogen is to remain in solution, a driving force, or effective hydrogen pressure, is required. The effective pressure is

$$P_{eff} = [(S_o/S) \exp(-Q_s/RT)]^2 \qquad [4]$$

The concept of representing the hydrogen activity as an effective pressure has been used to describe hydrogen induced effects during cathodic charging, corrosion, and acid cleaning of metals (4-6).

The diffusion of hydrogen generally involves interaction of the absorbed hydrogen with lattice defects, including alloy and impurity atoms (7). The sites for such interactions are traps and the equilibrium hydrogen concentration in the vicinity of the trap may be significantly higher than the true lattice solubility. Trapping causes the effective diffusivity to decrease and the apparent solubility to increase but has no effect on steady state conditions (8).

Trapping of hydrogen isotopes in Al-Li alloys will increase the tritium retention capabilities of the alloys. This can be illustrated through calculations of tritium retention in the Mark 22 targets that have been extensively used for tritium production at SRS.

The average isothermal diffusion distance (x) for hydrogen during time (t) is given by

$$x = \sqrt{Dt} \qquad [5]$$

where D is the diffusivity of hydrogen. Hydrogen diffusivity in aluminum, calculated from permeation type measurements (7), is given by

$$D = 0.011 \exp(-9{,}200/RT) \text{ cm2/sec.} \qquad [6]$$

A tritium atom, formed by a 6Li (n,a)3H reaction will begin to diffuse immediately after the nuclear reaction. The time required for tritium to migrate provides an estimate of the anticipated residence time for an untrapped tritium atom. These estimates show that without trapping, tritium atoms created within the targets would be released within days of operation at 100°C. This contrasts the operational experience which demonstrates months of irradiation at 100°C without measurable tritium release to the moderator.

The importance of trapping to tritium retention in Al-Li targets was established during the early SRS operations (see References 10 and 11 for example). This early work lead to the conclusion that lithium tritide is formed during irradiation and that the reaction between lithium tritide and aluminum,

$$LiT + Al \longrightarrow LiAl + T \qquad [7]$$

is the mechanism for release of tritium when the irradiated Li-Al alloy targets are heated.

These early arguments provide a basis to model for tritium release from aluminum clad, Al-Li alloys by assuming:

1. local equilibrium is maintained amount the phases in the Al-Li alloy, (These phases are face-centered cubic aluminum containing both lithium and tritium in solid solution, the intermetallic, LiAl, and lithium tritide),

2. the effective tritium pressure that establishes equilibrium pressure for decomposition of lithium tritide,

3. tritium release from the Al-Li alloy is determined by permeation through the aluminum cladding,

4. the effective pressures controlling tritium permeation through the cladding are the equilibrium pressure for decomposition of lithium tritide at the entrance surface and zero as the exit surface,

5. neutron irradiaiton does not significantly alter the permeability of aluminum alloys to hydrogen isotopes,

6. the intermetallic, LiAl is present in the Al-Li alloy throughout the irradiation process,

7. helium induced swelling and blistering are not a factor in tritium release, and

8. steady state permeation exists from the onset of irradiation.

The eight assumptions listed above are all included either directly or indirectly, in the model for tritium release illustrated in Figure 7.

Model Calculations

The temperature dependence of the equilibrium decomposition pressure was determined by a least squares fit of previously published data (12). The data was forced to an exponential function giving:

$$P_{equilibrium} = 351 \exp(-10{,}700/RT) \text{ atm} \qquad [8]$$

Individual data points are shown in Figure 8. The equilibrium decomposition pressure (P equilibrium) represents the effective tritium pressure in the Al-Li alloy.

The permeability of the cladding to tritium was calculated from previously published deuterium permeation data (9). The use of deuterium data should also provide an upper bound estimate of tritium permeation because classical isotope effects predict that the higher mass of the tritium atom will lower permeability. The permeability data used in the calculation were selected to minimize the potential for surface induced reductions in permeability. This selection was discussed in Reference 9 and the resulting permeability equation is

$$f = 1.9 \times 10^{-2} \exp(-22{,}400/RT) \text{ cc(NPT) atm}^{-1/2}\text{sec}^{-1}\text{cm}^{-1} \qquad [9]$$

The relationship may be combined with the anticipated cladding thickness, x, and the equation for the equilibrium decomposition pressure to obtain the temperature dependence of tritium release per square centimeter of target cladding. This maximum release rate, R, is given by

$$R = (0.355/x)\ \exp(-27{,}750/RT)\text{cc(NTP) cm}^{-2}\text{sec}^{-1}. \qquad [10]$$

where x and T are the clad thickness and temperature respectively.

CONCLUSIONS

Scoping tests to evaluate gravity casting, squeeze casting, and casting and swagging processes suggest that, based on fabricability and heat transfer considerations, squeeze casting was the preferred option for manufacture of aluminum clad-lead spallation targets with zero initial gap. The interior of the aluminum cladding should be anodized prior to the casting operation to minimize mercury - aluminium reactions resulting from metallurgical bonding across the core-clad interface.

The technical basis to model tritium release from aluminum clad, aluminum-lithium alloy targets as a function of temperature and clad thickness was developed. The model demonstrates that tritium release is governed by the equation:

$$R = (0.035/x)\ \exp(-27750/RT)\ \text{cc(NTP) cm}^{-2}\ \text{sec}^{-1} \qquad [11]$$

REFERENCES

1) H. B. Peacock, Concepts for Fabricating SILC Targets for the Accelerator Production of Tritium, Westinghouse Savannah River Company, WSRC-TR-93-452, August 31, 1993.

2) APT SILC Target Draft Preconceptional Design, APT Design Review Meeting March 1-4, 1993, Brookhaven National Laboratory, ATD/APT93-0007 (REV. 0).

3) Constitution of Binary Alloys, Max Hansen ed., Second Edition, p. 829, McGraw-Hill, New York, 1958

4) P. Rozenak and D. Eliezer, "Phase Changes Related to Hydrogen Induced Cracking in Austenitic Stainless Steels", Environmental Degradation of Engineering Materials III, edited by M. R. Louthan, Jr., R. P. McNitt and R. D. Sission, Jr., The Pennsylvania State University, p 149, 1987.

5) C. B: Bargeron and R. C. Benson, J. Electrochem Soc., Vol 119, p 1297, 1980.

6) R. Oriani and P. H. Josephic, Met. Trans. A, Vol 10A, p 1809, 1980 and J. W. Watson, Y. Z. Shen and M. Meshi, Met. Trans. A, Vol 19A, p 2299, 1988.

7) M. R. Louthan, Jr. and G. R. Caskey, Jr., International Journal of Hydrogen Energy, Vol.1, p 291, 1976.

8) G. R. Caskey, Jr., and W. L. Pillenger, Met. Trans., Vol. 6A, p 467, 1975.

9) M. R. Louthan, Jr., G. R. Caskey, Jr., and A. H. Dexter, Radiation Effects and Tritium Technology for Fusion Reactors, Vol. 4, p IV-117, Proceedings of International Conference held at Gatlinburg, TN, October 1975, Oak Ridge National Laboratory Report CONF-750989, March 1976.

10) L. H. Meyer and M. O. Fulda, Mode of Retention of Gases in Irradiated Li-Al Alloy, I-Distribution of Tritium and Helium Between Alpha and Beta Phases, DP-378, May 1959.

11) L. H. Meyer and M. O. Fulda, Mode of Retention of Gases in Irradiated Li-Al Alloy. II-Reaction Between Lithium Tritide and Aluminum, DP-397, July 1959.

12) J. H. Owen and D. Randall, Radiation Effects and Tritium Technology for Fusion Reactors, Vol. 3, p III-433, Proceedings of International Conference held at Gatlinburg, TN, October 1975, Oak Ridge National Laboratory Report CONF-750989, March 1976.

ACKNOWLEDGEMENTS

The authors acknowledge the support through Brookhaven National Laboratory and many helpful discussions with Dr. C. Czajkowski of BNL.

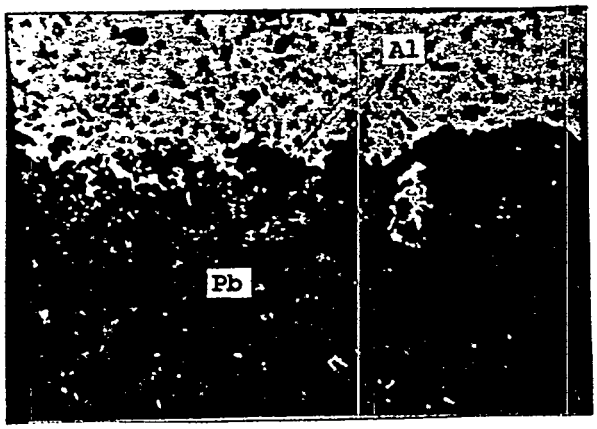

Figure 1: Typical Metallurgical Bond formed on Gravity Cast Pseudo Target

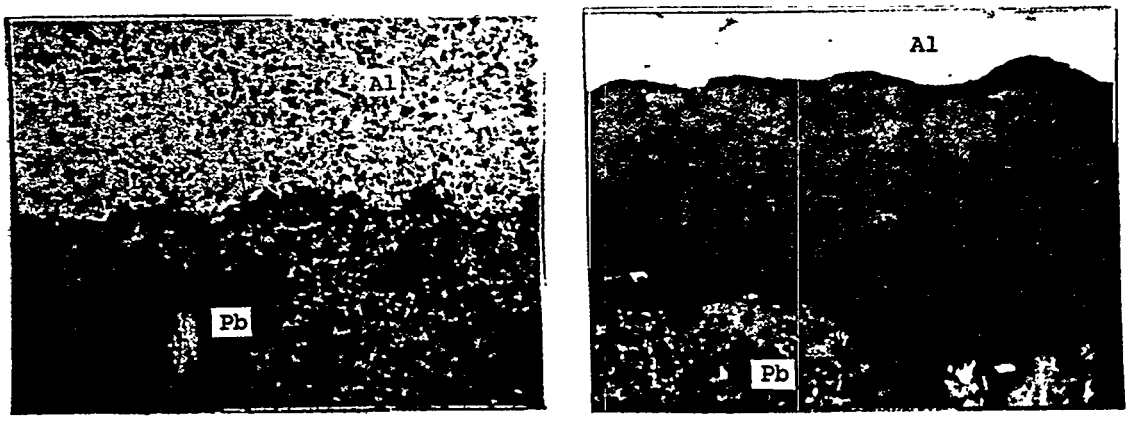

0.003 mm 0.043m

Figure 2: Typical Gaps Observed Between Core and Cladding of As-Cast Spallation target 1000x Magnification.

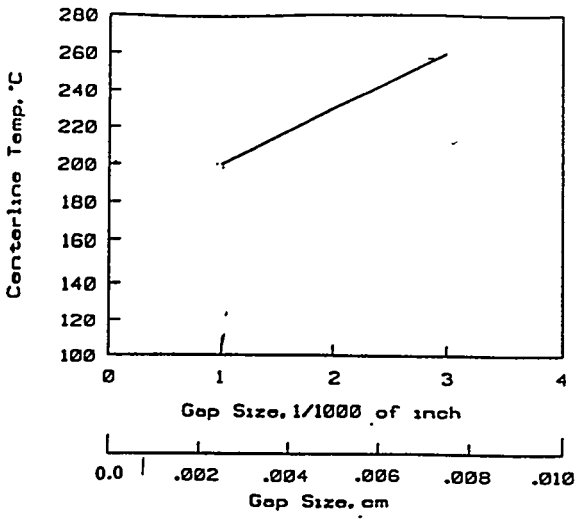

Figure 3: Centerline Temperatures vs. Gap Size for Lead (Q= 100 w/cc, Pellett Diameter = 1.27cm, Helium filled)

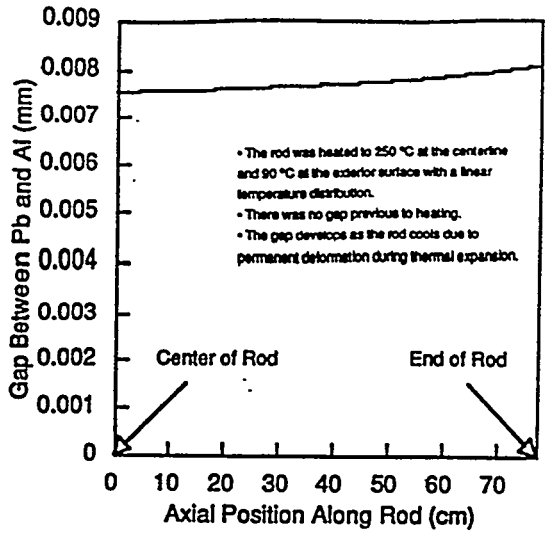

Figure 4: The Material Interface Gap After Heating

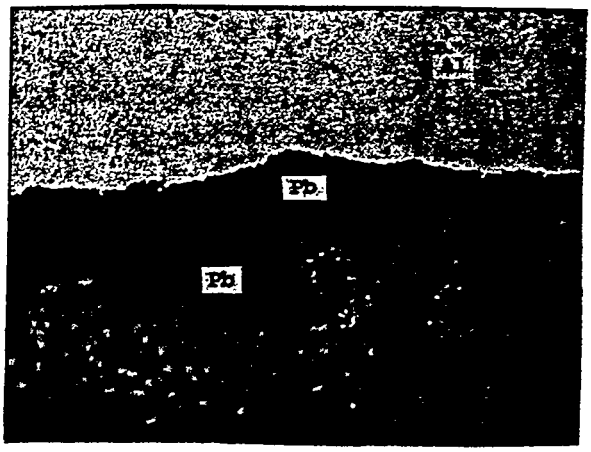

Figure 5: Cast and Swaged Spallation Target Indicating Bonding and Separation Between the Lead Core and Aluminum Cladding

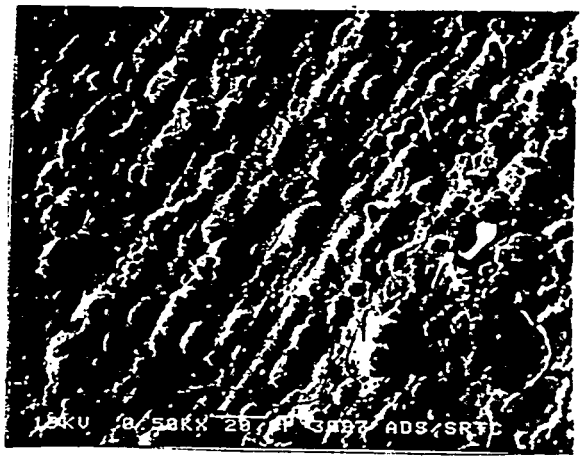

Figure 6: Anodized Aluminum Surface (Porous Film)

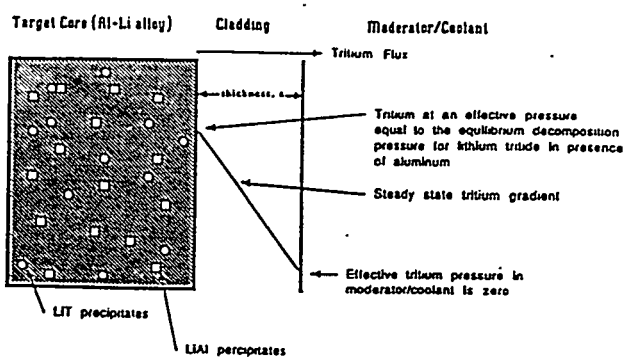

Figure 7: Model for Tritium Retention in, and Release from, Al-Li Alloys

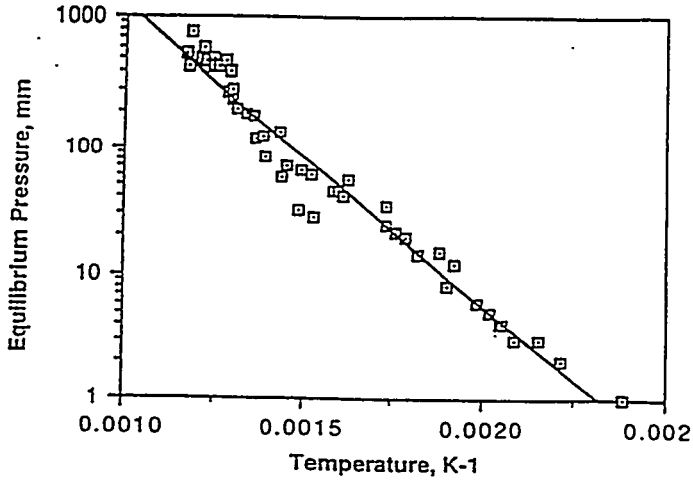

Figure 8: Temperature-Pressure Dependence of Decomposition of Lithium Hydride

Radiation-Induced Segregation in Materials: Implications for Accelerator-Driven Neutron Source Applications

Roy G. Faulkner and S. Song

Institute of Polymer Technology and Materials Engineering
Loughborough University of Technology
Loughborough
Leicestershire LE11 3TU
UK

Abstract. This paper reviews exisiting models for radiation-induced segregation to microstrucural interfaces and surfaces. It indicates how the models have been successfully used in the past in neutron irradiation situations and how they may be modified to account for accelerator-driven RIS. The predictions of the models suggest that any impurity with large misfit will suffer RIS and that the effect is heightened as radiation damage increases. The paper suggests methods to utilise the RIS in transmutation technology by dynamically segregating long life nuclides to preferred sites in the microstructure so that subsequent transmutations occur with maximum efficiency.

INTRODUCTION

Radiation induced segregation (RIS) occurs in materials because of the high non-equilibrium concentrations of point defects created during the irradiation process. In simple terms, the supersaturation of these point defects is relieved in regions of the microstructure which are good sinks, like grain boundaries and surfaces, but in other regions the supersaturation is maintained. There is a consequent concentration gradient produced for the point defects around the sink plane. This results in a net flux of defects towards the sink plane. There is evidence that a proportion of the defects will bind with misfitting impurity atoms and form point defect-impurity complexes. These complexes also move down the concentration gradients surrounding the defect sink plane. The net result is that a non-equilibrium concentration of complexed impurity atoms is created in the vicinity of the sink plane. The excess concentration will die away when the irradiation is switched off.

Various attempts have been made to model this process. The major model uses conventional non-equilibrium segregation theory, which has in the past been applied to thermally induced segregation situations. The model described by Faulkner (1) calculates the levels of point defects and associated complexes as a function of the irradiation conditions and assumes that the thermal equilibrium concentrations are maintained on the sink planes. The normal diffusion equations are then solved with these boundary conditions and a forecast of the expected composition profiles for the various impurity atoms around the sink is produced as a function of irradiation conditions. The model is most successful in predicting impurity segregation for dilute alloy conditions. For concentrations above 10%, the predictions are not so accurate. The outcome of this model is that any internal or external sink will attract impurity atoms during neutron or charged

particle irradiation. The effect is enhanced if the impurity has a large misfit with the matrix.

Alternative approaches apply rate theory, or inverse Kirkendall effect models (2,3). In this case the Fick's second law diffusion equations for all the participating defects and atoms are defined so that they will predict the variation of concentration with time at any predefined position. These partial second order differential equations are then solved simultaneously using a powerful computer. These models indicate the same trends as the non-equilibrium segregation model but they are able to take less account of microstructural variables such as grain size and dislocation density.

In this paper predictions of the non-equilibrium segregation model will be discussed in the light of making suggestions concerning the use of RIS in optimising transmutation technology with an accelerator-driven charged particle or neutron source.

MODELLING DETAILS

The non-equilibrium RIS model (1) is used in this paper. The model defines the point defect supersaturation as a function of dose rate. Recombination is considered and represented in a correction factor defining the number of freely migrating defects emerging from the collision cascades (4). Point defect annihilation at sinks such as dislocations and grain boundaries is accounted for in the Bullough equation for sink efficiency (5). A temperature dependency on dislocation density of the following form is assumed (6).

$$\rho = \rho_0 \exp\left(\frac{Ea}{kT}\right)$$

where ρ_0 is the original dislocation density and Ea is an energy of formation term connected with the creation of dislocations.

The result is an expression which defines the maximum enrichment of a sink plane with a given impurity. The rate at which these enrichments accumulate depends upon the diffusion characteristics of the point defects, the impurity atoms and the impurity-point defect complexes. The binding energy between the point defect and the impurity atom and the width of the sink plane are also important. The time factor in the calculations is equivalent to neutron dose.

The model predicts that eventually a steady state is reached during irradiation at a constant dose rate. The saturation time is dependent on the grain size, in the case of grain boundary RIS, and the relative diffusion rates of the complexed and uncomplexed impurity atoms in the matrix.

Binding energies between interstitials and impurities are always higher than those concerning the vacancies; 0.5 eV as opposed to <0.1 eV, and so the main complex considered in RIS is the interstitial-impurity complex.

Diffusion coefficient data are obtained by assuming that the interstitial complex diffuses with an entropy term approximating to 1 m^2 s^{-1} (7) The activation energy for migration of such complexes is calculated using a stress analysis approach aimed at defining the strain energy of the atoms at the saddle points envisaged in the diffusion mechanism (8). This idea is further used to calculate the binding energies for the complexes by estimating formation energies of the interstitial and impurity atom in the matrix and subtracting from the sum of these two quantities the formation energy of the complex configuration. This method relies only on the knowledge of the interstitial and impurity site locations in the matrix crystal lattice and the misfits between the various atomic species existing in the material.

Equilibrium segregation, which is a purely thermal effect, is also built into the model. The Mclean model (9) is used here and the major parameters involved are the binding energy of the impurity to the sink plane, which we assume in this case is the grain boundary (GB). There is also a small geometrical correction used to modify the segregation parameter. This type of segregation is equilibrium and so no critical time concept for saturation exists. Time is simply equivalent to dose.

MODEL PREDICTIONS

The model has successfully been applied to a number of alloy systems of interest to the nuclear industry. Useful indicators of Si segregation to grain boundaries (GB) in austenitic steels and ferritic-martensitic steels have been obtained (10,11) Si and Ni segregation to planar faults in austenitic steels has been observed by Kenik (12).

In this work we describe the behaviour of P in ferritic steel or alpha iron matrices. The necessary data are indicated in Table 1.

Table 1 Relevant Data Used in Model Calculations of Phosphorus in Alpha Iron

Activation energy for complex diffusion (13)	1.67 eV
Activation energy for solute diffusion (14)	2.39 eV
Activation energy of interstitial diffusion (15)	0.25 eV
Interstitial-solute binding energy (13)	0.72 eV
Entropy diffusion term for complexes and interstitials (7)	1.0 m^2 s^{-1}
Entropy diffusion term for solute (14)	2.9 cm^2 s^{-1}
Grain size	20 um
Interstitial Bias (5)	1.1
Dislocation formation energy (16)	0.1 eV
Matrix concentration	0.04 atomic %
Equilibrium segregation binding energy to grain boundary (17)	0.397 eV
Grain boundary width	1.0 nm

One of the best indicators of the non-equilibrium RIS-model's success is found by referring to Fig. 1. This shows the temperature dependence of the enrichment factor on GBs for P in an alpha iron matrix as predicted by the model. Several experimentally measured values taken from GBs in a ferritic steel within the temperature range 250-300°C are included. The model has used microstructural parameters appropriate to the alloy condition during irradiation and it is seen that a good fit is obtained.

Assuming the validity of the model, it is useful to predict how irradiation conditions may affect RIS in ferritic steels. Fig. 2 shows the effect of increasing the total dose with a fixed dose rate. It is seen that the peak segregation temperature is shifted to slightly lower levels and that there is an increase in the maximum enrichment factor.

Fig. 3 indicates the effect of varying dose rate. A lower dose rate leads to a lower peak segregation temperature. Increases in the dislocation density are shown in Fig. 4 to decrease the peak enrichment temperature.

MODEL MODIFICATIONS FOR ACCELERATOR-DRIVEN IRRADIATION

The primary difference between the conditions prescribed for modelling the radiation damage process so far and those in an accelerator is the particle energy spectrum. It is known that far higher charged particle or neutron energies will be found in accelerator beams and this implies that the proportion of freely migrating defects available per primary knock-on will be substantially affected. It is anticipated that this proportion will be increased and an example of the outcome for the model is shown in Fig. 5. It is clear that higher energies (higher B factors) will give rise to an increase in RIS and that the peak segregation temperature will be shifted to higher temperatures.

The temperature itself may be considerably dependent on the incident particle energy spectrum. At lower temperatures rises in material temperature could be over 100°C.

Other issues that need to be considered for higher energy spectra are 1) modification of the diffusion constants under high energy particle bombardment; and 2) alteration in interstitial bias under more severe irradiation conditions.

USE OF RIS IN TRANSMUTATION TECHNOLOGIES

The foregoing discussion of RIS effects has shown that trace impurities with large misfits will undergo substantial redistribution to sink planes during high energy particle irradiation. The elements which are likely to segregate to the greatest extent will be, for example, Mo, Nb, and most of the rare earths. These are precisely the elements whose isotopes have the long half lives that transmutation technology is seeking to destroy.

The main point of this paper is to indicate methods of harnessing RIS to optimise the efficiency of the transmutation process for the most dangerous nuclides in the radioactive waste. Clearly the objective is to arrange the spatial distribution of sinks in the

microstructure so that the unwanted nuclides are concentrated in the charged particle beam. The list of important sink types is as follows.

a) Grain boundaries.
b) Surfaces.
c) Dislocations.
d) Precipitate-matrix interfaces.
e) Planar faults, such as stacking faults.

a) and b) probably offer the most scope for improving transmutation efficiency. The models previously described can be adapted and applied to forecast the conditions necessary to produce maximum segregation at any of these sinks. It then remains to arrange these segregated regions of the microstructure in the most intense parts of the accelerator or neutron spallation source beam. Several scenarios are depicted in Fig.6.

Unidirectional structures can be produced by directional solidification. Such structures would provide the maximum grain boundary area on planes parallel to the irradiation beam. In this way maximum use can be made of GB RIS of long life nuclides.

Less complicated furnace procedures would be involved with producing fine grain surface microstructures. Such materials would have the advantage that GB RIS would be concentrated onto the grain boundaries more quickly in the fine grained structure close to the surface where the irradiation damage would be most severe. Fine grained surface structures can be produced by flame or flash heating processes.

Another approach requires the formation of the waste into powder. Surface RIS will then occur over a large surface area and the powder can subsequently be immersed in a suitable solvent to dissolve the layers containing the high levels of segregated long life nuclides. This will have the effect of concentrating the more harmful nuclides into a very small volume. For maximum efficiency of the powder RIS optimisation method the particles would need to be sub-micron and therefore some form of gas atomisation would be necessary.

CONCLUSIONS

The latest models of radiation induced segregation (RIS) are descibed and discussed. The applicability of the non-equilibrium model is demonstrated by application to an observed effect in low alloy ferritic steels. Several potential modifications to the non-equilibrium RIS model are proposed to account for the substantial difference between a reactor neutron energy spectrum and that of a charged particle acclerator beam or neutron spallation source.

The use of the RIS effect in microstructural optimisation of transmutation technologies is discussed and three different approaches are described:

a) unidirectionally solidified structures;
b) surface grain refinement; and
c) powder methods.

REFERENCES

1. R.G. Faulkner, N.C. Waite, E.A. Little and T.S. Morgan, Mat. Sci. and Eng., A171, 241, (1993).
2. R.A. Johnson and N.Q.Lam, Phys Rev, 13, 4364, (1976).
3. C.A. English, S,.M. Murphy and J.M. Perks, J. Chem. Soc. Faraday Trans., 86, 1263, (1990).
4. V. Naundorf, M-P. Macht and H. Wollenberger, J. Nuc. Mat., 186, 227, (1992).
5. R. K. Bullough, M.R. Hayns and M.H. Wood, J. Nuc. Mat., 90, 44, (1980).
6. T. Hashimoto and N. Shigenaka, J. Nuc, Mat., 189, 161, (1992).
7. N.Q.Lam, A. Kumar and H. Wiedersich, in 'Effects of Radiation on Materials', 11th Int. Conf. ASTM STP 782,, Eds, H.Brager and J.S. Perrin, ASTM, Philadelphia, 1982, p.985.
8. R.G. Faulkner, Mat. Sci. and Tech., 1, 442, (1985).
9. D. McLean,, 'Grain Boundaries in Metals'. Oxford Univ. Pr., London, 1957, p. 132.
10. T.S. Morgan, E.A. Little, R.G. Faulkner and J.M. Titchmarsh, ASTM STP 1125, Philadelphia, 1992, p.633.
11. C.M. Shepherd, J. Nuc. Mat., 175, 170, (1990).
12. E.A. Kenik and K. Hojou, J. Nuc. Mat., 191-194, 1331, (1992).
13. S. Song, 1994, Private Communication.
14. E.A. Brandes and G.G. Brook (eds.) Metals Reference Book 7th Ed. Butterworth-Heinemann, Oxford, 1992, 13-83.
15. F.W. Young, J.Nuc. Mat., 69-70, 310, (1978).
16. D. Hull and D.J. Bacon, 'Introduction to Dislocations', 3rd Ed., Pergamon, Oxford 1984, p.79.
17. T. Qgura, Trans. Japan. Inst. Met., 22, 109, (1981).

dan1

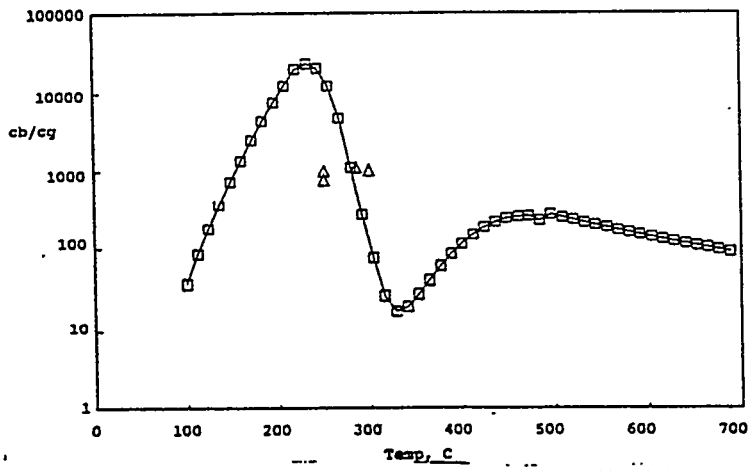

Fig. 1 The segregation of P in alpha iron, cb/cg, as a function of irradiation temperature, measured by FEGSTEM/ Auger methods (Δ), and as predicted by theory (□). Dose rate = 10 -9 dpa s-1, dose=0,01 dpa, dislocation density = 10 14 lines m-2, grain size = 20 um.

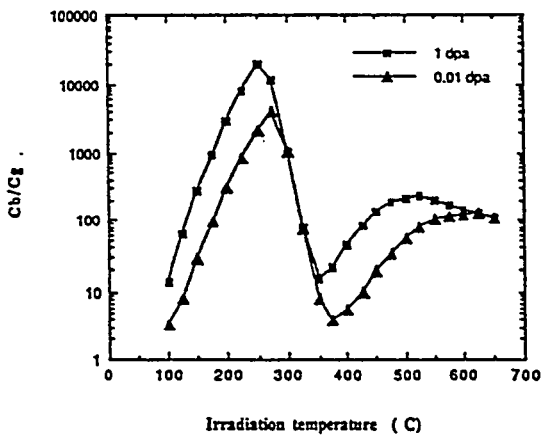

Fig. 2. The segregation degree of P in α-Fe, Cb/Cg as a function of irradiation temperature for different doses(Dose rate = 10^{-6} dpa/s, $\rho_o = 10^{16}$ m^{-2}, B =0.01 E_f^I = 3.0 eV).

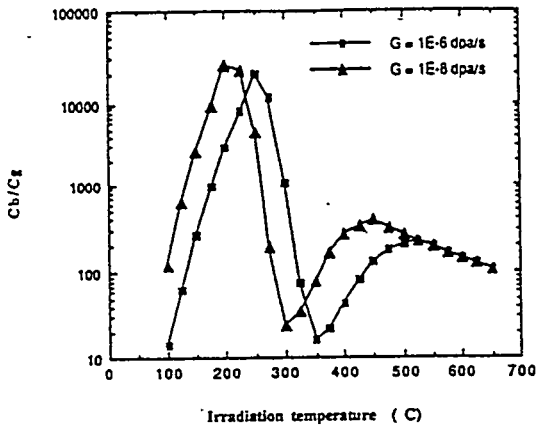

Fig.3 The segregation degree of P in α-Fe, Cb/Cg as a function of irradiation temperature at different dose rates(Dose = 1 dpa/s, $\rho_o = 10^{16}$ m^{-2}, B =0.01, E_t^I = 3.0 eV).

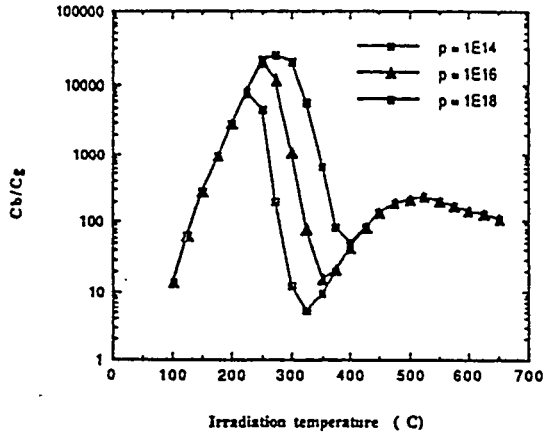

Fig. 4 The segregation degree of P in α-Fe, Cb/Cg as a function of irradiation temperature at different dislocation density constants(m^{-2})(Dose = 1 dpa/s, Dose rate = 10^{-6} dpa/s, B =0.01, E_t^I = 3.0 eV).

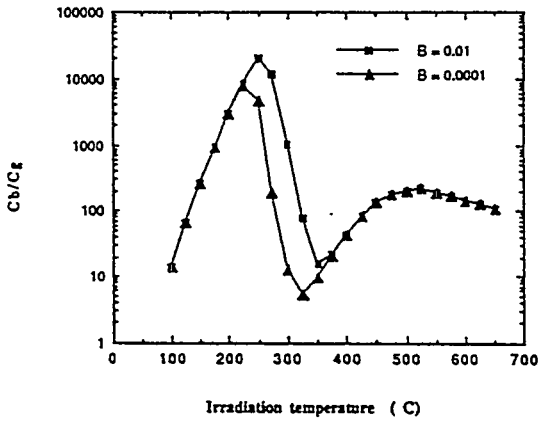

Fig. 5 The segregation degree of P in α-Fe, Cb/Cg as a function of irradiation temperature at different dose rate correct factors(Dose = 1 dpa/s, Dose rate = 10^{-6} dpa/s, $\rho_o = 10^{16}$ m-2, E_t^I = 3.0 eV).

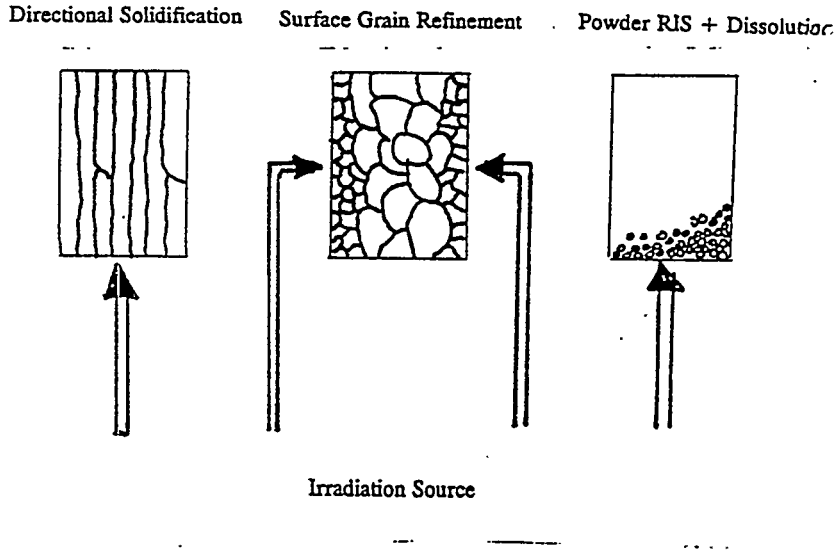

Fig. 6 Methods of using RIS to Optimise Transmutation Efficiency

Selection of Flowing Liquid Lead Target Structural Materials for Accelerator Driven Transmutation Applications

John J. Park and John J. Buksa
Reactor Design and Analysis Group (TSA-12), MS K551
Technology and Safety Assessment Division
Los Alamos National Laboratory
Los Alamos, NM 87545

Abstract. The beam entry window and container for a liquid lead spallation target will be exposed to high fluxes of protons and neutrons that are both higher in magnitude and energy than have been experienced in proton accelerators and fission reactors, as well as in a corrosive environment. The structural material of the target should have a good compatibility with liquid lead, a sufficient mechanical strength at elevated temperatures, a good performance under an intense irradiation environment, and a low neutron absorption cross section; these factors have been used to rank the applicability of a wide range of materials for structural containment. Nb-1Zr has been selected for use as the structural container for the LANL ABC/ATW molten lead target. Corrosion and mass transfer behavior for various candidate structural materials in liquid lead are reviewed, together with the beneficial effects of inhibitors and various coatings to protect substrate against liquid lead corrosion. Mechanical properties of some candidate materials at elevated temperatures and the property changes resulting from 800 MeV proton irradiation are also reviewed.

INTRODUCTION

Flowing liquid lead is the primary candidate target material for use as the compact, high-power spallation neutron source for the accelerator based conversion of plutonium/accelerator transmutation of waste (ABC/ATW) system at Los Alamos National Laboratory (LANL). The liquid lead target appears to be the best possible choice with its unique advantages including: high atomic number (Z = 82), moderate melting point (327°C), fast heat removal from the target, good neutron yield, low vapor pressure, and no worry about radiation damage to the target material. Lead was chosen over lead-bismuth eutectic because of the following undesirable properties of lead-bismuth eutectic. (1) Lead-bismuth eutectic produces α-radioactive ^{210}Po by capture of thermal neutrons in bismuth. (2) Lead-bismuth eutectic is more corrosive than lead, for example, the corrosion of steel in uninhibited bismuth is about 40 times greater than it is in uninhibited lead under similar conditions [1]. Materials known to be compatible with lead-bismuth have a high thermal neutron absorption cross section; preferred materials such as aluminum or zirconium are not considered compatible. (3) Lead-bismuth eutectic has unfavorable behavior of retained swelling after solidification. A simple test to measure this effect was conducted [2]. A 6.55-cm O.D. cylinder constructed from 0.175-cm thick chrome-steel was filled with molten Pb-Bi and then allowed to solidify. The diameter increased by a maximum of 0.35% over a period of 6 months with no measurable change of diameter at later times. The consequence of this test suggests that solidification of Pb-Bi may require additional structure beyond that required for mere fluid containment.

In the current preconceptual target design, liquid lead is circulated (400–500°C) through an active spallation region where it picks up sensible heat that is later transferred to a secondary coolant. This design is unique in that the beam window is an integral part of the target containment structure and is convectively cooled by the flowing lead. Consequently, the structural container for the molten lead will be exposed to a significant flux of high-energy protons and neutrons as well as an extremely corrosive environment. Selection of the container material will greatly affect the lifetime and safety of the target subsystem; the material should have good compatibility with molten lead, sufficient mechanical strength at operating temperatures, a low neutron absorption cross section, and good performance under an intense radiation environment. In this paper, an effort to

summarize the down-selection process that led to the selection of Nb-1Zr as the leading container material is made.

In selecting a structural material for use in any liquid metal application, a number of important factors must be considered including compatibility of the structural material with the liquid metal, the application's thermal and radiation environments, and the physical geometry of the container. In ABC/ATW system, operational conditions are very similar to those encountered in nuclear reactor system. The exception to this general analogy is in the spallation target region where a high-energy proton and neutron flux exists. Consequently, the large corporate knowledge base of liquid metal reactor systems is applicable, but not conclusive. For the particular application of a circulating molten lead spallation target, three factors have been used to rank the applicability of a wide range of materials for structural containment: good compatibility with liquid lead, sufficient mechanical strength under elevated temperature and intense irradiation, and good neutron yield.

MATERIALS COMPATIBILITY WITH LIQUID LEAD

One of the major factors limiting the design and lifetime of most elevated temperature liquid metal engineering systems is liquid metal corrosion. In contrast to aqueous corrosion, electrochemical reactions are generally not involved in liquid metal corrosion; however, chemical reactions combined with physical phenomena can occur readily in liquid-metal systems. Liquid metal corrosion tests are performed statically and dynamically. A static corrosion test simply involves the interaction of a solid metal specimen with a liquid metal for a suitable length of time at a desired temperature. A dynamic corrosion test usually employs circulation of the liquid through a temperature gradient to account for the mass transfer of the container material [3–5].

There are a number of different types of liquid metal corrosion: dissolution attack, temperature gradient mass transfer, concentration gradient mass transfer, impurity reactions, erosion, intergranular attack, alloying between the liquid metal and the solid containment metal, self-welding of solid metals, and liquid metal embrittlement. Of all the above mechanisms, temperature gradient mass transfer is usually the most damaging type in applications where there is a large temperature gradient in the system. The solubility of the container material in the liquid metal is a function of temperature. After a period of operation, solubility limits are reached and the temperature dependent solubility results in the transfer of the container material from the hottest location to the coldest location in the flowing loop. The effect in the circulating molten lead target is to dissolve container material from the window and deposit it in the heat exchanger. Both the thinning of the window and potential fouling of the heat exchanger are undesirable.

The relative resistance to mass transfer in liquid lead of 24 metals and alloys with a temperature gradient of 300°C (800–500°C) was measured by Cathcart and Manly [6], and the results are shown in Table 1. The materials tested were divided into three groups based on their relative resistance to mass transfer in a thermal convection loop test. The "heavy mass transfer" group included nickel, titanium, cobalt, chromium, iron, beryllium, Inconel, 304 stainless steel, and 310 stainless steel. The "usually little mass transfer" group included Hastelloy B, 410 stainless steel, 446 stainless steel, Fe-14Cr-2Si, Ni-25Mo, Co-45Cr, Fe-50Mo, Fe-37Cr-16Ni, and Fe-50Cr. Finally, the "no mass transfer" group included niobium and molybdenum. In an ORNL thermal convection loop test, Croloy 2-1/4 (Fe-2.25Cr-1Mo) exhibited 1–8 mils of attack at 593-654°C, and Nb-1Zr showed no attack after 5280 hrs exposure to lead at 760°C [7]. In another thermal convection loop test [8], chromium and austenitic steel showed 42–320 μm attack at 600 °C for 1000–2000 hrs; however, Nb, Nb-1Zr, Nb-5V, and V showed no attack at 625°C for 1858 hrs. The tests also showed that the corrosion attack was strongly increased due to stresses in material; the depth of corrosion attack was much higher in the bent region of U-shaped specimens than in the rest of the specimens. In conjunction with the LMFR program, BNL also ran a Croloy

2-1/4 loop containing 225 ppm Mg-inhibited (used as a deoxident) lead for over 27,765 hrs with a temperature differential of 105°C (550–445°C); no significant corrosion was observed [9]. A thermal convection loop test with a maximum hot-zone temperature of 550°C and a minimum cold-zone temperature of 470°C was performed on ferritic steels of Chromesco 3 (2-1/4 Cr) and EM 12 (10 Cr) [10,11]. The result showed that in the hot zone, the thickness loss of Chromesco 3 steel was about 90 μm, whereas, that of EM 12 was only 30 μm. In the cold zone, an abundant deposit of iron crystals up to several millimeters thick was formed on Chromesco 3 steel. On the other hand, a much thinner deposit of 0–35 μm of iron and magnetite was formed on EM 12. Asher et al. [12] have shown that, in their loops at 700°C with $\Delta T = 150$°C, Hastelloy N was severely attacked in only 4 days, and Croloy 2-1/4 was severely attacked in 15 days; however, molybdenum showed no attack in 282 days.

Dissolution attack is another important consideration for liquid metal corrosion. From the results of a static corrosion test, the evaluation of materials according to their resistance to attack by liquid lead has been studied [13,14], and is summarized in Table 1. At 600°C, the materials with good resistance included niobium, molybdenum, tantalum, tungsten, beryllium, iron, mild carbon steel, low chromium steel, and ferritic stainless steels. Aluminum, titanium, and zirconium exhibited limited resistance. Austenitic stainless steels, copper-base alloys, nickel, and nickel-base alloys showed poor resistance. In another static corrosion test of steels [10,11], austenitic steel (15Cr-15Ni) showed a strong attack with deep intergranular attack (up to 150 μm) at 530–600°C for 3000 hrs, whereas, ferritic steels (Chromesco 3 and EM 12) showed slight attack with no intergranular attack at 430–575°C for 1100–2100 hrs.

The loss of ductility and fracture strength experienced by a metal when stressed in tension while in contact with liquid metal is known as liquid metal embrittlement (LME). LME experiments with AISI 4145 steel showed that both fracture strength and ductility decreased in a continuous manner at temperatures considerably below the melting point of lead, and reached a minimum just above the melting point, and then increased rapidly [15]. Experiments with AISI 3340 steel showed loss of ductility in the temperature range of 315–427°C [16]. Chromesco 3 steel showed a slight decrease in the reduction of area (10%) and ultimate tensile strength in the temperature range between 327 and 350°C [10]. All of above data show that the ductility drop in steel is significant near the melting point of lead.

It has been found that the addition of 50–500 ppm of zirconium and titanium to liquid mercury and bismuth inhibits solution mass transfer of steels by reacting with nitrogen and carbon from the steel to form inert, adherent surface layers of ZrN, TiN or TiN + TiC [17]. As with bismuth and mercury, the corrosion of steels in lead was reduced significantly by the addition of 500 ppm of titanium. James and Trotman [1] reported that liquid lead containing 500 ppm titanium in combination with the low alloy steel with available nitrogen or carbon was the most corrosion resistant system among 0.3% carbon steel, mild steel, CRM-6, Fe-13Cr, and 18-8 stainless steel [1]. Asher et al [12] also showed that Croloy 2-1/4, although severely attacked in uninhibited lead for 4 days, did not show any attack in Ti-inhibited lead for 85 days.

The two effects of oxygen in lead have been discussed by Weeks [18]. Oxygen can form oxide layers on the surface of steels, especially those high in chromium, which reduce the corrosion rate. The lead oxide (PbO) is less stable than oxides of Fe and Cr, and is slightly soluble in liquid lead. Thus, there is a tendency for Pb to reduce Fe or Cr oxides in the hot leg of a loop and transfer oxygen to the minimum temperature of the system, where PbO precipitates from the solution and might form a plug. For these reasons, oxide films on a steel are only temporarily beneficial to its corrosion behavior, and could result in oxide plugs in the cold leg of the circuit. It appears that, from the result of BNL loop test, neutron irradiation does not increase corrosion or reduce the effectiveness of inhibitor [19].

Table 1. Properties of Selected Materials

Material	Density (g/cm^3)	T_m (°C)	ACS (barns)	Mass transfer	Resistance to attack	UTS (MPa)	UTS(500) (MPa)	YS(500) (MPa)
Be	1.85	1283	0.009	heavy	good	228-690	145-170	
Mg	1.74	650	0.063			90-220		
Al	2.70	660	0.215			40-140		
Ti	4.51	1668	5.6	heavy	limited	220	100	
V	6.09	1735	5.1			472-911		
Cr	7.19	1890	2.9	heavy		413	225-242	
Mn	7.44	1245	13.2		poor	496		
Fe	7.87	1539	2.53	heavy	good			
Co	8.89	1495	37	heavy		234-945		
Ni	8.91	1455	4.6	heavy	poor	317		
Cu	8.92	1083	3.69		poor	209-344		
Zr	6.51	1845	0.18		limited			
Nb	8.57	2415	1.1	no	good	210-334	200-290	90-120
Mo	10.22	2610	2.5	no	good	400-600	250-350	
Ru	12.48	2334	2.46					
Rh	12.44	1966	150			951-2068		
Hf	13.09	2222	115					
Ta	16.68	2996	21.3		good	250-400	200-300	
W	19.26	3410	19.2		good	560-3922	196-1667	
Re	21.03	3170	84			990-2400	1250	
Os	22.6	2700	14.7					
Ir	22.5	2454	430			990-2480	530	
Pt	21.45	1769	8.1		poor			
Th	11.66	1750	7			150-250	50-80	
304 ss	7.9	1425		heavy	poor	515-2240		
304L ss	7.9	1425			poor	480-620		
310 ss	7.9	1425		heavy				190
316 ss	8.0	1390			poor	515-1690		
316L ss	8.0	1390			poor	480-620		
347 ss	8.0	1412		heavy				
410 ss	7.7	1505		little		485-825	450	380
446 ss	7.6	1467		little			280	
Inconel	8.5	1410		heavy		697	650	
Inconel 718	8.19					995-1448	990-1200	
Hastelloy B	9.24	1335		little		583	531	
Hastelloy N	8.93					724	586	
Zircaloy-2	6.5	1817	0.193			570		
Zircaloy-4	6.5	1817	0.194					
Nb-1Zr	8.4	2467				280	200	130
PWC-11	8.4	2467				345	262	150
T-111	16.7	2977				690	379	
Mo-13Re	10.9	2537				550	530	
TZM	10.2	2610				552-883		
Croloy 2-1/4	7.9	1530				680	470	220
HT-9	7.7	1520					550-1500	500-1100

Density = density at 25°C in g/cm^3
T_m = melting point in °C
ACS = absorption cross section for 2200 m/s neutrons in barns/atom
Mass transfer = mass transfer in liquid lead from J. V. Cathcart and W. D. Manly
Resistance to attack = resistance to attack by liquid lead at 600°C from *Liquid Metals Handbook*
(good = rate of attack is less than 1 mil/year, limited = rate of attack is 1 to 10 mils/year,
poor = rate of attack is greater than 10 mils/year)
UTS = ultimate tensile strength at room temperature
UTS(500) = ultimate tensile strength at 500°C
YS(500) = 0.2% yield strength at 500°C
304 ss = Fe-(18-20)Cr-(8-12)Ni-2Mn-1Si-0.08C-0.045P-0.03S
304L ss = Fe-(18-20)Cr-(8-12)Ni-2Mn-1Si-0.03C-0.045P-0.03S
310 ss = Fe-(24-26)Cr-(19-22)Ni-2Mn-1.5Si-0.25C-0.045P-0.03S
316 ss = Fe-(16-18)Cr-(10-14)Ni-2Mn-1Si-0.08C-0.045P-0.03S-(2-3)Mo
316L ss = Fe-(16-18)Cr-(10-14)Ni-2Mn-1Si-0.03C-0.045P-0.03S-(2-3)Mo
347 ss = Fe-(17-19)Cr-(9-13)Ni-2Mn-1Si-0.08C-0.045P-0.03S-10 x % C min Nb + Ta
410 ss = Fe-(11.5-13)Cr-1Mn-1Si-0.15C-0.04P-0.03S
446 ss = Fe-(23-27)Cr-1.5Mn-1Si-0.2C-0.04P-0.03S
Inconel = 72Ni-15.5Cr-8Fe-1Mn-0.5Si-0.15C
Inconel 718 = 52.5Ni-19Cr-18Fe-5.2Nb-3.0Mo-1.0Co
Hastelloy B = 67Ni-28Mo-5Fe
Hastelloy N = 68Ni-17Mo-7Cr-5Fe
Zircaloy-2 = Zr-1.5Sn-0.14Fe-0.1Cr-0.06Ni
Zircaloy-3 = Zr-0.25Sn-0.25Fe-0.05Cr-0.05Ni
Zircaloy-4 = Zr-1.5Sn-0.17Fe-0.12Cr
T-111 = Ta-8W-2Hf
PWC-11 = Nb-1Zr-0.06C
TZM = Mo-0.5Ti-0.1Zr
Croloy 2-1/4 = Fe-2.25Cr-1Mo-0.15C
HT-9 = Fe-12Cr-1Mo-0.5Ni-0.5W-0.3V-0.2C

The use of coatings to protect substrate against lead corrosion has not been successful because of thermal expansion mismatch, with the exception of plasma sprayed molybdenum coating on Croloy and aluminized specimen of the same steel [12]. In the former case, the protection was attributed to the high corrosion resistance of molybdenum, and in the latter case, it was probably by the formation of protective oxide films.

MECHANICAL STRENGTH OF MATERIALS

A sufficient mechanical strength at service temperatures is also very important in the selection of structural materials for the circulating molten lead target. Preliminary design inlet and outlet temperatures of the flowing lead are 400 and 500°C, respectively. The mechanical properties of selected candidate materials are shown in Table 1. Note, however, that the strength of a material depends on many factors, primarily processing history and impurity levels; the mechanical strengths shown in Table 1 should not be regarded as absolute. In the preliminary target design, the maximum hoop stress in the container has been calculated to be approximately 28 MPa at a lower temperature region (400°C). At this high stress location, aluminum-base alloys will lose most of their strength because of their low melting point (around 660°C). As shown in Table 1, other common structural materials such as stainless steels, nickel-base alloys, zirconium-base alloys, refractory alloys, and iron-base heat resistance alloys (for example Croloy 2-1/4 and HT-9) will have enough strength at this location.

More importantly is the strength of the material at the highest temperature location. In the current design, it is estimated that the maximum temperature of the system will be approximately 900–1000°C at the point where the proton beam impinges on the window. At this temperature range, iron-base alloys are inadequate because they have melting points of 1400–1500°C and creep becomes significant problem at above half of the melting point of the material. Iron-base alloys are usually limited up to 650-700°C. Similarly, nickel-base and cobalt-base superalloys are marginally acceptable because they are limited up to 900–1000°C. Another consideration for the use of these superalloys is that nickel is incompatible with liquid lead, and cobalt has very high absorption cross section (37 barns). Refractory metals (Nb, Ta, Mo, W) are usually considered at service temperatures above 900°C.

Mechanical property change of materials upon intense proton irradiation is another factor to be considered. Samples of Fe, Ta, Fe-2.25Cr, and Fe-12Cr-1Mo were sealed inside capsules containing Pb-Bi, and were irradiated by 800 MeV proton beam by Brown et al. [20]. Room temperature tensile tests on these samples indicated that the strength increases and ductility decreases, which is consistent with the well-known effects of fission-neutron irradiation. Based upon the measured ductility and strength, it appeared that the two iron base alloys would be suitable for a proton beam window in contact with Pb-Bi as long as the window temperature does not exceed approximately 673 K. They have also performed mechanical tests of 304 stainless steels, alloy 718, molybdenum, and tantalum after low fluence 800 MeV proton irradiation in a separate experiment [21]. For 304 stainless steel and alloy 718, the ductility decreased approximately 30–40%. Tantalum still retained significant ductility, while several molybdenum specimens broke at less than 0.2% strain.

NEUTRON ABSORPTION CROSS SECTION

The candidate structural material should also have a low thermal neutron absorption cross section to offer maximum neutron yield. The neutron absorption cross section of selected materials are also included in Table 1. Beryllium has the lowest absorption cross section (0.009 barns); however, it exhibited heavy mass transfer in liquid lead [6]. Aluminum has a good absorption cross section (0.215 barns); however, it has a low melting point of 660°C. Zirconium has a good absorption cross section (0.18 barns), as does niobium (1.1 barns), iron (2.53 barns), and molybdenum (2.5 barns). Tantalum (21.3 barns), rhenium (84 barns), and tungsten (19.2 barns) have relatively high absorption cross sections.

SUMMARY

Nb-1Zr has been selected for use as the structural container for the LANL ABC/ATW molten lead target. It has been shown to be compatible with molten lead, it has sufficient mechanical strength at operating temperatures near 1000°C, and it has a low neutron absorption cross section. Because of these same attributes, Nb-1Zr was chosen as the primary structural material for the SP-100 space nuclear power system. It is readily available in all product forms from several commercial sources, and has a significant data base for fission irradiated performance. Molybdenum has a little higher mechanical strength and neutron absorption cross section than niobium, and has good compatibility with liquid lead. However, its brittle behavior following even a short-term irradiation of protons make it unattractive. Although ferritic steels showed significant resistance to mass transfer in liquid lead, their low strength at 1000°C make them unattractive as a window material. Ferritic steels are more corrosion resistant than austenitic steels, consequently, ferritic steels could be used with Mg- or Ti-inhibitor in lower temperature region of the system. Zirconium has some attractive properties such as a very low neutron absorption cross section and relatively high melting point (1845°C); however, its mass transfer behavior in liquid

lead is not known. Beryllium has very good absorption cross section, but it exhibited heavy mass transfer. Nickel and nickel base alloys have a very low resistance to mass transfer in liquid lead.

ACKNOWLEDGMENTS

The authors would like to express thanks to Walter Sommer and Carl Beard at LANL for their help during this work.

REFERENCES

[1] James, J. A., and Trotman, J., "Corrosion of Steels in Liquid Bismuth and Lead," *J. Iron and Steel Inst.* **194**, 319–323 (March 1960).

[2] Dubs, M., and Ulrich, J., "Design Considerations for the SINQ Target Window," in *Proceedings of the 11th Meeting of the International Collaboration on Advanced Neutron Sources (ICANS-XI)* (1990).

[3] Cathcart, J. V., and Manly, W. D., "A technique for Corrosion Testing in Liquid Lead," *Corrosion* **10**, n.12, 432–434 (1954).

[4] Epstein, L. F., "Corrosion by Liquid Metals," in *Proceedings of International Conference on the Peaceful Uses of Atomic Energy*, 1955, pp. 311-317.

[5] Manly, W. D., "Fundamentals of Liquid Metal Corrosion," *Corrosion* **12**, 336t-342t (1956).

[6] J. V. Cathcart and W. D. Manly, "The Mass Transfer Properties of Various Metals and Alloys in Liquid Lead," *Corrosion* **12**, 43–47 (1956).

[7] G. M. Tolson and A. Taboada, "A Study of Lead and Lead-Salt Corrosion in Thermal-Convection Loops," Oak Ridge National Laboratory report ORNL-TM-1437 (1966).

[8] I. Ali-Khan, "Corrosion of Steels and Refractory Metals in Liquid Lead," *Materials Behavior and Physical Chemistry in Liquid Metal Systems*, 1982, pp. 243–252.

[9] Romano, A. J., Klamut, C. J., and Gurinsky, D. H., "The Investigation of Container Materials for Bi and Pb Alloys: Part I. Thermal Convection Loops," Brookhaven National Laboratory report BNL 811 (July 1963).

[10] Broc, M., Sannier, J., and Santarini, G., "Experimental Studies on the Use of Liquid Lead in a Molten Salt Nuclear reactor," *Nuclear Technology* **63**, 197–208 (1983).

[11] Broc, M., Sannier, J., and Santarini, G., "Behavior of Ferritic Steels in the Presence of Flowing Purified Liquid Lead," *Liquid Metal Engineering and Technology*, London, 1984, vol. 1, pp. 361–368.

[12] Asher, R. C., Davies, D., and Beetham, S. A., "Some Observations on the Compatibility of Structural Materials with Molten Lead," *Corrosion Science* **17**, 545–557 (1977).

[13] R. N. Lyon (ed.), "Liquid Metals Handbook," Atomic Energy Commission, Department of the Navy, Washington, D. C., NAVEXOS P-733 (Rev.) (June 1952).

[14] Wilkinson, W. D., Hoyt, E. W., Rhude, H. V., "Attack on Materials by Liquid Lead," Argonne National Laboratory report ANL-5449 (October 1955).

[15] Breyer, N. N., and Johnson, K. L., "Liquid Metal Embrittlement of 4145 Steel by Led-Tin and Lead-Antimony Alloys," *J. Testing and Evaluation* **2**, 471-477 (1974).

[16] Dinda, S., and Warke, W. R., "The Effect of Grain Boundary Segregation on Liquid Metal Induced Embrittlement of Steel," *Materials Science and Engineering* **24**, 199-208 (1976).

[17] Kammerer, O. F., "Zirconium and Titanium Inhibit Corrosion and Mass Transfer of Steels by Liquid Heavy Metals," *Trans. of the TMS of AIME*, 20-25 (Feb. 1958).

[18] Weeks, J. R., "Lead, Bismuth, Tin and Their Alloys as Nuclear Coolants," *Nuclear Engineering and Design* **15**, 363-372 (1971).

[19] Waide, C. H. et al., "Uranium-Bismuth In-Pile Corrosion Test Loop," Brookhaven National Laboratory report BNL -736 (1961).

[20] Brown, R. D., Wechsler, M. S., Tschalaer, C., "Tensile Properties of Several 800 MeV Proton-Irradiated BCC Metals and Alloys," in *Effects of Radiation on Material Properties: 13th International Symposium (Part II, ASTM STP-956)*, 1987, pp. 131–140.

[21] Brown, R. D., and Cost, J. R., "Mechanical Properties of 800-MeV Proton-Irradiated Metals," *Effects of Radiation on Materials (ASTM STP 782)*, 1982, pp. 917–926.

Direct Irradiation of Long-Lived Fission Products in an ATW System

Thomas F. Carter*, Douglass Henderson°, and William C. Sailor+

*Department of Nuclear Engineering, *The University of Tennessee, Knoxville, TN 37919 and °The University of Wisconsin, Madison, WI 53706, +Los Alamos National Laboratory, Los Alamos, NM 87545*

Abstract. The feasibility of directly irradiating five long-lived fission products (LLFPs: ^{79}Se, ^{93}Zr, ^{107}Pd, ^{126}Sn, and ^{135}Cs, each with a half-life greater than 10,000 years), by incorporating them into the target of an Accelerator Transmutation of Waste (ATW) system is discussed. The important parameters used to judge the feasibility of a direct irradiation system were the target's neutron spallation yield (given in neutrons produced per incident proton), and the removal rate of the LLFP, with the baseline incineration rate set at two light water reactors (LWRs) worth of the LLFP waste per year. A target was constructed which consisted of a LLFP cylindrical "plug" inserted into the top (where the proton beam strikes) of a 30 cm radius, 100 cm length lead target. ^{126}Sn and ^{79}Se were each found to have high enough removal rates to support two LWR's production of the LLFP per year of ATW operation. For the baseline plug geometry (5 cm radius, 30 cm length) containing ^{126}Sn, 3.5 LWRs could be supported per year (at 75% beam availability). Furthermore, the addition of a ^{126}Sn plug had a slightly *positive* effect on the target's neutron yield. The neutron production was 36.83 ±.0039 neutrons per proton with a pure lead target having a yield of 36.29 ±.0038. It was also found that a plug composed of a tin-selenide compound (SnSe) had high enough removal rates to burn two or more reactor years of both LLFPs simultaneously.

INTRODUCTION

This paper discusses research concerning direct irradiation of five long-lived fission products (LLFPs) in an Accelerator Transmutation of Waste (ATW) [1] system. A 1600 MeV, 62.5 mA proton beam impinges upon a LLFP plug which is inserted into the top of a lead target. The five LLFPs examined are ^{79}Se, ^{93}Zr, ^{107}Pd, ^{126}Sn, and ^{135}Cs, each with a half-life greater than 10,000 years. The purpose is to determine the possibility of incinerating one or more of these LLFPs (which would otherwise be disposed of geologically) during the operation of an ATW system, without adversely effecting the ATW target's performance.

Two main parameters are used to judge target yield and thus the prospect of utilizing direct irradiation in an ATW system. The more important of these parameters is the target's neutron production, which is defined as neutrons produced per incident proton. The second parameter is that the target design burns two Light Water Reactor's (LWR's) production of the LLFP per year. This has been chosen because the baseline ATW system will burn two LWR's production of actinides, ^{99}Tc, and ^{129}I per year. If a target system is developed that does not degrade the performance relative to a standardized ATW target (to be defined later), while at the same time incinerating a LLFP(s), then this justifies more in-depth research into the feasibility of direct irradiation in an actual ATW system. This research will then determine if direct irradiation should be incorporated into current ATW target designs.

RESEARCH METHODS AND SOURCES OF ERROR

LAHET, a code for the transport of nucleons (as well as pions and muons), is used to track the complex reactions produced in a direct irradiation system. LAHET only treats nucleon interactions for energies greater than 20 MeV. Therefore, LAHET is coupled with the Monte Carlo code, HMCNP, which treats nucleon interactions for energies below 20 MeV. The history files written by LAHET and HMCNP are subsequently read by HTAPE, which performs the needed editing options. For research

concerning direct irradiation, the critical editing options are target neutron production and isotopic removal rate. LAHET, HMCNP, and HTAPE combined form what is termed the LAHET Code System (LCS) [2].

Two sources of error have been introduced due to a lack of complete cross-section information in LCS for the isotopes of interest. The first concerns the use of elastic scattering cross-section data in LAHET. Although this data has been recently updated at Los Alamos National Laboratory [3], it still lacks information for the LLFPs in question. However a good approximation can be made by using elastic scattering data for an element of similar or close atomic mass [3]. This has been done for each of the five LLFPs that are examined, and should result in negligible error.

The second source of error is present because HMCNP uses ENDF/B-based neutron cross-section libraries, which do not include data for the LLFPs ^{79}Se, ^{126}Sn, and ^{107}Pd. While this does not effect the determination of removal rates, it does effect determining the neutron production of the target. Furthermore, the two most important LLFPs turn out to be ^{79}Se and ^{126}Sn. Fortunately, cross-section data is available for natural tin, and this data has been used for ^{126}Sn. This should not significantly affect the overall results (in fact, a comparison of the multigroup cross-section files for ^{126}Sn and pure tin show that they are quite similar). Unfortunately, no such data exists for elemental selenium, and thus no neutron production data is available when ^{79}Se is incorporated into the ATW target.

TARGET DESIGN INCORPORATING A LONG-LIVED FISSION PRODUCT

An ATW target is constructed of a good spallation material, such as lead or tungsten. Both of these materials have the desirable properties of high atomic mass and high density. For this study the LLFP has been combined in an ATW target with liquid lead. Lead has been chosen for two reasons. First of all, the parasitic capture for lead in a thermal spectrum system is much less than tungsten. Secondly, the lead is a liquid that flows through a heat exchanger using well established technology.

The first target design for direct irradiation that is examined is a 30 cm radius, 100 cm length cylinder which is composed entirely of a LLFP in its pure, elemental form (in all target designs incorporating a LLFP it is assumed that the LLFP is separated from its other waste constituents). This so called pure LLFP target is chosen so that the second performance parameter could be tested. It is presumed that if a pure LLFP target will not incinerate two LWR's production of the LLFP per year then a composite target, composed of the LLFP with lead, will also not support two LWRs. Table 1 shows production and required removal rates for each of the five LLFPs [4]. The required removal rate is the

Table 1. Production and Required Removal Rates for each LLFP

LLFP	Production from 2 LWRs (kg/year)	Required Removal Rate (grams/hour)
Selenium 79	**0.40**	**0.0456**
Zirconium 93	47.9	5.46
Palladium 107	14.5	1.66
Tin 126	**1.02**	**0.208**
Cesium 135	20.00	2.28

rate, in grams of LLFP incinerated per hour, that will support two LWR's production of the LLFP per year. It can quickly be seen from Table 1 that ^{126}Sn and ^{79}Se have the greatest possibility of being incinerated at the required rate. Fig. 1 shows that this is indeed the case for a pure LLFP target (30 cm

radius, 100 cm length) operating at steady state with constant removal rates. Furthermore, it can be seen that the LLFPs ^{135}Cs, ^{107}Pd, and ^{93}Zr cannot be burned at the required rate of two LWR's production per year. Due to this fact, the remainder of this paper is restricted to examining direct irradiation of ^{126}Sn and ^{79}Se.

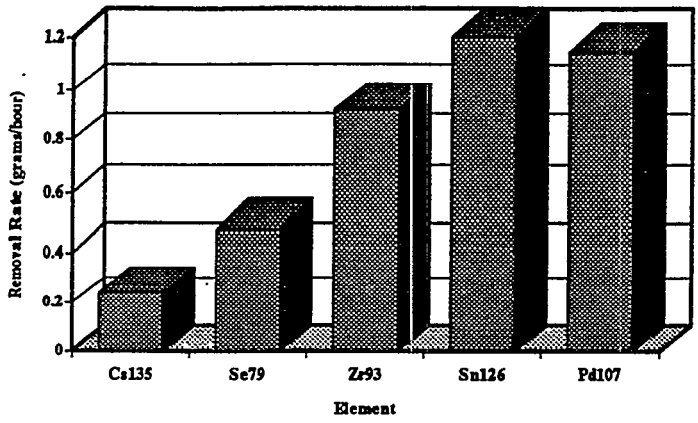

Fig. 1. Removal Rates for Each Long-Lived Fission Product

The ATW target that has been developed to incorporate a LLFP is shown in Fig. 2. As can be seen,

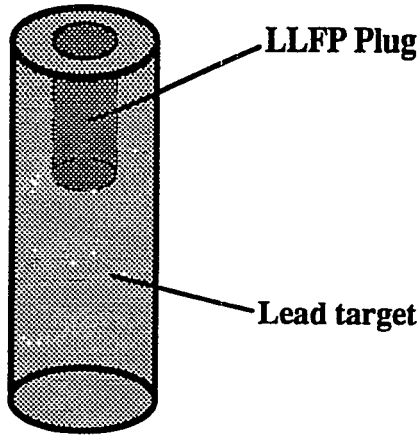

Fig. 2. Lead-Long-Lived Fission Product ATW Target Design

it consists of a cylindrical lead target with a LLFP "plug" inserted into the top, where the beam strikes. This target design has been chosen so that the LLFP is subjected to the full intensity of the proton beam, while being surrounded with an excellent spallation material. The actinides and fission products, as in a typical ATW design, flow through a blanket/moderator region surrounding the central target. For all LCS runs on this target design, the geometry of the lead is held constant as a 30 cm radius, 100 cm length cylinder. The performance of the target is then tested by setting the length of the LLFP plug at 7.5, 15, and 30 cm, and the radius at 2.5, 5, and 7.5 cm. Removal rates and target neutron production are determined for each of these plug geometries. As previously stated, the objective of this target design is to minimize the adverse effects on the neutron production while obtaining a high enough removal rate of the LLFP to incinerate two LWR's production of the waste per year.

LCS Results of Lead-LLFP Target

The first LLFP that is examined for use in the target design is ^{126}Sn. Since the melting point of tin is 232 °C, it is assumed to be in liquid form. This effects the density, an important factor when determining removal rates (generally, the higher the density, the greater will be the removal rate). LWRs supported per year (assuming 75% availability of the proton beam) as a function of plug geometry are shown for ^{126}Sn in Fig. 3. The base of the columns is referenced to two LWRs supported per year. It can be seen that the removal rates are high enough to incinerate two reactor years of ^{126}Sn per year of ATW operation for several different target geometries.

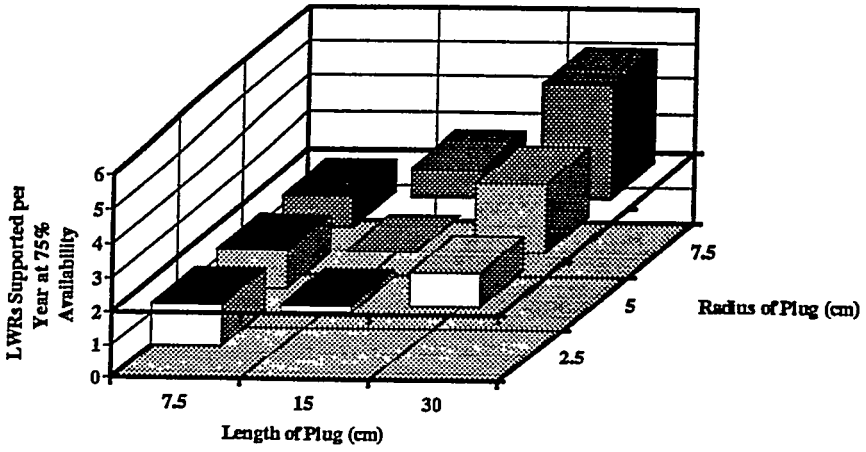

Fig. 3. LWRs per Year of ^{126}Sn Incinerated as a Function of Plug Geometry

The next factor is the affect on the neutron production of the ^{126}Sn plug in the target. For this target to be feasible in an ATW system, it should not have an adverse affect on the neutron production as compared to a target composed solely of lead. The neutron production across the radial surface of the lead given in neutrons produced per incident proton as a function of plug geometry is shown in Fig. 4.

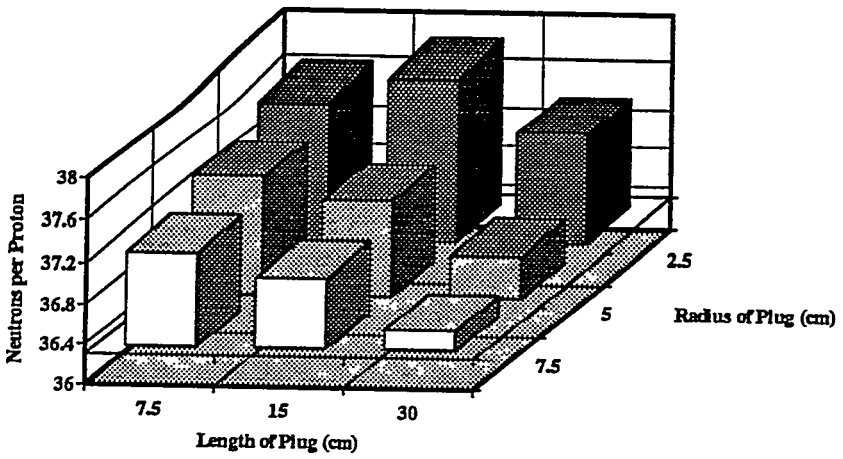

Fig. 4. Radial Neutron Production for Lead-^{126}Sn Target

The base of the columns is referenced to the neutron production from a pure lead target of similar geometry, which is 36.29 neutrons per incident proton. As can be seen, the neutron production actually *increases* for every plug geometry with the tin inserted. This is an interesting and unexpected result which shows that direct irradiation can be a beneficial modification to the ATW system. The advantages are two-fold. First, ^{126}Sn waste can be incinerated during the operation of the ATW system. Secondly, for the geometry shown, the neutron production will actually increase.

In order to explain this increase, it is important to note that there is a strong positive correlation between the density of a material and the resulting neutron production. In the lead-^{126}Sn target the tin is a less dense material than the lead. This leads to two main effects in the target which result in more neutrons produced per proton at the target's radial surface. First, there is less leakage (both neutrons and reflected protons) from the top of the target for a less dense material (i.e. the ^{126}Sn). Since the proton beam initially strikes the ^{126}Sn plug, most of the leakage is off of the lead face at the base of the tin plug. This results in the leakage that does occur off of the lead face to be "reabsorbed" back into the lead, and thus there are more spallation reactions in the target, which create more neutrons. Secondly, the mean path length that the neutrons must travel to escape to the radial surface of the dense lead is less where the LLFP plug is placed. As a result, neutrons passing through this annular surface will have a lower probability of being absorbed before reaching the target's radial surface. One might expect that, by following this line of reasoning, the greatest neutron production increase will occur with a vacuum in place of the plug. In fact, this does occur, and therefore it is suggested that this phenomenon be investigated in future research.

Another potential LLFP that can be burned during the operation of an ATW reactor is ^{79}Se. This LLFP, like ^{126}Sn, has a low melting point of 221 °C, and thus it is assumed to be in liquid form. Also like ^{126}Sn, this isotope does not need a very high removal rate to support two LWR's production of ^{79}Se waste per year. Fig. 5 shows removal rates for ^{79}Se as a function of plug geometry. As can be seen, a lead-^{79}Se target system can easily support two LWRs per year.

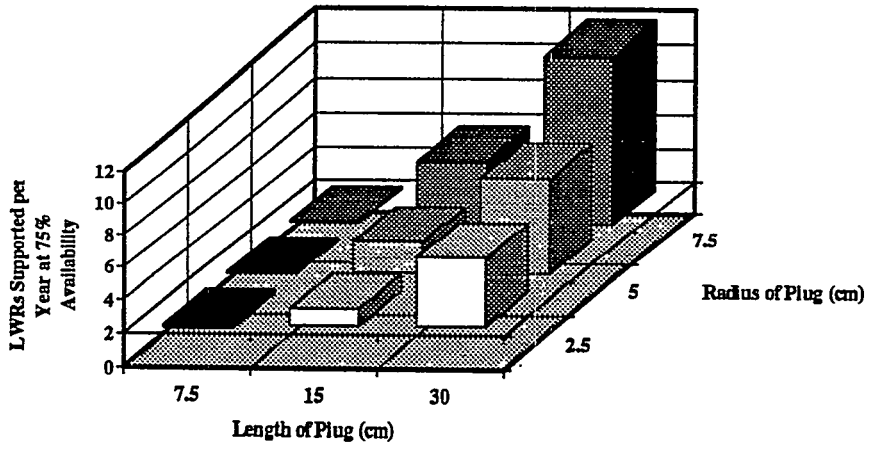

Fig. 5. LWRs per Year of ^{79}Se Incinerated as a Function of Plug Geometry

Neutron production results for selenium are not available, but it should be pointed out that ^{79}Se is a low density material (like tin). Furthermore, its multigroup absorption cross-sections are similar in

magnitude to tin. Therefore, it is expected that a lead-^{79}Se target will also have greater radial neutron production than a pure lead target of similar geometry.

Since both ^{126}Sn and ^{79}Se can be incinerated at the required rates, it was concluded that further research should be directed at a plug consisting of a composition of tin and selenium. The goal of examining a tin-selenide plug is to determine if an ATW target can be designed to incinerate both LLFPs while at the same time boosting the target's neutron production. Unfortunately, neutron production results for this target are not available (due to a lack of ^{79}Se cross-sections in HMCNP), but it is assumed, based on the previous discussion of ^{126}Sn, that the SnSe plug will have a positive effect. Therefore, the main parameter of interest is whether or not two reactor years of both LLFPs can be incinerated per year of ATW operation. Fig. 6 shows the results predicted by LCS. As can be seen, a plug length of 30 cm can incinerate both ^{79}Se and ^{126}Sn at or above the required rate for every plug radius.

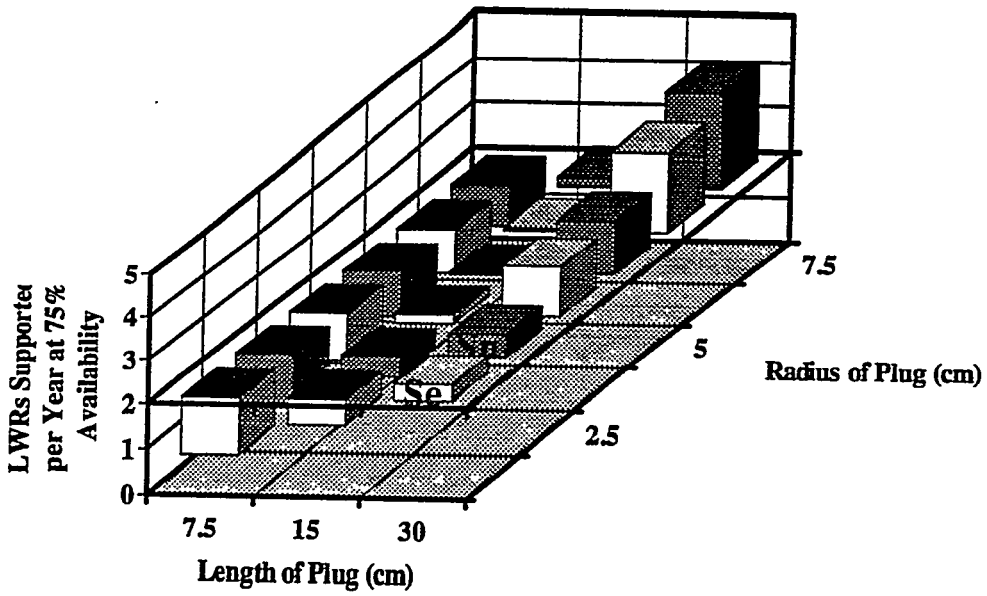

Fig. 6. LWRs per Year of ^{79}Se and ^{126}Sn Incinerated as a Function of Plug Geometry

SUMMARY

The feasibility of directly irradiating five long-lived fission products has been discussed. The purpose of direct irradiation is to incinerate long-lived nuclear waste without disposing of it geologically. In order to determine the feasibility, two performance parameters were utilized. The first was the neutron spallation yield of the target design, given as neutrons produced per incident proton. The second was that the target design incinerate two or more LWR's production of the LLFP per year of ATW operation. For the target design examined, a cylindrical plug composed of a LLFP plug inside a cylindrical lead target, both performance parameters were met for the LLFPs ^{126}Sn and ^{79}Se. Furthermore, it was found that the addition of a ^{126}Sn plug into a lead target results in a slightly greater neutron yield than for a pure lead target. The LLFPs ^{93}Zr, ^{107}Pd, and ^{135}Cs did not meet the second parameter, and therefore direct irradiation of these LLFPs is not achievable. Finally, it was discovered that a target including a LLFP

plug composed of a tin-selenide mixture could incinerate two or more LWR's production of both LLFPs simultaneously.

ACKNOWLEDGMENTS

The research discussed in this paper was supported by an undergraduate scholarship given to Thomas Carter. The scholarship was funded by the U.S. Department of Energy's Office of Environmental Restoration and Waste Management under the EMCORE program, which is administered by Associated Western Universities, Inc. The authors acknowledge Dr. Edward Arthur, host scientist of the EMCORE program at Los Alamos National Laboratory. Appreciation is also given to Barbara Devolder, Richard Prael, and Henry Lichtenstein, all of Los Alamos National Laboratory. Finally, the authors acknowledge Varien Tilton and Heidi Coker of EMCORE.

REFERENCES

[1] Bowman, C.D., Arthur, E.D., Lisowski, P.W., Lawrence, G.P., Jensen, R.J., Anderson, J.L., Blind, B., Cappiello, M., Davidson, J.W., England, T.R., Engel, L.N., Haight, R.C., Hughes III, H.G., Ireland, J.R., Krakowski, R.A.,LaBauve, R.J., Letellier, B.C., Perry, R.T., Russell, G.J., Staudhammer, K.P., Versamis, G., and Wilson, W.B., "Nuclear Energy Generation and Waste Transmutation Using an Accelerator-Driven Intense Thermal Neutron Source", Los Alamos National Laboratory, LA--UR-91-2601, 1991.

[2] Prael, R.E., and Lichtenstein, H., *User Guide to LCS: The Lahet Code System,* Los Alamos, N.M.: Los Alamos National Laboratory, 1989.

[3] R. Prael and H. Lichtenstein, private communications, Los Alamos National Laboratory, Los Alamos, N.M. 87545

[4] Benedict, M., Pigford, T., and Levi, H., *Nuclear Chemical Engineering,* McGraw-Hill Book Company, 1981.

THE CONCEPT OF ELECTRO-NUCLEAR FACILITY FOR USEFUL POWER GENERATION AND MINOR ACTINIDES TRANSMUTATION

B. R. Bergelson, S. A. Balyuk
ITEP, Moscow, Russia

The possibility is shown to design in principle the double-purpose liquid fuel electro nuclear facility for useful power generation and minor actinides transmutation in U-Pu fuel cycle conditions. D_2O and a melt of fluorine salts are considered as a working media for liquid fuel. Such facility replenished with depicted or natural uranium only makes it possible to generate power of 900 MW (c) for external consumers and serve 20 WWER-1000 reactors for transmutation of MA. The facility could be thought as an alternative to fast reactors since appr. 30% of the total power confined in uranium is utilized in it.

Reference

1. B. R. Bergelson, S. A. Balyuk. The long-lived radiotoxicity buildup in U-Pu fuel cycles and methods to reduce it. Proc. of the 2nd Int. Seminar on HLW Transmutation and Accelerator-Based Weapon-Grade Pu Conversion, May 23-27, 22994, Moscow, Russia.

529

Conception of Electron Beam-Driven Subcritical Molten Salt Ultimate Safety Reactor

S.S. Abalin, P.N. Alekseev, V.V. Ignat'ev, O.E. Kolyaskin,
L.I. Men'shikov, V.I. Mostovoi, V.N. Prusakov, and S.A. Subbotin ⋆

and

A.K. Krasnykh, Yu. P.Popov, V.T. Rudenko, and L.N. Somov ◇

and

N.S. Dikansky and A.V. Novokhatsky †

and

A.N. Dovbnia ‡

⋆ *Russian Research Center "Kurchatov Institute", Moscow, Russia*
◇ *Joint Institute for Nuclear Research, Dubna, Russia*
† *Institute of Nuclear Physics, Novosibirsk, Russia*
‡ *Kharkov Physical Technical Institute, Kharkov, Ukraine*

Abstract. This paper is a preliminary sketch of a conception to develop the "ultimate safety reactor" using modern reactor and accelerator technologies. This approach would not require a long-range R&D program. The ultimate safety reactor could produce heat and electric energy, expand the production of fuel, or be used for the transmutation of long-lived wastes. The use of the combined double molten salt reactor system allows adequate neutron multiplication to permit using an electron accelerator for the initial neutron flux. The general parameters of such a system are discussed in this paper.

INTRODUCTION

In the design of "*the safe reactor,*" the safety of the entire fuel cycle should be taken into consideration. This includes transportation, processing of the irradiated fuel, disposal of the radioactive waste, etc. A positive way to achieve these goals could be the following:

-- Adopt a system which will minimize the probability of thermal and nuclear accidents.

-- Prepare fuel by the use of simple technology right at the nuclear power plant (NPP) where the fresh nonirradiated material should be received.

-- Complete the fuel cycle at the NPP using a fuel cycle in which the nuclear fuel can be practically totally burned out. This way the natural fuels, chemical raw materials, and reagents which were prepared outside the NPP, can be shipped from suppliers in order to realize the closed fuel cycle. No nuclear waste products should be brought out from the NPP.

-- Allow NPP radiotoxic wastes (fission fragments) with half-life periods $\sim$ 30 years to decay in underground storage on the territory of the NPP directly.

This paper will show that these requirements could be achieved by the use of a subcritical Molten Salt Reactor (MSR) driven by an electron linear accelerator.

MOLTEN SALT REACTOR
and
COMBINED SUBCRITICAL MOLTEN SALT REACTOR

The major advantage of the molten salt reactor (MSR) is in the molten salt fuel. This type of fuel is the deciding factor when choosing the design of *"the safe reactor."* The fissioning and feedstock nucleii of the MSR are dissolved in molten salt (with a melting temperature of $\sim 500^oC$). The mixture is known as FLiBe; its composition is [1-3]

$$^7LiF + BeF_2(^7LiF + NaF) + MF_4,$$

where M is the fissioning and/or actinide nuclide. This composition simultaneously fulfills the functions of a fuel, a heat-transfer agent, and a medium where necessary chemical reactions can be produced. The experimental proven FLiBe properties are:

1. High radioactive hardiness.
2. Chemical inertia (less chemically aggressive than water).
3. Low stream pressure within the operating temperature range (the characteristic MSR temperature $(400 - 700^oC)$ is much less than the boiling temperature of FLiBe.)
4. The viscosity and heat conductiivity of FLiBe permit effective heat removal by natural convection.
5. A large negative temperature reactivity factor.
6. A high heat capacity.
7. Most fission products are dissolved in, and contained by the FLiBe so that so that efficient controlled chemical extraction of the fission products is possible.
8. Continuous extraction of fission products from the FLiBe eliminates the residual heat problem.
9. FLiBe-compatible materials in MSR performance conditions have been found and tested.

Due to these properties of FLiBe, thermal and nuclear accidents become highly unlikely.

The main idea of the MSR is the development of a type of reactor that does not produce nuclear wastes. For complete freedom from a nuclear accident, the reactor should work in the deep subcritical regime. It is for this reason that the external neutron source is needed. The subcriticality value is a function of reactor design and thus determines the power required from the neutron source.

In solid fuel reactors, the fuel composition should be changed no more than once per year. For this reason there is a large initial reactivity reserve in such reactor. Because of this reserve it is necessary that $k_{eff} \leq 1+15\beta$ where β is the fraction of delayed neutrons. As the nuclear fuel is depleted, the absorbing control rods are raised so that the critical regime can be maintained during the year. If such a reactor would be operated in the subcritical regime at the time of fuel transfer, then the subcriticality reserve would be more than the reactivity

reserve allowed for the year. The subcritical condition for this case should be approximately $1 - k_{eff} \leq 15\beta$. Only with this condition is the casual raising of absorbing cores safe. Hence for this reactor, an extraordinarily intensive neutron source would be required..

In the MSR case due to constant adjusting of the fuel composition, the initial reactivity reserve would not be required and therefore the performance could be safe with a sufficiently smaller subcriticality factor: $k_{eff} \leq 1 - \beta = 0.997$. A more detailed analysis [1,2,3] shows that in the MSR the reactivity could not accidentally increase by more than 0.5%. Thus, it can be concluded that in the MSR the following condition should be fullfilled: $k_{eff} < 0.99$.

We will now consider further the stronger safety condition of $k_{eff} < 0.98$. According to well known nuclear safety rules, under the condition $k_{eff} < 0.98$, a reactor does not require a control and safety system. Note however that this condition was made to apply to ordinary solid fuel reactors. Thus although for the MSR the condition $k_{eff} < 0.99$ is more reasonable, we will consider only $k_{eff} < 0.98$. Such a reactor could be stopped practically at the moment (within a couple of milliseconds) after a fast accelerator shut down. For the achievement of a final deep subcriticality state with $k_{eff} < 0.95$, both the absorbents injection and fuel salt ebb should be considered.

The average beam power W_b which is required to supply neutrons to a subcritical reactor whose thermal power is W_r, is

$$W_b = W_r \cdot C_n/(E_f \cdot N_f)$$

where N_f is the number of fission neutrons induced per initial neutron from the source, and is given by

$$N_f = 1/(\nu(1 - k_{eff})),$$

where ν is the fraction of neutrons leaving the system, $E_f = 200MeV$ is the energy output under one fission, and C_n is the beam energy expended for producing one neutron.

From the above formulae it follows that for $k_{eff} = 0.98$ the power of the proton beam should be $W_b = 28MW$ and for an electron beam this average power should be $W_e = 730MW$. It is clear that the proton beam power is reasonable and that the electron beam power is extraordinarily great. The concept that could be useful to reduce the beam power in both cases is well known [4]. The essence is the use of cascade neutron multiplication in two coupled reactor system with suppressed neutron feedback.

Let us consider an inside reactor #1 where the initial neutron is born. It produces n_1 neutrons in nuclear reactions. If ω_{12} is the probability that a neutron can pass from reactor #1 to an adjacent reactor #2 then $\omega_{12} \cdot n_1$ is the total number of passed neutrons. Assume that the probability of neutrons passing in the reverse direction is negligibly small, i.e. $\omega_{21} \simeq 0$. Finally, let each passed neutron produce n_2 neutrons inside reactor #2. Then the total neutron number n which have been arisen from each initial neutron is

$$n = \omega_{12} \cdot n_1 \cdot n_2.$$

If the probability ω_{12} is quite great ($\omega_{12} \geq 0.1$) then with respectively small values of n_1 and n_2 (i.e. in a deep subcritical reactor) a very great value of neutron flux could be achieved.

Thus coupled reactors allow the increase of the neutron multiplication and simultaneously allows ultimate nuclear safety [4].

In order to give to this system the character of inherent safety it is necessary that the coupled system be more subcritical during any conceivable accident when the neutron feedback barrier has been broken. For instance, consider two coaxial cylindrical reactors inserted one into the other, and using a molten salt fuel system. The electron beam produces initial photonuclear neutrons in reactor #1. The concentration of fissioning nuclei is quite great while its radius is quite small (smaller than the neutron attenuation distance, or transport distance until capture.) For fast or intermediate neutron spectre ($E_n > 100eV$), the value of ω_{12} is quite high. In contrast to reactor #1, reactor #2 is thermal with $E_n \sim 0.1eV$. In order to provide the condition $E_n > 100eV$ in reactor #1, there should be dissolved a high density of thermal neutron absorbing nuclei (for example lantanids: GdF_4, SmF_4). The neutron absorbing cross sections of these nuclei in the thermal range are extremely great ($\sigma_{n\chi} \sim 10^4$) and fall rapidly with neutron energy. Hence neutrons of reactor #1 (with $E_n > 100eV$), are not absorbed by these nuclei, while neutrons hitting from #2 to #1 are absorbed. Intrinsic safety has been guaranteed if two properties are assured:

1. The absorbent doesn't fall as a sediment when the reactor is processing.
2. If the tank barrier wall will be broken then the coupled reactor is stopped by itself.

There is experimental proof [1,3], that actinide florids, MF_4, are radioactively stable. The chemical properties of lantanids and actinides are practically identical, so that is why there are no sediments. The FLiBe inside reactor #1 is the neutron absorbent of the reactor #2.

The system could be much more stable if there would be two surrounding reactors. The coupled reactor system which is described below can be called a Combined Molten Salt Reactor (CMSR). For the first reactor, the radius shall be $\sim 0.15m$ and the height shall be $\sim 4.0m$. Radius and height of reactor #2 are approximately $4m$. The fission number N_f, in the reactor #1 is $N_f \simeq 0.24/(\Delta k_1 \cdot \Delta k_2)$ where Δk_1 and Δk_2 are the amounts by which each reactor is subcritical. It can be found that for $W_r = 2250MW$ and $W_b = 25MW$ the value of N_f is approximately 580. Thus it is found that $\Delta k_1 \cdot \Delta k2 = 4.3 \cdot 10^{-4}$. The cases $\Delta k_1 \sim \Delta k_2 \sim 0.02$ and $\Delta k_1 \sim 0.043$, $\Delta k_2 \sim 0.01$ could be also be possible. The nuclear fuel which must be added into reactor #1 or #2 to make the entire system critical ($N_f \to \infty$), can be characterized by the subcritical fuel coefficient $\xi = \Delta M_f / M_f$. In our case $\xi \simeq 1.7 \cdot \Delta k$ and for $\Delta k_1 \cdot \Delta k_2 \sim 0.2$ the subcritical fuel coefficients are $\xi_1 = \xi_2 \simeq 0.034$. Simalarly we get $\xi_1 = 0.07$ and $\xi_2 = 0.017$ for $\Delta k_1 \simeq 0.043$ and $\Delta k_2 \simeq 0.01$. This estimation shows that $W_1/W_2 \simeq 0.04$ and $W_1 \simeq 90MW$ for the typical NPP. This heat could be extracted from reactor#1 [1,3] but the system would be unnecessarily complicated.

There is the possibility to split reactor #1 into five similar parts. In this case five e-beams with 5 MW average power should irradiate each tank. Here the heat density would be approximately $100MW/m^3$ which was the same as on the molten salt ultimate safe reactor project. So, one could imagin two types of CMSR:

1. $W_r \sim 200MWe$, $W_b \sim 5MW$ (one accelerator, $5MW$ beam power).

2. High Power CMSR with $W_e \sim 1000MWe$ and $W_b \sim 25MW$ (five accelerators, each with $5MW$ beam power).

In the first case, one tank (reactor #1) is inserted in reactor #2; in the second case, five reactors are put into reactor #2. This is a preliminary sketch; it is obvious that more detailed investigations are required. However, it should be noted that the system has the capability for the transmutation of some long-lived radioactive nuclei and also that it can greatly extend the time beween fuel reproducing shutdowns.

It is well known that neither proton nor electron accelerator-driven sources can achieve the neutron flux which is found in existing reactors. The question is what kind of accelerator shall be used for the initial neutron source. Previously only the neutron price, i.e., dollar cost per neutron generated, had been considered. The comparison of these accelerators must of course include other aspects beside neutron price. This comparison has been done using the same conditions for both systems:

1. A CMSR with parameters $\Delta k_1 \cdot \Delta k2 = 4.3 \cdot 10^{-4}$ (i.e $N_f \sim 560$).
2. An MSR with $k_{eff} = 0.98$, i.e. as in the case of the CMSR with parameters $\Delta k_1 \sim \Delta k_2 \sim 0.02$.

The major results of the comparison are shown in Table 1 for the case of a subcritical 2250MWth MSR. For protons two cases are analyzed:

1. A CMSR with parameters $W_r = 2250MW$, $W_b = 25MW$, $N_f = 560$.
2. An MSR with $k_{eff} = 0.98$ and the same power as for the CMSR.

Table 1. Comparison of Proton- and Electron-Driven CMSR/MSR Systems

Case	p(CMSR)	e(CMCR)	p(MSR)
Energy, MeV	1000	50-100	1000
Accelerator Length, m	1000	$(30-50) \times 5$	1000
Cost, \$M	1000	$2 \times 5 = 10$	
Beam Power, MW	1	$5 \times 5 = 25$	30
Power consumption, MW	21	32	49
Power % of total	2.1%	3.2%	4.9%
Radioactivity 10 days after stopping, Ci/m	0.2	10^{-5}	6.
RF power dissipation, MW	20	1.3x5=6.5	
Accelerator lifetime, yr	~ 600	~ 50	20

As shown in Table 1, in the first case an accelerator like LANSCE (Los-Alamos) could be used to support the CMSR. In the second case a much more powerful accelerator is needed

(30MW), with a proton current of $30mA$. Long term R&D must take place before building such an accelerator. The problems which must be solved are well known. One of the major problems is connected with the lifetime of the facility. On acceleration, a small part of the proton beam is lost. Even if the beam losses are under 1%, the lifetime of the copper accelerator structure will be too short (around 20 years). The cost of electric power must take into account the amortization cost of the facility.

Loss of accelerated protons within the accelerator structure produces fission reactions in the copper nuclei. Deactivation of the copper would be very slow, and would require several tens of years after operations are stopped. It is clear that with increasing beam current, the proton losses will rise, and other operational problems will also appear. Thus for the proton accelerator, it appears that an expensive containment housing would be needed. The energy price of producing neutrons does not seem to be very important because the power consumption is no more than 5% of the power from the nuclear power plant.

GLOBAL PARAMETERS of the ELECTRON LINAC

Electron accelerators have important advantages compared to proton machines. Chief among these advantages are lower price, simplicity, safety, relatively small size, and the fact that for this application, neutron price is not a really significant parameter. At the present moment scientists at KhPhTI (Kharkov, Ukaine) and at JINR (Dubna, Russia) are carrying out calculations on designs of different kinds of electron accelerators for this purpose; both superconducting and classical 'warm' structures are considered in either CW or pulsed mode operation.

It is easy to show [5] that the physical limitation of accelerators to get high average power in the beam is determined by the simple formulae:

$$P_{av} \leq G^2 \cdot f/W_{tr} \text{ and } P_{av} \leq c \cdot B_z \cdot G \cdot f/W_{tr}$$

where: f is the repetition rate, G is the accelerating gradient, W_{tr} is a transverse wake potential determined by the geometry of the structure and the bunch length. The first formula results from the transverse instability (BBU-instability) limitation without external focusing magnet field B_z and second formula is with focusing. In both cases the average power of the beam is determined by the accelerating gradient and repetition rate, but does not depend on the length of the accelerator. Hence it is possible to increase the average power only by increasing the gradient of the accelerating field in the sections.

Right now the parameters of electron linac are not optimized for an accelerator driven reactor. Both the CMSR and the linac are under consideration and their parameters are flexibile. The rough design of the linac system with $100MW$ beam power and $100MeV$ beam energy of the CW mode operation is as follows. The accelerating structure is a periodically loaded structure with 40cm wavelength (frequency - 700 MHz). A travelling wave linac with phase velocity equal to velocity of light is adequate for beam injection. Cooling and temperature control are provided by distillated water with adjustments for power consumption. The accelerating module parameters are summarized in Table 2.

Table 2. Electron Linac Section Parameters

Effective section length, m	2	Shunt impedance, MOhm/m	15
Aperture, mm	130	Power attenuation constant	0.2
Cavity diameter ID, mm	345	Cavity diameter OD, mm	400
Operating temperature, ^oC	40	Input RF power, MW	1.0
Temperature tolerance, ^oC	± 2	Electron efficiency, %	95
Module weight, kg	300	Optimal current, A	0.8
Power dissipated in structure, kW	50	Energy gain per section, MeV	1.2
no beam, kW	100	with optimal beam current	
Power dissipated in load, kW	0.1	Power transmitted to	950
with no beam, kW	100	beam, MW	

The RF source should have approximately 0.5-1 MW DC power. Klystron technology is well known at the desired frequency in this power range. It should noted that both klystrons and sections need to have enough band width to get into the stable regime of acceleration by the use of a feedback system. The major linac parameters are shown in Table 4. The main power consumption in the chosen scheme should be the RF power supply system. To increase accelerator efficiency, the high voltage supply is provided by parallel connections to a 100 kV DC feeder. Each connection to the feeder has a 1 MW oil breaker. This scheme provides minimal power loss and the minimal number of components. The breaker is closed with full anode voltage before RF power is applied to the klystron. RF power control and response to blocking signals (such as high-voltage break down, overheating, or gross beam losses) is carried out by means of the input RF drive. Power consumption from the power supply line could be approximately 140 MW. Each power supply source dissipates $\sim 200kW$, each collector should take $\sim 190kW$, the klystron body should take approximately $10kW$, and $0.3kW$ would be dissipated in the power output ceramic window. Total power consumption for the rest of the linac system is shown in Table 3.

Table 3. Global Accelerator Parameters

Beam power, MW	100	Beam losses along linac, A	10^{-4}
Beam energy, MeV	120	Consumption power, MW	140
Beam current, A	0.8	Power loss in linac, MW	5
Number of sections	106	Power loss in RF power supply, MW	25
Accelerator length, with injector	330	Auxilliary power consumption, MW	3

Electrons with energy of $100MeV$ will penetrate in the molten salt to a depth of up to 20 cm (radiation length) losing about 10% of their energy by ionization loss. The volume

heat release shall be equal to $0.25 MW/liter$. The remaining beam power ($\sim$ 90%) should convert to bremstralung photons which would penetrate in molten salt up to 1.5 m.

JINR PULSED NEUTRON FACILITIES as EXPERIMENTAL TEST STANDS

JINR (Dubna) has a facility which could be named as the prototype of the future accelerator driven subcritical reactor. It is the LUE-40 & IBR-30 facility. Here the neutron multiplication coefficient of 200 from the coupled facilities allows the integral yield of 0.5×10^{15} neutrons per second at a pulse width of 4 μsec. This facility has now been in operation for 20 years and has been utilized extensivity by the international neutron community. In order to improve the parameters for new experiments, the Frank Laboratory of JINR is in the process of designing its new IREN project [5]. The IREN project is optimized for investigations with resonance neutrons and is designed to have the parameters given in Table 4 (for comparison the parameters of the existing LUE-40 & IBR-30 are also indicated).

Table 4. Comparison of IREN and IBR-30

Parameters	IREN	IBR-30	Parameters	IREN	IBR-30
Electron beam energy, MeV	200	40	Repetition rate, Hz	150	100
Average beam power, kW	10	2.5	Neutron gain	28	200
Electron pulse duration, ns	250	1600	Neutron yield, n/s	$1 \cdot 10^{15}$	$0.5 \cdot 10^{15}$
Neutron pulse duration, ns	400	4500			

Both old and new JINR facilities would be used for the experimental R&D programs on transmutation of wastes and the development of accelerator for this field of activity.

ACKNOWLEDGEMENTS

The authors thank various colleagues for their help and advice in preparing this paper. They especially thank the Los Alamos Scientific Laboratory for the hospitality afforded to one of us (Yu. Popov), and to the Stanford Linear Accelerator Center for similar hospitality to another of our group (A. Krasnykh). They also thank Bill Herrmannsfeldt, SLAC, for his help in preparing this report. Finally, they gratefully acknowledge the support of the George Soros Foundation for making it possible for two of us to attend this conference.

REFERENCES

1. Brown, A.B., "The development status of MSBR." Rep. ORNL-4812, August (1972).
2. Novikov, V.M., Ignatiev, V.V., "Molten Salt Reactors: outlooks and problems." Moscow: Energoatomizdat (1990).
3. Mays, G., "MSR Program Semianual Progress Report". Oak-Ridge Report ORNL/TM-5759 (1978).
4. Avery R., "Coupled reactors with suppressed feed back," Proc. of the 2-nd UN International Conf. Geneva, v.12, p.12 (1958).
5. IREN (Intense Resonance Neutron Source), Dubna, 1994.

Study of the Burning Capability of the Los Alamos ATW System

P.A. Landeyro,
ENEA, Innovative Reactor Department, C.R.E. CASACCIA
strada provinciale Anguillarese 301, 00100 Roma, Italy
A. Buccafurni, A. Orazi
ANPA, Safety and Health Protection Directorate,
via Vitaliano Brancati 48, 00144 Roma, Italy

Abstract. The aim of calculations is to evaluate the evolution of the infinite multiplication factor (k_{inf}) during the irradiation of minor actinides, High Level Waste (HLW) and Plutonium. The most important results are independently verified with Monte Carlo calculations. The relative importance of the main parameters affecting the k_{inf} was investigated by performing calculations with several minor actinide and plutonium concentrations as well as different ^{238}U decontamination factors for HLW. The merit figure value for minor actinide alone, considering a constant neutron flux indicates that the best results are reached for minor actinide concentration equal to PWR spent fuel. The best plutonium burning results are obtained for a concentration (50.23 g/l) equal to the half of PWR spent fuel one. The simulations lead to two different reactor concepts: one for HLW burning and the other for plutonium burning purposes. To burn the HLW the most suitable reactor is an homogeneous one. This kind of reactor can effectively be utilised to burn minor actinide in low concentration (namely the PWR spent fuel). On the other hand an heterogeneous reactor with channels filled by all actinides present in PWR spent fuel with the exclusion of U isotopes with a concentration of 50 g/l can be studied.

1. INTRODUCTION

The analysis of the Accelerator Transmutation of Waste (ATW) system was subdivided into three phases. The first one was focused on the validation of the calculation tools and the associated nuclear data. The second one, which is the object of the present paper, is performed with the purpose to estimate the range of nuclear design main parameters by one-dimensional calculations. The last one is planned to perform sensitivity analysis using a Monte Carlo model.

The aim of calculations is to evaluate the evolution of the infinite multiplication factor (k_{inf}) during the irradiation of minor actinides, High Level Waste (HLW) and Plutonium. The most important results are independently verified with Monte Carlo calculations.

The relative importance of the main parameters affecting the k_{inf} was investigated by performing calculations with several minor actinide and plutonium concentrations as well as different ^{238}U decontamination factors for HLW.

For all the considered fuel compositions, the maximum k_{inf} value during irradiation was firstly determined and after unit cell calculations was performed to estimate the channel pitch corresponding to a critical geometry ($k_{inf}=1$).

The minor actinides was assumed to be dissolved in heavy water, sodium fluoride, lithium seven fluoride or dispersed in void. This last set of calculations refer to a one-dimensional model of whole reactor used to determine the critical radius as well as the optimum one (design radius) from the safety and power distribution (constant neutron flux) point of view.

2. CROSS SECTION VALIDATION

To evaluate the adequacy of cross section libraries, the minimum critical masses of fissile minor actinides were calculated while, to separate the effect of each absorber actinide nuclide, two critical benchmarks were repeated by introducing, each time 1 gr/litre of one neutron poison minor

actinides; the last calculation set was able to quantify the negative reactivity introduced by each selected nuclide with a constant test concentration.

The data are taken from [1], they consist in spheres filled with homogeneous mixture actinide oxide and water, surrounded by 20 cm thickness of water.

Calculations were performed using the ANISN [2] code and the 4 group cross section library produced by EPRI, while, the MCNP [3] code with continue cross section library, generated by ENEA from JEF 2.2 and JEF 1 data for minor actinide and major actinides as well as fission products respectively,

The calculation results present a big spreading of values. ^{243}Cm Monte Carlo results are not satisfactory, JEF 2.2 nuclear data lead to k_{eff} estimations better than the ones calculated using ENDL-85 library. Finally can be useful to note that the ANISN calculation results are conservative (k_{eff} overestimation) except for ^{245}Cm.

Benchmarks number II and III of [4] were iterated by introducing each time 1 gr/litre of neutron poison actinide.

The results suggest the following observations:

- there exist good agreement for ^{237}Np calculations and ANISN calculations are conservatives;
- with reference to ^{243}Am, the ANISN results agree with MCNP ones calculated using ENDL 85 library while, the use of JEF 2.2 library lead to conservative results;
- the agreement between ANISN and MCNP with ENDL 85 library is confirmed also for ^{242}Cm, ^{244}Cm and ^{246}Cm; concerning this three isotopes all the calculations demonstrate that the negative reactivity introduced by them it is not so important.

The negative reactivities introduced by 1 gr/litre of ^{99}Tc, ^{129}I and ^{135}Cs are calculated with ANISN and MCNP with JEF cross section library. The agreement between both calculation sets is reasonable.

The intercomparison calculations were performed according to the NEACRP Burnup-Credit benchmark specifications [5].

The agreement between the JAERI and ENEA results seems to be quite reasonable with the following exceptions:

- ENDL 85 cross section data of ^{234}U, ^{236}U and ^{243}U and ^{243}Am lead to a poor results;
- some perplexities remain for the systematic over estimation of ^{16}O absorption (JEF 1 data);
- a more detailed analyses is necessary for the evaluations of JEF 1 data for ^{95}Mo, ^{101}Ru, ^{109}Ag and ^{143}Eu.

The final evaluations of the used cross section files by comparison of the results with all the other presented in the benchmark as well as the investigations in order to fix the JEF cross section for ^{234}U, ^{236}U and ^{243}Am is already started.

3. CALCULATION METHOD

The k_{inf} behaviour versus irradiation time was analysed to verify the maximum k_{inf} value reached during the burnup. ANISN code was also used for unit cell calculations as well as MCNP to check the critical configuration.

Flux calculations were performed with XSDRNPM [6] using the 27 group standard SCALE cross section library considering only the following actinide nuclides: ^{237}Np, ^{241}Am, ^{243}Am and ^{244}Cm.

All the above calculations deal only with actinide nuclides: fission products were not considered. Furthermore, ANISN cell calculations have been performed considering a 5 cm

cylindrical channel filled with D_2O or FNa actinide solution and surrounded by the moderator (D_2O). To evaluate the maximum k_{inf} for a a selected cell, same calculations was performed with the above geometry but filling the channel with actinides dispersed in void.

The actinide concentration evolution during the irradiation or cooling phase was calculated with ORIGEN2 generation and depletion code [7] using the CANDU cross section library.

In this work, PWR standard spent fuel means a 3.3 weight percent ^{235}U enriched UO_2 fuel irradiated 1100 days reaching a burnup of 33000 MWD/TU.

Assuming a multiply medium characterised by a $k_{eff} < 1.0$ and an external neutron source of 1 neutron per second, each neutron produce in the first generation k_{eff} neutrons, in the second generation k_{eff}^2, in the nth k_{eff}^n.

Then after n generations the rate of neutron production is:

$$M = 1 + k_{eff} + k_{eff}^2 + \ldots + k_{eff}^n = \frac{1}{1 - k_{eff}}$$

where M, multiplication, is defined as the total number of neutrons produced by one neutron introduced in the system.

The blanket of ATW system will work with k_{eff} in the 0.93-0.95 range, therefore the number of neutrons will be between 14 and 20 time the low-energy spallation neutrons. This means that the actinide burning will be determinate by the fission neutrons thereby the transmutation problem can be studied like a standard reactor burning.

The minor actinide concentration studied were 2.71 g/litre, 5.42 g/litre, 10.83 g/litre. The last concentration is that existing in a PWR spent fuel while the others two are a fraction of it (namely 1/4 and 1/2), other two minor actinide concentrations considered were 54.13 g/litre (5 time PWR spent fuel) and 108.25 g/litre (10 times PWR spent fuel).

4. MINOR ACTINIDE BURNING

To investigate the minor actinide burning problems, the following nuclides were considered as components for the initial fuel mixture: ^{237}Np, ^{241}Am, ^{242m}Am, ^{243}Am, ^{242}Cm, ^{243}Cm, ^{244}Cm, ^{245}Cm, ^{246}Cm and ^{247}Cm. While, to simulate the fuel composition evolution during the irradiation the following isotopes, generated by fuel transmutation, were also considered in the calculations: ^{238}Np, ^{238}Pu, ^{239}Pu, ^{240}Pu, ^{241}Pu and ^{242}Pu.

The initial minor actinides distribution is that of PWR spent fuel reprocessed after a cooling time of 10 years.

To design the main geometrical parameters of lattice, the cylindrical cell radius which leads to a maximum k_{inf} value equal to 1.0 during the whole irradiation time was assumed as reference safe value. In fact, taking into account the system neutron leakage, the overall effective multiplication factor will result always lower than the unit.

The k_{inf} behaviour respect the irradiation time presents an initial k_{inf} increasing due to the generation of ^{238}Np, ^{238}Pu, ^{239}Pu and ^{241}Pu from ^{237}Np and a final decreasing caused by the consumption of fissile nuclides. This is true for various minor actinide initial concentrations in heavy water.

There are good agreement between MCNP check calculation and the ANISN one performed for the fuel composition which lead to the maximum k_{inf} value during all the irradiation time.

The minor actinide concentration existing in PWR spent fuel (10.83 g/litre) leads to k_{inf} values greater than the unit. Every infinite lattices of cylinders filled with a minor actinide solution less or equal 1/2 the previous one are always safe from the criticality point of view. This last conclusion is valid also for homogeneous systems (not channels).

The curves of the k_{inf} dependence from the moderator cell radius at various irradiation times, for MA dissolved in D_2O concentrated 5 or 10 times PWR spent fuel (54.12 or 108.25 gr/litre respectively), are practically parallel to the time axis at low irradiation times and becoming more and more near to the ordinate axis for long irradiation times. The cell radius corresponding to k_{inf} = 1.0 decreases with irradiation time. The maximum cell radius will correspond to a few irradiation days.

The k_{inf} increases with MA concentrations, in D_2O. Comparing these data with figure 6 of [8] results that our calculations are conservatives respect to the Los Alamos ones.

The maximum k_{inf} value are produced for the minor actinides dispersed in void, this circumstance can be explained considering the spectrum change due to flashing of D_2O present in the channel.

The value of k_{inf} corresponding to 500g/litre of MA dissolved in ^7LiF are, in any case, lower to the ones corresponding to 50g/litre of MA dissolved in heavy water.

4.1. Final remarks

The fission contribution of ^{238}Np is about 31% , then a serious effort for the validation of ^{238}Np cross section should be necessary.

The design calculations performed at Los Alamos National Laboratory (LANL) assumed always actinides dissolved in heavy water. Such hypothesis is right from the safety point of view because the system is sub critical and it can be stopped down by switching off the proton beam. But considering an accidental scenario involving the D_2O flashing within the channel, it should be better consider actinide dispersed in void which lead to highest k_{inf} values.

5. HLW BURNING

These calculations were performed taking into account all the minor actinides present in PWR spent fuel while the and one U and Pu isotopes concentration is calculated assuming a reprocessing decontamination factor of 1%; a cooling time of 10 years was also assumed before the reprocessing phase.

The nuclear fuel obtained by dissolving such HLW in heavy water is excellent because it can maintain the reactor k_{inf} lower than unit and greater than 0.9 for more of 1000 days. The fuel performance can be enhanced by increasing 5 times the actinide concentrations: the system is always sub critical and k_{inf} lasts above 0.9 for more than 1700 days.

The industrial HLW contains both minor and major actinide and the presence of ^{238}U is the main responsible of waste burning effectiveness reduction. The worst case, higher k_{inf} value, is obtained with an ideal complete absence of Uranium in the HLW.

5.1. Final remarks

HLW are excellent nuclear fuel for energy production.

Because the isolated MA present the worst k_{inf} values and adding industrial U leakage does not significantly influence the critical geometrical parameters, isolated MA HLW represents a conservative material for safety design purposes.

6. PLUTONIUM BURNING

The calculations were carried out assuming PWR spent fuel actinide composition excluding the U isotopes at the reactor discharge.

The following actinide concentration were analysed: 10.05 g/l, 50.23 g/l, and 100.45 g/l.

Table 1 shows the cell radius and pitches dependence of the concentrations for k_{inf} =1. There is a minimum channel distance corresponding to a Pu concentration corresponding to 50.23 g/l.

Table 1. Cylinder infinite array, geometrical parameter corresponding to k_{inf} =1.

Solvent	Concentration (g/l)	Cell radius (cm)	Triangular pitch (cm)	Square pitch (cm)
D_2O	10.05	56.63	111.59	100.37
D_2O	50.23	12.87	25.36	22.81
D_2O	100.45	17.48	34.45	30.98
Void	10.05	56.70	111.73	100.50
Void	50.23	13.73	27.06	24.34
Void	100.45	18.49	36.44	32.77

7 MERIT FIGURES

It is defined as the product of the actinide concentration relative to the one of PWR spent fuel with the unit cell volume fraction filled by fissile solution and finally divided with the ratio between the actinide burning and generation time. This adimensional parameter represents the burning efficiency of the system.

The merit figure value for MA alone, considering a constant neutron flux indicates that the best results are reached for MA concentration equal to PWR spent fuel.

The best plutonium burning results are obtained for a concentration (50.23 g/l) equal to the half of PWR spent fuel one.

8. ONE DIMENSIONAL MODEL FOR AN HOMOGENEOUS REACTOR

8.1. Criticality analysis

In the criticality analysis the minor actinide concentration in PWR spent fuel after 40 irradiation days (maximum k_{inf} value) was chosen to fill the reactor core. The calculation performed considering two D_2O reflector thickness, 27 and 54 cm, assuming as independent variable the fissile zone size. As the critical configuration is reached for a fissile zone thickness of 500 cm for both cases, it can be concluded that the reflector dimensions do not significantly affect the k_{eff} value.

8.2. Fissile shell size optimisation

Considering that increasing the thickness of the annulus containing actinides the neutron flux will be more and more lowered in the outermost zone and that the effectiveness of actinides burning is higher for higher flux level as well as for higher fissile mass in the core, to reach the best results an optimisation has to be done between these two important system parameters. The analysis performed using the PWR spent fuel actinide concentration (maximum of fertile nuclide concentration) leads to a thickness of 136 cm.

8.3. Burning capability

The average neutron flux results about 1.0 10^{15} n/(cm^2 s) for a proton current of 50 mA. Introducing this value in ORIGEN2 with CANDU cross section library, the data presented in Table 2. were evaluated

Table 2. Burning capability.

Reactor type	homogeneous	heterogeneous
Burning material	MA	Pu
k_{eff}	0.70	0.95
Concentration (g/l)	10.83	50.23
Inventory (kg)	60.36	245
Burning capability (kg/y)	36	197

Taking into account the data from [8], it was determined, using MCNP, the neutron flux within each channel. The average value of this flux is about 1.0 10^{15} n/(cm^2 s) for 62.5 mA, that introduced in ORIGEN2 using CANDU cross section library gives the data in Table 2.

The burning capability underestimated in these calculations because, in both cases, the neutron spectra have an important epithermal component not considered using CANDU library. On the other hand, in the flux calculations for the homogeneous blanket, the maximum neutron absorption case (minimum flux) was considered.

9. CONCLUSIONS

The previous simulations leads to two different reactor concepts. One for HLW burning and the other for plutonium burning purposes.

To burn the HLW the most suitable reactor is an homogeneous one with a first guess thickness of 136 cm for the fissile zone. This kind of reactor can effectively utilised to burn minor actinide in low concentration (namely the PWR spent fuel).

On the other hand, an heterogeneous reactor with channels filled by all actinides present in PWR spent fuel (with the exclusion of U isotopes) at a concentration of 50 g/l can be successfully studied. A possible core configuration may be built by triangular channels module having a 27.06 cm pitch. Both configuration and concentration can be used for minor actinide burning analysis.

For both reactors, the actinide can be considered as dissolved in D_2O for neutron design purposes while, from safety point of view, the maximum k_{eff} value which can be reached during accidental situation must be evaluated considering the actinides dispersed in void.

It is safer to use ^{7}LiF as solvent for MA and Pu.

10. REFERENCES

[1] Clark, H.K., *Nucl. Technol.* **48**, 164-170, (1980).

[2] Ward W. Engle , Jr "A Users Manual for ANISN: a One Dimensional Discrete Ordinates Transport Code with Anisotropic Scattering", Report Number K - 1693, Oak Ridge National Laboratory, (1967).

[3] "MCNP - A General Monte Carlo Code for Neutrons and Photon Transport", LA - 7396 - M, Rev. 2, J.F. Briesmeister, Ed., Los Alamos National Laboratory (September 1986).

[4] Landeyro,P.A., Orazi, A., Santilli, A., *ENERGIA NUCLEARE* **1**, 67-82, (1993).

[5] M. Takano, M. Brady, "Burnup-credit Benchmark, Part. 1 Simple PWR Spent Fuel Cell Problem Specification)", NEACRP - L 337, November 1991.

[6] L.M. Petrie, N.M. Greene, "XSDRNPM: AMPX Module with One-Dimensional Sn Capability for Spatial Weighting", ORNL - TM - 3706, Oak Ridge National Laboratory (1976).

[7] A.G. Croff, "A User's Manual for the ORIGEN2 Computer Code", ORNL - TM - 7628, Oak Ridge National Laboratory, (1973)

[8] J.R. Ireland and M.N. Cappiello ,"Target/Blanket Conceptual Design for the Los Alamos ATW Concept", Specialist Meeting on Accelerator - Based Transmutation, Paul Scherrer Institute, Wuerelingen/Villingen, Switzerland, March 24-26, 1992.

Design Considerations and Evaluations of an Accelerator-Driven Fluid Fuel Transmuter

P. Lizana, F. Lypsch, Ch. Jansen, P.W. Phlippen
Institute for Safety Research and Reactor Technology, Research Centre Juelich
52425 Juelich, Germany

Abstract: A fluid fuel transmuter is proposed on the basis of circulating lead forming the fluid carrier material for long-lived actinides. Thermalization of neutrons is achieved by the use of graphite in the blanket leading to low actinide concentrations, typically around 100 g/l. An eigenvalue of 0.95 is aimed at and the extraneous source neutrons are provided by the interaction of 1.6 GeV protons with a central lead target (spallation process). Fuel depletion and neutron transport calculations are discussed with a view to the technical feasibility and possible advantageous design modifications.

INTRODUCTION

Transmutation offers a means of reducing the long-term radiological impact of nuclear waste. The general goal should be to reduce the hazard of the waste finally being deposited underground in such a way that after a certain time period the remaining hazard is equal to that of an equivalent amount of natural uranium. The above mentioned time period is determined by the lifetime of technical enclosures which can be assumed to last up to one thousand years [1,2,3].

The idea of reducing the hazard of nuclear waste implies that long-lived fission products (LLFP) have to be addressed in the transmutation concept. On the grounds of generally higher cross sections of LLFP in the thermal or epithermal region (resonances) thermal systems with specifically adapted incineration zones for fission products are well suited for transmutation. An essential further characteristic of the proposed fluid fuel transmuter is subcriticality which lessens the fuel constraints compared to critical reactors while providing an additional safety margin against criticality accidents. A subcritical device with a well thermalized spectrum offers further advantages in the neutronic potential [4].

DESCRIPTION OF THE REFERENCE DESIGN

General Layout

The general layout of the proposed design is depicted in **Fig. 1.** A proton beam impinges on a lead target and produces spallation neutrons, which are moderated in the surrounding subcritical blanket. The fluid fuel in the form of an actinide-lead suspension is pumped through appropriate tubes from the bottom to the top of the system and cooled in an external heat exchanger. The power density and the lead velocities in the tubes were adjusted so that an outlet temperature of 600 °C results yielding an efficiency rate of approximately 40 % for electrical power generation. A chemical separation and reprocessing facility is assumed extracting fission products (FP) and feeding actinides into the system in a quasi-continuous way. The external system feed consists exclusively of LWR-type waste and no isotopic separation is assumed.

The graphite-moderated blanket is subdivided into two regions: a "fission product region" directly surrounding the target and an "actinide region". Optionally, in a more refined design, adjacent to the side reflector a further fission product region is included. The fission product region consists of two kinds of cells: one containing iodine as an LLFP in an appropriate form and the other type containing actinides. The unit cell within the triangular lattice of the actinide region is shown in **Fig. 2.**

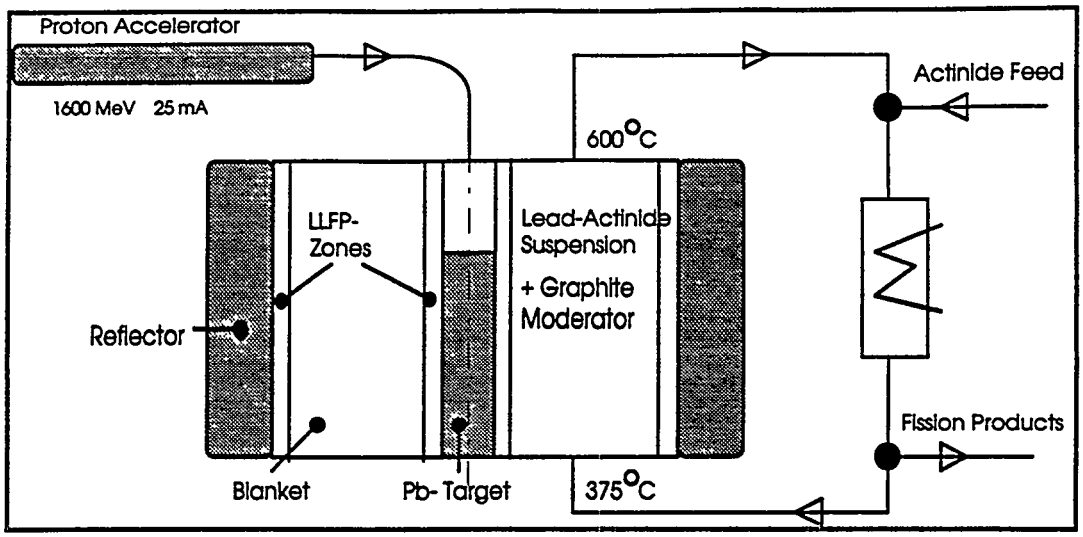

Fig. 1: Schematic overview of the fluid fuel transmuter

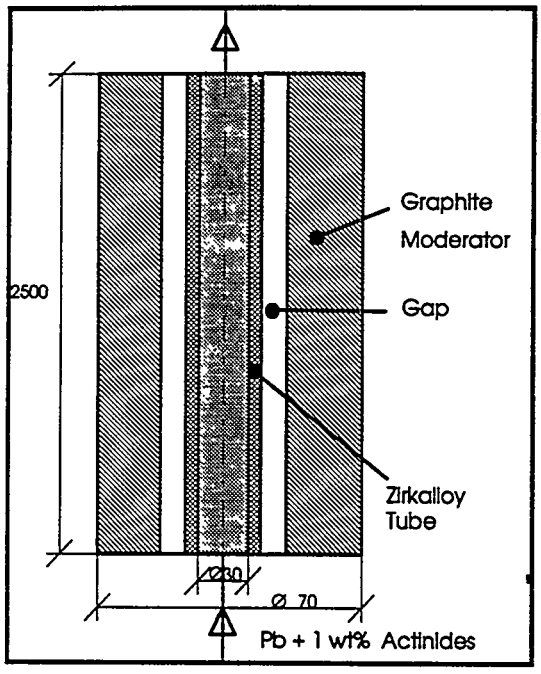

Fig. 2: Unit Cell in Actinide Region

In the initial neutronic calculations the tube consisted of zirconium and the gap between the tube and the graphite was assumed to be a vacuum. Alternative materials will be discussed in the frame of a technical evaluation. We chose a batchwise operation mode with variable cycle length. After each cycle a certain amount of the inventory consisting of actinides and fission products denoted by the reprocessing factor is removed from the system and reprocessed in a chemical facility. While the fission products are separated and conditioned in an appropriate form for intermediate or final storage, the actinides are treated in order to be recycled into the system after an appropriate and variable decay-time. Thus, the feed into the system at the beginning of each cycle consists of two streams: the recycled stream, which is the main part, and the external feed, which compensates the fissioned actinides.

The transmuter was optimized solely with regard to relevant neutron parameters like maximum actinide and LLFP destruction rates while maintaining minimum accelerator currents. As constant thermal power generation during a cycle was deemed best, a minimum decrease of the multiplication factor from the beginning of an equilibrium cycle (BOEC) ($k = 0.95$) to the end of the equilibrium cycle (EOEC) due to FP build-up was identified as a further significant goal.

Neutronic Performance

The aim of the neutronics calculation was to meet the above mentioned criteria. Considering the influence on neutronics behaviour of each design parameter we chose the following operation mode: reprocessing factor RP = 50 %; recycling 100 % of the actinides and no FP; cycle length Tz = 60 d; decay time t_Z = 120 d, and a power density in the fuel of 360 MW/m^3. The geometrical dimensions of the actinide cell are included in **Fig.2.**

The iodine cell in the FP-region has a rod diameter of 2.0 cm and is surrounded by actinide cells with characteristics as described. The number of actinide cells to iodine cells is assumed to be 4 and the isotopic composition of iodine is 25 % 127-I and 75 % 129-I. Iodine is exposed to the neutron flux in an elemental form. A graphite reflector of 60 cm thickness surrounds the actinide region (see **Fig. 3** for dimensions of the system).

The neutronics calculations were performed with modules from the SCALE 4.0 system [5], while the HETC code [6] computed the external neutron source. An operative equilibrium state is achieved approximately after 2.5 years. **Fig. 3** shows the radial neutron flux behaviour for a 1-dimensional calculation at the BOEC. The radial decrease of the thermal flux is accompanied by a radial decrease of power generation, which has to be optimized in a further step to avoid an adaptation of the fluid velocity to the flux gradient.

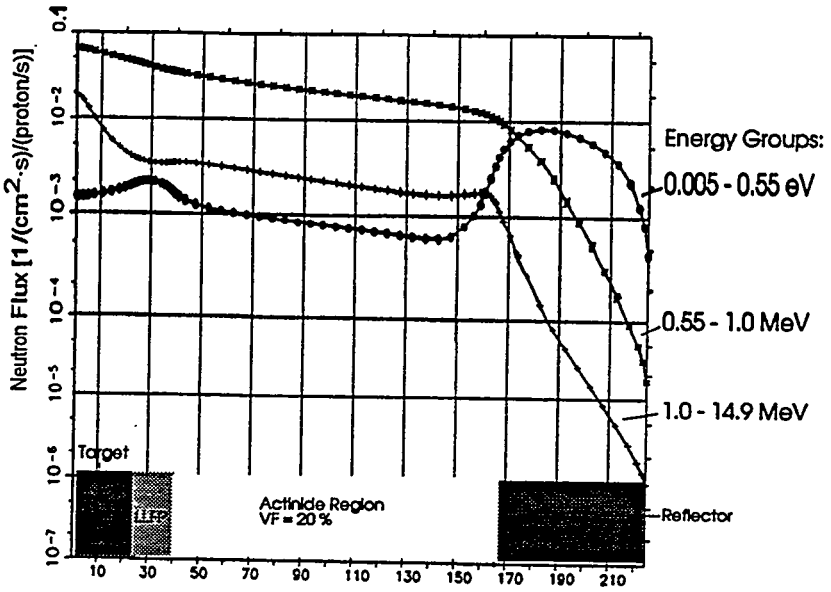

Fig. 3: Radial neutron flux distribution of the reference design

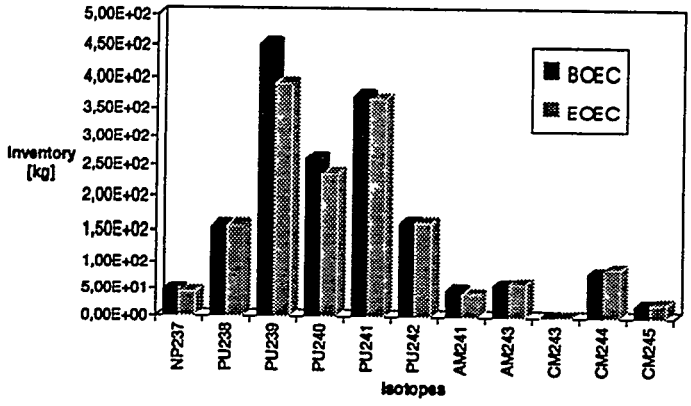

Fig. 4: Concentrations at BOEC and EOEC

The actinide compositon at BOEC and EOEC is shown in **Fig. 4.** At BOEC around 83 % of the actinides consist of plutonium-isotopes the rest being mainly minor actinides (MA). At EOEC the plutonium contribution decreases to approximately 80 %. Mainly plutonium (the isotopes Pu-239 and Pu-241) is fissioned. The incineration of MA occurs predominantly by fissioning the corresponding daughter nuclides. Additionally, an appropriate decay time outside the system offers furt her advantages to obtain fissile isotopes. The incineration of Am-241, for instance, is attained by fissioning Am-242M, Cm-243 or Pu-239, the last isotope resulting from an α decay of Cm-242 ($T_{1/2}$=162.8 d) via Pu-238. Main parameters characterizing the device at BOEC and EOEC are summarized in **Table 1.** All calculated inventories include the volume of the external piping system. A ratio of internal to total inventory of 1/4 was assumed.

543

Table 1: System parameters for the equilibrium cycle at constant power

	BOEC	EOEC
k_{eff}	0.960	0.935
I [mA]	25	40
Φ_{ave} [n/cm^2/s]	$2.24 \cdot 10^{15}$	$2.38 \cdot 10^{15}$
P [MW]	1530	1530
p_{fuel} [MW/m^3]	360	360

	Inventory [kg]	Transmutation rates [kg/a]
Actinides	1725	550
FP	155	-
LLFP	48	11
Actinide tubes	2408	
LLFP rods	25	

Technical Evaluations and Resulting Restrictions

Parallel to the neutronic calculations, the technical feasibility was assessed. Naturally, the high power density in the fuel of 360 MW/m^3 (approximately 70 MW/m^3 in the blanket) first focused attention on heat removal in the externally cooled system. Due to the high density and adequate heat capacity of liquid lead the fission heat can be transported out of the core rather easily. The required velocity is approximately 2.6 m/s limiting pressure drops to reasonable values. Thus, a system pressure of 1 MPa is sufficient even with regard to the higher velocities near the target (see the flux gradient in **Fig. 3**). The flow will be totally turbulent keeping the actinides in suspension.

A central question is how to determine the characteristics of the actinide-lead mixture, as it should be stable and homogeneous. It has to be admitted that no final conclusion could be reached at this stage though we would like to point out the basic features of the two alternatives:

- **a direct solution** of actinides in lead does not seem to be feasible below 600 °C since the solubility of uranium at 600 °C is just 10^{-2} at %, and not 1 at % as needed. Despite the fact that there is no uranium in the system, the extrapolation of solubility data to the transuranic elements is expected to give at least the order of magnitude.
- **a suspension** of actinides in the form of oxides or nitrides in lead seems to be promising especially if small particles (less than 15 μm) can be prepared. Low sedimentation rates would result and a recoil of fission products from the particle into lead would take place. Due to the density difference the fission products are expected to float meaning a simple and effective partitioning mechanism. Nevertheless, experimental data does not exist confirming such a suspension to be stable and not immediately agglomerating despite promising experiments with oxide suspensions in chemically similar bismuth [7].

Equally important is the tendency of the tube material towards corrosion. Zirconium is surely not best suited for containing liquid lead but it may have a thickness of 3 mm, whereas other materials have to be thinner in the proposed thermal system due to increased parasitic absorption. An alternative technically feasible possibility is to employ niobium tubes ($t \approx 0.5$ mm). Nb features favourable corrosion characteristics [8] and samples of pure Nb and Nb-1Zr have accumulated fast fluences up to $3.7 \cdot 10^{26}$ n/m^2 without exhibiting an explicitly brittle behaviour [9]. It should also be mentioned that external cooling requires no tubes at all and graphite is not wetted by pure lead. But with the uncertainties about the real performance of the suspension it was felt that tubes would define a necessary boundary at this stage.

The above described neutronics calculations assumed the gap between tube and graphite to be a vacuum which does not take into account graphite heating. One-dimensional n-γ calculations supposing a power density in the fuel of 360 MW/m^3 revealed that helium pressurized to 0.5 MPa is not an adequate coolant and will actually present a deterioration in safety. A better choice would be to fill the gap with pure lead resulting in lower stresses within the tube material due to negligible pressure differences. Consequently, the heat deposited in the graphite would be transported solely by thermal conduction to the central fluid lead column resulting in mean graphite temperatures of approximately 600 °C. These temperatures as well as all the other parameters can be tolerated so that the whole facility seems to be technically sound.

More problematic is the lifetime of the blanket which is assumed to be determined by the accumulated fluence of graphite at the computed temperature ($\approx 2 \cdot 10^{26}$ n/m^2 at E > 0.18 MeV [10]). Comparing it to the calculated fluxes the whole blanket can be estimated to last approximately 1 year. This cannot be adequate especially if you take into account that the blanket structure in the immediate vicinity of the target has to endure considerably higher fluxes (**Fig. 3**). Consequently, neutronic and technical improvements have to be initiated:

- improved designs should aim at an increased lifetime.
- the fuel power density distribution has to be homogenized to guarantee radially constant lead velocities with further positive effects on corrosion, thermal stresses, and irradiation damage.
- external cooling is an easy means of removing the heat from the core. But the required surface of the external heat exchanger and its necessary contents causes a comparatively high inventory, highly activated secondary components, and immense shielding requirements.

The following will deal with the problems described above and discuss possible solutions.

DESIGN OPTIONS

Neutronic Calculations

The shielding of the blanket structures from high energy spallation neutrons is one of the most important problems to be dealt with. A very powerful tool for protecting the graphite in the blanket from high fast neutron fluxes is to introduce a moderator layer of berryllium oxide (BeO) adjacent to the target structure. The thickness of this layer has to be adjusted in order to decrease the fast neutron flux around the BeO-layer to average cell values. Therefore, the lifetime of the blanket graphite is solely determined by fission neutrons, that is to say the power density in the fuel. Consequently, the graphite lifetime near the target can be increased by reducing the power density in the fuel. A BeO-layer of 5.0 cm thickness in combination with the reduced power density in the fuel (see **Table 2**) leads to a graphite lifetime of 4 years.

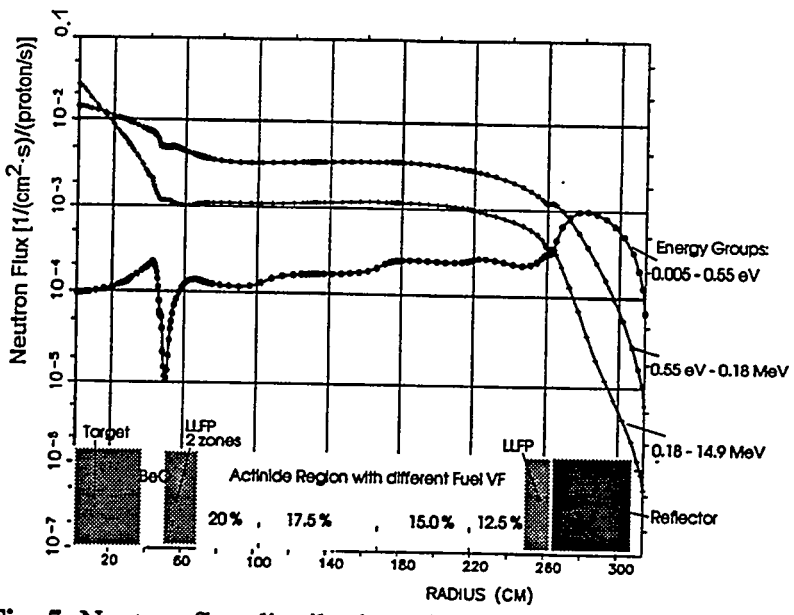

Fig. 5: Neutron flux distribution of the improved design

Radially different fluid velocities (see the pronounced flux gradient **Fig.3**) can be avoided by employing unit cells with different fuel VF in the actinide region. The proper way is to slowly increase the moderation ratio of the actinide cells with increasing radius yielding a more convenient flux distribution (see **Fig. 5**). The better thermalization is also equivalent to inserting additional reactivity into the system, thus enhancing the incineration of LLFP.

In this case the demanded radially constant power generation is linked to a radially increasing thermal flux, as the thermal fission cross section of the main fuel isotope (Pu-239), tends to decrease with softer neutron spectra, due to its relatively high resonance at 0.3 eV. The power peaking-factors for the calculated case are $p_{max}/p_{ave} = 1.15$ and $p_{min}/p_{ave} = 0.8$. With a view to reactor safety Pu-239 has a positive contribution to the net temperature coefficient. Fortunately, the system contains a relatively high amount of Pu-240,

which due to its resonance absorption at 1.0 eV leads to a net negative temperature-coefficient in the order of 10^{-6} /K according to computations for the actinide unit cell.

The operation mode has been taken from the basic design with the exception of a higher initial actinide loading (1.2 wt %). At two positions, directly surrounding the BeO-layer and adjacent to the reflector, additional incineration zones for LLFP have been employed. Iodine has been exposed in the form of PbI_2. The system parameters are summarized in Table 2.

Table 2: System parameters for the equilibrium cycle of the improved design

	BOEC	EOEC
k_{eff}	0.948	0.931
I [mA]	25	33.5
Φ_{ave} [n/cm^2/s]	$5.66 \cdot 10^{14}$	$5.78 \cdot 10^{14}$
P [MW]	1300	1300
p_{fuel} [MW/m^3]	165	165

	Inventory BOEC [kg]	Transmutation rates [kg/a]
Actinides	3800	510
FP	95	-
LLFP	94	8.4
Actinide tubes	4443	
LLFP rods	35	

Integral Heat Rejection Techniques

The way to obtain a smaller inventory is to reduce the time the suspension spends outside the core. As the reason for the time ratio spent inside and outside the core is the required mass of the heat exchanger, an interesting variation of the basic design is to circulate the central actinide-lead suspension at a high enough velocity just sufficient to have turbulent flow characteristics and to hold the actinides in suspension (**Fig. 6**).

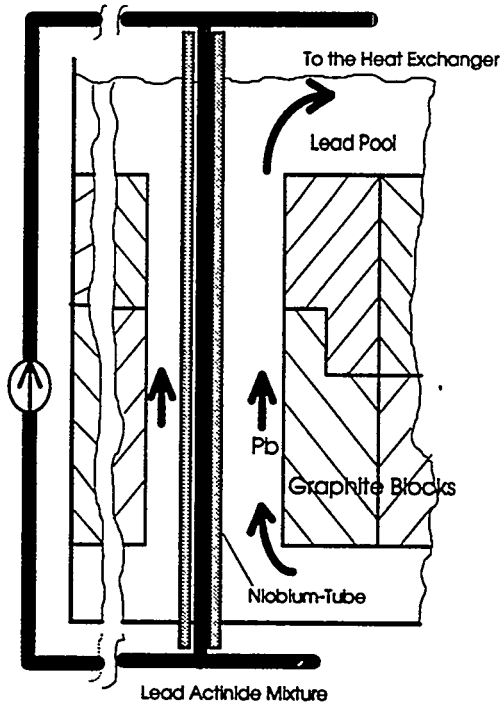

Fig. 6: Magnified unit cell and Heat Removal with external pumps

The fission heat could be conducted to the surrounding ring slot containing pure lead by a thin Nb-tube. At 1 m/s central lead velocity a simplified analysis yields temperatures in the hot part of the lead pool of approximately 500 °C (afterheat production outside the core zeroed in the simplified model). While the temperatures of the centrally circulating actinide-lead suspension (800 °C) are considerably higher than in the basic design, it could be noted that this circuit lacks a temperature gradient. Consequently with regard to the corrosion of niobium the negligible temperature difference means a lack of thermal gradient mass transfer which is normally an important corrosion mechanism. Thus, the system could have similarly good corrosion characteristics as the externally cooled system despite higher temperatures. The performance of the system can be further improved if a pipe system is designed to close the circuit by streaming upwards using tubes of the blanket, and downwards too. While further reducing the out-of-pile time, this design would also lessen shielding requirements since all the pipes could be immersed in a lead pool.

Preliminary analysis also indicates that the whole idea of designing a circuit for the lead actinide mixture may be superfluous as natural convection will stir up the fluid inside the niobium tube profoundly. Assuming according to [11] the effective thermal conductivity of lead to be roughly doubled, the central temperature of lead would be barely 1000° C.

All design alternatives discussed above assumed a fuel power density of 360 MW/m^3. They can be applied to lower power densities as well.

CONCLUSIONS

The discussion of subcritial accelerator-driven fluid fuel systems shows that they suit the purpose of transmutation and can be fed exclusively by LWR-type actinide waste. The neutronic performance strongly interrelates with the technical feasibility. Both demands are at least partially satisfied by design variations of a fluid fuel incinerator on the basis of liquid lead. Especially the following central advantages should be recalled:

- The combination of liquid lead with a graphite moderator allows the system to operate at a pressure only high enough to overcome the pressure drops.
- The quasi-continuous removal of a certain amount of fission products from the facility includes the advantage of a lower relative afterheat production in the subcritical design than in a reactor thus diminishing the accident potential of the system.
- In a thermal system a fuel dump offers a means of shutting down the facility in case of an emergency.
- The waste streams of the proposed system contain just short-lived fission products in addition to activation and spallation products, without at any stage producing materials suitable for nuclear weapons.

Further work will yield more refined and reliable data thus identifying additional design criteria. In particular, safety aspects will have to be addressed extensively as the shift of activities from final disposal to new innovative critical or subcritical systems should not diminish the safety performance of the whole nuclear fuel system.

ACKNOWLEDGMENT

One of the authors (P.L.) would like to thank the Konrad Adenauer Foundation for supporting his scientific work at the Research Centre Juelich.

REFERENCES

[1] Smailos, E. et al., *Untersuchungen zur Eignung keramischer Behälter als Korrosionsschutz für hochradioaktive Abfallprodukte bei der Endlagerung in Steinsalzformationen,* Kernforschungszentrum Karlsruhe, KfK 4244, April 1987

[2] Schwarzkopf, W. et al., *In-Situ Corrosion Studies on Selected High-Level Waste Packaging Materials under Simulated Disposal Conditions in Rock Salt Formations,* Kernforschungszentrum Karlsruhe, KfK 4324, January 1988

[3] Schwarzkopf, W. et al., *In-Situ Corrosion Studies on Cast Steel for a High-Level Waste Packaging in a Rock Salt Repository,* Materials Research Society Symp. Proc. **127** , 1989, pp. 411-418

[4] Salvatores,Slessarev,Uematsu, *A Global Physics Approach to Transmutation of Radioactive Nuclei,* Nucl. Sci. Eng. **116**,1-18 (1994)

[5] Hermann, O. W. et al., *SCALE 4.0 - A Modular Code System for Performing Standardized Computer Analysis for Licensing Evaluation* , ORNL, Radiation Shielding Information Center, 1990.

[6] Cloth,P. and Filges, D. et al., *HERMES - A Monte Carlo Program System for Beam-Materials Interaction Studies,* Research Centre Juelich, KFA-Report Jül-2203, 1988.

[7] Lane, MacPherson, Maslan, *Fluid Fuel Reactors,* Addison-Wesley Publ. Comp. Inc. ch. 3, p. 740, p. 945.

[8] Ali-Khan, I., "Corrosion of Steels and Refractory Metals in Liquid Lead" in *Material Behavior and Physical Chemistry in Liquid Metal Systems,* ed. H. U. Borgstedt, Plenum Press, New York, 1982

[9] Wiffen, F. W., " The Tensile Properties of Fast Reactor Neutron Irradiated BCC Metals and Alloys" in *Proceedings of the1973 Conference on Defects and Defect Clusters in B.C.C.Metals and Their Alloys,* p.176

[10] Haag, G. et al., *Development of Graphite,* Journal of Nuclear Materials **171**, 41-48, 1990

[11] Martens, McLain, *Reactor Handbook 2nd Edition,* J. Wiley & Sons, 1964, ch. 2, pp. 71-75

AN ACCLERATOR-BASED INSTALLATION OF SMALL POWER WITH THE LEAD-BISMUTH COOLANT

V.T.Gorshkov*, E.I.Yefimov, N.N.Novikova, E.A.Zemskov+

* - *Research and Development Bereau "Gidropress" Podolsk, Russia, 142103;*
+ - *Institute of Physics and Power Engineering, Obninsk, Russia, 249020.*

Abstract. The structure of the accelerator-based installation is described that includes the subcritical reactor-blanket with power 15 MW(h) cooled with lead-bismuth, the lead-bismuth flow target where a beam of α-particle is injected, the equipment of a primary and secondary curcuits. Some results of calculations and estimations are discussed that have been carried out to justify the target and blanket constructions. Some main characteristics of the installation are presented.

1. INTRODUCTION.

Nowdays the possibilities of development of advanced accelerator-based systems are actively discussed with high neutron flux in blanket mainly for purposes of actinides transmutation and plutonium utilization. The creation of such installation requires development and solution of a number of complicated scientific and engineering issues and it seems reasonable to develope at first stage a pilot installation of comparetively small power. Some technical arrangements useful for more powerful systems might be checked on such installations.

In this connection some preconceptual design of accelerator- based installation was carried out with subcritical blanket with power 15 MW(h) cooled with lead-bismuth where α-particle beam is injected from cycle accelerator with energy 6 GeV and mean current 0.1 mA.

Institute of Physics and Power Engineering, Research and Development Bureau "Gigropress" have gained a wide experience in development, creation and exploitation of NPP with lead-bismuth as a primary circuit coolant. This experience could be rather useful in development of both liquid metal targets for accelerator-based systems and systems itself [1,2].

To improve safety of the plant under heat removal accidents a number of non-traditional engineering solutions for NPP with lead- bismuth has been used in the presented design.

2. THE PLANT CONSTRUCTION.

The pilot plant of target-blanket complex (TBC) includes besides the α-particle guide the target and the blanket with heat removal circuit (the primary circuit) and steam generating circuit (the secondary circuit) with relevant equipment.

2.1. The target construction.

The target is made as an independent assembly tight separeted from the circulation circuit of the blahket (Fig. 1).

The low part 42 arranged in the center on the blanket axis is the target itself where α-particles injected on the guide 36 through diaphragm 41 generate neutrons in the lead-bismuth volume. To remove heat and to cool the window 41 the natural circulation circuit 40 of lead-bismuth is organized from the target itself up to the cooling coil 38. The heat removal to the cooling coil 38 is realized through the tight stable shell (wall) which separates the coil 38 from the circulation circuit, so if a breakdown of the coil tubes take place the steam will remove to a special condencer and the diaphragm 41 will not be subjected to excessive pressure.

The upper part of the target is filled with boron carbide which is both a heat insulator and radiation shield from neutron. There are channels for the guide and for six control rodes which are not shown in the picture.

2.2. The structure of the target-blanket complex.

The TBC has an integral arrangement of main equipment which including steam generator modules, circulation pumps, head and dump tanks is arranged in two-wall steel tight containment. (Fig.2).

In the fig.2 TBC includes: the blanket 1 with fuel asemblies, target 2 and control rodes 3; radiation shields 5; electropumps 6; steam generator modules 7 with evaporator 8, steam separator 9 and steam superheater 10; collectors 11, 12, 13; head tank 14 with nominal level 15; dump tank 16 with level 17 and 18 under nominal regime and shut-down pumps accordingly; coolant streams 19; tubes 20 of emergency heat exchanger; support plate 21 with supports 22 of the TBC vessel 23 with inner 24 and outer wall 25.

The blanket is a cilinder of sizes 907*860 mm with channel (diameter 300 mm) in the center for the target. Fuel elemehts are formed in blanket a triangle lattice with pitch 13.6 mm. Six control rodes are steel tubes ø 21*0.5 mm filled with boron carbide that has enrichment 80 % on boron-10. Control rodes are arranged in the centers of fuel assemblies on radius 389 mm from the blanket axis.

72 steam generator modules are unifed into 4 section which operate in parallel relative to the primary and secondary circuits. In the modules the feed water flow into nozzles of water-jet pumps, which arranged in evaporators beneath water level and realized multiple forced water circulation. The lead-bismuth flows down through annual channels flowing over the coil of steam superheater at first. In the low part the coolant flows over the wall of evaporator 8 and then it flows through holes and drops down to the dump tank 17 in the form of streams.

If the pumps 6 operate the circulation in the primary circuit takes place as a result of the coolant flow from the head tank 14 through steam generator modules into the dump tank 16. If the pumps 6 are shut down (for example in emergency case of loss of electricity supply) all the coolant will flow into the dump tank 16 covering partly the low part of steam generator heat transfer surface. In the dump tank 16 beneath the lead-bismuth level the heat transfer tubes 20 of emergency heat exchanger are arranged and natural circulation is established through this heat exchanger with heat transfer into atmosphere through containment walls.

3. SOME RESULTS OF PHYSICAL CALCULATIONS AND ESTIMATIONS.

The choice of α-particles as ions for neutron generation made a problem of calculation much more difficult than in the case of protons since both cross-section data and especially codes are available mainly for protons but

not for α-particles. Therefore calculations of secondary neutron generation, radiation energy releases in the target and structural materials were made for protons on the code MARS-10 modelling by Monte-Karlo method transport of high-energy particle in matter by inclusive approach [3]. In these calculations one α-particle with energy 6 Gev was considered as four protons with energy 1.5 Gev.

3.1. Secondary neutron field in the target.

The target diameter is 210 mm, the beam diameter is 100 mm, α-particle current is 0,1 mA that corresponds to equivalent proton intensity $1.25 \cdot 10^{15}$ p/s. The spectrum of neutrons with energy less than 14.5 Mev escaping into the blanket through the target lateral surface is presented in table 1. The total neutron leakage calculated on MARS-10 code is $5 \cdot 10^{16}$ n/s. Availability of steel construction between the target and the blanket with total thickness 8.5 mm was taken into account. Table 1. The spectrum of neutrons with energy less than 14.5 Mev escaping into the blanket through the target lateral surface

Table 1. Leakage neutron spectrum.

Energy interval, Mev	Part of neutrons, %	Energy interval, Mev	Part of neutrons, %
10.5 - 6.5	0.15	0.8 - 0.4	25.2
6.5 - 4.0	1.8	0.4 - 0.2	15.3
4.0 - 2.5	2.46	0.2 - 0.1	7.2
2.5 - 1.4	18.0	0.1 - 0.0465	1.6
1.4 - 0.8	27.9	0.0465 - 0.01	0.39

One can see that about 85% neutrons escaping into the blanket has energy in the interval 0.2÷2.5 Mev.

3.2. Radiation energy release.

The energy release distribution over the target volume was calculated on the code MARS-10. In cylindrical layers with Δr_1=0÷5 cm and Δr_2=5÷10 cm energy release power is 100 and 56 KW accordingly that is about half power of beam (300 KW) in sum. Energy release in the target steel window with thickness 1.5 mm is 0.75 KW.

3.3. Calculations of neutron fields in the blanket.

The problem of calculations of neutrons fields and energy release in an subcritical blanket with outer neutron source is not traditional in reactor physics. Therefore the calculations of the blanket were made in two stages with the use of codes that are available in Institute Physics and Power Engineering.

At the first stage the main physical and engineering characteristics of the blanket were determined as for a critical core in 26-group diffusion approximation in two-dimensional cylindrical geometry. The fast core cooled with lead - bismuth of BRUS-reactor type [1] was used as a prototype for the choice of fuel element construction and lattice pitch. The oxide fuel

reloading) was chosen 3 years. k_{ef} of the blanket was chosen 0.95.

In the course of the blanket life time reactivity and power of subcritical blanket decrease because of poisoning. The system of six control rods was calculated for compensation of this effect.

The calculations showed that maintenance of 5% subcritically requires U-235 charge 480 kg with mean fuel enrichment 21%. The reactivity change for 3 years $\Delta k=0.8\%$, maximum fuel burn-up 1.2%.

At the second stage neutron and energy release fields in subcritical blanket with known main characteristic were calculated with the use of small-group three (r,φ,z)- dimensional diffusion code RFZ-S [4]. The code allows to consider a subcritical core with a neutron source on cylindrical surface in the core.

These calculations showed in particular that irregularities in the energy release distribution in an subcritical blanket with outer neutron source is more than in critical core and they depend on subcriticality value. By subcriticality ~5% relevant discrepancies are comparatevly small.

Specific energy release power in the blanket is not high (30 KW/l)/ It seems that without change of the blanket sizes and some other characteristics transmutation of actinides can be realized, efficiency of control rods can be increased etc.

3.4. The assessment of the window life-time.

The window life-time was estimated about 3 years on conditions of radiation damage stability. The fast neutron fluence is about $\sim 10^{23}$ for this time. This value is not exceed the fluence on fuel element coatings in nuclear reactors.

Equivalent fluence of proton is $1.5 \cdot 10^{21}$ p/cm^2. Thre is the experience of exploitation LAMPF-accelerator in Los-Alamos where the window showed radiation damage stability by the proton fluence $3 \cdot 10^{21}$ p/cm^2 [5].

3.5. The estimation of polonium activity.

Specific activity of Po-210 in the primary circuit of the blanket is about 20 Ci/l (the circuit volume is - 5 m^3). This - activity in the target circuit is about 200 Ci/l (volume ~0.13 m^3). Because of (α,xn)-reaction on lead radioniclides of Po-209 ($T_{1/2}$=102 y) and Po-208 ($T_{1/2}$=2.9 y) are formed in the target circuit. After 3-years operating specific activity of Po-209 in the target circuit is ~0.01 Ci/l, Po-208 ~0.5 Ci/l.

4. SOME MAIN CHARACTERISTICS OF THE TARGET-BLANKET COMPLEX.

These characteristics are presented in the table 2. They were obtained as results of the calculations described above and additional assessments.

Table 2. Some main characteristics of TBC

NN	Characteristic	Value
1	2	3
1.	α - particle current, mA	0.1
2.	α - particle energy, GeV	6.0
3.	Diameter of α - particle beam, mm	100
4.	Diaphragm tnickness, mm	1.5
5.	Operating pressure on the diaphragm, kg/cm^2	2.5
6.	Permissible outer pressure on the diaphragm, kg/cm^2	46
7.	Maximum temperature in the diaphragm, ^oC	450
8.	Energy release power in the diaphragm, KW	0.75
9.	The target diameter, mm	210
10.	The target length, mm	860
11.	Lead-bismuth flow rate in the target circuit, m^3/h	7.15
12.	Temperature of lead-bismuth, ^oC	
	target circuit input	280
	target circuit output	367
13.	Heat power removed with natural circulation loop in the target, KW	265
14.	Feed water flow rate through the cooling coil in the target, m^3/h	3.1
15.	Feed water temperature, ^oC	
	coil input (pressure 40 kg/cm^2)	150
	coil output	240
16.	Maximum lead-bismuth velocity in the target circuit, m/s	0.14
17.	Lead-bismuth volume in the target circuit, m^3	0.13
18.	Target mass, t	3.325
19.	Blanket heat power, MW	15
20.	Lead-bismuth temperature in the blanket circuit, ^oC	
	input	300
	output	400
21.	Lead-bismuth flow rate through blanket, m^3/h	360
22.	Steam parameters on output of steam generator	
	temperature, ^oC	350
	pressure, kg/cm^2	37

1	2	3
23.	Steam generator capacity, t/h	22
24.	Feed water parameters on steam generator input	
	temperature, ^{o}C	150
	pressure, kg/cm^2	40
25.	Blanket sizes,	
	Equivalent diameter, mm	907
	Height of fuel, mm	860
26.	Sizes of fuel element coating, mmxmm	12x0.4
27.	Pitch of fuel elements arrangement in triangle lattice, mm	13.6
28.	Number of control rods in the blanket	6
29.	Mean lead-bismuth velocity in the blanket, m/s	0.66
30.	Mean specitic energy release power in the blanket, KW/l	30
31.	Maximum temperature of fuel element coating, ^{o}C	600
32.	Number of fuel elements	3355
33.	Fuel	UO_2
34.	Uranium-235 charge, kg	480
35.	Mean enrichment of the fuel, %	21
36.	Efficiency of 6 control rods, %	1,7
37.	Reactivity decrease for 3 years, %	0.8
38.	Initial Kef value	0.95
39.	Time between reloading, years	3
40.	Lead-bismuth volume in primary circuit, m^3	5.15

REFERENCES

1. Gromov B.F., Dekusar V.M., Yefimov E.I. et al. Lead-Bismuth as a perspective coolant for reactor and accelerator-Based Plants - Paper presented at International conference. ARS-94, Pittsburgh, April 17-21, 1994.

2. Gromov B.F., Gulevskij V.A., Yefimov E.I. et al. Some Problems of the Use of Lead-Bismuth or Lead in Flow Targets and Relevant Reactor Experience. - Paper presented at the 2-nd workshop on subproject "Target" for ESS. Switzerland, PSI, June 6-7, 1994.

3. Mokhov N.V. The MARS-10 Code System: Inclisive Simulation of Hadronic and Electromagnetic Cascades and Muon Transport. - Report. FN-509, FNAL, 1989.

4. Zemskov E.A. et al. The Code for Calculation of Critical Nuclear Reactor in (r,φ,z)-Geometry. Preprint - FEI-1223, Obninsk, 1991 (in Russian).

5. Capiello M. et al. ATW Aqueous Target/Blanket System Design, LANL, 1992.

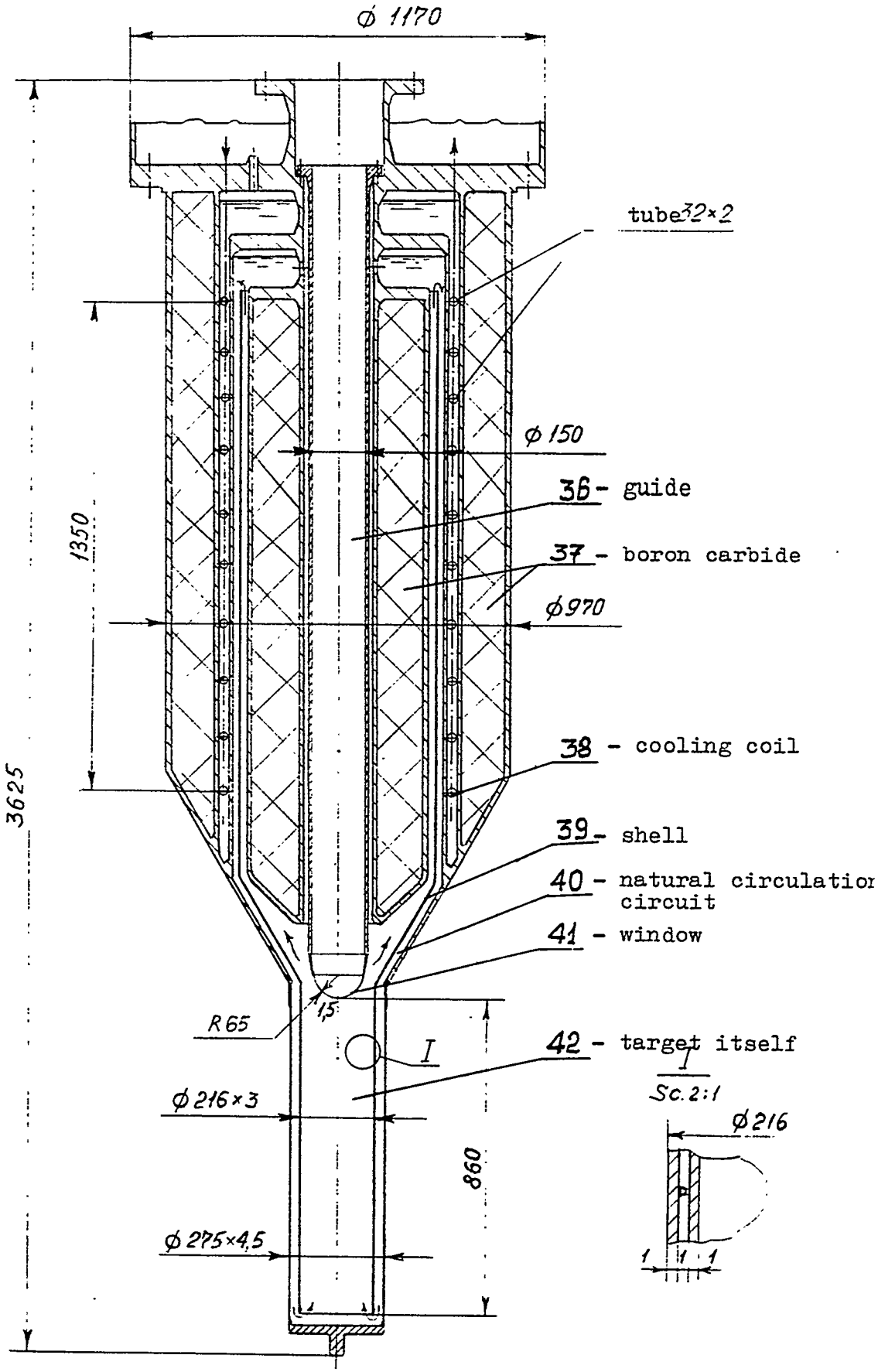
Ø 1170
tube 32×2
Ø 150
36 - guide
37 - boron carbide
Ø 970
38 - cooling coil
39 - shell
40 - natural circulation circuit
41 - window
42 - target itself
1350
3625
R 65
1,5
I
Ø 216×3
860
Ø 275×4,5
Sc. 2:1
Ø 216
1
1
1

Fig. 1.

Sc. 1:15

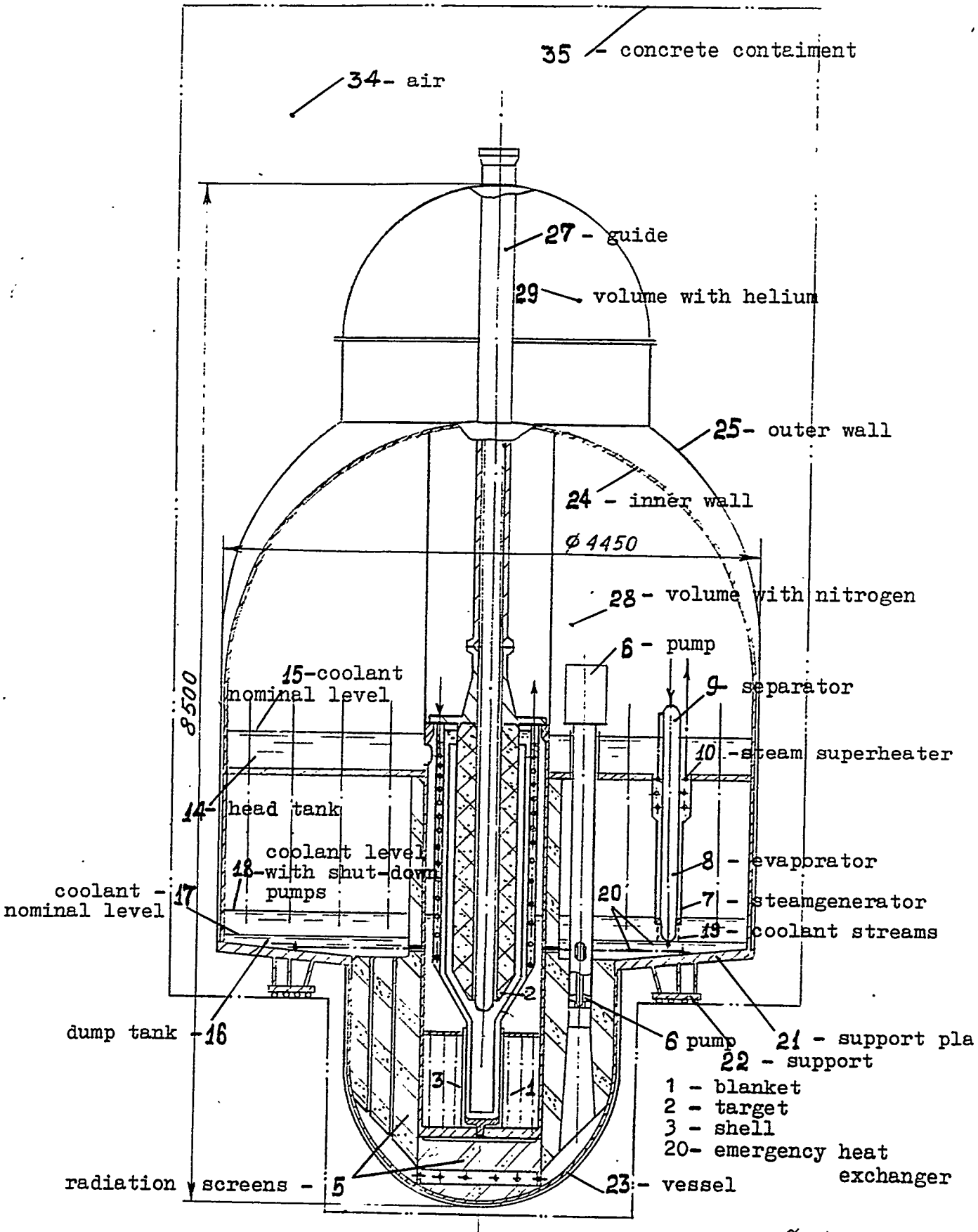

Fig.2.

Sc.1:40

555

Development and Analysis of a Metal-Fueled Accelerator-Driven Burner

F. Lypsch* and R. N. Hill**

**Institute for Safety Research and Reactor Technology, Research Centre Juelich, P.O. Box 1913, 52425 Juelich, Germany*

***Reactor Analysis Division, Argonne National Laboratory, Argonne, Illinois 60439*

Abstract: The purpose of this paper is to compare the safety characteristics of an accelerator driven metal-fueled fast system to a critical core on a consistent basis to determine how these characteistics are affected solely by subcriticality of the system. To accomplish this, an accelerator proton beam/tungsten neutron source model is surrounded by a subcritical blanket using metallic fuel and sodium as coolant. The consequences of typical accident transients, namely unprotected transient overpower (TOP), loss of heat sink (LOHS), and loss of flow (LOF) were calculated for the hybrid system and compared to corresponding results for a metal-fueled fast reactor. Results indicate that the subcritical system exhibits superior performance for TOP (reactivity-induced) transients; however, only in the critical system are reactivity feedbacks able to cause passive shutdown in the LOHS and LOF events. Therefore, for a full spectrum of accident initiators considered, the overall safety behavior of accelerator-driven metal-fueled systems can neither be concluded to be worse nor to be better than advanced reactor designs which rely on passive safety features.

INTRODUCTION

Numerous reactor research programs have focused on the transmutation of nuclear waste in order to reduce the hazards of high-level waste. An interesting variation seems to be a hybrid design consisting of a charged particle high energy accelerator, a target region making use of the spallation process, and a subcritcal blanket region [1,2].

Subcritical accelerator systems offer several potential advantages for transmutation applications. These systems can be operated with a low inventory since large fissile masses are not required for criticality. Moreover, this low inventory leads to low fuel concentrations which may allow the use of improved fuel forms, particularly for fluid fuel systems which are being investigated in current studies [3]. For the transmutation of fission products, the subcritical system is ideal because large capture rates can be tolerated; whereas, excess neutrons must be produced to offset parasitic capture in a critical system. The primary performance disadvantage of accelerator systems is the energy consumption of the accelerator, reducing the net energy production of the system.

Subcritical systems additionally differ from critical systems in their transient behavior. The reliance on extraneous source neutrons changes the worth of all temperature coefficients. For example, the large margin to any kind of criticality accident in accelerator systems has been widely recognized. However, subcriticality can also be expected to reduce the importance of the passive reactivity feedback mechanisms which have been exploited in advanced reactor designs.

The aim of this paper is to perform an overall safety performance evaluation to assess the impact of subcriticality by comparing the safety characteristics of an accelerator driven system to a critical core. In order to make the comparison as consistent as possible, the accelerator system was designed similar to a current reactor design. For this study, a metal-fueled fast reactor system proposed for transmutation [4] was chosen as the reference configuration. The development of a fast spectrum subcritical accelerator system using similar materials and geometry is described in the next section; ideally, the only difference between the two systems would be in the neutron criticality.

CONCEPTUAL DESIGN OF ACCELERATOR SYSTEM

The intended comparison of the subcritical design to a current reactor design greatly determined the configuration of the system. A 900 MWt IFR metal-fueled fast reactor [4] with a conversion ratio near 1 was chosen as the reference critical system. An eigenvalue of 0.95 and a cycle length of one year were targeted for the subcritical system. The eigenvalue reduction (compared to the critical system) was achieved by reducing the fuel volume fraction. The fuel parameters are enumerated in Table 1.

Table 1: Fuel Lattice Parameters

Fuel parameters	Inner Blanket	Outer Blanket	Critical Core
Height [cm]	200.0	200.0	96.5
Pin Diameter [cm]	0.508	0.546	0.724
Pin Pitch [cm]	0.838	0.846	0.854
Volume Fractions [%]:			
Fuel	20.0	23.0	38.5
Structure	25.3	25.3	25.6
Coolant	54.7	51.7	35.9
TRU/HM Enrichment [%]	20.5	20.5	24.6

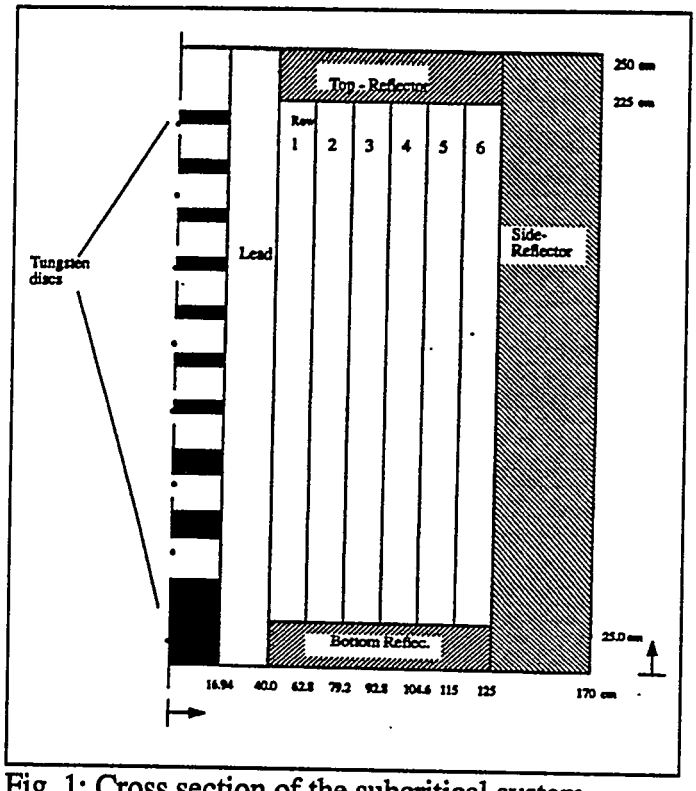

Fig. 1: Cross section of the subcritical system

The accelerator/target design resembles that of [5] and was only slightly adapted to our purposes. The main difference was the exchange of the heavy water coolant for sodium coolant in the target region. This modification should not change the overall conclusions of this study. The blanket region was configured to efficiently utilize the spallation neutrons. As shown in Fig.1, the height to diameter ratio of the blanket is nearly 1. The height was dictated by the axial size of the target design; and the radial dimension was scaled to provide adequate power production even in the outer rows. If the inner blanket zone is operated at power densities similar to a reactor system, the resulting power level of the entire blanket region is 1950 MWt. This power corresponds to a proton beam voltage of 1600 MeV and a current of 39 mA. The core was subdivided into two zones with a slightly higher fuel volume fraction in the outer regions to reduce the neutron flux gradient and to smooth the power density distribution. Finally, the fuel residence times were spatially varied to roughly conserve the discharge burnup at 100 MWd/kg; the row 1 fuel resides three cycles, and the row 6 fuel resides seven cycles.

THE NEUTRONICS OF THE STEADY STATE SYSTEM

The 1.6 GeV protons enter the target region from above (Fig. 1) and produce spallation neutrons in the various tungsten discs. The high energy reactions are modeled by HETC-KFA 2

[6] transporting protons and neutrons down to 14.2 MeV. Neutrons falling below that boundary form the source neutrons for the ensuing 9-group fixed source DIF3D calculations which compute the overall neutron balance and the flux distribution in the different regions [7]. Fuel burnup was modeled by the REBUS depletion code employing DIF3D and batch-averaged compositions [8].

Fig. 2 compares the flux distribution of the hybrid design to that of a 900 MWth metal-fueled fast reactor [4]. As expected, the source-driven flux distribution decreases with penetration into the blanket region; whereas, the flux is relatively constant in the fueled region of the reactor system. In addition, the subcritical flux decreases considerably during a fuel cycle. The average flux, that is to say the power, decreases considerably during a fuel cycle due to a change of the eigenvalue from 0.95 to 0.93. If the accelerator current is maintained at a constant level, the flux decrease with depletion results in a corresponding 33 % power decrease at EOEC.

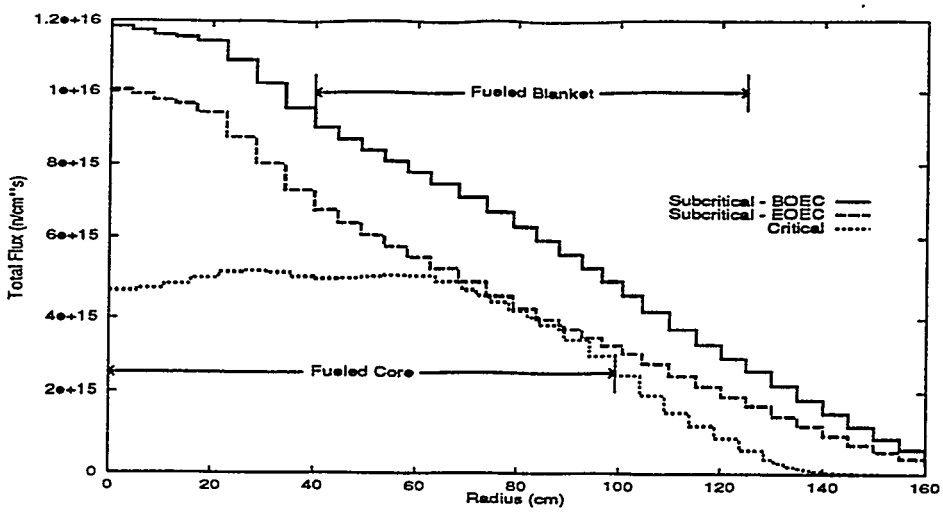

Fig. 2:Radial Flux Distribution of Subcritical Assembly and Typical Reactor

ANALYSIS OF THE SAFETY BEHAVIOR

Because the eigenvalue flux solution represents a non-physical situation (where the only source of neutrons is fission), changes in the eigenvalue are not useful for the evaluation of reactivity effects. Instead, a multiplication factor, k, is introduced to quantify neutron production:

$$k = \frac{\text{Prod.rate}}{\text{Absorp.rate} + \text{Leak.rate}}$$

Table 2: Reactivity Feedback Coefficients

	Accelerator	Core
Delayed Neutron Fraction	$3.31 \cdot 10^{-3}$	$3.53 \cdot 10^{-3}$
Prompt Neutron Lifetime [s]	$9.05 \cdot 10^{-7}$	$2.49 \cdot 10^{-7}$
Axial Expansion[cents/K]	-0.095	-0.11
Radial Expansion [cents/K]	-0.22	-0.22
Fuel Doppler [cents/K]	-0.099[a]	-0.099
Coolant Density. [cents/K]	+0.58	+0.18

[a]assumed equal to reactor values

where the reaction rates are determined using the fixed-source flux distribution. This multiplication factor also determines the correlation between the accelerator parameters (proton current and neutron yield per proton) and the power level.

Reactivity effects were calculated by evaluating changes in the multiplication factor for perturbations causing changes in radial dimensions, axial dimensions, and coolant density. The results are summarized in Table 2. The feedback coefficients are similar to those computed for the critical reactor system.

Using these reactivity feedback coefficients, the modeling of transient performance was conducted using a simplified version of the SASSYS code [9]. This code couples the neutronic behavior in each of the six fueled rows to the thermal behavior of the primary and secondary systems. Point kinetics are used to model the nuclear dynamics. This is sufficient for small perturbations where the flux shape does not change considerably; the modeling of transient behavior beyond the onset of sodium boiling (with large reactivity and thermal feedbacks) is beyond the scope of this calculational procedure. In the following section, results obtained for the high power region of the accelerator system (Row 1 in Fig. 1) are compared to typical reactor results for a variety of transient situations.

COMPUTATION OF THE TRANSIENTS

The accident analyses for both the critical and subcritical systems concentrated on three pertinent accidents generally investigated for reactor licensing,

- the TOP scenario (transient overpower) assumes a control rod failure and is simulated in the program by inserting an excess reactivity over a reasonable timescale. In a subcritical design control rods are not necessary, but they may be allocated to reduce the power drop between BOEC and EOEC
- the LOHS (Loss of Heat Sink) scenario is caused by failures in the steam generator system. All cooling in the secondary system is lost over a very short time period resulting in a temperature rise in the primary coolant.
- the LOF scenario (Loss of Flow) has its origin in the primary circuit due to a failure of all of the pumps, as the flow is reduced to zero after a certain amount of time depending on the pump inertial forces. A conceivable reason for this accident is an overall power failure accompanied by a general failure of the on-site auxiliary systems.

As expected, the subcritical system exhibits favorable responses to TOP (reactivity-induced) transients. As shown in Fig. 3, the subcritical system does not experience the rapid power rise exhibited by the critical system which activates the reactivity feedbacks; and the total power increase for a reactivity insertion of 1 $ is less than 10%. The secondary systems can readily discharge this additional heat and temperatures stabilize approximately 20 K higher than initial operational values.

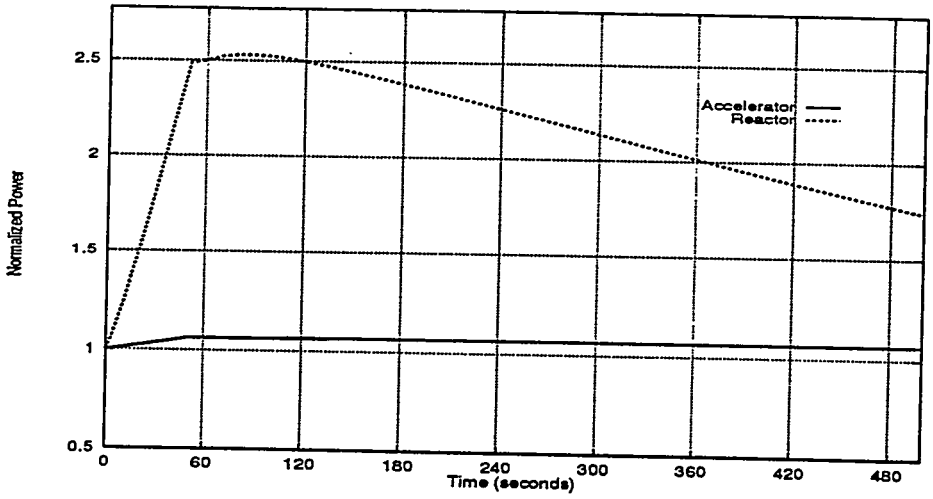

Fig. 3: Comparision of Power Transients for $1 TOP

The outcome of the LOHS event is shown in Fig. 4. The power increase in the subcritical system is caused by the large positive coolant density coefficient, which introduces significant reactivity as the system temperature rises; the relative contribution of the reactivity coefficients is illustrated in Fig. 5. The outlet temperature of the primary circuit is depicted in Fig. 6. Sodium boiling occurs in less than 350 seconds when the power of the system has already tripled. Since our design was not configured to minimize the sodium void coefficient, a case with a zeroed sodium coefficient was also run. In this case, the net reactivity effect is negative and the power decreases slightly with rising temperature (see Fig. 4). However, due to the constant number of extraneous source neutrons, the system continues to produce nearly full power unlike the critical system where the reactivity feedbacks effectively shut the system down (reduce to decay heat). As shown in Fig. 6, the lower power level of the zero-void-worth subcritical system does not prevent coolant boiling; but, the time to boiling is extended to beyond 1000 seconds. Conversely, the metal-fueled fast reactor avoids coolant boiling as long as adequate decay heat removal is provided.

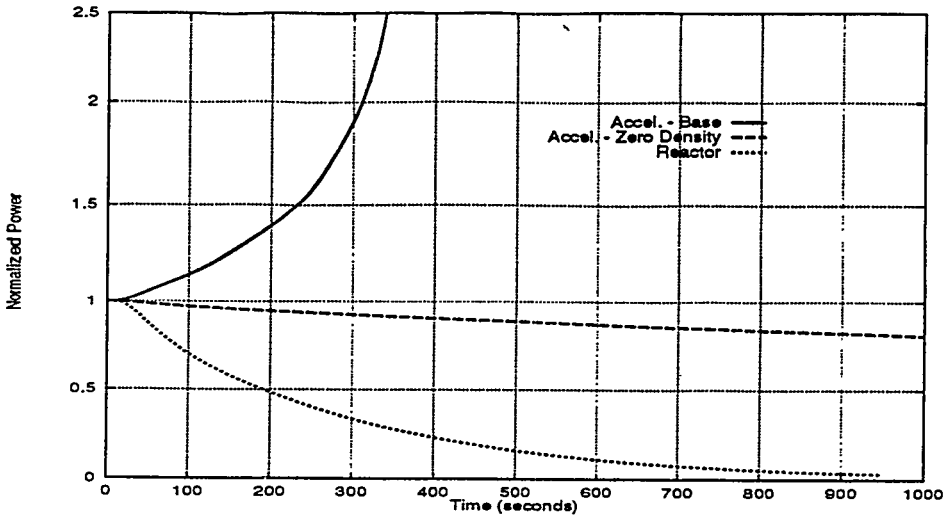

Fig 4:Comparision of Power Transients for LOHS

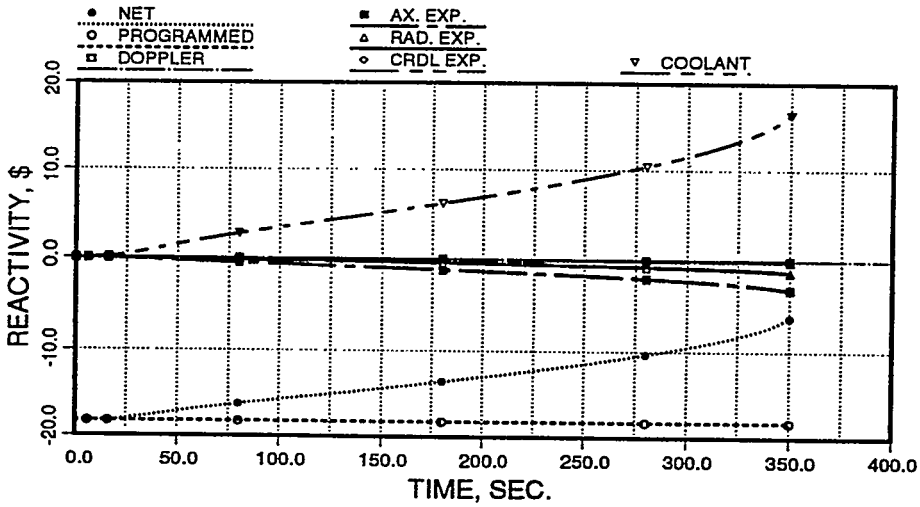

Fig 5: Reactivity Transients for Subcritical Assembly with Computed Sodium Coefficient (LOHS)

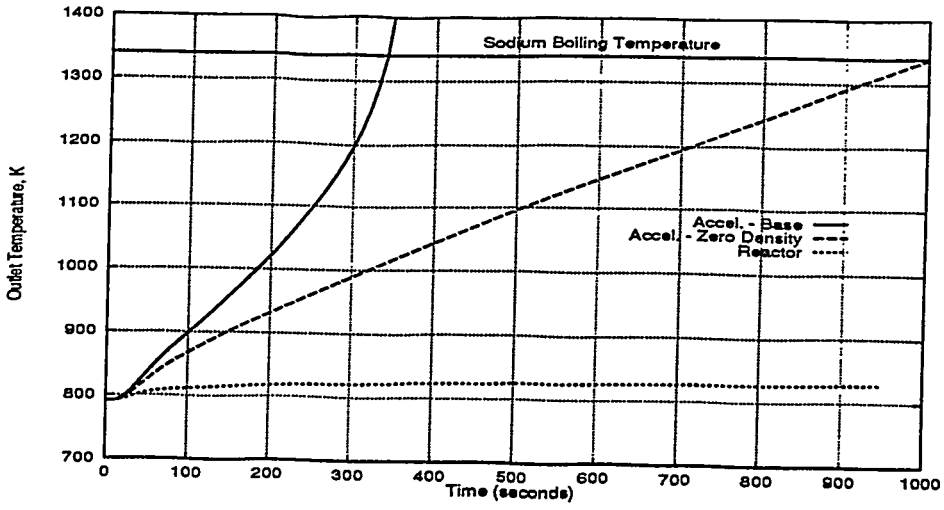

Fig 6: Comparison of Temperature Transients for LOHS

Because the power/flow mismatch is more severe in LOF events, the transient behavior is worse than in LOHS events. In Fig. 7, the response of subcritical and critical systems to a flow coastdown with a halving time of 6 seconds is shown. For the metal-fueled fast reactor, the initial coolant temperature rise is rapidly offset by reactivity feedbacks again leading to a passive shutdown after a short-lived temperature spike. A maximum coolant temperature of 950K is attained leaving a safety margin to boiling of 300K. In the subcritical system even with a zeroed sodium coefficient, the coolant temperature rises rapidly because reactivity effects do not sufficiently reduce the power level, and the outlet temperature reaches boiling only 20 seconds into the transient. However, this transient scenario is easily avoided for most initiating events. The principal initiating event for a rapid loss-of-flow is the general failure of offsite power; and this failure would imply an automatic shut-down of the accelerator if it is directly hooked into the grid. Thus, loss of offsite power instantaneously stops the production of source neutrons which zeroes the neutron flux and power density in the source-driven blanket. According to Fig. 7 the transient response is benign when accelerator operation ceases.

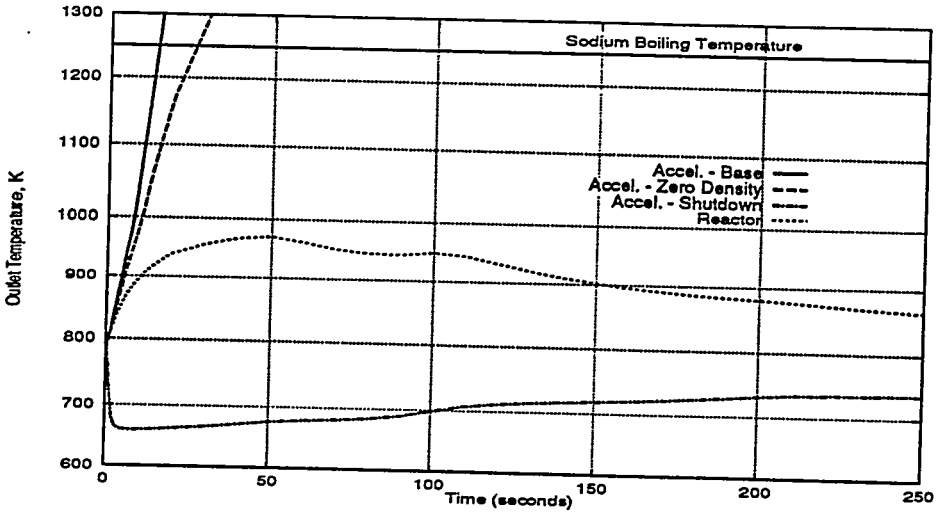

Fig 7: Comparison of Temperature Transients for LOF

SUMMARY AND CONCLUSIONS

The purpose of this paper was to compare a metal-fueled fast reactor design to an accelerator driven unit on a consistent basis with special regard to the safety issues. To accomplish this, a subcritical blanket using metallic fuel and sodium coolant was developed by modifying the lattice design of the reactor system (lower fuel volume fraction). The subcritical system is operated at a similar power density and fuel burnup; and identical heat removal systems are employed. Thus, performance differences between the two systems can be primarily attributed to the deviation from criticality.

Several nuclear performance issues were identified for the source-driven subcritical system. Large spatial gradients are observed in the neutron flux; thus, material zoning and/or residence time variation are needed to achieve favorable power shaping and depletion characteristics. In addition, subcritical operation leads to a decreasing flux level with depletion; in this study, the power decreased by 1/3 over a one year cycle. This depletion behavior could be compensated by either varying the accelerator current or controlling the neutron balance (e.g., insert poison material at BOEC).

The behavior of the subcritical system was analyzed for typical reactor accident scenarios, namely unprotected transient overpower (TOP), loss of heat sink (LOHS), and loss of flow (LOF) events. With regard to the TOP transient, the subcritical system exhibited much better performance than a critical system; even large reactivity insertions (up to 1$) lead to only small (<10%) power increases. However, the subcritical system does not passively shutdown for loss-of-cooling events. Some active measure (e.g., switching off the accelerator) is required. Otherwise, sodium boiling will occur in less than twenty minutes in the LOHS sequence, and less than one minute in the LOF event. In principal, these LOF events can be largely avoided by connecting the accelerator directly to the same power source as the coolant pumps.

In summary the overall safety behavior of this accelerator-driven metal-fueled system can not be considered to be obviously worse nor better than advanced metal-fueled reactor designs. The behavior of the subcritical system indicates different inherent strengths and weaknesses compared to a similar critical system. Reactivity-induced transients are particularly benign in the subcritical system. However, appropriate response to loss-of-cooling events is a more prominent issue for subcritical systems.

REFERENCES

[1] Takahashi, H. and Rief, H., "Concepts of Accelerator Based Transmutation Systems", presented at the Specialist's Meeting on Accelerator Based Transmutation, Wurenlingen, Switzerland, March 1992

[2] Takizuka, T. ,"Overview on Nuclear Design Problems of Accelerator-based Transmutation Systems with Emphasis on Target Facilities and their Interface with the Accelerator" presented at the Specialist's Meeting on Accelerator Based Transmutation, Wurenlingen, Switzerland, March, 1992

[3] Bowman, C. D;. Arthur E. D et al.: *Nuclear Energy Generation and Waste Transmutation using an Accelerator-Driven Intense Thermal Neutron Source*, Report, LANL, LA-UR-91-2601.

[4] Hill, R.N.; Wade, D. C.; Fujita , E. K. and Khalil, H.;" *Physics Studies of Higher Actinide Consumption in an LMR*" ,presented at the International Conference on the Physics of Reactors, Marseille, France, April 1990

[5] Ireland, J. and Cappiello, M.W., *Target/Blanket Conceptual Design for the Los Alamos ATW Concept* Report, LANL, LA-UR-92-46

[6] Cloth,P ; Filges D. et al, *HERMES - A Monte Carlo Program System for Beam-Materials Interaction Studies*, Research Centre Juelich, KFA-Report Jül-2203, 1988

[7] Derstine, K. L.,*DIF3D: A Code to Solve One-, Two, and Three-Dimensional Finite-Difference Diffusion Theory Problems*, Report, ANL, ANL-82-64, April 1984

[8] Toppel, B. J., *A User's Guide to the REBUS-3 Fuel Cycle Analysis Capability*, Report, ANL, ANL-83-2, March 1983

[9] Cahalan, J. E.; Tentner A. M. and Morris, E. M., "Advanced LMR Safety Analysis Capabilities in the SASSYS-1 and SAS4A Computer Codes" presented at the International Meeting on Advanced Reactor Safety, Pittsburgh, United States, April 1994

Accelerator-Driven Molten-Salt Blankets: Physics Issues

Michael G. Houts, Carl A. Beard, John J. Buksa, J. Wiley Davidson, Joe W. Durkee,
R.T. Perry, and David I. Poston
Los Alamos National Laboratory
Los Alamos, NM 87545

Abstract. A number of nuclear physics issues concerning the Los Alamos molten-salt, accelerator-driven plutonium converter are discussed. General descriptions of several concepts using internal and external moderation are presented. Burnup and salt processing requirement calculations are presented for four concepts, indicating that both the high power density externally moderated concept and an internally moderated concept achieve total plutonium burnups approaching 90% at salt processing rates of less than 2 m^3 per year. Beginning-of-life reactivity temperature coefficients and system kinetic response are also discussed. Future research should investigate the effect of changing blanket composition on operational and safety characteristics.

INTRODUCTION

Accelerator-driven molten-salt blankets are being considered for numerous applications, primarily plutonium destruction and nuclear waste transmutation. Blanket safety and performance should be optimized for each application, as the blanket is a major component of the overall system, and optimal blanket design will vary with the purpose of the system. The overall safety and performance of any target/blanket (T/B) concept depends on the nuclear physics, thermal-hydraulic, mechanical design, and other features of that system. The research reported in this paper focuses on the nuclear physics of subcritical molten-salt blankets designed for burning weapons-grade plutonium.

Two types of multiplying molten-salt blankets are under consideration: blankets with an internal graphite moderator and blankets with no internal moderator. These two concepts are used to highlight the important physics issues relevant to selecting a concept for conceptual design. Each blanket type has advantages and disadvantages. The difference in the performance of these two blankets is primarily caused by differences in neutron spectrum and leakage. Specific physics issues used to compare these two concepts include safety, blanket multiplication, blanket reactivity temperature coefficients, attainable blanket plutonium burnup, blanket control, and blanket neutron spectrum.

In selecting one concept for further design, maximum attainable burnup and safety (usually as related to the blanket reactivity temperature coefficient) are used in the initial screening process. Engineerability, waste stream generation, and other factors are used in the final selection process. Additional analyses are performed for point designs, including blanket flux distributions and the effect of various reactivity insertions. Reactivity insertion effects are evaluated by performing kinetics calculations that estimate blanket power, temperature, and reactivity throughout the transient. Reactivity effects of cooling and over-temperature accidents are also evaluated, as are methods for ensuring blanket shutdown.

TARGET/BLANKET DESCRIPTION

As previously mentioned, two blanket arrangements were initially screened for their attractiveness in terms of performance and safety. For both concepts, the T/B system consists of a molten lead target radially centered in the multiplying blanket, with the axial position optimized to produce the maximum effective number of neutrons for every incident proton. Salt enters at the bottom of the blanket and is pumped upward through the blanket. After exiting the active region, heat is transferred from the primary salt to a non-fissioning secondary salt. Various fission

products are removed from the salt through an active helium gas sparge system and metal fission product plateout at the heat exchangers. The volume of the active region ranges from 2 m^3 to 80 m^3, depending on design specifics and whether external or internal moderation is used. The first configuration, termed internally moderated (IM), is very similar to the reactor core of the ORNL molten-salt breeder reactor [1]. In this configuration the active blanket is comprised of 90% graphite and 10% molten fuel salt. Typical blanket dimensions are 5 m in diameter by 5 m tall, with the fuel salt traveling upwards through small (1- to 2-cm-diameter) circular channels cut directly into the graphite. A more detailed description of this concept can be found elsewhere [2,3]. The second configuration, termed externally moderated, consists of an all-fuel salt core surrounded by a stainless-steel-clad graphite vessel. A schematic of this configuration is shown in Figure 1. The size of this T/B is roughly 1.4 m in diameter and 1.4 m tall.

BURNUP

Burnup analyses were performed for four design concepts using a coupled Monte Carlo neutronic (MCNP) and depletion code (ORIGIN2) system. The first concept is a reference internally moderated design, described in reference [1]. The active region for this concept has a volume of approximately 80 m^3 (8 m^3 of fuel salt), and consists of salt flowing through channels in graphite blocks. The second concept is a low power density, externally moderated system (LPD/EM). The active region for this concept has a volume of 9 m^3, and consists entirely of fuel salt. A 1-m-thick graphite reflector/moderator surrounds the blanket, softening the neutron spectrum. The third concept is a high power density, externally moderated system (HPD/EM) with an active region (pure molten salt) volume of only 2 m^3. The fourth concept is a low power density system with no graphite reflector/moderator (LPD/NM). The active region for this concept has a volume of 9 m^3, and consists entirely of fuel salt.

In performing burnup calculations, several fission product classes are removed during operation, including noble gases (Kr and Xe), seminoble metals (Zn, Ga, Ge, and As), and noble metals (Nb, Mo, Tc, Ru, Rh, Pd, Ag, Cd, In, Sn, and Sb). Maximum burnup is limited by reactivity and solubility considerations. Reactivity limits are caused by the need to maintain a specified blanket multiplication (based on accelerator size and other factors). Solubility limits are caused by the need to ensure that plutonium and lanthanides remain dissolved in the salt during all operating conditions. Two solubility limits were considered: 75% of the solubility limit at the lowest projected blanket operating temperature (0.3 moles/liter at 850 K), and the solubility limit at the near freezing temperature of the salt (0.1 moles/liter at approximately 725 K).

Table 1 gives a summary of the results for the four systems evaluated. Burnup and cycle time for each of the four systems are shown for three conditions: at a total plutonium and lanthanide concentration of 0.1 moles/liter, at a total plutonium and lanthanide concentration of 0.3 moles/liter, and at peak burnup or 10 full power years (FPY). Table 1 contains several interesting results. First, the LPD/EM and LPD/NM systems achieve significantly lower peak burnups than the other two systems. Second, the peak attainable single-pass burnup (without the use of supplemental fissile material) is quite high (90%). Third, the IM and HPD/EM systems have very similar peak burnups, although this burnup is reached in less than half the time by the HPD/EM system. The decision on whether to use the IM or HPD/EM system will be made based on factors other than burnup. In Table 1, cycle time refers to the time at which the concentration limit is reached for the system.

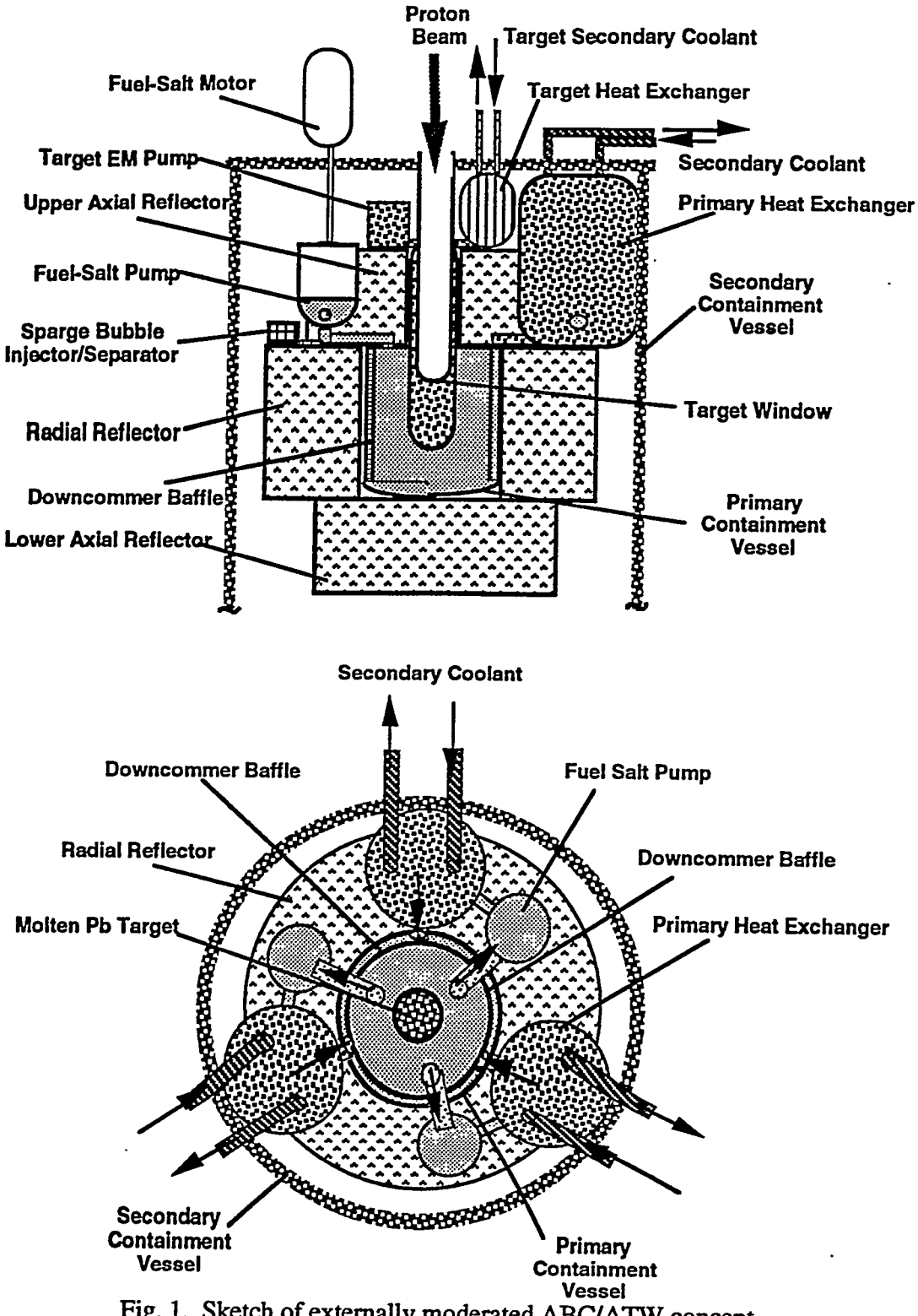

Fig. 1. Sketch of externally moderated ABC/ATW concept.

Table 1. Summary of plutonium burnup and cycle time for the four cases studied.

System	At 0.1 mole/liter Pu BU (%)	At 0.1 mole/liter Cycle Time (yr)	At peak or 10 FPY Pu BU (%)	At peak or 10 FPY Cycle Time (yr)	At 0.3 mole/liter Pu BU (%)	At 0.3 mole/liter Cycle Time (yr)
IM	81	3.2	88	10	~90	~12
HPD/EM	82	1.5	88	5.1	88	5.1
LPD/EM	76	2.3	80	~5.5	78	7.1
LPD/NM	69	1.9	73	~4.5	73	6.0

IM - Internally Moderated
EM - Externally Moderated
HPD - High Power Density
LPD - Low Power Density

Another parameter of interest is the salt processing requirement, summarized in Table 2. The rate at which salt must be processed will effect operating costs and other parameters. As shown in Table 2, the required salt processing rate for the HPD/EM system is slightly lower than for the other systems, especially at peak burnup.

Table 2. Summary of salt processing capacity requirement for the four cases studied.

System	At 0.1 mole/liter Salt Processing (m^3/yr)	At peak or 10 FPY Salt Processing (m^3/yr)	At 0.3 mole/liter Salt Processing (m^3/yr)
IM	5.81	1.86	1.55
HPD/EM	5.33	1.57	1.57
LPD/EM	6.04	2.53	1.96
LPD/NM	7.31	3.09	2.32

Salt Processing Capacity = cycle time x salt volume

REACTIVITY TEMPERATURE COEFFICIENTS

Another distinguishing factor between blanket concepts is the temperature coefficient of reactivity. This coefficient (RTC) will impact both safety and operation because if the RTC is either highly positive or highly negative, accidental criticality could result from overheating or overcooling accidents, respectively. The most desirable RTC is probably one that is near zero or slightly negative. Effects of burnup on the RTC are also very important as the composition of the fuel salt is changing as a function of operating history. This effect is currently being assessed.

The temperature coefficient of reactivity is strongly dependent on the neutron spectrum, making it dependent on plutonium concentration and the degree of neutron moderation. At the beginning of its life, the internally moderated system has a strong positive RTC, whereas the externally moderated systems have coefficients either near zero or negative. Temperature coefficients for the

internally moderated system are as high as +1.0e-4 dk/k/C, whereas temperature coefficients for systems with no additional moderator (internal or external) can be set at -1.5e-4 dk/k/C or below.

KINETICS

Unlike critical systems, subcritical multiplying blankets require an external neutron source to produce significant power. If the external source (accelerator) is turned off, the fission power in the blanket rapidly drops, and the decay of fission products becomes the only significant source of heat. In the systems being studied, the accelerator beam can be removed from the target quite rapidly (milliseconds), enabling rapid shutdown of the subcritical multiplying system.

Kinetics calculations have been performed on several point designs, and several observations have been made. First, from a criticality safety standpoint, even large positive temperature coefficients are acceptable, as long as k_{eff} does not approach unity at the maximum blanket temperature. Large positive temperature coefficients may also be acceptable from an overall safety standpoint if it is possible to rapidly remove the neutron source (by turning the accelerator off or directing the beam away from the target). However, from a safety and operational standpoint it appears most desirable to design a system with a near-zero or negative RTC. Scoping studies have shown that it is possible to design a system with a beginning-of-life RTC ranging from strongly positive to strongly negative. It may be possible to set the RTC at a desired value throughout the system life.

Subcritical multiplying blankets are characterized by a very benign response to reactivity insertion accidents. For example, in a plutonium-based multiplying blanket operating at a k_{eff} of 0.96, an instantaneous reactivity insertion of 5$ results in an increase in blanket power of less than 40% (assuming negligible feedback), which could be accommodated until the neutron source was removed. In contrast, a reactivity insertion of 5$ into a critical system could result in a severe accident, especially if there is no strong source of negative reactivity feedback. It should be possible to design a system that limits the maximum accidental reactivity insertion to values much lower than 5$, in which case the response of the subcritical multiplying blanket would be even more benign. General comments concerning the response of subcritical systems to reactivity insertions can be found in a companion paper [4].

SUMMARY

Accelerator-driven transmutation is a viable option for utilizing excess weapons plutonium. Two conceptual designs have been produced that allow plutonium burnups approaching 90% in a single pass. Plutonium extraction from the salt and other methods could be used to allow burnups exceeding 99%. Considerable future physics research is required to further develop blanket designs. First, blanket operating characteristics as a function of burnup must be determined.

REFERENCES

[1] Robertson, R. C., "Conceptual Design Study of a Single-Fluid Molten-Salt Breeder Reactor," Oak Ridge National Laboratory report ORNL-4541, June 1971.

[2] Venneri, F., "Overview of ADTT Target/Blanket Configurations," presented at the 1994 International Conference on Accelerator-Driven Transmutation Technologies and Applications, Las Vegas, Nevada, July 25–29, 1994.

[3] Buksa, J.J. et. al., "Conceptual Design of a Thorium Target for Molten Salt Transmutation Systems," presented at the 1994 International Conference on Accelerator-Driven Transmutation Technologies and Applications, Las Vegas, Nevada, July 25–29, 1994.

[4] Perry, R.T. et. al., "Kinetics of Accelerator Driven Devices," presented at the 1994 International Conference on Accelerator-Driven Transmutation Technologies and Applications, Las Vegas, Nevada, July 25–29, 1994.

"Transmutation efficiency calculation in the blanket on melted salts with central neptunium target"

V.F.Kolesov, S.K.Shtarev, V.Kh.Khoruzhiy, A.K.Zhitnik, B.Ya.Guzhovskii, E.F.Fomushkin
Russia Federal Nuclear Center - VNIIEF, Arzamas-16, Russia

In the limits of ABC project version of two-sectional reactor system in the form of combination of subcritical blanket on melted salts and multiplying target from threshold fissile material ^{237}Np is considered. This research is the development of the VNIIEF's earlier work's (Russia) investigating of usage possibilities in ABC project the conception of multisectional blankets with single-sided neutron coupling between sections. With the help of Monte-Carlo program the calculations results of system mentioned are given. The possibility of accelerator's considerable power reduction at the account of thorium target substitution with neptunium-237 multiplying target is shown.

One of the serious difficulties in realization of ABC project lie in too high requirements towards protons accelerator power. The theme of the report is testing of usage perspectives of single-sided multisectional reactors conception, allowing to reduce the mentioned requirements.

Beginning from the 50-th the multisectional reactors are the object of investigation in many works of different countries. R.Avery from Argonne National Laboratory, USA was the first who worked out the theory of this facilities and presented a paper in 1958 at the II Conference on peaceful uses of Atomic Energy held in Geneve [1].

Since the late 60-th the works on coupled systems concerning the aperiodic pulsed reactors began to carry out in VNIIEF (Russia). In this case the coupled reactors conception's usage opens the possibility of pulse's duration reduction.

It was shown that the most efficient way of pulses duration reduction in coupled system is the creation of one directional coupling between sections, at the same time in VNIIEF there was suggested the effective way of the realization of deeply one directional coupling on the basis of usage of threshold fissile material in one of the sections. In project of two-sectional booster-reactor BR-K with ^{237}Np as the material of one of the section (fig.1) developed in VNIIEF, almost 10-fold reduction of pulse's duration [3] is achieved.

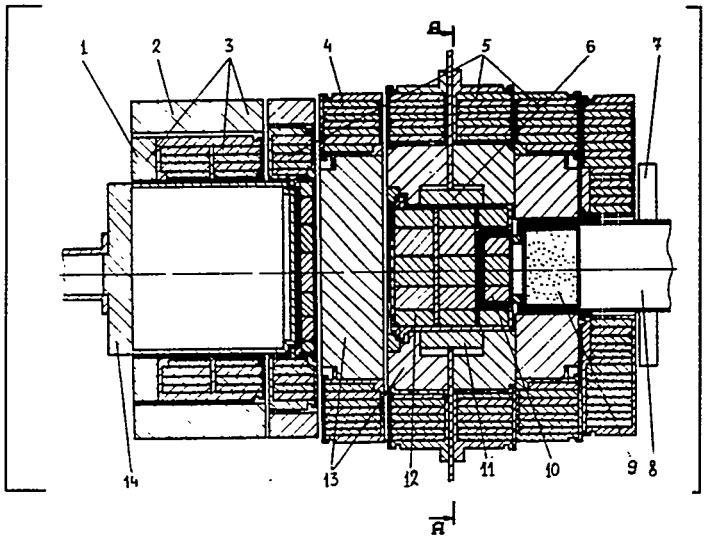

Fig.1 BR-K in axis section [3]: 1,2,3,6,7,10,11 - regulating and pulsed blocks; 4 - accident block; 5 - unmovable blocks of uranium core; 8 - channel for bremsstrahlung passing; 9 - neutrons moderator of ^{6}LiH type; 12 - unmovable block of neptunium core; 13 - tungstem's mass; 14 - container for inradiatedsamples.

In 1993 in VNIIEF the work on analysis of such one - directional facilities usage in the blanket of ABC project was carried out [4]. As the schematic variant of the proposal, the blanket presented in the fig.2 was considered. Threshold ^{237}Np of the inner section, ^{235}U and other nonthreshold and threshold fissile nuclides of the outer one are the fissile material in this scheme. The moderator's layer is placed between the sections. Neutrons originated in the inner section and after moderation in layer 5 found themselves into the outer section and easily initiate the fission. Neutrons originated in the outer section and passed the same moderation's phase are not able to initiate fissions in the inner section. It's precisely this fact that explains one-directional coupling given in the figure 2. On this basis one can also speak about multisectional blanket. Neutron characteristics of two-sectional blanket's scheme in the figure 2 and the similar multisectional schemes are derived in [4] on the basis of analytical solutions of equations for coupled reactors. The parameters of these systems, defining neutron characteristics are: total subcritically of $\Delta K=1-K$ system, subcriticallity of $\Delta K_1=1-K_{11}$ separate section and coefficients of neutron coupling K_{12},K_{21} (K_{ij} - multiplication factor in section i of neutrons, originated in section j).

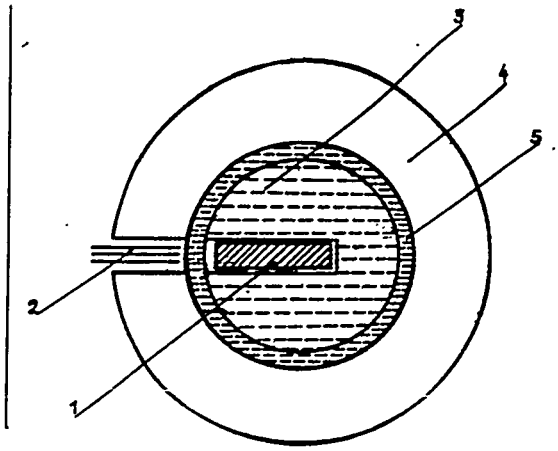

Fig.2 Realization variant of two-sectional blanket [4]: 1 - Accelerator's target; 2 - accelerator's protons beam; 3 - inner section with ^{237}Np; 4 - blanket's outer section with ^{235}U; 5 - moderator's layer.

It was shown that ratio of accelerator's power in cases of one-sectional and multisectional blankets (on the condition that transmutation efficiencies and subcriticality of the whole blanket will be equal in both cases) is equal to some value A, depending on subcriticality of the blanket ΔK, sections subcriticality ΔK_1 u coupling coefficients K_{12},K_{21}.

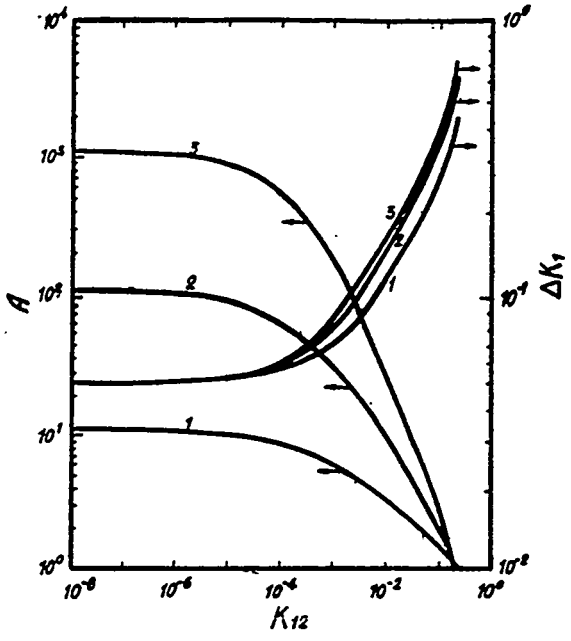

Fig.3 Coefficient's A and subcriticality's of one section's values ΔK_1 in dependence on K_{12} at $K_{21}=0.5$ and blanket's subcriticality $\Delta K=0.05$: 1 - two-sectional blanket; 2 - three-sectional; 3 - four sectional.

Values A in multisectional blankets with subcriticality 0.05 and K_{21}=0.5 depending on the coefficient K_{12} is presented in figure 3.

Data presented in figure 3 testify about the considerable advantages of multisectional blankets. The positive effect connected with the factor of blanket's multisection is significantly increasing with the sections number increase and blanket's subcriticality level decrease. But this positive effect in the whole is realized only at the large difference of coupling coefficients K_1 and K_{12}. Even K_{12} small difference from zero will lead to significant reduction of coefficient A is comparison with its limiting value at K_{12}=0.

On the basis of project's BR-K data there was made a conclusion that in scheme of blanket with ^{237}Np, considered, one can rely on the achievement of ratio K_{12}/K_{21} at the $3*10^{-3}$ level. In this case it was received that really achieved values A at K_{21}=0.5; ΔK=0.05 in the case of two-, three- and four-sectional blanket equals correspondently to 5; 4; 26 and 124.

The shown theoretical work on one directional multisectional blanket was as the initiator of the further calculations, connected with already concrete configuration of electronuclear facility in ABC project. These calculations task was formulated by Dr.A.Fasale from Grumman's Airspace Corporation (USA) together with Dr.V.F.Kolesov (VNIIEF, Russia). The conception of one-directional two-sectional system in this task was expressed in the form of combination of project blanket on plutonium melted salt (section 2) and ^{237}Np multiplying metallic target (section 1). Two-sectional system in the form of blanket's combination and multiplying target earther was discussed in K.F.Grebenkin's work [5] (VNIIEF, Russia).

The calculations of neutron characteristics of the mentioned system with neptunium, as well as the characteristics of project system with thorium target were provided. Besides in order to receive more complete idea about the factor's role of threshold fissionable material in system considered, there were carried out some calculations for system with project blanket and 90% enriched ^{235}U.

The main purpose of calculations consisted of determination of fission numbers ratio in blanket's plutonium, received in system with neptunium target and in system with thorium target at normalization on I proton from accelerator and at equality of total subcriticalities of both combinations.

Project blanket and ABC thorium target, presented in ABC review presentation [6] served as the supporting system for providing the calculations. During the calculations the project blanket and target were slightly simplified that was concluded, mainly, in structure's uniformity of core and in substitution of prismatic thorium target with equivalent cylindrical.

In the system with neptunium multiplying target its form because of its limitations on multiplication constant K_{11} differs from thorium target's form. The first one is the 90 cm in height cylinder. 10 cm in diameter region adjoining to axis is the continuum mass. Peripheric region with 10 and 40 cm inner and outer diameters is presented by five thin discs.

Uranium target's geometric form is accepted the same as thorium target. Protons beam's form is either 30 cm in diameter cylinder with protons current uniform distribution in cross section aligned with target, or the thin cord along the target's axis.

Reactions calculations in target and in blanket influenced by protons beam, the calculations of space distributions of primary neutrons sources and primary fissions, coefficients K_{11}, K_{22}, K_{12}, K_{21} were carried out with the help of several Monte-Carlo programs.

Monte-Carlo programs testing and testing of nuclear constant used in calculations was carried out at neutrons experimental yield from some plumbum and uranium targets.

Some primary neutrons calculations, calculations of primary fission and coupling coefficients data in systems are presented in Tables 1,2.

Table 1. Primary neutrons and primary fissions numbers, integral on target and blanket, normalized to I proton from accelerator

Form of protons beam	System	Zone	Numbers of primary		
			neutron $E_n \geq 15MeV$	neutron $E_n < 15MeV$	fissions
Cylinder	Np target and Blanket	Target	1.79	13.54	3.97±0.2
		Blanket	0.63	0.93	2.45±0.1
	Th target and Blanket	Target	3.35	22.6	0.73±.0.04
		Blanket	0.71	0.92	3.69±0.2
Axis cord	Np target and Blanket	Target	3.59	24.4	9.6±0.5
		Blanket	0.73	0.95	2.9±`0.15
	Th target and Blanket	Target	3.62	25.5	0.93±0.05
		Blanket	0.66	0.92	3.69±0.2

Table 2. Coupling coefficient values between sections in systems with Np, Th and U targets

System	K_{12}	K_{21}
Np target and blanket	$(1.7\pm0.17)*10^{-4}$	0.32±0.06
Th target and blanket	$(7.4\pm0.6)*10^{-6}$	0.29±0.06
U target and blanket	0.039±0.004	0.44±0.005

Total multiplication constant of neutrons in system K, fission complete numbers P_1,P_2 in target and blanket was analytically defined with the help of equations for coupled reactors solutions.

K and P_1,P_2 calculation with Monte-Carlo programs usage couldn't be made up because of very poor statistics of such calculations. This difficulty takes place due to coupling coefficient's K_{12} smallness at neutrons multiplication's considerability in each section.

Nevertheless with the help of Monte-Carlo program we succeeded in calculating the contribution in P_1,P_2 from the first six neutrons generation and with the help of this calculation we succeeded in resetting the necessary corrections in analytical solution.

The correction connected with possible deviation of neutrons real space distributions in sections in first generations from distributions of eigen functions.

Values P_2 optimal in K_{11}, K_{22} (and corresponding values P_1) for system with Np, Tp and U target and protons beams in the form of axis cord are presented in figure 3.

Values of coefficient B equaled to optimal P_2 ratio in the system with Np or U target to P_2 in the system with Th project target given in the same table. As it was already mentioned, the task of coefficient B values definition was the main goal of the work we are spoken about.

Table 3. P_1,P_2 values and coefficient B in the system with Th target and in systems with Np and U targets optimal in K_{11}, K_{22} in dependence on K-total multiplication constant of neutrons (neutrons beam in the form of axis cord)

System	K	Optimal values K_{11}, K_{22}	P_1	P_2	$B=P_2/P_2(Th)$
Np Target and blanket	0.93	$K_{11}=K_{22}=0.9225$	129	548	8.1
	0.95	$K_{11}=K_{22}=0.9425$	166	985	10.4
	0.97	$K_{11}=K_{22}=0.9625$	262	2330	14.7
	0.99	$K_{11}=K_{22}=0.9825$	660	12400	26.2
U Target and blanket	0.93	$K_{11}=0.784;K_{22}=0.812$	80.7	205	3.04
	0.95	$K_{11}=0.806;K_{22}=0.831$	109	301	3.2
	0.97	$K_{11}=0.825;K_{22}=0.852$	173	530	3.4
	0.99	$K_{11}=0.845;K_{22}=0.871$	482	1680	3.6
Th Target and blanket	0.93	$K_{11}=0.35;K_{22}=0.93$	1.06	67.5	I
	0.95	$K_{11}=0.35;K_{22}=0.95$	1.06	94.8	I
	0.97	$K_{11}=0.35;K_{22}=0.97$	1.06	158	I
	0.99	$K_{11}=0.35;K_{22}=0.99$	1.06	473	I

The calculation results made up testify about large level of difference in neutron coupling coefficients in system of blanket and Np target. Approximately 10-multiple difference in K_{12},K_{21} values is achieved due to geometric factor (calculation data system with U target point to this) and approximately 200-multiple - at the account of ^{237}N threshold. multiple increase of fission number in plutonium in the blanket on I proton from accelerator at project thorium target change on ^{237}N target is shown.

Thus, data received in this work testify the predicted on the basis of theoretical analysis the properties of two-sectional blankets with one directional neutron coupling between sections and ^{237}Np as the mean for providing deep one-directional coupling. These data received directly for electronuclear device in ABC project with blanket's project parameters, protons beams and target's configuration close to project, testify about possibility of significant reduction towards accelerator's power at the account of Th target substitution with multiplying target made of ^{237}Np - threshold fissile material. At the total subcriticality of blanket's system of 5%, transition to neptunium target will allow to reduce accelerator's power approximately by 10 times.

From work's it follows, that the most sample variant of realization of two-sectional electronuclear device in the form of blanket and multiplying target is, apparently, the most effective.

As it follows from analysis numerical data received, the mentioned advantage of this variant is the cause of primary neutrons loss's absent in it and the cause of geometric factor of the first section (target) small dimensions.

Report's data testify also about negative consequences of transitions of multiplying target - about its power. It means that thorium target's subsitution with neptunium will require the serious intensification of its cooling regime.

REFERENCES

[1]. Avery R. Theory of coupled reactors. Proceedings of the Second United Nations international conference on the peaceful uses of Atomic Energy, held in Geneva 1-3 Sept. 1958, v12, Geneva, 1958, p.182-191

[2]. Kolesov V.F., Malinkin A.A. Two-sectional booster-reactors kinetics with asymmetric neutron coupling between sections. - VANT, Series: Fizika yadernikh reactorov, 1991, issue 4, p.10-23

[3]. Pavlovskii A.I., Malinkin A.A., Kolesov V.F. "Two-sectional booster-reactor "Kaskad (BR-K) - VANT. Series: "Fizika yadernikh reactorov", 1992, issue 3, p.3-11

[4]. Kolesov V.F., Guzhovskii B.Ya. "About efficiency increase possibility of electronuclear transmutationas device on the basis of transition to blanket's multi-sectional structure. - Preprint VNIIEF N27-93, Arzamas-16, 1993

[5]. Grebenkin K.F. About one possibility of electronuclear reactor parameters improvement. - Preprint VNIIEF, N41, Chelabinsk-70, 1993

[6]. Bowman C., Toevs J., Arthur E. etal. The Los-Alamos Accelerator Based Conversion Concept for Plutonium Disposition (ABC). - JASON Review, La Jolla, CA, January 18, 1994

The work is carried out by the contract with Airspace Grumman Corporation N53-46726 on 07.02.94

LAMPF Reliability History And Program

Olin van Dyck
Accelerator Operations and Technology Division
Los Alamos National Laboratory, Los Alamos NM 87545

Abstract. Many years of service of the 800-MeV LAMPF H^+/H^- linac offers the opportunity to evaluate the long-term reliability characteristics of a high-power machine, which with up to 800-kW beam power available is as close to an ADTT machine as exists in the world today. Records from the last 15 years of operation were analyzed for trends and areas of deteriorating reliability or disproportionate downtime and used to support engineering judgment on facility refurbishment to regain beam availability. This round of analysis has helped define a further level of detail and automation to be implemented in availability recording. Interesting features which emerge from the history include a clear measurement of the lower availability in the first operating cycle following extended maintenance periods, and a consistent picture of the highest availability to be expected in extended operating periods with the facility as used and maintained. The results provide a starting point for informed discussion of reliability goals.

RELIABILITY HISTORY

Over the two decades of LAMPF operation, beam availability was logged automatically by the control computer and downtime was logged manually for about half-a-dozen major beam delivery systems in a fairly consistent manner. Readily-available records cover the last 15 years of operation and include downtime by major subsystem accumulated for 6-7 week operating cycles typically with 3-4 cycles per year, or 2000-4000 h/y.

Fig. 1 shows H^+ beam availability since 1979. The average availability is the horizontal line labelled *all;* also shown is the average availability for the *first* run cycle in each block and the *best* in each block. Availability appears to trend downwards through '92 and to recover in '93. The data refers to the portions of the system used for H^+ delivery, as shown in Fig. 2.

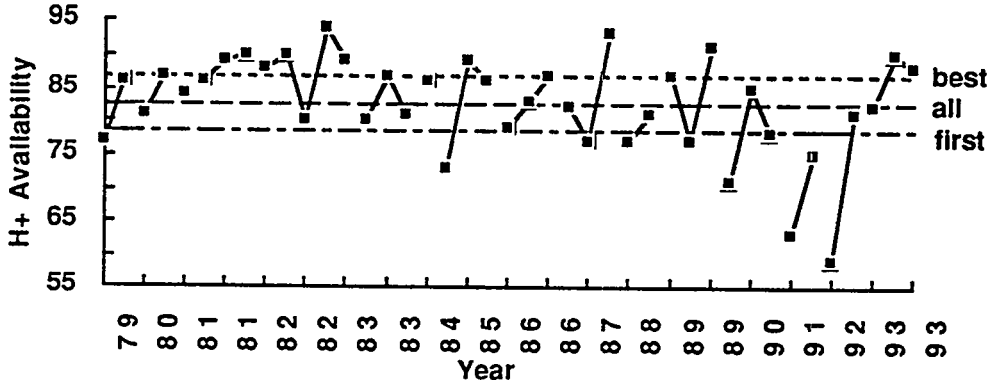

Fig. 1. H^+ Availability since 1979; points from contiguous run cycles connected by lines.

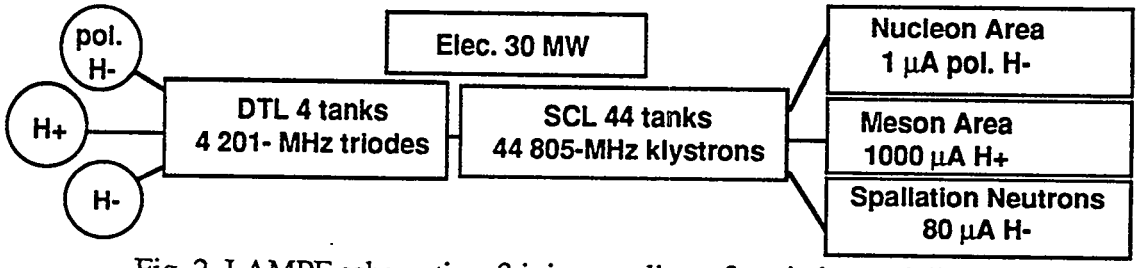

Fig. 2. LAMPF schematic – 3 injectors, linac, 3 main beam delivery areas.

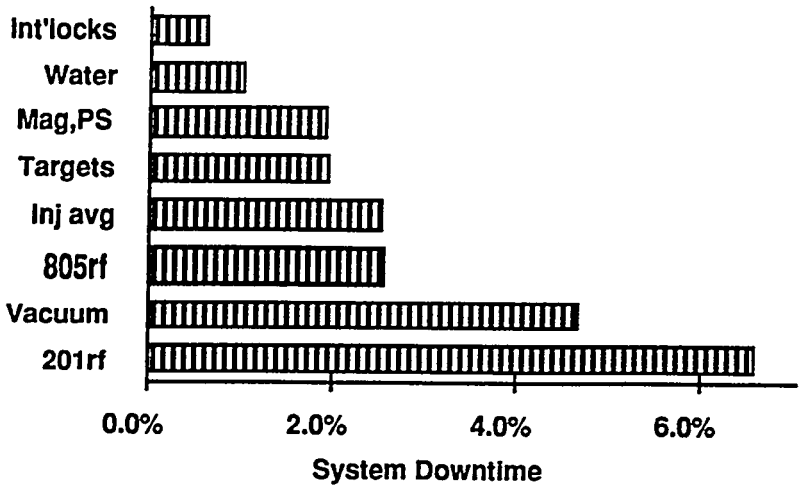

Fig. 3. Downtime by major systems.

Fig. 3 shows the system downtimes as a fraction of scheduled time averaged over the last five years, a period of nominally steady operation well past the Proton Storage Ring commissioning period. The injector downtime is shown averaged over the 3 injectors, to reflect average unavailability per beam, although the polarized and high-intensity H- injectors accounted for most of the time down. The equipment categories for logging downtime were established early in the facility lifetime and lack some of the detail one now sees as useful. For example, the vacuum system downtime includes the considerable downtimes experienced in the high-intensity target area. A more complete system would record downtime by major area as in Fig. 2 and by type of system (vacuum, magnets,...).

RF SYSTEM RELIABILITY

The 201rf system, which includes three ~2 MW power amplifier stages, had the highest unavailability of the major subsystems as they were defined. The DTL as a system would have had even larger downtime, because some of the downtime listed under distributed systems, such as vacuum, occurred in the DTL.

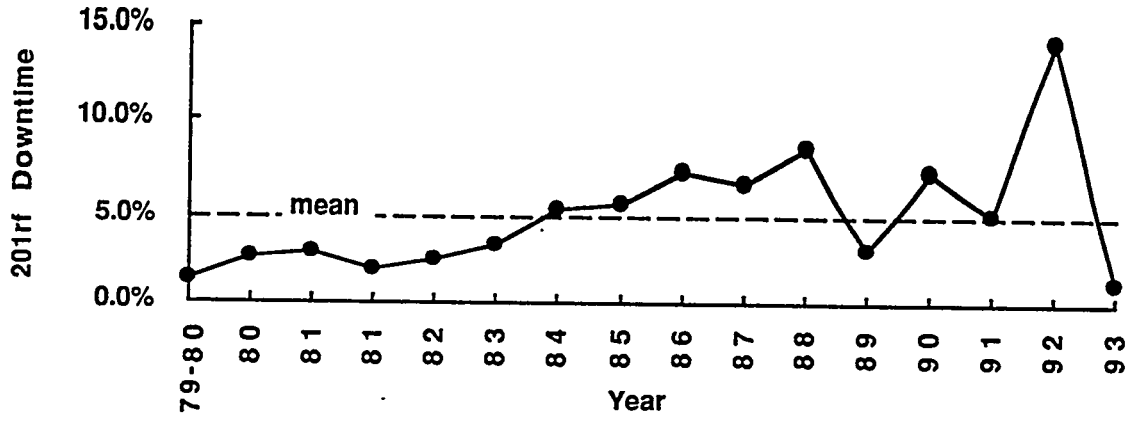

Fig. 4. 201rf downtime since 1979.

Fig. 4 shows the 201rf downtime since 1979. There appears to be a trend towards poorer reliability, with some dramatic swings. Of course there is an element of randomness in some of the fluctuations, and although some system improvements were made in '93, during most of the operating period no critical spares were available and the potential for extensive downtime was high.

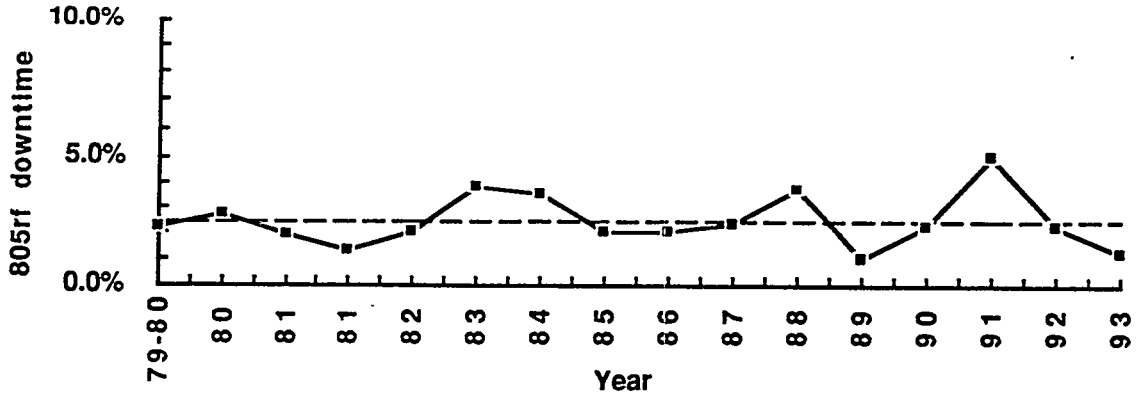

Fig. 5. 805rf downtime since 1979.

As a "control variable," 805rf downtime is shown in Fig. 5. There is no obvious correlation with time or 201rf performance, and system reliability remains high and relatively uniform. The system includes 44 klystrons.

One of the few measurable parameters expected to correlate with 201rf performance is duty factor (power dissipation). To examine this, 201rf duty factor and 201rf downtime are plotted in Fig. 6. The rf duty factor data was recreated partly from old log books and other records. Both the duty factor and the downtime are averages over cycle blocks (typically 2-3 run cycles per block).

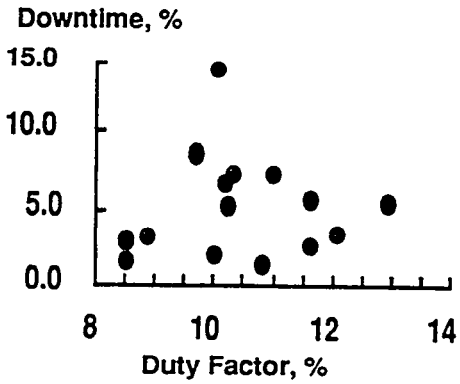

Fig. 6. 201rf downtime vs. duty factor.

Instead of showing a distinct upward-breaking curve, the data are scattered with only a weak correlation. Among factors reducing the expected correlation is the deliberate reduction in duty factor during episodes of poor rf reliability. This illustrates the point that although simple tracking and trending are valuable tools, they must be used together with engineering analysis to establish root cause and proper corrective action.

RELIABILITY PROGRAM

In response to increasing 201rf downtime, a modest upgrade effort was mounted in the last few years, and the rf stands were run very carefully in 1993. One significant improvement was a considerable increase in instrumentation. Instruments added included a calorimetric measure of Power Amplifier tube anode dissipation, to remove any doubt about this value in operation and how close it was to the 300-kW rated maximum, and to allow an accurate record to be accumulated on tube dissipation vs lifetime. Another monitoring capability added was the ability to capture the PA modulator tube current oscilloscope traces when hv power supply crowbars occurred; this allowed significant problems to be uncovered. This kind of capability tends to be very inexpensive compared to the value of the equipment concerned, the value of the production time saved, and the cost of the maintenance effort required during poor operation.

A rather scattered set of conclusions might be drawn from the 201rf reliability history, one being that a small capital investment skillfully applied can have a significant impact on performance. This suggests another conclusion, that typical accelerator systems may not have easily-characterized (or time-invariant) reliability. Finally, it appears that at least 13% rf duty factor (10% beam duty factor) can be run in this machine with average reliability under some conditions

(presumably these include modest peak power demand, e.g., moderate beam loading, and good maintenance).

The 201[illegible] reliability program will continue over the next several years in a catch-up mode. Improvements include a more detailed level of computer logging of performance, power supply modernization, improved modularity, and replacement of vacuum tube equipment by solid-state equipment as the state of the art allows. Unfortunately, redundancy in the high-power rf systems is expensive to implement.

LESSONS LEARNED

Lessons learned from our reliability experience include the usefulness of continuing performance oversight with measures, records, and analysis at the proper level of depth; the importance of a good operating team where management, engineering, and technician levels work together to ensure continuing high standards of system knowledge; and the payoff of sound design with adequate reserve and maintainability engineered in. In order to keep a facility in top operating shape, one should plan a continuing program of refurbishment and modernization perhaps at the level of 2-5% of the operating budget every year.

With the planned improvements and continuing maintenance, long-term linac availability in the range of 90% with beam power at the 1-MW level suitable for ADTT applications appears to be feasible.

RAMI ANALYSIS AND MODELING FOR THE LANSCE ACCELERATOR SYSTEMS

Robert J. Macek and Carol A. Wilkinson
Los Alamos National Laboratory, Los Alamos, NM 87545

Reliability, availability, maintainability, and inspectability (RAMI) have become important issues for the high-power machines being planned for applications such as accelerator transmutation of nuclear waste (ATW), accelerator production of tritium (APT) and the next generation spallation neutron source. Beam reliability and beam availability are vitally important specifications to the present users of accelerator-driven spallation neutron sources, synchrotron light sources and medical accelerators. At Los Alamos, improved beam availability is a key goal in the planned LANSCE improvement program. Clearly, the capability to adequately model and predict the reliability and availability of complex accelerator systems will be of great value in assessing and optimizing RAMI measures in accelerator design and improvement programs. To date, no major accelerator project has developed comprehensive reliability models although the Advance Photon Source at ANL has started work on reliability analysis for selected subsystems.

In this paper we will discuss our experience in developing RAMI analysis and modeling for the LANSCE Accelerator Systems. Progress has been made in developing suitable measures and functions to characterize user risk, in logging of needed data on failure rates and repair/down times, and in developing a first-pass RAMI model for selected subsystems. Plans have been made for a more complete RAMI model. In addition, we will discuss our experience in the use of probabilistic risk assessment (PRA) methodology for estimation of the reliability of active, instrumentation-based, radiation safety systems at LANSCE.

Reliability And Availability Considerations in the RF Systems Of ATW-Class Accelerators

Paul J. Tallerico, Michael T. Lynch, and George Lawrence
Los Alamos National Laboratory
Accelerator Operations and Technology Division
PO Box 1663, MS H-827, Los Alamos, NM 87545

Abstract. In an RF-driven, ion accelerator for waste transmutation or nuclear material production, the overall availability is perhaps the most important specification. The synchronism requirements in an ion accelerator, as contrasted to an electron accelerator, cause a failure of an RF source to have a greater consequence. These large machines also are major capital investments, so the availability determines the return on this capital. RF system design methods to insure a high availability without paying a serious cost penalty are the subject of this paper. The overall availability goal in our present designs is 75% for the entire ATW complex, and from 25 to 35% of the unavailability is allocated to the RF system, since it is one of the most complicated subsystems in the complex. The allowed down time for the RF system (including the linac and all other subsystems) is then only 7 to 9% of the operating time per year, or as little as 613 hours per year, for continuous operation. Since large accelerators consume large amounts of electrical power, excellent efficiency is also required with the excellent availability. The availability also influences the sizes of the RF components: smaller components may fail and yet the accelerator may still meet all specifications. Larger components are also attractive, since the cost of an RF system usually increases as the square root of the number of RF systems utilized. In some cases, there is a reliability penalty that accompanies the cost savings from using larger components. We discuss these factors, and present an availability model that allows one to examine these trade offs, and make rational choices in the RF and accelerator system designs.

INTRODUCTION

Availability considerations affect the accelerator and RF system design in several ways. First, only the most reliable, proven RF amplifiers may be used. This constraint makes the klystron the obvious choice as the RF amplifier for the main power systems, and forces the minimum frequency to be above 200 MHz. The accelerator itself can be designed to be more tolerant of RF system failures, by choosing a relatively small power requirement per RF generator. The smaller power also reduces the high voltage required, and this improves reliability. Availability will also depend on the choice of klystron, since the multiple beam klystron (MBK), for example, can produce a given output power at a significantly lower voltage than a single-beam klystron, and thus the MBK may have an availability advantage. The size and number of the dc power supplies will also influence the availability of the accelerator. Reliability and cost considerations drive the design towards very few, very large, utility-style power supplies, but the goal of being modular and more immune from single-point failures implies small power supplies. The smaller power supplies are easier to protect during an arc, and they are also useful in optimizing the electrical efficiency, since the power required per RF module varies by almost 50%. A large, 1000 MeV, 200 mA, CW proton accelerator for the accelerator production of tritium (APT) has been designed at Los Alamos[1], and this accelerator is also our baseline design for large waste transmutation applications. This baseline design uses a total of 376 1-MW CW klystrons (10 at 350 MHz and 366 at 700 MHz) to produce 254 MW of RF power for the accelerator. This APT machine is representative of only the largest ATW machines now contemplated. It is more likely that the first dedicated ATW accelerators will utililize between 50 and 150 MW of RF power, and be a more modest

scale-up of the largest existing CW RF systems, which produce about 20 MW now, and will move to 30 MW by 1995.

AVAILABILITY RESULTS IN EXISTING RF DRIVEN ACCELERATORS

The first question is whether a large RF driven accelerator may be operated for a major portion of each year. The world leader for large accelerators, in terms of reliability and availability, is the Photon Factory and TRISTAN injector linac at KEK in Japan. It is a 2.5 GeV machine that uses 48 S-band 30 MW, 3 μs-pulsed klystrons. In the latest 3 years for which data has been published [2](FY 90-92), this accelerator has been operated for an average of 5119.7 hours per year, with an average down time of 81.27 hours per year, or an average availability of 98.41%. This injector linac is pulsed rather than CW, and it accelerates electrons, not protons, but the excellent availability shows that high availability goals are achievable with good design, engineering, and operational procedures. This accelerator had an availability over 95% since 1988. Good availability tends to grow with time. The KEK klystrons fail most often from internal arcing, and window breakage is the second most common failure mode. Both failure modes have been reduced by improvements in the klystron design and processing. In Fig. 1 the average internal-arc rate, in arcs per day is plotted versus fiscal year for the KEK injector klystrons. A consistent improvement of a factor or 25 has occurred over the past 8 years, mostly from changing the cathode technology from oxide ,which can evaporate barium in the electron gun, to impregnated cathodes in which the processing is done in an external vacuum system, so the excess barium never gets into the electron gun. The gun geometry was also modified to reduce the electric fields.

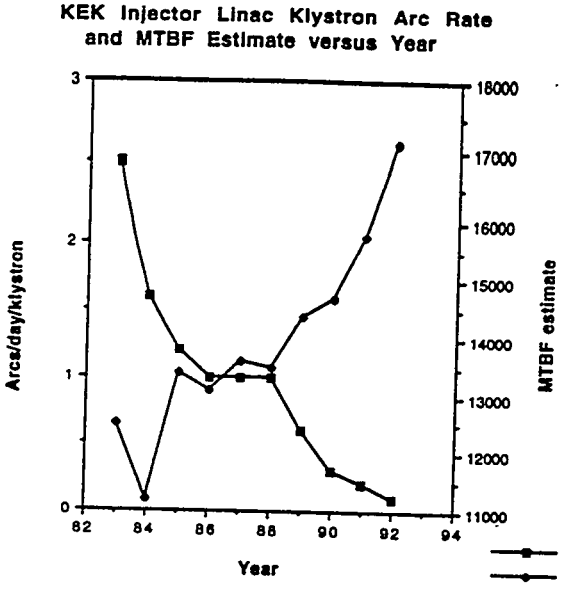

Fig. 1. The arc rate and the MTBF for the KEK injector klystrons for FY 83 to FY-92.

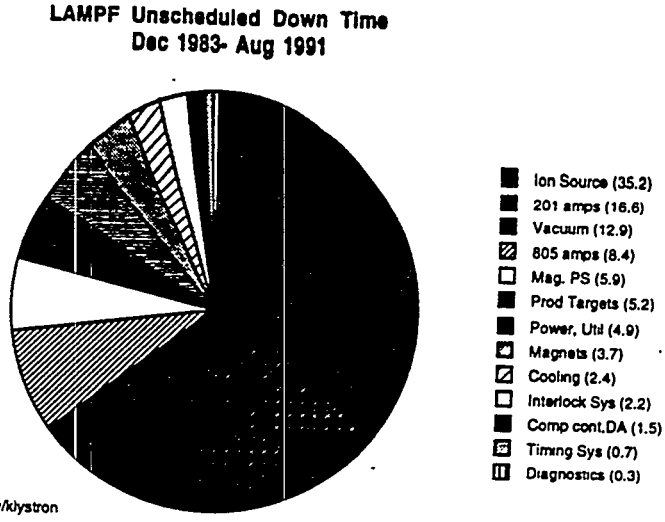

Fig 2. Unscheduled down time by subsystem for LAMPF.

The most pertinent availability and failure statistics for ATW machines come from high-power proton accelerators, so we have reviewed the records[4] at LAMPF for the interval from December 1983 to August 1991. The average availability for the H+ beam was 80.23% of the scheduled time, and the H+ beam was scheduled for an average of 3,272 hours each year. The causes of the unscheduled down time are shown in Fig. 2, and in the legend, the causes are ranked in order of down time. The numbers in parentheses in the legend are the percent of the unscreduled down time for each subsystem. For most of the interval under study, LAMPF operated with two or three beams, and the reported down times are exaggerated, since failures of certain components may only affect one beam.

The injector down times are especially over stated, since LAMPF has three injectors, and the failure of one only effects the beam that it produces. But the injectors and the RF systems, (especially the 201 MHz RF systems) were the major causes of down time. It must also be noted that the rising costs of electric power, and limited funding for LAMPF have forced major cuts in the maintenance funding for LAMPF. With proper funding of a maintenance program, the availability record for LAMPF would be better, but we expect the relative failure rates shown in Fig. 2 to remain valid. There are 12 to 24 power outages during the year at Los Alamos, and the reliability of the electrical supply at most other places is better. The electrical grid connections to Los Alamos are weak and long, and there are many thunderstorms in late Summer, during which the LAMPF machine is usually operating. Most sites for an ATW machine would have a stronger electrical power grid, and fewer thunderstorms, so the reliability of the line power would be greater.

KLYSTRON FAILURE RATES

The klystron is a key component in the analysis of the availability and reliability. Fortunately, there is reliability data available for a few types of klystrons used in accelerators. There are several methods of estimating the Mean Time Between Failures(MTBF) from a set of experimental life data. The simplest method is to simply divide the total operating hours by the observed failures. This estimate completely disregards all details of the actual life distribution, but it is valid when the hazard rate (the fraction failing in any time interval) is constant. A more sophisticated estimate can be obtained by fitting a distribution function to the observed fractional survival curve, or to the observed hazard rate. For most electron tubes, a Weibull distribution fits the observed cumulative failure distribution well. The two-parameter Weibull distribution is

$$F(t) = 1 - \exp\left(-(t/\alpha)^{\beta}\right) \tag{1}$$

where α is the time parameter and β is the shape parameter. When $\beta = 1$, the Weibull distribution reduces to the constant hazard distribution. The MTBF for a Weibull distribution is given by

$$MTBF = \alpha\Gamma\left(1+\frac{1}{\beta}\right) \tag{2}$$

By a least-squares fitting procedure, the observed cumulative failure distribution for over 2,880,000 hours of LAMPF klystron data provides the estimate that α= 101,566 hours and β=0.6431. With $\beta < 1$ the hazard rate is high initially, and the klystrons have a high infant mortality rate. From these parameters we calculate the MTBF as 140,400 hours, while with a constant hazard approximation, the MTBF estimate is 160,000 hours for the LAMPF klystrons, similar to the other estimate. The MTBF with the constant hazard assumption has been increasing steadily for the LAMPF klystrons, but even after 22 years of operation, this MTBF is still slowly changing. The MTBF for these LAMPF klystrons was only 56,533 hours in 1976 [3], but since the initial failure rate is so high from the infant mortality, the MTBF increases with age. We now are starting to see signs of aging in the LAMPF klystrons: the newest klystrons were purchased in 1972, and most of the new failures are vacuum leaks, with the basic physical cause of corrosion at the copper to stainless steel joints in the water system. We believe that the true MTBF will approach 80,000 hours as a result of this aging phenomenon. As another example of the trend towards increasing MTBF for the klystrons with klystron age, Fig. 1 also shows the growth of the MTBF for the TRISTAN injector klystrons versus fiscal year. In Table 1

below we have tabulated the constant hazard rate klystron MTBF's for several pulsed and CW accelerators.

Table 1. Mean Time Between Failures calculated with the constant hazard rate for Several Accelerator Klystrons

Accelerator	Total Hours	Klystron Failures	MTBF
TRISTAN Injector	1,936,215	113	17,135
LAMPF (Failures)	2,880,000	18	160,000
LAMPF (Removals)	2,880,000	140	20,571
SLAC	8,727,686	229	38,112
PEP	314,162	23	13,659
CERN LEP	272,000	6	45,333
TRISTAN Ring	712,000	32	22,250

The first four lines in Table 1 (TRISTAN through SLAC) are for pulsed klystrons, while the remaining three lines are for CW klystrons. Note that for the LAMPF entry, there only have been 18 klystron failures in 2,880,000 hours of klystron operation, but the next line shows that 140 klystrons have been removed from the accelerator during the same time. The removal rate is 7.8 times higher than the failure rate, but this is because the LAMPF klystron is located on top of a large modulator filled with oil for insulation, and whenever there is either a klystron or a modulator problem that cannot be repaired in a few minutes on the accelerator, the entire modulator and klystron assembly is removed, and sent to a repair shop. The causes for the LAMPF klystron and modulator removals are listed in Table 2, along with the removal rate. The system problems are removals that are done by correct analysis of incorrect data from a diagnostic, for example an interlock may say that there is no RF power from the klystron, so the klystron is changed, but the

Table 2. Removal Causes and Rates for LAMPF klystrons and Modulators.

Mechanism	Instances	Removals (/million hours)
System Problems	40	13.9
Water in Oil Tank	36	12.5
High-Voltage Arcing	29	10.1
Klystron Vacuum	17	5.9
Low Beam Current	10	3.5
Switch Tube Leakage	3	1.0
Human Error	3	1.0
Klystron Window	2	0.7

next klystron also shows no power output. A more detailed investigation shows that the power sensor is defective, and repairing that was required in the first place. In future systems we will have redundant diagnostics to eliminate this type of problem. We can also eliminate most occurrences of water in the oil tank by making the oil tank very small (it is 500 gallons at LAMPF!), and placing water lines and valves away from the tank. Many CW klystrons are air insulated, rather than oil insulated, and the high voltage is located high, and the water circuits located lower, so water leaks have a smaller chance of wetting a high voltage circuit. It also is a safety advantage to have all high voltage circuits at least 3 m above the floor.

AN AVAILABILITY MODEL

The RF system for the APT accelerator contains 376 klystrons, plus about 10 smaller amplifiers for the bouncers and funnel. The constant hazard rate approximation is used. To obtain initial availability estimates we study only the high power RF systems and will add the buncher systems and funnel at a latter stage. We require the hazard rates and repair times (mean time to replace or repair, or MTTR) for the various subsystems modeled. The first availability model utilizes only six subsystems to describe the accelerator high-power RF system: the klystrons, the power supply, the high voltage protection, the low-level RF system, the RF transport system, and the cooling system. A schematic diagram of the RF system is shown in Fig. 3. Two very large power supplies

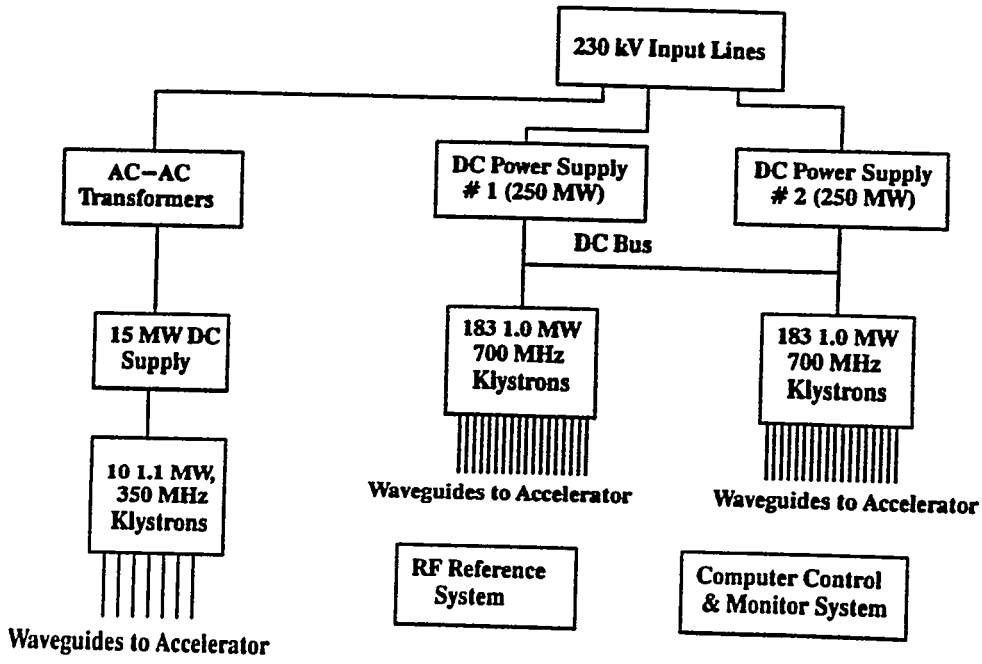

Fig 3. Schematic diagram of the power system for an APT/ATW accelerator.

and one smaller one were selected to operate the whole facility. These facilities are similar to half of the ac to ac power converters that are used to connect large power grids. They are very reliable, and can be made with redundancy. Based on similar units produced for the power utilities industry, an industrial partner has estimated a MTBF of 2912 hours for the power supply, with an MTTR of 6 hours. The MTBF for the last three lines of CW klystrons in Table 1 are averaged to estimate a MTBF of 27,320 hours for the klystron. We believe that this estimate is conservative, since two of the three CW klystrons in Table 2 were designed at least 10 years ago, and the technology has been improving. The MTBF for UHF television tubes is approximately 35,000 hours, but the television tubes are an industrial commodity, and there is little incentive for the manufacturers to improve the tube life, provided that the life is acceptable. Based on experience at LAMPF, the time to replace is estimated at 4 hours for the klystron. The time to repair the klystron may well be weeks, but it is done off line, and this time only affects the number of spares required. The high voltage protection module is a series switch and crowbar combination that isolates each set of 8 klystrons from the main power bus whenever one of the 8 klystrons arcs. An industrial partner has made a first design of

the high-voltage protection units, and has estimated a failure rate of 9.7 failures per million hours based on a major component count. These units will be rich in diagnostic circuits and telemetry, so we have doubled this failure rate to account for all the lower power components, arriving at a failure rate of 19.4 per million hours or a MTBF of 51,500 hours. The partner estimates a 5 hour mean time to repair the protection units. The low-level RF system, the RF transport system, and the cooling systems MTBF and MTTR are estimated based on our experience at LAMPF and other accelerators, and are given in Table 3 below.

The mathematics of the availability calculation is straightforward, but it is presented here for reference. The constant hazard approximation means that in a period of time t, given n identical components with a failure rate λ, the probability of no failures in this time interval is (disregarding common mode failures)

$$P_0(t) = \exp(-n\lambda t), \tag{3}$$

where $\lambda = 1/MTBF$. The probability of exactly q (q>0) failures in the time interval t is then

$$P_q(t) = n\lambda t P_{q-1}(t)/q. \tag{4}$$

The expected number of failures in the interval t is

$$E_{x(failures)}(t) = n\lambda t, \tag{5}$$

and the expected values of the time to repair is

$$E_{x(MTTR)}(t) = MTTR \cdot E_{x(failures)}(t). \tag{6}$$

The overall availability of the RF system is found by applying Eqn. (6) to each component, and summing the expected value of the mean times to repair. Although most accelerators are operated for periods of about 6 weeks before maintenance work, we are currently planning on one 8 hour maintenance shift per week for the APT machine. During the maintenance shift, everything that can be left operating will be, and only subsystems that need to be worked on, plus the proton beam itself, will be shut down. We also plan to instrument the RF system more heavily than is now done, and use this data to anticipate failures. This is done in some accelerators already. For example at LAMPF we had a rather short-lived modulator switch tube that would fail by not shutting off completely between pulses. This leakage current was no problem for either the switch tube or the power supply, but it caused X-rays that could become a safety hazard. The leakage current increased gradually over time, and at first we did not monitor this leakage current. By installing a leakage current monitor, we could observe the leakage current increase, and replace the switch tube in about 80% of the cases before the leakage current limit was reached. Thus, the unavailable time from this source was reduced to about 20% of the value without this circuit. In the klystron, the gain may slowly decrease with time due to intercepted electrons changing a cavity gap, or the modulating anode current or filament power may increase with time due to changing surface conditions within the klystron. By monitoring these variables, and observing a time series of the data, one can anticipate which klystrons will probably fail in the next week, and change them out in a maintenance period.

Sub-system	MTBF (1000 h)	Installed (#)	Failures (#/week)	% Anti-cipated	Unanti-cipated (#/week)	MTTR (hours)	Time out per week (hours)
Klystron	27.32	376	2.312	75	.578	4	2.312
Power Convert.	2.912	2	0.115	25	0.0865	6	0.519
High V Protect.	51.5	47	0.153	75	0.0383	5	0.192
Low Lev RF	100	376	0.632	50	0.316	2	0.632
RF Transp.	150	376	0.421	50	0.211	4	0.842
Cooling	40	47	0.197	50	0.0987	5	0.494
Total Unanticipated Down Time per Week							**4.99 hours**

Table 3. Unscheduled outage time budget for the APT/ATW RF system.

Table 3 shows that excellent avialability of over 97% is obtainable without redundancy in the RF system for a large ATW RF system. Even without the anticipation factors, the power system down time per week is only 14.636 hours, or an availability of 91.28%. We have, however, used and anticipation factor on all subsystems, but we beleive that this is well within the ranges of possibility. Redundancy is utiliized in the water cooling system, but the details do not show at this low level of analysis.

The conclusion is that power system availabilities above 90% are possible with minimal redundancy for up to several hundred MW of CW power. By anticipating failures with well diagnosed power systems, the availability can be increased above 97%, again with minimal redundancy. The techniques advocated here are used on a very small scale in existing power systems, but we propose to accelerate the evolution to achieve major availability gains.

REFERENCES

[1] Los Alamos National Laboratory, Brookhaven National Laboratory, Sandia National Laboratories, APT Accelerator Topical Report, Volume 1, Revision 1, Los Alamos Report LA-CP-94-48, March 1994.

[2] Photon Factory Activity Report #8, 1990; #9,1991; #10, 1992, National Laboratory for High-Energy Physics, KEK, Tsukuba, Japan; 1991, 1992, and 1993.

[3] Paul J. Tallerico, "Reliability and Operating Experience of the LAMPF 805-MHz RF System", Proc. Sixth European Microwave Conference, Rome, Italy, pp. 715-719, Sept. 14-17, 1976.

[4] Progress at LAMPF, yearly progress reports for 1983 to 1991.

Structural Activation Calculations Due to Proton Beam Loss in the APT Accelerator Design

S.K. Lee, C.A. Beard, W.B. Wilson, L.L. Daemen, D.J. Liska and L.S. Waters
Los Alamos National Laboratory
Los Alamos, New Mexico 87545

M.L. Adams
Texas A&M University

Abstract. For the new, high-power accelerators currently being designed, the amount of activation of the accelerator structure has become an important issue. To quantify this activation, a methodology was utilized that coupled transport and depletion codes to obtain dose rate estimates at several locations near the accelerator. This research focused on the 20 and 100 MeV sections of the Bridge-Coupled Drift Tube Linear Accelerator. The peak dose rate was found to be approximately 6 mR/hr in the 100 MeV section near the quadrupoles at a 25-cm radius for an assumed beam loss of 1 nA/m. It was determined that the activation was dominated by the proton interactions and subsequent spallation product generation, as opposed to the presence of the generated neutrons. The worst contributors were the spallation products created by proton bombardment of iron, and the worst component was the beam pipe, which consists mostly of iron. No definitive conclusions about the feasibility of hands-on maintenance can be determined, as the design is still not finalized.

INTRODUCTION

In recent years, a significant interest has developed in the design and use of high-power linear accelerators (LINACs). Several different efforts have been initiated that would require the use of such power, including the Accelerator Production of Tritium (APT) project [1], the Accelerator Transmutation of Waste (ATW) program[2,3], and the Accelerator Based Conversion of plutonium (ABC) program[4], among others. Each of these projects requires the generation of an intense neutron source to drive the system, which translates into a need for a high-energy (800-1600 MeV), high-current (100-250 mA) accelerator operating with a high availability (>90%).

All of the accelerators for these programs are still in the design phase. The APT design, however, is the most complete to date. High-power accelerators make activation of the accelerator structure and its surrounding containment a serious concern. This activation is a direct result of beam loss occurring during normal operation: lost incident particles interact with the structure, producing a variety of radioactive species. These radioactive species could potentially create large dose rates in the immediate area. Accelerator operators would like to avoid this scenario, as it could preclude hands-on maintenance of the structure. The ability to perform hands-on maintenance is highly desirable, as it avoids the additional expense and complication of developing and utilizing remote maintenance technology. For currently operating accelerators, operators rely on manual measurements for information regarding the safety of the surrounding environment. But since these new high-power accelerators are still in the design stage, manual measurements cannot be made.

The activation, therefore, has not yet been quantified for accelerators of this high power. It should, however, be an important consideration before a design is finalized and constructed. Having the ability to predict the activation would save a significant amount of time and money. Knowing the level of activation associated with a certain amount of beam loss occurring during steady-state operation will allow for possible design changes or additional safeguards to enable hands-on maintenance of the machine. The general methodology used in determining the activation could also be used to test design variations in future revisions.

Since the activation cannot be directly measured, computational methods must be used. Methods are now available to perform these calculations and obtain reasonable results. The computational method used in this work couples transport and depletion codes to obtain estimates of dose rates near the accelerator.

This research focused on the Bridge Coupled Drift Tube LINAC (BCDTL) section of the APT accelerator design. As the APT design represents the most complete linear high-power accelerator design in the world at current standing, it was chosen as the baseline model for research described here. This design has the added advantage of being applicable to the several other accelerator projects in progress. The BCDTL accelerates charged particles from 20 to 100 MeV and is comprised of several sections. For this effort, two sections were modeled, one each at the beginning and end of the BCDTL.

Hence, the purpose of this work was to develop a model to predict the structural activation of the BCDTL portion of a high-power linear accelerator, and to use this model to estimate dose rates resulting from the activation. The activation was calculated for several operational histories. Three irradiation periods were considered, for one hour, one week, and one year. For each irradiation period, results were obtained for four separate decay times: ten seconds, one hour, one week and one year.

CALCULATIONAL METHODOLOGY

In order to determine the structural activation due to proton beam loss, a calculational method incorporating several codes was utilized. The structural activation was quantified in terms of dose rates. Figure 1 outlines the general procedure followed for this research.

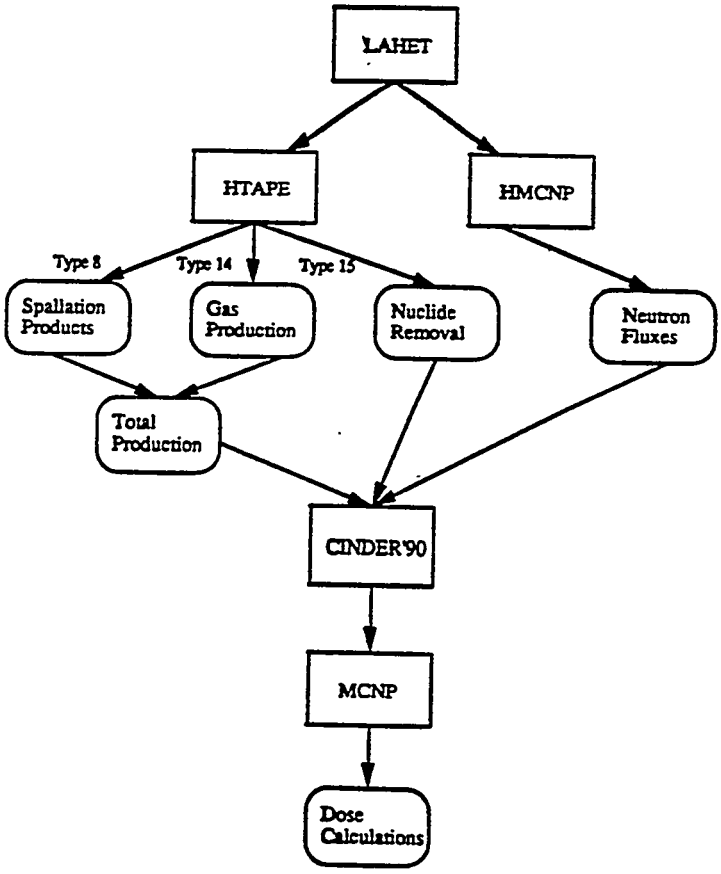

Fig. 1. Flowchart for calculational methodology.

This methodology makes use of the LAHET Code System (LCS)[5] developed at Los Alamos National Laboratory. The main code in the LCS, LAHET[5], was used to transport the incident high-energy protons, compute the resulting nuclear interactions, and transport particles emitted with energies greater than 20 MeV. Though the theoretical basis for the code relies on particles of energy of at least 50 MeV, for the activation problem, the code will be used for particles in the range of 20 to 100 MeV. LAHET, therefore, was benchmarked in that energy range to determine its useful ranges and limitations. In the benchmarking, the code must accurately predict three quantities: the magnitude of the neutron yield generated through proton interactions, the angular and energy distributions of the resultant neutrons, and the residual nuclei produced by the proton interactions (spallation products). In each case, the calculated results were compared with experimental results found in literature, and one of two materials was used, copper or iron, as they make up the majority of the accelerator structure.

For protons incident on copper, the difference between the calculated and experimental yields did not exceed 30% in the proton energy range of 5–25 MeV, and the yields predicted by LAHET for 5-25 MeV protons on copper can be assumed to be within this margin. For protons incident on iron, the yields determined by LAHET are at worst accurate within a factor of three in the proton energy range of around 6 MeV. For most of the range (12–25 MeV), however, the calculated yields appear to be accurate within 50%. The next quantities studied were the energy and angular distributions of the neutrons produced by the activation of the accelerator components. LAHET accurately predicts the energy distribution of the resultant neutrons. The differences are larger at energies below about 8 MeV, but still within a factor of three. This overprediction at lower energies will lead to a conservative estimate: the lower energy neutrons cause greater amounts of activation. For the angular distribution, the LAHET results are more forward-peaked than are the experimental results. Hence, any axial spatial dependence observed in the results must be treated with caution. Finally, several spallation product reactions were studied, and LAHET predicted the spallation product yield fairly accurately. As expected, the results can be considered accurate for proton energies above 50 MeV. At less than 50 MeV, all of the yields can be considered accurate to within a factor of four.

In the LAHET calculations, generated neutrons of energies below 20 MeV were written to a source file. This file then served as the source for subsequent transport of the neutrons using HMCNP[5] (a version of the Monte Carlo transport code, MCNP[6]), which then determined the neutron flux in the accelerator structure.

In addition to the neutron flux, it is also important to know the quantities of spallation products generated and nuclides destroyed, as all three are key inputs used in the later depletion calculations. To obtain these results, HTAPE [5] (another code in the LCS) was utilized. HTAPE is designed to edit the history file created by LAHET. The history file is a record of the outcome of every event. It includes such information as the type of event, the location of the event, the energy of the incident particle, and a description of any particles introduced into the system. There are different edits available in HTAPE, including quantities of residual nuclides and gas produced.

Once the total spallation product yield and neutron flux distribution were known, CINDER'90[7] was used to determine gamma production rates in the structures of interest. CINDER'90 is a code designed to determine radionuclide inventories and their subsequent decay. Once CINDER'90 had determined gamma production rates, the resulting gammas were transported using MCNP, which determined the desired dose rates.

MODEL DEVELOPMENT

In order to be able to determine the structural activation associated with accelerator beam loss, a baseline accelerator design had to be chosen to create a new computer model. The APT design was selected, and this research was focused on the BCDTL section of the accelerator. This section operates at twice the original frequency (700 MHz) and current (200 mA) and is comprised of 61 separate tanks. As previously stated, in the BCDTL the beam particles are accelerated from 20 to 100 MeV over a length of almost 94 m. This section is an innovative design that was incorporated to accommodate high frequency by using a bridge coupler. Figure 2 provides a more detailed view of the BCDTL components and layout.

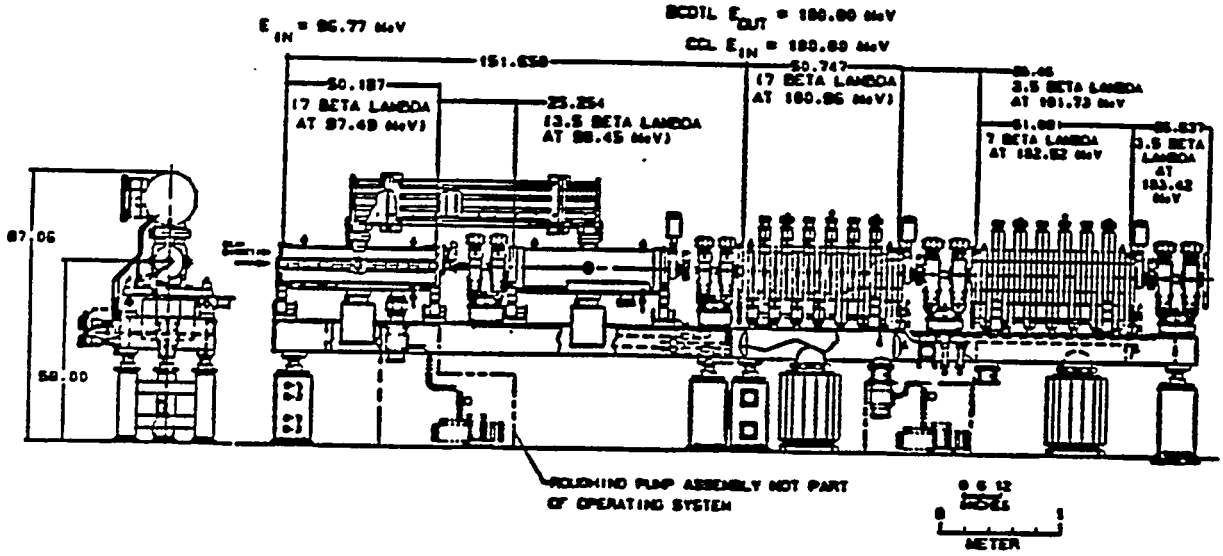

Fig. 2. BCDTL schematic diagram for 100 MeV section.

Using the detailed engineering drawings of the accelerator design from the APT project, simplified three-dimensional computer models were created. The 20 and 100 MeV sections were modeled to provide meaningful bounds for the activation levels in this portion of the accelerator. It was neither practical nor beneficial to completely model the structure to the level of detail contained in the engineering drawings. Instead, the modeling effort focused on the most important accelerator components. For each energy (20 and 100 MeV), the model included the quadrupoles, a tank assembly on either side for symmetry, and the entire associated bridge coupler, including the water channels used for its cooling. The 20 MeV section, however, has multiple bridges, so its model also contained a portion of the two additional bridges, located symmetrically about the quadrupoles. All known components containing water or other neutron-moderating materials were included in order to properly model increased activity due to neutron capture. Minor components, such as individual bolts, were omitted as was any support structure located too far away to be of interest. It was also not practical to include surrounding structures, such as possible coolant pipes in the accelerator tunnel, as their location in completely undetermined. Figures 3 and 4 show a side view of the 20 and 100 MeV section computer models, respectively.

One challenge in this effort was modeling the steady-state beam loss. During the CCL effort [1], experiments performed at Los Alamos Meson Physics Facility (LAMPF) showed that the quadrupole was the most significant place for activation [1]. Figure 5 shows the results of the measurements for the 200 MeV portion of the CCL, which was the lowest energy portion of the accelerator that was measured. The LAMPF design does

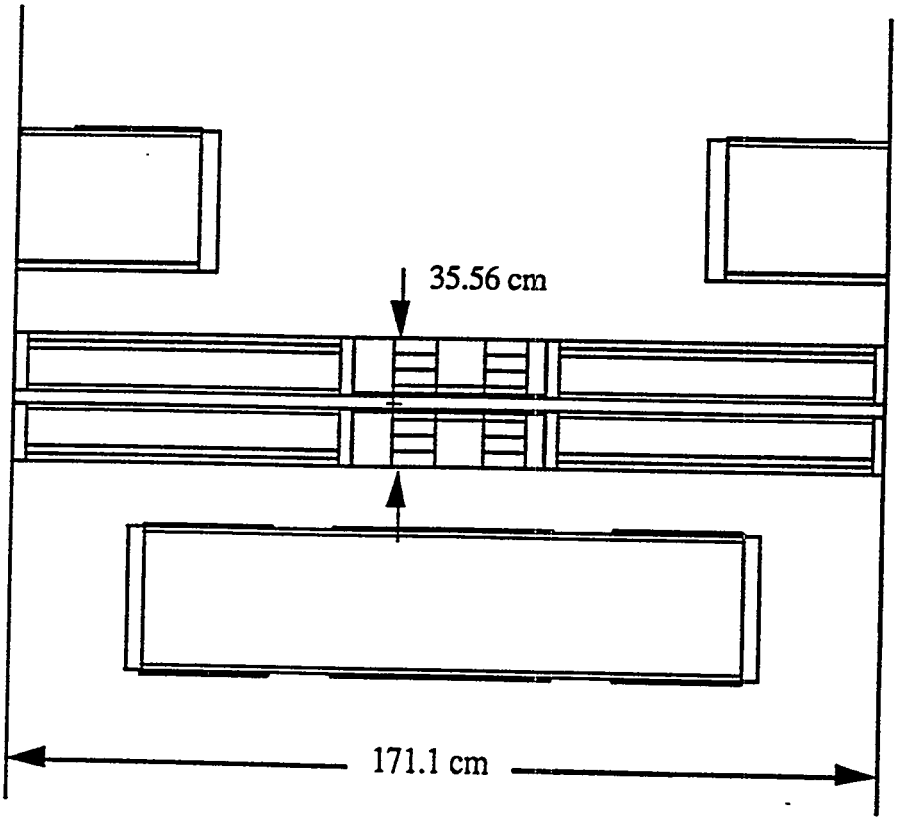

Fig. 3. Side view of 20 MeV BCDTL section computer model.

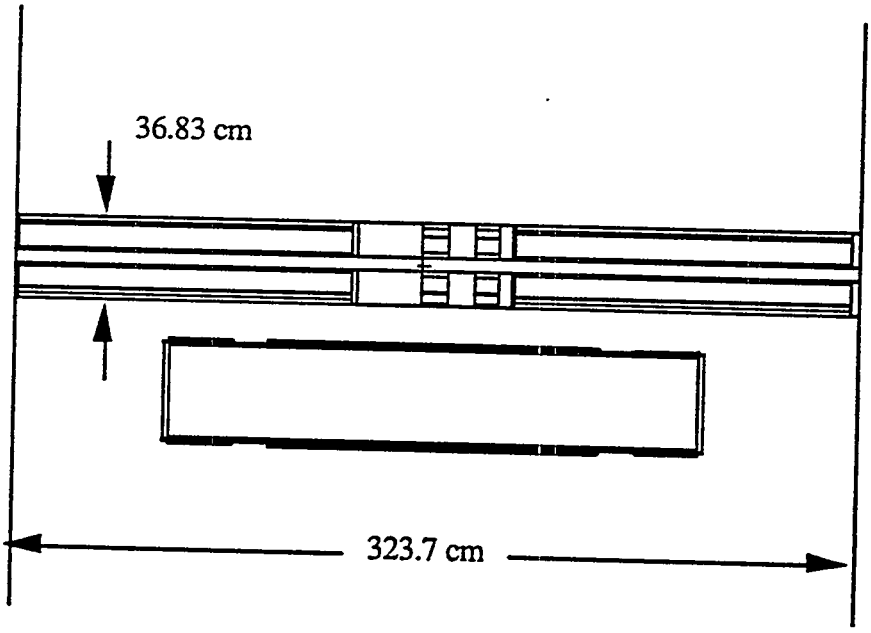

Fig. 4. Side view of 100 MeV BCDTL section computer model.

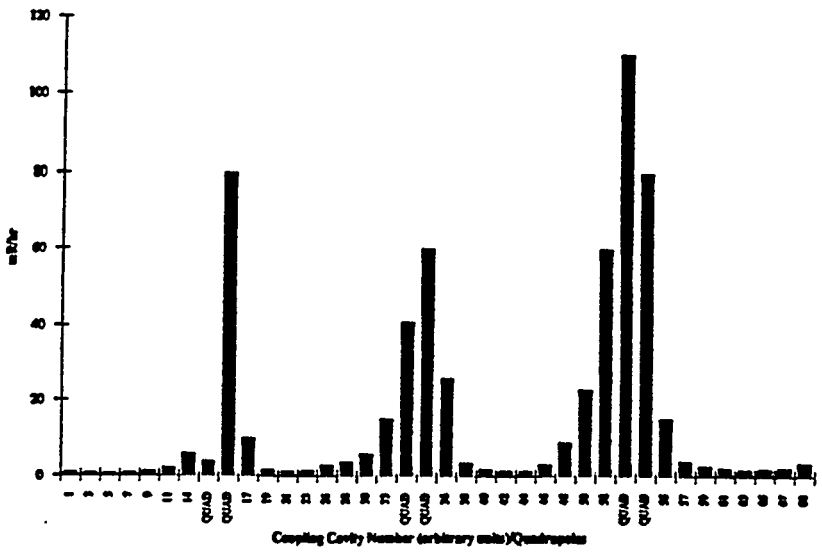

Fig. 5. Dose rate as measured for LAMPF CCL (200 MeV).

not incorporate a BCDTL, so measurements of this structure were not possible. However, since the quadrupole design for the BCDTL is similar to that in the LAMPF CCL, the activation behavior should also be similar. Furthermore, the shape of the beam dictates that beam loss is most likely to occur in the quadrupole because there the beam spreads out and becomes less focused. Based on these considerations, the beam loss was assumed to occur at the beginning of a quadrupole pair. In actuality, beam loss will occur all along the accelerator line. Assuming that the entire beam loss in the modeled sections occurs at a single point maximizes the peak dose produced and therefore yields a conservative result.

To model this beam loss, protons were initiated at the front edge of the first quadrupole. This position was designated as zero on the axial scale. The protons were introduced at a single point just inside of the beam tube material (approximately one-tenth of a millimeter deep), traveling parallel to the beam line. The location of the loss in the pipe is not significant, as the photon source calculated for the dose calculations will be evenly distributed in the cell. This beam loss model provides a reasonable approximation of the small angle of impact of the protons with the structure that is assumed to dominate the beam loss. Although a small angle of incidence difference can yield significantly different results, it was determined that for this research, it would not be a major concern. A calculation was performed that simulated proton loss in an "infinite" amount of the same material. For the 20 MeV protons, no significant increase in spallation yield was detected. For the 100 MeV protons, the yield was only 20% higher than that used in these calculations.

A beam loss of 1 nA was arbitrarily assumed for the CINDER'90 calculations. This assumption was based on an estimated loss of 1 nA/m for the APT accelerator [8], which has an operating current of 200 mA. As this design is not yet finalized, however, the actual loss has yet to be determined. This value should be close enough to allow a reasonable comparison.

Point detector tallies were used in MCNP to determine the resulting gamma fluxes, which were then converted to dose rates using the 1977 ANSI/ANS conversion factors [9] specified in the MCNP user's manual [6]. Radial locations of 25 and 100 cm were chosen, each having detectors at five separate axial locations, equally spaced. Figure 6 is a simple schematic of the accelerator with the detector positions indicated. These detectors provide a spatially dependent dose rate, both axially and radially.

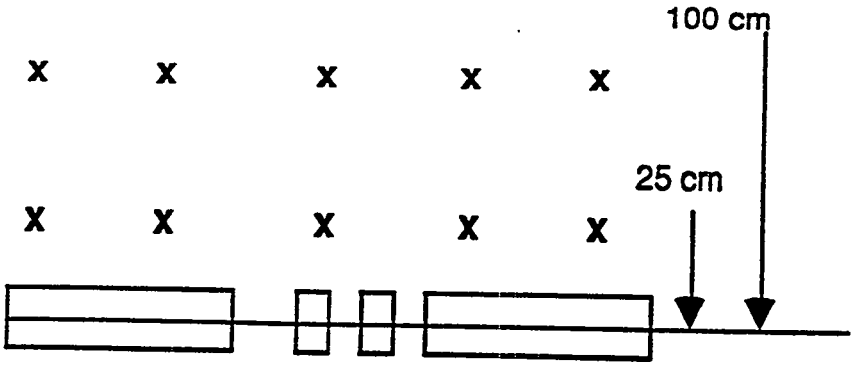

Fig. 6. Point detector locations for dose rate calculations

RESULTS

It is of interest to know the peak dose rate in each section of the accelerator, both the numerical value and its location. Calculations show that the 100 MeV results are higher than those for the 20 MeV section. It is therefore expected that the peak dose rate for the BCDTL section will be found in the 100 MeV results. Furthermore, the results show that the maximum dose occurs after the longest irradiation time (one year) and the shortest decay time (ten seconds) of the several times considered for this study. Figure 7 shows the axial distribution of this peak photon dose rate at each of the two radial locations. For this specific scenario, the peak photon dose rate occurs at the central detector at the 25-cm radius and its numerical value is approximately 6 mR/hr. The dose rate is approximately an order of magnitude smaller at the same axial location for the 100-cm radius.

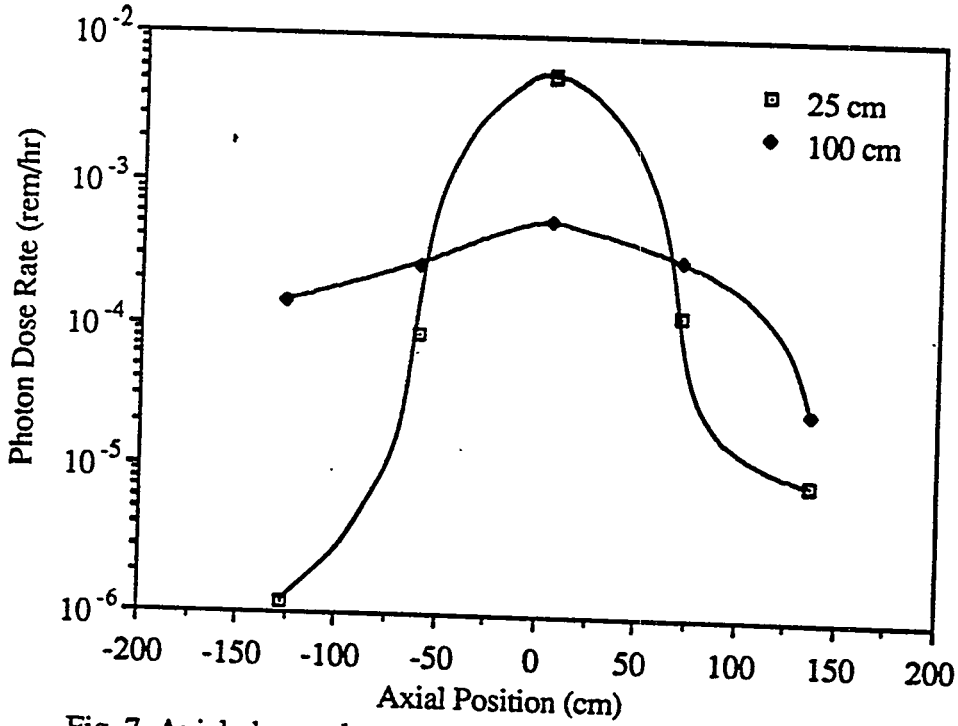

Fig. 7. Axial photon dose rate distribution for 100 MeV BCDTL section at two radial locations (one year irradiation and ten seconds decay).

The dose rate as a function of time is also of interest, because an initially high dose rate might not be so troublesome if it decays away fairly quickly, avoiding the need for remote maintenance. Figure 8 shows a comparison of the decay rates for each energy (20 and 100 MeV) at the 25-cm radial location. For simplicity's sake, only one irradiation time was used, arbitrarily chosen as one year. Since dose (based on energy deposition) can be proportional to decay power (energy emitted), the extensive results produced by the CINDER'90 calculations can be analyzed to attempt to determine the dominant dose producing nuclide(s). CINDER'90 generates several tables that rank the isotopes according to the parameter of interest, one of which is decay power. Table 1 shows the decay power of these isotopes for the 100 MeV section after one year of irradiation for each of the four decay times.

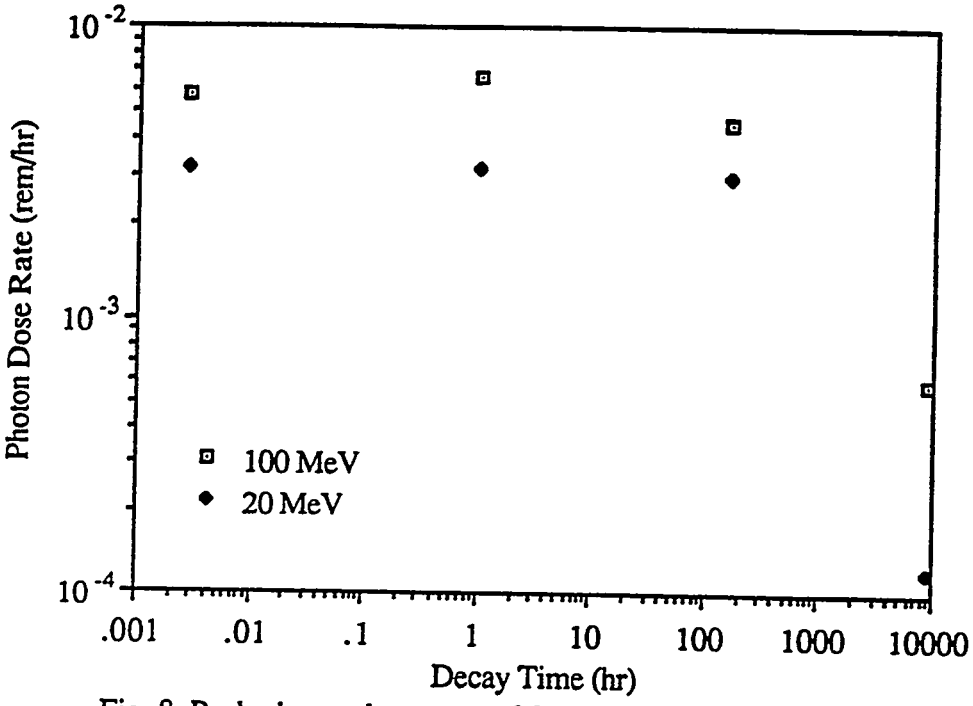

Fig. 8. Peak photon dose rate at 25 cm as a function of decay time.

Table 1. Decay Power of Ten Worst Isotopes at Each Decay Time at 100 MeV.

Ten Seconds		One Hour		One Week		One Year	
Isotope	Decay Power (W)	Isotope	Decay Power (W)	Isotope	Decay Power (W)	Isotope	Decay Power (W)
Mn-52	1.4827e-5	Mn-52	1.4753e-5	Mn-52	6.2362e-6	Mn-54	2.0332e-6
Cu-62	1.1073e-5	Cu-61	7.7466e-6	Co-56	4.6230e-6	Co-56	1.8515e-7
Cu-61	9.4884e-6	Co-56	4.9209e-6	Mn-54	4.5022e-6	Co-60	8.1163e-8
Fe-53	5.6173e-6	Mn-54	4.5723e-6	V-48	9.5504e-7	Zn-65	2.2547e-8
Co-56	4.9227e-6	Cu-64	1.4946e-6	Co-58	4.2843e-7	Fe-55	1.6838e-8
Mn-54	4.5727e-6	V-48	1.2888e-6	Cr-51	1.1928e-7	Co-58	1.2947e-8
Cu-64	1.5878e-6	Mn-56	1.1291e-6	Co-60	9.2324e-8	Co-57	1.1832e-8
Cu-60	1.5851e-6	Co-55	6.7109e-7	Zn-65	6.2376e-8	Sc-46	1.6815e-9
Mn-56	1.4762e-6	Cu-62	6.5834e-7	Sc-46	3.2479e-8	V-49	1.3269e-9
V-48	1.2911e-6	Co-58	4.5843e-7	Co-57	2.9487e-8	Ni-63	1.3219e-10

For this case, Mn-52 is the dominant isotope for up to a week of decay. With a half-life of 5.591 days [10], there will be a negligible amount after only about two weeks. Cu-61 also makes a significant contribution in the early decay times, but with a half-life of only 3.35 hours [10], it does not remain for long. After longer periods of decay, on the order of one year, Mn-54 becomes the dominant isotope, with a half-life of 312.2 days [10]. Co-56 also makes a contribution, but its half-life is only 77.3 days [10]. For the 20 MeV case, Co-56 is the dominant isotope throughout the decay period.

With the exception of Cu-61 and Cu-64, these isotopes are all spallation products created by proton bombardment of the iron present in the accelerator structure. The Cu-61 isotope is also a spallation product, created by proton bombardment of copper, whereas the Cu-64 isotope could either be a spallation product of Cu-65 or created by neutron capture in Cu-63. These results, therefore, provide indication that the activation of the structure is mainly the result of the proton loss and the subsequent creation of spallation products, as opposed to the presence of the generated neutrons.

Finally, in addition to the dominant isotopes, it is important to identify the specific accelerator components that contribute significantly to the activation. The worst-case scenario, after one year of irradiation and ten seconds of decay for each section, was studied further. For the central detector at the 25-cm radius of the 100 MeV section, MCNP output showed that the beam pipes in the quadrupole section were the worst of the components, contributing almost 99% of the total dose rate (5.7 mR/hr out of 5.76 mR/hr total). The remaining components' contributions were all at least two orders of magnitude lower.

The worst-case scenario for the 20 MeV section was also analyzed. Again, the worst component was the beam pipes in the quadrupole region. At this energy the beam pipes completely dominate the total dose rate, and the remaining components all have dose rates several orders of magnitude smaller.

CONCLUSIONS

The peak dose rate of 6 mR/hr occurs at the detector closest to the quadrupoles at a radius of 25 cm, also the closest to the location of the modeled beam loss. The component determined to have the highest amount of activation, the beam pipe in the quadrupole section, was also the closest component to the beam loss. The location of the beam loss plays a major role in the distribution of the dose. Hence, the results obtained here cannot be considered definitive. These results, however, are useful in that most of the beam loss is expected to occur in the quadrupoles, due to the shape of the beam at that point. Also, because the major contributor is the beam pipe, which is present throughout the modeled portion of the accelerator, the dose characteristics should be similar regardless of the beam loss location.

Another important conclusion drawn from these results is that the activation in this energy range is dominated by the proton interactions and the subsequent spallation product generation, particularly from spallation of iron. Iron is the main element in the composition of the beam pipe, which has been shown to be the most activated component in the accelerator structure.

When using these results, caution must be taken to consider their degree of accuracy. Most of the spallation products that were found to dominate the activation were analyzed in the benchmarking effort. It was determined that LAHET accurately predicts the presence of the spallation products to within a factor of four. This can then be assumed to be true for the overall dose rates.

Therefore, multiplying the obtained result by a factor of four yields a peak photon dose rate of approximately 24 mR/hr. As the APT design has not been finalized yet, however, the amount of maintenance required is still unknown. Therefore, no definitive conclusions can be drawn about the feasibility of performing hands-on maintenance for this particular design. This dose rate does appear reasonable, however, when compared

with the LAMPF measurements shown in Figure 5, which exhibit peaks as high as 100 mR/hr.

There are several additional areas in the field of accelerator activation that need to be studied before a complete characterization is achieved. Several design variation studies would be of interest. These and other comparisons (such as the use of different materials) can all be easily performed with this methodology. A similar study of the higher energy portion of the APT design (100-1000 MeV) is currently underway and should be completed soon.

REFERENCES

[1] *APT ^{3}He Target/Blanket Topical Report*, LA-12670-MS, Los Alamos National Laboratory, I-II (1993).

[2] Bowman, C.D. et al., *Nucl. Instr..*, A230, 336 (1992).

[3] Arthur, E. et al., *The Los Alamos Accelerator Transmutation of Nuclear Waste (ATW) Concept*, LA-UR-92-2020, Los Alamos National Laboratory (1992).

[4] "The Los Alamos Accelerator Based Conversion Concept for Plutonium Disposition (ABC)", presented at the JASON Review, La Jolla, CA, 1994.

[5] Prael, R.E., and Lichtenstein, H., *User Guide to LCS: The LAHET Code System*, Los Alamos National Laboratory (1979).

[6] Breismeister, J.F. ed., *MCNP - A General Monte Carlo Code for Neutron and Photon Transport*, LA-7396-M Revised, Los Alamos National Laboratory (1981).

[7] Wilson, W.B. et al., "Accelerator Transmutation Studies at Los Alamos with LAHET, MCNP and CINDER'90," presented at the Workshop on Simulating Accelerator Radiation Environments, Santa Fe New Mexico, January 11, 1993.

[8] Liska, D., Los Alamos National Laboratory, Private Communications (1994).

[9] ANS-6.1.1 Working Group, *American National Standard Neutron and Gamma-Ray Flux-to-Dose Rate Factors*, ANSI/ANS-6.1.1-1977 (N666), American Nuclear Society (1977).

[10] Walker, F.W., Miller, D.G., and Feiner, F., *Chart of the Nuclides*, Thirteenth Edition, General Electric Company (1984).

A New Approach To Modeling Linear Accelerator Systems

George H. Gillespie*, Barrey W. Hill* and Robert A. Jameson†
*G. H. Gillespie Associates, Inc., P.O. Box 2961, Del Mar, CA 92014, U.S.A. and
†Los Alamos National Laboratory, P. O. Box 1663, Los Alamos, NM 87545, U.S.A.

Abstract. A novel computer code is being developed to generate system level designs of radiofrequency ion accelerators with specific applications to machines of interest to Accelerator Driven Transmutation Technologies (ADTT). The goal of the Accelerator System Model (ASM) code is to create a modeling and analysis tool that is easy to use, automates many of the initial design calculations, supports trade studies used in assessing alternate designs and yet is flexible enough to incorporate new technology concepts as they emerge. Hardware engineering parameters and beam dynamics are to be modeled at comparable levels of fidelity. Existing scaling models of accelerator subsystems were used to produce a prototype of ASM (version 1.0) working within the Shell for Particle Accelerator Related Code (SPARC) graphical user interface. A small user group has been testing and evaluating the prototype for about a year. Several enhancements and improvements are now being developed. The current version of ASM is described and examples of the modeling and analysis capabilities are illustrated. The results of an example parameter trade study, for an accelerator concept typical of ADTT applications, is presented and sample displays from the computer interface are shown.

INTRODUCTION

The development of a variety of accelerator-driven concepts to meet differing requirements for a spectrum of transmutation related applications [1]-[3] has placed increased demands on accelerator designers to explore a rapidly expanding region of the parameter space available to accelerators. Overall system efficiency, performance optimization and cost minimization are of critical importance in establishing the feasibility of many of these applications. System level tradeoffs of the type needed for ADTT applications require computer models capable of tracking the large numbers of parameters involved and their relationships to each other. A computer model that also offers the ability to change the conceptual design of the accelerator can provide designers with a new paradigm for carrying out system studies. The Accelerator System Model (ASM) is a computer program developed specifically to model proton and deuteron radiofrequency linear accelerators and to assist accelerator designers in carrying out system-level trade studies. An object oriented approach has been used that provides flexibility to the users in changing, and comparing, the conceptual designs for accelerator systems.

Several programs have been developed to model ADTT accelerator systems and ASM has similarities to some of these other codes. The LIDOS code system [4] developed at the Moscow Radiotechnical Institute represents one of the most developed and integrated packages for ion linac beam dynamics design. LIDOS provides for different levels of accelerator modeling and utilizes an expert help system to assist scientists in developing designs. The LINACS program [5] written at Los Alamos National Laboratory also provides for different levels of modeling and incorporates engineering models. ASM focuses on one level of modeling, but includes both beam dynamics and engineering. ASM features an advanced graphical user interface with some expert system type features to facilitate ease of use. One approach to incorporate multi-level modeling is to integrate ASM with other programs working within the same graphical interface environment [6]. Another approach is to incorporate more detailed accelerator system models into user defined ASM modules. In this vein, Grumman is working with us to utilize in ASM the engineering models available from their ABSOC program [7].

ASM OVERVIEW

ASM consists of two primary parts: (1) a set of accelerator physics and engineering models and (2) a graphical user interface. The physics and engineering models are written in FORTRAN and the interface is written in C. Both parts of the program are modular, or object oriented. The modules on the FORTRAN side of ASM correspond to specific accelerator "subsystems," such as the ion source, radiofrequency quadrupole (RFQ) or drift tube linac (DTL). The interface side incorporates object-oriented structures that correspond to the same subsystems. A baseline set of modules was developed for the prototype version (1.0) of ASM for test and evaluation. In addition to the set of built-in baseline modules, the current version (1.1) of the program contains a large number of user definable modules. Table 1 summarizes the modules available in ASM version 1.1. In a joint effort with Grumman, we are developing new ASM modules to be incorporated in the future.

Table 1. Accelerator Modules Available in ASM Version 1.1

Module Types	Accelerator Subsystems	Number of Modules
Linac Baseline		
	Ion Source	3
	Low Energy Beam Transport (LEBT)	2
	Radiofrequency Quadrupole (RFQ)	2
	Drift Tube Linac (DTL)	1
	Coupled Cavity Linac (CCL)	1
	Funnel	2
User Defined Linac		
	Ion Source	4
	Low Energy Beam Transport (LEBT)	4
	Radiofrequency Quadrupole (RFQ)	4
	Drift Tube Linac (DTL)	4
	Coupled Cavity Linac (CCL)	4
	Funnel	4
	"Black Box" Transport Line	4
	"Black Box" Accelerator Component	4
Advanced Linac Baseline		
(in development)	IMS, BCDTL, ...	4
Baseline Support Systems		
	Radiofrequency (RF) Power	4
User Defined Support Systems		
	Radiofrequency (RF) Power	1
	Vacuum	1
	Thermal Management (Cooling)	1

Accelerator Physics and Engineering Models

The beam physics parameters and engineering parameters in ASM are represented by two vectors for each of the linac components listed in Table 1. These vectors are referred to as the Beam Vector (BV) and Engineering Vector (EV). A given module in ASM generates a BV and EV as the primary output.

The BV represents the state of the beam at each point in the accelerator and the vector's elements are physical properties of the beam at that point. Versions 1.0 and 1.1 of ASM use an eight-dimensional representation of the BV:

$$\mathrm{BV} = [E,\ I,\ \langle x^2\rangle,\ \varepsilon_{t,rms}^2,\ \langle \Delta p^2\rangle,\ \varepsilon_{l,rms}^2,\ \alpha_t,\ \alpha_l] \quad . \tag{1}$$

Here, E is the beam energy, I the current, $\langle x^2\rangle$ the mean-square extent of the beam (envelope), $\varepsilon_{t,rms}$ and $\varepsilon_{l,rms}$ the normalized (rms) transverse and longitudinal emittances, Δp the momentum dispersion and α_t and α_l are the transverse (magnitude) and longitudinal Twiss parameters. The quadratic form for several parameters was suggested by the types of models used. Note that although because only one transverse dimension is included in the definition in BV, it is intended that the BV be used to represent the beam at points of cylindrical symmetry near the exit of each device, where $\langle y^2\rangle = \langle x^2\rangle$, $\varepsilon_{x,rms}^2 = \varepsilon_{y,rms}^2 = \varepsilon_{t,rms}^2$, and either $\alpha_x = \alpha_y = \alpha_t$ or $\alpha_x = -\alpha_y$ with $\alpha_t = |\alpha_x| = |\alpha_y|$. Internally, within a given module, any expanded parameter set may be used. The parameter set defined by the BV is used only to described the beam out of, and into, each module.

The EV is used to describe the requirements of the accelerator component that produces the beam defined by Equation (1). In the current version of ASM, the EV is also eight dimensional:

$$\mathrm{EV} = [L,\ V,\ M,\ P,\ x,\ y,\ \mathit{Conf},\ \mathit{Cost}] \quad . \tag{2}$$

The EV elements shown in Equation (2) are: L device length, V device volume, M device mass, P device power requirement, x the maximum horizontal and y vertical dimensions of the component, as measured from the beam axis, *Conf* a confidence factor for the device as modeled, and *Cost* a cost estimate for the device.

The basic requirement for each module in ASM is that the input BV, in the form of Equation (1), be mapped into an output BV of the same form, and that an EV of the form given by Equation (2) be generated by the module. Other outputs can be generated, and are for all baseline modules, but the minimum requirement for a linac module to work within the ASM framework is that these two vectors be created. The two vectors are used for interfacing to other ASM linac and support system modules. It is beyond the scope of this paper to describe the ASM modules individually, but we will briefly describe the structure of the interfacing between modules.

For the baseline modules, a matrix is used to represent the effect on the beam of each device of the linac system (e.g., RFQ, DTL, etc.). This matrix maps the input BV into an output BV by matrix multiplication. In addition to this matrix, the baseline modeling uses the addition of a column vector which augments the output BV by vector addition. For a particular accelerator component, this matrix and its associated augmentation vector are labeled the device matrix (DM) and the device vector (DV). They define the component's effect on the BV. The general model equation for each device is:

$$[BV_o] = [DM]\,[BV_i] + [DV] \quad . \tag{3}$$

Equation (3) need not be linear. The elements of the DM and DV can, and in most ASM models do, depend upon elements of the input BV. Although ASM uses the matrix formulation for the data structure of the built-in baseline models, the ASM program does not require a matrix representation. For a particular device, any set of formulae mapping the input BV into the output BV will suffice. Formally, the flexibility of this approach to accelerator modeling is easy to visualize. One starts by specifying numerical values of the beam vector at any point $(BV)_i$ in the system. By repeated application of the matrix Equation (3), one can advance the beam to any further position along the system.

The EV is used to store the engineering and other systems data for the individual components. The individual component EVs are utilized in a set of system integration algorithms to combine this information into an overall system EV. For example, the overall length and power requirement of the linac are generated. These are not simple additions of the corresponding vector components. The geometry associated with funneling must be taken into consideration and the nature of the power required (dc or rf, pulsed or continuous, etc.) for each component must be addressed.

The types of mathematical models used for the baseline modules of ASM are frequently referred to as scaling models [5]. This means that most computations are algebraic and program execution times are fast, permitting a highly interactive mode for the use of ASM. One compromise associated with this approach is a limit on the detail and accuracy in the accelerator component modules. Our goal for the level of accuracy in the primary outputs (described below) from the baseline ASM modules is in the 10-20% range. Benchmarks against existing accelerators, and accelerator designs, are used to assess how well this goal is achieved [X6] and to develop modifications in the modeling algorithms. However, the user definable modules offer the analysts the ability to improve this accuracy by incorporating higher fidelity models. The object oriented approach requires that users adhere to certain guidelines in developing individual modules, but the guidelines are sufficiently flexible that relatively sophisticated models of accelerator components can be incorporated into the program. This is currently being demonstrated in a joint project with Grumman [7].

Graphical User Interface

The graphical user interface (GUI) for ASM is provided by the Shell for Particle Accelerator Related Codes (SPARC). SPARC [6] is a unique software environment that includes the basic elements needed to support a GUI: specialized windows, palettes, menus, icons, etc. The interface is written in C, but is easily linked with FORTRAN programs. For ASM, the configuration of a linac is set up by selecting icons representing the components from a palette and dragging them to a Document Window. Parameter values for the components are entered using Data Tables in Piece Windows for each linac component. The Data Tables are constructed so that expert system rules may be incorporated. For example, guidance limits are displayed for input parameters, that incorporate design rules of thumb, and alert users when their input data may have impractical consequences. Default input parameters may be automatically scaled using other rules of thumb. Other GUI features also support system design, including: (a) different options for units, including "smart units," (b) multiple linac Document Windows open at once and (c) copying and pasting groups of linac components between windows. SPARC has been described in detail elsewhere [6] so we now discuss a specific example of using ASM.

USING ASM

Figure 1 illustrates a typical computer screen for ASM. In this example a linac system has been constructed by selecting accelerator components, from the vertical palette bar shown on the left, and dragging them to the Model Space pane (lower part) of the Document Window, which occupies the majority of the illustration. The example linac system, or model, includes a funneled beamline. Each leg of the funnel consists of an electron-cyclotron resonance (ECR) ion source, an electromagnetic solenoid (EMS) low energy beam transport section for matching and one of the radiofrequency quadrupole models (RFQ2) available in ASM. A funnel component and drift tube linac (DTL) complete the accelerator model for this example. An alternative model for the legs of the funnel is shown on the Work Space pane of the Document Window. The Work Space pane is useful for temporarily storing components when comparing different linac concepts.

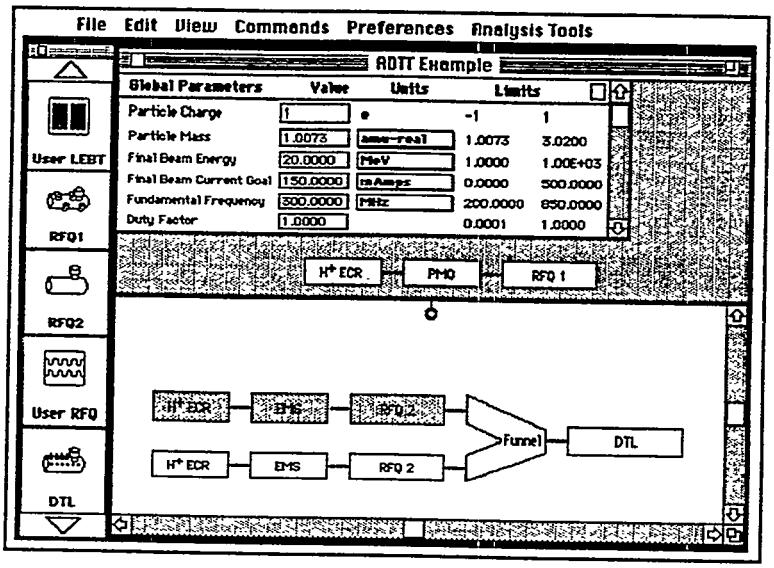

Figure 1. Example of computer screen for the Accelerator System Model (ASM) program.

System parameters such as the particle charge and mass, the fundamental radiofrequency of the accelerator, and other Global Parameters are assigned using the Data Table shown in the top part of the Document Window. Input parameters for an individual component are set using Piece Windows accessed by double clicking the icon of the component. Scaling options for input parameters are also set using the component Piece Windows. Figure 2 illustrates the Piece Window for the RFQ of the example and shows how the user accesses the scaling options.

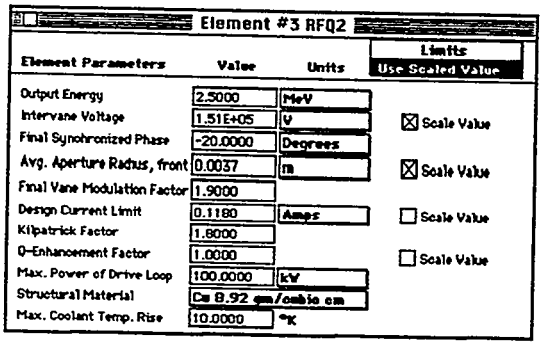

Figure 2. Piece Window for the input of RFQ parameters. The use of scaling options for two inputs, the Intervane Voltage (based on the Kilpatrick Factor) and the Average Aperture Radius at the front of the RFQ (i.e. radial matching section), is illustrated.

Parameter variations, useful for carrying out system trade studies, are automated in ASM by using one of the selections available from the Analysis Tools menu shown in Figure 1. Special windows, which contain a duplicate graphic image of the current linac model, are used for running a parameter variation. Figure 3 illustrates the set up of a parameter variation analysis. The user may select any Global Parameter to be varied, or an individual component parameter may be selected by clicking on the icon of the desired component.

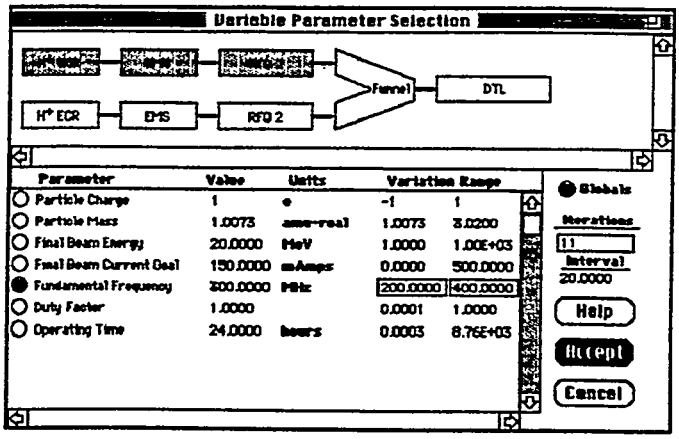

Figure 3. Selecting the independent variable for an ASM trade study. In the example shown, the Fundamental Frequency of the linac is to be varied between 200 and 400 MHz, in ten equal steps of 20 MHz. Outputs to be plotted as a function of the frequency are selected using a similar window.

A window similar to that shown in Figure 3 is used to select the outputs, from any BV or EV, that are to be plotted as a function of the independent parameter. Figure 4 shows the results, for the example parameter variation, when the final longitudinal and transverse emittances are selected for plotting.

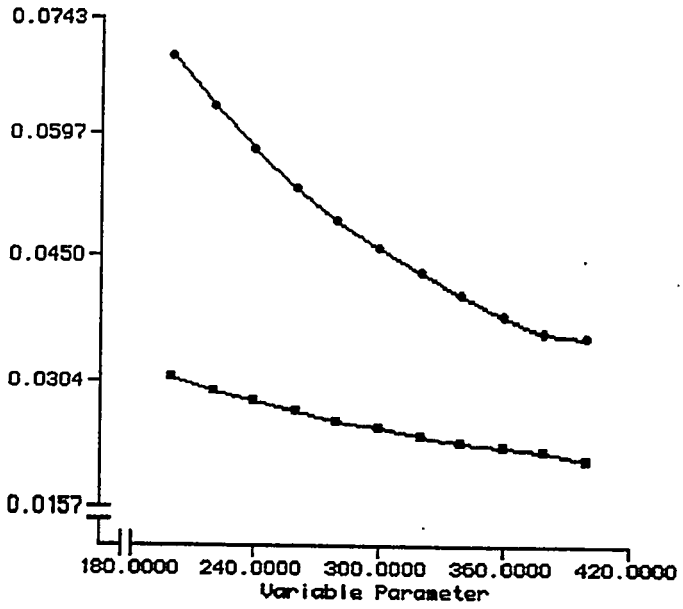

Figure 4. Final emittances in the longitudinal (circles) and transverse (squares) planes as a function of the linac frequency between 200 and 400 MHz. Units are π-cm-rmad, rms, normalized. An arbitrary number of such graphs, with up to four curves each, may be displayed in individual windows. The graphs may also be copied and pasted directly into other documents.

The results shown in Figure 4 quantify the characteristic decrease in normalized emittances, as the linac frequency is increased, for the example accelerator shown in Figure 1. This example only takes a few minutes to set up and run, and illustrates the power of the computer program we

are developing. The precise details depend upon the parameters used and the scaling options selected. Analyses of this type are currently being used to benchmark the ASM modules, but will provide the basis for carrying out future trade studies of ADTT concepts. A collaboration with Grumman [7] is integrating ASM into an overall ADTT facility systems model.

SUMMARY

A new computer code for modeling radiofrequency accelerator systems has been described. Beam dynamics and engineering parameters are incorporated on an approximately equal footing. An advanced graphical user interface makes the program easy to use and provides interactive tools for supporting trade studies and other analyses important in system design. The formalism used for describing the accelerator components is sufficiently flexible that relatively sophisticated models of linac technology can be used. Additional work is on-going to bring ASM up to the standards necessary to provide accelerator scientists with a comprehensive system design tool for ADTT applications. The progress to date is encouraging and demonstrates the usefulness of the approach being taken.

ACKNOWLEDGEMENTS

The authors are indebted to George Lawrence, Carl Paulson, Mike Peacock and Alan Todd for constructive comments on ASM version 1.0 and for useful suggestions that have lead to improvements incorporated into version 1.1. This work has been supported in part by subcontract 9119K0014-9Q with the Los Alamos National Laboratory, under contract W-7405-ENG-36 with the U. S. Department of Energy.

REFERENCES

[1] T. P. Wangler, G. P. Lawrence, T. S. Bhatia, J. H. Billen, K. C. D. Chan, R. W. Garnett, F. W. Guy, D. Liska, S Nath, G. H. Neuschaefer and M. Shubaly, "Linear Accelerator for Production of Tritium: Physics Design Challenges," *Proceedings of the 1990 Linear Accelerator Conference*, LA-12004-C, 548-552 (1990)

[2] R. A. Jameson, "Accelerator-Driven Neutron Sources for Materials Research," *Nucl. Instr. Meth. Phys. Res.* B56/57, 982-986 (1991).

[3] G. P. Lawrence, "High-Power Proton Linac for Transmuting the Long-Lived Fission Products in Nuclear Waste," *IEEE Particle Accelerator Conference Record* 4, 2598-2600 (1991).

[4] B. I. Bondarev, A. P. Durkin, B. P. Murin, G. T. Nikolaishvili and O. Yu. Shlygin, "LIDOS - Unconventional Helper for Linac Beam Designing," *AIP Conference Proceedings* 297, 377-384 (1993).

[5] R. A. Jameson, et al, "Scaling and Optimization in High-Intensity Linear Accelerator," Los Alamos National Laboratory Report No. LA-CP-91-272, Section III (1991).

[6] G. H. Gillespie, "The Shell for Particle Accelerated Related Codes (SPARC) - A Unique Graphical User Interface," *AIP Conference Proceedings* 297, 576-583 (1993).

[7] A. M. M. Todd, C. C. Paulson, M. A. Peacock and M. F. Reusch, "A Beamline Systems Model for Accelerator-Driven Transmutation Technology (ADTT) Facilities," these proceedings.

A Beamline Systems Model for Accelerator-Driven Transmutation Technology (ADTT) Facilities†

Alan M. M. Todd, C. C. Paulson, M. A. Peacock and M. F. Reusch
Grumman Research and Development Center,
4 Independence Way, Princeton, New Jersey 08540-6620, USA.

Abstract. A beamline systems code, that is being developed for Accelerator-Driven Transmutation Technology (ADTT) facility trade studies, is described. The overall program is a joint Grumman, G. H. Gillespie Associates (GHGA) and Los Alamos National Laboratory effort. The GHGA Accelerator Systems Model (ASM) has been adopted as the framework on which this effort is based. Relevant accelerator and beam transport models from earlier Grumman systems codes are being adapted to this framework. Preliminary physics and engineering models for each ADTT beamline component have been constructed. Examples noted include a Bridge Coupled Drift Tube Linac (BCDTL) and the accelerator thermal system. A decision has been made to confine the ASM framework principally to beamline modeling, while detailed target/blanket, balance-of-plant and facility costing analysis will be performed externally. An interfacing external balance-of-plant and facility costing model, which will permit the performance of iterative facility trade studies, is under separate development. An ABC (Accelerator Based Conversion) example is used to highlight the present models and capabilities.

1. INTRODUCTION

The system complexity, coupled with the large capital and operating costs of Accelerator-Driven Transmutation Technology (ADTT) facilities makes optimization with respect to life cycle and capital cost essential. Additionally, the reliability and maintainability of the system components must be considered, since this can have a critical impact on the operating and hence facility life cycle cost. Such optimization of ADTT facility designs requires consideration of many diverse issues. Accelerator and nuclear engineering/physics dominate beamline and target/blanket trade studies, but relatively mundane labor and economic considerations in the balance-of-plant (BOP) subsystem can overwhelm the impact of beamline or target trades that may appear significant within their own context.

The best strategy to effectively model the various subsystems at a meaningful technical depth with applicable reliability and costing data, while balancing their impact within the overall system analysis, is not immediately obvious. We have chosen to approach this problem by developing three separate but interfacing optimization codes. These are a top level code that addresses the overall system, and two separate more technically detailed codes for beamline and target/blanket optimization, respectively. The beamline and target codes will perform local optimization based on input requirements from the top level code, as well as employing greatly simplified BOP and costing models to approximate the overall system consequence of local optimization. They can also be driven to output parameterized trade study data that can be input to and used by the top level analysis to perform overall system optimization. At the present time, progress has been made in the development of the top level [1] and beamline codes, but the remainder of this paper will only discuss the models, status and future plans for the beamline systems model. At present, work has not begun on target/blanket modeling.

The choice of a beamline system model framework was made to accommodate the widest possible segment of the community involved in ADTT systems design. Los Alamos has been supporting the Accelerator Systems Model (ASM) [2,3] of GHGA[4] for this function. Because of its appropriate structure and ease of use, we chose to adopt the ASM framework for the development of our beamline systems model, and build upon the ADTT relevant models already developed by GHGA for ASM. Los Alamos and GHGA continue to develop their own ASM based systems models. GHGA, Los Alamos and Grumman have agreed to cooperate in this effort, and to share the various models developed in the ASM framework for ADTT modeling.

† This work is supported by the Grumman Aerospace Corporation

Over the last several years, under Strategic Defense Command and internal funding, Grumman developed a series of ion accelerator systems codes for application to the Neutral Particle Beam (NPB) program. This effort culminated in the creation of a systems code named ABSOC (Accelerator Based Systems Optimization Code) [5]. Whereas the prior ASM focus has been on accelerator and beam transport physics models, and the GUI (Graphical User Interface) I/O (Input/Output) structure, ABSOC had evolved to feature fairly complex engineering models of the beamline systems with less emphasis on beamline physics models. Our first task therefore, was to incorporate the best of the ABSOC engineering and certain useful physics models within ASM. Thereafter, we began the development of those new models required to complete an ADTT beamline systems evaluation.

Section 2 discusses the overall structure of the ADTT systems analysis effort, and briefly describes a few Grumman component models presently available within the ASM framework. Section 3 then illustrates the application of these models to the proposed Accelerator Based Conversion (ABC) [1] system. Finally, in section 4, we present our conclusions and future plans.

2. ADTT SYSTEMS ANALYSIS FRAMEWORK AND MODELS

Figures 1 and 2 illustrate the framework and calculational flow of the ADTT code. The GUI of ASM controls the beamline design layout, user input data and constraints, as shown in figure 1. The detailed component models communicate with the GUI via the SPARC module [2]. At present, the interfaces with the external codes, that will control the application of constraints and permit iterative facility optimization, are not implemented. Table 1 lists the currently proposed component models, the origin of the source coding and the status of the models. In some cases, such as the Drift Tube Linac (DTL), multiple models (denoted by greater than "1" in the status column of the table) exist which have been added by different contributors. In others, no models (denoted "0") are presently implemented. The present paper will focus on the general code architecture and model implementation, specifically engineering model development, while avoiding details of the individual engineering and physics models employed.

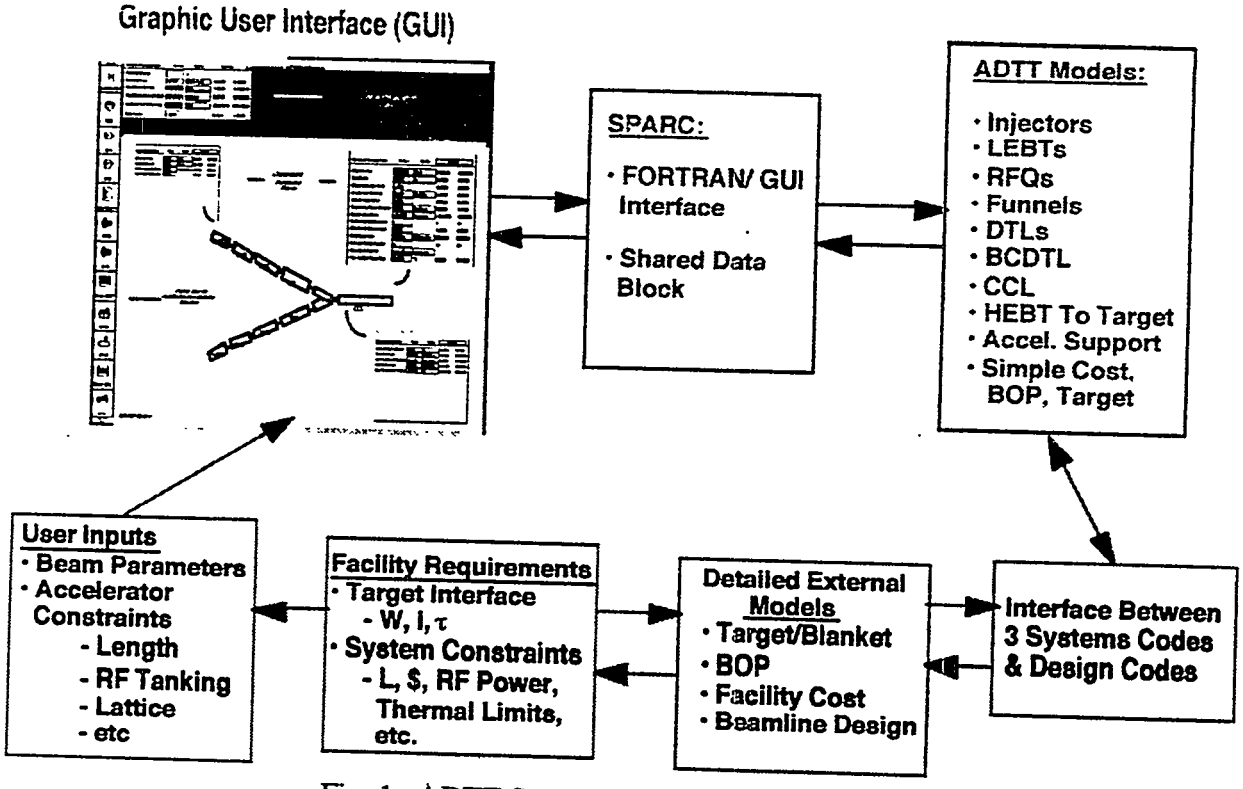

Fig. 1. ADTT Systems Analysis Architecture.

Table 1. Beamline Model Status

Component	Status (# Models)	Source
Ion Source	3	GHGA
Low Energy Beam Transport (LEBT)	2	GHGA
Radio Frequency Quadrupole (RFQ)	2	GHGA
Low Energy Funnel	1	GHGA
Drift Tube Linac (DTL)	2	GHGA/Grumman
High Energy Funnel	1	GHGA
Bridge Coupled DTL (BCDTL)	1	Grumman
Coupled Cavity Linac (CCL)	2	GHGA/Grumman
HEBT (Transport to Target)	1	Grumman
Matching Section	0	Grumman
Doublet,Electromagnetic Quad.(EMQ)	1	Grumman
RF, Thermal, Vacuum	1	Grumman
HILBILAC / Other Accelerator	0	Grumman
Internal Target / Blanket	0	Grumman
Internal BOP / Costing	0.5	Grumman
External Target / Blanket	0	Grumman
External BOP / Costing	1	Grumman
Interface Coding	0	Grumman

Figure 2 shows the analysis flow within the beamline systems code. It illustrates that communication between modules is accomplished by assigning critical physics and engineering parameters to arrays, which are tracked and updated from component to component and compiled into system level output. These include the beam vector (BV), the engineering vector (EV), the inventory vector (IV), the cost vector (CV), and system vectors for the inventory (SIV), the layout (SLV), the cost (SCV) and the engineering (SEV). This concept originated in ASM but has been expanded by us for ADTT applications.

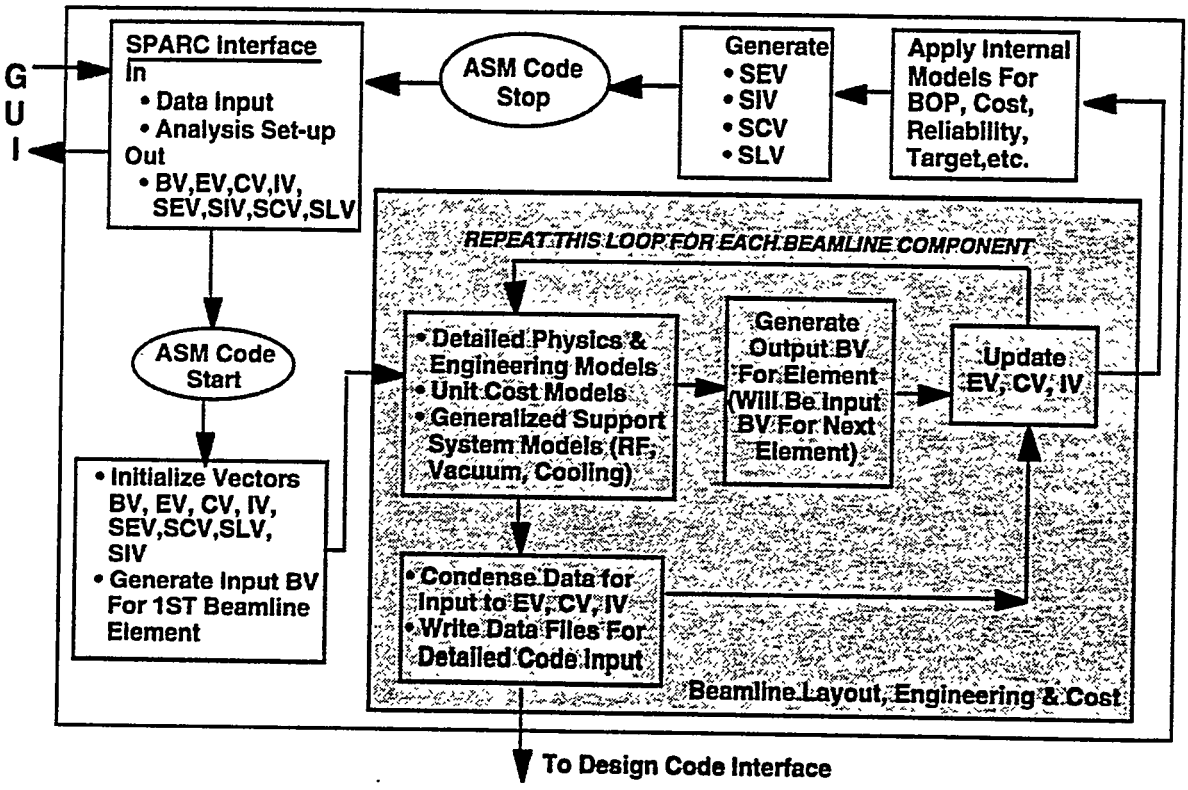

Fig. 2. ADTT Beamline Code Analysis Flow

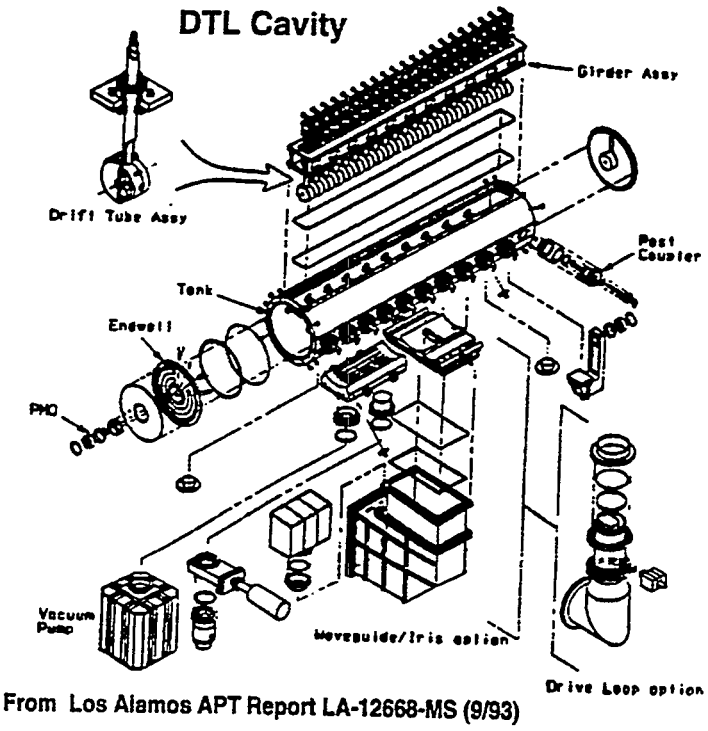

Modeling Objectives

- Model all major components of each beamline element
- Model all major support system interfaces
- Provide data useful to detailed design codes
- Provide inventory & unit costs for major components
- Provide reliability & performance data

Fig. 3. Beamline Modeling Objectives

Generalized Heat Transfer Model

$$Q = kA_{Surface}\left(\frac{\Delta T_{Cond.}}{t}\right) \quad (1)$$

$$Q = hA_{Surf.}\Delta T_{Film} \quad (2)$$

$$Q = \dot{m}\Delta H_{Total} \approx \dot{m} C_p \Delta T_{Cool.} \quad (3)$$

$$\dot{m} = \rho V_{Flow} A_{Flow} \quad (4)$$

$$T_{Surface} - \Delta T_{Conduction} - \Delta T_{Convection} = T_{\substack{Coolant \\ Inlet}} + \Delta T_{Coolant} \quad (5)$$

$$(\Delta T_{Convection} + \Delta T_{Coolant}) = T_{Surface} - T_{\substack{Coolant \\ Inlet}} - \Delta T_{Conduction} \quad (6)$$

Coolant Distribution Scheme

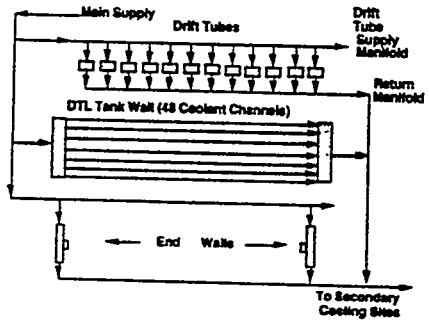

Drift Tube Coolant Flow Path & Pressure Loss

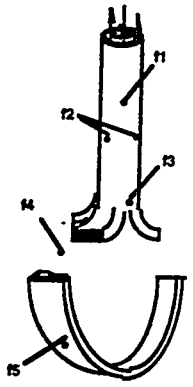

$$F = [(f1 + f2 + f3 + 2nf4 + nf5 + f6)]$$

$$\Delta P = (F) \times \frac{\rho \bar{V}^2}{2g} + \frac{[\dot{m}(Vout - Vin)]}{A_{FLOW}\ (g)}$$

Friction Loss — Momentum Loss

Fig. 4. Thermal Engineering Model

The goal of each component model is to provide the kind of information identified in figure 3. Here, we take a DTL example to illustrate the level of detail we seek in our inventory vector, IV. We note the importance of the inventory for cost purposes, system interfaces, design data suitable for detailed physics and engineering design input, as well as reliability and performance predictions. An attempt is being made to develop all the ADTT models to this level of detail.

Figure 4 is included to give a flavor of the new cooling model as applied to a DTL. The governing heat transfer equations, coolant distribution system concept, flow paths and related pressure loss analysis are indicated. These kinds of models and the driving code architecture are used for the ABC comparison in the next section.

3. ABC BENCHMARKING

The baseline ABC top level design parameters, with which we have begun benchmarking studies, are shown in figure 5 [6]. At present, although sufficient individual component models exist for end-to-end analysis of the beamline, we are still tuning these individual component models to the more detailed physics and engineering parameters of the design. Nevertheless, many of the models are already yielding good agreement with the baseline design.

For instance, figure 6 shows the cavity power loss distribution as a function of beam energy gain for ABC constraints. The spikes in the DTL section are the end wall losses, that we calculate separately from the cell/tank impedance generated thermal losses, and which identify the two DTL tanks. The BCDTL cavity power is similarly calculated, but in this case, the end wall spikes have been suppressed for clarity. The break in cavity power near the center of the BCDTL results from a step change in tank parameters at that point in order to optimize the structure impedance [7]. The CCL has been arbitrarily truncated in the figure in order to preserve some the detail of the low energy accelerator tanking. In the CCL case, the individual cells are calculated including all the wall losses. Although some of the cavity power models are somewhat elementary, these results are not inconsistent with the more detailed ABC calculations, and the models are being further refined.

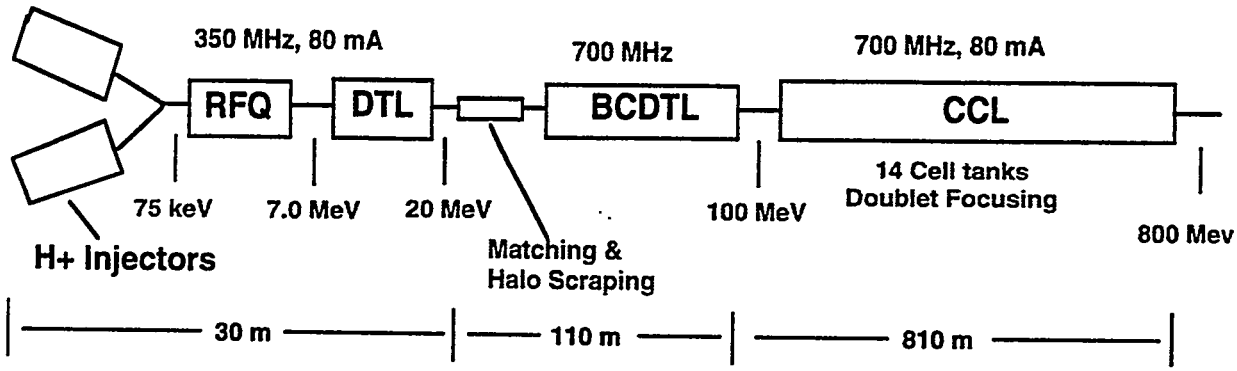

Parameters

Beam Power	64 MW
Total RF Power To Linac	107 MW
RF to Beam Efficiency	0.60
AC to RF efficiency	0.58
RF Transport Efficiency	0.95
AC to Beam Efficiency	0.33
AC Power Requirement	214 MW
Average CCL Gradient	1.0 MV/m
Transverse output emittance	< 0.04 π-cm-mrad
CCL aperture / beam-size ratio	> 13-26

Fig. 5. ABC Baseline

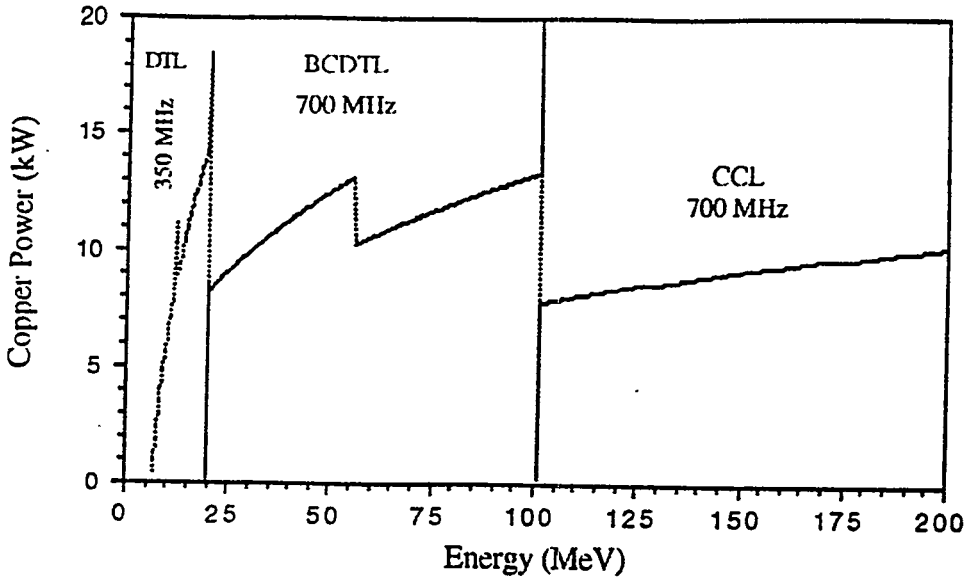

Fig. 6. ABC Cavity Power Loss Calculations

BCDTL Detailed OutPut

MPW Shell

Summary Tables

******** BCDTL TOTALS ********

Total Accelerator Length	106.8086	m
Total Accelerator Mass	14548.80	kg
Total Accelerator Envelope	127.3068	m3
Required RF Power	9.410145	MW
Required AC Power	25.46499	MW
Total Power Dissipation	24.32745	MW
Required Coolant Mass Flow	616.8194	kg/s

********** BCDTL INVENTORY **********

Total # Of BCD Cavities 65.00000
Total # Meters Of Tank Wall 62.74819
Total # Drift Tubes 390.0000
Total # End Walls 130.0000
Total # Stems 390.0000
Total # Tank Coolant Manifolds 130.0000
Total # RF Drive Loops 130.0000
Total # Tank Supports 65.00000
Total # Coupling Cavities 63.00000
Total # Quadruploe 130.0000
Total # Inter Tank Diagnostic Sets 65.00000
Total # Variable Tuners 65.00000
Total # Rail Tuners 65.00000
Total # Ion Pumps 130.0000
Total # Drift Tube Coolant Feeds 390.0000
Total # End Wall Coolant Feeds 520.0000
Total # Meters Of Cryostat 0.0000000

********** BCDTL COST **********

Cost Of BCDTL Cavities $ 16,250,000.
Cost Of Drift Tubes $ 8,580,000.
Cost Of End Walls $ 5,200,000.
Cost Of Coupling Cavities $ 5,775,000.
Cost Of RF Drive Loops $ 11,700,000.
Cost Of Tank Support Stands $ 6,500,000.
Cost Of Quadrupole Doublets $ 9,750,000.
Cost Of Inter Tank Diagnostics $ 2,275,000.
Cost Of Variable Tuners $ 2,925,000.
Cost Of Rail Tuners $ 325,000.
Cost Of Ion Pumps $ 3,250,000.
Cost Of Misc. Fittings & Connectors $ 50,000.
Cost Of RF Power For BCDTL $ 29,393,000.

Total BCDTL Cost $ 101,973,000.

Fig. 7. ABC BCDTL Engineering Summary

In figure 7, we show a BCDTL model engineering summary that compares favorably with the baseline of figure 5, and where the desired engineering detail has been captured. The engineering model for this component is not finalized. In particular, the costs presented should be treated with caution since the BCDTL benchmarking process is incomplete. Figure 7 is an example of the component level output summaries and detailed layout sheets that are available for each design element. The summaries present physics, engineering and systems data, which is further compressed into overall beamline summary data tables.

Other than the missing models identified in table 1, an area that requires particular attention is the development of a generic matching section model and associated top level lattice definition coding. This will assign the lattice to each accelerator and beam transport element, subject to appropriate matching constraints. At present, the lattice for each element is input from external matching calculations performed by the user.

4. FUTURE PLANS AND CONCLUSIONS

The near term goal of this activity is to provide a useful level of ADTT facility modeling in this fiscal year. In order to achieve this goal, we need to complete the validation of the existing beamline models, and incorporate the presently missing internal BOP and target/blanket models. A planned near term study will be to analyze the optimum RF configuration for the ABC system.

Beyond this immediate goal, we need to integrate models for systems engineering, reliability and maintainability; improve the internal engineering, physics and costing models; complete the interfaces with the external existing facility optimization model and the new target/blanket model. New models, such as for the high current, low energy Russian HILBILAC accelerator [8], are needed for some ADTT applications, in addition to the required improvements to existing ones. As noted above, a specific need is the completion of a top level lattice selector that matches the beam throughout the various accelerator and beam transport components in a self-consistent manner.

In conclusion, a beamline systems modeling code for application to ADTT facilities, based on the GHGA Accelerator Systems Model code, is being developed. Physics and engineering models have been implemented for most ADTT beamline components, and benchmarking against the existing ABC concept has begun. Continued collaboration with GHGA and Los Alamos to develop a "standard" ADTT systems model, based on the ASM framework, is planned.

6. REFERENCES

[1] D. Berwald, A. Favale, T. Myers and J. McDaniel, "Potential Role of ABC-Assisted Repositories in U.S. Plutonium and High-Level Waste Disposition", these Proceedings.

[2] G. H. Gillespie, B. W. Hill and R. A. Jameson, "Progress in Development of an Accelerator System Modeling Code", to appear in the Proceedings of the International Workshop on Beam Dynamics and Optimization, St. Petersburg, Russia, July 4-9, 1994.

[3] G. H. Gillespie et al., "A New Approach to Modeling Linear Accelerator Systems", these Proceedings.

[4] G. H. Gillespie Associates Inc., P. O. Box 2813, Del Mar, California 92014.

[5] M. A. Peacock and C. Piaszczyk, priv. comm.

[6] G. Lawrence, "Los Alamos High-Power Proton Linac Designs", these Proceedings.

[7] R. Garnett, priv. comm.

[8] B. Bondarev et al., "Experimental RF Proton Accelerator with Beam Focusing by Means of a Superconducting Solenoid", Preprint 8901, Moscow Radio Technical Institute, Moscow (1989) - In Russian.

Specialized Beam Diagnostic Measurements for an ADTT Accelerator Funnel

John Douglas Gilpatrick*
M.S. H808, LANL
Los Alamos, NM, 87545

Abstract. Los Alamos National Laboratory has proposed several CW-proton-beam facilities for accelerator-driven transmutation technologies (ADTT) with beam-current densities greater than 5 mA/mm^2. The primary beam-diagnostics-instrumentation requirement for these facilities is to provide sufficient beam information to understand and minimize beam-loss. To accomplish this task, the beam diagnostics instrumentation must measure beam parameters such as the projected centroids and profiles, total integrated current, and particle loss. Because of the high specific energy loss in materials at beam energies less than 20 MeV, interceptive measurements such as wire scanners or fluors cannot be used to determine beam profiles or centroids. Therefore, noninterceptive techniques must be used for on-line diagnosis of high-intensity CW beam at low energies. The beam funnel area of these proposed accelerator facilities provide a particular interesting beam measurement challenge. In this area of the accelerator, beam measurements must also sense how well the two funnel input-beams are matched to each other in phase space. This paper will discuss some of the measurement requirements for these proposed accelerator facilities and the various noninterceptive techniques to measure dual-beam funnel operation.

INTRODUCTION

A new generation of cw H^+-beam accelerators have been proposed whose primary purpose is to either produce tritium or transmute nuclear waste [1,2]. These accelerator designs have common components. Typically, the low energy beamlines contain a dc injector, and a 350-MHz radio frequency quadrupole (RFQ) and drift tube linac (DTL). The output beams from the DTLs are combined using various electromagnetic lenses to match and interleave the two beams. This transport area, known as the funnel, contains an RF deflector cavity which interleaves and bends each of the input beams to form a single output beam of twice the input bunching frequency. This bunched beam is further accelerated by two other 700-MHz accelerator structures. A bridge-coupled drift-tube linac (BCDTL) is injected with the funnel output beam and accelerates this beam to 100 MeV. The coupled cavity linac (CCL) accelerates the beam from 100 MeV to 1 GeV. The funnel output beamline also has a dc bending magnet which bends the beam into an offset beamline that is used to fully measure the beam entering the BCDTL.

Since these accelerators are production facilities, an overall facility requirement is that hands-on maintenance is necessary. To meet this requirement, the accelerator is designed with a beam radius 8 to 13 times smaller than that of the beam pipe radius. The combination of a smaller beam, high beam currents, and cw operation increases the average beam power density at the accelerator output to 8 MW/mm^2 (see Table 1).

Beam Diagnostics Requirements

Beam diagnostic measurements for these accelerators consist of two types of beam instrumentation. Those beam measurements that characterize the beam during the initial start of the beam facility or during off-normal beam operation, and those beam measurements that are used during normal beam operation. The operational or on-line beam diagnostics measurements sense only the portion of the beam phase space required to establish and maintain normal daily beam operations. Due to the large quantity of beam energy deposited into robust materials like graphite (shown in Table 1), the on-line measurements are either non- or minimally-interceptive and therefore sense the beam without interfering with beam operation or increasing the amount of beam loss.

Table 1. Summary of the cw beam parameters for a 2-mm-rms wide beam (i.e., peak current densities of 8 mA/mm^2) from the output of each accelerator structure.

Acc. Structure	Avg. Current (mA)	Bunch Freq. (MHz)	Energy (MeV)	Power Density (kW/mm^2)	Dep. Power* (W)
Injector	100	DC	0.075	0.3	220
RFQ	100	350	7	28	48
DTL	100	350	20	80	21
Funnel	200	700	20	160	42
BCDTL	200	700	100	800	12
CCL	200	700	1000	8000	3

* Average beam power deposited in a 1-mmW x 1-mmH x 1-μmD volume of graphite by a cw proton beam.

The characterization beam diagnostics are capable of fully measuring the transverse or longitudinal beam phase-space and either fully or partially intercept the beam. Due to their interceptive nature, the characterization beam measurements must be operated under low-current-density or low-duty-factor pulsed-beam conditions. These operation conditions reduce their usefulness during normal beam operation. An offset beamline in the funnel output section has both on-line and characterization beam diagnostics.

Typically, the accelerator operator needs are nearly satisfied if the on-line beam diagnostics measure the first and second moments of the projected distributions for all six dimensions of the beam's phase space, number of particles contained in the beam, and the number of particles lost to the structure. However, in reality, there are a limited number of measurements that can be performed for these beam currents. Typical on-line measurements include beam current, beam loss, transverse and longitudinal centroids, transverse width and angular distributions. The longitudinal phase-space beam-parameters are difficult to measure without directly intercepting the beam[3].

BEAM FUNNEL MEASUREMENT CHALLENGES

Specialized Beam Measurement

One of the more challenging beam measurements required for the ADTT facilities is the wide-bandwidth measurements that sense differences between two funnel input beams. If one of these input beams has a different phase-space density distribution than its counterpart, the resulting beam will have a phase-space modulation at one half of the merged beam's frequency. This "every other beam bunch" modulation may occur in the first and second moments in all dimensions of the merged beam's phase-space.

If left undiagnosed and uncorrected, this beam modulation may result in increased beam emittance. These higher-emittance beams could also result in increased beam halos and loss - the beam parameters that must be minimized so that "hands-on" maintenance may be performed on the accelerator beamline components.

It is clear that these input beam differences must be detected with beam diagnostics. But why not just measure these input-beam differences with standard beam diagnostics instrumentation during single beam operation of the funnel? First, standard beam instrumentation do not have sufficient accuracy and repeatability. To perform these

measurements under single beam operation and match the two input beams to the required amount, the standard beam instrumentation will need a factor of ten improvement in accuracy and repeatability. Secondly, without modification, standard beam instrumentation are not sensitive to merged-beam mismatched-phase-space errors (i.e., standard instrumentation cannot detect a mismatch between the two input beams' phase-space moments, they will only provide an average of the two beams' phase-space moments). Third, single beam operation does not provide sufficient peak beam current to address high current beam-tuning issues, such as rf cavity loading effects. Finally, under single beam operation, tuning of the funnel will take much longer to accomplish than under dual-beam operation using beam modulation instrumentation. The general requirements for the beam modulation instrumentation are as follows:

1.) These measurements must be non-interceptive. Not only because of the deposited beam power-density issues but because these are tuning measurements. Therefore, these measurements must be capable of detecting mismatched merged-beam errors under normal dual-beam funnel-operation.
2.) The measurement bandwidths must be sufficiently wide to detect the input beam errors in a "real-time" fashion (i.e., bandwidths greater than a few 100 kHz).
3.) It is preferred that the modulation measurements have the capability to detect which beam is in error and in what direction (i.e., that it detect the magnitude and sign of the error).

The last two items are extremely important if these measurement were used in a feedback loop to maintain beam stability within the funnel.

DUAL-BEAM FUNNEL MEASUREMENT TECHNIQUES

Beam Current Modulation Measurements

Several different types of beam modulation may occur in the funnel output leg. The most fundamental modulation is that of beam current. If one of the funnel input beam's has a different current, then the resulting merged beam current will have a modulation in beam current of half the merged bunched-beam frequency. This modulation is then detectable by sensing the beam image currents with an image-current probe designed to be insensitive to beam position and by measuring the magnitude of the components at 0.5 and 1.5 times the merged bunched-beam frequency (see Figure 1). This amplitude modulation of the merged bunched-beam, requires that

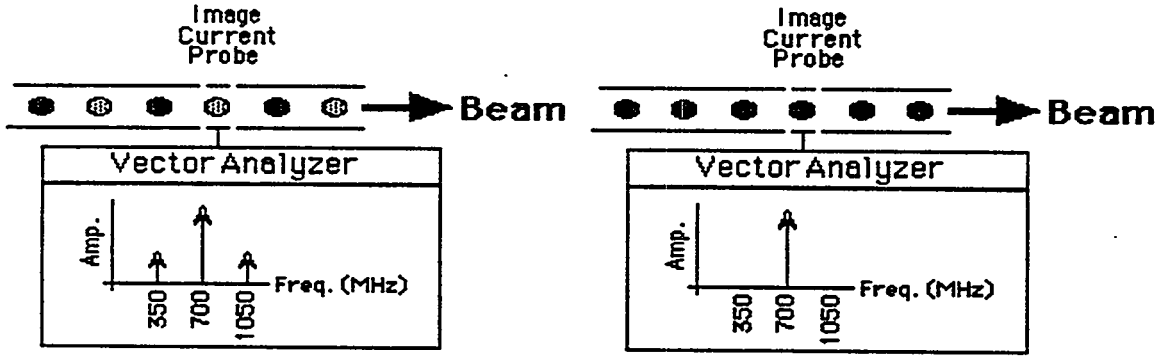

Fig. 1. The left figure shows the signal spectrum of an image current probe sensing a beam with "every other beam bunch" current modulation. The right figure shows the same image current signal spectrum without this modulation.

both of the side components will have the same sign. The amount of beam current differences between the two input beams that is feasibly detectable is approximately 0.1% of the average beam current.

Transverse Centroids Modulation Measurements

If one of the funnel input beams is missteered into the deflector cavity, that particular beam may either have a different position or trajectory angle from the other beam once the two beams are merged. This disagreement in beam position or angle results in a beam modulation of half the merged bunched-beam frequency and more importantly also results in an effective increase in the merged beam's transverse emittance with respect to either of the two input beams. However, in order to detect this type of modulation, an image-current probe that is sensitive to beam position must be used. A four-lobe microstrip or capacitive probe whose lobes are on two orthogonal axes is one example of a beam position sensitive probe. As shown in Figure 2, the signals from opposite lobes of these types of probes are processed with a high frequency power difference processor. The spectral output from this processor is then analyzed. With this processing technique, the position modulation is displayed as an amplitude modulation much like the current modulation. If there is "every other beam bunch" position modulation, side spectral components will appear at 0.5 times and 1.5 times the merged beam frequency. For angular modulation, two probes at two locations along the beamline provide the beam position information. From these two sets of beam position information, the trajectory angle disagreement between the two input beams may be determined. The resolvable magnitudes of position and trajectory angle errors are typically <10μm and <50 μrad.

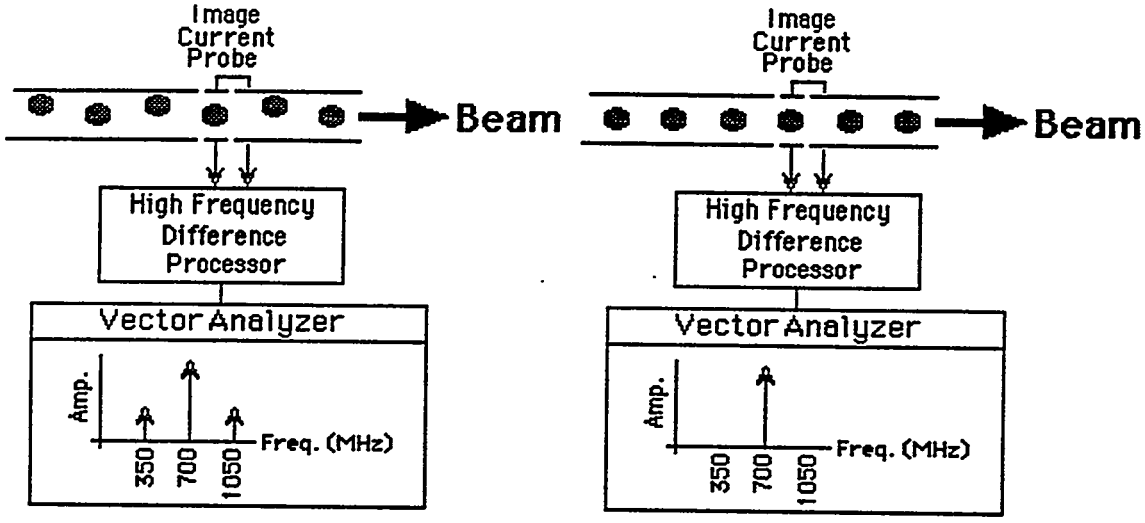

Fig. 2. The left figure shows the signal spectrum of an image current probe sensing a beam with "every other beam bunch" position modulation. The right figure shows the same image current signal spectrum without this modulation. Note that a position-sensitive beam probe and high frequency processor are necessary to detect the beam position modulation.

Longitudinal Centroids Modulation Measurements

If the two input beams are not exactly out of phase with each other by π or if their beam energies do not agree, the merged output beam will look similar to the left portion of Figure 3.

The resultant disagreement results in a phase modulation of half the merged bunched beam frequency. It also results in an effective increase in the longitudinal emittance with respect to the two input beams. The detection of the phase modulation is much like that of the beam current modulation. Again, an image-current based probe that is insensitive to beam position is used and the signals are detected using spectral analysis. As Figure 3 illustrates, the primary difference between beam-phase modulation versus beam-current modulation is that one of the side frequency components will have an opposite sign. Like its transverse centroid counterpart, beam-energy modulation measurements that use probes at two locations along the beamline, provide beam phase information. From these two sets of beam phase information, the beam energy disagreement between the two input beams may be determined. The resolvable magnitudes of beam phase and energy errors are typically <0.1° and <0.005% of the merged beam energy.

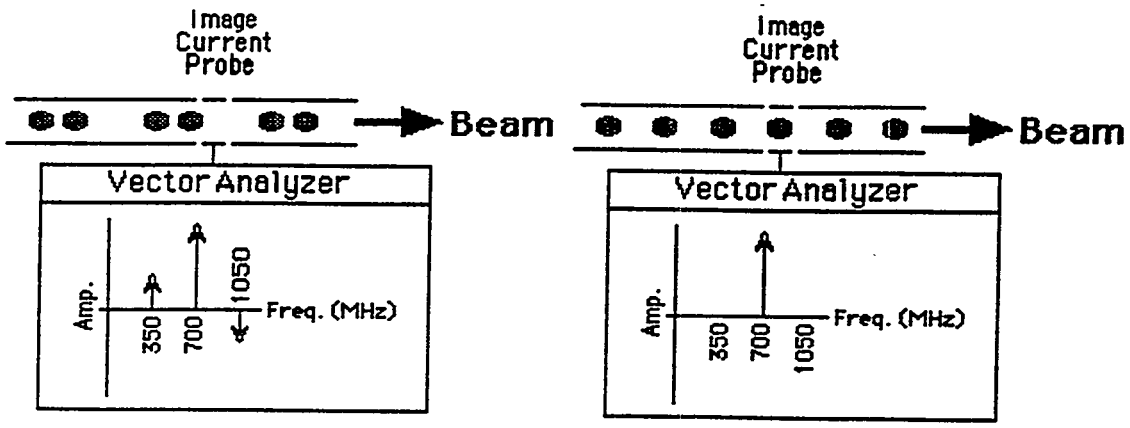

Figure 3. The left figure shows the signal spectrum of an image current probe sensing a beam with "every other beam bunch" phase modulation. The right figure shows the same image current signal spectrum without this modulation. Note that unlike amplitude modulation that was seen in the beam current modulation, beam phase modulation changes the sign of one of the side components.

Other Moments Modulation Measurements

Besides beam current and phase-space centroid modulations, second moment modulations may also exist in a merged funnel beam. These modulations can take four forms. In transverse phase space, the beam width and divergence of the two funnel input beam need not match. This condition could result in mismatched beams, increased emittance and beam halo production. In longitudinal pahse space, the phase and energy spread of the input funnel beam may also disagree and therefore cause similar mismatch conditions.

These second-moment modulation errors are very difficult to detect with wide bandwidth measurements. Presently, there are no real-time detection methods available for these second moment errors. Therefore, the present method for detecting the second moment errors does not use dual beam operation (i.e., measure each of the input beam's second moments separately during single beam operation). In reality, some mixture of all of the modulation errors is likely so it will be necessary that these measurements distinguish between each type of beam modulation. Furthermore, a beamline tuning procedure will be necessary to distinguish the various modulations.

Funnel Tuning Procedure

The first-order funnel tuning procedure that reduces error between the two input beams has the following steps.

1.) Set each individual input beamline to the nominal approximate beam current and transverse and longitudinal centroid using standard diagnostic measurements.
2.) Set each individual input beamline to the nominal approximate beam profile using standard diagnostic measurements.
3.) Null differences between the two input beam positions and trajectory angles using the transverse centroid modulation measurements.
4.) Null differences between the two input beam phase and energy using the longitudinal centroid modulation measurements.
5.) Null differences between the two input beam currents using the modulation measurements.
6.) Measure the transverse beam profiles and emittances for each input beam under single beam operation. Adjust the magnetic lenses for minimum differences.
7.) Check independent beam loss measurements for minimum loss.

Although this procedure does not have any iterations built into the list, several iterations are likely to minimize all of the possible modulation conditions.

SUMMARY

The on-line beam diagnostic measurements for these very intense beam facilities must be noninterceptive. This is due to the amount of peak beam power density deposited in any material that should come in contact with the beam. One of the beam measurement challenges for these facilities is that of matching the two input beams of the funnel. If mistuned, the funnel will be the source of much beam loss. To minimize this loss, thereby improving the capability of performing hands-on maintenance, the funnel input-beam's current and first and second moments must be matched. The match of these beam parameters should be achieved by using various types of "every other beam bunch" modulation measurements in the output funnel beamline. Several detection techniques for centroid and current modulation were discussed in this paper. However, we do not presently have a wide bandwidth method to detect second moment modulations during dual beam operation (i.e., single beam detection with standard instrumentation will be necessary). Finally, a funnel tuning procedure was proposed using these beam modulation measurements.

REFERENCES

[1] George Lawrence, "Los Alamos High-Power Proton Linac Designs," to be published in the *International Conference on Accelerator-Driven Transmutation Technologies and Applications Proceedings,* Las Vegas, Nevada, July, 1994.
[2] K.C. Dominic Chan, et.al., "Accelerator Performance Demonstration Facility in Los Alamos," to be published in the *1994 Linear Accelerator Conference Proceedings* , Ibaraki, Japan.
[3] J. D. Gilpatrick, et.al., "Experience with the Ground Test Accelerator Beam-Measurement Instrumentation," *1993 Beam Instrumentation Workshop*, Santa Fe, NM, October, 1993.

MOLTEN FLUORIDE FUEL SALT CHEMISTRY

L. M. Toth, G. D. Del Cul, S. Dai, and D. H. Metcalf
Chemical Technology Division
Oak Ridge National Laboratory
Oak Ridge, Tennessee 37831-6181

Abstract

The chemistry of molten fluorides is traced from their development as fuels in the Molten Salt Reactor Experiment with important factors in their selection being discussed. Key chemical characteristics such as solubility, redox behavior, and chemical activity are explained as they relate to the behavior of molten fluoride fuel systems. Fission product behavior is described along with processing experience. Development requirements for fitting the current state of the chemistry to modern nuclear fuel system are described. It is concluded that while much is known about molten fluoride behavior, processing and recycle of the fuel components is a necessary factor if future systems are to be established.

Introduction

Molten fluoride fuel salts were developed and utilized more than twenty five years ago originally for use in the Aircraft Nuclear Project and finally, in the Molten Salt Reactor Experiment, MSRE. A considerable R&D effort was devoted to these systems during the 1950's and 1960's which culminated in the construction and operation of the MSRE during the late 1960's. After shutdown of the MSRE in late 1969, research on fluoride systems was drastically curtailed, even in fundamental studies. However, after a 25 year hiatus, there has been renewed interest in utilizing molten fluoride solutions in nuclear applications because of the same unique advantages that were recognized decades ago.

This paper will summarize the key features in molten fluoride chemistry that makes it desirable for application to such nuclear systems. The significant chemical characteristics of molten salts will be described along with their impact on the design of a molten salt reactor system. The presentation of these characteristics will be integrated with fundamental chemical principles which help to determine them and the necessary measurements will be listed. In addition, the final post-mortem experience will be discussed in view of the fundamental inorganic chemistry which has evolved since 1970. Finally, the current needs in further molten fluoride R&D will be addressed in order to fulfill the goals in utilizing molten fluorides for Accelerator Based Conversion, ABC, requirements.

Much of the development of MSRE molten fluoride chemistry was under the leadership of the late, Warren E. Grimes. This presentation follows much of the plan he had initially outlined and many of the results which were obtained by him; and, therefore, it is fitting that this be dedicated to his memory.

Molten Salt Reactor Experiment

Figure 1 shows a cutaway of the MSRE which consists of a primary loop containing approximately 4 tons (4650Kg or approximately $2m^3$) of molten salt, LiF-BeF_2-ZrF_4-UF_4(64.5-

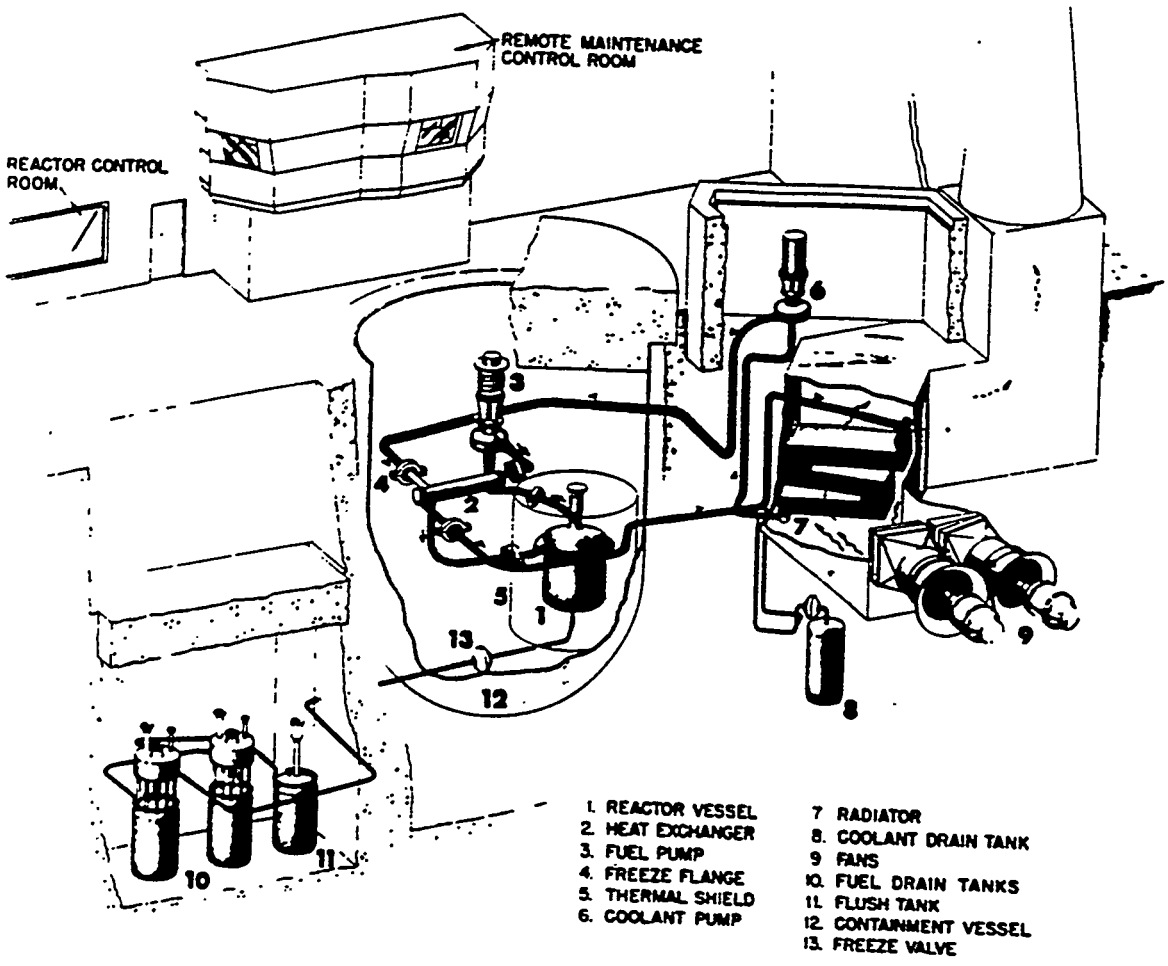

Fig. 1. Cutaway view of the Molten Salt Reactor Experiment circuitry.

30.3-5.0-0.13 mole%) which was pumped through the core by the fuel pump and on to the heat exchanger. The 2610Kg of coolant salt was pumped by the coolant pump from the heat exchanger to the radiator where fans blew the 7.5MWt power generated up the stack. The molten fuel mixture varied from 550 - 650°C in the circuit. Two significant features of this system should be noted: First, the fuel pump not only provided the circulation of the fuel but also provided ready access to salt sampling and addition through the pump bowl cavity. (See Fig. 2 discussion in the following paragraph.) Second, at termination of the MSRE experiment in 1969 the fuel salt was split by draining into the two fuel drain tanks and allowed to solidify. It has remained there for the past 25 years.

A cutaway drawing of the pump bowl is shown in Fig. 2. It provided easy access for routine sampling, fuel additions and inert gas sparging. The first two operations were achieved by lowering a sample capsule attached to a wire cable down an access pipe and into the sample capsule cage. There the sample capsule would flood with salt (for sampling) or release its contents by melting (for additions). The access point was farthest from the high radiation levels in the reactor vessel and, thus, could be routinely used on a weekly/monthly basis. Finally, inert gas sparging of the pump bowl contents through the bubbler enabled the removal of the noble gases, Kr and Xe into the offgas line.

General Requirements for the Molten Salts

A molten salt reactor makes the following stringent minimum demands upon its fluid fuel. The fuel must consist of elements of low (and preferably very low) capture cross section for neutrons typical of the energy spectrum of the chosen design. The fuel must dissolve more than the critical concentration of fissionable material at temperatures safely below the temperature at which the fuel leaves the heat exchanger. The mixture must be thermally stable and its vapor pressure must be low over the operating temperature range. The fuel mixture must possess heat transfer and hydrodynamic properties adequate for its service as a heat-exchange fluid. It must be relatively non-aggressive toward some otherwise suitable material— presumably a metal — of construction and toward some suitable moderator material. The fuel must be stable toward reactor radiation, must be able to survive fission of the uranium — or other fissionable materials — and must tolerate fission product accumulation without serious deterioration of its useful properties. In order to be economical, there must be a low fuel cycle cost which presupposes a cheap fuel and an effective turn-around of the unburned fissionable material or (more reasonably) an effective and economical decontamination and reprocessing scheme for the fuel.

Choice of the Fuel Composition

Of all the compounds that could be used as high temperature fluids in reactor systems, fluorides best emcompass the properties of stability, low vapor pressure, reasonable melting points, and low neutron cross section. These characteristics are summarized in Table 1 for several candidate fluorides from which the LiF, BeF_2 , and ZrF_4 components were optimal. (The inclusion of ZrF_4 will be discussed later in more detail.) Chlorides could offer another possible route to molten salt systems but when (1) usefulness of the element, Cl, without isotope seperation, (2) better neutron economy, (3) higher chemical stability, (4) lower vapor pressure,

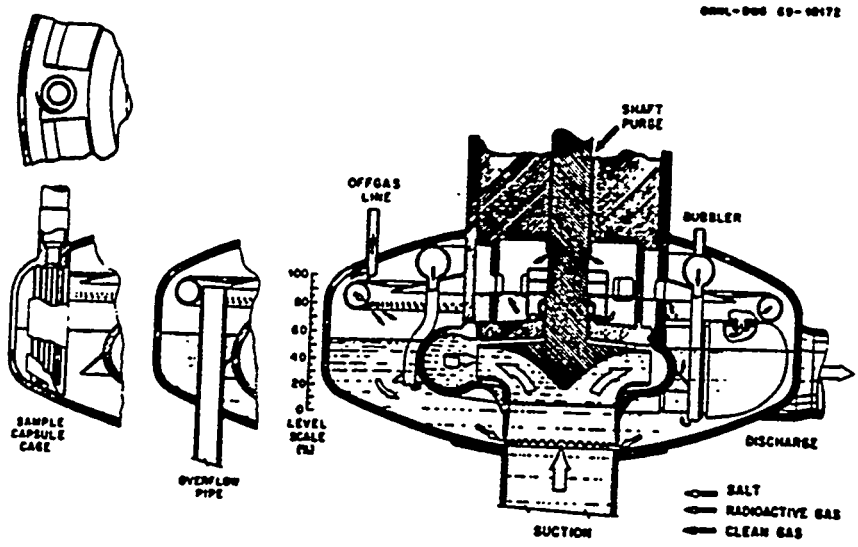

Fig. 2. Cutaway view of the Molten Salt Reactor Experiment fuel pump bowl.

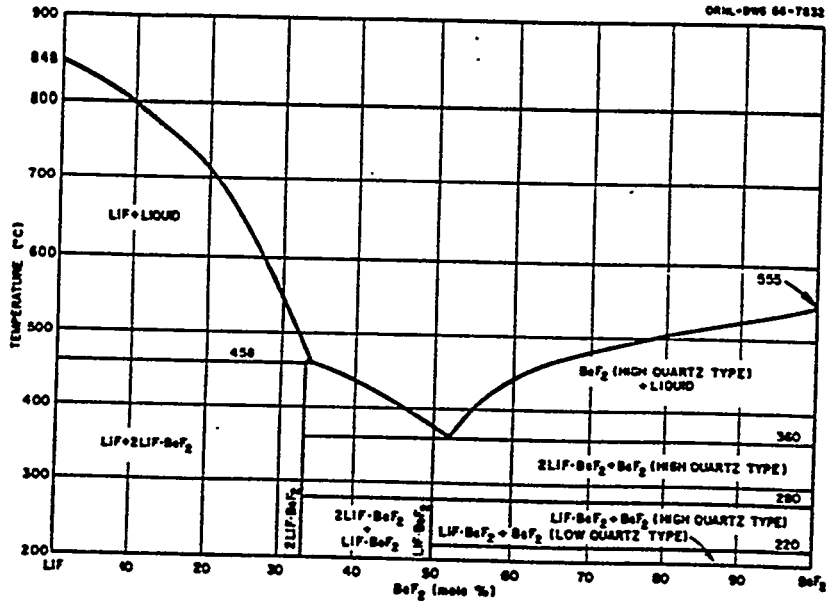

Fig. 3. Phase diagram of $LiF-BeF_2$

Table 1. Relevant Properties of Fluorides in the Selection for use in High Temperature Reactors

Compound	Free Energy of Formation[a] at 1000°K (Kcal/mole F atoms)	Melting Point (°C)	Absorption Cross Section[b] for Thermal Neutrons (barns)
Structural Metal Fluorides			
CrF_2	-74	1100	3.1
FeF_2	-66.5	930	2.5
NiF_2	-58	1330	4.6
Diluent Fluorides			
CaF_2	-125	1330	0.43
LiF	-125	848	0.033[c]
BaF_2	-124	1280	1.17
SrF_2	-123	1400	1.16
CeF_3	-118	1430	0.7
YF_3	-113	1144	1.27
MgF_2	-113	1270	0.063
RbF	-112	792	0.70
NaF	-112	995	0.53
KF	-109	856	1.97
BeF_2	-104	548	0.010
ZrF_4	-94	903	0.180
AlF_3	-90	1404	0.23
SnF_2	-62	213	0.6
PbF_2	-62	850	0.17
BiF_3	-50	727	0.032
Active Fluorides			
ThF_4	-101	1111	-
UF_4	-95.3	1035	-
UF_3	-100.4	1495	-

[a]Reference state is the pure crystalline solid; these values are, accordingly, only very approximately those for solutions in molten mixtures.
[b]Of Metallic ion.
[c]Cross section for ^7Li.

and (5) higher heat capacity per unit weight or volume are considered, fluorides have an obvious advantage.

Chemical Considerations

Three important chemical concepts play a major role in controlling the behavior of the MSRE fuel. These are solubility, redox chemistry, and chemical activity.

Solubility. Solubility takes on a broad meaning in molten salt considerations since the major concern is to keep the components, especially the fuel entity, in a homogeneous molten solution during reactor operation. For pure, unreacting salts solubility is determined by the melting point of the mixture and consequently, the determination of such melting point as a function of salt composition played a dominant role in the early R&D stages of reactor design. The phase diagram of the two major MSRE solvent components is shown in Figure 3.

As seen by the composition vs. temperature relationships a lower melting solution can be obtained with mixtures of the salts as opposed to the pure components. Furthermore, the composition dependence of *insolubility* is better understood by examining the figure where it is seen that for compositions such as LiF-BeF_2(80-20 mole %) pure LiF would be the insoluble component (or "primary phase") if the melt fell below 710°C. On the other hand, at the 60-40 mole % composition, Li_2BeF_4 would be the insoluble phase if the temperature fell below 440°C. For criticality control and safety, it is highly desirable that the primary phase (the first solid phase that precipitates out on cooling) not contain the fuel component. While this was achieved with the MSRE for the UF_4 component, it is less certain for PuF_3 fuels which have apparent solubilities of approximately 1 mole % in most molten fluoride solvents at typical operating temperatures.

From melting point (or solubility) considerations alone the LiF-BeF_2 (48-52 mole %) eutectic composition would be most desirable with its 360°C melting point. However, for this particular system the melt viscosity becomes progressively higher due to the formation of a -BeF_4- network in the fluoride-deficient environment where fluoride atoms are shared between adjacent Be atoms while satisfying the necessary four coordination requirement of Be. (See the discussion on chemical activity.) Therefore the 2:1 ratio of LiF:BeF_2 composition offers the best compromise between acceptable melting point and viscosity. (At this composition, there is ample fluoride to satisfy the four coordinate requirement for Be, ie. BeF_4^{2-} without sharing F^-.

In addition, chemical reaction of the fluoride with impurities (eg., moisture) or system components (eg., graphite) can form metal oxides or carbides which have a much higher melting points and therefore appear as insoluble components at operating temperatures. Reactions of the fuel component with water vapor:

$$2H_2O_{(g)} + UF_4 \rightleftarrows UO_2 + 4HF_{(g)} \qquad (1)$$

are of particular concern because they result in the formation of the insoluble oxide. Because this occurrence would have disastrous consequences on the operation of a circulation fuel solution, a means on insuring against it was essential. The most direct method of preventing the fuel oxide formation is through the addition of ZrF_4 which reacts in a similar fashion with water vapor:

$$2H_2O_{(g)} + ZrF_4 \rightleftarrows ZrO_2 + 4HF_{(g)} \qquad (2)$$

The net reaction, by subtracting the two above would be:

$$ZrF_4 + UO_2 \rightleftarrows ZrO_2 + UF_4 \qquad (3)$$

The concentrations at equilibrium for Eq. 3 are shifted far to the right with the consequence that

ZrO_2 is formed, preferentially, to UO_2, providing there is enough ZrF_4 in the solution. The molten fluoride solution for the MSRE contained 5.0 mole % of ZrF_4 and was more than adequate to handle any oxide impurity problems. Even though there was enough ZrF_4 in the system to react with a 55 gal. drum of (liquid) water, no significant oxide was ever formed during the operating experience of the MSRE; and, consequently, it is practical to consider reducing the ZrF_4 concentration (to fulfill other solution requirements) if the oxide control system is as reliable as that for the MSRE.

Reactions of the fuel or solvent with the other system components such as the metal container or the moderator graphite can also produce insoluble components. These reactions are largely governed by the second major chemical factor, redox behavior, and will be discussed in the context of how it was used to control both insolubility and corrosion mechanisms.

Redox Control. Corrosion of the metal container for molten fluoride reactor systems was also a major concern during the development of the MSRE. As a result, much effort was given to the development of a suitable metal alloy, namely, Hastelloy N, which contains, in addition to the nickel base composition, the following percentages of: Mo, 15-18; Cr, 6-8; Fe, 5; C, 0.04-0.08; Mn, 1.0; Si, 1.0; W, 0.5; Al+Ti, 0.5; Cu, 0.35; Co, 0.2; P, 0.015; S, 0.02; B, 0.01; Others, 0.5. Since the most reactive of the metal alloy components is Cr, the following corrosion reaction could be expected in a uranium fueled system:

$$Cr + 2UF_4 \rightleftarrows 2UF_3 + CrF_2 \qquad (4)$$

Realizing that this is an equilibrium, the corrosion reaction can be controlled by adding a substantial quantity of UF_3 to the solution. The addition was however accomplished by the beryllium reduction of the UF_4 already in solution according to:

$$Be + 2UF_4 \rightleftarrows BeF_2 + 2UF_3 \qquad (5)$$

Beryllium was conveniently added by placing the metal in a sample capsule and lowering it down the access tube into the sample cage of the pump bowl. Controlled additions of Be metal reductant were made in order to maintain the UF_3/UF_4 ratio at 0.01. These Be additions could be made on a weekly or monthly basis to maintain, while monitoring the CrF_2 content of salt samples taken from the pump bowl. In this manner the corrosion of the MSRE Hastelloy N was kept at a negligible value — a fact that was substantiated by analysis of metal parts taken from the reactor after shutdown in 1969.

Other corrosion reactions are possible with the solvent components if they have not been thoroughly pretreated prior to usage:

$$Cr + NiF_2 \rightleftarrows CrF_2 + Ni \qquad (6)$$

$$Cr + 2HF \rightleftarrows CrF_2 + H_2 \qquad (7)$$

These reactions were never a problem due to the hydrofluorination pretreatment of the solvents which eliminated metal ion concentrations such a NiF_2 and dissolved gases such as HF by final inert gas sparging.

Chemical reaction of the fuel components with the moderator graphite were also of concern and involved:

$$4UF_4 + C \rightleftarrows 4UF_3 + CF_4 \quad (8)$$

$$4UF_3 + xC \rightleftarrows 3UF_4 + UC_x \quad (9)$$

From thermodynamic values, the reaction in equation 8 is expected to produce $<10^{-8}$ atm of CF_4 and none was ever seen giving assurance that graphite oxidation was unimportant. The formation of uranium carbides, as indicated in equation 9, could occur if the UF_3/UF_4 ratio became too large. Careful control of this ratio between 0.007 and 0.02 prevented the formation of carbides, if too reducing, and corrosion products via equation 4, if too oxidizing.

For plutonium fueled reactors, similar redox control will be necessary but will be more difficult because the Pu(III)/Pu(IV) redox couple is outside the range of stability in contact with the other reactor components. It is anticipated that redox control in plutonium fueled systems could be accomplished with Ce(III)/Ce(IV) additions or, preferably, by sparging with a redox gas mixture such as HF/H_2.

The importance of redox control is so important to the chemical behavior of molten salt reactor systems that numerous analytical techniques were developed to monitor the status. These techniques include spectrophotometry and electrochemistry (to determine the UF_3/UF_4 concentration ratio) as well as grab samples using the sampling procedure in the pump bowl followed by wet chemical analysis for U(III), U(IV) and Cr contents of the fuel salt. Inline spectrophotometry or electrochemistry is expected to play a significant role in future operating systems.

Redox control would be a simple matter were it not for the fact that the fission of the actinides produces changes in the redox potential of the melt. This arises because, for example, in the case of UF_4 fissioning, the net oxidation state of the fission products is less than four and yet four fluorine atoms are released, leaving a slightly oxidizing event for each fission. In the case of PuF_3 fission, it is expected that the net oxidation state of the fission products will be slightly greater than three while only three fluorine atoms are released to produce a slightly reducing event for each fission. This is clearly a matter that requires further investigation if plutonium fuels are to be used in future designs.

In addition to changes in the redox potential due to fission, transmutation of LiF and BeF_2 in high neutron fluxes is expected to produce redox changes and oxide impurities which will require further consideration in future systems.

Chemical Activity. Chemical activity, per se, in the molten salt system was not of prime concern during the MSRE development. Rather, such changes were represented as shifts in the equilibrium quotients for the various metal ions in equilibrium with each other, realizing all the while that these equilibrium shifts were controlled by changes in the chemical activity. It is believed that a better understanding of the coordination chemistry of these metal ions since that time has permitted a change of focus to those factors which alter the chemical activity.

Because each metal ion tends to coordinate with ligands (ie., F^-, in this case) according to their size and charge, usually discrete coordination numbers can be given for each ion, for example, Be(II): 4, Zr(IV): 6-7, U(IV):7-8. In a Lewis acid/base concept, these are Lewis acids. Alkali metal fluorides are not so strongly attached to their corresponding fluoride ions and readily give these up so such acidic ions.. Alkali metal halide melts are then thought of as basic while those deficient in fluoride ion are acidic. Equilibria such as:

$$2F^- + BeF_2 \rightleftarrows BeF_4^{2-} \quad (10)$$

$$2F^- + ZrF_4 \rightleftarrows ZrF_6^{2-} \quad (11)$$

with the F^- supplied by the alkali metal fluoride, determine whether the solution is acidic or basic. The mixture LiF-BeF_2(66-34 mole %) if fluoride ion neutral while the mixture LiF-ZrF_4(50-50 mole %) is acidic.

Changes in the chemical activity are defined by:

$$a = \gamma \cdot [\,] \quad (12)$$

where γ is the activity coefficient and [ ] is the concentration of the ion in solution. Coordination equilibria similar to those indicated in equations 10 and 11 can occur for U(IV), U(III), and any other ions in solution and over the composition range of the phase diagram, these changes can account for activity coefficient changes of several orders of magnitude. The net impact is that the equilibrium chemistry of ions in solution can change dramatically as the solvent system is varied from acidic to basic conditions. Typically, the experience with molten salt systems is with the very basic (ie., F^- rich) to neutral solutions. Solvent changes to very acidic systems are expected to bring on great changes in the chemistry of the system and would require much additional R&D development if they were to be used as reactor fuels. One of the most noticible changes on going to acidic systems is a great increase in volatility of those species which are normally volatile in pure form, eg., Zr(IV) and Be(II), because there are not enough F^- present to adequately solvate them in solution.

Fission Product Behavior/Processing

Although there was some salt processing for purposes of fission product removal in the MSRE, there still remains much to be developed for more current applications. The fission-product Kr and Xe were readily removed by the helium gas sparge in the pump bowl. The operation was simple because these inert gases show very low solubilities in molten mixtures such as LiF-BeF_2(66-34 mole %).

Other fission products such as Rb, Cs, Sr, Ba, Zr, Y, and Ln form stable fluorides and are soluble in the molten salt solution. While acceptable for MSRE operations, the removal of these in current applications would be necessary for recycle of the solvent or for ultimate disposal.

The least understood are the fission products, Mo, Nb, Ru, and Te. Some, notably the first two, form cluster compounds with metal-metal bridges as in Nb_6F_{15} upon reduction from the higher oxidation states. They are expected to show a variety of unusual reaction characteristics with increasing insolubility and volatility as the reduction process continues. Disproportionation of intermediate valence states can produce insoluble lower valences accompanied by very volatile high valence species. During the operation of the MSRE, this unusual behavior was perhaps incorrectly attributed to metal fogs in the system. Still much chemical R&D is required to clarify this chemical behavior as a function of redox and solvent acid/base conditions.

Chemical processing in MSRE was under development primarily for intermediate removal of Pa during the ^{232}Th breeding cycle. Difficulties encountered in this development can be avoided because such processing will probably not be necessary in current applications. Processing operations on molten chloride solutions as related to systems such as the Integral Fast

Reactor fuel processing gives much encouragement that similar processes can be developed for molten fluoride processing. Removal of the lanthanides will probably be required to maximize neutron economy. Batch processing off line will probably be first utilized, only to be followed by continuous inline processing as the current systems develop.

Summary

The experience with the MSRE demonstrates that most of the molten fluoride chemistry is well known and controllable. The chemical stabilities and volatilities were easily controlled due to a well designed fuel/solvent system. Fission product behavior and separation is a major need which will require considerable R&D. The use of plutonium fuels will lead to several uncertainties including solubility and redox control and these, along with the effects of high neutron fluxes on the molten fluoride behavior, will require further study. The future for molten salt reactor systems will certainly be driven largely by waste concerns as other systems are already experiencing. Without such an answer to the waste question, which includes recycle and adequate separation of fission product, the promise for such devices will be compromised. Ultimately, batch and/or continuous processing will become a prime necessity.

Acknowledgement

Research sponsored by the Division of Chemical Sciences, U.S. Department of Energy under contract DE-AC05-84OR21400 with Martin Marietta Energy Systems, Inc.

USE OF PYROPROCESSING IN THE PREPARATION OF SPENT FUEL FOR TRANSMUTATION

James J. Laidler
Chemical Technology Division
Argonne National Laboratory
Argonne, Illinois 60439

Pyrochemical processing, or "pyroprocessing," of spent fuel offers a number of unique advantages, particularly in comparison with conventional aqueous solvent extraction techniques. Pyroprocessing, in its present version, has been under development for nearly ten years. Emphasis has been placed on the development of a simple, efficient process that features compact, inexpensive process equipment. Particular attention has been paid to the minimization of waste volumes and to the development of a process that is both economic and environmentally sound as well as proliferation-resistant.

The key element of the pyroprocess is the electrorefining step, during which the actinide elements are separated from the fission products. Electrorefining is carried out in a mild steel vessel at a temperature of 500°C. The process utilizes a molten salt electrolyte that is a eutectic mixture of lithium and potassium chlorides. The metallic spent fuel materials are electrolytically dissolved in a perforated basket that is made anodic, and the uranium present in the spent fuel is collected on a simple steel rod cathode. The uranium deposited at this cathode is free of fission product contamination and contains no residual transuranic elements. The transuranics must be collected in a different type cathode, because their chlorides are more stable than UCl_3 and the TRU elements will not deposit as metals on the rod cathode in the presence of UCl_3 in the electrolyte. The transuranics are collected by causing them to deposit in the presence of liquid cadmium as intermetallic compounds with cadmium. The transuranics are later purified by distillation and recycle of the cadmium, but it is not possible to produce a pure TRU product. Owing to the equilibrium thermodynamics of the process, the liquid cadmium cathode product contains about 30 weight percent uranium and a few thousand ppm of the rare earth fission products.

The chemically active fission product elements (those that form stable chlorides), such as Cs, Sr, Ba and I, remain in the electrorefiner salt phase. They are subsequently removed from the salt by ion exchange and placed in a mineral waste form. Those fission product elements that do not form stable chlorides, including Ru, Tc, the noble metals, and most of the rare earths, remain as a residue in the anode baskets, where they are collected for inclusion in the metallic waste form. This natural separation of the actinide elements and the important fission products makes the pyroprocess highly attractive in an accelerator-based partitioning and transmutation system, especially when consideration is given to the overall economics of the system.

BRIEF OVERVIEW OF THE LONG-LIVED RADIONUCLIDE SEPARATION PROCESSES DEVELOPED IN FRANCE IN CONNECTION WITH THE SPIN PROGRAM

Charles MADIC*[1], Jacques BOURGES* and Jean-François DOZOL**

CEA, Direction du Cycle du Combustible
**DRDD, CEN-FAR, B.P. N°6, 92265 Fontenay-aux-Roses, France;*
*** DESD, CEN-CAD. Cadarache, France.*
1/ Author to whom correspondence should be addressed.

Abstract. To reduce the long-term potential hazards associated with the management of nuclear wastes generated by nuclear fuel reprocessing, one alternative is the transmutation of long-lived radionuclides into short-lived radionuclides by nuclear means (P & T strategy). In this context, according to the law passed by the French Parliament on 30 December 1991, the CEA launched the SPIN program for the design of long-lived radionuclide separation and nuclear incineration processes.
The research in progress to define separation processes focused mainly on the minor actinides (neptunium, americium and curium) and some fission products, like cesium and technetium. To separate these long-lived radionuclides, two strategies were developed. The first involves research on new operating conditions for improving the PUREX fuel reprocessing technology. This approach concerns the elements neptunium and technetium (iodine and zirconium can also be considered). The second strategy involves the design of new processes ; DIAMEX for the co-extraction of minor actinides from the high-level liquid waste leaving the PUREX process, An(III)/Ln(III) separation using tripyridyltriazine derivatives or picolinamide extracting agents ; SESAME for the selective separation of americium after its oxidation to Am(IV) or Am(VI) in the presence of a heteropolytungstate ligand, and Cs extraction using a new class of extracting agents, calixarenes, which exhibit exceptional Cs separation properties, especially in the presence of sodium ion. This lecture focuses on the latest achievements in these research areas.

1. INTRODUCTION

Nuclear-generated electricity accounts for about 17 % of all the electricity produced worldwide. This industry is faced today with a problem of managing the wastes, which is considered acute by public opinion in the different nuclear countries and, in general, by world public opinion. Depending on national policy, these wastes consist either of irradiated fuels, in which case the energy materials (uranium and plutonium) are considered as wastes, or of the mixture of fission products, minor actinides and activation products resulting from the reprocessing of the fuels to recover the uranium and plutonium for recycling. To simplify and to lower the cost of the treatment and conditioning of spent fuel reprocessing wastes, and perhaps also to improve the public acceptance of nuclear power, considerable efforts have been mounted, with the aim of decreasing the unit volume of solid wastes (per ton of fuel reprocessed), particularly those intended for disposal in deep geological repositories. In this field, COGEMA has emerged as the prime mover of this strategy. At the reprocessing plants in La Hague, the unit volume of solid wastes generated in reprocessing operations, which justify deep geological disposal, is around 1.5 m^3/t today, or about half of the volume initially defined in the process book. Following modifications to the PUREX process and the application of new processes, this unit volume is due to decrease drastically by the end of the century, when it should be around 0.465 m^3/t [1]. The single distinguishing feature of nuclear waste management is their extreme danger, which, depending in particular on the nuclear properties of the radionuclides that they contain, may be spread over considerable periods of time. Faced with the growing opposition of public opinion to very long-term radwaste disposal techniques and the difficulty of the scientists to predict the behavior of the geological barriers for periods exceeding one hundred thousand or even one million years, it has become necessary to study and propose some technical solutions to this problem.

The separation and incineration of long-lived radionuclides by nuclear means, which lies at the source of the problem, in order to convert them to short-lived radionuclides, exhibiting higher activity, but which can feasibly be stored over a short period of time, is considered one possible solution to the problem. The situation is regarded with extreme caution in France, where more than 75 % of the electricity consumed is nuclear-generated. A law was accordingly passed by the French Parliament on 30 December 1991, ordering research to be conducted over a fifteen-year period, aimed in particular to determine the experimental conditions for the conversion of certain long-lived radionuclides present in the nuclear fuels to short-lived radionuclides by nuclear means. In this connection, the CEA launched the SPIN (SéParation/INcinération) program for the definition of long-lived radionuclide separation processes and for their destruction, chiefly by fast-neutron reactors [2]. This "intensive reprocessing" strategy is also being investigated in Japan, which launched the OMEGA program in 1988 [3], with objectives similar to those of the SPIN program.

This paper describes the main research guidelines selected at the CEA, aimed at the separation of long-lived radionuclides, and the latest experimental results obtained are briefly described.

2. PROBLEM ANALYSIS AND RESEARCH OBJECTIVES

The high-level wastes generated by irradiated fuel reprocessing, and intended for disposal in deep geological repositories, today include short- and long-lived radionuclides belonging to the families of fission products, minor actinides and activation products. It is universally acknowledged that the half-life identifying the borderline between short- and long-lived radionuclides is thirty years (half-life of ^{137}Cs). In fact, it is considered possible to develop safe disposal methods for periods of up to three centuries, or ten times the "borderline" period, the time necessary for the "total" decay of the short-lived radionuclides. After three centuries, the radionuclides which subsist in the stored wastes, particularly in the most active among them (nuclear glasses) will be the long-lived radionuclides. For the UOx reference fuel, irradiated to a burnup of 33 GWd/t and cooled for three years, Table 1 lists the long-lived radionuclides present, their abundance and some of their nuclear and radiotoxicological properties [4].

A glance at the data in Table 1 shows that the potential hazard of long-lived radionuclides is chiefly due to the minor actinides, and particularly the americium isotopes. This situation prevails for several tens of thousands of years. Consequently, efforts to develop separation methods will mainly concern the minor actinides, and especially americium. However, another way to tackle the problem is to consider the residual toxicity at the outlet of the geological formations where the nuclear wastes may be stored. This is currently being examined, particularly as part of the European exercice called PAGIS [5]. In this case, the doses delivered to the population in the neighborhood of the disposal site, although considerably lower than the standards currently in force, are mainly due to certain fission products, whose migration rates, with the water vector in the subsoil, are much greater than those of actinides. In consequence, a part of the research efforts is also focused on the separation of certain fission products, particularly technetium and cesium. Since long-lived radionuclides were also certainly not completely destroyed during a nuclear incineration cycle, it is also essential to guarantee the "reprocessability" of the targets or nuclear fuels which will contain these materials.

Table 1. Main characteristics of the long-lived radionuclides present in an irradiated fuel (UOx type fuel ; burn-up : 33 GWd/t ; cooling time : 3 years)

Radio-nuclide	t½ (years)	Abondance ($g/t_{H.M.}$)	Specific activity (Bq/g)	Dose factor for ingestion (Sv/Bq)	Isotopic %	Total element ($g/t_{H.M.}$)
Fission products						
^{14}C	$5.7\ 10^{3}$	0.13	$1.05\ 10^{11}$	$5.7\ 10^{-10}$	100	0.13
^{79}Se	$6.5\ 10^{4}$	4.7	$2.58\ 10^{9}$	$2.3\ 10^{-9}$	8.6	54.6
^{93}Zr	$1.5\ 10^{6}$	714	$9.3\ 10^{7}$	$4.2\ 10^{-10}$	20.5	3617
^{99}Tc	$2.1\ 10^{5}$	814	$6.3\ 10^{8}$	$3.4\ 10^{-10}$	100	814
^{107}Pd	$6.5\ 10^{6}$	200	$1.9\ 10^{7}$	$3.7\ 10^{-11}$	16.1	1240
^{126}Sn	$1.0\ 10^{5}$	20.3	$1.0\ 10^{9}$	$5.1\ 10^{-9}$	39.8	51
^{129}I	$1.6\ 10^{7}$	169	$6.5\ 10^{6}$	$2.4\ 10^{-8}$	81.2	208
^{135}Cs	$2.3\ 10^{6}$	1312	$4.2\ 10^{7}$	$1.9\ 10^{-9}$	37.2	3521
Minor actinides						
^{237}Np	$2.1\ 10^{6}$	434	$2.6\ 10^{7}$	$1.0\ 10^{-6}$	100	434
^{241}Am	$4.3\ 10^{2}$	217	$1.3\ 10^{11}$	$1.2\ 10^{-6}$	66.8	325
^{243}Am	$7.4\ 10^{3}$	102	$7.4\ 10^{9}$	$1.2\ 10^{-6}$	31.4	325
^{245}Cm	$8.5\ 10^{3}$	1.2	$6.3\ 10^{9}$	$1.2\ 10^{-6}$	4.7	25.5
Activation products						
^{59}Ni	$7.5\ 10^{4}$	36.1	$3.0\ 10^{9}$	$5.4\ 10^{-11}$	--	36.1
^{63}Ni	$1.0\ 10^{2}$	6.6	$2.1\ 10^{12}$	$1.5\ 10^{-10}$	--	6.6
^{94}Nb	$2.0\ 10^{4}$	4	$6.9\ 10^{9}$	$1.4\ 10^{-9}$	--	4

The objectives of separative chemistry research connected with the SPIN program are listed in Table 2.

Table 2. Research objectives in separation processes [6]

Nature of the objectives	Importance
° Am separation (99 %)	Very important
° Ability for reprocessing	
° MOx (LWR, FNR)	Very important
° Am targets (FNR ?)	Very important
° Cm, Pu, Np separation (99 %)	Important
° Ability for reprocessing	
° Fuels with Np (FNR ?)	Important
° Cm targets (FNR ?)	Important
° Long-lived F.P. separation	Secondary

3. SEPARATION OF LONG-LIVED RADIONUCLIDES

3.1. Strategy

Before presenting the strategic guidelines concerning the separative methods to be developed for some of the long-lived radionuclides mentioned above, it is essential to review the behavior of these materials in current nuclear fuel reprocessing operations. Table 3 presents this information for the specific case of COGEMA's UP3 plant at La Hague.

Table 3. Behavior of some long-lived radionuclides at COGEMA's UP3 plant at La Hague [4]

Long-lived radionuclide	Behavior
Minor actinides	
^{237}Np	° 70 to 90 % extracted in the first U+Pu co-extraction cycle ° Np extracted separated in second U cycle ° All the Np is finally mixed with FP
$^{241,243}Am$, ^{245}Cm	° Not extracted, remains with FP
$^{239\text{ to }242}Pu$	° 0.12 % of losses with wastes
Fission products	
^{99}Tc	° $\simeq$ 30 % of Tc is insoluble in fuel dissolution ° Soluble Tc is co-extracted with Zr(IV) and then Pu(IV) (and U(VI)) in the first U+Pu co-extraction cycle, and then separated by special washing and mixing with FP
^{135}Cs	° Not extracted, remains with FP

In consequence, the separation strategies adopted are divided into two categories.

* Definition of operating conditions of the PUREX process (in the broad sense of the term) for the separation of some long-lived radionuclides. This strategy concerns ^{237}Np and ^{99}Tc. It could also be applied to ^{93}Zr and ^{129}I.

* Definition of specific separation processes. This concerns $^{241,243}Am$, ^{245}Cm and ^{135}Cs.

Due to its outstanding ability to solve separation problems in the nuclear industry, all the processes investigated are based on liquid/liquid extraction. For the difficult separation of

americium and curium, the process being investigated has several cycles involving different extractants, whereas cesium can be separated using a single extractant.

3.2. Separation of long-lived radionuclides using the PUREX process

^{237}Np

As stated above, most of the neptunium is extracted in the first U+Pu co-extraction cycle (1CUPu) applied at the UP3 plant in La Hague, and this fraction of extracted neptunium is mainly separated in the second uranium purification cycle (2CU). Hence the current research objective is to determine the physicochemical conditions of the PUREX process required to boost the neptunium extraction yield in 1CUPu. Two types of study are undertaken in this program : consolidation of the PAREX code used to predict the behavior of neptunium in the different steps of the PUREX process, and especially in the 1CUPu and 2CU cycles, and experimental investigations, in the laboratory, aimed to consolidate the knowledge of the redox reactions between the Np(V)/Np(VI) and HNO_2/HNO_3 pairs, and, in a test loop, to qualify the PAREX code for the behavior of neptunium. One may well ask why new studies appear necessary for the new objective, whereas the behavior of neptunium in the PUREX process has been investigated for many years. The answer is that the objectives previously assigned were chiefly aimed to prevent the uranium and plutonium end products from being polluted by neptunium, so that only an "overall" knowledge of neptunium behavior was then necessary, whereas the new objective implies a much closer understanding of this behavior.

The equation of the basic reaction allowing a "rough" interpretation of neptunium behavior in 1CUPu is the oxidation of Np(V) to Np(VI) by nitric acid, a reversible reaction catalysed by nitrous acid produced by reaction.

$$NpO_2^+ + 3/2H^+ + 1/2NO_3^- \Leftrightarrow NpO_2^{2+} + 1/2HNO_2 + 1/2H_2O \qquad (1)$$

This reaction, which has been investigated for many years by Siddall and Dukes [7], Swanson [8] and Moulin [9], does not yet appear to have revealed all its aspects. One unanswered question is its kinetics in the presence of highly concentrated uranyl nitrate and of the solvent.

Valid methods nevertheless appear to be developing : increasing the temperature and the nitric acidity during extraction in 1CUPu should help to achieve the objective of quantitative neptunium extraction in 1CUPu without requiring the addition of a special reagent to oxidize the Np(V). This also represents the analysis of Yamana [10].

^{99}Tc

The behavior of technetium present in the fuel dissolution liquor (which accounts for about two-thirds of the Tc inventory of irradiated fuel) is unusual (in comparison with the other metallic species) during the operations of the PUREX process. The technetium exists in solution in oxidation state VII, in the form of the TcO_4^- ion. In this form, Tc(VII) is co-extracted with Zr(IV) (Tc(VII) playing an identical role to that of the nitrate anions), and then with Pu(IV) and U(VI) after washing of the Zr(IV) contained in the solvent. It is then possible to transfer Tc(VII) to the aqueous phase by washing with concentrated nitric acid (NO_3^-/TcO_4^- competition effect) [11]. The behavior of the soluble fraction of Tc can therefore be considered to be under control. In consequence, research must focus on the understanding of the behavior of Tc in the irradiated fuel dissolution step, in order to identify simple methods that can be used to make the solubilization of the Tc quantitative. Investigations currently under way are designed to determine the precise metabolism of the Tc in the overall PUREX

process which is a problem due to analytical difficulties, and to improve the Tc dissolution yield from the dissolution residues.

3.3. Separation of long-lived radionuclides with new processes

3.3.1. Minor actinides

Assuming the implementation of an "intensive reprocessing" strategy, the high-level raffinate leaving the "modified" 1CUPu(Np) will only contain, as actinides, in addition to traces of uranium, neptunium and plutonium, the entire fuel inventory of americium and curium. The CEA is investigating two types of process to extract and separate these minor actinides from the FP : the first is based on the extraction of the actinides in their stable oxidation state in nitric medium, i.e. An(III), and the second process is mainly concerned with the separation of americium, and is based on its selective oxidation to Am(IV) or Am(VI) in the presence of a heteropolytungstate ligand, followed by selective extraction (SESAME process).

A common feature of these two processes is that, if they are applied directly to the raffinate from the PUREX process, after being subjected to a minimal modification of its composition. No decrease in the nitric acidity of the effluent is in fact intended, for preventing any risks of undesirable FP precipitation. In the first process, it is necessary to use several extraction cycles to achieve the objectives : first co-extraction cycle of minor actinides by the DIAMEX process (DIAMide EXtraction), applied to the raffinate from the PUREX process. In this step, the lanthanides (Ln(III)), which account for about one-third of all the FP, are co-extracted, and the mixture of An(III) + Ln(III) is obtained, free of strongly hydrolysable ions, such as traces of Pu(IV) and U(VI). The second An(III)/Ln(III) separation cycle uses an extractant with a nitrogen donor atom, such as the alkyl derivatives of tripyridinetriazine or picolinamides, allowing their separation by selective extraction of An(III) the least abundant metallic entities, so that only a minimal extraction capacity is required from the solvent. The third Am/Cm separation cycle could be applied either by the DIAMEX process or by the SESAME process. Note also that, for the first process, all the reagents to be employed (extractants, diluents, chelatant reagents present in aqueous solution) will display the feature of being totally incinerable into gases releasable into the environment, thus helping to eliminate any generation of secondary solid waste. Consequently, these reagents will consist exclusively of C, H, N and O atoms.

DIAMEX

The extraction of the An(III) (Am and Cm) from the high-level raffinate produced by the PUREX process is difficult because of the low extraction capacity of the An(III) nitrates and by the high concentration of nitric acid, which induces strong competition in the extraction of the An(III) nitrates. The diamide extractants, proposed by Musikas [12], and particularly those belonging to the sub-class of malonamides, which have a single carbon that forms a bridge between the two amide groups, offer a solution to this problem of extraction. With the general formula $(RR'NCO)_2CHR''$, where R, R' and R" are alkyl or oxyalkyl radicals, these compounds are bidentate oxygen donors, forming an extremely stable six-link ring with the metallic ion. The extraction mechanism essentially concerns the extraction of neutral molecules, and corresponds to the following equation :

$$M^{3+} + 3NO_3^- + \overline{nE} \Leftrightarrow \overline{M(NO_3)_3 E_n} \qquad (2)$$

where E is the diamide extractant (the species present in organic phase are overlined).

The value of n, the number of diamide molecules solvating the An(III) nitrate, is two at saturation of the organic phase. However, using the conventional slope method, the value of n found exceeds two, reflecting the non-ideality of the organic solutions of diamide, an occurrence often encountered in the extractive chemistry of the amides.

For a given extractant concentration in the organic phase, the direction and intensity of An(III) transfer is governed by the nitrate ion concentration in the aqueous phase : at high concentration, the affinity of the solvent is high and hence allows the extraction of the An(III) nitrates (and especially of the U(VI) and Pu(IV) nitrates, which are generally better extracted), whereas, at low nitrate ion concentrations (in the form of HNO_3), the affinity of the solvent for An(III) nitrates is weak. This makes it possible to define an An(III) extraction/stripping cycle. Diamides, which are oxygenated donors ligands, consequently have extractive properties for Ln(III) which are similar to those displayed for An(III) nitrates. Since the Ln(III) concentration in the raffinates to be processed is fairly high (~ 10^{-2} mol/l), and since the diamide can also extract a large quantity of nitric acid, it was necessary to examine the third phase mechanism (i.e. demixing of the organic phase after extraction of macro-concentrations of solutes). Note also that the organic diluent selected for the DIAMEX process is TPH (hydrogenated tetrapropylene), an aliphatic diluent used at La Hague for the PUREX process. To minimize third-phase mechanisms during the extraction of nitric acid and metallic nitrates (chiefly Ln(III)) by organic solutions of diamide in TPH, it was decided to adjust the structure of the diamide extractant by varying the R, R' and R" radicals. Thus the diamide serving as the present basis for the development of the DIAMEX process, dimethyldibutyltetradecylomalonamide (DMDBTDMA), with the semi-developed formula :

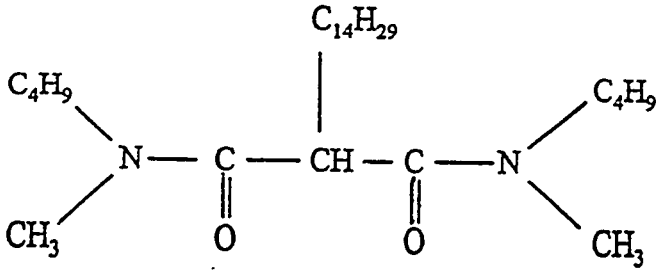

(3)

displays acceptable properties for this requirement. For example, the load limits at 21°C of a solution of 0.65 mol/l of DMDBTDMA in TPH are equal to 5.7 mol/l for aqueous nitric acidity, and 0.041 mol/l for organic Nd(III) nitrate in the presence of an aqueous 4 mol/l nitric solution.

The diamide was therefore selected for the development of a first version of the DIAMEX process. The first active tests of the DIAMEX process took place in June 1993 and concerned the treatment of a high-level raffinate produced by the reprocessing of an MOx fuel. The objectives set for the three active tests were essentially achieved, demonstrating the feasibility of the process [13].

Research currently under way in this area concerns :

* optimization of the diamide extractant formula to improve its properties with respect to third-phase mechanisms and solvent degradation/regeneration,
* consolidation of the first version of the DIAMEX process, based on the use of DMDBTDMA : studies are currently under way on the development of washing methods of Mo(VI) and Zr(IV) from loaded solvents, on the selective chelation of Ru to prevent its extraction, and on the hydrolytic and radiolytic stability of the solvents.

An(III)/Ln(III) separations

After the DIAMEX process is applied, the An(III) is present in the aqueous dilute nitric acid solution mixed with the Ln(III), which are much more abundant because the molar ratio R = number of moles of Ln/number of moles of An is close to 50. An elegant process for An(III)/Ln(III) separation must therefore permit the selective extraction of An(III). To simplify the industrial implementation of such a process, it seems important for this separation to be feasible using aqueous solutions with fairly high nitric acidity (0.2 to 0.5 mol/l), to overcome problems such as the hydrolysis of traces of metallic species contaminating the An(III)/Ln(III) mixture. This separation problem is made even more acute because of the choice to use exclusively reagents that are totally degradable into gas. To achieve this difficult separation, it seems indispensable to pick extractants that have one or more nitrogen donor atoms, which display greater affinity for An(III) than for Ln(III), and which are capable of forming chelates, in order to guarantee a sufficient affinity of the solvents for the An(III) salts.

Two types of system are being investigated.

The first is based on the use of derivatives of tripyridinetriazine R_3TPTZ [14], answering to the following semi-developed formula :

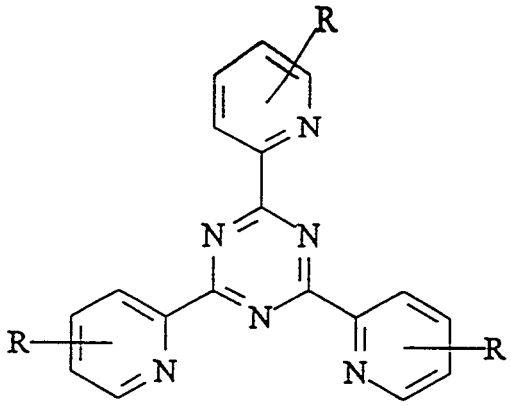

(4)

To be effective, the extractant R_3TPTZ must be employed in synergistic combination with an HA acid extractant, a source of more lipophilic anions than nitrate ions. The extraction equation is then written :

$$M^{3+} + \overline{nB} + \overline{3HA} \Leftrightarrow \overline{MB_nA_3} + 3H^+ \qquad (5)$$

The current research direction, pursued jointly with the team of Dr. M.J.Hudson of the University of Reading (UK), concern the synthesis of alkyl derivatives of TPTZ that are sufficiently hydrophobic and the synthesis of HA acids with low pK_a.

The second system concerns the use of picolinamide extractants, answering to the following general semi-developed formula :

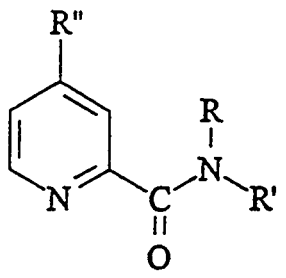

(6)

As demonstrated by Cordier [15], pyridine 2 carboxamide, for which R, R' and R" = H, a soluble reagent in the aqueous phase, is a selective chelatant of Am(III) with respect to Nd(III). The grafting of alkyl groups, R, R' and R", helps to reinforce the lipophilic properties of the molecules and accordingly to enhance their ability as selective extractant for An(III).

The extraction equation is written :

$$M^{3+} + 3NO_3^- + \overline{nE} \Leftrightarrow \overline{M(NO_3)_3 E_n} \qquad (7)$$

Current research directions in this area are aimed to strengthen the affinity of picolinamides for An(III) nitrates, particularly in order to counteract the strong competition due to the extraction of nitric acid.

SESAME (Selective Extracting Separation of Americium by Means of Electrolysis)

Another alternative to separate americium, either directly form the raffinate produced by the PUREX process, or from the An(III)/Ln(III) mixture produced by the DIAMEX process, or even from the Am(III)+Cm(III) mixture, consists of its selective oxidation to Am(IV) or Am(VI) followed by its extraction. The chief difficulty to be overcome in this connection is the oxidation of Am(III) in nitric medium with acidity greater than 1 mol/l. In the case of the Am(III)/Am(IV) pair, in fact, this impossibility is thermodynamic (E_0 Am(III)/Am(IV) = 2.6 V/NHE), whereas it is rather kinetic in the case of the Am(III)/Am(VI) pair. By contrast, it is possible to oxidize Am(III) by chemical or by electrochemical means, subject to the presence in aqueous solution of a powerful ligand belonging to the heteropolytungstate family. For example, the ligand $P_2W_{17}O_{61}^{10-}$ is extremely effective for this purpose. Present in a concentration higher than of Am(III), it allows the oxidation of the americium to Am(IV), whereas for molar ratios lower than 1, the americium is oxidized to Am(VI). Other heteropolytungstate ligands are also satisfactory, such as silicotungstates. After oxidation, the americium can be extracted, either by amine salts in the case of Am(IV), or by bis-2,6 dimethyl-4 heptyl phosphoric acid for Am(VI). In these conditions, neither the lanthanides (except for cerium) nor the curium is oxidized, and is therefore easily separated from the americium. This is the basis of the SESAME process [16].

Active tests of the SESAME process are currently under way at Fontenay-aux-Roses, on raffinates from the PUREX process, and on an An(III)/Ln(III) mixture generated in 1993 during active tests of the DIAMEX process.

3.3.2. Fission products

Among the long-lived fission products that need to be separated, only ^{135}Cs is now the subject of intensive study at the Cadarache Nuclear Center, for the definition of a separation process. The extractant molecule expected to permit the separation of Cs(I), either from a 1 mol/l nitric acid solution, concentrated with sodium nitrate (4 mol/l), like the solution

generated by evaporation processes for radioactive effluents, or a high-level raffinate produced by the application of the PUREX process, has been selected in the family of calixarenes. These molecules, in the form of a calix (hence their name) are pre-organized structures which, by the grafting of adequate functional groups, either on the upper rim or on the lower rim of the structure, help to define specific chelatants for ionic species considered as targets. The use of these substituents also makes it possible to impart hydrophilic or lipophilic properties to the molecules, thus enabling them to act as chelatants or extractants. The research project, conducted jointly with several European universities under a contract with the CEC, consisted of a screening of the different synthesized calixarenes for their aptitude for Cs(I)/Na(I) separation followed by the extraction of Cs(I) from nitric solutions. Spectacular performance was observed in these two areas with the following calixarenes : mono-ring calix[4]arenes and bis-ring-n calix[4]arenes. Very high separation factors $SF_{Cs/Na}$ close to 4.10^4 were obtained with certain molecules[17]. These molecules lend themselves well to extraction in the form of supported liquid membranes (SLM), which therefore help to perform separations with a very small quantity of extractant.

Research under way at Cadarache in this area is concerned with :

* the demonstration of the feasibility of the extraction of ^{135}Cs (in a mixture with the other cesium nuclides) from a high-level effluent produced by the PUREX process,
* the search for specific calixarenes for the minor actinides, allowing selective separation of An(III)/Ln(III).

4. CONCLUSIONS

Studies under way at the CEA in connection with the SPIN program aimed at the separation of long-lived radionuclides for their subsequent nuclear "incineration" (P & T strategy) have yielded promising results, both in the areas of the DIAMEX and SESAME processes, and in the selective separation of cesium. Yet the road is a long one before the definition of the flow diagrams of a facility that would implement these intensive reprocessing technologies. While it is possible to reasonably predict the feasibility of a process such as DIAMEX, this cannot be said of An(III)/Ln(III) separations, which are certainly more difficult to achieve, or of the SESAME and "calixarene" processes, which are still in the basic research or early development stage. It also appears clear that economic considerations will have to be taken into account when the process decisions are made. For the time being, criteria of simplicity and reliability will certainly prevail in these decisions. While it is possible to predict that the chemists will find solutions to these complex problems of long-lived radionuclide separation, it is also clear that considerable efforts will have to be made to develop industrially-viable solutions.

ACKNOWLEDGEMENTS

A portion of the work mentioned in this article was carried out under European contracts of the "Fourth Research Development Programme on the Management and Disposal of Radioactive Wastes" : (*1*) ***DIAMEX, An(III)/Ln(III) separations*** - Contract No. F12W-CT-0112 with the CEA, CEN-Fontenay-aux-Roses (C. Madic), conducted jointly with the University of Reading (UK) (Dr. M.J. Hudson) ; (*2*) ***Calixarenes*** - Contract No. F12W-CT-90 0062 TSTS with the CEN-Cadarache (J-F. Dozol), conducted jointly with the Universities of Belfast (UK) (Professor M.A. McKervey), Parma (Italy) (Professor R. Ungaro), Barcelona (Spain) (Professor L. Lopez Calahorra), Mainz (Germany) (Professor W. Böhmer), Strasbourg (France) (Dr. J. Vicens & Professor M.J. Schwing), and Twente (Netherlands) (Professor D.N. Reinhoudt).

REFERENCES

[1] Ricaud, J-L., "Main Issues of the fuel cycle back-end" in *Proceedings of RECOD'94*, Vol. I, The Fourth International Conference on Nuclear Fuel Reprocessing and Waste Management, London, 24-28 April, (1994).

[2] Rouyer, H., "The french law on R & D at the back-end of the fuel cycle in the nuclear industry. Consequences and effects" in *Proceedings of RECOD'94*, Vol. I, The Fourth International Conference on Nuclear Fuel Reprocessing and Waste Management, London, 24-28 April, (1994).

[3] Kubota, M., "Research activities on the partitioning and transmutation at JAERI under the framework of the OMEGA program in Japan" in *Proceedings of RECOD'94*, Vol. I, The Fourth International Conference on Nuclear Fuel Reprocessing and Waste Management, London, 24-28 April, (1994).

[4] Boullis, B., Personnal communication.

[5] *"Performance Assessment of Geological Isolation Systems for Radioactive Waste, PAGIS"*, Commission of the European Communities, EUR 11775 EN, (1988).

[6] Viala, M., Personnal communication.

[7] Siddall, T.H.III, Dukes, E.K., *J. Am. Chem. Soc.*, 81, 2, 293 (1972).

[8] Swanson, J.L., *B. N. W.*, 1017 (1969).

[9] Moulin, J-P., Rapport CEA, R 4912, (1977).

[10] Yamana, H. "A calculational study on the recovery of Np into Pu nitrate product in the PUREX process" in *Proceedings of RECOD'94*, Vol. I, The Fourth International Conference on Nuclear Fuel Reprocessing and Waste Management, London, 24-28 April, (1994).

[11] Baron, P., Boullis, B., Germain, M., Gué, J-P., Miquel, P., Poncelet, F., Dormant, J-M., Dutertre, F., "Extraction cycles design for La Hague plants" in *Proceedings of GLOBAL'93*, September 12-17, (1993), Seattle, Washington, (USA), vol. I, 63-70, Editors, Am. Nuc. Soc. Inc., La Grange Park, Illinois, 60525 USA.

[12] Musikas, C., *Inorg. Chim. Acta*, 140, 197-206 (1987).

[13] Madic, C., Blanc, P., Condamines, N., Baron, P., Berthon, L., Nicol, C., Pozo, C., Lecomte, M., Philippe, M., Masson, M., Hequet, C. and Hudson M.J., "Actinide partitioning from high level liquid waste using the DIAMEX process" in *Proceedings of RECOD'94*, Vol. I, The Fourth International Conference on Nuclear Fuel Reprocessing and Waste Management, London, 24-28 April, (1994).

[14] Vitart, X., Musikas, C., Pasquiou, J-Y. and Hoel, P., *Journal of the Less Common Metals*, 122, 275-286 (1985).

[15] Cordier, P-Y., Condamines, N., Berthon, L. and Madic, C., "New molecules for the separation of actinides (III) : the picolinamides" in *Proceedings of the "Journées des Actinides"*, Obergurgl (Austria), April 15-19, (1994).

[16] Adnet, J-M., Brossard, P. and Bourges, J., "The selective extraction of oxidized minor actinides ; a possible route for the ACTINEX program", in *Proceedings of GLOBAL'93*, September 12-17, (1993), Seattle, Washington, (USA), vol. II, 1008-1014, Editors, Am. Nuc. Soc. Inc., La Grange Park, Illinois, 60525 USA.

[17] Hill, C., "Applications des calixarènes fonctionnalisés au traitement des effluents radioactifs par membranes liquides supportées", Thèse de Doctorat, Université L. Pasteur, Strasbourg (France), 20 Mai, (1994).

Electrochemical Separation of Actinides and Fission Products in Molten Salt Electrolyte

R. L. Gay, L. F. Grantham, S. P. Fusselman, D. L. Grimmett, and J. J. Roy
Rockwell International/Rocketdyne Division
Canoga Park, CA 91309-7922

Abstract. Molten salt electrochemical separation may be applied to accelerator-based conversion (ABC) and transmutation systems by dissolving the fluoride transport salt in LiCl-KCl eutectic solvent. The resulting fluoride-chloride mixture will contain small concentrations of fission product rare earths (La, Nd, Gd, Pr, Ce, Eu, Sm, and Y) and actinides (U, Np, Pu, Am, and Cm). The Gibbs free energies of formation of the metal chlorides are grouped advantageously such that the actinides can be deposited on a solid cathode with the majority of the rare earths remaining in the electrolyte. Thus, the actinides are recycled for further transmutation.

Rockwell and its partners have measured the thermodynamic properties of the metal chlorides of interest (rare earths and actinides) and demonstrated separation of actinides from rare earths in laboratory studies. A model is being developed to predict the performance of a commercial electrochemical cell for separations starting with PUREX compositions. This model predicts excellent separation of plutonium and other actinides from the rare earths in metal-salt systems.

INTRODUCTION

The development of accelerator-based conversion and transmutation systems will require actinide and fission product separation technology for head-end preparation of spent fuel and for processing of the ABC salt. The separation of rare earths from actinides is an important step in enabling transmutation technologies to be successful. The presence of rare earth fission products acts as competition for the transmutation neutrons and increasing concentration of rare earths lowers the efficiency of the transmutation process. Rockwell International, together with the Univ. of Missouri, the Central Research Institute of Electric Power Industry (of Japan), and Kawasaki Heavy Industries, has been developing a molten salt separation process for PUREX waste over the past six years. This process, called TRUMP-S (TRansUranic Management by Pyropartitioning Separation), is a pyrochemical waste management process that uses a series of processing steps to achieve a final electrolytic separation of actinides from fission products in molten eutectic LiCl/KCl solution. Molten salt electrolytes are attractive due to their radiation resistance and stability, especially as compared to organic and aqueous solutions. The TRUMP-S process is shown schematically in Fig. 1.

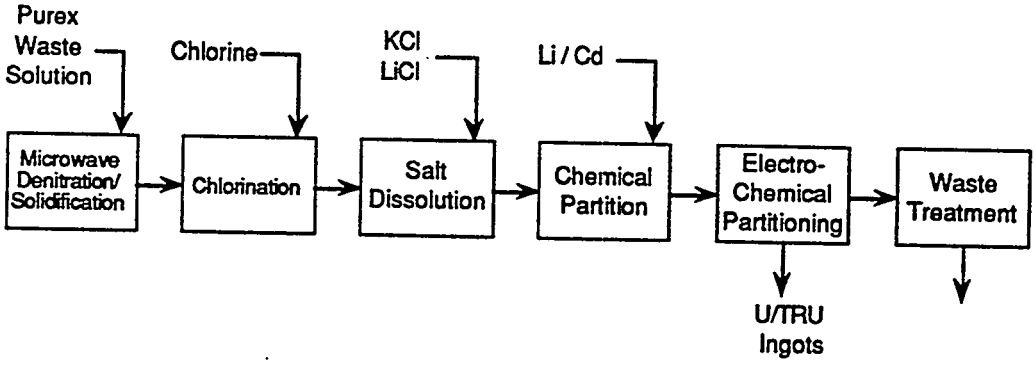

Fig. 1. Diagram of the TRUMP-S process for separating actinides and rare earth fission products

TRUMP-S is designed to take the nitrate residues from PUREX processing and convert the nitrates to oxides by microwave denitration. The oxides are catalytically converted into chloride salts and mixed with lithium metal for an initial separation of the more noble elements. The resulting chloride mixture consists of fission product rare earths (La, Nd, Gd, Pr, Ce, Eu, Sm, and Y) and actinides (U, Np, Pu, Am, and Cm). The LiCl/KCl eutectic is used as the electrolyte for electrochemically separating the actinides from the rare earths. The Gibbs free energies of formation are grouped advantageously such that the actinides can be deposited on a solid cathode with the majority of the rare earths remaining in the electrolyte. Thus the cathodes containing the actinides are removed and the actinides are recovered for further treatment. In an ABC system this treatment would consist of further transmutation by accelerator-based conversion.

CHEMICAL THERMODYNAMICS

Electrochemical separation of the rare earths from the actinides is attractive because a natural separation of potentials occurs for the chlorides of these elements. These potentials are related directly to the Gibbs free energy of formation by Equation (1).

$$\Delta G_f^\circ = -nFE^\circ \tag{1}$$

As shown in Fig. 2, the rare earth fission products are grouped together, as are the actinides. A potential difference of about 150 mV separates the closest rare earth (Gd) from the nearest actinide (Am).

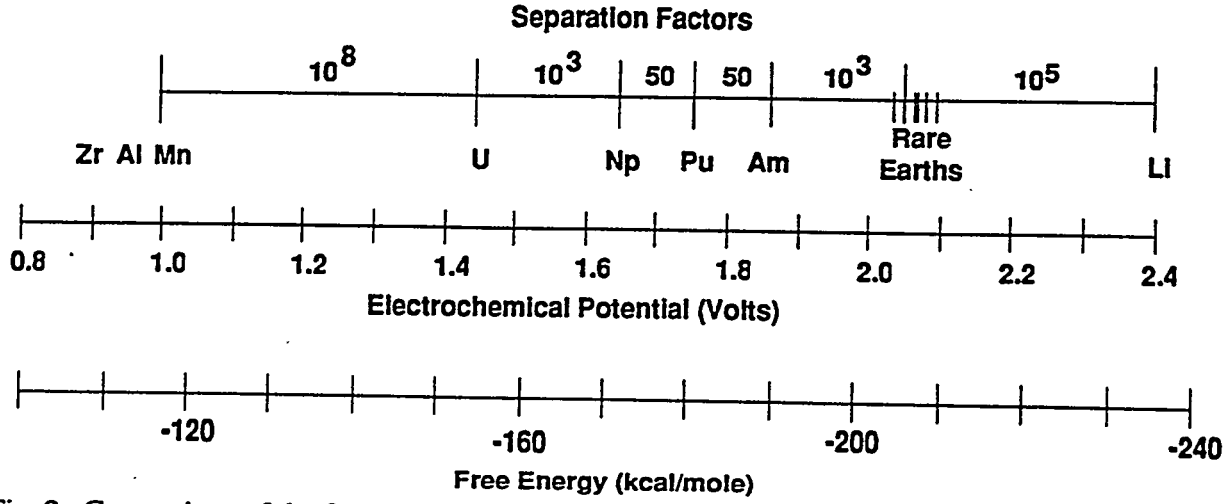

Fig. 2. Comparison of the free energies of formation of actinide and rare earth chlorides indicating the natural grouping of the elements

The electrochemical potential of the elements can be related to concentration by the Nernst equation, Equation (2).

$$E = E^\circ_{MCl_3} + \frac{RT}{nF}\ln X_{MCl_3} + \frac{RT}{nF}\ln \gamma_{MCl_3} \tag{2}$$

The metals are assumed to form trichlorides (the americium and the rare earths actually form both trivalent and divalent states), and the standard potential refers to a hypothetical supercooled liquid reference state where mole fraction =1 and activity coefficient = 1. The potential in a cell, E, is related to both mole fraction X and activity coefficient γ. The Nernst equation can be used to

predict that a theoretical equilibrium separation of an order of magnitude (a factor of 10) can be achieved for every 48 mV difference in potential for trivalent ions of equal concentrations at 723 K. The actual separation in molten salt processing can be enhanced by careful selection of solvent composition, temperature and process conditions. For some of the actinides, especially uranium and plutonium, separation by many orders of magnitude appears feasible due to the large potential separation from the nearest rare earth fission product.

MEASUREMENT CAPABILITIES

In order to determine the feasibility of developing an electrochemical separation process using molten salts, it became necessary to redetermine the potentials of lanthanide and actinide metal chlorides in LiCl-KCl eutectic. A comprehensive list of the standard potentials for most of the metal chlorides as measured at 723 K (450 C) existed [1], and thermodynamic values of the standard free energies of formation based on thermal data were also available [2]. However, we found sufficient discrepancies between the electrochemical data and thermal data that meaningful evaluation of the TRUMP-S separation concept could not be made. Together with our partners, we constructed laboratories and developed the techniques needed to make these new measurements under carefully controlled conditions.

Experimental Facilities

Measurements were made using small scale electrochemical cells located in high-purity argon glove boxes[3]. Cell designs and experimental techniques were developed at Rockwell's Los Angeles laboratories using non-radioactive materials. These designs and techniques were used at the University of Missouri, Columbia in a specially-designed alpha laboratory for actinide testing located at the Missouri University Research Reactor (MURR). The test conditions at both locations were extremely well-controlled. The argon atmosphere in the glove boxes was continually purified and contained less than 0.1 ppm O_2, 0.01 ppm H_2O, 10 ppm H_2, and 10 ppm N_2. The temperature of the electrochemical cell was controlled by proportional controllers to a fixed set point (usually in the range of 400 to 500 C), and a large copper block around the cell assured isothermal conditions. Equilibrium potentials were typically recorded when temperature changed less than 0.1 C and the potentials changed less than 0.5 mV over a 15-minute period. The laboratory at Rockwell was equipped with an ICP-AES (inductively-coupled plasma atomic emission spectrometer), scanning electron microscope, and X-ray diffractometer for aid in analysis. The MURR alpha laboratory had a dedicated ICP-AES for analysis of actinides, rare earths, and solvent salts.

Several cell designs were developed. Most non-radioactive measurements were made in a cell containing approximately 50 g of electrolyte and 100 to 1000 mg of active metal chloride. Radioactive measurements used a small cell with about 5 g of electrolyte and up to 50 mg of active metal chloride. The small cell design minimized the exposure to personnel and allows many tests to be performed with a very small inventory of actinide material.

Experimental Results

Thermodynamic Data

Rockwell and its partners measured the Gibbs free energies of formation of the metal chlorides of interest (rare earths and actinides), the activity coefficients of the metal chlorides in the molten salt, and performed separation measurements of rare earth-actinide mixtures [4-7]. The rare earth fission products expected to be of significant concentration are lanthanum, neodymium, gadolinium, praseodymium, cerium, europium, samarium, and yttrium. The actinides of interest are uranium, neptunium, plutonium, americium, and curium. Tests were performed with all of the above elements except for curium (due to extreme cost).The elements expected to be of most importance in separating PUREX residues are neodymium and americium. Significant differences

in literature data were found for yttrium, neodymium, neptunium and americium. The lanthanides were also found to exhibit some divalent character in the LiCl-KCl solvent. Good agreement was found between measurements for uranium and plutonium and literature data. The chemistry of americium was extremely important for development and evaluation of the TRUMP-S process. Literature data was unclear regarding the divalent and trivalent character of Am in LiCl-KCl. We have resolved this chemistry by making cyclic voltammetry measurements which show the existence of both valence states. These voltammetry measurements also provide values for the potentials of the divalent and trivalent reactions. An example of cyclic voltammetry of Am is shown in Fig. 3.

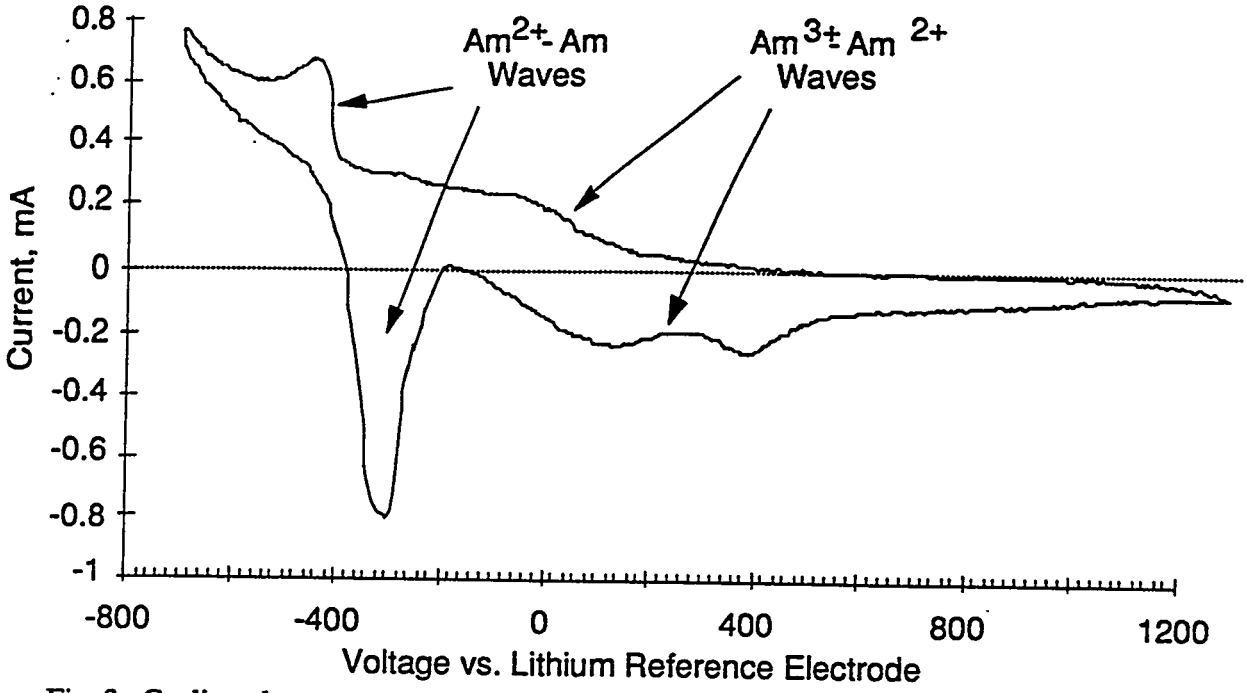

Fig. 3. Cyclic voltammetry measurements of americium showing the divalent and trivalent character of americium chemistry

Separation Studies

In order to evaluate the feasibility of using molten salt electrochemistry to separate the actinides from rare earths the TRUMP-S testing is now focusing on separation studies.The two rare earths expected to be nearest in potential and concentration to the actinides are neodymium and gadolinium. Electrodeposition tests have been made of the individual actinides U, Pu, Np, and Am in mixtures of $NdCl_3$ and $GdCl_3$ in an electrolyte of LiCl-KCl [8]. The actinides were collected on solid cathodes in these tests. Initial and final concentrations of actinide, Gd, and Nd indicate that depletion of about 99% of the actinides is possible. The ratio of uranium to gadolinium or neodymium on the cathode in these tests was consistently greater than 100. The ratios of neptunium and plutonium were progressively less. This ordering, U>Np>Pu>Am, is consistent with the measured ordering of potentials from our thermodynamic data. These tests confirmed the feasibility of electrochemical separation. Further work is in progress with more complex mixtures and optimization of the deposition techniques.

Modeling

TRUMP-S testing has been accompanied with development of an analytical model to aid in application of the process to complex actinide/rare earth mixtures, to assist in design of the experiments for improved performance, and to better understand the physical processes taking place. The model has been anchored by comparison to test data. Table 1 below shows a comparison of predicted and measured separations for Gd/La, Pr/La, and U/Gd mixtures. Very good agreement was found in this comparison.

Table 1. Comparison of TRUMP-S Separations--Model and Experiment

Element Pairs	Model	Experiment
Gd/La	76	72
Pr/La	22	20
U/Gd	10E+13	>200[a]

[a]Exceeded analytical limit

The TRUMP-S model was applied to the residues from PUREX processing of spent nuclear reactor fuel. The results of this modeling are shown in Fig. 4. The results predict nearly 100% removal of U, Np, and Pu from the electrolyte. Americium and curium are removed more slowly but still over 99% removal is predicted before significant rare earth deposition begins. Americium is predicted to be the most difficult element to separate from the rare earths in the electrolyte.

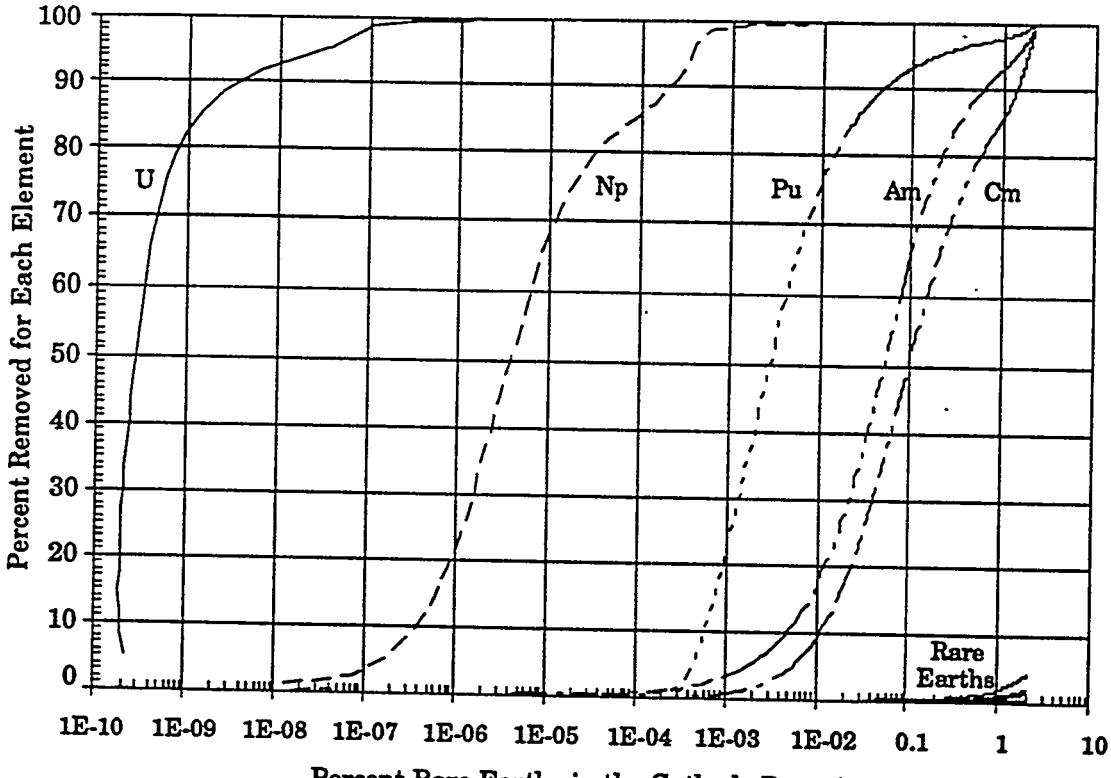

Fig. 4. Modeling of TRUMP-S treatment of PUREX residue indicating separation of actinides from rare earths

APPLICATION TO ABC SYSTEMS

PUREX residues contain larger concentrations of uranium, neptunium, and rare earth fission products than expected in the transport salt from ABC processing of plutonium. The majority of ABC salt is the carrier salt consisting of $LiF\text{-}ZrF_4$, which may contain BeF_2. Actinides and rare earths are dissolved in small concentrations in the transport salt. The ABC salt from 10 years of conversion treatment is expected to contain 10^{-5} to 10^{-6} mole/L of U and Np. However, the concentrations of plutonium, americium and curium will be larger than typical PUREX residue. These three elements are expected to be in the 10^{-2} moles/L range. Typical concentrations of rare earth fission products in 10-year ABC salt are significant, with La, Ce, Nd, Pr, Gd, and Sm in the 10^{-2} mole/L range. Thus, separation of rare earths from the actinides will be necessary and potentially difficult. The high concentrations of Am and Cm, due to neutron capture, may increase this difficulty.

The actinides and rare earths in ABC salt will be present as fluoride salts. The fluorides may be dissolved in LiCl-KCl eutectic solvent salt as a means of performing electrochemical separation similar to TRUMP-S. (The fluorides may slightly change the potentials of the various elements. Further studies would be needed to examine this effect.) The solution of fluorides and chlorides will behave predominantly as a chloride mixture. The TRUMP-S model was applied to the expected ABC salt from 10 years of conversion. The results of this modeling are shown in Fig. 5. The modeling shows that cathodes containing approx. 99% Pu can be recovered with less than 0.001% rare earth content. As deposition continues the americium and curium will deposit and rare earths will begin to deposit. Since process parameters affect separation, this model is only an indication of the possible results. Significant separation of the actinides from the rare earths is predicted.

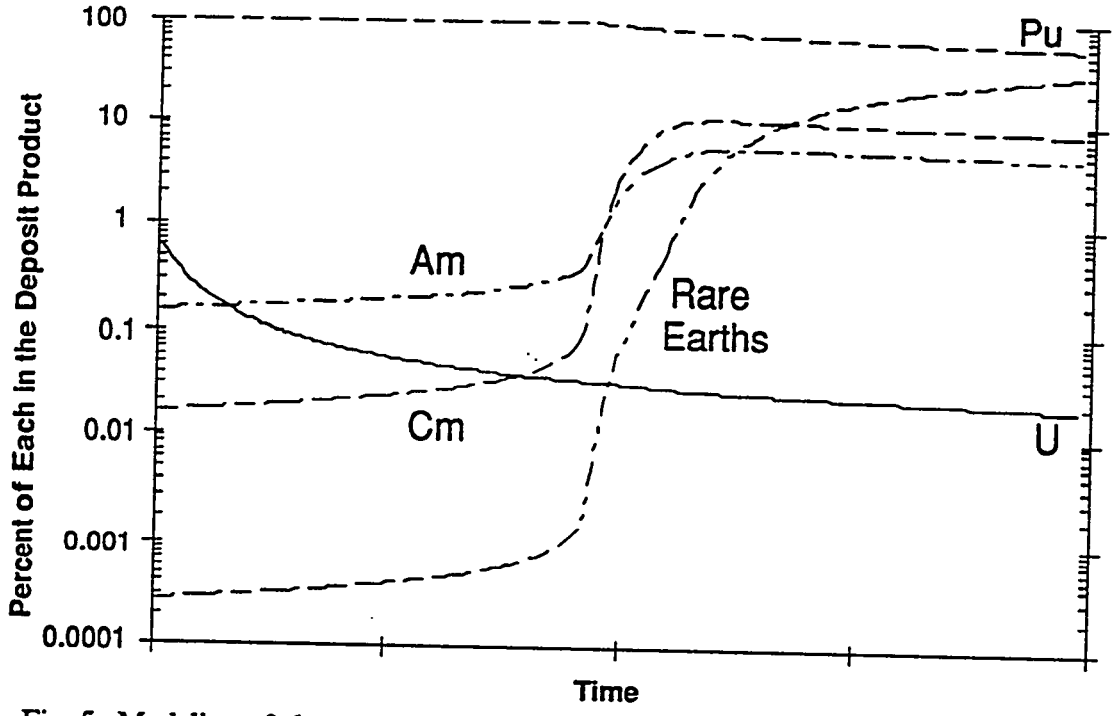

Fig. 5. Modeling of electrochemical separation of accelerator-based conversion salt

CONCLUSIONS

Molten salt electrochemistry holds promise for providing the necessary separation needed for ABC systems. Rockwell and its partners are developing a process for treatment of PUREX

residues, called TRUMP-S, for actinide-rare earth separation in LiCl-KCl solvent. The laboratories, hardware, measurement techniques and analytical models of TRUMP-S may be applicable to ABC needs. Application of TRUMP-S results through its analytical model indicates that excellent separation of plutonium and other actinides may be accomplished. Much further work is needed to confirm these predictions.

ACKNOWLEDGMENTS

Financial support for TRUMP-S was received from Kawasaki Heavy Industries, Ltd. and the Central Research Institute of the Electric Power Industry of Japan.The US Department of Energy provided the actinide metals. This project was made possible through the cooperation of the Missouri University Research Reactor staff.

REFERENCES

[1] Plambeck, A., *Encyclopedia of Electrochemistry of the Elements*, New York: Marcel Decker, Inc., 1976, Chapter X.

[2] Pankratz, L.B., *Bulletin 674*, U. S. Bureau of Mines, Albany, Oregon (1986).

[3] Roy, J. J., et al., "Standard Potentials of Lanthanide and Actinide Trichlorides in Molten Eutectic LiCl-KCl Electrolyte," *Materials Science Forum* 7 4, 547-554 (1991).

[4] Krueger, C. L., et al., "Standard Potential and Thermodynamic Properties of Trivalent Actinides in LiCl-KCl Eutectic," presented at the 180th Meeting of the Electrochemical Society, Phoenix, Arizona, October 13-18, 1991.

[5] Krueger, et al., "Measurement of the Standard Potential of the Np(III)/Np(0) Couple in LiCl-KCl Eutectic," *J. Electrochemical Soc.* 138, 1186 (1991).

[6] Grimmett, D. L., et al., "Cyclic Voltammetry of Lanthanide and Actinide Chlorides in LiCl/KCl Eutectic," presented at the 183rd Meeting of the Electrochemical Society, Honolulu, Hawaii, May 17-20, 1993.

[7] Grantham, L. F., et al., "The Standard Potential of Am/$AmCl_2$," presented at the 183rd Meeting of the Electrochemical Society, Honolulu, Hawaii, May 17-20, 1993.

[8] Fusselman, S. F., et al., "Separation of Actinides (U, Np, Pu) from Lanthanides (Gd, Nd) Utilizing Electrodeposition in Molten LiCl/KCl Eutectic," presented at the Ninth International Symposium on Molten Salts, San Francisco, California, May 22-27, 1994.

The Extraction of Some Trivalent Elements with Aliquat-336

Anders Landgren, Jan-Olov Liljenzin and Mats Skålberg
Department of Nuclear Chemistry
Chalmers University of Technology, S-412 96 Göteborg, Sweden

Abstract. The extraction behaviour of some trivalent elements in the Aliquat-336-1,3-diisopropyl benzene-nitric acid system has been investigated. For most of the elements a maximum in the distribution ratio occur at about 2 molar nitric acid. At 0.20 molar Aliquat-336 lanthanum attained the highest distribution ratio, about 0.05, of all investigated elements. It was found that nitric acid to a large extent influences the distribution ratio of trivalent elements since it competes with metal nitrate complexes for the extractant molecules. A first approach to a model describing the extraction system is derived.

INTRODUCTION

The way of creating high neutron fluxes by using accelerators has opened new possibilities to transmute the most long lived nuclides in radioactive waste into short lived or stable nuclides. Although high neutron fluxes can be achieved, separation of untransmuted material from transmuted, is necessary. Different separation techniques are discussed, but all have in common that they must achieve a high quantitative as well as a high qualitative separation yield. Losses of untransmuted material to different waste streams cannot be tolerated.

The Los Alamos National Laboratory have suggested a baseline aqueous based separation process using Aliquat-336[1] (tricaprylmethylammonium nitrate) and HDEHP (bis-(2-ethylhexyl) phosphoric acid) as extractants [1], [2], [3]. In the first part of the separation process neptunium, plutonium, technetium and palladium are extracted with Aliquat-336 in diisopropyl benzene from a 2 molar nitric acid solution and in the second part (Reversed Talspeak process) the trivalent elements americium, curium and the lanthanides are extracted from a nitric acid solution with HDEHP.

Not many experiments have been performed in order to investigate the behaviour of trivalent elements in the Aliquat-336-nitrate system. Although trivalent elements are poorly extracted with Aliquat-336, their behaviour in the separation process must be known so that no unexpected enrichment will occur. The extraction of trivalent elements with Aliquat-336 has therefore been studied as an initial part of a project to evaluate the applicability of the Aliquat-336-diisopropyl benzene-nitric acid system in connection with partitioning and transmutation.

THEORY

Aliquat-336 is a quaternary ammonium salt extracting anionic species as ion pairs or neutral species as adducts. The ability of the trivalent elements to form anionic or neutral nitrate complexes in the aqueous phase strongly influences the distribution ratio. Formation of the i:th nitrate complex in the aqueous phase is given by equation (1) where i is an integer greater than or equal to zero. β_0 is by definition equal to 1.

---

[1] In this paper the nitrate form is considered.

$$M^{3+} + iNO_3^- \overset{\beta_i}{\rightleftharpoons} M(NO_3)_i^{3-i} \quad (1)$$

If the extraction is considered as an ion pair formation (equation 2) or as an adduct formation (equation 3) which takes place in the organic phase or at the liquid-liquid interface, different reaction paths are obtained but the same product results. In equations (2) and (3) i is an integer greater than or equal to zero.

$$\overline{iR_3R'N^+} + M(NO_3)_{i+3}^{i-} \overset{\delta_i}{\rightleftharpoons} \overline{(R_3R'N)_iM(NO_3)_{i+3}} \quad (2)$$

$$\overline{iR_3R'NNO_3} + \overline{M(NO_3)_3} \overset{\alpha_i}{\rightleftharpoons} \overline{(R_3R'N)_iM(NO_3)_{i+3}} \quad (3)$$

To form neutral or negatively charged complexes a high nitrate concentration is needed. The solution behaves thus as a non-ideal system and therefore one has to consider activities instead of concentrations when describing the extraction system. Activities are, however, difficult to determine experimentally and they are therefore replaced with concentrations as a first assumption. If it is further assumed that no polynuclear complexes are formed and that the extraction proceeds by the adduct formation mechanism in the organic phase, the distribution ratio for trivalent elements is given by equation (4)

$$D_{M^{3+}} = \frac{\left[M^{3+}\right]_{org,tot}}{\left[M^{3+}\right]_{aq,tot}} = \frac{\sum_{i=0}^{P} \alpha_i \left[\overline{R_3R'NNO_3}\right]^i}{\sum_{i=0}^{N} \frac{\beta_i}{\lambda_3\beta_3}\left[NO_3^-\right]^{i-3}} \quad (4)$$

where α_i is given by equation (3), β_i and β_3 are given by equation (1), λ_3 is the distribution constant for the uncharged trivalent metal nitrate complex between the organic and aqueous phases, N is the maximum number of nitrate ions coordinating to the metal ion in the aqueous phase and P is the maximum number of Aliquat-336 molecules coordinating to the metal nitrate complex in the organic phase.

EXPERIMENTAL

Nitric acid solutions were prepared from concentrated (65 % by weight) nitric acid of analytical grade (J.T. Baker). Nitrate solutions were prepared from lithium nitrate of analytical grade (Fluka) dissolved in distilled water. The organic solutions were prepared by dissolving Aliquat-336 in the nitrate form (Fluka) with 96 % 1,3-diisopropyl benzene (Janssen Chimica). 5 volume-% 1-dodecanol (Merck) was added to the organic solutions as a third phase inhibitor.

The following radionuclides were used in the experimental investigation: ^{46}Sc, ^{59}Fe, ^{114m}In, ^{140}La, ^{141}Ce, ^{142}Pr, ^{147}Nd, ^{147}Pm, ^{153}Sm, ^{152}Eu, ^{241}Am and ^{244}Cm. The radionuclides ^{46}Sc, ^{114m}In, ^{140}La, ^{142}Pr, ^{147}Nd and ^{153}Sm were prepared by neutron irradiation of metal oxides. All radioactive tracer stock solutions were either prepared as or converted to 0.50 molar nitric acid.

3.98 ml of the aqueous phase and 20 µl of the radionuclide stock solution was added to a test tube which always gave a metal concentration less than 0.001 molar. The aqueous phase was allowed to "equilibrate" for one hour, where after 4.0 ml of the organic phase was added to the test tube. After shaking the tube vigorously for five minutes the phases were separated in a centrifuge at about 4000 rpm. A sample of suitable volume was withdrawn from each phase and transferred to a measuring vial. ^{46}Sc, ^{59}Fe, ^{114m}In, ^{141}Ce, ^{147}Nd, ^{153}Sm and ^{152}Eu were analyzed by γ-spectrometry using a HPGe-detector. ^{142}Pr, ^{147}Pm, ^{241}Am and ^{244}Cm were measured by liquid scintillation counting using a LKB WALLAC 1219 RACKBETA. ^{140}La was measured in a NaI(Tl) scintillation detector, Intertechnique model CG-4000. Extraction of nitric acid was investigated by potentiometric titration of hydrogen ions using sodium hydroxide and by analyzing the nitrate concentrations using an ion chromatograph, DIONEX DX-100.

RESULTS

When equal volumes of nitric acid with a concentration larger than 1 molar and pure 0.20 molar Aliquat-336 in 1,3-diisopropyl benzene were contacted with each other, three liquid phases resulted. All experiments must therefore be done by addition of 5 volume-% 1-dodecanol to the organic phase which prohibits the formation of third phase.

Distribution ratios for some trivalent elements as a function of the initial nitric acid

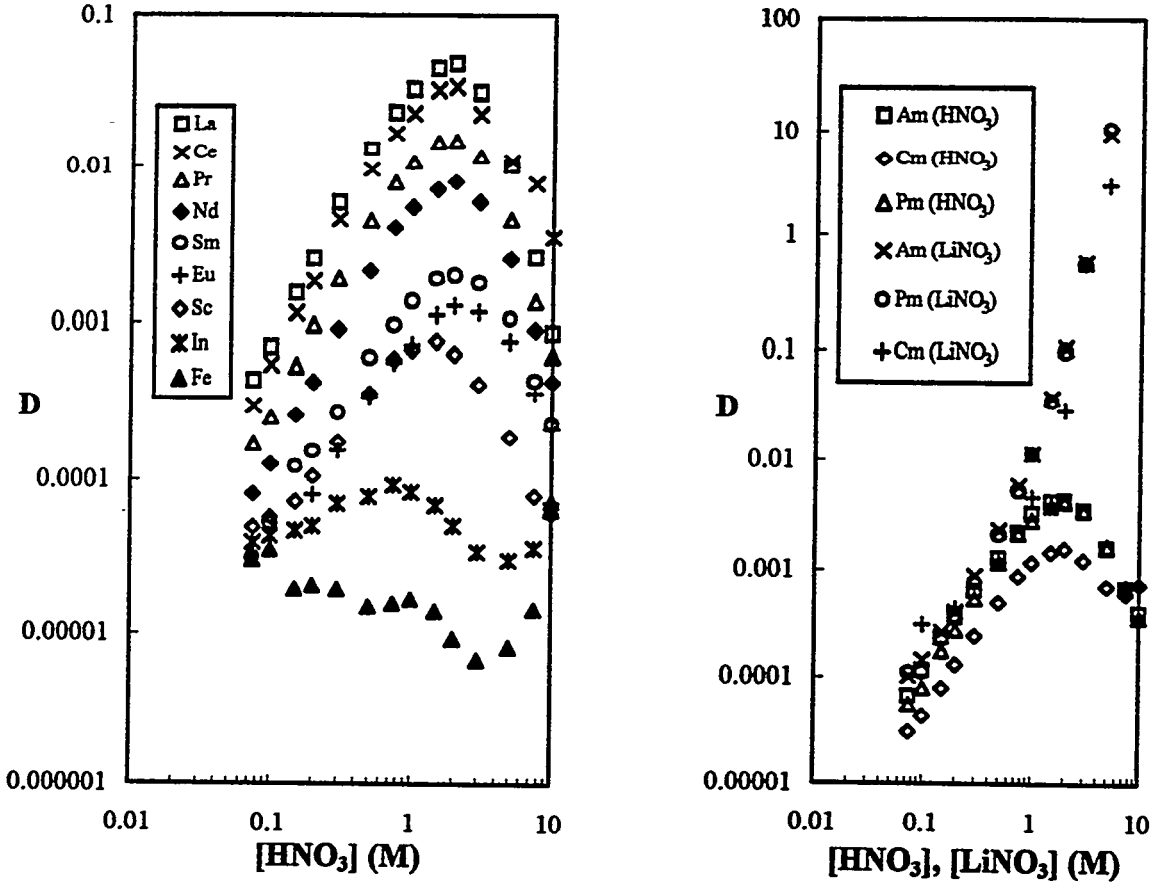

Fig. 1. Distribution ratios for some trivalent elements as a function of the initial nitric acid or lithium nitrate concentration using 0.20 M Aliquat-336 dissolved in 1,3-diisopropyl benzene.

concentration are given in Fig. 1. The distribution ratios obtained when nitric acid was replaced with lithium nitrate, are also included for promethium, americium an curium.

Experiments were performed in order to determine the extraction of nitric acid. It was found that the distribution ratio increased as the initial nitric acid concentration in the aqueous phase was increased to about 2 molar. From 2 to 10 molar nitric acid, the distribution ratio was rather constant, about 0.06.

The influence of the Aliquat-336 concentration on the extraction of trivalent metals was investigated at three different nitric acid concentrations, 0.30, 2.0 and 7.5 molar. These nitric acid concentrations were selected because they represent three locations on the extraction curve, i.e. where the distribution ratio increases, at the maximum and when the distribution ratio decreases, see Fig. 1. The results obtained for promethium are given in Fig. 2.

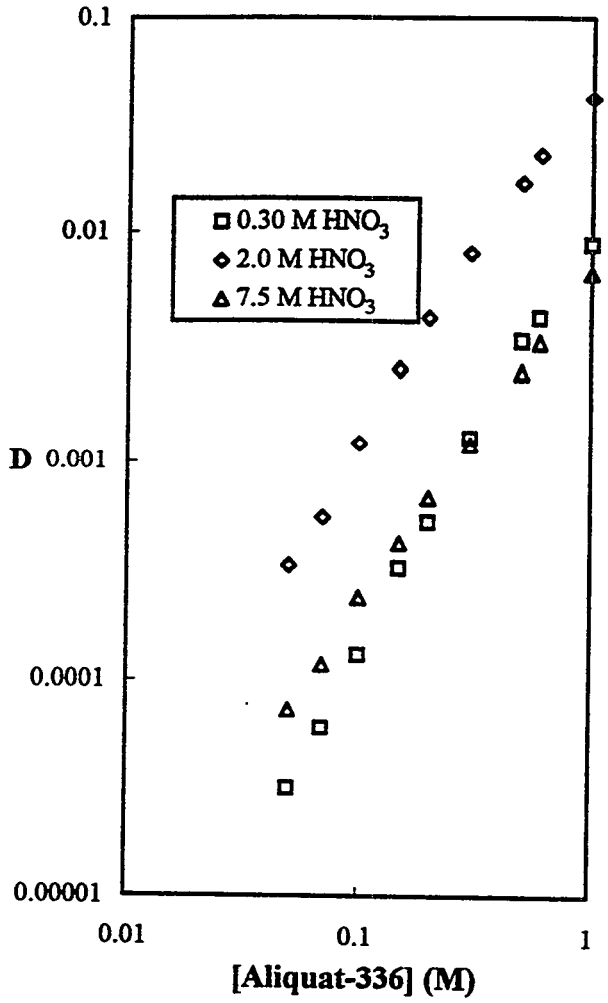

Fig. 2. Distribution ratios for promethium as a function of the initial Aliquat-336 concentration. Extraction data were determined at 0.30, 2.0 and 7.5 molar nitric acid.

Results obtained for the other elements are given in table 1 as slopes of the logarithmic values. The slopes were estimated with a 95 % confidence interval.

Table 1. Slopes obtained from the Aliquat-336 dependence.

Element	$\left.\frac{\partial \log D}{\partial \log[\text{Aliquat-336}]}\right\|_{[HNO_3]=0.30M}$	$\left.\frac{\partial \log D}{\partial \log[\text{Aliquat-336}]}\right\|_{[HNO_3]=2.0M}$	$\left.\frac{\partial \log D}{\partial \log[\text{Aliquat-336}]}\right\|_{[HNO_3]=7.5M}$
Sc	1.6 ± 0.05	1.4 ± 0.05	-
Fe	-	1.3 ± 0.3	-
In	2.7 ± 0.3	2.1 ± 1.2	2.8 ± 0.5
La	2.0 ± 0.2	1.8 ± 0.1	1.5 ±0.1
Ce	1.8 ± 0.2	1.6 ± 0.15	1.2 ± 0.45
Pr	1.9 ± 0.15	1.7 ± 0.1	1.4 ± 0.05
Nd	2.1 ± 0.2	1.7 ± 0.15	1.5 ± 0.1
Pm	1.9 ± 0.1	1.6 ± 0.1	1.5 ± 0.1
Sm	1.8 ± 0.1	1.6 ± 0.1	1.5 ± 0.05
Eu	-	1.6 ± 0.15	-
Am	1.7 ± 0.1	1.6 ± 0.1	1.3 ± 0.05

DISCUSSION

Up to about 2 molar nitric acid there is an increase in the distribution ratio (except for iron) when the initial nitric acid concentration is increased (Fig 1) and above 2 molar the distribution ratio decreases. The distribution ratio ought to increase as the nitric acid concentration is increased due to an increasing number of extractable metal nitrate complexes. As can be observed from Fig. 1 no decrease in the distribution ratio occurred when nitric acid was replaced by lithium nitrate. Competition between extractable metal nitrate complexes and nitric acid for extractant molecules can explain this behaviour. Thus, the extraction of nitric acid strongly influences the distribution ratio of trivalent elements. It is therefore important to know the extraction behaviour of nitric acid. The shape of the extraction curve for nitric acid can be explained if it is assumed that nitric acid extracts according to equation (5).

$$\overline{HNO_3} + \overline{R_3R'NNO_3} \underset{}{\overset{k_H}{\rightleftharpoons}} \overline{R_3R'NH(NO_3)_2} \qquad (5)$$

and that no micelle formation occurs. Then the total Aliquat-336 concentration in the organic phase is a sum of the free Aliquat-336 concentration and Aliquat-336 coordinating nitric acid. This is expressed in equation (6).

$$\left[\overline{R_3R'NNO_3}\right]_{tot} = \left[\overline{R_3R'NNO_3}\right]\left(1 + \lambda_H k_a^{-1} k_H \left[NO_3^-\right]^2\right) \qquad (6)$$

where λ_H is the distribution constant for nitric acid, k_a is the dissociation constant for nitric acid and k_H is given by equation (5). Up to about 2 molar nitric acid the distribution ratio was increasing with increasing nitric acid concentration in the aqueous phase and above 2 molar the distribution ratio was constant. For a nitric acid concentration higher than 2 molar the Aliquat-336

is saturated with nitric acid. Therefore a distribution of pure nitric acid between the two phases takes place. With use of equation (6) the extraction of nitric acid can be expressed as

$$D_{HNO_3} = \frac{\lambda_H k_a^{-1}\left[NO_3^-\right]\left(1+\frac{k_H\left[R_3R'NNO_3\right]_{tot}}{1+\lambda_H k_a^{-1} k_H\left[NO_3^-\right]^2}\right)}{1+k_a^{-1}\left[NO_3^-\right]} \qquad (7)$$

A property of Aliquat-336 that complicates the description of the system, is the ability of forming micelles in inert diluents. According to Rydberg and Sekine [4] these aggregates seem to behave like monofunctional species, each extracting only one metal nitrate complex. The aggregation can be reduced by using aromatic diluents or by adding a strong Lewis base. In this investigation micelle formation was supposed to be negligible because an aromatic solvent (1,3-diisopropyl benzene) was used as a diluent and 1-dodecanol acting as a Lewis base was added to the organic phase. The decrease in distribution ratio among the lanthanides is due to the lanthanide contraction. When the ionic radius [5] decreases, the formation of extractable complexes also decreases. Americium and promethium have about the same ionic radius and these two elements behave almost identical, as can be observed in Fig. 1.

In Fig. 1 it can be seen that the distribution ratio of cerium exceeds that for lanthanum at 5 - 10 molar nitric acid. Formation of tetravalent cerium may explain this behaviour since the tetravalent elements are better extracted than the trivalent.

The maximum in the distribution ratio occurs at about 2 molar nitric acid. Shabana and Ruf [6], [7] also investigated the extraction of some trivalent elements with Aliquat-336. They found that cerium and europium had a maximum in the distribution ratio at about 2 molar nitric acid whereas no maximum was found for americium. Koch [8] found a maximum in the distribution ratio for cerium at about 1.3 molar nitric acid.

As can be observed from Fig. 2 there is almost a linear relationship between the logarithmic values of the distribution ratio and the Aliquat-336 concentration. The slope decreases somewhat with increasing Aliquat-336 concentration. According to equation (4) is it possible to determine the extraction stoichiometry from the slope, i.e. the number of Aliquat-336 molecules per metal atom in the organic phase, if it is assumed that only one type of metal complex dominates in the organic phase. In table 1 it can be observed that the slope is about 2 for the lanthanides and americium at 0.30 molar nitric acid. This can be interpreted as 2 Aliquat-336 molecules are needed for each trivalent metal atom.

A model describing the extraction of trivalent metals with Aliquat-336 is complex. A first approach to a mechanistic model in which activities are replaced with concentrations is given in equation (8).

$$D = \frac{\lambda_3\beta_3\alpha_2\left[R_3R'NNO_3\right]_{tot}^2}{\left(1+\lambda_H k_a^{-1} k_H\left[NO_3^-\right]^2\right)^2 \sum_{i=0}^{N}\beta_i\left[NO_3^-\right]^i} \qquad (8)$$

It is further assumed that no polynuclear complexes are formed, two Aliquat-336 molecules are needed to extract one trivalent metal atom and the extraction of nitric acid is assumed to proceed according to equation (5). In equation (8) λ_3 is the distribution constant for the uncharged metal nitrate complex, β_i is given by equation (1), α_2 is given by equation (3), k_H is given by equation (5), λ_H and k_a are the distribution constant for nitric acid and the dissociation constant for nitric acid, respectively. Equation (8) is an attempt to describe the system in a very simple way. The extraction behaviour of nitric acid is, however, poorly investigated and an experimental investigation ought to be done in order to determine the extraction mechanism of nitric acid before the model can be further tested.

CONCLUSIONS

The investigated extraction system becomes complex even though it originates from a few components. It can be concluded that the extraction of nitric acid strongly affects the distribution ratio and therefore it must be included in extraction model.

According to Jarvinen et al [1] the aqueous feed to the first extraction step, in the LANL's baseline separation process, consists of 2 molar nitric acid. The results obtained for the trivalent elements except iron and indium show that they have their maximum distribution ratio at about 2 molar nitric acid. It is observed in Fig. 1 that no distribution ratio exceeds 0.05, in the nitric acid system. The trivalent elements will probably not interfere with the extraction of plutonium, neptunium, technetium and palladium according to present extraction data. To be able to understand the extraction system and to determine more extraction data some of the tetra-, penta- and hexavalent elements will be investigated.

ACKNOWLEDGMENTS

The authors are very grateful to the Swedish Nuclear Fuel and Waste Management Co., SKB, for their financial support.

REFERENCES

[1] Jarvinen, G.D., Marsh, S.F., of Development Schroeder, N., Smith, B.F., Villarreal, R., Walker, R.B., Yarbro, S.L. and Yates, M.A., *Baseline Actinide Blanket Processing Flowsheet for the Accelerator Transmutation of Waste (ATW) Program*, Los Alamos National Laboratory, Report LA-UR-92-63 (1992)

[2] Walker, R.B., *Flowsheet Report for Baseline Actinide Blanket Processing for Accelerator Transmutation of Waste*, Los Alamos National Laboratory, Report LA-UR-92-1241 (1992)

[3] Dewey, H.J., Jarvinen, G.D., Marsh S.F., Schroeder, N.C., Smith, B.F., Villareal, R., Walker, R.B., Yarbro, S.L. and Yates, M.A., Status of Actinide Blanket Processing Flowsheets for Accelerator Transmutation of Nuclear Waste, in *Proceedings of the Conference* on Future Nuclear Systems: Emerging Fuel Cycles and Waste Disposal Options Global '93, 1993, pp. 985-997

[4] Rydberg, J., Sekine, T., Eds.: Rydberg, J., Musikas, C., and Choppin G.R., *Principles and Practices of Solvent Extraction*, New York, Basel, Hong Kong: Marcel Dekker, Inc., 1992, ch. 4, pp. 136-139

[5] Seaborg, G.T. and Loveland, W.D., *The Elements Beyond Uranium*, New York, Chichester, Brisbane, Toronto, Singapore: John Wiley & Sons Inc., 1990, ch. 3, pp. 80-82

[6] Shabana, R. and Ruf, H., *Radiochimica acta* **23**, 148-151 (1976)

[7] Shabana, R. and Ruf, H., *Radiochimica acta* **24**, 15-18 (1977)

[8] Koch, Von G., *Kerntechnik* **7**, 394-399 (1965)

LITHIUM ACTINIDE RECYCLE PROCESS DEMONSTRATION

G. K. Johnson, R. D. Pierce, and C. C. McPheeters
Chemical Technology Division
Argonne National Laboratory, Argonne, Illinois 60439

Several pyrochemical processes have been developed in the Chemical Technology Division of Argonne Laboratory for recovery of actinide elements from LWR spent fuel. The lithium process was selected as the reference process from among the options. In this process the LWR oxide spent fuel is reduced by lithium at 650°C in the presence of molten LiCl. The Li_2O formed during the reduction process is soluble in the salt. The spent salt and lithium are recycled after the Li_2O is electrochemically reduced. The oxygen is liberated as CO_2 at a carbon anode or oxygen at an inert anode. The reduced metal components of the LWR spent fuel are separated from the LiCL salt phase and introduced into an electrorefiner. The electrorefining step separates the uranium and transuranium (TRU) elements into two product streams. The uranium product, which comprises about 96% of the LWR spent fuel mass, may be enriched for recycle into the LWR fuel cycle, stored for future use in breeder reactors, or converted to a suitable form for disposal as waste. The TRU product can be recycled as fast reactor fuel or can be alloyed with constituents of the LWR cladding material to produce a stable waste form.

The lithium process offers several potential advantages over other options that were studied. These advantages include lower temperature, a less corrosive environment, and waste salt that can be treated by established processes. Laboratory work on the lithium system is focused on small-scale experiments to demonstrate the process steps and to select conditions for engineering-scale tests.

A demonstration of the lithium process starting with 0.5 kg of simulated LWR fuel, which contained UO_2, TRU's, and representative fission products, has been conducted. The demonstrated steps include reduction, electrorefining, consolidation, and electrowinning.

The reduction step convereted the uranium, TRU's and noble fission products from oxides to metals. The electrorefining step produced pure uranium and a TRU-rich salt. The consolidation step conducted in a retort furnace produced a uranium ingot. The electrowinning step conducted on the reduction salt used a graphite anode to decompose the LI_2O into lithium and CO_2.

652

CHEMICO-TECHNOLOGICAL SUPPORT OF TRANSMUTATION OBJECTIVES: SOLID, MOLTEN SALT AND LUQUID BLANKET.

V. I. Volk, B. S. Zakharkin, A. Yu. Vakhrushin

VNIINM, Moscow, Russia

Chemical and technological provision for the transmutation process, independantly on the scheme of its conduction, includes: fuel composition separation for fractions of components, subjected to annihilation; their transition into chemical form, in which they are present in the reactor; discharge and return into the form, convenient for chemical reprocessing, providing for the transmutation products separation from the components being transmutated and transferring of short-lived isotops into the form of their temporary storage.

When carring-out transmutation in the fast reactors, using solid fuel composition, it is advantageous to organize chemical reprocessing similar to the operating Purex-process, within the framework of which all the problems enumerated are basically solved. Currently the content of composition being transmutated (individual Np, Am, Cm; their mixture or their mixture at the presence of their actinides, for example, uranium) is not clear, in connection witn that it is difficult, but, apparently, it will be slightly different from the high-level waste fractioning patterns developed. Heat release will have same restricting effect on the component concentration in the process flows, however, the list of safe operation requirements for these systems hasn't been formulated up till now.

Main variant of chemical form for the component arrangement in fuel composition is their oxides, which production technology can be formed as the technology of mixed uranium-plutonium fuel production. The difficult using is to choose solid chemical form to arrange iodine and technetium, for which there is currently no ready technical solutions.

Among the problems requiring solution for this alternative

transmutation implementation the following should be noted:

- cooling of irradiated fuel composition and its shipment to the place of reprocessing, including possible creation of new transporting container;

- safe solution of the problems of fuel assembly cutting and fuel composition dissolving, taking into account the intensive heat realease in assemblies and their relatively great mass;

- creation of the chain for the composition aqueous-extraction reprocessing likewise the unit of HlW fractioning or this unit adaption to the technology of the components being transmutated purification from decay products;

- development and creation of technology for oxide or alternative compositions production for fuel element equipment;

- creation the line of fuel element remote equipment and fuel assemblies production, (possibly, according to the technology of fuel consolidated by vibration);

- solution of problems of fuel assemblies monitoring and security at fuel elements loss of tightness the reactor.

Implementation of the given alternative transmutation is facilitated by the operating reactor available, if its use for these purposes doesn't violate the conditions of safe operation, however, it is characterized by a greatly protacted in-reactor process cycle, a great amount of reagent expenditures, and, therefore, secondary wastes being formed. Thus, taking into account the fact that not more then 10% of actinides subjected to transmutation is annihilated for one act of irradiation, burning-up of 1 kg of long-lived isotopes will resulted in the formation of up to 10 kg of irradiated constractional materials and such a quantity of salts contaminated with radionuclides, being formed at fuel composition dissolution and oxide re-precipitation. Besides the increase of equipment units, required for the process cycle conditions, all these operations have their own volume of cycle in the form of process scrap, subjected to secondary reprocessing.

At first consider the situation with chemical-technological supply of reactors with blanket on the basis with molten salts loop, and formulate approaches to its reprocessing. First of all, the fact should be taken into account that only the fractioning technology built on aqueous-extraction methods, and primarily, reprocessing of Purex-process nitrate solutions, can be technically realizable in

the nearest future.

If go along the path accepted in the uranium industry: production of oxides with their subsequent fluorization, then the formation of secondary salts contaminated with radionuclides, is inevitably.

The situation can radically be solved only if the classical Purex-process is abandoned and the methods of pyrochemistry are used for irradiated nuclear fuel technical investigations, particularly in the field of separation elements of actinide and lanthanide series close by properties.

Reprocessing of salt loop can be organized in stationary mode: continuous introduction of the components being transmutated into the reactor loop and removal of part of salt flow in the amount, necessary for the decay products drawal. At the initial stage the technology of aqueous-extraction fractioning of high lewel wastes can be used after salt carrier separation and actinides and decay products conversion into nitrate form, taking into account the relationship of the element-by-element composition of this flow and products, being discharged from transmutation cycle. Later, this technology can be supplemented with its own elements, relying on the methods of pyrochemistry, extraction with metal melts, metal light-melting-point eutectics, etc. However, it is apparently imposible to complectely abandon hydrometallurgical techniques in reprocessing cycle, as the methods for secure fising of short-lived radionuclides (vitrifications, storage in mineral-like materials and metal ceramic composition) provide for the production of oxide forms for the components being disposed. It should be noted here that the known methods of equipment decontamination for preventive inspection and repair are using as well the processing with aqueous solutions.

To realize this variant of transmutation, not technical but complex problems should be solved, among them the followings can be noted:

- constructional materials;
- phase stability of salt melts and physical-chemical process, taking place in them under irradiation;
- stuctural safety when working with the crystallizing systems;
- technology and implementation of the melt chemical reprocessing;
- technology and managment with the process wastes, including

problems of waste disposal;

- emergency conditions and elimination of their consequences.

Such problems are removed form the agenda when the reactor with heavy water loop is used.

Variant of introduction the components being transmutated in the form of dispersed fuel (stabilized suspension of oxides or other solid forms) has the previously noted short comings of salt waste formation as a result of chemical form conversion operations. Moreover, specific safety problems arise, caused by the possible loss of the system phase stability and uncontrolled advent of local of the system phase stability and uncontrolled advent of local places with high actinide concentration ("the overgoing" of the installation units). These problems are particularly urgent in the case of transmutation fission materials (plutonium) or materials, that can become fission ones (neptunium) in neutron fluxes of high density, where the nuclear safety is of primary importance (prevention of spontaneous chain reaction). The simplicity of transfer the component being transmutated from the water medium into the reactor heavy water loop, is an attractive aspect of this transmutation variant.

The use of reactor with nitrate salt solution loop in heavy water is nowadays an obvious way for minimizating the amount of secondary wastes, being formed within the full process conversion. To successfully realize this variant it is important to effectively solve the problem of actinide nitrate transport from the flux after Purex-process high level waste fractioning into the reactor heavy water loop and back, and also transmutation products recycling to use the cycle of fractioning for separation the components being transmutated from the decay products. The transport task can be successfully solved with using membrane-extractional transfer procedure. Requires to the transfer selectivity are determinated by fractioning efficiency and, correspondingly, at sufficient selectivity, transfer may be realized through typical for hydrometallogy moderately selective extractants of main classes: acid, neutral and base.

Structure of chemico-technological support of transmutation tasks.

Main tasks are:

- fuel composition separation on fractions of component;
- their transmutation into chemical form, in which they are present in the reactor;
- discharge and return into the form, convenient for chemical reprocessing;
- transferring of short-lived isotopes into the form of their temporary storage.

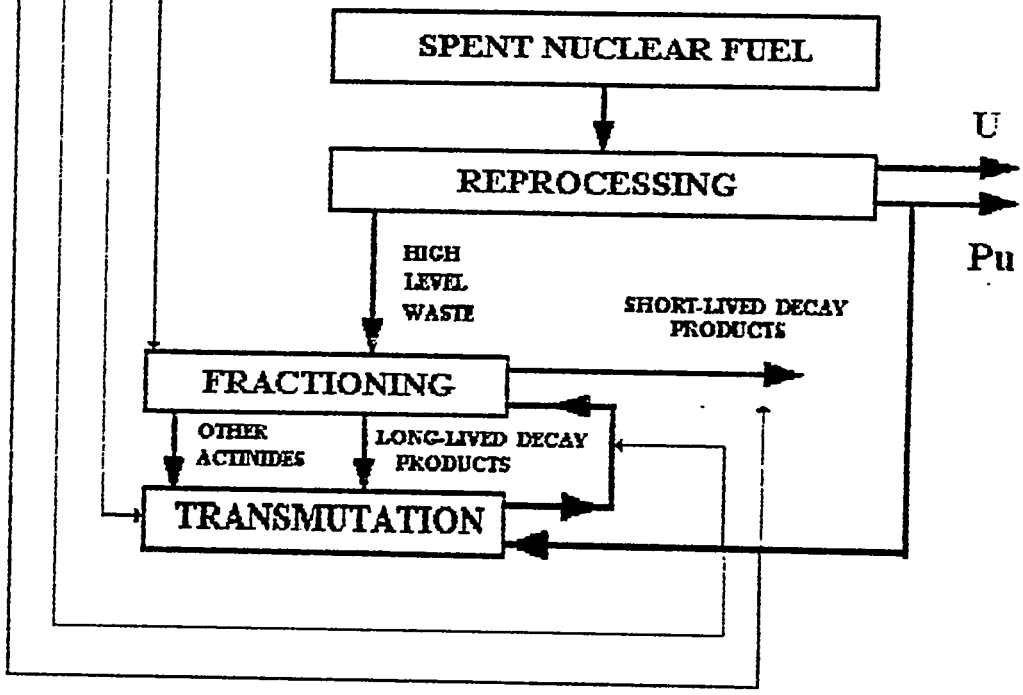

Fig. 1.

657

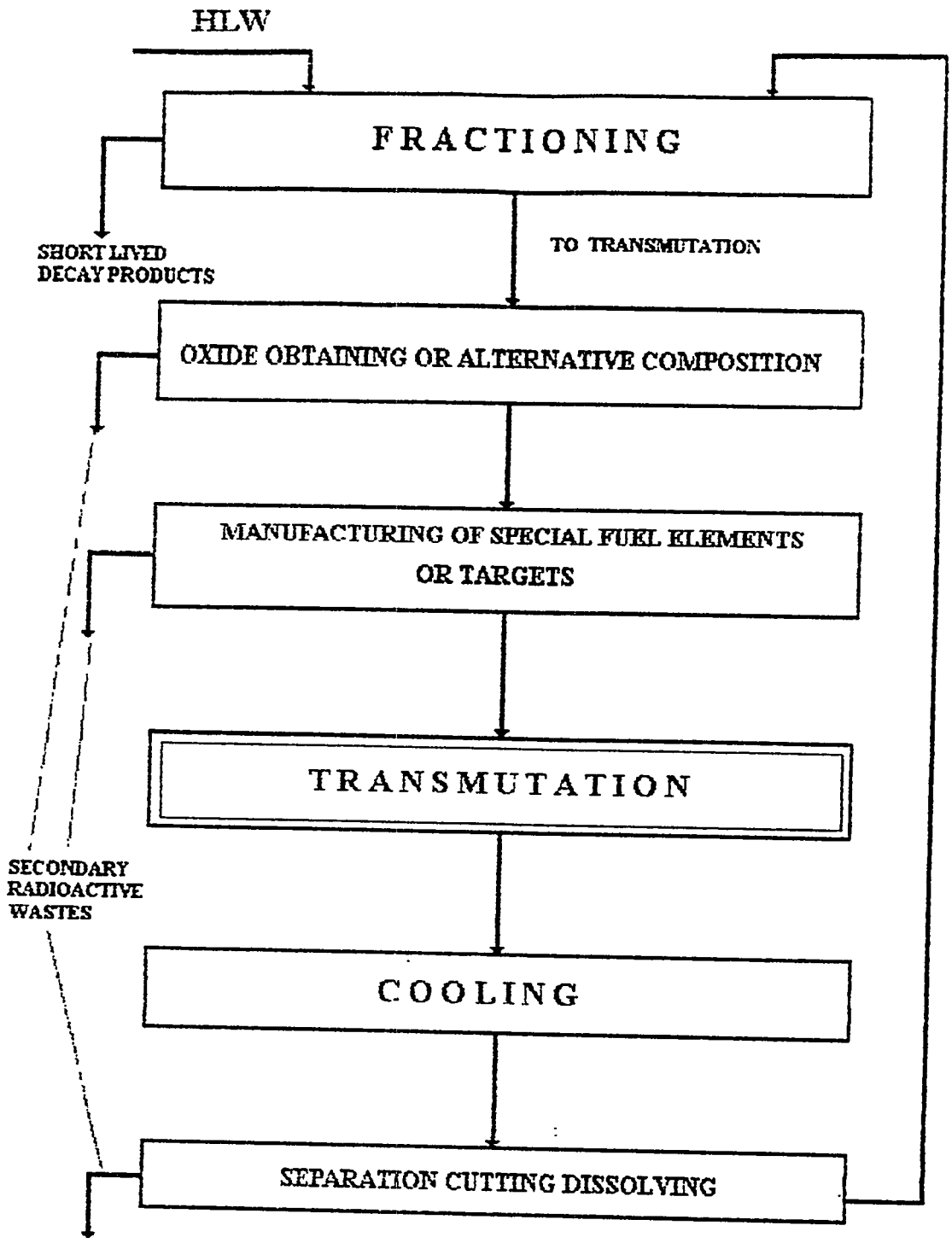

Operations of chemico-technological transmutation support with solid blanket.

Fig. 2

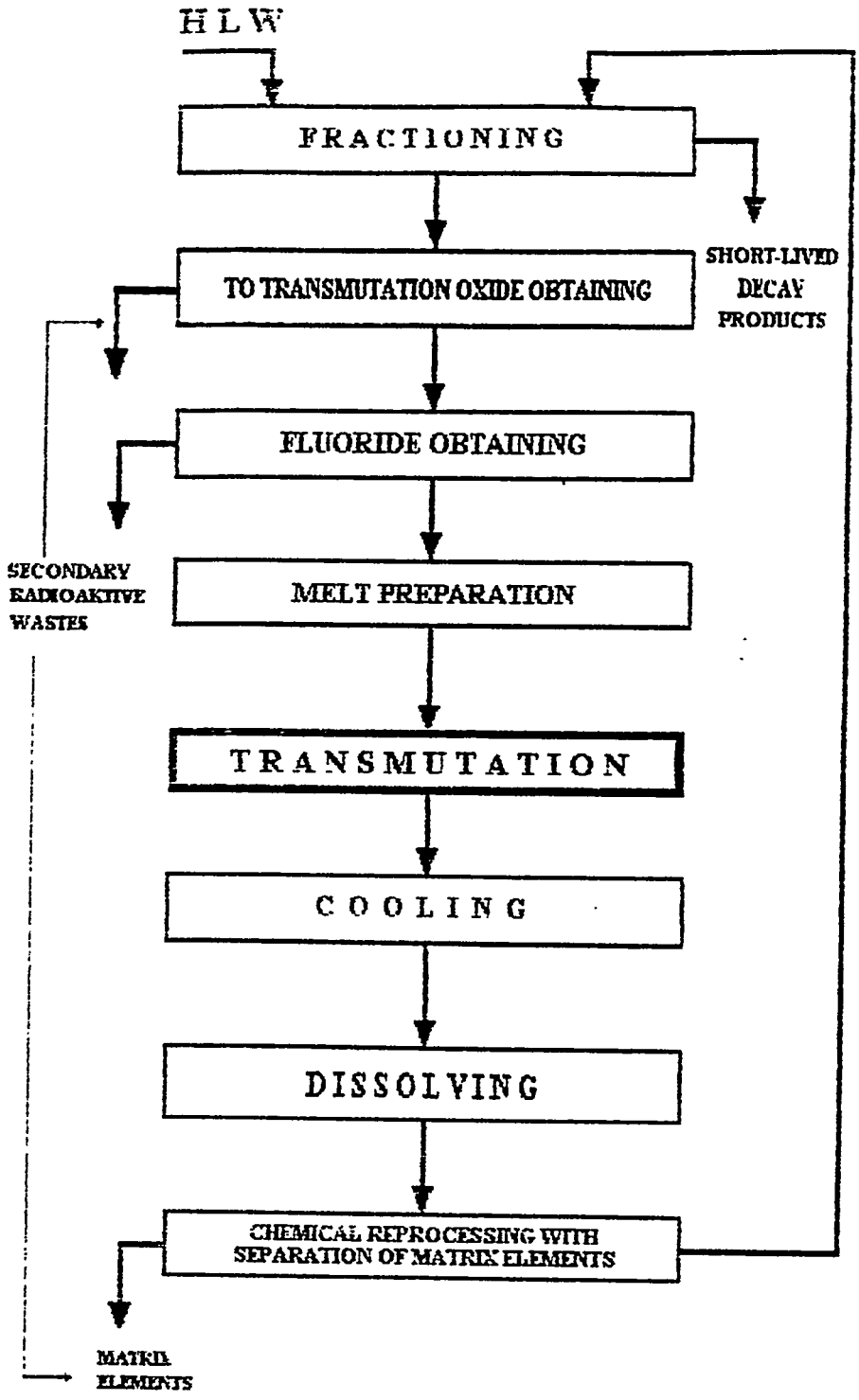

Operations of chemico-technological transmutation support with molten salt blanket.

Fig. 3

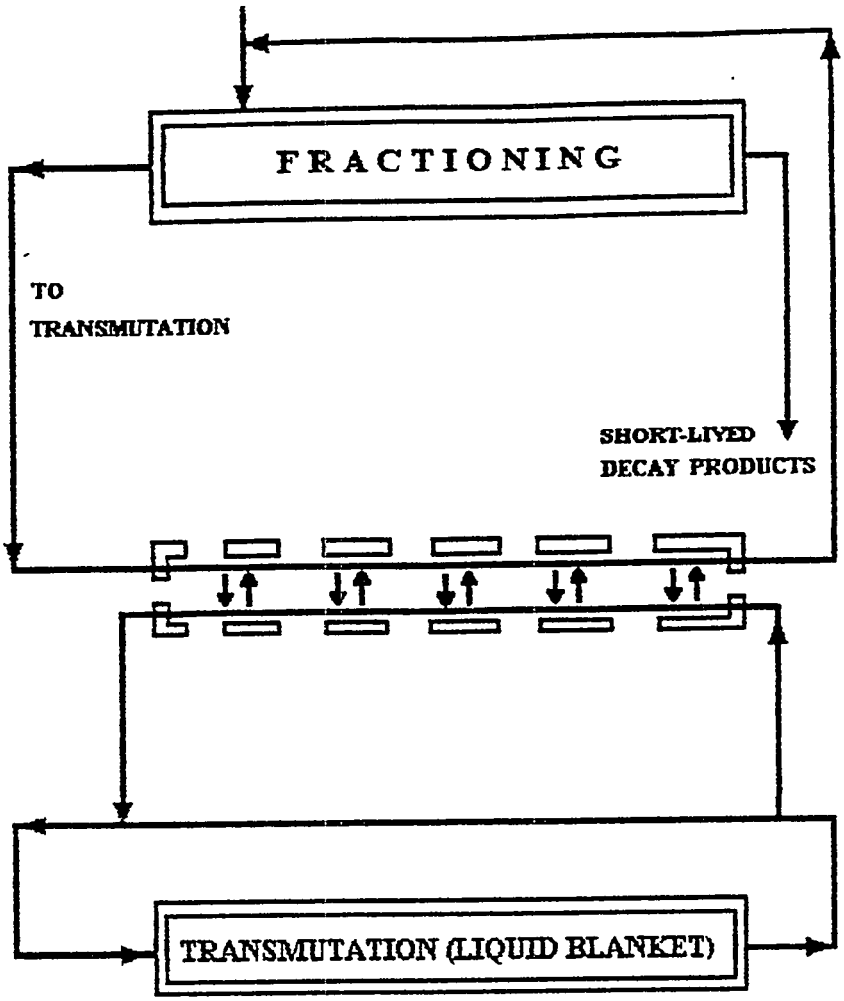

Operations of chemico-technological transmutation support with heavy water homogenous blanket.

Fig. 4

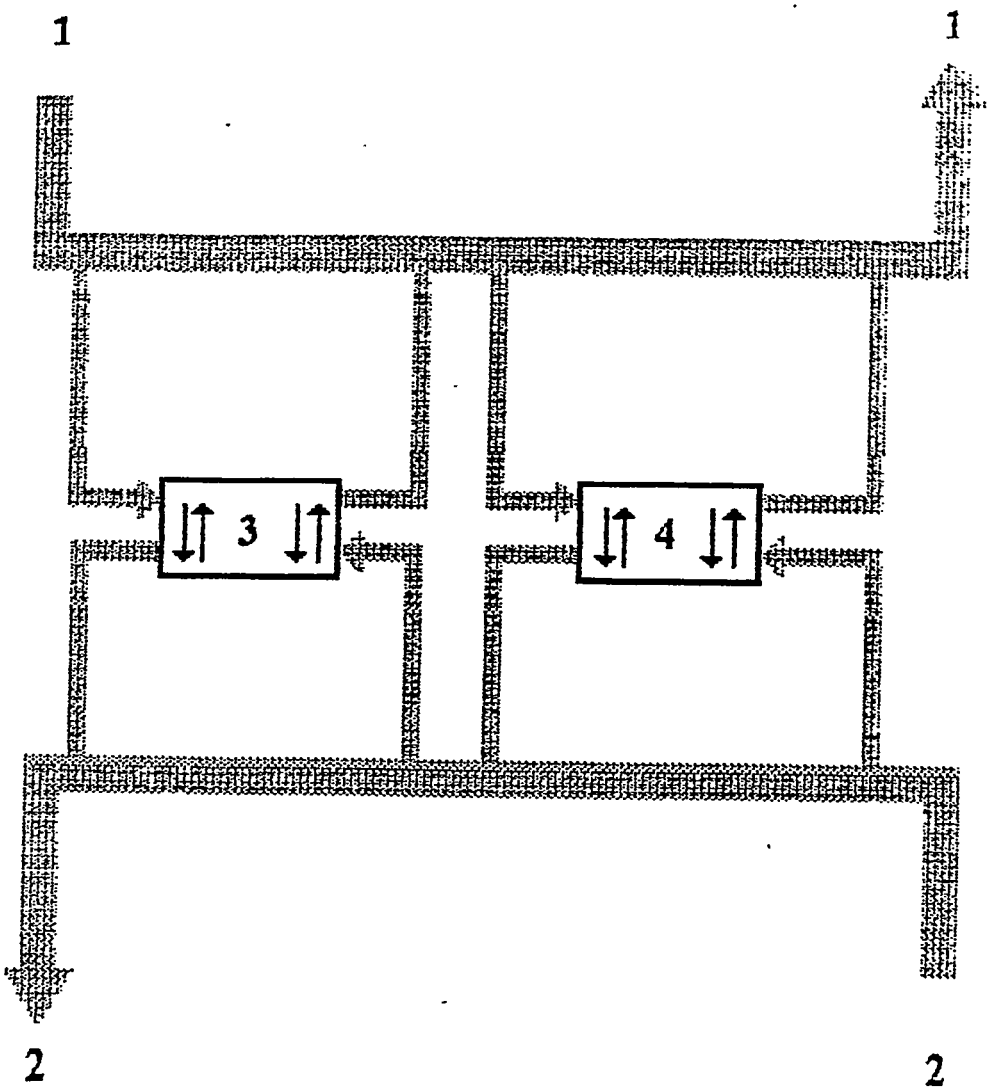

1 - partial flow from fractioning operation
2 - partial heavy water blanket flow
3 - transport block to the blanket
4 - transport block from the blanket

Principal scheme of membrane - extraction transport.

Fig. 5

A Small Scale Accelerator Driven Subcritical Assembly Development and Demonstration Experiment at LAMPF

S. A. Wender, F. Venneri, C. D. Bowman, E. D. Arthur, E. Heighway
C. A. Beard, R. R. Bracht, J. J. Buksa, W. Chavez, B. G. DeVolder, J. J. Park,
R. B. Parker, C. Pillai, E. Pitcher, R.C. Potter, R. S. Reid, G. J. Russell,
D. A. Trujillo, D. J. Weinacht, W. B. Wilson, K. A. Woloshun

Los Alamos National Laboratory
Los Alamos, NM 87545

Abstract

A small scale experiment is described that will demonstrate many of the aspects of accelerator-driven transmutation technology. This experiment uses the high-power proton beam from the Los Alamos Meson Physics Facility accelerator and will be located in the Area-A experimental hall. Beam currents of up to 1 mA will be used to produce neutrons with a molten lead target. The target is surrounded by a molten salt and graphite moderator blanket. Fissionable material can be added to the molten salt to demonstrate plutonium burning or transmutation of commercial spent fuel or energy production from thorium. The experiment will be operated at power levels up to 5 MW_t.

I. Introduction

The coupling of a neutron producing accelerator with a sub-critical fission assembly has been proposed at Los Alamos as a method of addressing several issues of current importance. This type of subcritical system can be operated in a much larger parameter space than an ordinary reactor. Because of this increased flexibility in operating conditions, an accelerator driven subcritical fission system can be used to 1) destroy weapons grade plutonium with little actinide residue, 2) burn spent fuel from commercial reactors with reduced waste stream and 3) generate power using the thorium/uranium cycle. Because the fuel does not need to be enriched, it appears that the system can be made more proliferation resistant than other proposed systems that address these issues.

At present the system concept for an accelerator driven transmutation technology (ADTT) system consists of a 500 MW_t module driven with 15 mA of 800 MeV proton

5. It will demonstrate control of molten salt chemistry, material solubilities, material deposition and plate out problems.

6. It will demonstrate the helium sparging techniques for handling and removing the evolved fission product gases and the containment of tritium.

7. At a reduced flux level, it will verify the integrity of the materials and the design concepts used.

8. It will demonstrate the control of environment, safety and health (ES&H) issues related to the operation of the integrated system.

II. Molten Lead Target

The neutron production target consists of a cylindrical container that holds the molten lead, a lead-to-helium heat exchanger that is located above this cylinder and a reservoir below the target volume. A window on the side of the target allows the proton beam to enter the target volume and internal baffling directs the flow of the lead against the window to ensure proper cooling. A liquid lead target provides the following advantages:

1. Higher beam powers can be used compared to solid targets. The beam power in solid targets is limited by the ability to cool them. This limits the beam power to approximately 1 MW. Many ADTT concepts as well as spallation targets for material science research involve power levels substantially greater than 1 MW. Development of this technology will have wide and future applications. Similar liquid lead targets are being developed at PSI for the SINQ spallation source.[1]

2. Because the bulk of the material is liquid, the target is not subject to the same radiation damage issues that are present in solid target designs. Radiation damage concerns are only present in the container and window of the target. In addition, the molten lead can removed and reused if the container needs to be replaced.

3. Because a liquid lead target does not have to be cooled by the salt it can be decoupled from the salt tank and physically isolated from it. This means the target can have its own container and can be removed without having to open up the salt volume that may contain highly radioactive and fissionable material. In addition, removal of the target will be much easier because its volume and mass are only small part of the salt blanket system. The tank that contains the molten salt does not require a window for the beam.

Two types of molten lead targets are possible: pure lead and lead-bismuth eutectic (LBE). LBE has the advantage of a lower melting point. LBE has a melting point of approximately 125°C which is considerable lower than the 325 °C of pure lead. This

beam (12MW) incident on a neutron production target. The neutron production target is at the center of a LiF-BeF_2 molten salt (MS) and graphite moderator blanket. In the case of plutonium destruction, plutonium can be added to the molten salt. Other applications such as energy production (EP) and accelerator transmutation of waste (ATW) will probably use the same basic technology and design philosophy. In these cases thorium or spent fuel could be added to the molten salt to demonstrate energy production or spent fuel transmutation.

Considerable knowledge and experience exists on the operation of MS systems from the Molten Salt Reactor Experiment (MSRE) that was operated at the Oak Ridge National Laboratory (ORNL) in the 1960's. At the conclusion of the MSRE, the researchers at ORNL felt that they had satisfactorily demonstrated the basic requirements of MS operation. In the design of this experiment we have assumed that the major technical issues have been satisfactorily addressed by this work at ORNL. As we design and fabricate the experiment, we will continuously evaluate the technology and update it where possible or necessary.

As a crucial step towards developing a 500 MW_t prototype module, we are proposing a small scale demonstration experiment. The experiment consists of a phased sequence of development and demonstration activities that begin with the development of a molten-lead target and techniques for molten salt handling. The experiment will culminate in the operation of an integrated accelerator-target/blanket subcritical fission assembly that can operate at power levels of up to 20 MW_t, although significant progress can be made at lower power levels.

This experiment will demonstrate many of the important aspects of ADTT and will be modeled on the preconceptual design of a single 500 MW_t module. The experiment will take advantage of the high power 800 MeV proton beam from the Los Alamos Meson Physics Facility (LAMPF) accelerator and will be located in experimental Area-A. Proton beam currents of up to 1 mA (800 kW) will be incident on the neutron production target. The experiment has the following ultimate goals:

1. It will demonstrate the integrated operation of a high-power particle beam used to produce neutrons coupled to a subcritical fission assembly. The power levels will be high enough to show significant transmutation processes.

2. It will test the analytical, diagnostic and control instrumentation that will be developed to monitor and operate the system. It will verify predicted system responses, time constants and reactivity behavior of the integrated system.

3. It will demonstrate the operation and performance of the neutron production target both alone and coupled to the molten salt blanket. It will also demonstrate the beam window technology necessary to inject the beam into such a target.

4. It will demonstrate techniques for large scale molten salt handling. It will provide a test bed for gaining safety related experience in molten salt operations.

reduced temperature will simplify some of the materials issues in the operation of the target. The major disadvantage of LBE is that the production of radioactive Po is approximately 1000 times greater than that of molten lead.[2] We are presently evaluating the choice of lead for this target.

Figure 1 shows a schematic drawing of the liquid lead target. A detailed description of the target design and operation is given by the Beard et. al [3] in this conference. The present choice of a material for the target container is Nb with 1% Zr. This choice is based on its excellent compatibility with molten lead and is discussed in a contribution by Park et. al[4] in this conference.

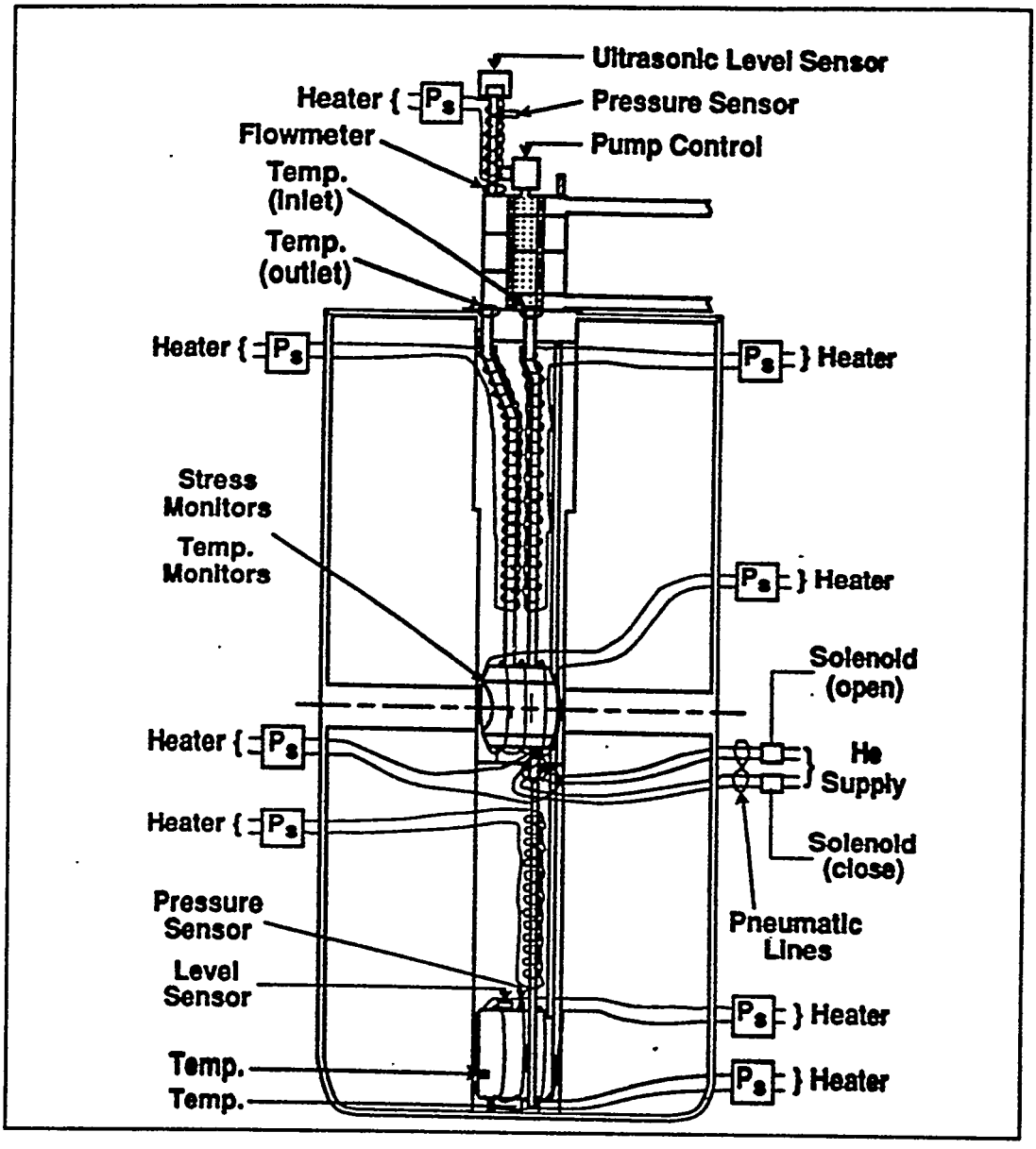

Figure 1. Drawing of the molten lead target for the accelerator driven subcritical assembly

The lead is stored in a reservoir below the target volume when not being irradiated. Lead is pumped into the target volume with pressurized argon. During normal operation the valve between the reservoir and the target volume is closed and the lead circulates between the target volume and the heat exchanger. The lead is returned to the reservoir to cool and is stored there.

III. Site Selection

We chose to locate the experiment at the LAMPF accelerator because LAMPF presently has the highest beam power of any accelerator in the world and the beam energy is similar to that being proposed for the actual modules. A beam current of 1 mA is about the right intensity to test many of the issues associated with the development of the 500 MW_t module and will not require significant expenditure that going to higher currents will require. The proposed location for the experiment is after the A1 and A2 pion production targets (between the A3 and A4 targets). This location was chosen for the following reasons:

1. The proton beam transport and shielding for up to 1 mA of beam already exists.

2. There is relatively easy access to the proton beamline through stackable shielding, with little or no modification of existing structures necessary.

3. Because this location has never been the site of a production target it is relatively unactivated.

4. There is a large area near the beamline to stage the experiment. This area can be used to set up the experiment prior to its placement in the beam. The support infrastructure such as cooling and electrical power that will be installed for these initial test can be used in the actual experiment.

5. There is good access to the experimental and setup areas with a large forklift and there is a 30 ton overhead crane in both the setup and the experimental areas.

IV. Molten Salt Blanket

Figure 2 shows a conceptual design of the experimental tank for the experiment. It consists of a 3.6 m diam, 4.2 m high cylinder with a hole in the center for the target cell. The entire tank is fabricated from Hastelloy N and contains the molten $LiF\text{-}BeF_2$ salt and an array of carbon moderators. Hastelloy N has been shown in the MSRE to have excellent compatibility with molten salt. The lithium in the salt will be enriched to 99.9% in ^7Li to reduce the absorption of neutrons due to of the large thermal capture cross section of ^6Li. The beam passes through the tank and enters the molten lead target cell on the side through a window. The molten salt is heated to a temperature of

approximately 600°C and is circulated through the carbon moderators and cooled by heat exchanges located inside the molten salt tank. An external cooling loop, that uses a NaF-LiF molten salt with boron added cools the primary heat exchanger in the tank. The secondary loop is cooled by an independent heat exchanger. Some of the physical properties of the system are listed in table 1.

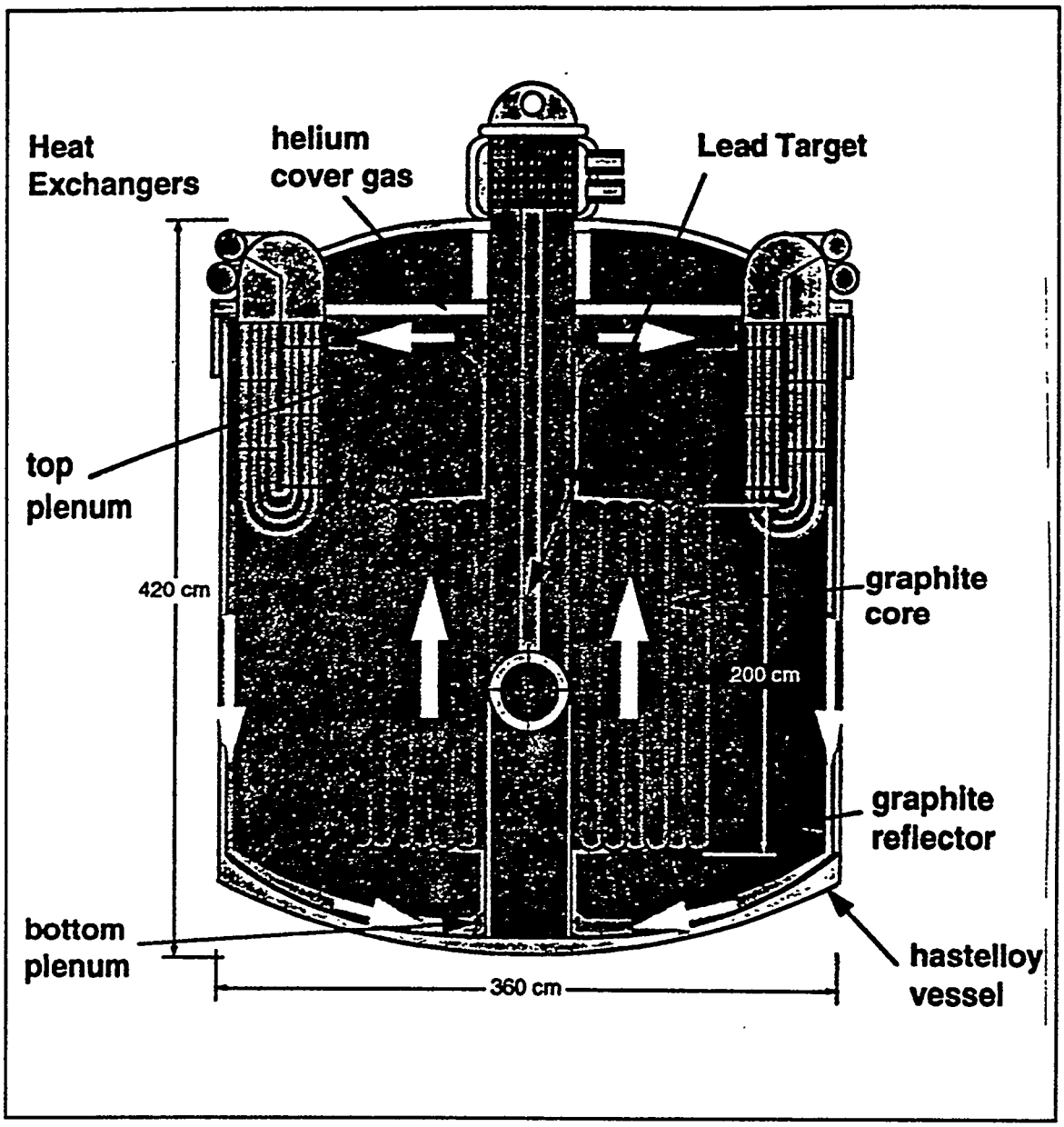

Figure 2. A conceptual system layout of the molten salt blanket for the accelerator driven subcritical assembly.

Table I

Physical Properties of Experiment

Volume of salt	1 m^3
Volume of carbon	10 m^3
Operating temperature of salt	600 °C
Lead Target volume	60 ℓ
Operating temperature of target	500°C

There will be a small pipe installed in the tank to allow the removal of small amounts of salt during the experiment to monitor the oxidation state of the Pu and the build up of fission products (FP). Small amounts of material will be added to the salt blanket to adjust the redox potential of elements in the molten salt blanket. The control of the salt flow through this drain pipe will be via freeze plugs that have been used successfully in the MSRE. There will be provisions to supply approximately 1 MW of electrical power to the MS tank to heat the salt during initial setup when there is no power being supplied by the beam.

V. Experiment Schedule

The experiment will proceed in three stages. The first stage involves the development of the molten lead target. In the second stage, the molten salt tank is constructed and the technology for molten salt operation is developed. In the final stage, fissionable material is added to the molten salt target/blanket and actual transmutation processes are demonstrated. In this stage, small amounts of fissionable material will be added and the response of the system will be measured. The measurements will be compared to the predicted behavior. If the calculations are verified, more fuel may be added to the blanket and the power increased.

At each stage, the systems will be developed first in off-line test stands. Following complete testing, each system will be installed in the LAMPF beamline and tested in-beam. For the case of the molten lead target, the radiation testing will occur at the LAMPF beam stop location. In the case of the molten salt tank, the testing will occur in the new target area in the location described in section III.

VI. System Performance

We have calculated the performance of a fueled molten salt subcritical target\blanket system based on the conceptual design of this experiment. Figures 3 and 4 shows calculations of initial blanket power and initial k_{eff} following the addition of ^{239}Pu

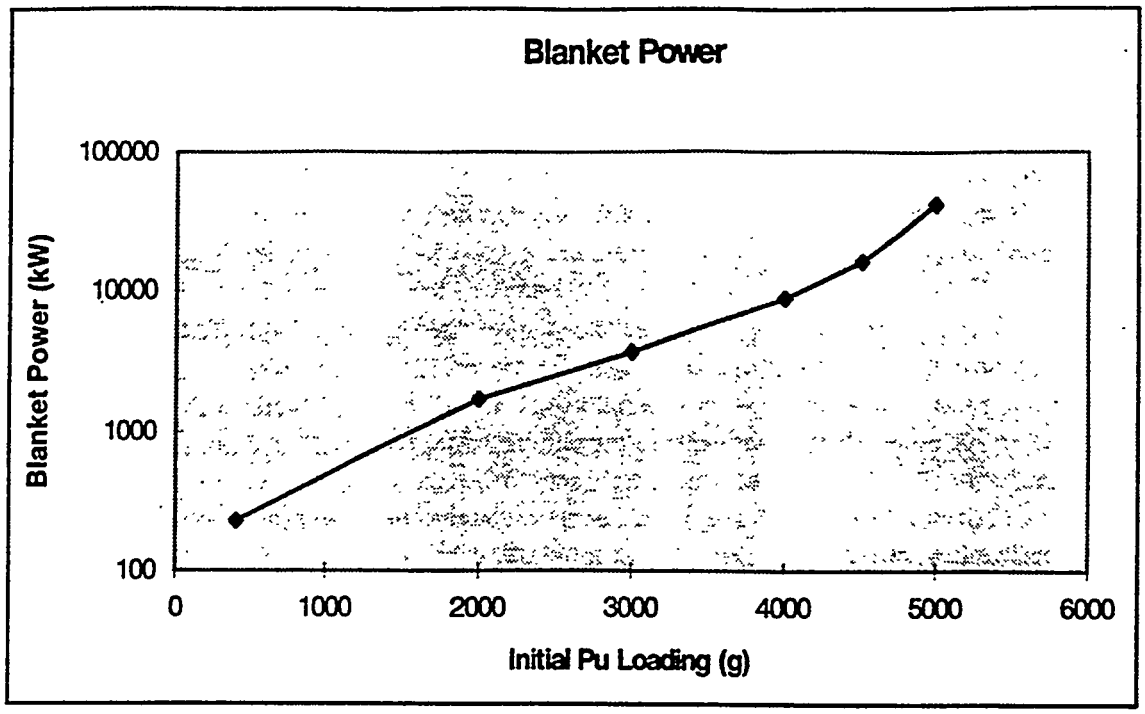

Figure 3. Initial blanket power for various initial plutonium loadings in the molten salt.

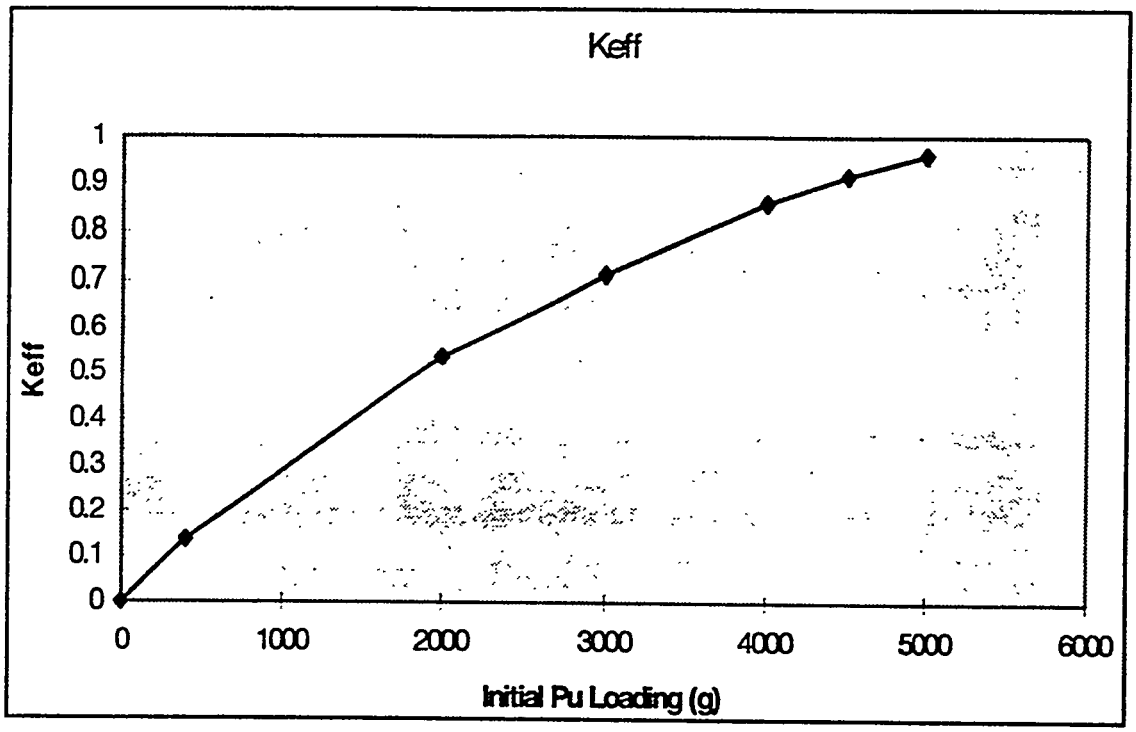

Figure 4 Initial k_{eff} for different initial plutonium loading in the molten salt blanket.

to the molten salt blanket. For these calculations we have assumed 1 mA of proton beam with a neutron production target that produces 21 neutron /proton. For an initial loading of 3 kg of ^{239} Pu, the power in the blanket is calculated to be approximately 4 MW and k_{eff} is approximately 0.7.

Energy production from thorium is shown in figure 5. The solid squares show the time dependence of the blanket power when the MS blanket is loaded with 1000 kg of thorium. The open circles show the performance of the system for the case where 2 kg of ^{239} Pu is added to the 1000 kg of thorium. For comparison, the triangle curve shows the time dependence of the blanket when only 2 kg of pure ^{239} Pu is added. As seen from the figure (squares), the power from the fission of ^{233}U slowly rises when only thorium is used in the blanket. The power output and the breeding rate of ^{233}U can be increased with the addition of ^{239} Pu . The fact that the curve for thorium and plutonium increase above the curve for pure plutonium is an indication of power generation using the thorium/uranium breeding cycle.

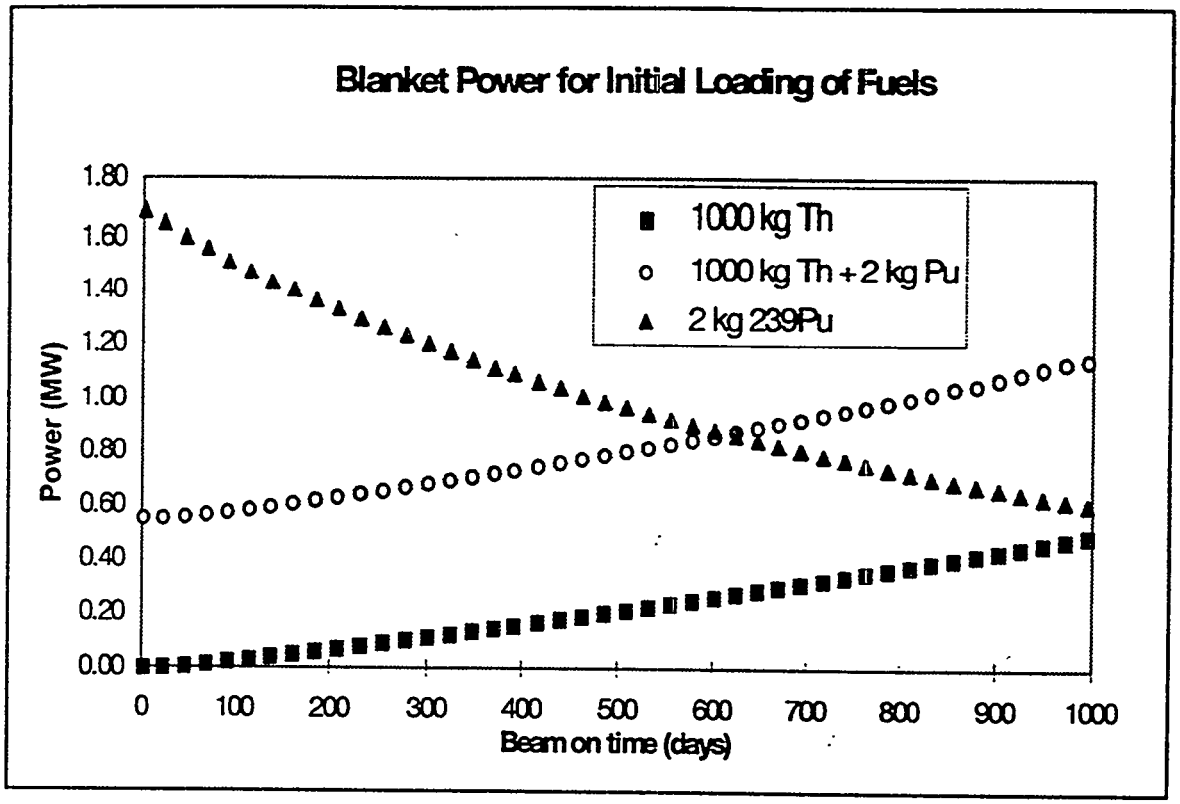

Figure 5 The blanket power for various initial fuel loadings of the blanket. The solid squares are for an initial loading of 1000 kg of thorium. The open squares is for an initial loading of 1000 kg of thorium and 2 kg of ^{239}Pu. For comparison. the triangles show the blanket power for 2 kg of ^{239}Pu alone.

VII. Conclusion

This small scale demonstration experiment is a crucial step towards the development of a full scale ADTT system. The experiment addresses many key issues in ADTT technology and will demonstrate the following new technologies:

1. Molten lead neutron production targets
2. Integrated operation of a neutron production target and a subcritical fission blanket assembly.
3. Integral heat exchangers and pumps
4. On-line criticality measurements
5. Helium sparging to remove volatile fission product gases
6. Plutonium burn up
7. Energy production using the thorium/uranium breeding cycle.

References

1. Nucl. Sci. and Eng. **113** (1993) 287.

2. V.T. Gorshkov et. al, "An Accelerator Based Installation of Small Power with the Lead-Bismuth Coolant", this conference 1994.

3. C. A. Beard et. al, "Flowing Lead Spallation Target Design for Use in an ADTT Experimental Facility Located at LAMPF", this conference 1994.

4. J. J. Park et. al, "Selection of Flowing Liquid Lead Target Structural Materials for Accelerator Driven Transmutation Applications", this conference, 1994.

SPALLATION STUDIES AT SATURNE

J. Fréhaut
Commissariat à l'Energie Atomique, Centre d'Etudes de Bruyères-le-Châtel
BP 12 - 91680 Bruyères-le-Châtel, France

Abstract. SATURNE is a synchrotron accelerator which can deliver particles of momentum P and charge Z up to P/Z = 4 GeV/c. Monokinetic neutron beams of momentum up to 2 GeV/c can be produced. The spallation studies deal with measurements of : (i) differential neutron production cross sections from thin targets, (ii) neutron multiplicity distribution for proton and ^{3}He induced reactions, and (iii) nuclide production in thin targets. Measurements on thick or composite targets are under consideration.

OVERVIEW OF SATURNE

SATURNE is a French National Laboratory funded and operated jointly by the Commissariat à l'Energie Atomique and the Centre National de la Recherche Scientifique. Located at Saclay, it has been in operation since 1978 [1].

SATURNE consists of two concentric synchrotrons. The inner one, MIMAS is an accumulator and accelerator matched to the ion sources in which protons can be accelerated up to 45 MeV. The outer one, SATURNE, is fed by MIMAS with 100 % transfer efficiency. After acceleration, particles are delivered through slow resonant extraction. The cycle duration can be varied in the range from 0.8 to 3.6 s, and the duty cycle decreases from 40 % at 1 GeV to 12 % at 2.9 GeV.

All the temporal microstructure of the beam is washed out so that time-of-flight techniques cannot be used.

Projectiles Accelerated in Saturne

Three ion sources are currently in use. DIONE delivers heavy ions up to krypton, HYPERION delivers polarized protons and deuterons, and AMALTHEE provides proton, deuteron, ^{3}He and ^{4}He beams. The mean characteristics of light ion beams [1] are given in table 1.

Table 1. Light Ions Accelerated in SATURNE

Projectile	A	Q	Intensity (part/cycle)	Max Energy (GeV/u)
p	1	1+	8.10^{11}	2.95
d	2	1+	5.10^{11}	1.15
He	3	2+	2.10^{11}	1.69
He	4	2+	2.10^{11}	1.15
$\bar{p}$	1	1+	2.10^{11}	2.95
$\bar{d}$	2	1+	3.10^{11}	1.15

Monokinetic Neutron Beams

Stripping of deuterons in a light target can be used to produce quasi-monokinetic neutrons. Due to the relatively large average distance between proton and neutron inside the deuteron, which is of the same order of magnitude as the dimension of a light target nucleus, the probability for both nucleons in the deuteron to interact with the constituants of a same nucleus is small. Most of the time, only one of the nucleons will interact, which allows one to define a spectator nucleon and to use the impulse approximation to determine its momentum distribution inside the deuteron.

The angular and momentum distributions of the spectator nucleon in the laboratory then result from the Lorentz transformation of these quantities from the deuteron rest frame to the laboratory frame. Therefore the energy and angular spread in the laboratory for the spectator nucleon are smaller at higher incident deuteron energy as can be seen in Fig. 1.

Good quality neutron beams with momentum between 1 and 2 GeV/c have been obtained at SATURNE using a 18 cm thick Be target [2]. Remaining deuterons and stripping protons were swept away from the beam using a dipole magnet to obtain a pure neutron beam. About 0.2 neutrons per deuteron were produced at 1.5 GeV/c with a transmission of the order of 5.10^{-4} within a 1 mrad half-angle cone centered on the incident deuteron beam direction. The neutron beam intensity at 0° varies linearly with the square of the neutron momentum. The contamination from inelastically produced neutrons in the momentum region of stripping neutrons is negligible. Absolute neutron flux calibration to within ± 5 % was obtained using ^{12}C activation and data from the $n + p \rightarrow d + \pi^\circ$ reaction.

Although deuteron stripping and Coulomb dissociation cross sections are more important for heavy nuclei, these cross sections are not of practical use for producing neutrons in thick targets because of deuteron multiple Coulomb scattering and secondary reactions in the target.

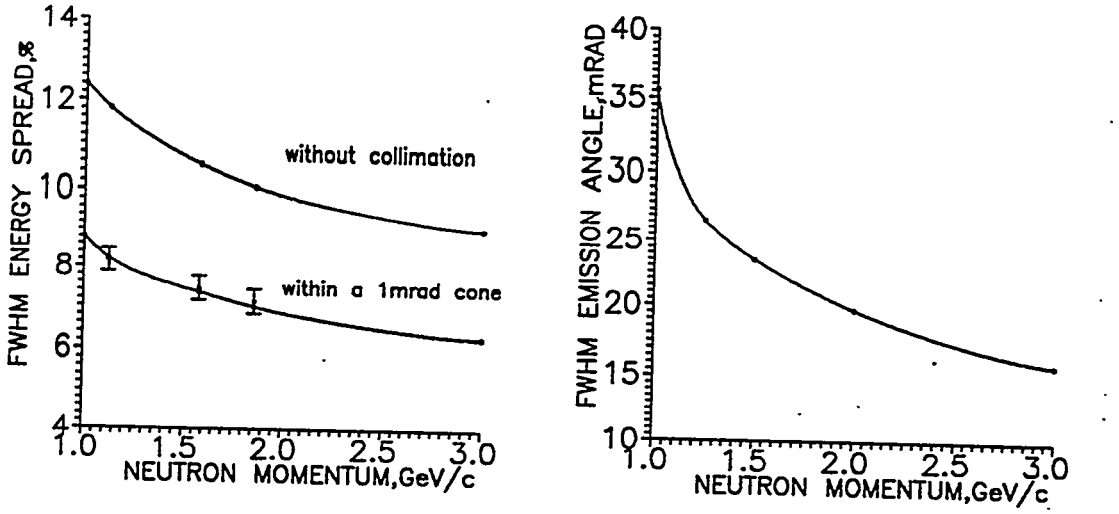

Fig. 1. Deuteron stripping on Be : energy and angular spread of emitted neutrons as a function of their central momentum. Taken from Ref. [2].

SPALLATION EXPERIMENTS AT SATURNE

Most of SATURNE scientific programmes deal with the study of strong interactions, nuclear structure experiments and heavy ion physics. However taking advantage of the specific beams delivered by SATURNE. [2], applied experiments dealing with spallation physics have been recently planed and allocated a significant fraction of beam time. A review of these experiments is now presented.

Differential Neutron Production Cross Sections

Differential (p, xn) cross sections, $d^2\sigma/d\Omega.dE_n$, have been measured from thin targets of a selected number of elements mainly for incident protons in the energy range below 800 MeV. Above 800 MeV, as well as for other incident particles, the data are very scarce [3].

An experimental program to extend the existing data for incident protons and deuterons in the energy range up to about 2 GeV is under development at SATURNE as a result of a cooperation between several french laboratories with an active participation of Uppsala University. Time structure of the beams delivered by SATURNE does not allow to use time-of-flight techniques which moreover are less and less efficient as the neutrons become more and more relativistic. The principle of a measurement at 0° for the high energy part of the spectrum, as adopted in previous measurements at SATURNE [4], is shown in Fig. 2.

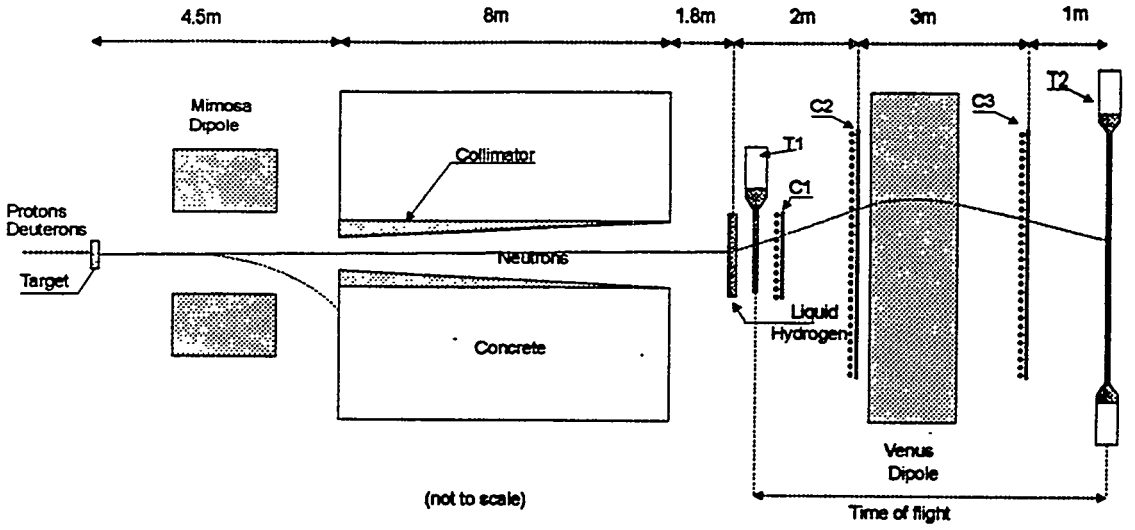

Fig. 2. Experimental set-up for measurements at 0° of the high energy part of a neutron spallation spectrum.
C1, C2, C3 : Multiwire proportionnal counters.
T1, T2 : plastic scintillator detectors.

After interaction with the target, the incident beam as well as the charged spallation particles from the target are swept away by the MIMOSA dipole. Neutrons are collimated on to a 14 cm diameter liquid hydrogen target. Since there is a direct correspondance between the energy of an incident neutron and the energy of the elastically scattered proton at a given angle in the hydrogen target, the neutron spectrum can be obtained from the measurement of the double differential proton spectrum. The angle of emission and the momentum of the scattered protons

are obtained using three multiwire proportionnal counters C1, C2 and C3, each with a spatial resolution of 2 mm, and a magnetic deflection in the VENUS dipole.

Other reactions are also taking place in the hydrogen target. Deuterons can be produced through the reaction $n + p \rightarrow d + \pi^\circ$ for which the cross section is very well known [4]. In order to discriminate between protons and deuterons having identical momentum and trajectory, a time-of-flight measurement using the signals from two thin plastic scintillator detectors T1 and T2 is also performed.

Inelastically scattered protons are also present in the proton spectrum as shown in Fig.3. By using a deuteron beam incident on a Be target to produce monokinetic incident neutrons, elementary response functions will be measured. At the same time deuterons from the secondary $n + p \rightarrow d + \pi^\circ$ reaction will provide an efficiency calibration of the detection line.

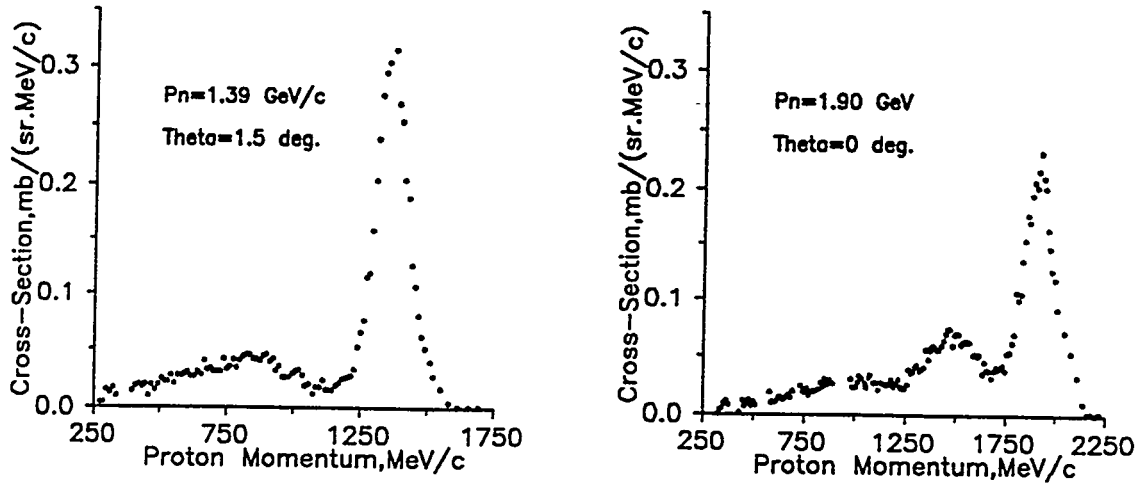

Fig.3. Experimental proton momentum distribution from the inclusive reaction $n\,p \rightarrow p\,x$ at final proton lab angle Theta for incident neutrons of momentum 1.39 and 1.90 GeV. Taken from Ref. [4].

Due to proton energy losses in air and detectors, this apparatus is limited to the analysis of the incident neutron spectrum region above about 200 MeV. The experimental method used for lower energies is shown in Fig. 4. A thin plastic scintillator placed in front of the target will be used to tag the incident particles, and a liquid scintillator will detect the neutrons at the exit of the collimator. The time-of-flight measurement between tagged incident particles and detected neutrons will provide the neutron energy spectrum. Tagging imposes a reduction of the incident charged particle flux down to about 10^6 per cycle. To reduce random coïncidences in the time-of-flight measurement, we plan to tag again with a thin plastic scintillator the swept charged particles behind the MIMOSA dipole. This is intended to identify those incident particles which have not interacted with the target and therefore cannot be at the origin of a detected neutron.

The whole experiment is presently settled for a detection angle of 0° and calibrations are in progress. The first data acquisition is planned for November 94. In this experiment, we will study 0.8 and 1.2 GeV protons incident on a lead target. In the near future, measurements on tungsten, lead and structural materials for incident protons and deuterons are planned. Minor modifications

of the experimental apparatus will then allow us to perform measurements at angles up to 20°. This is possible at SATURNE by changing the beam axis on the target using a movable magnet.

Measurements at larger angles will require important modifications of the experimental area to be worked out.

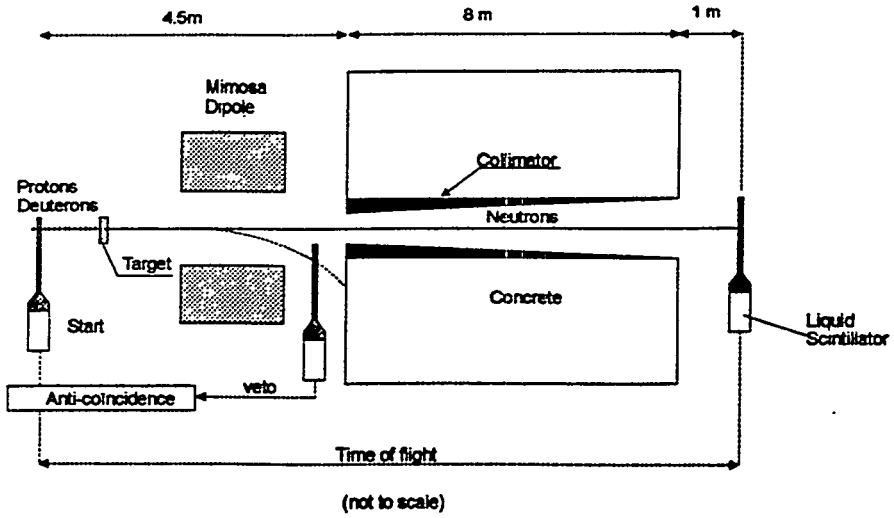

Fig.4. Experimental set-up for measurements at 0° of the low energy part of a neutron spallation spectrum.

Neutron Multiplicity Distribution Measurements

Neutron multiplicity distribution measurements have been performed at GANIL [5] to study the formation and decay of hot nuclei formed from the interaction of energetic heavy ions with a range of targets. However, the interpretation of the data was complicated by the presence of collective excitation modes which can be strongly excited in nucleus-nucleus collisions. Light energetic projectiles then appeared as an interesting alternative to investigate hot nuclei and their limit of stability. This latter experiment was performed at SATURNE [6] using the GANIL 4π neutron detector ORION. It consisted in measuring, event after event, the number of emitted neutrons in correlation with the characteristics of the light charged particles (p, d, t, He), intermediate mass fragments (Li, Be, B, C, ...), and fission fragments also emitted.

The experimental set-up is shown in Fig.5. ORION is a 4 m^3 Gd-loaded liquid scintillator viewed by 24 photomultiplier tubes. A thin target surrounded by the charged particle detectors is placed in a central hole and irradiated by a collimated incident beam of reduced intensity. A start detector placed 30 meters ahead of the target is used to tag the incident particles. Neutrons originating from a spallation event in the target are slowed down in the scintillator giving rise, together with emitted γ-rays, to a prompt pulse at the output of the photomultiplier tubes. A coïncidence between this prompt pulse and the start detector identifies the spallation event. The slowed down neutrons migrate in the scintillator until their capture by a gadolinium nucleus. Capture γ-rays cause scintillations which are detected by the photomultiplier tubes. Due to the low Gd concentration, the time distribution of capture events (Fig. 5(a)) is large enough for the captures to be detected one by one within a 100 μs time interval following an event when up to ~50 neutrons are emitted.

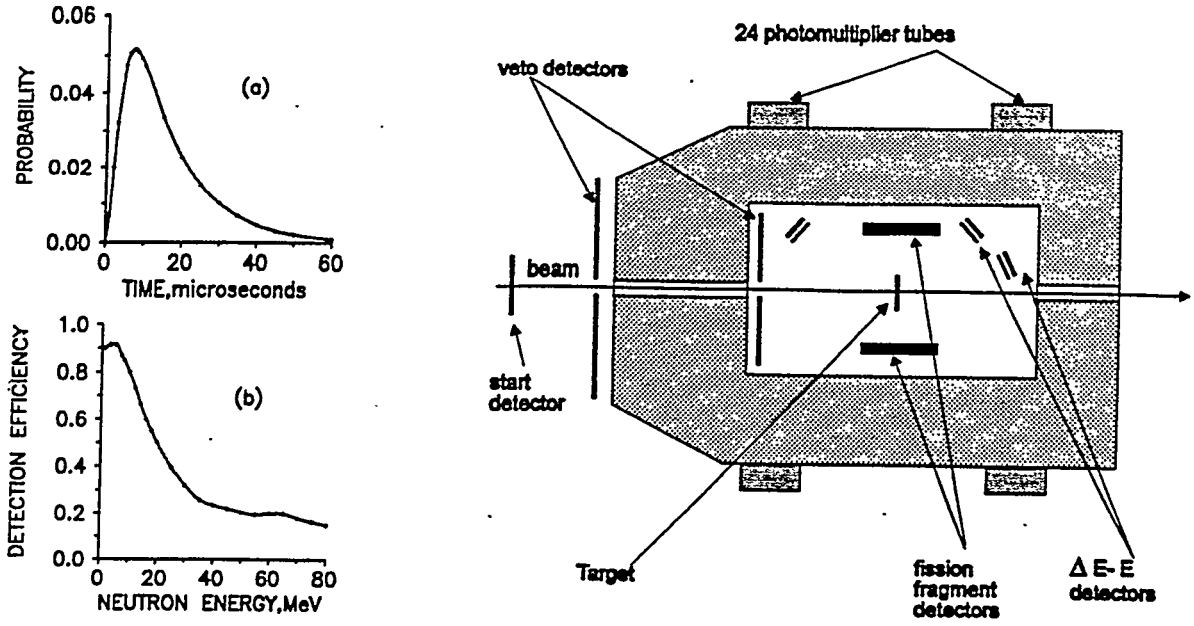

Fig.5. Principle of the ORION experiment for spallation neutron multiplicity distribution measurements. Taken from Ref. [5].
(a) Time distribution of neutron detection.
(b) Energy dependance of neutron detection efficiency.

Fig.5(b) shows the calculated detection efficiency for an isotropic source of neutrons placed at the center of the detector, as a function of their energy : ORION is mainly sensitive to evaporation neutrons. The calculated average detection efficiencies (about 75 %) using double differential neutron spectra as calculated by HETC are nearly independent of the nature of incident particles, their energy, and of the target.

Neutron multiplicity distributions have been measured [6] for Ag, Au, Bi and U for incident protons of 475 MeV and 2 GeV and for ^{3}He ions of 2 GeV. The measured distributions are shown in Fig.6. They exhibit a similar shape with a maximum at low multiplicity resulting from peripherical collisions, and a broad maximum at higher multiplicity corresponding to more central collisions. The number of neutrons increases with projectile energy for a given target, as well as with target mass for a given projectile energy. The distributions are very similar for protons and ^{3}He at 2 GeV. If this behavior is confirmed at lower energy, ^{3}He could be a good candidate for spallation projects because it would require shorter linear accelerators. These data are fairly well reproduced by HETC calculations made is our laboratory.

The experiment also provides useful information about the energy spectrum and multiplicity distribution of light charged particles. The multiplicity of the evaporation component of these charged particles is strongly correlated to the measured neutron multiplicity.

The ORION detector is furthermore divided into 5 sectors optically independent. Thus it can be used to deduce a rough information about the angular distribution of emitted neutrons.

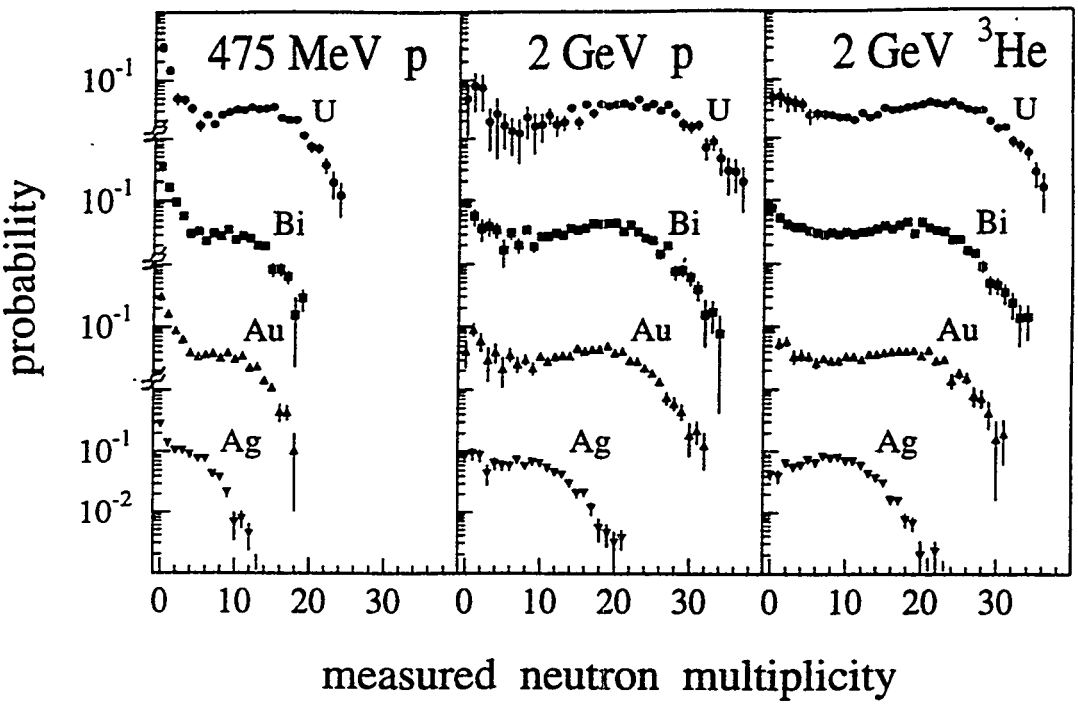

Fig.6. Neutron multiplicity distributions as measured for 3 different types of projectile impinging on U, Bi, Au and Ag targets. Taken from Ref. [6].

Residual Nuclide Production

Accurate knowledge of the radioactive species produced as a result of spallation reactions in target and structure materials is necessary to evaluate the potentialities of systems based on spallation neutron sources. A program to measure residual nuclide production was set up several years ago at SATURNE [7] with the aim of interpreting the observed abundance of cosmogenic nuclides. These nuclides result from the interaction of solar and galactic cosmic rays with matter. Induced proton reactions on thin targets of C, N, O, Mg, Al, Si, Ca, Ti, Mo, Fe, Ni, Rb, Sr, Y, Zr and Ba have been investigated at incident energies up to 2.6 GeV.

A complete set of excitation functions for a number of radioactive nuclides have been measured. Using this data base together with spectra of secondary particles calculated with transport codes such as HETC, nuclide production in thick targets could be reproduced with uncertainties better than 5 % [7].

An extension of this program at SATURNE aimed at including thin targets of materials of interest for spallation neutron sources has been accepted. Some other elements have also been included for nuclear systematics. Measurements will cover the following elements : C, N, O, Na, Cr, Zn, Cu, Y, Zr, Nb, Rh, Ba, Ta, W, Re, Os, Ir, Au, Pb, Bi. Up to 20 different thin-target stacks, mounted on a light aluminium support, and separated by a distance of about 20 cm to reduce interferences from secondary particles, will be irradiated at the same time.

It is intended to cover the incident proton energy range from 200 MeV to 2.6 GeV. Measurements have already been made at 0.6, 0.8, 1.2 and 1.6 GeV. Other measurements are planned for 1995.

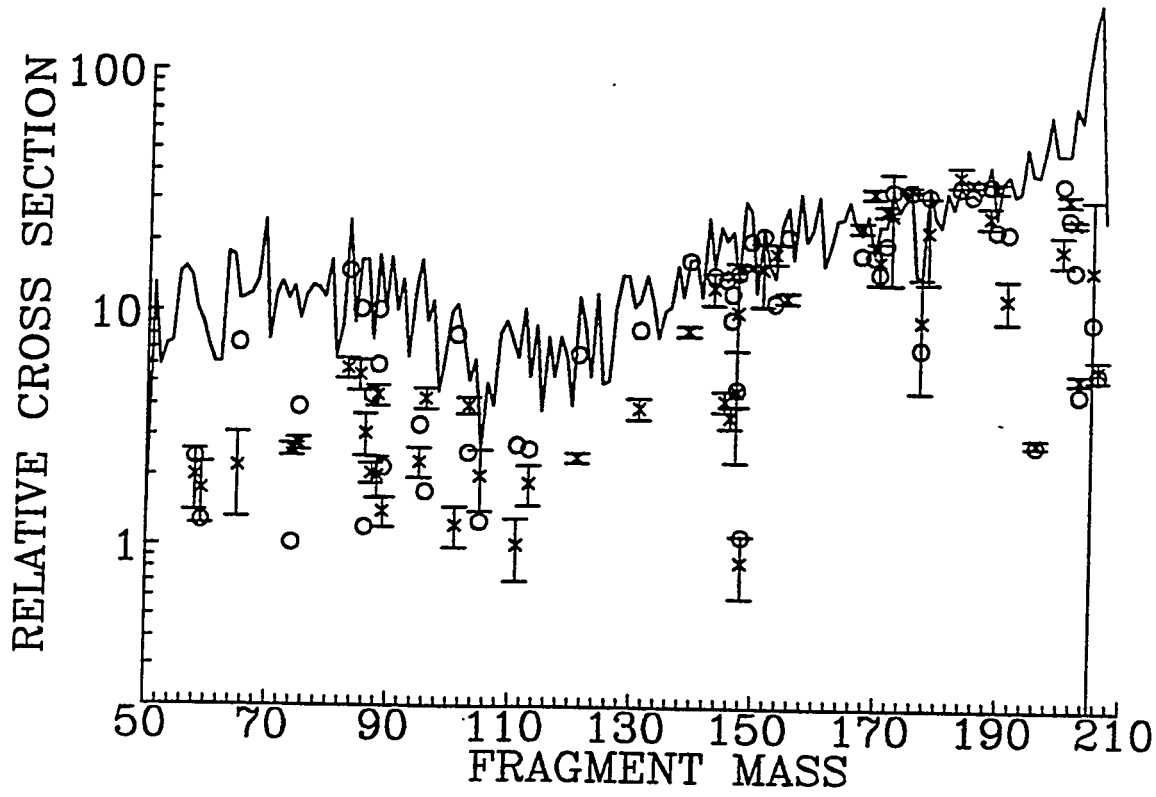

Fig.7. Residual nuclide production in a Pb target irradiated by 1.3 GeV protons :
× experimental data.
o simulation of the experiment using the results of a HETC calculation (histogram) and allowing for decay of short half-life nuclei.

The Radiochemistry Division at C.E. Bruyères-le-Châtel has now joined the collaboration. In the recent measurements on natural targets of W, Pb and U performed at 0.6 and 0.8 GeV proton incident energies, more than 150 nuclides are seen on a Germanium detector spectrum 15 hours after irradiation, and about 70 nuclides remain after 10 days. Chemical separation is used to separate elements of low activity or emitting low energy γ-rays.

Fig.7. presents results of a demonstration experiment on a Pb target irradiated by 1.3 GeV protons. Gamma-ray counting started only 9 days after irradiation. Experimental data are compared to a simulation made with the HETC code and taking into account the decay of short half-life isotopes for which all direct information was lost. Since the incident proton fluence has not been measured accurately, calculated values were renormalized on to experimental values.

Fluctuations of a factor between 0.5 to 2 are observed between experiments and calculations, but on the average fission as well as spallation residual nuclei are reproduced with a correct amplitude.

Measurements should be extended in the near future to a larger range of incident energies and to other targets such as Th and possibly Pu.

FURTHER PERSPECTIVES

Measurements of the absolute neutron production rate on thick targets are not given presently a high priority. As a follow-up of experiments already made at LAMPF, there is an ATW proposal to investigate several targets incorporating stopping lengths of high-Z (lead), low-Z (Lithium) and combinations of high-Z and low-Z neutron converters (thoria, lithium carbonate and teflon). The main objective is to establish the absolute neutron production function for the various incident particles available at SATURNE (p, d, ^{3}He) in an energy range between 0.4 and 1.5 GeV in order to test the predictive capability of the codes and to establish the foundations for designing composite targets for applications.

In these experiments the target is a cylinder 25 cm in diameter and 200 cm long surrounded by a 60 cm diameter lead blanket. The target-blanket assembly is surrounded by a large tank filled with a 1 % solution of $MnSO_4$ in light water. The absolute proton to neutron production rate is determined with an on-line germanium detector that monitors the γ-ray emission from the ^{56}Mn that is produced by thermal neutron capture in the manganese sulfate solution.

Despite of a common scientific interest, this experiment has been postponed due to a lack of support.

Another possibility under investigation is to use an ORION type detector adapted to house the large target and blanket assemblies. The neutron energy spectra from thick targets being softer than those from thin targets, an overall large detection efficiency should be obtained. Very low incident particle fluxes are needed (~10^3 per second).

Most of the fast secondary particles from spallation are neutrons. Data on spallation for thin targets with neutrons as projectiles would be useful, in particular for residual nuclide production [7]. The monokinetic neutron beams delivered at SATURNE seem to be intense enough to consider such measurements.

REFERENCES

[1] Boyard, J.L., Radvanyi, P., Soyeur, M., Nucl. Phys. News **2**, 15 (1992).

[2] Bizard, G., Bonthonneau, F., Laville, T.L., Lefebvres, F., Malherbe, J.C., Regimbart, R. ,Duflo, J., and Plouin, F., Nucl. Instr. and Meth. **111**, 451 (1973).

[3] Cierjacks, S., "Cross Section Measurements, Integral Validation Experiments and Nuclear Model Code Developments of Importance to Accelerator-Based Transmutation", in Proceedings of the OCDE/NEA Specialist'Meeting on Accelerator-Based Transmutation, PSI, Switzerland, March 92, PSI-Proceedings 92-02,556.

[4] Bizard, G., Bonthonneau, F., Laville, T.L., Lefebvres, F., Malherbe, J.C., Regimbart, R. ,Duflo, J., and Plouin, F., Nucl. Phys. **B108**, 189 (1976).

[5] Jiang, D.X., et al., Nucl. Phys. **A503**, 560 (1989).

[6] Pienkowski, L. et al.,"Hot Nuclei in Reactions Induced by 475 MeV, 2 GeV ^{1}H and 2GeV ^{3}He ", preprint Ganil P9410, accepted for publication in Phys. Lett. B (1994).

[7] Michel, R., "Nuclear Data for the Interpretation of Cosmic Ray Interactions With Matter", Proceedings of International Conference on Nuclear Data for Science and Technology, Gatlinburg, Tenessee, USA May 9-13 (1994).

LANL Sunnyside Experiment: Study of Neutron Production in Accelerator-Driven Targets[1]

G. Morgan, G. Butler, M. Cappiello, S. Carius[2], L. Daemen, B. DeVolder, J. Frehaut[3], C. Goulding, R. Grace, R. Green, P. Lisowski, P. Littleton, J. King, N. King, R. Prael, T. Stratton, S. Turner[4], J. Ullmann, F. Venneri, and M. Yates
Los Alamos National Laboratory
Los Alamos, NM 87545

Abstract. Measurements have been made of the neutron production in prototypic targets for accelerator driven systems. Studies were conducted on four target assemblies containing lead, lithium, tungsten, and a thorium-salt mixture. Integral data on total neutron production were obtained as well as more differential data on neutron leakage and neutron flux profiles in the blanket/moderator region. Data analysis on total neutron production is complete and shows excellent agreement with calculations using the LAHET/MCNP code system.

INTRODUCTION

A key factor in the design of any accelerator-driven transmutation system is the neutron production in the target system. Transport codes, including high energies, will be the main tool used in these designs. It is crucial to the development of accelerator-driven systems that data be provided to benchmark the ability of these codes to accurately predict neutron production. We have therefore studied neutron production in several assemblies which have dimensions and compositions similar to likely candidates for actual production targets. These experiments included the measurement of quantities with both integral and differential natures. The most important of these was the accurate determination of the total neutron yield. In addition, on two of the targets we studied the energy spectra of neutrons leaking from the assembly and profiled the neutron flux inside the blanket and moderator surrounding the target.

The four types of targets were selected to give information relevant to systems which are under consideration for various transmutation schemes. These include solid lead, solid lithium, a thorium-salt mixture, and a series of separated tungsten plates. While some of the results of these experiments are still being analyzed, the principle integral measurement, the neutrons per incident proton, has been completed and will be compared with calculations using the LAHET/MCNP [1] code system. These data will be the focus of this report, with some indication given as to the status of the neutron leakage and flux profile work.

EXPERIMENTAL PROCEDURE

In order to facilitate the study of several targets, a standard design was adapted for all the targets. They were required to fit inside a 25 cm diameter by 335 cm long aluminum tube. This tube was then placed inside a lead blanket which was 200 cm long by 60 cm outside diameter. The measurement of neutrons / proton was carried out using the manganese bath technique. In this technique, the neutrons produced in the target are trapped and moderated in the water and a

---

[1]Work performed under the auspices of the U. S. Department of Energy.
[2]Uppsala University.
[3]Commissariat a l'Energie Atomique.
[4]University of Michigan

fraction are captured in the manganese to form ^{56}Mn, which has a half life of 2.6 hours and emits an easily detected gamma-ray of 846 keV energy. The target-blanket assembly was surrounded by a water moderator tank 2.5 m in diameter and 3.0 m long. The system is illustrated in Fig. 1. The tank was constructed in three sections for ease of handling. The upper section could be drained and removed to permit opening of the blanket and changing of the target. The lower two tank sections contained water with a 1% $MnSO_4$ while the upper section contained only pure water. While this arrangement compromised the symmetry of the experiment, it was necessary to insure that the target could be changed without the possibility of spilling any water containing the radioactive ^{56}Mn. Note also that since most of the ^{56}Mn is produced near the target, it is necessary to carefully mix the water before extracting a sample for counting in order to be able to accurately determine the total ^{56}Mn production. This mixing was accomplished with a circulation system using two pumps, each of which removed water from the outer region of one section and injected it into the central region of the other section through a pipe running the length of the tank and having orifices designed to maximize turbulence. A high resolution germanium detector was mounted in a shielded box in contact with one of the circulating pipes about 3 m from the tank. It was used to monitor the ^{56}Mn activity in the circulating water after an irradiation. This allowed us to ascertained that the water was completely mixed by observing that the decrease in activity in the line accurately tracked the half-life of ^{56}Mn.

This experiment was carried out in the Target 2 area at the Weapons Neutron Research facility of the Los Alamos Meson Physic Facility. Target 2 is a shielded room approximately 12 m in diameter and with a series of flight paths radiating from the center of the room (see Fig. 4). Proton beams from LAMPF of up to 100 nA can be accommodated. Proton beams exit the beam line through a thin stainless steel window and enter the target system in air. Figure 1 shows the details of the target, blanket, and moderator assembly. As noted in the figure, the blanket and moderator tank contain tubes parallel to the proton beam direction and at various radii which permit the introduction of activation foils which can be used to map the neutron flux. With the tank drained or removed (a separate stand was built to support the target and/or target-blanket assemblies), neutrons leaking from the system could be observed through four flight paths at angles of 7.5, 30, 60, and 150° with respect to the incident proton beam.

Details of the targets are shown in Fig. 2. The upper is a solid lead cylinder, 120 cm in length (note that stopping length for 800 MeV protons is about 40 cm). The front of the lead was 20 cm upstream of the center of the assembly. The extra 80 cm behind the stopping length served to trap and multiply forward going high energy neutrons produced in the primary interaction region. The second target consisted of 170 cm of ^{7}Li metal contained in seven sections, each sealed in a stainless steel can. The stopping power of Li is low and this length was sufficient to stop only 400 MeV protons, so the beam energy was lowered to this value for the Li target measurements. The third target was intended to mock-up a mixture of thorium in molten salts with lithium and fluorine. It contained a mixture of thorium oxide, lithium carbonate, and Teflon. This target was fabricated on short notice when additional beam time became available and the as-built target did not have the expected density leading to insufficient length to stop 800 MeV protons. To remedy this situation a Teflon plug was added ahead of the main target. The last target studied was a series of separated tungsten plates with increasing thickness. A cylinder of lead was located behind these plates.

Extensive calculations were carried out to aid in design of the experiment. These indicated that for a system of this size the maximum neutron leakage from the moderator tank would be

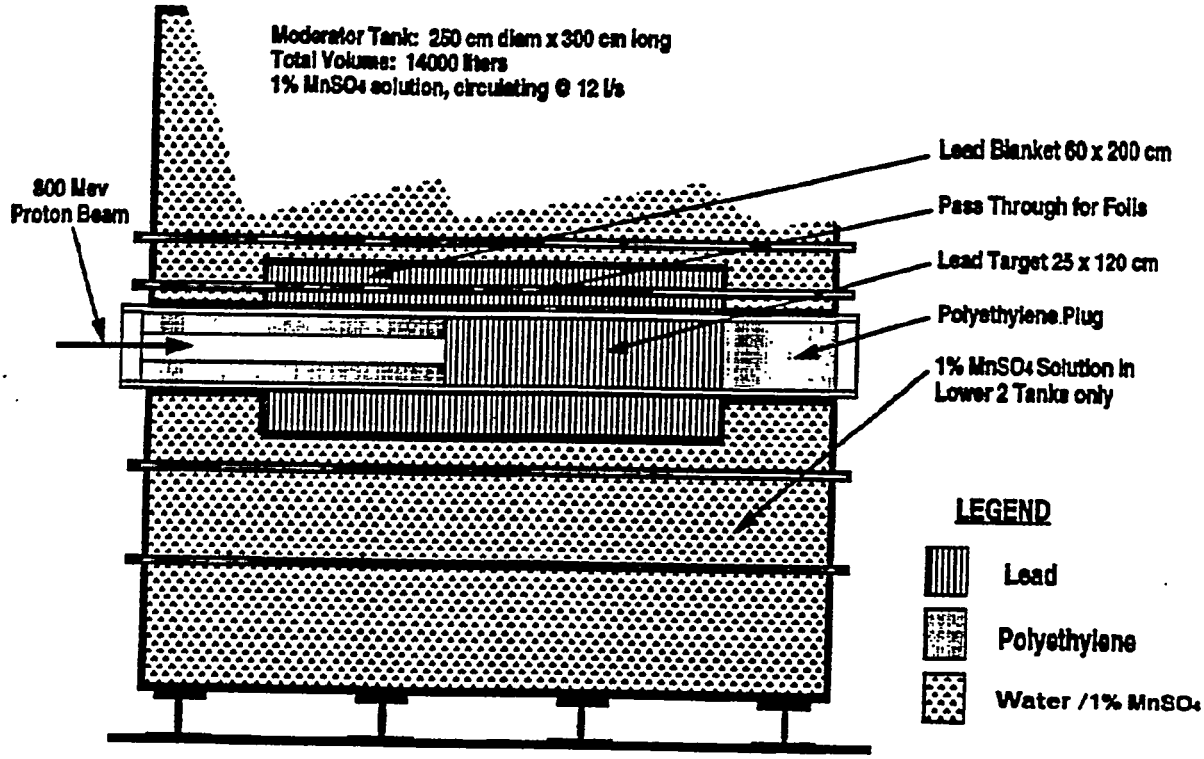

Fig. 1. Schematic diagram of the target assembly, lead blanket, and water moderator tank.

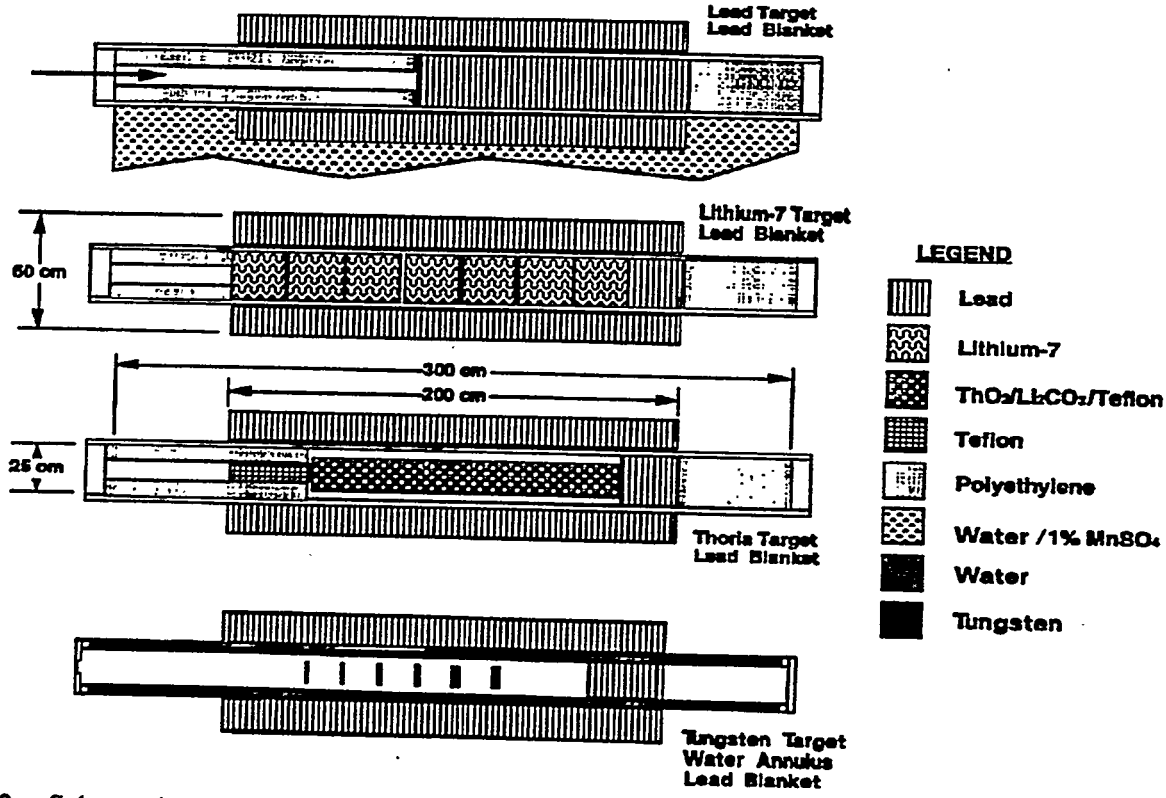

Fig. 2. Schematic diagrams of the four types of target / blanket assemblies studied here.

only 1.7% for the lithium target and much less for the other systems. With manganese only in the lower two sections, a 5 cm vertical displacement of the proton beam from the center of the target would result in a 15% change in ^{56}Mn production. It was therefore necessary to carefully monitor the proton beam position. To accomplish this a system was implemented to image the proton beam spot on the front face of the target. It is shown in Fig. 3 and consisted of a Cr doped aluminum oxide phosphor indexed and accurately mounted on the target. A thin aluminized mylar pellicle reflected the light from this phosphor into a lens system which relayed the image to a mirror and then into a shielded camera system. This camera system contained a wavelength filter to help remove stray light, a gated image intensifier, and a CCD video camera. This system permitted both real-time observation of the beam size and position and also recording of the beam intensity profiles during the course of the irradiation. The image was relayed to the accelerator control room and permitted the operators to quickly correct any diffuse or dislocated beam spots. In all cases, any dislocation of the beam was corrected within 5 minutes of the beginning of irradiation. In all cases the beam spot was maintained within 0.5 cm of the target center.

Also shown in Fig. 3 are the systems used to determined the total number of protons incident on the target during the course of an irradiation. These consisted of an aluminum foil whose activation cross sections at 800 MeV are accurately known [2] and an integrating current transformer which permitted the charge in each micropulse to be measured and recorded. The current transformer responds to beam pulses with less than 1 ns width and produces an output pulse with a width of about 20 ns and a charge proportional to the beam charge. This signal was fed into a charge-sensitive preamplifier, then to a linear shaping amplifier, and finally to an analog-to-digital converter. Each micropulse (separation was greater than 15 microseconds) was digitized and stored as a histogram during the irradiation. The total charge could be obtained by calculating the weighted integral of this histogram. The system was calibrated using a precision step pulse generator driving a accurately known charge terminating capacitor which was connected to a loop through the transformer. Comparison of the beam charge determined with the transformer and the Al activation agreed on average to 2%. The ratio had a variance of about 2.2% which was attributed to the transformer. For the measurements at 800 MeV, the Al activation was taken as the primary determination of number of protons. A correction factor (about 2%) was derived for the transformer and it was used to determine the number of protons for the measurements at 400 MeV where the Al activation cross sections are not as well known.

An irradiation proceeded as follows. A fresh Al foil was mounted in the beam in front of the target assembly. If they were not already running, the circulating pumps were started. Two water samples were taken to establish background activity levels. The integrating current transformer and its associated electronics were calibrated. The imaging system was activated and the data acquisition computer for the current transformer was turned on. The accelerator operators were requested to begin beam delivery. The time was recorded. As soon as beam was on target, the operators observed the beam spot with the imaging system and made any adjustments necessary to center and focus the beam. A typical irradiation for the lead target was about 30 minutes at 50 nA beam current. At the end of irradiation, the time was recorded and a series of short counts were begun with the gamma-ray detector on the circulating line. The circulating pumps were run for at least 45 minutes and then two water samples were obtained. Any activation foils in the blanket and moderator were removed at this time. The gamma-ray detector on the circulating line continued to operate to track the decay of the ^{56}Mn. The two water samples were taken to calibrated counters in another location and accurately measured amounts of water were removed

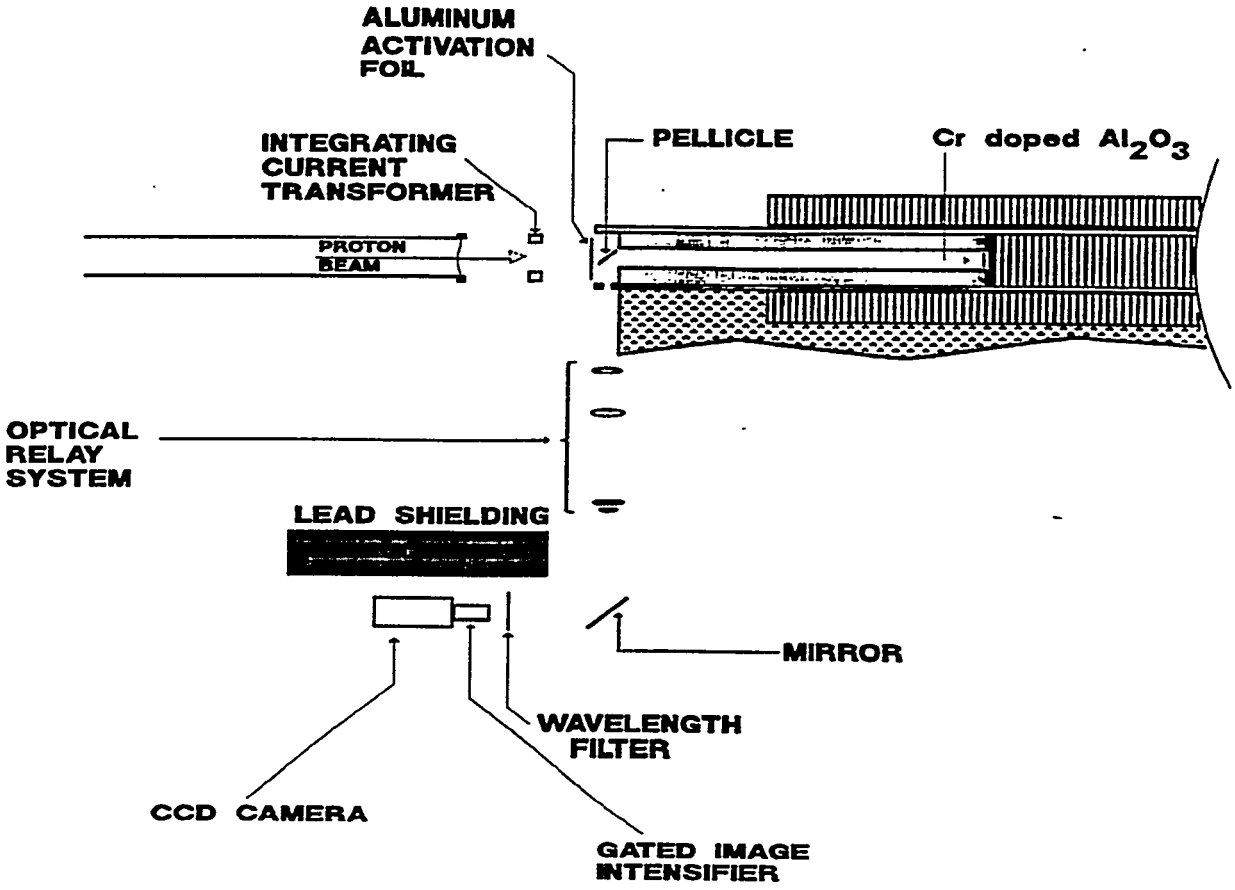

Fig. 3. Details of the systems used to monitor proton beam intensity and position.

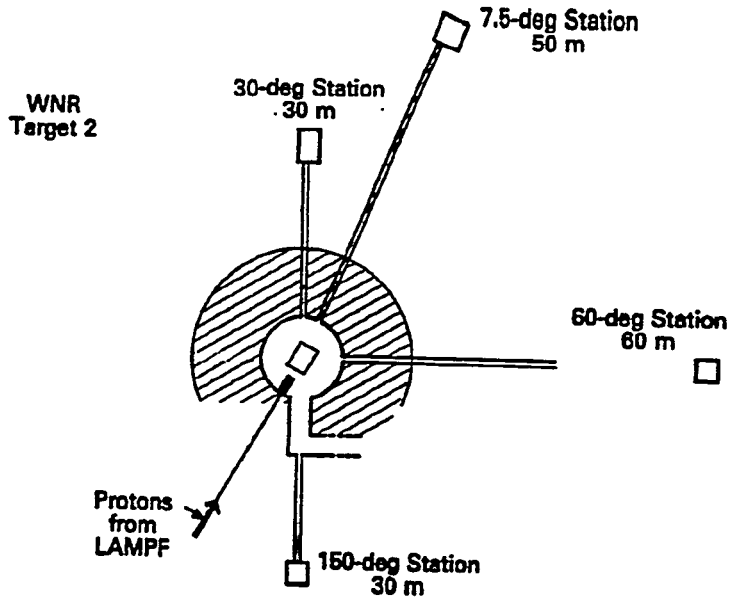

Fig. 4. Schematic diagram of Target 2 with the associated neutron flight paths used to measure neutron leakage from the target assemblies.

from the samples and counted to determine activity. The measured activities were corrected for decay after and during irradiation and scaled to total volume of water in the moderator system to determine the total number of ^{56}Mn atoms produced. The aluminum activation foil was removed and counted at the same location to determine the total number of protons using the measured cross sections with appropriate corrections for the decay of the activation products.

RESULTS

Having the total number of ^{56}Mn atoms and the total number of protons, one can determine the number of ^{56}Mn atoms produced per incident proton. This number was the experimentally measured quantity which could be compared to that calculated by the LAHET / MCNP code and used to test the neutron yield per proton generated by the code.

The statistical uncertainties from the counting of the various activities were generally less than 2%. Additional systematic uncertainties arise from the calibration of the counters used to measure the ^{56}Mn and Al activation, the uncertainty in the total volume of water in the system, the concentration of $MnSO_4$, and the cross sections for proton activation of Al at 800 MeV [2]. The quadratic combination of all these systematic uncertainties is estimated to be 4.2%.

Table 1 gives the results of the yield determinations with their total uncertainties and compares them to the calculated values. Agreement is very good for all systems except the thorium-salt mock-up. This disagreement is probably attributable to problems with the fabrication of this target which caused its actual make-up to be poorly determined. With this exception, the experiment demonstrates the accuracy of LAHET / MCNP in predicting the total neutron production over a range of elements and proton energies.

Table 1. Neutron/Proton Measurements Compared to LAHET / MCNP

Target	Energy (Mev)	^{56}Mn/proton (Experiment)	Uncertainty (Absolute)	^{56}Mn/proton (Calculated)	Neutron/Proton (Calculated)
Lead	800	0.2046	0.0089	0.204	22.2
Lithium	397	0.0458	0.0022	0.0459	4.35
Tungsten	800	0.1255	0.0055	0.126	18.2
Th-Li-F	800	0.1094	0.0049	0.1243	12.6

A separate paper at this conference [3] will present results of the flux mapping done with a series of activation foils in the blanket and moderator. In addition, measurements of the neutron leakage spectra were obtained for the lead and lithium targets and are presently being analyzed. These data sets will provide test of a more differential nature.

Fig. 4 shows a schematic of Target 2 with the associated neutron flight paths. Calibrated plastic scintillators [4,5] were used to measure neutron time-of-flight spectra from 0.5 to 800 MeV at four angles with respect to the incident proton beam. The availability of additional beam time permitted the acquisition of data for the bare lead target and lead target/blanket combination without the water tank in place. ^{6}Li loaded glass scintillation counters were used along with the plastic scintillators and produced data over the energy region from 0.01 to 800 MeV.

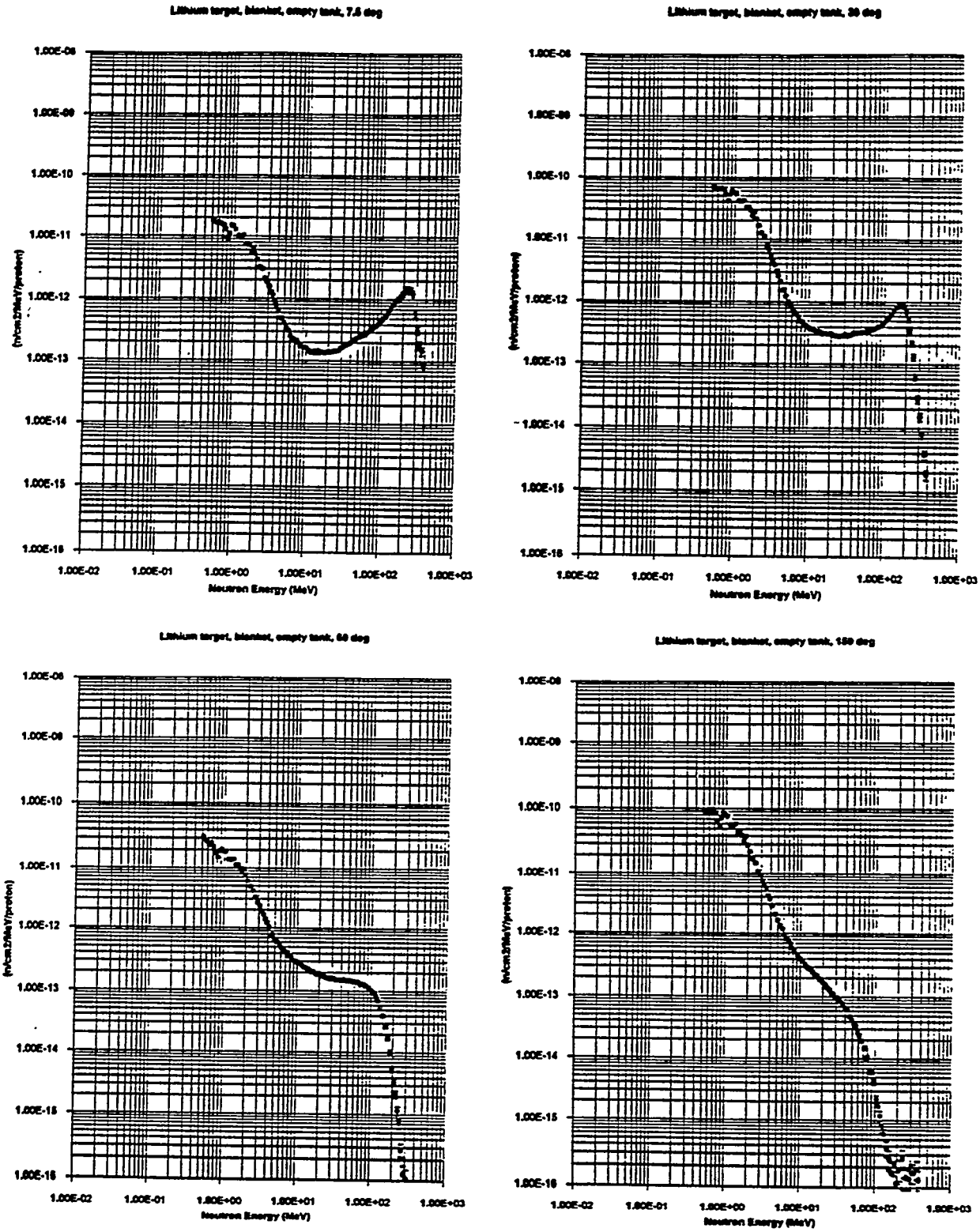

Fig. 5. Neutron leakage fluxes at the detector positions for the lithium target plus blanket. The empty water tank was in place for these measurements.

Examples of leakage spectra for lithium target are shown in Fig. 5. The data shown here are the neutron fluxes at the detector positions, normalized to unit incident proton. These results are for detectors distances of 51.15, 29.85, 59.4, and 31.51 m at angles of 7.5, 30, 60, and 150°, respectively. The corresponding fields-of-view at the center of the target assemblies are 11.07, 11.71, 10.64, and 12.09 cm in diameter. These results are in the process of being compared to calculations with LAHET / MCNP.

REFERENCES

[1] Prael, R. E., and Lichtenstein, H., *Los Alamos Report LA-UR-89-3014*, 1989.

[2] Cumming, J. B., Agoritsas, V., and Witkover, R., *Nuclear Instruments and Methods* **180** , 37-44 (1981).

[3] Butler, G. W., "ATW Neutron Spectrum Measurements at LAMPF", presented at the International Conference on Accelerator-Driven Transmutation Technologies and Applications, Las Vegas, Nevada, July 25-29, 1994.

[4] Amian, W. B, Meier, M. M., Byrd, R. C., Goulding, C. A., and Moss, C. E., *Nuclear Instruments and Methods* **A281**, 353-358 (1989).

[5] Amian, W. B., Meier, M. M., Byrd, R. C., Goulding, C. A., Morgan, G. L., and Moss, C. E., *Nuclear Instruments and Methods* **A313**, 452-456 (1992).

800-MeV Proton Irradiation of Thorium and Depleted Uranium Targets

G. J. Russell, T. O. Brun, E. J. Pitcher, and L. L. Daemen
Manuel Lujan, Jr. Neutron Scattering Center (LANSCE)

W. B. Wilson
Nuclear Theory and Applications Group

Los Alamos National Laboratory
Los Alamos, NM 87545

As part of the Los Alamos Fertile-to-Fissile-Conversion (FERFICON) program in the late 1980's, thick targets of the fertile materials thorium and depleted uranium were bombarded by 800-MeV protons to produce the fissile materials ^{233}U and ^{239}Pu, respectively. The amount of ^{233}U made was determined by measuring the ^{233}Pa activity, and the yield of ^{239}Pu was deduced by measuring the activity of ^{239}Np. For the thorium target, 4 spallation products and 34 fission products were also measured. For the depleted uranium target, 3 spallation products and 16 fission products were also measured. The number of fissions in each target was deduced from fission product mass-yield curves. In actuality, axial distributions of the products were measured, and the distributions were then integrated over the target volume to obtain the total number of products for each reaction.

We have re-analyzed the FERFICON conversion experiments with the latest versions of the Los Alamos LAHET/CINDER'90 code package. Some of the major changes in LAHET (compared to HETC which was used in the first experimental analysis) are inclusion of: a) elastic scattering; b) an optional pre-equilibrium model; c) a Fermi breakup model for light nuclei; and d) an energy-dependent level density formulation. The CINDER'90 code is being modified to handle fissionable materials. We will give an overview of the FERFICON experiments, and present the comparisons between our latest calculated results and measured values.

ATW NEUTRON SPECTRUM MEASUREMENTS AT LAMPF*

G. W. Butler, P. E. Littleton, G. L. Morgan, T. F. Stratton, and M. A. Yates
Los Alamos National Laboratory
Los Alamos, NM 87545

Accelerator transmutation of waste (ATW) is a proposal to use a high flux of accelerator-produced thermalized neutrons to transmute both fission product and higher actinide commercial nuclear waste into stable or short-lived radioactive species in order to avoid long-term storage of nuclear waste. At LAMPF we recently performed experiments that were designed to measure the spectrum of neutrons produced per incident proton for full-scale proposed ATW targets of lead and lithium. The neutrons produced in such targets have a spectrum of energies that extends up to the energy of the incident proton beam, but the distribution peaks between 1 and 5 MeV. Transmutation reactions and fission of actinides are most efficient when the neutron energy is below a few eV, so the target must be surrounded by a non-absorbing material (blanket) to produce additional neutrons and reduce the energy of high energy neutrons without loss. The experiments with the lead target, 25 cm diameter by 40 cm long, were conducted with 800 MeV protons, while those with the lithium target, 25 cm diameter by 175 cm long, were conducted with 400 MeV protons. The blanket in both sets of experiments was a 60 cm diameter by 200 cm long annulus of lead that surrounded the target. Surrounding the blanket was a steel water tank with dimensions of 250 cm diameter by 300 cm long that simulated the transmutation region. A small sample pipe penetrated the length of the lead blanket and other sample pipes penetrated the length of the water tank at different radii from the beam axis so that the neutron spectra at different locations could be measured by foil activation. A selected set of activation foils and threshold detector foils were inserted in the sample pipes for each irradiation to measure the moderated neutron spectra at a few radial and axial positions. The foils that were used included Au, In, (cadmium ratios were measured for Au and In foils), Dy, Lu, Mo, Ti, and W foils. Irradiation times were typically 20 minutes at 50 nA to achieve adequate activation to yield 3% counting statistics. After irradiation the activated foil sets were extracted and counted with calibrated high resolution germanium gamma ray detectors at the Los Alamos nuclear chemistry counting facility.

These experiments provided neutron spectrum measurements in full scale experimental geometries that closely correspond to those proposed for ATW. The results will provide a benchmark for verifying modeling calculations of these large scale accelerator-based reactor concepts.

*Work performed under the auspices of the U. S. Department of Energy

690

Resonance Enhancement in the Accelerator Transmutation of 1.3-day ^{232}Pa and 2.1-day ^{238}Np

M. S. Moore* and Y. Danon†

**Group P-15, Mail Stop D-406, Los Alamos National Laboratory*
Los Alamos, New Mexico 87545
and
†Department of Nuclear Engineering and Engineering Physics
Gaerttner Linac Laboratory, Rensselaer Polytechnic Institute
Troy, NY 12180-3590

Abstract. The suggestion that the transmutation of actinide waste into fission products might best be done with thermalized spallation neutrons and odd-odd target materials such as ^{238}Np has been studied. During the 1993 LAMPF/PSR cycle, we measured the fission cross section of 1.3-day ^{232}Pa and 2.1-day ^{238}Np from 0.01 eV to 40 keV at the LANSCE facility, and have carried out a preliminary resonance analysis of the observed structure and of the thermal region, with a 1/v representation above a few eV. In the present study, we calculate the reaction rates of these two species and ^{247}Cm in a "resonance reactor," an accelerator-driven assembly whose slowing-down properties are well known. Our model is a 1.8 m^3 block of lead with a helium-cooled tungsten target in the center, i.e, the Rensselaer Intense Neutron Source (RINS). We include the effects of adding moderator outside an idealized lead slowing-down assembly, giving resonance enhancement factors for ^{232}Pa and ^{238}Np, and present parameters for the accelerator required to drive such an assembly to accomplish actinide burnup of these species.

INTRODUCTION

The suggestion was first made by Bowman et al [1] that the transmutation of actinide waste into fission products might be optimized by burning odd-odd target materials such as ^{238}Np and ^{242}Am in an assembly driven by a spallation neutron source. Because of the expected large fission widths of the odd-odd target isotopes, fission of these species would be the dominant reaction. It was also conjectured that the close spacings of the resonances could lead to a cross-section shape over the thermal Maxwellian that could be significantly different from 1/v, and that low-lying resonance structure could lead to a substantial enhancement of the burnup properties. In order to assess such effects, a measurement of the resonance fission cross section of these short-lived odd-odd targets is required. Of interest also, in connection with the Th-^{233}U fuel cycle, is the fission cross section of 1.3-day ^{232}Pa in the resonance region.

During the 1993 cycle of the Los Alamos Clinton P. Anderson Meson Physics Facility (LAMPF), we measured the fission cross sections of ^{232}Pa and ^{238}Np on a 5-m flight path at the Los Alamos Manuel J. Lujan Neutron Scattering Center (LANSCE). The samples were prepared by irradiating thick metal targets of ^{232}Th or ^{238}U with 19-MeV deuterons at the Los Alamos Ion Beam Facility (IBF), followed by radiochemical separation of the proactinium or neptunium produced by this irradiation. This material was then deposited onto a thin titanium backing that was inserted as one of the electrodes into a parallel plate fission chamber. The chamber was then transported to LANSCE facility, positioned in the neutron beam line, and the fission-fragment pulses were recorded over the next few days as a function of fission-fragment pulse height and neutron time of flight. The development of the technique, and a preliminary reduction and analysis of the data obtained, were described at the recent International Conference on Nuclear Data for Science and Technology. [2]

As part of the present study, we have carried out a final data reduction and a more elaborate analysis of the data from 0.01 eV to 40 keV, with a 1/v extrapolation to 100 keV. This parameterization was then used to calculate the reaction rates of these two species, and of another material of interest, ^{247}Cm, in an accelerator-driven assembly whose slowing-down properties are similar to those of the Rensselaer Intense Neutron Source (RINS), a 1.8 m^3 cube of pure lead with a helium-cooled tungsten target in the center. [3] We calculated the neutron flux in a similar-sized cylindrical lead assembly, and studied the effects of adding a moderator blanket on the outside. We found that the resonance enhancement factors in this latter assembly, with a D_2O blanket, can be significant. However, the accelerator required to drive such an assembly in order to accomplish efficient burnup of these short-lived actinides may be beyond present technology.

DATA REDUCTION AND ANALYSIS

We found that production of the odd-odd samples ^{232}Pa and ^{238}Np by the (d,2n) reaction with ten to fifteen μA of 19-MeV deuterons on thick samples of ^{232}Th and ^{238}U, respectively, gives a few tens of nanograms of the isotopes of interest, which is an adequate amount to permit us to carry out the measurement. There is a competing reaction, the (d,n), which has about four times the integrated cross section, and produces four times as much ^{233}Pa and ^{239}Np as ^{232}Pa and ^{238}Np. The presence of these isotopes is not a problem with fresh samples, as they are subthreshold fissioners, and their fission contribution is small compared to the statistical spread of the data and can be neglected. However, these isotopes are also reasonably short-lived, and their decay products are fissile; ^{233}Pa decays into ^{233}U with a 27.0-day half life, and ^{239}Np into ^{239}Pu with a 2.35-day half life. While the presence of these fissile decay products causes a serious background problem, in another sense it is an enormous advantage: we can normalize the ^{232}Pa fission cross section, through the radiochemically measured protactinium isotopic ratios and the half lives, to well-known resonances in ^{233}U, and the ^{238}Np fission cross section to resonances in ^{239}Pu. The results are summarized in Table 1; in both cases, the thermal (2200 m/s) fission cross sections are found to be substantially higher than those reported in the Mughabghab compilation. [4]

Table 1. Contents of the Fission Chambers[a] and Normalization Results.

Fission Chamber Number	Contents	Amount of Isotope of Interest[a]	Amount of Other Isotope[a]	Normalizing Resonances Used (eV)	2200 m/s Cross Section
1	Protactinium	33 ng ^{232}Pa	137 ng ^{233}Pa	1.8 + 2.3 ^{233}U	1500±100 b
2	Neptunium	5.9 ng ^{238}Np	33 ng ^{239}Np	0.296 ^{239}Pu	2600±200 b
3	Neptunium	3.2 ng ^{238}Np	14.8 ng ^{239}Np	0.296 ^{239}Pu	--

[a]At the time of the final radiochemical separation from uranium or plutonium.

The actual content of the isotope of interest in the fission chambers during the course of the experiment ranged from about 90 % at the beginning of data taking to between 10 and 30 % at the end. In order to take account of the decay of the isotope of interest and the growing in of the fissile decay-product isotopes, we automatically read out the data to disk every hour. Because of the wide

variability of the neutron beam intensity, we found it necessary to process each of these short runs, and to average the results, reduced to fission cross section for the isotope of interest and weighted according to the product of the average amount of sample material present during that hour and the number of counts recorded by a ^{235}U foil mounted in the same chamber. It is important to emphasize that the ^{235}U fission monitor served only as a beam-intensity and flux-shape monitor; the data normalization being done through the ^{233}U or ^{239}Pu fission cross sections as described above.

By far, the largest source of background was the fission of the decay products. We found that for the ^{238}Np data, an adequate correction for ^{238}Pu and ^{239}Pu fission could be achieved by using a broadened ENDF/B-VI fission cross section. For the ^{232}Pa data, the representation in ENDF/B-VI for ^{232}U and ^{233}U did not give satisfactory results. Some of the ^{232}U resonances were overcorrected, e.g., the one at 6 eV, while others were undercorrected. We ended up using a tabulated fission cross section for ^{233}U, that of Moore et al [5], which had been measured with very similar resolution conditions. For ^{232}U, we fitted the present data to obtain a new set of neutron widths, with the resonance energies and fission widths listed in BNL-325. The background-corrected data are shown in Figs. 1 and 2 for ^{232}Pa and ^{238}Np, respectively.

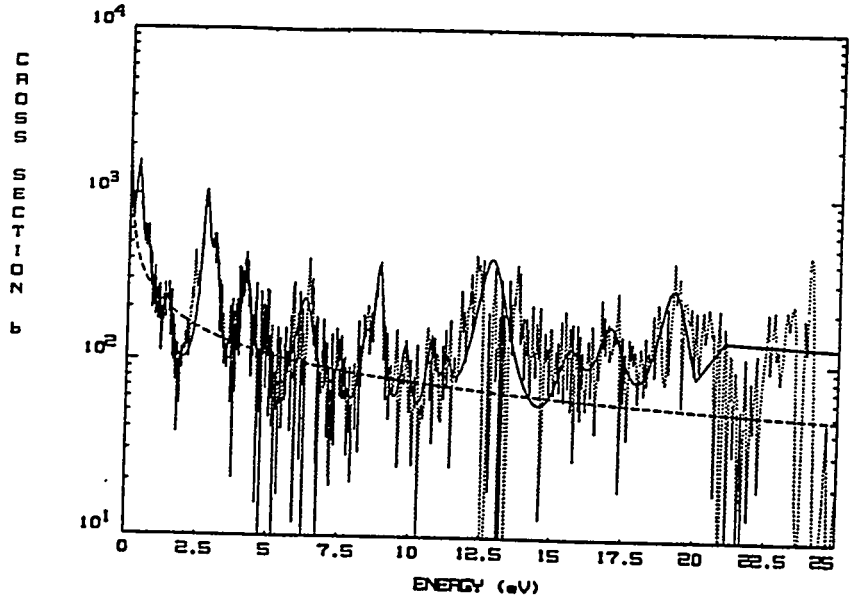

Fig. 1. The fission cross section of ^{232}Pa from 0.01 to 25 eV. The solid line shows a single-level broadened representation that preserves the area. The dashed line is a 1/v curve that passes through the 2200 m/s value.

The resonance structure shown in Fig. 1 was parameterized by a single-level broadened representation of the data below 20 eV that preserves the area. Above 20 eV, we have chosen to use a 1/v curve that preserves the area below 220 eV, which is the upper limit of the known resonance parameters for ^{232}U. Above 220 eV, for purposes of this study, we use the same 1/v curve to 100 keV and above.

Below 8 eV, the resonance structure shown in Fig. 2 is also parameterized by a single-level broadened representation that preserves the area. Above 8 eV, we have chosen to use a 1/v curve that preserves the area in the region below 100 eV. For purposes of this study, we use an extrapolation of this 1/v curve for ^{238}Np as a representation to 100 keV and above. The dashed line

in both Figs. 1 and 2 is a 1/v curve that passes through the measured fission cross section at the thermal (2200 m/s) value. We define resonance enhancement as the ratio of the reaction rate calculated with the resonances included to that calculated from the 1/v curve only.

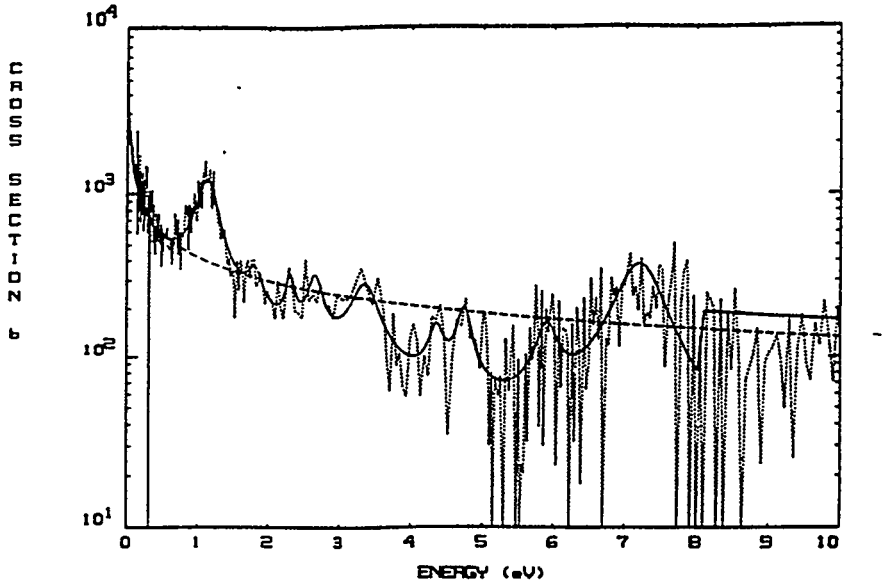

Fig. 2. The fission cross section of ^{238}Np from 0.01 to 10 eV. The solid line shows a single-level broadened representation that preserves the area. The dashed line is a 1/v curve that passes through the 2200 m/s value.

A SIMPLE ACCELERATOR-DRIVEN ASSEMBLY

The experience gained in the calculation of the measured neutron slowing-down spectrum in the RINS, the Rensselaer Intense Neutron Source, suggests that, if the accelerator-driven assembly we choose in this study of resonance enhancement is not too different from the RINS, then the same calculational technique should give a reasonable estimate of the neutron slowing-down properties. The RINS consists of a 1.8-m cube of pure lead, driven by a helium-cooled tantalum electron-bremsstrahlung target in the center. The flux has been measured many times: every fission cross-section measurement in this assembly requires a flux measurement. The flux has also been successfully calculated, with the MCNP code [6], a study that gave new insight into the resolution properties of the RINS.

The present study began with a simple cylindrical scaled-down copy of the RINS: a 1.5-m D and 1.5-m high solid cylinder of pure lead, again we calculated the slowing-down properties as if it were to be driven with an electron-bremsstrahlung neutron source. The resulting calculated flux shape, as shown in Fig. 3, was a bit disappointing in the thermal region; we modified it by adding a 75-cm thick D_2O blanket. The geometry and dimensions of this simple array, for the MCNP calculations, are described in Table 2. Finally, we tested, in a very crude way, whether this calculation might be appropriate for a proton-driven spallation source, by introducing a 19-MeV point source of neutrons instead of the electron-bremsstrahlung source. The results were a factor of 2 larger than those in Fig. 3, which is reasonable agreement for such a study as this.

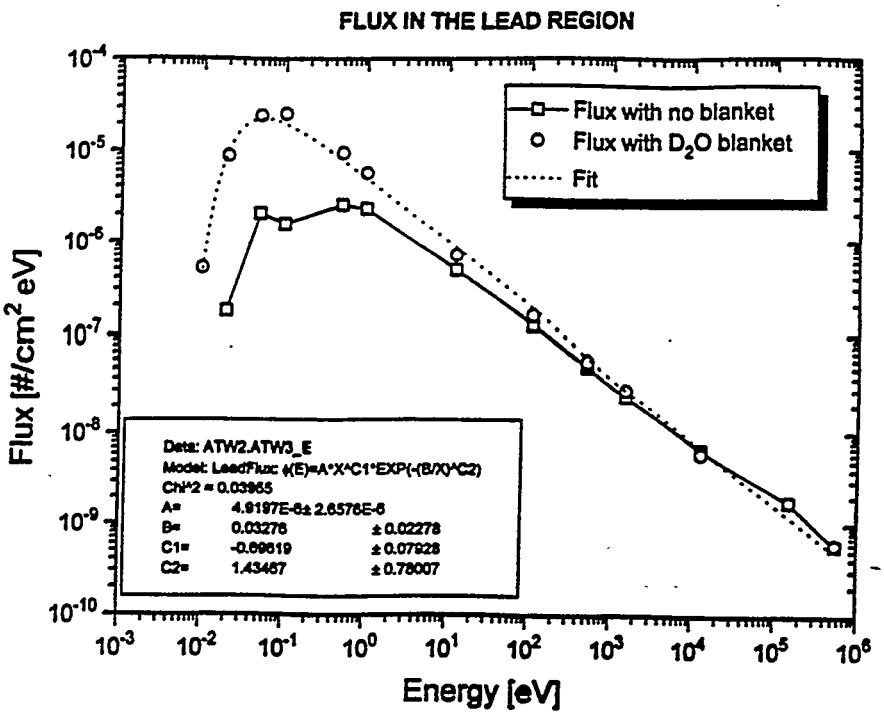

Fig. 3. Calculated neutron flux, driven by one neutron per unit time, for the pure lead assembly with D_2O moderator described in Table 2.

Table 2. Geometry and Dimensions of the Lead Cylinder and D_2O Blanket for MCNP.

Cell Number	Description	Height	Radius (Thickness)
1	Lead Cylinder	150 cm	75 cm
2	Flux Tally Region	20 to 40 cm	(20 cm)
3	D_2O Moderator	150 cm	(75 cm)

As is shown in Fig.3, the fit to the calculated flux with the D_2O blanket is given by

$$\Theta(E) = (4.9197\text{ e-}6)\,E^{**}(-0.69619\exp(-(0.03276/E)^{**}1.43467)), \qquad (1)$$

where the flux has the units of neutrons/cm^2-eV per unit time, and is driven by a neutron production rate of 1 neutron per unit time. The reaction rate is given by $\int\sigma_f(E)\cdot\Theta(E)\,dE$. We define the resonance enhancement factor as the ratio of the above quantity to the integral $\int(C/\sqrt{E})\cdot\Theta(E)\,dE$, where the constant C is chosen to be equal to $\sigma_f(0.0253\text{ eV})\cdot\sqrt{0.0253}$. The energy dependence of the calculated reaction rates in the simple assembly of Table 2, with resonances included and for the 1/v dependence of the cross sections for ^{232}Pa, ^{238}Np, and ^{247}Cm, another actinide of interest to ATW, are listed in Table 3. The resonance enhancement factors are the ratios of the pairs of entries in the bottom line of Table 3, 1.84 for ^{232}Pa, 1.13 for ^{238}Np, and 8.07 for ^{247}Cm in this assembly. Even though the resonances in ^{247}Cm have a very large relative effect on the reaction rate, the value of this quantity is still only about half that of the odd-odd isotopes.

695
696

Table 3. Calculated Reaction Rates for ^{232}Pa, ^{238}Np, and ^{247}Cm in the Assembly of Table 2.

Energy range (eV)	^{232}Pa with resonances	^{232}Pa as 1/v	^{238}Np with resonances	^{238}Np as 1/v	^{247}Cm with resonances	^{247}Cm as 1/v
0 to 0.01	4.8 e-6	4.8 e-6	8.3 e-6	8.3 e-6	5.8 e-7	5.8 e-7
0.01 to 0.1	0.00192	0.00179	0.00308	0.00313	0.00021	0.00022
0.1 to 1	0.00622	0.00334	0.00581	0.00582	0.00041	0.00041
1 to 10	0.00309	0.00218	0.00466	0.00380	0.00547	0.00050
10 to 100	0.00338	0.00138	0.00314	0.00243	0.00139	0.00027
10^2 to 10^3	0.00232	0.00088	0.00200	0.00154	0.00081	0.00017
10^3 to 10^4	0.00151	0.00057	0.00130	0.00100	0.00084	0.00007
10^4 to 10^5	0.00094	0.00036	0.00081	0.00062	0.00075	0.00004
$> 10^5$ [a]	(0.00110)	0.00022	(0.00095)	0.00037	(0.00087)	0.00002
0 to 10^5	0.01934	0.01053	0.02081	0.01835	0.01033	0.00128

[a] Numbers in parentheses are estimates, based on an electron-bremsstrahlung neutron spectrum.

ACCELERATOR REQUIREMENTS

The fluxes and reaction rates above were calculated for a neutron production rate of one neutron per unit time. The next step is to calculate the Bateman equation to see if the assumed assembly can be driven in such a way as to accomplish burning of actinides by fission of ^{238}Np or ^{232}Pa. The differential equation for the production and removal of, e.g., ^{238}Np is given by

$$dN_{238} = ((N_{237} \cdot \sigma_\gamma^{237} \cdot \Theta) - \lambda_{238} - (\sigma_f^{238} + \sigma_\gamma^{238}) \cdot \Theta)\, dt, \qquad (2)$$

where N_{237} is the number of ^{237}Np atoms present at time t, σ_γ^{237} is the capture cross section of ^{237}Np (i.e, the production cross section for ^{238}Np), Θ is the neutron flux, λ_{238} is the decay constant and σ_f^{238} and σ_γ^{238} are the fission and capture cross sections of ^{238}Np. In order to convert actinides to fission products in an efficient way through ^{238}Np, two conditions must obtain. First, the ^{238}Np fission cross must be much larger than the capture cross section, and second, the product of the fission-plus-capture cross section and the flux must be much larger than the decay constant. The closed-form solution of this equation is well-known; Fig. 4 shows a family of curves giving the number of atoms of ^{238}Np as a function of time for five decades of flux level ranging from 2·e13 to 2·e17 n/cm^2-s in the accelerator-driven assembly of the previous section. In Fig. 4, Curves A and B show the characteristic behavior when the flux level is too low. Curve E, at the highest flux level, shows a different behavior: the amount of ^{238}Np peaks and is reduced rapidly as the ^{237}Np disappears.

Can we burn ^{238}Np in an efficient way? The answer appears to be "No", at least not with the simple assembly we have chosen to calculate. Let us suppose we drive such an assembly with 1A of 800 MeV protons, and that we have solved the problem of dissipating the 800MW of heat produced. If we use the usual number of 22 neutrons produced in liquid lead by each proton [7], then the production rate is 22/(1.6 e-19) n/s, which, multiplied by the appropriate entry in the bottom line of Table 3, gives a value of 2.9 e-6 per second for the fission reaction rate $\sigma_f \cdot \Theta$. The decay constant λ_{238} for a 2.117-day half life is 3.8 e-6 per second, implying that in this case actinide burning is about 40% efficient. We have seen that a factor of two increase in the flux may be

expected if we use a more realistic neutron driving spectrum; this increases the actinide burning to 60%. Other factors of two may be possible; we need a factor of 10 to 100.

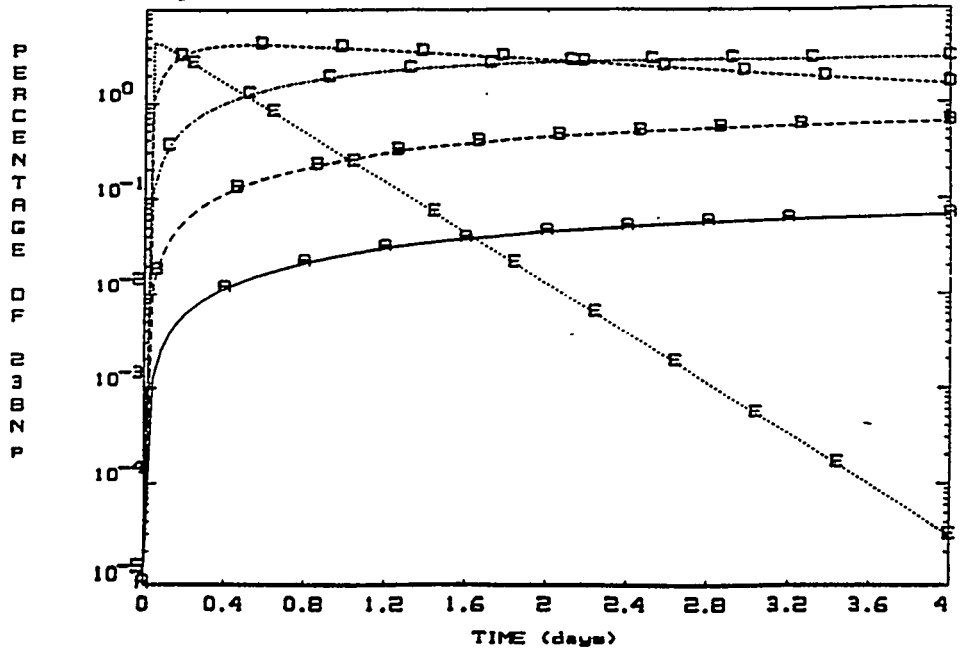

Fig. 4. The number of atoms of ^{238}Np, relative to the number of ^{237}Np atoms present at t = 0, as a function of time in days, for five decades of neutron flux ranging from 2-e13 (Curve A) to 2-e17 n/cm^2-sec (Curve E).

ACKNOWLEDGEMENTS

The authors would like to acknowledge the encouragement and support of C. D. Bowman and E. D. Arthur of the ATW Program office. This study would not have been possible without the efforts of our collaborators who measured the ^{232}Pa and ^{238}Np cross sections: Paul Littleton, Geoff Miller, Marty Ott, Larry Rowton, Wayne Taylor, Jerry Wilhelmy and Mary Anne Yates of the Los Alamos National Laboratory, Allan Carlson of the National Institute for Standards and Technology, Ron Harper and Bob Hilko of EG&G, Inc, and Nat Hill and Paul Koehler of the Oak Ridge National Laboratory.

REFERENCES

[1] Bowman, C. D., Arthur, E. D., et al., *Nuc. Inst. Meth. in Physics Research* A320, 336-367 (1992).
[2] Moore, M. S., et al., "Development of a Technique for Measuring Cross Sections of Interest to ATW," in *Proc. Int. Conf. on Nuclear Data for Science and Technology, Gatlinburg, TN,* 1994, paper 15B.4.
[3] Slovacek, R. E., et al., *Nuc. Sci. Eng.* 62, 455, (1977).
[4] Mughabghab, S. F., *Neutron Cross Sections, Vol.1, Neutron Resonance Parameters and Thermal Cross Sections, Part B; Z=61-100,* New York, Academic Press, 1984.
[5] Moore, M. S., et al., "Slow Neutron Total and Fission Cross Sections of ^{233}U, USAEC Report IDO-16576 (1959).
[6] Fisher, H. M., "Monte Carlo Feasibility Assessment of the Lead Slowing-Down Time Spectrometer..." PhD Thesis, Rensselaer Polytechnic Institute (1985).
[7] Bowman, C. D., "Accelerator-Driven Transmutation for Resolution of Waste Issues Facing Nuclear Technology" in *Proc. Int. Conf. on Nuclear Data for Science and Technology, Gatlinburg, TN,* 1994, paper 16.2.

CROSS-SECTION ACTIVATION MEASUREMENT FOR U-238 THROUGH PROTONS AND DEUTERONS IN ENERGY INTERVAL 10-14 MeV

B.Ya. Guzhovskii, S.N.Abramovich, A.G.Zvenigorodskii,
V.S.Rudnev, S.V.Trusillo.
Russia Federal Nuclear Centre - VNIIEF
607200, Arzamas-16, Nizhny Novgorod region Russia

Abstract. There were presented results of cross-section measurements for nuclear reactions $^{238}U(p,n)^{238}Np$, $^{238}U(d,2n)^{238}Np$, $^{238}U(d,t)^{237}U$, $^{&238}U(d,p)^{239}U$ and $^{238}U(d,n)^{239}Np$. Interval of projectile energy was 10-14 MeV. For measurements of cross-sections it was used the activation methods. The registration of β- and γ-activity was made with using of plastic scintillation detector and Ge(Li)-detector.

INTRODUCTION

In connection with actinide transmutation problem it is requirement for renewal of nuclear data among their number for short-lived actinides. The generation of these nuclei for indicated nuclear data measurement can be realized on charged particle accelerators through nuclear reactions resulted in nuclei with atomic numbers, which differ from atomic number for nucleus-target. It simplify sharply the problems for manufacture of targets from generated nuclei for following measurements, because discharge of the generated nuclei may be realized by chemical processes of separation. It is much cheaper and less labour-intensive process than isotope separation, which is necessary with generating through (n,γ), (n,2n) reaction, although these can provide the much greater productivity by using the greater neutron flux in the reactors and by the greater cross-section. For estimation of the need generation capacity of these nuclei on ion beams it is necessary to know cross-section for these reactions. Besides, interest with these reactions were caused necessary of consideration for role of secondary reactions caused fast proton and deuteron for estimation of heavy actinide yields in a thermonuclear explosion [1,2]. Specifically, nuclear reaction with U-238 result to formation of odd isotopes of Np and Pa, which have the greater capture cross-section than U-238. Ground cause for appearance of fast proton and deuteron in nuclear explosion is process of elastic scattering for DT-neutrons on protium and deuterium. The greatest energy for proton is 14 MeV, and for deuteron is 12,5 MeV. In presence work it is considered the interval of projectile energies E=10-14 MeV.

METHODS OF MEASUREMENT

Irradiation conditions

At irradiation of U-238 by protons and deuterons it is generated mainly short-lived β-radioactive nuclei. It is convenient for detection of isotopes ^{238}Np, ^{239}Np and ^{237}U in conditions of our measurements. Therefore, we have measured cross-sections for reactions $^{238}U(p,n)^{238}Np$, $^{238}U(d,2n)^{238}Np$, $^{238}U(d,t)^{237}U$ and the sum of cross-section for two reactions $^{238}U(d,p)^{239}U \rightarrow {}^{239}Np + {}^{238}U(d,n)^{239}Np$. The methods of measurement consisted in a consecutive irradiation of set of thin targets in scattering chamber, in which monitor of coulomb scattering was installed under

angle 20° to beam direction. There were installed the detectors for fission fragments and elastic scattered projectile, too. All irradiation run was continued several hours. After completion of irradiation the scattering chamber was opened. The irradiated targets were extracted from it for measurement β- and γ-spectra. The targets were manufactured by evaporation of U-238 dioxide on thin backing from Al_2O_3. The used uranium was impoverished relatively U-235. The counting of the coulomb monitor is proportional product of projectile flux, thick of target relativity U-238 and coulomb scattering cross-section under angle 20°. In such away, the coulomb monitor makes it possible to connect of measurement results for different targets for different projectile energy, and to obtain relative run for the all measurement cross-section. At moment of measurement there were left in the targets only radioactive nuclide with $T_{1/2} \gg 1$ hour.

The measurement of β and γ -spectra.

β-spectrum measurements were made by plastic scintillation detector. Thickness of detector was chosen accordingly with the range of the greatest β-particle energy. A contribution of γ-ray was counted up in background measurements with Al filter, which had got thick 2 mm.

γ-spectrum measurements were made by Ge(Li)-detector with depletion volume $\approx$ 45 cm^3 and resolution $\approx$ 3 keV on γ - lines of ^{60}Co. The spectrum measurements were repeated regularly during several weeks to obtain decay curves for all detected β- and γ-transfers.

MEASUREMENT RESULTS

Volume of activation cross-section for i^{th} nuclide σ_{ai} was estimated by expression:

$$\sigma_{ai}(E) = \sigma_f(E,\theta) * \frac{2N_{ai}\Omega_f}{N_f(E,\theta)},$$

there $\sigma_f(E,\Theta)$ - fission differential cross-section by protons or deuterons with energy E under angle Θ;

Ω_f - solid angle of fission fragment detector;

N_{ai} - number of nuclei for i^{th} nuclide generated in the target. The using known fission cross-section [4,5,6] allows to exclude errors connected with thick targets and projectile numbers. N_{ai} was estimated for γ - spectra by a count for total absorption peaks for according γ-lines. For this it was used absolutely efficient $\epsilon\Omega(E_\gamma)$ of γ-detector, probability of γ-transfer I_γ, constant of decay λ for i^{th} nuclide and time t from irradiation end to beginning of measurement:

$$N_{ai} = \frac{N_\gamma * e^{\lambda t}}{(\epsilon\Omega)_\gamma * I_\gamma}.$$

The similar expression was used for β-spectra, but I_γ was changed on I_β, and $(\epsilon\Omega)_\gamma$ - on $(\epsilon\Omega)_\beta$.

The results of measurements are placed on table and shown on figures 1 and 2.

Table 1. Measurement results.

E_p MeV	σ_{pn} mb	E_d MeV	σ_{dp+dn} mb	$\sigma_{d,2n}$ mb	σ_{dt} mb
9,97	3	10	85,6	25,8	6,6
10,99	4,7	10,98	137,5	47	16,4
11,4	5,1	11,97	190	57,5	27,3
11,94	5,8	13,0	182	51	33,5
12,98	7,5	-	-	-	-
13,9	8,8	-	-	-	-

ERRORS OF MEASUREMENTS

The errors for relativity projectile energy runs of cross-section were conditioned mainly by statistic errors of counts, which were less 5%. Statistic errors of monitor and fission fragments detector counts were less 1%. Systematical errors of cross-sections consisted of following components:

- Error of absolute efficient for Ge(Li) detector. It was conditioned by errors of standard sources $\approx$ 4%.
- Errors of branching ratio for γ- and β - decay for Np-238,239 and U-237 from [3] - less 2%.
- Errors of decay constants from [3] - less 1%.
- Errors fission cross-section σ_{pf} and σ_{df} from [4,5,6] - less 2%.
- Error of solid angle for fission fragment detector - less 3%.

Total errors activation cross-section in table and figures 1,2 make 8-10%.

REFERENCES

1. J.Bell, Phys.Rev.139B(1965)1207.
2. J.Bell,Phys.Rev.158(1967)1127.
3. Table of Isotopes (seventh edition), Editor C.M.Lederer and V.S.Shirley.N.-Y.,1978.
4. G.Bate,J.Huizenga,Phys.Rev.133B(1964)1471.
5. G.Bate,R.Chaudhry,J.Huizenga,Phys.Rev. 131(1963)722.
6. G.Choppin,J.R.Meriweetter,J.Fox,Phys.Rev.131(1963) 2149.

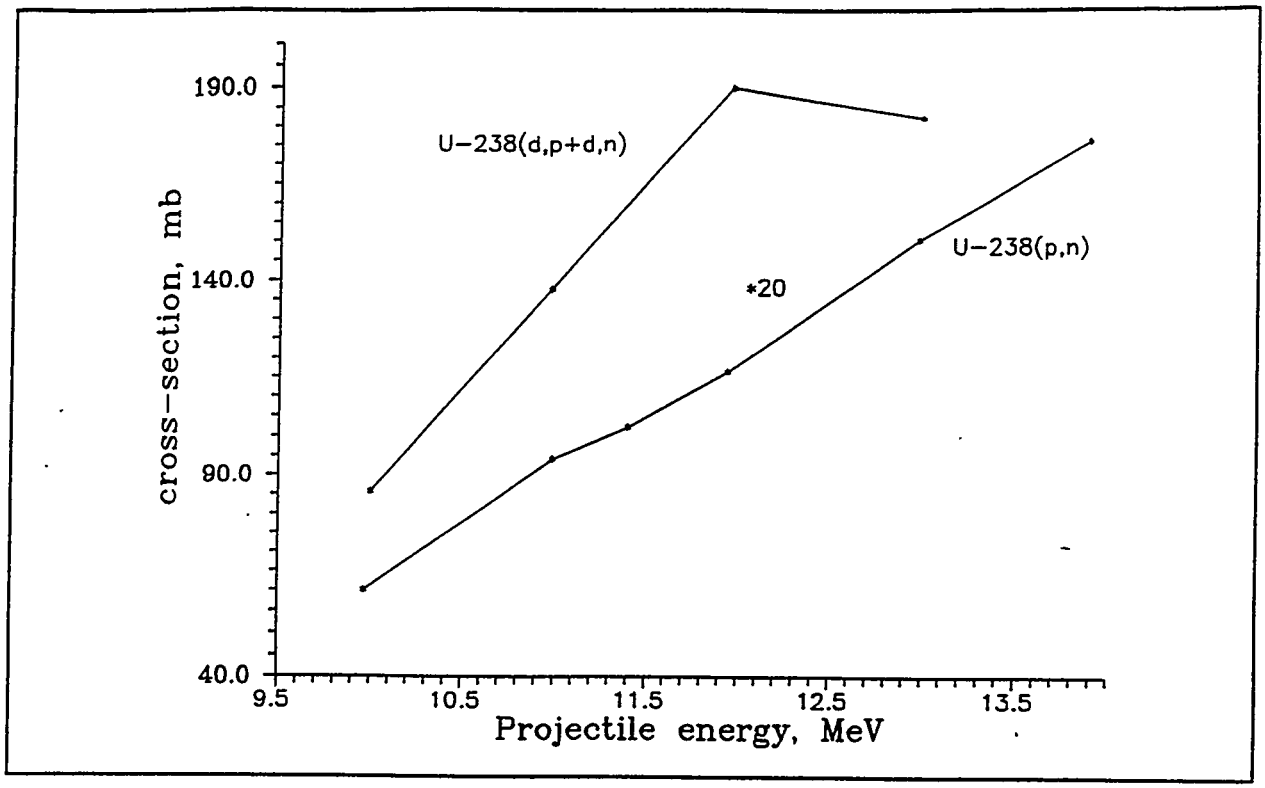
190.0
140.0
90.0
40.0
cross-section, mb
U-238(d,p+d,n)
U-238(p,n)
*20
9.5
10.5
11.5
12.5
13.5
Projectile energy, MeV

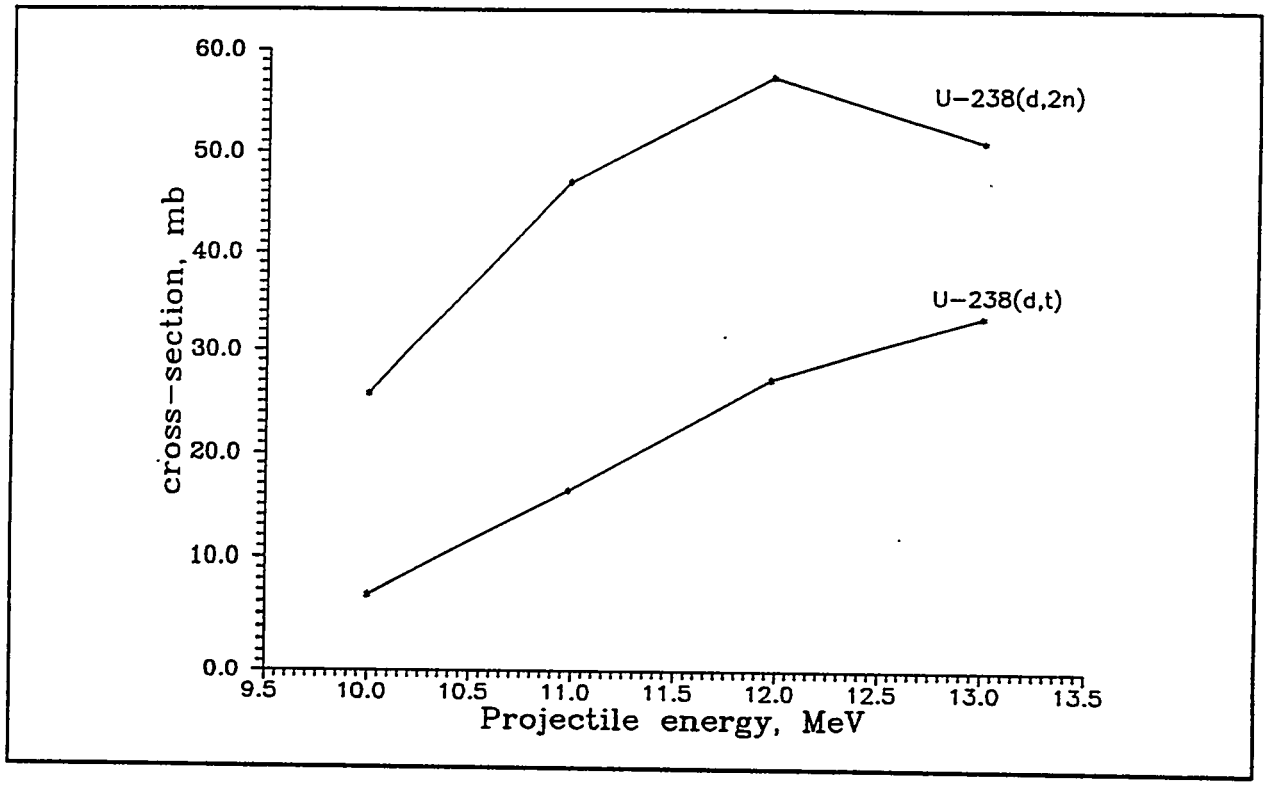
60.0
50.0
40.0
30.0
20.0
10.0
0.0
cross-section, mb
U-238(d,2n)
U-238(d,t)
9.5
10.0
10.5
11.0
11.5
12.0
12.5
13.0
13.5
Projectile energy, MeV

Nuclear Data Requirements for Accelerator-Driven Transmutation Systems

P. G. Young and W. B. Wilson
Nuclear Theory and Applications Group, MS B-243
Los Alamos National Laboratory
Los Alamos, NM 87545

and

M. B. Chadwick
Nuclear Data Group, MS L-412
Lawrence Livermore National Laboratory
Livermore, CA 94551

Abstract. The possibilities of several new technologies based on use of intense, medium-energy proton accelerators are being investigated at Los Alamos National Laboratory. The potential new areas include destruction of long-lived components of nuclear waste, plutonium burning, energy production, and production of tritium. The design, assessment, and safety analysis of potential facilities involves the understanding of complex combinations of nuclear processes, which in turn places new requirements on nuclear data that transcend the traditional needs of the fission and fusion reactor communities. In this paper an assessment of the nuclear data needs for systems currently being considered in the Los Alamos Accelerator-Driven Transmutation Technologies program is given. The importance of developing neutron and proton cross section libraries in the incident particle energy range of 20 MeV to approximately 200 MeV for transport applications is discussed, and new theoretical methods for developing cross section libraries at higher incident neutron and proton energies are summarized.

INTRODUCTION

Recent progress in high-power accelerator technology, materials separations, and neutron sources has enabled new accelerator-based systems that can impact important problem areas. Several such systems are currently being investigated in the Accelerator-Driven Transmutation Technology (ADTT) program at Los Alamos National Laboratory (LANL). These include tritium production, plutonium disposition, destruction of long-lived components of nuclear waste, and ultimately long-term energy supply requirements.

In this paper we give an assessment of the nuclear data needs for systems currently being considered in the Los Alamos ADTT program. Nuclear data needs for potential target materials, coolants, moderators, blankets, and structural materials are included, as well as requirements for spallation and fission products. The status of the experimental data base and the adequacy of evaluated data libraries such as the Evaluated Nuclear Data File (ENDF/B) for transmutation system design applications are also addressed. Areas where experimental and theoretical information is required are summarized, and the importance of developing neutron and proton cross section libraries in the incident particle energy range of 20 MeV to approximately 200 MeV for transport applications is considered. New theoretical methods for developing cross section libraries at higher incident neutron and proton energies are summarized, and validation calculations are compared to experimental data.

Comprehensive reviews have been written by Koning on the availability of high energy nuclear data and model codes for accelerator transmutation of waste (ATW) problems [1] and on the requirements for evaluated data for such problems [2]. Because we specialize our considerations to LANL ADTT systems, some materials that Koning includes are omitted in our review. We also introduce a few new materials and consider some of the more important neutron data needs at lower energies, whereas Koning concentrates on the region above $E_n = 20$ MeV. In general, however, our findings are consistent with and complementary to those of Koning.

GENERAL REQUIREMENTS FOR NUCLEAR DATA

In each of the Los Alamos ADTT concepts, there is a target region where materials (target, target cladding, breeding material, etc.) are exposed to direct beam protons and secondary neutrons ranging in energy from the primary beam energy down to thermal energies. Surrounding the target area are salt fuel materials, blanket and moderator materials, coolants, and structural materials that are not exposed to the direct proton beam but which are irradiated by a high flux of neutrons ranging from a very hard spectrum with a significant number of medium-energy neutrons, to an intermediate energy neutron spectrum , and finally to essentially a thermalized neutron spectrum.

For all materials present in significant quantities in the target and surrounding region, neutron-induced data adequate for neutron transport calculations are required. These data are needed to calculate the energy distributions of down-scattered neutrons that drive the transmutation reactions in the blanket/moderator regions and, perhaps even more demanding, that can be used in shielding calculations for these complex, medium-energy neutron systems. Additionally, individual nuclide production or spallation yields are required, together with information on recoil nuclei energy distributions that can be used to obtain DPA and damage cross sections up to high energies for structural materials. Lastly, transmutation and activation cross sections are necessary for neutron-induced reactions, including cross sections for formation of isomeric states. In terms of nuclear reactions, the data required are neutron total, elastic and inelastic scattering, double differential (n,xn) and (n,xp), (n,γ), (n,f), (n,x), and (n,xγ) cross sections, plus production cross sections for individual nuclides as functions of Z and A with isomeric state production included.

For actual target materials, that is, materials that are exposed to the direct proton beam, essentially the same data requirements exist for proton-induced reactions as described above for neutron-induced reactions. Most importantly, (p,xn) and (p,xp) production cross sections are required as functions of incident energy and emission angle and energy for all materials directly exposed to the particle beam. Spallation product yields, recoil nuclei energy distributions, and (p,xγ) are needed, as well as information on isomer production. Proton-induced data would also be useful for materials that are not directly exposed to the proton beam, but these data are of lower priority than the incident neutron data.

Target materials under current (or recent) consideration in Los Alamos designs are W, Pb, Th, and U. These elements, plus the hastelloy and zircalloy target cladding (Cr, Fe, Ni, Zr, Mo, Sn), a breeding material (^{3}He), and heavy water (^{2}H, O), are exposed to both the direct proton beam and high-energy neutrons from (p,xn) reactions, depending on the particular ADTT concept. The remaining materials in and around the target region, including the molten salt fuel carrier materials (Li, F, Be, Zr), structural materials (C, Al, Si, P, Cr, Fe, Mn, Ni, Zr, Mo, Sn), salt coolant (Na, B), and blanket/ moderator materials (^{1,2}H, Be, C, O), are irradiated by neutrons from (p,xn) reactions, with a significant hard component near the target and becoming a moderated fission spectrum further into the blanket region. Additionally, significant amounts of reactor fission-product and actinide waste are loaded into the ATW blanket region, plus ^{239}Pu in the case of the plutonium-burning application. Important higher actinides are ^{232,233}Pa (for the ^{232}Th - ^{233}U fuel cycle), ^{237,238}Np, $^{241\text{-}244,242m,244m}$Am, and $^{242\text{-}248}$Cm.

Transmutation/activation cross sections and decay data are required for all nuclides that are products of spallation, fission, absorption, activation, (n,x), (n,xn), etc., reactions, including nuclides that are formed in isomeric states. The magnitude of this requirement is better envisioned from Fig. 1, in which the range in neutron and proton number of spallation products formed by 800-MeV proton reactions on a tungsten target is superimposed on the Chart of the Nuclides. The N,Z distribution of fission products from thermal neutron fission of ^{235}U is also included in the display. Obviously, there is a good deal of overlap between the fission and spallation product ranges, except that the latter cover a much broader range in Z and N. Fission products are more important than spallation products in the concepts that include actinides, although both types of data are required for all concepts.

The list of materials requiring transmutation/activation/decay data is obviously quite extensive and is the reason that massive (>10000 reactions) data libraries are under development [3]. This is

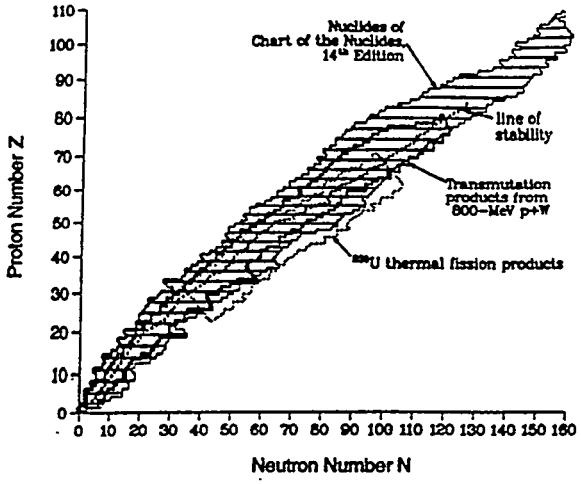

Fig. 1. Range in Z and N of spallation products from 800-MeV protons on tungsten.

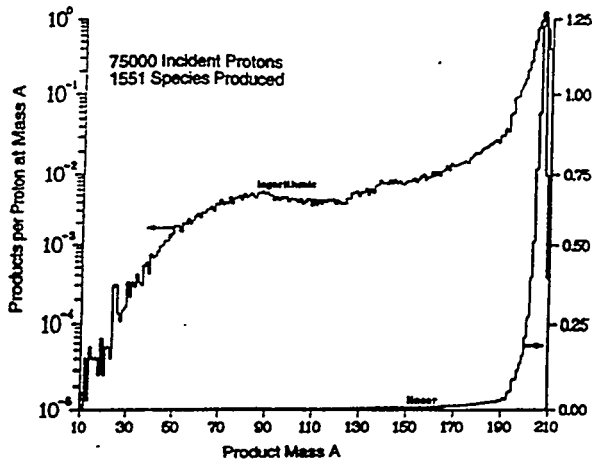

Fig. 2. Mass distribution of spallation products from 1-GeV protons on a lead target.

further illustrated in Fig. 2, which shows the distribution of spallation products as a function of product mass from 1-GeV proton bombardment of Pb. From the distribution in Fig. 2 we surmise that transmutation data for spallation and fission products should roughly cover the mass range $10 \leq A \leq A_{target} + 2$, with the mass range from the upper limit down to $A_{target} - 20$ clearly being the most important region. A list of the more important long-lived fission products that are transmutation candidates is given in Table 1, together with summary information on low energy cross sections and resonance parameters from the compilation of Mughabghab [4].

Regarding transmutation of actinides, data are required for nuclides important in the ^{232}Th - ^{233}U energy-production cycle and in burning ^{239}Pu, as well as the higher actinides in fission reactor waste that would be introduced into an ATW system for destruction, as detailed above. Considering all the actinides that must be included in analyses of these systems, the list is truly extensive but fortunately reasonable evaluated data exist for many of them from the fission reactor program, at least up to incident neutron energies of 20 MeV. A qualitative assessment of evaluated data in the ENDF/B-VI file for important higher actinides is given in Table 2, including thermal cross sections from Mughabghab's compilation [4]. Note that there are presently no evaluations in the ENDF/B-VI file for ^{232}Pa, ^{244}Cm, or ^{244m}Cm, and that the evaluations for ^{238}Np, ^{242}Am, ^{242}Cm, and ^{247}Cm are regarded as "weak."

Table 1. Long-Lived Fission Product Transmutation Candidates*

Nuclide	Half Life (Years)	Thermal Capture Cross Section (b)	Resonance Integral (b)	V6 Resonance Parameters?
^{79}Se	6.5×10^4	(10)?	-	No
^{93}Zr	1.5×10^6	2.5 ± 1.5	-	~ No
^{99}Tc	2.1×10^5	$20. \pm 1.$	340 ± 20	Yes
^{107}Pd	6.5×10^6	1.8 ± 0.2	86.6	Yes
^{126}Sn	1.0×10^5	(0.14)?	-	No
^{129}I	1.6×10^7	$27. \pm 3.$	36 ± 4	Yes
^{135}Cs	3.0×10^6	8.7 ± 0.5	62 ± 2	No

*The cross sections are from Mughabghab [4] and the resonance parameter comment refers to ENDF/B-VI.

Table 2. Higher Actinide Transmutation Candidates

Nuclide	Half Life	Thermal $\sigma_{n,\gamma}$ (b)	Thermal $\sigma_{n,f}$ (b)	ENDF/B-VI Quality
^{237}Np	2.1×10^6 y	176 ± 3	21.5 ± 2.4	Good
^{241}Am	433 y	587 ± 12	3.2 ± 0.1	Reasonable
^{243}Am	7370 y	75.1 ± 1.8	0.198 ± 0.004	Need Update
^{242}Cm	163 d	16 ± 5	< 5	Very Weak
^{244}Cm	18 y	15.2 ± 1.2	1.04 ± 0.20	Reasonable
^{246}Cm	470 y	1.22 ± 0.16	0.14 ± 0.05	Need Update
^{247}Cm	1.6×10^7 y	57 ± 10	81.9 ± 4.4	Weak
^{248}Cm	3.5×10^5 y	2.63 ± 0.26	0.37 ± 0.05	Need Update
		MOST SERIOUS DATA PROBLEMS		
^{232}Pa	1.3 d	700 ± 100	464 ± 95	None
^{238}Np	2.1 d	~ 300	2088 ± 30	Very Weak
^{242}Am	16.1 h	?	2100 ± 200	Very Weak

DATA LIBRARY FOR PARTICLE TRANSPORT

Design and feasibility studies for ADTT systems obviously require detailed transport calculations of radiation associated with the stopping of protons of energy 1.0 GeV in various target materials. As outlined above, such calculations require information on nuclear interactions by protons and neutrons from essentially zero energy up to the primary beam energy with target materials, coolants, cladding and structural materials, moderator and blanket materials, fission and spallation products, and actinides. Such transport calculations are currently done at Los Alamos in the following manner: (1) the LAHET Monte Carlo transport code [5] tracks neutrons from the highest energy down to a lower energy cutoff of 20 MeV, using on-line nuclear models to calculate cross sections; (2) all neutrons born or scattered below 20 MeV are recorded as source particles for subsequent Monte Carlo transport calculations with the high energy version of the general Monte Carlo code MCNP [6], using tested cross section libraries from the national evaluated data file, ENDF/B-5; (3) reaction products and fluxes are tallied and passed to a separate code, CINDER-90 [7], for transmutation calculations, utilizing a large activation cross section and decay data library.

The above procedure is satisfactory for scoping calculations. It is well known, however, that the nuclear physics in the LAHET code is most applicable for particles in the medium energy range, whereas using the on-line nuclear models down to 20 MeV is not appropriate, most especially for lighter elements. As a result, a significant and unnecessary component of error is introduced in such calculations, and it affects subsequent calculations that utilize neutron fluxes from LAHET/MCNP analyses, e.g., radiation damage, transmutation, nuclide inventories, engineering design, shielding, and safety calculations.

A straightforward way to circumvent this problem is to extend the validated neutron transport data library (now ENDF/B-V) from the current energy limit of 20 MeV to a more appropriate higher energy where the models in LAHET are expected to be more reliable. This extension could be accomplished utilizing experimental data, systematics, and nuclear theory. An upper energy limit in the range 100 - 200 MeV appears feasible and adequate for this purpose.

To summarize, the two nuclear data libraries of major importance to the ADTT projects are the neutron transport library and the transmutation/activation/decay data library. Efforts have been directed at developing a transmutation/activation/decay data library [3]. While such libraries still need improvement, considerable progress has been made, and a significant library validation effort using reaction cross section data has been undertaken at Los Alamos [8]. In the case of neutron

transport data, a limited library up to 100 MeV was developed in 1990 [9]; however, a comprehensive library with enough materials to be useful only exists at present to 20 MeV (ENDF/B-VI).

The third nuclear data component that is crucial in analyses performed at Los Alamos is the LAHET code [5] and the intranuclear cascade/preequilibrium/evaporation modeling that is built into the code. Significant efforts have been directed at validating and improving the double-differential proton-induced neutron emission spectra calculated with the code [10] by comparing calculations with both thin and thick targets. A problem area that still needs improvement deals with the calculation of distributions of spallation products. Recent measurements by Ullmann et al. [11] of mass yields from 800-MeV proton bombardment of W are compared with LAHET calculations in Fig. 3. It is found that approximately 52% and 38% of the calculated mass yields disagree with the two measurements presented by a factor of 2 or greater.

A second feature in LAHET calculations of spallation yields that should be addressed concerns the fact that all product nuclei are created in their ground states. Isomers are known to be present in fission products, and we have observed significant isomeric state branching as well in calculations of spallation reactions with the GNASH code [12]. For example, branching ratios are shown in Fig. 4 for several Pb isomers calculated for neutron reactions on ^{208}Pb at incident energies up to 150 MeV. The branching ratios tend to increase rapidly with incident neutron energy near their thresholds but then flatten out at higher energies. Because the branching ratios are so large (between 0.4 and 0.8 at higher energies), we feel that these effects should be included in the spallation calculations that are used in design studies.

NUCLEAR THEORY FOR CALCULATING TRANSPORT LIBRARIES

Considerable progress has been made in recent years in the development of nuclear theory and model codes for calculating nuclear data in the incident neutron/proton/γ-ray energy range from 10 to ~ 200 MeV. In a collaborative Los Alamos/Livermore activity, we have developed a new model code, called FKK-GNASH [13], which combines a quantum mechanical preequilibrium model from Feshbach, Kerman, and Koonin (FKK) [14], with a statistical Hauser-Feshbach reaction theory code, GNASH [12], that makes use of phenomenological and semiclassical models and that has long been used to provide nuclear data at lower incident energies. The addition of the FKK capability greatly enhances the predictive capability for calculations at higher energies,

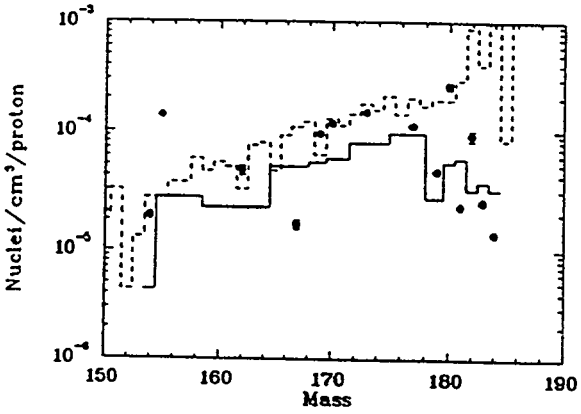

Fig. 3. Comparison of measured and calculated (LAHET) summed mass yields for 800-MeV protons on W [10]. The dashed line indicates calculated yield summed over all nuclei at the given mass; the solid line is the calculated sum over only those nuclei that were observed and should be compared to the data.

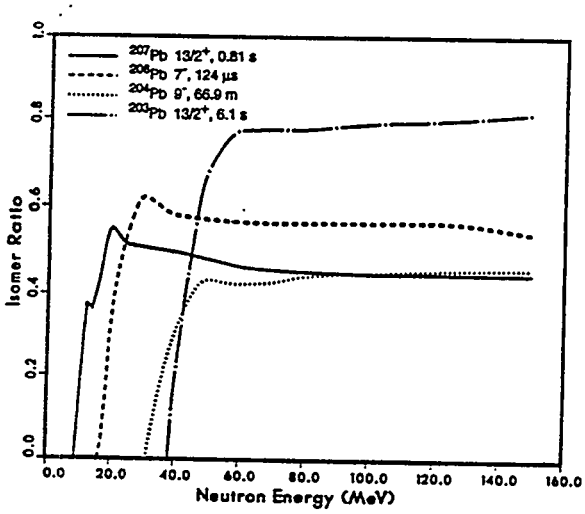

Fig. 4. Isomer ratios calculated with the GNASH code for four isomeric states in Pb isotopes formed by neutron reactions with ^{208}Pb.

whereas the inclusion of the older GNASH modules allows the reliable calculation of all relevant reaction chains, including gamma-ray emission. Other improvements made to the code system include the addition of modeling for multiple preequilibrium effects, more appropriate optical and level density models for higher energy calculations, and better estimates of angular momentum distributions from preequilibrium reactions [15]. The code system has been tested extensively in an Nuclear Energy Agency sponsored *International Code and Model Intercomparison for Intermediate Energy Reactions*, and found to give reliable results for proton reactions up to at least 160 MeV with ^{90}Zr and ^{208}Pb [16]. An example of angle-integrated and angle-dependent spectra calculated for 160-MeV protons on ^{90}Zr is compared to experimental data in Fig. 5.

CONCLUSIONS

In addition to the summary of nuclear data needs in the previous sections, a number of more general conclusions and recommendations are possible from this brief assessment of nuclear data needs for ADTT systems.

- Nuclear models in LAHET should be improved as needed when neutron emission and spallation mass distribution measurements are available.
- Effects of direct formation of isomeric states in spallation process should be assessed.
- Results from new cross section experiments (^{232}Pa, ^{238}Np, etc.) should be incorporated into evaluated data libraries as they become available.
- The impact of nuclear data on safety questions should be carefully assessed. For example, the uncertainty in delayed neutron fractions for higher actinides could be important.
- Full neutron data evaluations adequate for transport calculations should be provided for all materials that are present in significant quantity.
- Improvements should be made in the massive activation cross section and decay libraries used in transmutation calculations, especially for reactions leading to isomeric states, for (n,γ) reactions in general, and for isomer target nuclei. Systematic use of modern theory codes is recommended.
- Extension of neutron data files to higher energies is desirable, so that the transition from LAHET to MCNP calculations would occur in the 100 - 200 MeV range rather than the present energy boundary of 20 MeV. The physics used to determine cross sections would be much better, especially for lighter elements, and transport calculations with state-of-the-art transport codes like MCNP would be possible to much higher energies.

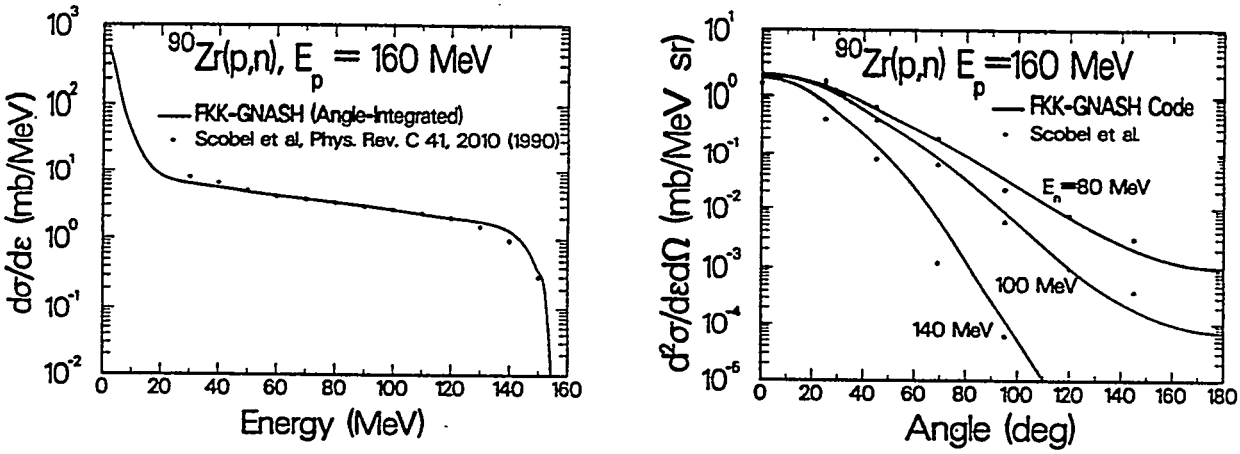

Fig. 5. Neutron angle-integrated spectrum and angular distributions from 160-MeV proton bombardment of ^{90}Zr.

ACKNOWLEDGMENTS

We wish to thank E. D. Arthur, C. A. Beard, J. W. Davidson, M. S. Moore, G. L. Morgan, and J. L. Ullmann for several useful discussions. This work was performed under the auspices of the U.S. Department of Energy by Los Alamos National Laboratory under contract No. W-7405-Eng-36 and by Lawrence Livermore National Laboratory under contract No. W-7405-Eng-48.

REFERENCES

1. A. J. Koning, "Review of High Energy Data and Model Codes for Accelerator-Based Transmutation," Netherlands Energy Research Foundation report ECN-C--93-005 (1993).

2. A. J. Koning, "Requirements for an Evaluated Nuclear Data File for Accelerator-Based Transmutation," Netherlands Energy Research Foundation report ECN-C--93-041 (1993).

3. J. Kopecky, H. A. J. van der Kamp, et al., "The European Activation File EAF-3 with Neutron Activation and Transmutation Cross Sections," Netherlands Energy Research Foundation report ECN-C--92-058 (1992).

4. S. F. Mughabghab, M. Divadeenam, and N. E. Holden, *Neutron Cross Sections*, V. 1, Part A, Z = 1-60 (Academic Press Inc., 1981) and Part B, Z = 61-100 (Academic Press Inc., 1984).

5. R. E. Prael and H. Lichtenstein, "User Guide to LCS: The LAHET Code System," Los Alamos National Laboratory informal report LA-UR-89-3014 (1989).

6. J. F. Briesmeister, "MCNP - A General Monte Carlo N-Particle Transport Code," Los Alamos National Laboratory report LA-12625-M (1993).

7. W. B. Wilson, T. R. England, E. D. Arthur, C. A. Beard, C. D. Bowman, L. N. Engel, et al., "Accelerator Transmutation Studies at Los Alamos with LAHET, MCNP, and CINDER'90," Proc. Workshop on *Simulating Accelerator Radiation Environments*, Jan. 11, 1993, Santa Fe, New Mexico (LA-UR-93-3080].

8. D. W. Muir and W. B. Wilson, "Validation of a Large Activation Cross-Section Library," Proc. Int. Conf. on *Nuclear Data for Science and Technology*, May 9-13, 1994, Gatlinburg, Tennessee, to be published.

9. P. G. Young, E. D. Arthur, M. Bozoian, T. R. England, et al., "Transport Data Libraries for Incident Proton and Neutron Energies to 100-MeV," Los Alamos National Laboratory report LA-11753-MS (July 1990).

10. R. E. Prael, "LAHET Benchmark Calculations of Differential Neutron Production Cross Sections for 113 MeV and 256 MeV Protons," Los Alamos National Laboratory informal report LA-UR-89-3347 (1989); R. E. Prael, "LAHET Benchmark Calculations of Neutron Yields from Stopping-Length Targets for 113 MeV and 256 MeV Protons," Los Alamos National Laboratory informal report LA-UR-90-1620 (1990).

11. J. L. Ullmann, et al., "Thick Target Spallation Product Yields from 800 MeV Protons on Tungsten," Proc. Int. Conf. on *Nucl. Data for Sci. and Tech.*, May 9-13, 1994, Gatlinburg, Tennessee, to be published.

12. P. G. Young, E. D. Arthur, and M. B. Chadwick, "Comprehensive Nuclear Model Calculations: Introduction to the Theory and Use of the GNASH Code," Los Alamos National Laboratory report LA-12343-MS (1992).

13. M.B. Chadwick and P.G. Young, *Phys. Rev. C.* 47, 2255 (1993).

14. H. Feshbach, A. Kerman, and S. Koonin, *Ann. Phys. (N.Y.)* 125, 429 (1980).

15. For example, M.B. Chadwick, H.M. Blann, P.G. Young and D.C. George, "Multiple Preequilibrium Processes in FKK Theory," to be published, *Phys. Rev. C* (1994).

16. M.B. Chadwick and P.G. Young, "Progress in Applying the FKK Multistep Reaction Theory to Intermediate-Energy Data Evaluation," Proc. OECD/NEA Specialist Meeting on *Intermediate Energy Nuclear Data*, Issy-les-Moulineaux, France, 30 May - 1 June, 1994, to be published.

Transmutation of High-Level Radioactive Waste and Production of ^{233}U Using an Accelerator-Driven Reactor

Hiroshi Takahashi, Hirofumi Takashita, and Xinyi Chen
Department of Advanced Technology
Brookhaven National Laboratory, Upton, New York 11973

Abstract. An accelerator-driven fast reactor (700 MWt), run in a subcritical condition, and fueled with MOX can generate ^{233}U more safely and efficiently than can a critical reactor. We evaluate the production of ^{233}U, ^{239}Pu, and the transmutation of the long-lived fission products of ^{99}Tc and ^{129}I, which are loaded with $YH_{1.7}$ between the fast core and blanket, by reducing the conversion factor of Pu to ^{233}U. And we assessed the rates of radiation damage, hydrogen production, and helium production in a target window and in the surrounding vessel.

INTRODUCTION

Reactor safety, the disposal of high-level nuclear waste, and nonproliferation of nuclear material for military purposes are the problems of greatest concern for nuclear energy. Technologies for accelerators developed in the field of high-energy physics can contribute to solving these problems [1]. For reactor safety, especially for that of a Na-cooled fast reactor, the use of an accelerator, even a small one, can enhance the safety using a slightly subcritical reactor [2].

There is growing concern about how we can deal with weapons-grade Pu, and about the large amount of Pu accumulating from the operation of commercial reactors. It has been suggested that this Pu could be incinerated, using the reactor and a proton accelerator. However, because Pu is a very valuable material with future potential for generating nuclear energy, we should consider transforming it into a proliferation-resistant material that cannot be used for making bombs, rather than simply eliminating the Pu.

^{233}U Production and Minor-Actinide Transmutation

At the last international fuel-cycle evaluation (INFCE), several options for producing ^{233}U were proposed; however, this study was carried out before the collapse of Soviet Union, and the use of Pu was not considered. In this paper, we discuss the production of ^{233}U from ^{232}Th using an accelerator-driven Na-cooled fast reactor in a slightly subcritical condition to transmute minor actinides (MAs) and long-lived fission products (LLFPs). It is well known that ^{233}U has superior properties to ^{235}U in a thermal reactor. However, ^{233}U does not exist naturally, but has to be made from ^{232}Th by neutron capture.

When ^{233}U is produced, ^{232}U, which emits strong gamma radiation, also will be produced by the (n,2n) reaction from ^{233}U; the latter is a more theft-resistant fissile material. Any ^{233}U produced in the core and near the spallation target is a strong gamma emitter; however, ^{233}U produced in the blanket region is a weak gamma emitter because the neutron-energy spectrum in the blanket is much softer than the one produced in the core region. Due to this emission of gamma radiation, the fuel-processing operation has to be heavily shielded, and hence, it becomes expensive. When a pyrolitic system such as that applied to a metal fuel [3] can be employed, then

the processing plant can be small, and processing is less expensive. Improvements can be made in the method of using a metal fuel in a fast reactor to make a much harder neutron spectrum, and in increasing the neutron economy to produce ^{233}U (or ^{239}Pu). Also, by running the reactor in a subcritical condition, safety problems associated with criticality can be avoided.

One option in producing ^{233}U from the ^{232}Th is to use spallation neutrons generated by injecting medium-energy protons into a thorium target. This approach suppresses fission but requires large proton currents. As part of our study of the accelerator-breeder concept, we investigated a method of producing ^{233}U in which high currents of protons and injected into a thorium-oxide fuel in pressure tubes [4].

^{233}U can be produced in a thorium blanket in the thermal reactor (or by using thorium oxide fuel instead of uranium-oxide fuel) with Pu-mixed fuel. However, a large percentage of Pu material mixed in with the uranium-oxide fuel creates a positive temperature coefficient of reactivity because of the resonance located at neutron energy of 0.3 eV; therefore, we cannot burn a large amount of Pu in the thermal reactor.

^{233}Pa produced from ^{232}Th has large thermal-neutron capture cross section; thus, when a thermal neutron reactor is operated at a high flux level to get a high rate of production of ^{233}U, ^{233}Pa is converted to ^{234}Pa before decaying to ^{233}U; in this reaction neutrons are lost, and so it is undesirable from the point of view of neutron economy.

When ^{233}U is produced in a fast-neutron reactor, this loss of neutrons is small because of the small neutron-capture cross section of ^{233}Pa. As a material for making bombs, ^{233}U is more effective than ^{239}Pu; to prevent this and confer resistivity, the ^{232}Th should be mixed with a small amount of ^{238}U.

Another problem facing the nuclear energy field is the accumulation of minor actinides (MAs) which are long-lived alpha emitters. To transmute these MAs, the use of a fast reactor [5] has been promoted. Mixing MAs with the fuel in a fast reactor hardens the neutron spectrum, and makes the fission of MAs more effective, rather than transforming them into other MAs in a soft neutron spectrum, such as in the thermal reactor. Since the η value of ^{239}Pu increases as the neutron energy increases, the neutron economy improves, but the void coefficient of the sodium coolant in the MA-fueled fast reactor becomes more positive than in a reactor without MA. To reduce this positive coefficient, the fast reactor can adopt a very neutron-leaky core such as the flattened core (D/H = 3-7). However, this change worsens the neutron economy. Furthermore, in a reactor with a hard neutron spectrum, the lifetime of the neutrons becomes small, as does that of the delayed neutrons which are vital in operating a critical reactor. Therefore, a very careful operation is needed. When a reactor is operated in a subcritical condition instead of a critical one, the creation of a positive Na void coefficient is not a danger, because the transient behavior of the subcritical reactor is gentle, as we discussed in our paper [6], even in a small subcritical operation.

Figure 1 shows the geometry of the fast-neutron ^{233}U producer and transmutor of MA which uses conventional mixed-oxide fuel blended with MAs; the thorium oxide is placed in the blanket region in the Prototype of the 700 MWt fast reactor [7].

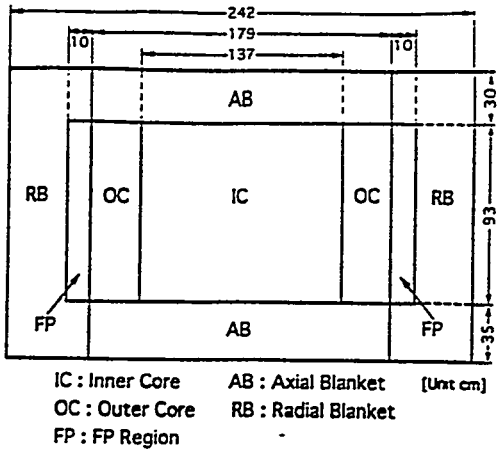

Fig. 1 Geometry of the Fast Neutron ^{233}U Producer and Transmutor of MA and LLFP when it is operated by subcritical condition, the lead target is installed in the center of the core

Table I shows the initial production rate of ^{233}U and ^{239}Pu, multiplication factor, neutron lifetime, and initial breeding ratio for various blanket materials. When ^{232}Th is included in the blanket region, the production rate of the total amount of ^{233}U created by the ^{232}Th blanket plus the ^{239}Pu created in core region is not much different from the total production of ^{239}Pu in a ^{238}U system. When ^{232}Th is put in the core region, the ^{233}U production increases, but the multiplication factor, k, is reduced substantially; thus, a larger core volume is required. When MA is added into the fuel, the production of ^{239}Pu increases, but the k value is slightly reduced.

Table I. Multiplication Factor, Neutron Life-Time, Production of ^{239}Pu & ^{233}U, Transmutation of MA and LLFP, and Initial Breeding Ratio of Various Configuration of Reactor

	*Multiplication Factor Neutron Life time**	*Production of ^{239}Pu &^{233}U transmutation MA or LLFP***	*Initial Breeding Ratio*
a) Uranium Blanket	1.0343+-.0043 129.4	^{239}Pu 243.8Kg	0.96026
b) Thorium Blanket	1.0275+-0.0045 134.56	^{239}Pu 123.8 ^{233}U 122.4	0.9765
c) Thorium Blanket Core	.9503+-.0046 123.94	^{233}U 265.5	1.0528
d) Thorium Blanket 5w/0 MA in core	.9808+-.0042 123.49	^{239}Pu 122.2 ^{233}U 106.2 Ma(cap) 41. Ma(fis) 10.9	1.02716
e) Thorium Blanket ^{99}Tc	.9920+-.0012 353.77	^{239}Pu 112.7 ^{233}U 60.1 ^{99}Tc 34.7	0.698
f) Thorim Blanket ^{129}I (30%)	1.002+-.006 462.18	^{239}Pu 173.6 ^{129}I 34.4	0.7014

a) Uranium-oxide(UO2) in core and blanket(BL), b) Thorium-oxide(ThO2) in BL, c) ThO2 in core and BL, d) ThO2 in BL & 5w% MA in core, e) ThO2 in BL & 99Tc with YH1.7, f) UO2 in BL &129I(30%) with YH1.7. * unit of 10^{-4}sec, ** in unit of Kg

Transmutation of LLFPs

As discussed in our previous paper [8], which investigated the energy requirements, thermal heat generation, and proton current in the transmutor, the LLFPs produced by the fission reaction are substantially high, even without FP, such as ^{137}Cs and ^{90}Sr. Thus, to transmute LLFPs without reducing the conversion factor, the reactor has to have a good neutron economy.

To transmute 16.46% of LLFP made from ^{99}Tc, ^{129}I, ^{85}Kr and ^{93}Zr, but not ^{137}Cs and ^{90}Sr, a subcriticality less than 0.33 achieved with a proton accelerator can produce more thermal energy than that consumed for accelerating the protons. Energy-wise, it is not so difficult to transmute the LLFP; however, the proton currents needed are rather large with such a large subcriticality, and many problem are created that are associated with a high proton current, such as radiation damage, and localized heat generation. To reduce this, we need a subcritical reactor with small subcriticality.

We assessed the possibility of transmuting the long-lived fission products (LLFPs) ^{99}Tc and ^{129}I in a this prototype fast reactor. As shown in figure 1, ^{99}Tc is mixed with yttrium hydride ($YH_{1.7}$), and the mixture is loaded between the core and the radial blanket. Iodine in the form of CeI_3 and an iodine's concentration of 25% ^{127}I and 75% ^{129}I, which correspond to the anticipated isotropic inventories in the long-cooled spent fuel from LWRs, are mixed with $YH_{1.7}$. We calculated the transmutation rate and quantity of LLFP that could be transmuted for various LLFP to $YH_{1.7}$ volume ratios, using the MCNP code. The nuclear data for ^{99}Tc, ^{129}I, and Ce were calculated from the ENDF/B Library, using the NJOY code. Table I shows the results. This-700 MWt reactor transmutes 34.7 kg of ^{99}Tc and 34.4 kg of ^{129}I in one year. Therefore, this reactor can deal with the annual 29.3 kg of ^{99}Tc generated at one 1 GWe LWR, in addition to its own generation of this isotope. For transmuting ^{129}I, the reactor transmutes the ^{129}I generated in about seven 1 GWe LWRs in addition to the amount it generates itself.

When the LLFP is transmuted to a nucleus which has a large neutron capture cross section, the neutron economy worsens due to additional neutron capture. For example ^{99}Tc ($\sigma_{n,\gamma} = 20$ barns) will be converted to ^{100}Tc by neutron capture, and ^{100}Tc (15.8 sec half-life) decays to ^{100}Ru, which has a significant thermal-neutron capture cross section of 5.1 barns. Therefore, it is desirable to remove the LLFPs as soon as this isotope is created. LLFP can be removed by using particle LLFP, as also is the case with liquid LLFP. The variation in reactivity associated with removing the LLFPs can be safely handled in subcritical operation. However, in the case of critical operation much more care should be taken.

The prototype MOX fast reactor with a thermal power of 700 MWt can transmute a substantial amount of LLFP, but the breeding ratio is reduced from about 0.96 to 0.7 because of the large number of neutrons that are consumed during transmutation. The economy of such transmutation should be studied more rigorously.

Radiation Damage to the Proton Target Area

Because accelerated protons produce spallation neutrons and protons in the target and window areas with energies above that requested for atomic displacement, and also produce hydrogen and helium, the problem of radiation damage is expected to be substantial when a high-power accelerator is used to drive a large subcritical reactor. To alleviate this problem, in our first conceptual design we spread the high-current proton beam over a large area. However, this

requires a long, expansion section of the beam-transport line, and shielding of the holraum becomes problem. Also, the neutron economy is worse due to a large neutron leakage from the exposed surfaces. Using a small proton current associated with small subcriticality avoids this serious problem.

We assessed the radiation damage to a lead target system installed in the center of a MOX fuel fast transmutor (reactor). Damage to the structural materials of a proton-accelerator-driven reactor is being investigated using the Monte Carlo simulation codes LAHET, HMCNP, and HTAPE. For comparison, calculations were made with the MCNP code for the critical reactor, which has a softer spectrum than the accelerator-driven subcritical reactor. The atomic displacement (DPA), H, and He production rates, and the energy deposition were evaluated using the cross sections calculated by the TRANSX2 code for neutrons with energies less than 20 MeV, and the values given by Kolovin, et al., [9] for the cross sections for neutrons with energies above 20 MeV. In our previous study of radiation damage to particle fuel (PFT) and MOX fuel (MFT) caused by varying the thickness of the core, we showed that the extent of damage is rather insensitive to the k_{eff} because the proton current is reduced while getting the same power density. When the overall size of the reactor is fixed, and subcriticality is increased, the proton current increases in proportion, and the radiation damage becomes proportionally greater.

The lead target, the structural walls, and the core were divided into small cells, as shown in Figure 2, to estimate the positional dependence characteristics of radiation damage; for PFT and MFT, they are almost the same. Table II shows the extent of radiation damage when a proton current of 16.8 mA is injected into the subcritical MOX Fuel transmutor. Cell #5 of the lead target shows a large DPA of 320.3, (if a solid lead target is used) as do the beam window (cell #9) of 160.7 DPA, and a side structural wall near the window section (cell #12) of 167.7 DPA. These findings indicate that, in designing the proton-accelerator based transmutor, the radiation damage not only to the beam widow section but to the side walls of the target should be investigated carefully. The contributions to DPA by neutrons with energies below 20 MeV are dominant to those with energies above 20 MeV for the fast-neutron reactor. Further, the DPA in the accelerator-driven reactor with a subcriticality of $K_{eff} = 0.9$, which requires a proton current of 15 mA, is about 1.5 times larger than that of the critical reactor. However, this value for DPA is not unusually large because this fast reactor has less power and a harder neutron spectrum which produces the higher DPA effect.

Our analysis shows that the rates of H and He production depend on the proton beam current, as expected, because these rates reflect the high-energy neutron and proton reactions. A higher beam current will give larger values for energy deposition, except in the core because, here, fission energy is mainly deposited, and the total fission energy mostly depends on the power density, not on the proton beam current. The beam window (cell #9) and the lead target near the beam window (cell #5) have the largest rates of energy deposition and of H and He production. However, the rate of production of He is smaller than that of H. The radiation damage DPA caused by protons was not calculated, but it is not as high as that caused by neutrons, because the cross sections for both are of about the same order in the high-energy range and the DPAs of neutrons with energies above 20 MeV are small, as discussed above.

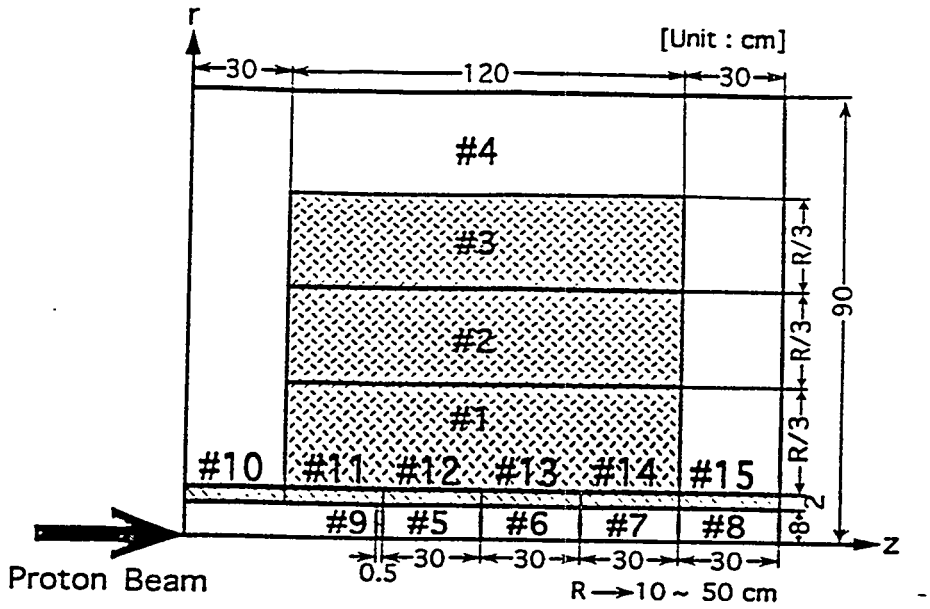

Fig. 2 The lead target, the structural walls, and the core were divided into small cells

Table II. The Radiation Damage when a Proton Current of 16.8 mA is Injected Into a Subcritical MOX Fuel Transmutor

(c) $R^{a)}$ = 30cm, k_{eff} = 0.858, $P^{b)}$ = 300MW_{th}, $I_p^{c)}$ = 16.8mA

Cell #	Material	DPA[d] (dpa/yr) below 20MeV[e]	DPA[d] (dpa/yr) above 20MeV[f]	DPA[d] (dpa/yr) Total	W[g] (W/cm^3)	H[h] ($mol/cm^3/yr$)	He[i] ($mol/cm^3/yr$)
1	Fuel	88.5	2.0	90.5	600.1	2.7×10^{-5}	5.3×10^{-6}
2	Fuel	71.1	0.9	72.0	503.2	8.8×10^{-6}	3.3×10^{-6}
3	Fuel	51.4	0.5	51.9	481.6	4.2×10^{-6}	1.2×10^{-6}
4	Stainless	5.3	3.5×10^{-2}	5.3	0.1	1.1×10^{-6}	6.1×10^{-8}
5	Lead	273.1	47.2	320.3	1322.1	3.1×10^{-3}	6.3×10^{-4}
6	Lead	98.1	10.8	108.9	242.7	3.5×10^{-4}	4.5×10^{-5}
7	Lead	33.6	1.0	34.6	2.4	1.3×10^{-5}	3.6×10^{-6}
8	Lead	6.6	0.2	6.8	6.0×10^{-2}	$< 10^{-6}$	$< 10^{-8}$
9	Stainless	145.5	15.2	160.7	1003.8	4.9×10^{-3}	1.6×10^{-4}
10	Stainless	15.6	0.2	15.8	0.1	1.6×10^{-6}	$< 10^{-8}$
11	Stainless	66.6	1.3	67.9	3.4	2.9×10^{-5}	3.2×10^{-6}
12	Stainless	158.2	9.5	167.7	34.4	2.7×10^{-4}	9.7×10^{-6}
13	Stainless	93.2	3.6	96.8	33.1	1.2×10^{-4}	9.7×10^{-6}
14	Stainless	39.4	0.4	39.8	0.4	6.5×10^{-6}	$< 10^{-8}$
15	Stainless	8.6	3.0×10^{-2}	8.6	$< 10^{-6}$	$< 10^{-6}$	$< 10^{-8}$

a) Core thickness in the radial direction, b) Total thermal power, c) Proton beam current required to operate the transmuter continuously, d) Atomic displacement, e) DPA by neutron with energy below 20 MeV, f) DPA by neutron with energy above 20 MeV, g) Energy deposition, h) H production rate, i) He production rate.

Although this analysis was made for a fast-neutron reactor, when the thermal-neutron reactor is used as an accelerator-driven reactor, the DPA due to spallation neutrons will be much higher than that in the critical reactor because the neutron spectrum in the latter is much softer.

ACKNOWLEDGEMENTS

The authors would like to express their thanks to Drs.H.Rief, H.Harada for valuable discussions, and for providing him the information for writing this report, and Dr. Woodhead for editorial work. This work was performed under the auspices of the U.S. Department of Energy under Contract No. DE-AC02-76CH00016, and under The Power Reactor and Nuclear Fuel Development Corporation.

REFERENCES

[1] H. Takahashi, "The Role of Accelerator in the Nuclear Fuel Cycle" Proc. of 2nd Int. Symp. in Advanced Nucl. Energy Research. p. 77, Mito, JAERI, Jan. 24-26, (1990).

[2-a] H.Takahashi and H.Rief."Concept of Accelerator Based Transmutation System" Proceeding of the OECD Specialist Meeting on Accelerator based Transmutation March,25-16,1992. Paul Scherrer Institute, Switzerland Edited by H.U.Wenger, p.2-26

[2-b] H. Takahashi " A Fast Breeder and Incinerator Assisted by a Proton Accelerator" Fusion Technology, 20, 657,1991.

[3] C.E.Till and Y.I.Chang "Progress and Status of the Integral Fast Reactor (IFR); Fuel Cycle Development", Inter. Conf. on Fast Reactor and Related Fuel Cycles(ICFRRFC). I-6, Oct.28-Nov.1,1991 Kyoto Japan

[4] H.Takahashi, J.Powell, and H. Kouts;" Accelerator Breeder with Uranium and Thorium Target" ,; Atomkernenergie- Kerntechnik, 44, (1978) 329.

[5] C.L.Cockey and M.L.Thompson " ALMR Potential for Actinide Consumption",(ICFRRFC).P3.4-1,

[6-a] H. Rief and H.Takahashi, Safety and Control of accelerator-driven Subcritical System. This conference.

[6-b] H.Rief and H.Takahashi, Some Physics Consideration in Actinide and Fission Product Transmutation" Proc. Int. Conf. on Reactor Physics and Reactor Computations, edited By Y. Ronen and E.Elias, Tel-Aviv, Jan 23-26,1994.Ben-Gurion Unv. of the Negev Press (1994).

[7-a] H. Takashita, H.Harada, H.Takahashi, A.Aronson,"Transmutation of Long Lived Radio-active Nuclide" p-797,Proc. Global Conf. Sep, 1993. American Nuclear Society, Inc. La Grange Park,Illinois.60525,USA. }

[7-b] H.Takashita, H.Takahashi and A. Aronson "Study on the Transmutation of Minor Actinides and Fission Products in a Prototype Fast Reactor with Mixed-Oxide Fuel". International Conference of Emerging Nuclear Energy System (ICENES)-93.

[8] H.Takashita, H.Takahashi, A. Aronson; Submitted to Nuclear Science Engineering[9]. Yu. A. Korovin, A.Yu. Konobeyev and V.N.Sonin."Biserm, Neutron and Proton Data Library for Evaluation of Irradiation Effects in Structural Material in the Energy Range up to 800 MeV" to be published.

Some Nuclear Safety Aspects of the Los Alamos Accelerator Based Conversion Concept

Waclaw Gudowski*, Erik Möller* and Francesco Venneri†

*Department of Physics,
Royal Institute of Technology, 100 44 Stockholm
Sweden
and
† Los Alamos National Laboratory
Los Alamos, New Mexico 87 545
USA

Abstract. The detailed analysis of the few parameters important for the safety of the accelerator-driven plutonium burner concept developed at Los Alamos National Laboratory was performed. The plutonium load, optimal thermalization of the neutron spectrum and temperature reactivity coefficients were investigated. The calculations revealed the strong positive temperature reactivity coefficient. The ways to solve this problem are suggested.

INTRODUCTION

In the last few years Accelerator-Driven Transmutation Systems have gained significant public and scientific attention offering several potential advantages over the reactors for transmutation applications and possibly even for the energy production. Aiming at reducing long time hazards of nuclear wastes the safety hazards of the transmutation system have to be evaluated very carefully. The long time risks of the waste handling (e.g. storing in the geological repository) should be compared with the short term risks connected with the operating of the accelerator-driven facility and in the case of energy production with the conventional nuclear reactor or other energy generating facilities. In this paper we focused our investigations on the analysis of the temperature reactivity coefficients of the accelerator system designed for the weapon plutonium incineration, so called Accelerator Based Conversion (ABC) concepts developed at Los Alamos National Laboratory [1]. The temperature reactivity coefficient is an important safety parameter also for the subcritical systems like ABC, it may limit the subcriticality margins and determine the stability of this system.

COMPUTATIONAL MODEL OF ABC

The 3-D computational geometry of the ABC system was simulated as close as possible to geometry of the Los Alamos conceptual design of ABC [1]. The MCNP4A Monte-Carlo code was used to perform the neutronic and reactivity calculations for the typical 500 MW_{th} ABC blanket assembly - graphite pile (core) of 4.5 m diameter and 5 m height. At this stage the spallation neutron source was assumed to be a point source located in the Th target. The energy of spallation neutrons was assumed to be of 2 MeV. Fig. 1 shows the horizontal cross section of the two parts of the core, Fig. 1a - the central part of the core surrounding the target assembly; Fig. 1b - model of the hexagonal graphite moderator block with fuel channels.

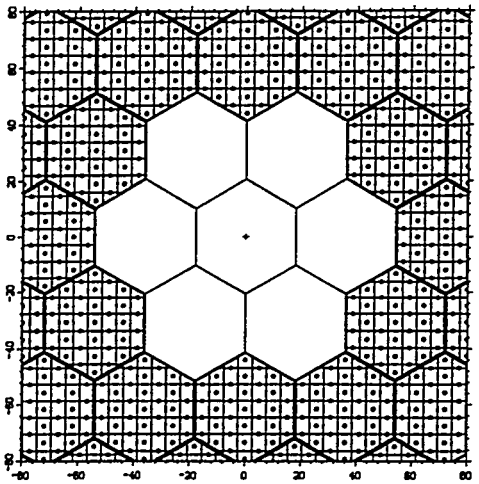

a) the central part of the blanket surrounding the target assembly

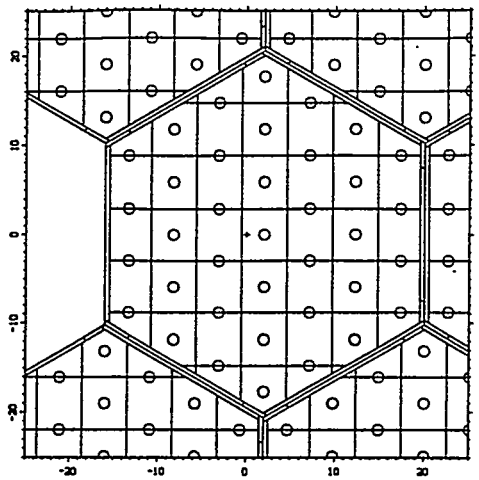

b) the hexagonal graphite block with fuel channels

Fig. 1. The computer model of the blanket geometry. Horizontal cross section of the central part of the blanket.

Molten salt circulating through the fuel channels consists of the mixture of Be-Li-Zr and Pu fluorides with the concentration given in the Table 1.

Table 1. Composition of the ABC molten salt fuel

Fuel component	Weight fraction
LiF	65%
BeF_2	29%
ZrF_4	5%
Pu	~0.1%

PLUTONIUM LOADING LIMITS

To ensure the subcritical mode of ABC operation the concentration of Pu in the molten salt should be kept on the desired level. The simulations were performed to determine the Pu concentration margins for the subcritical operation. Fig. 2 presents a MCNP neutronics analysis of how k_{eff} of the ABC system varies with Pu loading in the molten salt.

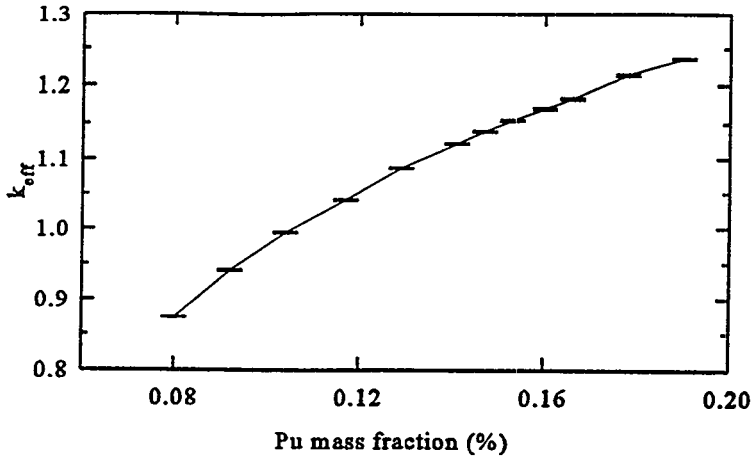

Fig. 2. k_{eff} as a function of the Pu concentration in the molten salt loop. BoL (Beginning of Life) of the system: fresh fuel, no fission products. The temperature - 880 K. The error bars indicate the uncertainty of the k_{eff} calculations.

This plot shows that the Pu concentration of about 0.1% (mass fraction) is the upper limit for subcriticality at 880 K. The next important issue is the question if the system with 6 mm radius fuel channels - as proposed by Los Alamos [1] - is the optimal one, i.e. if this system is well moderated. Fig. 3 presents the results of the simulations in which k_{eff} was calculated as a function of two variables - fuel channel radius and the graphite temperature. The analysis of this 3D-plot along the axis of the fuel channel radius indicates that the system with 6 mm radius channels is not optimal from the k_{eff}
point of view, it is overmoderated. The optimum size of the fuel channels is about 11 mm radius which corresponds to 14 % of the salt volume fraction (see Tab. II). The total mass of plutonium was constant for all simulations (~20 kg), salt volume fractions was varying due to the variation of the fuel channel radius as shown in Table 2.

Table 2. Salt volume fraction corresponding to different size of the fuel channel radius in the graphite moderator.

Fuel channel radius (mm)	Salt volume fraction (%)
6	3.8
11	14
19	57

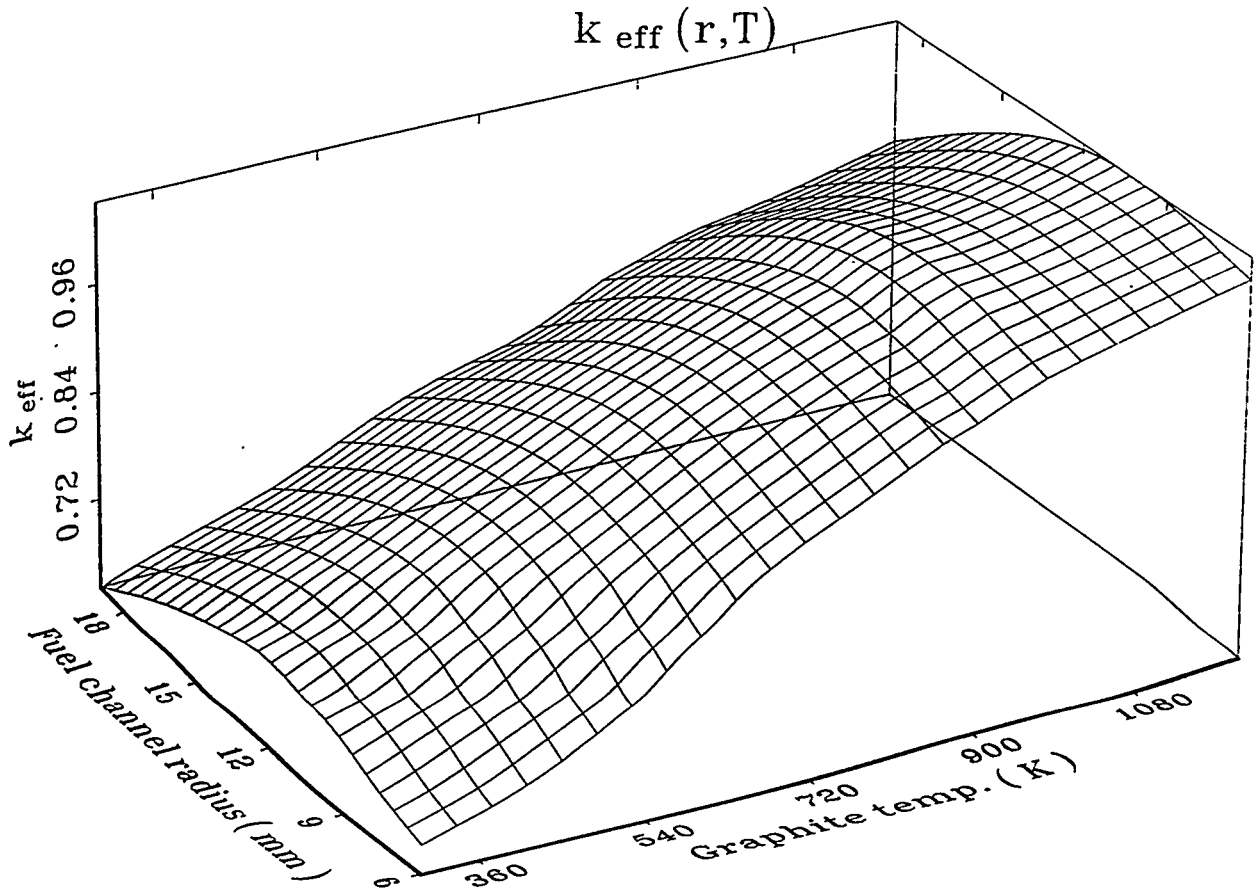

Fig. 3. k_{eff} as a function of the fuel channel radius and the graphite temperature. Constant plutonium loading in the system - ~20 kg.

Fig. 3 demonstrates the existence of the significant safety concern connected with the ABC system - the raise of the k_{eff} with the temperature. It indicates the strong positive reactivity coefficients.

TEMPERATURE COEFFICIENTS OF REACTIVITY

In order to determine the temperature coefficients of reactivity the calculations of k_{eff} were performed as a function of the salt and the graphite temperature. The results of these investigations are presented in Fig. 3, Fig. 4 and summarized in the Table 3.

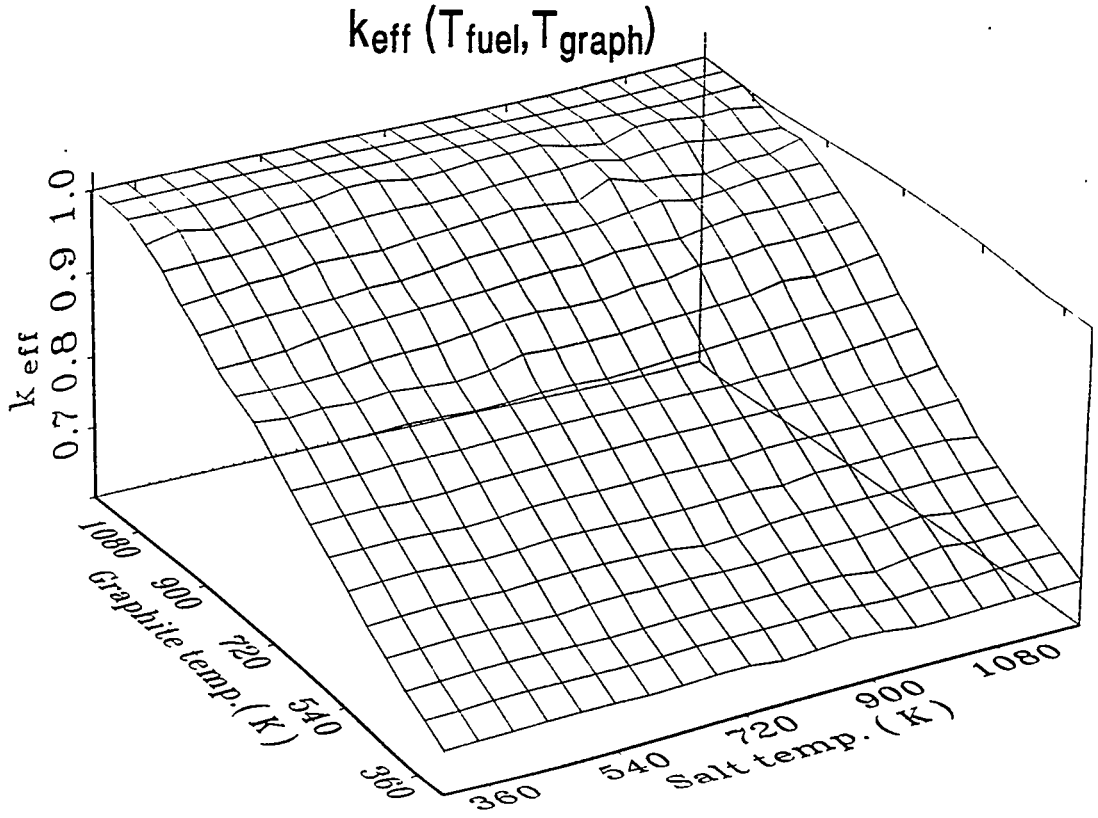

Fig. 4. k_{eff} as a function of the molten salt and the graphite temperature. Constant plutonium loading in the system - ~20 kg.

Table 3 Temperature coefficient of reactivity for ABC-system, r - radius of the fuel channels.

Temp. coefficient of reactivity (pcm)	r=6 mm (overmoderated)			r=11 mm (optimal)		r=19 mm (under-moderated)
	fresh fuel			fresh fuel	1% of fission products[a]	fresh fuel
$\partial\rho/\partial T_{moderator}$	45			42	36	34
	300K	800K	1000K			
$\partial\rho/\partial T_{fuel}$	-0,2	1,5	1			

[a] - effect of the fission products was simulated with the average cross-section data for the fissions products from plutonium fission (see MCNP4A cross section data description [2].

It is clear that the ABC system shows very strong, positive temperature dependence on the moderator temperature. Even for the subcritical system this situation is unacceptable. As shown for the r=11 mm situation does not change with the increased amount of the fission products. 1% concentration of the fission products does effect significantly the temperature reactivity coefficient.

In order to understand what is the physical mechanism responsible for this strong raise of the reactivity with the temperature, one can perform very simple analysis of the different parameters which effect the reactivity of the system. Similarly as for the classical nuclear reactors we can assume that in the first approximation k_{eff} can be described as a function of 5 independent parameters [3]:

$$k_{eff} = \eta f p \epsilon P \qquad (1)$$

where:

η	effective number of fission neutrons per absorption in fuel,
f	thermal utilization factor,
p	resonance enhancement factor (for LWR it is usually called resonance passage factor, determined mainly by absorption in ^{238}U; for ABC - Pu burner - we may call it resonance enhancement factor),
ϵ	fast multiplication factor,
P	probability to avoid escape(fast+thermal).

Defining a parameter H as the effective number of fission neutrons per absorbed thermal neutron - $H=\eta f$ and assuming that ϵ does not depend on the temperature, we may assume that the reactivity temperature coefficient is equal to:

$$\frac{\partial \rho}{\partial T} \sim \frac{\Delta H}{\Delta T H} + \frac{\Delta p}{\Delta T p} + \frac{\Delta P}{\Delta T P} \qquad (2)$$

Fig. 5a shows the effective number of fission neutrons per absorbed thermal neutron - H(T). It is clear that H(T) gives the negative contribution to eq. (2) in the relevant temperature range due to the 0.3 Pu cross-section resonance. The capture resonance increases faster than fission one. Fig. 5b demonstrates the escape fraction of the neutron flux. Increasing number of neutrons with the temperature raise gives leads to decreasing of the probability to avoid escape. It gives the negative contribution to the reactivity temperature coefficient. The conclusion is that the strong positive temperature dependency of the reactivity is driven by the plutonium resonances - i.e. by Doppler broadening which shows to be much stronger for the fission cross sections that for capture.

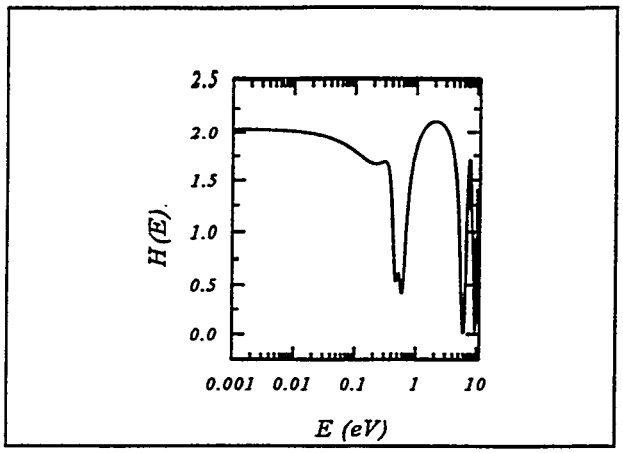

a) The effective number of fission neutrons per absorbed thermal neutron

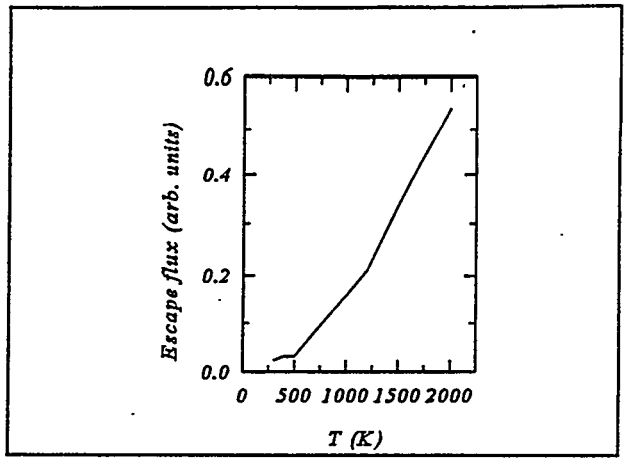

b) The escape probability for thermal and fast neutrons as a function of temperature

Fig. 5. Energy (temperature) dependence of the parameters contributing to eq. (2).

CONCLUSIONS

The ABC system shows very strong positive reactivity temperature coefficient - of the order of 40 pcm per K, it does not change significantly with increase of the fission product concentration in the fuel. This effect is caused by the Doppler broadening of the plutonium cross-sections. More detailed studies on how to reduce this effect are necessary, the most straight forward way to cure this problem could be:

1. Avoiding to run the system on the pure plutonium. Addition of e.g. ^{238}U or higher isotopes of plutonium could reduce the problem.
2. Introducing the resonance poisons like ^{167}Er may be a solution. This idea is to be studied in details.

Acknowledgments

W. Gudowski and E. Möller acknowledge the support for this research from the Swedish Nuclear Fuel and Waste Management Board Co.

REFERENCES

1. "The Los Alamos Accelerator Based Conversion Concept for Plutonium Disposition (ABC), Jason Review, La Jolla, CA, Jan. 18, 1994.
   F. Venneri, "The Physics Design of Accelerator-Driven Transmutation Systems, International Conference on Accelerator-Driven Technologies and Applications, July 25-29, 1994, Las Vegas.

2. J.F. Briesmeister, editor, "MCNP- A General Monte Carlo N-particle Transport Code", Version 4A, LA-12625, 1993.

3. Any book in reactor physics, e.g. D.J. Bennet, J.R. Thompson,"The elements of nuclear power", Longman Scientific & Technical, 1989.

Kinetics Of Accelerator Driven Devices

R.T. Perry, John Buksa, and Michael Houts
Los Alamos National Laboratory
Los Alamos, NM 87545

Abstract. Kinetic calculations were made to show that subcritical accelerator driven devices are robust and stable. The calculations show that large changes in reactivity that would lead to an uncontrollable excursion in a reactor would lead only to a new power level in a subcritical device. Calculations were also made to show the rate of power changes resulting from startup and shutdown, and that methods also exist for continuously monitoring the reactivity of a subcritical system.

INTRODUCTION

Any device containing fissile material will be in one of four operating regimes: subcritical, critical, delayed critical, or prompt critical. Both delayed and prompt critical are referred to as "supercritical." In the absence of an external source, the power of a subcritical device always decreases. In a critical device, the power is constant. If a device is delayed critical, the power is increasing with the rate of increase limited by the time constants, on the order of minutes, that are associated with the delayed neutrons. A prompt critical device has time constants associated with the prompt neutron lifetime, which is on the order of milli- to microseconds. The time behavior of any of these devices can be approximated by the point reactor kinetics equations.

The point reactor kinetics equations are given below:

$$\begin{aligned} dn/dt &= ((\rho(t) - \beta) / \Lambda)\, n(t) + \Sigma \lambda_i C_i(t) + S, \\ dC_i/dt &= (\beta_i/\Lambda)\, n(t) - \lambda_i C_i(t), \\ \rho(t) &= (k(t) - 1) / k(t). \end{aligned} \tag{1}$$

where:

- $n(t)$ = neutron population as a function of time - note that it is proportional to power
- t = time
- β = fractional yield of delayed neutrons per fission neutron
- β_i = fractional yield of the i^{th} group of delayed neutrons
- Λ = prompt neutron lifetime
- λ_i = decay constant of the i^{th} group of delayed neutron group
- $C_i(t)$ = the concentration of the i^{th} group of delayed neutron precursors as a function of time
- S = fixed source - here neutrons produced from the accelerator protons, and
- $k(t)$ = reactivity of the reactor as a function of time.

The neutrons born in a fissile material containing device will have two separate origins. The prompt neutrons are born of fission and comprise a fraction greater than 0.99, i.e. $(1-\beta)$, of these neutrons. The prompt neutron lifetime, Λ, refers to the time it takes from the neutrons birth to the fission resulting from its capture. The delayed neutrons are born from the decay of a fission fragment and appear seconds to minutes following the fission in which the fission fragment was born. Source neutrons from protons are independent of these prompt and delayed neutrons.

An examination of the kinetics equations delineates the various operating regimes. The prompt critical regimes occur when ρ is greater than β. The rate of change of power is positive independent of contributions from delayed neutrons. The time constant, Λ, is on the order of micro- to milli-seconds. The doubling times are such that the reactor could not be controlled.

When ρ is positive, but less than β, the reactor is in the delayed critical regime, and the rate of change of power is positive only with contributions from the delayed neutron term with the time constants, $1/\lambda_j$, being on the order of seconds to minutes. The power doubling times are much longer, and the device is clearly controllable. The critical reactor is the regime where ρ is zero. Each fission will subsequently produce only one fission, thus the power is constant, i.e. dn/dt=0.

If the device is capable of maintaining constant power or increasing in power, without a external source of neutrons, it is a reactor. If the device requires a external source to maintain constant power, then it is referred to as a subcritical reactor. The reactivity, ρ, of a subcritical reactor is negative. Note that in the absence of a source, the power of a subcritical reactor decreases indefinitely with time constants $1/\lambda_j$. In the subcritical regime, the larger portion of a power change resulting from a change in the external source or a change in reactivity occur with the time constant, Λ, associated with the prompt neutrons. The delayed neutrons which follow, slowly increase the power slightly by adding a tail to the major power change.

The power of a subcritical reactor results from a multiplication of the neutrons from the external source, S. The source multiplication is described by the following equation:

$$M = 1/(1-k) \qquad (2)$$

where:

M = multiplication factor
k = reactivity.

The power of a subcritical accelerator driven reactor then is determined by the reactivity of the device and the proton beam strength that produces the neutrons.

Thus, an important safety feature of accelerator driven devices is that they cannot undergo unlimited power excursions. The maximum power is limited to the subcritical multiplication of the source. In this paper we demonstrate this with our initial calculations describing the kinetic behavior of an accelerator driven device. Comparisons are also made between the power changes in a critical reactor and an accelerator driven device resulting from the same ramp input of reactivity.

It is important in accelerator driven devices to constantly monitor the reactivity of the system to ensure that it remains in the subcritical mode and to design the system in such a way that deposition or precipitation of fissile material does not lead to a supercritical system. Kinetic calculations are then made to demonstrate that the time rate of change of the power as a function of reactivity and source strengths give a clear indication of the reactivity the blanket (1).

Kinetic calculations are also made to describe the startup and shutdown of accelerator driven devices. These calculations show the rapid initial rise or drop in power followed by a slowly changing power level.

METHODS

A modified version of the kinetics code AIREK III [1] was used to make the calculations. Among the important input parameters to a kinetic codes are reactivity, prompt neutron lifetime, and the delayed neutron fraction. Note that parameters such as geometry, materials, or fissile enrichment are not included. Thus, a given set of input parameters could describe a large envelope of devices. The startup and shutdown cases used parameters consistent with a system containing fissile uranium. The remaining cases used parameters consistent with a blanket utilizing a ^{239}Pu containing salt, e.g., (65%LiF / 29%BeF_2 / 5%ZrF_4 / x%PuF_3) where percents

---

1) George Lawrence, Los Alamos National Laboratory, suggested these calculations be made and that they could possibly provide a method for measuring the reactivity of subcritical devices.

are mole percent and "x" represents 1% or less. The Li is 99.99 a/o ^{7}Li.

Parameters were established as reasonable through a set of k calculations using one- and two-dimensional S_n transport codes in which subcritical devices with salt containing blankets were modeled. In these calculations, it was established that in highly thermal systems, small changes in Pu concentration lead to large changes in reactivity. For example, a change of 0.1 mole percent of Pu lead to a reactivity change of greater than 1\$ (ρ / β = reactivity in units of dollars) in a blanket containing 5% salt and 95% carbon. These calculations indicate that in certain reactor systems, large accidental excursions are possible.

CALCULATIONS / RESULTS

The first calculations demonstrated a startup, shutdown, and steady state case for a subcritical device. These cases were run with β of 6.1e-03, Λ of 1.e-04 s, and initial k for the subcritical device of 0.95 The steady state subcritical reactor power is 3000 MW.

In Fig. 1, these startup, shutdown and steady state cases are shown. The shutdown occurs form turning off the source while the device is at steady state power. The startup occurs when the source is turned on when the device is at a low power level. The initial time rate of change of the power for startup or shutdown is related to the prompt neutron lifetime and the tail to the decay constants of the delayed neutrons.

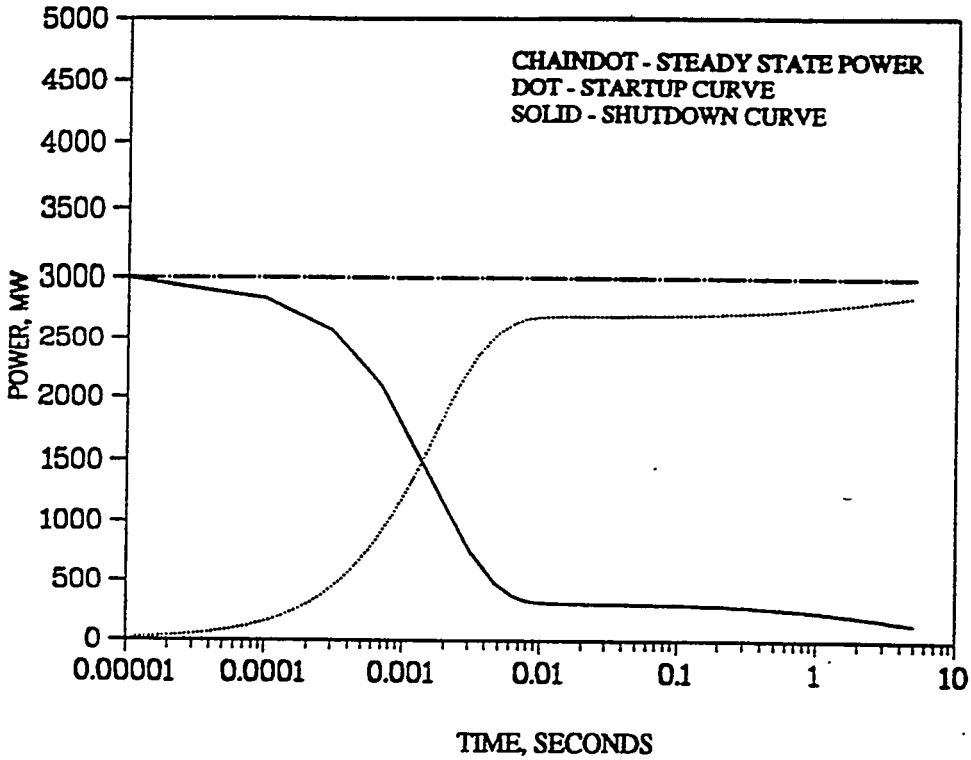

Fig. 1. Startup, Shutdown and Steady State Power

These calculations were followed by a comparison of the power change of a subcritical device to that of a reactor both having a 1\$/s reactivity ramp insertion with a maximum insertion of 1\$, i.e. $\rho = \beta$. These cases were run with β of 2.18e-03 and Λ of 1.e-04 s. The initial k for the subcritical device was 0.96 and initial k of the reactor was 1 (critical). The steady state reactor power was 500 MW. The source strength for the subcritical device is such that it operated at a steady state power of 500 MW.

In Fig. 2, the results of the calculations are shown. The reactor goes prompt critical one second into the excursion while the subcritical device's power is only increased by approximately 5% . This power change for the subcritical system can hardly be seen in Fig. 2, but is clearly noted in Fig. 3. In this scenario, the reactors become uncontrollable, while the accelerator driven device simply levels off at a new, higher power level.

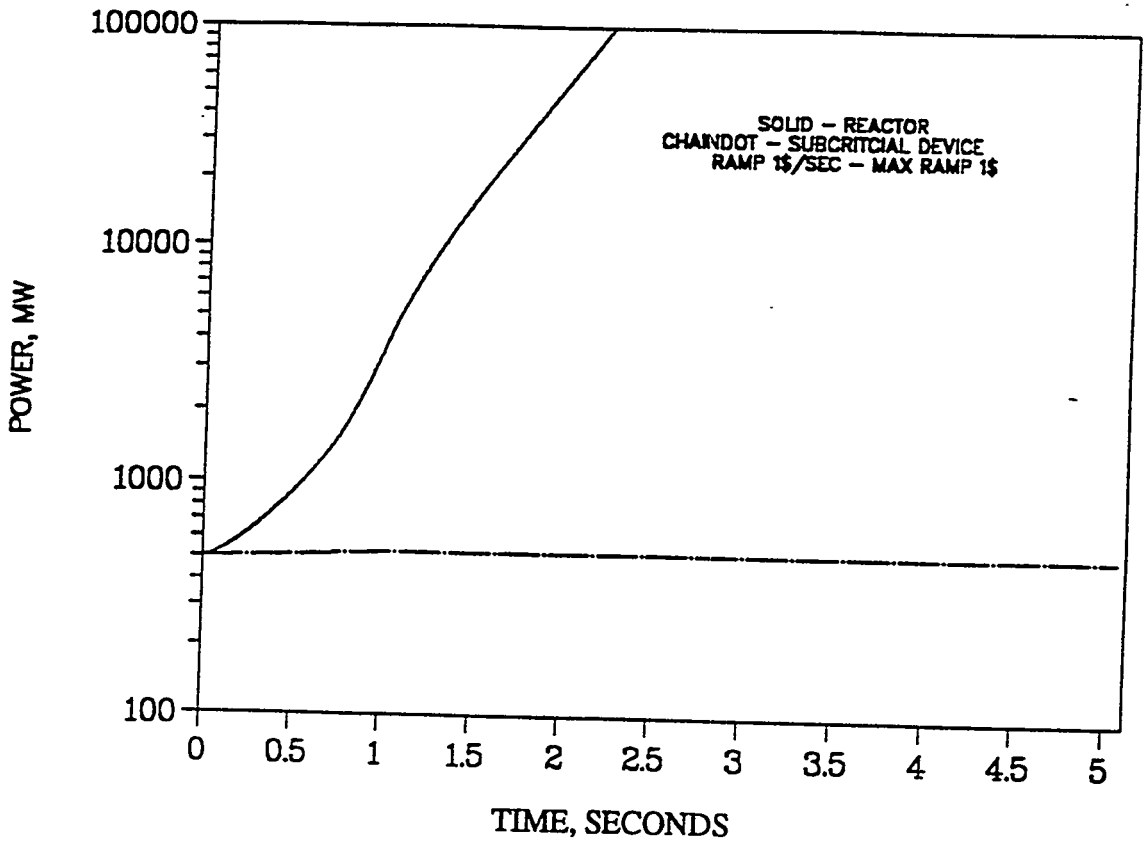

Fig. 2. Ramp Reactivity Input Into Critical Reactor and Subcritical Device

Next, shutdown calculations for several initial values of k for a 500 MW reactor were made. For these calculations β of 2.18e-03 and Λ of 1.e-04 s were used. These results are shown in Fig. 4. Note that the k at which the reactor was operating clearly determines the shape of the shutdown curve, which may be measured. Note also that the source needs to be turned off only very short periods of time to establish the curve shape. Such measurements could clearly establish the reactivity of the device and could be used to ensure the subcritical status of the system.

CONCLUSION

Clearly, subcritical systems are robust devices. Calculations show that large changes in reactivity that would lead to an uncontrollable excursion in a reactor would lead only to a power change in a subcritical device. Methods also exist for continuously monitoring the reactivity of a subcritical system. Thus, a subcritical device may have several advantages over a critical device in the areas of safety and operability.

REFERENCES

[1] L.R. Blue and M. Hoffman "AIREK-III," Atomics International document AMTD-131 (1963)

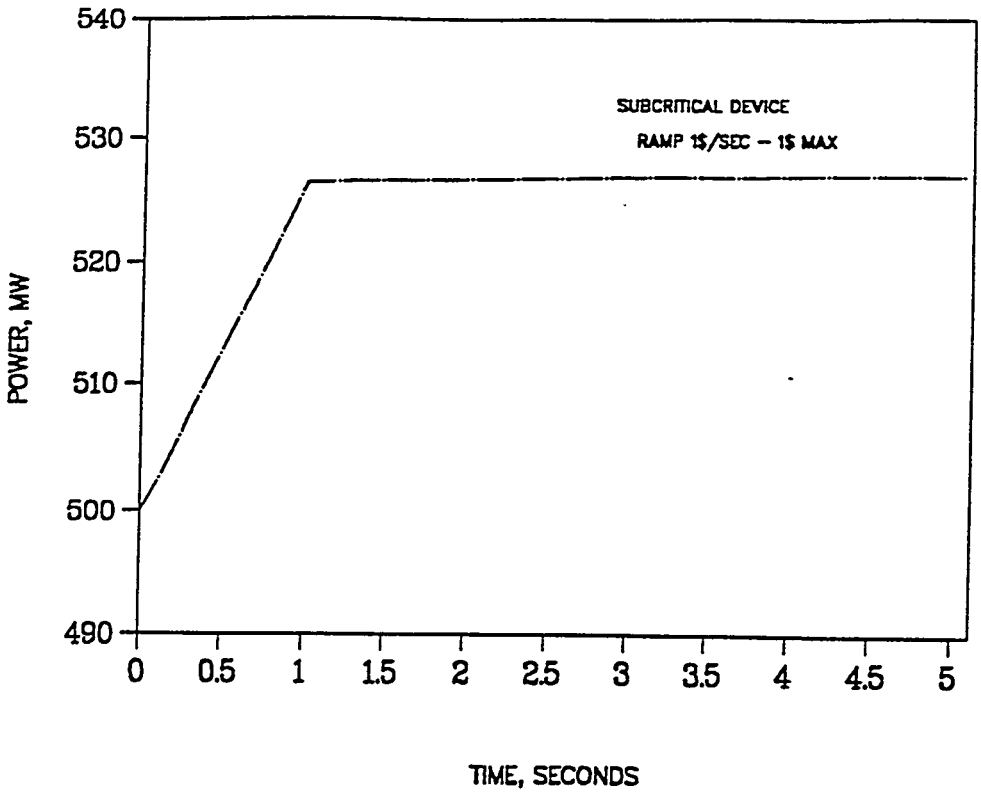

Fig. 3. Ramp Reactivity Input Into Subcritical Device

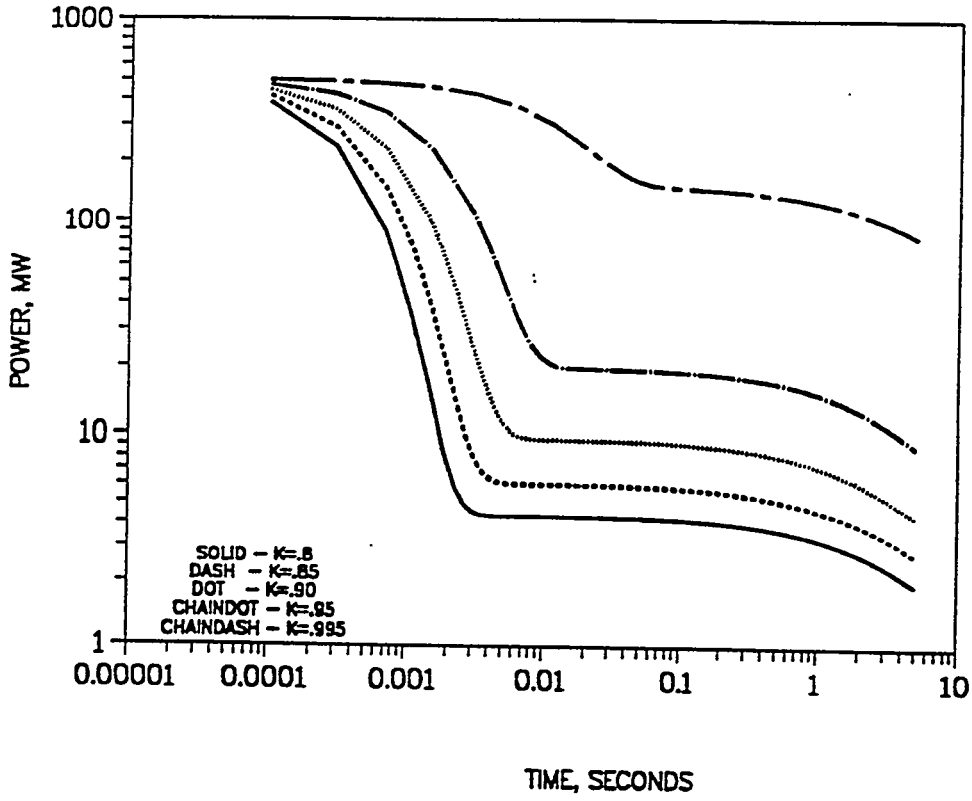

Fig. 4. Shutdown curves for blankets with various values of k.

The Neutronics of an Accelerator-Driven Energy Amplifier

Erik Möller and Waclaw Gudowski
Department of Physics,
Royal Institute of Technology, 100 44 Stockholm
Sweden

Abstract. This study has been focused on an Accelerator-Driven Energy Amplifier, based on the concept proposed by the CERN-group. To analyze the performance of this system the extensive optimization of the core lattice was done, the temperature coefficients of reactivity were investigated, reactivity budget and power distribution were estimated

INTRODUCTION

Accelerator-driven Energy Amplifier (ADEA) proposed last year by Carminati et al [1] gained a great public attention and generated vigorous discussion in many European countries. The idea of using a particle accelerator to drive the subricitical reactor is neither new [2] nor recently revived [3], the strong public response to the ADEA-idea and its great appeal was caused by the fact that:

1. Rubbia [1] stressed the cleaner and safier nuclear energy production compared to the conventional nuclear reactors, especially concerning long-lived nuclear wastes and operational safety of new systems.
2. The ADEA-idea is based on well known and proven nuclear technology applied eg. in light water reactors with fixed fuel-assemblies like in PWRs or BWRs. As an advantage was also stressed the low neutron flux mode of operation. The accelerator proposed for driving of ADEA is the isochronus proton cyclotron which compared to the LINAC has the advantage of the smaller size and much lower cost. It is believed that no significant technological development is required for the industrial construction of the 10-mA machine

For some European countries, where the conventional nuclear power is today publicly unacceptable or like in Sweden, where the development of new reactor-based nuclear power is prohibited by the law, this idea seemed to be even more attractive and plausible to implement in the near future.

In order to evaluate the feasibility of the ADEA-system we made very extensive calculations of the neutronics with some emphasis to the nuclear safety features and economy of this system. The calculations were performed using the Monte-Carlo simulation with MCNP-code [4] and ORIGEN2 depletion code [5].

MODEL OF ADEA

The analysis of the performance of ADEA was begun with extensive calculations

aimed to find the optimal moderator to fuel ratio. Based on the standard PWR construction we assumed the following parameters:

Tab. I Parameters of the Accelerator -Driven Energy Amplifier

Fuel	ThO_2 enriched 1.32 - 1.35 % ^{233}U
Fuel pellet diameter	8,2 mm
Fuel cladding	Zircalloy
Fuel rod diameter	9.5 mm
Fuel lattice	Triangular or semi-triangular (Fig. 1)
Moderator:	H_2O
Operating parameters:	
Pressure:	$9.8 \cdot 10^6$ N/m^2
Moderator temp.	300 °C
Fuel temp.	1400°C
H_2O density at 300°C and pressure $9.8 \cdot 10^6$N/m^2	716 kg/m^3

The numerical model of the fuel lattice used in the calculations is presented on Fig. 1

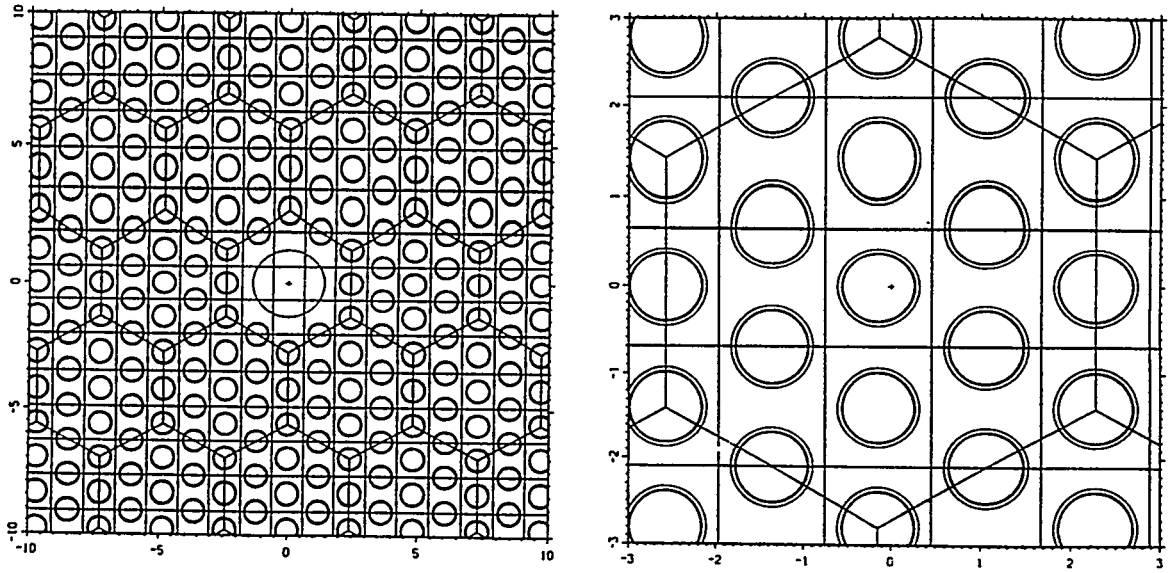

Fig. 1. Semi-triangular fuel rods configuration in the ADEA-core. Horizontal cross-section of the part of the core around the target (bigger circle on the left picture) and the details of fuel rods (the

right picture). Inner circles - fuel, outer circles - cladding, the rest - light water.

Optimization of the blanket/core lattice

The calculations of the optimal moderator/fuel ratio were performed by varying the rod pitch in the core/blanket lattice. Fig. 2 presents these results as the variation of k_{inf} as a function of rod pitch (bottom X-axis) and corresponding moderator/fuel volume ratio (top X-axis). k_{inf} calculated as a k_{eff} of the very large core (radius of ab. 10 m). The maximum k_{inf} corresponds to the rod pitch 15 mm and moderator to fuel ratio of 1.13.

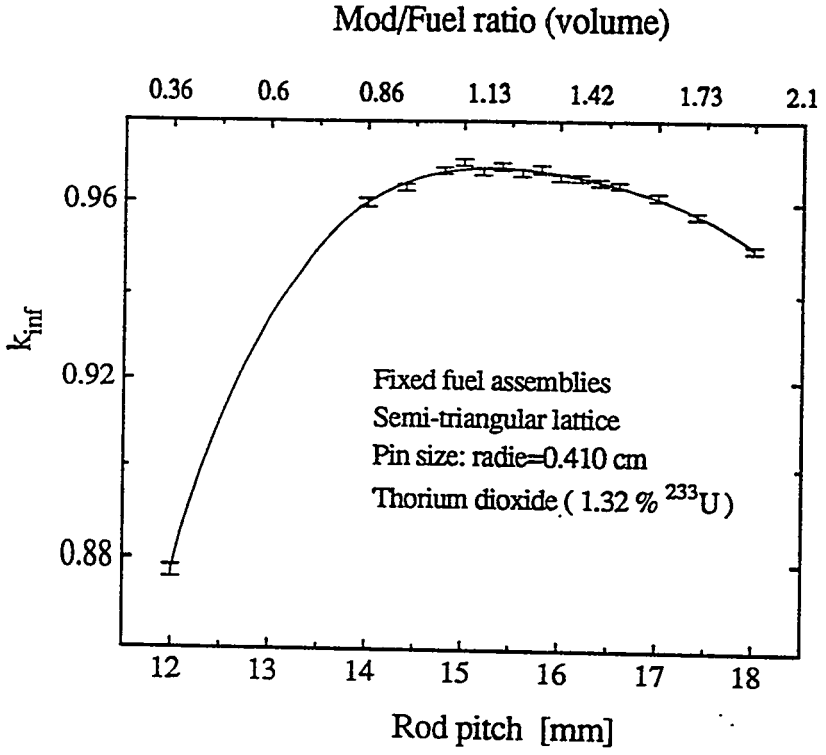

Fig. 2. k_{inf} as a function of rod pitch. Top X-axis describes the moderator/fuel volume ratio corresponding to rod pitch.

This curve indicates also that the desired by Rubbia et al [1] ratio 0.8 can be achieved for the rod pitch of 13.5 for this type of fuel lattice, the reactivity cost of this undermoderation is about 1%.

The fuel pellets radius was chosen - in similarity to conventional nuclear reactors - to be 4.1 mm. To analyze if this dimension is optimal from the neutronics point of

view series of calculations were performed to investigate k_{eff} as a function of fuel pellet radius. Calculation were performed on such a way that the optimal moderator/fuel ratio of 1.13 was kept constant.

Fig. 3 indicates that the optimal radius of the fuel pellet is much larger than 4.1 mm and should be in the range of 10 - 11 mm. The reactivity gain on the fuel pellet size is ~1%. However it is probably heat exchange process which imposes stronger constrains on the pellet diameter.

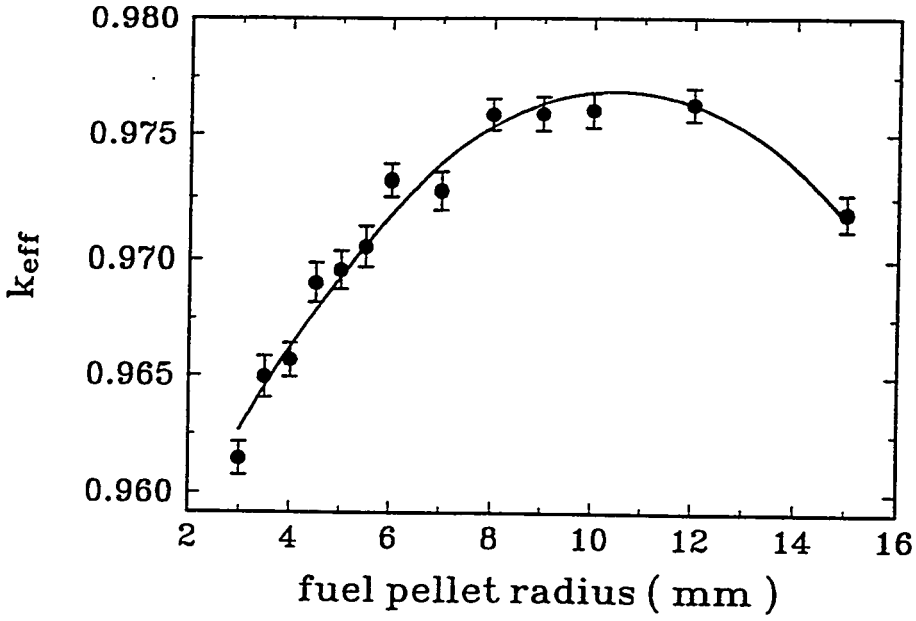

Fig. 3. k_{eff} as a function of fuel pellet radius.

The influence of moderator/fuel ratio and the fuel pellet radius on the thorium breeding ratio has to be analyze separately because it may influence the overall optimization.

TEMPERATURE COEFFICIENTS OF REACTIVITY

One of the most important parameters of the nuclear power system are the temperature coefficients of reactivity. They can strongly affect the reactivity budget of the system and the nuclear safety margins. The contribution from the raise of the fuel and moderator temperature has been analyzed separately. Fig. 4 shows k_{eff} as a function of the fuel temperature. Doppler broadening of ^{233}U resonances is responsible for this effect. It can be calculated from this plot that the fuel temperature coefficient of reactivity is fairly low ~0.3 pcm/°C and corresponds to 0.5% of the reactivity loss during reactor start up.

3-D plot on Fig. 5 presents k_{eff} as a function of the operational parameters of the ADEA-system, namely, pressure and temperature of the light water moderator. It is clear from this picture that the system has negative moderator temperature coefficient

of reactivity, its value is about 2.8 - 3 pcm/°C. The reactivity loss due the temperature raise during reactor start-up is of the order of 1%.

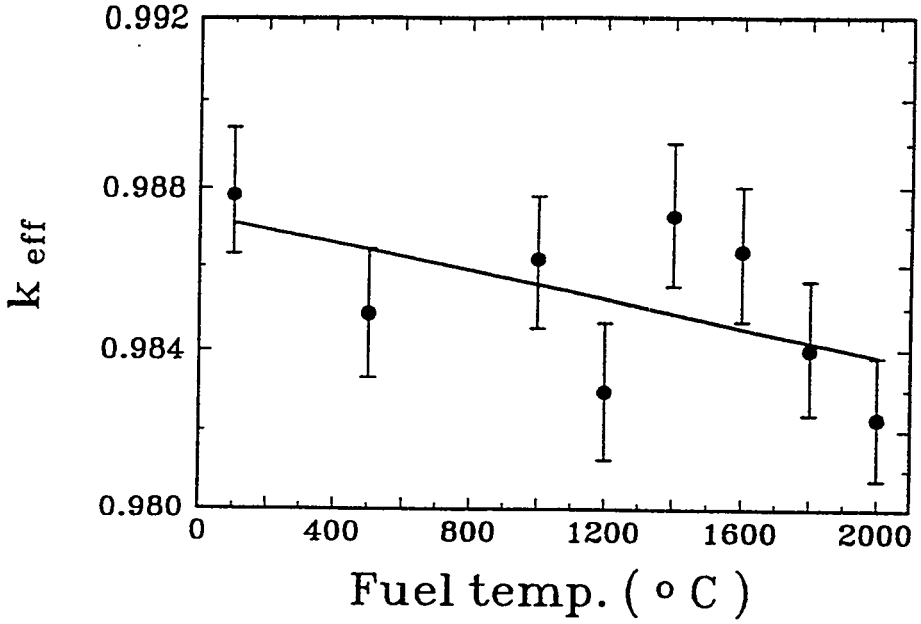

Fig. 4. k_{eff} as a function of the fuel temperature raise.

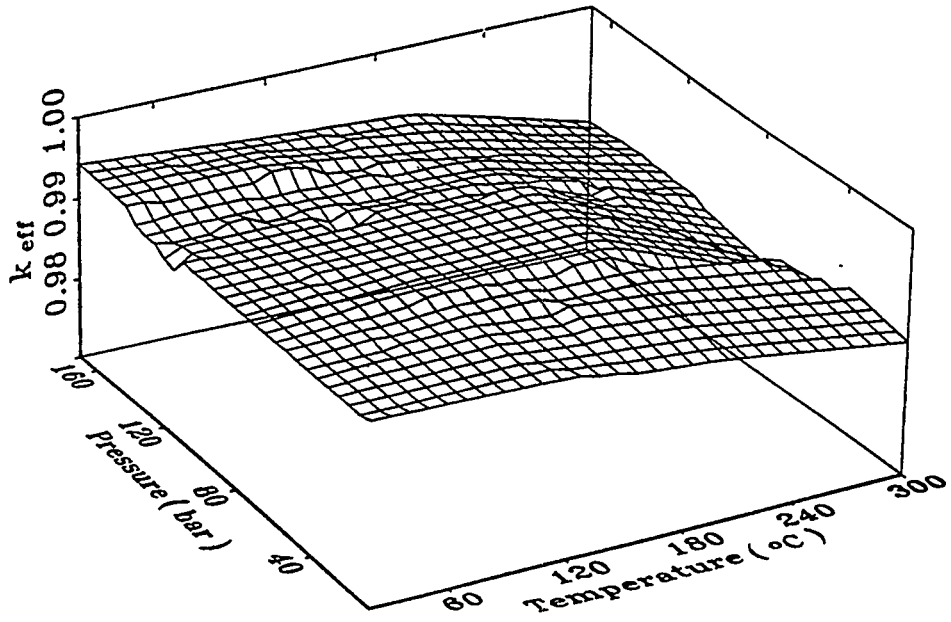

Fig. 5. k_{eff} as a function of the moderator temperature and pressure.

REACTIVITY BUDGET OF ADEA

An important contribution to the reactivity balance in this system after shut-down comes from the ^{233}Pa decay. ^{233}Pa, an intermediate isotope in the breeding chain, β-decays with the half-life of 27 days. During ADEA operation ^{233}Pa is in equilibrium with ^{233}U [1], ^{233}Pa fractional content is on the level of 0.15%. After shutdown, protactinium decays increasing ^{233}U enrichment, which finally reaches 1.5%. The reactivity contribution from the protactinium decay is presented on Fig. 6. Fig. 6 shows the dependence of k_{eff} on ^{233}U-enrichment, 1.5% corresponds - after couple of months - to the complete ^{233}Pa decay, which gives reactivity increase of 5%.

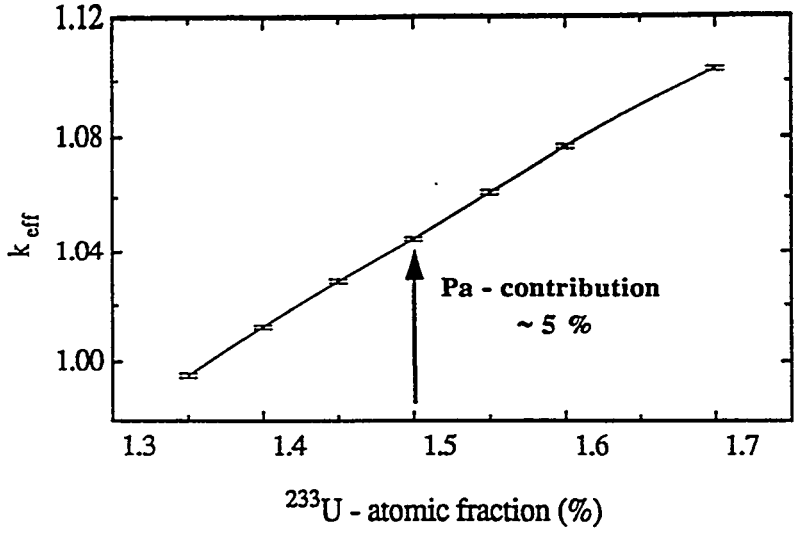

Fig. 6. k_{eff} as a function of ^{233}U enrichment. Assuming equilibrium enrichment 1.35 %, 1.5% corresponds to the complete ^{233}Pa decay a couple of months after ADEA shutdown .

In order to estimate the reactivity margins to ensure the safe and smooth operation of the ADEA the reactivity budget has to be estimated. In Table II we have listed the most important contributions to the reactivity variation in ADEA during its operation.

Table II ADEA reactivity budget (in parenthesis the sign of contribution)

Fuel temperature raise	(-)0.5%
Moderator temperature raise	(-)1.0%
^{233}Pa decay	(+)5.0%
Xe - poisoning	(-)3.5% (ORIGEN2)
Sm-poisoning	(-).75% (ORIGEN2)
Shut-down margin	(-)~1%
Burn-up	0% ("equilibrium breeding")
TOTAL (absolute)	~12.0%

It is very important to stress that these contributions have **different signs** and **different time scales**, which makes possible to optimize some reactivity controls. However it seems that the regulatory authorities would probably require that the reactivity control of this system would be on the level of 12 %. The reactivity increase due to the ^{233}Pa decay could be e.g. controlled by inherent safety mechanisms based on PIUS II - ideas [6] .

POWER DISTRIBUTION

Solid fuel in the nuclear energy system put strong requirements on the power peaking factor and if one wants to avoid frequent refueling, the power peaking factor should as low as possible. Having a system without selfsustaining chain reaction with a spallation target as primary neutron source makes situation even more difficult. Fig. 7 shows the fission density (power distribution) of the ADEA-system with one and two targets as a function of radial distance along the radius on which targets are placed.

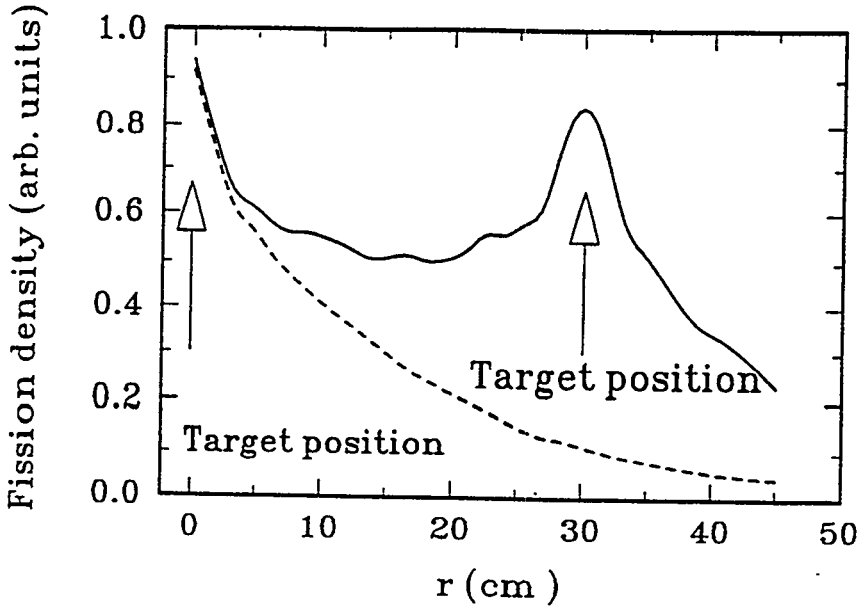

Fig. 7. Fission density as a function of radial distance from the central spallation target. Dashed line - one target system, solid line - two target system. Arrows indicate the position of the spallation target; $k_{eff.}$= 0.97

This figure indicates clearly that one target system has - due to the neutron diffusion length in light water - a very small energy generating volume. It could be flatten up by increasing k_{eff} but safety constrains contradict this requirement. Another solution, which improves the power distribution is a multiple target system - two target system presented in solid line on Fig. 7 shows the radical improvement along the line between these targets. However to achieve this result in the entire core of ADEA minimum 9-10 targets are required. This alters radically the economy of the system and makes the construction much more difficult if not impossible.

SPENT FUEL

Using thorium cycle together with accelerator opens the breeding option from thorium which is - as well known - more abundant, one isotope and cheaper element. It reduces very drastically the formation of higher actinides, especially plutonium, which are of the great concern for the U-Pu fuel cycle. However, it should be remembered that ADEA does not address the transmutation of fission products and the spent fuel from ADEA contains about 10 kg of ^{233}U/tonne fuel (half life 160 000 years), 2 kg of ^{234}U (245 000 y half life). ^{208}Tl is quite frequently mentioned as a troublesome isotope in reprocessing of the spent fuel in the thorium fuel cycle. This danger seems to be exaggerated - after 5 years of the ADEA operation it builds-up only few micrograms of ^{208}Tl with 10^{13} Bq radioactivity. ^{208}Tl in spent fuel is responsible only for maximum 2-3% of radioactive hazards, reaching this maximum after about 20 years.

Special attention should be also paid to the radioactivity generation in the spallation target (targets).

CONCLUSIONS

Using accelerators for safer and cleaner nuclear energy production opens new options and broadens the parameter space of different nuclear energy systems. Subcritical reactor, functioning as a " slave" to the accelerator seems to be a very attractive and appealing idea. But summarizing our analysis one should conclude:

1. The reactivity budget analysis of this system shows that it is virtually impossible to construct ADEA without external reactivity control systems. The idea of the subcritical system with k_{eff} inherently lower than 1 seems to be irreconcilable with the physics of this system and economical requirements

2. Solid fuel and light water moderator require multiple target due to the power density peaked around the targets. It makes the construction of ADEA much more difficult and more expensive (multiple cyclotrones, target window problems etc.).

3. To make the construction of ADEA economically possible it seems to be necessary to reevaluate the requirements of the inherent subcriticality. Instead, better safety mechanism could be invented (or re-invented) and applied to ensure safe operation. Very high k_{eff} of the level of .99 should be reconsider if one wants to proceed with light water and the solid fuel.

ACKNOWLEDGMENTS

This research is supported by the Swedish Nuclear Fuel and Waste Management Board Co and the Royal Institute of Technology.

REFERENCES

1. F. Carminati, R. Klapisch, J.P. Revol, CH. Roch, J.A. Rubio and C. Rubbia, "An Energy Amplifier for Cleaner and Inexhaustible Nuclear Energy Production Driven by a Particle Accelerator, CERN/AT/93-47 (ET) (1993)

2. C.M. van Atta, J. LEE and W. Heckrott, Lawrence Livermore Laboratory, UCRL-52144, 1976
C.M. van Atta, "A brief History of the MTA Project MTA Project", ref.(3), 20 (1977)

3. e.g. : Bowman, C. D. et. al. , Nuclear energy generation and waste transmutation using an accelerator driven intense thermal neutron source. LA-UR-91-91-2601, Los Alamos National Laboratory (1991);
G.P. Lawrence, R.A. Jameson, S.O. Schriber, Accelerator Technology for Los Alamos Nuclear-Waste-Transmutation and Energy-Production Concepts, LA-UR-91-2797, Los Alamos National Laboratory (1991).

4. J. F. Briestmeister (Editor), MCNP - A General Monte Carlo N-Particle Transport Code, ver. 4A, LA-12625 (1993)

5. RSIC Computer Code Collection, ORIGEN2 - Isotope Generation and Depletion Code, NEA Data Bank (1991)

6. C. Mileikovsky et al., private communication.

ACCELERATOR-BASED TRANSMUTER-BREEDER AND ENERGY PRODUCER FROM TRANSURANIC ACTINIDES AND THORIUM

Guennadii I.Batskikh, Arkadii P.Fedotov, Boris P.Murin, Ratmir G.Vassil'kov

Moscow Radiotechnical Institute
Russia Academy of Sciences
Moscow, Russia, 113519

Abstract. A concept of an accelerator-driven subcritical blanket with Pb or molten salt (heavy chloride) as the primary target, a graphite moderator-reflector to produce high-density thermal neutron fluxes and a fluid fuel carrying TUA actinides and Th-U, is being studied at MRTI. A driver is CW H^+/H^- linac: 1 GeV, 200 mA, SIU-DTL-D&W structure energized by regotron as RF power supply.

For the last 45 years an interest to the accelerator way of large-scale neutron production (electronuclear method, EN) arose more than once, every time being summoned by some new needs. Ironically, while in the end of 40-ies and the beginning 50-ies one was eager to do much fissile materials by means of high-current accelerators of deuterons/protons of energy of hundreds MeV (e.g. [1]), in the beginning of 90-ies we intend to burn down quickly (within 30-50 years), also with hydrogen ion accelerators but still more powerful, a hundred tons of really existing weapon grade Pu [2], which has been produced, however, in fission reactors, and giving rise now to serious problems [3].

The use of nuclear energy for the last half-century revealed along with well known merits of this high-potential energy source also a number of conspicuous difficulties that are due to, so to say, the initial conditions. 40-50 years ago political, military, technological situation was of such a kind that nuclear fuel cycle has been started on the basis of ^{235}U with a production of ^{239}Pu. Additionally to the principal aims the cycle grounded expectations for a near realization of the fast neutron breeding, thereby providing a fuel base of nuclear power industry for many centuries. As to the hopes for practical mastering more efficient (in thermal neutron systems) Th cycle, they were put off till the future.

The choice made has predetermined an accumulation of a quantity of waste minor actinides and, naturally, Pu for the sake of which the very U-Pu cycle was selected as a matter of fact. A drastic alteration of political situation in the world brings to releasing hundreds tons of weapon Pu, and the problem of Pu breeding ceases to be a live issue. At the moment principal concern is not restricted fuel resources to produce nuclear power, but the problem of nuclear waste management, i.e. the problem on a resolving of which the very further destiny of nuclear power depends on. By now, the U-Pu NFC has given rise to dissatisfaction and anxiety of public opinion, whereas the Th cycle looks more and more attractive (despite of its some obvious drawbacks, say, a rising up ^{232}U): its essentially higher fuel efficiency, no complications due to a production of bulk quantity of Pu, a formation of transuranium actinides (TUA) would be by about hundreds times less and the fuel base is much broader.

We digress here from a question, how costly the simultaneous performing of two NFC (in limited time period) might be, and discuss only possible approach to technical mastering of Th cycle. A decade ago Teller [4] reminded four known ways: HWR, MSR, HFR and thermonuclear underground explosion ("pacer"). But one should add more the fifth one, viz. high-energy high-current hydrogen ion accelerator to produce spallation neutrons, which for some reason or other

was not mentioned by Teller (evidently,not through forgetfulness or ignorance) and to which, nonetheless, an attention was paid long ago [5,6].

At present the method seems to be feasible, being suitable to do several jobs at once: incinerating TUA in order to pump neutrons released into $^{232}Th \Rightarrow ^{233}U$, utilization of TUA fission energy to produce power, destroying a part of fission products. Its combination with already proved technology of molten salt reactor [7,8] promises to be especially advantageous. It turned out to be elucidated from times of the EN "boom" of 1976-78, when various types of real fission reactors have been analyzed from the standpoint of their application as subcritical blankets, driven with beams of accelerated protons/deuterons [9].

Lately MRTI works at a version of three-purpose spallation neutron generator (TUA transmuter, ^{233}U/energy producer) on the basis of CW proton linac (E_p=1.0 GeV, I_p=0.2 A). The linac would drive through the primary target (liquid Pb/Pb-Bi, its combination with W/Th, or heavy molten salt $PbCl_2$-$ThCl_4$-[TUA]Cl_3 [10]), a subcritical blanket, which is consisted of graphite moderator and fuel in the form of molten fluoride salt ^{7}LiF-BeF_2-ThF_4-^{233}U (k_{eff}= 0.86-0.92).

From the very beginning of our studies [11] carried out during 1962-1969 a flow of liquid Pb/Pb-Bi was believed to be the most probable interface between an ion beam and a blanket. So, in experiments at Dubna accelerators the nuclear data were being acquired both on thin Pb targets and very thick extended ones (Fig.1,2) among others heterogeneous assemblies combining Pb primary

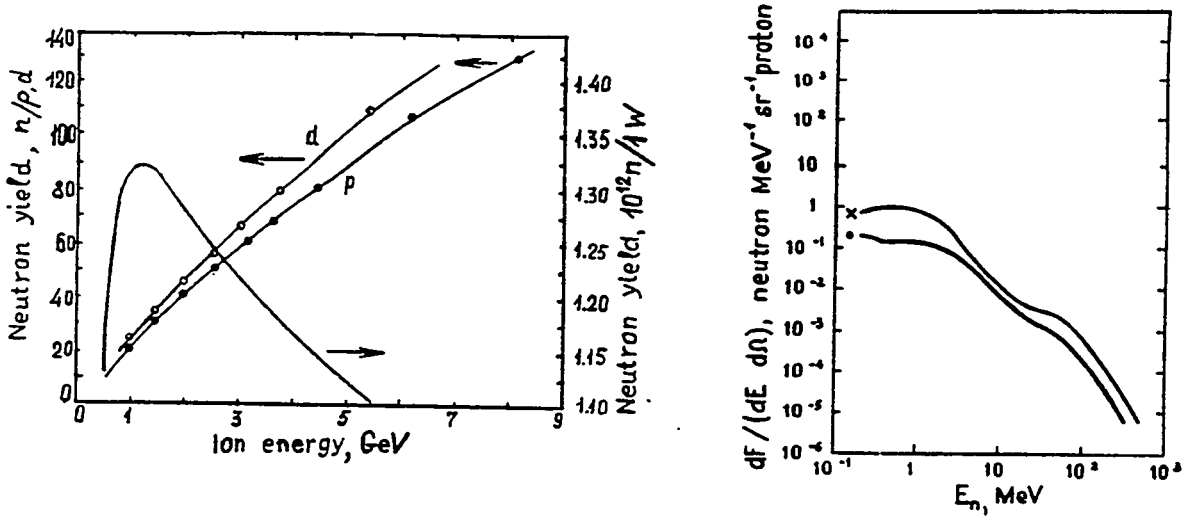

Fig.1. Some examples of the experimental data, acquired for validating calculational methods describing the high energy radiation transport in bulky lead targets: a) E_p-dependence of neutron yields per incident deuteron/proton (left ordinate) and per unit of proton beam power, neutrons releasing from Pb target ø20x60 cm ; b) double differential distributions of neutrons $(d^2Y/dEd\theta)$ emitted from Pb targets 8x8x8 cm^3 (o) or ø20x20 cm (x) bombarded with 2-GeV protons (time-of-flight technique).

target with Be,depleted U, reactor graphite [11,12]. The data acquired [11-14] have permitted to select unequivocally (on the quantitative basis) the type of projectiles and their initial kinetic energy, up to which acceleration of them would be expedient (fig.2 a, b); the values of this initial energy for proton and deuteron are close to each other (≈1.2 GeV), and would be hardly shifted when substituting liquid Pb/Pb-Bi for W, Th or chloride molten salt.

The latter option ($PbCl_2$-$ThCl_4$-[TUA]Cl_3) one should keep in mind as a li-

kely way to raise spallation neutron yield/heat release per unit of beam power (as compared to fluoride molten salt) and to make the target less transparent for protons. If molten fluoride salt ^{7}LiF-BeF$_2$-ThF$_4$-[TUA]F$_3$ is used as the pri-

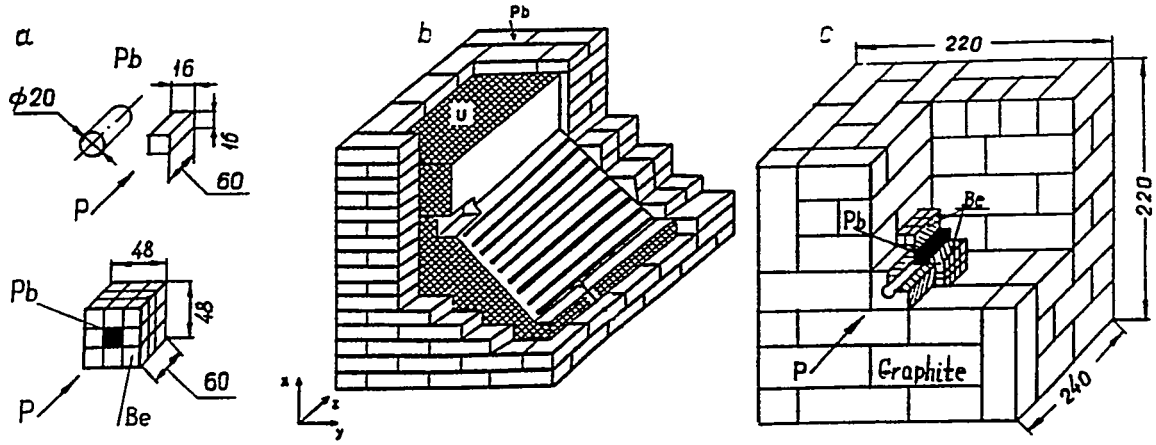

Fig.2. Spallation neutron targets (assemblies) that were studied in order to ascertain total numbers/maximum thermal neutron flux densities under the action of 0.66-GeV proton beam: a) bar Pb targets 16x16x60 cm^3, ø10-26 cm and Pb target 16x16x60 cm^3 surrounded by Be blanket-multiplier, wall being variable thickness, or depleted U wall 8 cm thick; b) 3.4-ton metal natural/depleted U blanket around Pb primary target; c) Pb target 16x16x60 cm^3 inside Be multiplying cavity, wall thickness 16 cm, both surrounded by a graphite moderator-reflector 80 cm thick; in this assembly thermalized neutron flux densities $(3.8\text{-}8.6)\cdot10^{-3}$/cm^2·sec·proton (±15%) have been obtained.

mary target, i.e. light substance ($\rho\approx3,3\div3.5$ g/cm^3), giving few neutrons under the action of protons, then deuteron should be chosen as bombarding particle. Owing to large stripping cross section of deuteron on light nuclei (85-90% of molar content of the salt) its ionization loss before nuclear interaction is small, so arising neutron/proton have almost all deuteron initial energy and can be effectively multiplied in a heavy matter convertor, e.g. in a mixture of Th with TUA (but preferably not in ^{238}U in order to avoid piling-up of TUA). This convertor-multiplier is placed between the primary target and blanket, its principal performances might be roughly estimated by means of spectrum averaged one-group actinides fission cross sections, measured in spallation neutron field of "standard" lead target (ø20x60 cm) when irradiating with protons and deuterons of energies 1.0÷3.7 GeV [15].

The blanket is a graphite moderator (with channels in experiments, but pebble-bed in full-scale system) with molten salt LiF-BeF$_2$-ThF$_4$-^{233}UF$_4$ fuel in loops inside. The liquid fuel-coolant enables to ensure higher level of safety (for example, incidents of the LOCA type would be impossible) and better neutron economy, if fission products and ^{233}Pa are separated from irradiated salt under operation. Improvements of neutron economy remain to be a live issue for subcritical systems too. Thermodynamic properties of molten salts form more one important advantage more, which is high outlet temperature of salts amounting to 900^{0}C, and combined with already proved technology of helium gas turbines it would yield to 50% efficiency of electricity production on NPP. The experience gained in dealing with molten fluoride salts after the MSRE program [7] and on reactor stands in Kurchatov' Institute for Atomic Power [8] enables to rely on this technology, although on-line chemistry of irradiated ^{7}LiF-BeF$_2$-ThF$_4$-^{233}UF$_4$ fission products, ^{233}Pa and ^{233}U will have to be demonstrated.

Unfortunately, by now there exists only scarce knowledge concerning nucle-

ar properties of the molten salts (even fluorides), solubilities of relevant actinides in them. Therefore, at present we are going to undertake detail experimental studies of molten salt target neutronics on 0.7÷2-GeV proton beam, the same plans referring to W, Th and to Pb-chloride (fluoride) compound targets containing Th-U.

In a series of experiments [11] done during 1966-69 on 0.66-GeV proton beam at the JINR Synchrocyclotron (Dubna) we acquired some experience dealing with a neutron multiplying assembly (composed of Pb, Be and reactor graphite) bombarded by protons. Now, such a system may be interesting as a basis for developing the molten salt EN facility to burn Th, to transmute TUA (and some fission products) and to produce commercially attractive quantities of energy. The very idea to resort to Th-graphite blanket was inspired by just those our old experimental data [11], that have shown that one could get quite high neutron fluxes even in rather primitive multiplying target assemblies. In experiments [11] done at the Dubna 660-MeV proton Synchrocyclotron on a reactor graphite cube of 2.2x2.2x2.6 m^3, the multiplier was a Be cavity (or depleted U wall, 8 cm thick) around Pb prism 16x16x60 cm^3, Be wall being of variable thickness (Fig.2).

The thermal neutron flux density in a graphite layer of 3÷15 cm, adjoining Be wall amounted to $(3.8\div8.6)\cdot10^{-3}$ /cm^2sec/p (±15%). If proton energy and current would be of 1.0 GeV and 200 mA respectively, the value of specific neutron flux would amount to $(4\div6.4)\cdot\cdot10^{15}$/$cm^2$sec/p taking into account an increase of the target-multiplier size and spallation neutron multiplication in a possible heavy material multiplier. Because an application of metal Be in intense fluxes of neutrons of energies ~MeV would be impracticable and we want to avoid making of use ^{238}U in the system, the multiplier for our design is chosen in the form of mixture Th+TUA (say, Th80%+^{237}Np20%). A primitive scheme of the blanket is given in fig. 3. Realization of such high flux densities of thermalized neutrons needs a reliable and efficient high-energy high-current CW proton linear accelerator. A choice of the linac parameters is based on the data partly presented in Fig.1c, where E_p-dependence of the neutron energy cost $\mathcal{E}$ on the initial proton kinetic energy E_p for Pb targets of two size, one of them being quasi-infinite (ø80x100 cm). The lowest value of $\mathcal{E}$ corresponds to $E_p \approx$ 1.0 GeV, only slightly depending on target size and material.

At the same time the data base was being created and effective methods were being developed for neutron transport calculations in integral assemblies [16]. Techniques developed in [16] prove to be the most effective on stages of research of the problem in question and of conceptual designing when accelerator and target-blanket parameters are being optimized and a lot of calculational runs are necessary to test alternative compositions/geometries and sets of input values. Methods of prompt Monte-Carlo simulation do not seem to be in such cases practical and efficient, whereas approaches in [16] were originally developed to do calculations for bulky extended targets in broad intervals of the input parameters.

The region of E_p values where $\mathcal{E}$ rises not more than, say, by 1-2% swings from ≈1.0 to 1.8 GeV. The linac length and output proton energy diminishing, its technical/operating characteristics ameliorate as well as its economics, so the optimum value of E_p turnes out to be near the lower edge of above-mentioned interval of E_p, i.e. near 1 GeV. Owing to beam loss one should restrict the proton current by a level of 200 mA (CW).

Acceleration rate was chosen proceeding from the highest efficiency of accelerating cavities when capital cost is not very high. One may estimate a cavity efficiency by known relation

$$\eta_c = [1+E_a/I_b Z_{eff}\cos^2\phi_s]^{-1},$$

where I is proton current, E_a is electrical tension determining the energy gain

of proton per unit length of linac, Z_f- effective shunt resistance of unit cavity length, ϕ_s- equilibrium phase. As one can see from I_b-dependence of η_c for three E_a values and typical values Z_{eff}=40 MOhm/m ϕ_s= 30° (Fig.4), cavity efficiency η_c is 0.88 if I_b = 0.25 mA, E_a = 1 MeV/m. If efficiency of RF power sup-

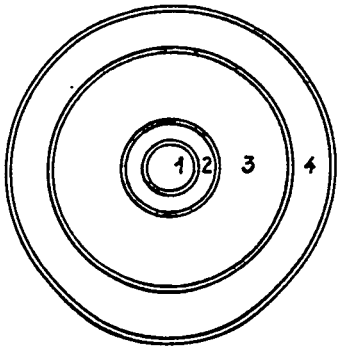

Fig.3

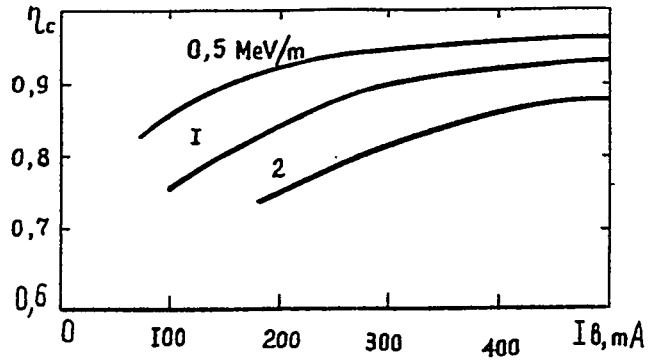

Fig.4

Fig.3. A calculational scheme of an accelerator-driven target-blanket: 1: Pb/ /Pb-Bi target (an option is heavy chloride molten salts carrying TUA), 2: neutron multiplier (Th 80%+TUA 20%), 3: graphite moderator with molten salt fuel (Th- ^{233}U), 4: graphite reflector.

Fig.4. A dependence of the cavity efficiency η_c on proton current for three values of acceleration rate.

ply device is 0.7, the total linac efficiency would exceed 0.5. Beam current decreasing, economy efficiency diminish. Some general problems concerning linacs of such a kind were discussed in [8-10]. If necessary, a linac of parameters like these would be capable to drive at least five target stations dividing up the outgoing beams of H^+/H^- ions among them.

Thus, we accept linac energy of 1 GeV and proton current of 0.2 A as the optimum ones, CW beam power being of 200 MW. A scheme of the MRTI linac (Fig.5) includes sources of ions H^+ and H^- of energies of 0.2 MeV which are accelerated in opposite RF half-waves. Its initial part accelerating protons up to 3

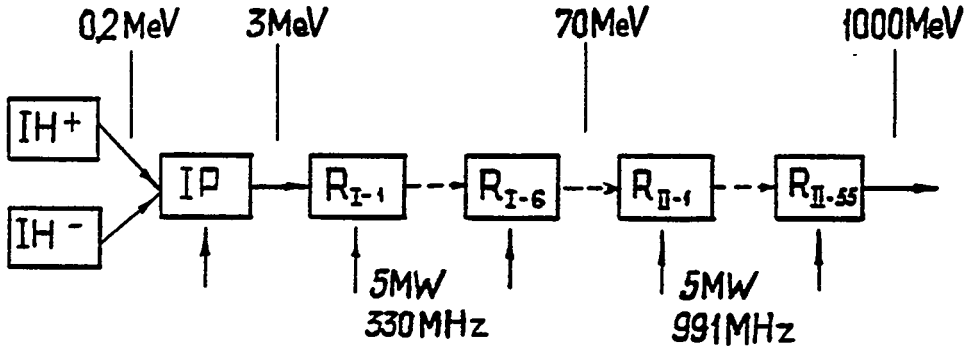

Fig.5. A scheme of the MRTI CW linac. IH^+/IH^-: injectors of ions H^+/H^-; IP: initial part (a cell with strong axial magnetic field focusing), RI-1-RI-6: cavities of the first part (DTL), RII-1- RII-55: cavities of the second part (D&W). Focusing system is permanent magnet quadrupole lenses.

MeV is being built on H-cavities with a focusing by strong longitudinal magne-

tic field. As our experience shows, such an accelerator would enable to accelerate beam currents of 1 A and even higher.

The first part of the linac comprises drift tubes running at frequency of 330 MHz, output proton energy of 70 MeV. In its second (main) part cavities with disks and washers (D&W) are used [11], energized by the regotron [9], which is RF power generator, the focusing being performed by single permanent quadrupole magnets (PMQ); a scheme of standard module is presented in fig.6, the principal features of the MRTI linac are given in the following table.

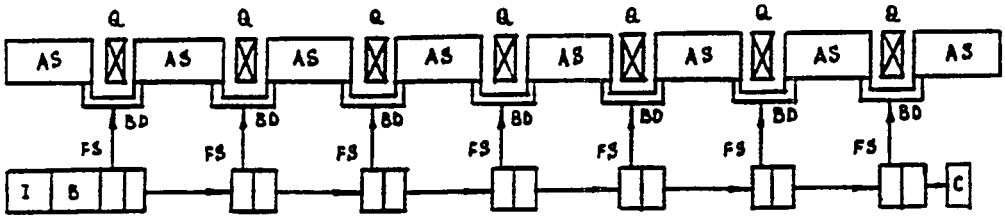

Fig.6

Standard module of the MRTI linac main part. I: regotron injector, B: its buncher, AS: accelerating cell, Q: quadrupole, BD: bridge device, FS: feeder system.

Table. Parameters of the MRTI Linac

	Linac part		
Parameter	**Initial**	**First**	**Second**
Inj. energy, MeV	0.2	3	70
Output energy, MeV	3	70	1000
Frequency, MHz	330.3	330.3	991
Length, m	3	70	900
Accel. rate, MeV/m	1	1	1
Aperture diam., mm	13⇒20	30	30⇒40
Focusing structure	LMF[a]	FODO	FODO
Focusing lenses type	SCS	PMQ	PMQ
Limit current, A	0.9	0.9	1.0
Acceptance, πcm·mrad	2.5	3.0	4.5
Emittance, πcm·mrad	0.5	1.0	3.0
Bunch phase length[b]	60°	25°	20°
Synchronous phase	90°⇒40°	30°	30°

[a] Longitudinal magnetic field
[b] 330.3 MHz

REFERENCES

1. *Status of the MTA Project.* Lawrence Radiation Laboratory, report LRL-102, Livermore, California, USA, 1954.
2. The Los Alamos Accelerator-Based Conversion Concept for Plutonium Disposition (ABC). JASON Review, La Jolla, California, January 1994.
3. Management and Disposition of Excess Weapons Plutonium (executive summary). Committee on International Security and Arms Control, National Academy of Sciences, Washington, D.C., 1994.
4. Teller E., Remarks on Thorium Cycle. *Annals of Nuclear Energy* 5, 287 (1978).
5. Lewis W.B. Intense Neutron Generator and Future Factory-Type Ion Accelera-

tors. Atomic Energy of Canada Limited,report AECL-3190, october 1968.
6. Vassil'kov,R.G., Goldanskii,V.I., Dzhelepov,V.P.,and Dmitrievskii,V.P., The electronuclear method of neutron generation and production of fissile materials. *Atomnaya energhiya,*29, 151 (1970).
7. An Evaluation of the Molten Salt Breeder Reactor. Prepared for the Federal Council on Science and Technology R&D Goals Study by the US Atomic Energy Commission,Division of Reactor Development and Technology,WASH-1222, UC-80, September 1972.
8. Novikov,V.M., Ignatiev,V.V., Fedulov,V.I.,and Cherednikov,V.N., *Liquid-salt nuclear power facilities: prospects and problems.* Moscow: Energoatomizdat, 1990.
9. Mynatt,F.R., "Accelerator Molten-Salt Breeder Concept", in *Proceedins of an Information Meeting on Accelerator Breeding,*held at BNL 17-18 January 1977, Upton,New York, p.211.
10. Desyatnik,V.N., Vorobey,M.P., Kurbatov,N.N. et al., *Atomnaya energhiya* 38, 173 (1975).
11. Vassil'kov,R.G.,Goldanskii,V.I., Kogai,S.S.,Pimenov,B.A.,and Sokolov,L.N., a) "Neutron yields and thermalized neutron fluxes in a system Pb-Be-H2O bombarded with high-energy protons",report N^0 3/743,1970; b)"Thermal neutron flux in a model heterogeneous assembly bombarded with protons of energies 400, 500 and 660 MeV",report N^0 2/0368, 1971. Institute for Chemical Physics of the USSR Academy of Sciences and Moscow Institute of Physical Engineering (to be published).
12. Vassil'kov,R.G., Goldanskii,V.I., Pimenov,B.A., Pokotilovskii,Yu.N., and Chistyakov L.V., "Neutron multiplication in uranium bombarded by protons with energies 300-660 MeV", *Atomnaya energhiya* **44**,329 (1978).
13. Vassilkov,R.G., Yurevich,V.I. "Neutron Emission from Extended Pb Targets under the Action of Light Ions in the GeV Region", in *Proceedings of the ICANS-XI Meeting,* KEK,Tsukuba,Japan, 22-26 october,1990.
14. Nikolayev,V.A., Vassil'kov,R.G.,Yakovlev,R.M., Yurevich,V.I.,"Neutron production in thick lead target by 1-3.7 GeV protons and deuterons",in *Proceedings of the ICANS-XI Meeting*, KEK,Tsukuba, Japan, 22-26 october 1990.
15. Nikolayev,V.A., Vassil'kov,R.G., Yakovlev,R.M., Yurevich,V.I., "The fission transmutation of ^{237}Np in a field of spallation neutrons emitted from thick lead target bombarded by 1-3.7-GeV protons and deuterons",in *Proceedings of the Specialists' Meeting on Accelerator-Based Transmutation*, PSI, Villigen,Switzerland, 24-26 March,1992.
16. Gelfand E.K.,Man'ko B.S.,Serov A.Ya.,Sychev B.S., "The Brief Review of the Nuclear Physics Aspects of Radiation Field Simulation on High Energy Accelerators",presented at the ABC/ATW Conference Chelyabinsk-70,Russia, 1993.
17. Batskikh,G.I. et al., "On the Way to High-Power Linear Proton Accelerator for the Long-Life Radionuclides Transmutation",in *Proceedigs of the ICANS-XI,* KEK,Tsukuba,Japan, 1990, pp. 199-209.
18. Batskikh G.I.,Fedotov A.P.,Murin B.P.,"Linear Accelerator for Burner-Reactor", in *Proceedins of the 1990 Linear Accelerator Conference,* LANL, Albuquerque, New Mexico, USA.
19. Andreev V.G. et al., "Basic Principles of Burner-Reactor Linac Design", in *Proceedings of the Specialist Meeting on Accelerator-Driven Transmutation Technology for Radwaste and other Applications,* 1991, Saltsjobaden, Stockholm, Sweden.
20. Andreev V.G. *Journal Technicheskoy Fiziki* **41**, 788-797 (1971).
21. Murin B.P. et al., "Superhigh-Power RF Regotron-type Generator for Linear Accelerator with High Mean Currents",in *Proceedings of the 1990 Linear Aclerator Conference*, LANL, Albuquerque, New Mexico, USA, p. 584-586.

Plutonium(TRU) Transmutation and ^{233}U Production by Single-Fluid Type Accelerator Molten-Salt Breeder(AMSB)

Kazuo Furukawa*, Yoshio Kato*1, and Sergey E. Chigrinov*2
*Inst. of R & D, Tokai University, Hiratsuka, Kanagawa 259-12, Japan
*1Dept. Chem. of Fuels Research, Japan Atom. Ene. Res. Inst., Tokai, Ibaraki 319-11, Japan
*2Radiation Phys. & Chem. Problems Inst., Academy of Science, Sosny, Minsk, Belarus

Abstract For practical/industrial disposition of Pu(TRU) by accelerator facility, not only physical soundness and safety but also the following technological rationality should be required: (1) few R&D items including radiation damage, heat removal and material compatibility; (2) few operation/maintenance/processing works; (3) few reproduction of radioactivity; (4) effective energy production in parallel. This will be achieved by the new modification of Th-fertilizing Single-Fluid type Accelerator Molten-Salt Breeder (AMSB), by which a global nuclear energy strategy for next century might be prepared.

INTRODUCTION

In the Pu disposition issue, our target in final stage should be put on: (1) nearly complete elimination of the world's Pu stocks (cf. US·NAS report [1]), achieving the followings:
(2) economical utilization of energetic potentiality of Pu(and TRU), and
(3) rational global nuclear-energy industry establishment in the next century.

For the complete disposition of weapon-head Pu or reactor-grade Pu, the application of Th-^{233}U fuel recycle system will be the best. However, its practical/economical realization should depend on fluid-fuel concepts due to the high gamma activity of ^{233}U fuel, which is highly efficient for the prohibition of nuclear-proliferation and terrorism.

The only one, that is, Molten Fluorides Fuel, among several fluid-fuel concepts has been verified the practicality by the long effort of Oak Ridge National Laboratory in 1947-80 [2]. They aimed to establish a Fission Breeding power station (MSBR). However, it has several serious difficulties in design and global application in future. Therefore, our group is proposing more rational approach, Th-breeding synergetic system: THORIMS-NES ("Thorium Molten-Salt Nuclear Energy Synergetics") [3], which is composed of [I] simple fission power stations [Molten-Salt Reactor (MSR) : FUJI-series] [4], which is a fuel self-sustaining reactor without continuous chemical processing and core-graphite exchange, [II] fissile-fuel producers by spallation/fission reactions of 1 GeV-proton [Accelerator Molten-Salt Breeder (AMSB) : ASO-series] [5], and [III] dry process plants.

GENERAL SCHEME OF PU-DISPOSITION BY THORIMS-NES

The complete Pu disposition by this THORIMS-NES might be established in the following three plans:

(1) D-plan: Pu (and Trans-Uranium elements [TRU]) separation Dry-process from the spent solid-fuels all. Not only depending on the present Purex, the new Dry-process by Molten-Fluoride technology should be developed improving economy and diversion resistance, and finally supplying their fluoride salts for F- and A-plans. The technological basis has been examined by French, Russian, etc..

(2) F-plan: Pu-burning and ^{233}U-production by MSR [FUJI-Pu]. The most rational safe technology for the effective Pu-incineration will be an application of MSR fertilized by Th [6]. Already a simple system: FUJI-Pu has been studied verifying the rapid and continuous Pu-burning by the stepwise isolation of ^{233}U, which is

produced for the next Th-U cycle operation [7], [8].

(3) A-plan: Pu-burning and ^{233}U-production by AMSB-Pu [ASO*-Pu]. In parallel with F-plan, spallation/fission reactions in AMSB will be applicable for the same purpose. A new design named AMSB-Pu or ASO-Pu has been developed predicting the efficient production of ^{233}U 2-3 times higher than the incinerated Pu, and of some excess-electricity [9], [8].

In the final stage, we would have an orthodox THORIMS-NES fully depending on pure Th-^{233}U fuel cycle. This system might realize an idealistic global Nuclear Energy Industry, which characteristics are: (a) safe: no severe accidents; (b) anti nuclear-proliferation and -terrorism; (c) very few Radio-wastes by the facts of nearly no TRU and few maintenance/operational works; (d) very few nuclear materials transportation; (e) small R&D cost owing to few items; (f) high economical potential; and (g) real establishment of idealistic Breeding Fuel Cycle, resulting a small need of Th of only about 2 M tons for about 1000 TWe•Year production in the next century [cf. the past nuclear production of 2 TWe-Year] [8].

SEVERAL MODIFICATIONS OF AMSB

The basic idea of AMSB was invented on 1980 depending on the single phase Molten-Salt target/blanket concept [10], which is significantly simple in configuration [cf. Fig. 1].. Therefore, several serious technological problems related with (i) radiation-damage, (ii) heat removal, (iii) spallation chemistry, (iv) shuffling of target, etc. are mostly able to solve already except the proton-beam injection port engineering, which might be solved by the real beam test increasing intensity step by step [11,12].

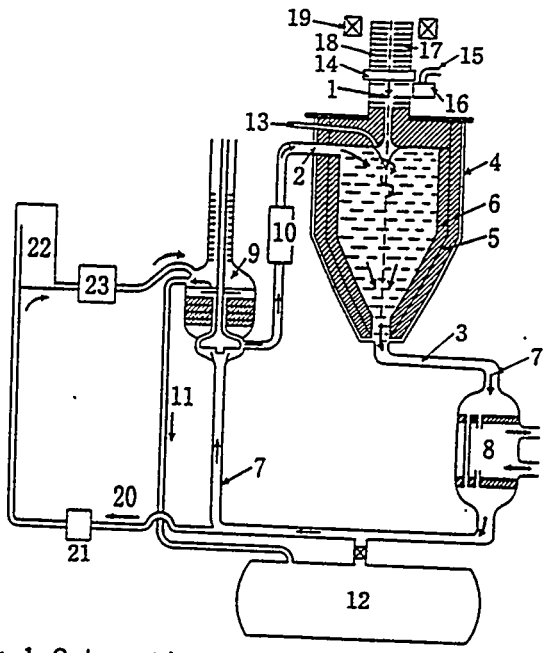

Fig. 1. Schematic set-up of single-fluid-type Accelerator Molten-Salt Breeder (AMSB).
1:Proton beam; 2:Salt inlet; 3:Salt outlet; 4:Reactor vessel; 5,6:Graphite; 7:Primary loop; 8:Heat exchanger; 9:Main salt pump; 10:Throttle valve; 11:Overflow line; 12:Storage tank; 13:High-pressur salt inlet; 14:Gate valve; 15:Vacuum line; 16:Vapor trap; 17:Duct; 18:Orifice; 19:Focussing magnet; 20:Bypath for salt processing; 21:Pump; 22:Process facility; 23:Filter.

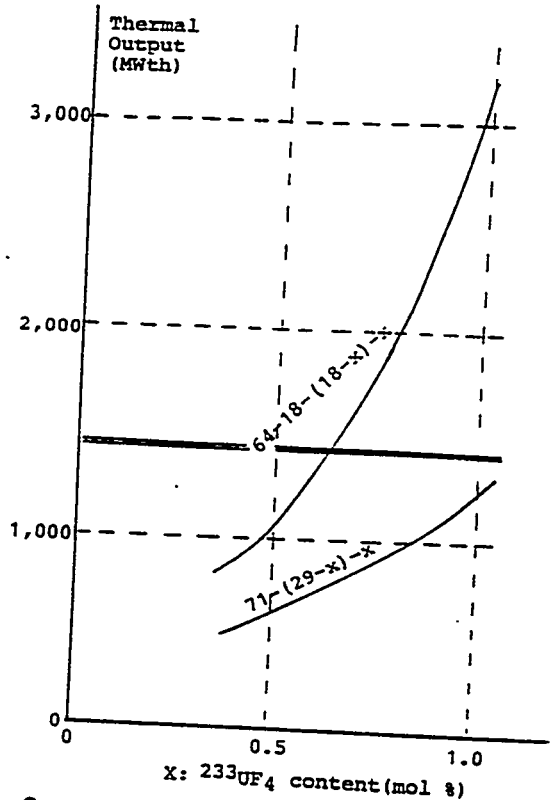

Fig. 2. Relation between thermal output and $^{233}UF_4 = X$ in target salt of AMSB : ^7LiF-BeF_2-ThF_4-$^{233}UF_4$
[Double line shows an accelerator sustaining power.]

This concept AMSB has been proposed the several modifications such as (A) Standard AMSB [AMSBst], (B) Highgain AMSB [AMSBhg], (C) Supergain AMSB [AMSBsg], (D) Highgain Pu-burn AMSB [AMSB-Puhg], (E) Supergain Pu-burn AMSB [AMSB-Pusg]. The words "standard", "highgain" or "supergain" mean non, medium or high contents of fissile components in target salts, respectively, which would result few, medium or significant fission events, respectively, accompanying fissile production and heat generation in several grads..

The relation between fissile content and total thermal output in 1 GeV-300 mA proton facility will be understood from the Fig. 2. The operation of such facility will need about 600 MWe, converted from the generated heat of 1400 MWth. The initial stage, hg-type one will be easier in development, but in the matured stage, sg-type mode could be operated supplying an excess electricity such as 1 GWe to public and improving economy.

In here, (D) Highgain Pu-burn AMSB [AMSB-Puhg] and (E) Supergain Pu-burn AMSB [AMSB-Pusg] have an important relation with Pu disposition. Their performance has been preliminarily examined in 1993 [8], [3]. The conservative values are presented in Table 1 with the performance of FUJI and FUJI-Pu.

Table 1. Preliminary Performance of FUJI [per 1GWe] and AMSB [1GeV-300mA]

	Pu-inv.	^{233}U-inv.	Pu burn/Y	^{233}U prod./Y	Elec. output
FUJI-Pu	3 t		0.86 t	0.7 t	1 GWe
FUJI		2 t		self-sust.	1 GWe
AMSB-Puhg	4 t	3 t	0.35 t	0.7 t	0 -
AMSB-Pusg	5 t	5 t	0.6 t	1.0 t	0.5-1 GWe

OPENING THE "THORIUM ERA" DEPENDING ON PU DISPOSITION

The global nuclear energy demand for the next century would be huge as predicted in Fig. 3 [3] [8] extending the original work of Marchetti [13], because it will not be enough to solve even the CO_2 Greenhouse effect yet.

U-Pu cycle system could not produce even the amount shown by the dotted curve in Fig. 3 (B), and would not be real due to the huge Pu handling. However, to realize the 1,000 TWe-Year production in the next century, there are many scenario depended on THORIMS-NES applying the above D-, F- and A-plans. Here, a simple example has been shown in Fig. 4 and Table 2.

Tentatively the system size of U-Pu cycle power stations might be imagine as 4 times larger in maximum than the present, decreasing from the dotted curve in Fig. 3 (B). Even so low this will still produce more than 10,000 ton Pu till 2050, which will be separated by Purex or D-plan process accompanying TRU in all in the more proliferation-resistant form, because the storage is not solution.

Pu (TRU) disposition could be started from 2010 by F-plan, and from 2020 by A-plan in parallel. The former activity will become 500 GWe in maximum scale about 2030, burning about 7,400 ton Pu (TRU) or more. The latter will become 400 facilities in peak about 2040, burning about 3,000 ton Pu (TRU) or more.

The duty of FUJI-Pu will be finished until 2050. However, it can be operated as proper Th-^{233}U power stations till the end of reactor life. The technological development of AMSB-Pu will be significant among 2020 and 2050. The initial will be AMSB-Puhg in lower grade not producing any outer electricity. The next AMSB-Pusg will produce about 0.5 GWe/facility, gradually improving in performance till 1 GWe or 2 GWe/facility.

In general, FUJI-Pu will be more economical than AMSB-Pu for Pu disposition. However, after the middle of 2040's decade, in which Pu would be almost eliminated, AMSB-Pu should be gradually replaced by AMSMsg of high performance

depending on near critical condition. This is essential to establish the THORIMS-NES. On 5-10 years before the peak position of nuclear energy demand curve (Fig. 3), which would be 2055-65 in our tentative prediction, AMSB-Pusg will be dismantled recovering ^{233}U fissile, which is useful to increase FUJI power stations more. Therefore, the main leading role of AMSB will be only less than 40 years, although it will be useful for radio-waste incineration as a minor work [5].

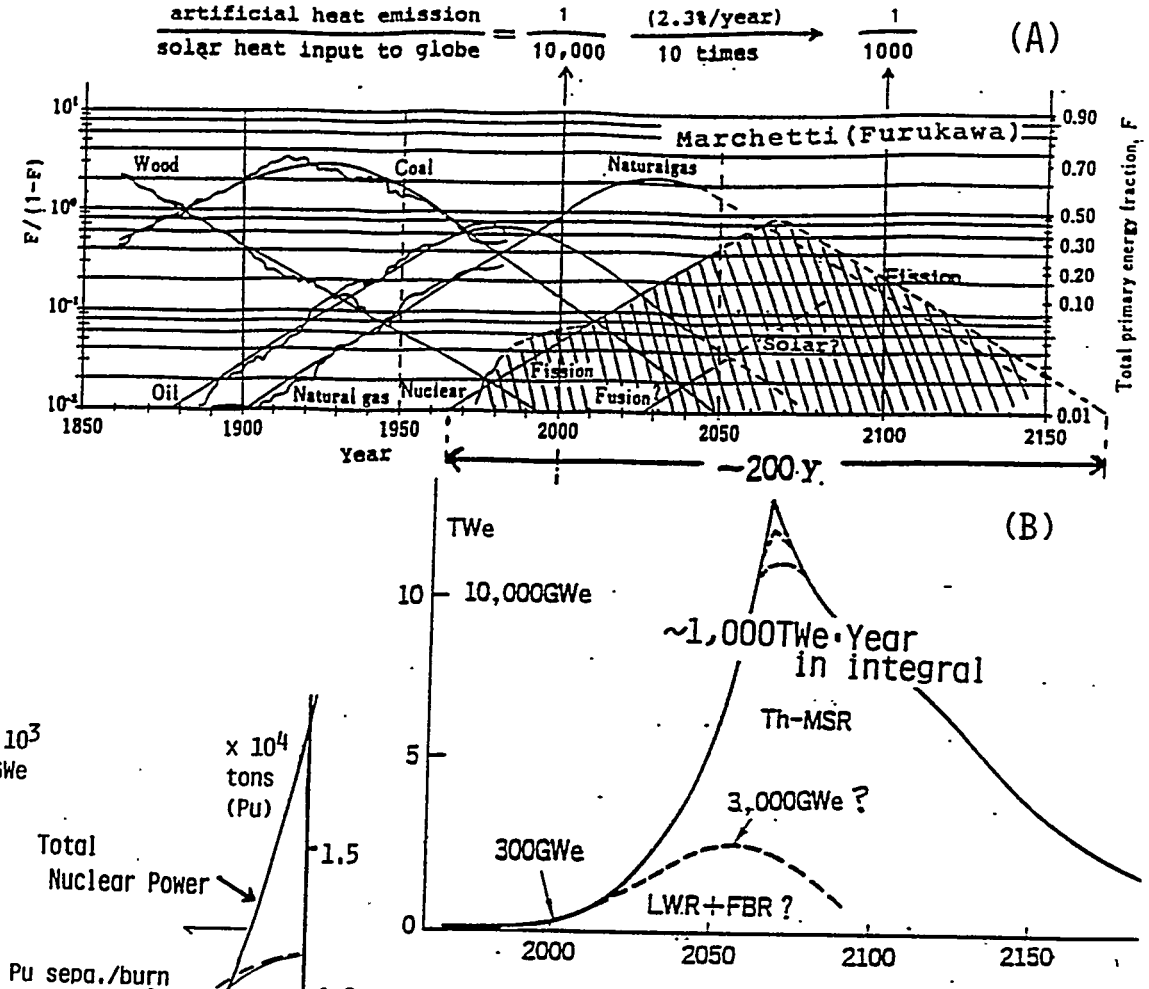

Fig. 3. Global future energy prediction.
(A) Logistic functional prediction based on Marchetti's original work (1985).
(B) Nuclear energy demand depending on the curve in (A) and assumed yearly energy growth rate of 2.3 %/year.

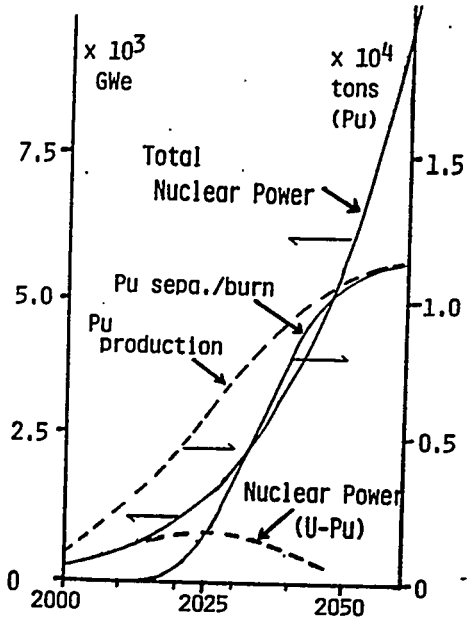

Fig. 4. A scenario for Pu disposition in early next century [cf. Table 2].

Table 2. Complete Pu Elimination by THORIMS-NES and Replacement of U-Pu Reactors by Th-U Reactors [cf. Fig. 4]

	Total Capacity (GWe)	U-Pu Stations (GWe)	Cumulative Pu (ton)	D-Plan Pu supply (t/10Y)	F-Plan FUJI-Pu, FUJI (GWe)	A-Plan AMSB-Pu (fac./10Y)
2000	300	300	1,200			
2010	550	550	2,500	start	start	
2020	1,000	750	4,400	990	200, 50	start
2030	1,850	800	7,000	4,170	500, 550	hg: 100
2040	3,460	550	9,300	5,920	300, 2,210	sg: 400
2050	6,800	200	10,600	0	0, 6,200	sg: 400*

	Th-U Stations (GWe)	Pu burn (t/10Y)	^{233}U produc. (t/10Y)
2000			
2010			
2020	250	390	310
2030	1,050	2,870	2,450
2040	2,910	4,320	4,480
2050	6,600	3,090	7,380*

[/10Y : cumulative values in 10 years till the date]

[* : replacing by improved AMSBsg gradually]

R & D PROGRAM

Its technological basis of F-plan has been prepared by the excellent efforts of ORNL among 1947-76. Therefore, the commercialization of FUJI in smaller size (100-300 MWe) will be performed in 15 years at least. Such public nuclear power stations should be simpler in configuration/operation/maintenance, and power-size flexible not like as Fission or Spallation Breeding power stations [MSBR or AMSB].

Depending on this initial developmental effort of MSR basic technology, A-plan developing AMSB-Pu will be proceeded in about 10 years delay from FUJI. The most important items for R&D of AMSB-Pu will be the followings:

(A) 1 GeV, 100-300 mA proton Linear Accelerator: In the target/blanket salt system a little lower voltage, 1 GeV, will be convenient due to deeper beam penetration, which is effective for heat removal, although it should be optimized in final design.

As a long term program, more economical non-monochromatic beam accelerator development should be encouraged as an industrial machine than Linac.

(B) Injection port engineering: It is a most serious unclear item. However, the vapor of salt might be mostly condensable on duct wall (cf. Fig. 1), applying several additive techniques such as electrostatic collection. Gaseous species in molten salt should be carried away to be separated in outside of reactor core.

(C) Accuracy of neutronic calculations: The target/blanket salt system of AMSB contains several kind of nuclei including light ones. Therefore, neutronic calculation is not easy and low accuracy in reaction products yield and in heat generation rate. Furukawa and Kato unsuccessfully aimed to proceed the experimental analysis of large target salt block getting the help of SIN (now PSI) group in 1981, but now again planning it under the cooperation with Russian group. It will be valuable for the development of spallation theorem in general, too.

(D) Reactor chemical aspects: Several chemical issues relating with "spallation chemistry" has been successfully examined [11, 12, 5] depending on chemical basis of MSR developed by ORNL. The chemical processing procedures of salt will be more

flexible in our substantially subcritical system. The transmutation of hazardous radioisotopes could be proceeded by the minimum separation work simply circulating through target/fuel salt cycle in THORIMS-NES.

(E) System engineering design optimization: The size of target/blanket system is important relating with [a] radiation damage of reflector graphite and reactor vessel wall, [b] inventory of fissile, fertile and reaction products for resulting the most important optimal reactor performance, and finally [c] total economy.

Its optimization connecting with salt composition and the operation purpose of this facility should be improved depending on the progress of several technological items.

The time schedule of developmental program has been shown in Table 3.

Table 3. Developmental Program of THORIMS-NES for Pu Disposition

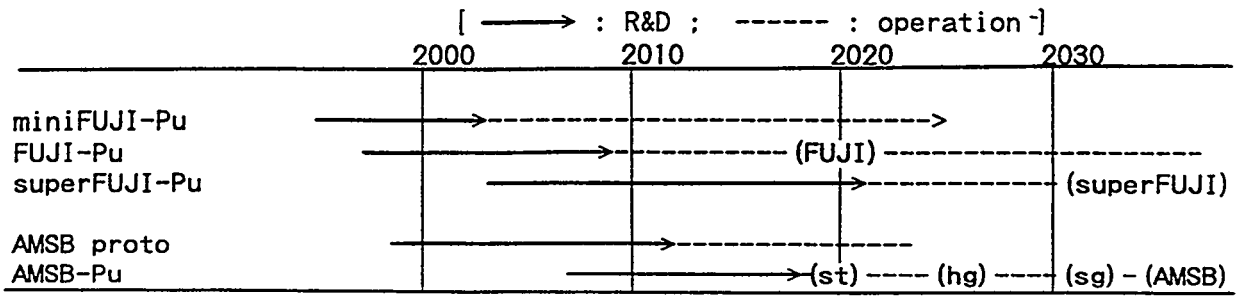

CONCLUSIONS

For the practical industrialization of Pu (TRU) disposition, it should be constructed as a positive work depending on not only the minimization of negative steps in separation, target-fabrication, -transportation, -dismantling & -refabrication, and R&D work only necessary for Pu disposition, but also the modification such as resulting a new rational nuclear energy system without Pu (TRU).

In here, one of the most promising approaches, that is THORIMS-NES, has been proposed briefly, including a scenario of realistic elimination of all Pu produced by U-fueled solid reactors in the past, present and near future. This might be an useful example to verify the feasibility of complete Pu elimination and huge nuclear energy production, and to judge the facility performance necessary for that purpose.

The main facilities composed of fission MSR (FUJI and superFUJI): public power stations and proton beam AMSB are not developed yet. However, their R&D will be not difficult and not costly, and their further improvements will be hopeful by few efforts, promising the world-wide application to solve the energy, environment and North-South problems opening a new nuclear era.

ACKNOWLEDGEMENTS: The authors wish to express sincere thanks to Dr. Y. Nakahara, JAERI, and Dr. M. Odera on their cooperation for this study, and also to Mr. F. Atchison, PSI, Drs. H. Takahashi and P. Grand, BNL, Dr. C. Marchetti, IIASA, Drs. I. Chuvillo and G. V. Kiselev, ITEP, and many Japanese and foreign friends on their encouragement and helps for developing this work.

REFERENCES

[1] Comm. Int. Security & Arms Control, Nat. Acad. Sci., "Management & Disposition of Excess Weapons", Washington: Nat. Acad. press, 1994, pp. 2-3.
[2] Rosenthal, M. W., Haubenreich, P. N., Briggs, R. B. :ORNL-4812 (1972) ; Engel, J. R., Grimes, W. R., Bauman, H. F., McCoy, H. E., Dearing, J. F., Rhoades, W. E. :ORNL/TM-7207 (1980).
[3] Furukawa, K., Lecocq, A., Kato, Y & Mitachi, K. : J. Nucl. Sci. Tech., 27, 1157 (1990).
[4] Furukawa, K., Minami, K., Oosawa, T., Ohta, M., Nakamura, N., Mitachi, K., Kato, Y. : Emarg. Nucl. Energy System, p. 235, World Sci. (1987) ; Furukawa, K., Mitachi, K., Kato, Y. : Nucl. Engineering & Design, 136, 157 (1992).
[5] Furukawa, K., Lecocq, A., Kato, Y. and Mitachi, K. : LA-12205-C, pp. 686-697 (1991) : Furukawa, K. :Atomkernenergie/Kerntech., 44, 42-45 (1984).
[6] Gat, U., Engel, J. R. & Dodds, H. L., Nucl. Tech., 100, 390-394 (1992).
[7] Mitachi, K., Furukawa, K., Murayama, M. and Suzuki, T. :"Nucl. charac. of a small M. S. power reac. fueled with Pu", in Emerging Nucl. Energy Systems, World Sci., 1994, pp. 326-331.
[8] Furukawa, K., Chigrinov, S. E., Kato, Y., & Mitachi, K. ; "Accelerator Molten-Salt Breeding Power Reactor useful for Pu-burning and ^{233}U-production", in Emerging Nucl. Energy Systems, World Sci., 1994, pp. 429-433.
[9] Chigrinov, S., Kievitskaya, A., Petlitski, V., Rutkovskaya, K. and Furukawa, K. : "Calcu. method of energy systems based on high energy particle and nuclei accelerators", in Emerging Nucl. Energy Systems, World Sci., 1994, pp. 434-438; Kato, Y., Furukawa, K., Mitachi, K. and Chigrinov, S. E. : "Fuel trajectory in Accel. M. S. Breeding Power Reactor system including Pu burning", in Emerging Nucl. Energy Systems, World Sci., 1994, pp. 439-443.
[10] Furukawa, K., Tsukada, K. and Nakahara, Y. :Proc. 4th ICANS, 1980, pp. 349-354; J. Nucl. Sci. Tech., 18, 79 (1981) ; JAERI-M83-050 (1983)
[11] Furukawa, K., Kato, Y., Ohomichi, T. & Ohno, H. : Thorium Fuel Reactors, "Proc. Japan- U. S. Semi. Th Fuel Reactors", Nara, 1982, Atomic Ene. Soc. of Japan, 1985, pp. 271-280.
[12] Furukawa, K. et al., First Int. Sympo. on Molten Salt Chemistry & Technology (April, 1983, Kyoto) Proceedings, 1983, J-303 pp. 405-408, J-304 pp. 409-413, K-210 pp. 497-499.
[13] Marchetti, C. & Nakicenovic, N. :RR-79-13, IIASA, (1987) ; Marchetti, C. :Nucl. Sci. Eng., 90, 521 (1985).

Actinide and Xenon
Reactivity Effects in ATW High Flux Systems

M. Woosley,* K. Olson,† D.L. Henderson,† and W.C. Sailor‡
*Department of Mechanical, Aerospace, and Nuclear Engineering
University of Virginia, Charlottesville, VA 22903
†Department of Nuclear Engineering and Engineering Physics
University of Wisconsin, Madison, WI 53706-1687
‡Los Alamos National Laboratory, Los Alamos, NM 87545

Abstract. In this paper, initial system reactivity response to flux changes caused by the actinides and xenon are investigated separately for a high flux ATW system. The maximum change in reactivity after a flux change due to the effect of the changing quantities of actinides is generally at least two orders of magnitude smaller than either the positive or negative reactivity effect associated with xenon after a shutdown or start-up. In any transient flux event, the reactivity response of the system to xenon will generally occlude the response due to the actinides.

INTRODUCTION

The central objective of the Los Alamos developed Accelerator Transmutation of Waste (ATW) system is to destroy the actinides and long-lived fission products that have been produced by commercial light-water reactors. In addition to burning its own wastes, the base-line 400 MW_e ATW system can handle the fission product and actinide waste from 2.5 conventional LWR's [1]. A proton accelerator is used to produce an intense thermal neutron source from a tungsten target. Surrounding the target is a blanket which contains, depending on the design, either a flowing slurry of actinide oxide (AcO_2) in heavy water or a graphite-moderated solution of actinides in molten salt. In addition there is a separate region in the blanket for the transmutation of long-lived fission products.

It has always been clear that xenon (^{135}Xe), with its huge thermal neutron cross section, would have important reactivity effects in the presence of flux changes in an ATW system. However, the response of the transuranics to flux changes, and the effect on the reactivity of the system has not been as clear. It has been suggested that in the presence of a flux increase in a very high flux system, an unstable positive reactivity growth could be caused by the change in actinide concentrations alone [2].

This paper develops two models. One to measure the reactivity effects of the actinides and one to measure the reactivity effects of xenon. The actinide model (ACTRHO) measures the response of a system of 25 actinides to a change in flux. The xenon model (HIXE) follows the concentrations of xenon, iodine, and a single generic actinide (^{239}Pu).

ACTINIDE MODEL

There has been some concern about the dynamics of the actinides under high transient fluxes [2]. Generally, equilibrium concentrations of the well fissioning nuclides grow with increasing flux. For example, under the condition of a pure neptunium feed, a step increase in the flux will cause an increase in the ratio of fissile ^{238}Np to non-fissile ^{237}Np as the capture in ^{237}Np becomes more important. Reference 2 suggests that this could lead to an unstable positive reactivity growth. In the paper, the author estimates that the positive rate of reactivity insertion due to a flux increase in the presence of a pure non-fissile feed (^{237}Np) could be as much as 1000 times as great as the negative insertion due to a step increase in flux in the presence of a pure fissile feed (^{235}U).

151

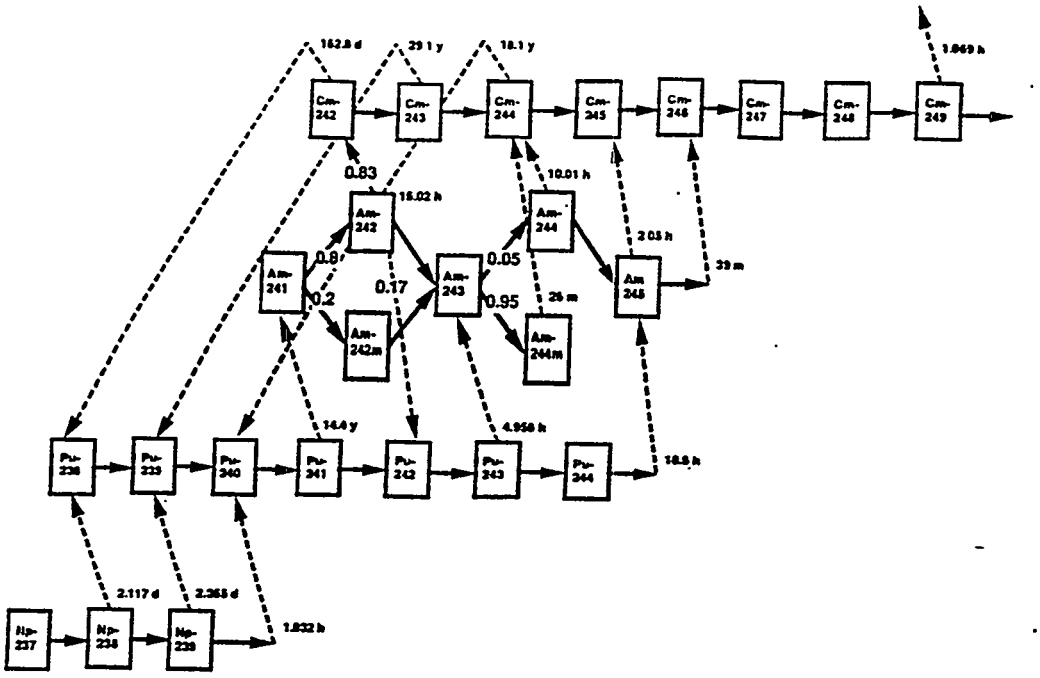

Fig. 1. The set of 25 actinides species considered in the actinide reactivity analysis.

The possibility of an unstable positive reactivity growth is unpleasant; however, preliminary calculations suggest that the magnitude of the reactivity insertion due to ^{237}Np could be lower than that calculated in Ref. 2. A model is needed that can calculate the time response to an increase in flux of the entire set of actinides in a general way, allowing for more species than just neptunium. In this manner, the time response of the system - a plot of fuel composition and reactivity versus time - can be calculated after a change in flux is made. The effects of fission products can also be included.

Figure 1 shows the 25 actinide isotopes that are considered important in the transmutation process of a waste burner. The fuel or feed streams in the system might be the plutonium and higher actinides separated from the uranium and fission products in LWR waste. The governing equation for the number of moles of species k implied by Fig. 1 is

$$\frac{d\,N_k}{d\,t} = F_k - \lambda_k\,N_k - \phi\,\sigma_k\,N_k + \sum_{i=1}^{25} \sigma_{i\to k}\,\phi\,N_i + \sum_{i=1}^{25} \lambda_{i\to k}\,N_i. \qquad (1)$$

where N_k is the number of moles, F_k is the feed rate, λ_k the decay constant for species k to all channels, ϕ the flux, σ_k the absorption cross section. The summations are source terms from decay and capture on other actinides. Thus $\sigma_{i\to k}$ is the cross section for the capture on species i leading to species k. To model the entire 25 species, there are 25 such equations coupled by the summation terms.

In order to model the transmutation of actinides in Fig. 1, the computer code ACTRHO, written in Fortran, was developed. ACTRHO calculates the equilibrium concentration of isotopes for a specified feed at a given spatially independent flux by setting the left hand side of Eqn. 1 to zero. Using these isotope concentrations as an initial condition, it calculates the time dependent solution to the coupled set of 25 first order differential equations suggested by Eqn. 1 for a step change in the flux from the steady state value.

152

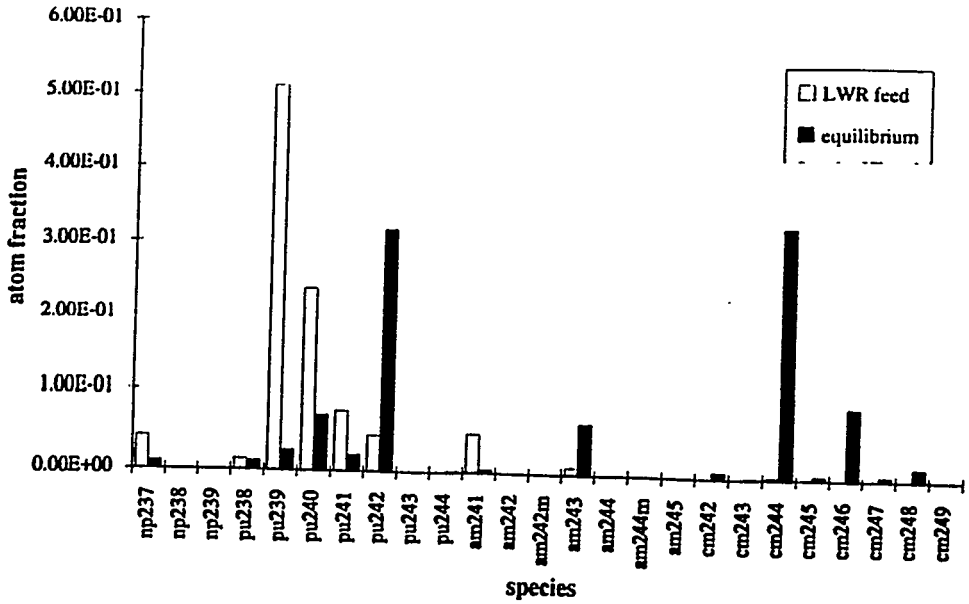

Fig. 2. Concentrations in the LWR discharge feed and at equilibrium at a flux of 1×10^{15} n/cm^2-s.

ACTINIDE RESULTS

Equilibrium Response of the System to Differing Feeds

The steady state concentrations are, in general much different than the initial feed. Figure 2 shows the feed and the equilibrium atom fractions for the ATW system designed to burn commercial LWR waste. The feed reflects the relative quantities of the 25 actinide isotopes in the actinides separated from spent LWR fuel. The equilibrium composition depends on the 1 group cross section and flux level in the blanket. Although the feed is 51% ^{239}Pu, the equilibrium fraction is only about 3%. At equilibrium, the non-fissile species ^{242}Pu, ^{243}Am, and ^{244}Cm make up the majority of the composition. These species have relatively small cross sections.

Figure 3 shows the rates of decays, captures, and fissions each species experiences at equilibrium. The figure is based on the LWR feed brought to equilibrium at a flux of 1×10^{15} n/cm^2-s. Fission occurs predominantly in ^{239}Pu and ^{241}Pu with about 9% occurring in ^{245}Cm. Some fast fission occurs in the even numbered Plutonium and Curium isotopes and in fissile ^{244m}Am. With the exception of ^{243}Am and ^{244}Cm, the plutonium species also undergo most of the capture reactions.

Short Time Reactivity Analysis

Reference 2 develops a framework for estimating the change in reactivity for a "small" step increase in the flux for non-fissile/fissile isotope pairs such as ^{237}Np/^{238}Np or fissile/non-fissile pairs such as ^{235}U/^{236}U. If the pair of isotopes are in equilibrium, a flux increase will cause a positive reactivity for the neptunium pair because the proportion of fissile ^{238}Np is increased by capture. The opposite is true for the uranium pair.

Exact reactivity as a function of time was calculated with the ACTRHO program for a variety of initial conditions. The results agree with Ref. 2 in that the initial rate of change of reactivity is indeed linear: Figure 4 shows the reactivity response for the first ten minutes after the flux is increased from 1×10^{15} n/cm^2-s to 2×10^{15} n/cm^2-s for a pure ^{237}Np feed.

153

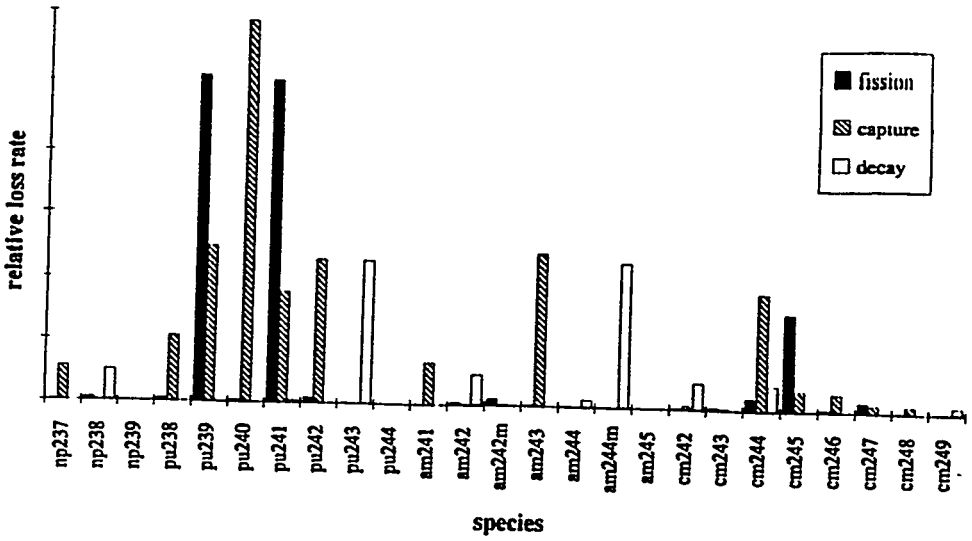

Fig. 3. Relative importance of decay, capture and fission at equilibrium in a flux of 1×10^{15} n/cm^2-s. 99% of the fission events occur in^{239}Pu, ^{241}Pu, and ^{245}Cm.

Figure 5 shows the reactivity response for 5 other feeds under the same conditions, but for the first ten hours after the flux change. The LWR discharge shows the earliest departure from linearity: the reactivity curve begins to saturate after about 30 minutes.

The time rate of change of reactivity can be cast in the following form

$$\frac{\delta\rho}{\delta t} = r\frac{\Delta\phi}{\phi} \tag{2}$$

where r is directly proportional to the initial flux [2]. The results in Table 1 are from Ref. 2.

Table 2 shows the initial rate of change of reactivity for a variety of materials irradiated at 2×10^{15} n/cm^2-s. All of the values in Table 2, with the exception of the last, are for pure

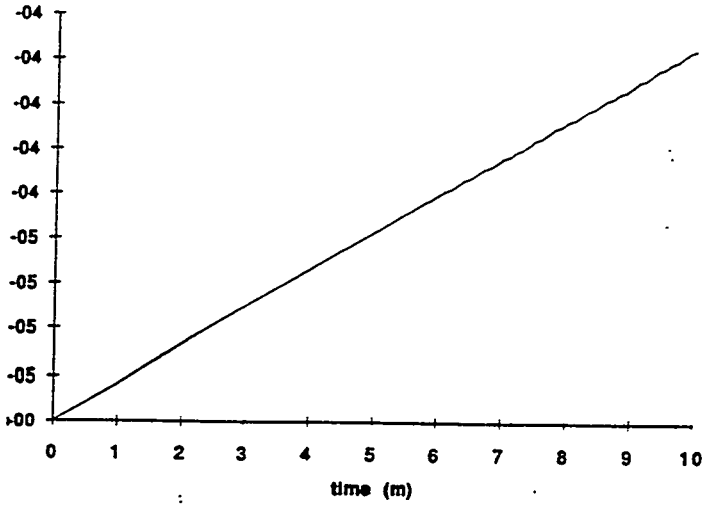

Fig. 4. Initial 10 minute response of a pure ^{237}Np feed to a flux jump from 1×10^{15} n/cm^2-s to 2×10^{15} n/cm^2-s.

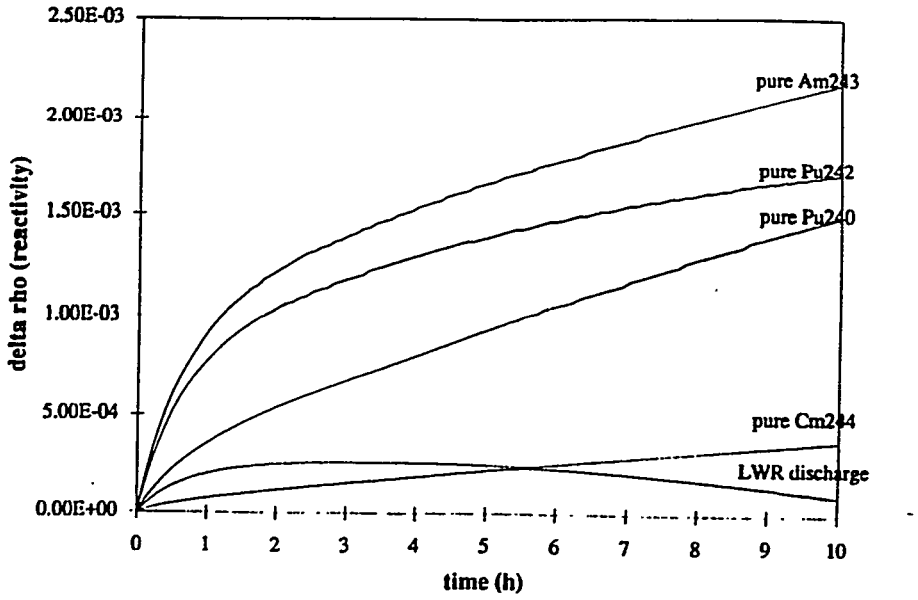

Fig. 5. Response of a pure feeds and LWR discharge to a flux jump from 1×10^{15} n/cm^2-s to 2×10^{15} n/cm^2-s. The species were all brought to equilbrium before the flux jump.

Table 1. Reactivity coefficients for step flux increase at short times [2]

Initial Isotope	Initial Flux	r value
^{235}U	10^{14}	-3.8×10^{-9}
^{237}Np	10^{15}	3.5×10^{-6}
^{237}Np	10^{16}	6.7×10^{-6}

isotope (or LWR) initial conditions, not feed. The last entry is for LWR discharge material brought to equilibrium at 1×10^{15} n/cm^2-s. These numbers differ from the r-values in Table 1 in two respects: First, Table 1 uses 2200 m/s cross sections and Table 2 uses ATW thermal cross sections. Next, Table 1 reports r while Table 2 reports $\delta\rho/\delta t = r\Delta\phi/\phi$. However, $\Delta\phi/\phi \sim 1$ and the values in Tables 1 and 2 can be compared on order of magnitude.

Note that the first entry in Table 2 for ^{237}Np is comparable to the second line in Table 1. On the other hand, the rate of reactivity increase for a realistic ATW composition which contains a mixture of fissile and non-fissile isotopes (LWR feed at equilibrium) is an order of magnitude smaller than that for a single non-fissile isotope. It is much more important to look at the whole system of actinides than any one individual isotope.

For the pure feed conditions, the non-fissile isotopes always show a positive reactivity upon irradiation, while the fissile isotopes show negative reactivity. Reference 2 mentions that the non-fissile isotope ^{237}Np is about 1000 times as reactive as fissile ^{235}U, and in the positive direction. This is misleading because a flux of 10^{14} n/cm^2-s was used for the uranium while a flux of 10^{15} n/cm^2-s was used for the neptunium. Table 2 suggests that the non-fissile actinides are indeed more reactive to a flux change than the fissile isotopes, but usually only by a factor of ten to one hundred. Notice that the LWR feed has a negative response to a flux increase, while the LWR feed at equilibrium has a positive response: the mixture becomes more reactive over time. This is due to the high quantities of non-fissile isotopes such as ^{240,242}Pu and ^{244}Cm in the equilibrium LWR material (Fig. 2).

755

Table 2. Initial reactivity for actinide system at 2×10^{15} n/cm^2-s for various initial conditions.

Initial Condition	$\delta\rho/\delta t$ (/s)
^{237}Np	2.8×10^{-6}
^{238}Np	-2.3×10^{-6}
^{238}Pu	9.1×10^{-7}
^{239}Pu	-9.8×10^{-8}
^{240}Pu	1.3×10^{-6}
^{241}Am	8.0×10^{-6}
^{242}Am	-2.2×10^{-7}
^{243}Am	4.2×10^{-6}
^{242}Cm	6.0×10^{-7}
^{243}Cm	-8.4×10^{-9}
^{244}Cm	1.9×10^{-6}
LWR initial condition	-1.3×10^{-8}
LWR feed at equilibrium	1.1×10^{-7}

Reactivity Time Evolution: An Example

ACTRHO was used to evaluate the actinide system response to an increase in flux over time [3]. One case tested was LWR feed. The feed was irradiated to equilibrium at 1 $\times 10^{15}$ n/cm^2-s and then, at time zero, the flux was increased to 2×10^{15} n/cm^2-s. Figure 6 shows the evolution of $\Delta\rho$ over three time scales.

When the flux is increased, reactivity quickly increases and remains positive for about 35 hours. This is because the concentrations of the fissile isotopes ^{243}Pu, ^{242}Am, ^{244}Am, ^{244m}Am, and ^{245}Cm all increase significantly after the flux jump. For example, the quantity of ^{244m}Am doubles within three hours. After a few hours, the reactivity curve begins to bend over at about 35 hours, the reactivity becomes negative. This is apparently due to the gradual decrease in the relative concentration of the fissile isotope ^{239}Pu. After roughly two and a half years, the reactivity becomes positive again due to the gradual recovery in relative concentration of most of the fissile elements, particularly ^{239}Pu, ^{241}Pu, and the isotopes ^{242}Am and ^{242m}Am which have very high fission cross sections. Also significant is the fact that the relative concentrations of the non-fissile isotopes ^{242}Pu and ^{244}Cm which collectively comprise more than 60 percent of the fuel at equilibrium (see Fig. 2) are decreasing steadily.

XENON MODEL

^{135}Xe is an important fission product poison because of its large thermal cross section of 2.7×10^6 barns. Although xenon itself does not have a large direct fission yield (1.09%), one of its precursors, ^{135}I, does (6.1%). Because of its large thermal absorption cross section and the significant amount of ^{135}Xe that is produced, xenon can substantially lower the thermal neutron flux and thereby decrease the burn-up rate of the long-lived fission products and actinides. Xenon in addition has a substantial effect on the ATW during a transient by decreasing, as much as 50%, the steady state thermal neutron flux. For these two reasons, it is important to analyze the system response due to ^{135}Xe during transient and steady state operation.

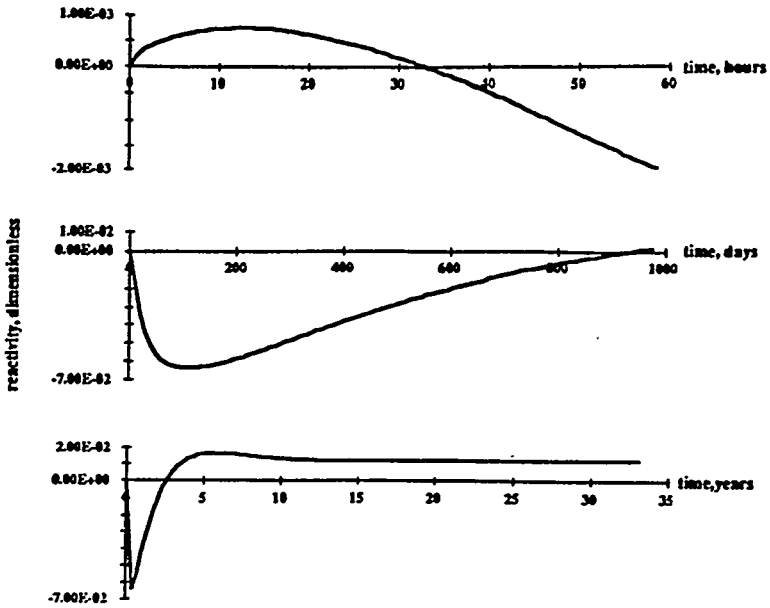

Fig. 6. Time evolution of reactivity for LWR discharge system taken from equilibrium at a flux of 1×10^{15} n/cm^2-s, jumped to 2×10^{15} n/cm^2-s at time zero. (a) up to 60 hours -, (b) up to 1000 days -, and (c) up to 33 years - after the flux jump.

Calculational Procedure

A simplified spatial model of the ATW is used in which the system is modeled as two regions; blanket region and an external heat exchanger region. The fluid flows through the blanket region of the reaction vessel where it is exposed to the extense thermal neutron flux produced in the ATW system. In this region, it is assumed that ^{135}I is produced from fission with a yield, γ_I, and only removed by decay into the ground state of ^{135}Xe. ^{135}Xe is produced by fission with a yield, γ_{Xe}, and by the decay of ^{135}I and is removed by neutron absorption or by beta decay. Within this region the neutron flux is considered spatially uniform. With these assumptions the rate equations for iodine and xenon within the neutron flux region are [4]:

$$\frac{\partial I}{\partial t} = \gamma_I \Sigma_f \Phi - \lambda_I I, \quad \text{and} \quad \frac{\partial Xe}{\partial t} = \gamma_X \Sigma_f \Phi + \lambda_I I - \lambda_X Xe - \sigma_a^X \Phi Xe. \tag{3}$$

Once the actinide containing fluid has passed outside the neutron flux region (blanket), it enters an intermediate heat exchanger. ^{135}I is no longer produced and is only removed through natural decay. ^{135}Xe is produced through the decay of iodine and is similarly removed through beta decay. The rate equations for xenon and iodine outside the neutron flux are the following:

$$\frac{\partial I}{\partial t} = -\lambda_I I, \quad \text{and} \quad \frac{\partial Xe}{\partial t} = \lambda_I I - \lambda_X Xe. \tag{4}$$

The actinides contained in the fluid are modeled as one generic actinide, "Ac", having the nuclear properties of ^{239}Pu. For the present analysis it is assumed that the actinide concentration is a constant in the fluid. The cycle time of the fluid through the system is 1 second [1].

The system of first order differential equations described by ^{135}Xe, ^{135}I, and the generic actinide, "Ac", both in the blanket and the heat exchanger regions, can be written as matrix

157

equations. To model the nuclide concentrations correctly as they circulate through the system, the matrix equations are coupled through the initial nuclide vector for each matrix equation after each circulation. Using the methods of fundamental matrices [5] and for the fluid cycle time considered within the ATW system, the complicated matrix solution attained after n circulations (cycles) through the system reduces to the following simple solutions for the equilibrium concentration of xenon and iodine as a function of the fraction of time, f, that the actinides spend within the blanket region [6];

$$Xe_{\infty} = \frac{(\gamma_I + \gamma_x)\,\Sigma_f \Phi_0 f}{\lambda_x + \sigma_a^{Xe}\Phi_0 f}, \quad \text{and} \quad I_{\infty} = \frac{\gamma_I \Sigma_f \Phi_0 f}{\lambda_I}. \tag{5}$$

If the fraction of time spent within the blanket region is unity, the equilibrium concentrations are just the steady state solutions to the rate equations in Eqn. 3. For the steady state neutron flux of 1.7×10^{15} n/cm^2-s [1], the equilibrium concentrations of ^{135}Xe and ^{135}I are 4.4×10^{14} and $5.99\times10^{14}\cdot f$ Atoms/cm^3, respectively. Note that for the high thermal flux level attained in the ATW system, the equilibrium xenon concentration is relatively independent of the actinide residence time. The iodine and xenon equilibrium concentrations are used as initial system conditions for the equilibrium xenon transient analysis.

Numerical Algorithm

A Fortran code (HIXE) was developed to calculate the concentrations of ^{135}Xe, ^{135}I, negative reactivity, and the themal flux during transient events. The simplified spatial model discussed previously was used. Following the fluid around one cycle, it first enters into the neutron flux of the ATW fluid blanket region. In this region the rate equations in Eqn. 3 describe the concentrations of ^{135}Xe and ^{135}I. The one speed time-dependent neutron diffusion equation,

$$\frac{1}{v}\frac{\partial \Phi}{\partial t} + \Sigma_a \Phi + \sigma_a^{Xe} Xe(t)\Phi = 0.95\,\nu\Sigma_f \Phi + S_0\,,$$

characterizes the neutron flux. The above system of first order differential equations was solved using a fourth order Runge-Kutta algorithm [7]. After the fluid spends a time t seconds within the ATW blanket, it flows outside the neutron flux into the external heat exchanger. In this region the actinides are no longer exposed to the intense neutron flux found within the blanket region. The relevant set of equations are now just those given in Eq. 4. The analytical solution to these equations is utilized to compute the concentrations.

Two different transient scenarios were investigated. The first case considers the possibility of a shutdown in the ATW system preceded by steady-state operation. The length of the shutdown period was 11 hours after which the ATW was restarted and run for 50 hours.

The second scenario considers the possibility that the ATW is forced to shutdown before equilibrium concentrations of xenon and iodine are established. The ATW in this case begins operation with a clean core, no fission products, and after four hours of operation it is shutdown. As in the first scenario, the duration of shutdown is 11 hours. Again the ATW is restarted and run for 50 hours.

Qualitatively, one would expect that the ATW would behave in a manner similar to light-water reactors [4]. Once the reactor is shutdown, the concentration of ^{135}Xe should build to a maximum and then slowly decay. In particular, one should note that for several hours after shutdown the negative reactivity caused by ^{135}Xe will be sizable.

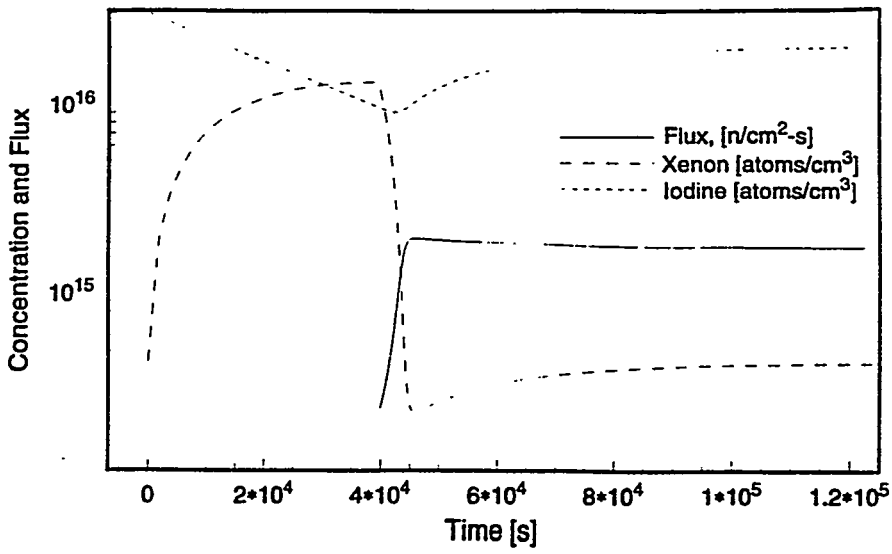

Fig. 7. Neutron flux, iodine, and xenon concentrations in ATW after an 11 hour shutdown period following steady state operation.

RESULTS

Several cases with varying actinide residence times in the blanket region ($f = 0.25$ to 0.5) for both the above mentioned scenarios were analyzed [6]. For all cases the xenon concentration was found to reach a maximum approximately 11 hours after shutdown. The cases of most interest are those that resulted in the largest amount of negative reactivity which correspond to the actinides spending half their cycle time ($f = 0.5$) in the blanket region.

Xenon Transient Starting from Equilibrium System Condition

Figure 7 shows the neutron flux, iodine, and xenon concentrations in the ATW after an 11 hour shutdown period following steady state operation. The actinides spend 0.50 seconds in the reaction vessel. As is evident from Figure 7, once the ATW is turned off the concentration of iodine decays away exponentially. Conversely, as the iodine decays into ^{135}Xe, the concentration of xenon increases and reaches a maximum approximately 11 hours after shutdown.

Once operation is re-established (i.e. neutron production resumes) the iodine builds back up to its steady state value. The xenon burns up quickly and drops below its steady state concentration before slowly building back up. The neutron flux overshoots its equilibrium value of 1.7×10^{15} n/cm^2-s and then slowly decreases. For all quantities the steady state conditions are restored within 50 hours.

Figure 8 shows the negative reactivity due to xenon. The largest negative reactivity should occur when the xenon concentration reaches a maximum as the two values are directly proportional, which is confirmed by this figure. As shown the negative reactivity can reach substantial values, the maximum $\Delta k/k$ is approximately -0.65.

Clean System Start-up Condition

Figure 9 depicts the neutron flux, ^{135}I and ^{135}Xe concentrations, negative reactivity for a 4 hour operation followed by a 11 hour shutdown period. These figures are qualitatively

759

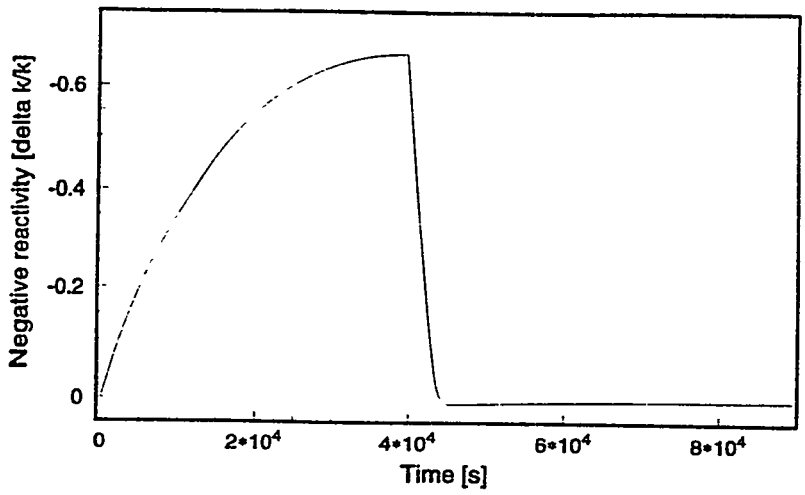

Fig. 8. Negative reactivity in ATW after an 11 hour shutdown period following steady state operation.

similar to those presented previously. As shown in Figure 9, upon startup from a clean system, one that does not contain any fission products, the concentration of iodine and xenon quickly build. However in this case, the ATW is shutdown before obtaining equilibrium concentrations.

As before the iodine decays decreasing its concentration while building the concentration of xenon within the fluid. After 11 hours the concentration of xenon is near its maximum value. At this point operation resumes and the concentration of xenon quickly decreases, again overshooting its equilibrium value. After approximately 50 hours the ATW is again operating at steady state. The behavior of the reactivity curve mirrors the xenon concentration curve as in the previous case. However because the concentration of iodine and

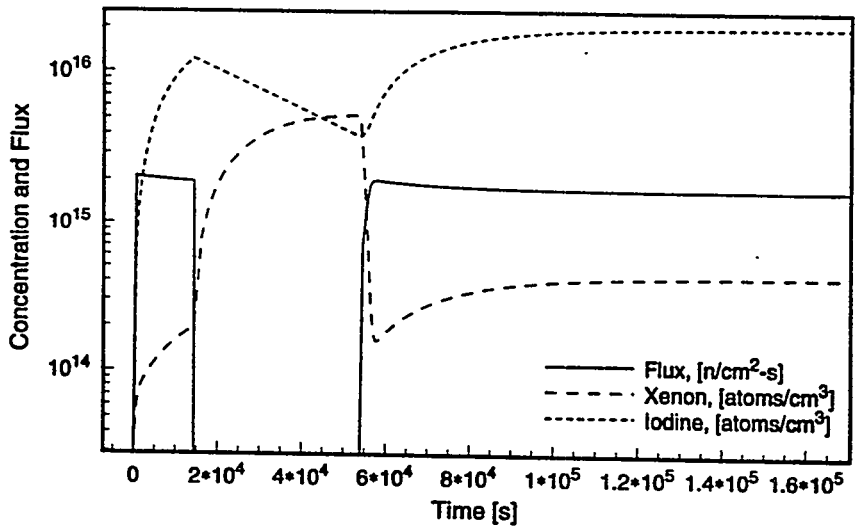

Fig. 9. Neutron flux, iodine, and xenon concentrations in ATW after an 11 hour shutdown period following 4 hours of operation.

760

xenon at the start of the shutdown is less than that of the steady state case, the maximum $\Delta k/k$ is only -0.25.

CONCLUSIONS

When the full system of 25 actinides depicted in Fig. 1 is considered, the initial reactivity insertion has been found to be an order of magnitude smaller than the value reported in Ref. 1 for a single isotope. Furthermore, the reactivity change for LWR feed, which is actually negative from 35 hours to 2.5 years after the flux change, saturates at a finite positive value. Finally, the possibility of an unstable positive reactivity insertion has been shown to be much smaller than the effect associated with xenon.

For an unexpected shutdown after steady state operation, the concentration of ^{135}Xe is the greatest approximately 11 hours after shutdown. The thermal neutron flux rises to within 5% of its steady state value approximately one hour after the ATW is restarted for shut down periods of less than 100 hours. The largest negative reactivity is produced by the fluid circulation case for which the actinides spend the largest fraction of each cycle within the reaction vessel (f= 0.5). Equilibrium values of ^{135}Xe, ^{135}I and the flux are re-established within 50 hours after an unexpected shutdown.

The maximum reactivity change seen for actinide composition changes in the short run was +0.0007 which occurred about 12 days after doubling the flux in an LWR fed system. On the other hand, the maximum reactivity change due to xenon buildup during shutdown was about -0.65, and the maximum change due to xenon burn-off during startup was +0.0182. Xenon reactivity effects will generally occlude actinide reactivity effects.

ACKNOWLEDGMENTS

Ken Olson, an undergraduate student, was supported during this research on a scholarship funded by the U.S. Department of Energy's Office of Environmental Restoration and Waste Management under the EMCORE program. EMCORE is administered by Associated Western Universities, Inc. Support for Michael Woosley was provided in part by the U.S. Department of Energy's Nuclear Engineering and Health Physics fellowship program administered by Oak Ridge Institute for Science and Education (ORISE). The authors acknowledge Dr. Edward Arthur, ATW Project Leader, who was the host scientist for the research performed at Los Alamos National Laboratory.

REFERENCES

[1] Sailor, W.C. and Beard, C.A., "Neutronics Analysis for an Accelerator-Based Nuclear Waste Transmuter," in *Proceedings of the Global '93 Conference*, American Nuclear Society, Seattle, Sept. 12-16, 1993.

[2] Rabotnov, N.S., et al., "The Reactor Aspects of Electronuclear Transmutation of Actinides in the Heavy Water High Flux Blankets, Analysis of Problems," Psi Switzerland, March 1992.

[3] Woosley, M.L., et al., "Response of Actinides to Flux Changes in High Flux Systems," LA-UR-93-3668, 1993.

[4] Duderstadt, J.J., and Hamilton, L.J., *Nuclear Reactor Analysis*, New York: John Wiley and Sons, 1976.

[5] Boyce, W.E., and Diprima, R.C., *Elementary Differential Equations and Boundary Value Problems*, 3rd ed., New York: John Wiley and Sons, 1977.

[6] Olson, K., and Henderson, D.L., "Xenon Poisoning in the ATW System," LA-UR-94-1089, 1993.

[7] Cheny, et al., *Numerical Mathematics and Computing*, Belmont, CA: Brooks/Cole, 1985.

761

TRANSMUTATION AND INVENTORY ANALYSIS IN AN ATW MOLTEN SALT SYSTEM

J. E. Sisolak, M. T. Truebenbach, and D. L. Henderson
Department of Nuclear Engineering and Engineering Physics
University of Wisconsin-Madison, Madison, Wisconsin 53706-1687

Abstract: As an extension of earlier work to determine the equilibrium state of an ATW molten salt, power producing, reactor/transmuter, the WAIT code provides a time dependent view of material inventories and reactor parameters. By considering several cases, we infer that devices of this type do not reach equilibrium for dozens of years, and that equilibrium design calculations are inapplicable over most of the reactor life. Fissile inventory and k_{eff} both vary by factors of 1.5 or more between reactor startup and ultimate convergence to equilibrium.

INTRODUCTION

One variant ATW (Accelerator Transmutation of Waste) Molten Salt [1] reactor endeavors to both burn waste and produce power on a commercial scale. Earlier work [2] studied the equilibrium state of such reactors, and provided a means to compare various designs based on several criteria: total inventory (total mass in the molten salt medium), total fissile inventory, α (capture to fission ratio), and the residence times t_{hfr} and t_{lfr} (see Fig. 1). While useful, equilibrium information does not apply early in the reactor life. More importantly, the definition of "early." in this sense, varies among different ATW systems and is usually unknown. This work addresses these questions by calculating the reactor history, so that comparisons between different designs can be made during any part of reactor life, and by seeking to minimize the approach to equilibrium (*ATE*), defined as the time required for the ^{232}Th inventory to reach 90% of its equilibrium value. It is important to keep in mind that the ATW reactors considered herein, in addition to transmuting waste, are constrained by a minimum required power output of 3000 MW. In fact, the designs in question should be considered primarily power producers, with transmutation being an added benefit.

METHODS

The ATW Molten Salt concept embodies two features which complicate the calculation of transmutation rates and waste inventory. First, the ATW molten salt design introduces large amounts of ^{232}Th, used to breed ^{233}U, to ensure 3000 MW of power. Second, in order to attain reasonable ^{233}U breeding rates, at least two distinct regions are required in the system: a high flux region (*hfr*, in which most of the neutron induced transmutation occurs) and a low flux region (*lfr*, in which ^{233}Pa decay occurs).

It is also desirable to include a third region, the feed flux region (*ffr*), where extraction and feed-stream mixing take place. The circulating waste stream has different residence times in each region—about a month or more—which are chosen to balance conflicting desires to minimize total actinide inventory, minimize the production of new waste isotopes not present in the original feed, minimize α (capture to fission ratio), and maximize the overall transmutation rate.

Model

Fig. 1 shows a schematic of the ATW design, indicating the significance of the various terms. Each region (*ffr, hfr, lfr*) is divided into a number of subregions, each with a "width" of one time step; that is, after one time step, a given slug of molten salt has advanced one subregion. Thus, in the figure, Δt_{hfr} equals Δt_{lfr}. Marching through the reactor history, a point calculation (i.e. one assuming a constant flux) is done for each time step, and the new power and inventory of each isotope are calculated.

All mixing takes place in the *ffr*, which is typically chosen to be one time step wide, since the volume in which mixing occurs is assumed to be small. However, batched systems, in which the feed region residence time is significant, could also be modeled. Either approach should give approximately the same results, since the feed region is expected to be maintained at low flux, and can be viewed as a short extension of the *lfr* for most problems.

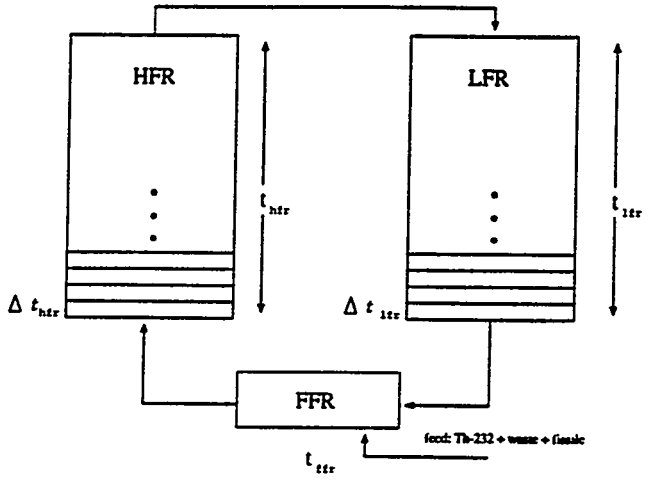

Figure 1: Schematic of the System Modeled

Code

The WAIT (Waste Actinide Inventory and Transmutation) code, written specifically for ATW molten salt calculations, takes an arbitrary, time dependent feed (^{232}Th plus waste) and computes the inventory, activity, and power production for both steady state and transient scenarios. Also, by fixing a desired power level, it is possible to calculate a consistent, but non-unique, feed rate for each fissile isotope contributing to the target power. In such cases, it is found that the system behavior depends on t_{hfr} and t_{lfr} (residence times in the high and low flux regions), and varies considerably over the life of the transmuter.

The transient portion of the code chooses only *one* of many paths the reactor could take toward equilibrium. It should be noted that the transient problem is under-determined, and has infinitely many solutions, since there are multiple, adjustable, feed streams. WAIT obtains a unique solution by first determining the equilibrium feed rate of ^{232}Th (which is unique and independent of the initial mass in the system) for the residence times in question. It then fixes this feed rate and adjusts the feeds of all other fissile isotopes by a common ratio to converge the power.

Input Parameters

A time step of 1 day was chosen, although it was found that 2 - 5 day time steps gave approximately the same results. Very short time steps (minutes) significantly increase execution time, and may cause a breakdown of the numerical method, as described in reference [3]. Shorter time steps would be desirable for detailed, minute-by-minute tracking of such isotopes as ^{233}Th, with a half-life of 22.3 minutes, but have negligible effect on the predictions of overall system behavior. To help detect the onset of numerical instability, all results were compared at double and quadruple precision, with minimal differences.

Choice of optimal residence times obviously requires knowledge external to the reactor, such as a quantification of the relative merits of low inventory and high transmutation rates. A parametric study of various residence times ($\Delta t_{hfr}, \Delta t_{lfr}$ pairs, with Δt_{ffr} fixed at 1 day) was undertaken for both the equilibrium and transient cases, with the intent of providing design guidelines. Cases are designated as, for example, 1.30.60, meaning 1 day in the *ffr*, 30 days in the *hfr*, and 60 days in the *lfr*. The reference values for most of the diagrams herein are 1.30.30, since this is representative of the shorter *ATE* cases. Typical fluxes for the *hfr* and *lfr* are $\phi_{hfr} = 10^{15}$ n/cm^2-s, and $\phi_{lfr} = \phi_{ffr} = 10^{11}$ n/cm^2-s, and these were used as reference values for all calculations described below.

WAIT tracked thirty-seven nuclides (see Fig. 2 for a list), ranging from ^{232}Th to ^{249}Cm, and these were more than adequate to illustrate the general differences between equilibrium and transient behavior, as most appear only in small quantities.

The transient calculations were the most important new feature of this study, since it became evident after only a few trials that it requires a *significant* fraction of the device lifetime to attain equilibrium. Consider, for example, Fig. 3 showing the total inventory (sum over all 37 isotopes) and fissile inventory (isotopes with $\sigma_f > 10b$). After 200 cycles, the curve levels off, and by cycle 300 (not shown), convergence has been attained and the curve becomes flat at the equilibrium value of 10523 kg, of which 94% is ^{232}Th. The 90% mark is reached just after cycle 100, and since each cycle is $1 + 30 + 30 = 61$ days long, this represents almost 17 years of operation. In view of this, everything was run to at least 300 cycles to ensure equilibration.

RESULTS

Although the primary focus of this study was the transient phenomena, it was necessary first to extend the equilibrium work of Truebenbach [2]. A sample equilibrium configuration is provided below, to provide some reference values for the transient discussion.

Equilibrium Results

The lessons from Fig. 3 are twofold: (1) a great number of cycles must be allowed to get close to equilibrium, and (2) if the *ATE* is to be minimized, short residence times are desirable. However, we are constrained, since too short a value of t_{lfr} will cause excess ^{233}Pa (half-life 27 days) to loop back into the *hfr* and be transmuted into actinides, instead of decaying to ^{233}U and subsequently fissioning. It was determined in reference 2, and confirmed with the WAIT code, that *lfr* residence times outside the range $30 - 60$ were undesirable: shorter times produce excessive inventory since much of the Thorium feed is "wasted," and

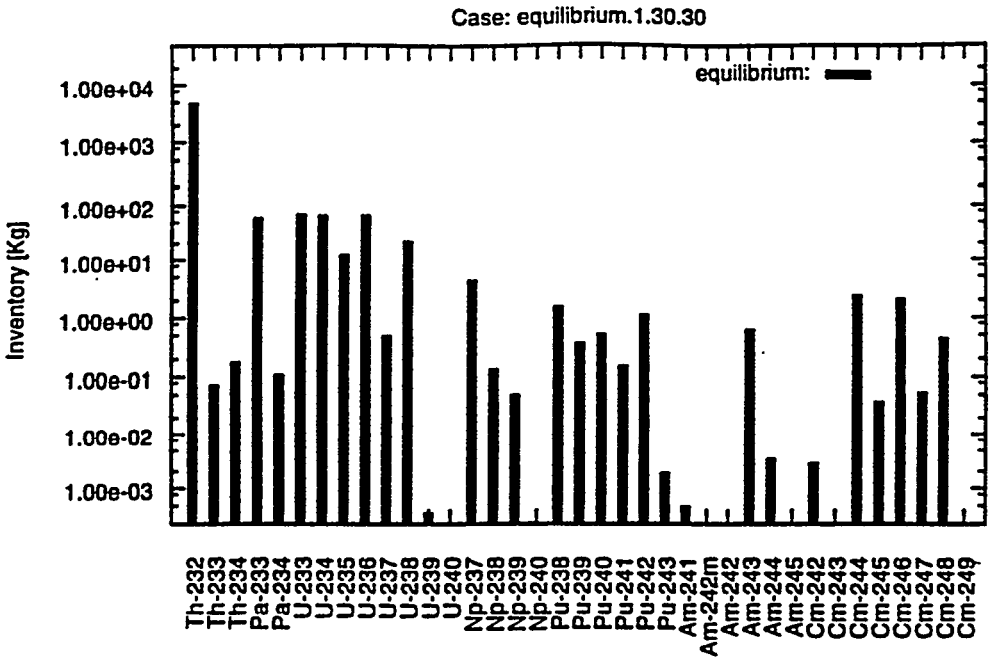

Figure 2: Total Equilibrium Inventories

does not end up as ^{233}U; longer times increase α and thus reduce k_{eff}. The desirable range for the *hfr* is $30 - 45$ days.

An optimal configuration is impossible to define without using additional information, such as economic and safety considerations, to weigh the relative importance of low inventory on the one hand, and low capture to fission ratios on the other.

Figure 2 shows equilibrium inventories for all the tracked isotopes for the 1.30.30 case. Note that the dominance of ^{232}Th necessitates a log scale.

Transient Results

Because of the large *ATEs*, equilibrium data must be viewed as reference values only, and are unsuitable for design calculations. If constant power is maintained, the relative abundances of ^{232}Th and actinide waste in the feed stream change considerably over the first several years of operation, so a transient analysis becomes necessary.

In all power producing systems studied so far, at least 15 years (often much longer, depending on $(\Delta t_{hfr}, \Delta t_{lfr})$) was required before attaining 90% of equilibrium. It is also worth mentioning that even after the dominant ^{232}Th equilibrates, shifting of the less prevalent isotopes still occurs, and the power sharing among ^{233}U and the actinides takes many more years to stabilize. This redistribution is illustrated by Fig. 4, in which the inventory of each isotope is shown at 4 different times. Again, note the logarithmic y-axis. Thus, for the 1.30.30 case, our value of 17 years was based on a conservative definition of "equilibrium."

Other interesting aspects of the approach to equilibrium are the fissile feed needed to maintain constant power, and α, the capture to fission ratio. In these cases, the fissile feed of ^{235}U, allows us to maintain a reasonably small Thorium input, and correspondingly low inventory, while still producing 3000 MW. Not surprisingly, the ^{235}U feed drops off with an exponential-like curve as the concentration of ^{233}U and other fissile isotopes builds up (Fig. 5).

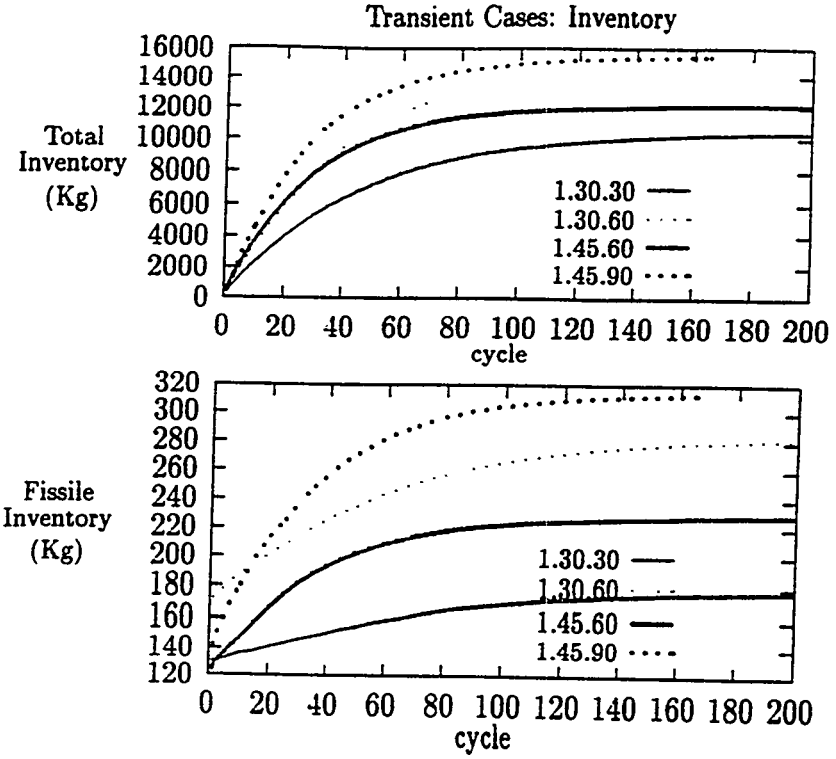

Figure 3: Total and Fissile Inventories

Notice that α changes by as much as a factor of 4. (Fig. 5) and has large design implications, since the neutronic properties of ATW systems will vary dramatically during the first several years. Following standard ATW approximations [4], we can estimate k_{eff} as

$$k_{eff} = \frac{\overline{\nu}}{1 + \alpha + S},$$

where $\overline{\nu}$ is about 2.5 neutrons generated per fission (for a Th/^{233}U mix), α is the capture to fission ratio, and S is the sum of all other loss terms, estimated to be between 0.26 and 0.96 [4].

From Fig. 5 we see that α varies from about 0.4 early in the reactor life, to almost 1.5 at equilibrium. Hence, we can calculate:

$$\frac{k_{eff-bol}}{k_{eff-eol}}(S = 0.96) = 1.46 \qquad \frac{k_{eff-bol}}{k_{eff-eol}}(S = 0.26) = 1.66$$

using the upper and lower estimates of S, respectively, so that we can expect k_{eff} to change by a factor of about 1.5 over the reactor life.

Finally, observe from Fig. 3 that for fixed t_{hfr}, smaller values of t_{lfr} decrease inventory, whereas for fixed t_{lfr}, the reverse holds. Unfortunately, the benefits of small t_{lfr} disappear below 27 days (half-life of ^{233}P), and the benefits of large t_{hfr} are offset by increased values of α.

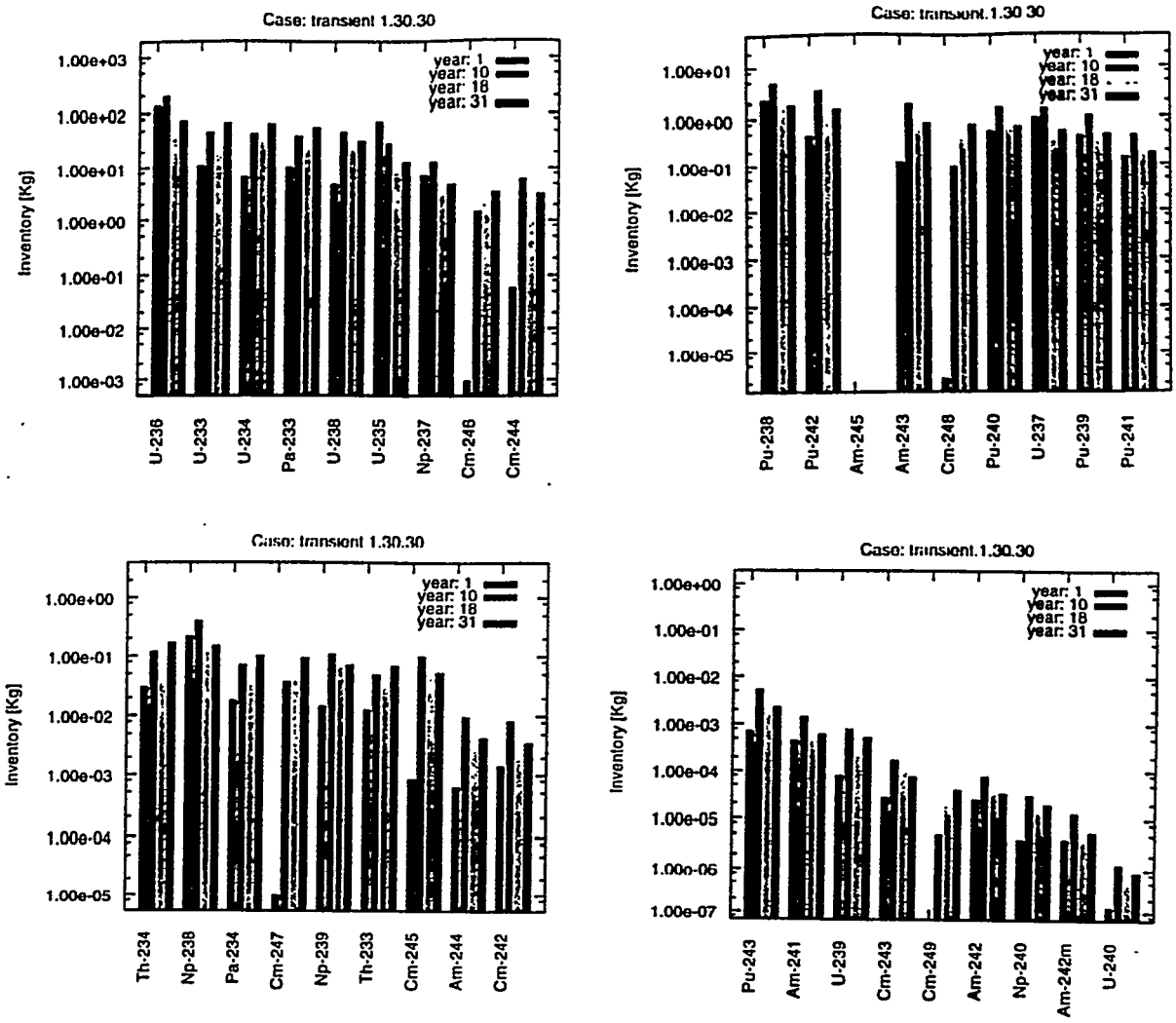

Figure 4: Transient Inventories at Several Times

CONCLUSIONS

It seems clear that operation of an ATW reactor at equilibrium conditions is unrealistic. Obtaining such a configuration within a reasonable time, even 5 years, would require a highly variable, and carefully planned, ^{232}Th feed rate. While such a system is possible in principle, it suffers from 3 major drawbacks. First, the enormous ^{232}Th feeds early on would severely curtail the number of neutrons available for waste transmutation. Second, they would drive up the total reactor inventory, and also the fissile inventory, and third, any extended shutdown for maintenance or inspection would disrupt the feed-schedule. Additional work, still in the preliminary stage, suggests that attaining equilibrium before 5 years would require prohibitively high feed rates of ^{232}Th.

ACKNOWLEDGMENTS

The authors wish to acknowledge Dr. Edward Arthur, ATW Project Leader, who was the host scientist for research performed at Los Alamos National Laboratory, and sponsor for this paper. During this work, Mike Truebenbach, an undergraduate, received a U.S. Department of Energy scholarship through the Office of Environmental Restoration and

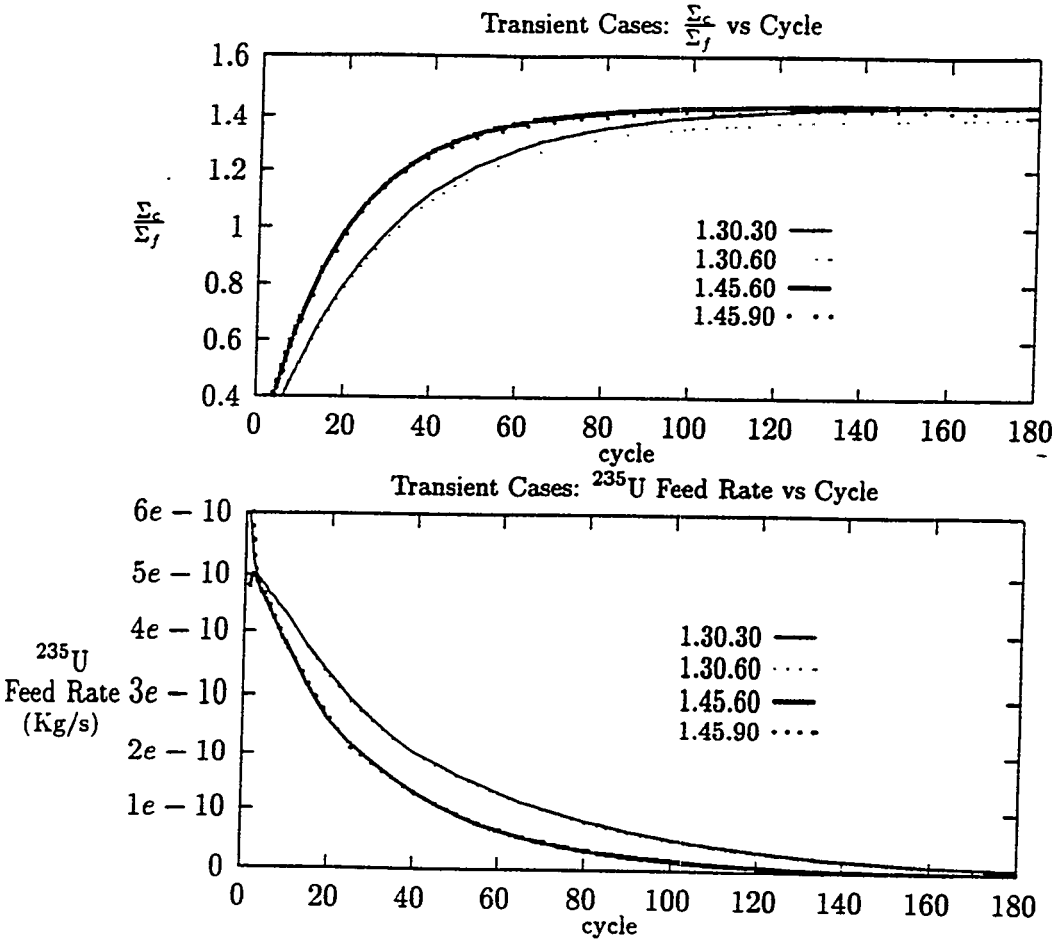

Figure 5: Capture to Fission Ratio ($\frac{\Sigma_c}{\Sigma_f}$) and Feed Rate (^{235}U)

Waste Management under the EMCORE program. EMCORE is administered by Associated Western Universities, Inc..

REFERENCES

[1] Bowman, C.D., et al., "Nuclear Energy Generation and Waste Transmutation Using an Accelerator-driven Intense Thermal Neutron Source," Nucl. Inst. Meth., A320, 336-367 (1992).

[2] Truebenbach, M.T.., et al., "A Thorium/Uraninium Fuel Cycle for an Advanced Accelerator Transmutation of Nuclear Waste Concept," *Proceedings of the International Conference on Technology and Future Nuclear Systems 'Global 93'*, 1993, p.774ff.

[3] Sidell J., "Extra: A Digital Computer Program for the Solution of Stiff Sets of Ordinary Initial Value, First Order Differential Equations," UK Atomic Energy Authority, AEEW – 799, June 1972.

[4] Arthur, E.D., "The Los Alamos Accelerator Transmutation of Waste (ATW) Concept," *Presentations to the STATS Transmutation Subpanel*, LA-UR-92-2020, April 15-16, 1992.

The Concept of the Double-Purpose Electro-Nuclear Facility

B.P. Bergelson, S.A. Balyuk
Institute of Theoretical and Experimental Physics
Moscow 117259, Russia

Abstract. The parameters have been determined on a conceptual level of the electro-nulear facility intended for electric power generation and MA transmutation.

Introduction

Electro-nuclear facilities (ENFs) are being developed without apparent success for many years. The main difficulties are associated with high accelerator cost and absence of their own cleary defined place for ENFs in the nuclear-power complex. In the recent years, however, the situatuation has changed in many aspects in connection with the rise in safety requirements for nuclear power industry and because of the necessity to decrease the equilibrium level of the long-lived radiotoxicity in particular. In our opinion double-purpose ENFs designed for power generation and transmutation of minor actinides (MA) are promising. The results of conceptual investigations for such facility being operated on liquid fuel in condition of uranium-plutonium fuel cycle are given below.

Parameters of the double-purpose ENF

Let us consider the double-purpose ENF where the blanket is replenished with MA and U-238 (or natural uranium). The range of thermal neutron fluxes in blanket considered is equal to $\varphi = (1\text{-}5)\cdot 10^{15}$ neutron/cm$^2\cdot$s. At substantially lower neutron fluxes the process of transmutation becomes ineffective. The calculations show that for equilibrium solution of uranium and MA in heavy water at various values of q_2/q_1 and ε (q_1 is the rate of

uranium supply in solution, q_2 is the same rate for MA, ε is the residence time of solution in zone irradiated by neutrons) $K_\infty < 1$. If structural componenets will be placed in such medium for removal of high potential energy (pressure > 10[illegible] MPa), K_{eff} will be sufficiently lower which makes the achivement of objectives to be sought impossible.

Good neutron multiplying properties of the solution necessary for placement of structural components in blanket could be achieved in a facility with two targets and two blankets. The blanket 1 is replenished with uranium only and designed for Pu-239 production as result of absorption in uranium of neutrons with energy close to that in U-238 range of resonances. In blanket 1 there is no any amount of sizable multiplication of neutrons being generated in target 1 (K_∞ is significantly less than 1). The blanket 2 is replinished with Pu-239 from the blanket 1 and with MA from power reactors. In the medium that fills blanket 2 there is an effective neutron multiplication being generated in the target 2. K_∞ is sufficiently higher than 1 which makes it possible to place structural components for removal of highly potential energy in blanket 2. A diagram of such facility is shown in Fig. 1

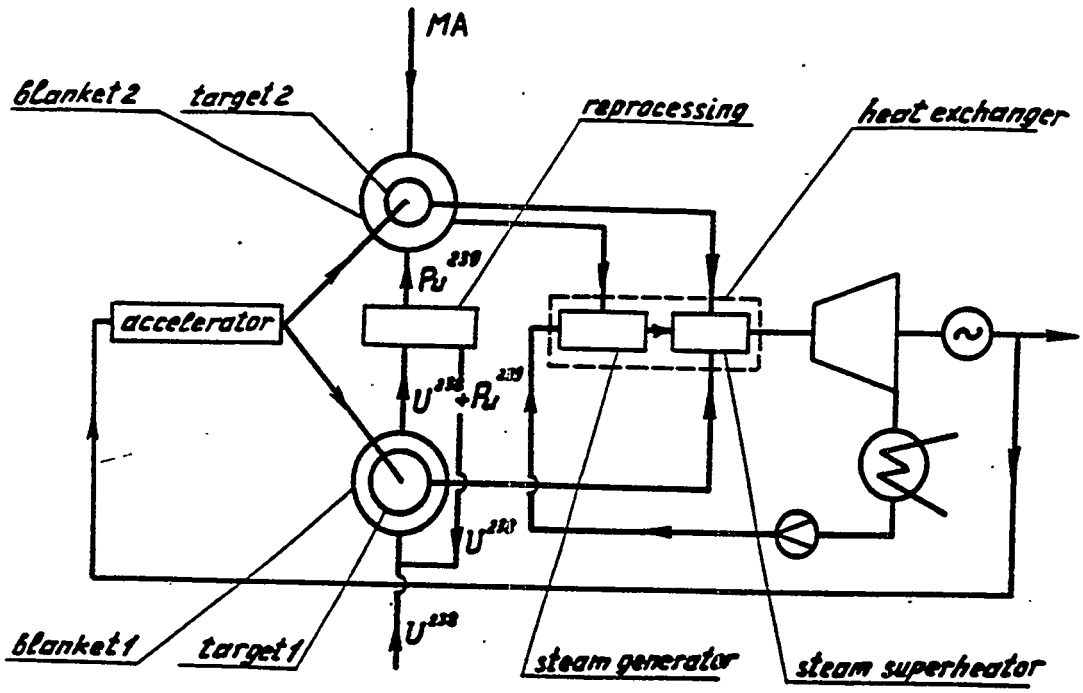

Fig. 1

A relationship establishing a one-to-one correspondence between N_{fac} (facility's electric power) and N_{ace} (electrical power consumed by accelerator) could be written for the facility with two targets and blankets.

$$N_{fac} = N_{ace} \cdot \left[1 + x \cdot \frac{E_f}{E_p} \cdot \alpha \cdot \left(1 + \frac{q_2}{q_1} \right) \right] \cdot \eta_1 \cdot \eta_2 > 1 \quad (1)$$

$$x = \left[1 + \nu \cdot \left(1 + \frac{q_2}{q_1} \right) \cdot \frac{1 - K_{eff}}{K_{eff}} \right]^{-1} \quad (2)$$

E_f is fission energy; E_p is proton energy; η_1, η_2 is accelerator's efficiency and thermal power conversion in electrical; α is a conversion ratio of protons into neutrons; K_{eff} is effective factor of neutron multiplication in blanket 2. The value of N_{fac}/N_{ace} at $K_{eff} = 0.95$; $E_p = 1.6$ GeV; $\alpha = 55$; $\nu = 2.9$; $\eta_1 = 0.5$ are tabulated in Table 1 for various ratios of replenishment between Pu-239 and MA.

Table 1. ($K_{eff} = 0.95$)

$q_2/q_2 + q_1$		0	0.33	0.50	0.67	1.0
x		0.87	0.81	0.76	0.67	0
$\frac{Nfac}{N_{ace}}$	$\eta_2 = 0.4$	1.4	1.9	2.3	2.9	8.6
	$\eta_2 = 0.3$	1.1	1.4	1.7	2.2	6.5

At $q_2 = 0$ the facility produces the electric power only in quantity of 40% from that consumed by accelerator. Because of high accelerator cost the facility has shown very little promise.

Two versions of the liquid fuel for blanket 2 were considered:

1. The solution (or suspension) of Pu + MA in heavy water. The close packaging of zirconium tubes (100 x 100) designed for the

pressure of 10ρ MPa has been taken as structural material.

2. The melt of fluoride salts consisting salts of Pu and MA [1]. The blanket 2 is 80% full with graphite (without tubes) and has 20% of molten salts. The dependence of the average specific power generation in liquid fuel q_v of the average thermal neutron flux φ in blanket 2 has been calculated at various q_2/q_1 values and $K_\infty = 1$.

The parameters of the double-purpose facility with heavywater liquid fuel has been determined from condition q_v = 100 kW/litre and are tabulated in Table 2.

Table 2.

Parameters	Dimension	Transmutation		Electric power without transmutation
		with external power comsumption	without ext. power consumption	
Accelerator elec. power	MW	1000	1000	1000
Electric power for external consumers	MW	900	-	400
Number of 1000 MW(e) power react. serviced	-	20	18	-
Average thermal neutron flux in blanket 2	neutr/cm^2 s 10^{-15}	0.6	1.8	2.4

Of three versions of the double-purpose facility which parameters are shown in Table 2 the version without use of electric power by external users is the most easy from feasibility viewpoint and has the highest nuclear safety. This is caused by high subcriticality of the blanket 2 for this version (K_{eff} = 0.75).

At q_v = 123 kW/litre of molten salts (the warm-up in blanket is equal to 100°C) the facility parameters are close to those indicated in Table 2. If q_v = 250 kW/liter (the warm-up in blanket

is 200 °C), the parameters of the facility with molten salts is sufficiently better. In this case the electric power is appr. 50% higher, and the number of reactors served are almoust twice higher. The use of molten salts, however, is associated with the necessity to solve serious technological problems: the purification from fission products, circulation of melt with relatively high rates, compact blanket and heat exchangers, etc.

In double-purpose ENF long-lived fission products (Tc-99, J-129) could be in principle transmuted too. For this purpose blanket 1 should consist of two sections. The external section of such blanket with high subcriticality is replenished with uranium and internal section with low subcriticality - with nuclear fuel and fission products being transmuted. The solution of the optimization problem will allow us to determine the most advantageous relationship between quantity of MA and fission products being transmuted.

The quantity of useful power obtained from a single nucleus of uranium which replenishes the blanket 1 is

$$E = \{ [1 + X \cdot \frac{E_f}{E_p} \cdot \alpha \cdot (1 + \frac{q_2}{q_1})] \cdot \eta_1 \cdot \eta_2 - 1 \} \cdot \frac{E_p}{X \cdot \alpha \cdot \eta_1 \cdot \eta_2} \quad (3)$$

For pure power version ($q_2 = 0$) this value exceeds 30% of electrical power that could be obtained at fission of one uranium nucleus (E_f = 200 MeV) at $\eta_2 = 0.4$. E, the useful power increases when $\chi \cdot E_f / E_p \cdot \alpha \cdot \eta_1 \cdot \eta_2$ complex increases and the limiting value of E is equal to E_f. This means that similar facilities can be considered as alternative ones to fast reactors.

The following characteristics are shown in Fig. 2:

1. The build up in a long-term storage facility for the radiotoxicity of MA being recovered from PWR (50%) and LMBFR (50%) per 1 GW(e).

2. The increase (during appr. 200 years) in radiotoxicity of the same MA, if they are loaded in standard PWR and LMBFR for transmutation. The rise in radiotoxicity occurs as a result of the transformation of the long-lived MA into relatively small ones (Pu-238, Cm-244) [2].

3. The drastic decrease in equlibrium long-lived radiotoxicity at MA load in a specialized transmuter with thermal neutron flux in blanket higher than 10^{15} neutron/cm^2·s [3].

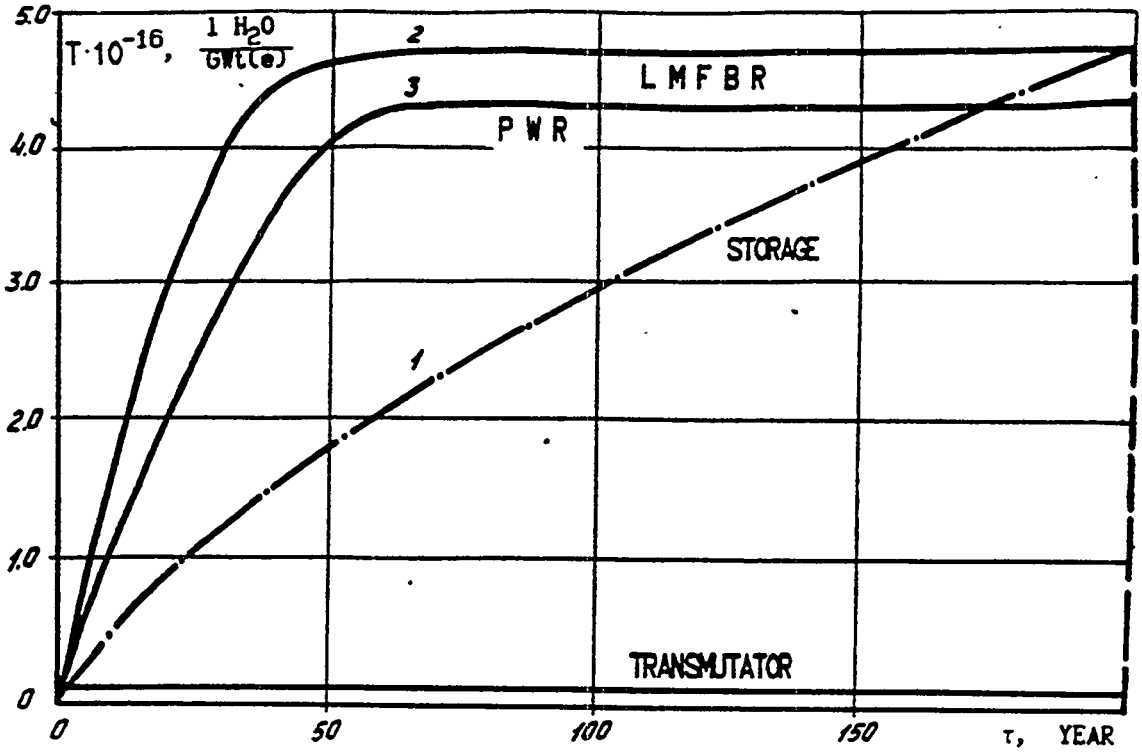

Fig. 2

It follows from curves in Fig. 2 that MA transmutation in modern PWR and LMBFR is inadvisable.

Conclusion

The results of conducted investigations make it possible to draw a conclusion that development of double-purpose facilities designed for electric power generation and MA transmutation is promising. This conclusion is based on the following:

Double-purpose liquid fuel ENFs operated in conditions of the closed cycle have low specific nuclear fuel loadings (thermal neutron flux is approximately 10^{15} neutron/cm^2·s) and short fuel cycle (there is no need for fuel elements to be manufactured). The application of such facilities makes it possible to reduce the equilibrium level of the long-lived radiotoxicity more than

10 times and by doing so to increase the ecological safety of nuclear power industry. Along with effective destruction of the long-lived radiotoxicity the double-purpose ENF being replenished with depleted or natural uranium only generates electric power for external users. In doing so the unit useful facility's power is close to 1 GW(e).

The cost of the accelerator construction is the price which have to be paid for achieving indicated objectives.

References

1. Williamson Mark A. *Actinide Burning Concept: Fuel Salt Chemistry*, LANL, Los Alamos, NM, USA, 1994.

2. Bergelson B.R., Balyuk S.A. *Long-lived Radiotoxicity Build-up Under U-Pu Fuel Cycles And Methods To Decrease It.* Paper presented at the 2-nd Int. Seminar on Weapon-Grade Plutonium Conversion and HLW Transmutation, Moscow, Russia, 23-27 May, 1994.

3. Bergelson B.R., Balyuk S.A. *Parameters of the MA transmutation facility without use of the nuclear fuel and with small plutonium additions*, Moscow, Russia: ITEP preprint No. 10-94, 1994.

The Influence of External Source Intensity in Accelerator/Target/Blanket System on Conversion Ratio and Fuel Cycle

Boris P. Kochurov
Institute for Theoretical and Experimental Physics,
B.Cheremushkinskaya, 25, Moscow, Russia, 117259
e-mail:kochurov@vxitep.itep.msk.su
Fax:7-(095) 123 6584

Abstract. The analysis of neutron balance relation for a subcritical system with external source shows that a high ratio of neutron utilization (conversion ratio, breeding ratio) much exceeding similar values for nuclear reactors (both thermal or fast spectrum) is reachable in accelerator/target/blanket system with high external neutron source intensity. An accelerator/target/blanket systems with thermal power in blanket about 1850 Mwt and operating during 30 years have been investigated. Continual feed up by plutonium (fissile material) and Tc-99 (transmuted material) was assumed. Accelerator beam intensity differed 6.3 times (16 mA - Case 1, and 100 mA - Case 2). Conversion ratio (CR) was defined as the ratio of Tc-99 nuclei transmuted to the number of Pu nuclei consumed. The results for two cases are as follows:

	Case 1	Case 2
CR	0.77	1.66
N(LWR)	8.6	19.1
Power MWt(el)	512	225

where N(LWR) - number of LWRs(3000 MWt(th)) from which yearly discharge of Tc-99 is transmuted during 30 years. High value of conversion ratio considerably exceeding 1 (CR=1.66) was obtained in the system with high source intensity as compared with low source system (CR=0.77). Net output of electric power of high source intensity system is about twice lower due to consumption of electric power for accelerator feed up. The loss of energy for Tc-99 transmutation is estimated as 40 Mev(el)/nuclei. Yet high conversion ratio (or breeding ratio) achievable in electronuclear installations with high intensity of external source can effectively be used to close fuel cycle (including incineration of wastes) or to develop growing nuclear power production system.

INTRODUCTION

In many recent works devoted to subcritical systems with external neutron source produced by spallation reactions of proton beam with target material one of the advantages of such systems is outlined - a possibility to have small inventories of fissile and transmuted materials or fertile materials.

Small inventories provide high flux at a given power output [1,2,3]. High flux is supposed to lead to high productivity of installation. Indeed it is true if short-lived fissile materials are involved in transmutation chains (Np238). However for transmutation of such types of long-lived radionuclides as Tc99, I129 there is no need in a high flux, as well as for production of fissile materials say U233 from Th232. In these cases the productivity of installation is determined by neutron utilization factor x in a balance equation [4]:

$$\nu + (n,2n)/F + S/F = 1 + \alpha + q + q_{FP} + x + L' \qquad (1)$$

ν - mean number of emitted neutrons per fission,
(n,2n) - number of (n,2n) reactions in the system,
S - external neutron source,

F - number of fissions,
C - number of captures in all the materials,
α - mean ratio of capture/fission in fissile materials,
q - ratio of parasitic capture to fission rate F,
q_{FP} - ratio of captures in fission products (produced in fissile materials) to F,
x - ratio of useful captures (in transmuted nuclides) to fissions F
$L' = L(1 + C/F)$, L - leakage of neutrons

The productivity of installation is determined by the product

$$Px$$

where P is the thermal power output, that is at a given P, - by neutron utilization factor x. The higher is the loading of fissile material, the less is q and usually leakage L, that is with fixed left part of equation (1) the value x grows with the increase of loading and consequently grows the productivity of installation. It was demonstrated in [4] - Case 1 and Case 2, - with different Pu loadings in the blanket, that with the decrease of Pu loading 5 times the flux increased 5 times, but the productivity essentially decreased due to parasitic loss of neutrons and higher leakage.. The other reason, influencing the productivity of accelerator/target/blanket system- the value of external source S, the term S/F in the left side of equation (1) - and this is a new and essential feature of accelerator fed neutron subcritical system as compared to nuclear reactors.

Power output of blanket is determined by the relation

$$P \approx S/(1/K_{eff} - 1)$$

that is proportional to neutron source and inversely proportional to subcriticality level $1-K_{eff}$, $K_{eff}<1$. The level of subcriticality determines safety properties of installation, and at a given power output it determines the level of external source, so that with low level of subcriticality (if it is acceptable by safety considerations) the source level can be decreased together with proton beam current. However from balance equations it follows that the term S/F is also decreased and consequently neutron utilization factor x.

Below an example is presented that demonstrates the influence of source term (and proton beam current) on the conversion ratio and net electric power output of installation. Taking account of electric energy necessary for conversion of electric energy to proton beam energy of accelerator (with an efficiency about 50%) the system with increased proton beam current and consequently higher level of subcriticality is a system with lower net electric power production, but with a higher conversion ratio, that can resolve the problem of closure of fuel cycle including the elimination of wastes produced in the process of nuclear fuel utilization.

THE MODEL

The key parameters of 2 systems were chosen as follows:

Accelerator
Proton energy 1.6 GeV
Proton beam current 0.016 A (System A);
0.100 A (System B)
Target - lead, radius 0.28 m,

Blanket
Height 2.5 m
Buffer layer , thickness 2 cm
Thermal power about 1850 MWt

The fuel (with about 1% Pu content) is supposed to flow inside pressure tubes as solutions or slurries. Fission products are continually removed, except Xe. Number of tubes 250. Tc-99 is

dissolved in heavy water moderator and continually fed up into the system, while its products - Ru isotopes are continually extracted. The rate of fissile material and transmuted material (Tc99) feed up is taken to keep the necessary level of subcriticality. Proton beam intensity and consequently the intensity of external source differed 6.3 times. Subcriticality levels of two systems were different correspondingly. The installation was under operation during 30 years (effective). Conversion ratio C was defined as the ratio of transmuted nuclides of Tc99 (with the consumption of 1 neutron/ 1 nuclide transmuted) to the number of nuclides of Pu (weapons composition) eliminated by fissions and by captures of neutrons.

THE RESULTS OF CALCULATIONS

The results of calculations by a modification of computer code TRIFON [5] are presented in tables 1A, 1B through 4A, 4B (BoC, EoC - begin, end of cycles).

System A

Table 1 A. Thermal power (MWt), K_{eff} and Tc99 loading, dependence on time

Time (yr)	Power (Mwt)		K_{eff}		Tc99 kg	
	BoC	EoC	BoC	EoC	BoC	EoC
0-5	1860.	2079.	0.9743	0.9713	3746.4	1812.4
5-10	1877.	2070.	0.9716	0.9749	2190.5	2214.6
10-20	1842.	1865.	0.9719	0.9720	2413.1	2074.8
20-30	1858.	1993.	0.9719	0.9737	2074.8	1713.9

Table 2 A. Isotopic content (kg) in blanket , dependence on time

Isotope	0	5	10	20	30
PU8	0.0000+0	0.1095+1	0.6901+0	0.4274+0	0.2908+0
PU9	0.2926+3	0.1943+3	0.1326+3	0.1151+3	0.9632+2
PU0	0.1175+2	0.9777+2	0.3389+2	0.4380+2	0.3546+2
PU1	0.4426+0	0.4897+2	0.3448+2	0.2904+2	0.2449+2
PU2	0.0000+0	0.2238+3	0.5745+2	0.8012+2	0.6194+2
AM1	0.0000+0	0.9223+0	0.5913+0	0.4075+0	0.2955+0
AM2	0.0000+0	0.8602-2	0.5999-2	0.4918-2	0.4053-2
AM3	0.0000+0	0.6649+1	0.3413+2	0.2575+2	0.2574+2
CM2	0.0000+0	0.1311+1	0.9137+0	0.7397+0	0.6021+0
CM3	0.0000+0	0.2981-1	0.2067-1	0.1617-1	0.1283-1
CM4	0.0000+0	0.2086+2	0.1604+3	0.2880+2	0.8204+2
CM5	0.0000+0	0.7446-1	0.6074+1	0.4103+1	0.3253+1
CM6	0.0000+0	0.1127+0	0.2536+2	0.5293+2	0.5263+2
CM7	0.0000+0	0.5543-2	0.1780+1	0.3845+1	0.3632+1
CM8	0.0000+0	0.2064-2	0.1274+1	0.6146+1	0.9360+1
BK9	0.0000+0	0.5251-4	0.3596-1	0.1481+0	0.2094+0
CF0	0.0000+0	0.2466-4	0.1854-1	0.8341-1	0.1238+0
CF1	0.0000+0	0.1556-4	0.1128-1	0.4617-1	0.6462-1
CF2	0.0000+0	0.7523-4	0.9071-1	0.6861+0	0.1333+1

Table 3A. Neutron balance for different time points (see eq. (1))

Time, yr	ν	S/F	l	α	q	q_{FP}	x	L'
0 BoC	2.8784	0.0852	1	0.4638	0.0782	0.0000	1.3686	0.0531
5 EoC	2.8917	0.0762	1	1.0496	0.0833	0.1049	0.6505	0.0796
5 BoC	2.8917	0.0844	1	1.0533	0.0833	0.1049	0.6779	0.0568
10 EoC	2.9722	0.0766	1	0.8980	0.0985	0.1078	0.8685	0.0760
10 BoC	2.9722	0.0860	1	0.9022	0.0985	0.1077	0.8859	0.0639
20 EoC	2.9516	0.0850	1	0.8733	0.1093	0.1104	0.8626	0.0809
20 BoC	2.9516	0.0853	1	0.8735	0.1093	0.1104	0.8627	0.0809
30 EoC	2.9457	0.0795	1	0.8900	0.1226	0.1126	0.7948	0.1052

Table 4A. Feed up of fissile material (kg) and transmuted material (kg), transmutation rate ΔTc99, kg, for different time intervals .

Time interval, yr	Pu9	Pu0	Pu1	Tc99	ΔTc99
0 - 5	3175.9	205.0	20.6	-468.0	1466.2
5-10	2431.2	157.0	15.8	1064.4	1040.3
10-20	5470.1	353.4	35.5	1709.8	2047.7
20-30	5456.2	352.5	35.4	1577.5	1938.1

System B

Table 1B. Thermal power (MWt) , K_{eff} and Tc99 loading, dependence on time

Time, yr	Power (Mwt)		K_{eff}		Tc99 kg	
	BoC	EoC	BoC	EoC	BoC	EoC
0-5	1851.	1912.	0.8219	0.8272	5340.7	3346.2
5-10.	1853.	1785.	0.8227	0.8201	3495.7	3337.0
10-15.	1760.	2013.	0.8180	0.8374	3523.7	3432.6
15-20.	1955.	1697.	0.8333	0.8122	3604.2	3218.8
20-25.	1651.	1920.	0.8081	0.8302	3423.7	3093.7
25-30.	1838.	1741.	0.8240	0.8163	3278.9	3157.9

Table 2B. Isotopic content (kg) in blanket , dependence on time, yr

Isotope	0	5	10	15	20	25	30
Pu8	0.1214-7	0.7346+0	0.4055+0	0.4092+0	0.2472+0	0.2456+0	0.2202+0
Pu9	0.2926+3	0.1270+3	0.1291+3	0.1139+3	0.9037+2	0.9580+2	0.9092+2
Pu0	0.1175+2	0.4697+2	0.4763+2	0.3469+2	0.2898+2	0.4098+2	0.3342+2
Pu1	0.4426+0	0.3223+2	0.3316+2	0.2812+2	0.2247+2	0.2418+2	0.2304+2
Pu2	0	0.1566+3	0.6327+2	0.6465+2	0.4809+2	0.7739+2	0.5671+2
Am1	0	0.5957+0	0.4009+0	0.3867+0	0.2504+0	0.2614+0	0.2357+0
Am2	0	0.5669-2	0.5509-2	0.4759-2	0.3689-2	0.3929-2	0.3716-2
Am3	0	0.4355+1	0.3284+2	0.2510+2	0.2184+2	0.2520+2	0.2511+2
Cm2	0	0.8662+0	0.8172+0	0.7141+0	0.5440+0	0.5778+0	0.5438+0
Cm3	0	0.2047-1	0.1787-1	0.1594-1	0.1186-1	0.1229-1	0.1162-1
Cm4	0	0.1548+2	0.1572+3	0.2454+2	0.6896+2	0.4469+2	0.6331+2
Cm5	0	0.5492-1	0.4152+1	0.4228+1	0.3072+1	0.3104+1	0.3294+1
Cm6	0	0.8498-1	0.2498+2	0.5311+2	0.4965+2	0.5511+2	0.5755+2
Cm7	0	0.4589-2	0.1608+1	0.4082+1	0.3618+1	0.3641+1	0.3919+1
Cm8	0	0.1806-2	0.1549+1	0.6461+1	0.9265+1	0.1078+2	0.1156+2
BK9	0	0.5166-4	0.3786-1	0.1704+0	0.2299+0	0.2308+0	0.2588+0
CF0	0	0.2384-4	0.2120-1	0.9528-1	0.1328+0	0.1402+0	0.1563+0
CF1	0	0.1575-4	0.1148-1	0.5357-1	0.7211-1	0.7023-1	0.7922-1
CF2	0	0.7759-4	0.1310+0	0.7975+0	0.1528+1	0.1628+1	0.1880+1

Table 3B. Neutron balance for different time points (see eq. (1)).

Time, yr	ν	S/F	1	α	q	q_{FP}	x	L
0 BoC	2.8785	0.6239	1	0.4746	0.0905	0.0000	1.9404	0.0032
5 EoC	2.8915	0.6040	1	0.9235	0.1203	0.1073	1.3359	0.0086
5 BoC	2.8916	0.6234	1	0.9246	0.1199	0.1072	1.3585	0.0047
10 EoC	2.9496	0.6471	1	1.0671	0.1159	0.1118	1.2961	0.0059
10 BoC	2.9496	0.6563	1	1.0628	0.1154	0.1118	1.3141	0.0019
15 EoC	2.9534	0.5736	1	0.8454	0.1228	0.1105	1.4362	0.0121
15 BoC	2.9534	0.5908	1	0.8462	0.1223	0.1104	1.4576	0.0076
20 EoC	2.9446	0.6806	1	0.8816	0.1440	0.1136	1.4744	0.0116
20 BoC	2.9446	0.6993	1	0.8845	0.1434	0.1135	1.4964	0.0061
25 EoC	2.9420	0.6015	1	0.9636	0.1371	0.1140	1.3142	0.0146
25 BoC	2.9420	0.6282	1	0.9710	0.1368	0.1139	1.3397	0.0088
30 EoC	2.9471	0.6634	1	0.9287	0.1423	0.1148	1.4122	0.0125

Table 4B. Feed up of fissile material (kg) and transmuted material (kg) for different time intervals, transmutation rate ΔTc99, kg, for different time intervals .

Time interval, yr	Pu9	Pu0	Pu1	Tc99	ΔTc99, kg
0-5	2072.7	133.7	13.4	1931.8	3926.2
5-10	3567.4	230.5	23.1	1777.5	1936.2
10-15	2733.5	156.6	15.7	1708.8	1799.9
15-20	2727.5	156.2	15.7	1705.1	2090.7
20-25	3080.2	199.0	20.0	1488.6	1818.6
25-30	3072.0	198.5	19.9	1802.7	1923.7

COMPARISON OF SYSTEMS A AND B

The difference in the loadings of Pu, heavy isotopes and Tc at the beginning and at the end of 30 years period - DifPu, DifHis, DifTc, the amount of consumed Pu - DPu, the amount of transmuted Tc99 - DTc and conversion ratio C are given in table 5.

Table 5. DifPu, DifHis, DifTc - the difference in the loadings of Pu, heavy isotopes and Tc at the beginning and at the end of 30 years period, DPu - the amount of consumed Pu, DTc -the amount of transmuted Tc99, C -conversion ratio

	System A	System B
DifPu	86.3	100.0
DifHis	-93	-67.4
DifTc	2030	2180
DPu	17800	18500
DTc	6490	13500
C	0.881	1.76

Mean power during 30 years of operation

System A 1856 Mwt

System B 1818 Mwt

Under a supposition that the amount of TC99 accumulated in the system per power unit is the same as in LWR the amount of Tc99 accumulated is as follows:

System A 419 kg

System B 411 kg

If one supposes that in the system long-lived FP Tc99, I129, Se, Sm(partly) are to be transmuted then an equivalent amount of transmuted Tc99 is estimated as [6]:

System A 419/0.53 = 790 kg

System B 411/0.53 = 775 kg

If the rest neutrons are spent for breeding, then conversion ratio CR is equal

System A 0.77

System B 1.66

Under a supposition of 30% efficiency of thermal power conversion to electric power and accelerator efficiency 50% the electric power consumed for accelerator feed up is equal

System A 44 Mwt
System B 320 Mwt
and net electric output is
System A 512 Mwt
System B 225 Mwt
From energy balance the loss of energy for Tc-99 transmutation can be estimated as 40 Mev(el)/nuclei.

CONCLUSION

Comparative analysis of two systems with accelerator beam current differing 6.3 times has shown that an accelerator/target/blanket installation with high value of external neutron source can be characterized by a high value of conversion ratio, much exceeding 1. Electric power production in such a system is about twice lower than in the system with small accelerator current. Yet high conversion ratio can provide the agvantages for the development of growing nuclear power industry and for closure of fuel cycle including incineration of long-lived radio-wastes.

REFERENCES

[1] Bowman, C.D. et. el., "Nuclear energy generation and waste transmutation using an accelerator-driven intense thermal neutron source" Nuclear Instruments and Methods in Physics Research A320, 1992, pp. 336-367

[2] Ireland, John R., "Overview of Los Alamos Concepts for Accelerator Transmutation of Nuclear Waste (ATW)",
Paul Scherrer Institute Villigen, Switzerland March 24-26, Los Alamos National Laboratory, 1992

[3] Davidson , J.Wiley, " Status of the Aqueous-Based ATW/ABC Target-Blanket Design and Analyses", Russian-US Meeting on Methods and Data for ABC Chelyabinsk-70, Russia, June 1-3, 1993

[4] Kochurov, B.P., "Some Calculational Results for Transmutation of Plutonium and Wastes in Blankets of Accelerator-Based Systems" , *Contributed Paper Proceedings, Volume 3 of 3 International Nuclear Congress,* October 3-3, 1993, Toronto, Ontario, Canada, C20.4.

[5] Kochurov, B.P., Kwaratzhely, A.Yu., Computer code abstract: TRIFON, VANT, Ser: PHTYAR, 1985, N 4, pp. 45-47.

[6] Galanine, A.D., "Transmutation of Long-Lived Fission Products in a High-Flux Heavy Water Reactor", Preprint ITEP, 132-90, Moscow, 1990.

CHEMISTRY OF PYROPROCESSING FOR NUCLEAR WASTE TRANSMUTATION

John P. Ackerman
Chemical Technology Division
Argonne National Laboratory

Pyrochemical treatment of spent nuclear fuel is an attractive approach for separating the transuranium (TRU) elements neptunium, plutonium, americium, and curium because of its simplicity, diversion resistance, and potentially low cost.

In pyrochemical processing, molten salt electrorefining provides a natural and convenient separation of transuranium elements from uranium and fission products; this separation follows directly from the stabilities of the various chlorides. The TRU trichlorides are all more stable than uranium trichloride. Pure uranium is thus deposited at a solid cathode, even with a large excess of TRU chlorides over UCl_3 in the salt.

Although the uranium-cadmium intermetallic decomposes above 746 K, the TRU metals form stable (~40 kcal/mol) intermetallic compounds with cadmium at the 775 K process temperature. Because of this stabilization, the TRU metals predominate in a liquid cadmium at the 775 K process temperature. Because of this stabilization, the TRU metals predominate in a liquid cadmium cathode. The relative amount (~10% and up) of uranium in the cadmium cathode product is selected by controlling the concentrations of the uranium and TRU chlorides.

Fission products with highly stable chlorides (rare earths, alkalis, alkaline earths, e.g. ^{135}Cs and ^{90}Sr) remain in the salt along with the halogen (^{129}I) and chalcogen anions. We have shown that all these can be removed by mean of ion exchange with zeolite. A; It should be possible to extract and concentrate them relatively easily.

The noble metal fission products (mostly transition metals, including ^{99}Tc and ^{126}Sn) have such unstable chlorides that the metals are not oxidized in the electrorefining process. They remain in the anode container as finely divided metal. This relatively small amount of noble metal fission product rapidly decays to a level where processing for, say, technetium removal would be feasible by aqueous methods.

THE CHEMISTRY OF ABC

Reed J. Jensen
Los Alamos National Laboratory, Los Alamos, NM 87545

ABC stands for accelerator based conversion of Pu. It is a unique approach to Pu destruction that allows for a well controlled and complete burn of Pu as may be required by treaty or policy.

The central idea of the approach is to provide a spallation source of neutrons that allows the operation of a fissioning system without a critical mass and at a K effective less than one Material to be fissioned is suspended in a molten salt medium for high temperature control and on-line removal of neutron absorbing fission products.

This paper discusses the issues associated with the selection and operation of a molten salt chemical system: redox control, product removal, material feed, solubilities, deposition control, and a host of operational procedures.

The salt selected is LiF with either BeF_2 or ZrF_4 as a freezing point depressant. The implications of this selection will be discussed.

An important issue is that of separation and remediation of the salt at the end of the experiment. Oxide precipitation is a method that is simple and perhaps amendable to stepwise separations that could be desirable as an on-line separation method. Precipitants can be chosen, based on thermodynamics, to selectively precipitate certain groups of elements, but not others. The method will be discussed.

ACTINIDE REMOVAL FROM MOLTEN SALTS BY CHEMICAL OXIDATION AND SALT DISTILLATION

James A. McNeese, Eduardo Garcia, Vonda R. Dole, Walter J. Griego
Nuclear Materials Processing-Chloride Systems, NMT-3 MS E511
Nuclear Materials Technology Division, Los Alamos National Laboratory
Los Alamos New Mexico, 87545

Abstract

Actinide removal from molten salts can be accomplished by a two step process where the actinide is first oxidized to the oxide using a chemical oxidant such as calcium carbonate or sodium carbonate. After the actinide is precipitated as an oxide the molten salt is distilled away from the actinide oxides leaving a oxide powder heel and an actinide free distilled salt that can be recycled back into the processing stream. This paper discusses the chemistry of the oxidation process and the physical conditions required to accomplish a salt distillation. Possible application of an analogous process sequence for a proposed accelerator driven transmutation molten salt process is also discussed.

Introduction

Plutonium metal preparation and purification processes have been primarily performed by pyrochemical methods. These methods are typically performed in molten salts, such as equi-molar sodium chloride potassium chloride (NaCl-KCl) and calcium chloride ($CaCl_2$). The processes include the preparation of plutonium metal by the direct calcium reduction of plutonium oxide PuO_2 in calcium chloride (DOR) and the electrorefining (ER) of the prepared metal in a NaCl-KCl salt system. An americium separation process called molten salt extraction (MSE) was used to oxidize ingrown americium with plutonium ions in molten salts systems. During the pyrochemical processing of the plutonium, large volumes of spent pyrochemical salts were generated that required recovery of the actinide species contained in the salt as a result of the pyrochemical process. The traditional method of recovery of the actinides has been aqueous dissolution of the salts with subsequent recovery of the actinide by ion exchange of the dissolved plutonium salt solution followed by precipitation of the actinide from the ion exchange eluate. The aqueous systems were very efficient in the actinide recovery, but corrosion of glove box systems and large volumes of acidic solutions were required to treat the actinide residue.

In order to minimize waste and increase process yields, Los Alamos National Laboratory has maintained a pyrochemical process development effort to investigate molten salt techniques for the removal of actinides from pyrochemical residues and to recycle the salt reagents whenever possible. Initial attempts to recover actinides from the molten salts included adding a reductant to the molten salt and recovering the stripped product as a metal button. The reduction stripping although somewhat successful did not completely remove the actinides from the salt due to problems with metal coalescence and reduction of the salt matrix with the reductant. Metal coalescence was inhibited by the presence of oxide films on the metal product resulting from moisture and oxides contained in the processed salt matrix. Another drawback to reduction processes was the generation of pyrophoric metals in the stripped salt which were not acceptable for disposal at the Waste Isolation Pilot Plant (WIPP). WIPP Waste Acceptance Criteria (WAC)

restricted the amount of free metals allowed in discarded salts destined for WIPP. A process was developed whereby, oxygen was introduced into the molten salt to react with the free metals in solution and precipitate them as oxides, thereby, inerting the salts for WIPP WAC. It was found that the sparging process was also effective in oxidizing actinide chloride species to the oxide or oxychloride. Most of actinide metal in the oxygen sparged system remained as metal in the precipitated oxide layer that was formed during the precipitation process. Oxygen sparging was somewhat effective in actinide removal, but only addressed the available soluble species in the melt. Alternative methods for oxidizing actinide components to the oxide were investigated.

Chemical Oxidation

In order to convert the all the actinide species to the oxide, various oxidizing agents were added to salt melts. Sodium carbonate and calcium carbonate were found to be effective in converting the actinides to the oxide which are insoluble in the molten salt. The following reactions are summarized as to the chemistry that occurs in a system with plutonium metal plutonium chloride and plutonium oxychloride in an equi-molar NaCl-KCl salt.

$$3\ Pu + 2\ Na_2CO_3 \rightarrow 3\ PuO_2 + 2\ C + 4\ Na \quad (1)$$

$$3\ PuCl_3 + 2\ Na_2CO_3 \rightarrow 3\ PuO_2 + 4\ NaCl + 2\ C + Cl_2 \quad (2)$$

$$2\ PuOCl + Na_2CO_3 \rightarrow 2\ PuO_2 + CO + 2\ NaCl \quad (3)$$

$$Cl_2 + 2\ Na \rightarrow 2\ NaCl \quad (4)$$

$$Na_2CO_3 + 2\ C \rightarrow 2\ Na + 3\ CO \quad (5)$$

The overall reaction for 2 moles of PuO_2 formed with reasonable concentrations of the plutonium metal, plutonium trichloride and plutonium oxychloride is:

$$1.26\ Pu + 0.43\ PuCl_3 + 0.31\ PuOCl + 1.69\ Na_2CO_3 \rightarrow 1.37\ CO + 1.80\ Na + 0.32\ C + 1.58\ NaCl + 2.00\ PuO_2 \quad (6)$$

In the calcium carbonate system the following reactions were predicted:

$$2\ PuCl_3 + 3\ CaCO_3 \rightarrow 2\ PuO_2 + 3\ CaCl_2 + 2\ CO_2 + CO \quad (7)$$

$$Pu + 4\ CaCO_3 + 1\ CO_2 \rightarrow 5\ PuO_2 + 4\ CaO + 5\ C \quad (8)$$

$$2\ PuOCl + CaCO_3 \rightarrow 2\ PuO_2 + CaCl_2 + CaO \quad (9)$$

$$CO_2 + C \rightarrow 2\ CO \quad (10)$$

Overall reaction: Based on 2.00 moles of plutonium in acceptable concentration is listed below

$$1.26\ Pu + 0.43\ PuCl_3 + 0.31\ PuOCl + 1.79\ CaCO_3 \rightarrow$$
$$0.69\ CO + 1.10\ C + 0.80\ CaCl_2 + 0.99\ CaO + 2.00\ PuO_2 \quad (11)$$

Similar reactions will occur with americium compounds.

In both sets of reaction chemistries, graphite is formed and the only predicted plutonium species is plutonium dioxide. Experimental results on equi-molar NaCl-KCl with plutonium metal, oxychloride and plutonium trichloride present in the salt were successful in converting the majority of the plutonium into the oxide. Similar results were obtained with the calcium chloride salt system. In both cases the objective was to convert all of the plutonium to the oxide which is the least volatile species for a subsequent distillation process. To verify the predicted reactions, chemical oxidation experiments were performed by incremental additions of the oxidizing compounds. Grab samples of the molten salt mixture were obtained after each addition by removal of the molten salt through a sample tube. Extent of reaction of the soluble plutonium species was obtained in a stepwise manner. Table 1. is a summary of one of the sets of experiments with carbonate addition.

Table 1. Chemical Analysis of Carbonate Oxidation Samples

Sample ID	Oxidant	Oxidant wt. Added (g) Cum. Total.	Calculated Soluble Pu Conc. (ppm)	Analyzed Pu Concentration (ppm)	Analyzed Am Concentration (ppm)
199S1	Na_2CO_3	0	22323	7130	8.45
199S2	Na_2CO_3	20	748	7370	9.68
199S3	Na_2CO_3	40	0	536	0.512
199S4	Na_2CO_3	60	0	677	0.321
200S1	$CaCO_3$	0	22437	170000	199
200S2	$CaCO_3$	20	12265	8440	11.9
200S3	$CaCO_3$	40	2095	126	0.16
200S4	$CaCO_3$	60	0	53.9	0.063
Top phase	$CaCO_3$	60		18.5	0.023
Bottom phase	$CaCO_3$	60		110000	107
201S1	Na_2CO_3	0	22109	20400	24.5
201S2	Na_2CO_3	10	11424	9650	12.9
201S3	Na_2CO_3	20	741	5300	7.27
201S4	Na_2CO_3	30	0	672	0.59
201S5	Na_2CO_3	40	0	609	0.63
Top phase	Na_2CO_3	40		58	0.064
Bottom phase	Na_2CO_3	40		74000	76

Salt Distillation

Distillation is based on a very simple physical process where more volatile components are removed from less volatile components. A process that uses the extremely large differences in vapor pressure between the chloride salts and the actinide oxides has a likelihood of success.

The basis for this separation is the large difference in vapor pressure between the chloride salts and actinide oxides. From the kinetic theory of gases it can be shown that the rate of the mass of a gas incident on a unit area per unit time is

$$W = CP\left(\frac{M}{2\pi RT}\right)^{\frac{1}{2}} \quad (13)$$

Where

W = gas incident rate (g cm $^{-2}$ sec^{-1})
M = molecular rate (g mol $^{-1}$)
R = gas constant (8.325 x 10 ^{7} ergs K^{-1} mol $^{-1}$)
T = Temperature (K)
P = Vapor pressure at temperature T (torr)
C = Conversion factor (1333 dyne cm $^{-2}$ torr $^{-1}$)

Employing the units shown in parentheses the equation can be rewritten as:

$$W = 0.0583P\left(\frac{M}{T}\right)^{1/2} \quad (14)$$

If the temperature of the surface the gas strikes is much colder than the temperature of the gas vapor then condensation will occur with a sticking coefficient of 1. Under these conditions the condensation rate is equal to the rate gas molecules strike the surface. Therefore, the amount of material deposited can be estimated by equation (14). In the case of distillation of molten salts the condenser temperature will be much lower than the temperature at which the material is evaporating so that equation (14) is applicable. Calculations can be made for the rate of deposition of this molten salts system since the vapor pressure of the various components with one exception is known. Table 2 lists the vapor pressures of compounds of concern in the discussed molten salt system.

Table 2 Log Vapor pressure (torr) of pyrochemical salt components

Compound	850 °C	950 °C	1050 °C
NaCl	-0.063	-0.64	1.2
KCl	0.23	0.90	1.5
$MgCl_2$	0.27	0.97	1.6
$CaCl_2$	-2.9	-1.9	-1
CaF_2	-7.7	-6.1	-4.7
Pu	-8	-7	-5
$PuCl_3$	-1.8	-0.86	-0.086
PuO_2	-15.7	-13.5	-11.7
PuOCl	*	*	*

* The vapor pressure of PuOCl is not known but we have preliminary experiments that indicate a vapor pressure similar to that of plutonium metal.

The extremely low values for calcium fluoride and plutonium oxide have not been measured at these temperatures and the values listed are extrapolations from higher temperature data. It is obvious from these vapor pressures that the best separation can be achieved between plutonium dioxide and the chloride salts. Similar values are indicated for vapor pressure of americium oxide. The distillation process is therefore most amenable to systems where the actinide compounds have been oxidized prior to the distillation operation. In this case, it is accomplished by the carbonate addition mentioned earlier.

Distillation Rate

Equation (14) can be used to give a more quantitative value for the possible separation as well as the length of time needed to run the process on a practical scale. Table 3 lists the rate of deposition of the various compounds listed in table 1. It should be noted that these are calculated rates and in distillation processes actual rates have been found to be slower and sometimes slower by some orders of magnitude, nevertheless it appears that all of the chlorides salts, except calcium chloride, can be distilled at acceptable rates below 900°C.

Table 3 Deposition rate (g hr^{-1}) from 100 cm^2 area

Compound	850°C	950°C	1050°C
NaCl	4100	20000	75000
KCl	9100	41000	140000
$MgCl_2$	11000	55000	200000
$CaCl_2$	9	85	560
CaF_2	$10^{-3.9}$	$10^{-2.3}$	$10^{-1.0}$
AmO_2	10^{-11}	10^{-9}	$10^{-7.2}$
PuO_2	10^{-12}	$10^{-9.6}$	$10^{-7.8}$
Pu	$10^{-3.7}$	$10^{-2.4}$	$10^{-1.4}$

The distillation process has been used successfully to distill NaCl-KCl salt away from actinide oxides by heating the salt system above the melting point and applying moderate vacuum to the molten salt. The salt is distilled away from the actinide oxide and is collected in cool areas of the furnace. Experimental results on actual plutonium pyrochemical process residue salts shows very low levels of actinide in the distilled portion and the distillation "heel" is essentially clean of salt as evidenced by a pourable powder and chloride chemical analysis. We are currently developing the distillation process in conjunction with the chemical oxidation process to remove the molten salt in the system as a below low level waste discard. In our actinide system that means that the level of plutonium in the salt is less than 0.2 ppm and the americium level is below .03 ppm. The success of the process will allow for concentration of actinide oxides in a storable form and the removal of large volumes of salt as low level waste.

As part of the molten-salt breeder reactor (MSBR) program, a low pressure distillation process was developed at Oak Ridge National Laboratory to remove rare earth fission products from a lithium fluoride, beryllium fluoride, and zirconium fluoride salt stream.[1] This process was demonstrated on a 12 liter batch size of salt with the rare earth fission products remaining in the distillation heel. The distilled fluoride salt stream was intended for recycle. As a alternative method, the combination of a oxidation reaction followed by distillation as described above may

minimize the amount of salt in the heel leaving the rare earth fission products and all other oxidized species. An analysis of oxidation of metals and fluoride compounds in the designated fluoride salts matrix could be performed with a hoped for separation of fission product oxides from the fluoride salt distilled product. An oxidation process for fluorides has not been investigated, but when a melt containing only LiF BeF_2 and UF_4 is treated with a reactive oxide (such as H_20) precipitation of transparent ruby crystals of $UO_{2.00}$ results. In the presence of ZrF_4, UO_2 only precipitates after the ZrF_4 is oxidized to ZrO_2 and the concentration of ZrF_4 approaches that of UF_4. [2] It is obvious that this system is sensitive to the oxide concentration and the amount of precipitated ZrF_4 in the molten salt.

Acknowledgments

The work described here-in is sponsored by the DOE office of Technology Development and Stockpile Support.

References

1. Hightower, J. R. Jr, McNeese, L. E., "Low Pressure Distillation of Molten Mixtures of Lithium Fluoride, Beryllium Fluoride, and Zirconium Fluoride for Removal of Rare-Earth Fission Products", *Industrial Engineering Chemical Process Design Development*, Vol. 12, No 3, 1973, pp. 232-236.

2. Grimes, W. R. "Molten Salt Reactor Chemistry", *Nuclear Applications & Technology*, Vol. 8, February 1970, pp. 137-155.

The Possibility of Fuel Cycle Design for ABC/ATW Complex with Molten Fuel on LiF-BeF_2 Basis

V.S. Naumov and A.V. Bychkov
Federal Scientific Center of Russia Research Institute of Atomic Reactors (RIAR)
Russia, Dimitrovgrad 433510

Abstract. The experience gained in the field of the development of molten salt reactors (MSR) can be made a basis of chemical processing of the ABC/ATW liquid fuel.

The following combination of two processing principles are proposed for the ABC/ATW fuel (LiF-BeF_2-$PuF_{3,(4)}$ - MAF_n):
- continious removal of radioactive gases, volatile impurities and "noble fission products";
- portion-by-portion electrochemical processing with removal of rare earth elements and some other fission products at an autonomous plant.

After processing the fuel salt is brought back to the blanket of the ABC/ATW complex.

The analysis of information previously published in different countries allows for a safe assumption that the ABC/ATW fuel cycle with liquid fuel salt is feasible and can be demonstrated experimentally.

INTRODUCTION

One of the ways for handling the problem of utilization of the excess of plutonium and long-lived actinides is creation of electro nuclear power plants using accelerator and liquid fuel blanket.

The investigations performed in the Oak Ridge National Laboratory (ORNL) within the framework of these projects demonstrated the principal feasability of conversion methods and liquid salt fuel processing.

On developing the ABC/ATW fuel cycle the following issues investigated within the MSRE and MSBR projects should be taken into account:
- study on physical-chemical properties of LiF-BeF_2 molten salts/1,2/;
- study on the behavior of molten salt fuel in reactor /1,3/;
- engineering development on some issues of fuel salt processing (e.g. gas removal/1,4/).

1. FUEL CYCLE REQUIREMENTS

Untill now only one complex example of the nuclear power system fuel cycle with molten salt fuel has been described elsewhere - this is the MSBR project /1,5/.

The principles of its structure are similar in many respects with those of the LWR fuel cycle which fuel was used to be processed completely enough. The MSR fuel cycle aimed at the following technological tasks:
- removal of noble gases from fuel;
- removal of Pa and rare earths;
- removal of uranium for further usage.

This presentation peraues the following aims:
- definition of the knowledge level for further development of fuel processing process based on LiF - BeF_2;
- development of the preliminary flow-sheet of fuel processing based on LiF - BeF_2 .

2. PROPOSALS ON THE ABC/ATW FUEL CYCLE

The external ABC/ATW fuel cycle can be realized under several options.

From the point of view of the extent of fuel processing the following three technological options are possible:

A. Complete fuel salt processing with sufficiently high purification from fission products;
B. Partial fuel salt processing. In this case two approaches are possible:

- only removal of radioactive gases, noble, seminoble metals and solid particles from liquid salt fuel;
- removal of radioactive gases, noble metals, solid particles and reduction of the neutron poison content.

C. No fuel salt processing. Salt processing will be performed after a long-term ABC/ATW operation without continuous processing.

From technological standpoint the following two approaches to fuel salt processing are possible:
- continuous processing of the flux passing through the processing circuit (as it was proposed for MSBR/1/ and DMSR/6/);
- processing of salt portions at a special facility on their withdrawal from the circuit and returning back to the circuit afterwards.

The aim of processing is provision of the shortest technological way for restoration of nuclear-physical characteristics of fuel.

1. Fuel processing with a sufficient decontamination level from the reactor physics standpoint (removal of corrosion-active impurities and neutron poisons). Usage of fuel with a low level fission products decontamination decreases the probability of unauthorized use of fissile materials.

2. Provision of the minimum radioactive waste (RAW) volume in the fuel cycle as a whole and at its individual stages. Processing of irradiated fuel should lead to the formation of waste in compact form suitable for storage and disposal in small volumes.

The external MSBR fuel cycle flow-sheet, developed in ORNL/6/, is well known. Fig. 1.1 presents the flow-sheet . This flow-sheet practically copies that of the MSBR project.

The flow-sheet was developed based upon the task of complete processing of LiF-BeF_2-ThF_4 fuel salt with an increased plutonium content.

On fuel reprocessing several different methods are used for treatment of the melt:
- fluorination with removal of UF_6 (implying the availability of a special zone in the system for gas preparation, absorption and utilization of UF_6 with absorption and recirculation of HF);
- extraction of some fission products and fissile components with Bi-Li alloy followed by the extraction into fresh fuel;
- treatment and removal of rare earths using the above alloy and molten chloride;
- hydrofluorination of the alloy.

From the uptodate standpoint such a variety of methods is the main disadvantage of the flow-sheet resulting in:
- a lot (from 15 up to 30) of analytical monitoring places.

In addition it should be noted that the line process application in molten salt technology has been developed much worse than that of batch-by-batch processes. It will accomplish the realization of the irradiated fuel processing technology in remote conditions since they require the equipment capable of a long-term continuous operation. The development of such an equipment is a difficult task at the present level of developments on the high-temperature processes.

Partial fuel processing can provide the plant operation, provided the activity in the blanket will gradually increase due to generation of rare earths fission products and Cs, Sr, Rb in fuel.

In this case two options of the technological approach are possible:

The first option: only removal of radioactive gases, noble and half-noble fission products and also solid particles from the molten fuel salt flow.

Gaseous fission products are removed by purging with pure inert gas using the devices developed for the MSRE project /7/. In this case it is recommended to use argon instead of helium.

Removal of noble and half-noble fission products is required to prevent their deposition on metal and graphite surfaces inside the reactor and heat exchanger.

The following methods can be used for this purpose:

The first one is interaction between fuel and chips (or another crushed form) of more active metal as melt components. The unit, where the deposition takes place, can be renewable, besides, it can be based on the "cold trap" principle, as it has been developed in the fast reactor technology for removal of oxides and fission products from sodium coolant /8/.

Fig. 1.1.

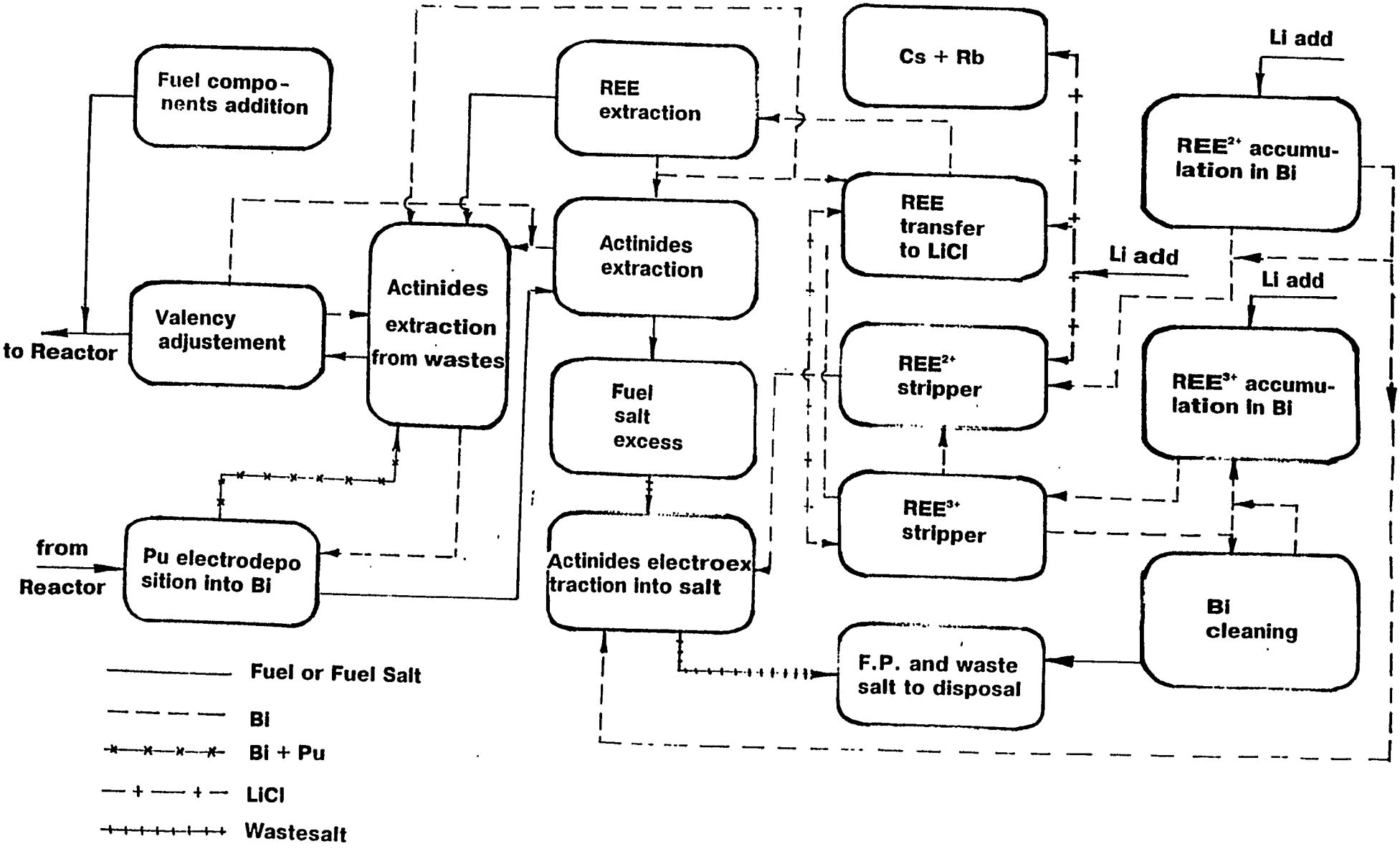
Fuel compo-
nents addition
REE
extraction
Cs + Rb
Li add
REE²⁺ accumu-
lation in Bi
REE
transfer
to LiCl
Actinides
extraction
Li add
Li add
Actinides
extraction
from wastes
Valency
adjustement
to Reactor
REE²⁺
stripper
REE³⁺ accumu-
lation in Bi
Fuel
salt
excess
REE³⁺
stripper
from
Reactor
Pu electrodepo
sition into Bi
Actinides electroex
traction into salt
Bi
cleaning
F.P. and waste
salt to disposal
Fuel or Fuel Salt
Bi
Bi + Pu
LiCl
Wastesalt

193

Another method is the usage of finely dispersed plutonium alloy for the exchange interaction. In this case plutonium will replace noble and half-noble fission products in fuel salt.

The third method is introduction of finely divided suspensions into the cooled fuel and their separation from the melt.

All these methods provide decontamination of fuel salt from harmful fission products and development of simple, compact and efficient equipment for their technical realization. Basically, this fuel cycle will decontaminate fuel from the following fission product groups:

Noble gases - Kr, Xe;

Noble and seminoble metals - Zn, Ga, Ge, As, Se, Nb, Mo, Tc, Ru, Rh, Pd, Ag, Cd, In, Sn, Sb and Te;

Corrosion products - Ni, Fe and Cr.

In the case of realization of this procedure it is useless to tackle the decontamination level of fuel from the above-listed impurity groups since the determining factor of the decontamination efficiency will be the residual amount of the element in the melt. The removal rate of these impurities will depend on the velocity of fuel travelling through the processing units.

The described procedure can be denoted the one without fuel processing.

The second option: removal of radioactive gases, noble metals, solid particles and reduction of the content of rare earth neutron poisons (Fig. 1.2).

The first two stages of this option are similar with those of the previous one (Fig. 1.1): removal of gases and noble fission products.

But in this option it is proposed to direct a portion of fuel salt to processing performed at a separate facility portion-by-portion. The facility can be isolated and receive fuel both in liquid and solid form.

The facility should include at least two following devices.

The first one is designed for electrolytic precipitation of all actinides (and, evidently, some rare earths and fission products) into the liquid metal melt that need not be based upon Bi. The salt from this apparatus (the electrolyzer) is brought to the second device designed for the removal of rare earths from fuel salt. The procedure can be based upon two methods:

- precipitation of the rare earths oxides with an inert oxide matrix followed by separation of solid particles from the melt and electrochemical treatment of the melt aimed at the removal of oxygen-bearing impurities;
- exchange interaction with the alloy containing Li until the rare earths are completely removed.

After the purification the salt is returned to the first apparatus again for the electrochemical separation of actinides into the fuel salt, more electropositive elements (for these system they are, for instance, Zr, Mo, Fe etc.) being accumulated in the alloy.

After processing the fuel salt returns to the blanket circuit of the ABC/ATW plant again.

After the complete removal of actinides the metal alloy in the first apparatus should be periodically removed from it for disposal or electrochemically treated to transfer the accumulated fission products into the melt. The melt with the fission products should be processed in the second apparatus until they are separated there in the form of compact oxide precipitates or another metal alloy.

Such technology will make it possible to maintain a particular content of fission products and rare earths that will depend on the molten fuel volume subjected to reprocessing.

The range of the expected separation factor of Pu from rare earths is **20 - 50** and that of the salt from impurities is **100-500.**

From the data obtained it is impossible to define exactly the degree of separation of Am and Cm from rare earths but it is expected to be from 2 to 5 times over. In the case the alloy will be chosen having the highest selectivity of separation of Am and Cm from rare earths Although, there are no sufficient data in literature to estimate this separation precisely.

This flow-sheet provides for the use of electrochemical methods allowing the development of the compact technology and elimination of the variety of the processing methods applied.

Thus, there is a number of methods providing, by that way or another, realization of the ABC/ATW fuel cycle with the following fuel compositions: LiF-BeF_2-PuF_3(PuF_4) and LiF-BeF_2 -PuF_3(PuF_4)-MAF_n (where, MAF_n - NpF_3, NpF_4, AmF_3 and CmF_3).

Fig. 1.2.

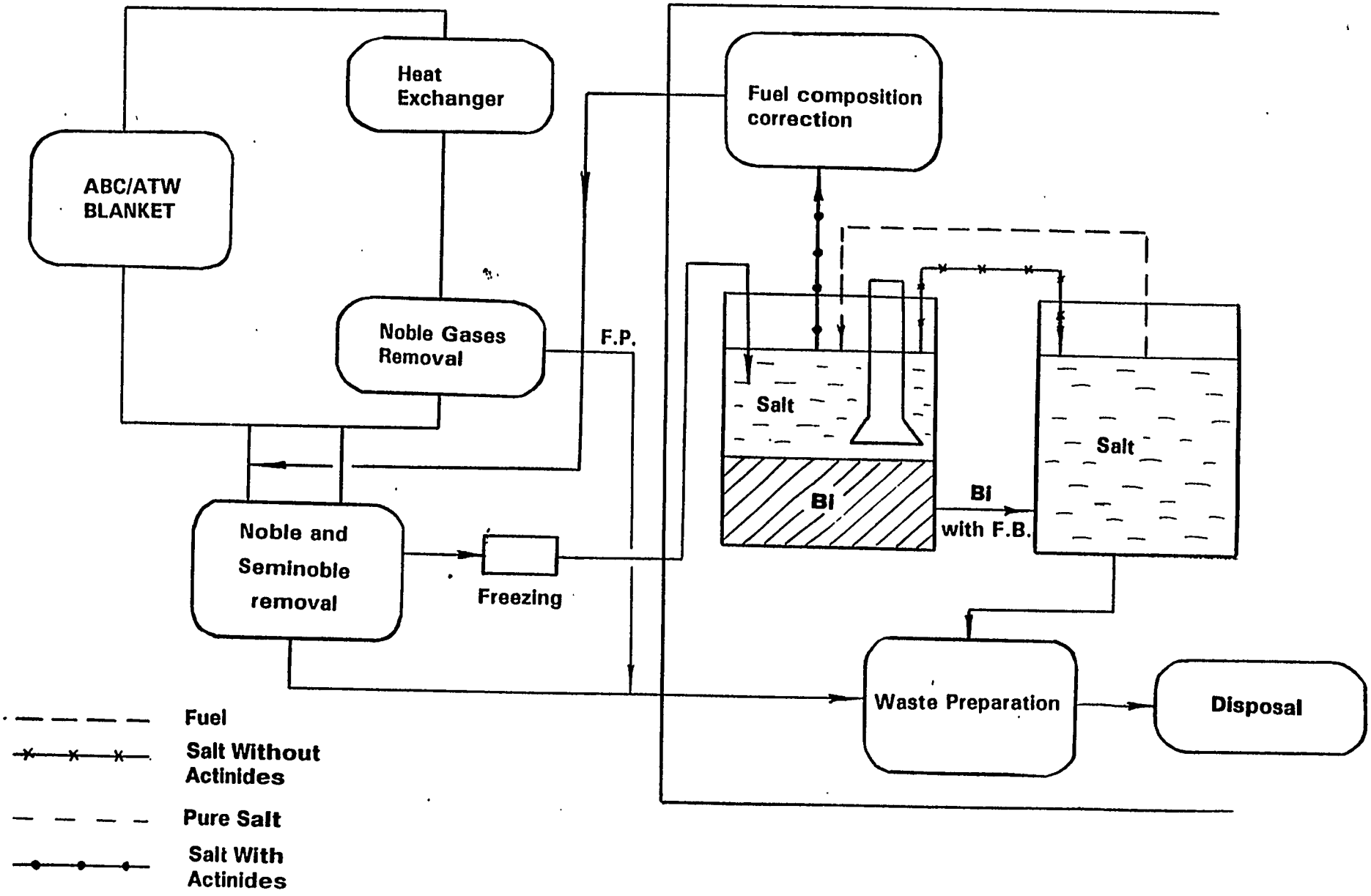
Heat Exchanger
ABC/ATW BLANKET
Noble Gases Removal
F.P.
Noble and Seminoble removal
Freezing
Fuel composition correction
Salt
Bi
Bi with F.B.
Salt
Waste Preparation
Disposal
Fuel
Salt Without Actinides
Pure Salt
Salt With Actinides

3. PROPOSALS ON FURTHER RESEARCH

The greatest scope of fundamental research should cover the development of chemical processes for fuel processing.

In the literature lacks the required data on Am and Cm behavior in molten fluorides and low-melting metal alloys. The data volume on Pu and Np behavior is not sufficient for the comprehensive analysis of the system.

To perform further research and development of the actinide and fission product separation processes by electrochemical or exchange methods the following experimental data are required:

- electrochemical properties of the actinide fluorides and some rare earths in $LiF-BeF_2$ melt;
- actinide fluorides behavior on their interaction with low-melting metals (Bi, Cd, Pb, Zn and Sn) in the $LiF-BeF_2$ environment;
- characteristics of the actinide alloy-formation with low-melting nonferrous metals (solubility in the alloying agent and activity coefficient).

These data will make it possible to choose the best system for fission products and actinides separation and on its basis to develop the fuel salt processing procedure.

Although, at the first stage it is possible to perform a range of experiments providing sufficient data for the developing of the processes. The data obtained on the equilibrium distribution of the elements in the systems with a liquid Li alloy and low-melting metal (Bi, Cd, Pb, Sn and Zn) will provide for calculation of the required distribution coefficient values of the elements for a particular system.

CONCLUSIONS

The consideration and analysis of the information published with regard to the fulfillment of the programs on the MSR research and the data on the other molten fluorides investigations allow for the following conclusions:

- investigations confirming the principal realization of the molten fluoride fuel cycle have been performed and described;
- information on the transuranium chemistry is not sufficient but the general approaches developed in the ORNL can be applied to the ABC/ATW fuel;
- obtaining of the adequate data for the primary estimation of the fuel cycle processes will not require a great experimental program;
- on obtaining the data on the transuranium element chemistry (solubility of fluorides in the melt and alloys-melt interaction) the calculated estimation of the fuel cycle processes can be completed;
- other issues are, mainly, of technical and engineering character;

There are strong grounds for believing that the ABC/ATW fuel cycle using molten $LiF-BeF_2$ fuel can be realized and demonstrated experimentally.

ACKNOWLEDGMENTS

This work was performed by supported of the U.S. LANL under contract 5058L0013-9Y.

REFERENCES

1. Rosental M.W., Haubenreich P.N., Briggs R.B. The Development Status of Molten-Salt Breeder Reactors, ORNL-4812, USA, 1972.
2. Гримс У.Р. Проблемы подбора материалов для реакторов с расплавленными солями - В кн.: Материалы и горючее для высокотемпературных ядерных энергетических установок.- М.: Атомиздат, 1966,с.69-100.
3. Grimes W.R. Molten-Salt Reactor Chemistry.- "Nucl. Appl. Technol.",8, N2, p.137-155, 1970.
4. Molten-Salt Reactor Program, 1976, ORNL-5132.

5. Блинкин В.Л., Новиков В.М. Жидкосолевые ядерные реакторы. -М.:Атомиздат, 1978. -112с.
6. J.R.Engel, W.A.Rhoades, W.R.Grimes. Molten-Salt Reactors For Efficient Nuclear Fuel Utilization Without Plutonium Separation.-"Nucl. Technol.", **46**, N11, p.30-43,1979.
7. Новиков В.М., Игнатьев В.В., Федулов В.И., Чередников В.Н. Жидкосолевые ЭУ: перспективы и проблемы.-М.: Энергоатомиздат, 1990. -192с.
8. Чечеткин Ю.В., Кизин В.Д., Поляков В.И. Радиационная безопасность АЭС с быстрым реактором и натриевым теплоносителем.- М.: Энергоатомиздат, 1983. - 128с.

Centrifugal Separation for Miscible Solutions: Fundamentals and Applications to Separation of Molten Salt Nuclear Material

Ning Li,[1,3] Roberto Camassa,[2,3]
Robert E. Ecke,[1,3] and Francesco Venneri[4]

[1] *Materials Science and Technology Division MST-10*, [2] *Theoretical Division T-7*,
[3] *Center for Nonlinear Studies*, and [4] *ADTT*
Los Alamos National Laboratory, Los Alamos, NM 87545

Sept. 19, 1994

Abstract

We report on the physical separation of dilute solutions using centrifugal techniques. We use numerical simulations of the diffusion and sedimentation dynamics of centrifugation to model the approach to an equilibrium concentration profile. We verify experimentally the equilibrium profiles for aqueous solutions of different salts under rotation at 25000 rpm corresponding to centrifugal accelerations of about 57,000 g and 75,000 g in two different commercial centrifuges. These measurements provide ratios of sedimentation and diffusion coefficients. We show experimental results for the dynamics of separation that confirm the predictions of the theoretical model. We also measure the mass diffusion coefficient for several solutions. Although the relaxation to equilibrium is long, we have determined a method for efficiently extracting enriched components from a ternary mixture based on fast dynamics at early times. These dynamics are modeled in numerical simulations with realistic fluid parameters. Based on these studies we show that a multistage centrifugal separation process could provide efficient physical separation of actinides and fission products from a molten-salt solution in proposed transmutation/energy-production systems. We consider technical issues in the design of such a separation system.

1 Introduction

There is a critical need in both the United States and the international community for safe, efficient energy production and transmutation of nuclear waste. A novel scheme that holds great promise for such an energy source is a molten-salt based, accelerator-driven nuclear reactor[1]. It has advantages over conventional reactors in its inherently safe design and potentially low waste stream. Many of the fundamental questions involving the feasibility of such a reactor have been addressed but several pose significant challenges. One is the purification of the reactor blanket of fission products which can poison the nuclear reaction. For a number of reasons including nonproliferation issues, physical separation methods are preferred over more conventional chemical techniques. Recently, Bowman[2] has suggested that solutions could be separated using strong centrifugal forces to produce significant concentration gradients in the molten salt solutions. His analysis showed that the equilibrium concentrations obtainable from centrifugal forces having a magnitude of about 10^5 g would provide adequate separation efficiency. Such centrifugal forces have been realized in biological centrifuges[3] and scaling them up to larger containers should be technologically achievable. The major unresolved question regarding this method was the dynamics of concentration evolution and the potentially destabilizing effects of adverse temperature gradients due to radioactive heating. In addition, few experiments exist on the equilibrium profiles and virtually none on the dynamics of centrifugal separation. In order to firmly establish the legitimacy of this physical separation technique, experiments must verify the theory and the dynamics must be addressed.

In this paper, we present measurements, theory, and modeling which focus on these issues. We find experimental profiles that match the theoretically-predicted ones. Our theoretical and numerical modeling provides a good picture of the separation process and suggests an alternative scheme to provide efficient separation that does not require waiting for equilibrium concentration profiles to develop. We have made preliminary experimental tests of the relaxation dynamics and find reasonable agreement with our models. Based on our analysis and experiments we have determined a method for centrifugal separation of molten-salt based nuclear materials. The proposed procedure does not separate actinides during the intermediate steps. Such a process would certainly have applications in other areas of nuclear materials handling and disposal. Although we have to a large degree established the fundamentals of centrifugal separation of molecular solutions, much work on the technological challenges remains.

2 Theoretical model

The basis for a theory of molecular separation is the equations of mass and heat transport[4]. Since we have established that the thermally induced hydrodynamic instabilities can be suppressed through careful design[5], and that the coupling between the concentration and temperature gradients (Soret effect[6]) is small, we will treat only the isothermal centrifugation case in this paper.

The basic equation for isothermal centrifugation is the Lamm differential equation:

$$\frac{\partial c}{\partial t} = \frac{1}{r}\frac{\partial}{\partial r}\left(rD\frac{\partial c}{\partial r} - s\Omega^2 r^2 c\right) \tag{1}$$

where the mass diffusion coefficient D and the sedimentaion coefficiant s are assumed to be independent of the radial position r. The boundary conditions are such that there is no mass flux across the end surfaces:

$$\frac{1}{c}\frac{\partial c}{\partial r}\Big|_{r_i} = \frac{s\Omega^2}{D} r_i, \quad i = 1, 2. \tag{2}$$

where r_1 and r_2 correspond respectively to the inner and outer radii of the cylinder. The steady-state solution to (1) is known as the Archibald solution and describes the equilibrium concentration profile:

$$\frac{c(\varrho)}{c_0} = \frac{(\varrho_2 - \varrho_1)}{[exp(\varrho_2) - exp(\varrho_1)]} exp(\varrho) \tag{3}$$

where $\varrho = s\Omega^2 r^2/2D$, $\varrho_i = s\Omega^2 r_i^2/2D$ for (i = 1,2). Without further knowledge of the sedimentation dynamics, this equilibrium profile can be used to estimate the ratio of enrichment a centrifugation unit can achieve, which in turn will determine the number of centrifugation stages needed to reach a set separation goal.

The relation between s and D can be complicated in the most general case. However, for dilute nonelectrolyte binary systems, the widely used Svedberg equation holds,

$$\frac{s}{D} \equiv \rho k_p/(pc) = \frac{M_s(1 - \rho_0/\rho_s)}{RT} \tag{4}$$

where M_s and ρ_s are the molecular weight and density of the solute, ρ_0 is the density of the pure solvent, and R is the gas constant. The nonideality correction is a multiplicative factor of $1/(1 + c_s(\partial \ln y_s/\partial c_s)_{T,p})$ on the left-hand side, where y_s is the activity coefficient of the solute and c_s is the concentration of the solute. This correction can be neglected at this stage of consideration given that the concentrations in the carrier molten salt are small.

A useful further simplification of the Lamm differential equation is to take advantage of the Svedberg equation. We nondimensionalize (1) by using a characteristic mass diffusion time $\tau \equiv t/(d^2/D)$ and a characteristic length $\xi \equiv r/d$ where d is the annular gap distance $r_2 - r_1$:

$$\frac{\partial \theta}{\partial \tau} = \frac{1}{\xi}\frac{\partial}{\partial \xi}\left(\xi\frac{\partial \theta}{\partial \xi} - S\xi^2\theta\right) \tag{5}$$

C-20

where $\theta \equiv c/c_0$ and $S \equiv (s/D)\Omega^2 d^2$ is a dimensionless number. This description can be used to classify the numerical simulation results in one combined parameter S for a given geometry. A very useful result from this classification can be stated as the following: a higher $S \equiv (s/D)\Omega^2 d^2$ results in a steeper concentration gradient, and a larger D with a fixed S leads to a higher sedimentation speed. We will use this criterion in the design section.

The time scale in (5) is inversely proportional to D which can be determined from an independent experiment. We discuss briefly the one-dimensional solution of the 1D diffusion equation. For an infinite system and an initial concentration profile of $c = 0$ for $x < 0$ and $c = c_0$ for $x > 0$, the solution is an error function erf(x) of the form:

$$\frac{c(x)}{c_0} = \frac{1}{2\sqrt{\pi Dt}} \int_{-\infty}^{x} dy \; exp\left(-\frac{y^2}{4Dt}\right) \tag{6}$$

It is more convenient for experimental data to consider the derivative of erf(x) which is a Gaussian:

$$\frac{1}{c_0}\frac{dc(x)}{dx} = \frac{1}{2\sqrt{\pi Dt}} exp\left(-\frac{x^2}{4Dt}\right) \tag{7}$$

We will use this form in Sec. 3 to extract D from experimental data.

We take (1) and (3) as the starting point for a numerical study of the equilibrium concentration profiles and the dynamics of the process. Before turning to our numerical results we should address the validity of the assumptions we have made especially in light of the huge pressure gradients generated by centrifugal forces equivalent to $200,000g$. Possible difficulties are that the coefficients in (1) or in (5) depend on r through the pressure and concentration. Another difficulty is that for the aqueous solutions considered in the experiments the system is an electrolyte where the components dissociate and one must consider a more complicated set of equations for the diffusion of the ions. There are certainly other possible difficulties as well. For now we ignore these details and proceed. To a great extent our comparisons of the numerical model and the experiment will justify or invalidate our approach.

3 Numerical Results

Our numerical simulations of centrifugal separation can be divided into two parts. The first, separation in a binary mixture, is relatively simple and can be used for direct comparison with experimental separation in aqueous solutions discussed in the next section. The second is a simulation of a ternary mixture of one solvent and two solutes of very different molecular densities, roughly modeling the actinides and fission products as individual components. This latter simulation should be quite reasonable for the proposed reactor solution since the concentrations of the constituents are sufficiently small that each can be treated to first approximation as a non-interacting component. This allows us

501

to approximate the ternary mixture as two binary mixtures and use independent Lamm equations (1) for each component. In the simulations for the molten-salt mixture, we use experimentally-determined coefficients when available and reasonable estimates for those that have not been experimentally measured.

The simulations were performed using a partial-differential-equation-solver package PDELIB[7]. The equations were integrated in time with a variable order, variable timestep ordinary differential equation solver to a tolerance of $1.0e-7$ per unit time. The spatial operators were approximated with 2nd-order finite-difference methods on a uniform grid. The number of spatial points was varied between 50 and 400 to ensure that the numerical results were converged; typically we used 200 points.

For simulations of the Lamm equation we have two materials parameters in (1), the mass diffusion coefficient D and the sedimentation coefficient s. We have taken "typical" values of $D = 10^{-5}$ cm^2/sec and $s \approx 10^{-13}$ sec for simulation purposes. The conclusions of our analysis do not depend qualitatively on these choices although, of course, the quantitative results will. In Fig 1 we show a family of curves with $s = 0.5 \times 10^{-13}$ sec for the concentration field $c(r,t)$ normalized by the initial concentration c_0 which is uniform in r. The inner and outer radii are taken to be $r_1 = 15$ cm and $r_2 = 20$ cm respectively, similar to the geometry anticipated for a realistic centrifuge for nuclear material separation. The most important thing to notice in this plot is the nonuniform evolution of the concentration profile. Whereas the concentration close to the inner and outer boundaries differs substantially from c_0 at short times, the evolution in the central region is much slower. A similar plot, Fig 2, for $s = 1.0 \times 10^{-13}$ sec. shows the same trend at small time but overall faster profile evolution as expected[1]. There is appreciable dependence on the values of the inner and outer radii. In Fig 3, we show the normalized concentration $c(r,t)/c_0$ with $r_1 = 10$ cm and $r_2 = 20$ cm. In this case the concentration evolution is even slower in the middle relative to the extremes. The distinguishing feature of the middle region at short times is the plateau of rather constant concentration.

Another way to illustrate the separation is to look at the approach to equilibrium at several values of r as a function of time, see Fig 4. At the same radius with different s the decay time is shorter for larger s and for r closer to the inner and outer radius the relaxation is much faster. The early relaxation cannot be approximated by a pure exponential function but a stretched exponential of the form $A\ exp\left(at^{-\beta}\right) + c_\infty$ works reasonably well. There is no theoretical basis for this functional form but empirically it gives some insight. We found that the exponent β is about 0.8 near the walls whereas in the center it is about 1.2. In Fig 5, the dependence of β on r is shown. Values of β less than one mean that at early times the decay is faster than exponential whereas $\beta > 1$ implies slower than exponential relaxation for short times. For later times, the relaxation dynamics can be closely approximated by a simple exponential. This regime of concentration evolution is useful if one wants to reach a high ratio of enrichment of one species over the other – the concentration of one of them has to change significantly from the original value. In the next section, we present experimental results which we compare with our theoretical model and numerical simulations. This is absolutely crucial since an *a priori* evaluation of the validity of the assumptions in the theory is difficult.

[1] we found out later that the above set of numbers was closer to that of the actinides and fission products in an aqueous solution at room temperature

802

4 Experiments

The experiments we performed were designed to test the equilibrium profiles established by centrifugal acceleration and also to determine the dynamics of the sedimentation process. In principle, one would like to have real time information about the concentration along the radius which would require a special purpose apparatus. For initial studies we used a commercial ultracentrifuge[8] capable of rotation speeds up to 41,000 revolutions per minute in a vacuum environment. Aqueous solutions of CsCl, $CuSO_4$, $ZnCl_2$, $AuCl_3$, NaCl, $SrCl_2$, and $FeCl_3$ were prepared with molar concentrations of less than 5%. Although we have used a number of solutions most of our results will be for CsCl which has long been a favorite of the biomedical community for establishing known density gradients for separation of large molecules[9]. The centrifuge we used had a swing-bucket rotor with 6 metallic vessels. Soft chemically-inert plastic vials containing the solutions were placed into the vessels and the vessels were sealed against the centrifuge vacuum which was typically less than 10 micron. Once good vacuum was achieved in the centrifuge, the rotor was spun up to the operating rotation rate in about 5-10 minutes. The rotor was temperature controlled at about 25°C during the entire operation. After a certain time at full speed the rotor was decelerated, the system was repressurized and the samples were removed for measurement. Several precautions needed to be taken to ensure undisturbed separation. Inadequate vacuum or too rapid deceleration could result in mixing and destroy the centrifugally-induced concentration profile. The latter was the most troublesome, completely destroying the separation effect if the system brake was on. Instead we turned off the brake and let the rotor decelerate under the influence of the natural friction that arise from a variety of sources including bearing friction and viscous drag. This increased the spin-down time from about 5 minutes to about 30 minutes. Even with this precaution some mixing could occur during spin-down. Further work will be required to quantify the mixing effects but our measurement suggest they are small with the present procedure. Finally, one might be concerned that the separated solution could mix owing to the effects of mass diffusion. This is not a problem because mass diffusion is extremely slow in ordinary gravity. As a result, a separated solution is stable for hours if the environment is reasonably isothermal. Since the measurements are typically done well within an hour after removal of the samples, no significant mixing is expected.

Once the solution was sedimented under the action of the centrifugal force, we measured the concentration profile using the density dependence of the index of refraction. The vial containing the solution was removed from the metal container and a small amount of solution was extracted from different heights using a syringe. The depth from which the fluid was taken corresponded to a radial position when the vial was being rotated. A superior method, using a peristaltic pump and a fraction collector, is currently being implemented so as to improve the reproducibility of our measurements. The method used here, however, gave quite good results as we now show.

The concentration of each sample was determined using a commercial refractometer[10] capable of resolving differences in index of refraction of about ± 0.0001 out of 1.4000. The sample volume was temperature controlled at 25°C using a refrigerator/circulator. The concentration was calibrated against density according to published data[11] or our own calibration results. Normalizing by the initial radially-uniform concentration c_0, we obtain the quantity $c(r_i)/c_0$. The measurements for different total times allow a deter-

803

mination of the dynamics at a modest number of discrete times.

We also independently determined D by preparing a stratified aqueous solution layer of concentration c_0 below a layer of pure water. This initial condition evolved under the action of mass diffusion so that in typically several hours the concentration profile had a sigma-function shape. Such a profile is shown in Fig 6 for CsCl along with the center-difference derivatives of the experimental data and a fit to a Gaussian function of the form (7) from which one obtains $D = 1.7 \times 10^{-5}$ cm^2/sec. We show in Fig 7 similar data for NaCl for which $D = 1.7 \times 10^{-5}$ cm^2/sec. The value of D for NaCl compares reasonably with published data ($D \approx 1.5 \times 10^{-5}$ cm^2/sec)[12]. Slightly larger values from our experiments might be the result of initial disturbances to the interface during preparation.

The results of one centrifugation run lasting 135 hours and 35 minutes for several different solutions are in Fig 8, which shows the concentration profiles for $HAuCl_4 \cdot 3H_2O$ (the initial molar fraction $x_0 = 0.0022$, MW = 393.9), CsCl ($x_0 = 0.032$, MW = 168.4) and NaCl ($x_0 = 0.030$, MW = 58.4). The difference in the profiles reflects the difference in the material properties: the gold chloride, with the heaviest molecular weight and thus the highest sedimentation coefficient, had the steepest concentration gradient; sodium chloride, being the lightest, established a very gentle profile while cesium chloride's resultant gradient was in the middle. For the CsCl data, one can extract the ratio s/D from a fit to the expected equilibrium profile, Eq. (3). We obtain a ratio $s/D = 1.4 \times 10^{-9}$ sec^2/cm^2. This agrees well with the published result in the manual for our Beckman ultracentrifuge ($s/D = 1.38 \times 10^{-9}$ sec^2/cm^2)[8].

The experiments on the separation dynamics show good qualitative agreement with expectations derived from the numerical simulations. We have data on the dynamics for aqueous solutions of NaCl ($x_0 = 0.03$, MW = 58.4), CsCl ($x_0 = 0.032$, MW = 168.4), and $AuCl_3$ ($x_0 = 0.0022$, MW = 393.9, the crystal form before dissolution is $HAuCl_4 \cdot 3H_2O$). As shown in Figs. 9, 10, and 11, there is a plateau region at short times that softens with increasing time. The qualitative features of these data are the same as the simulations. Furthermore, one can fit the data to the same stretched exponential form as we used for the numerical simulations to obtain a more quantitative comparison. In Fig 12, the evolution of the normalized concentration is shown for values of r in the middle, at the inner radius, and at the outer radius. The solid lines show the stretched exponential fits. For a sequence of these fits at increasing r one obtains values for β shown in Fig 13. The correspondence with the numerical data in Fig 5 is striking and supports the consistency of both the numerical and experimental results. One problem associated with the stretched exponential form is the absence of a characteristic time for the decay. That means that there is no straightforward way to relate the relaxation to the sedimentation coefficient s. A more complicated comparison between the experimental data and the numerical simulations is required and is currently in progress.

On the basis of the experiments reported here we see that there is qualitative and perhaps semi-quantitative agreement between theory/numerics and experiment. These comparisons give us confidence in the short time dynamics that shows up in the numerics and on that basis we proceed to a description of how we can use this information to design an efficient centrifugal separation process applicable to the separation of nuclear

804

materials in molten-salt solution. We plan to perform more extensive measurements to make quantitative comparisons with the theory, in particular we will make separation measurements of ternary solutions to check the more realistic case appropriate to nuclear separation. Index of refraction measurements are not enough for determining concentrations of multiple species solutions so we will use spectrophotometry for that purpose.

5 Design for Centrifugal Separation

Based on the above understanding of the sedimentation and diffusion dynamics in a centrifuge, we propose the following process for partitioning the fission products and actinides in the molten-salt carrier. This process is illustrated in Fig 14, in which we plot the result of the evolution of concentration profile $c_1(r,t)$ for the light solute (e.g. fission products) for a ternary system and the ratio of this concentration to that of the heavy solute (e.g. actinides). The parameters are chosen based on the Svedberg relation and the Einstein relation for the sedimentation coefficients and mass diffusion coefficients, and the known material properties from an ORNL report[14]. The initial variations of the concentration and ratio are much faster near the inner and outer cylinder, although it takes a very long time to reach the equilibrium. For extracting the light-component-rich solution, one operates close to the inner end. Since the evolution toward the equilibrium or higher ratio is nearly (stretched) exponential, it is not economical to wait much longer after the initial fast evolution of concentrations near the ends. Instead, one should utilize the fast initial changes in the concentration ratios to obtain separation with a relatively low separation ratio and use multiple stages of centrifugation to achieve final separation of high ratios. To this end, we can, for example, extract solution with 2:1 ratio of light to heavy components at a single stage, and use 10 stages to reach 1024:1 ratio (if their initial concentrations are equal).

Similar arguments can be applied to the outer end where the heavy component is enriched. It can be seen that the ratio very quickly jumped to a value which changes slowly later on. For the molten-salt fuel, this would correspond to a quick enrichment of the actinides versus the fission products. This enriched portion would be extracted and fed back to the fuel cycle directly.

The interconnection of the multiple stages of centrifugation is rather complicated and has not been worked out in detail yet. We also need to understand the hydrodynamics of the extraction process. The actual processing flux of a centrifugation separation unit will depend quantitatively on these details but the approximate processing efficiency can be estimated at this stage.

We estimate the extraction rate using the extraction scheme shown in Fig 14. This scheme has used the following estimated material properties: for fission products, $s/D = 1\times10^{-9}$ sec^2/cm^2, $D = 3.4\times10^{-6}$ cm^2/sec, and for the actinide fluorides, $s/D = 3\times10^{-9}$ sec^2/cm^2, $D = 3.4\times10^{-6}$ cm^2/sec. The geometry is given by the inner and outer radii of $r_1 = 15$ cm, $r_2 = 20$ cm, a length $l = 50$ cm and 4 centrifuges at each stage. The (nonvolatile) fission product production rate is assumed to be 100 kg/yr = 3.2 mg/sec.

805

After a time of 3×10^5 sec, the concentration ratio of the fission products to actinides reached 2:1 at $r = 15.2$ cm. If we extract the fluid within a layer of $\delta r = 0.5$ cm, corresponding to a volume of 9.6×10^3 cm^3, the concentration of the fission products is $c_F/c_{F0} = 0.62$. This gives an extraction rate of fission products of $0.62 c_{F0} \times 9.6 \times 10^3$ cc/3×10^5 sec $= 2 \times 10^{-2} c_{F0}$ (g/sec). If a concentrator stage is used at each centrifugation stage to concentrate the diluted extraction back to the input concentration, then the equilibrium extraction rate $2 \times 10^{-2} c_{F0} = 3.2$ mg/sec, or $c_{F0} = 0.16$ g/cc, which is approximately 2% molar fraction. This is the initial concentration of the fission products required to maintain the balance between production and extraction. The fission products concentration inside the reactor can be lower if this 2% molar concentration is reached with a concentrator stage outside. This leads to higher fluxes which may be desirable for some ADEP applications.

It is important to recognize the limiting factors in determining the extraction rate. From the discussion in the numerical simulation section, we understand that for a given geometry and rotation speed, s/D determines the steepness of the concentration profiles: the larger the s/D, the steeper the profiles and hence the larger the ratio of enrichment that can be achieved for each stage. Since s/D is inversely proportional to T (the Svedberg relation), the elevated temperature of the molten salt is unfavorable for high-ratio separation. The time scale is proportional to D which, according to Einstein's relation, is inversely proportional to the dynamic viscosity of the solution. Since the viscosity of the molten salt is almost 5 times that of water at room temperature, this constitutes another unfavorable factor for efficient extraction in the molten salt solutions.

For comparison purposes, let's examine the extraction rate for the following property parameters: for the heavier component, $s/D = 1 \times 10^{-8}$ sec^2/cm^2, $D = 1 \times 10^{-5}$ sec and for the lighter component, $s/D = 0.5 \times 10^{-8}$ sec^2/cm^2, $D = 1 \times 10^{-5}$ sec. These values are very close to the parameters for the actinides and fission products in an aqueous solution at room temperature. Using the simulated concentration evolution dynamics shown in Fig15 and extracting at a ratio of 2:1, we arrive at the following conclusion: for the same geometry we used in the previous discussion, after a time of 0.2×10^5 sec, the concentration ratio of the fission products to actinides reached $2:1$ at $r = 15.2$ cm. If we extract the fluid within a layer of $\delta r = 0.5$ cm, this corresponds to a volume of 9.6×10^3 cm^3; the concentration of the fission products is $c_F/c_{F0} = 0.55$. This gives an extraction rate of fission products of $0.55 c_{F0} \times 9.6 \times 10^3$ cc/0.2×10^5 sec$= 0.26 c_{F0}$ (g/sec). If a concentrator stage is used at each centrifugation stage to concentrate the diluted extraction back to the input concentration, then the equilibrium extraction rate $0.26 c_{F0} = 3.2$ mg/sec, or $c_{F0} = 0.012$ g/cc, which is approximately 0.15% molar fraction. This low concentration corresponds to a much lower fission products inventory in the system, because the extraction rate is much higher. With these material properties, it is even possible to go to higher ratios of enrichment at each stage. For instance, if we choose to extract at 5:1 ratio, then we can reach this ratio after 2.0×10^5 sec at $r = 18.8$ cm. The extraction volume is 1.17×10^4 cc; the concentration of the fission products is $c_F/c_{F0} = 0.9$. This gives an extraction rate of fission products of $0.9 c_{F0} \times 1.17 \times 10^4 cc/2.0 \times 10^5 sec = 0.053 c_{F0} (g/sec)$. If a concentrator stage is used at each centrifugation stage to concentrate the diluted extraction back to the input concentration, then the equilibrium extraction rate $0.053 c_{F0} = 3.2$ mg/sec, or $c_{F0} = 0.061$ g/cc, which is approximately 0.76% molar fraction. With this kind of extraction, one needs 5 stages to reach a separation ratio of 3125 : 1.

206

6 Conclusions

We have analyzed the problem of centrifugal separation of solutions without thermal effects. The theoretical model and numerical simulations that we used have developed a firm foundation for understanding centrifugation. Our experiments in aqueous solutions confirm the validity of the model and quantitatively demonstrate the important phenomena associated with separation. On the basis of the model and the experiments we have developed a process for separation of actinides and fission products from realistic molten salt solutions. Further work is needed to test the hydrodynamics of continuous separation, the effects of multiple component solutions and of nonideal solutions, and the influence of a realistic non-aqueous molten-salt solution with dissolved heavy compounds. Some additional details, including the derivation of the Lamm equation and consideration of thermal effects are presented in [5].

7 Acknowledgements

This project was funded by the ADTT program and would not have been possible without the support and seminal contributions of Charlie Bowman. We would also like to thank Mac Hyman (T-7) and Don Stark (CNLS) for assistance with the numerical simulations and Rick Reynolds (LS-1) for helping us make the initial measurements of separation in a modern ultracentrifuge when our older one broke down.

807

References

[1] F. Venneri (unpublished).

[2] C. Bowman, Technical report, Los Alamos National Laboratory (unpublished).

[3] T. Svedberg and K. O. Pedersen, *The Ultracentrifuge* (Oxford At the Clarendon Press, Briton, 1940).

[4] Landau and Lifshitz, *Fluid Mechanics* (Pergamon, Oxford, 1959).

[5] L. Ning, R. Camassa, R. Ecke and F. Venneri, Technical report (LA-UR-94-3197), Los Alamos National Laboratory.

[6] H. Tyrrell, *Diffusion and Heat Flow in Liquids* (Butterworths, London, 1961).

[7] M. Hyman, LAUR-79-740 .

[8] Model L3-50 Ultracentrifuge with SW-41 Ti Rotor, Beckmann.

[9] H.-W. Hsu, in *Separations by Centrifugal Phenomena*, Vol. 16 of *Techniques of Chemistry*, edited by E. S. Perry (John Wiley & Sons, New York, 1981), .

[10] Model ABBE-3C refractometer, Milton Roy.

[11] J. Ifft, D. Voet, and J. Vinograd, J. Phys. Chem. **65**, 1138 (1961).

[12] *Handbook of Chemistry and Physics* (CRC Press, 1983).

[13] H. Fujita, *Mathematical Theory of Sedimentation Analysis* (Academic Press, New York, 1962).

[14] Technical report, Oak Ridge National Laboratory (unpublished).

808

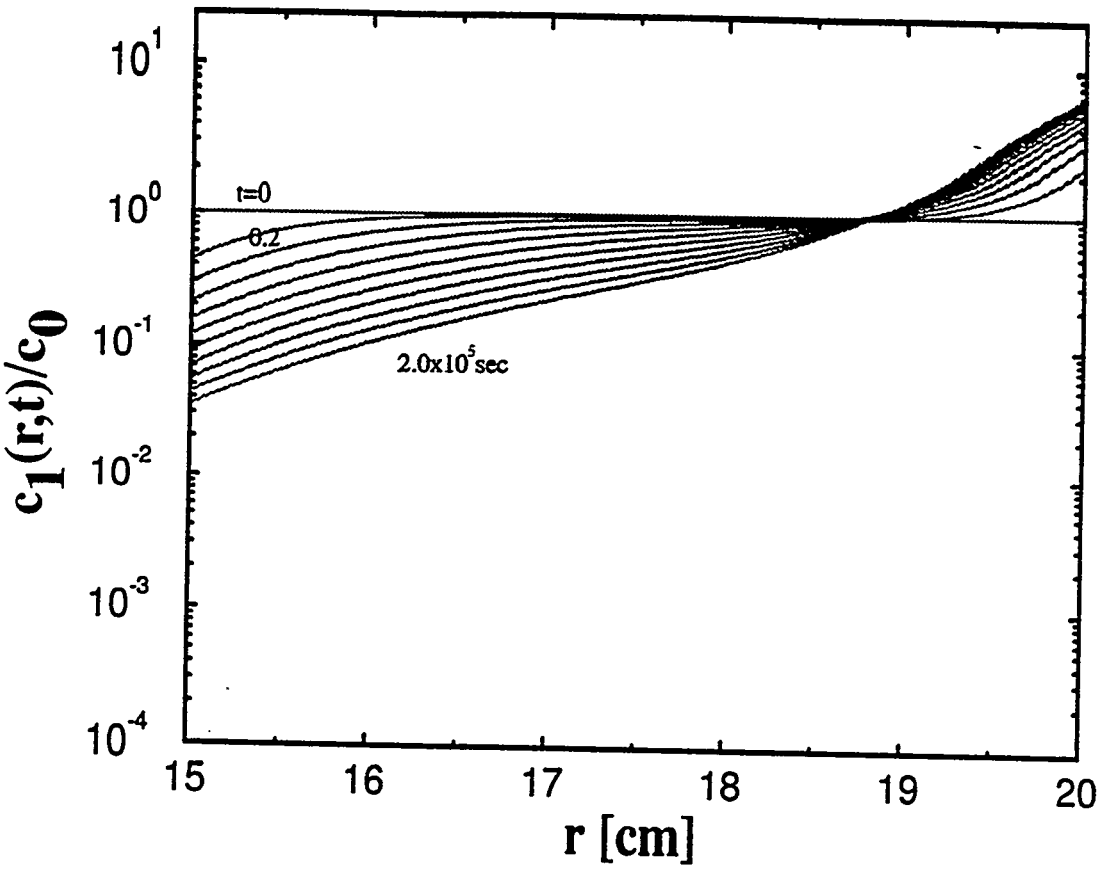

Figure 1: $c_1(r,t)/c_0$ vs r with $s = 0.5 \times 10^{-13}$ sec for different times showing the evolution of the concentration field. The separation between individual curves is 0.2×10^5 sec, r_1 = 15 cm, and r_2 = 20 cm.

809

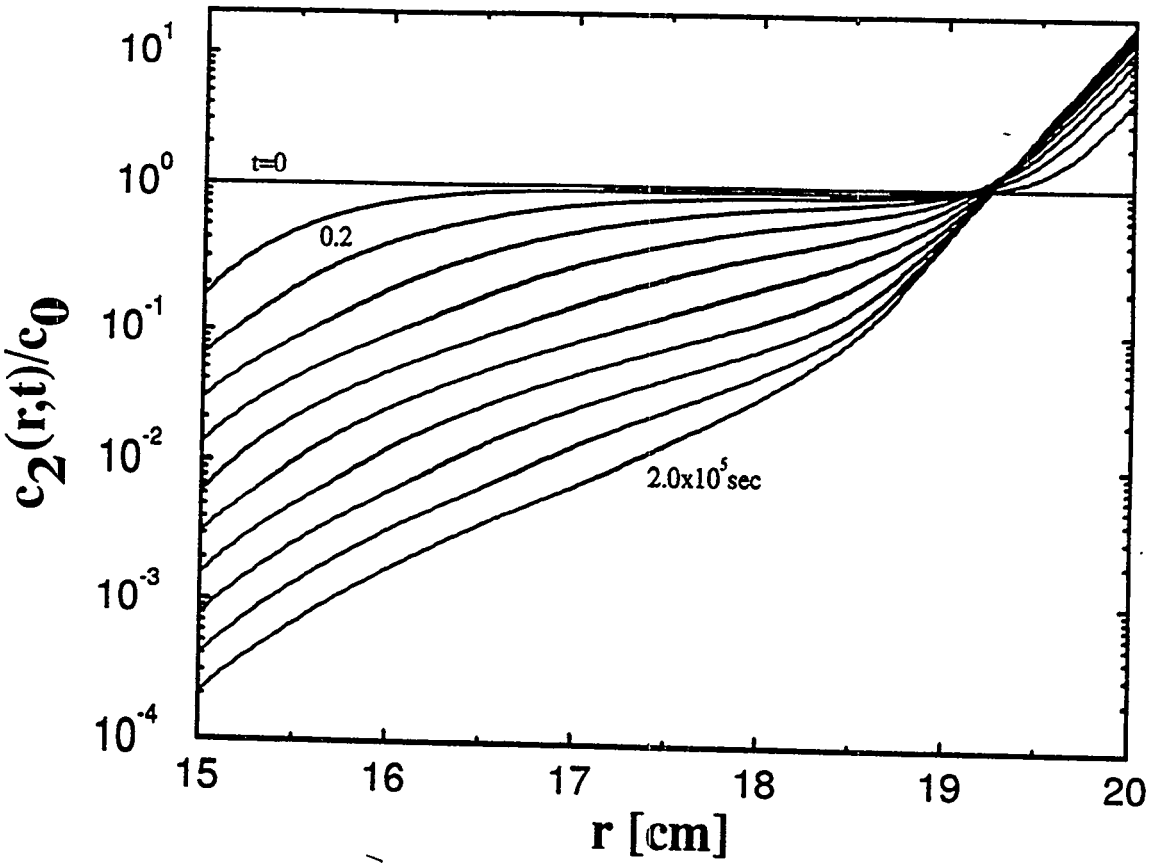

Figure 2: $c_2(r,t)/c_0$ vs r with $s = 1.0 \times 10^{-13}$ sec for different times showing the evolution of the concentration field. The separation between individual curves is 0.2×10^5 sec, r_1 = 15 cm, and r_2 = 20 cm.

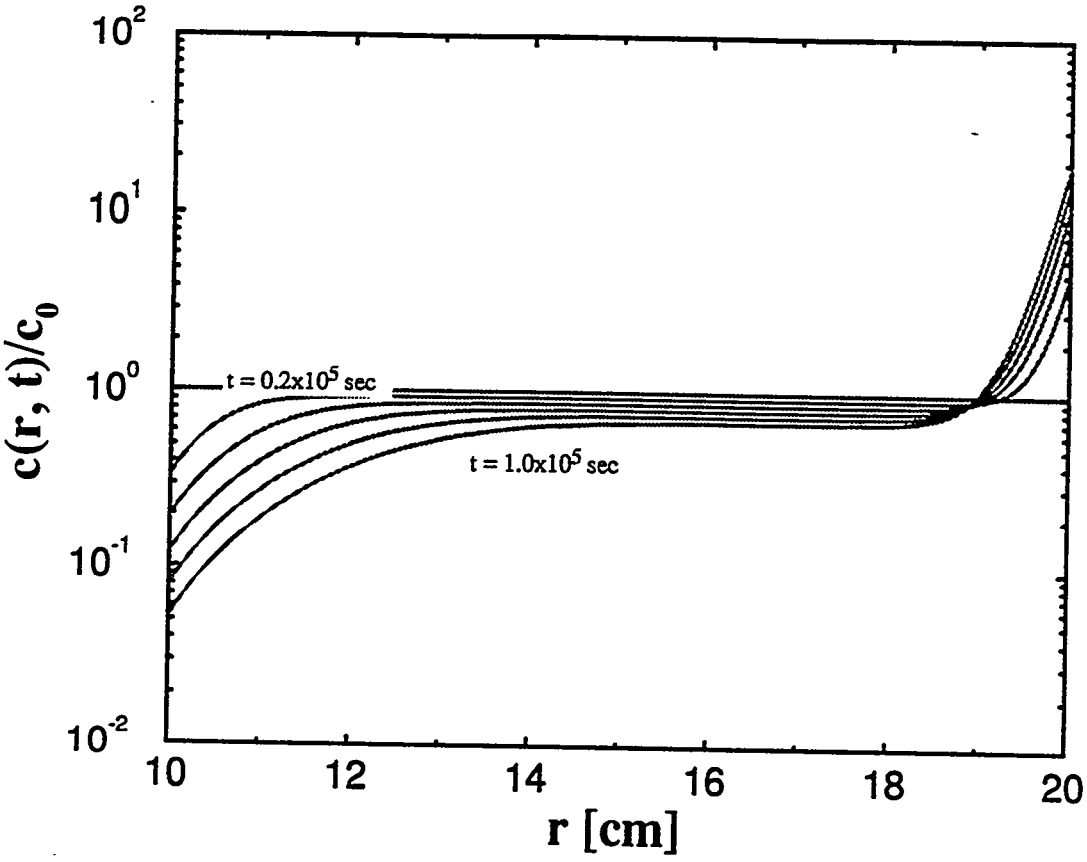

Figure 3: $c(r,t)/c_0$ vs r with $s = 0.5 \times 10^{-13}$ sec for different times showing the evolution of the concentration field. The separation between individual curves is 0.2×10^5 sec, r_1 = 10 cm, and r_2 = 20 cm.

811

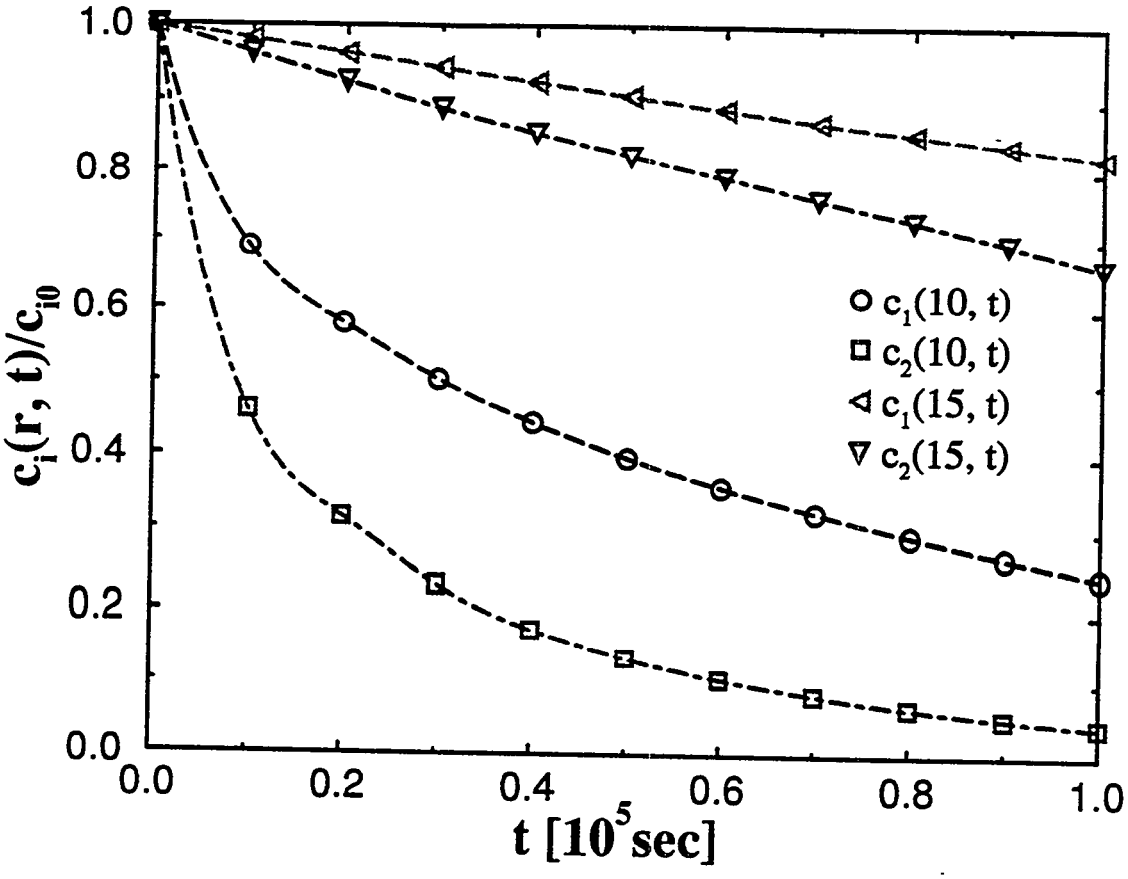

Figure 4: $c(r,t)/c_0$ vs t for $s = 0.5 \times 10^{-13}$ sec, $r = 10$ (o), $s = 1.0 \times 10^{-13}$ sec, $r = 10$ ($\Box$), $s = 0.5 \times 10^{-13}$ sec, $r = 15$ ($\triangleleft$), and $s = 1.0 \times 10^{-13}$ sec, $r = 10$ ($\triangle$). For all data $r_1 = 10$ and $r_2 = 20$

$8/7$

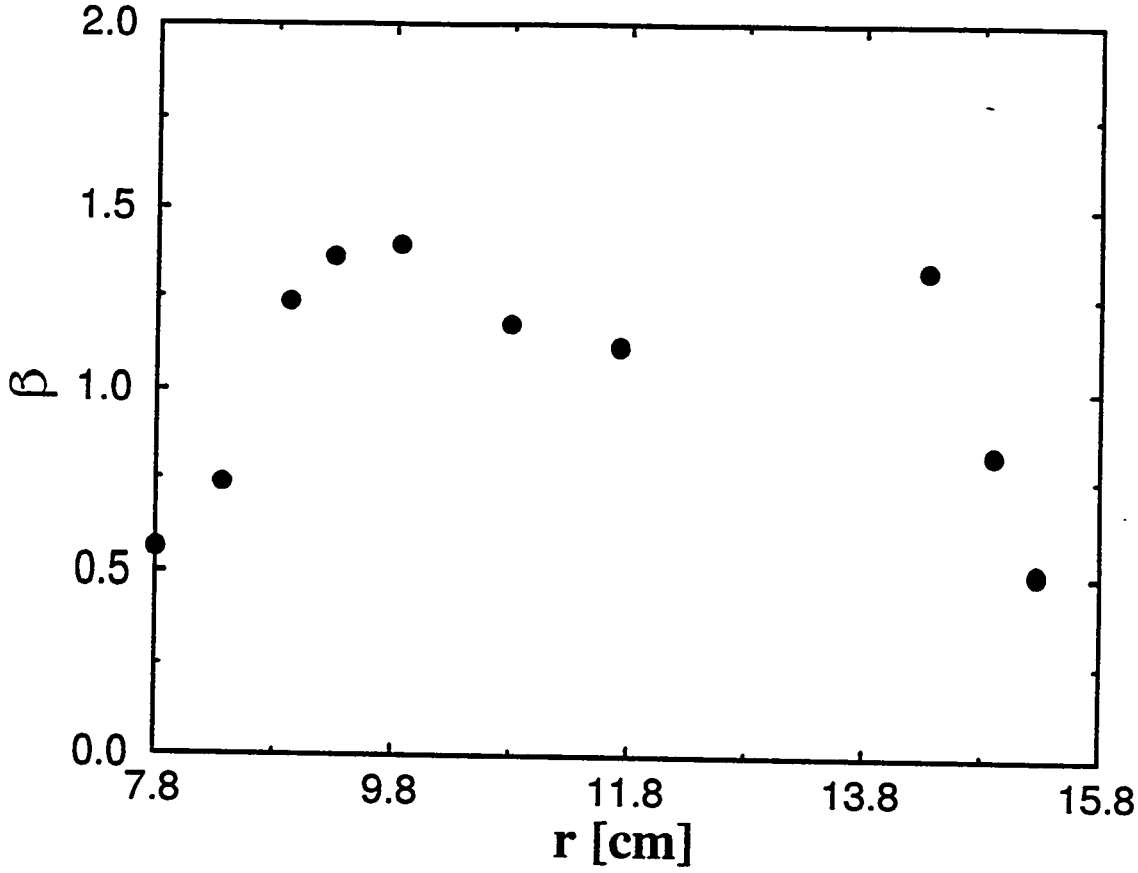

Figure 5: β vs r for numerical data.

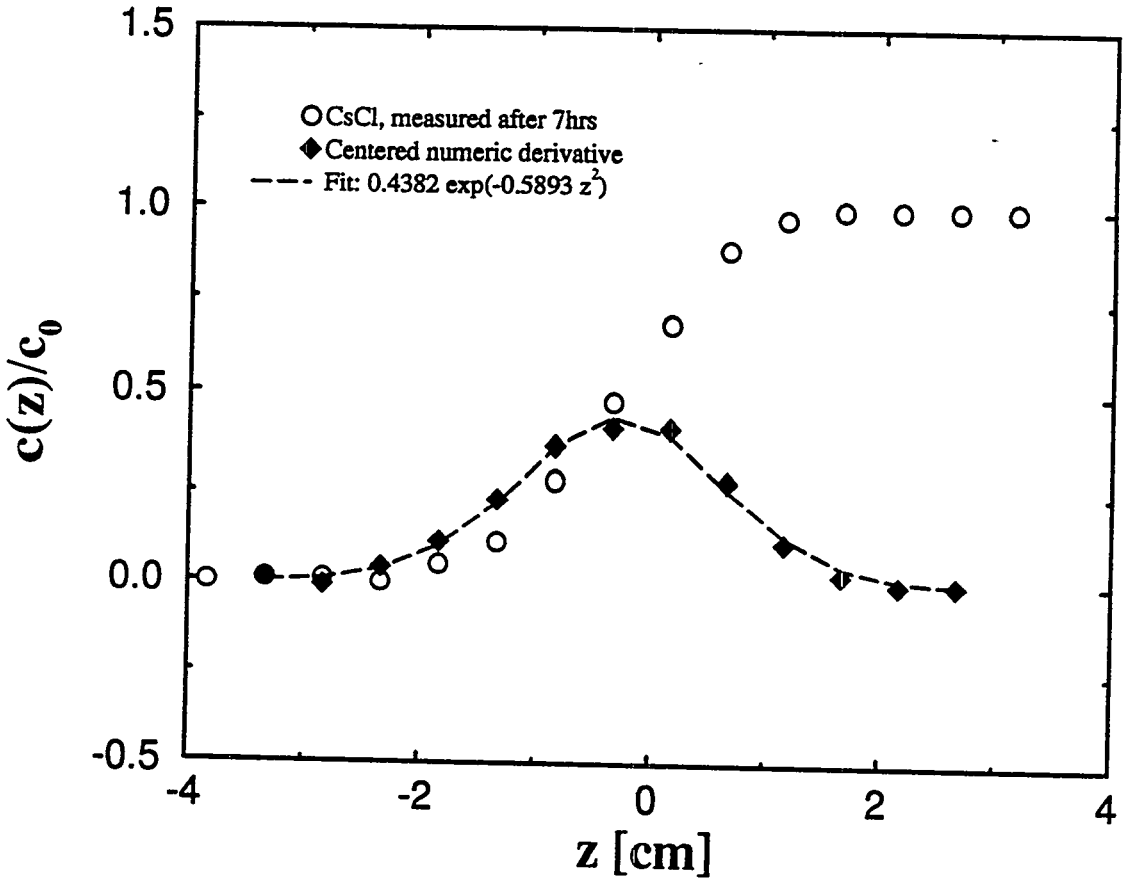

Figure 6: $c(z)/c_0$ (o) vs z for CsCl, numerical derivative ($\diamond$), and fit to Gaussian function (- - - -).

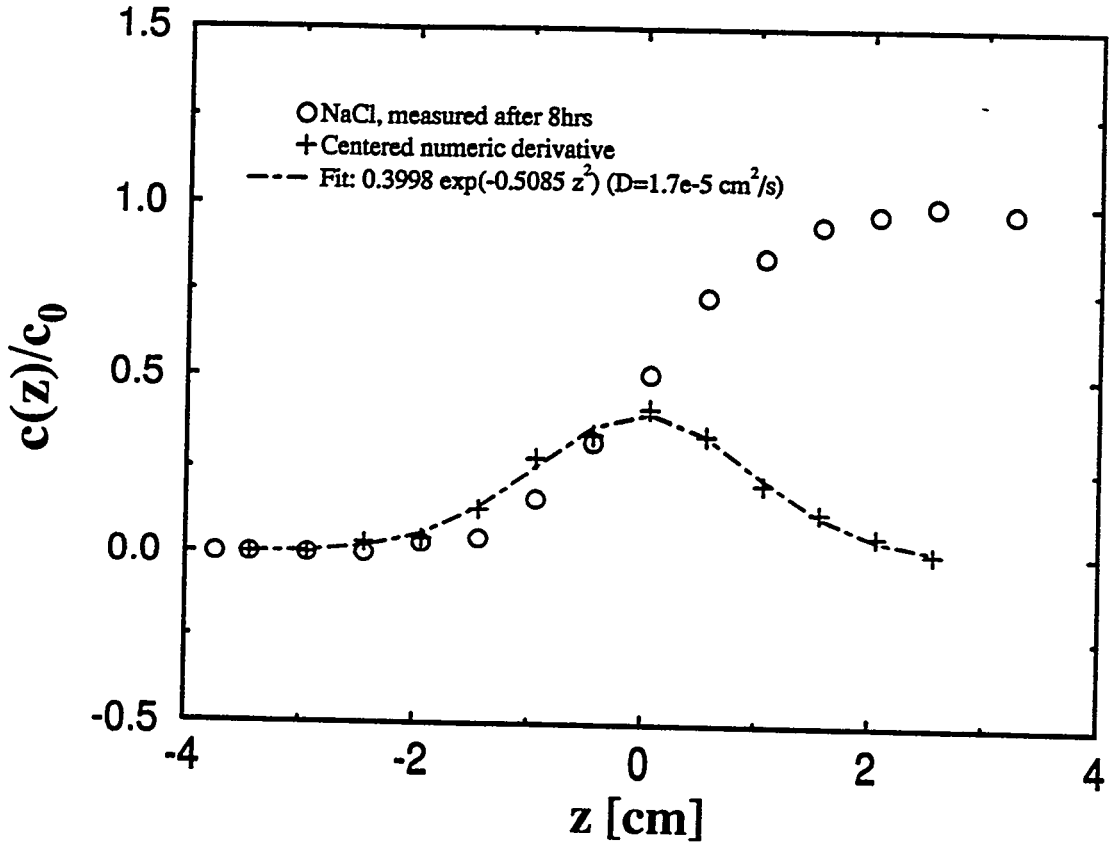

Figure 7: $c(z)/c_0$ (o) vs z for NaCl, numerical derivative (+), and fit to Gaussian function (- - - -).

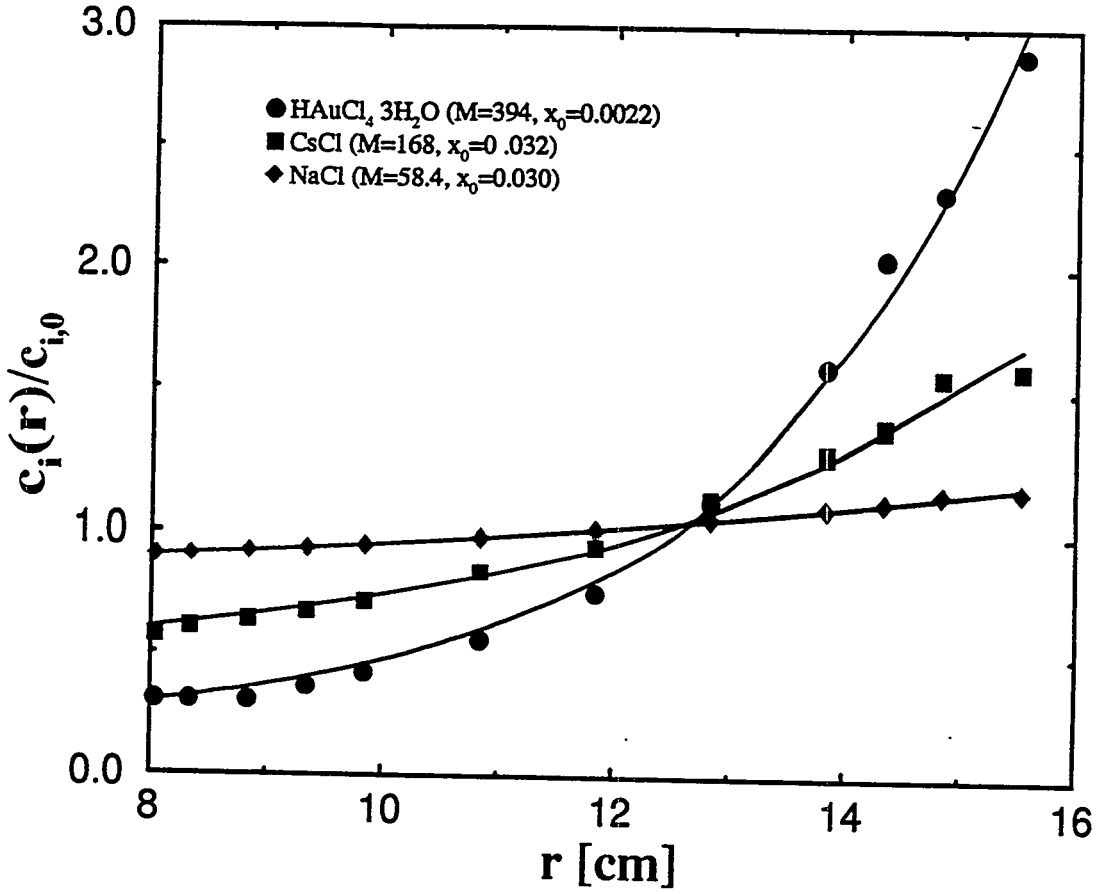

Figure 8: $c(r,t)/c_0$ vs r for $HAuCl_4 \cdot 3H_2O$ (o), CuCl (□), and NaCl (◇). The solid lines are the fitted results to the Archibald solution.

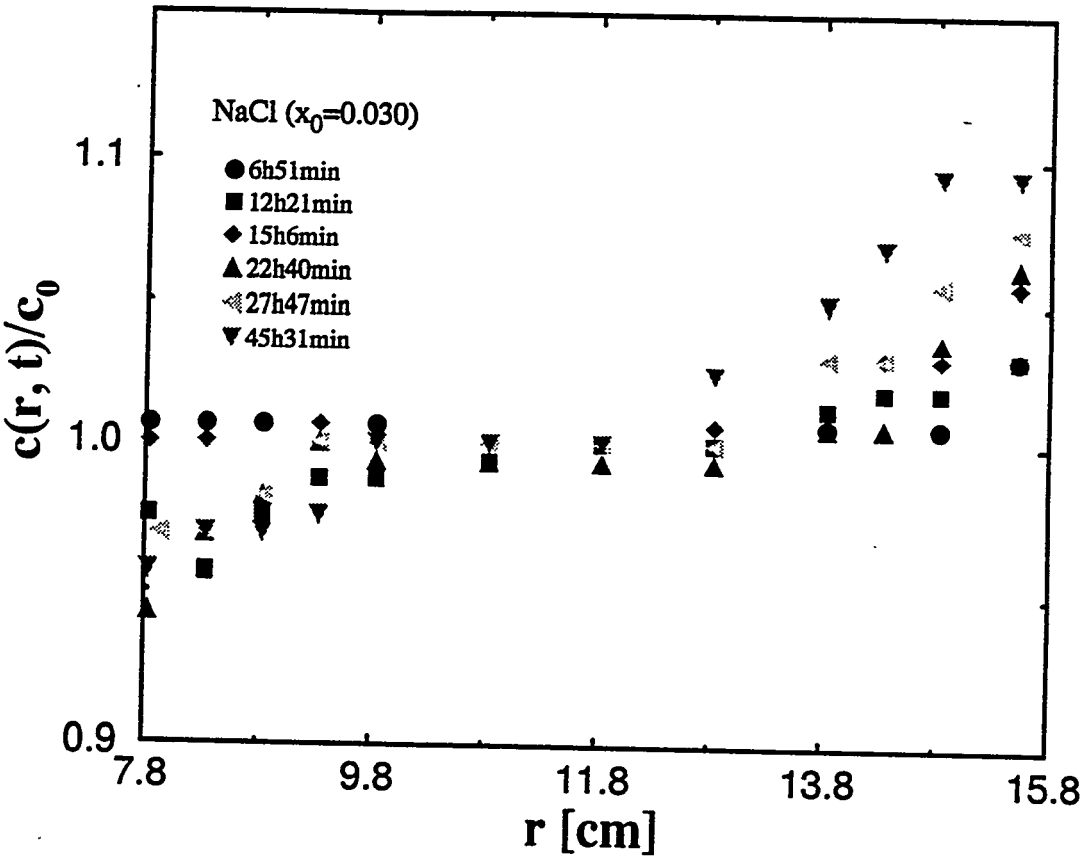

Figure 9: $c(r,t)/c_0$ vs r for NaCl with total separation time 6.8 h ($\bullet$), 12.3 h ($\square$), 15.1 h ($\diamond$), 22.7 h ($\triangle$), 27.8 h ($\triangleleft$), and 45.2 h ($\triangledown$).

817

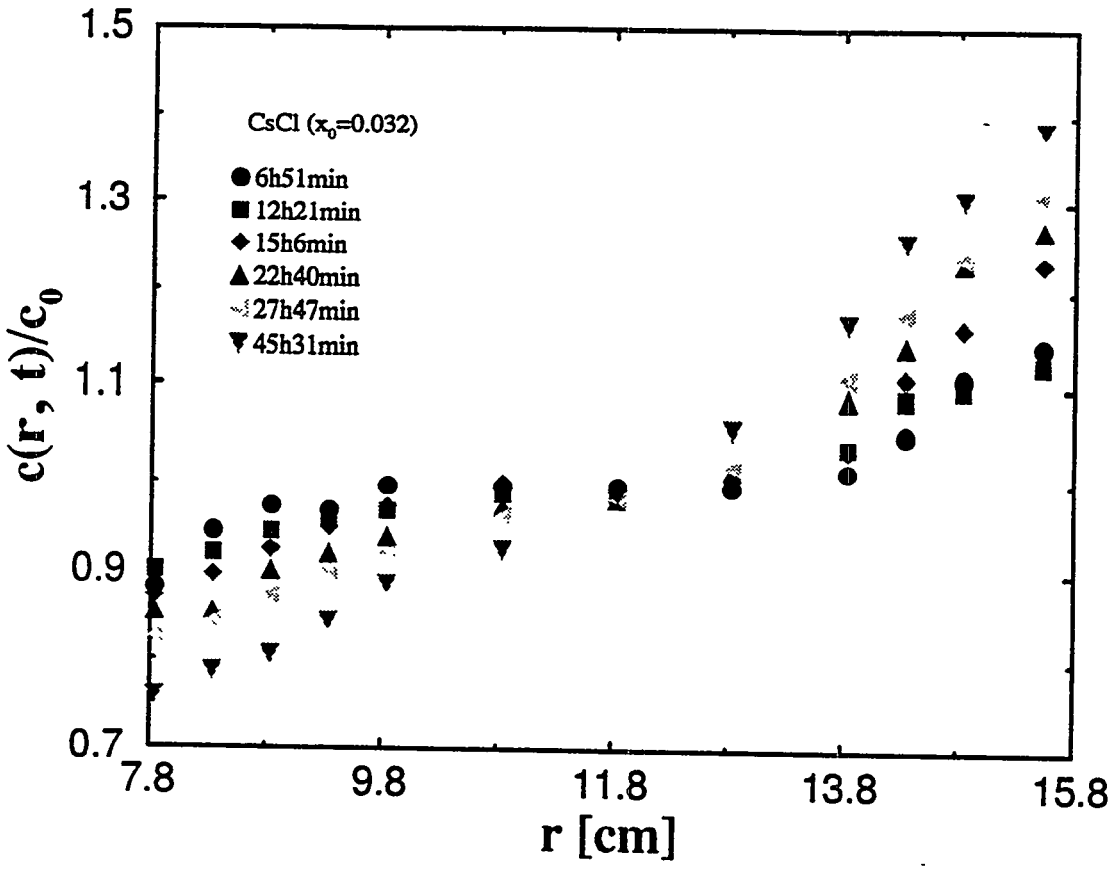

Figure 10: $c(r,t)/c_0$ vs r for CsCl with total separation time 6.8 h (•), 12.3 h (□), 15.1 h (◇), 22.7 h (△), 27.8 h (◁), and 45.2 h (▽).

818

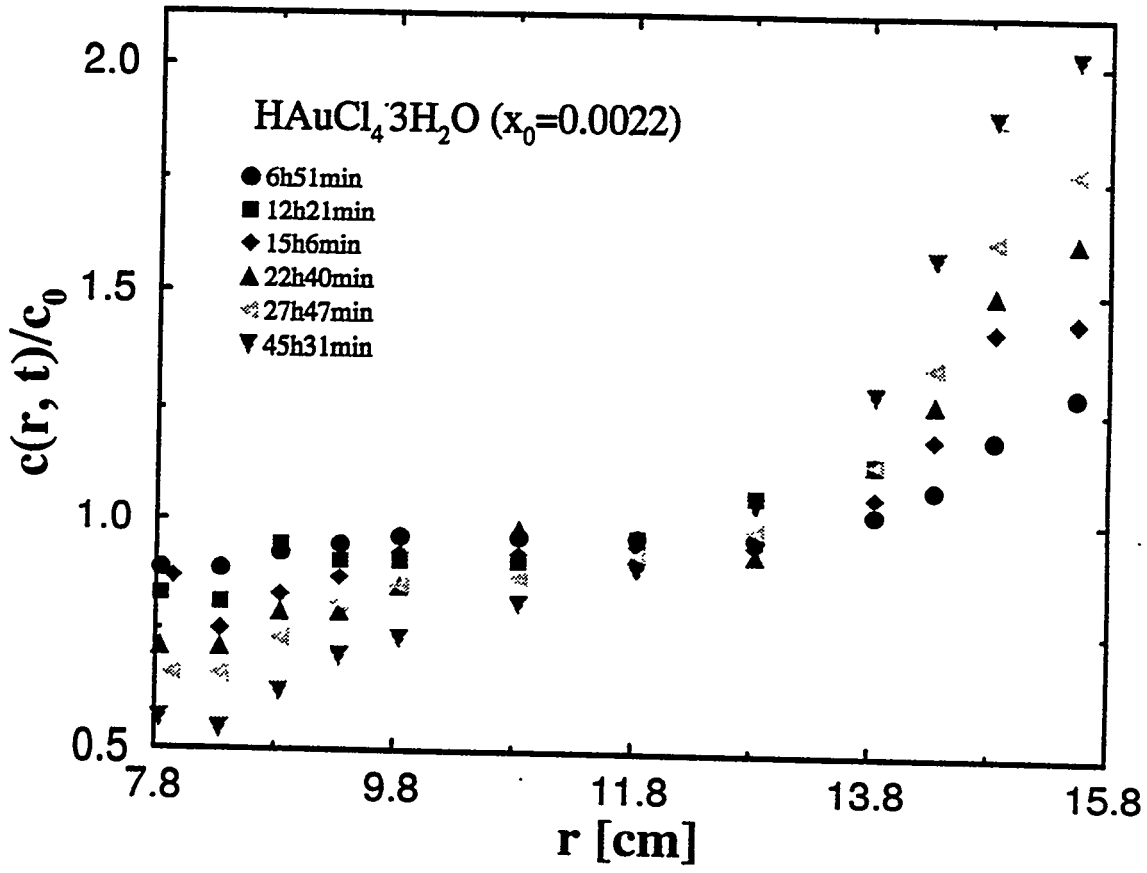

Figure 11: $c(r,t)/c_0$ vs r for AuCl with total separation time 6.8 h (•), 12.3 h (□), 15.1 h (◇), 22.7 h (△), 27.8 h (◁), and 45.2 h (▽).

8/9

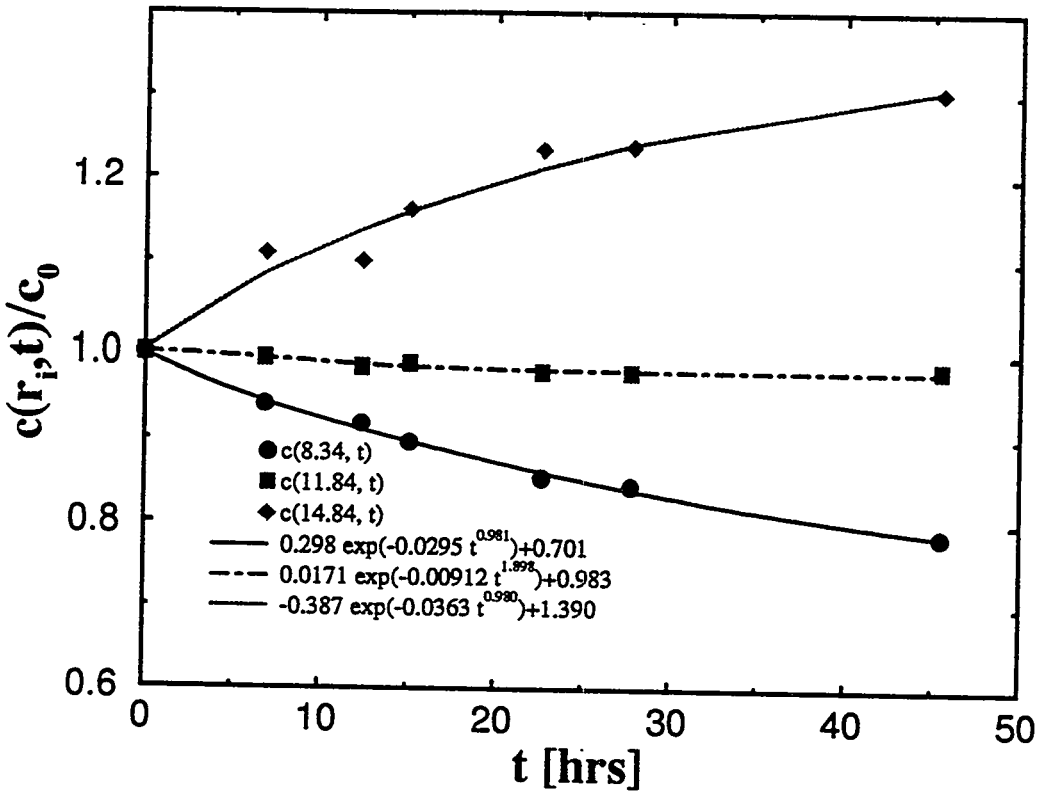

Figure 12: $c(r,t)/c_0$ vs t for CsCl for r = 8.3 (•), r = 11.8 (□),and r = 14.8 (◇). Solid lines are fits to stretched exponential form.

820

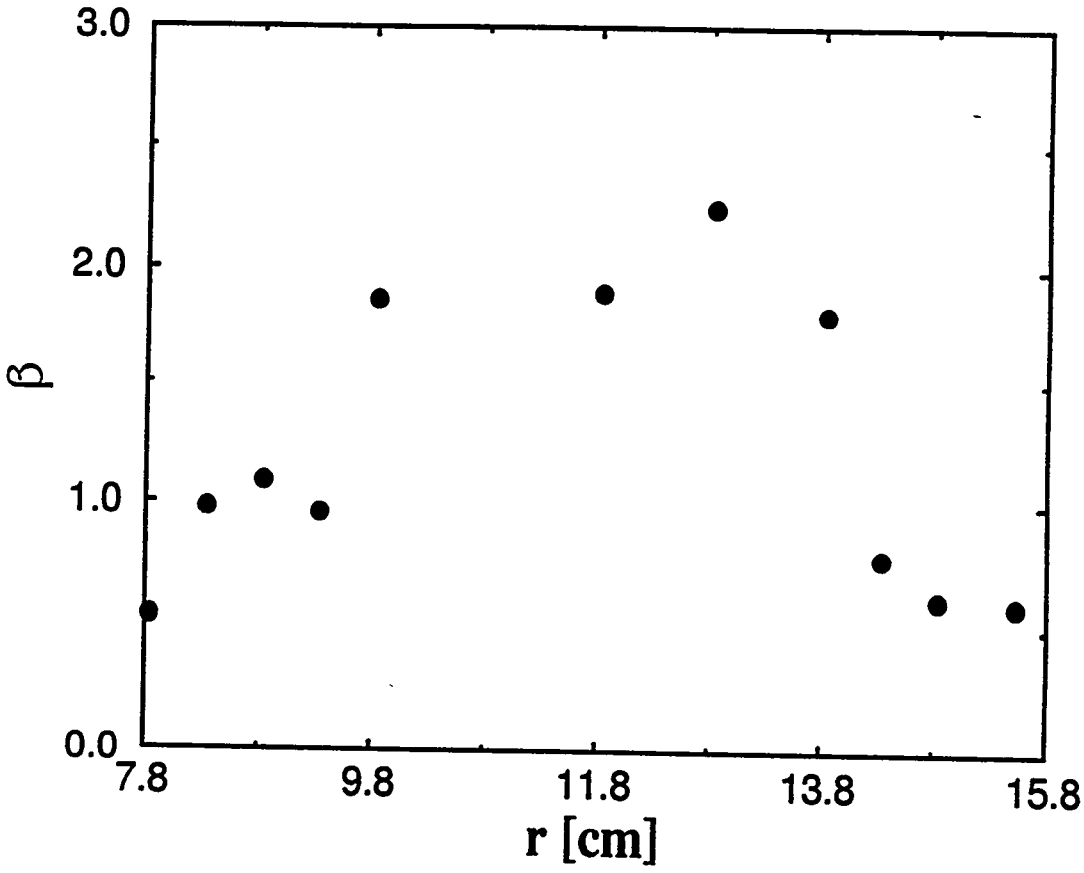

Figure 13: β vs r for experimental data with CsCl.

871

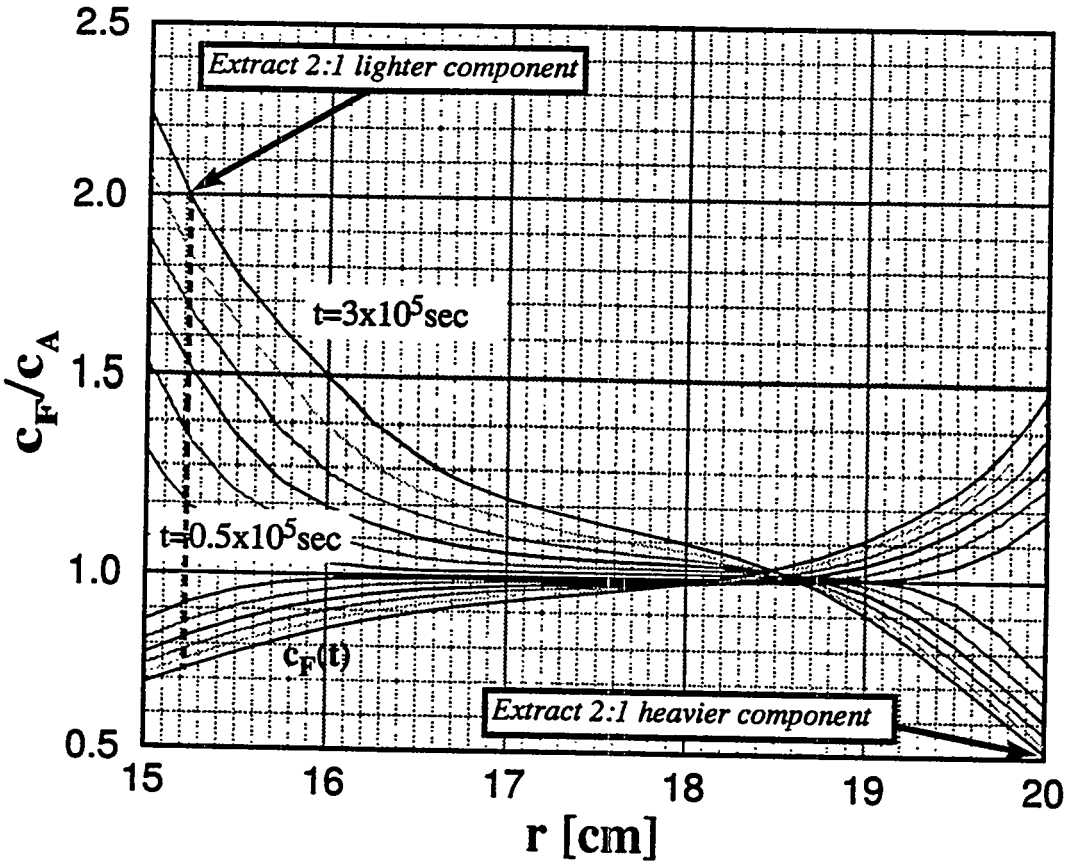

Figure 14: Illustration of a possible extraction process based on the estimated material properties in the molten salt solutions at the operational temperature.

428

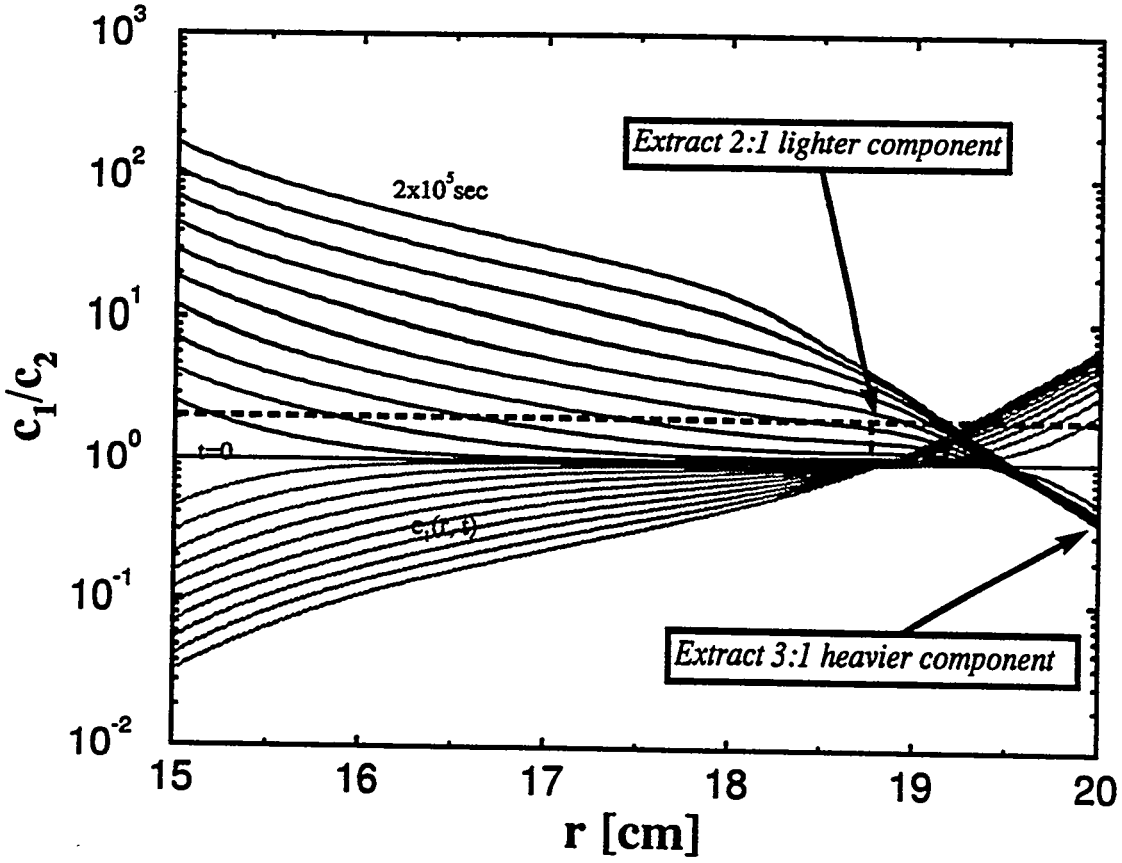

Figure 15: Illustration of a possible extraction process based on the estimated material properties in aqueous solutions at room temperature.

823

CONVECTIVE INSTABILITIES IN LIQUID CENTRIFUGATION FOR NUCLEAR WASTES SEPARATION

Roberto Camassa
Los Alamos National Laboratory, U. S. A.

The separation of fission products from liquid solutions using centrifugal forces may prove an effective alternative to chemical processing in cases where radioactive materials necessitate minimal mixed-waste products or when allowing access to sophisticated chemical processing is undesirable. Our investigation is a part of the effort to establish the feasibility of using liquid centrifugation for nuclear waste separation in the Accelerator Driven Energy Production (ADEP) program.

A number of fundamental issues in liquid centrifugation with radioactive elements need to be addressed in order to validate the approach and provide design criteria for experimental liquid salt (LiF and BeF2) centrifuge. We concentrate on one such issue, the possible onset of convective instabilities which could inhibit separation.

We study a set of coupled diffusion equations to assess whether in the course of the evolution out of physical initial conditions adverse temperature gradients ("fluid heated from below") can occur thereby leading to convective instability. These equations govern the temperature and concentration behaviour of a binary solution in a rotating cylindrical geometry under the condition of equilibrium (zero macroscopic velocity field and hydrostatic pressure). The smallest (in absolute value) eigenvalue of the corresponding stationary problem provides a simple estimate of the time scale needed to achieve separation for a given centrifugal force field.

When the heating from radioactive decay is due to the heavier component of the solution, we show that generation of adverse temperature gradients can occur before reaching equilibrium with the centrifugal field. According to a linear stability analysis, convective motion between the heavier fluid (outer with respect to the centrifugal force) and lighter (inner) fluid would then ensue. This convective flow would cause remixing of the separating components which could significantly inhibit separation. A few simple methods to defeat the tendency of the system to convective motion are briefly examined.

SUBCRITICAL NEUTRON GENERATOR - TEST FACILITY FOR NUCLEAR WASTE TRANSMUTATION STUDIES

I. V. Chuvilo, A. A. Kolomiets, A. M. Kozodaev, N. V. Lazarev, Yu. G. Orlov, V. K. Plotnikov, A. M. Raskopin, O. V. Shvedov, V. S. Skachkov, V. V. Vassiliev, R. M. Vengrov, S. G. Yaramishev
ITEP, 25, Bolshaja Cherjomushkioskaya, Moscow 117259, Russia

The development of the optimal design of high power facility for NPP transmutation and for a number of applications can not be carried out without of preliminary tests of much cheaper prototypes. It has been proposed to combine in new test facility 36 MeV Linac ISTRA constructed in ITEP, original Be target and subcritical blanket that will be mounted on the place of partly disassembled heavy water ITEP experimental reactor. The basic parameters of Linac, schemes of the target and blanket are described. It will provide the direct experiments on installation which can be considered as prototype future linac driven high power facilities.

Presently, 150 mA beam has been accelerated in RFQ and first DTL resonator up to 10 MeV at low duty cycle. For assembly second DTL cavity there are all drift tubes and all other parts. Linac average current can be rised up to 1 mA by increasing of duty factor. The existing cavities allow to achieve such (and fourfold) regime, it is necessary only to upgrade the RF system.

The preliminary estimation of project parameters of the proposed facility (flux of thermalize neutrons 10^{12} - 10^{15} n/cm^{2}s in experimental channels zone) shows that it could be very useful for a number applied and research program.

825
822

Measured Radionuclide Production From Copper, Gold and Lead Spallation Targets

Theodore A. Parish and Anthony P. Belian
Nuclear Engineering Department
Texas A & M University
College Station, TX 77843-3133

Abstract. Spallation target materials are chosen so as to produce large numbers of neutrons while at the same time avoiding the creation of long-lived radioactive wastes. While there has been considerable research to determine the number of neutrons produced per incident particle for various target materials, there has been less effort to precisely quantify the types and amounts of radionuclides produced. Accurate knowledge of the radioactive species produced by spallation reactions is important for specifying waste disposal criteria for targets. In order to verify the production rates calculated by LAHET, a study has been conducted using the Texas A& M University (TAMU) Cyclotron to measure radionuclide yields from copper, gold, and lead targets.

INTRODUCTION

Spallation neutron sources have been proposed for radioactive waste transmutation [1]. Spallation reactions are induced when high energy particles from accelerators slam into targets. For transmutation applications, the primary particles are usually assumed to be 500 Mev to 3 Gev protons, or in some cases, deuterons. The term "spallation reactions" refers to those inelastic nuclear reactions in which 1) at least one of the two colliding nuclei is a complex nucleus and 2) the energy available far exceeds the typical interaction energy between nucleons in a nucleus [2]. Generally, any nucleon - nucleus reaction in which the incident energy exceeds 50 MeV per amu is termed a spallation reaction.

At high incident energies, the "compound nucleus" model for describing nuclear reactions is no longer adequate and the explanation of spallation reactions requires an improved two step model due to Serber. In the first step, termed the intranuclear cascade, the incident particle interacts with individual nucleons within the target nucleus, and in so doing, a few nucleons are knocked out of the target nucleus. These particles are more energetic and less isotropically distributed than those emitted later by the residual nucleus. Some of the nucleons emitted in the first step may have sufficient energy to induce "spallation" in other target nuclei. In the second step, the residual nucleus, which contains fewer nucleons and is in an excited state, de-excites by emitting single nucleons or small clusters of nucleons through an evaporation process leaving behind a final (potentially radioactive) nucleus. Particles and gamma rays emitted in the second step are more isotropic and less energetic (less than 10 MeV) than those emitted in the first step [3].

Spallation reactions are capable of producing a wide variety of particles and final nuclei. Particularly, when transmuting long-lived fission products, like Tc^{99} and I^{129}, it is essential that the quantity of waste radionuclides produced as a result of the beam-target interactions should be small. The choice of spallation target material is therefore dictated by the needs 1) to produce large numbers of neutrons and 2) to avoid the creation of long-lived wastes. The radioactive

species produced as a result of spallation reactions are important in determining the disposal options for the targets from accelerator driven transmutation systems.

One modern code used to predict the types and amounts of spallation products produced as a result of beam-target interactions is called LAHET (Los Alamos High Energy Transport) [4]. LAHET is an improved and modernized version of HETC which was originally developed at Oak Ridge National Laboratory. The system of codes consisting of LAHET, its data libraries and post-processors, is designated as the LAHET Code System (LCS). In LAHET, an alternative intranuclear cascade model has also been adapted from the ISABEL code [5], which allows deuterons, helium ions and antiprotons to be modeled as source particles. In order to verify the spallation product distributions computed by LAHET, experimental irradiations of thin copper, gold and lead targets have been performed and the resulting radioactivities are reported here.

PROCEDURE

The accelerator used for the irradiations was the TAMU Cyclotron. This machine with its superconducting magnets is capable of accelerating particles to a maximum energy of 60 MeV per amu. This is significantly less than the energies desired for most accelerator driven transmutation applications, but is nonetheless, above the (somewhat arbitrary) energy threshold (50 MeV per amu) for classifying the induced target reactions as "spallations". Without any modifications, the TAMU Cyclotron can produce beams of 120 MeV deuterons at currents up to 10 nanoamperes. While higher particle energies would have been desirable, 120 MeV is the maximum deuteron energy achievable with the TAMU Cyclotron.

Two irradiations were performed using 120 MeV deuterons. In the first, a 1 mm thick lead sample was bombarded for two hours at a beam current of 1 nanoampere. The experimental setup is shown in Fig. 1. In the second, copper and gold samples with thicknesses of .15 mm and .0635 mm, respectively, were irradiated at 8 nanoamperes for 15 min. After the irradiations, gamma

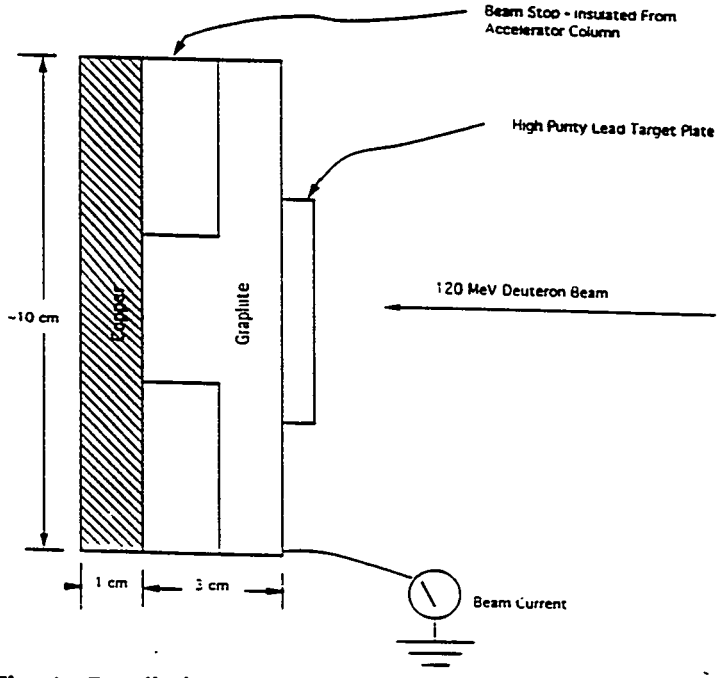

Fig. 1. Irradiation Setup for TAMU K500 Cyclotron.

827

rays emitted from the samples were counted using a well calibrated, high purity germanium detector. The germanium detector was absolutely calibrated using a mixed gamma (Eu^{152}) standard. Spectra from all of the samples were collected several times during the weeks following the irradiations. The earliest useful multichannel spectra from the copper and gold foils were obtained about 6 hours after the end of irradiation. For the lead sample, the earliest useful spectrum was obtained about 12 hours after the irradiation and the last useful spectrum was accumulated 14 months after the irradiation. Using customized emission libraries that included those nuclides that were expected to be produced by the spallation reactions, the gamma ray peak and identification software, GENIE PC, was used to determine the types and amounts of the radioactive species in the samples. The measured activities were also compared to the calculated activities which were determined from the LAHET production rates and calculations employing appropriate radioactive decay equations for various decay chains.

The procedure for calculating the amount of a particular nuclide as a function of time consisted of two parts. First, LAHET was used to model the experimental irradiation in order to obtain the production rate per incident deuteron for each radionuclide. Second, coupled differential equations for each decay chain were set up and solved for the buildup and decay of the radionuclides both during and after the irradiation. The software package Maple was used to solve the resulting coupled differential equations. An example of a typical three member decay chain from the gold irradiation is shown in Figure 2.

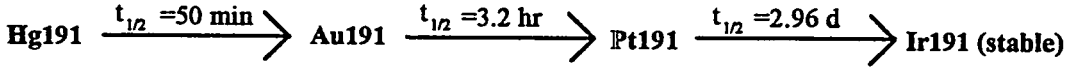

Fig. 2. Decay structure of mass chain 191.

Equations 1, 2, and 3 are used to determine the amounts of each nuclide as a function of time during irradiation.

$$\frac{dN_a(t)}{dt} = I * Y_a - \lambda_a * N_a(t) \quad (1)$$

$$\frac{dN_b(t)}{dt} = I * Y_b + \lambda_a * N_a(t) - \lambda_b * N_b(t) \quad (2)$$

$$\frac{dN_c(t)}{dt} = I * Y_c + \lambda_b * N_b(t) - \lambda_c * N_c(t) \quad (3)$$

Where 'a' denotes Hg^{191}, 'b' denotes Au^{191}, 'c' denotes Pt^{191}, 'I' is the beam current (deuterons per second), 'Y_X' is the nuclide yield taken from LAHET for nuclide X (atoms per deuteron), and 'λ_X' is the decay constant of nuclide X (inverse seconds). The equations that determine the amounts of each nuclide as a function of time after irradiation are the same as the above equations except that 'I' is taken to be equal to zero. The solutions to the three coupled differential equations of the mass-191 decay chain are too large to be included here, but other necessary data to solve these equations are the initial amounts (zero) and the time of irradiation (seconds). Using a spreadsheet, the activities of each radionuclide were calculated as a function of time and graphs were produced comparing the calculated and measured results.

RESULTS

Activities from Copper and Gold

Table 1 presents the measured and calculated activities for all of the identifiable radionuclides in the copper and gold foils. Note that the LAHET production rates, in general, lead to activities within a factor of two of the measured values. Since the observed activity varies according to the time of counting, the results in Table 1 were not taken from a single set of counting data, but instead reflect "typical" agreement over four sets of counting data.

Table 1. Calculated and Measured Activities of the Copper, Gold and Lead Foils

Foil	Nuclide	Calc. Activity (μCi)	Meas. Activity (μCi)	Ratio (calc/meas)
Copper	Mn54	1.6020E-04	6.2082E-04	0.26
	Mn56	1.7738E-02	6.4747E-02	0.27
	Fe59	4.4029E-04	6.0194E-04	0.73
	Co55	1.0245E-03	7.5072E-03	0.14
	Co56	8.4904E-04	1.6793E-03	0.51
	Co57	1.2606E-03	2.0374E-03	0.62
	Co58	8.0631E-03	1.0476E-02	0.77
	Co60	1.6268E-04	2.0744E-04	0.78
	Ni57	2.6069E-03	7.6751E-03	0.34
	Cu61	1.9056E+00	1.1213E+00	1.70
	Zn62	4.5185E-02	1.3118E-02	3.44
Gold	Ir186	2.2702E-02	1.7198E-02	1.32
	Pt188	1.0483E-02	2.4475E-02	0.43
	Pt189	4.2034E-01	5.4619E-02	7.70
	Pt191	2.4957E-01	1.7386E-01	1.44
	Pt197	1.0944E-02	1.0239E-01	0.11
	Au191	2.3774E+00	2.2610E+00	1.05
	Au193	7.3203E-01	4.9804E-01	1.47
	Au194	1.7731E-01	1.2571E-01	1.41
	Hg192	2.1433E-01	2.2342E-01	0.96
	Hg197	1.4117E-02	9.6793E-02	0.15
Lead	Au195	1.5000E-04	2.4000E-04	0.63
	Bi207	3.7000E-04	1.3000E-04	2.85

Copper consists of two naturally occurring isotopes, Cu^{63} (69.17%) and Cu^{65} (30.87%). A total of eleven isotopes, produced by the irradiation, were identified and quantified from the

gamma ray spectra from the copper foil. Figure 3 presents a comparison of the measured and calculated activities of Co^{56} as a function of time after irradiation. This plot is representative of those obtained from the counting data for the other copper spallation products that are listed in Table 1. Based on the activities in Table 1, it can be seen that two isotopes, Cu^{61} and Zn^{62}, of the eleven copper spallation products are close in mass to the copper isotopes that constitute the target. The calculated activities of both Cu^{61} and Zn^{62} were overestimated relative to the measured activities. For the observed copper spallation products with masses (A) of 60 or less,

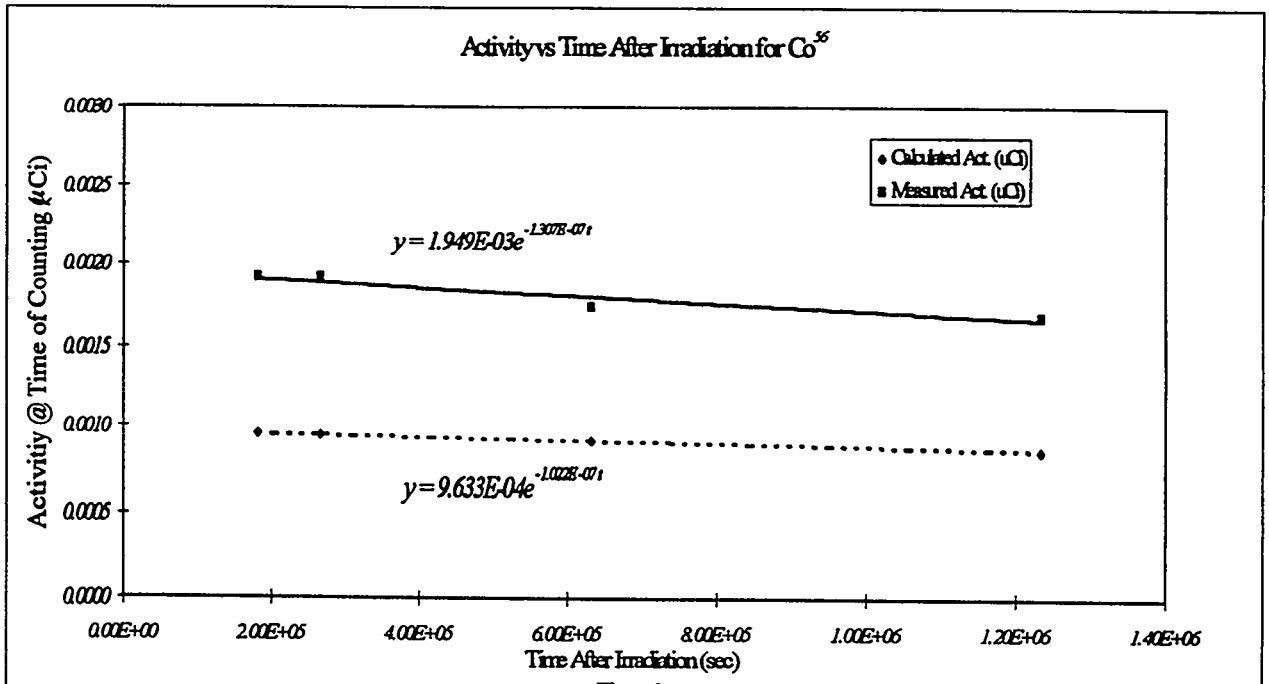

Figure 3.

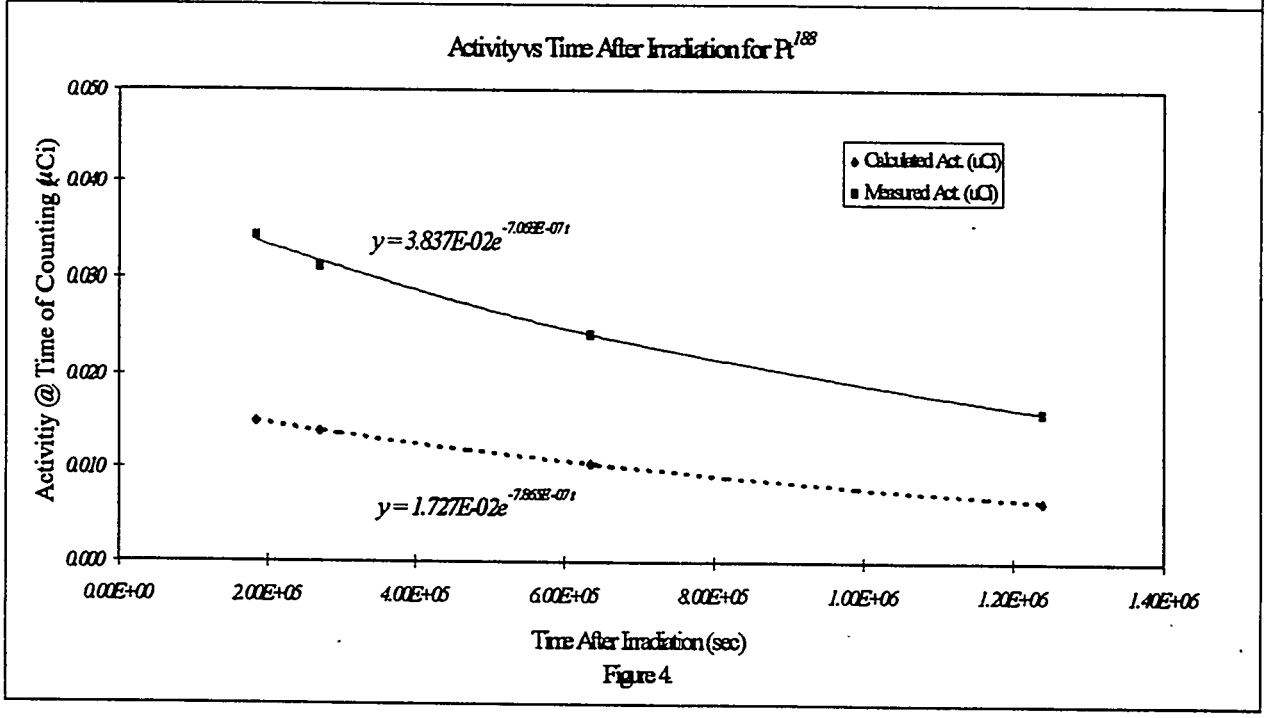

Figure 4.

the calculated activities based on the LAHET production rates were lower than the measured values.

Naturally occurring gold consists of a single isotope, Au^{197}. Based on the gamma ray spectra obtained from the irradiated gold foil, a total of ten spallation products were identified. As can be observed from Table 1, agreement between the calculated and measured values were reasonably good for seven of the product isotopes. Figure 4 displays a plot of the measured and calculated activities for Pt^{188} as a function of time after irradiation. This plot is typical of those obtained for the other gold spallation products. In the case of Pt^{189}, the calculated activities were about eight times larger than the measured values. In the cases of Hg^{197} and Pt^{197} , the calculated activities were about eight times smaller than the measured values. It is worth noting that Hg^{197} and Pt^{197} have the same "key" gamma which could account for the inflated measured activities of both nuclides since the GENIE PC software does not account for gamma rays of the same energy from more than one source isotope.

Agreement between the measured and calculated activities of the spallation products from both gold and copper were generally good, with the calculated activities typically being too small for copper and too large for gold. Spallation product activities for lead obtained in an earlier experiment were also comparable to those reported here. Thus, the LAHET (ISABEL) model for spallation product generation appears applicable over a target mass range from ~63 to ~208 for irradiations with relatively low energy (120 MeV) deuterons.

Activity from Lead

The activities of the identified radionuclides from the lead sample with half lives less than 15.3 days have been reported previously [6]. Eleven nuclides in eight different decay chains (masses from 199 to 206) were found and quantified using spectra obtained during the first two weeks after the end of irradiation. Subsequent gamma ray spectra obtained over one year after irradiation have led to the identification and quantification of two additional products, Bi^{207} and Au^{195}, which are reported here for the first time. The measured and calculated activities of these long-lived species, half lives of 32.2 years and 183 days, respectively, are also listed in Table 1.

One of the most important long lived radiospecies produced as a result of spallation reactions in lead is Bi^{207}. The measured amount of Bi^{207} was .00013 μCi, while the value predicted based on LAHET was .00037 μCi. Both results have fractional standard deviations that were estimated to be ~10 %. The standard deviation of the measured value is primarily due to counting statistics. It is worth noting that Bi^{207} is close in both Z and A to the most plentiful isotopes of the lead target, i.e. Pb^{206}, Pb^{207} and Pb^{208}.

In accelerator transmutation applications, one of the spallation products of greatest concern is Hg^{194} with its 520 year half life. The activity of Hg^{194} was not measured directly in the experiment reported here. However, Au^{195} which is contained in the decay chain that is only one mass unit greater than the decay chain containing Hg^{194} was observed. The calculated and measured activities of Au^{195} were .00015 μCi and .00024 μCi, respectively. Both the measured and calculated activities of Au^{195} were estimated to have fractional standard deviations of ~25%. The gamma ray spectra from the lead sample indicate that LAHET generally can be used to predict the activities of spallation products within factors of 2-3 of the measured values even for species like Au^{195} that have masses over 10 amu less than the dominant isotopes in the target.

CONCLUSIONS AND RECOMMENDATIONS

For each of the three types of samples irradiated, approximately eleven radioactive spallation products were identified and compared to predicted activities based on the production rates from LAHET. Counting of the lead sample over one year after the end of irradiation has also led to the identification of two long lived products, Bi^{207} and Au^{195}. Sufficient time has not yet elapsed since the end of the irradiation of the copper and gold samples to determine if long lived activity will be observable. Agreement between the measured activities and those predicted based on the LAHET production rates was generally within a factor of two. In the case of the lead experiment, the induced activity of Hg^{194} (520 year half life), which emits no gamma rays, was not observed. However, the activity of Au^{195} was observed and agreed reasonably well with the value predicted based on LAHET. For 120 MeV deuteron irradiations, the differences between the measured and predicted activities were of approximately the same size over the target mass (A) range from 63 (copper) to 208 (lead). Irradiations at higher deuteron energies are needed to verify that LAHET is applicable to transmutation system design. However, it appears that LAHET is most probably already sufficiently accurate to be used in estimating residual radioactivity of spallation targets for waste disposal classification purposes.

REFERENCES

[1] W.C. Sailor, C. A. Beard, F. Venneri and J.W. Davidson, "Comparison of Accelerator-Based With Reactor-Based Nuclear Waste Transmutation Schemes," *LA-UR-94-1001*, Los Alamos National Laboratory (1994).

[2] B.S.P. Shen and M.Merker, *Spallation Reactions and Their Applications*, Dordrecht,Holland / Boston,USA, D. Reidel Publishing Company (1976).

[3] G.S. Bauer, "Spallation Neutron Sources: Basics, State of the Art, and Options for Future Development," *Journal of Fusion Energy*, Vol.8, Nos. 3/4 (1989).

[4] R.E. Prael and H.Lichtenstein, "Users Guide to LCS: The LAHET Code System," *LA-UR-89-3014*, Los Alamos National Laboratory (1989).

[5] Y. Yariv and Z. Fraenkel, *Phys. Rev. C, 24* (1981), p. 488

[6] T. A. Parish, R. G. Cochran and C. A. Beard, "Spallation Products From a Lead Target Bombarded by 120 MeV Deuterons: Calculations and Measurements," *Transactions of the American Nuclear Society*, Vol. 68 (November 1993).

NEUTRON DATA LIBRARY FOR TRANSACTINIDES AT ENERGIES UP TO 100 MEV

Yu.A.Korovin, V.V.Artisyuk, A.Yu.Konobeyev, P.E.Pereslavtsev, V.I.Plyaskin, A.Yu.Stankovski

Obninsk Institute of Nuclear Power Engineering 249020, Obninsk, Russia

Abstract. New neutron data library for transactinides is briefly described. The library includes evaluated cross-sections for fission and threshold neutron induced reactions for isotopes of U, Np and Pu at energies 0-100 MeV.

To study processes of activation and transmutation of transactinides irradiated by fast neutrons new data library WIND has been elaborated. The library containes evaluated neutron induced fission reaction cross-sections, cross-sections for threshold reactions (n,xn), (n,pxn) and (n,αxn) for uranium, neptunium and plutonium isotopes at energies from 0 to 100 MeV. The WIND includes the cross-sections for 576 reactions taking place in neutron irradiation of ^{232}U, ^{233}U, ^{234}U, ^{235}U, ^{236}U, ^{237}U, ^{238}U, ^{237}Np, ^{239}Np, ^{236}Pu, ^{237}Pu, ^{238}Pu, ^{239}Pu, ^{240}Pu, ^{241}Pu, ^{241}Pu, ^{243}Pu, ^{244}Pu.

The detailed description of method to obtain cross-sections contained in the library is given in Ref.[1].

The evaluation of cross-sections includes the calculation of preequilibrium particle spectra on the basis of geometry dependent hybrid exciton model and using energy-independent experimental and calculated relations of neutron and fission widths Γ_n/Γ_f for description fission-evaporation competition.

The calculation of nonequilibrium nucleon spectra was carried out taking into account multiple pre-compound emission in accordance with [2]. Nucleon-nucleon interaction cross-sections with the correction for the Pauli principle were used to calculate the rate of intranuclear transitions (λ_+). Normalization coefficient for the calculation of λ_+ value was taken to be equal to unity.

The calculation of pre-compound α-particle spectra was performed within the frame of the coalescence pick-up model combined with the hybrid exciton model, as described in Ref.[3].

Neutron to fission width relation Γ_n/Γ_f and fission barriers B_f were taken from known systematics and empirical compilations.

The probability of γ-emission was calculated using average radiation widths with their energy dependence taken according to Ref.[4].

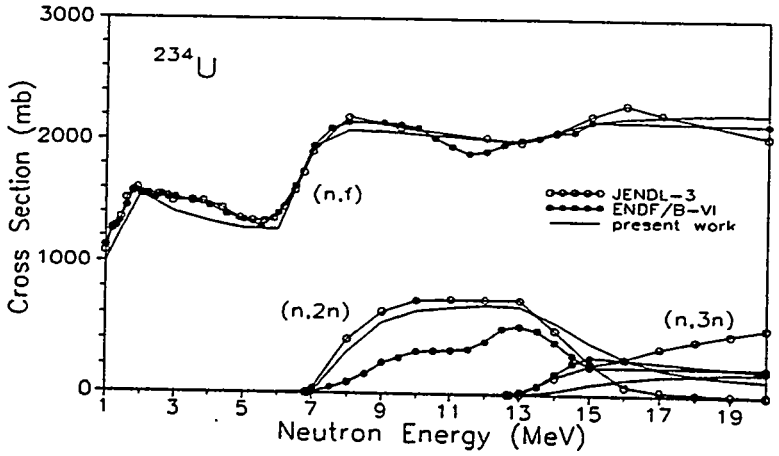

Figure illustrates typical result of present evaluation compared to the data from libraries ENDF/B-VI and JENDL-3.

The catalogue of WIND includes information about target nucleus, type of reaction, residual nucleus and brief commentary for method to obtain cross-section. The fragment of WIND catalogue is presented below.

The library is distributed in ENDF-6 format. All files are available from authors after request.

Fragment of catalogue

Target	Reaction	Product	Q-value	Comments
92-U -235	(N,2N)	92-U -234	-5.298E+00	Below 20 MeV BROND; GDH, *EXPR Gn/Gf*
92-U-235	(N,3N)	92-U -233	-1.214E+01	Below 20 MeV BROND; GDH, EXPR Gn/Gf
92-U -235	(N,4N)	92-U -232	-1.790E+01	GDH, EXPR Gn/Gf
92-U -235	(N,5N)	92-U -231	-2.515E+01	GDH, SYST Gn/Gf
92-U -235	(N,6N)	92-U -230	-3.105E+01	GDH, SYST Gn/Gf
92-U -235	(N,7N)	92-U -229	-3.872E+01	GDH, SYST Gn/Gf
92-U -235	(N,8N)	92-U -228	-4.481E+01	GDH, SYST Gn/Gf
92-U -235	(N,9N)	92-U -227	-5.254E+01	GDH, CALC Gn/Gf
92-U -235	(N,10N)	92-U -236	-5.892E+01	GDH, CALC Gn/Gf
92-U -235	(N,P)	91-PA-235	-0.621E+00	GDH; NORMALIZED TO EXPR 14.5 MEV
92-U -235	(N,PN)	91-PA-234	-6.723E+00	GDH, EXPR Gn/Gf
92-U -235	(N,P2N)	91-PA-233	-1.193E+01	GDH, EXPR Gn/Gf
(see full content in a special file)				

REFERENCES

[1] A.Yu.Konobeyev, Yu.A.Korovin, V.I.Plyaskin, *Kerntechnik 59* (1994) 87
[2] M.Blann, H.K.Vonach, *Phys. Rev. C28* (1983) 1475
[3] A.Yu.Konobeyev, Yu.A.Korovin, *Kerntechnik 59* (1994) 72
[4] H.Maletski, A.B.Popov, K.Tshchetsyak, *Yadernaya Fizika 37* (1983) 284

STATUS OF NUCLEAR DATA FOR ACTINIDES

Boris Ya. Guzhovskii, Vladimir P.Gorelov, Andrey N.Grebennikov, Gennady G. Farafontov and Vladimir I.Il'in.

Russia Federal Nuclear Centre - VNIIEF

607200, Arzamas-16, Nizhny Novgorod region, Russia

Abstract. Nuclear data required for transmutation problem include many actinide nuclei. In present paper the analysis of neutron fission, capture, (n,2n) and (n,3n) reaction cross sections at energy region from thermal point to 14 MeV was carried out for Th, Pa, U, Np, Pu, Am and Cm isotops using modern evaluated nuclear data libraries and handbooks of recommended nuclear data. Comparison of these data indicates on substantial discrepancies in different versions of files, that connect with quality and completeness of original experimental data.

INTRODUCTION

The investigation of actinide nuclear property has been started more half century ago. Two prominent problems of twenty century - the creation of nuclear weapons and power reactors - were the principal stimulus for realization of such a long research program. The main attention was directed on acquisition of nuclear data for a small set of nuclei used as power reactor fuel or nuclear weapon material or produced in noticeable amount by neutron capture. It is the main nuclear group, which includes the ^{232}Th, ^{233,235,238}U, ^{237}Np and $^{238\text{-}242}$Pu nuclei. They have enough long half life and are produced in sufficient great amount. These circumstances alleviated their experimental investigation using particle accelerators and research reactors as neutron sources.

The second actinide nuclei group includes such long lived nuclei as ^{231}Pa, ^{232,234,236}U, ^{244}Pu, ^{241,242m243}Am, $^{243\text{-}248}$Cm, which are accumulated by neutron irradiation of nuclear fuel. They are less important for fuel cycle than first nuclei group and therefore they have not been explored adequately.

The third actinide nuclei group includes following short-lived nuclei: ^{232,233}Pa, ^{233}Th, ^{237,239}U, ^{238,239}Np, ^{243}Pu, ^{242g,244g,244m}Am and ^{242,249}Cm, which are produced by transmutation of original fuel. The equilibrium amount of these nuclei in fuel is very small, therefore their neutron data has no influence practically on fuel cycle. Last time new nuclear power direction are discussed, for example, the problem of long lived radioactive waste (second group) along closed fuel cycle.

The transmutation facility differs from ordinary power reactors by more high level of neutron flux needed for high enough transmutation rate. The typical neutron flux is about 10^{15} - 10^{16} n/cm^{2}s for different estimations.In this case transmutation life time is about 1 - 10 days for capture cross-section of 10^3 barn. This life time is comparable with the half life for β-decay of the third nuclei group. Therefore it is necessary to take into account the competition of two branches: radioactive decay and nuclear reactions. The fuel composition for transmutation facility also differs from power reactor fuel. Second group nuclei are the main fuel component for transmutation. The transmutation facility based on accelerator, target and subcritical blanket differs from ordinary power reactor also by original neutron spectrum formed by spallation (p,xn) reaction. Spallation neutrons are faster than fission spectrum ones (average neutron energy is $\approx$ 20 MeV and $\approx$ 2 MeV, respectively). As a result for transmutation problem the main nuclear data requirements displace from the first to the second and third nuclei groups. The first

nuclei group materials will be used as an amplifier of initial neutron flux, therefore it is necessary to know nuclear data particularity in fast neutron region.

EVALUATED NUCLEAR DATA ANALYSIS

We have considered evaluated nuclear data state for actinide nuclei from the point of view of requirements arisen from transmutation problem. Evaluated neutron data from main modern libraries: ENDL-82, ENDF/B-6 (USA), JENDL-3 (JAPAN) and BROND-2 (former SU) and recommended data from [1,2] in ordinary energy region below 20 MeV were taken by us as a basis for analysis. We distinguished four specific subregion within it: thermal, resonance, fission spectrum and around 14 MeV. The comparison of nuclear data from various libraries was carried out by the most economic method permitting, nevertheless, fully judge of available uncertainties in the knowledge of competitive nuclear data which are important from the point of view of transmutation problem in various energies neutron flux. The following characteristics were considered:

- fission and capture cross-sections at thermal point (E =0.0253 eV) below designated as σ_{fo} and $\sigma_{\gamma o}$, respectively;
- infinitely dilute resonance integrals (hereafter resonance integrals) of fission and capture designated by I_f and I_γ;
- averaged on ^{252}Cf spontaneous fission neutron spectrum cross-sections of fission, capture and the (n,2n) reactions, designated as $\bar{\sigma}_f$, $\bar{\sigma}_\gamma$ and $\bar{\sigma}_{2n}$;
- cross-sections of fission and the (n,2n), (n,3n) reactions at the point En = 14 MeV, designated as σ_f, σ_{2n} and σ_{3n}.
- fission and capture resonance integrals for a interval of sets with the increasing upper (E_{max}) and lower (E_{min}) limits of integral denoted as ΔI_f and ΔI_γ;
- averaged cross-sections

$$\langle \sigma_\gamma \rangle = \int_{E_{min}}^{E_{max}} \sigma_\gamma(E)\, dE / (E_{max} - E_{min})$$

for the processes of fission (γ=f) and capture and number of sets of integration limits (E_{max}, E_{min}).

Before the comparison of various data let us note some comments. Experimental cross-section values at thermal point can be obtained by some various methods:

1. the measurements by time-of-flight method for neutron energy 0.0253 eV;
2. the measurements on Maxwell spectra with the average energy 0.0253 eV in thermal columns;
3. the measurements on reactor spectra having the average energy 0.0253 eV.

The experimental results of the first group have priority over the rest ones. The discrepancies between the data of these groups are observed in practice, and the data of the third group are met more often. As an illustration there is a Table 1 where the comparison of cross-sections at thermal point is given for a set of actinides with the use of the first and second methods.

Table 1. The values of σ_{f_0} and σ_{γ_0}, in barn

nucleus	σ_{f_0}		σ_{γ_0}	
	method 1	method 2	method 1	method 2
U -234	0	0	94,7	84,1
U -236	0	0	8,54	7,66
Np -237	-	-	151	161
Pu -238	17,5	-	500	434
Pu -240	0,06	0,05	246	235
Pu -241	950	1030	345	390
Pu -242	-	-	15,7	14,3
Am -241	2,91	3,49	622	800
Am -243	0	0	142	147
Cm -244	0	0	9	8

According to the method of data obtaining experimentally evaluated resonance integrals may be classified into the following most common groups :

1. calculation on measured differential data;
2. measured by activation method with Cd-shield for relatively "clean" samples data;
3. measured on the reactor by various ways data;The list of evaluation methods is discussed in more detail in [2] and the data of the first and second groups have priority in this case.

The values of I_f and I_γ depended on the choice of E_{max} and E_{min}. Dependence on E_{min} is important both for I_f and I_γ under strong resonance distinctions in energy dependencies of corresponding cross-sections . In the experiments E_{min} changes from 0.3 to 0.68 eV. The value of E_{min} =0.5 eV is the mostly used value and it will be taken by us for our further estimations. The choice of E_{max} is most important for fission reaction, particularly, in case of the threshold structure of this reaction. As it was noted in [2] the calculations for ^{243}Am has shown that the change of E_{max} = 10 MeV by E_{max} = 20 MeV increases the I_f value a 1.5 times. However at comparison of results of experimental evaluation of resonance integrals obtained either on thermal columns, or immediately in reactors, one should remember that neutrons with the energy En > 10 MeV are practically absent in the reactors. Therefore we have restricted ourselves to the energy E =10 MeV. It must be noted also, that I_f values obtained at the reactors may contain an error that was caused by the differences of reactor spectra at En > 100 keV from Fermi ones and was not taken into account.

The calculation of $\bar{\sigma}_f$, $\bar{\sigma}_\gamma$ and $\bar{\sigma}_{2n}$ was carried out with the help of approximation of spectrum of ^{252}Cf spontaneous fission neutrons from [3], that was recommended by US National Bureau of Standard as a standard reference.

At least, the comparison of ΔI_f, ΔI_γ, $< \sigma_f >$ and $< \sigma_\gamma >$ values for various (E_{max}, E_{min}) pairs was carried out for visual identification of energy intervals where the differences of competitive versions of evaluated data are of a great significance. RECONR code was used under the recovery of energy dependence of cross-sections in resonance region. The accuracy of recovery corresponded to the ERR = 0.05 value of parameter in all cases, except ^{232}Th and ^{238}U. In case of ^{232}Th we were forced to restrict ourselves by the value ERR = 0.1 and for ^{238}U this limit was

equal to 0.5. Thereat the I_f and I_γ calculation error was less than that of recommended values of these quantities.

The region of thermal and resonance energy is more convenient and effective from the point of view of transmutation because of joint action of two factors: high level neutron flux (to 10^{16} n/cm^2s) and high level values of capture and fission cross-section (to several thousands of barn). Fission process dominates in fission spectrum region. The threshold (n,xn) reaction give essential contribution (less than fission reaction) around 14 MeV region.

Neutron data for first group nuclei are the most completely and thoroughly studied. They are included practically in all references libraries and handbooks. Maximal neutron cross-section differences are limited by 10%. This situation is rather successful. Neutron data for the second group nuclei are known with great discrepancies (up to 50%)and are not complete. These data should be refined and completed by direct measurements and nuclear model calculations. The most unsuccessful situation is for the third group nuclei. It is connected with a very difficult measurement conditions for short lived target nuclei and with a slight interest of these nuclear data. If the half life is much less than that of transmutation, nuclear data for short lived nuclei may be considered as not essential ("momentary" b-decay). It is necessary to take into account nuclei transmutation probability for high level neutron flux (to 10^{16} n/cm^2s) and cross-section (to thousand barn) and half life more than 1 day. Unfortunately, neutron cross-section for short lived actinide nuclei are practically absent or measured near thermal point with great errors. The information about file presence in reference libraries is given in Table 2 for illustration. The values of $\sigma_i^{max}/\sigma_i^{min}$ ratio for different cross-sections showing maximal discrepancies between the values of different libraries are also included.

Ratio of fission cross-section at thermal point and resonance integrals of fission are particularly large in cases where there is fission threshold and fission probability is small. Capture cross-section ratio has large discrepancies in the region of fission spectrum, where capture cross-sections fast decrease with energy increasing. Average fission cross-section is determined well enough in this region. Maximal difference among average values are not more than 5% for the first nuclei group and 10% for the second one. Near 14 MeV fission cross-section ratio has small difference (not more 10%). Situation in this region is much worse for the (n,2n) and (n,3n) cross-sections. Cross-section ratio of various libraries differ several times. Spallation neutron spectrum is very fast, therefore it is necessary to know the (n,xn) process probability with high precision in order to describe the conversion of original neutron spectrum to more slower one of secondary neutrons.

CONCLUSION

The transmutation rate for actinide nuclei is determined, first, by region of thermal and resonance neutrons, where neutron flux maximal level and fission and capture cross-sections may be reached. These data for the third nuclei group are unknown or determined roughly. Therefore it is necessary to carry out new experiments and investigations first and foremost for such nuclei as $^{232,233}Pa$, ^{237}U, $^{238,239}Np$ and ^{242g}Am in thermal and resonance region, where fission and capture cross-sections are high enough. In unresolved resonance region there is good cross-section approximation by modern nuclear model calculations. Fast neutron contribution of fission and (n,xn) reaction to the common rate of actinide transmutation is small. Summary absorption cross-section is about 3 barn for 14 MeV that is several hundred times below than that in thermal and resonance regions. Fast neutron reactions are essential for creation of excess

neutrons to good advantage for transmutation after moderation. Therefore it is necessary to know with high precision the cross-sections of neutron multiplication for corresponding materials (from the first or second groups), that will be used in target blanket systems.

Application of subcritical blanket with K_{eff} =0.95-0.98 provides a possibility to increase neutron flux 20-50 times. However, in this case it is necessary to have easily accessible reliable subcritical level for all stages of transmutation process with account of change of blanket composition. These conditions impose heavy demands on precision of neutron data needed for K_{eff} correct calculation. The choice of main blanket materials essentially depends on proposed conception. On the other hand, the choice of one or other blanket type is mainly determined by nuclear data for specific fissionable materials. In the light of transmutation problem the nuclear data status for actinides is considered to be unsatisfactory. Great work is to be done to create special-purpose library of evaluated nuclear data for actinides on a basis of new experimental data and calculations, that will permit to eliminate completely the main drawbacks and gaps in available data.

References

1.Mughabghab S.F.- Neutron Cross Sections, v.1, part B, N.Y.- London: Academic Press, 1984.

2.Belanova T.S., Ignatyuk A.V., Pashchenko A.B., Plyaskin V.I., - Radiative capture of neutrons: Handbook, Moscow, Energoatomizdat, 1986.

3.La Bauve R.J., Madland D.G., - Transactions of APS, v.44 - N1, 1983, p.538.

Table 2 Nuclear data information for actinides

nn	Nuclei	1	2	3	4	5	6	7	8	9	10	11	12
1.	Th-232	+	+	+	+	15,6	1,01	1,06	1,12	1,05	1,16	1,04	1,32
2.	Th-233	+	+	-	-	1	1,07	7,7	1,61	1,15	1,13	1,21	1,55
3.	Pa-231	-	+	+	-	3,3	1,14	76,5	2,86	1,18	1,38	1,06	1,83
4.	Pa-232	-	+	-	-	1	1,64	1	1,04	-	-	-	-
5.	Pa-233	-	+	+	-	-	1,06	2,24	1,05	1,45	1,55	1,66	2,79
6.	U-232	-	+	+	-	1,05	1,03	1,33	1,84	1,23	3,54	1,92	11,4
7.	U-233	+	+	+	+	1,01	1,05	1,06	1,06	1,05	1,19	1,04	2,50
8.	U-234	+	+	+	-	77,4	1,04	1,44	7,02	1,02	1,57	1,03	1,89
9.	U-235	+	+	+	+	1,03	1,05	1,03	1,14	1,01	1,05	1,02	1,56
10.	U-236	+	+	+	+	10,6	1,06	1,67	2,5	1,04	1,89	1,05	3,42
11.	U-237	+	-	+	-	5,7	1,25	10,6	4,14	1,07	1,29	1	1
12.	U-238	+	+	+	+	436	1,02	1,02	1,08	1,03	1,15	1,02	1,06
13.	U-239	+	-	-	-	1	1	-	-	-	-	-	-
14.	Np-237	+	+	+	-	1,43	1,07	1,15*	1,12	1,05	1,10	1,10	1,04
15.	Np-238	+	-	+	-	1,03	4,72	1,64	10,6	-	-	-	-
16.	Np-239	-	+	+	-	-	2,08	1	1,03	-	-	-	-
17.	Pu-238	+	+	+	+	1,10	1,02	1,38	1,15	1,04	1,45	1,03	4,70
18.	Pu-239	+	+	+	+	1,01	1,01	1,03	1,10	1,01	1,41	1,06	2,23
19.	Pu-240	+	+	+	+	2,13	1,05	1,17	1,06	1,08	1,18	1,07	4,6
20.	Pu-241	+	+	+	+	1,02	1,13	1,08	1,39	1,10	1,7	1,08	4,75
21.	Pu-242	+	+	+	+	2,84	1,04	9,1	1,17	1,11	1,21	1,10	1,69
22.	Pu-243	+	-	+	-	1,09	1,47	1,09	1,03	1	1	1	1
23.	Pu-244	-	-	+	-	-	1,08	-	2,6	-	-	-	-
24.	Am-241	+	+	+	+	1,09	1,58	1,81	1,25	1,08	2,3	1,18	2,9
25.	Am-242g	-	+	+	+	1,38	21,8	2,04	17,0	1,04	1,77	1,05	2,14
26.	Am-242m	+	+	+	+	1,10	1,59	1,34	1,76	1,21	5,95	1,07	2,14
27.	Am-243	+	+	+	+	2,7	1,09	1,67	1,31	1,05	4,46	1,05	11,0
28.	Am-244g	-	+	-	-	1	-	-	-	-	-	-	-
29.	Am-244m	-	+	-	-	1	-	-	-	-	-	-	-
30.	Cm-242	+	+	+	+	1,67	1,26	7,85	1,49	1,78	4,5	1,18	29,4
31.	Cm-243	+	+	+	-	1,15	6,75	2,53	2,07	1,07	6,1	1,16	6,45
32.	Cm-244	+	+	+	+	2,5	1,49	2,94	1,11	1,15	3,3	1,32	5,65
33.	Cm-242	+	+	+	-	1,22	1,16	1,16	1,21	1,06	1,56	1,18	1,44
34.	Cm-246	+	+	+	-	2,7	1,29	1,67	1,38	1,12	1,36	1,15	11,0
35.	Cm-247	+	+	+	-	1,30	1,58	1,53	2,2	1,08	1,76	1,02	2,41
36.	Cm-248	+	+	+	-	4,2	1,56	1,19	1,15	1,10	1,63	1,28	1,55
37.	Cm-249	-	+	-	-	-	-	-	-	-	-	-	-

Descriptions for table 2:

1) - ENDL-82; 2) - JENDL-3; 3) - ENDF/B-6; 4) - BROND-2;

5) - $\sigma_{f_0}^{max}/\sigma_{f_0}^{min}$; 6) - $\sigma_{\gamma_0}^{max}/\sigma_{\gamma_0}^{min}$; 7) - I_f^{max}/I_f^{min}; 8) - $I_\gamma^{max}/I_\gamma^{min}$;

9) - $\bar{\sigma}_f^{max}/\bar{\sigma}_f^{min}$; 10) - $\bar{\sigma}_\gamma^{max}/\bar{\sigma}_\gamma^{min}$; 11) - $\sigma_f^{max}/\sigma_f^{min}$; 12) - $\sigma_{2n}^{max}/\sigma_{2n}^{min}$.

Measurement of ^{238}Np fission cross-section by neutrons near thermal point (preliminary results)

S.N. Abramovich, M.F.Andreev, Yu.M. Bol'shakov, V.V. Gavrilov, B.Ya.Guzhovskii, N.G. Krylov, I.K.Kunitsina, G.F.Novoselov, V.I. Serov, E.F.Fomushkin.

Russia Federal Nuclear Centre- All Russia Scientific Research Institute of Experimental Physics (VNIIEF)

607200, Arzamas-16, Nizhny Novgorod Region, Russia.

Abstract. Measurements have been carried out of ^{238}Np fission cross-section by thermal neutrons. The isotope ^{238}Np was built up through the reaction ^{238}U (p,n) on an electrostatic accelerator. Extraction and cleaning of the sample were done by ion-exchange chromatography. Fast neutrons were generated on the electrostatic accelerator through the reaction ^{9}Be(d,n); a polyethylene block was used to slow down neutrons. Registration of fission fragments was performed with dielectric track detectors. Suggesting that the behavior of ^{238}Np and ^{238}U. Westscott's factors are identical the fission cross-section of ^{238}Np was obtained: σ_{f0} =2110 ± 75 barn.

INTRODUCTION

In the works of Los Alamos National Laboratory (LANL) it was shown [1],that transmutation of odd-even actinides (^{231}Pa,^{237}Np,^{241}Am and others) into fission fragments in intense fields of thermal neutrons may be considerably enhanced. A radiation capture of a neutron by such a nucleus leads to formation of a compound odd-odd nucleus having a quite high fission cross-section by thermal neutrons. To apply successfully this property of the odd-odd actinides one needs high enough density of thermal neutrons flux ($10^{15} \pm 10^{16}$ n/cm^2*sec) to provide a series capture of the second neutron and formation of high-excited odd-even compound nucleus prior the β-decay of an intermediate odd-odd nucleus. Life-times of the nuclei, being of interest (^{232}Pa, ^{238}Np, ^{242}Am and others) don't exceed several tens of hours, for example, $T_{1/2}$(^{238}Np)=50.87 ± 0.05 hour [2].

To choose optimum parameters of such actinides transmutation one needs for reliable data on fission cross-sections of corresponding short-half-life odd-odd isotopes Pa, Np, Am and others with short life-times. However this data are few and in some cases are completely absent. For example, for ^{238}Np fission cross-section by thermal neutrons all the data represented in the neutron constant libraries are based on measurement [3],carried out in 1969 in Savannah River Laboratory (SRL): σ_{f0}(^{238}Np) = 2070 ± 30 b., with supposition - σ_{f0}(^{235}U) = 562.3 b.

In 1993 in LANL there were performed measurements of energy dependence ^{238}Np fission cross-section in the neutron energy range 0<E<2eV. The measurements were performed by time-of-flight method. For the thermal point E=0.0253 eV a value was obtained, which exceeds the generally accepted one.

At our Institute a cycle of integral measurements has been carried out of σ_{f0} value for ^{238}Np with the use the polyethylene block and the electrostatic accelerator as a neutron source.

The work is being fulfilled in accord with the contract with LANL.

The goal of the present report is the discussion of some experimental details and representation of preliminary measurement results of ^{238}Np fission cross-section by thermal neutrons.

BUILDING UP, PURIFICATION AND PRODUCTION OF THE ^{238}NP SAMPLE

Subnanogramm quantity of the ^{238}Np isotope was accumulated through the reaction ^{238}U(p,n)^{238}Np on the electrostatic recharged accelerator of VNIIEF. The accelerator operation mode: proton energy Ep=12MeV, beam current 0.6÷0.8 μA, beam diameter ≤6 mm.

By present two series of building up of ^{238}Np and following measurement have been performed. In the first series the irradiation of ^{238}U sample took 59 hours, during the second one - 88 hours.

The central part of the uranium target, under proton irradiation, was etched with a small quantity of the hot concentrated $HN0_3$ up to the moment a rapid reaction begins. Then this part of the target was treated two times during two minutes with a hot 6 M HCl. The walls of the vessel, where the etching was carried out were rapidly washed with concentrated HNO_3 and water. All the solutions were collected into a glass and then were evaporated to dryness. The sediment was dissolved in 7.5 M HNO_3, after this Np was stabilized in four-valency state with hydrogen peroxide. The solution was absorbed on anionite AB-17-8 (analog to Dowex-1). The chromatographic column was washed with 7.5 M HNO_3 to separate uranium and fission products. For the purpose of further cleaning the column was washed with 10 M HCl, then neptunium was extracted with 4 M HCl. Eluate was evaporated to dryness, dissolved in 6 M HCl, formic acid was added to the solution to stabilize Np in the four-valency state. Then the solution was absorbed from 10 M HCl on the anionite AB-17-8. The column was washed with 10 M HCl, then Np was desorbed with 4 M HCl, and eluate was evaporated to dryness. The dry precipitate was treated with 0.1 M HNO_3 and placed into an electrolytic cell, then it was made up to the required volume (pH 2.5) with water.

Electrolysis was carried out during 1.5-2 hours at current density 120÷140 μA/cm^2 and voltage 100 V. The obtained layer of ^{238}Np was washed and heated.

During the first series the process of ^{238}Np extraction, cleaning and layer production took 22 hours, during the second one - 18.5 hours.

QUANTITY MEASUREMENTS OF ^{238}NP NUCLEI IN THE LAYER AND OPERATING SOLUTIONS

"Weighing" of the ^{238}Np layer was performed by two methods. At the initial stage immediately after production and during irradiating the method of gamma-spectrometry was applied. During the final stage after practically full β-decay of ^{238}Np the methods of alpha-spectrometry were used.

Gamma-spectrometry

In the work the Ge(Li)-detector was used with the crystal volume 65 cm^3, as well as the standard complex of electronic apparatus, including the multichannel analyzer of pulses "Canberra" (series 85). The energy scale calibration of the spectrometer and efficiency of gamma-

quanta registration measurement was carried out with Standard Spectrometric Gamma Sources (SSGS-3), certified by the Government Metrologies Service.

Energy spectrometer resolution ΔE_γ=3÷4 keV. The energy dependence of registration efficiency for E_γ>200 keV was reproduced by the function $\varepsilon(E_\gamma) \sim E_\gamma^{-B}$. The registration efficiency also depends on geometry conditions of gamma-spectrum measurement, i.e. on the registration solid angle Ω. For the standard conditions of measurement $\Omega*\varepsilon(E_\gamma)=A*E_\gamma^{-B}$, where $A=1.29*10^{-4}$, B=1.12.

Gamma-spectra measurement results for the samples ^{238}U and ^{238}Np

For the ^{238}Np preparation a sample of poor ^{238}U was used with thickness 0.5 mm. The ^{235}U content in this sample was defined by the intensity of gamma-lines of these isotopes. In regard to self-absorption of gamma-quanta the value of the ^{235}U relative content in the sample was obtained: $N_{235U}/N_{238U}=(2,2\pm0,2)*10^{-3}$.

The content of ^{238}Np and ^{239}Np in the operating layer and solutions were defined by ^{238}Np lines intensities: E_γ=882.6; 924.0; 941.0; 984.5;1028 keV and ^{239}Np lines: E_γ=228.2; 277.6 keV. According to the gamma-spectrometry results in the first series the ^{238}Np layer contained after production immediately $(7.96\pm0.28)*10^{11}$ atoms of ^{238}Np and $(2.20\pm0.28)*10^{10}$ those of ^{239}Np; in the second series - $(9.12\pm0.20)*10^{11}$ atoms of ^{238}Np and $(2.63\pm0.38)*10^{10}$ those of ^{239}Np.

Gamma-spectrometry of solutions at different stages of extraction, cleaning and ^{238}Np covering allowed to determine losses of the isotope, presented at every stage. In the first series these losses comprised 5.5%; therewith

a) at the primary etching of the uranium target -1.85%;

b) in chromatographic columns under neptunium extraction -2.19%;

c) under electrolytic covering of ^{238}Np on the backing of stainless steel-1.5%.

In the second series ^{238}Np losses were somewhat higher.

It should be noted, that the procedure development of express chemical separation of neptunium and uranium was performed with gamma-spectrometry method and with dielectric track detectors. Two mixtures were prepared: ^{237}Np and ^{233}U; ^{237}Np and ^{235}U. In these preliminary investigations the coefficient of neptunium extraction wasn't worse than 86%, and the coefficient of uranium suppression $< 5*10^{-6}$.

Alpha spectrometry

There were used surface-barrier silicon detectors with energy resolution $\Delta E_\alpha \sim$ 40 keV, as well as the standard complex of electronic apparatus. To calibrate the energy scale and to "weigh" the operating layers Standard Spectrometric Sources of Alpha-Radiation (SSSAR) were used, certified by the Government Metrologies Service.

The weighing results of the operating layers with alpha-activity of ^{238}Pu with precision up to statistical and apparatus errors and with regard to time shifts agree with the gamma-spectrometry data.

With the help of alpha-spectrometry in the ^{238}Np layers the nuclei of ^{236}Pu were discovered, the product of ^{236}Np β-decay, being formed in the reaction ^{235}U(p,γ). The number of ^{236}Np nuclei relative to ^{238}Np was $< 10^{-4}$.

The Neutron Source

For the measurement of ^{238}Np fission cross-section by thermal neutrons the electrostatic accelerator EGP-10 was used and the slowing-down polyethylene block. To generate fast neutrons the reaction ^{9}Be(d,n) was used. The operation mode of the accelerator: Ed=11.5 MeV, I=1 μA. A beryllium plate 1 mm thick was used as the target; the output accelerator device was cooled with water. The slowing-down polyethylene block represented itself a cylinder with diameter 32 cm, length 30 cm with a central channel, diameter 4.5 cm. The beryllium target of the accelerator was placed inside the polyethylene block at 8 cm distance from the block face.

To investigate the thermal neutron field in the polyethylene block a miniature ionizing chamber was used with the calibrated ^{235}U layer. The maximum flux density of thermal neutrons of ~$4*10^8$ n/cm^2*sec was observed at the distance of 3 cm from the beryllium target along the cylinder block axis. Cadmium ratio for the ^{235}U fission reaction in this position comprised Rcd=41.9±0.5. In measurements the cadmium filter was used with thickness 0.45 mm.

PROCEDURE OF FISSION CROSS-SECTION MEASUREMENT

Dielectric Track Detectors

To register fission fragments the dielectric track detectors were used: a polymer film (polycarbonate) and a silicate glass. The use of such detectors allows to eliminate fully the background, related with α, β, γ - and neutron-radiation, electromagnetic induction and so on. The ^{238}Np layer with diameter 8.12 mm was placed in a special miniature assembly (a track chamber) with a polymer film with diameter 8.52 mm, the distance between the layer and the film is 1.47 mm. All the geometrical sizes of the assembly were controlled with the measuring microscope. The fragment registration efficiency in the track chamber is defined by the solid angle Ω of system: the source (layer) - the detector (film). Value Ω is calculated by the methods of geometrical possibilities. For the sizes, mentioned, Ω=0.5416±0.0056; the error is caused by possible irregularity of fissionable material distribution along the layer surface.

The ^{235}U layer, used as a standard, was placed in the track chamber with the glass detector. The solid angle of registration for such a chamber can be also calculated. In the previous years a set of such chambers was calibrated on the Institute laboratory neutron sources; the chambers were certified by the Institute metrologies service, and were used many times in nuclear explosion measurements [5].

Track chamber with the ^{238}Np and ^{235}U layers irradiation

The chambers with layers back-to-back were placed in the slowing-down block channel at the distance of 3 cm from the beryllium target. A free channel space in the block was filled with polyethylene. Irradiation cycle duration as a rule took 1-3 hours under irradiation without the cadmium filter and it took 5-10 hours to do it with the cadmium filter. In doing so the chamber with the ^{238}Np layer registered several hundred of fission fragments, depending on the ^{238}Np layer "age". The neutron yield in every cycle of irradiation was controlled by a "long" counter of Mac Cabbies and an integrator of deuteron current on the beryllium target. In the first series of

measurements 12 cycles were performed of irradiation by thermal neutrons; the time range of the experimental points was in total 5.20 - 420 hours (fig.). In the second series the attention was paid to the resonance (supercadmium) neutrons. That is why only 6 experimental points were obtained in the range 4.70 -165 hours (fig.2). The purification of the neptunium fraction from plutonium was accepted as the origin of the count. This process took place during neptunium washing-out from the chromatographic columns by the 4 M HCl solution (see above).

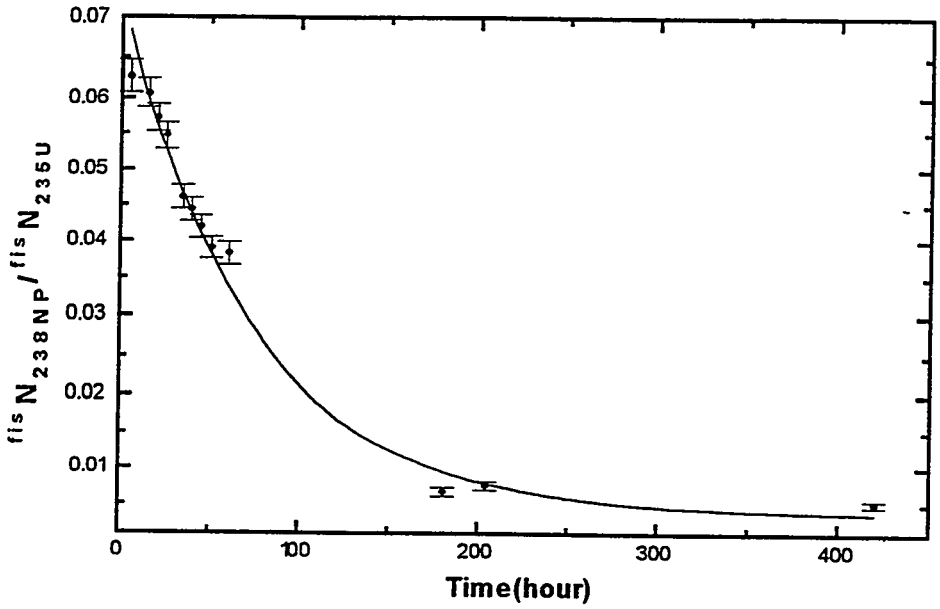

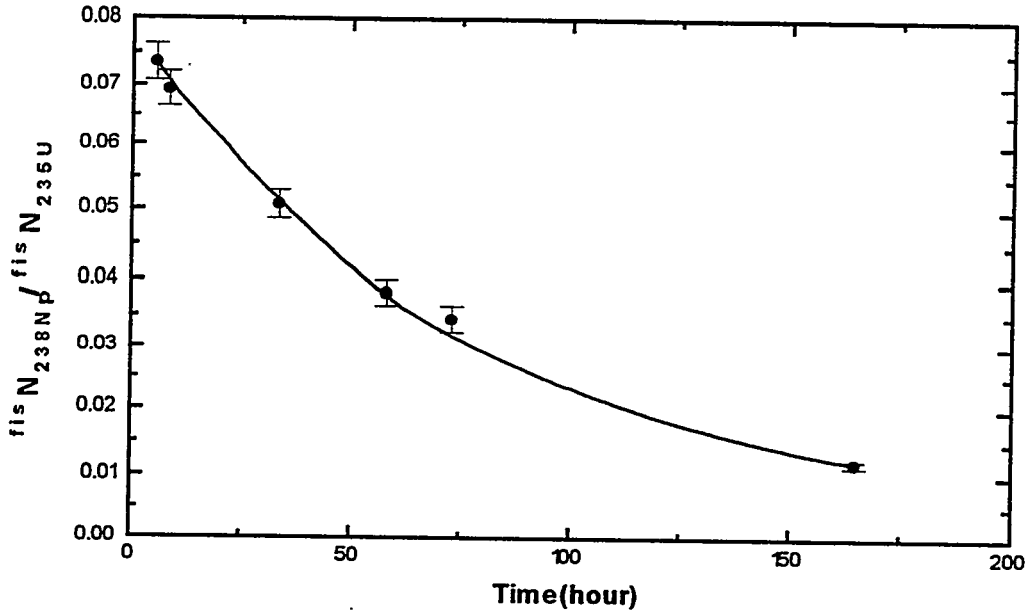

Fig. 1, 2. Time dependence of ($^{fis}N_{238Np}/^{fis}N_{235U}$)-value; 1-st and 2-nd series.

Data processing

During the following treatment of the results the value was used: $Z={}^{fis}N_{238Np}/{}^{fis}N_{235U}$,i.e. a normalized number of ^{238}Np fission by thermal (subcadmium) neutrons.

The time dependence of this value for two series of measurements is shown in fig.1.2. The results are also shown of approximation of experimental values by the dependence:

$$Z(t)=Z(0)*\exp(-0.013626*t)+C\ ,$$

where the value 0.013626[1/hour] - ^{238}Np β-decay constant [2].The values of approximation parameters, obtained (for the first series), are: Z(0)=0.06948±0.00106, C=0.00355±0.00033.

The constant component C is probably caused by the fission of ^{235}U nuclei remained in the ^{238}Np layer after chemical separation, the fission of ^{239}Pu nuclei, accumulated due to ^{23}9Np β-decay, and the fission of ^{236}Np nuclei, formed in the uranium target through the reaction ^{235}U(p,γ). A more detailed analysis of these components will be performed later.

Reasoning from the experimental data, obtained, one can define the ratio $[g(T)*\sigma_{f0}]^{238}Np/[g(T)*\sigma_{f0}]^{235}U$, where g(T) - Westcott's factor. Suggesting that Westcott's factors are identical for ^{238}Np and ^{235}U and $\sigma_{f0}(^{235}U)$=582.25 barn, one obtains the value

$$\sigma_{f0}(^{238}Np)=2110\pm75 \text{ barn.}$$

This result practically coincides with the data of Spencer and Baumann (SRL) [3].

CONCLUSION

The results, represented, are preliminary. Probably one more series of ^{238}Np accumulation and fission cross-section measurements will be carried out. Corrections will be introduced for the time dependence of ^{239}Pu accumulation in the operating layer, as well for remaining ^{235}U and others. The resonance integral value will be estimated on the base of the data obtained and the results of forthcoming measurements.

REFERENCES

[1] C.D.Bowman, E.D.Arthur et al. Nucl. Instr. Meth., A 320, 336 (1992).

[2] Decay Data on the Transactinium Nuclides. Techn. reports series N 261, IAEA, Vienna, p.157 (1986).

[3] J.D.Spencer, N.P.Baumann. Trans. Am. Nucl. Soc., v.12, N 1, p.284 (1969).

[4] M.S.Moore, A.D.Carlson, Y.Danon et al. International Conference on Nuclear Data for Science and Technology. May 9-13 1994, Gatlinburg, Tennesee, USA.

[5] E.F.Fomushkin, G.F.Novoselov, V.V.Gavrilov, Yu.I.Vinogradov. Proc. of Intern. Conf. on Nuclear Data for Science and Technology, May 13-17 1991, Julich, FRG, p.439-441 (1992).

ON THE PREEQUILIBRIUM EMISSION OF CLUSTERS

Lunev V.P.
Institute of Physics and
Power Engineering.
249020, Obninsk, Russia.
(084)399-8813

Masterov V.S.
Institute of Physics and
Power Engineering.
249020, Obninsk, Russia.
(084)399-8813

Pronyaev A.V.
Institute of Physics and
Power Engineering.
249020, Obninsk, Russia.
(084)399-8813

Shubin Yu.N.
Institute of Physics and
Power Engineering.
249020, Obninsk, Russia.
(084)399-8611

ABSTRACT

An approach for the description of the preequilibrium emission of light composite particles in the framework of the exciton model is proposed. The description is analogous to the Iwamoto-Harada[1,2] (I-H) model in which formation factors (FF) of clusters are obtained and the possibility of pick up process is taken into account. In the model proposed phase-space volume corresponding some arbitrary type of cluster with fixed excitation energies of nucleons picked up below and above Fermi Surface (FS) is calculated. This allows us to obtain the correct distribution of excitation energy between particle and hole degrees of freedom in the final state density of system: compound nucleus - cluster. The simple factorized form of the final state density of system can be obtained by introducing the average values of excitation energy of cluster constituent particles. The result of I-H treatment is valid only if we neglect the hole energy of picked up m particles, and thus it results in the overestimation of final states density and correspondingly overestimates cross-sections in comparison with the approach proposed. The numerical calculations of modified formation factors (MFF) of alpha particle and tritium are performed.

I. INTRODUCTION

As well known, the pre-equilibrium processes give dominant contribution to the high-energy part of particle's spectra emitted in reactions of light projectiles with nuclei. Overall such preequilibrium models as exciton[3] or hybrid[4] describe well many experimental data, but there exist some complications in description of cluster emission. A few publications proposing various ways of account of cluster internal structure, formed in compound nucleus at the pre-equilibrium stage of reactions are devoted to this problem.[1,5,6] The most successful and at the same time simple approach accounting also the possibility of pick-up of cluster components under Fermi surface (FS) is a model proposed by I-H. The cluster FF are explicitly calculated in this model while obtaining the density of final states. Weak dependence of cluster formation probability from characteristics of particular compound nucleus makes this approach almost nearly universal. In order to get a simple factorized form of final state density, it is argued in I-H that the part of excitation energy carried out by cluster components picked up under FS can be neglected. Influence of this approximation on the final result is not discussed there. The concepts given in I-H and their further development related with correct accounting of energy of pick-up particles is presented in this paper. The approximations used in framework of I-H approach are also analyzed.

II. CLUSTER PREEQUILIBRIUM EMISSION MODEL

This approach is based on exciton pre-equilibrium model of the I-H form . The differential emission cross section of the x-type cluster (x – is a number of constituent nucleons) is given by formula:

$$\frac{d\sigma}{d\varepsilon_x} = \hbar \cdot \sum_{n,l+m=x} \sigma_n \frac{W^{(n)}_{x(l,m)}(\varepsilon_x)}{\Gamma^{tot}_n}, \qquad (1)$$

notations are obvious. The primary object of the work is $W^{(n)}_{x(l,m)}(\varepsilon_x)$, the probability of emission of cluster with energy ε_x. Here l,m are the numbers of x-cluster constituents picked up correspondingly above and below FS (l+m=x). From the detailed balance principle we have:

$$W^{(n)}_{x(l,m)}(\varepsilon_x) = \frac{2s_x+1}{\pi^2\hbar^3}\mu_x\varepsilon_x\sigma^{abs}_x \cdot \frac{\omega^*}{\omega(p,h,E)}. \qquad (2)$$

Residual nucleus will have p-l particles and h+m holes after formation of cluster with l particle above and m below FS. However, because degrees of freedom, cor-

responding to m constituents of cluster are explicitly accounted in the cluster phase volume while calculating FF, the p-l particle and only h hole degrees of freedom have to be taken into account in the state density formula for residual nucleus. Correspondingly we have for $\omega^*\equiv\omega^*(p\text{-}l,h+m,U;l,m,\varepsilon_x)$ following formula:

$$\omega^* = F_{l,m}^{(x)}(\varepsilon_x)\cdot\omega(p-1,h,U) \qquad (3)$$

where $U=E-(\varepsilon_x+S_x)$ is excitation energy of residual nucleus. S_x is cluster separation energy. As mentioned in,[1] the use in (3) excitation energy of the residual nucleus U is the approximation and in fact we have to take into account that the part of excitation energy uplifts m nucleons participating in the cluster formation under the FS.

The cluster formation factors $F_{lm}(\varepsilon_x)$ with given l, m composition are calculated in I-H for determination of cluster constitution into the final state density. Phase volume of the particle system comprising cluster in the ground state is calculated in Fermi-gas model in harmonic-oscillator well.

For correct account of hole energy let us introduce the excitation energy E_l of l particles which pick-up m nucleons below FS and form new m holes with excitation energy E_m. They are related with cluster energy ε_x by relation $\varepsilon_x+S_x=E_l-E_m$. It is correct to use the excitation energy $U^*=E-E_l=U-E_m$ instead of U. To do this, let us introduce modified formation factors $F_{l,m}(e_x,E_m)$ in which apart from ε_x, the excitation energy of m (l) nucleons E_m (E_l) is also fixed. MFF are calculated as

$$F_{l,m}^{(x)}(\varepsilon_x,E_m) = \oint d\Omega\cdot\delta\{E_m - \sum_{e_i<e_f}(e_f-e_i)\}\ , \qquad (4)$$

in the same manner as in I-H. They are related with ordinary FF by apparent relation:

$$F_{l,m}^{(x)}(\varepsilon_x) = \int dE_m F_{l,m}^{(x)}(\varepsilon_x,E_m). \qquad (5)$$

Therefore we get the following formula for the density of final states:

$$\omega^* = \int dE_m F_{l,m}^{(x)}(\varepsilon_x,E_m)\omega(p-1,h,U-E_m)\ . \qquad (6)$$

This formula is free from double account of identical degrees of freedom and from neglecting final energy reduction by amount of hole excitation energy. It is clear that for such a correct account of excitation energy there must be correlation between different parts of the system: residual nucleus with cluster. For simplicity we can introduce the mean energy of hole excitation by cluster:

$$\overline{E}_m(\varepsilon_x) = \int dE_m E_m\cdot F_{l,m}^{(x)}(\varepsilon_x,E_m)\Big/F_{l,m}^{(x)}(\varepsilon_x)\ , \qquad (7)$$

and we get factorization of ratio (6):

$$\omega^* = F_{l,m}^{(x)}(\varepsilon_x)\cdot\omega(p-1,h,U-\overline{E}_m(\varepsilon_x))\ . \qquad (8)$$

The result of I-H can be obtained when the energy of hole excitation by cluster is relatively small, but this presumption is not realistic one as shown in the next section.

II. NUMERICAL RESULTS AND CONCLUSION

The calculation are performed by Monte-Carlo method of integration. All graphs corresponds to $S_x=0$ value, so for the corresponding nucleus shift on current value of S_x must be done. All results are obtained both for alphas and tritons, but only last one are represented here.

The numerical results of I-H are well reproduced for FF. The results of numerical calculations of MFF are represented on Figs. 1,2. Their normalization satisfies condition (5). The surface plots have some common features: while cluster energy ε_x increases the hole energy E_m region, giving rise the cluster formation, reduces. The internal energy of alphas and tritons is relatively large and therefore the excitation energy of holes is not negligible. This fact is apparently demonstrated by calculation of mean hole excitation energy $\overline{E}_m(\varepsilon_x)$ as function of kinetic energy ε_x. Fig. 3 shows that energy of hole degrees of freedom is not negligible in the whole range of cluster energies where corresponding FF are not very small.

If we reduce cluster energy, the part of excitation energy corresponding to constituents under FS tends to particle energy. That is why the model, developed in I-H neglecting part of excitation energy of hole degrees of freedom, overestimates cross-sections of cluster emission. This overestimation is connected with dependence of residual nucleus state density on excitation energy, as well on incoming and outcoming energies. This statement can be shown by (n,α) and (n,t) spectra, Figs. 4,5. We see that the difference between I-H approach and its modification is significant and can attain an order of magnitude. So the refinement of theory, seems to be correct, withdraws it from experiment and shows its drawback: pure account of cluster formation media - nucleus, absence of direct knock-out type mechanisms. This factors must be considered in the correct physical theory. Probably there is some influence of nuclear coupling in the nucleus.

REFERENCES

1. A.Iwamoto, K.Harada, *Phys. Rev.* **C26**, 1821 (1982).
2. K.Sato, A.Iwamoto, K.Harada, *Phys. Rev.* **28**, 1527 (1983).
3. J.J.Griffin, *Phys. Rev. Let.* **17**, 478 (1966).

4. M.Blann, *Phys. Rev. Let.* **27**, 337 (1971).
5 C.K.Cline, *Nucl. Phys.* **A193**, 417 (1972).
6. J.J.Hogan, *Z. Phys.* **A295**, 169 (1980).
7. S.M.Qaim, G.Stöcklin, *Nucl. Phys.* **A257**, 233 (1976).
8. S.Sudar, J.Csikai, *Nucl. Phys.* **A319**, 157 (1979).
9. F.E.Bertrand, R.W.Peelle, *Phys.Rev.* **C8**, 1045 (1973).

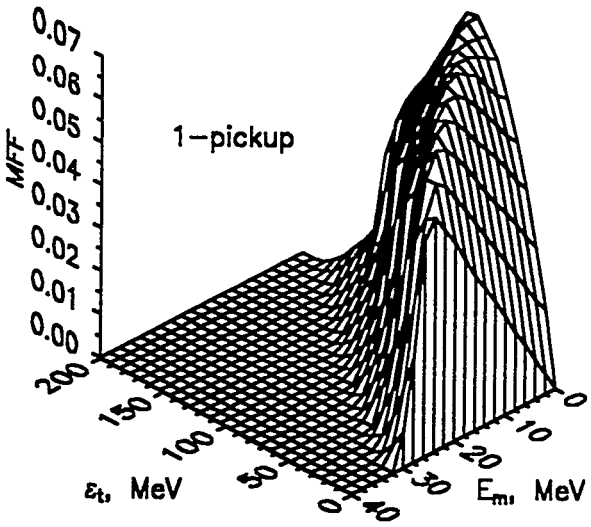

Fig.1 Modified formation factors of triton for 1−pickup case.

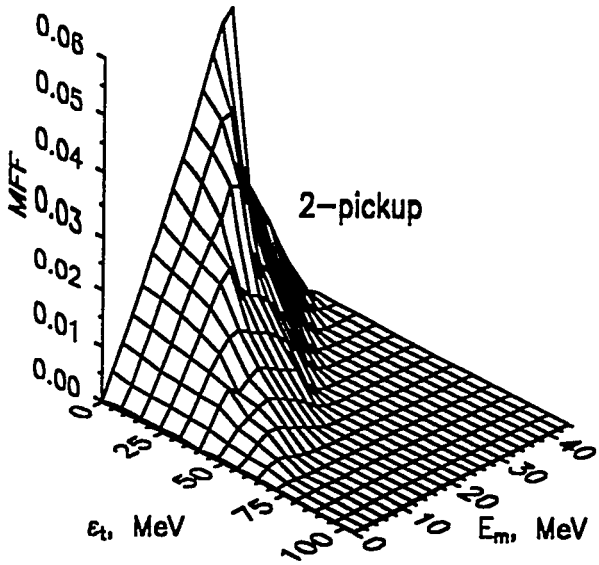

Fig.2 Modified formation factors of triton for 2−pickup case.

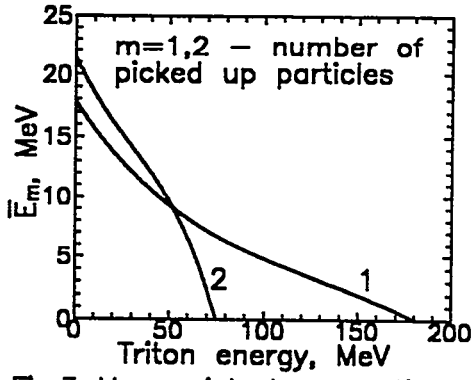

Fig.3 Mean picked up particles energy for triton.

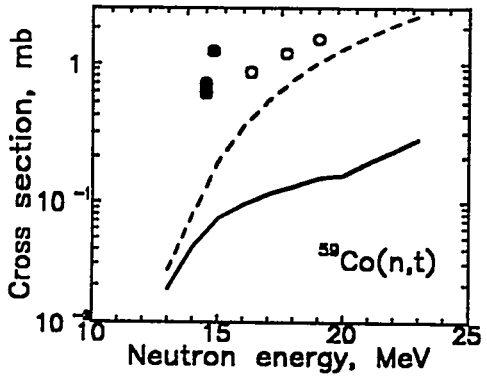

Fig.4 Excitation function of triton.
solid − calculation with MFF
dashed− calculation with FF
symbols− experimental data [7,8]

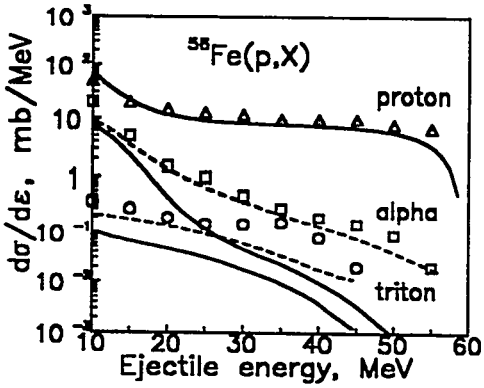

Fig.5 Angle−integrated spectra.
solid − calculation with MFF
dashed − calculation with FF
symbols− experimental data[9]

TRANSMUTATION OF FISSION PRODUCTS AND ACTINIDE WASTE AT HANFORD

L.L. Daemen, E.J. Pitcher, and G.J. Russell
Los Alamos National Laboratory

We studied the neutronics of an ATW system for the transmutation of the fission products (^{99}Tc in particular) and the type of actinide waste stored in several tanks at Hanford. The heart of the system is a highly-efficient neutron production target. It is surrounded by a blanket containing a moderator/reflector material, as well as the products to be transmuted. The fission products are injected into the blanket in the form of an aqueous solution in heavy water, whereas an aqueous actinides slurry is circulated in the outer part of the blanket. For the sake of definiteness, we focussed on ^{99}Tc (the most difficult fission product to transmute), and ^{239}Pu, ^{237}Np, and ^{241}Am. Because of the low thermal neutron absorption cross-section of ^{99}Tc, considerable care and effort must be devoted to the design of a very efficient neutron source.

We applied successfully the concept of a split-composite neutron production target to the design of the transmuter. The present target consists of a pattern of W rods in flux trap geometry plus a Pb lateral target zone. It is surrounded by a $LiTcO_4$ solution in D_2O. This assembly is immersed in a large reflector/moderator D_2O tank. A Zircaloy-4 backstop ranges out the proton beam, and contributes modestly to neutron production. Various engineering details such as tanks, canisters and cooling plena were included in the model. The rod bundles, Pb slabs, and the backstop are cooled with D_2O. The actinides slurry is contained in a number of in-blanket heat exchangers. ^{239}Pu is transmuted mostly via fission reactions, ^{237}Np and ^{241}Am are converted via (n,γ) reactions. Nonetheless, we have enough fission reactions taking place in ^{239}Pu to increase significantly the rate of the fission products transmutation while keeping the entire system well below criticality.

Two criteria drove the neutronics design of the transmuter. First of all, because of the relatively small amount of technetium available at Hanford, the ^{99}Tc inventory in the transmuter should be kept as low as possible to guarantee that an adequate concentration of ^{99}Tc can be maintained during most of the plant's lifetime. We aimed at having anywhere between 15 % to 20 % of the total Hanford inventory of 2100 kg in the transmuter at all times. Second, the transmutation rate should be kept above a minimum level to burn the waste in a reasonable amount of time, namely 30 to 40 years. We optimized a fission products transmuter, as well as a more complex system where the fission products and the actinides waste are transmuted simultaneously.

850
847

A PROTON-DRIVEN,INTENSE,SUBCRITICAL,FISSION NEUTRON SOURCE FOR RADIOISOTOPE PRODUCTION

Yves Jongen
President
Ion Beam Applications s.a.
Chemin du Cyclotron, 2
B-1348 Louvain-la-Neuve
(Belgium)

Abstract. ^{99m}Tc, the most frequently used radioisotope in nuclear medicine, is distributed as $^{99}Mo \Rightarrow ^{99m}Tc$ generators. ^{99}Mo is a fission product of ^{235}U. To replace the aging nuclear reactors used today for this production, we propose to use a spallation neutron source, with neutron multiplication by fission. A 150 MeV, H^- cyclotron can produce a 225 kW proton beam with 50% total system energy efficiency. The proton beam would hit a molten lead target, surrounded by a water moderator and a graphite reflector, producing around 0.96 primary neutron per proton. The primary spallation neutrons, moderated, would strike secondary targets containing a subcritical amount of ^{235}U. The assembly would show a k_{eff} of 0.8, yielding a fivefold neutron multiplication. The thermal neutron flux at the targets location would be $2\ 10^{14}$ n/cm^2.s, resulting in a fission power of 500 to 750 kW. One such system could supply the world demand in ^{99}Mo, as well as other radioisotopes. Preliminary indications show that the cost would be lower than the cost of a commercial 10 MW isotope production reactor. The cost of operation, of disposal of radiowaste and of decommissioning should be significantly lower as well. Finally, the non-critical nature of the system would make it more acceptable for the public than a nuclear reactor and should simplify the licensing process.

1. INTRODUCTION

Technicium 99-m is, by a large extent, the most widely used radioisotope in nuclear medicine. In Europe only, approximatively 7 million ^{99m}Tc studies are conducted each year. The ^{99m}Tc is normally supplied to the hospital as $^{99}Mo \Rightarrow ^{99m}Tc$ generators. The ^{99}Mo has a half life of 66 hours, versus 6 hours for the ^{99m}Tc, making the logistics of distribution much more practical for the ^{99}Mo generator than for the short-lived ^{99m}Tc. Most of the ^{99}Mo used in nuclear medicine is obtained as a fission product of ^{235}U. The chain of 99-mass radioisotopes is obtained in 6.074 % of the fissions made by thermal neutrons.

The world production of fission ^{99}Mo is today essentially concentrated in the hands of two producers : Nordion in Canada and IRE in Belgium. Nordion alone holds approximatively 80% of the world production of ^{99}Mo. There is, today, no domestic producer of ^{99}Mo in the USA. This reliance of the US domestic market on a very small number of foreign sources has been, in the recent years, a subject of major concern for the nuclear medicine community in the USA [1].

This concern is compounded by the fact that the present production of fission ^{99}Mo is made in a very small number of research reactors which are getting quite old and are due, in the next years, for a major refurbishment or for decommissioning.

To face this planned shortage of isotope production reactors, Atomic Energy of Canada Ltd. (AECL) had started the design and construction of a 10 MW reactor dedicated for radioisotope production : the MAPLE-X. However, as a result of cost overruns and of a legal dispute between AECL and Nordion, the construction of the MAPLE-X prototype is now interrupted [2] [3].

The problems related to the future availability of reactors suitable for the production of medical radioisotopes, mainly ^{99}Mo, has prompted a renewed interest on alternative, accelerator based methods of production.

2. THE DIRECT ACCELERATOR PRODUCTION OF ^{99m}Tc AND ^{99}Mo

M.C. Lagunas-Solar has studied the direct accelerator production of ^{99m}Tc or of ^{99}Mo by proton bombardment of ^{100}Mo between 15 and 70 MeV[4].

Although the "direct" ^{99m}Tc yield is high, the ^{99}Mo generator yield is low and the resulting product is unlikely to be separable from the ^{100}Mo target material. The proton bombardment of ^{100}Mo offers thus no alternative to the present neutron production of ^{99}Mo.

Due to its short 6 hours half life, the directly made ^{99m}Tc would require a fundamental change in the logistics of distribution. An "Instant Tech." production unit could only be a regional scale facility. A loss of 2...3 half life or 75% to 85% of the produced activity seems unavoidable. The specific activity of "Instant Tech." is expected to be lower than that of generator ^{99m}Tc at the time of use and further investigations are needed to know if this lower specific activity meets the clinical needs. In any case, it is very likely that the diagnostic radio pharmaceuticals that have been FDA licensed to be labelled with generator produced ^{99m}Tc, would require a significant relicencing if used with "instant Tech".

These reasons explain why this method hasn't been yet adopted by the industry. In all instances, a ^{99}Mo source will always be needed to supply remote areas.

It should however be pointed out that the main obstacle to the development of the direct production of ^{99m}Tc is the availability of abundant and cheap fission ^{99}Mo. The above mentioned problems, related to the availability of suitable reactors could possibly radically alter the picture in the future.

3. AN ACCELERATOR BASED SOURCE OF FISSION ^{99}Mo

A number of reasons favor the continued use of ^{235}U fission reaction for the production of ^{99}Mo.

- The high production yield, resulting from the large cross-section of fission of ^{235}U by thermal neutrons.
- The very high density of activity in the irradiated samples, allowing to perform the separation chemistry on reasonably low amounts of material. The saturation yield of ^{99}Mo for pure ^{235}U irradiated in a thermal neutron flux of $2*10^{14}$ n/cm^2 is around 335 Ci/gram. The total world production of 2.7 10^4 Ci/week requires to process around 100 gr of irradiated ^{235}U each week. This is a quite reasonable amount.
- The possibility to continue to use the existing - and very expensive - fission ^{99}Mo chemical separation facilities.
- The possibility to avoid or minimize the re-licencing process for all radioactive diagnostic drugs labeled with ^{99m}Tc from ^{99}Mo=>^{99m}Tc generators.

There are, however, downsides to the use of ^{235}U fission ^{99}Mo.

- Many other fission radioisotopes are produced at the same time as ^{99}Mo. Fortunately due to the relatively short irradiation time of a target (typically one week), the production of long lived radioisotopes is, relatively, minimized. However the process produces significant amounts of short and medium lived radioactive waste.
- To minimize the amount of material to be chemically separated, and to minimize the production of actinides by neutron capture on ^{238}U, the targets use high enrichment, bomb grade ^{235}U. Despite the small amount used, this is undesirable from a non proliferation stand-point and imposes a strict security for the use, transport, inventory and accounting of the target material.

We present here an accelerator based neutron source for the production of fission ^{99}Mo, and of other fission or reactor produced isotopes. This production system includes the following elements :

1. a H^- cyclotron, able to accelerate 1.5 mA of beam at 150 MeV with low acceleration losses and almost 100% extraction efficiency.
2. a beam transport system, transporting the proton beam without losses to one of several possible neutron sources
3. a primary beam target, where the proton beam strikes a molten lead target, producing spallation (mostly evaporation) neutrons. The expected neutron yield at 150 MeV is 0.96 neutron/proton
4. a water moderator surrounding the lead target
5. a number of secondary targets made of highly enriched ^{235}U. The mass of ^{235}U in the system - approximatively 120 grams - would produce a subcritical assembly with a k_{eff} of 0.8, resulting in a five-fold multiplication of the primary spallation neutrons by fission neutrons. Because the mass of ^{235}U is strictly subcritical, and arranged so as to produce the highest possible reactivity, any perturbation to the system would reduce the reactivity. The mechanical layout of the system would be such that the introduction of additional targets would be a mechanical impossibility.
6. The target assembly would be surrounded by a thick graphite reflector.

The proposed target assembly is illustrated in fig.1

4. THE 150 MeV, 1.5 mA H^- CYCLOTRON

The description of the 150 MeV, 1.5 mA H^- cyclotron is not the subject of this presentation. However, the company of the author (Ion Beam Applications s.a. in Belgium) has built more than 15 lower energy (30 MeV), high current (0.5 mA) H^- cyclotrons for radioisotope production. Such cyclotrons are used today by all major radiopharmaceutical companies for the production of medical radioisotopes. The current design of the CYCLONE 30 is being upgraded to increase the beam current to 1mA or, in the future, to 1.5 mA. A key component of this upgrade is higher brightness H^- multicusp ion sources developed for IBA by AEA Technology in Culham (G.B.) [5].

Recently the author presented experimental results and calculations [6] showing that the space charge limit for current designs of H^- cyclotrons was between 5 and 10 mA of beam current. These results show also that very high beam loadings of the cyclotron RF system - up to 80% - are possible. The results of another IBA accelerator, the Rhodotron [7] show that mainline to RF

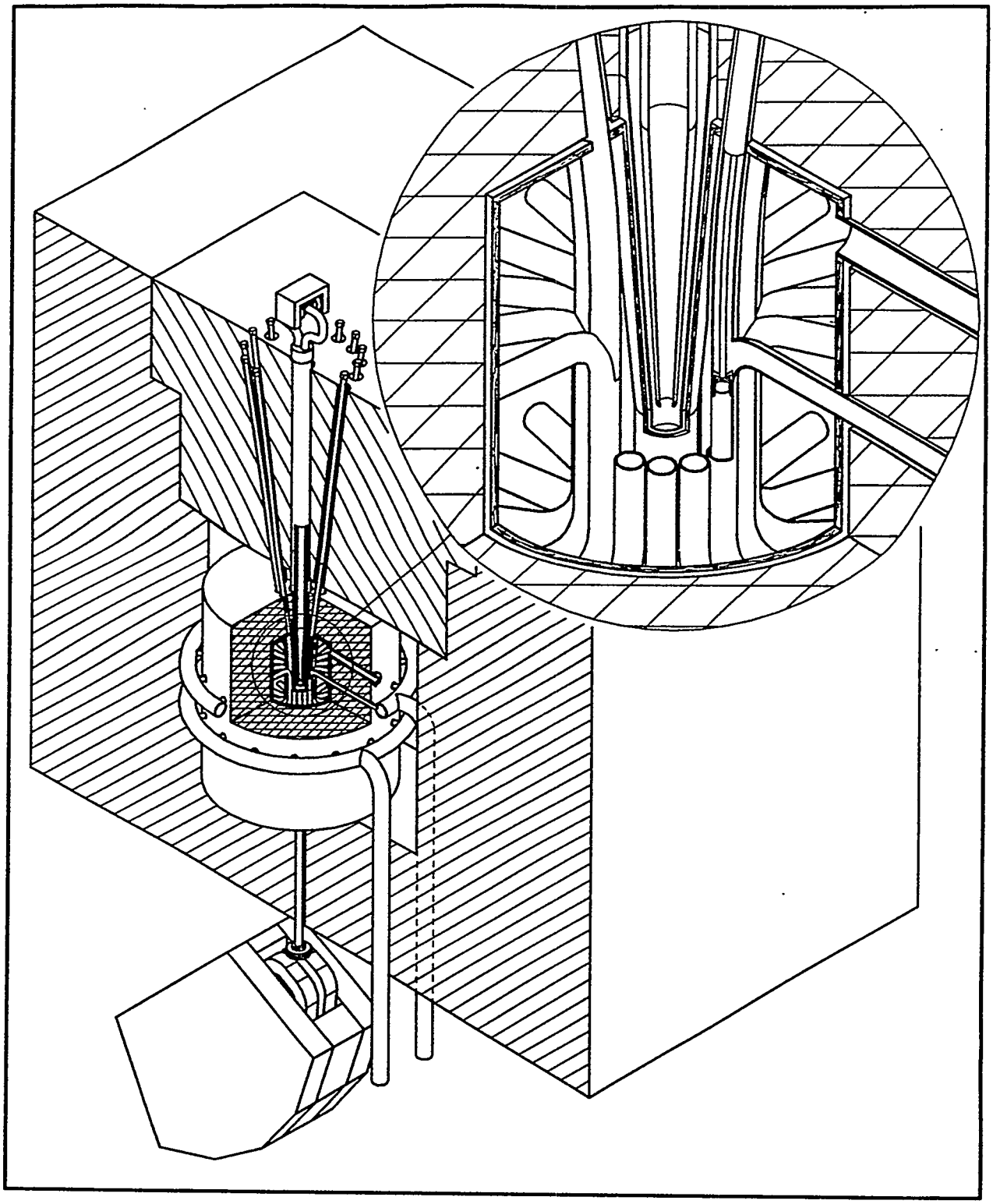

Figure 1 :Axonometric view of the proposed system with a blow-up of the core region, showing the coaxial feed for the molten lead target, the surrounding cooling tubes containing the ^{235}U targets and the graphite refector. The concrete walls are 1.5 m thick.

efficiencies in excess of 70% can be achieved at 200 kW RF power and 107 MHz.

The total power efficiency of such a 150 MeV, 1.5 mA H^- cyclotron could therefore reach 50%, i.e. a total electrical power of only 450 kW for 225 kW of beam power.

The problem of the electromagnetic dissociation of H^- imposes the use of lower magnetic fields at higher energies. For a 150 MeV cyclotron, the maximum sector field would be 1.1 T, and the average field .6 T at the center. This would result in a pole radius of 2.75 m, and an external diameter of 8 m for the accelerator.

5. THE PRIMARY SPALLATION TARGET

The 150 MeV, 150 to 225 kW proton beam is used to produce spallation neutrons in a molten lead target.

The neutron production yield from protons on lead targets has been measured by Bell et al. [8] at energies below 80 MeV, and by Carpenter [9] between 0.5 and 1.5 GeV. Using the cross-sections of [8] at low energy, assuming a constant cross-section of 1.61 Barn above 70 MeV and fitting the neutron multiplicity at higher energies to meet the results of [9], we find the following neutron yield/incident proton in the 0-200 MeV range.

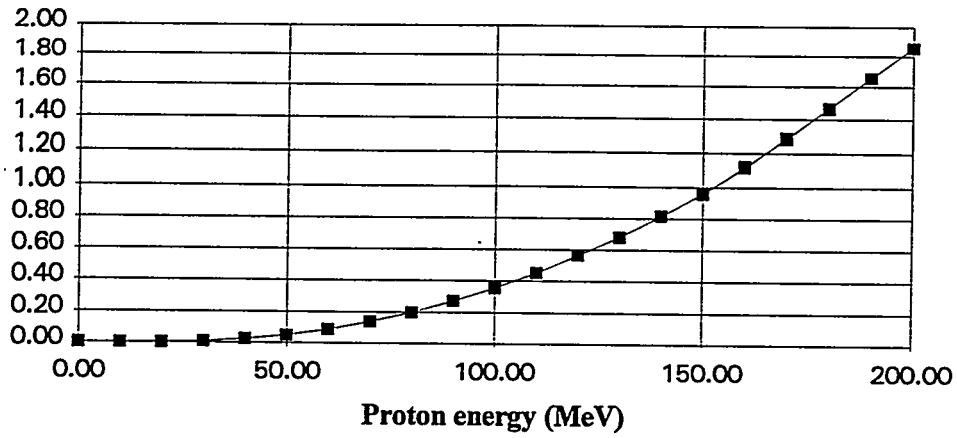

Incidentally, a measurement of the total neutron yield at 100 MeV made by Lone et al. [10] shows a value of 0.35 neutron/incident proton at 100 MeV, in excellent agreement with our crude calculation.

To handle the 225 kW beam power, a flow of approx. 40 l/min of liquid lead will be maintained through the target, resulting in a temperature rise of 200°C. The liquid lead will be circulated in closed loop by a magneto-hydro-dynamic pump. Such a pump, without any moving part, can operate reliably in high radiation environment for many years. A system of hot air circulating in the small gap between the lead target and the water moderator tank will be used to melt the lead at start-up.

6. MODERATOR, REFLECTOR, SECONDARY TARGETS AND NEUTRON CALCULATIONS

The primary target will be surrounded in all directions by a water moderator, in order to thermalize the primary spallation and secondary fission neutrons. The secondary targets, made of highly enriched ^{235}U encapsulated in an appropriate cladding, are tube shaped in order to improve the heat dissipation. Each secondary target is placed at the end of a special handling rod, and located in an individual aluminium water cooling tube providing high velocity water cooling. The secondary targets are located at close distance (8 cm) from the primary spallation target, and are surrounded by a thick (30 cm) graphite reflector.

The neutron transport, thermalisation and multiplication in this assembly are presently simulated using numerical neutron transport codes. Dr. Hamid Ait Abderrahim of the nuclear fuel group of the Nuclear Research Center in Mol (Belgium) is performing those calculations. Although the neutronics calculations should be best described today as "work in progress", initial results using the DORT code show that a k_{eff} of 0.554 is obtained with 15 targets containing each 4gr of ^{235}U, or a total of 60 gr of ^{235}U. We expect that by raising this amount to 100 ... 120gr of ^{235}U, a k_{eff} of 0.8 will be obtained, yielding a neutron multiplication factor of 5, but staying far enough from a critical mass.

In this case, using a 1 ... 1.5 mA beam of 150 MeV protons on the primary lead target, a thermal neutron flux of 2 10^{14}n/cm^2.s should be obtained at the secondary fission targets. The resulting thermal fission power would be 600 ... 720 kW.

In a flux of 2 10^{14}n/cm^2.s, a properly designed ^{235}U target would reach a saturation activity of 335 Ci of ^{99}Mo/gram. With a loading of 100 gr, and replacing the targets on a weekly basis, the weekly production of ^{99}Mo would be 2.77 10^4 Ci, or 6,000 Ci/week with a 6-day post calibration. This amount represents approximatively the world weekly demand in ^{99}Mo.

It should be noticed that the decay time of ^{235}U in a thermal neutron flux of 2 10^{14}n/cm^2.s is approximatively 160 days. By replacing the targets on a weekly basis, the reactivity of the assembly will hardly vary, and most of the ^{235}U content of the targets will be unused and could be recycled. The short irradiation time, and the small amount of ^{238}U in the targets will minimize the production of actinides and, generally, of low lived radioisotopes.

7. CONCLUSION

We have shown the possibility to replace the nuclear reactors currently used for the production of fission-based radioisotopes by a cyclotron driven spallation neutron source, with neutron multiplication by fission. The system would be far enough from a critical mass and would present, therefore, an unquestionable safety. One such system could supply the world demand in ^{99}Mo, and would cost significantly less than a commercial, 10 MW isotope production reactor. Costs of operation, radioactive waste management and decommissioning would be significantly lower also. Finally, the non critical nature of the system would make it more acceptable for the public opinion than a nuclear reactor, and should simplify the licensing process as well.

ACKNOWLEDGMENTS

The 99Mo production specialists of the National Institute of Radioelements in Belgium (IRE), specially Dr. B. David, A.Debauche, J. Finn and E. Constant provided very useful data on the problem to be solved. Dr. Miles Wagner and Dr. Janet Sisterson from the Harvard Cyclotron Laboratory were very kind to provide me with very useful published and unpublished data on the production of neutrons by protons in lead. Last, but not least, Dr. Hamid Ait Abderrahim of the nuclear fuel group of the Nuclear Research Center in Mol (Belgium) performed the neutron transport calculations.

REFERENCES

[1] "Isotope supply : Subcommittee focuses on DOE plans, actions" in *Nuclear New*, May 1994, p.71

[2] "Maple, AECL : Isotope reactor is economically unfeasible" ibidem

[3] "Canadian isotope spat could cause price hike" in *Diagnostic Imaging Scan*, Vol 7, number 22, Nov. 17, 1993, pp. 3-4 (published by Miller Freeman, Inc. 600 Harrison St. San Francisco, CA 94107)

[4] Manual C. Lagunas-Solar "Cyclotron production of NCA 99mTc and Mo. An alternative non reactor supply source of instant 99mTc and 99Mo => 99mTc generators", *Appl. Radiat. Isot.*, Vol. 42, N°7, pp. 643-657,1991

[5] R. Mc Adams, R.F. King, G. Proudfoot and A.J.T. Holmes, "Pure and Cesiated CW Volume Source Performance at the Culham Ion Source Test Stand", *Proceedings of Sixth Intl. Symposium on Production and Neutralisation of Negative Ions and Beams*, Brookhaven, nov. 1992, AIP conf. proceedings N° 287, pp. 353-367.

[6] Y. Jongen, "Extremely High Intensity Cyclotrons for Radioisotope production" *Proceedings of EPAC 94*, London, July 1994, (to be published)

[7] Y. Jongen, M. Abs, D. Defrise, F. Genin, J.M. Capdevilla, O.Gal, A. Nguyen, "First beam tests results from the 10 MeV, 100 kW Rhodotron" (ibidem, to be published)

[8] R.E. Bell and H.M. Sharsgard, "Cross-sections of (p,xn) reactions on the isotopes of lead and Bismuth" in *Can. Journal of Physics*, Vol 34 (1956), pp. 745-766.

[9] J.M. Carpenter, "Pulsed spallation sources for slow neutron scattering" *NIM 145* (1977) pp.91-113

[10] M.A. Lone et al. "Total neutron yields from 100 MeV protons on Pb and 7Li targets" *NIM 214* (1983) pp. 333-339.

Some Basic Advantages of Accelerator-Driven Transmutation of Minor Actinides and Iodine-129

A.N.Shmelev, V.A.Apse, G.G.Kulikov
Moscow Engineering Physics Institute,
Kashirskoe shosse 31, Moscow 115409, Russia

Abstract. The blanket of accelerator-driven facility designed for I-129 transmutation doesn't contain fissile and fertile materials. So the overheating of iodine compounds transmuted is practically excluded. The efficacy of I-129 transmutation is estimated. Curium being accumulated in nuclear reactors can be incinerated in blanket of accelerator-driven facility. The deep depletion of curium diluted with inert material can be achieved.

THE BASIC ADVANTAGE OF ACCELERATOR-DRIVEN TRANSMUTATION OF IODINE - 129

The long-lived radionuclide I-129 ($T_{1/2} = 16*10^6$ years) is characterized by low value of radioactivity. Nevertheless that nuclide is considered to be very dangerous because of its high mobility in an environment [1].

An iodine and its compounds are characterized by high volatileness and have a property of decomposing with elevation of temperature. Consequently, the safe I-129 transmutation requires that possibility of iodine compounds overheating has to be ruled out. In nuclear reactors that utilise solid fuel with accumulated fission products there is always some possibility of overheating caused by loss of heat removal (for example, loss of coolant circulation). In blanket of accelerator-driven facility (ADF) without fissile and fertile materials the residual heat generation is practically excluded. Such blanket has a basic advantage for the safe I-129 transmutation.

The layout of ADF blanket for I-129 transmutation is shown in Fig.1. The liquid metal (lead or lead-bismuth eutectic) is used as a coolant both in target and in blanket. It should be noted that utilization of the liquid metal both in the target and in the blanket allows to simplify the problem of insulation the target and blanket volumes. The stainless steel tubular structure is used for this purpose. The "barrier" surrounding the target region contains liquid Pb (or Pb-Bi) and beryllium (or graphite) blocks. The purpose of barrier is to form the resonance neutron spectrum for effective I-129 transmutation and for decreasing of the structural materials' damage dose. There is a I-129 transmutation zone outside the barrier.

This zone has a thickness sufficient for effective utilization of neutrons. The lattice of graphite tubular elements containing iodine compounds is located in the I-129 transmutation zone. The graphite tubular elements were supposed to be filled by lead with PbI_2 dispersed. The graphite reflector surrounds the I-129 transmutation zone from the outside.

Neutronics calculations were carried out for one-dimensional spherical model of ADF blanket by means of code "TIME-26" (multi-group diffusion approximation with distributed external neutron source). Evaluated nuclear data library ABBN-78 and code ARAMACO-C1 [2] were applied for preparing the group cross-sections. The neutron balance in the blanket is shown in Table 1. It can be seen that 71 - 75% source neutrons is consumed by iodine isotopes (I-129 and I-127 from fission products).

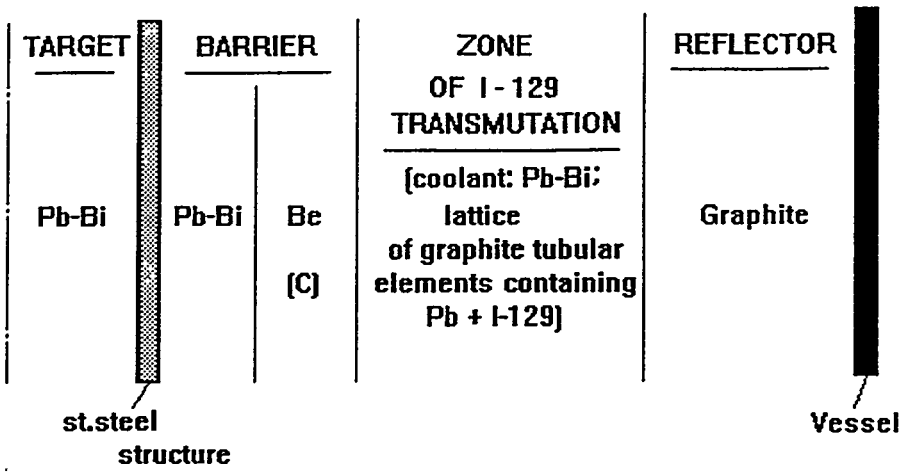

Fig.1. Layout of accelerator-driven blanket for I-129 transmutation, coolant - Pb-Bi.

Table 1. The neutron balance in ADF blanket for I-129 transmutation (proton energy -1.6 GeV; beam current -100mA; neutron yield n/p = 55)

Liquid metal	Pb	Pb-Bi
Thickness of "barrier" (liquid metal/beryllium), cm	18 / 16.2	18 / 16.2
Neutron source	100.0	100.0
Neutron consumption:		
I - 129	61.3	65.3
I - 127	10.1	10.6
Liquid metal	17.8	12.2
Graphite	0.3	0.3
Beryllium	5.3	5.6
Stainless steel	5.2	6.0

As is known the melt point of lead-bismuth eutectic is 125 C, it means that coolant temperature in the blanket must be sustained at level of 200 C. In case of lead coolant (melt point is 327 C) its temperature in blanket is estimated as 350-400 C.

The neutron characteristics of the ADF blanket for I-129 transmutation are shown in Table 2. The annual damage dose of stainless steel used as beryllium cladding (if any) is about 110 dpa. It means that the residence time of that structural material may be more than one year. The maximum damage dose of graphite tubular elements that contain iodine compounds is estimated as 10.4 dpa per annum. Taking into account the reloading of graphite tubular elements during irradiation the residence time of that elements in the blanket is assumed to be two (maybe more) years. During this time of irradiation about 30% of iodine-129 load is being transmuted into stable xenon isotopes.

Table 2. Some neutron characteristics of the ADF blanket for I-129 transmutation (coolant Pb-Bi; proton energy - 1.6 GeV; beam current - 100mA; neutron yield n/p = 55)

Spherical geometry	BARRIER		ZONE FOR I - 129
	Pb - Bi	Be	TRANSMUTATION
Thickness, cm	18	16.2	60
Annual fluence, $*10^{22}$ n/cm^2 ($E_n > 50$ keV)		6.3 * ($E_n > 1$ MeV)	1.7 *
Displacements per atom, dpa/year		110 * ($E_n > 1$ MeV)	10.4 * (graphite)
σ_c, barn I - 129			11.2
I - 127			9.4

*The value is given for the 5-cm. layer of corresponding zone.

As is known the yield of I-129 is 0.77% and I-127 is 0.13% per fission of U-235 by thermal neutrons; yield of I-129 is 1.5% and I-127 is 0.5% per fission of Pu-239 by thermal neutrons. Neutron losses in xenon isotopes during irradiation in blanket are about 15% under conditions of 50%-iodine load transmutation.

The values of load and transmutation capability are shown in Table 3. It can be seen that blanket utilizing Pb-Bi as a coolant is capable to transmute about 85 kg (I-129 + I-127) per annum. Taking into account that annual production of iodine isotopes in PWR-type reactor (1 GWe.) is about 8.5 kg (I-129 + I-127) it may be concluded that ADF blanket is capable to transmute radioiodine produced by total electrical net capacity 10.4 GWe of PWR-type reactors. The iodine load for such blanket can be accumulated for 7 years.

The decay heat of radioiodine is negligible. The removal of heat generating as a result of neutron capture reactions is needed. The natural circulation of liquid metal is expected to be used for heat removal.

Table 3. The iodine load in the blanket and I-129 transmutation rate (proton energy - 1.6 GeV; beam current - 100 mA, neutron yield n/p = 55 ; liquid metal - Pb-Bi)

The load in the blanket, tonne	I - 129	0.48
	I - 127	0.12
	Pb - Bi	34.6
Iodine transmutation rate, kg per annum	I - 129	71.0
	I - 127	14.0

If efficiency of the electricity conversion into beam energy is assumed to be 50% the consumed electrical power of the accelerator is 320 MWe, i.e. 3.1% of total electrical net capacity of attended nuclear reactors.

THE BASIC ADVANTAGE OF ACCELERATOR-DRIVEN BLANKET FOR CURIUM BURN-UP

Curium isotopes represent a relatively small fraction of minor actinides (MAs) contained in radiowastes [3]. However, due to its high radioactivity the handling of curium isotopes in external part of nuclear fuel cycle will be complicated [4]. The difficulties are related with high heat generation of radioactive decay and with high neutron emission caused by spontaneous fission and (α,n) reaction. High heat generation is mainly connected with isotope Cm-244 (half-life equals to 17 years);the specific heat generation of its radioactive decay is about 2800 W/kg. It means that if we put a limit of 10 W/kg for fuel heat generation (such value is allowable for "dry" handling operations with spent fuel assemblies of light-water reactors [5]) then the contents of Cm-244 in fuel must be no more than 0.3-0.4%. So the curium incineration requires its dilution with large amounts of fuel or inert material. It will become feasible, for instance, in case of functioning of fast power reactors system with corresponding scale of their fuel cycle industry. But there is a principal possibility to solve this problem independently on plans and schedule of wide involvement of fast breeder reactors into nuclear power.

Fuel cycle of ADF designed for curium incineration may be characterized as adaptable to various conditions of MAs burn-up. Irradiation elements of ADF blanket may consist of the inert dilutant (matrix) containing small portion of curium isotopes. There are two reasons explaining why ADF possesses the conceptual capability to operate in regime of deep curium depletion.

Firstly, neutron source in ADF is connected not only with fission of incinerated curium but with spallation reactions in target also. Presence of the external neutron source enables us to perform a prolonged irradiation despite of the certain neutron losses due to capture in fission products and structural materials.

Secondly, high dilution of curium with inert material permits to avoid the restriction imposed on duration of MAs exposure and connected with accumulation of fission products.

Quantity of fission products that must be separated from under-burnt nuclides of curium-berkelium-californium isotopic chain by reprocessing of the irradiated elements will be significantly less than that generated in fuel elements of nuclear reactor intended for MAs incineration.

The layout of the blanket is the same as that for I-129 transmutation, i.e. the pool-type blanket filled with liquid lead (or Pb-Bi). Irradiation elements and blocks of graphite reflector are immersed into liquid lead. Target region is surrounded by "barrier" zone of the same liquid metal that fills the blanket. Although MAs are incinerated more effectively in the hard neutron spectrum but in such spectrum the cladding material of irradiation elements (graphite and stainless steel) accumulates the damage dose rapidly and leads to reducing the duration of exposure. So the "barrier" may be considered as certain trade-off of the second factor against the first one. Behind the "barrier" there is the "hard" sub-zone in form of lattice of irradiation elements containing aluminium matrix with dispersed MAs in steel cladding. Behind the "hard" sub-zone there is the "soft" sub-zone also in form of lattice of irradiation elements containing aluminium matrix with dispersed MAs in graphite cladding (cylindrical capsules). Further, the blocks of graphite reflector are located.

Curium incineration in described blanket was proceeded successively at first in the "hard" sub-zone and then - in the "soft" sub- zone. Such succession was chosen in order to compensate the reduction of neutron flux amplitude on periphery of blanket by softening of the neutron spectrum that can result in increasing of fission and capture reaction rates. Remained under-burnt

MAs after exposure in the "soft" sub-zone were recycled to the "hard" sub-zone for recurring incineration. Before reloading of irradiation elements into sub-zones the reprocessing was carried out to separate fission products and to add the portion of fresh MAs into recycled fuel of the "hard" sub-zone. In refabrication of the irradiation elements the contents of MAs in inert matrix was chosen by such a way that temperature of element during technological and transport procedures would not be too high. In considered case it was supposed that for cylindrical element with diameter 3 cm, in conditions of heat removal by natural convection of air, the temperature difference between surface of cladding and environmental air must not exceed 100 C. From analysis of the balance between neutron production and consumption obtained for steady-state isotopic composition of blanket it can be seen that contribution of neutrons produced in fission of MAs into total neutron source is about 73%. MAs fission consumes near 19% of neutrons and MAs absorb about 45% of neutrons.

Neutronics parameters of blanket are presented in Table 4. It can be seen that for irradiation time in the "hard" and in the "soft" sub-zones of 345 and 443 days, respectively, more than half of loaded MAs is incinerated over one cycle of irradiation in each sub-zones. Average specific power generated in the "hard" and in the "soft" sub-zones are 19.4 and 39 kW/l, respectively, that allows to hope the removal of that heat is feasible by natural circulation of liquid metal.

Note that deep depletion of MAs in the "hard" sub-zone provides the preconditions to decrease the heat peak ratio by the intra-zone transpositions of the irradiation elements.

Volume fraction of MAs in aluminium matrix of elements loaded into blanket does not exceed 1%. Such low contents of MAs limited by the heat of its radioactive decay can't lead to such amount of fission products accumulated that would be able to impact violently structure of matrix. Constraint on MAs exposure duration is caused by the increase of neutron losses during MAs burn-up and by accumulation of damage dose in cladding materials (see Table 4).

Data of Table 4 shows also that after irradiation in the "soft" sub-zone the certain quantity of MAs is discharged. It is supposed that these under-burnt MAs were recycled into the "hard" sub-zone after mixing with portion of curium from PWR. The steady-state isotopic composition of MAs is established in the multi-cycle process of irradiation, reprocessing, inter-zone reloading and mixing with portion of curium from PWR.

Data of Table 4 show that rate of curium incineration in considered ADF blanket is 328 kg per annum. Typical PWR of 1000 MWe power utilizing uranium fuel produces about 1 kg of curium annually [3]. So, such ADF blanket is capable to incinerate curium inventory produced by nuclear power of Russia, Europe and USA taken together. However, it should be noted that in the nearest future the need to solve this problem will hardly arise. Obviously, it strongly depends on the scale of plutonium involvement into fuel cycle of thermal reactors. Conversion of thermal reactors into utilization of MOX-fuel leads to drastical increasing of curium production rate up to 28 kg per annum [3]. Then, the considered ADF blanket will be capable to incinerate curium produced by thermal reactors of 11.7 GWe total power. Curium needed for loading of such blanket is produced by these reactors for ~1.4 year.

If conversion efficiency of electricity supplied for accelerator operation into power of proton beam is 50% then power consumed by accelerator will be 320 MWe. So fraction of uranium-fuelled reactors' power used for accelerator's feed is very low, about 0.1%. If reactors utilise the MOX-fuel then 2.8% of reactors' power is needed for accelerator feed. Thermal power of ADF is equal to about 980 MW. It is formed by 96 MW generated in target and 880 MW generated in blanket. If this thermal power removed by liquid metal is converted into electricity with efficiency

33% then such ADF will be self-sustaining on electrical power.

Table 4. Some neutron characteristics of the blanket for curium burning-up (coolant - Pb; proton energy - 1.6 GeV; beam current - 100 mA; neutron yield n/p = 55).

Spherical geometry	BARRIER Pb	ZONE OF CURIUM TRANSMUTATION	
		"hard" sub-zone	"soft" sub-zone
Thickness, cm	35	150	12
MA-flow rate, kg per annum (in / out)		421 / 191	191 / 93
Maximum specific heat, kW / l		68	54
Heat peak ratio		3.51	1.39
Time of MA-irradiation, day		337	525
Annual fluence, $*10^{22}$ n/cm^2 ($E_n > 50$ keV)		36.5*	1.2
Displacements per atom, dpa / year		104*	7.5

*The value is given for the 1-cm. layer of corresponding zone.

REFERENCES

[1] Rawlins J.A., Holmes J.J. et al. CURE: clean use of reactor energy. - Westinghouse Hanford Company, WHC-EP-0268, 1990.

[2] Abagyan L.P., Bazazyanc N.O., Nikolaev M.N., Tsibulya A.M. Group constants for calculation of reactors and radiation shields. M., Energoisdat, 1981.

[3] Koch L. Status of transmutation. - *Proceedings of a Specialists Meeting* "Use of fast reactors for actinide transmutation", held in Obninsk, Russian Federation, 22-24 September, 1992, IAEA-TECDOC-693, March 1993, pp. 13-17.

[4] Gai E.V., Ignatyuk A.V., Rabotnov N.S. et al. Reactor aspects of electronuclear transmutation of actinides in the heavy water high flux blankets. Analysis of problems. - *Proceedings of a Specialists Meeting* "Use of fast reactors for actinide transmutation", held in Obninsk, Russian Federation, 22-24 September, 1992, IAEA-TECDOC-693, March 1993, pp. 49-55.

[5] Sinev N.M. Nuclear power economics. The principles of technology and economics of nuclear fuel fabrication. Economics of nuclear power plants. M., Energoatomizdat, 1987.

[6] Bowman C.D., Arthur E.D., Lisowski P.W. et al. Nuclear energy generation and waste transmutation using an accelerator-driven intense thermal neutron source. - LA-UR-91-2601, Los Alamos, USA, 1991.

Target/Blanket Design For The Los Alamos Apt System

Michael Cappiello, Paul Lisowski, Gary Russell, and Sewell C. Rose, Jr.
Technology and Safety Assessment Division
Los Alamos National Laboratory
Los Alamos, NM 87545

Abstract: The Accelerator Production of Tritium (APT) concept proposes the production of tritium by means of an accelerator and target system. The Los Alamos APT design incorporates a high-energy, high-current proton accelerator, a tungsten neutron source, a lead neutron multiplier, and a moderating blanket that contains ^{3}He for the production of tritium. This innovative system makes use of existing spallation neutron source technology, and proven design concepts. Inherent safety and environmental features include low decay heat, the absence of fissile or fertile material, no criticality concerns, no potential for overpower transients, and the fact that no high level waste is produced.

INTRODUCTION

In late 1989, an APT concept was reviewed by the DOE's Energy Research Advisory Board for the 1988 goal requirement, and more recently, by a JASON panel in 1992 for a reduced requirement equal to 3/8 to 1/2 of the 1988 goal [1,2]. Both reviews were positive about the APT technology but pointed out the need for a program of confirmatory engineering and development to resolve key technical issues and demonstrate performance in critical areas. The JASON report stated, "The Panel believes that APT is a technology that appears feasible and practical for producing tritium in the quantities specified, and with a start-up date consistent with the currently projected national goal."

As an alternative to the reactor concepts, and in response to the panel reviews, the US Department of Energy is now supporting development of a reference preconceptual design for an accelerator-driven spallation-neutron facility to produce tritium. Los Alamos, Brookhaven, and Sandia National Laboratories formed a team together with several industrial participants that include Bechtel, Northrop/Grumman, Babcock & Wilcox, Westinghouse, Maxwell, and General Atomics, to develop the APT design. The National Laboratories provide the in-depth expertise and experience in the science and technology, while the industrial participants complement the laboratories with unique and extensive experience related to APT in the design and construction of high technology facilities.

The APT tritium-supply option consists of a powerful linear accelerator that bombards a spallation target with high-energy protons. Neutrons are produced in the spallation target and are absorbed in a blanket material to produce tritium. Two spallation targets are currently under investigation: (1) a tungsten neutron source proposed by Los Alamos and (2) a lead neutron-source proposed by Brookhaven. In the tungsten neutron source concept, the neutrons are captured by gaseous ^{3}He an isotope of helium, which is circulated through the system, thus producing tritium. In the Brookhaven concept, the centrally located solid lead neutron source is surrounded with a blanket of lithium-aluminum. Tritium is produced by capture in ^{6}Li.

THE ^{3}HE TARGET/BLANKET CONCEPT

The ^{3}He target/blanket system is depicted in Fig. 1. The incident proton beam is expanded to a "beam spot" size of 0.5 m by 1.0 m. The beam passes through a double-wall vacuum interface window that is constructed of inconel, and is cooled with D_2O. The protons then enter a 1.3-m diam. by 3.5-m long vessel also made of inconel that contains ^{3}He at moderate pressure, and approximately 100 tungsten rod bundles that are distributed along the length of the vessel. The protons impinge on the tungsten and produce high-energy neutrons through the process of

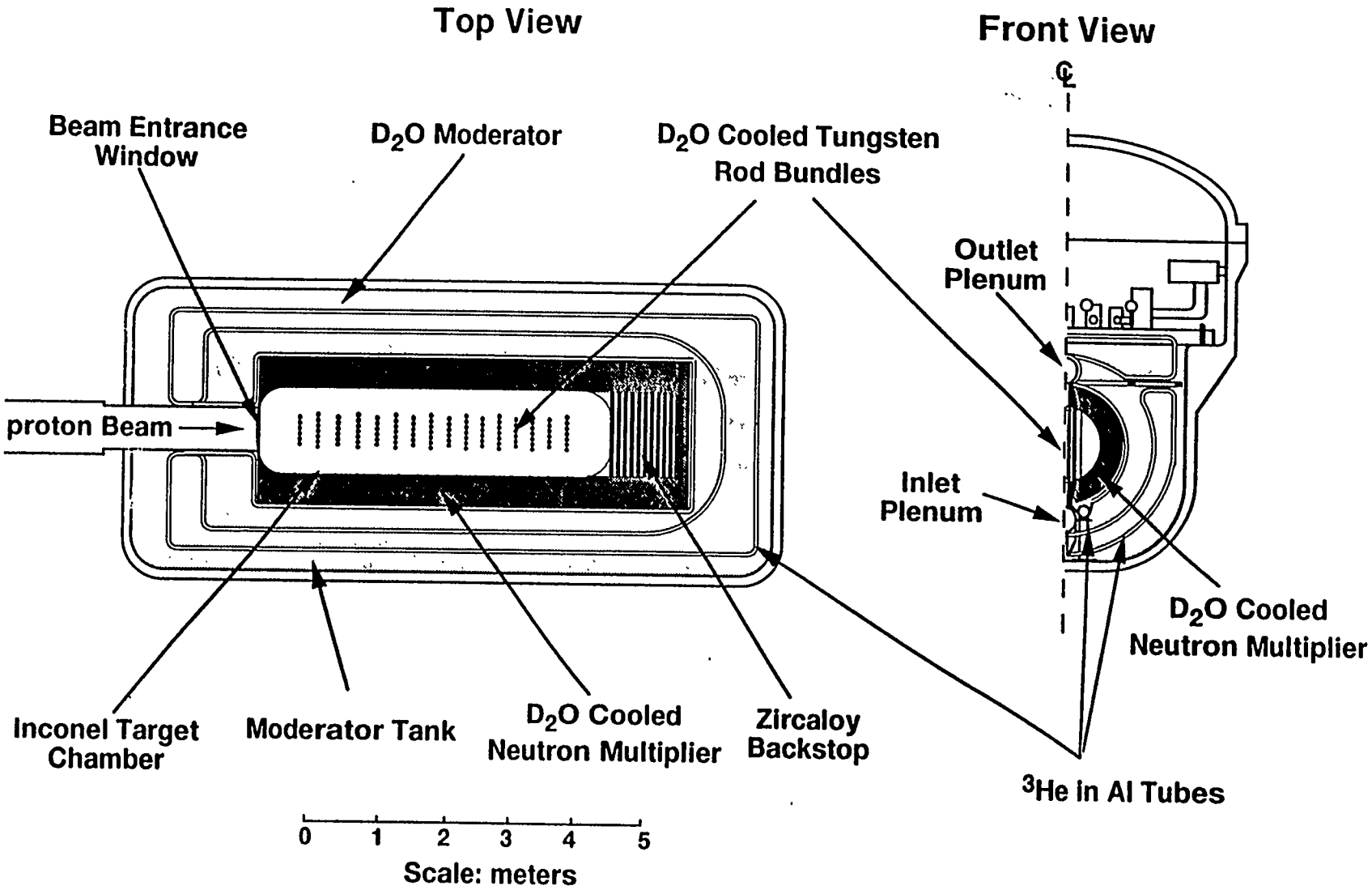

Fig. 1. Target/blanket layout.

spallation. Behind the inconel vessel is a proton backstop made of zirconium and lead that provides an additional source of neutrons, and fully stops the proton beam.

The inconel vessel is surrounded by an annulus of lead that is cooled with D_2O. Neutron multiplication occurs in the lead through additional spallation and (n,xn) reactions. Surrounding the lead is a thin annulus of ^3He contained in aluminum tubing, a D_2O moderator, another annulus of ^3He, and a D_2O reflector. Neutrons are moderated to near thermal energies in the D_2O. Tritium is produced through neutron capture in ^3He that is circulated and processed continually. Thermal neutrons that are scattered back into the neutron source are preferentially captured in the ^3He, thereby reducing the parasitic capture in the tungsten. The entire assembly of the neutron source vessel and surrounding blanket of lead, ^3He and D_2O, are contained in a steel vessel. The ^3He is processed continually to remove the tritium.

The preconceptual design of the beam entrance window and the choice of structural material for the neutron source is based on the extensive experience at the Los Alamos Meson Physics Facility (LAMPF), where the beamstop window is a double-walled inconel-718 structure with water cooling. The APT window will operate at similar stress levels and proton fluence. The lifetime estimate for the neutron source is 2.2 years at 75% capacity. At this time, the beam entrance window will achieve a proton fluence of about 1.5 by 10^{22} p/cm^2. This is similar in magnitude to the proton fluence that the LAMPF window had experienced when it was taken out of service. The LAMPF window had not failed and could have perhaps operated much longer. It is therefore possible that we could safely operate the target/blanket much longer than 2.2 years.

The choice of tungsten as the neutron source was made based on the extensive experience with tungsten spallation sources at the Los Alamos Neutron Scattering Center, its high temperature capability, and its high neutron production rate. The disadvantage of tungsten is its moderate neutron absorption cross section. This is overcome in the design by increasing the potential for leakage of high energy neutrons from the tungsten and decoupling the thermal neutrons using the ^3He gas.

The tungsten neutron source is in the form of rod bundles that are cooled with low pressure D_2O. Each bundle is hexagonal with 91 rods per bundle. The tungsten operates at a peak power density of about 2 MW/l. To provide adequate surface area for cooling, the rods are approximately 0.317 cm in diameter. Recent experiments at Los Alamos have verified the thermal-hydraulic design with both cold and hot flow tests. These tests confirm that even at the peak power conditions, a power increase of a factor of 2.3 is required to reach boiling.

Heat is generated in the target/blanket components because of proton, neutron, and other high-energy particle interactions. Separate heat removal systems have been designed for the tungsten neutron source and the moderator because the heat removal requirements are different in each system. In addition, the moderator acts as the heat sink for the beam entrance window; the target lead; the proton beam backstop region; the ^3He in the chamber and in the blanket tubes; and the moderator tank structural components. The coolant systems operate at low temperatures and pressures.

The target/blanket Heat Transport Systems consist of three separate and independent heat transport systems that remove the thermal energy from various components of the target/blanket system under normal and off-normal conditions. These systems are: (1) tungsten heat transport systems, (2) moderator tank heat transport systems, and (3) ^3He heat transport systems. Together, these systems remove the thermal loads under normal operations and provide cooling capability for anticipated operational occurrences, design basis events, and selected beyond design basis events for the target/blanket

In the design of these systems, there were several important considerations. These include safety, reliability, operation, maintenance, and the use of existing technology. The target/blanket heat transport systems are based on the "defense-in-depth" principle, and utilize both active and passive cooling systems with redundancy to provide high assurance that important safety functions are achieved. For example, the tungsten and moderator heat transport systems use two 50% loops

to remove the energy generated in these systems and to mitigate the effects of large-break loss-of-coolant-accidents (LBLOCAs). Active residual heat removal in each of these systems is provided by two 100% forced-flow cooling systems (only one system is needed to remove the decay heat) that allow small piping sizes and the use of existing nuclear reactor technology. Two independent active residual heat removal systems prevent the complete loss of cooling from a single failure.

In addition, the tungsten and moderator coolant systems have been designed for passive decay heat removal by natural circulation in the event that the active systems are unavailable. The design for natural circulation is provided by establishing sufficient thermal center elevation differences between the primary heat sources, the primary heat exchangers, the secondary heat exchangers, and the water-to-air heat exchangers in the secondary loop. Redundancy in passive decay heat removal is provided because only one loop in natural circulation is required to remove the decay heat. No operator action, valve motion, or active system responses are required to accomplish the transition to natural circulation decay heat removal. Detailed system analyses show that during an unprotected LBLOCA, which is a beyond design basis event, the rod bundles are cooled by natural circulation in the unbroken loop, and remain below 160°C (320°F).

The ^{3}He heat transport systems remove and transport the energy generated in the ^{3}He in the neutron source assembly and blankets to the moderator in the moderator tank. The use of the moderator as a heat sink for the ^{3}He simplifies the overall system design and reduces the costs of separate additional systems.

The target/blanket heat transport systems also provide intermediate loops or barriers between the primary loops and the third loops that dump the heat to the atmosphere to reduce the probability of radionuclide leakage from the plant to the environment. This, combined with the very low decay heat (0.9% of full power) and high temperature materials, provides a significant safety margin.

SUMMARY OF APT ADVANTAGES AND DISADVANTAGES

Environmental Discriminators. APT has several environmental advantages over nuclear reactor technology for tritium production. Nuclear reactors generate significant annual amounts of high-level and transuranic wastes requiring on-site management, reprocessing and/or storage, and eventual disposal, whereas APT does not generate any such wastes. Elimination of the need to produce enriched uranium will have significant environmental advantage within the nuclear weapons complex. Most of the radioactive waste from APT will result from the target materials. Existing facilities can provide final disposal of these materials as mixed solid waste with acceptable impacts.

Safety Discriminators. APT is inherently safer than a nuclear reactor. The lack of fissile material avoids all criticality concerns, and eliminates reactivity accidents and overpower transients. In the APT concept, the accelerator can be shut down very quickly (approximately 0.1 ms), providing a unique safety advantage. APT has much lower stored energy, decay heat, and radioactive material inventory than a reactor. This will simplify the design and operation of safety systems in the APT compared with a reactor. For the worst conceivable accidents, the source term will be low relative to a reactor producing the same amount of tritium. Nevertheless, the APT design will include engineered safety systems to prevent and mitigate the consequences of potential accidents.

Other Advantages. Development of the APT concept will enhance the United States' leadership position in a new technical field, namely accelerator-driven transmutation technology useful for other applications including nuclear waste disposition, plutonium disposition, isotope production, and materials research.

Disadvantages. A significant concern for APT is the electricity requirement to power the accelerator. The amount of power required is currently available now and in the foreseeable future from the grid at several sites. In more advanced accelerator designs, the potential exists to reduce

this power requirement by 20% to 40%. Also, lower tritium production requirements reduce the power demand, making the accelerator option more attractive.

CONCLUSION

The APT concept is a new tritium-supply option that does not require the use of nuclear reactors. The Los Alamos ^{3}He target/blanket concept incorporates a water-cooled tungsten neutron source, a lead neutron multiplier, and a heavy water moderator. Helium-3 gas circulating through the system creates tritium, and reduces the parasitic capture in the tungsten. The design makes use of existing spallation neutron source technology, and proven design concepts.

The thermal-hydraulic design of the neutron source has been verified with experiments showing a significant margin of safety. The APT is a low temperature and pressure system, making the release of radionuclides a low probability in the event of an accident. Inherent safety features include the low decay heat, absence of criticality concerns and overpower transients, and low-level waste production. The conservative coolant system design provides cooling during all potential design basis and beyond design basis events. Because of safety and environmental advantages, the APT offers a low impact and cost competitive approach compared with reactors for tritium production.

REFERENCES

[1] Papay, L.T. et al, "Accelerator Production of Tritium (APT)," Energy Research Advisory Board Report, DOE/S-0074 (February 1990).

[2] Drell, S. et al, JASON Report, JSR-92-310 (January 1992).

SILC Target Design for Accelerator Production of Tritium (APT)*

Michael Todosow
Department of Advanced Technology
Brookhaven National Laboratory, Upton, New York 11973

Abstract. An accelerator-driven spallation neutron-source target/blanket system has been developed for the production of tritium. The system employs a proton linear accelerator, and a lead neutron-producing target, surrounded by tritium-producing blankets based on the lithium-aluminum technology employed at Savannah River for tritium production since the 1950's. The target/blanket configuration is referred to as the SILC target, for Spallation-Induced Lithium Conversion. In this concept, tritium is produced without the presence of fissionable materials; therefore, no high-level waste is produced, and the ES&H concerns are significantly reduced compared to reactor systems. A preconceptual design has been completed for the SILC target, and the attractive performance and ES&H characteristics demonstrated. Experiments were also performed in support of the target design to confirm materials performance, safety, and to validate the nuclear design methodology.

INTRODUCTION

The SILC APT target concept has been developed at BNL over a number of years. It is based on two distinct nuclear processes: 1) the generation of neutrons from proton-induced spallation reactions in a heavy (high-Z) material, and 2) the production of tritium through neutron capture in a suitable target material. The target designs developed by BNL have been predicated throughout on adherence to three major criteria:

- the maximum use of reactor-like, and demonstrated technology in terms of mechanical and thermal-hydraulic design, materials, fabrication, and performance in proton/neutron radiation and thermal environments
- a demonstrated physical mechanism for generating the tritium and retaining it *in situ* in a reactor-like radiation and thermal environment
- a demonstrated extraction process for removing the tritium from the target material and subsequent handling

The above criteria resulted in the selection of lead for the neutron-producing spallation-source material, and lithium-aluminum as the tritium-producing blanket material based on its use for over 40 years at the Savannah River Site.

A number of successful and practical target designs have been developed over the past ~7 years. These designs have been previously reviewed by the DOE's Energy Research Advisory Board (ERAB) in 1989 and more recently by the JASON panel in 1992. Both reviews were positive about the technology, but pointed out the need for a research and development program.

As a result of these reviews, DOE sponsored a preconceptual design activity beginning in the Spring of 1992 to develop the APT technology sufficiently to serve as a viable alternative to the conventional reactor-based approach for production of needed tritium. The overall APT program consists of a multilaboratory team (Los Alamos, Sandia, and Brookhaven), collaborating

* This work was performed under the auspices of the U.S. Department of Energy

with several industrial partners (Bechtel, Babcock & Wilcox, Grumman, General Atomics, Maxwell Balboa, and Merrick). In the context of reduced U.S. weapons' stockpile requirements, APT offers significant safety, environmental, and production flexibility advantages compared to reactor systems, and can be developed in time to meet the U.S. defense tritium requirements of the 21st century. An alternative target/blanket to the SILC concept is being developed by Los Alamos [1].

DESCRIPTION OF SILC TARGET

The APT accelerator/target complex is shown schematically in Figure 1. The proton beam exiting from the linear accelerator is diverted to one of two identical target stations. When one target and/or blanket have reached their design cycle-life, the beam is moved to the second target, permitting the first to cool, be disassembled, and processed to remove the tritium, and then refurbished to serve as a spare, or be available when the second target/blanket has successfully completed an operating cycle. With this approach, availability should be enhanced, especially if a target can be processed and refurbished in significantly less time than a standard operating cycle.

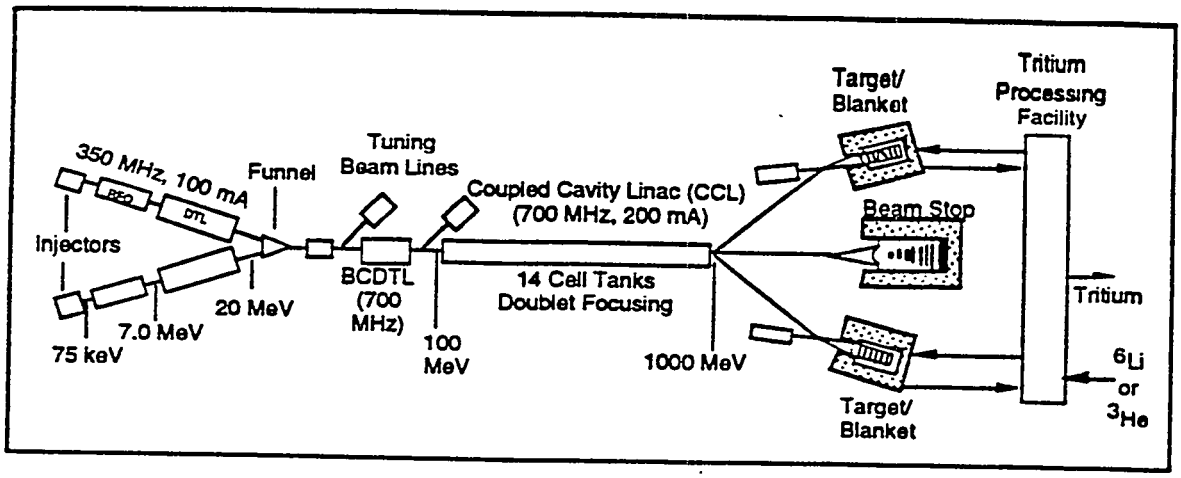

Fig. 1. Schematic Diagram of the APT System (not to scale)

Mechanical Design

The SILC target is shown in exploded form, and as assembled in Figures 2 and 3, respectively. The target consists of the following components:

- A **Target Cavity** which contains the target during operation and shutdown cooling prior to removal for tritium extraction. The cavity is formed by an appropriate arrangement of shielding sections, and contains the connections to the target cooling systems, shielding, and structural interfaces to the target components. The entire Target Cavity can be flooded in the event of a Loss-of-Coolant-Accident to preclude overheating of target components.
- A **Neutron-Source Array (NSA)** where neutrons are generated via spallation reactions induced by the incident proton beam. The NSA consists of an array of pressure tubes containing lead rods, clad in aluminum, and cooled by heavy water.

- Two **Blankets (U- and L-)** composed of aluminum clad lithium-aluminum plates, and cooled by light-water, surround the NSA on five sides. The neutrons leaking from the NSA are thermalized, and captured in the lithium producing tritium via the $Li^6(n,\alpha)H^3$ reaction.
- A **Beam Expander Duct** which provides a vacuum chamber in which the initial narrow proton beam is magnetically expanded such that it has a uniform footprint on the Source Array of ~1.5m x 1.5m. Protons enter the open end of the Expander Duct and exit through the Beam Window, an aluminum membrane integral to the end of the Beam Expander Duct. The Expander Duct is fabricated of lithium-bearing aluminum plates identical to those used in the blanket modules described above. Therefore it also serves as a source of tritium production by capturing the neutrons leaking from the front face of the NSA that would otherwise be lost.

Note that the target/blanket modules are configured so as to ease handling, and permit removal of the tritium-producing modules from the target chamber without removing the Neutron-Source Array; this capability makes different operating cycles for the target and blanket feasible, thereby reducing the cost and waste streams.

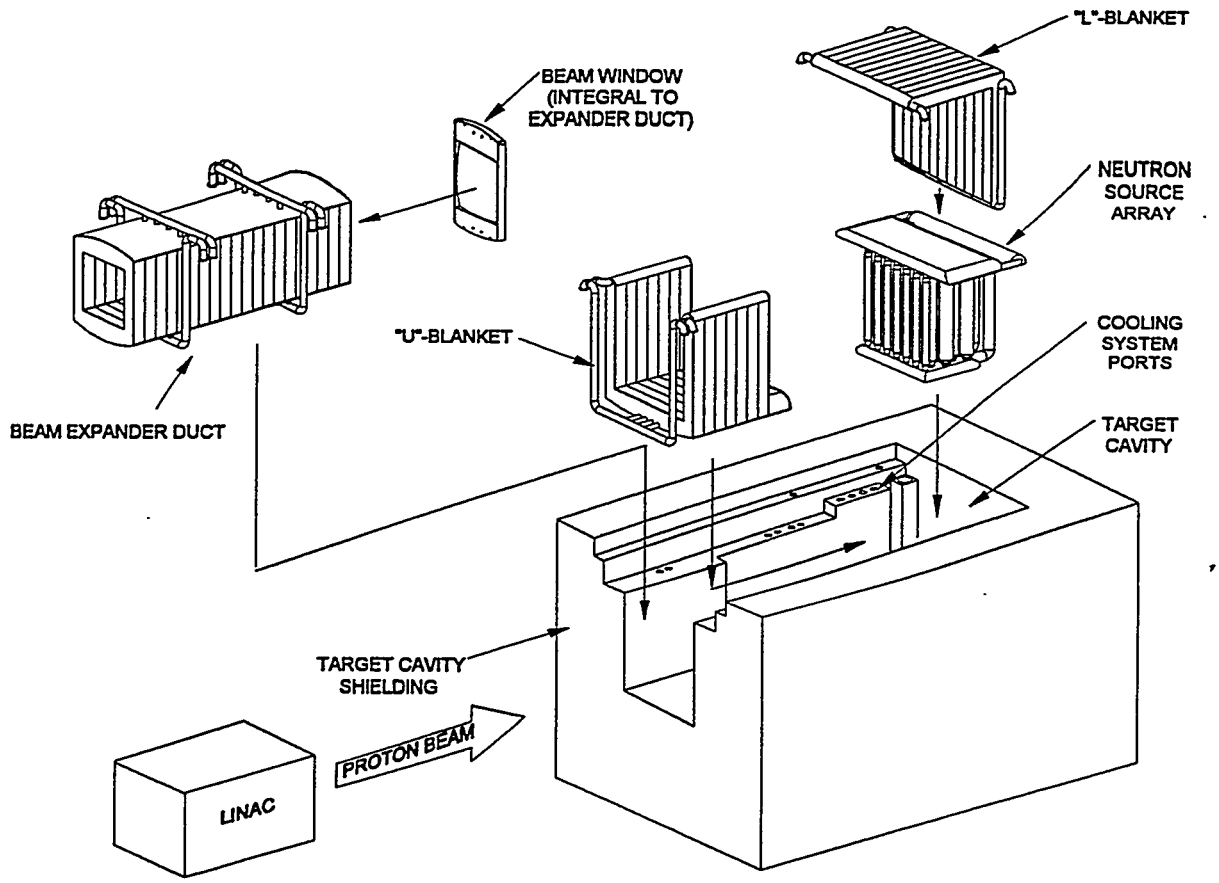

Fig. 2. Exploded View of SILC Target Components

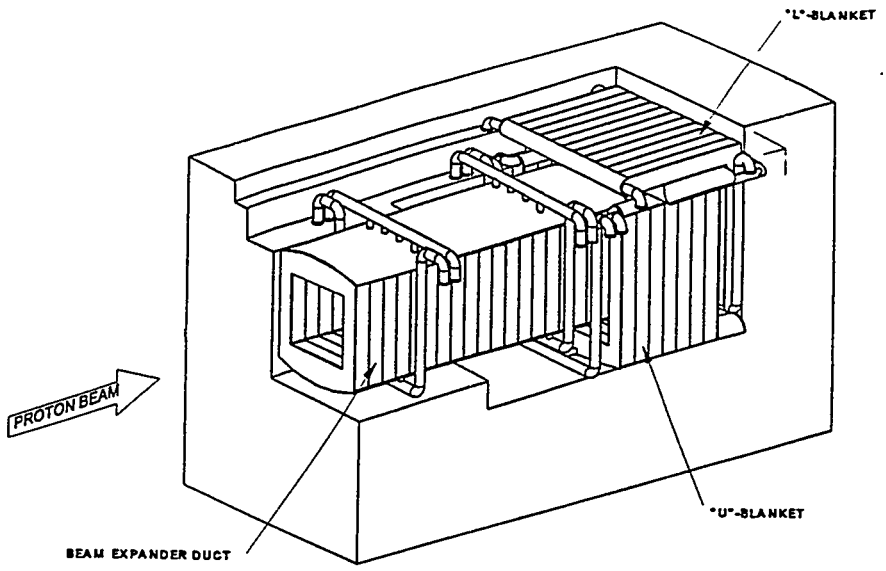

Fig. 3. View of SILC Target Installed in Target Cavity

Nuclear Design

The methodology employed for the nuclear evaluation of the APT/SILC target includes the LANL-developed LAHET Code System (LCS) [2] and the ORIGEN2 [3] and CINDER90 codes. The LCS consists of LAHET, a modified version of the HETC intranuclear cascade code for evaluations above 20 MeV, and HMCNP, a modified version of the well-known MCNP transport code for calculations from 20 MeV down to thermal energies. Time-dependent calculations to determine the build-up and decay of isotopes produced from spallation and neutron capture, as well as activity and decay power, were performed with a BNL-modified version of the industry-standard ORIGEN2 code, or the LANL CINDER90 program.

An extensive validation effort to confirm the ability of these methods to simulate the nuclear performance of the SILC target system accurately, and quantify uncertainties, has been an integral part of the APT program. This effort included a series of experiments performed as part of the APT program at BNL and LANL, and included measurements of n/p, and isotopic production and decay heat vs. energy and target material. Simulations of experiments with the standard design methodology suggest an uncertainty in the predictions in the range of ~20% for parameters such as tritium production, up to a factor of ~10 for the production of individual spallation isotopes. As the design efforts at both BNL and LANL continue, and new experimental data become available for both simple geometries and more prototypic configurations, the uncertainties should be reduced. Indeed, preliminary interpretation of recent experimental results, and calculational simulations suggest that current estimates of uncertainty are too conservative.

The current baseline operating cycle for a given target/blanket assumes that the tritium-producing blankets will be removed after one year of operation and processed. The Neutron-Source Array will remain in the target cavity, and after a one year beam-off period, the target

would be reconstituted with fresh blankets, and operated for an additional year. The major spallation products produced, and activity and decay heat in the neutron source region after two years of beam-on operation (not accounting for a capacity factor) are shown in Figures 4, 5 and 6, respectively. These results were obtained with the BNL-modified version of the ORIGEN2 code, with the latest version of the CINDER90 nuclear data libraries, and considers the entire source array. Note that both the activity and the decay heat drop off rapidly with the beam off, and that there is no significant build-up of activity or decay heat between the two cycles reflecting the short half-lives of the most-abundant radioactive isotopes. Also, both the activity and decay heat are significantly lower than for a comparable heavy-water production reactor.

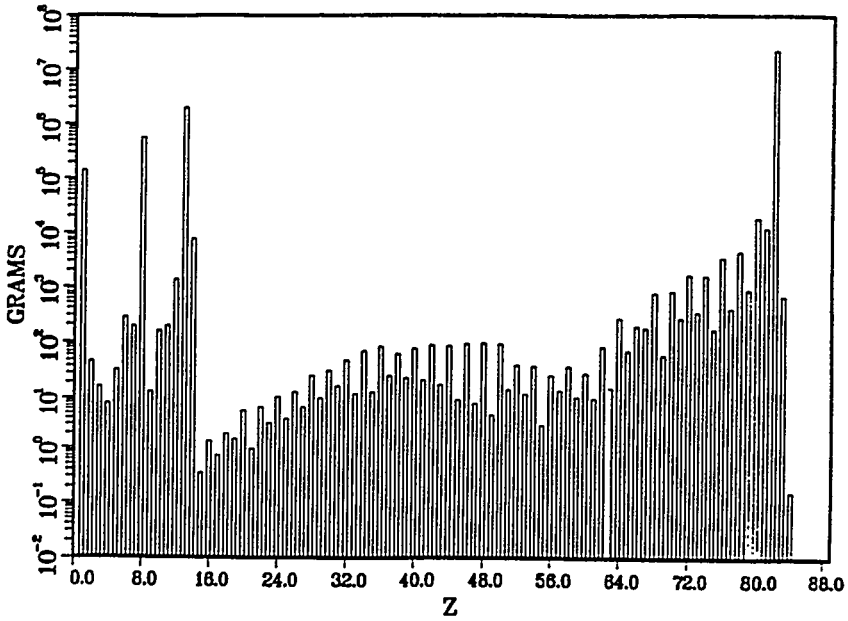

Fig. 4. Elements in Neutron-Source Array After Two Full Irradiation Cycles

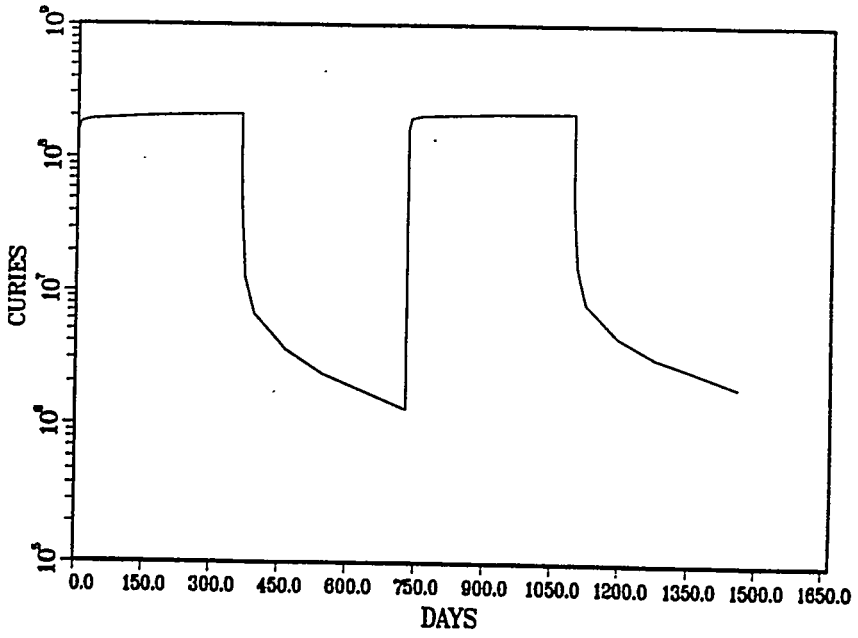

Fig. 5. SILC Target Activity (Curies) For Two Full Irradiation/Cooling Cycles

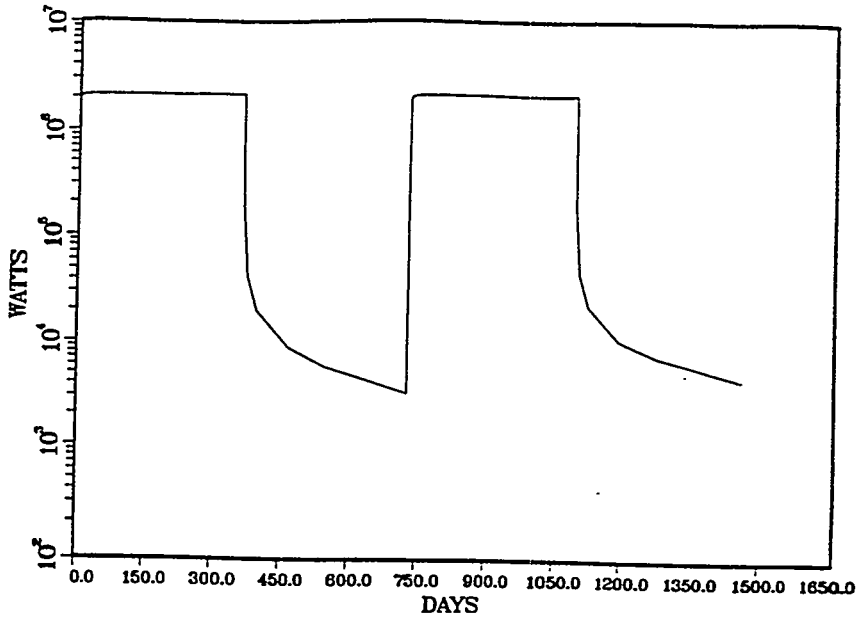

Fig. 6. SILC Target Decay Heat (MW) For Two Full Irradiation/Cooling Cycles

Cooling and Heat-Removal System, and Target Safety

A cooling and heat-removal system has been designed to provide cooling for the source, blankets, and window of the SILC target system. The system contains multiple loops, heat-exchangers, and many redundancies and safety features to provide a high degree of safety and investment protection during normal operations, and off-normal/accident scenarios. Instrumentation to monitor key parameters and provide timely detection of upset conditions, combined with a prompt and highly reliable beam trip at the initiation of accident scenarios, ensure that the cooling system provides adequate protection. A confinement boundary is provided as a further barrier against the release of radioactive species to the environment. Safety analyses for a severe loss-of-coolant-accident scenario with conservative assumptions regarding availability of mitigating systems, result in ~27% of the lead in the NSA melting. However, preliminary results from a related experimental effort to measure the potential release of mercury from the molten lead falling through heated air have shown that none of the mercury spallation products (which could dominate the accident source term) should be released from the lead. These studies are continuing.

Materials and Fabrication

Extensive testing of the SILC target/blanket materials following proton and neutron irradiation have been performed. While study of the effects on the materials properties continue, no problems have been identified to date. In particular, results from experiments on heated samples of mercury-doped lead suggest that mercury embrittlement of aluminum should not be a concern at the expected levels of mercury in the Neutron-Source Array following the present baseline two-year irradiation cycle. In addition, fabrication technologies for the Pb rods, and lithium-aluminum plates have been identified, and have been evaluated by the Savannah River Technology Center (SRTC), and B&W, respectively.

Tritium Extraction and Waste Stream

Tritium extraction continues to be based on the newest technology recommended by Savannah River. Basically, the lithium-aluminum plates will be cut to appropriate size, placed in crucibles, and heated to drive off the tritium, which is then purified and stored for use; the crucibles containing the residue from the plates are sealed and sent for final disposal.

Waste-stream management should be largely routine with the exception of lead, where one encounters a mixed-waste problem, i.e., the waste issues involve both chemical and radiological restrictions, and thus institutional ambiguities. The current assumption is for disposal of the lead whenever the aluminum cladding and/or pressure tubes reach the end of their useful lifetimes. However, it is believed that the initial lead loading could serve for several decades, and some reprocessing options are likely available. The bulk of the waste is generated in the tritium extraction process. However, as noted earlier, all the waste falls into the low-level, mixed, or hazardous categories; there is no high-level or transuranic waste produced.

SUMMARY

An accelerator-based system, Accelerator Production of Tritium (APT), is now being considered by the DOE as an alternative to a reactor for the production of needed tritium. BNL has developed a target based on the use of lead for production of neutrons, and lithium-aluminum for the production of tritium, that has attractive performance, safety, ES&H, and economic benefits. The system does not use fissile material, and therefore, reactor-related issues such as reactivity transients, nuclear criticality, and disposal of high-level radioactive spent fuel are not concerns in the design and operation. In addition, the inherent rapid-shutdown capability of the accelerator, combined with the low decay-heat rate of the APT/SILC target and blanket, greatly diminish many of the traditional safety concerns associated with a reactor facility.

ACKNOWLEDGEMENTS

The following individuals contributed to the successful design effort for the APT/SILC target: G. J. Van Tuyle, C. L. Snead, D. M. Cokinos, C. Czajkowski, E-M Franz, G. A. Greene, P. Kroeger, N. Tutu, R. Youngblood, N. Tsoupas, E. Schmidt, A. Hanson, J. Heiser, B. Boyer, M. Zucker, and G. Bozoki at Brookhaven National Laboratory; R.V. DeMars, S. M. Trepanitis, D. W. Bell, D. Hildreth, D. Mensink, B.E. Bingham, and T. L. Lotz at Babcock & Wilcox; E.L. Albenesius, C.B. Goodlett, P. Grand, and O.A. Towler at Amparo Corporation; and L.K. Heung, and J.H. Owen at the Savannah River Technology Center.

REFERENCES

[1] Cappiello, M., et.al.,"Target/Blanket design for the Los Alamos APT System," International Conference on Accelerator-Driven Transmutation Technologies and Applications, Las Vegas, July 25-29, 1994.

[2] Prael, R.E., and Lichtenstein, H.,"User Guide to LCS: The LAHET Code System", LA-UR-89-3014, Los Alamos National Laboratory (September, 1989).

[3] Croff, A.G.,"ORIGEN2.1-Isotope Generation and Depletion Code, Matrix Exponential Method," CCC-371, Radiation Shielding Information Center (1991).

LONG-LIVED ISOTOPES PRODUCTION IN Pb-Bi TARGET IRRADIATED BY HIGH ENERGY PROTONS

Yu.A.Korovin, A.Yu.Konobeyev, P.E.Pereslavtsev

The Obninsk Institute of Nuclear Power Engineering
249020, Obninsk, Russia

Concentration of long-lived isotopes has been calculated for lead and lead-bismuth targets irradiated by protons with energy 0.4, 0.8, 1.0 and 1.6 GeV. The time of irradiation is equal from 1 month up to 2 years.

The data libraries BROND, ADL and MENDL have been used to obtain the rate of nuclider transmutation. All calculations have been performed using the SNT code [1].

1. Yu.A.Korovin, A.Yu.Konobeyev, P.E.Pereslavtsev: Voprosy Atomnoi Nauki i Techniki (Problems of Nuclear Science and Technology), Series: Nuclear Data, 3-4 (1992) 117

876

ABOUT THE POSSIBILITY OF USE OF DIFFERENT TYPES OF TARGETS AS A NEUTRON SOURCE FOR SUBCRITICAL NUCLEAR REACTOR DRIVEN BY PARTICLE BEAM ACCELERATOR

E.F.Avdeev, S.L.Dorokhovich, I.A.Chusov

The Obninsk Institute of Nuclear Power Engineering
249020, Obninsk, Russia

The schemes of jet gas and liquid targets as well as the gastargets with a solid phase dispersion are introduced to use to receive the neutrons admited to a subcritical reactor core. The possible variants of target position in the reactor are considered, target characteristics are calculated. The authors pay a great attention to the estimation of radioactive products yield receiving due to the interaction of the beam with the target.

Behavior of Structural and Target Materials Irradiated in Spallation Neutron Environments

J.F. Stubbins[1], M. Wechsler[2], M. Borden[3], and W.F. Sommer[4]
[1]*Department of Nuclear Engineering, University of Illinois, Urbana, IL 61801,* [2]*Department of Nuclear Engineering, North Carolina State University, Raleigh, NC 27695,* [3]*Accelerator Technologies Section and* [4]*Materials Science and Technology Section, Los Alamos National Laboratory, Los Alamos, NM 87545*

Abstract. This paper describes considerations for selection of structural and target materials for accelerator-driven neutron sources. Due to the operating constraints of proposed accelerator-driven neutron sources, the criteria for selection are different than those commonly applied to fission and fusion systems. Established irradiation performance of various alloy systems is taken into account in the selection criteria. Nevertheless, only limited materials performance data are available which specifically related to neutron energy spectra anticipated for spallation sources.

INTRODUCTION

The development of accelerator-driven neutron sources provides advantages over fission and fusion neutron sources in terms of source accessibility and control, but presents some unique challenges regarding the selection and use of structural and target materials. Many advantages of proposed systems lie in the fact that the neutron production is confined to the target material or the target material surrounded by a neutron multiplier. In some configurations, for instance the power-producing accelerator transmutation of waste system, a fission-based multiplying medium surrounds the target region to produces additional neutrons in a fission blanket. However, even with the fission source present, the system is subcritical and is easily shut down by stopping the accelerator-driven neutron supply.

Because of these attributes, accelerator-driven neutron systems are much different than present fission reactor systems and proposed fusion reactor systems. In the case of fission reactors, the most widely utilized designs, light water reactors, operate at high pressures (from 1000 to 2200 psi depending on the design) and moderate temperatures (~300°C) for metallic (i.e. non-fuel) components. These operating constraints, which are set by neutron moderation and heat removal requirements, mean that those systems require large, thick section pressure vessels, which in turn restricts materials selection to medium yield strength steels with high fracture toughnesses. The principal safety issue for those systems is related to the fracture resistance of the pressure vessel, which is known to degrade with neutron irradiation.

Fusion systems designs are still not yet well enough established to uniquely quantify materials operating constraints. However, major attention is being directed to materials capable of handling high intermittent heat fluxes. The first wall of the fusion chamber must not only provide a hard vacuum seal, but also be able to conduct away large heat impulses during plasma burn periods, and withstand large numbers of the associated thermal-mechanical load cycles.

Accelerator-driven systems tend not to be restricted by high pressure and in many cases high temperature, except local to the target material, which serves only minor structural capacity. This opens the possibility of selecting from a much wider group of materials for structural service because of the relatively less stringent requirements regarding potential fracture and high temperature applications. Nevertheless, other structural material selection restriction apply due to

the unique nature of the operating environments in proposed accelerator-driven neutron sources. These restriction will be discussed here in light of the understanding of materials performance in similar spallation neutron environments, and in fission neutron and other spectra. The relevant materials database is small, but some generalizations can be drawn from existing information, and plans for the development of experimental programs to start to acquire other relevant information can be drawn.

PROBLEM DEFINITION

Materials selection for accelerator-driven neutron sources is highly dependent on the influence of the irradiation field on materials properties. It is, therefore, necessary to examine a number of open issues which affect this performance, and for which significant experimental programs have been developed to address these issues in fission and fusion applications. The major issues affecting irradiation stability can be listed as follows: 1. the initial atom displacement process, 2. the efficiency of the damage production - surviving defects and their configuration, 3. the agglomeration of defects into defect clusters, and 4. defect cluster evolution with fluence, and 5. the influence of the numbers and nature of the defect clusters on physical and mechanical properties of the material. Due to the differences of the irradiating and secondary particle energies from high energy proton-induced spallation sources, it is not immediately clear to what extent present understanding of these issues in fission and fusion applications can be extrapolated to the spallation case. In any case, other materials application issues, such as strength, fracture resistance, corrosion resistance, etc. must also be accounted for in the selection process. This helps to define the number of potential materials systems by virtue of their use and applicability in other similar situations.

IRRADIATION DAMAGE AND TRANSMUTATION ISSUES

The field of irradiation damage has received much attention over the past 40 years, and has resulted in a much better understanding of the role of point defect (e.g. interstitials, vacancies, transmutants) production, migration and agglomeration on materials physical properties and mechanical performance. A companion paper in this conference deals directly with the calculation of the atomic displacement crossections and their use for establishing the initial numbers of defects produced given the neutron or proton energy spectrum [1]. Once the initial defect numbers are established, it is necessary to determine how many survive the initial quenching phase and in what form. This is critical issue for comparison of radiation damage between fission, fusion, and spallation spectra. Again, much effort has been expended to address this issue, particularly with regard to the fission-fusion correlation where a large part of the fusion materials irradiation performance database has been developed in fast or mixed spectra fission reactors. Three basic approaches have been used to try to bracket the problem: computer simulation calculations of displacement cascades and annealing effects, direct observation of defect clusters by transmission electron microscopy, and comparisons of physical or mechanical properties changes in various spectra (i.e. properties-properties correlations). The computer calculations were first to indicate the potential for direct comparison of damage structures in cascades due to highly energetic incident particles [2]. This is because, above a certain incident particle energy, the cascades 'break-up" to form sub-cascades, where the sub-cascade size is nearly constant.

Thus higher energy incident particles form larger numbers of subcascades, but the subcascades which do form are directly comparable to those formed through lower energy knock-ons as long as the energies are above the cut-off. Direct observation of this effect has been made in certain materials [3,4], and has also been confirmed by properties-properties correlations in other systems [5]. This comparability of cascade structure bodes well for allowing useful materials performance data and trends to be obtained from the large body of fission irradiations.

One major difference between spallation-based sources and fission sources is the differences in the amounts and types of transmutation produces. Many transmutation reaction require a threshold neutron energy which is on the order of 2 to 10 MeV, usually above most fission neutron energies, but well within the range of neutron produced in DT fusion or by spallation. Particular concerns have been expressed regarding the amounts of H and He produced in materials systems under irradiation with highly energetic incident particles. A good deal of effort has been put forward to assess the extent of this problem for fusion applications. Presently opinions of the effect vary since it is postulated that insoluble inert gasses, particularly He, will stabilized void formation, and possibly contribute to high temperature embrittlement by collection along grain boundaries. Evidence to support this picture has been presented, but the extent of the effect seems not to be as damaging as first postulated. The production of these and other types of transmutants in spallation sources has been investigated [6].

Based on the foregoing, it should be evident that previous materials investigations and application experience for neutron environment uses provides a insight for spallation source application, with caution.

MATERIALS PERFORMANCE AND SELECTION CRITERIA

Materials performance can be generalized by considering various ranges of temperature over which properties apply. Table 1 gives approximate characterizations of issues of selection which are of concern over various temperature ranges. Since several of the properties depend on thermal activation and the mobility (or lack thereof) of point defects, the generalization can be very useful for identifying properties which control materials performance.

Table 1. Temperature Regimes of Interest and Associated Materials Performance Concerns

$T < 0.3\ T_m$ (T_m is the melting temperature)

No or low swelling
Embrittlement (Ductility)
Hardening (Strength)
Thermal creep not a concern, transient irradiation creep may occur
H embrittlement may be important
He effects may be important
Irradiation-induced precipitation, segregation minimal
Corrosion minor concern
Fatigue and Crack Growth

$0.3\ T_m < T < 0.55\ T_m$

Swelling
Creep and Irradiation Creep
Hardening and Embrittlement (Ductility)

H effects less than at low temperature, H attack
He effects are important
Irradiation-induced precipitation and segregation are important
Corrosion important
Fatigue and Crack Growth

$\underline{T > 0.55\ T_m}$

Smaller swelling, but rate effects and He effects may contribute
Hardening less concern
Embrittlement by radiation-induced segregation and He
Low mechanical strength
Thermal creep
High corrosion rates

Based on several years of research, development and application of a variety of materials systems for neutron environments, several classes of alloys are worthy of consideration for spallation environments. These are listed in Table 2.

Table 2, Classes of Materials for Examination

Structural Materials
- Aluminum and Alloys
- Ferritic and Martensitic Steels (Fe and Fe-Cr base)
- Stainless Steels and High Alloy Fe-Ni-Cr Materials
- Zirconium and Alloys
- Vanadium and Alloys
- Titanium and Alloys

Target Materials
- Pb-Bi, Pb (liquid or solid)
- High Z refractories and Alloys (W)
- U and Alloys
- Others, Th

Barrier and Coating Materials
- Ceramics
- Coatings/Cladding

Advanced Applications
- Composites for enhance radiation performance and NDE: Al/SiC, SiC/SiC, C/C

The selection and use of barrier and coating materials, and the potential for use of advanced materials systems including metal-matrix and ceramic-matrix composites will not be considered directly here. However, based on the time scale of the development of several of the proposed accelerator-driven technologies, advance materials systems should be available for use at the time of demo-scale plant construction.

IRRADIATION PERFORMANCE OF POTENTIAL STRUCTURAL MATERIALS

The irradiation performance of several of the structural materials are now presented with reference to their durability and limitations by virtue of use or experimental findings in neutron irradiation environments. As will be clear, much of the characterization of performance is based on irradiations in a fission reactor neutron spectra, but limited data are also available for exposure in spallation neutron environments. The spallation neutron irradiation experience is reviewed in another paper in detail [7]. Attention will be directed here a more general overview of the performance of certain classes of materials in neutron environments.

Aluminum and Alloys

Aluminum and it alloys have been of interest for nuclear applications since early fission reactor designs. This material is low Z and has minimal activation problems. High strength structural alloys are available, and are used extensively in applications where high temperature is not a concern. The low melting point of Al and its alloys is the one significant drawback to its use in energy conversion systems where strength at moderately high temperature is important.

Most of the relevant high fluence radiation experience at 55°C with aluminum alloy 6061 (T6 heat treatment) is available from the HFBR at Brookhaven reactor. Al6061 is precipitation strengthened by Mg_2Si. The BNL experience parallels other experimental irradiation work on that alloy. The principal finding of those studies is that the alloy continues to strengthen but loose ductility under irradiation until dose of around 10^{23}n/cm^{2}s are reached when the strengthening and ductility level out. The mechanical properties changes are associated with the thermal neutron transmutation reaction of Al → Si. The additional Mg reacts with the Si to form further precipitates.

The main concern regarding the use of precipitation strengthened aluminum alloys under irradiation is the unresolved question regarding the stability of Mg_2Si (or other) precipitates during neutron versus proton irradiation. One possibility is that the dissolution may be uniquely tied to the radiation-induced cascade structure where the mix of cascade size and number of freely migrating defects affect the precipitate stability. The question of precipitate stability under irradiation requires further consideration.

Table 3. Aluminum Alloy Irradiation Performance

Alloy	Irradiation	Comment	Ref.
6061	n, HFBR-BNL	Thermal n: Al-Si; plateau in prop. changes	[8]
6061	n, HFIR	Thermal n: Al-Si	[9]
5154	n, Petten	GB Mg_2Si embrittlement	[10]
6061	p,n, LAMPF	Mg_2Si dissolution; decrease in strength	[11]
6061, 5054	p,n, LAMPF	Results similar to BNL and ORNL	[12]
6061	He-ions	(Work not completed)	[13]
Others			

Leading Factors:

Limited to low temperature applications (T_m = 660°C)
Influence of thermal neutrons on Al → Si conversion
Influence of high energy neutron/proton irradiation, particularly on precipitate stability

Ferritic and Martensitic Steels

Certain ferritic and martensitic steels, HT-9 in particular, have been shown to be highly radiation damage resistant. Some of this resistance has been explained to be due to intrinsic differences in the properties of body centered cubic (bcc) versus face centered cubic (fcc) alloys. The ferritic martensitic alloy HT-9 has been shown to be high resistant to swelling and to have minimal changes in ductile brittle transition temperature (DBTT) after extended irradiations (> 100 dpa) at temperatures at and above 400°C. However, at temperature around 55°C, the same alloy has been shown to experience substantial shifts in DBTT due to radiation hardening [14,15].

Table 4. Selected Fe-Cr Alloys Irradiation Performance

Alloy	Irradiation	Comment
HT-9	Extensive	Low swelling at 400°C to very high doses (>200 dpa)
9Cr-1Mo	Extensive	Similar to, but worse than HT-9
Other	Extensive	Many other Fe-Cr alloys have been investigated Low activation (for fusion) versions are being developed

Leading Factors:
Low temperature performance
Ductile - Brittle transition

Stainless Steels and High Alloy Fe-Ni-Cr Materials

A very large data base exists for austenitic stainless steels in fission reactor applications. These data are primarily for fast fission and fusion reactors with hard neutron spectra. Reactors with a large thermal flux are problematic for high Ni alloys due to a large absorption crossection, and the two step $^{58}Ni(n,\gamma)^{59}Ni$, $^{59}Ni(n, \alpha)^{56}Fe$ reaction which can produce copious amounts of He in large thermal neutron spectra with all of the accompanying problems due to He. Furthermore, activation of these alloys tends to be higher than other acceptable classes of alloys. Because of this experience, austenitic stainless steels and other high nickel Fe-Ni-Cr alloys are often downplayed for nuclear application. However, because of the familiarity with their use, and their relative ease of fabricability and joining, the often end up as the material of choice.

It should be mentioned that certain Fe-Ni-Cr base alloys have been of use in certain spectra anticipated for the ADTT concepts. In particular, Inconel 718 has been used for long periods without problem as a beam window material at LAMPF. Inconel 718 is also use in LWR fuel elements, that is high thermal neutron fluxes, for spring materials in the fuel pin plenum region.

Table 5. Irradiation Performance Selected Fe-Ni-Cr Alloy

Alloy	Irradiation	Comment
316 SS	Extensive	Swells a 1%/dpa between 375 and 525°C, after about 20 dpa incubation dose
304 SS	Extensive	similar to 316SS
Inconel 718	LAMPF, LWRs, others	
Other	Extensive	Many other Fe-Ni-Cr alloys have been investigated.

	The incubation dose for swelling increases with Ni content. Swelling is highly sensitive to small amounts of alloying element additions.

Leading Factors:

High He production in thermal neutron fluxes
High swelling at high doses
Radiation-induced segregation influences on aqueous corrosion and stress corrosion cracking

Zirconium and Alloys

Zirconium and its alloys have a long standing history of use in water cooled and moderated thermal fission reactor technology. The principal use is as fuel cladding in LWR applications, and for pressure tube and other structural applications in HWRs. The performance of these alloys is well documented. Some typical compositions and applications are listed below.

Table 6. Selected Zirconium Alloy Irradiation Performance

Alloy	Application	Comment
Zircaloy 2	BWR Cladding	Extensive Use
Zircaloy 4	PWR Cladding, IPNS U-clad	Extensive Use
Zr-2.5 Nb	CANDU Pressure Tube Material	Extensive Use
Zirlo	Zr-1Nb-1Sn-.1Fe, PWR Cladding	Now In Use
Zr-1Nb	Cladding in Eastern Block Countries	
Ohzennite	Cladding in Eastern Block Countries	

Problems with zirconium and alloys have been established from extensive fabrication and processing histories. Principal problems and solutions are shown below. Comparisons of mechanical properties and corrosion performance have been made [16].

Table 7. Zirconium Performance Problems and Solutions

	Problem	Solution
1.	Hydride Embrittlement	Control H content and texture in fabrication Assure low H uptake in service (improves with Nb content)
2.	Radiation Growth	Controlled by heat treatment during processing
3.	I-induced SCC	Stress corrosion cracking (SCC) can be induced by interaction with fission product I. This process is sensitive to the precipitate structure in the alloy which can be controlled through initial processing
4.	Loss of ductility	Radiation-induced strengthening and concomitant loss of ductility is common and is taken into account in cladding design life calculations. Zirlo composition my less sensitive to this problem than the others.
5.	High T Reactions	TMI-2 showed that Zr reactions with H_2O and UO_2 quickly produced H_2 and other unwanted products

that lead to severe accident reactor safety issues. This is not an issue for ADTT systems.

Corrosion compatibility with aqueous solutions is adequate. Relatively poor thermal conductivity of this material should not be a concern for ADTT applications, except perhaps for basket materials in a solid pellet target configuration.

Vanadium and Alloys

Vanadium and several of its alloys are of high interest for fusion applications due to the low activation issues. However, vanadium has a very large thermal transmutation crossection V $\rightarrow$ Cr which renders V unsuitable for mixed spectra reactors. Some of the ADTT applications, particularly the ATW concept, rely on a highly thermalized neutron spectrum. In those cases, the use of V-based alloys may be precluded due to the transmutation problems. Furthermore, swelling in V alloys and the increase of ductile to brittle transition temperature have been shown to be highly sensitive to alloying content. In particular, undersized solutes present severe irradiation effects problems. Present V alloy development has focused on a composition near V-4Ti-4Cr which seems to show good swelling resistance, and only small increases of DBTT with irradiation. There are other limitations for the large scale use of this alloy since there is little or no experience with the production of large forgings or castings of this material. Efforts are underway in the fusion program to address this issue.

Table 8. Irradiation Performance of Vanadium Alloys

Alloy	Irradiation	Comment
V-4Ti-4Cr	Fast Reactor	Lead candidate composition for fusion applications
Several	Fast Reactor	Can control swelling and embrittlement by alloying additions

Leading Factors:
- Large thermal crossection for V $\rightarrow$ Cr
- High sensitivity to swelling and segregation with undersized solutes
- Ductile - Brittle Transition, Low Fracture Toughness

Titanium Alloys

Titanium alloys have not been the focus of a large research effort for neutron environment application. Thus, the understanding of the performance of this alloys system in neutron environments is limited. Nevertheless, this class of materials has made a significant contribution to the aerospace and aircraft industry where structural demands are also extreme and may have potential for certain applications in ADTT systems. [17]

TARGET MATERIALS SELECTION

There are several outstanding issues for potential target materials, particularly if solid targets are adopted. Table 9 list potential materials and selection considerations.

Table 9. Target Materials

Candidates:
- Pb-Bi, Pb (liquid or solid)
- High Z refractories and Alloys (W)
- U and Alloys
- Others, Th

Issues:
- Liquid Metal:
  - Impurity (transmutant) element effects
  - No structural damage due to irradiation
- Solid:
  - High dpa/s, transmutations/s,
  - Embrittlement
  - Coating/cladding for compatibility
  - Energy Deposition and thermal/mechanical cycles
  - Dimensional stability (U)
  - Transmutation/Activation effects

The issue of target material selection is complex particularly due to the requirements for efficient neutron production and, for solid targets, heat removal considerations. These issues are beyond the scope of the present paper, and are presently being addressed in on-going research work.

SUMMARY

This paper has presented an overview of several aspects of materials selection and potential candidate materials classes primarily for structural application in accelerator-driven transmutation technologies. On one hand, it is helpful that similarities and guidance can be drawn from the now vast irradiation damage and materials selection experience for fission and fusion systems. On the other hand, the fission and fusion experience has shown that materials selection is complex, and must be accounted for early in the design and development process. Due to the complexity of the conditions and constraints for use, sufficient data for materials performance assessment is often lacking. Focused experimental programs also need to be directed at the prototypic materials performance characterization early in the design and development process.

ACKNOWLEDGMENTS

The authors would like to acknowledge the support of the Department of Energy, and their respective institution in the pursuit of this work.

REFERENCES

[1] Wecshler, M.S. and Sommer, W.F., Basic Aspects of Spallation Radiation Damage to Materials, this proceedings.

[2] Heinisch, H.L., Singh, B.N., . J. Nucl. Mater., 179-181 (1991) 893.

[3] Muroga, T. Heinisch, H.L., Sommer, W.F., and Ferguson, P.D., J. Nucl. Mater., 191-194 (1992) 1150.

[4] Kiritani, T., Yoshie, T., Kojima, S., and Satoh, Y., Rad. Eff. Def. Sol., 113 (1990) 75.

[5] Heinisch, H.L., 'Correlation of Mechanical Properties Changes in Neutron Irradiated Pressure Vessel Steels on the Basis of Spectral Effects," FRM-SPR-0313/9 (1990) 69.

[6] Wechsler, M.S., Ramawarapu, R., Dougherty, E.L., Palmer, R.C., Bullen, D.B., and Sommer, W.F., J. Nucl. Mater. 212-215 (1994) 849.

[7] Sommer, W.F., 'Materials Performance Experience at Spallation Neutron Sources," this proceedings.

[8] J. R. Weeks et al., ASTM STP 1046, V. II, p. 441, 1990

[9] K. Farrell and R. T. King, ASTM STP 683 (1979) 440-449.

[10] E. Lijbrink et al., ASTM STP 782 (1982) 765-778.

[11] W. Lohman et al., Rad. Effects, 101 (1987) 301.

[12] Dunlap, J., Borden, M., Sommer, W.F., and Stubbins. J.F., 17th Effects of Radiation on Materials, ASTM, Sun Valley, ID, June 1994, to be published.

[13] Lohmann, W., Ed., 'Materials Investigations for the SNQ Target Station-Progress Report 1984," SNQ 3 J./BC 22 02 85, Feb. 1985.

[14] Hu, W-L. and Gelles, D.S., ASTM STP 1046 p. 453, v II

[15] Huang, F., ASTM STP 1046 p. 459, v II

[16] L. Castaldelli et al., ASTM STP 754 (1982) 105-126.

[17] Victoria, M., private communication.

MATERIALS ISSUES IN NUCLEAR ENVIRONMENTS: A HISTORY OF UNANTICIPATED PHENOMENA

F. A. Garner
Pacific Northwest Laboratory

The development of spallation neutron sources for plutonium conversion, transmutation of waste or energy production will most likely lead to designs and/or materials that exceed the envelope of existing knowledge concerning the response of such materials in the new irradiation environment. If previous history can be used as a guide, it is inevitable that some previously unanticipated phenomenon will arise, requiring the development of an irradiation test program to define the behavior and limitations of the materials.

Each of the major energy-producing concepts has encountered such surprises. Examples are the low-dose embrittlement of light water reactor pressure vessels, creep and growth of zirconium base alloys in the Canadian CANDU reactors, irradiation creep and swelling of austenitic steels in liquid metal fast breeder reactors, various types of high-dose embrittlement in breeder and fusion reactor concepts, and finally, transmutation-related phenomena in a variety of reactor concepts.

Development of programs to provide the necessary data for spallation neutron sources can be patterned on the groundwork laid by earlier programs, but unique challenges exist in developing new test programs in today's environment. The major problems arise due to the declining number of test reactors, space limitations in those that remain, and environmental concerns limiting the choice of construction materials. Some suggestions are presented on how to address these challenges.

THE PIREX PROTON IRRADIATION FACILITY

M. Victoria
CRPP-EPFL Fusion Technology-Materials, Association EURATOM - Confederation Suisse, 5232 Villigen PSI, Switzerland

The proton Irradiation Experiment (PIREX) is a materials irradiation facility installed in a beam line of the 590 MeV proton accelerator at the Paul Scherrer Institute. Its main purpose is the testing of candidate materials for fusion reactor components. Protons of this energy produce simultaneously displacement damage and spallation products, amongst them helium and can therefore simulate any possible synergistic effects of damage and helium, that would be produced by the fusion neutrons.

After extraction of the 390 MeV proton beam an electrostatic septum is used to split 10 - 20 μA off the main beam for transport to the PIREX beam line. This line has been designed so that a variety of target geometries can be irradiated with luminosities of up to 4 μA mm^{-2} of a positionable and spatially stable beam, focused by a quadrupole doublet onto the plane of the specimen being irradiated.

The irradiation head is inserted vertically into a double wall vacuum container, isolated from the beam line vacuum. Up to three specimen targets can be irradiated simultaneously. The targets can be either flat, 0.3 mm thick tensile probes or tubes of 0.3 mm wall thickness, normally used for fatigue testing. The specimens are cooled by a stream of helium gas from a loop, with a cooling power of 120 W cm-2. An in-beam testing head is also available, which also tests tubular specimens on beam, under tensile, relaxation, creep or fatigue conditions and is used for studies of the dynamical interactions of beam damage, helium and stress.

The construction of the facility has been partially financed by the European Fusion Technology Program.

689

An Overview of the PIREX Proton Irradiation Facility and its Research Program

M. Victoria and D. Gavillet
CRPP - EPFL Fusion Technology Division - Materials, Association EURATOM - Confederation Suisse, 5232 Villigen PSI, Switzerland.

Abstract. The main design characteristics of PIREX (Proton Irradiation Experiment) are described. The facility is installed in the 590 MeV proton beam of the PSI accelerator system. Its main task is the irradiation and testing of fusion reactor candidate materials. Protons of this energy produce simultaneously in the target material displacement damage and impurities, amongst them helium. They can therefore simulate possible synergistic effects between helium and damage that would result from irradiations with the fusion neutrons.
The research program being developed includes studies on both materials of technological interest, such as martensitic stainless steels and Mo - based alloys and basic radiation damage research on pure metals. The facility is also being used for actinide transmutation studies, in the so called ATHENA experiment. The main directions of the research program are described and examples of present results are given.

1. INTRODUCTION

The displacement damage in materials exposed to a flux of 14 MeV fusion neutrons is produced by a high energy recoil spectra jointly with impurities introduced through nuclear reactions. Helium and hydrogen are produced in particular. The radiation effects resultant from these conditions can only at present be imperfectly simulated, since there is no intense source for fusion neutrons. The simulation with intermediate energy protons can be taken as an upper bound: the recoil spectra is a factor 5 to 10 harder than that produced by the fusion neutrons, while the helium production is typically, depending on the target material, five times higher. On the other hand, both damage and helium are produced in the bulk of the material, so that the specimen thickness is limited only by the heat extraction and no directional effects are expected. As it will be described below, a part of the research program is dedicated to a comparison of the defect microstructures obtained after irradiation with energetic protons and to that of other irradiation sources. These results have provided the initial means for extrapolating to the fusion neutron conditions.

2. THE PIREX FACILITY

2.1 The beam line

The decision to build a new beam line was early taken based on two conditions which were thought of primary importance for the use of the facility: (i) the possibility of using different beam geometries and densities according to target design and to control this beam independently and (ii) the change of target should be performed in as much as possible without interfering with other accelerator users and with adequate radiation protection for the operators. An earlier description of the facility, which started operating in March 1987, has been given in [1]. The present report includes the modifications performed since then.

890

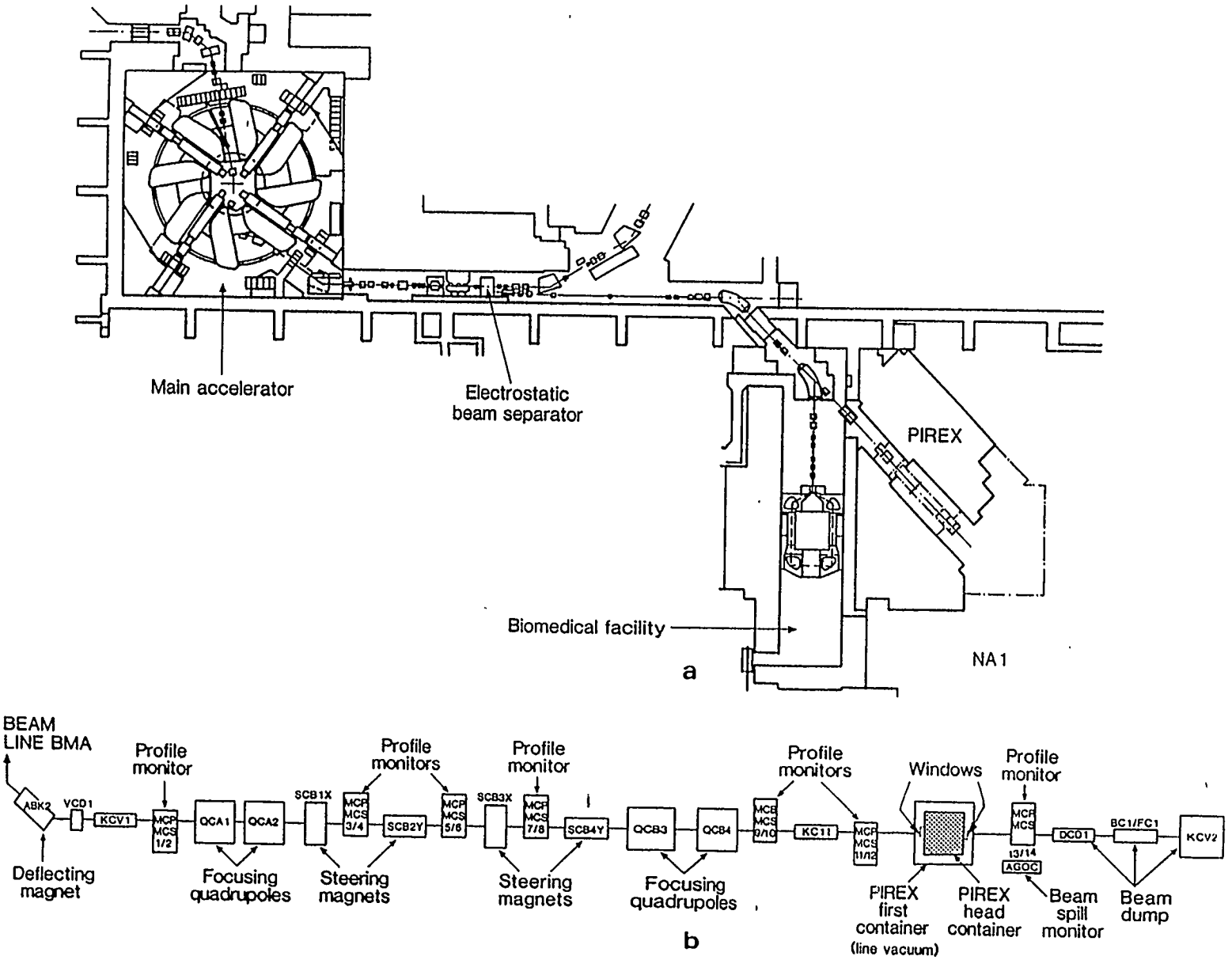

Fig. 1.(a) The PIREX beam line (b) PIREX beam components

As shown in Fig. 1a, the 590 MeV proton beam (~ 700 μA at present) is extracted from the main cyclotron. An electrostatic septum can split off up to 20 μA, which are directed to the PIREX beam line. This beam is focused on the plane of the target with a quadrupole doublet, QCA1, QCA2, QCB3, QCB4 in Fig. 1b. The beam position in both horizontal and vertical axis is defined by two sets of steering magnets (SCB1X, SCB2Y, SCB3X and SCB4Y) and controlled to 0.1 mm on the target plane by a set of fourteen profile and centre of gravity monitors (MCP and MCS 1 to 14). The beam luminosity at the target is controlled by a beam spill monitor (AGOC). In order to further improve the dose distribution on the target specimen, an electronic ramp control has been installed in SCB4Y, so that the beam can be displaced around the centre point of the specimen with frequencies of up to 2 Hz. Control software has been developed, so that beam transport calculations, based on measurements of the control monitors, provide the beam size or the magnet settings necessary to produce the desired beam geometry.
The resulting beam has a Gaussian profile and luminosities of up to 4 $\mu A\ mm^{-2}$ have been produced. Beam spatial and time stability has been tested by integrating beam distribution on aluminium foils. The results show that a positioning within 0.3 mm can be maintained for periods of more than 200 hours.

2.2 Irradiation head, cooling system and specimen geometry

The irradiation head is inserted vertically into a double wall vacuum container, isolated from the beam line vacuum. The beam is transported through 100 μm thick aluminium windows and can be discarded in a water cooled dump behind the target. The beam line is surrounded by 3.5 m of iron shielding.

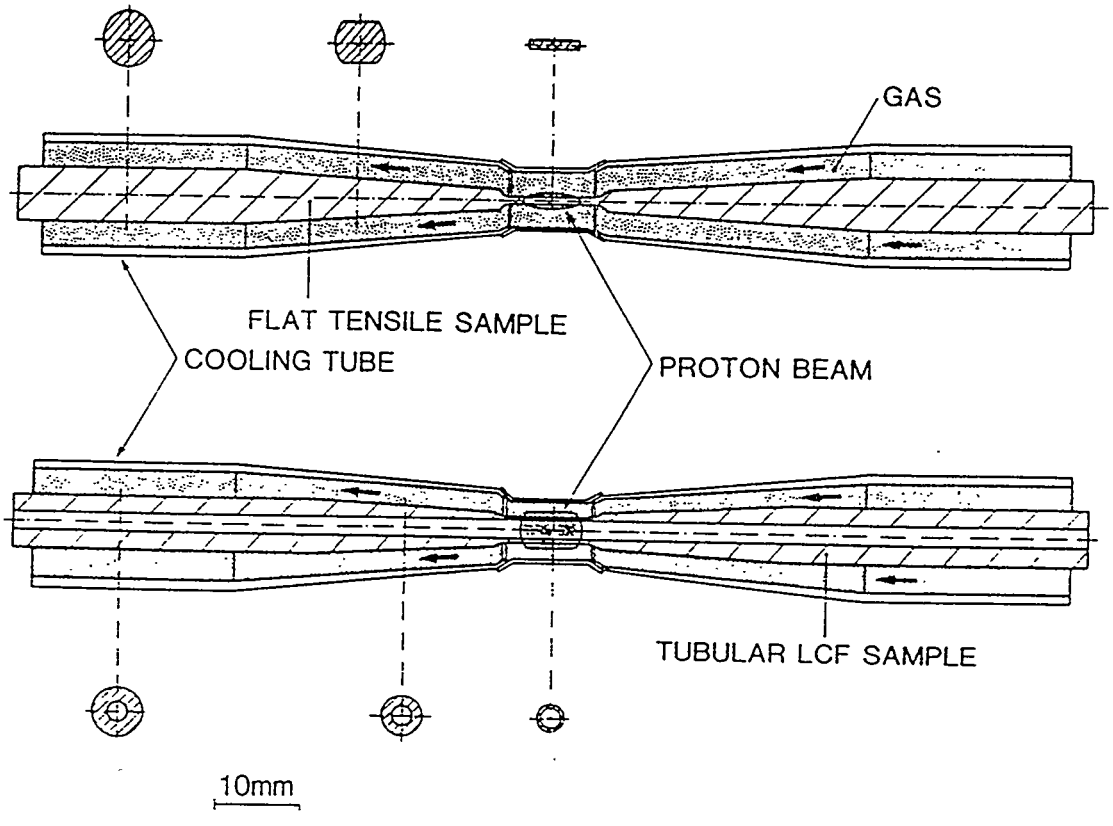

Fig. 2: Specimen and

A large amount of heat, between 2 and 11 $kW.cm^{-3}$ according to the target material, is generated by the beam. The cooling and temperature control of the specimen constitutes then one of the main problems to be solved. In the PIREX facility, a stream of helium gas, circulating at a velocity of 80 - 120 $m.s^{-1}$ and pressures up to 40 bars, is used to obtain cooling powers of the order of 120 $W.cm^{-2}$. The temperature of the gas is regulated by a 29 kW counterflow heat exchanger that cools the gas as it exits the specimen region and a 9 kW electrical heater that can preheat the input gas. As shown in Fig. 2, the gas circulates between the specimen surface and an external tube in which the specimen is centred. The evolution of the diameter of this external tube is calculated to maintain laminar flow on the surface of the specimen. The helium loop is provided with a large purifier, that can continuously purify up to one third of the circulating gas at full flow. At the exit of the purifier O, N and C impurities can be reduced to less than 1 ppm in volume.

Since thermocouples degrade very rapidly in the beam, no direct measurement of the temperature is made on the region being irradiated. A series of thermohydraulic simulation experiments were performed, with the specimen being ohmically heated, in which the transfer coefficient between gas and the surface of the specimen was measured. The temperature can then be calculated for fixed geometry and gas parameters. The validity of the calculation was checked by mounting a 0.2 mm diameter in a coaxially centred hole drilled in the gauge length of a flat specimen, so the standard cooling geometry is preserved. For a section Gaussian beam distribution, the difference between calculated and measured values was found to be about 5° C. The maximum difference found for other beam geometries or off-centre beam positions is 25° C. Irradiation temperatures in the range 310 - 800 K can be obtained.

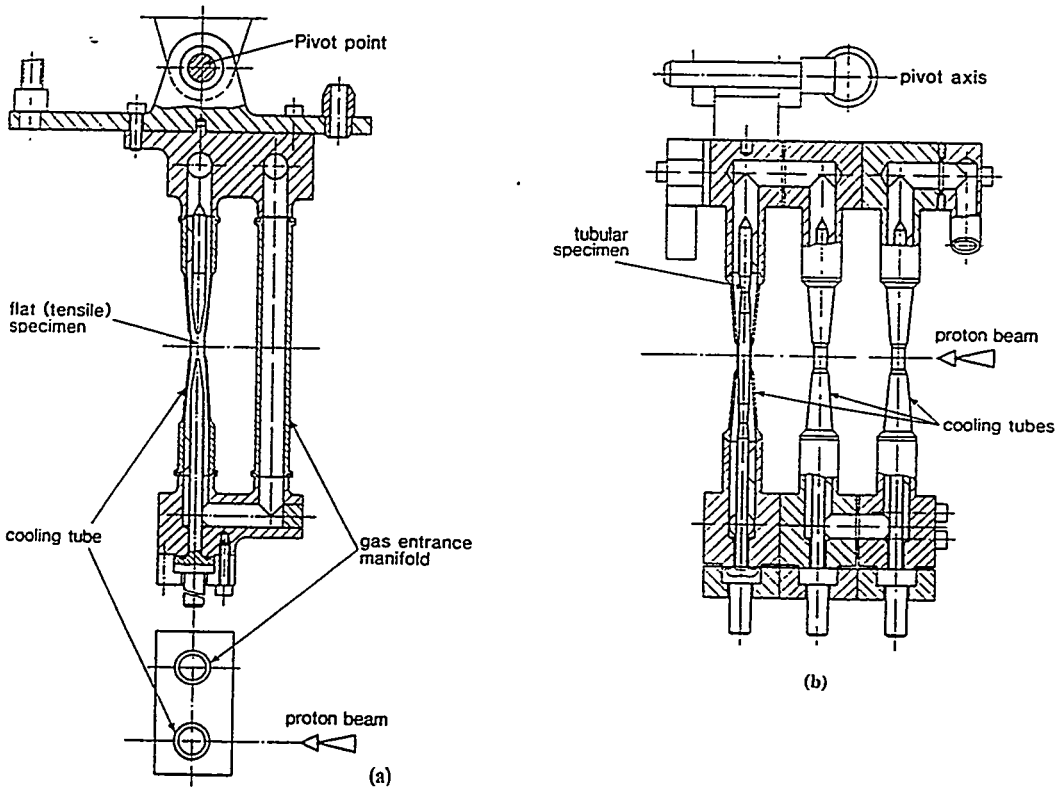

Fig.3: (a) single specimen cooling tube (b) Three specimen configuration

A biological shield is placed above the heat exchanger, followed by a vacuum flange that closes the vacuum container. Above this flange, a mechanical device that can be operated remotely, operates both as a switch for all electrical, gas and vacuum connections from the head to the exterior as well as a clamp holder to the transport shielding bottle. The overall structure of the irradiation head is sketched in Fig.4

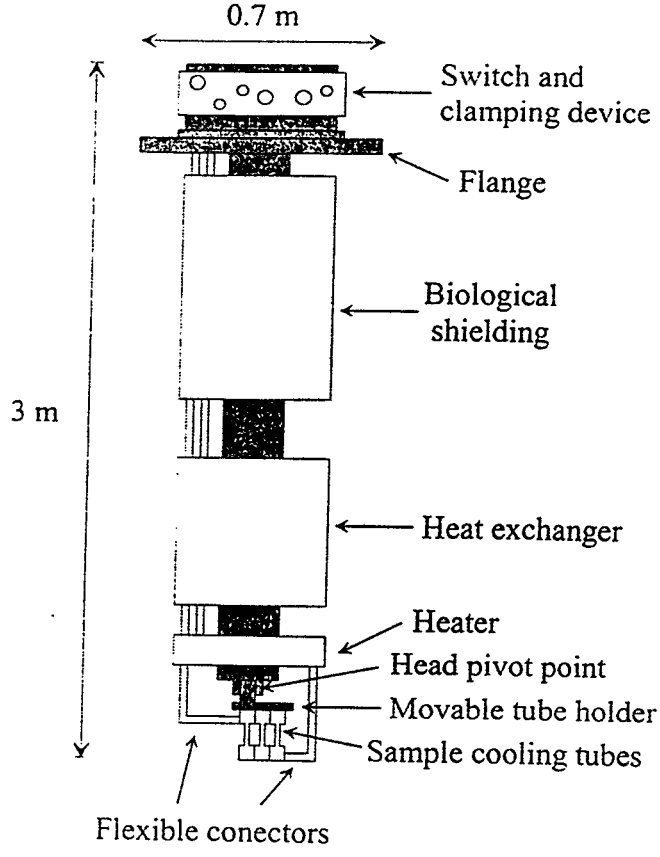

Fig. 4: Schematic drawing of the irradiation head

Two types of specimen target geometry are normally used and are shown schematically in Fig. 2. They are either (i) flat, tensile type specimens, in which the irradiated region is typically 0.3 mm thick, 6 mm wide and 9 mm long, or (ii) thin walled tubes, 3.4 mm external diameter, 0.3 mm wall thickness and 9 mm long, that are used for fatigue testing. An extension can be screwed to the specimen so that they can be placed and centred in the cooling tube with the manipulator of a hot cell. The complete manifold is shown in Fig 3a. Up to three such tubes can be irradiated in series, as indicated in Fig. 3b.

More recently, an in-beam testing head has been developed. The specimen is in this case also tubular, with an irradiated region of the same size as the postirradition fatigue sample described above, but the cooling gas circulates now inside the specimen tube. It is also provided with a cooling gas exchanger and an input gas heater, so that specimen irradiation temperatures can be controlled. A computer driven system allows testing of the specimen under beam, for tensile, relaxation, creep or fatigue deformation conditions. An overall view of the testing head and control system is shown in Fig. 5.

The radioactivities induced by the proton irradiation are high: typically ~ 1 Ci $gr^{-1}dpa^{-1}$ for a martensitic steel at the end of irradiation. They have to be

managed in a hot cell. A shielded transport bottle is used to move conveniently the specimen and irradiation head. It is made of 150 mm steel walls and weights 18 tons. It contains a motor driven clamp system with remote control that extracts the irradiation head from the vacuum container and holds it in the bottle. The bottle is then transported to a hot cell with a convenient interface, so that the whole irradiation head is inserted in the hot cell and the specimen extracted with manipulators.

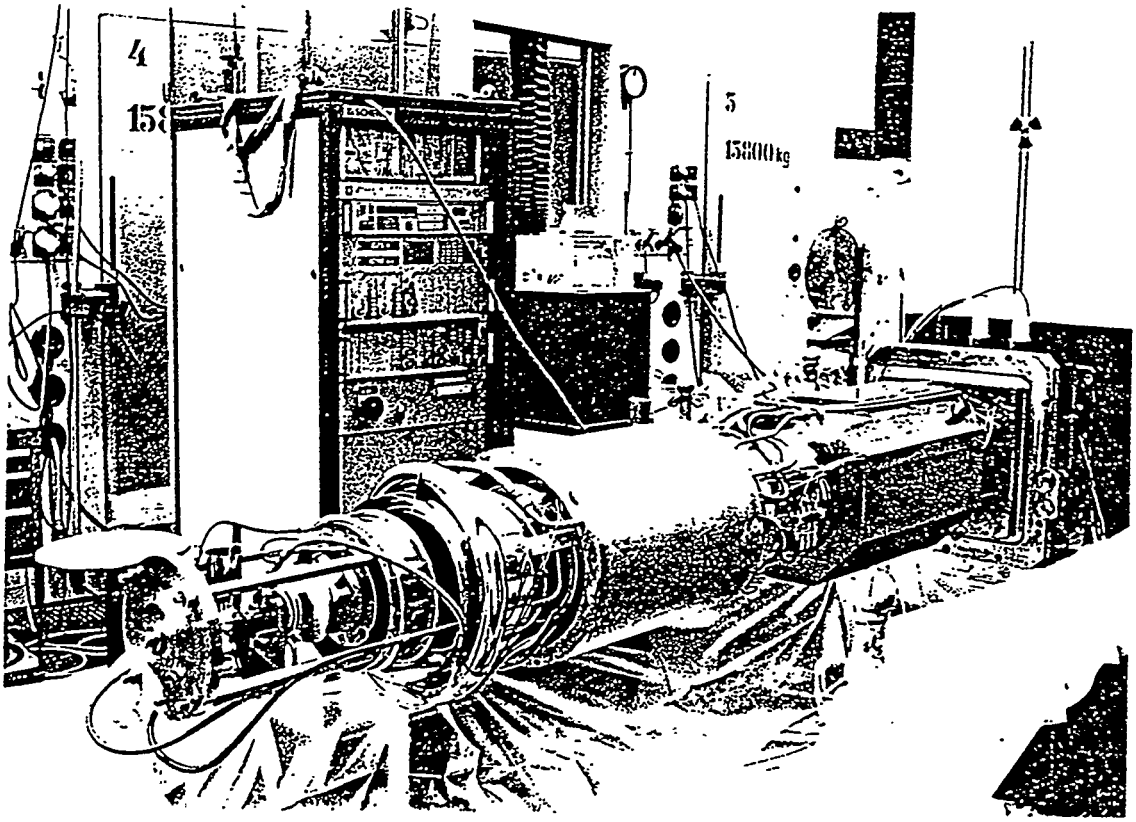

Fig. 5: The in-beam testing head and its control unit

3.THE PIREX RESEARCH PROGRAM

3.1 Damage in metals and alloys

The research program is divided in two main parts. (i) Basic radiation damage studies are performed on pure materials, to describe the radiation effects produced by intermediate energy protons. A number of numerical simulation procedures have been developed in order to model these effects and extrapolate the results to more complex alloys. (ii) Both the microstructure and the post irradiation and in-beam mechanical properties of fusion reactor candidate alloys are investigated.

The main damage parameters are first calculated using a modified version of the High Energy transport Code (HETC). The code incorporates the intranuclear cascade - evaporation model as described earlier by Serber [2]. It should be noted that the He is produced isotropically during the evaporation phase. The main agent of displacement damage is the recoiling nucleus resulting from the spallation process. A treatment for fission events has also been included in the calculation.

HETC produces a listing of the type, energy, location and direction of each particle produced by each proton interaction. Cascade nucleons with energy greater than 20 MeV are transported and may produce further interactions before they are carried out

of the target thickness. The resulting recoil energy distribution is obtained. The Robinson formulation [3]of the Lindhard model [4] is then used to determine the partition of the recoil energy between electronic excitation and displacement damage. This damage energy is combined with the calculated production cross section for each isotope and added to give the total damage energy cross section. This late value is used together with the NRT [6] modifiication of the Kinchin - Pease model to relate the proton beam fluence to displacements per atom (dpa) in the target material.

The recoil energy spectra extends well into the MeV region, with a maximun around 1-3 MeV depending on the target material [6]. This spectra is much harder than that produced by 14 MeV neutrons, which typically (i.e. for Cu) has a maximun in the 100 KeV region. The question arises of wether this substantial difference in recoil energy will affect the damage microstructure produced in the target material.

A series of proton irradiations at doses low enough so that there is no overlapping of single displacement cascade effects, have been performed in high purity Al, Si, Cu, Pd, Au and Mo, in both single and polycrystalline form at 310 K. The displacement doses are in the range 10^{-4} - 10^{-1} dpa. The resultant microstructure has been observed in the electron microscope, using the weak beam technique to improve the visibility of the defects. A series of observations for Cu single crystals are shown in Fig. 6. Small (~ 2 nm) defect clusters are visible and their volume density increases with dose. The irradiated crystals were also deformed in tension and in Fig. 6d a slip channel with a (111) trace, which results from dislocations destroying the defect structure can be clearly seen.

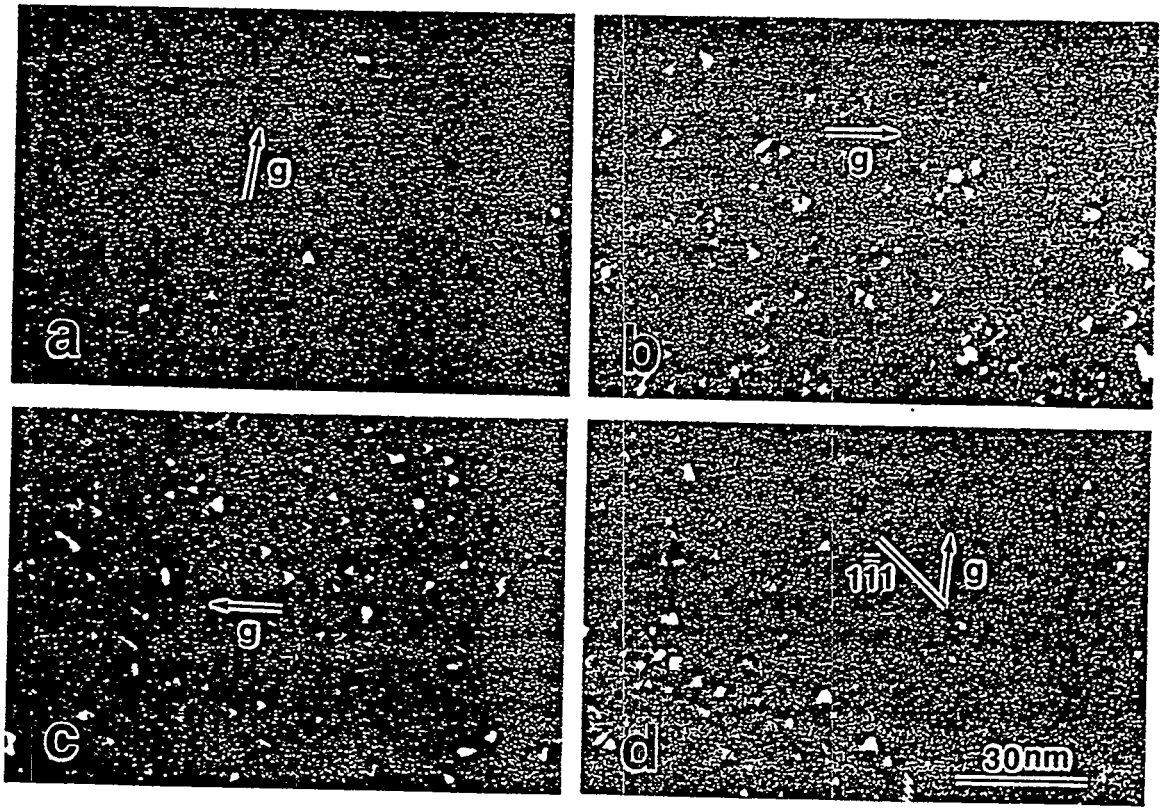

Fig. 6: Defect microstructures in 590 Mev proton irradiated Cu single crystals under WB condition (g, 6g), g=200. B=011. (a) 9.7 10^{-4} dpa, (b) 1.3 10^{-2} dpa, (c) 4.6 10^{-2} dpa and (d) 3.9 10^{-2} dpa after 46 % deformation

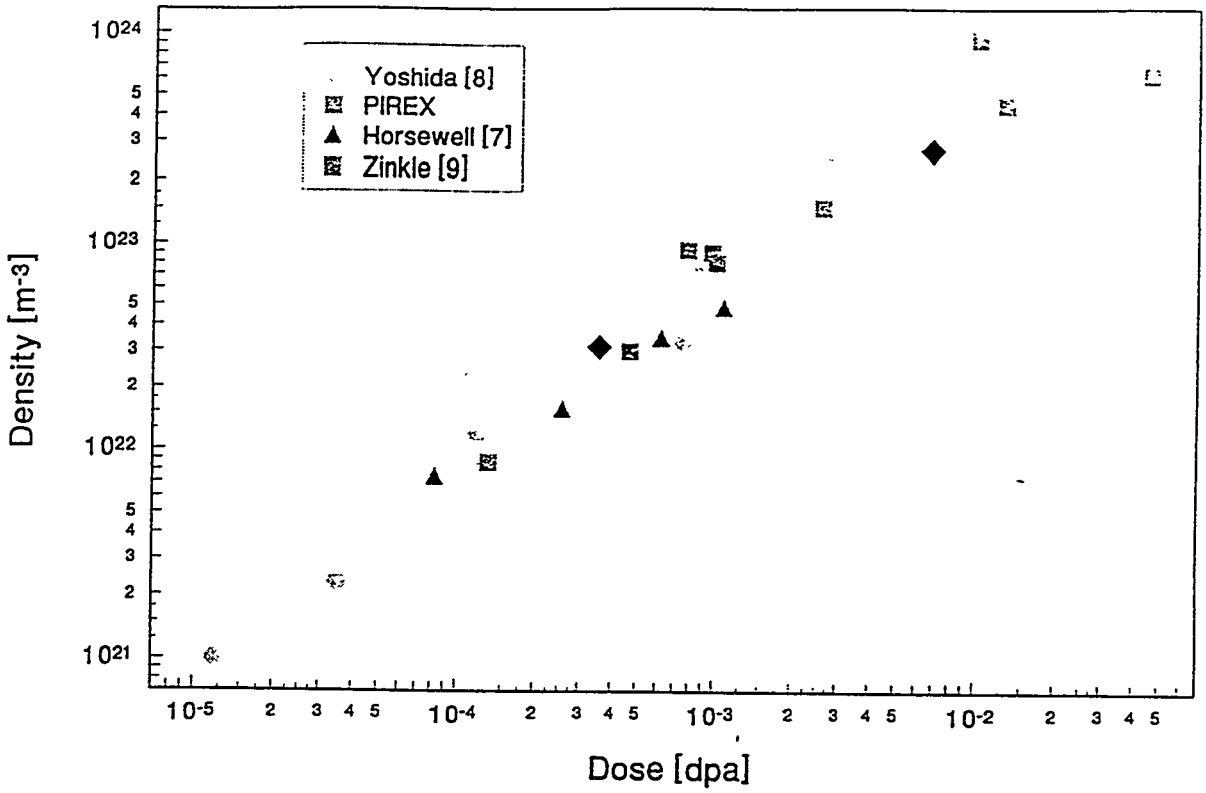

Fig. 7: Defect cluster number density as a function of dose in Cu irradiated with particles with different recoil spectra

The measured number densities are plotted in Fig. 7 as a function of the displacement dose. Values available from the literature for 14 MeV neutrons (RTNS II) [7,8,9] and fission reactor neutrons [7] have also been included for comparison purposes. All values fall within the same type of dependence with dose, indicating that at least for irradiations performed around room temperature, there is no substantial difference in the defect microstructure produced by different recoil spectra.

The martensitic 9-12 Cr steels have been extensively investigated within the European Fusion Technology Program, in particular a cast based in the DIN 1.4914 composition known as the MANET steel [10-12]. It has been shown that this steels undergoes strong radiation hardening, which diminishes with irradiation temperature to practically disappear at 700 K. Another property of particular importance for its use in a pulsed reactor is its fatigue life. In the non irradiated steel it is found that the total stress in the fatigue cycle diminishes with the number of cycles, as shown in Fig. 8. In the irradiated case, the total stress also decreases but starting from a higher value due to the initial radiation hardening and softening at higher rate, an indication that the moving dislocations redisolve the defect clusters that are responsible for the radiation hardening. A clear indication of the importance of the in-beam tests is given by the result shown also in Fig. 8: the dislocation annealing mechanism is strong enough that practically no hardening builds up. In fact, the in-beam test is practically superimposed on that of the non irradiated steel.

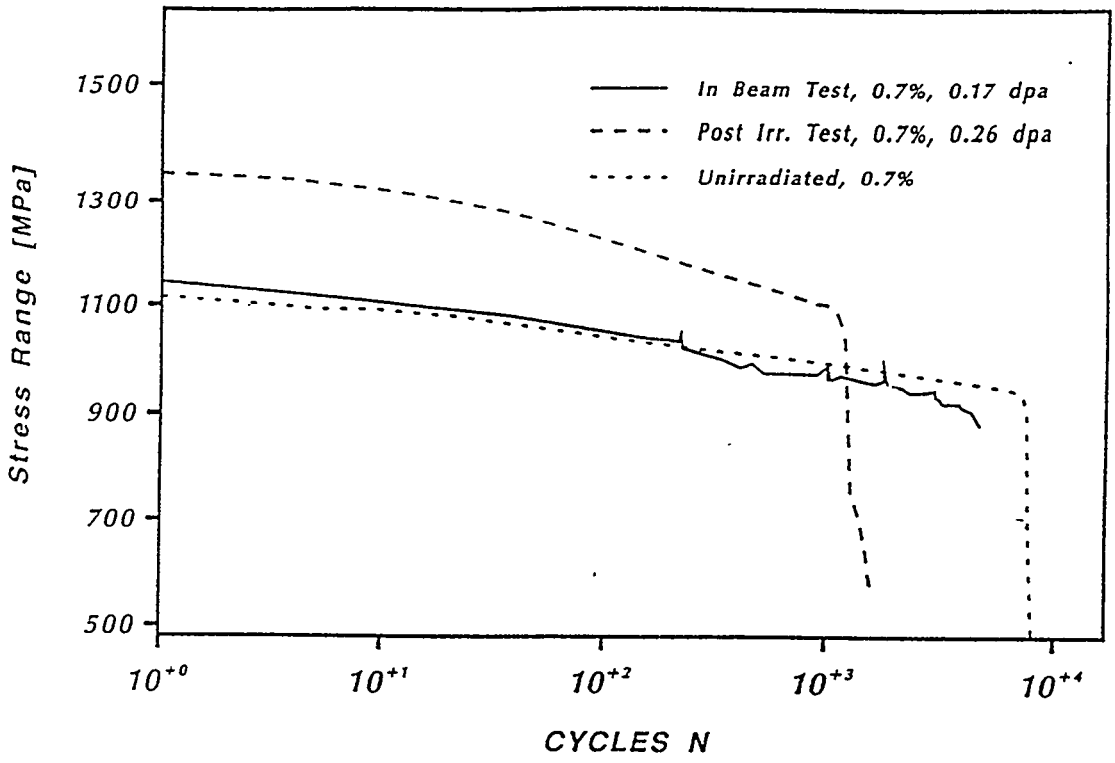

Fig. 8: The fatigue behaviour of the MANET steel

3.2 Dosimetry measurements

A number of dosimetry experiments have been performed with the following goals. The first was to measure the effective production cross section of some isotopes in all the materials currently irradiated in PIREX in order to be able to calculate the irradiation dose (in dpa or proton/cm2) in any specimen by measuring the activity of some isotopes after irradiation. A second objetive was to compare these experimental values with the values of the production cross section calculated by HETC. Finally, by measuring the helium contained in the irradiated specimens, a helium production rate can be obtained. This part of the program has been part of a fruitful collaboration with LAMPF and the first results have already been published [13].

Sandwiches of thin discs (0.01 to 0.1 mm thick, 3 mm diameter) of a number of materials were irradiated with an Al disc in front, whichis used to determine the proton fluence through the well known production cross section of ^{22}Na [14]. The end of beam (EOB) activity of medium to long lived isotopes (more than few days) in each individual disc is determined by g-spectrometry measurements.

The specimen set-up was irradiated with a beam of 590 MeV protons with an average flux of about 2.7 10^{14} protons s^{-1} cm^2 (43.3 $\mu A/cm^2$) in the centre. The shape of the beam intensity was gaussian with an elliptic cross section and a $4\sigma_y$ of 8 mm and a $4\sigma_x$ of 7 mm along the horizontal axis. The specimen set-up was kept at 310 K.

Four specimens containing three sandwichs each, one in the centre and two 4 mm symmetrically away from the centre along the vertical axis, have been irradiated. Due to the shape of the beam the centre sandwich had a higher irradiation dose than the two off center ones. In all the sandwiches, the first specimen was always an aluminium disk of 0.1 mm thick. Proton doses between 1.6 10^{19} proton cm^{-2} and 4.0 10^{19} proton cm^{-2} were obtained.

Table 2 : **Measured effective production cross-section and calculated production cross section at EOB for different isotopes in different metals**

Target	Isotope	Measurement		Calculation	
		X-Sect [mb]	S.Dev. [%]	X-Sect [mb]	S.Dev. [%]
Cu	^{51}Cr	28.7	1.9	20.11	1.56
	^{54}Mn	21.7	1.8	19.79	1.33
	^{56}Co	9.3	2.5	15.45	2.22
	^{57}Co	25.7	3.8	24.62	1.89
	^{58}Co	30.9	2.2	24.81	2.29
	^{60}Co	10.3	5.0	10.26	4.89
Zr	^{65}Zn	5.1	8.6	6.9	2.2
	^{67}Ga	7.5	8.2	6.9	0.6
	^{75}Se	27.1	4.1	12.3	3.2
	^{83}Rb	50.8	3.5	14.9	6.6
	^{88}Zr	35.2	1.9	34.0	0.7
	^{95}Zr	2.1	1.0	3.0	2.9
Au	^{172}Hf	37.0	15.6	7.5	2.9
	^{175}Hf	46.3	7.2	3.4	8.5
	^{184}Re	0.7	6.5	2.6	6.8
	^{185}Os	59.0	2.7	10.2	3.4
	^{189}Ir	73.4	1.2	7.8	7.3
	^{196}Au	62.8	6.7	176.1	1.9

The number of gama rays detected in a target increases with its mass. In the case of the high Z materials, a number of ray overlap, making a quantitative analysis very difficult. Also,s in the high Z material the number of γ-rays emitted by each isotope increases making the respective emitter determination more arduous. As an example, in the Cu specimens on an average of 35 γ-peaks detected, it was possible to measure with a reasonable precision 30 and to determine the emitter for 28 of them, but in the Au specimens, with an average of 80 lines detected, 60 were measured and only 45 identified.

The HETC calculations were performed in pure materials on a 1 cm thick target irradiated with 600 MeV protons. In each materials 3 to 5 runs, with each 1'000'000 incident protons were made with different random number initiator in order to obtain a idea of the statistical variation of the results.

As a typical example, the effective production cross-section of some isotopes detected in Cu, Zr and Au are presented in table 2 with the corresponding calculated values.

It can be seen that the effective production cross section obtained in Cu are in very good agreement with the calculated ones, but in higher Z materials the results from HETC seem to become less reliable.

Two basic reasons can explain this discrepancy. First, in high Z material the number of short lived isotopes being a parent of the measured isotope increase rapidly (0 for ^{54}Mn in Cu, 3 for ^{75}Se in Zr, 5 for ^{95}Zr in Zr, 9 for ^{189}Ir in Au). So the effective

production cross section, being the addition of the production cross section of all these isotopes, is no more representative of the production crossection. Second, the model of the atom target in HETC for high Z materials is not optimized.

3.3 The ATHENA Experiment

Simple code comparisons for the irradiation of thin samples of actinides with high energy protons have revealed considerable differences in the total yield and the shape of the mass distribution for both spallation and fission products.
The ATHENA experiment (Actinide Transmutation using High Energy Accelerators) has been designed to validate transport codes such as HETC and its modifications. for irradiation of actinides with medium energy protons
As a first test, a specimen of 258 mgr of UO_2 encapsulated in stainless steel has been irradiated in PIREX for about 40 hours with a typical beam density of $.2.0\ 10^{14}$ protons s^{-1} cm^{-2}. Three techniques have been used for the determination of the type and quantity of isotopes produced by transmutation during the irradiation: γ-spectrometry for radioactive isotopes, Total Reflection X-ray Fluorescence and mass spectrometry.
A list of radioactive isotopes produced by transmutation has been established using γ-spectrometry, but the quantitative analysis is made very difficult for the same reason that was pointed out in the dosimetry experiment for high Z materials. The two other techniques have demonstrated a very high detection sensibility but the dose was not high enough and also the purity of the sample was not sufficient for a conclusive analysis. A new higher current irradiation is programmed this fall.

Acknowledgements

The authors would like to acknowledge fruitful discussions on the results with other group members: Drs. F. Hegedus, P. Marmy, F: Paschoud and with graduate students Mr. G. Müller and Mr. D. Yong. The most recent information on the ATHENA experiment was discussed with Prof. R. Chawla.

References

[1] Marmy, P., Daum, M., Gavillet, D., Green, S., Green, W.V., Hegedus, F., Proennecke, S., Rohrer,U., Stiefel, U. and Victoria, M., Nucl. Instr. & Meth. **B47**, 37-47 (1990).
[2] Serber, R., Phys. Rev. **72**, 1114 (1947).
[3] Robinson, M.T., "The dependence of radiation effects on the primary recoil energy", in Proceedings of a Conference on Radiation Induced Voids in Metals, Corbett, J.W. and Iannello, L.C., Eds., CONF 710601, National Technical Information Service, U.S.A., 1972, pp 397-429.
[4] Lindhard, J., Nielsen, V. and Scharff, M., K. Dan. Vidensk. Selsk. Mat.-Fys. Medd. **36**, No.10 (1963).
[5] Norgett, M.J., Robinson, M.T. and Torrens, I.M., Nucl. Eng. Des. **33**, 50 (1974).
[6] Victoria, M., Alurralde, M., Caro, A., Horsewell, A. and Proennecke S., Mat. Sc. Forum **97-99**, 541-552 (1992).
[7] Horsewell, A., Singh, B.N., Proennecke, S., Sommer, W. and Heinisch, H.L., J. Nucl. Mater. **179-181**. 924 (1991).
[8] Yoshida, N., Akashi. Y., Kitajima, K. and Kiritani, M., J. Nucl. Mater. **133-134**, 405 (1985).
[9] Zinkle. S.J.. J. Nucl. Mater. **150**. 140 (1987).
[10] Marmy. P.. Ruan Yuzhen and Victoria, M., J. Nucl. Mater. **179-181**. 679 (1991)

[11] Marmy, P. and Victoria, M., J. Nucl. Mater. **191-194**, 862 (1992).
[12] Gavillet, D., Marmy, P. and Victoria, M., J. Nucl. Mater. **191-194**, 890 (1992).
[13] Green, S.L., Green, W.V.,Hegedus, F.H., Sommer, W.F.and Oliver, B.M.,J. Nucl. Mater.**155-157**, 1350-1353 (1988).
[14] Van Ginneken, A. and Walpole, P.H.; Phys. Rev. **C14**, 1506 (1976)

THE CURRENT STATUS AND POSSIBLE FUTURE OF THE LOS ALAMOS SPALLATION RADIATION EFFECTS FACILITY

Michael J. Borden, Walter F. Sommer
Los Alamos National Laboratory, Los Alamos, NM, 87545, USA

The Los Alamos Spallation Radiation Effects Facility (LASREF) has been configured for both proton and spallation neutron irradiations since 1985. The facility makes use of the Los Alamos Meson Physics Facility 1 mA 800 MeV proton beam. Environment controlled proton and neutron irradiations have been demonstrated over the past nine years. The current copper beam stop configuration produces a maximum measured neutron flux of 4.6×10^{17} m^{-2} s^{-1} for energies greater than 1 KeV. The maximum proton flux at the center of the Gaussian shaped beam is 1.2×10^{14} protons cm^{-2} s^{-1} with a beam spot diameter of 3.5 cm at 2σ. Previously published work has shown that the neutron flux can be increased by a factor of ten by changing the beam stop to tungsten and decreasing the diameter. Expertise exists at Los Alamos to further optimize this design to tailor neutron production and spectrum. Consideration and preliminary planning has also been done for increasing the LAMPF proton current from 1 mA to a few mA with a possible maximum of 10 mA. An upgrade of this type would produce current densities comparable to those proposed for the Accelerator-Driven Transmutation Technologies (ADTT) programs.

LASREF can currently be used to do in situ measurements with controlled atmospheres and temperature. A volume of $0.12 \times 0.25 \times 0.50$ m^3 is available at 12 neutron irradiation positions and a volume of 150 cm^3 at each of three proton irradiation positions.

The LASREF design is modular and can be configured to do very elaborate experiments, such as those proposed for the ADTT programs. Materials characterization and proof of principle experiments are possible and highly desirable.

902

MATERIALS PERFORMANCE EXPERIENCE AT SPALLATION NEUTRON SOURCES

Walter F. Sommer
Los Alamos National Laboratory

There is a growing, but not yet substantial, data base for materials performance at spallation neutron sources. Specially designed experiments using medium energy protons (650 MeV) have been conducted at the Proton Irradiation Experiment (PIREX) facility at the Swiss Nuclear Institute accelerator (SIN). Specially designed experiments using 760-800 MeV protons as well as a spallation neutron flux at 90° from a copper target have been completed at the Los Alamos Spallation Radiation Effects Facility (LASREF) at Los Alamos Meson Physics Facility (LAMPF). An extensive materials testing program was initiated at LASREF in support of the German spallation neutron source (SNQ) project, before it terminated in 1985.

Considerable phenomenological materials performance data has been obtained at the TRIUMF facility in Canada, ISIS at Rutherford Appleton Laboratory in England as well as at SIN and LAMPF, including the Los Alamos Neutron Scattering Center (LANSCE). Most emphasis has been placed on neutron producing targets; uranium and tantalum at ISIS, copper at LAMPF and tungsten at LANSCE. Additional studies have focused on metal beam-entry windows; aluminum at SIN, stainless steel and Inconel at ISIS, LAMPF and LANSCE. Adequate performance to doses as high as $10^{22}/cm^2$ has been observed for some components. Work is presently underway on tungsten and tungsten alloys irradiated at LASREF.

Studies of the basic mechanisms of radiation damage effects due to medium energy protons and spallation neutrons have been aimed at an understanding of the differences from those observed and extensively studied in fission reactor environments where the neutron energy is generally < 10 MeV. Comparisons for aluminum alloys have been made.

Computational methods such as the Los Alamos High Energy Transport Code package (LAHET), coupled to radiation damage codes, are being used to predict the displacement and impurity production rates in materials selected for spallation neutron sources. There is a need to design and perform benchmark experiments to test these codes as well as codes under development that predict microstructural evolution as a function of fluence and spectrum.

For both liquid metal and solid metal-water cooled target systems there is a need to measure the ionization effect of medium energy particles on corrosion and mass transport.

Summary and Concluding Presentations Made at the International Conference on Accelerator Driven Transmutation Technologies and Applications

Two special presentations were made at the conclusion of the ADTT International Conference. The first was by A. Favale of the Northrop-Grumman Corporation and provided a summary of the conference highlights. The second presentation was given by C. Miliekowski of Skandatronix (Sweden). It provided a view of the future for ADTT systems and along with immediate needs that should be addressed for concept development. No papers are available for these talks; instead vugraph copies are included in these proceedings.

Accelerator Driven Transmutation Technologies Conference Wrap-Up

Anthony J. Favale
Grumman Aerospace Corporation

Las Vegas Nevada

29 July 1994

Accelerator Driven Transmutation Technologies

- Symposium Overview -

Why are they needed?

- new environmental mission for national laboratories
- Reduce the nuclear danger
- potential impact on geological repository
- new energy system for the future

What technologies are involved?

- Accelerators
- Target/Blankets
- Separations
- Materials

What countries have shown interest?

US	Sweden	Czech Republic
Russia	Germany	Netherlands
France	Italy	Others?
Japan	Spain	

What are the issues?

- economic impacts
- safety
- public perception
- regulatory impacts
- government interests
- government policy

What are the underlying drivers?

- Do we need Nuclear Power
- is Plutonium a *waste* or a *resource* ?

Environmental Mission for National Laboratories

What has happened?

- the cold war is over
- environmental concerns are coming into dominance

Mission of Laboratories

- maintain stockpile
- dispose of weapons materials
- clean up environment

Comment on ADTT

- no scientific barriers
- can we make the overall system work (technically, economically, environmentally)
- we must establish balance between systems engineering and experiments

Environmental Mission for National Laboratories - Continued

Problems for nuclear energy

- safety
- waste

These are difficult times for new technologies

- public skeptical about new solutions
- Resources are very scarce
- we must widen interest in ADTT

THIS CONFERENCE IS A GOOD STEP TOWARD WIDENING INTEREST

Reduce the Nuclear Danger

Danger

Use of nuclear weapons brings mankind's future to question. We must ensure the stability of the stockpile.

Reduce the Danger

Make final material physically unavailable

Dilemma

If nuclear power is to play a continuing role, how to develop the nuclear option and maintain low world inventory of fissile materials

Reduce the Nuclear Danger - Continued

Visions

Have a world with no fissile material and adequate power.

ADTT

- Develop technology ~20 years
- Burn all Plutonium
- Replace reactors with ADTT systems (Thorium/Uranium cycle: Bowman, Rubbia)

Testing Visions

- is the objective correct?
- is it achievable?
  - technically
  - politically
- are there better ways?

Reduce the Nuclear Danger - Concluded

Other approaches

- MOX
- reactors
- burial
- nuclear - no longer an option

Challenges for ADTT community - Develop a global posture

- inventory control
- use control
- international agreements & agencies

Accelerator-based conversion can have the following beneficial effects on repository

Effect	Qualitative Impact
1. Smaller source term of Pu, Np, Am, Tc, I	1. • Reduced releases. Np dominates the aqueous releases; actinides dominate releases by human intrusion and volcanic modes. • Reduce criticality safety concerns and constraints on emplacement.
2. Opportunity to convert ^{14}C and other nuclides into more stable forms.	2. Reduced ^{14}C gaseous releases.
3. Reduce decay heat that repository must accommodate.	3. • Reduce complexity of repository; decreased risk and costs associated with licensing. • Reduced releases of all nuclides. • Increased repository capacity; delay or eliminate need for second repository.

Materials Potentially Reporting to Yucca Mountain Exceed its Capacity

- Some materials being designated by DOE and other generators for Yucca Mountain are not acknowledged in repository plans. These include:

  - HEU spent fuel (DOE and foreign research reactors)
  - Surplus weapons Pu/other fissile materials
  - DOE LEU spent fuel
  - GTCC Wastes (including reactor decommissioning)
  - Depleted tails from enrichment plants

- Studies by Cowell et al. indicate that capacity of Yucca Mountain may need to be increased by 2x to accommodate all of the expected commercial spent fuel, defense HLW, and other items (above)

- Current estimates are that capacity of Yucca Mountain could be increased by 4 - 4.9x by actinide transmutation

Reference: Cowell, B. S., M. H. Fontana, and G. E. Michaels, "Incentives and Techniques for Increasing the Capacity of the Geologic Repository," to be presented at Spectrum '94, Atlanta, Georgia, (August 1994).

Summary

1. In current analyses, Np dominates the aqueous releases from Yucca Mountain. Accelerator-based transmutation of Np would eliminate the major source of health risk.

2. Yucca Mountain Project assessments underestimate the aqueous and gaseous releases due to neglected effects

   - waste package alteration/corrosion above 100°C
   - steam hydrolysis of waste glass
   - increased mobility of actinides in colloids

3. Actinides dominate releases by human intrusion and volcanic explosion. Transmutation would eliminate the source term for the major releases by these modes.

4. Accelerator-based transmutation could benefit the repository by reducing/eliminating the massive thermal perturbation to the site's hydrology and geology

   - Objective should be to eliminate gas phase flow in repository and maintain temperatures below 70°C
   - Requires reduction of actinide inventory by 10 - 100x
   - Pre-emplacement cooling times for Cs and Sr should be > 30y
   - Releases of all radionuclides would likely be reduced in a "cold" repository

New Energy Systems for the Future

- C. Bowman (LANL)

  Energy production utilizing the thorium uranium cycle. System employs a subcritical molten salt liquid fuel blanket driven by a high energy LINAC. (THERMAL REACTOR)

- C. Rubbia (CERN)

  Energy amplifier concept utilizing the thorium-uranium cycle. System employs a subcritical solid fuel blanket driven by a high energy cyclotron. (FAST REACTOR)

Advantages:

Systems would supply nuclear power for centuries with a very minimum nuclear waste. Possibility exists for negating the need of a repository.

National Involvements in ADTT

- Demonstrated at this conference -

These interests are guided by:

- **whether or not nuclear power is needed**
- **whether plutonium is considered a waste or a resource**
- **public concerns for nuclear waste**

<u>Countries represented at conference</u>

US	**Sweden**	**Czech Republic**
Russia	**Germany**	**Netherlands**
France	**Italy**	**others?**
Japan	**Spain**	

Observations on Panel Discussion

- Very Sobering Remarks -

Alan Croft

- This community must maintain credibility
  - must address the many obstacles (safety, chemistry, etc.)
  - must substantiate claims
  - must answer the question: *"Why use an accelerator?"*
- Did not appear to concur with G. Michaels comments though his published papers would appear to strongly back partitioning and transmutation.

Max Blanchard

- Tale of woes concerning 13 years process so far with Yucca Mt.
- ADTT too late to impact Yucca Mt.
- Nuclear power in US is ***DEAD*** so no need to worry about second repository

Observations on Panel Discussion - continued

John Rawlings

- We should look for opportunity to impact new DOE mission statement, HLW mission statement
- Los Alamos concept appears more real than fusion
- Question is whether we want nuclear power

Waclaw Gudowski

- Believes ADTT concept for energy (Bowman/Rubbia) very attractive for European countries where nuclear reactors are unpopular
- ATW is very appealing for Sweden
- Strong impact of Environmentalist

Problems of (Nuclear) Technologies

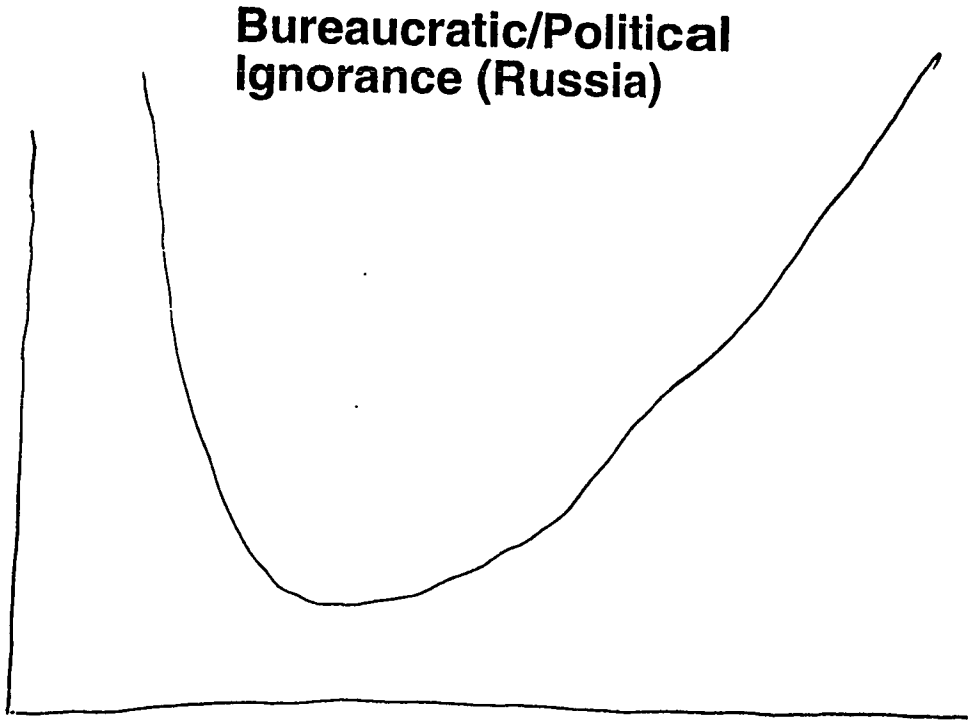

"Not in my Backyard " Philosophy (US?)

Licensing problems due to public acceptance!

More and more complicated issues to be explained to less and less competent (broader) audience

General Comments

- Excellent attendance, participation, community spirit evidenced by large amount of international collaboration. Remarkable in light of political and economic climate: Anti-nuclear, anti-technology, no money.
- Excellent symposium setting groundwork for why partitioning and transmutation is needed.
- Substantial technology base evident, directly applicable to ADTT. Preliminary indications ==> no show stoppers. Continued basic technology research, development, analysis, and testing is required.
- The community needs to formulate very sound arguments why accelerators are the preferred option for transmutation.
- We need to build on the international interest.
- We need to sell our governments on the concepts.
- There is a need for a systematic approach for evaluating the many options for accelerators, targets, and blankets.
- Plutonium is central to ABC, ATW, repository, which should be viewed as one integrated system. It drives the hazard, heat, proliferation. Assisted repository (Wagner, Michaels, Berwald)
- Insitu thorium cycle breeder has a lot of long term benefits (less short and long term hazard, proliferation resistance) and considerable interest. (Bowman/Rubbia).

General Comment - Continued

- Real technical progress in accelerator design (Lawrence)
- Cyclotrons: look interesting but can they carry the current? (Rubbia)
- HILBILAC: also interesting (Batskikh)
- Los Alamos getting second order effects on molten salts designs. Performance remains excellent (Bowman, et. al.)
- Others, concerned about development (chemistry, materials) are pursuing alternative technologies involving fixed fuels, aqueous slurry, carbides, etc. (Rubbia, ITEP: Chuvilo, Kazaritsky, Van Tuyle)
- Lots of interest in Pb and Pb-Bi targets. Obninsk brings real experience.
- Several serious attempts to get at safety issues for subcritical systems. Some include assessments of reactivity feedback coefficients for plutonium fueled systems. Preliminary results indicate that it should be possible to operate safely in 0.95-0.98 regime. However, if there is a LOCF or LOC accident, it must be sensed and the accelerator must be turned off. This should be addressed in future designs. (Los Alamos, BNL, Julich/ANL)
- Debate over fast versus thermal systems continues. Rubbia and Salvatores prefer fast systems. Bowman prefers thermal systems. New 238 NP (n,f) thermal sec measurement helps case for thermal blanket, but debate goes on.

General Comments - Concluded

- Neutron diode concepts discussed by several authors. (VNIIEF, RFNC-ITP) Mostly neutronics. No practical designs yet.
- To extent that all of these blankets have very high keff, accelerator current is minimized (in some cases to extent that cyclotron can be used). *However, the question of why not make them critical assemblies requires an explanation.* Solutions which have been suggested include: increased flexibility, better response to positive reactivity feedback for plutonium, less sensitivity to reactivity swings, ability to achieve full burnup, higher flux, ... Need point design to put this in perspective (including fission point design -- Salvatores, Croft, Van Tuyle, Venneri)

Future Directions for ADTT Concepts

C. Miliekowski

Scandatronix Corporation

ADTT Conference
Las Vegas, Nevada

July 29, 1994

Nuclear Power in the OECD Countries

				Connected to the grid Dec. 1993		Under construction 1993 or finally committed				Planned 1993			
		Electric Generation Nuclear 1993		Electric Capacity Nuclear		Units	Cap GWE	%	%	Units	Cap GWE	%	%
Country	Pop Millions	TWh	%	GWe	%			of tot electr cap	of nucl. cap			of tot electr cap	of nucl. cap
United States	253	622	19,6	99,0	13,2	5	5,9	0,79	6,0	–	–	–	–
Canada	27	88,8	17,2	15,5	14,3	–	–	–	–	–	–	–	–
Belgium	10	39,5	59,0	5,6	39,4	–	–	–	–	–	–	–	–
France	57	350,2	77,7	59,0	55,1	4	5,8	5,4	9,2	8	11,6	10,8	19,7
Germany	80	145,2	29,7	22,6	19,5	–	–	–	–	–	–	–	–
Netherlands	15	3,5	4,8	0,5	2,6	–	–	–	–	2	1,2	6,2	240
Spain	39	53,9	35,3	7,4	16,4	–	–	–	–	4	3,0	6,6	41
Switzerland	7	22,0	37,9	3,0	19,4	–	–	–	–	–	–	–	–
United Kingdom	57	80,3	26,7	11,9	18,2	1	1,2	1,84	10,0	–	–	–	–
	545	1.405,4		224,5		10	12,9			14	15,8		
Japan	125	234,0	30,2	36,7	19,7	8	7,4	4,0	20,2	22	243	13,0	66
S. Korea	44	58,1	40,2	7,6	28,0	9	8,1	30	107	8	7,4	27	97
	169	292,1		44,3		17	15,5			30	31,7		
Sweden	9	58,9	41,8	10,0	29,3	–	–	–	–	–	–	–	–
Finland	5	18,8	32,4	2,3	18,3	–	–	–	–	–	–	–	–
	14	77,7		12,3		–	–	–	–	–	–	–	–
Austria*	7	0		0		–	–	–	–	–	–	–	–
Italy*	56	0		0		–	–	–	–	4	4,0	6,4	∞
Australia	12	0		0		–	–	–	–	–	–	–	–
Denmark	5	0		0		–	–	–	–	–	–	–	–
Greece	10	0		0		–	–	–	–	–	–	–	–
Iceland	0,3	0		0		–	–	–	–	–	–	–	–
Ireland	3,5	0		0		–	–	–	–	–	–	–	–
Luxemburg	0,4	0		0		–	–	–	–	–	–	–	–
New Zealand	3,5	0		0		–	–	–	–	–	–	–	–
Norway	4,3	0		0		–	–	–	–	–	–	–	–
Portugal	11	0		0		–	–	–	–	–	–	–	–
Turkey	57	0		0		–	–	–	–	2	2,0	9,9	∞
	170	0		0		–	–	–	–	6	6,0		
OECD	898	1.775,2	24,8	281,1	16,5	27	28,4	1,67	10,1	50	53,5	3,14	19

General interest in ADTT for many years was rather cool but recently speeded up by:

- The advent of powerful accelerators.
- The expected surplus W-Pu from 40,000 nuclear weapons.
- The general recognition that also commercial Pu can be used as a material for making nuclear charges.
- The recognition of problems with deep waste repositories.

ADTT stands, in some ways, before an up-hill struggle, for example:

- National policy against reprocessing and against breeders as in some countries like the US and Sweden.
- Thermal neutron ADTT requiring very high neutron fluxes with new challenges in materials technology and partition/separation.
- Fast neutron machines are particularly unpopular in many countries.
- Safety is difficult to prove and to explain.

Nuclear Waste Policies

Nuclear Waste Policy I:

No Reprocessing. Among nations with this policy: USA, Sweden....
- Spent fuel elements not opened
- After intermediary cooling off final repository in deep rock

Proponents' arguments:
- Pu-bombs impossible to make without reprocessing
- Proliferation difficult thanks to the very high radioactivity
- Uninterrupted containment minimizes health hazards

Back end cycle cost within ~ 10 % of kWh$_e$ cost

Nuclear Waste Policy II:

Reprocessing important cornerstone. Nations with this policy: France, Great Britain, Russia, Japan etc.
- Spent fuel elements are opened and treated
- Partitioning and separation etc are performed.

Proponents' arguments:
- Fissile materials (Pu and actinides) burned for their destruction and for improved economy
- Possibility to reduce or eliminate sources of long lived rad. waste by reactors or ATW

Nuclear Waste Policy III:

Limited processing, in front end, on line processing thereafter. Suggested by Los Alamos ADTT group.
- Spent fuel elements opened, zircalloy cladding and uranium removed.
- Remaining mixture introduced in molten salt in liquid metal, molten salt spallator

Proponents' arguments:
- Compatible with Policy II
- Hoped to be compatible also with Policy I, fullfilling the basic purpose of Policy I

COMPETING NON-PROLIFERATION POLICIES

A policy can be advantageous for the more distant future but have some disadvantages in the near future, or vice versa.

- Reprocessing reduces proliferation risks later on, but may increase them during the period of reprocessing.

- A once-through cycle policy (no reprocessing) reduces the near term risk but leaves a higher risk to the future.

The choice, different in different countries, is in most countries not made on the basis of proliferation only, but also on economic and radiation safety considerations.

THE IMPORTANT ADTT ISSUES

Qualification Area	Present Situation	Decision Makers
Technical Feasibility	Very Probably	The technical experts
Safety	Can be made very good but not so extreme as often stated	The NRC is in respective countries
Proliferation Safety	Can be made better than with present reactors but International Inspection absolute condition	The governments
Cost and Competitiveness	Surprisingly, this area is still being largely neglected	The utilities
The Public's Trust	It is hoped that the portion of the Public trusting nuclear power will increase with ADTT but we do not know	The Public

4. REACTIVITY SWING AND REACTIVITY BUDGET FOR A Th-U CYCLE LIGHT WATER COOLED AND MODERATED LARGE SPALLATOR.

Which is the highest permissible k_{eff} of the cold unpoisoned core such that the machine will remain under $k_{eff} = 1{,}00$ after shut down at full power, i.e. when hot and poisoned? And what is the necessary reactivity to be supplied for start-up after shut-down late in the fuel cycle? These are important values because the economy of the plant depends strongly on them.

Physical changes after shut down (a - f) and influence of FP and stable U isotopes generated by multiple neutron capture after 4 - 5 years of the fuel cycle (h - i).		Spontaneous reactivity increase after shut-down from full power, caused by the physical changes:		Necessary reactivity increase to be supplied by accelerators for start-up after shut-down from full power 4 - 5 years into the fuel cycle:	
		LWR	Thorium H_2O cooled + moderated spallator	LWR	Thorium * spallator
a. Fuel element temperature decreases (500°)	$(\Delta k)_{FT}$	+ 1%	+ x%	+ 1%	+ x%
b. Moderator temperature decreases	$(\Delta k)_{MT}$	+ 3%	+ y%	+ 3%	+ y%
c. Xenon poisoning first increases, but soon disappears by decay	$(\Delta k)_{Xe}$	+ 3%	}+ 2% **	+ 3%	}+ 2% **
d. Samarium poisoning disappears by decay	$(\Delta k)_{Sm}$	+ 1%		+ 1%	
e. Protactinium disappears by decay	$(\Delta k)_{Pa}$	0	+ 5,3% **	0	+ 5,3% **
f. U^{233} grows up from Pa^{233} decay	$(\Delta k)_{U}$	0	+ u%	0	+ u%
g. Shut down margin	$(\Delta k)_{SDM}$	+ 1%	+ 1%	+ 1%	+ 1%
h. Effect of FP after 4 - 5 years at flux 10^{14} n/cm^2	$(\Delta k)_{FP}$	n.a.	n.a.	+ 3%	+ q%
i. Effect of U^{234}, U^{235}, U^{236} and U^{238} after 4 - 5 years	$(\Delta k)_{Ucap}$	n.a.	n.a.	n.a.	+ 2,5% **
	$(\Delta k)_{Tot}$	+9%	8,3+x+y+u%	+12%	10,8+x+y+u+q%

* It is assumed that only accelerators are used for regulation and shut-down (and a simple scram system)

** according to Rubbia et al, CERN Nov. 1993 n.a. = not applicable.

Conclusion: The accelerator capacity must be large enough so that the 1 GeV proton beam current is sufficient to overwin the reactivity gap of $10{,}8 + x + y + u + q$ %. Thus k_{eff} must not exceed $1 - \frac{10{,}8+x+y+u+q}{100}$, which leads to a high kWh_e cost even at relatively high z-values (z = number of spallation neutrons per proton). The Swedish group is in the process of calculating x, y, u and q and other (Δk):s. Thereafter the result can be integrated into the Matrix, giving the relation $\frac{\text{Spallator } kWh_e \text{ cost}}{\text{LWR } kWh_e \text{ cost}}$ as a function of z.

DIAGRAM OF THE MATRIX, showing Rrel as function of z and keff.
Blanket technology; light water cooling and moderator.

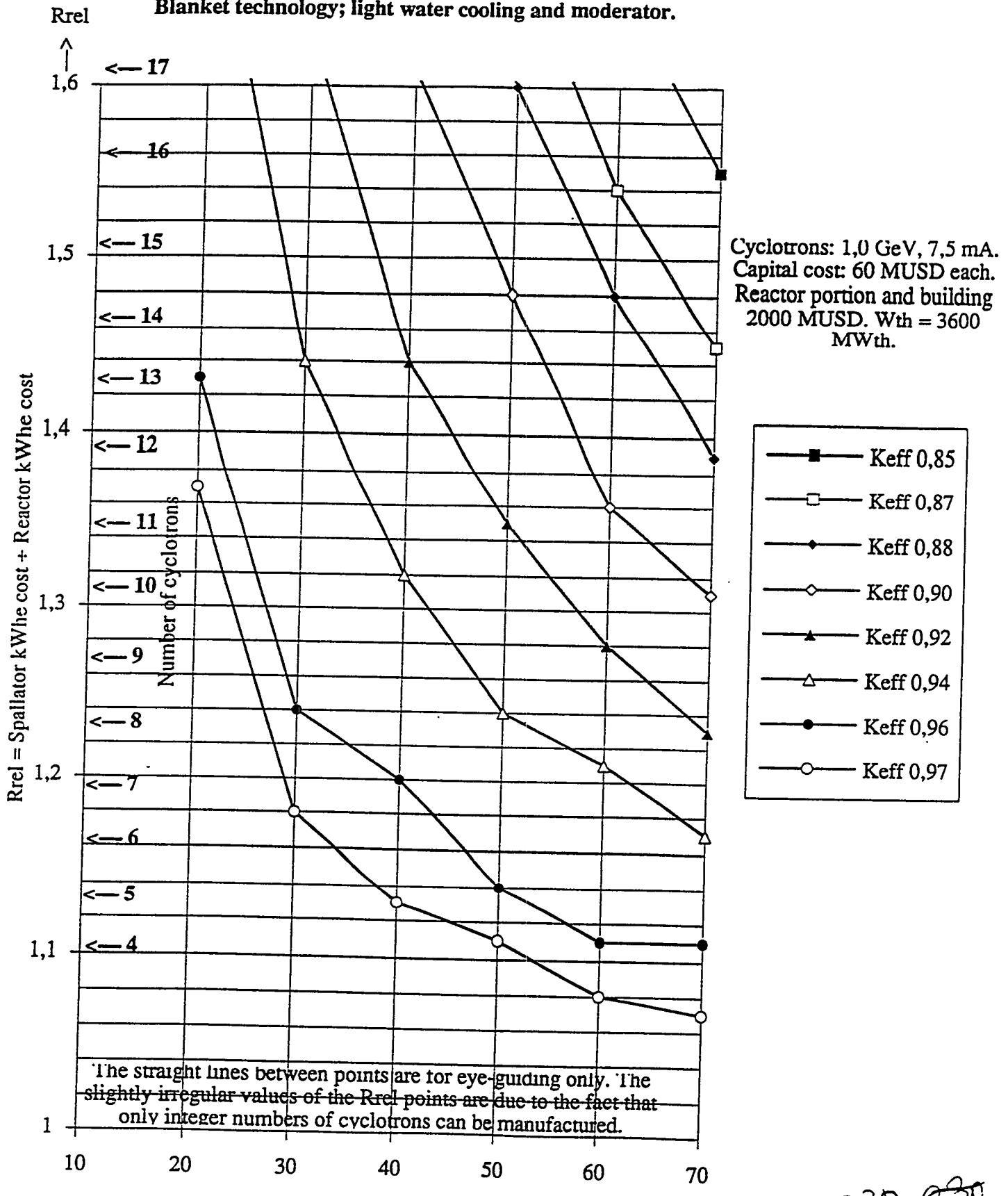

CONTINUED PROJECT RELATED WORK

After the chosen purpose and the capacity goal for the concept studied having been precisely specified, the foremost need is to

- use more reactor expertise for the target//blanket.
  (Neutronics heat transfer, mechanical eng., accident analysis)

- do more physics, neutronics, kinetics, operational analysis of consequences of shut down and restart etc. to check required accelerator capacity with respect to both safety and cost.

The next steps would then include:

- Detailed engineering design, heat transfer, mechanical design, particularly for a complete target/blanket.

- Plant lay out including buildings and containment, also for the accelerator.

- Cost calculation based on detailed design and lay out.

- Cost comparisons and competitively estimate.

- Technological tests and small demo plant for validations.

- Thorough non-proliferation analysis.

Rather detailed safety analysis of the type NRC would require for various accidental malfunctions the above work cost money. Sufficient funding has to be secured.

Studies like this are important for getting the vision come true – the financing and construction of a large demonstration plant.

Yucca Mountain is currently being evaluated, might be modified so as to be able to handle larger quantities of waste; thus delaying for several decades, or even eliminating, the need for siting and constructing a second repository.

Recent total system performance assessments for the proposed Yucca Mountain site [8,9], (which assumes that spent fuel is directly emplaced in the repository without reprocessing and transmutation), has substantially altered the technical picture upon which much of the previous transmutation assessments were based. The intention of this paper is to provide a qualitative update of the benefits of transmutation to the U.S. high-level waste repository to reflect the recent advances in understanding of repository performance. It is suggested that transmutation may provide very significant benefits to the repository by removing the long-term heat source posed by actinides and by eliminating the radionuclides that dominate the projected environmental releases.

Actinides as a Source of Heat

It is a standard assumption in repository assessments that spent fuel is emplaced after cooling times of 10 years after irradiation. At 10 years, approximately 77% of the thermal power in spent fuel originates from the decay of ^{137}Cs and ^{90}Sr and their daughters, with almost all of the remaining heat from actinide decay. In the short term, such as cooling times less than 50 years, the decay of ^{90}Sr and ^{137}Cs continues to produce the majority of the overall heat from spent fuel. However, over periods longer than 100 years, it is the alpha decay of various actinides, principally Pu and Am, that dominates the total heat output of spent fuel. Figure 1 shows the calculated total heat energy (that is, the thermal power integrated over time) for LWR spent fuel with the actinides present and with the actinides removed. The actinides account for about 80% of the heat that is generated over the first 1000 years. For time frames beyond 1000 years, actinides contribute about 99% of the additional heat generated in a repository.

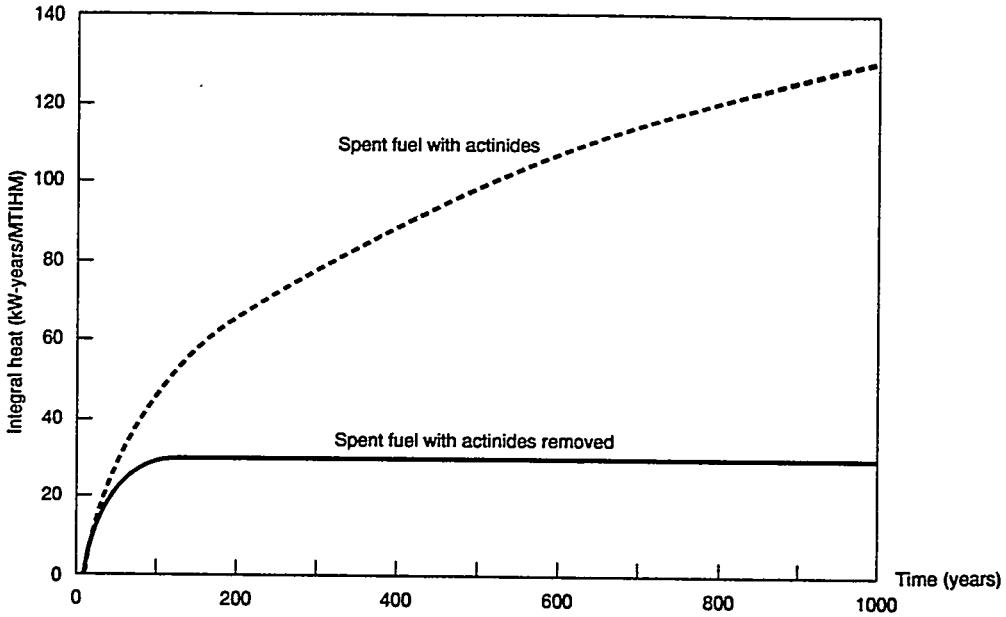

Fig. 1. Total integral heat to be accommodated by a geologic repository. Heat values were calculated with ORIGEN2 model and are based on PWR fuel with an assumed burn-up of 30 GWd/MTIHM and 10 years cooling.

These longer time frames are important, because heat is expected to move relatively slowly through the geologic media. Bulk rock temperatures in and around the repository at any given time will depend upon the heat produced over long periods of time. As an example, rock temperatures at the so-called far-field location in the geologic media (about 50 meters from the emplaced waste) is not expected to reach its peak value until 700 years after emplacement of spent fuel [5]. Thus, in the context of overall bulk temperatures of large volumes of the repository site, it is the decay heat of the actinides in spent fuel that is the dominate heat source, not the decay of fission products such as Cs or Sr.

The Effect of Decay Heat upon Yucca Mountain

The proposed repository at Yucca Mountain would be at an elevation of about 200 meters above the water table but at about 300 meters below the surface of the mountain. Standardly [10,11], water is envisioned as contacting the surface of the mountain through rainfall or snowmelt and moving slowly downward through the repository region until it percolates into the aquifer, or water table, below. The standard scenario for releases from the repository involves water contacting the waste packages and accelerating their failure rate, followed by the alteration of the spent fuel by water, the subsequent dissolution of radionuclides within the groundwater, and the transport by aqueous pathways to the water table, where it is then assumed to have been released to an environment accessible to humans. The rock of Yucca Mountain above the water table has a moisture content that does not fill 100% of the rock pore volume; thus, it is said to be unsaturated. The relatively low level of moisture in the rock (70-90% saturated) and the slow speed at which water is able to move through the rock to the accessible environment are aspects of the Yucca Mountain site that were originally thought to contribute to the minimization of radionuclide releases for any given emplacement period.

However, the existence of the decay heat from spent fuel is now expected to substantially perturb the unsaturated zone of Yucca Mountain. It is now reported [8,9,12-15] that the hydrology and geochemistry of the site will be dominated by the heat of the spent fuel. Given the thermal-loading densities of spent fuel now considered for Yucca Mountain, a significant volume of the mountain will be raised in temperature above the boiling point of water. Thus, buoyant gas phase convection of water vapor will become an important feature of groundwater movement and of heat transport. Heat-driven buoyant vapor will transport water to a cool region above the emplaced waste where the water will condense and then be driven by gravity downward toward the repository. The resulting mountain-scale convection cells between the hot, above-boiling repository and the cooler, subboiling regions will create thermo-hydrologic phenomena not currently found in the ambient-temperature site. The mountain hydrology will change significantly over thousands of years as the mountain rock first heats up after waste emplacement and then cools because of the long-term reduction of the decay heat source term.

A schematic of the potential heat-driven effects upon the Yucca Mountain hydrology at the mountain-scale is shown in Figure 2. This figure is modified from Figure 10-1 of Reference 8 and is intended to show a physical picture of the thermally-driven hydrology as it has been developed by the U.S Yucca Mountain project. The schematic presents a snapshot in time of the mountain-scale phenomena..

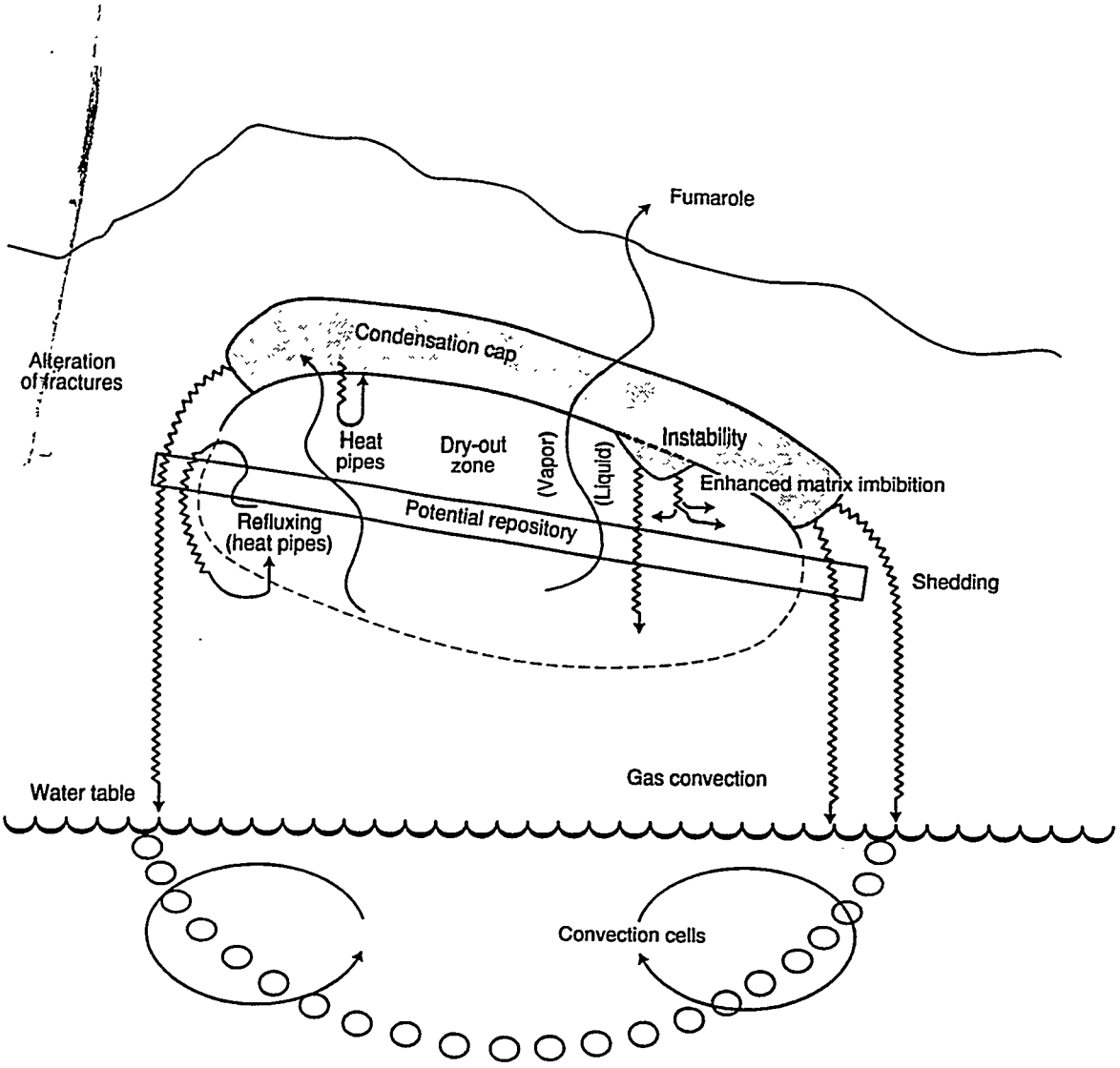

Fig. 2. Schematic of thermally-driven processes that are expected to affect the hydrology of Yucca Mountain. Heat of decay of the actinides is the predominant source term that drives these processes. Some of the phenomena depicted are not yet included in repository performance calculations. Note that the so-called "dry-out zone" will actually retain non-zero levels of liquid saturation/humidity for long periods of time. Based on Figure 10-1 from Reference 8.

Some of the relevant aspects are:

- A saturated zone above the repository will arise from condensation of thermally-driven buoyant water vapor. This is often called the condensation "perch" of the repository. The size and characteristics of the perch will vary in time and spatially, according to the spatial inhomogeneity of rock characteristics and of the thermal conditions. The saturated condensation zone may be tens of meters in depth and exist over hundreds of acres within the rock.

- Depending upon assumptions, the so-called dryout zone will only include the center portion of the emplaced waste, thus exposing the edges of the repository to near-boiling liquid water. Accelerated degradation of the waste packages from subboiling liquid condensation in the end regions of the repository is a concern.

- The so-called dryout zone will probably not be absolutely dry. First, the elevation of temperatures above boiling simply converts liquid phase water into the vapor phase; but, the resulting steam will leave the above-boiling region rather slowly [12,16] under most conditions and assumptions. Thus, the initial effect of heat is to create a hot (above-boiling), humid environment in which liquid film formation on the waste packages could lead to their accelerated failure. Additionally, aqueous phase water that is shed from the condensation perch will travel via fractures underneath the dryout zone and may be transported by heat pipe refluxing back into the dryout region, thus providing a mechanism for rewetting of the packages.

- A variety of possible phenomena could cause transport of liquid phase water from the condensation perch back into the waste package region. Instabilities in the surface of the condensation cap, arising from geologic or heat source heterogeneities, may cause fracture flow of liquid phase water into the repository or enhanced imbibition of water into the local rock matrix (see Figure 2). Heat pipe effects may also affect transport of water around the condensation cap.

- The elevation of the rock to temperatures of 130°C or higher may cause alteration of the structure of fractures within the rock. This is important, because flow through rock fractures is currently believed to be the dominant transport mechanism for groundwater.

- Convection cells may arise within the water table. The geochemistry of the aquifer may be affected.

- The pH and chemistry of the groundwater may be greatly altered by the increase in temperatures due to the strong dependence of dissolution rates and solubility upon temperature and due to the introduction of flowing steam through the rock matrix.

In addition to these mountain-scale phenomena, there will exist potentially important heat-driven phenomena at the spatial scale of the waste packages. During heatup and cooldown of the repository region, liquid phase convection cells can arise between neighboring waste packages, greatly altering the local groundwater hydrology. Additionally, Buscheck and Nitao [12] have developed a conceptual model of heat-driven vapor and condensate flow between two neighboring packages that are in regions of sharply varying bulk permeability; i.e., one package is in relatively unfractured impermeable rock and the second package is in rock that is significantly fractured. In the Buscheck-Nitao model, vapor-phase pressure differentials drive vapor flow into the fractured rock region where it condenses and drains, possibly causing persistent two-phase refluxing conditions that may "drench" the waste package. Such phenomena may generate a need to characterize the heterogeneity of fractures in the rock over the approximately thousand acres of the repository for the 10,000 to 30,000 waste packages.

Other temperature dependent phenomena important to repository performance will also be driven by repository heat. These include: solubility of the radionuclides, rates of corrosion pitting and microbial attack of the waste package, oxidation of the spent fuel, and transport time of $^{14}CO_2$ through the repository. An example of the latter consideration is shown in Table 1.

Given the 5450 year decay half life of ^{14}C, the difference in transport times of $^{14}CO_2$ from the packages to the accessible environment may be significant because of the potential for decay of the radionuclide during transport.

Table 1. Retarded Travel Times of ^{14}C from the Repository to the Atmosphere

Peak Bulk Temperature of Repository at Release Time	Average ^{14}C Travel Time to Atmosphere*	
	tuff permeability = $10^{-11}m^2$	tuff permeability = $10^{-12}m^2$
~50°C	1250 years	11,000 years
~130°C	250 years	4,500 years

*Values of travel time are derived from Figures 12-5 and 12-8 of Reference 8. Temperature values were obtained from Figure 12-6 of the same reference.

Implications of Actinide Heat for Repository Licensing

Licensing of a hot repository will require extensive analysis and characterization of a massively perturbed geologic system. Essentially, site characterization studies can only characterize the properties, hydrology, and chemistry of the unperturbed system. The licensing effort will need to rely upon computer models to extrapolate the existing mountain system to the massive-perturbed system that must be relied upon for isolation of the wastes from the accessible environment. Small-scale experiments may be able to provide helpful information, but the spatial scale of many of the discussed phenomena would appear to make their experimental characterization impractical. Thus, computer modeling will be required as a licensing basis.

For repositories that are above-boiling or near-boiling in temperature, the fact that heat transport will likely be dominated by multiphase convective processes rather than by conduction [12] will require enormously greater complexity in calculations of temperature. Similarly, the transport of water and radionuclides in these systems will be driven by nonisothermal, multiphase flow with critically important [13,14] nonequilibrium flow processes between the fractures and the rock matrix. The modeling of these phenomena will require theoretical advances in flow modeling [12].

Another aspect of the effects of actinide heat upon the repository is the potential importance of heterogeneity to the performance calculations. The requirements for characterizing the heterogeneity of the mountain are unclear, but may well be very costly, and might be impractical. The issue of heterogeneity is further complicated by the possibility of heat altering the properties of the media; i.e., by alteration of fractures.

The temporal nature of the thermally-driven perturbation to the mountain system also introduces unfavorable complexity into the licensing process. Calculations by Buscheck and Nitao [15] indicate that repository heat-driven changes in the hydrology can persist for more than 100,000 years. The licensing requirements are expected to call for characterization of the performance of the mountain over a time period of 10,000 years or longer.

The combination of these factors: (1) theoretically complex heat transport and flow phenomena; (2) the importance of heterogeneity; (3) the diverse spatial scales of the processes, and (4) the long time periods over which the phenomena must be described, may make the licensing of Yucca Mountain very complex and uncertain of success.

In this context, it may be that destruction of the actinides by transmutation with either accelerator-driven systems or in reactors, in combination with longer surface cooling times for Cs and Sr, would permit the emplacement of waste in an ambient-temperature repository that might be licensed in a more rapid and cost-effective manner. This "cold" repository concept would need to be studied further to determine its benefits and to define the requirements for actinide burning. It seems likely that the actinides would not need to be completely eliminated from the repository, but that reduction in actinide quantity by more than a factor of 10, but less than a factor of 100, might be required. Thus, transmutation systems would not need to address every waste stream that is to be emplaced in the repository in order to achieve the benefits of a cold repository — but only the majority of the actinide-bearing streams. This simplification is a potentially important aspect of a transmutation-enabled "cold" repository concept.

The projected benefits of a "cold" repository may be fully achievable only if both far-field and near-field temperatures are maintained at subboiling levels. Thus, transmutation-enabled cold repository concepts may require surface cooling times for Cs and Sr that are longer than 10 years in order to meet near-field temperature limits. This may be a potential problem for the cold repository concept and needs further study. Surface storage time requirements up to 50 years may be acceptable, and indeed may match well the lag storage times that will be required anyway as transmutation systems are developed, constructed, and brought into operation. However, Cs and Sr storage times greatly in excess of 50 years may present institutional issues for a transmutation-enabled cold repository concept. Clearly, better quantification of cooling time requirements for Cs and Sr are needed.

Methods other than actinide transmutation may exist for avoiding the above-mentioned thermal complexity issues. These methods may include:

- finding a repository waste emplacement strategy and configuration for which the repository performance is insensitive to the theoretically difficult aspects of heat transport and flow that are expected for the hot repository.

- decreasing the areal loading density of waste to maintain repository temperatures below the threshold for buoyant gas-phase flow processes. This repository strategy must result in temperatures that are significantly below "subboiling," e.g., peak temperatures below 70°C. This option would have unfavorable impacts on repository capacity.

The discussion of these other options is beyond the scope of this paper.

Results of Recent Repository Performance Assessment

Two total-system performance assessments of Yucca Mountain have been recently published [8,9]. These two assessments appear to agree on major conclusions, but the models and assumptions used by Wilson, et al. [8] appear to be more completely documented and the work appears to involve more detailed and comprehensive treatment of effects and uncertainties. For this reason, we use the work of Wilson, et al. as a basis for these discussions.

A major change from previous assessments [1,2,10,11] is the reevaluation of the values used for actinide solubility in the Yucca Mountain groundwater. These previous assessments used very low values for actinide solubility, with the result that the calculated magnitude of the releases for the actinides was very low. However, these previously-used values of solubility were the solubilities of the actinide elements in ionic forms; whereas, the relevant values are now assumed to be the solubilities of the actinides as oxides. This point has proved to be very important, because the solubilities of the actinide oxides are larger than the ionic solubility by several orders of magnitude.

Table 2 shows the mean values for actinide solubility currently used in the Sandia Total System Performance Assessment (TSPA)-1993 [8] and compares them with the values formerly used in performance assessments conducted in 1991.

Table 2. Assumed Values of Actinide Solubility (moles/liter) in Repository

	1991 Performance Assessments		TSPA-1993	
U	$10^{-7.7}$	(b)	$10^{-4.5}$	(a)
Np	10^{-9}	(c)	10^{-4}	(a)
Pu	$10^{-12.4}$	(b)	$\sim 10^{-7}$	(a)
Am	$10^{-8.2}$	(b)	$\sim 10^{-7}$	(a)

(a) mean values of solubility parameter distributions assumed in Sandia TSPA-1993 calculations [8].
(b) base scenario solubility assumptions at 100°C from Table 3.3 of PNL-8444 [11].
(c) mean value of solubility parameter distribution assumed in Sandia TSPA-1991 [10].

As a result, the actinides are now calculated by the Yucca Mountain Site Characterization Project to dominate releases by the aqueous pathway. This point is acknowledged in both of the recent total-system performance assessments [8,9] sponsored by the Yucca Mountain project. Table 3 shows the calculated relative dose, by radionuclide, from aqueous releases as reported in one of the TSPA-1993 reports [8]. Note that ^{237}Np dominates the dose and that ^{231}Pa (a daughter of ^{235}U) and ^{234}U are the next largest contributors. The projected releases of the long-lived soluble isotopes, ^{99}Tc and ^{129}I, have dropped somewhat from the values calculated in past assessments. This fact, in combination with the calculated increase in releases from the actinides, has made the ^{99}Tc and ^{129}I releases relatively less important.

Table 3. TSPA-1993* Results for Doses from Aqueous Releases

Relative Radionuclide Contributions to Peak Individual Dose from Aqueous Releases

10,000 years		1,000,000 years	
^{237}Np	(84.7%)	^{237}Np	(87.1%)
^{231}Pa	(6.0%)	^{231}Pa	(6.5%)
^{234}U	(3.8%)	^{234}U	(4.6%)
^{99}Tc	(2.1%)	^{99}Tc	(1.9%)

*Reference 8, Table 15-4, page 15-36.

It is noteworthy that isotopes of Pu, which are now identified as being somewhat more soluble than in the past, still do not contribute significantly to the projected aqueous releases from the repository. This is due to the tendency of ionic Pu to be less mobile in the geologic media; i.e., Pu is expected to be highly sorbed by chemical interactions with the medium. Np is more soluble and less highly sorbed than Pu and thus tends to dominate radionuclide releases.

The ^{14}C gaseous releases are still reported as dominating the overall projected releases when judged against the EPA release limits [17]. A portion of those projected releases originate from the fraction of ^{14}C that is projected to be in the fuel-cladding gap and thus assumed to be readily releasible subsequent to waste package degradation and cladding breach.

Considered in the context of the hot repository, releases from human intrusion are approximately of the same order as the aqueous releases [8]. These releases are dominated by the actinides as well.

Given the baseline Yucca Mountain Site Characterization Project models, the absolute magnitude of the calculated releases are lower than the EPA release limits. Inherent in the modeling methodologies are several conservative assumptions that tend to overpredict the release. However, these model calculations also currently omit many phenomena that may increase the magnitude of calculated releases. Several of the omitted phenomena may be quite important to the calculation of radionuclide releases. The assumption of zero humidity at temperatures of 100°C and higher used by Wilson et al. [8] will underestimate the waste package corrosion rates. The effects of steam hydrolysis on the vitrified high-level waste has not been considered; steam hydrolysis is known to rapidly degrade borosilicate glass under some conditions. Colloid formation could increase the mobility of radionuclides such as Pu and Am, causing these releases to be greater than calculated. Alteration of the groundwater chemistry by thermal effects and by climate change can affect the radionuclide solubilities, increasing or decreasing them by at least an order of magnitude. In the words of the authors of TSPA-1993 [18]:

"Many potentially important features, processes, and events have yet to be included in our models, and many model simplifications have not yet been evaluated to determine whether they cause us to underestimate releases."

For this reason, it is premature to dismiss the radionuclide releases from the Yucca Mountain site as being acceptably low. Quantitative evaluations of the omitted phenomena are needed to determine whether the proposed Yucca Mountain repository will pose an acceptable health risk to the public.

Benefits of Transmutation Systems to Repository Health Risk

Transmutation of actinides and of ^{99}Tc and ^{129}I has the potential to significantly reduce the health risk of the repository from all identified release mechanisms and to reduce the uncertainties in health risk from phenomena that are incompletely evaluated.

Aqueous releases of radionuclides could be greatly reduced.

- the radionuclide that dominates peak individual health risk from aqueous releases in current assessments is ^{237}Np. Complete transmutation of this nuclide would reduce the overall risk by over 80%. Additionally, transmutation of ^{99}Tc, ^{129}I, and use of alternative disposition methods for uranium could reduce the projected individual risk from aqueous releases by as much as two orders of magnitude, or more.

- transmutation of Pu and Am would reduce the long-term source of heat in the repository. This has the potential to reduce the aqueous releases of all radionuclides by eliminating the undesirable effects of high-temperature such as accelerated waste package corrosion in hot, humid environments, steam hydrolysis of vitrified waste forms, reduced sorbing properties of geologic media at higher temperatures, and the effects of thermally-driven alteration of the fracture system on groundwater velocity.

Gaseous releases of ^{14}C could be greatly reduced.

- the waste processing associated with transmutation concepts would provide the opportunity to use a waste form for ^{14}C that has superior performance characteristics relative to spent fuel. In particular, the relatively rapid release of the free ^{14}C in the fuel-cladding gap of emplaced spent fuel can be avoided.

- transmutation of Pu and Am would reduce the long-term source of heat in the repository, which in turn would increase the travel time of gaseous ^{14}C to the accessible environment. Longer travel times for ^{14}C have the potential to reduce ^{14}C emissions by as much as a factor of two, due to decay of the ^{14}C radionuclide during the travel period.

Releases of radionuclides due to human intrusion and volcanic expulsion could be greatly reduced.

- As pointed out by Forsberg [2], intrusive and expulsive release mechanisms have the potential to bypass the relatively slow aqueous migration modes of release by directly placing radionuclides into the accessible environment. Transmutation of Pu, Am, Np and other actinides would eliminate the most radiotoxic components of emplaced waste that tend to dominate health risk from intrusive and expulsive methods.

- Transmutation of Pu would reduce or eliminate the potential for intentional intrusion of the repository for recovery of Pu; i.e., using the repository as a Pu mine. Such intentional intrusion poses the potential for either deliberate or inadvertent releases of radionuclides to the environment.

Releases due to colloid formation could be greatly reduced.

- Colloid formation may be difficult to characterize or quantitatively predict but has the potential to increase the releases of all radionuclides, and in particular, those radionuclides that are currently projected to be strongly sorbed by the geologic media. Transmutation of Pu and Am might significantly reduce potential releases from colloid formation.

Uncertainties in aqueous releases due to climate change could be greatly reduced.

- Despite the fact that climate change is currently assessed as occurring 45,000 years in the future in current repository performance assessments, climate change is cited as the second most sensitive parameter uncertainty in assessments of aqueous releases [19]. The potentially unfavorable attributes of climate change might be an increase in the water infiltration rate at Yucca Mountain and a change in the groundwater chemistry, which in turn would affect radionuclide solubilities. Transmutation of the radionuclides that dominate aqueous releases, such as Np, would reduce the leverage that climate change would have on health risk uncertainties.

CONCLUSIONS

1. In performance assessments published by the Yucca Mountain Site Characterization Project, Np and other actinides are now found to be the dominant sources of health risk for aqueous releases from the Yucca Mountain site. Thus, actinide transmutation would have the potential to reduce or eliminate the major health risk source terms that are identified in current calculations of repository aqueous releases.

2. Transmutation of actinides has the potential to greatly reduce the quantities of radionuclides released and the health risks from all identified release pathways from the repository.

3. Transmutation of actinides and long-lived water-soluble fission products has the potential to greatly reduce the uncertainties associated with the effects on repository releases of repository heat, climate change, and colloid formation.

4. Many potentially important features, processes, and events have yet to be included in repository performance models, and many model simplifications have not yet been evaluated to determine whether they underestimate radionuclide releases. For this reason, it is premature to dismiss the radionuclide releases from the Yucca Mountain site as being acceptably low. Quantitative evaluations of the omitted phenomena are needed to determine whether the proposed Yucca Mountain repository will pose an acceptable health risk to the public.

5. Licensing of a repository at the Yucca Mountain site may be very expensive and may be uncertain of success due to the substantial perturbations to the mountain hydrology and geology caused by actinide decay heat. The heat of the actinides may have the following implications:

   - heat transfer calculations will not be focused upon theoretically-simple conduction processes, but instead will address multiphase, convective processes that are sensitive to spatial variability in the heat source term and in the geologic medium properties.

   - groundwater transport calculations will not be based solely on currently observable figures-of-merit such as groundwater percolation rates. Instead, thermally-driven processes will dominate the hydrology, and the licensing process will need to extrapolate multiphase flow processes with critically important disequilibrium processes between fractures and the rock matrix. These calculations will likely be sensitive to spatial variations in geologic media properties over hundreds of acres and may depend upon ability to forecast thermally-induced alterations of fractures in the mountain.

   - these theoretically-difficult processes will vary in time, and thus modeling of the massively perturbed mountain system must be performed for periods of 10,000 years or greater.

   Transmutation of actinides, in combination with longer cooling times for ^{137}Cs and ^{90}Sr, may create an opportunity to design a relatively high capacity repository with peak temperatures below 70°C. Such a cold repository concept requires significant additional evaluation to determine whether it offers significant benefits. However, transmutation-enabled cold repositories have an intuitive appeal, because their licensing may be more directly based upon currently observable characteristics of the site and because their licensing may not depend upon unprecedented success with modeling of very complex phenomena over very long periods of time which are sensitive to small-scale system heterogeneities.

REFERENCES

[1] Pigford, T. H., Actinide Burning and Waste Disposal, UCB-NE-4176, October 5, 1990.

[2] Ramspott, L. D., J. Choi, W. Halsey, A. Pasternak, T. Cotton, J. Burns, A. McCabe, W. Colglazier, and W. Lee, Impacts of New Developments in Partitioning and Transmutation on the Disposal of High-Level Nuclear Waste in a Mined Geological Repository, UCRL ID-109203, March 1992.

[3] Forsberg, C. W., "Health and Environmental Risk-Related Impacts of Actinide Burning on High-Level Waste Disposal," Oak Ridge National Laboratory, Report ORNL/M-1822, May 1992.

[4] Michaels, G. E., "Reexamination of the Incentives for Partitioning-Transmutation for High-Level Radioactive Wastes and Spent Nuclear Fuel," presented at the 205th American Chemical Society National Meeting, Denver, Colorado, March 28-April 2, 1993.

[5] Croff, A. G., "A Concept for Increasing the Effective Capacity of a Unit Area of a Geologic Repository," *Radioactive Waste Management and the Nuclear Fuel Cycle,* June, 1994.

[6] Cowell, B. S., M. H. Fontana, and G. E. Michaels, "Incentives and Techniques for Increasing the Capacity of the Geologic Repository," presented at the Spectrum '94 International Meeting on Nuclear and Hazardous Waste Management, Atlanta, Georgia, August 14-18, 1994.

[7] Private communication from B. S. Cowell, Oak Ridge National Laboratory, Oak Ridge, Tennessee, July 1994.

[8] Wilson, M., et al., *Total-System Performance Assessment for Yucca Mountain - SNL Second Iteration (TSPA-1993), SAND93-2675*, Sandia National Laboratories, April 1994.

[9] Andrews, R. W., T. F. Dale, and J. A. McNeish, *Total System Performance Assessment - 1993: An Evaluation of the Potential Yucca Mountain Repository,* B00000000-01717-2200-00099-Rev.01,INTERA, Inc., Las Vegas, NV, March 1994.

[10] Barnard, R. W., et al., "TSPA 1991: An Initial Total-System Performance Assessment for Yucca Mountain," *SAND91-2795*, Sandia National Laboratories, Albuquerque, NM, 1992.

[11] Pacific Northwest Laboratory, *Preliminary Total-System Analysis of a Potential High-Level Nuclear Waste Repository at Yucca Mountain, PNL-8444*, Richland, Washington, Westinghouse Hanford Company, January 1993.

[12] Buscheck, T. A., and J. J. Nitao, "The Impact of Buoyant, Gas-Phase Flow and Heterogeneity on Thermo-Hydrological Behavior at Yucca Mountain," American Nuclear Society, *Proceedings of the Fifth Annual International High Level Radioactive Waste Management Conference*, Vol. 4, Las Vegas, NV, May 22-26, 1994, pp. 2450-2474.

[13] Buscheck, T. A., J. J. Nitao, and D. A. Chesnut, "The Impact of Episodic Nonequilibrium Fracture-Matrix Flow on Geological Repository Performance," *Proceedings American Nuclear Society Topical Meeting on Nuclear Waste Packaging (Focus 91)*, Las Vegas, NV, September 30-October 2, 1991. Also, *UCRL-JC-106759*, Lawrence Livermore National Laboratory, Livermore, CA, 1991.

[14] Nitao, J. J., T. A. Buscheck, and D. A. Chesnut, "Implications of Episodic Nonequilibrium Fracture-Matrix Flow on Repository Performance," *Nuclear Technology*, Vol. 104, No. 3, pp. 385-402, 1993.

[15] Buscheck, T. A., and J. J. Nitao, "The Impact of Thermal Loading on Repository Performance at Yucca Mountain," American Nuclear Society, *Proceedings Third International High-Level Radioactive Waste Management Conference*, Las Vegas, NV, April 12-16, 1992. Also, *UCRL-JC-109232*, Lawrence Livermore National Laboratory, Livermore, CA, 1992.

[16] Mishra, Srikanta, "Far-Field Thermohydrologic Calculations," Appendix A in *Total System Performance Assessment - 1993: An Evaluation of the Potential Yucca Mountain Repository,* B00000000-01717-2200-00099-Rev.01, INTERA, Inc., Las Vegas, NV, March 1994.

International Conference on Accelerator Driven Transmutation Technologies and Applications

Breakout Group Summaries

935 933

Summary of The Accelerator Part of The International Conference on Accelerator-Driven Transmutation Technologies and Their Applications.

Thomas P. Wangler

November 15, 1994

During the past 15 years many advances have been made in the technology of high-power accelerators, and in the understanding of the beam-physics issues associated with their high-performance requirements. These developments have contributed significantly to the high level of confidence in the practicality of the applications that were the central point of the international Accelerator-Driven Transmutation Technologies (ADTT) Conference. Even so, there are many accelerator topics that needed to be addressed, and the Conference provided the opportunity to address these issues.

At present, the beam requirements are usually specified as a nominal 1-GeV energy, with average beam currents for accelerator transmutation of nuclear wastes (ATW) or commercial energy production that ranged from 10 to 100 mA. This wide range of beam currents is the result of different applications and different system concepts. At present the required beam current for one target-blanket for ATW is about 15 mA, but, typically, one may want to irradiate as many as six targets at one facility. Thus, nominal beam current of 100 mA for ATW is not unreasonable. Other desirable accelerator requirements include a) high electrical efficiency, b) low capital and life-cycle costs, and c) high availability and reliability (numbers ranging from 85% to 95% were discussed as a desirable goal). Availability is generally defined as the fraction of actual running time, excluding the time for scheduled maintenance. The accelerator presentations and the discussions in an accelerator breakout session, were organized into four broad topics, a) accelerator design concepts, b) accelerator systems and components, c) accelerator operations and system modeling, and 4) beam physics.

The room-temperature rf-linac approach has been studied thoroughly at LANL, especially for the tritium production (APT) application, and has undergone several reviews. This continuous-wave (cw or 100% duty factor) high-power linac concept, presented by G. Lawrence, provides a 1-GeV proton beam of 200 mA. The beam power of this linac is 200 MW, the total rf power required is about 250 MW, and the total ac power for the accelerator is 490 MW. The high beam current is achieved by using two electron-cyclotron resonance (ECR) ion sources, and funneling the beams with an rf funnel at 20 MeV. The funnel and the status of this technology was described in more detail in talks by S. Nath, and F. Krawczyk. At the lower beam currents of interest for ATW, the beam-power to ac-power efficiency for this concept would be smaller, but could be restored by pulsing the linac. The beam funnel

required high average currents can be achieved. The cyclotrons may be of interest for the lower end of the scale of beam currents. The PSI cyclotron facility operates in a cw mode at 1 mA, and is presently being upgraded to 1.5 mA. The total beam loss rate appears to be comparable to that of LAMPF. How high the current limits for cyclotrons can be pushed is not completely clear, but because of the inherently weaker focusing compared to the linac, especially at low velocities, it is not expected to compete favorably with linacs at high currents. An untested concept that was also mentioned is the separated orbit cyclotron, which is thought to be capable of accelerating up to 10 mA. Finally, an electron-driven subcritical reactor concept was presented by A. Krasnykh of the Joint Institute for Nuclear Research, Dubna, Russia. This idea, if feasible, would replace the proton accelerator with a simpler, and cheaper electron version.

C. Bohn discussed the prospects of a superconducting rf-linac for ADTT. In addition to reducing the rf power required for the accelerator, the superconducting linac would lead naturally to lower frequency cavities with larger radial apertures that could help reduce beam losses on the cavities. Superconducting solenoids could be used for strong focusing. The system is modular, being composed of many independent superconducting cavities and solenoids, and it is from this modularity that a high reliability can be achieved. By comparison with the room-temperature accelerator, higher accelerating gradients are possible in cw operation, leading to a shorter accelerator, and lower capital and operating costs. However, at the present time for high-current applications the rf power couplers limit the gradients. Furthermore, much more experience is needed for high-current operation of superconducting cavities; presently the experience is limited to several tens of milliamperes of relativistic electron beams. It is generally agreed that more R&D is needed to achieve the full potential provided by the superconducting option.

The beam-physics talks concentrated on the topics of design philosophy, beam halo, and the implications for control of beam loss. From the high-availability requirement, it follows that beam losses must be limited to avoid radioactivation that would complicate routine maintenance. Fractional beam loss rates should be controlled to below 10^{-8} m^{-1}, to ensure that hands-on maintenance is feasible. This requirement is hard to guarantee, until the beam distribution, including the beam halo is better understood. M. Reiser argued that the prevailing strategy for rf-linac design is incompatible with hands-on maintenance, because it results in a beam that is intrinsically unstable. He proposed a strategy in which the beam is continually equipartitioned, and always in thermal equilibrium. To achieve this state it is necessary to reduce the transverse focusing as the energy increases, resulting in a beam that is more space-charge dominated. Beam simulation studies should be carried out to investigate the implications of this suggestion.

937 95

demonstrate the long-term reliability. G. McMichael from Argonne reviewed the Continuous-Wave Deuterium Demonstrator (CWDD) project, a 7.5 MeV, 80-mA, cw, deuteron linac, which is a legacy from the SDI program. The facility was nearly completed when the funding ended, and is being retrofitted as a water-cooled, proton linac, and has been renamed the Argonne Continuous-Wave Linac (ACWL). Possible applications include a testbed for cw linac engineering. D. Chan described the proposed Accelerator Performance Demonstration Facility (APDF) at LANL, intended as a front end prototype for an APT. A summary of the new 7-MeV RFQ model, and other new developments, including a new intermediate-velocity structure, known as the coupled-cavity drift-tube linac (CCDTL) were discussed.

The high average intensity meson factories, such as LAMPF (800 MeV, 1 mA, and 6-12% duty factor, 82% availability), are most similar to the accelerators that we need for the ADTT. The operational experience from the LAMPF linac was reviewed by O. Van Dyck. Over the most recent five year period the accelerator availability was rated at 82.5%, although there was a steady downward trend. Comparison of the reliability of the different components showed the highest failure rate for the 201-MHz rf system. This situation improved significantly after repairs were made, and more instrumentation was introduced in 1993. The predominant 805-MHz rf system has shown no such deterioration. Progress was made through a combination of statistical analysis and engineering input. The lesson to be learned is that one needs a continuing program of refurbishment, and if this is done, there is no reason why the accelerator availability should not exceed 90%. The discussion of reliability continued in the presentation of P. Tallerico, who reviewed the rf system issues. Reliability has two components a) mean time to failure, and b) the mean time for repair. Stress and loading are the main causes of failure. The usual remedy for control of thermal stress, which is to increase the dimensions, is limited for rf components, where the sizes are fixed proportional to the wavelength. Instrumentation is important to provide warning before failure occurs.

Recent work on accelerator system models, helpful for optimizing the accelerator design and for making cost estimates, were presented by G. Gillespie of Gillespie Associates, and A. Todd of Grumman. Gillespie demonstrated such a computer code that runs on a Macintosh computer. Gillespie and Todd have shared many of their developments. The important topic of an accelerator cost model was also presented by R. McAdams of AEA Technology, Culham, UK.

The two-hour accelerator breakout session provided a forum for a continuing discussion of all the above topics. Perhaps the most important recommendation was that an integrated high-current, low-energy, front-end linac is needed to address the cw reliability and availability issues. One needs to design for high reliability, establish a data-base of long-term cw operation,

Summary of the Materials Breakout Group

International Conference on Accelerator Driven Transmutation Technologies and Applications

Chairpersons
Frank Garner, Batelle-Pacific Northwest Laboratories
Walt Sommer, Los Alamos National Laboratory

This breakout group discussed the following topics and reached a number of recommendations summarize later. The topics of discussion included

1) a comparison of expected materials response at spallation sources to experience with fission reactors;
2) synergistic effects from high-energy particle radiation, corrosion, and cyclic stresses;
3) estimates, based on experience with materials developed for fission and fusion reactors, for
- materials testing needs;
- facilities for materials development, both available and needed;
- candidate materials;
- time frame for material qualification; and
- expected program costs.

A summary of experience with materials at accelerator target stations and dedicated experiments was presented in the Breakout Group that contained the following information:

Material	Fluence or Irradiation
Inconel718	$> 10^{21}$ protons/cm^2
Copper	$> 10^{21}$ protons/cm^2
Tungsten	$> 10^{21}$ protons/cm^2
304L Stainless Steel	$\sim 10^{22}$ neutrons/cm^2
Aluminum (AC-100)	6×10^{21} protons/cm^2
Aluminum alloys (6061, 5052, 2219)	4 to 7 x 10^{20} protons/cm^2 4 x 10^{20} neutrons/cm^2
Glidcop ($Cu + Al_2O_3$)	2 dpa
Copper	low dose and 0.5 dpa
Tantalum	5 x 10^{20} protons/cm^2
HT-9 (Fe 12Cr 1Mo)	5 x 10^{20} protons/cm^2
Carbon Steel	low dose
Tungsten and alloys	4 x 10^{20} protons/cm^2
Pure materials	low proton and neutron dose
304 Stainless Steel	5 x 10^{20} protons/cm^2

Continuing or new materials irradiation tests are underway at the LAMPF facility (summer/fall 1995) and in the Proton Irradiation Experiment (PIREX) at the Paul Scherrer Institute in Switzerland. Materials irradiation to high dose values continue for relevant neutron spectra in reactors in the United States, Japan, Europe, and Russia.

Recommendations, conclusions, and observations from the Materials Breakout Group were the following.

1) An early emphasis on materials behavior in response to irradiation should accompany any new program.
2) Both "surrogate" and surveillance activities should be included.
3) A high-level of participation of materials specialists from the reactor community should occur and collaborations should be developed with Russian and Japanese scientists in order to conduct tests in their reactors. This can help the material testing community address a difficulty associated with the closing of most test reactors in the United States.
4) With respect to radiation performance of "new" materials, ignorance of their behavior is often taken as a sign that the material will perform as required.
5) Materials chosen primarily on the basis of desired neutron properties are frequently those found to be most prone to either environment and/or radiation-induced degradation.
6) One difficulty for future materials testing is that the United States is shutting down most of its test reactors.
7) All nuclear-related activities now proceed in an ever more restrictive regulatory environment, requiring scientists and engineers to recognize and participate in what is now referred to as a "culture change".
8) There is a growing sensitivity to safety issues and perceptions of safety. There is a growing sophistication of DOE and other agencies on the role of radiation-induced degradation as a crucial element of safety. Thus in the current political and regulatory environment, it is counterproductive to attempt to minimize the potential impact of radiation-induced degradation in any new system.
9) Development of spallation-based devices will most likely exceed the envelope of existing knowledge concerning the radiation response of chosen materials. If conditions of high displacement rates and elevated temperatures exist in accelerator-driven systems, these could propel materials into a non-equilibrium regime of microstructural evolution having profound impacts on materials phase stability. They could also lead to the initiation of dimensional instability and mechanical and physical property changes.
10) Each major existing energy producing concepts has encountered unanticipated phenomena arising from radiation damage. Often these become a life limiting factor for the concept.

Summary of the Target-Blanket Breakout Group

International Conference on Accelerator Driven Transmutation Technologies and Applications

Chairpersons
Mike Capiello, Los Alamos National Laboratory
Charles Bell, Los Alamos National Laboratory
Wolfgang Barthold, Barthold and Associates

This breakout group discussed a number of topics and issues pertaining to target and blanket concepts for accelerator-driven systems. This major component area is one marked by a broad spectrum of technical approaches. It is therefore less defined than other major component areas such as the accelerator and is at an earlier stage of technical needs and task specification. The working group did reach a number of general conclusions and recommendations that will be summarized later.

The Conference and the Target/Blanket Breakout Group provided a first opportunity for people working on a variety of missions and concepts to get together and exchange information. A number of subcritical systems applicable for a spectrum of missions were proposed at the Conference and discussed in the Breakout Group. Missions included plutonium disposition, energy production, waste destruction, isotope production, and neutron scattering. These, along with target-blanket concepts proposed for them, appear in Table 1.

Abroad spectrum of target/blanket approaches are being investigated world wide in varying stages of analyses and sophistication. These efforts are primarily aimed at establishing the feasibility of subcritical systems with the emphasis on physics performance. Little actual engineering detail has been included thus far in most analyses. However real progress has been made on establishing the framework for solving problems of level of subcriticality, reactivity coefficient behavior, materials requirement definition, etc. Current analysis codes appear to be sufficiently accurate for beginning design activities. There is a follow-on need for sophisticated production/depletion codes such as CINDER90 to be made available for follow-on design activities. As can be seen from the list of target/blanket concepts in Table 1, there is real interest for many applications for liquid lead as the spallation target material.

An important topic area common to all such blanket analyses centered around issues associated with subcriticality. Subcritical operation provides conditions where the is less performance sensitivity to xenon decay, in contrast to reactor environments. The need to measure subcriticality level during system operation was established as an important one. Also since such systems are subcritical, reactivity feedback mechanisms that provide capabilities for levels of passive control in newer reactor designs have diminished importance. The accelerator system must rely on the fact that the level of subcriticality is sufficient to account for unforeseen reactivity insertions. Off-normal events must be sensed so that the accelerator beam can be turned off. The shut down reliability needs to be similar to passive reactor shutdown features proposed for advanced reactors. Finally, there is a need for understanding of accelerator operation in terms of possible effects on target/ blanket operation resulting from accelerator upsets, flicker, etc.

The Target/Blanket Breakout Group also defined areas where parameters and data should be addressed as target/blanket design activities become more detailed and sophisticated. This list is contained in Table 2.

Table 1 - ADTT Target/Blanket Concepts Presented at the Conference

Mission	Target	Blanket /Fuel	Neutron Spectrum
Pu Disposition	Liquid Pb	Fluoride salt	Thermal, epithermal
	Liquid Pb	Chloride salt	Epithermal
	Liquid Pb	HTGR	Epithermal
	Water cooled Pb	Particle bed	Fast
	Na cooled W	Na cooled metal fuel	Fast
Energy	Liquid PbBi	UO_2, Pb-Bi cooled	Fast
	Liquid Pb	Th-U, Pb cooled	Fast
	Liquid Pb	Th-U fluoride salt	Epithermal
Waste Destruction	Liquid Pb	Pu fluoride salt	Thermal, epithermal
	Th-Pu-Pb chloride	Th-Pu-Pb chloride	Fast
	Na cooled W	Na cooled metal	Fast
	Actinide chloride	Coated particle, He cooled	Fast
	Liquid Pb	Pb slurry	Thermal
Isotope Production	Water cooled lead	Light water	Thermal
	Water cooled tungsten	Heavy water	Thermal
Neutron Scattering	Water cooled W		
	Water cooled Zr		
	Water cooled Pb		
	Rotating Pb		
	Liquid Pb		

Table 2 - Parameters and Data Needs for More Sophisticated Design Efforts

GENERAL DESIGN PARAMETER NEEDS
Application
Accelerator energy
Blanket power
Target material and type (solid or liquid)
Blanket material and type (solid or liquid)
Front-end partitioning partition and processing needs
Potential changes required in laws or regulations for system operation
Waste Stream
Cost and Schedule

TARGET DESIGN DETAILS
Material
Structural material
Peak power density
Window material
Coolant type
Coolant flow rate, temperature regime, pressure

Component lifetime

BLANKET DESIGN DETAILS
Fuel type
Structural material
Moderator
Total power
Peak power density
Spectrum
Coolant type
Coolant flow rate, temperature regime, pressure
Average and peak fluxes
Component lifetime

PERFORMANCE
Rate and efficiency of mission objectives (material destruction, electricity generation, etc.)
Accelerator power requirements
Cost projections
Projected availability

SAFETY
Degree of subcriticality
Doppler coefficient behavior
Temperature coefficient
Design basis events
Containment requirement and defense in depth

TECHNOLOGY MATURITY
Fuel
Structures
Coolant
Moderator
Processing
Components
Nuclear data

DEVELOPMENT REQUIREMENTS
Feasibility issues
Near-term experiments
Long-term experiments
Test facility requirements

Summary of the Separations Breakout Group

International Conference on Accelerator Driven Transmutation Technologies and Applications

Chairperson
Reed Jensen, Los Alamos National Laboratory

The Separations Breakout Group reviewed the wide spectrum of separations technologies available for application to ADTT systems. Separations processes play a key role in areas associated with preparation of feed materials for introduction into ADTT, removal of fission products and other transmutation by products that build into the fuel during operation, and in the preparation of wastes ("polishing") for discharge from ADTT systems so as to meet appropriate waste disposal criteria. General separations technologies addressed by the group included aqueous, fluoride salt, and chloride salt approaches.

A top level question associated with separations needed for ADTT systems was whether they can achieve required performance (separation) levels with minimized waste production. Simultaneously such operations must achieve public acceptance driven primarily by safety and environmental perspective. Both specialists in aqueous and molten salt believed the answer to this feasibility question to be yes.

The area of aqueous technology has seen a long-period (decades) for development with successful operation demonstrated mainly overseas in large plants such as Thorp and La Hague. In the United States, aqueous-based separations suffer from negative perceptions associated with their use in the past at governmental sites such as Savannah River and Hanford. The technology has been demonstrated at scale, can be adapted to continuous processing, and avoids use of moving parts. Key improvement areas for aqueous processing include the development of more efficient methods for actinide/lanthanide separations, improvement of the performance of reagents in high radiation environments, and overall reduction of waste generation, particularly low-level wastes.

Molten salt separations have seen a significant level of recent development through the Argonne National Laboratory and Rockwell Corporation's work in pyroprocessing of actinides and fission products in chloride salt mixtures. Beginning flowsheets have been defined for ADTT systems but a number of significant gaps exists in components associated with actinide/lanthanide separations. Candidate methods include liquid metal extraction investigated by Oak Ridge as part their Molten Salt Reactor Program, precipitation-based methods proposed by Los Alamos, and a novel centrifugation-based approach, also proposed by Los Alamos. Most of these flowsheet component definitions lack real engineering. Finally with respect to salt-based processing there are questions concerning the real level of waste generation, particularly the mixed waste category because of beryllium and cadmium involved in such processes.

The following development needs were identified by the Breakout Group. These would primarily occur before moving to pilot-scale experience and would be preceded by more detailed flowsheet specification and development. Next stage development needs include

-acquisition of electrochemical experience in fluorides;
- improved trivalent actinide/lanthanide separation technique development both for aqueous and molten salt media;
- determination of chemical behavior in salts as a function of redox potential and of Lewis basicity;

Summary of the Experiments and Data Breakout Group

International Conference on Accelerator Driven Transmutation Technologies and Applications

Chairperson
Steve Wender, Los Alamos National Laboratory

The Experiments and Data Breakout Group addressed status of experiments directed towards, or relevant to, ADTT system development. Such experiments are the bridge between ideas and reality. They simultaneously cross cut all major technology and components of ADTT systems -- accelerators, target/blanket, separations, and materials. At this Conference the large majority of papers dealing with experiments were on nuclear data and cross sections. No separate papers were presented on materials experiments although data were included in papers presented at the several sessions on materials.

Nuclear data and cross section presentations included cross sections for proton and neutron induced reactions on relevant ADTT materials. Data were also presented for spallation product cross sections and for cross sections involving reactions on unstable nuclei. One conclusion from the breakout group was that there are too many cross sections needed over too large an energy range. Since direct measurements cannot supply all data needed for ADTT system design, calculational tools will supply the vast majority of the needed data. Such codes must be carefully benchmarked with relevant data. One recommendation from this breakout group was the formation of a group to collate and prioritize data needs and to provide input to existing data centers (IAEA, OECD/NEA, ...).

Some of the discussion related to materials damage in this breakout group overlapped that of the Materials Breakout Group. Experimental areas identified by the group included corrosion, radiation damage (gas production, embrittlement), radiation-enhanced corrosion, new materials development, compatibility, qualification/certification, and environmental issues. In this area, similar to the situation for nuclear data, issues arise that are associated with dissemination of material needs and the availability of facilities for materials testing, particularly those with high neutron fluences.

Beginning engineering experiments were also discussed which could address issues such as neutronics performance and code benchmarking, handling of special products through processes such as sparging of volatiles, determination of thermal hydraulics performance, and beginning safety performance.

Larger scale experiments will also be required for ADTT system development. One such example is a proposed experiment that would be a coupled accelerator/target/blanket demonstration that could be performed at the Los Alamos Meson Physics Facility. Such an experiment would demonstrate neutronics performance, diagnostics, control mechanisms, and coupling of several complex systems plus support features such as pumps, heaters, heat exchangers, etc. Issues include how to involve a wide spectrum of participants from national laboratories, industry, and universities. The status of other facilities amenable to such integrated tests is also uncertain. Finally the importance of LAMPF either in the context of engineering tests or integrated demonstrations was noted as essential.

- identification of materials to be used in salt processing that are compatible and corrosion resistant;
- demonstration of redox control of plutonium fluoride salt systems;
-development of plutonium fluoride salt mixture phase diagram data;
- improved control of neptunium in PUREX processes;
- improvement in the performance and waste generation characteristics of front-end processes to ADTT; and
- improvements in instrumentation, particularly methods that allow determination of material composition of flowing process streams.

Author Index

M

N

O

P

R